

ADHESION SCIENCE AND ENGINEERING - 2

Series Editor: A.V. Pocius

SURFACES, CHEMISTRY & APPLICATIONS



Edited by M. Chaudhury and A.V. Pocius

ELSEVIER

ADHESION SCIENCE AND ENGINEERING – 2

Series Editor

A.V. Pocius

The cover displays a micrograph of glass particles on a plasticized polystyrene substrate showing adhesion-induced viscous flow of the substrate and encapsulation of the particle. The crater is the deformed substrate after a particle had been removed. The micrograph was taken by Ray Bowen and was supplied by Dr. Donald Rimai.

ADHESION SCIENCE AND ENGINEERING – 2

SURFACES, CHEMISTRY AND APPLICATIONS

Edited by

M. Chaudhury

*Department of Chemical Engineering
Center for Polymer Interfaces
Lehigh University
111 Research Drive
Bethlehem, PA 18105
U.S.A.*

A.V. Pocius

*3M Adhesive Technologies Center
3M Center, Building 201-4N-01
St. Paul, MN 55144-1000
U.S.A.*



2002

ELSEVIER

Amsterdam – Boston – London – New York – Oxford – Paris – San Diego
San Francisco – Singapore – Sydney – Tokyo

ELSEVIER SCIENCE B.V.
Sara Burgerhartstraat 25
P.O. Box 211, 1000 AE Amsterdam, The Netherlands

© 2002 Elsevier Science B.V. All rights reserved.

This work is protected under copyright by Elsevier Science, and the following terms and conditions apply to its use:

Photocopying

Single photocopies of single chapters may be made for personal use as allowed by national copyright laws. Permission of the Publisher and payment of a fee is required for all other photocopying, including multiple or systematic copying, copying for advertising or promotional purposes, resale, and all forms of document delivery. Special rates are available for educational institutions that wish to make photocopies for non-profit educational classroom use.

Permissions may be sought directly from Elsevier Science via their homepage (<http://www.elsevier.com>) by selecting 'Customer support' and then 'Permissions'. Alternatively you can send an e-mail to: permissions@elsevier.com, or fax to: (+44) 1865 853333.

In the USA, users may clear permissions and make payments through the Copyright Clearance Center, Inc., 222 Rosewood Drive, Danvers, MA 01923, USA; phone: (+1) (978) 7508400, fax: (+1) (978) 7504744, and in the UK through the Copyright Licensing Agency Rapid Clearance Service (CLARCS), 90 Tottenham Court Road, London W1P 0LP, UK; phone: (+44) 207 631 5555; fax: (+44) 207 631 5500. Other countries may have a local reprographic rights agency for payments.

Derivative Works

Tables of contents may be reproduced for internal circulation, but permission of Elsevier Science is required for external resale or distribution of such material.

Permission of the Publisher is required for all other derivative works, including compilations and translations.

Electronic Storage or Usage

Permission of the Publisher is required to store or use electronically any material contained in this work, including any chapter or part of a chapter.

Except as outlined above, no part of this work may be reproduced, stored in a retrieval system or transmitted in any form or by any means, electronic, mechanical, photocopying, recording or otherwise, without prior written permission of the Publisher.

Address permissions requests to: Elsevier Science Global Rights Department, at the fax and e-mail addresses noted above.

Notice

No responsibility is assumed by the Publisher for any injury and/or damage to persons or property as a matter of products liability, negligence or otherwise, or from any use or operation of any methods, products, instructions or ideas contained in the material herein. Because of rapid advances in the medical sciences, in particular, independent verification of diagnoses and drug dosages should be made.

First edition 2002

Library of Congress Cataloging in Publication Data

A catalog record from the Library of Congress has been applied for.

British Library Cataloguing in Publication Data

A catalogue record from the British Library has been applied for.

ISBN: 0 444 51140 7 (set)

♾ The paper used in this publication meets the requirements of ANSI/NISO
Printed in The Netherlands.

Preface

Volume I of Adhesion Science and Engineering dealt with the mechanics of adhesive bonds and the rheology of adhesives. Volume II deals with the other two disciplines that make up adhesion science, surfaces and chemistry. In addition, this volume describes several applications of adhesion science and engineering.

The volume begins with discussions of aspects of surface science and how they relate to adhesion science. Methods based on surface thermodynamics have been powerful tools in the hands of adhesion scientists. Berg introduces us to the topics of interfacial thermodynamic and practical adhesion and shows how the critical predictive parameters of adhesion can be obtained from wetting, solution theory and group contribution methods (UNIFAC). It becomes clear from Berg's presentation that the predictions of adhesion strengths by the traditional wet chemical methods are somewhat empirical. This limitation can be partially overcome by the methods of contact mechanics as pioneered by Johnson, Kendall and Roberts, which allows direct measurements of the surface energies of deformable solids. These methods, as shown by Mangipudi and Falsafi, have played a very important role in developing a deeper understanding of the relationship between adhesion and the chemical composition of surfaces and complement the chapters describing contact mechanics found in Volume I. Rimai and Quesnel extend this discussion to the interaction of powdered solids and give us an in-depth view of the types of intermolecular forces that control adhesion of solid surfaces. The chapter by Wahl and Syed Asif explores the behavior of adhesion and contact mechanics at the nanoscopic level. This chapter not only complements the above three but also describes additional techniques that may be used to probe the properties of surfaces. Surface roughness, which could be examined by some of the probe techniques described in Chapter 4, is discussed by Packham. Spectroscopic techniques useful for examination of the chemistry of surface and interfaces are described by Boerio (Chapter 6).

Other aspects of interfacial science and chemistry are examined by Owen and Wool. The former chapter deals with a widely used chemistry to join disparate surfaces, that of silane coupling agents. The latter chapter describes the phenomenon of diffusion at interfaces, which, when it occurs, can yield strong and durable adhesive bonds. Brown's chapter describes the micromechanics at the interface when certain types of diffusive adhesive bonds are broken. The section on surfaces ends with Dillingham's discussion of what can be done to prime surfaces for adhesive bonding.

The section on chemistry of adhesives evolves from rubber-based adhesives to semi- structural and finally to structural adhesives. Everaerts and Clemens provide a thorough description of chemistry and applications of pressure sensitive adhesives and Kinning and Schneider describe an enabling technology for pressure

sensitive adhesive tapes, release coatings. Martín-Martínez reviews the chemistry and physical properties of rubber-based adhesives with an emphasis on the materials properties of the components of those adhesives. Silicone chemistry provides products that range from pressure sensitive adhesives to sealants to semi-structural adhesives and is described by Parbhoo et al. in Chapter 14. Progressing into more semi-structural and structural adhesives, the chapters by Paul and by Frisch describe the chemistry and properties of hot melt adhesives and polyurethane adhesives, respectively. The remainder of this section deals with structural adhesives beginning with discussions of acrylate chemistry by Righettini and then Klemarczyk. The adhesives described in these two chapters are some of the most easy to use structural adhesives available. One of the oldest technologies in modern adhesive chemistry, phenolic chemistry is described by Detlefson and one of the newer chemistries, bismaleimides is discussed by Kajiyama.

The final section in this volume deals with applications of adhesion science. The applications described include methods by which durable adhesive bonds can be manufactured by the use of appropriate surface preparation (Davis and Venables) to unique methods for composite repair (Lopata et al.) Adhesive applications find their way into the generation of wood products (Dunky and Pizzi) and also find their way into the construction of commercial and military aircraft (Pate). The chapter by Spotnitz et al. shows that adhesion science finds its way into the life sciences in their discussion of tissue adhesives.

The editors wish to express their sincere thanks to the contributing authors for their invaluable contributions to this volume. Their collective expertise represents many years of industrial and academic experience in the field of Adhesion Science and Engineering. We would also like to thank the employers of each of the contributors for allowing them to take on the extra tasks associated with the completion of their contribution to this volume. We would also like to acknowledge the contribution of Mr. Theodore Reinhart of the University of Dayton Research Center to the initial organization of this volume. An unfortunate illness prevented him from completing his work on this project. Assistance from the Department of Chemical Engineering and the NSF sponsored IUCRC of the Polymer Interface Center at Lehigh University are gratefully acknowledged. Finally, we thank our spouses for their patience as we compiled and edited this volume.

ALPHONSUS V. POCIUS
Editor

Corporate Scientist
3M Company
St. Paul, MN, USA

MANOJ CHAUDHURY
Associate Editor

Professor of Chemical Engineering
Director, Center for Polymer Interfaces
Lehigh University
Bethlehem, PA, USA

Contents

Preface	v
---------------	---

Surface Science

Chapter 1. Semi-empirical strategies for predicting adhesion <i>J.C. Berg</i>	1
Chapter 2. Direct estimation of the adhesion of solid polymers <i>V.S. Mangipudi and A. Falsafi</i>	75
Chapter 3. Particle adhesion <i>D.S. Rimai and D.J. Quesnel</i>	139
Chapter 4. Surface mechanical measurements at the nanoscale <i>K.J. Wahl and S.A. Syed Asif</i>	193
Chapter 5. Micro-mechanical processes in adhesion and fracture <i>H.R. Brown</i>	221
Chapter 6. Surface analysis in adhesion science <i>F.J. Boerio</i>	243
Chapter 7. Surface roughness and adhesion <i>D.E. Packham</i>	317
Chapter 8. Diffusion and autohesion <i>R.P. Wool</i>	351
Chapter 9. Coupling agents: chemical bonding at interfaces <i>M.J. Owen</i>	403
Chapter 10. Priming to improve adhesion <i>G. Dillingham</i>	433

Chemistry

Chapter 11. Pressure sensitive adhesives <i>A.I. Everaerts and L.M. Clemens</i>	465
Chapter 12. Release coatings for pressure sensitive adhesives <i>D.J. Kinning and H.M. Schneider</i>	535
Chapter 13. Rubber base adhesives <i>J.M. Martín-Martínez</i>	573
Chapter 14. Fundamental aspects of adhesion technology in silicones <i>B. Parbhoo, L.-A. O'Hare and S.R. Leadley</i>	677
Chapter 15. Hot melt adhesives <i>C.W. Paul</i>	711
Chapter 16. Chemistry and technology of polyurethane adhesives <i>K.C. Frisch, Jr.</i>	759
Chapter 17. The chemistry of bis-maleimides used in adhesives <i>M. Kajiya</i>	813
Chapter 18. Structural acrylics <i>R.F. Righettini</i>	823
Chapter 19. Cyanoacrylate instant adhesives <i>P. Klemarczyk</i>	847
Chapter 20. Phenolic resins: some chemistry, technology, and history <i>W.D. Detlefsen</i>	869

Applications

Chapter 21. Surface treatments of metal adherends <i>G.D. Davis and J.D. Venables</i>	947
Chapter 22. Electron beam processed adhesives and their use in composite repair <i>V.J. Lopata, A. Puzianowski and M.A. Johnson</i>	1009

Chapter 23. Wood adhesives	
<i>M. Dunky and A. Pizzi</i>	1039
Chapter 24. Tissue adhesives and hemostats: new tools for the surgeon	
<i>W.D. Spotnitz, D. Mercer and S. Burks</i>	1105
Chapter 25. Applications of adhesives in aerospace	
<i>K.D. Pate</i>	1129
<i>Author Index</i>	1193
<i>Subject Index</i>	1195

Chapter 1

Semi-empirical strategies for predicting adhesion

JOHN C. BERG *

Department of Chemical Engineering, University of Washington, Seattle, WA 98105-1750, USA

1. Predicting adhesion: is it a reasonable objective?

1.1. The scope of the question

1.1.1. The meaning of adhesion, adhesive failure and interfacial strength

Adhesion refers to a complicated set of inter-connected phenomena that is far from completely understood, and it therefore makes sense at the outset to inquire into the reasonableness of any attempts to ‘predict’ it using semi-empirical methods. To preserve the hope of a positive answer, it is first necessary to narrow the scope of the question. There may be ambiguity with respect to what is to be predicted. It may refer, on one hand, to the strength of an isolated adhesive joint as determined by some carefully crafted mechanical test in which the joint is destroyed, or it may, on the other hand, refer to the strength of a more complex global structure, such as a multi-layer laminate, or a fiber-reinforced or particle-filled composite. The present chapter focuses mainly on the individual adhesive joint rather than on global structures in which interfaces exist. Even when attention is focused on single joints, it must be noted that these may be stressed to failure in different modes and at different rates, leading to different results. In fact, understanding of the different interfacial rate processes involved in adhesion is just beginning to emerge [1].

Another distinction to be made is illustrated with the peel test shown in Fig. 1. Application of stress may cause the joint to fail either ‘adhesively’ or ‘cohesively’. Adhesive failure, shown in Fig. 1a, is thought ideally to correspond to a perfect

* Corresponding author. E-mail: berg@cheme.washington.edu

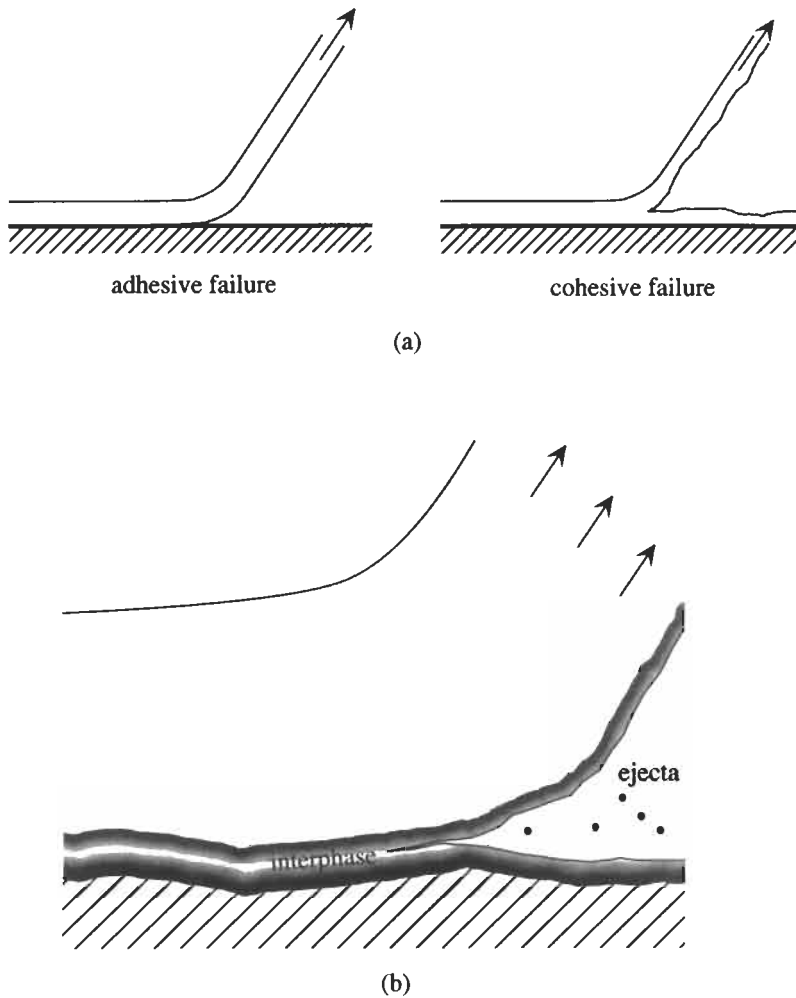


Fig. 1. (a) Adhesive vs. cohesive failure. (b) Close-up view of adhesive failure in the presence of an 'interphase.' The locus of failure may be adjacent to or within the interphase (as shown), and particles of material may be ejected during the debonding process.

separation of the two phases meeting at the interface. Sharpe [2] has argued persuasively, however, that such 'adhesive' or 'interfacial' failure almost never occurs in practice. Owing to the geometric complexity of any real interface at the microscopic level, it would be highly unlikely for the system to disjoin precisely along its contours. One would expect instead to find at least fragments of the opposing material on each of the separated surfaces, and indeed some of the material may be ejected and lost as microparticles during the disjoining process [3]. Furthermore, Sharpe argues that true interfaces, in the mathematical sense, dividing phases which are homogeneous right up to the interfaces, almost never

exist between joined solid phases. Instead there is generally a transition zone of finite thickness, perhaps as thin as 1 nm, but possibly as thick as several micrometers, separating the bulk phases. Called *interphases*, they may be caused by the interdiffusion or interdigitation of the materials, or they may be simply the result of structuring of the adhesive layer adjacent to the interface due to the asymmetric molecular forces existing at the boundary between the phases. Such an 'interphase' has a structure, and possibly a composition, distinct from that of either of the bulk phases. Recognizing the ubiquitous presence of interphases, the following definition of terms will be used in this chapter: when the locus of failure occurs within or immediately adjacent to the interphase, it will be referred to as 'adhesive' or 'interfacial' failure, as shown in Fig. 1b. The word 'interface' is thus used loosely in that it may be referring to an interphase. When failure of the joint occurs in material outside the interphase, i.e. in one of the bulk phases, it will be designated as 'cohesive' failure. Even with this distinction having been made, some cases involve a mixture of adhesive and cohesive failure. The design or choice of a structural adhesive thus may depend on both high interfacial strength and high cohesive strength of the adhesive. The present chapter concerns adhesive failure, and therefore focuses on 'interfacial strength' in accord with the above definition.

It must also be recognized that adhesive interfaces are not static entities, but may deteriorate or even strengthen over time, and often it is the time course of interfacial strength or durability under different conditions and in different environments that is of greatest concern [4]. As important as durability issues are, they too will not be a direct concern of this chapter.

It remains to be determined if even the more modest scope suggested above may profitably be pursued. To address this question, we note that 'adhesive interfaces' refer to those dividing solid phases across which intermolecular forces are engaged over all or a significant portion of the interfacial area. With the exception of clean, atomically smooth solid surfaces (as might be obtained when Muscovite mica is freshly cleaved in vacuo), this cannot be achieved by simply bringing two solid surfaces together. Their inherent roughness and contaminability prevent it. Thus at least one of the phases must be a liquid (or a polymer sufficiently above its glass transition temperature to be fluid-like) when the two materials are brought together to form the interface. The 'liquid' phase is designated as the *adhesive*, and the solid surface to which it is applied is the *adherend*. The adhesive interface is finally formed when the adhesive 'cures'. In most cases, curing results in solidification of the adhesive, although pressure sensitive adhesives may remain in a viscoelastic state. In most cases, solidification results in the development of significant internal residual stresses at the interface owing to the mismatch in thermo-mechanical properties of the adhesive and adherend [5,6]. In some cases, these are great enough to cause interfacial failure without the application of any external stress at all. In any event, the presence and magnitude of internal residual

stresses must be taken into account in the analysis of the results of mechanical measurements of interfacial strength. Residual stresses do not directly influence the *intrinsic* interfacial strength, but instead contribute to the total of the stresses existing at an interface in a mechanical test.

In a mechanical test, interfacial strength may be quantified in terms of either the minimum load required for interface disruption or the total integral energy or work expended. In many situations, due to non-uniformity of chemical or morphological conditions over the area of the interface or to non-uniformity of the applied stress in a given test [7], the two criteria are different. The investigator must thus strive to minimize or deal with both of the above complications, i.e. the interfaces studied should be chemically and morphologically uniform, and the stresses applied in the test should be uniform or distributed in way which is quantitatively describable.

1.1.2. Optimizing adhesion

The adhesion scientist or technologist has two general variables at his or her disposal in seeking to increase or control adhesive interfacial strength: (1) the chemical formulation of the adhesive; and (2) the chemistry and morphology of the adherend surface. The adhesive may be chosen, for example, to be made up of species capable only of Lifshitz–van der Waals (LW) intermolecular interactions (referring to predominantly dispersion or London's forces, but also including a possible small contribution to permanent dipole interactions), or it may be made to be acidic or basic, or acid–base bifunctional, or it may be designed to interact covalently with the adherend (reactive adhesion). Its surface tension may be lowered or its viscosity altered through the use of additives. Most adhesives are polymeric, and for a given chemistry of the repeat unit, the molecular weight and the structure (linear vs. branched, etc.) may be important. Thermosetting adhesives (e.g. epoxies, polyurethanes, bis-maleimides, etc.) are designed to crosslink internally, leading to enhanced cohesive strength (outside the scope of the present discussion), but may also produce covalent bonding with the adherend *across* the interface [8]. The morphology of the adherend surface may be altered by roughening or texturizing (e.g. acid-etching, grit-blasting, anodization, etc.), and its chemistry may be altered through plasma treatment, corona treatment, etc. or the use of finishes, conversion coatings, primers or coupling agents, either physically adsorbed, coated onto or covalently bonded to the surface.

It is only in the context of the systematic variation of the properties of the adhesive and/or the adherend surface in a set of otherwise identical specimens subjected to a given mechanical testing procedure that it is reasonable to think of predicting *relative* interfacial strength.

In the above narrowed context, 'prediction' refers to the development of system descriptors which can be measured independently in some rather simple and inexpensive way (in terms of time and instrumentation), or it may refer to ab

initio calculations based on readily available handbook data and requiring no experimental measurements at all. Both approaches are examined in this chapter. The objective may be to screen candidate adhesive formulations and/or adherend surface treatments for the purpose of eliminating unpromising candidates for what is generally tedious and costly mechanical testing. The results of such attempts may vary from the formulation of simplistic, but nonetheless useful, 'rules of thumb', to more sophisticated optimization schemes. Such guidelines may be useful even when all of the above-mentioned *caveats* are not observed.

1.2. 'Practical' vs. 'ideal' adhesion

1.2.1. Practical adhesion

The measure of adhesive interfacial strength is the result of a properly conducted mechanical test which leads to a predominantly adhesive failure of the specimen. This leads to a measure of what is termed 'mechanical', or 'practical' adhesion. Many different such tests are described in detail elsewhere in this text series, as well as in standard texts on adhesion [9–11]. As noted above, however, even for a given material interface, different tests carried out under the same thermodynamic conditions, or the same test carried out at different rates (normalized in accord with WLF theory, described elsewhere in this text series), will in general lead to different values for the failure stress or for the energy per unit area required to disjoin the interface. The recent emergence of the method of 'contact mechanics', reviewed recently by Chaudhury [12], permits the quantitative mechanical determination, under idealized circumstances, of both the energy required to separate two surfaces as well as the energy gained by adjoining them, and the results indicate that there is a sizable difference between the two ('adhesion hysteresis') [13]. Thus any valid comparisons of practical adhesion between material systems whose properties are varied as suggested above must pertain to the same test, carried out under the same conditions at the same normalized rate. Even when these requirements are stringently met, the results may show significant variation, as has been demonstrated in a round-robin program in 1993 involving 12 different laboratories measuring the interfacial shear strength of the same fiber/matrix interface with the same set of techniques [14]. Fig. 2 shows the results of this effort, revealing variations within any given test method of approximately a factor of two amongst the different laboratories. Thus the objective of predictions must be recognized as a somewhat blurred target, although it may be hoped that results for practical adhesion obtained in any given laboratory for a series of properly conducted tests may be validly compared.

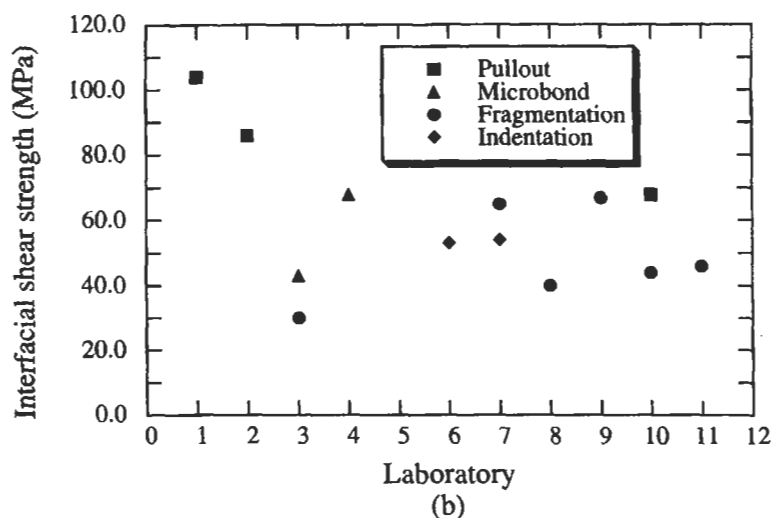
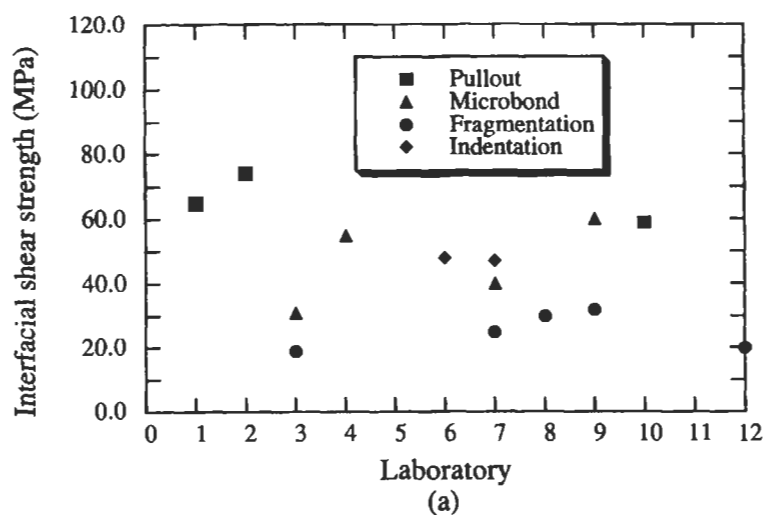


Fig. 2. Results of interfacial shear strength measurements of the same fiber/matrix systems using four different micro-mechanical tests during a round-robin program involving 12 different laboratories. (a) Results for untreated, unsized carbon fibers. (b) Results for carbon fibers with the standard level of surface treatment. Redrawn from ref. [13].

1.2.2. Ideal adhesion

Most of the various strategies which have been proposed to 'predict' relative adhesive interfacial strength are based on thermodynamics. One may define, without ambiguity, as shown in Fig. 3, a thermodynamic 'work of adhesion', W_A ,

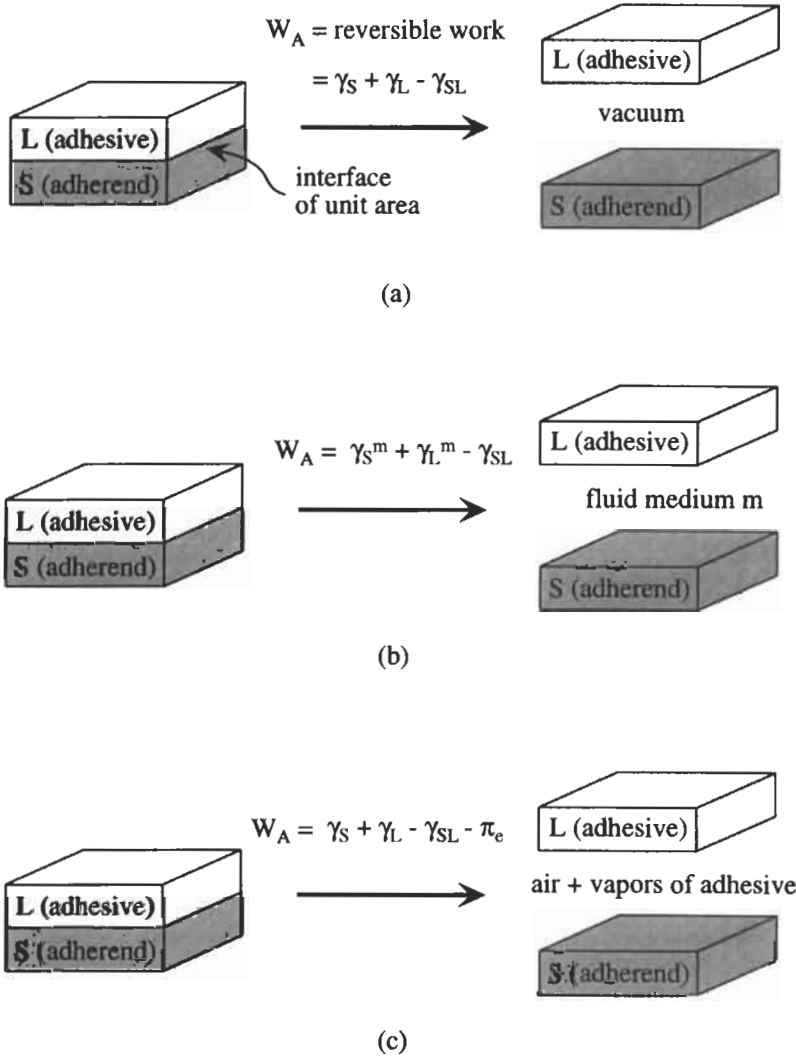


Fig. 3. Definition of thermodynamic work of adhesion, W_A : (a) disjoining surfaces in vacuum; (b) disjoining surfaces in fluid medium m ; and (c) disjoining surfaces in presence of vapors from adhesive.

as the reversible work required to perfectly disjoin a unit area of interface between an adherend S (solid) and adhesive L (liquid) in some fluid medium m , as given by the Dupré equation:

$$W_A = \gamma_S^m + \gamma_L^m - \gamma_{SL}, \quad (1)$$

where γ_L^m is the surface or interfacial tension of the adhesive (liquid) in the fluid medium m , γ_S^m is the interfacial free energy/area of the adherend (solid)/medium

interface, and γ_{SL} is the interfacial free energy/area of the adhesive/adherend interface. W_A is thus the free energy/area of the surfaces created minus that of the interface destroyed in the disjoining event. This is equivalent to the negative free energy change associated with the contacting event, that is, $W_A = -\Delta G^{E_{adhesion}}$. It is seen to depend not only upon the adhesive and the adherend, but also upon the fluid medium in which the system resides. It is usually assumed that this medium is air, whose components are assumed to adsorb but negligibly on the surfaces of either the adhesive or the adherend. While this is generally true, complications arise when the air contains water vapor or when the adhesive is volatile, and its vapors adsorb onto the otherwise dry adherend. Water vapor may adsorb to the adherend surface reducing its energy, so that any accounting of such energy must take this into consideration. Any adsorption of vapors from the adhesive also reduces the surface energy of the adsorbent, by an amount at equilibrium termed the equilibrium spreading pressure, π_e , so that the Dupré equation becomes:

$$W_A = \gamma_S + \gamma_L - \gamma_{SL} - \pi_e. \quad (2)$$

It is common to neglect the effect of equilibrium spreading pressure, particularly for ‘low surface energy’ adsorbents [15,16], but there is some evidence that it may not be negligible even under such circumstances [17,18]. It can certainly be neglected for polymeric liquids, owing to their non-volatility. Whether π_e is taken into account or not, the work of adhesion is thought to be a measure of the ‘thermodynamic’ or ‘ideal’ adhesion for a given adhesive/adherend system. One must next inquire: (1) whether W_A is conveniently measured; and (2) if it relates in any meaningful way to practical adhesion, defined earlier.

While the surface tension of the adhesive, γ_L , is easily measured in the laboratory, the other terms in W_A , by themselves, are not. A second easily measurable property associated with the solid–liquid–air system, however, is the contact angle, θ , the angle, drawn in the liquid, between the solid–liquid and the liquid–air interfaces, drawn in the plane perpendicular to the three-phase interline, as shown in Fig. 4. Minimization of the free energy of the solid–liquid–air

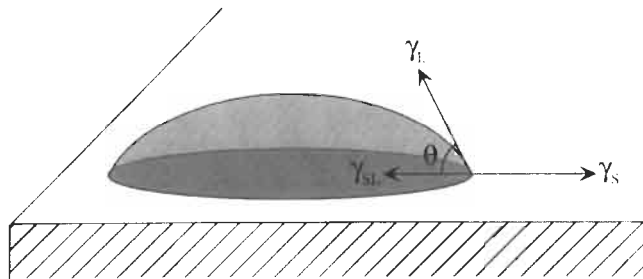


Fig. 4. Definition of contact angle showing the derivation of Young's equation, Eq. 3, using a balance of horizontal forces at the three-phase interline.

system with respect to θ leads to a relationship between the contact angle and the free energies of the interfaces meeting at the three-phase interline, viz. Young's equation:

$$\cos \theta = \frac{\gamma_S - \gamma_{SL}}{\gamma_L}. \quad (3)$$

Eq. 3 may also be derived heuristically by making a balance of horizontal forces on a small section of the interline as shown in Fig. 4. This treats the solid surface and the solid-liquid interface as though they were in states of tension given by their respective surface energies. The vertical force $\gamma_L \sin \theta$ in such a construction is balanced by stresses in the underlying solid.

If equilibrium spreading pressure is to be included, it must be subtracted from the right hand side of Eq. 3, i.e.

$$\cos \theta = \frac{\gamma_S - \gamma_{SL}}{\gamma_L} - \pi_e. \quad (3a)$$

Since $-1 < \cos \theta < 1$, Young's equation is valid only when the right hand side of Eq. 3 or Eq. 3a lies between these limits, i.e. the observed contact angle is finite. In the event that the measured contact angle is 0° , i.e. full spreading occurs, one may conclude only that

$$\frac{\gamma_S - \gamma_{SL}}{\gamma_L} \quad \text{or} \quad \frac{\gamma_S - \gamma_{SL}}{\gamma_L} - \pi_e \geq 1 \quad (4)$$

Substitution of Eq. 3 into Eq. 1 leads to the Young-Dupré equation:

$$W_A = \gamma_L (1 + \cos \theta), \quad (5)$$

which suggests that thermodynamic adhesion is quantifiable in terms of the readily measured values of γ_L and θ , at least for the situation in which the contact angle is finite.

The technique of contact mechanics has also been applied to the direct mechanical determination of solid-fluid interfacial energies, and the results compare favorably with those obtained by contact angle measurements [19].

If equilibrium spreading pressure is to be accounted for, it is added to the right hand side of Eq. 5, giving:

$$W_A = \gamma_L (1 + \cos \theta) + \pi_e. \quad (5a)$$

Determination of the equilibrium spreading pressure generally requires measurement and integration of the adsorption isotherm for the adhesive vapors on the adherend from zero coverage to saturation, in accord with the Gibbs adsorption equation [20]:

$$\pi_e = RT \int_0^p \Gamma(p) d \ln p, \quad (6)$$

where $\Gamma(p)$ is the adsorbed amount (moles/area) as a function of the adsorbate partial pressure, p , and p^s is the saturation value. The needed data are not so easily obtained as those of contact angle and surface tension. A second difficulty with using the Young–Dupré equation to estimate the work of adhesion is that it presumes the use of an appropriate stable *equilibrium* contact angle. In practice, one measures either an advancing angle or a receding angle, and the hysteresis between them is significant. Both refer to metastable states [21]. It is common practice to use the static advanced angle to compute the work of adhesion, but this cannot be rigorously justified.

One may also be able to determine the work of adhesion for cases in which the contact angle is zero by using *probe liquids*, as described later in this chapter. There are also other ways of determining the work of adhesion, such as inverse gas chromatography, which do not depend solely on capillary measurements (surface tension and contact angle). This too will be discussed later.

1.2.3. The relationship between practical adhesion and the work of adhesion, W_A

Assuming the work of adhesion to be measurable, one must next ask if it can be related to practical adhesion. If so, it may be a useful predictor of adhesion. The prospect at first looks bleak. The perfect disjoining of phases contemplated by Eq. 1 almost never occurs, and it takes no account of the existence of an ‘interphase’, as discussed earlier. Nonetheless, modeling the complex real interphase as a true mathematical interface has led to quantitative relationships between mechanical quantities and the work of adhesion. For example, Cox [22] suggested a linear relationship between W_A and the interfacial shear strength, τ , in a fiber–matrix composite as follows:

$$\tau = kW_A = \frac{1}{\lambda} \left(\frac{E_m}{E_f} \right)^{1/2} W_A, \quad (7)$$

where E_m and E_f are the elastic moduli of the matrix and the fiber, respectively, and λ is a universal length (≈ 0.5 nm). This has led to a number of successful interpretations of fiber fragmentation tests on these types of systems described later.

The most-often cited theoretical underpinning for a relationship between practical adhesion energy and the work of adhesion is the generalized fracture mechanics theory of Gent and coworkers [23–25] and contributed to by Andrews and Kinloch [26–29]. This defines a linear relationship between the mechanical work of separation, w_m , and the thermodynamic work of adhesion:

$$w_m = C(\dot{\alpha}, T, \varepsilon) \cdot W_A, \quad (8)$$

where w_m is the work of separation (per unit area) and C is the mechanical loss factor, which accounts for the effects of geometry and rheology, and depends on

the crack growth rate (\dot{a}), temperature (T) and maximum strain level (ε). The theory was developed for elastic adhesives against hard (brittle) solid adherends, and is limited to slow (quasi-equilibrium) rates of detachment [7]. The format of Eq. 8 has been corroborated with experiments in which only the work of adhesion factor was changed. For example, Gent and Schultz [25] measured the peel strength of a polybutadiene film on Mylar under a variety of solvent media (air, water, butanol, etc.) and found it to vary in proportion to the work of adhesion as computed using Eq. 1 with contact angle values evaluated in the solvent media. Similar results have been found more recently for cases involving acid–base effects [30].

Combination of Eq. 7 or Eq. 8 with the Young–Dupré equation, Eq. 3, suggests that the mechanical work of separation (and perhaps also the mechanical adhesive interface strength) should be proportional to $(1 + \cos\theta)$ in any series of tests where other factors are kept constant, and in which the contact angle is finite. This has indeed often been found to be the case, as documented in an extensive review by Mittal [31], from which a few results are shown in Fig. 5. Other important studies have also shown a direct relationship between practical and thermodynamic adhesion, but a discussion of these will be deferred until later. It would appear that a useful criterion for maximizing practical adhesion would be the maximization of the thermodynamic work of adhesion, but this turns out to be a serious over-simplification. There are numerous instances in which practical adhesion is found not to correlate with the work of adhesion at all, and sometimes to correlate *inversely* with it. There are various explanations for such discrepancies, as discussed below.

1.3. The mechanisms of adhesion

The above discussion has tacitly assumed that it is only molecular interactions which lead to adhesion, and these have been assumed to occur across relatively smooth interfaces between materials in intimate contact. As described in typical textbooks, however, there are a number of disparate mechanisms that may be responsible for adhesion [9–11,32]. The list includes: (1) the adsorption mechanism; (2) the diffusion mechanism; (3) the mechanical interlocking mechanism; and (4) the electrostatic mechanism. These are pictured schematically in Fig. 6 and described briefly below, because the various semi-empirical prediction schemes apply differently depending on which mechanisms are relevant in a given case. Any given real case often entails a combination of mechanisms.

1.3.1. Adsorption mechanism (contact adhesion)

In the adsorption mechanism, adhesion is modeled as occurring across a well-defined interface by molecular interaction across that interface, and is often

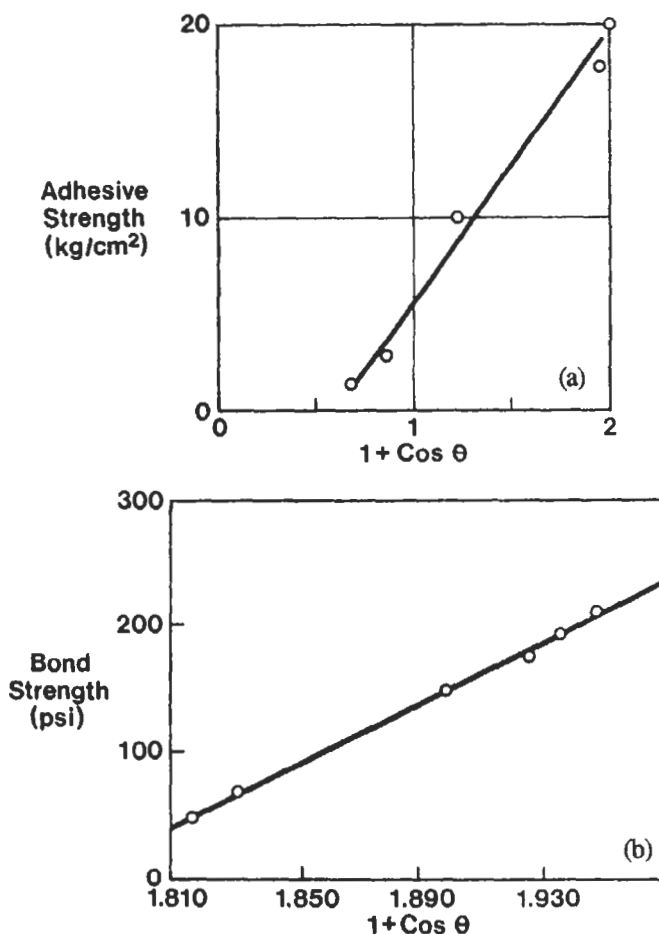


Fig. 5. Examples of the correlation between measured adhesive strength and $(1 + \cos \theta)$. (a) Plot of data from Raraty and Tabor [171] for adhesion of ice to various solids. (b) Plot of data of Barbaris [172] for adhesion of a mixture of epoxy and polyamide resin to low density poly(ethylene) treated in various ways. Both figures from ref. [31], by permission.

referred to as 'contact adhesion'. Because of the rather short-range nature of molecular interactions, they occur principally between the outermost molecular layers of the adherend and the molecules of the adhesive immediately adjacent to them and are said to be 'adsorbed' to the adherend surface. Such adsorption may be purely physical (physisorption), or it may involve the formation of covalent bonds across the interface (chemisorption). The mobile molecules or chains of the adhesive will orient themselves at the interface to maximize whatever interactions are possible and thereby minimize the free energy of the system. The types of interactions may be classified as follows. Lifshitz-van der Waals

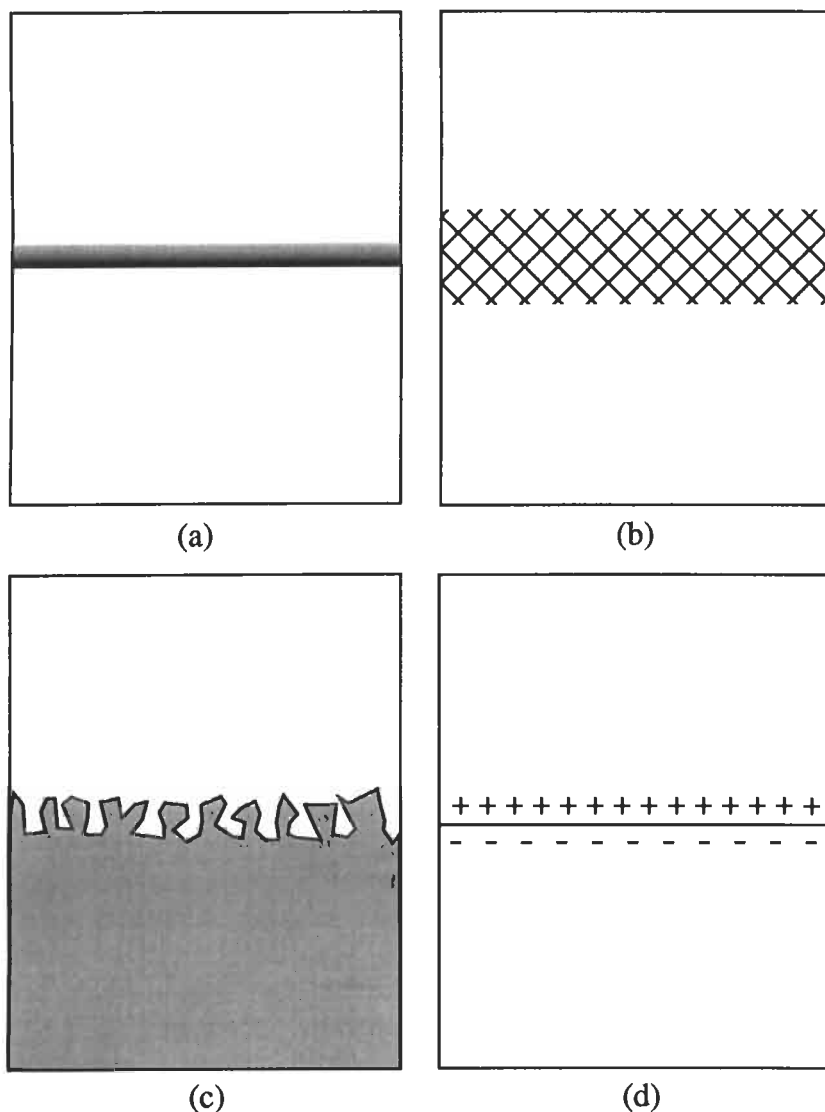


Fig. 6. Four mechanisms of adhesion. (a) The adsorption mechanism (contact adhesion). (b) The diffusion mechanism (diffusion interphase adhesion). (c) The mechanical interlocking mechanism. (d) The electrostatic mechanism.

(LW) interactions refer to the purely physical London's (dispersion), the Keesom's (polar) and Debye's (induced polar) interactions and correspond to magnitudes ranging from approximately 0.1 to 10 kJ/mol (but in rare cases may be higher). The polar forces *in the bulk* of condensed phases are believed to be small due to the self-cancellation occurring in the Boltzmann-averaging of the multi-body

interactions there [33,34], but some investigators prefer to retain it as a separate term to account for possible dipole orientation at the interface. In addition to the universally present LW interactions, there may be acid–base, i.e. donor–acceptor, interactions. These occur when an electron donor (Lewis base) shares an electron pair with an electron acceptor (Lewis acid) to form an acid–base complex (adduct) [35]. Acid–base interactions include hydrogen bonding and are usually characterized by energies in the range of 10–25 kJ/mol (but may be higher). These physical interactions contrast with covalent bond energies that are typically an order of magnitude larger still. There is ample evidence that, despite the lower energy associated with them, LW interactions are adequate under the right circumstances to produce very large interfacial strengths. For example, Fowkes [36] computed the theoretical strength of a polyethylene/steel interface at over 1000 MPa, based on LW forces alone.

More often than not, as Sharpe points out [3], during curing of the adhesive, a structured layer, i.e. an interphase, is formed in the adhesive adjacent to the interface. We may call such a layer a *contact interphase*. This type of interphase contrasts with that formed when the two phases interpenetrate and obscure the original interface between them, and both types are shown schematically in Fig. 7. A contact interphase may be the result of organization or the crystallization (transcrystalline growth) of a polymer in contact with a hard, impenetrable surface, such as glass, a metal or a metal oxide, or even against a highly polar medium such as water [37]. For thermosetting polymers, the degree of crosslinking is often very different near the interface, thus forming an interphase, and dependent on the nature of the adherend. Another example arises in the exposure of polyethylene to radio-frequency excited glow discharge in noble gases reported by Schonhorn and Hansen [38], a process they termed CASING (Crosslinking by Activated Species of Inert Gases). The result was a tough, crosslinked skin on the PE of thickness ranging from 300 Å to 1 µm, depending on exposure time, with a 5-s exposure time yielding a thickness (about 500 Å) sufficient to maximize joinability of the PE to an epoxy adhesive. Interfacial failure may occur along the boundary or within the contact interphase. The role of interfacial forces would appear to be indirect in the latter case, but in the view of Sharpe [2], they provide “the driving force for the many and varied processes that create [contact] interphases.” It is thus still appropriate to seek correlations between interfacial forces and ‘interfacial strength’.

The two issues that are dominant in determining the interfacial strength in the case of contact adhesion are: (1) the completeness and intimacy of contact between the adhesive and adherend at the interface; and (2) the strength of the intermolecular interactions across the interface. Methods for predicting both of these factors are discussed below.

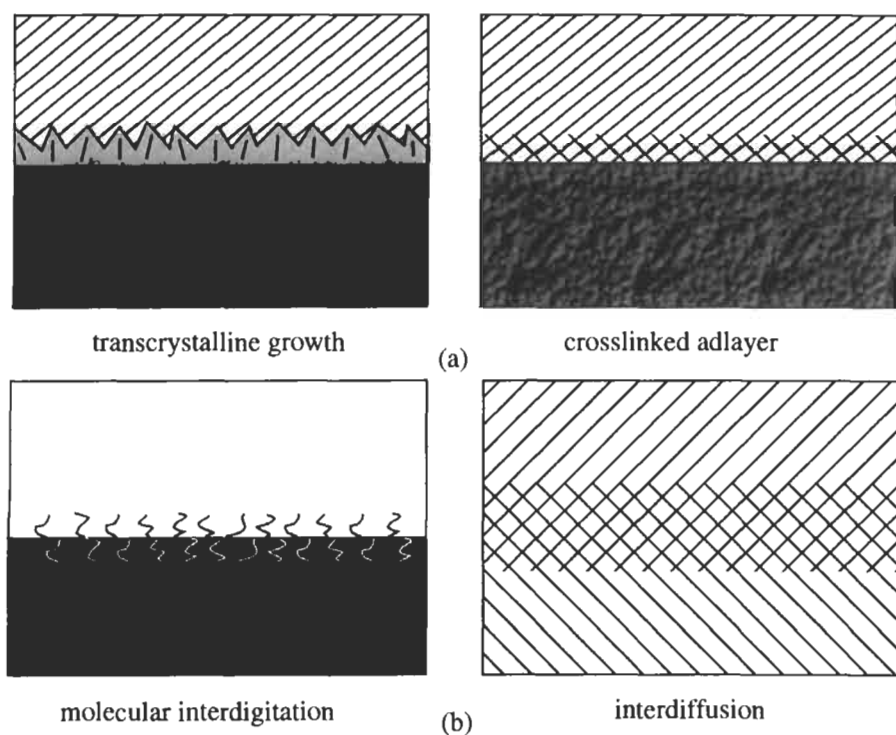


Fig. 7. Different types of interphases. (a) Contact interphases, as produced for example by transcrystalline growth or enhanced adlayer crosslinking in the adhesive phase. (b) Diffusion interphases, as produced by interdigitation or interdiffusion of chains from either or both phases.

1.3.2. Diffusion mechanism (diffusion interphase adhesion)

A situation distinct from contact adhesion described above often arises in the bonding of polymeric adherends and adhesives, in particular in the bonding of specimens of the same polymer together (autoadhesion). In such cases, if there is adequate thermodynamic compatibility (in the sense of mutual solubility) between the polymers, the polymer molecules are mobile (e.g. not locked into a tightly crosslinked or crystallized structure), and there is adequate contact time, the chains of the polymers will interdiffuse, leading to the formation of an interphase through diffusion or interdigitation. This is different from the interphase formed exclusively in the adhesive during contact adhesion, and may be denoted a *diffusion interphase*. Across it, the composition and properties vary continuously from those of one phase to those of the other, and the resulting adhesion may be termed *diffusion interphase adhesion*. Indirect evidence of the diffusion mechanism dates back to the work of Voyutskii [39], its earliest proponent. He noted that for various polymer–polymer systems he investigated,

the dependence of the interfacial strength on time, temperature, compatibility, and molecular weight were consistent with the diffusion theory. Vasenin [40] developed a model of the diffusion theory showing that the penetration depth should vary directly as the square root of the effective polymer diffusivity and as the fourth root of time. Direct experimental evidence of a diffusion interphase by a variety of techniques leaves no doubt of its existence [41–45]. The thickness of the interphases may be as great as 10 μm , but Voyutskii and Vasenin argue that layers as thin as 1–2 nm should be sufficient to produce order-of-magnitude increases in joint strength.

Initial intimacy of contact between the adhesive and adherend must of course precede the formation of a diffusion interphase, but in contrast to contact adhesion, the issue which is dominant is not the maximization of the work of adhesion but instead must be some appropriate measure of the phase *compatibility*, in the sense of mutual solubility.

1.3.3. Mechanical interlocking mechanism

A mechanism thought to explain the improvement in bond strength achieved by roughening the adherend surface is that of mechanical interlocking. The liquid adhesive penetrates the cavities in a rough or porous adherend surface and upon solidification forms effective hooks holding the phases together. Wood, paper, cloth and many other materials are inherently porous, and adhesion to such media inevitably involves such considerations. In a now classic study, Arrowsmith [46] investigated the role of adherend surface topography in determining the peel strength of the resulting joints. He prepared electroformed copper and nickel foils of various topographies, including dendrites, pyramids of various aspect ratios, with and without dendrites, and mushroom-like nodular structures, by altering the electroforming conditions. The dendritic pyramids and the mushroom nodules, both capable of true hooking, produced the greatest enhancement of the peel strength of the metal foils against glass-cloth reinforced epoxy laminates, but the simpler topographies also produced significant enhancement. Aside from any hooking or holding effects, roughness increases the surface area across which intermolecular forces act, and it may induce microstructural changes (possibly increased crystallinity) in the cured adhesive, both of which may act to increase joint strength. Perhaps most importantly, the roughness may increase the energy dissipation in the adhesive during joint failure. It is evident how in this way even moderate surface roughness might produce adhesion enhancements in shear mode since the applied force cannot be exerted everywhere tangentially along the interface. As the force is diverted away from the interface, it is dissipated viscoelastically and plastically in the bulk adhesive. Finally, when surfaces are roughened prior to the formation of an adhesive bond, the primary effect may be to clean the surface of debris (plasticizers, mold release agents, low molecular weight

polymer fragments, lubricants or other processing aids, etc.) which might interfere with the intimacy of adhesive/adherend contact or produce a weak interlayer. While all of the above factors may be important, roughness probably has only a minor effect on the intrinsic interfacial strength.

1.3.4. Electrostatic mechanism

Finally, it has been proposed by Derjaguin [47] that electrostatic interactions across interfaces play a key role in adhesion. Such forces may be familiar to the reader from the experience of rubbing different surfaces together, such as silk against glass, or rubber against wool, and noting that the surfaces subsequently will cling together. The rubbing action assists in contacting the surfaces permitting the transfer of electrons (triboelectricity) from the more electronegative to less electronegative surface by direct tunneling. The surfaces in contact form an 'electrical double layer', analogous to a capacitor. Electrical discharges may be observed when the surfaces are separated. Electrical double layers are generally formed at liquid/solid interfaces by a variety of different mechanisms. Their contribution to interfacial strength, however, is thought to be small ([10], p. 78).

In what follows, particular attention is given to semi-empirical strategies for optimizing contact adhesion and diffusion interphase adhesion. The former centers around maximizing the strength of intermolecular interactions across a true interface, while the latter seeks to maximize thermodynamic compatibility between the phases.

1.4. The general importance of wetting

1.4.1. Wetting requirement for intimacy of contact

Regardless of which, or which combination, of the above mechanisms is responsible for adhesion in a given case, intimate molecular contact between the adhesive and adherend is required. This means that the contact angle of the liquid adhesive against the adherend surface should be as low as possible, and preferably 0° .¹ For the case of contact adhesion, this is immediately evident, but in cases where mechanical interlocking is the primary mechanism for adhesion it is also the case because the adhesive must first be able to flow or wick into the pores of the

¹ The author has found but one reference to a situation in which good adhesion was achieved in the absence of good wetting. Liston [48] reported good adhesion for a contact angle as high as 95° for a polyphenyl sulfide (Ryton[®] R-4)/epoxy system treated by $\text{CF}_4 + 5\% \text{O}_2$ plasma. It was speculated [49] that even a small amount of residual fluorine on the surface could cause the observed high advancing contact angle while the concentration of surface C-O groups could still be high enough to give good adhesion.

adherend sufficiently completely to form the interlocking structure needed. If the mechanism of diffusion interphase formation is responsible for the adhesion, it is still necessary that intimate contact first be established so that the diffusive interphase structure can form.

We have seen that in accord with the Dupré equation, Eq. 5, for the case of finite contact angle, minimum contact angle corresponds to a maximum in the work of adhesion. The minimization of the contact angle, however, is important for reasons other than the maximization of the work of adhesion. Sharpe and Schonhorn [50] report convincing data that wetting is important aside from its effect on the work of adhesion. In an experiment involving epoxy resin and polyethylene, they found the adhesion to be poor when liquid (uncured) epoxy resin was deposited as an adhesive on the polyethylene substrate. On the other hand, if the epoxy was first cured, and then molten polyethylene were applied to it as the adhesive, the adhesion was excellent. Since the same interface was created in both cases, one would assume that the work of adhesion would be the same, but the results were dramatically different. The difference is that the polyethylene solid has rather low surface energy and is not wet by the epoxy liquid ($\theta > 0^\circ$), while the low surface tension molten polyethylene spontaneously spreads over the epoxy adherend ($\theta = 0^\circ$). The strong implication is that if spontaneous spreading does not occur, interfacial contact, even over nominally smooth surfaces, will be incomplete. There are thus two primary reasons that one seeks to minimize the contact angle of the adhesive against the adherend:

- (1) minimum contact angle (optimally 0°) corresponds to maximum area and intimacy of contact between the phases; and
- (2) minimum contact angle (optimally 0°) corresponds to a maximum in the thermodynamic work of adhesion.

In the case of structural adhesives, there is an additional factor not included in the above criteria. Fig. 8 shows that the magnitude of the stress concentration factor in a stressed lap joint increases quite sharply with contact angle beyond about 30° [51]. Furthermore, the locus of the stress concentration moves out toward the edge of the adhesive layer as the contact angle increases. Such stress concentrations are not unlike those which exist at the sites of vapor inclusions or voids between the adhesive and rough or porous surfaces, and the latter are more likely to be present the poorer the wetting. The presence of a row of such voids can lead to a zippering type of failure, as shown in Fig. 9a [52]. Voids are also a serious problem in the formation of fiber–matrix composite materials, as pictured in Fig. 9b. Macroscopic voids may occur in the bulk of the matrix, spanning the fibers, or may occur in the microscale roughness elements on the fiber surfaces, such as the axial cusp-shaped crenulations commonly found on carbon fibers. Recent results of Connor et al. [53] correlated the measured transverse flexural strengths of unidirectional carbon fiber reinforced laminates of poly(ether ether ketone) (PEEK) and glass fiber reinforced laminates of poly(ether imide) (PEI)

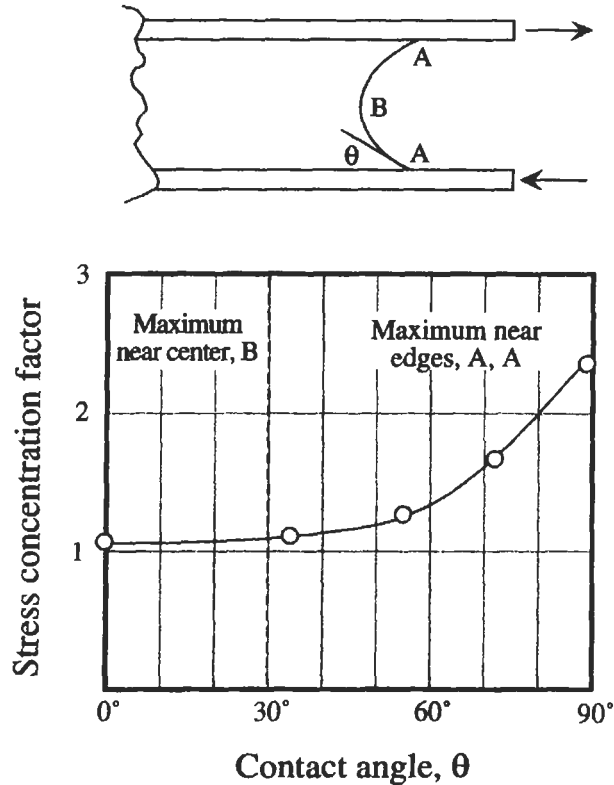


Fig. 8. The dependence on contact angle of the magnitude and location of maximum stress concentration in a lap shear test. As the contact angle decreases, the stress concentration decreases, and its locus moves toward the center-plane of the adhesive phase. Redrawn from ref. [51].

with the contact angles measured for the molten resins against the fibers. This study showed the direct relationship between the mechanical properties and the void morphology within the laminates after consolidation.

In seeking to minimize the contact angle or to promote wetting of the adherend by the adhesive, one must consider the effects both of the chemistry of the components and of the morphology of the adherend surface on the observed contact angle. Finally, comment must be made on the dynamics of the wetting process and the factors upon which it depends.

1.4.2. The relationship between wetting and solid surface energy

The effect of the chemical makeup of the adhesive/adherend system on contact angle and wetting is manifest through the influence of such chemistry on the surface free energies of the adhesive–air (or other fluid medium), adherend–air

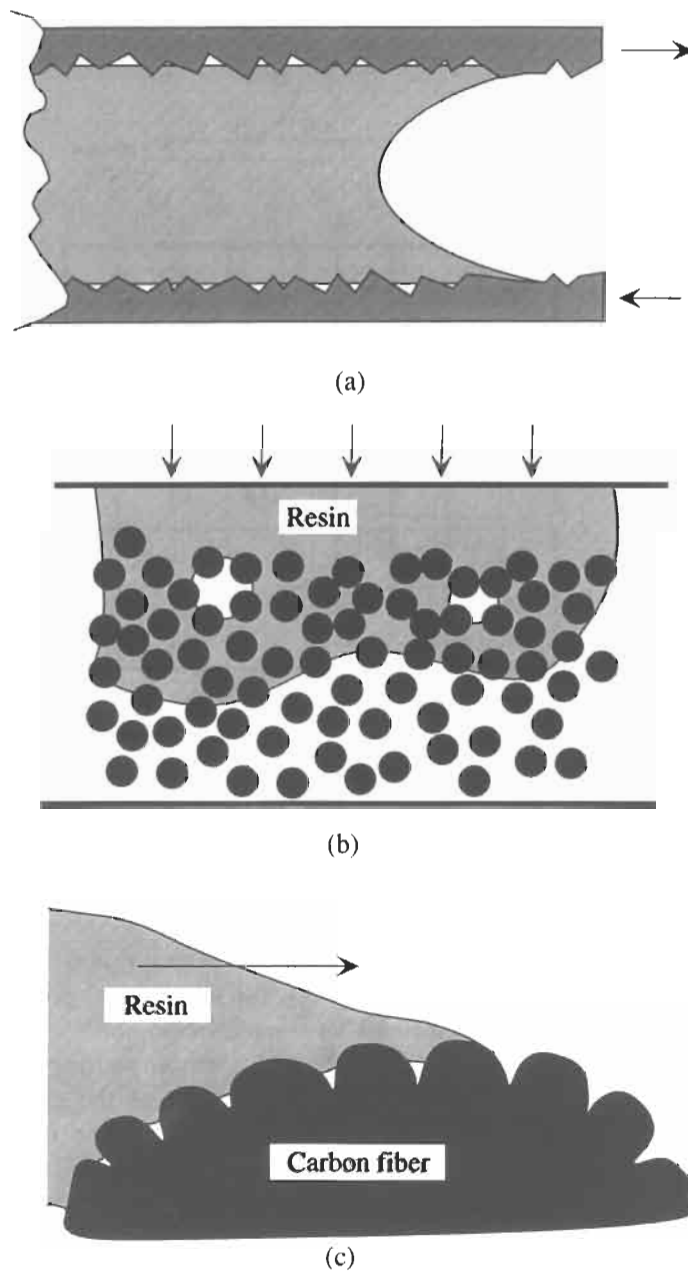


Fig. 9. The effect of voids due to poor wetting on adhesive strength. (a) The zippering effect of voids aligned in the plane of shear. (b) Macro-voids in the resin formed during the manufacture of a carbon fiber reinforced prepregs. (c) Micro-voids caused by axial crenulations along carbon fiber surfaces.

(or other medium) and adhesive–adherend interfaces. For the case of a smooth adherend, Young’s equation, Eq. 3, provides the relationship between equilibrium wetting behavior and the free energies of the three interfaces meeting at the adhesive–adherend–medium (usually air) interline. It is evident that wetting is favored, i.e. low θ , or high $\cos\theta$, when the surface energy term ($\gamma_S - \gamma_{SL}$) is large, and the surface tension of the adhesive, γ_L , is low. Liquid surface tension is readily measured, and it is known that water has a value of approximately 70 mN/m, while most organic solvents have surface tensions between 20 and 40 mN/m. (Note that 1 mN/m = 1 mJ/m² = 1 dyne/cm = 1 erg/cm².) Only silicone liquids and fluorocarbons have surface tensions substantially below 20 mN/m. Water’s surface tension may be reduced to values comparable to organic solvents through the use of surface-active agents. The solid surface energy term is inferred through measurements of the contact angle of various liquids against it, and the following generalizations can be made. Clean metal, metal oxide and other ‘hard’ mineral surfaces are wet out ($\theta = 0^\circ$) by water and organic solvents and thought to have ‘high energy’ surfaces, while softer minerals, such as graphite and sulfides are only partially wet by water and wet out by some, but not all, organic liquids. Organic polymers generally have ‘low energy’ surfaces which are poorly wet by water and often only partially wet by most organic solvents. The softer, low energy surfaces thus provide the principal challenge with respect to wetting, and much effort has gone into quantitating their behavior in this respect.

Zisman and coworkers [54] provided many contact angle data for such systems using optical goniometry. They noted that if for a given solid one plotted $\cos\theta$ (static advanced angle) against the surface tension of the liquid for a series of liquids of different surface tension, they would fall on a single straight line (except for the higher γ values, associated with hydrogen-bonding liquids), as shown schematically in Fig. 10. Such lines are known as *Zisman plots*, and they permit extrapolation to $\cos\theta = 1$ ($\theta = 0^\circ$). Zisman plots are best prepared for a given smooth solid surface using only pure, apolar liquids which do not dissolve or swell the solid. The extrapolated value of the surface tension on the Zisman plot has the practical significance of being the surface tension of a liquid at or below which the solid will be wet out. Zisman noted that the value of γ_c was independent of the liquids used and was therefore characteristic of the solid alone. He designated it as the ‘critical surface tension’ of the solid, γ_c , and regarded it as a measure of the surface energy of the solid.

Although Zisman plots are strictly empirical, one may attempt to give the critical surface tension values theoretical significance. Under conditions where $\gamma_L \rightarrow \gamma_c$ ($\cos\theta \rightarrow 1$), $\gamma_c = (\gamma_S - \gamma_{SL})$. Since this surface energy difference contains a term involving the liquid, it appears incorrect to state it as property of the solid alone. It may be rationalized, however, using models developed by Girifalco and Good [55] and by Fowkes [36] for evaluating the interfacial energy between a pair of phases in terms of the surface energies of the phases. They stated that the

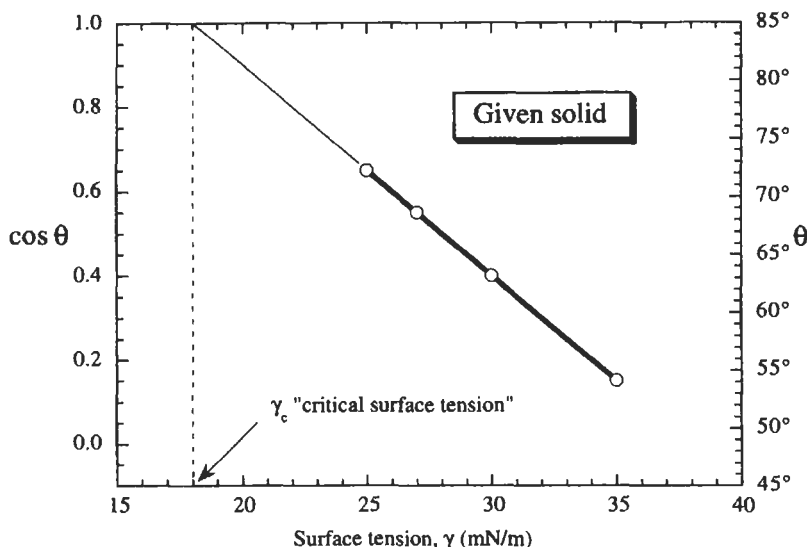


Fig. 10. A schematic Zisman plot for a given solid specimen. When the cosine of the static advancing contact angle is plotted against the surface tension for a series of apolar liquids against a test solid, a straight line results. Its extrapolation to $\cos \theta = 1$ yields the 'critical surface tension' of the solid.

interfacial energy should equal the sum of the two surface energies, minus the attractive intermolecular energy across the interface. Girifalco and Good wrote:

$$\gamma_{SL} = \gamma_S + \gamma_L - 2\Phi \sqrt{\gamma_S \gamma_L}, \quad (9)$$

where Φ is a correction factor accounting for any deviation from the geometric mean mixing rule for the molecular interactions between species across the interface. If only dispersion forces were involved, $\Phi = 1$. Fowkes proposed that the surface free energies of materials, particularly with reference to the surface tension of liquids, could be split into terms representing the various forces that might act between the molecules [56] viz.

$$\gamma = \gamma^d + \gamma^p + \gamma^i + \gamma^h + \dots, \quad (10)$$

where γ^d represented the contribution of dispersion (London's) forces, γ^p permanent dipole (Keesom's) forces, γ^i induced dipole (Debye's) forces, γ^h hydrogen-bonding forces, etc. He further argued that (in the absence of cross-interface hydrogen bonding) only dispersion forces could operate across the interface, in which case only the dispersion-force components of the surface energies should be taken into account in the mixing term, so that:

$$\gamma_{SL} = \gamma_S + \gamma_L - 2\sqrt{\gamma_S^d \gamma_L^d}. \quad (11)$$

For the case in which the molecules of both the solid as well as the liquids used in preparing the plot interact only through dispersion forces, either Eq. 9 or Eq. 11 may be used to express γ_{SL} , giving:

$$\gamma_C = \gamma_S - [\gamma_S + \gamma_L - 2\sqrt{\gamma_S\gamma_L}]. \quad (12)$$

Substituting $\gamma_L \rightarrow \gamma_C$, and simplifying leads to $\gamma_C = \gamma_S$. If the molecules of the solid interact with one another through more than dispersion forces, but the molecules of the liquids still interact only via dispersion forces so that $\gamma_L = \gamma_L^d$, one may apply Eq. 11 to obtain γ_{SL} , which leads to $\gamma_C = \gamma_S^d$, i.e. the Zisman critical surface tension gives the dispersion (or more generally, Lifshitz–van der Waals) component of the solid surface energy. Finally, we should note that the γ_C -values obtained from Zisman plots correspond strictly to γ_S^m , or to $(\gamma_S^d)^m$, rather than to the surface energy of the solid in vacuo. The difference between γ_S and γ_S^m (if any) is the equilibrium spreading pressure, π_e . Thus we would expect $\gamma_C \leq \gamma_S^m \leq \gamma_S$.

It should be noted that one may obtain an estimate for the surface energy of a solid from a single contact angle measurement by combining Eq. 9 or Eq. 11 with Eq. 3. One then has:

$$\gamma_S = \frac{\gamma_L (1 + \cos\theta)^2}{4\Phi^2}, \quad \text{or} \quad (13a)$$

$$\gamma_S^d = \frac{\gamma_L^2 (1 + \cos\theta)^2}{4\gamma_L^d}. \quad (13b)$$

Such equations are generally successful only for the case of apolar liquids and solids, for which $\Phi = 1$, $\gamma_S = \gamma_S^d$ and $\gamma_L = \gamma_L^d$, giving:

$$\gamma_S = \frac{1}{4} \gamma_L (1 + \cos\theta)^2. \quad (13c)$$

Thus apolar probe liquids of sufficiently high surface tension to yield finite contact angles against many surfaces are especially valuable for this purpose. Popular examples of these include diiodomethane, with a surface tension of 50.8 mN/m at 23°C, and α -bromonaphthalene, with a surface tension of 44.4 mN/m at the same temperature. One should be cautioned, however, that both are sufficiently volatile that the π_e -effects may not be negligible with their use.

Zisman critical surface tension values have been found for a wide variety of materials. The range of interfacial composition and structure studied was greatly expanded by the fact that it is only the uppermost surface monolayers which govern wetting behavior. Some critical surface tension data for various materials are summarized in Table 1 [54]. Noting the very low surface energy associated with Teflon, viz. 18 mJ/m², it is clear why it is difficult to find anything that will stick to it. The low surface energies of the hydrocarbons, such as polyethylene or polypropylene, also show why it is comparatively difficult to

Table 1

Critical surface tension data for low-energy surfaces of varying surface chemistry obtained from Zisman plots

Surface	Surface chemical structure	Critical surface tension γ_c (mJ/m ²)
Perfluorolauric acid, monolayer	-CF ₃ , close-packed	6
Perfluorokerosene, thin liquid film	-CF ₂ - and some -CF ₃	17
Poly (terafluoroethylene), Teflon [®] , solid	-CF ₂ -	18
Octadecylamine, monolayer	-CH ₃ , close-packed	22
<i>n</i> -Hexadecane, crystal	-CH ₂ - and some -CH ₃	29
Poly(ethylene), solid	-CH ₂ -	31
Poly(vinyl chloride), solid	-CH ₂ -CHCl-	39
Poly(ethyleneterephthalate), solid	C ₆ H ₆ , -CH ₂ -, ester	43
Nylon, solid	-CH ₂ -, amide	44
Benzoic acid, monolayer	C ₆ H ₆ , edges and faces	53

Data from ref. [54].

find good adhesives for them. Using extensive data of this type, it was possible to build up generalizations about the surface energy attributable to various chemical functionalities as shown. In fact, it was possible to construct a series of ascending surface energies based on the atomic constitution, viz.



The underlying explanation for a series of the above type may be given in part by the how the electrons are held by the atomic nucleus. The more closely and tightly they are held, particularly as exemplified by fluorine, the more difficult it is for these electrons to be shared or for the atom to be polarized. In any event, a series such as that above provides valuable information on how one should modify surface chemistry in order to achieve desired changes in wetting behavior. The rationale for many of the treatments commonly used to prepare hydrocarbon or fluorocarbon adherends for adhesion can be understood by the above results. Plasma, corona, flame, E-beam and other treatments often have the effect of planting oxygen functionality on the surfaces of such materials, increasing their surface energy and improving their wettability. In addition, a variety of surface wet chemical treatments may be used for this purpose. As an example, Keller et al. [57] treated Kevlar, a polyamide, with strong acid or base, as shown in Fig. 11. The treatment produced a population of carboxyl or amino groups, conferring hydrophilicity to the surface, and improved bondability to epoxy adhesives.

A requirement underlying the validity of Zisman plots is that there be no specific interactions, such as acid-base interactions, between the solid surface and the probe liquids. Such interactions, however, can, in principle, be taken into account by Young's equation, provided the contact angle remains finite. Their

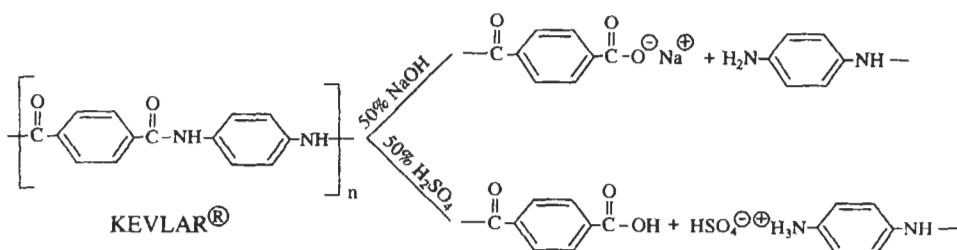


Fig. 11. Chemical treatment of Kevlar to increase hydrophilicity and bondability to epoxy resin matrices. Treatment with either strong base or strong acid causes chain scission at the surface. From ref. [57].

presence will be manifested through the value of the solid–liquid interfacial free energy, γ_{SL} . When these interactions are strong, such as in the case of a strongly acidic liquid interacting with an adherend possessing strongly basic functional groups, it might be anticipated that γ_{SL} can take on negative values, resulting in low values of the contact angle. Acid–base interactions are considered in greater detail later.

1.4.3. Spreading and spreading dynamics

Complete wetting, i.e. spontaneous spreading should always be sought to maximize adhesion. This condition occurs when, with reference to Fig. 4, it is not possible to satisfy the horizontal force balance, i.e. $\gamma_{\text{S}} > \gamma_{\text{L}} + \gamma_{\text{SL}}$. The thermodynamic driving force for the spreading process is the spreading coefficient, $S_{\text{L/S}}$:

$$S_{\text{L/S}} = \gamma_{\text{S}} - (\gamma_{\text{L}} + \gamma_{\text{SL}}). \quad (14)$$

For spontaneous spreading to occur, $S_{\text{L/S}}$ must be positive (or at least non-negative). It is clear that this implies a 0° contact angle. In actual application, adhesive is usually forcibly applied to the adherend surface either by blading, dipping, rolling, injecting, pressing, spraying, etc. so that the major portions of the area are covered. But one depends on spontaneous spreading to effect the filling of surface irregularities and providing the ultimate completeness and intimacy of contact needed. Thus the rate of spreading is also of importance.

When spontaneous spreading occurs, the bulk of the advancing liquid is preceded by a precursor film, usually a few millimeters in width and a few hundred nanometers or less in thickness [58], as pictured in Fig. 12. The observed dynamic contact angle is that which is made by the bulk liquid against the precursor film, and it itself depends on the rate of the advance of the nominal interline. The relationship between the rate of spontaneous spreading, i.e. the rate of movement of the nominal interline normal to itself, U , and the dynamic contact

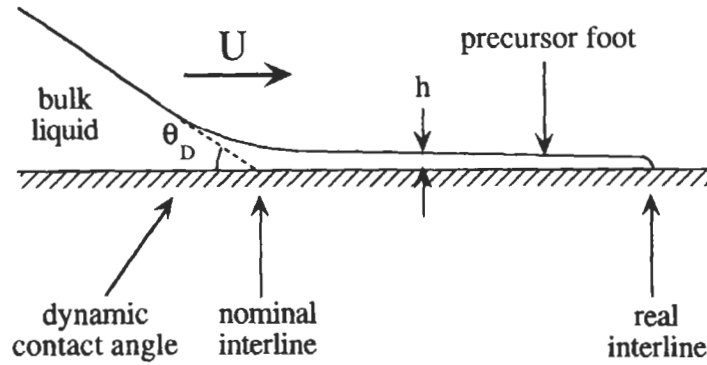


Fig. 12. The morphology of spreading. Liquid advances over the solid by means of a precursor foot (usually a few to a few hundred nanometers in thickness) moving out typically several millimeters ahead of the nominal bulk liquid interline.

angle, θ_d , has been found to be the same as that between θ_d and U for forced spreading [59]. Both theoretical and empirical studies of this rate process have been reported [60–62], and most conform to what is now known as Tanner's Law [63]:

$$\theta_d^3 \propto Ca = \left(\frac{\eta U}{\gamma} \right), \quad (15)$$

where η is the viscosity, and Ca is the Capillary number (a ratio of viscous to surface tension forces). Eq. 15 is in good agreement with the extensive data of Hoffman [64] for the steady forced movement of silicone oils in glass capillaries, for the case of $Ca \leq 0.1$. If the spreading liquid is in the form of a circular cap, and θ_d is small ($\ll \pi/2$), it can readily be shown that the radius, r , of a spreading circular drop varies with time, t , in accord with a $1/10$ th power law [65]:

$$r(t) \propto t^{1/10}, \quad (16)$$

where the prefatory coefficient is dependent upon the original drop size, surface tension, and inversely on the viscosity, but is independent of the magnitude of the spreading coefficient, provided it is positive. The important result is that as the spreading distance increases, the rate of spreading slows precipitously. Although descriptions of spreading morphology and spreading laws of the type of Eq. 15 or Eq. 16 are based mainly on data for low viscosity Newtonian liquids, similar descriptions hold for the spreading of polymeric liquids [66], even those of molecular weight beyond the three-dimensional entanglement threshold [67].

1.4.4. Roughness and chemical heterogeneity

Actual solid surfaces are always rough at some level and are also generally chemically non-uniform (amorphous vs. crystalline portions of a polymer surface,

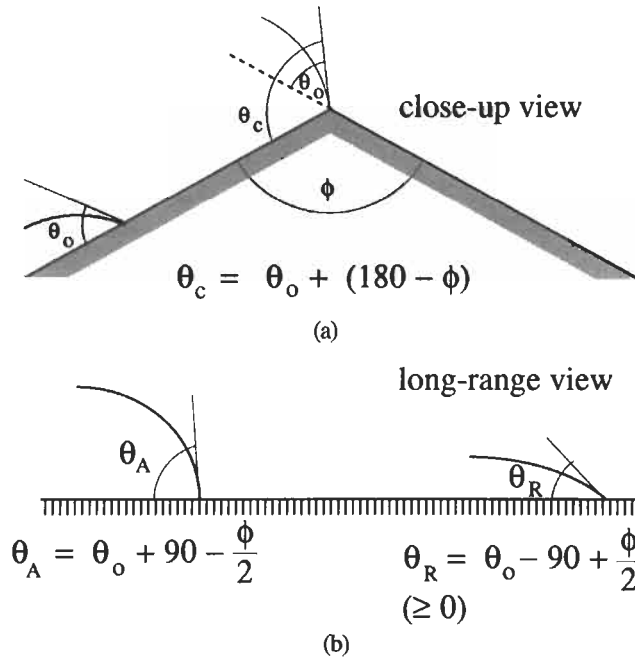


Fig. 13. Motion of a liquid interline across a sharp edge. (a) Close-up of movement over the sharp edge shows that the liquid must exhibit the appropriate contact angle against the surface in front of it in order to advance over the edge. (b) Contact angle hysteresis resulting from the sharp edge.

surface lattice defects on mineral surfaces, patchy contamination, etc.). These factors lead to considerable hysteresis between the advancing and the receding contact angles, and to a stick-slip type of motion when the interline advances or recedes over the solid surface. When it comes to rest, the interline will locate itself at the edges between patches of different kinds of surface. Small liquid masses may be completely pinned by such irregularities, unless external forces are applied to overcome them.

The size scale of the surface heterogeneities is important. When these are large and regular, the hysteresis may take on a predictable character. Fig. 13 shows the slow motion of a liquid interline across a straight sharp edge. In order to cross over the edge, the advancing angle made by the liquid against the upstream surface must be augmented by $(180 - \phi)^\circ$, where ϕ is the angle of the asperity. For a system in which the intrinsic contact is θ_o , a sharp edge of this type would produce an apparent advancing angle of $\theta_A = \theta_o + 90 - \phi/2$, and a receding angle of $\theta_R = \theta_o - 90 + \phi/2$ (≥ 0).

On the other hand, when the size scale of the heterogeneities is sufficiently small (generally $\ll 1 \mu\text{m}$) and uniform, another type of analysis may be used. In this case it is assumed that the interline will be able to adjust its position to

minimize the system free energy and produce a preferred contact angle different from the preferred contact angle that would be observed on a smooth or uniform surface of the same material, θ_0 . The free energy ‘barriers’ between the various metastable interline positions are assumed to be sufficiently small that ever-present small disturbances will eventually lead the system to assume the preferred (stable equilibrium) configuration. Based on such assumptions, treatments have been given to predict the observed equilibrium contact angle in terms of the intrinsic contact angle(s) for both rough and chemically heterogeneous surfaces.

Wenzel [68] considered rough surfaces and supposed that the true solid surface area could be related to the nominal area by a ‘rugosity factor’, \mathfrak{r} :

$$A = \mathfrak{r} A_{\text{smooth}}; \quad \mathfrak{r} = A/A_{\text{smooth}} > 1. \quad (17)$$

The minimization of total system free energy leads to a modified form of Young’s equation, viz.

$$\cos \theta_{\text{app}} = \mathfrak{r} \frac{(\gamma_S - \gamma_{SL})}{\gamma_L}, \quad (18)$$

known as Wenzel’s equation. Although $(\gamma_S - \gamma_{SL})$ is not known independently, this equation is useful in assessing the effect on the apparent (thermodynamically preferred) contact angle of roughening a given solid surface. What we see is that one should be able to *increase* the wettability of a surface which is already wet ($\theta_0 < 90^\circ$) by a given liquid, or *decrease* the wettability of a solid by a liquid that does not wet it. Since $\mathfrak{r} > 1$ for a roughened surface, if $\cos \theta_0$ is positive ($\theta_0 < 90^\circ$), the roughened surface will have a larger $\cos \theta_{\text{app}}$, viz.

$$\cos \theta_{\text{app}} = \mathfrak{r} \cos \theta_0. \quad (19)$$

If the liquid is non-wetting, $\cos \theta_0$ is negative, and $\cos \theta_{\text{app}}$ will become more negative if the surface is roughened. This is illustrated in Fig. 14. The ability to change wetting characteristics by roughening is important in several applications. In particular, if θ_{app} can be made to go to 0° , spreading will occur. The rugosity factor required for this to occur is $\mathfrak{r} = \cos^{-1} \theta_0$, and since \mathfrak{r} -values up to two can readily be achieved, this is often possible.

A treatment similar to Wenzel’s has been given by Cassie and Baxter [69] for chemically heterogeneous surfaces. For the case of a surface consisting of two types of patches, for which the intrinsic contact angles are θ_1 and θ_2 , respectively, minimization of the system free energy leads to the Cassie–Baxter equation:

$$\cos \theta_{\text{app}} = f_1 \cos \theta_1 + f_2 \cos \theta_2, \quad (20)$$

where f_1 and f_2 are area fractions for the two types of surface. The equation is readily extended to the case of many different types of patches. One important case is that in which pores in the surface lead to vapor gaps across which the liquid

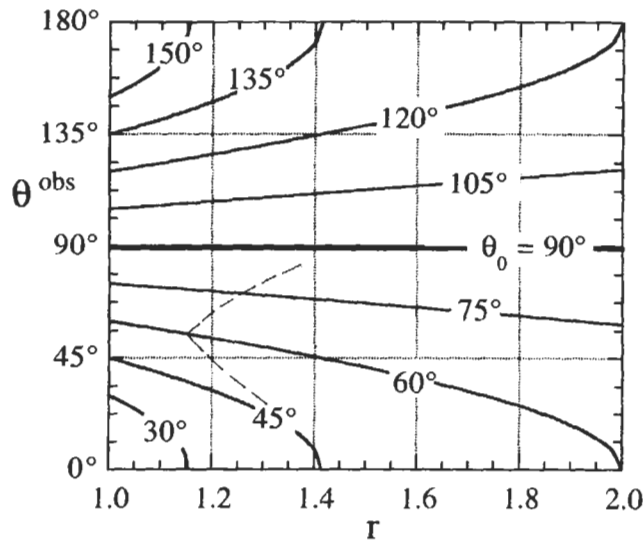


Fig. 14. The effect of micro-roughness on the preferred contact angle. The observed contact angle is shown as a function of rugosity $r = A/A_{\text{nominal}}$ for various intrinsic contact angles, θ_0 . Larger scale roughness leads to hysteresis as indicated by the dashed lines diverging from the $\theta_0 = 60^\circ$ curve, with the top line corresponding to the advancing angle, and the lower line corresponding to the receding angle.

does not contact the solid. The effective contact angle over such gaps is 180° , and if the area fraction of them is f_2 , the Cassie–Baxter equation becomes:

$$\cos \theta_{\text{app}} = f_1 \cos \theta_1 - f_2. \quad (21)$$

The deceptive simplicity of Wenzel's equation and the Cassie–Baxter equation depends on the accessibility of the thermodynamically preferred (equilibrium) configuration. If this is not the case, one may observe widening hysteresis with increasing roughness, i.e. advancing angles may show increases under all circumstances, while receding angles show decreases under all circumstances, as suggested in Fig. 14. For the chemically heterogeneous surface, one is likely to obtain results as pictured in Fig. 15, where due to pinning effects, the observed advancing and receding curves break away sharply from the Cassie–Baxter curve. For a given case, the advancing contact angle curve is in the upper right hand side of the diagram, and the receding angle is shown at the lower left. Both are shown for a surface with high energy portions ($\theta_2 = 0^\circ$) and low energy portions ($\theta_1 = 120^\circ$) as a function of the fraction of the surface occupied by the high energy sites. Note that the advancing angles closely reflect the low surface energy behavior, while the receding angles reflect the high energy behavior. Such results suggest that the removal or covering of either high or low energy portions of a surface may drastically affect its wettability. One example of this is furnished by

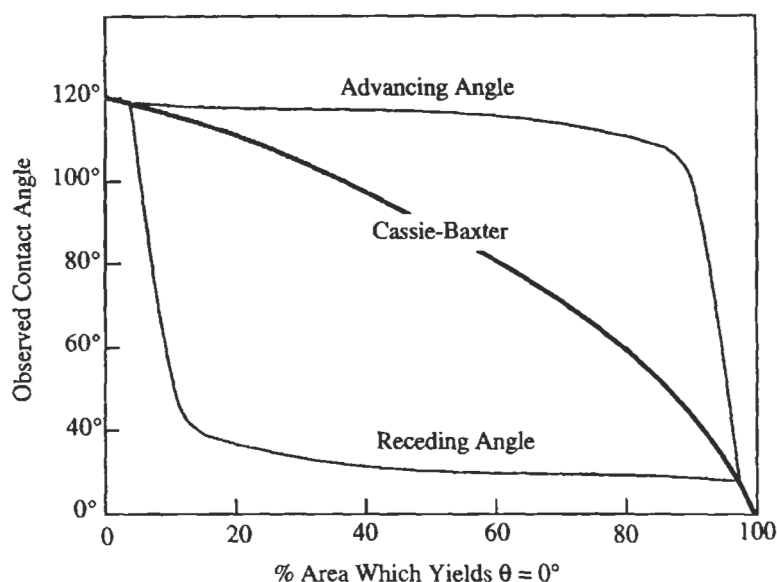


Fig. 15. Wetting of a chemically heterogeneous surface. Micro-heterogeneities produce behavior described by the Cassie–Baxter equation, Eq. 20. Larger scale heterogeneities lead to hysteresis, with the advancing contact angle reflecting the wettability of the low surface energy parts of the surface and the receding angle reflecting the high surface energy parts of the surface.

the patchy application of sizing to paper surfaces [70]. Application of sizing was seen to cover only the small portion of the high-energy sites on the surface but producing large increases in contact angle.

2. The optimization of contact adhesion

2.1. Lifshitz–van der Waals (LW) interactions

2.1.1. Surface energy criteria and polarity matching

In view of the foregoing discussion, it is clear that good wetting (contact angle of adhesive against adherend, $\theta \rightarrow 0^\circ$) is a requirement (but not necessarily a guarantee) of good practical adhesion. Also, in view of the Cox theory, Eq. 7, or the Gent–Andrews–Kinloch continuum fracture mechanics theory, Eq. 8, the optimum practical contact adhesion should correspond to a maximum in the thermodynamic work of adhesion, W_A . The Young–Dupré equation, Eq. 5, suggests that as long as the contact angle is finite, these two requirements are consistent with one another, and the ample database assembled by Mittal [31],

showing the positive correlation between practical adhesion and $(1 + \cos\theta)$ in a variety of different systems appears to bear this out. This may, however, reflect nothing more than an increase in the fractional area of intimate contact between the phases occasioned by better wetting, as suggested by the classical experiment of Sharpe and Schonhorn cited earlier [50].

Good wetting is of course not a sufficient criterion for good contact adhesion because it takes no account of the factors that influence the mechanical loss factor, C , in Eq. 8, nor does it account for residual stress development during cure. But aside from these factors, one might inquire into the validity of the correlation between practical contact adhesion and W_A ‘beyond 0° contact angle’, i.e. can any distinction be made based on W_A between different adhesives, all of which perfectly wet the adherend?

It can be shown, in the context of the assumption that only dispersion forces operate across the interface (i.e. $\gamma_L = \gamma_L^d$ and $\gamma_S = \gamma_S^d$), that optimal wetting and maximal work of adhesion may *not* be criteria consistent with one another. Either Eq. 9 or Eq. 11 gives for these conditions:

$$\gamma_{SL} = \gamma_S + \gamma_L - 2\sqrt{\gamma_S\gamma_L}. \quad (22)$$

Substitution of Eq. 22 into Eq. 1 gives:

$$W_A = 2\sqrt{\gamma_S\gamma_L}, \quad (23)$$

i.e. the work of adhesion expresses directly the molecular interactions across the interface, given in terms of the geometric mean of the surface energies. If it is to be maximized for a given adherend surface, it appears that γ_L should be made as large as possible, but with the limitation that the spreading coefficient, Eq. 14, remain positive:

$$S_{L/S} = \gamma_S - (\gamma_L + \gamma_{SL}) = 2\sqrt{\gamma_S\gamma_L} - 2\gamma_L \geq 0. \quad (24)$$

This requires that $\gamma_L \leq \gamma_S$, so that the maximum value of W_A achievable subject to the constraint of Eq. 21 occurs when:

$$\gamma_L = \gamma_S. \quad (25)$$

Thus the optimum contact adhesive for a given adherend is that whose surface tension is as high as possible, without exceeding the surface energy of the adherend. This is an important criterion when seeking adhesives for bonding to low-energy adherends, such as polymers, carbon, sulfide minerals, etc. Some convincing evidence for it was given by Dyckerhoff and Sell [71]. They studied smooth steel adherends upon which fatty acids of varying chain lengths were adsorbed, producing low-energy surfaces whose γ_S -values ranged between 20 and 53.2 mN/m, and various plastic adherends with γ_S -values from 19 to 42 mN/m. These surface energies were obtained using Eq. 13c with apolar probe liquids

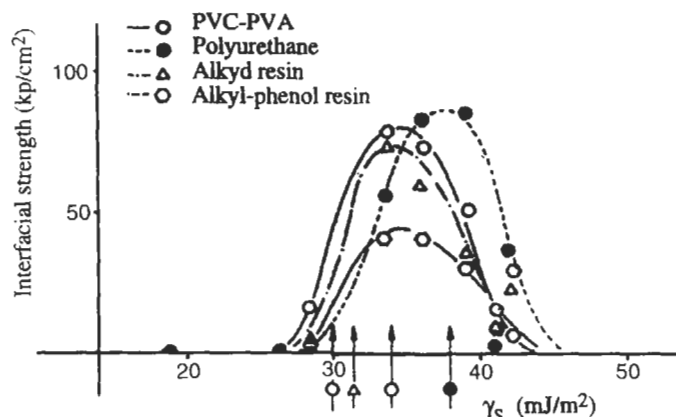


Fig. 16. The results of Dyckerhoff and Sell for interfacial strengths measured by butt-tensile tests for various lacquers (adhesives) against various plastics as a function of the surface energy, γ_s of the plastics. Arrows indicate the surface tensions of the adhesive, γ , used in the generation of each curve, showing rough agreement with the requirement that a maximum in adhesion is achieved when $\gamma_L \approx \gamma_S$ ($1 \text{ kp/cm}^2 \approx 0.1 \text{ MPa}$). Redrawn from ref. [71].

of sufficiently high surface tension to yield finite contact angles. Four different adhesives were used (and it should be noted that the values used for γ_L were those for the *cured* adhesives, which were sometimes different from those of the adhesives in liquid form). In all cases, the systems were likely to be subject only to LW forces. The results for various adhesives against various plastic adherends are shown in Fig. 16. The ordinate is the measured adhesive bond strength from butt-tensile tests. While exact adherence to Eq. 25 at the point of maximum practical adhesion was not observed, it appeared to be qualitatively true. Results similar to those of Dyckerhoff and Sell have been reported by Iyengar and Erickson [72], Mittal [73] and Zosel [74], the last of whom investigated the adherence of polyisobutylene against a number of adherends both in air and in various liquids. An alternate way of stating the criterion of Eq. 25 is that adhesion is enhanced as γ_{SL} is reduced, with maximum adhesion corresponding to $\gamma_{SL} = 0$. Thus we conclude that the continuum fracture mechanics theory expressed by Eq. 7 or Eq. 8 is valid only for cases in which full wetting of the adherend by the adhesive occurs.

In view of the above, the optimum adhesive for contact adhesion to a given adherend is the *spreading* liquid which yields the maximum work of adhesion. This is achieved when the surface tension of the adhesive is made as high as possible without exceeding the surface energy of the adherend ($\gamma_L \rightarrow \gamma_S$), or alternatively, when the adhesive–adherend interfacial energy approaches zero ($\gamma_{SL} \rightarrow 0$). On the other hand, the optimum adherend (as modified through surface treatment) for a given adhesive is simply that which maximizes the work of adhesion.

There is much evidence that there are many cases in which the interaction between liquids and solids cannot be described in terms of dispersion forces alone. For example, Dann [75] found significant ‘non-dispersion-force’ contributions to the work of adhesion between ethanol/water mixtures, mixed glycols, and polyglycols and a mixture of formamide and 2-ethoxyethanol against a variety of solids. The nature of these ‘other interactions’, however, were at first the subject of some dispute. We may account for them in a general way with a term I_{SL} inserted into Eq. 11:

$$\gamma_{SL} = \gamma_S + \gamma_L - 2\sqrt{\gamma_S^d \gamma_L^d} - I_{SL}, \quad (26)$$

from which it is immediately evident that if these interactions are strong enough, the indicated energy of the solid–liquid interface may become zero or even negative. Upon substitution into Dupré’s equation for the work of adhesion, one obtains

$$W_A = W_A^d + I_{SL} = 2\sqrt{\gamma_S^d \gamma_L^d} + I_{SL}. \quad (27)$$

Owens and Wendt [76] and Kaelble [77] suggested that surface energies consist of contributions due to dispersion forces plus those due to polar effects (and ignoring other possible contributions):

$$\gamma = \gamma^d + \gamma^p, \quad (28)$$

and that the latter may act across the interface with the same geometric mean mixing rule as is valid for dispersion forces. It should be noted that neither assumption is theoretically valid [78]. This yields:

$$W_A = W_A^d + W_A^p = 2\sqrt{\gamma_S^d \gamma_L^d} + 2\sqrt{\gamma_S^p \gamma_L^p}, \quad (29)$$

and W_A is maximized when the ‘fractional polarity’ of the adhesive and the adherend are equal, i.e.:

$$\frac{\gamma_S^p}{\gamma_S^d} = \frac{\gamma_L^p}{\gamma_L^d}. \quad (30)$$

Wu [79] has suggested that the cross-dispersion as well as the cross-polar interactions are more appropriately expressed using harmonic rather than geometric means, so that

$$W_A = W_A^d + W_A^p = \frac{4\gamma_S^d \gamma_L^d}{\gamma_S^d + \gamma_L^d} + \frac{4\gamma_S^p \gamma_L^p}{\gamma_S^p + \gamma_L^p}. \quad (31)$$

The use of the harmonic mean often leads to better predictions of interfacial tensions between polymers and better contact angles between liquids and polymer solids, but the criterion for maximization of the work of adhesion is the same as

that of Eq. 30. This so-called ‘polarity matching’ condition is consistent with ‘de Bruynes’ rule’, which states that optimum adhesives for non-polar materials are non-polar and for polar materials are polar [80]. The adherend surface (‘treated’ or otherwise) may be ‘characterized’, i.e. given values of γ_S^d and γ_S^p , by using a pair of probe liquids, each with known γ_L^d and γ_L^p values. These are widely tabulated or may be determined from interfacial tension measurements against apolar liquids [81]. The work of adhesion values of these probe liquids against the solid are measured from their contact angles against the solid and their surface tensions:

$$W_{Ai} = \gamma_i(1 + \cos\theta_i) = 2\sqrt{\gamma_i^d \gamma_S^d} + 2\sqrt{\gamma_i^p \gamma_S^p} \quad \text{and} \quad (32a)$$

$$W_{Aj} = \gamma_j(1 + \cos\theta_j) = 2\sqrt{\gamma_j^d \gamma_S^d} + 2\sqrt{\gamma_j^p \gamma_S^p}, \quad (32b)$$

providing two equations in the two unknowns γ_S^d and γ_S^p . (A similar set of equations based on the harmonic mean may be used.) As an example, this method has been applied in the assessment of various surface treatments of cellulose fibers [82]. The polarity matching criterion has achieved some measure of qualitative success in optimizing contact adhesion.

The criteria for optimization of contact adhesion have been formulated in terms of surface energetics, and the only means implied thus far for their determination have been capillary measurements, i.e. surface tensions and contact angles. Such methods for determining solid surface free energies are limited to those materials of low surface energy because of the unavailability of appropriate high surface tension probe liquids. Solids whose surface free energy exceeds approximately 50 mN/m are thus inaccessible. Furthermore, the use of probe liquids even for the case of lower free energy solids is potentially problematic owing to the possible importance of equilibrium spreading pressure, which would be different for each probe. Fortunately, high surface energy solids are likely to be well wet by candidate adhesives for contact adhesion, so precise knowledge of their surface energy is often less important. Nonetheless, it is desirable to have a convenient alternate means for their determination.

2.1.2. Inverse gas chromatography (IGC)

There are numerous techniques which provide information related to the surface energy of solids. A large array of high-vacuum, destructive and non-destructive techniques is available, and most of them yield information on the atomic and chemical composition of the surface and layers just beneath it. These are reviewed elsewhere [83,84] and are beyond the scope of the present chapter. From the standpoint of their effect on wettability and adhesion, the property of greatest importance appears to be the Lifshitz–van der Waals (\approx dispersion) surface energy, γ_S^{LW} . This may be measured by the simple but elegant technique of

inverse gas chromatography (IGC) [85], which will be briefly described here. It is conventional gas chromatography with respect to the equipment and techniques involved, but is called ‘inverse’ because it is the solid stationary phase, rather than the gas phase, whose properties are to be investigated. The stationary phase may be in the form of a powder, fiber mass, or thin coating on the wall of the column. The technique measures the adsorption of probe gases of various kinds on the test solid, and the characteristics of the resulting adsorption isotherms are related to the surface energetics and chemistry of the solid. Probe gases, such as the alkanes, known to adsorb only through dispersion interactions, may be used to determine the dispersion force component of the of the solid surface energy.

The simplest mode of IGC is the ‘infinite dilution mode’, effected when the adsorbing species is present at very low concentration in a non-adsorbing carrier gas. Under such conditions, the adsorption may be assumed to be sub-monolayer, and if one assumes in addition that the surface is energetically homogeneous with respect to the adsorption (often an acceptable assumption for dispersion–force-only adsorbates), the isotherm will be linear (Henry’s Law), i.e. the amount adsorbed will be linearly dependent on the partial saturation of the gas. The proportionality factor is K_{eq} , the adsorption equilibrium constant, which is the ratio of the volume of gas adsorbed per unit area of solid to its relative saturation in the carrier. The quantity measured experimentally is the *relative retention volume*, V_N , for a gas sample injected into the column. It is the volume of carrier gas required to completely elute the sample, relative to the amount required to elute a non-adsorbing probe, i.e.

$$V_N = j F_{col}(t_R - t_{ref}), \quad (33)$$

where F_{col} is the volumetric flow rate of the carrier gas, t_R is the retention time (time required to elute the sample, which for a dilute sample is taken as the time to reach the peak of the elution curve), and t_{ref} is the time required to elute the non-adsorbing reference gas (often taken as methane). j is the ‘James-Martin correction factor’, used to correct for any pressure drop in the column. The relative retention volume is directly related to the slope of the adsorption isotherm [86]:

$$V_N = K_{eq} A_{tot}, \quad (34)$$

where A_{tot} is the total area of the solid in the column.

The standard molar free energy change upon adsorption of the probe gas is thus given by

$$\Delta G_{ads}^{Eo} = -RT \ln K_{eq} + C_1 = RT \ln V_N + C_2, \quad (35)$$

where C_1 and C_2 are constants dependent upon the standard states chosen and the adsorbent surface area. Finally, the standard free energy of adsorption is related to

the work of adhesion by

$$W_A = \frac{-\Delta G_{\text{ads}}^{\text{Eo}}}{a_{\text{mol}}} + C_3, \quad (36)$$

where a_{mol} is the molar area of the adsorbate gas, and the constant accommodates the choice of standard states. If the only interaction between the adsorbate and the adsorbent is of the Lifshitz–van der Waals (i.e. dispersion force) type, the geometric mean mixing rule applies, and

$$W_A = 2\sqrt{\gamma_S^d \gamma_L^d}, \quad (37)$$

where γ_S^d is surface energy component of the solid we seek, and γ_L^d refers to the dispersion portion of the surface tension of the liquid. For apolar probes, the latter is simply the surface tension. Combining the above four equations leads to:

$$RT \ln V_N = 2a_{\text{mol}}\sqrt{\sigma_S^d \sigma_L^d} + C_4, \quad (38)$$

from which γ_S^d could be evaluated if one had knowledge of the trailing constant. The need for it is avoided, however, by using a series of chromatograms and extracting γ_S^d from the slope of a plot of $RT \ln V_N$ vs. $a_{\text{mol}}\sqrt{\gamma_L^d}$, as shown in Fig. 17. An homologous series of alkane probes is generally used because good values for their adsorbed molar areas are available [87]. The linearity of the plot (the ‘alkane line’) lends credence to the procedure.

Values of γ_S^d obtained by IGC can be compared with those obtained by wetting measurements, and are usually found to be larger. A recent example is the characterization of the energetics of both the liquid state and the solid state of two commercially available epoxy resins as a function of temperature [88]. They may be brought largely into agreement, however, when proper account is taken of the equilibrium spreading pressure [18]. Finally, it has been shown how IGC may be used to obtain complete adsorption isotherms by working beyond the infinite dilution regime, and from them to derive site energy distribution functions for (energetically heterogeneous) solids [89].

Inverse gas chromatography has been used by Harding and Berg [90] to characterize the dispersion force component of the surface free energy of silica treated with various silane coupling agents to varying degrees of coverage. Surface energy decreased with coverage in all cases, reaching a final minimum value for each silane when coverage was complete. The fractional coverage could be determined from the inferred surface energy as follows:

$$\text{Fractional coverage} = \frac{(\gamma_S^d)_o - \gamma_S^d}{(\gamma_S^d)_o - (\gamma_S^d)_m}, \quad (39)$$

where $(\gamma_S^d)_o$ refers to the uncovered silica, and $(\gamma_S^d)_m$ refers to full monolayer coverage. The authors also prepared highly filled composites of the treated and

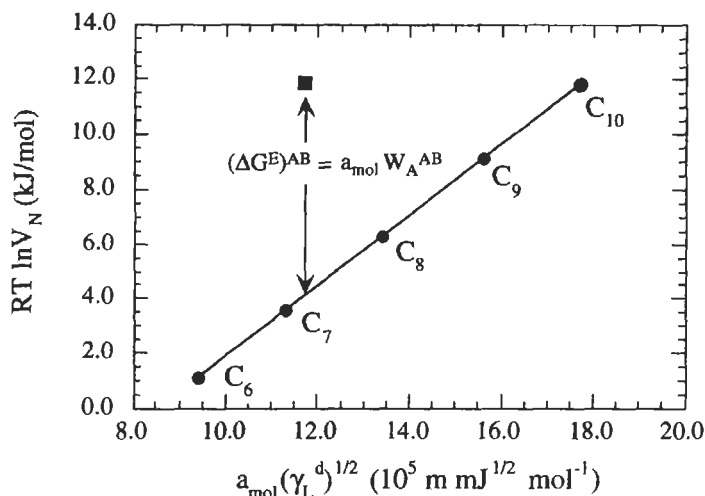


Fig. 17. A schematic of the 'alkane line' obtained by inverse gas chromatography (IGC) measurements. The relative retention volume V_N of carrier gas required to clute a series of alkane probe gases is plotted against the molar area of the probe times the square root of its surface tension. The slope of the plot is $2(\gamma_S^d)^{1/2}$, yielding the dispersion component of the surface energy of the solid. The point (■) represents a probe vapor showing acid–base interactions with the solid surface. Its displacement from the alkane line yields the acid–base component of its free energy of interaction with the solid surface, which gives W_A^{AB} .

untreated silica particles in the rubbery thermoplastic matrix poly(vinyl butyral) (PVB), and specimens of the composite were stressed to failure in a three-point bend test. Electron micrographs revealed that the failure was adhesive in all cases. The surface free energy of the PVB was also determined using IGC, so that the work of adhesion for a series of specimens could be computed in accord with Eq. 38, for cases thought to involve only dispersion interactions. Yield stresses were found to correlate linearly with the work of adhesion for the case of methyl silane and octyl silane treatments, for which only dispersion interactions were assumed, as shown in Fig. 18. The results are of special interest because the value found by IGC for the surface energy of the PVB was 39.8 mJ/m^2 , lower than that of the treated silica in all cases except that corresponding to 100% coverage (for which the values of γ_S^d were found to be 36.2 and 32.6 mJ/m^2 for the methyl and octyl silanes, respectively). Thus full wetting could be assumed for all points in Fig. 18 except those for full coverage by the silanes, so that the correlation of the yield stress with W_A could not be attributed solely to differences in wetting. When an aminosilane was used, the yield stress was found to correlate *inversely* with the work of adhesion, a result attributed to the formation of a diffusion interphase mediated by acid–base interactions discussed below.

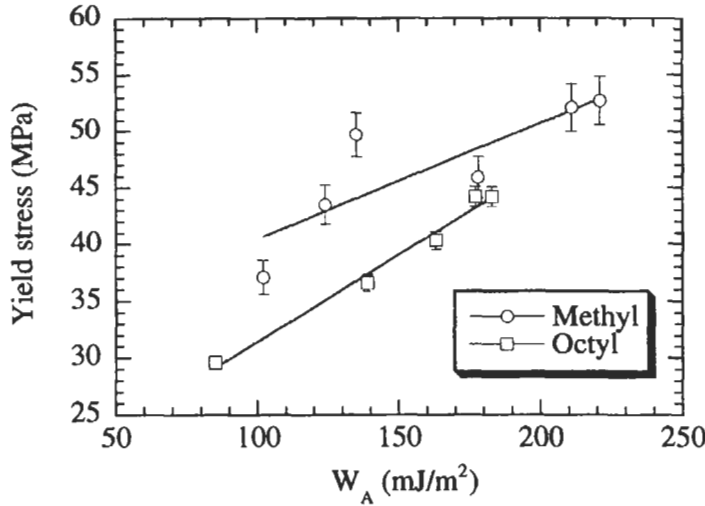


Fig. 18. Yield strengths in three-point bend tests of highly filled composites of poly(vinyl butyral) and silica particles treated with methylsilane and octylsilane coupling agents to varying degrees of surface coverage vs. work of adhesion measured independently using IGC. Redrawn from ref. [90].

2.2. Acid–base (AB) effects

2.2.1. Acid–base contributions to the work of adhesion

An alternative view of the work of adhesion was proposed by Fowkes and coworkers [91] beginning in 1978, and developed significantly in the following years [78]. What had been identified above as ‘polar’ interactions, it was claimed, were more likely to be due to H-bonding, or more generally, to ‘acid–base interactions’. Some liquids could be identified as acids, some as bases, and many as capable of acting as both acids and bases (bifunctional). A brief listing is given in Table 2. The contribution of permanent dipole interactions was considered sufficiently small as to be rolled into the dispersion force term, which is now referred to more generally as the Lifshitz–van der Waals (LW) term. The surface tension of a liquid would be given, in contrast to Eq. 10, by

$$\gamma = \gamma^{\text{LW}} + \gamma^{\text{AB}}, \quad (40)$$

where γ^{AB} was the result of acid–base *self-association*. Monofunctionally acidic or basic liquids would have surface tensions given exclusively by their LW interactions. The possibility of acid–base interactions across the interface leads to a further elaboration of Eq. 27:

$$W_A = W_A^{\text{d}} + W_A^{\text{p}} + W_A^{\text{AB}} \approx W_A^{\text{LW}} + W_A^{\text{AB}}, \quad (41)$$

Table 2

Various solvents sorted in accord with their acid–base functionality

Solvent	Functionality	Solvent	Functionality
Chloroform	Acidic	Aniline	Bifunctional
Methylene chloride	Acidic	Benzaldehyde	Bifunctional
Phenol	Acidic	Dimethyl sulfoxide	Bifunctional (leans basic)
Dioxane	Basic	Ethanol	Bifunctional
Ethyl acetate	Basic	Formamide	Bifunctional
Pyridine	Basic	Methanol	Bifunctional
Tetrahydrofuran	Basic	Nitrobenzene	Bifunctional
Triethylamine	Basic	Propionitrile	Bifunctional
Acetic acid	Bifunctional	Pyrrole	Bifunctional (leans acidic)
Acetone	Bifunctional (leans basic)	Water	Bifunctional

Acid–base interactions in the most general ‘Lewis’ sense occur whenever an electron pair from one of the participants is shared in the formation of a complex, or an ‘adduct’. They include hydrogen bonding as one type of such a bond. The bond may vary from an ionic interaction in one extreme to a covalent bond in the other. Acid–base interactions and their importance in interfacial phenomena have been reviewed extensively elsewhere [35,78] and will be described only briefly here.

The augmentation of the work of adhesion by acid–base effects has, as a consequence, an effect on wettability properties. Identifying I_{SL} in Eq. 26 as W_A^{AB} , and substituting it into Eq. 3 and Eq. 14, respectively leads to:

$$\cos \theta = \frac{2\sqrt{\gamma_S^d \gamma_L^d} + W_A^{AB}}{\gamma_L} - 1 = (\cos \theta)^{LW} + \frac{W_A^{AB}}{\gamma_L}, \quad \text{or} \quad (42)$$

$$S_{L/S} = 2\sqrt{\gamma_S^d \gamma_L^d} - 2\gamma_L + W_A^{AB} = (S_{L/S})^{LW} + W_A^{AB}, \quad (43)$$

which it can be seen how acid–base interactions may augment either $\cos \theta$ or the spreading coefficient.

Eq. 42 shows how capillary measurements may be used to determine W_A^{AB} -values for various acid–base functional liquids against a given solid. An apolar (non acid–base functional) probe liquid giving a finite contact angle against the given solid is used to deduce γ_S^d . Then the measured contact angles of acid–base test liquids, for which γ_L and γ_L^d are known, yield the corresponding values of W_A^{AB} . Fowkes et al. [92] measured contact angles for various acidic liquids (phenolic solutions) on acidic solids (copolymers of acrylic acid) and basic liquids on basic solids (pyridine on vinyl acetate sites) and found for all such cases $W_A^{AB} \approx 0$. Acidic liquids on basic solids, and vice versa, however, led to a appreciable values for W_A^{AB} . Similarly, Vrbanc and Berg [93] found negligible

W_A^{AB} -values for bromoform and pyrrole, acidic liquids, against poly(vinyl chloride), an acidic polymer, and dimethyl sulfoxide, a predominantly basic liquid, against poly(methyl methacrylate), a basic polymer, but large values for the acidic liquids against PMMA and the basic liquid against PVC. 2-Iodoethanol, a bifunctional liquid, showed appreciable W_A^{AB} -values with both polymers. Despite these results in line with expectations, other results based on wettability measurements are not so clear-cut. For example, Vrbanac [94] found significant apparent acid–base interactions of various aromatic liquids against poly(ethylene), presumably a neutral substrate.

2.2.2. The correlation of W_A^{AB}

Once again, capillary measurements are limited to low energy surfaces. As described below, IGC measurements can be used to deduce W_A^{AB} -values, as described below, but with its own difficulties. Considerable effort has gone into attempts to *predict* W_A^{AB} -values using information available in published databases, and the format of these attempts has been useful in interpreting both IGC and other data. It is clear that W_A^{AB} cannot be expressed simply in terms of the surface energies of the adhesive and adherend, but depends on their specific chemistry. In particular, it depends on the presence *and accessibility* of acidic or basic functional groups on the solid surface. Fowkes suggested [95] a format relating W_A^{AB} to the database and correlations available for the heats of acid–base adduct formation, viz.

$$W_A^{AB} = f \cdot n^{AB} \cdot (-\Delta H^{AB}), \quad (44)$$

where ΔH^{AB} is the enthalpy (per mole) of acid–base adduct formation between the acid or base functional groups on the adherend and in the adhesive, n^{AB} is the number (moles) of accessible functional groups per unit area of the adherend, and f is an enthalpy-to-free energy correction factor (which Fowkes assumed to be ≈ 1). In view of the above equation, what should really be sought for maximum adhesion is not a ‘polarity match’, but rather complementarity, i.e. acidic adhesives for basic surfaces and vice versa. Most ‘polar’ materials have both an acid *and* a base character, as shown in Table 2. They include water, alcohols, amides, carboxylic acids and many more, and as liquids, are self-associated. Only a minority of materials may be regarded as monofunctional i.e. exclusively acids (such as chloroform) or exclusively bases (such as most ketones). Thus whenever a monofunctional or bifunctional adhesive interacts with a solid with bifunctional groups, or vice versa, there will be an acid–base interaction. Materials capable of entering acid–base interactions are often thought of as ‘polar’ (even though their dipole moments may be nil), and it is easy to see the origin of the fortuitous success of the Owens–Wendt–Kaelble approach. That approach misidentified the

acid–base interaction: $f \cdot n^{AB} \cdot (-\Delta H^{AB})$ as a ‘polar’ interaction: $2\sqrt{\gamma_S^p \gamma_L^p}$, and the probe liquids used and/or the adherends were generally bifunctional so that *some* interaction was detected. Conspicuous, i.e. qualitative, failures of the old theory would occur only for the relatively uncommon cases when a monofunctional acid interacted with a monofunctional base.

It is clear that the existence of acid–base interactions as quantified by W_A^{AB} between an adhesive and an adherend should improve wetting and spreading, in view of Eqs. 42 and 43, and that they should add to the magnitude of the work of adhesion. These concepts have met with some qualitative successes relevant to adhesion, as documented by Fowkes [94]. There is hope that the prediction of acid–base effects might eventually achieve semi-quantitative status, but that is definitely not the case at present. One may initiate the attempt starting with Eq. 44. Among the difficulties for its direct use are that the factor n^{AB} is not known for any given solid of interest, and evidence from the author’s laboratory suggests that the enthalpy-to-free energy factor, f , *cannot* be assumed to be unity [93]. Nonetheless, some guidance in optimizing acid–base interactions may be obtained by examining the strength of the relevant acid–base enthalpies (ΔH^{AB}). One possibility for assessment of the acid–base contribution to adhesion, particularly between a finely divided particulate filler in a polymer matrix, would be a direct calorimetric measurement of the immersional heat of the filler in a liquid consisting of the monomers from which the polymer is formed, and then comparing the result to an appropriate measure of the adhesion, such as the yield stress of the filled polymeric composite subjected to a bending test. Such experimentation seems not to have been reported.

Much attention has been given to correlating ΔH^{AB} against properties of the interacting species. Two of the most common are the Gutmann [96] *donor number*, DN, or *acceptor number*, AN, scales and the Drago [97] ‘*E & C*’ formulation. The donor number, DN, quantifies the Lewis basicity of a variety of solvents and was defined for a given base B as the exothermic heat of its reaction with the reference acid, antimony pentachloride, in a 10^{-3} M solution in a neutral solvent (1,2-dichloroethane). The units are (kJ/mol). Specifically:

$$DN_B = -\Delta H(\text{SbCl}_5 : B). \quad (45)$$

The dimensionless acceptor number, AN, ranked the acidity of a solvent and was defined for an acidic solvent A as the relative ^{31}P NMR downfield shift ($\Delta\delta$) induced in triethyl phosphine when dissolved in pure A. A value of 0 was assigned to the shift produced by the neutral solvent hexane, and a value of 100 to the shift produced by SbCl_5 . Gutmann suggested that the enthalpy of acid–base adduct formation be written as:

$$-\Delta H^{AB} = \frac{(AN_A)(DN_B)}{100}, \quad (46)$$

where the factor 100 converts the tabulated AN to a decimal fraction of the SbCl_5 value. A considerable data base for donor and acceptor numbers (corrected for solvent effects) [98] is available. Drago expressed the enthalpy of AB complex formation in apolar organic solvents as:

$$-\Delta H^{\text{AB}} = E_{\text{A}}E_{\text{B}} + C_{\text{A}}C_{\text{B}}, \quad (47)$$

where E_{A} and E_{B} represent the 'hardness' or electrostatic contribution, and C_{A} and C_{B} the 'softness' or covalent contribution to the exothermic heat. The E and C constants are obtained experimentally from calorimetric or other measurements, with iodine chosen as a reference acid having $E = 1.00$ and $C = 1.00$ (kcal/mol)^{1/2}. Materials with E much larger than C are termed *hard* acids or bases, while those with C much larger than E are termed *soft* acids or bases. E and C constants for many liquids are presently available, but those for a given solid of interest must generally be obtained experimentally.

The technique of IGC may be employed to obtain acid–base information, as suggested by Schultz and Lavielle [99], by using acid and base probe gases on a solid for which the alkane line has already been obtained. If acid–base interaction is involved in the adsorption, the retention volume should be greater than that corresponding to the dispersion force interaction alone, which should be the same as that of the 'equivalent alkane', i.e. the hypothetical alkane for which the value of $a_{\text{mol}}\sqrt{\chi_{\text{L}}^{\text{d}}}$ is the same. The acid–base component of the work of adsorption is given directly by the difference in the $RT \ln V_{\text{N}}$ values:

$$W_{\text{A}}^{\text{AB}} = \frac{RT}{a_{\text{mol}}} \ln \frac{V_{\text{N}}}{(V_{\text{N}})_{\text{alkane}}}, \quad (48)$$

as shown schematically in Fig. 17. When such data are obtained over a range of temperatures they may be Gibbs–Helmholtz differentiated to yield values of $(-\Delta H^{\text{AB}})$.

Using a method suggested by Saint-Flour and Papirer [100], Schultz and Lavielle obtained ΔH^{AB} -values for the interaction of several vapors of differing donor numbers and acceptor numbers with various treated and untreated carbon fibers used in the preparation of carbon fiber–epoxy matrix composites. ΔH^{AB} was expressed as:

$$\Delta H^{\text{AB}} = K_{\text{A}} \cdot \text{DN} + K_{\text{D}} \cdot \text{AN}, \quad (49)$$

where K_{A} and K_{D} are numbers presumably describing the acid and base characteristics of the fibers and matrices. Writing Eq. 49 as

$$\frac{\Delta H^{\text{AB}}}{\text{AN}} = K_{\text{A}} \frac{\text{DN}}{\text{AN}} + K_{\text{D}}, \quad (50)$$

and plotting $\Delta H^{\text{AB}}/\text{AN}$ vs. DN/AN yielded different straight lines for each fiber and matrix type, permitting determination of their respective K_{A} and K_{D} values.

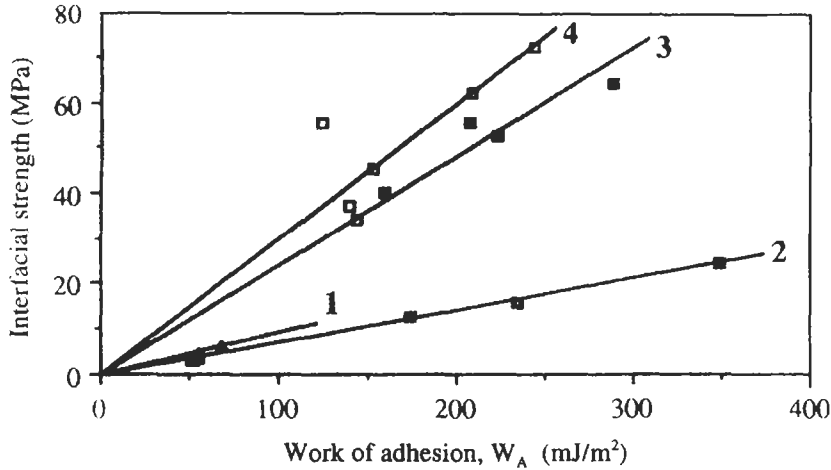


Fig. 19. Interfacial shear strengths of various fiber/matrix composites as a function of the work of adhesion as determined by IGC. 1, glass fiber–poly(ethylene); 2, carbon fiber–epoxy B; 3, carbon fiber–epoxy A; and 4, carbon fiber–PEEK. Redrawn from ref. [102].

Then a parameter A , proportional to ΔH^{AB} , was computed for each fiber (f)–matrix (m) combination:

$$A = K_{A(f)}K_{D(m)} + K_{A(m)}K_{D(f)}, \quad (51)$$

and finally plotted against interfacial shear strength, as determined by fiber fragmentation tests on the composites. Good straight lines were obtained in all cases, in contrast to the correlation obtained with W_A computed on the basis of LW interactions alone.

Nardin and Schultz [101,102] have produced a convincing demonstration of the direct relationship between the work of adhesion (including the contribution of acid–base effects) and measured interfacial shear strength in contact adhesion. IGC measurements were used as detailed in the foregoing paragraph to obtain both the dispersion and the AB contributions to the work of adhesion for glass fiber–poly(ethylene) composites, two carbon fiber–epoxy composites and carbon fiber–PEEK composites, with the fibers subjected to different surface treatments. The composites were then subjected to mechanical tests yielding the interfacial shear strength τ . The results are summarized in Fig. 19. Good straight lines passing through the origin were found for each system, in agreement with Eq. 7 or Eq. 8. In accord with Eq. 7, the authors plotted a normalized interfacial shear strength, $\tau(E_m/E_f)^{1/2}$ vs. W_A and were able to collapse all of the data of Fig. 19 onto a single straight line.

The literature also contains other less quantitative but direct indications of the importance acid–base effects in contact adhesion [35,78,103].

In concluding the discussion of contact adhesion, the near universal presence

of an interphase must be recalled. While the structure and properties of this interphase, derived from the adhesive phase, are often shown to have decisive influence on the adhesive 'interfacial' strength, it is believed that the interfacial forces discussed above provide the driving forces for the formation of the interphase and thus indirectly determine the strength of contact adhesion.

3. The optimization of diffusion interphase adhesion

3.1. General characteristics of diffusion interphase adhesion: coupling agents

As described briefly earlier, the mechanism of contact adhesion differs significantly from that which usually occurs when a polymer adhesive and adherend are bonded. In the latter case, chains from both polymers migrate across what was initially an interface to produce eventually an interphase of interpenetrating chains, as pictured in Fig. 6b. This situation is termed 'diffusion interphase adhesion' to distinguish it from adhesion due to the formation of an interphase by means other than diffusion. In this case, the strength of adhesion is dependent upon the depth and areal density of interpenetration and the strength of molecular interactions between the chains originating in the opposing phases. While true entanglement between linear polymer chains requires chain length-to-width aspect ratios of approximately 30 [104], this may not be required to form strong bonding. In the latter case, it may be presumed that the molecular interactions are strong. In some cases, crosslinking occurs amongst chains of either or both types, producing an interpenetrating *network* (IPN). Diffusion interphase adhesion may occur not only across polymer-polymer interfaces, but also across polymer-nonpolymer interfaces or multi-component polymer interfaces. Polymer-nonpolymer interfaces comprise polymer-metal, polymer-ceramic and polymer-biological interfaces, and diffusion interphases can be formed in such systems when they are strengthened with the aid of primers, such as the silane coupling agents [105], which bond covalently to the metal or ceramic surface and offer organofunctional groups for penetration into the polymer phase, as shown in Fig. 20. These may be oligimeric or even polymeric but are usually lower molecular weight entities. Multi-component polymer interfaces generally refer to incompatible polymers bonded together with the aid of compatibilizers, which are generally block copolymers or co-oligimers which have different blocks compatible with the polymers to be bonded. The polymer surfaces to be bonded are often pretreated with swelling solvents to assist in the subsequent interphase formation [106].

One of the most important choices for the adhesion technologist is the choice of an appropriate coupling agent or compatibilizer for a given system. The choice of a copolymer for bonding two polymers together or a swelling solvent for pretreatment amounts to identifying functional blocks or solvents which will

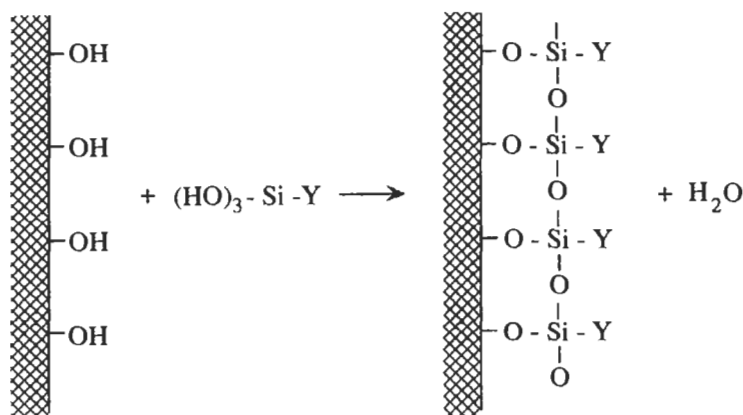
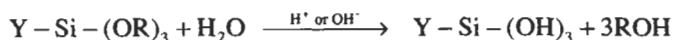


Fig. 20. Schematic representation of the hydrolysis of silane coupling agents and their subsequent interaction with hydroxylated mineral surfaces.

dissolve and penetrate into the substrate polymers. An obvious choice is a copolymer whose blocks match identically with the bulk polymers to be joined. For the case of metal-matrix or ceramic-matrix systems in which the matrix is polymeric, one seeks the appropriate choice of organo-functional group. The most important category of coupling agents of this type are the silane coupling agents, whose synthesis, application and properties are described in great detail in the monograph by Plueddemann [107] and in the more recent compilation of Mittal [108]. They have the generic formula: $Y-Si-(OR)_3$. Upon contact with water, the alkoxy groups (OR) form a triad of -OH groups on the silicon atom, which subsequently condense with other silane molecules and with -OH groups on glass or mineral surfaces to form a laterally crosslinked layer attached to the surface by ether linkages, as shown in Fig. 20. (Other types of coupling agents have similar chemical structure and include zirconium based, zircoaluminates and other metal alkoxides, most commonly the titanates.) Y is the organo-functional group, such as methacrylate, amine, epoxy, styrene, etc., chosen to be compatible with a given polymeric material. A partial list of commercially available compounds is given in Table 3. If the organo-functional group is compatible with the polymer, it is expected to penetrate it or interdigitate with it, leading possibly to significant enhancement of 'interface' strength. If this does not occur, the chief effect of the coupling agent may be to alter the free energy of the surface to which it is covalently bonded. In this case, the mechanism of adhesion would be that of contact adhesion, discussed earlier. In many cases leading to the

Table 3

Examples of organo-functional groups for silane coupling agents

Organofunctional silane	Chemical structure of organofunctional group	Functional groups used
Octylsilane	$-(CH_2)_7CH_3$	7 CH_2 and 1 CH_3
Chloromethylsilane	$-CH_2Cl$	1 CH_2Cl
Chloropropylsilane	$-(CH_2)_3Cl$	2 CH_2 and 1 CH_2Cl
Iodosilane	$-(CH_2)_3I$	3 CH_2 and 1 I
Mono-aminosilane	$-(CH_2)_3NH_2$	2 CH_2 and 1 CH_2NH_2
Di-aminosilane	$-(CH_2)_3NH(CH_2)_2NH_2$	3 CH_2 , 1 CH_2NH , and 1 CH_2NH_2
Tri-aminosilane	$-(CH_2)_3NH(CH_2)_2NH(CH_2)_2NH_2$	4 CH_2 , 2 CH_2NH , and 1 CH_2NH_2
3-Methacryloxysilane	$-(CH_2)_3COO(CH_3)C=CH_2$	3 CH_2 , 1 CH_3 , 1 COO , and 1 $CH_2=C$
Phenylaminosilane	$-(CH_2)_3NHPh$	5 ACH , 1 AC , 2 CH_2 , and 1 CH_2NH
Dihydroimidazolesilane	$-(CH_2)_3C_3N_2$	3 CH_2 , 2 CH_2N , and 1 CH

strongest interphases, the organo-functional groups react chemically, producing covalent bonds with the polymer. These are the 'reactive silanes', and methods for predicting the ultimate 'interfacial' strength in such cases is outside the scope of this chapter. It should also be mentioned that silane coupling agents are also often used not so much for the purpose of increasing the initial joint strength as for improving its durability under conditions of high temperature and/or humidity. This issue too is outside the scope of the present chapter. There are many situations, however, in which adhesion depends solely upon physical interactions, including acid-base interactions, between the coupling agent and the matrix, and in which enhancement of the initial bond strength is the objective. In any event, strong physical interaction between the coupling agent and the matrix polymer is a prerequisite to achievement of any other advantages to be gained from their use.

Whatever the specific system or situation, the key issue in diffusion interphase adhesion is physical *compatibility*. This is once again, a thermodynamic issue and may be quantified in terms of mutual solubility. Most of the strategies for predicting diffusion interphase adhesion are based on thermodynamic compatibility criteria. Thus it is appropriate to review briefly the relevant issues of solution thermodynamics and to seek quantitative measures of compatibility between the phases to be bonded.

3.2. The thermodynamics of solutions

A solution is a single-phase mixture of more than one compound, and the driving force for its spontaneous formation from the pure compounds at constant T and p is the negative Gibbs free energy change of the mixing process, $-\Delta G^{EM}$, as

any spontaneous process constrained to constant T and p seeks a minimum in the system's Gibbs free energy. ΔG^{EM} in general has both an energetic (enthalpic) and an entropic component:

$$\Delta G^{\text{EM}} = \Delta H^{\text{M}} - T \Delta S^{\text{M}}, \quad (52)$$

where ΔH^{M} is the enthalpy change of mixing (the heat of mixing), ΔS^{M} is the entropy change of mixing, and T is the absolute temperature. For 'ideal' solutions, the strength of the molecular interactions between like species and unlike species is the same, so that ΔH^{M} is zero, and the packing of the molecules in the solution is fully random, so that ΔS^{M} reflects the increase in the number of arrangements of the species over the available volume of the solution as compared to the number of such arrangements when the components exist in the pure state. Full randomness of the mixing process requires that the molecules be all of the same size and shape (generally spherical). For the formation of one mole of a binary *ideal* solution of two components, 1 and 2,:

$$\Delta S^{\text{M(ideal)}} = -R(\phi_{\text{m1}} \ln \phi_{\text{m1}} + \phi_{\text{m2}} \ln \phi_{\text{m2}}), \quad (53)$$

where R is the gas constant, and ϕ_{m1} and ϕ_{m2} are the component mole fractions in the solution. We note that $\Delta S^{\text{M(ideal)}}$ is always positive, so that

$$\begin{aligned} \Delta G^{\text{EM(ideal)}} &= \Delta H^{\text{M(ideal)}} - T \Delta S^{\text{M(ideal)}} \\ &= 0 - [-RT(\phi_{\text{m1}} \ln \phi_{\text{m1}} + \phi_{\text{m2}} \ln \phi_{\text{m2}})] \\ &= RT(\phi_{\text{m1}} \ln \phi_{\text{m1}} + \phi_{\text{m2}} \ln \phi_{\text{m2}}) < 0. \end{aligned} \quad (54)$$

Thus the formation of an ideal solution from its components is always a spontaneous process. Real solutions are described in terms of the difference in the molar Gibbs free energy of their formation and that of the corresponding ideal solution, thus:

$$G^{\text{Ex}} = \Delta G^{\text{EM}} - \Delta G^{\text{EM(ideal)}}, \quad (55)$$

where G^{Ex} is termed the *excess* Gibbs free energy of the solution. Theories of solution are formulated in terms of G^{Ex} as a function of T , p and composition. The magnitude of G^{Ex} is a direct measure of the *incompatibility* of the components forming the solution, and when it is zero (or negative), the components may be regarded as fully compatible.

One may distinguish at least five categories of non-ideal solutions in terms of the nature of the intermolecular interactions that dominate their behavior:

- (1) Regular solutions
- (2) Athermal solutions
- (3) Associated solutions
- (4) Electrolyte solutions
- (5) Metallic solutions

The categories are by no means all-inclusive, nor are they free of overlap, but their definitions assist greatly in taking the first steps toward constructing models for their description. The first two refer to non-associating, non-electrolyte solutions. The measure of the solution non-ideality is given by the excess Gibbs free energy, G^{Ex} , which may be split into energetic and entropic contributions:

$$\begin{aligned} G^{\text{Ex}} &= H^{\text{Ex}} - TS^{\text{Ex}} \\ &= \Delta H^{\text{M}} - T[\Delta S^{\text{M}} - \Delta S^{\text{M}(\text{ideal})}]. \end{aligned} \quad (56)$$

In the first category of solutions ('regular solutions'), it is the enthalpic contribution (the heat of mixing) which dominates the non-ideality, i.e. $G^{\text{Ex}} \approx H^{\text{Ex}}$. In such solutions, the characteristic intermolecular potentials between unlike species differ significantly from the average of the interactions between like species, i.e.

$$\Gamma_{12} \neq \frac{1}{2}(\Gamma_{11} + \Gamma_{22}), \quad (57)$$

but the packing of the molecules into the solution is essentially the same as it is in the pure components. *Regular solutions* thus refer best to solutions of approximately spherical molecules of approximately the same size, which differ with respect to the energetics of their pair interactions. A typical example of a solution approaching these conditions would be that of neopentane and carbon tetrachloride.

In the second category ('athermal solutions'), it is the non-ideal (i.e. non-random) entropy of mixing which is chiefly responsible for non-ideality: $G^{\text{Ex}} \approx -TS^{\text{Ex}}$. Non-randomness in the packing of the molecules into solutions of this type results from the difference in molecular size and/or shape as well as from differences in the energetics of the interactions between components. It thus is particularly applicable to solutions of macromolecules (polymers) in low-molecular-weight solvents of the same chemical type. In the simplest of these solutions, the energetics of the interactions are assumed to be the 'same' as those in the pure components, thus leading to no absorption or evolution of heat when the solution is formed. Thus they are termed 'athermal'. A typical example of a solution approaching these conditions would be a high molecular weight saturated hydrocarbon dissolved in a low molecular weight saturated hydrocarbon solvent, whose molecules are essentially the same as the repeat units of the polymer.

It is evident that many solutions fall between these limiting categories, with both energetic and entropic effects contributing to solution non-ideality. For example, if the energy of interaction between unlike species in a solution is highly favored over like-like interactions, it is obvious that these interactions will be preferred, a fact which *in itself* will lead to non-randomness of the packing in the solution.

The third category ('associated solutions') refers to solutions in which molecular *complexes* may form, either through association of like or unlike species, or

dissociation of solution components. Hydrogen bonding or other acid–base adduct formation would lead to solutions of this type. In terms of the ‘appropriate species’ (i.e. accounting for the complex formation), these solutions are sometimes treated as ideal. Finally, the distinction between a strong physical interaction and the formation of a ‘complex’ is often difficult to make, and it is frequently an arbitrary call, based on convenience.

The fourth category (‘electrolyte solutions’) usually refers to dilute solutions of solutes (usually in water) which dissociate into ions. Their behavior is dominated by the long-range Coulombic interactions between the ions. The dissociation may be either ‘strong’ (i.e. complete) or ‘weak’ (i.e. incomplete). The last category (‘metallic solutions’), exemplified by amalgams, are best described as systems in which a ‘sea’ of electrons moves about freely in the cationic metallic matrix, leading to strong cohesion of the system. The present discussion will not consider electrolyte or metallic solutions further.

3.3. Regular solutions, the solubility parameter and Scatchard–Hildebrand theory

A theory of regular solutions leading to predictions of solution thermodynamic behavior entirely in terms of pure component properties was developed first by van Laar and later greatly improved by Scatchard [109] and Hildebrand [110,111]. It is Scatchard–Hildebrand theory that will be briefly outlined here. Its point of departure is the statement that $G^{\text{Ex}} \approx \Delta H^{\text{M}}$. It is next assumed that the volume change of mixing, ΔV^{M} , is zero, so that

$$G^{\text{Ex}} \approx \Delta H^{\text{M}} = \Delta E_{\text{int}}^{\text{M}} + p\Delta V^{\text{M}} = \Delta E_{\text{int}}^{\text{M}}, \quad (58)$$

where $\Delta E_{\text{int}}^{\text{M}}$ is the internal energy change of mixing. $\Delta E_{\text{int}}^{\text{M}}$ is formulated in terms of the molar *configurational* internal energies as follows for a binary solution:

$$\Delta E_{\text{int}}^{\text{M}} = E_{\text{int-m}}^{\text{C}} - \phi_{\text{m1}} E_{\text{int-1}}^{\text{C}} - \phi_{\text{m2}} E_{\text{int-2}}^{\text{C}}, \quad (59)$$

where the $E_{\text{int}}^{\text{C}}$ terms are the ‘configurational’ internal energies, i.e. the difference between the molar internal energies possessed by the species in their condensed form and the corresponding internal energies of the species as ideal gases. The configurational energy is thus that which is associated with the proximity of the molecules (their ‘configuration’) and not with the molecules themselves, i.e. their translational, rotational and vibrational energies. It is a negative quantity whose magnitude expresses the energy of *cohesion* of the molecules. For a given liquid species 1

$$-E_{\text{int-1}}^{\text{C}} = E_{\text{int-1}}^{\text{ideal gas}} - E_{\text{int-1}}^{\text{liquid}}, \quad (60)$$

which may be evaluated from an appropriate equation of state for the substance or

may be estimated in terms of the molar heat of vaporization:

$$-E_{\text{int-1}}^{\text{C}} \approx \Delta E_{\text{int-1}}^{\text{vap}} \approx \Delta H_1^{\text{vap}} - RT. \quad (61)$$

Scatchard and Hildebrand defined the *cohesive energy density* $E_{\text{coh-11}}$ of a liquid 1 as the negative molar configurational energy divided by its liquid molar volume, V_1 :

$$E_{\text{coh-11}} = \frac{-E_{\text{int-1}}^{\text{C}}}{V_1}. \quad (62)$$

The cohesive energy density has units of pressure and is a measure of the strength of cohesion of the molecules in the liquid. The molar excess Gibbs free energy (which is the same as the molar internal energy change of mixing) is then expressed in terms of the cohesive energy densities for a binary solution as:

$$G^{\text{Ex}} = \Delta E_{\text{int}}^{\text{M}} = \phi_{\text{m1}} V_1 E_{\text{coh-11}} + \phi_{\text{m2}} V_2 E_{\text{coh-22}} - V_{\text{m}} E_{\text{coh-m}}, \quad (63)$$

where V_{m} and $E_{\text{coh-m}}$ refer to the mixture. Consistent with the assumption that the volume change of mixing is zero,

$$V_{\text{m}} = \phi_{\text{m1}} V_1 + \phi_{\text{m2}} V_2. \quad (64)$$

The mixture cohesive energy density, $E_{\text{coh-m}}$, was not to be obtained from some mixture equation of state but rather from the pure-component cohesive energy densities via appropriate mixing rules. Scatchard and Hildebrand chose a quadratic expression in *volume fractions* (rather than the usual mole fractions) for $E_{\text{coh-m}}$ and used the traditional geometric mean mixing rule for the cross constant:

$$E_{\text{coh-m}} = \phi_{\text{v1}}^2 E_{\text{coh-11}} + 2\phi_{\text{v1}}\phi_{\text{v2}} E_{\text{coh-12}} + \phi_{\text{v2}}^2 E_{\text{coh-22}}, \quad (65)$$

where ϕ_{v1} and ϕ_{v2} are volume fractions defined by

$$\phi_{\text{v1}} = \frac{\phi_{\text{m1}} V_1}{\phi_{\text{m1}} V_1 + \phi_{\text{m2}} V_2}, \text{ etc., and} \quad (66)$$

$$E_{\text{coh-12}} = \sqrt{E_{\text{coh-11}} E_{\text{coh-22}}}, \text{ so that} \quad (67)$$

$$E_{\text{coh-m}} = \left(\phi_{\text{v1}} \sqrt{E_{\text{coh-11}}} + \phi_{\text{v2}} \sqrt{E_{\text{coh-22}}} \right)^2. \quad (68)$$

Then:

$$\begin{aligned} G^{\text{Ex}} = & \phi_{\text{m1}} V_1 E_{\text{coh-11}} + \phi_{\text{m2}} V_2 E_{\text{coh-22}} \\ & - (\phi_{\text{m1}} V_1 + \phi_{\text{m2}} V_2) \left(\phi_{\text{m1}} \sqrt{E_{\text{coh-11}}} + \phi_{\text{m2}} \sqrt{E_{\text{coh-22}}} \right)^2, \end{aligned} \quad (69)$$

which after some algebra reduces to:

$$G^{\text{Ex}} = (\phi_{\text{m1}} V_1 + \phi_{\text{m2}} V_2) \phi_{\text{v1}} \phi_{\text{v2}} (\delta_{\text{s1}} - \delta_{\text{s2}})^2, \quad (70)$$

Table 4

Solubility parameters and liquid molar volumes for various solvents and polymers (25°C)

Liquid solvent/polymer	Solubility parameter, δ_s (J/cm ³) ^{1/2}	Molar volume, V (cm ³ /mol)
<i>Liquid solvent</i>		
Benzene	18.7	89
Carbon disulfide	20.5	61
Carbon tetrachloride	17.6	97
Chloroform	19.0	81
Dioxane	20.5	86
Ethyl ether	15.1	105
Ethylbenzene	18.0	123
Fluoro- <i>n</i> -octane	11.7	253
Methyl chloride	17.6	56
Methylene iodide	24.1	81
Neopentane	12.8	122
<i>n</i> -Hexadecane	16.4	295
Nitromethane	25.8	54
<i>n</i> -Octane	15.4	164
<i>Polymer</i>		
Poly(tetrafluoroethylene)	12.7	
Poly(ethylene)	16.0	
Poly(styrene)	18.0	
Poly(vinyl chloride)	19.8	
Poly(ethylene terephthalate)	20.5	
Epoxy resin	22.3	

where δ_{s1} and δ_{s2} are the square roots of the cohesive energy densities and are termed the *solubility parameters* of components 1 and 2. Eq. 70 is termed the Scatchard–Hildebrand equation.

Large databases for the solubility parameter exist, most notably Barton's 'Handbook of Solubility Parameters and Other Cohesive Parameters' [112]. A small listing of values is given in Table 4. The units used are those of (J/cm³)^{1/2} \equiv (MPa)^{1/2}, although the older literature uses units of (cal/cm³)^{1/2}. The units are related by:

$$2.0455\delta_s [\text{cal/cm}^3]^{1/2} = \delta_s [\text{J/cm}^3]^{1/2}. \quad (71)$$

Solubility parameters are generally tabulated, together with the corresponding liquid molar volumes, only at 25°C. Although solubility parameters are themselves temperature-dependent, the combination of quantities in Eq. 70 is not. Differentiating Eq. 70 with respect to temperature gives $-S^{\text{Ex}}$, the excess entropy, a quantity which has been assumed to be zero in accord with the definition of a regular solution. Thus only data at 25°C are needed. Solubility parameters may be

estimated using group contribution methods, as first suggested by Dunkel in 1928 [113], but since developed and used by others [112,114]. Recent studies have used this device to follow the evolution of the solubility parameter with time during the isothermal curing process of epoxy resins [115,116].

Eq. 70 suggests that ideal solution behavior, i.e. full compatibility is achieved when the solubility parameters are equal, and that the degree of incompatibility should scale as $(\delta_{s1} - \delta_{s2})^2$. One of the critical assumptions made in the derivation of the Scatchard–Hildebrand equation is the validity of the geometric mean mixing rule, Eq. 67, for the cross cohesive energy density. This rests on the assumption of the dominance of dispersion forces, for which the rule is valid on theoretical grounds. However, in view of the relatively minor importance of permanent dipole interactions in condensed media, discussed earlier, it is not surprising that Eq. 70 predicts compatibility quite well even when polar molecules are involved. Secondly, the use of volume fractions rather mole fractions for expressing the mixture cohesive energy density permitted the description of solutions of molecules of different sizes. Differences in molar volume of up to a factor of two are easily tolerated. Scatchard–Hildebrand theory is *not* designed to describe associated solutions, including those in which hydrogen bonding occurs. This would exclude aqueous solutions. It is nonetheless often misapplied to these situations, but only with mixed and coincidental success.

The Scatchard–Hildebrand theory was not designed to describe solutions of polymers in low molecular weight solvents, nor to describe solutions involving polymers at all, owing to the large differences in molecular size and/or shape involved. Nonetheless, use of the solubility parameter concept to predict the compatibility of polymers with solvents has met with much success. The solubility parameter for a polymer cannot be obtained from its definition as given above owing to its non-volatility. Furthermore, it would be expected to represent the chemistry and morphology of the repeat unit rather than that of the polymer molecule as a whole. In practice, the solubility parameter of a polymer is most often obtained using a lightly crosslinked form of the polymer and measuring the degree of its swelling by a range of solvents of different solubility parameter [119]. The δ -value of the solvent producing the maximum swelling of the polymer is assigned to the polymer. A large database for the solubility parameters of different polymers, obtained in this way, is given in the Polymer Handbook [117], a few values of which are listed in Table 4. They may also be estimated using group contribution methods. One can generally predict that a polymer (2) will be soluble in a solvent (1) if $(\delta_{s1} - \delta_{s2})^2 \leq 1 \text{ (J/cm}^3)^{1/2}$. Larger values of $(\delta_{s1} - \delta_{s2})^2$ correspond to diminishing degrees of compatibility.

The solubility parameter concept has found widespread use in predicting the compatibility of components used in paints and coatings, and the patent literature contains numerous references to the solubility parameter or solubility parameter ranges in specifying formulations. Its use in predicting adhesion should apply in

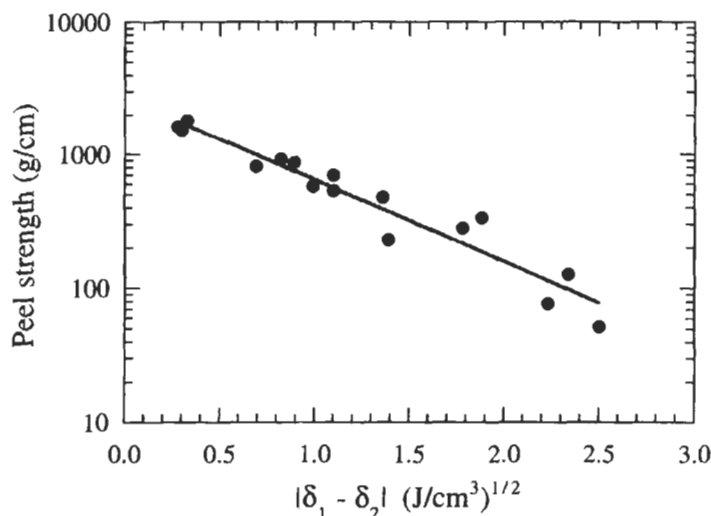


Fig. 21. Peel strengths of various adhesives against poly(ethylene terephthalate) adherends vs. the solubility parameter difference between adhesive and adherend. Drawn using data from ref. [72].

instances when a diffusion interphase is formed. In fact, a fracture energy analysis of interphases created by the interdiffusion of molecular segments, as developed in the monograph by Wu ([79], pp. 396), leads to a quantitative relationship between the fracture strength, σ_f , and the solubility parameter difference, viz.:

$$\sigma_f = p \exp[-q |\delta_{s1} - \delta_{s2}|], \quad (72)$$

where p and q are constants. A convincing demonstration of the applicability of Eq. 72 is given by data of Iyengar and Erickson [72] for the peel strengths of a series of adhesives on poly(ethylene terephthalate), shown in Fig. 21, in which it is seen that $\log \sigma_f$ varies linearly with the solubility parameter difference between the PET and the adhesives. Similar results for the relationship for the peel strength between various polymers and rubbers and $|\delta_{s1} - \delta_{s2}|$ are reported by Wu ([79] p. 400).

A further example applies to the use of silane coupling agents. An interphase solution may be assumed to form between the organo-functional group of the silane coupling agent and the matrix polymer, so that a close match in solubility parameter between the two should be necessary for good adhesion. An early attempt at this was published by Plueddemann [118], with the results shown in Fig. 22. Laminates of polystyrene and glass treated with various silane coupling agents with solubility parameters ranging from 6 to 11.9 (cal/cm³)^{1/2} (as determined from whole-molecule homomorphs of the organo-functional groups) were prepared, and the adhesive strength rating reported was based on the sum (in psi $\times 10^{-3}$) of the dry and wet flexural strengths and the dry and wet compressive

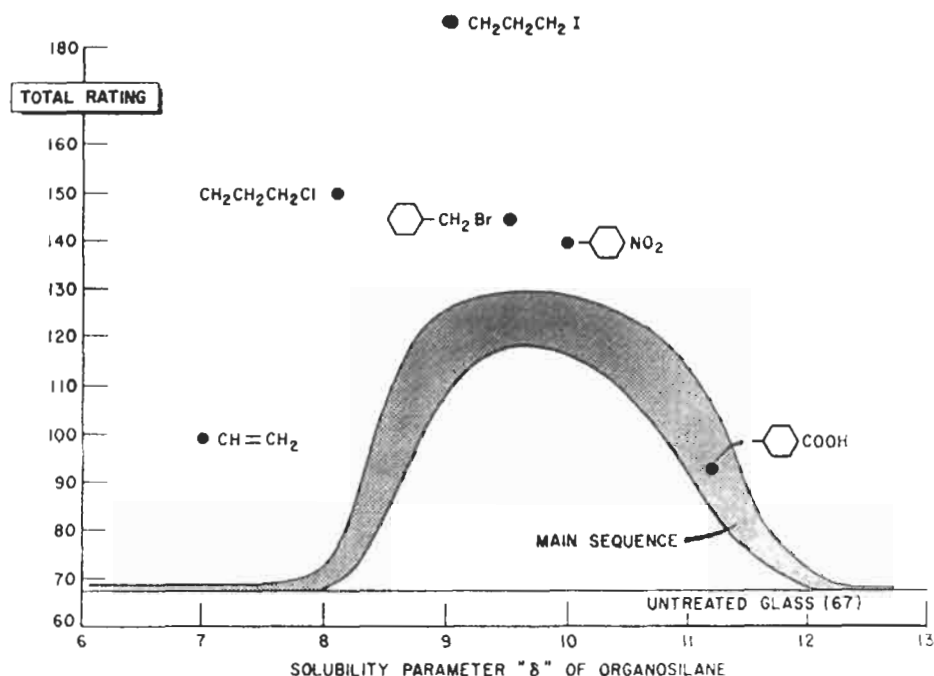


Fig. 22. Adhesion rating based on flexural strengths of laminates of poly(styrene) with glass treated with various silane coupling agents vs. solubility parameter of the organo-functional group of the coupling agent. From ref. [117], by permission.

strengths of the laminates. Most of the results fell within the band indicated 'main sequence', with specific compounds identified as being suspected of chemically reacting with the matrix. Most of the non-reacting silane cases showed optimum performance when the solubility parameter lay between approximately 9 and 11 $(\text{cal}/\text{cm}^3)^{1/2}$, in reasonable agreement with the value of 9.1 $(\text{cal}/\text{cm}^3)^{1/2}$ tabulated for polystyrene.

Numerous reports of comparable levels of success in correlating adhesion performance with the Scatchard-Hildebrand solubility parameters can be found in the literature [116,120–127], but failures of this approach have also been documented [128–132]. Particularly revealing are cases in which failure was attributed to the inability of the Scatchard-Hildebrand solubility parameter to adequately account for donor-acceptor (acid-base) interactions [130,132]. Useful reviews of the use of solubility parameters for choosing block copolymer compatibilizers have been prepared by Ohm [133] and by Gaylord [134]. General reviews of the use of solubility parameters in polymer science have been given by Barton [135], Van Krevelen [114], and Hansen [136].

3.4. The 'three-dimensional' solubility parameter

Hansen [137–139], and later van Krevelen [114] proposed the generalization of the solubility parameter concept to attempt to include the effects of strong dipole interactions and hydrogen bonding interactions. It was proposed that the cohesive energy density be written as the sum of three terms, viz.

$$E_{\text{coh}} = E_{\text{coh-d}} + E_{\text{coh-p}} + E_{\text{coh-h}}, \quad (73)$$

representing dispersion, polar and H-bonding contributions, respectively. The solubility parameter was decomposed accordingly:

$$\delta_s^2 = \delta_{\text{sd}}^2 + \delta_{\text{sp}}^2 + \delta_{\text{sh}}^2, \quad (74)$$

with δ_s representing the Scatchard–Hildebrand solubility parameter, and the terms on the right hand side designated the 'three-dimensional' solubility parameters. The idea was that better predictions of solubility might be found if matches were sought not just of the overall solubility parameter but of its components. For a series of solvents, Hansen determined the dispersion solubility parameter, δ_{sd} , as equal to that of a hydrocarbon homomorph of the molecule. Then the sum of the squares of the polar and hydrogen bonding terms could be found by subtraction from the square of the experimentally measured total solubility parameter. Different methods have been used to determine the polar contribution, sometimes employing measured dipole moments. In other cases, group contribution methods are used. The hydrogen-bonding component is then finally obtained by subtraction. It is becoming more common to use group contribution methods, as outlined in Van Krevelen [114], for all of the terms, and different sets of values of them have been published. Extensive compilations are given in Barton [112], Van Krevelen [114] and Brandup and Immergut [117]. Once determined for a series of solvents, the three-dimensional solubility parameters could be determined for polymers using solubility or swelling measurements. The degree of compatibility of any given compound, polymeric or otherwise, with a series of different solvents could be characterized by the 'distance' between the δ_{sd} , δ_{sp} , and δ_{sh} coordinates of the compound of interest and those of the various solvents. Thus for any compound of interest one could define a 'compatibility sphere' in three-dimensional solubility parameter space, based on some objective level of compatibility, such as complete solubility, as pictured in Fig. 23. Best results were obtained by defining this radius a

$$R^2 = 4(\delta_{\text{sd1}} - \delta_{\text{sd2}})^2 + (\delta_{\text{sp1}} - \delta_{\text{sp2}})^2 + (\delta_{\text{sh1}} - \delta_{\text{sh2}})^2, \quad (75)$$

from which it is evident that the dispersion component is given special weighting. If the criterion for the definition of R was complete solubility, then all solvent points for which complete solubility is achieved should lie inside this 'sphere'.

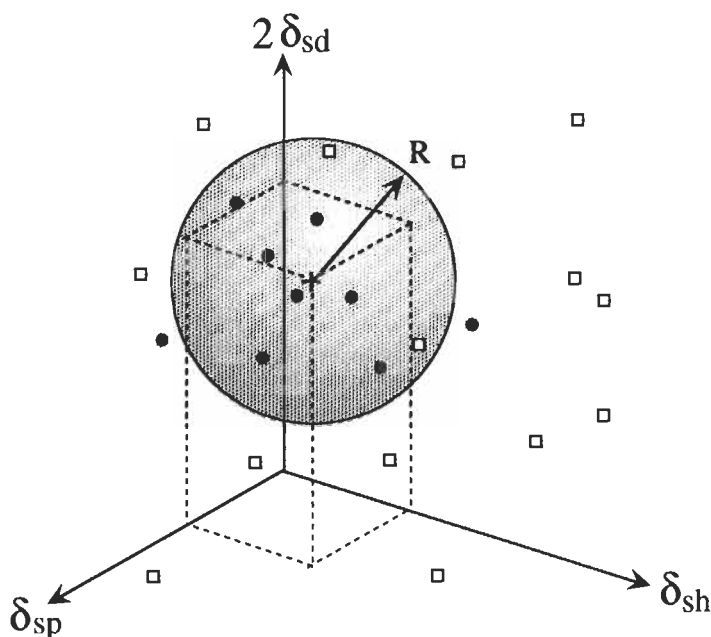


Fig. 23. The 'compatibility sphere' defined by the 'three-dimensional solubility parameters'. +, the solubility parameter coordinates of a given polymer; •, coordinates of solvents showing a high degree of compatibility (e.g., full miscibility) with the polymer; □, solvents showing a lower degree of compatibility.

Lower levels of compatibility, for example swelling to 25%, may be defined by larger values of the radius.

As a matter of convenience, Van Krevelen suggests that the dispersion and polar solubility parameter terms be rolled together into a 'van der Waals' term, δ_{sv} , such that

$$\delta_{sv}^2 = \delta_{sd}^2 + \delta_{sh}^2, \quad (76)$$

and the 'sphere' has been reduced to a 'circle' with

$$R^2 = \delta_{sv}^2 + \delta_{sh}^2 \quad (77)$$

in which no special weighting to the van der Waals term is given.

Extensive use of the three-dimensional solubility parameters for predicting adhesion seems not to have been made, although its additional flexibility should make it successful over a wider range of conditions than the single-parameter approach. Some recent studies involving dental adhesion employed the method with success. Asmussen and Uno [140] successfully correlated the shear bond strength of various dental adhesive resins, characterized in terms of their three-

dimensional solubility parameters, against two different dentin conditioners. In a similar study, Miller et al. [141] successfully correlated the relationship between the Hansen solubility parameters for etched dentin and those for various candidate adhesive primer solutions against the measured adhesive bond strength.

Despite its purported ability to account for specific interactions such as hydrogen bonding, the three-dimensional solubility parameter approach often fails to do so adequately. Many studies document this. The inability of the method to describe compatibility when aqueous phases are involved is recognized by Hansen himself [136], although it is suggested that improvement is achievable if one limits the investigation to the compatibility of aqueous media with pure solvents only. Barton writes in his review of applications of solubility parameters [135]: "The most important situation where caution is required in using Hildebrand parameters or Hansen parameters is where the extent of donor-acceptor (Lewis acid-Lewis base) interactions (particularly hydrogen bonding) within a component is very different from that between the components." The Scatchard-Hildebrand framework is built on the assumption, among others, of no intermolecular complexation. Examination of Eq. 70 shows that it is only capable of predicting positive deviations from ideality, i.e. $G^{\text{Ex}} > 0$, regardless of the relative values of the solubility parameters and regardless of whether or not the factor $(\delta_{s1} - \delta_{s2})^2$ is replaced by the more complex formulations of Eq. 75 or Eq. 77. If one is concerned only with systems in which the molecules of one of the components is acid-base bifunctional and self-associates while the other does not, the theory of associating solutions [142] indicates that one again obtains positive deviations. Even in cases where both components self-associate, and therefore are capable also of associating with one another, the strength of self-association may be greater in both components, and once again one may obtain positive deviations. In such cases it may be possible to achieve some degree of correlation between solubility parameter differences and measures of compatibility, but in cases where acid-base interaction between unlike species (solvation) predominates, such correlation would be impossible. This refers especially clearly to cases of interactions between monofunctional acids and bases. These situations produce (sometimes large) *negative* deviations from ideality. These cases are relatively uncommon as most acid-base capable materials are bifunctional, and the situation is somewhat analogous to the fortuitous success of misidentifying acid-base interactions as polar effects in the description of wetting behavior. It is clear that a more general formulation is needed to describe solution component compatibility.

3.5. Flory-Huggins theory

Another formal shortcoming of Scatchard-Hildebrand theory, or any of its variants, is its requirement that the interacting molecules be of essentially the same size and shape. This disallows an accounting for any non-randomness of the pack-

ing of the molecules in the solution, a shortcoming of considerable importance for solutions involving polymers.

The simplest type of solutions which exhibit non-randomness are those in which the non-randomness is attributable solely to geometric factors, i.e. it does not come from non-ideal energetic effects, which are assumed equal to zero. This is the model of an *athermal* solution, for which

$$G^{\text{Ex}} \approx -T S^{\text{Ex}}. \quad (78)$$

One needs then to compute S^{Ex} based on differences in molecular size and shape.

Both Flory [143] and Huggins [144] in 1941 addressed themselves to this problem with the initial aim of describing solutions of linear polymers in low molecular weight solvents. Both used lattice models, and their initial derivations considered only polymer length (rather than shape, i.e. branching, etc.) The derivation given here will also limit itself to differences in molecular size, but will be based on an 'available volume' approach.

Consider the entropy change in forming one mole of solution at constant T from ϕ_{m1} moles of 1 (of molar volume V_1) and ϕ_{m2} moles of 2 (of molar volume V_2). In the pure state, the ϕ_{m1} moles of 1 occupy (or have available) the volume: $\phi_{m1} V_1$, and the ϕ_{m2} moles of 2 have available the volume: $\phi_{m2} V_2$. However, when the solution is formed, both the ϕ_{m1} moles of 1 and the ϕ_{m2} moles of 2 have available to them the entire volume of the solution: $\phi_{m1} V_1 + \phi_{m2} V_2$. The entropy change experienced by component 1 due to this 'available volume' change is

$$\phi_{m1} \Delta S_1 = \phi_{m1} \int dS = \phi_{m1} \int_{V_{(1)}}^{V_{(2)}} \left(\frac{\partial p}{\partial T} \right)_V dV. \quad (79)$$

Since the molecules are in an energy-neutral environment, the entropy change experienced is the same as that which would be experienced by an equivalent ideal gas, i.e.

$$\left(\frac{\partial p}{\partial T} \right)_V = \frac{R}{V}$$

and

$$\phi_{m1} \Delta S_1 = \phi_{m1} R \ln \frac{V_{(2)}}{V_{(1)}} = \phi_{m1} R \ln \frac{\phi_{m1} V_1 + \phi_{m2} V_2}{\phi_{m1} V_1} = -\phi_{m1} R \ln \phi_{v1}. \quad (80)$$

Similarly, $\phi_{m2} \Delta S_2 = -\phi_{m2} R \ln \phi_{v2}$, and the entropy of mixing is given by

$$\Delta S^{\text{M}} = \phi_{m1} \Delta S_1 + \phi_{m2} \Delta S_2 = -R [\phi_{m1} \ln \phi_{v1} + \phi_{m2} \ln \phi_{v2}]. \quad (81)$$

Subtracting $\Delta S^{\text{M}}(\text{ideal}) = -R [\phi_{m1} \ln \phi_{m1} + \phi_{m2} \ln \phi_{m2}]$ gives

$$S^{\text{Ex}} = -R \left[\phi_{m1} \ln \frac{\phi_{v1}}{\phi_{m1}} + \phi_{m2} \ln \frac{\phi_{v2}}{\phi_{m2}} \right], \quad \text{and} \quad (82)$$

$$\begin{aligned}
 G^{\text{Ex}} &= -TS^{\text{Ex}} = RT \left[x_1 \ln \frac{\phi_{v1}}{\phi_{m1}} + x_2 \ln \frac{\phi_{v2}}{\phi_{m2}} \right] \\
 &= RT \left[\phi_{m1} \ln \frac{1}{\phi_{m1} + r\phi_{m2}} + \phi_{m2} \ln \frac{r}{\phi_{m1} + r\phi_{m2}} \right], \quad (83)
 \end{aligned}$$

where $r = V_2/V_1$. It is to be noted that if $V_2 = V_1$, $\phi_{v1} = \phi_{m1}$ and $\phi_{v2} = \phi_{m2}$, and $G^{\text{Ex}} = 0$, so the solution is ideal. Note also that the Flory–Huggins athermal solution equation always predicts *negative* deviations from ideality.

Real solutions are rarely completely athermal, even when there is considerable similarity between the nature of the molecules. For cases in which *some* energy effects must be taken into account, Flory introduced an additional term into the expression for excess Gibbs free energy. Adapting the format of the Scatchard–Hildebrand equation, the additional contribution to the excess Gibbs free energy is assumed to be of the form:

$$G^{\text{Ex}}|_{\text{energy}} = (\phi_{m1} V_1 + \phi_{m2} V_2) \phi_{v1} \phi_{v2} (\delta_{s1} - \delta_{s2})^2 = \chi \phi_{m1} \phi_{v2}, \quad \text{so that} \quad (84)$$

$$G^{\text{Ex}} = RT \left[\phi_{m1} \ln \frac{\phi_{v1}}{\phi_{m1}} + \phi_{m2} \ln \frac{\phi_{v2}}{\phi_{m2}} + \chi \phi_{m1} \phi_{v2} \right], \quad (85)$$

where χ is the Flory–Huggins interaction parameter, or simply the ‘ χ -parameter’, introduced to account for non-ideal energy effects of mixing but in practice a fitting parameter. Since χ was supposed to account for energy effects, interpretations are often given for it in terms of the Scatchard–Hildebrand expression for such effects, viz.

$$\chi = \frac{V_1}{RT} [\delta_{s1} - \delta_{s2}]^2, \quad (86)$$

from which it is evident that χ depends directly on the molar volume of the solvent and is an inverse function of temperature. Both observations are borne out qualitatively by experimental determinations of χ in many cases. It should be recalled, however, that such expressions as Eq. 86 come out of solution models based on assumptions which contradict those of Flory–Huggins theory. Thus predictions for χ based on the Scatchard–Hildebrand theory are seldom accurate. χ thus accounts not only for energy effects but also for imperfections in the rather simplified accounting of entropy effects given by the Flory–Huggins athermal model. As such, however, it has been extremely valuable for the *correlation* of data for polymer or oligomer solutions in ordinary solvents, but cannot be computed from knowledge of pure-component properties alone. The Flory–Huggins equation is thus not predictive, but databases exist for the χ -parameter for many polymers in many different solvents [117]. Inverse gas chromatography (IGC) has also been shown to provide convenient access to this property [145].

It is evident that as a criterion for compatibility between a polymer and a solvent the χ -parameter should be as low as possible. For high molecular weight polymers, a value of $\chi = 0.5$ gives $G^{\text{Ex}} = 0$, and a value of $\chi = 0$ produces an athermal solution. If there are strong net acid–base interactions between the polymer and the solvent, χ will assume negative values. If one extends the Flory–Huggins equations to describe solutions of polymers in polymers, such that $r \approx 1$, the negative entropic contribution to G^{Ex} is diminished, but the contribution of the χ -term may become enormous. In view of Eq. 86, if the ‘solvent’ is polymeric, V_1 and hence χ itself become very large even for the slightest difference in solubility parameters. This is indeed found to be the case: in general, polymers are found to be mutually immiscible. The only way around this is for χ to become zero or negative by virtue of specific (acid–base) interactions between the segments of the different polymers. These interactions must be on the average greater than the tendency of segments from the same polymer to associate. The existence of such interactions in polymers which do mix has been demonstrated by several investigators, including Kwei et al. [146], who spectroscopically quantified acid–base interactions in a variety of miscible polymer mixtures.

3.6. Group contribution methods: UNIFAC

Although the Flory–Huggins equation did not produce a means for prediction of the thermodynamic properties of solutions from pure component properties, its format suggested numerous useful semi-empirical correlative equations which have proven enormously useful in describing vapor–liquid equilibrium [147]. It finally set the stage for the development of a successful theory of solutions based on the contributions of the chemical functional groups that make up the molecules of the solution. It is capable of accounting for all types of physical molecular interactions, including acid–base interactions and including the effects of differing molecular sizes and shapes.

Functional groups are the building blocks from which molecules are constructed, and a partial listing of such groups is shown in Table 5. For the computation of pure-component properties such as solubility parameter, a group contribution value to that property is assigned to each group, and these are summed to give the molecular property. The application of group contributions to describe the properties of *solutions*, however, is more challenging in that not only are the individual group contributions required but also *group interaction parameters*. Molecular interactions are then computed as appropriately weighted group-interactions. In particular for present purposes, we seek expressions for the excess Gibbs free energy, G^{Ex} of solutions as functions of composition. Historically, the use of group contributions for solutions was first suggested by Langmuir in 1925 and first carried out by Wilson and Deal in 1962 [148], leading to a method referred to as ASOG (analytical solution of groups). But the method that

Table 5
Examples of chemical functional groups used in UNIFAC

Main group	Subgroups	Main group	Subgroups
1 'CH ₂ '	CH ₃ CH ₂ CH C	15 'CNH'	CH ₃ NH CH ₂ NH CHNH
2 'C=C'	CH ₂ =CH CH=CH CH=C CH ₂ =C	19 'CCN'	CH ₃ CN CH ₂ CN
3 'ACH' (AC = aromatic carbon)	ACH AC	21 'CCl'	CH ₂ Cl CHCl CCl
5 'OH'	CH ₂ CH ₂ OH CHOHCH ₃ CHOHCH ₂ CH ₃ CH ₂ OH CHCH ₂ OH	26 'CNO ₂ '	CH ₃ NO ₂ CH ₂ NO ₂ CHNO ₂

has become widely adopted was proposed in 1975 by Fredenslund et al. [149] and termed UNIFAC (universal functional activity coefficient). It is described in detail in Fredenslund et al. [150] and will be presented here only in outline form.

One first must consider the nature and number of functional groups to be used. The method is necessarily an approximation because the action of a given functional group will be somewhat different when it is part of one molecule as opposed to another. This difference is reduced the larger and more complex is the functional group, and the ultimate functional group is the molecule itself. If we err on this side, we get too large a group database to be manageable. At the other extreme is the individual atom, whose use would not allow prediction of the anything, as 'atomic functionality' depends absolutely on the atomic environment. The initial presentation of UNIFAC involved a list of about 60 structural units, grouped into 25 'main groups'. The main groups refer to structural units of a given chemical type, and the individual structural units are termed 'subgroups'. In its present form UNIFAC has more than twice as many subgroups sorted into 50 main groups. Interaction parameters are evaluated only between main groups, but even this requires a data matrix of $C_2^{50} = 1225$ entries. At present, it is about half filled.

UNIFAC was built on the framework of a contemporary model for correlating the properties of solutions in terms of pure-component molecular properties and fitting parameters, viz. UNIQUAC (the universal quasi-chemical) model

proposed by Abrams and Prausnitz [151]. The term ‘quasi-chemical’ refers to its ability to account for all types of energetic interactions, including donor–acceptor interactions. The starting point in the method is to divide the purely geometric (‘combinatorial’) effects from the non-ideal energetic (‘residual’) effects. Thus:

$$G^{\text{Ex}} = G^{\text{Ex}}(\text{combinatorial}) + G^{\text{Ex}}(\text{residual}), \quad (87)$$

where $G^{\text{Ex}}(\text{combinatorial})$ is due to differences in molecular size and shape (geometric considerations) and the resulting nature of the packing. It thus depends only on pure-component properties and composition. $G^{\text{Ex}}(\text{residual})$ is due to non-ideal energetic interactions, and depends in part on interactions between unlike species. It was reasonable to suppose that the combinatorial effects should be expressible in terms of volume fractions and *area* fractions (to account for molecular shape effects), and hence to be dependent on molecular volumes and ‘molecular areas’, while the residual effects should depend on effective molecular areas alone. The latter is appropriate because it is across the pseudo-surfaces between molecules that energetic interactions occur, rather than between the masses of the interacting molecules. Based on these ideas, the following *tabulated* [152] molecular parameters r_i and q_i were employed:

$$\begin{aligned} r_i &= \text{relative molecular volume parameter} \\ &= \frac{V_{wi}}{V_{ws}} = \frac{\text{“van der Waals” molar volume}}{\text{vol. of 1 mol } (-\text{CH}_2-)_{298} = 15.17 \text{ cm}^3} \end{aligned} \quad (88)$$

and

$$\begin{aligned} q_i &= \text{relative molecular area parameter} \\ &= \frac{A_{wi}}{A_{ws}} = \frac{\text{“van der Waals” molar area}}{\text{std. molar area} = 2 \times 10^9 \text{ cm}^2} \end{aligned} \quad (89)$$

When values for the relative molecular volumes and areas are not available for the molecules of interest, they may be constructed from group contributions.

For a binary solution, we define:

$$\phi_{v1} = \text{volume fraction} = \frac{\phi_{m1} r_1}{\phi_{m1} r_1 + \phi_{m2} r_2}, \quad \text{etc.} \quad (90a)$$

$$\theta_1 = \text{area fraction} = \frac{\phi_{m1} q_1}{\phi_{m1} q_1 + \phi_{m2} q_2}, \quad \text{etc.} \quad (90b)$$

Putting these together in accord with the ‘quasi-chemical’ approach gives:

$$\frac{G^{\text{Ex}}(\text{comb.})}{RT} = \phi_{m1} \ln \frac{\phi_{v1}}{\phi_{m1}} + x_2 \ln \frac{\phi_{v2}}{\phi_{m2}} + \frac{z}{2} \left(q_1 \phi_{m1} \ln \frac{\theta_1}{\phi_{v1}} + q_2 \phi_{m2} \ln \frac{\theta_2}{\phi_{v2}} \right) \quad (91a)$$

$$\frac{G^{\text{Ex}}(\text{res.})}{RT} = -q_1 \phi_{m1} \ln (\theta_1 + \theta_2 \tau_{21}) - q_2 \phi_{m2} \ln (\theta_2 + \theta_1 \tau_{12}) \quad (91b)$$

where

$$\tau_{12} = \exp \frac{-a_{12}}{T} \quad \text{and} \quad \tau_{21} = \exp \frac{-a_{21}}{T}, \quad (92)$$

z is the coordination number, generally set equal to 10, and a_{12} and a_{21} are molecular interaction parameters. Note that $a_{12} \neq a_{21}$, so that $\tau_{12} \neq \tau_{21}$. These are ultimately adjustable parameters, derived from the regression of vapor–liquid equilibrium data.

In UNIFAC, one constructs the molecular parameters r_i and q_i from the appropriate group contributions for computing the combinatorial G^{Ex} , and computes the residual contribution to G^{Ex} in terms of *group fractions*. The latter requires the energetics of the interaction between main groups m and n in the form:

$$\psi_{mn} = \exp \left(\frac{-a'_{mn}}{T} \right), \quad \text{and} \quad \psi_{nm} = \exp \left(\frac{-a'_{nm}}{T} \right), \quad (93)$$

where a'_{mn} and a'_{nm} are the *group* interaction parameters. They too are regressed primarily from large databases on vapor–liquid equilibrium, such as the Dortmund Data Bank (DDB), Dortmund, Germany. Both the database of interaction parameters and the structure of UNIFAC have been updated and refined over the years since its inception [153–163].

The details of UNIFAC are complex for hand calculations, but it is resident to such simulation packages as ASPEN (Aspen Technology, Inc., Cambridge, MA). Furthermore, programs for the computations are available on the internet. For example, a UNIFAC Calculator prepared by the University of Sydney, Sydney, Australia, is presently available at: <http://www.chem.eng.usyd.edu.au/pgrad/bruce/unifacal/calc.htm>. Use of group contribution methods such as UNIFAC should have considerable advantages over solubility parameter methods for quantifying compatibility in diffusion interphase adhesion. It is built on a structure which accounts for all types molecular interactions, including acid–base effects, and accounts also for differences in molecular size and shape.

Tseng et al. [164] successfully used UNIFAC to optimize polymer–solvent interactions in three-solvent systems, determining polymer activity as a function of the solvent composition. The composition yielding the minimum in polymer activity was taken as the criterion for optimum interaction, and it compared well with experimental measurements of dissolution rate and solution clarity. Better agreement was obtained using UNIFAC than using solubility parameter methods.

UNIFAC has been used recently by Miller et al. [165] to quantify the compatibility of the interface between glass spheres treated with a range of different silane coupling agents and a matrix polymer, poly(vinyl butyral) PVB, and to correlate the compatibility parameter against measured interfacial strength. Mechanical measurements were performed using the single-particle composite method of Harding and Berg [166], pictured schematically in Fig. 24. A single 650- μm -diameter silane-treated spherical glass bead was imbedded at the center

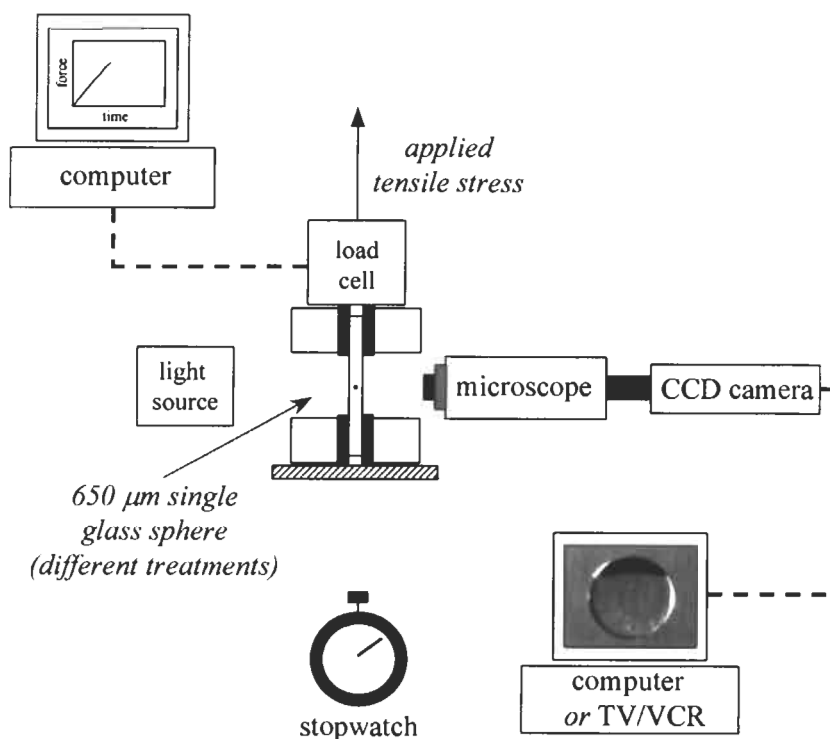


Fig. 24. Experimental set-up of Harding and Berg for testing the single-particle composites. The digital video image shows an example of a failed interface for a silane-treated glass bead in polymer matrix. Redrawn from ref. [166].

of a 9-mm-thick rectangular specimen of the polymer which was then subjected to uni-axial tensile stress with a mechanical tester. The specimen was strained until interfacial failure occurred at one of the particle poles (detected optically), with the applied stress at that point being recorded. Interfacial failure was clearly evident as a debonded cap of definite size. In the case of cohesive failure, a crack could be detected away from the interface. In related experiments [161], failure events were detected acoustically rather than optically. The radial stress at the pole, σ_{rr} , for the case of interfacial failure, is related analytically to the tensile stress, σ_d , applied to the specimen by the theory of Goodier [167], which when applied to this situation takes the form:

$$\frac{\sigma_{rr, \text{ pole}}}{\sigma_d} = f(\nu_1, \nu_2, G_1, G_2), \quad (94)$$

where ν_1 , ν_2 , G_1 and G_2 are the Poisson's ratios and the shear moduli for the matrix and particle, respectively. Eq. 94 takes no account of thermal stresses that exist at the interface (prior to tensile testing) caused by differences in the thermal expansion coefficients for the two materials. Thus Harding and Berg used the

solution of Beck et al. [168] to account for these effects. The radial component of these stresses at the sphere surface is given by:

$$\sigma_{rr, \text{ thermal}} = \frac{4(\alpha_2 - \alpha_1)(1 + \nu_2)G_1G_2}{6(1 - 2\nu_2)G_1 + 3(1 + \nu_2)G_2} \Delta T, \quad (95)$$

where α is the thermal expansion coefficient, and ΔT is the sample annealing temperature and the testing temperature. Since $\alpha_1 > \alpha_2$, the thermal stresses were compressive. Since the interface of the glass particle was strained to failure, the measured value of $\sigma_{d, \text{ fail}}$ is used with the theory of elasticity to compute the interfacial strength as:

$$\text{Interfacial strength} = \left(\frac{-\sigma_{rr, \text{ pole}}}{\sigma_d} \right) \sigma_{d, \text{ fail}} + \sigma_{rr, \text{ thermal}}. \quad (96)$$

At least 11 repetitions of the mechanical test were made for each silane.

The silane coupling agents used are those listed in Table 3. In each case, full monolayer coverage, as verified by IGC measurements of surface energy, was achieved. The compatibility criterion for the interaction between the organo-functional group of the silane and the matrix polymer was defined as the (negative) Gibbs free energy of mixing for an equimolar mixture of the organo-functional group and the repeat unit of the matrix polymer $(-\Delta G^{\text{EM}})_{0.5}$, at 50°C. UNIFAC was then used to calculate $(-\Delta G^{\text{EM}})_{0.5}$ in terms of the functional groups making up the polymer and the particular organo-functional group in each case. The groups used for the PVB were five CH_2 , two CH , two CHO , one CH_3 and one OH . The groups used for each coupling agent are listed in the last column of Table 3. The results of correlating the measured interfacial strength against the compatibility criterion $(-\Delta G^{\text{EM}})_{0.5}$, computed using UNIFAC are shown in Fig. 25. The error bars correspond to the 95% mean confidence interval. A very reasonable trendline is achieved considering all the results, but it is noteworthy that if the points for the tri-amino-, phenylamino-, and 3-methacryloxysilanes are excluded, an excellent correlation exists. All three of the above silanes show greater-than-expected adhesion enhancement, and there may be reasons to explain this behavior. Aside from the octylsilane, which is marginally incompatible with the polymer, the three silanes lying above the line of Fig. 25 have the largest molecular dimensions, suggesting additional steric effects associated with disjoining interphases in which these groups are imbedded. Additionally, in the case of the tri-aminosilane, one expects the formation, on average, of two acid-base adducts per organo-functional group in contrast to the mono- and di-silanes [169]. There is also some evidence that the 3-methacryloxysilane may be able to engage in covalent bond formation with the matrix polymer [170].

Recent unpublished results from the author's laboratory, shown in Fig. 26, confirm the good correlation obtainable between mechanically measured interfacial strengths, as detailed above, and UNIFAC calculations of $(-\Delta G^{\text{EM}})_{0.5}$ for

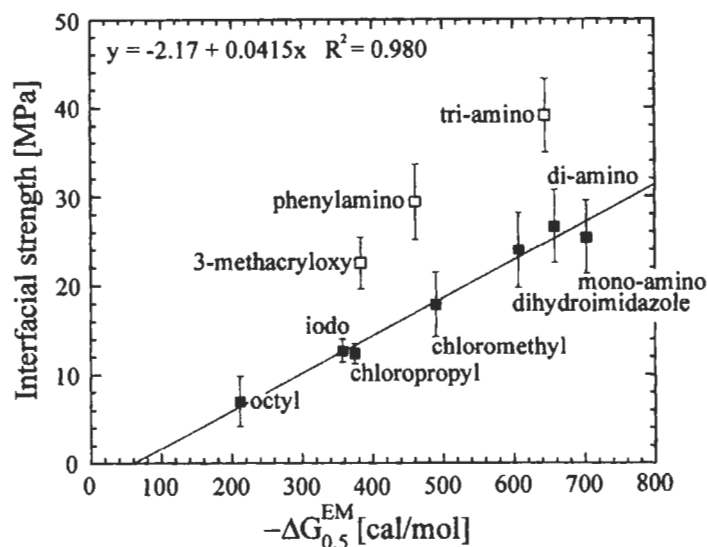


Fig. 25. Relationship between the measured interfacial strength and the (negative) Gibbs free energy of mixing, $(-\Delta G^{EM})_{0.5}$, for glass beads treated with various silane coupling agents embedded in a PVB matrix. Error bars correspond to 95% mean confidence intervals. Redrawn from ref. [165].

a second matrix system, viz. poly(methyl methacrylate). In this set of studies, iodosilane and bromosilane produced interfacial strengths higher than predicted by the trendline. These are the result of covalent bonding which occurs when the iodo-alkyl and bromo-alkyl bonds are cleaved permitting attack of the resulting free radicals on the O-CH₃ bonds of the PMMA.

4. Caveats and future prospects

While adhesion is extremely varied and complex, it appears to be possible to make a number of useful semi-empirical generalizations based on thermodynamic surface and interfacial energetics and adhesive/adherend compatibility which may serve as guidelines in designing adhesion systems. The caveat to be observed is that in general, many factors other than those of interfacial energetics and compatibility are involved in the formation and disruption of an adhesive bond. Thus, in using semi-empirical guidelines based on thermodynamic parameters, these 'other factors' must be constant. The unfortunate fact is, however, that in changing an adhesion system, it is almost never possible to change only one factor by itself.

An apparently universal truth is that intimate contact between adhesive and adherend is a necessary (but not sufficient) requirement for good adhesion,

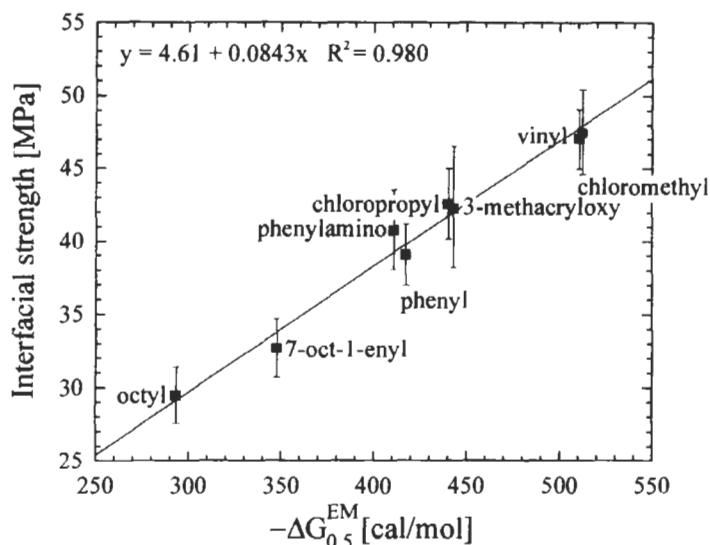


Fig. 26. Relationship between the measured interfacial strength and the (negative) Gibbs free energy of mixing, $-\Delta G_{0.5}^{EM}$, for glass beads treated with various silane coupling agents embedded in a PMMA matrix. Error bars correspond to 95% mean confidence intervals.

regardless of the mechanism by which adhesion is effected. The intimacy of contact, in turn, depends on the completeness of the wetting of the adherend by the (liquid) adhesive, i.e. spontaneous spreading, and the latter requires that the surface energy of the adhesive (equal to its surface tension, γ_L) be less than the surface free energy of the adherend, γ_S . A conservative measure of γ_S is given by the Zisman critical surface tension of the solid, γ_c , as obtained through wetting measurements using apolar probe liquids, or as the dispersion component of the surface energy, γ_S^d , as obtained by IGC measurements using alkane vapor probes. The stringent requirement that $\gamma_L < \gamma_c$ or γ_S^d for spreading may be overcome in many cases through the engagement of acid–base interactions between the adhesive (if it is acid–base functional) and functional groups on the surface of the adherend. Reliable semi-quantitative strategies for ab initio prediction of the magnitude of these acid–base effects are presently not available, but qualitative guidelines based on the chemistry of the components involved are useful in choosing materials for which these effects should occur.

In developing criteria for the ranking of adhesive formulations or adherend surface treatments or primers, it is necessary to distinguish between two different situations. In one case (contact adhesion), a true interface is believed to exist across which intermolecular forces are engaged, while in the other, an interphase is formed by diffusive interpenetration or interdigitation between the adhesive and the adherend (diffusion interphase adhesion). Even in the case of contact adhesion, more often than not, an *interphase* of macroscopic thickness forms on

the adhesive side of the interface before or during the curing the adhesive joint, and 'adhesive' failure may occur *within* this interphase more often than at the 'true' adhesive/adherend interface. Nonetheless, it is believed that the strength of the interphase (and hence, the 'interfacial' strength) is the result of the driving force for its formation, which in turn is directly related to the forces developed between molecules on opposing sides of the interface before and during cure. Under such circumstances, it makes sense, among the cases that produce spontaneous spreading, to seek the adhesive/adherend system which maximizes the work of adhesion. For the case of dispersion interactions alone (apolar materials), this leads to the criterion that there be a match between the adhesive surface tension and the adherend surface energy (or equivalently, that $\gamma_{SL} \approx 0$). The work of adhesion is often significantly enhanced through the engagement of acid–base interactions across the interface, and the qualitative advice offered by thermodynamics is that acid–base complementary adhesive/adherend systems be employed.

For diffusion interphase adhesion, the criterion for optimum adhesion is not a maximization of the work of adhesion, but rather a maximization in bulk *compatibility* between the adhesive and adherend. In this case, matching of the Scatchard–Hildebrand solubility parameters, or the 'three-dimensional' solubility parameters has proven useful in gauging compatibility. Since the materials to be interdiffused or interdigitated are often both polymeric, effectively matching solubility parameters is often inadequate to guarantee compatibility, and the only way to achieve it is through acid–base interactions. These are not adequately accounted for by solubility parameters, even the three-dimensional variety, which offer a 'hydrogen-bonding' component. Generalized group contribution methods, as exemplified by UNIFAC have recently shown significant promise for predicting compatibility, even in cases where acid–base effects play a dominant role. The database comparing the predictions of such methods to adhesion strength measurements must be expanded for a full assessment of the promise of this approach.

The continued pursuit of semi-empirical methods for the prediction of adhesion is a worthy, if somewhat risky, enterprise. It may well lead to improved and more streamlined methods of finding new materials and methods, but lacking that, even its failures, if honestly evaluated, should lead to improved understanding of the complex phenomena of adhesion.

References

1. Ghatak, A., Vorvolakos, K., She, H., Malotky, D.L. and Chaudhury, M.K., *J. Phys. Chem. B*, **104**, 4018 (2000).
2. Sharpe, L.H., *J. Adhes.*, **67**, 227 (1998).
3. Sharpe, L.H. In: Akovali, G. (Ed.), *The Interfacial Interactions in Polymeric Composites*.

- Kluwer Academic, Dordrecht, 1993, p. 1.
4. Pape, P.G. and Plueddemann, E.P. In: Mittal, K.L. (Ed.), *Silanes and Other Coupling Agents*. VSP, Utrecht, 1992, p. 105.
5. Lange, J., Hult, A., Toll, S. and Månson, J.-A.E., *Polymer*, **809** (1997).
6. Lange, J., Toll, S., Hult, A. and Månson, J.-A.E., *Polymer*, **36**, 3135 (1995).
7. Ahagon, A. and Gent, A.N., *J. Polym. Sci.*, **13**, 1285 (1975).
8. Anderson, G.P. and DeVries, K.L. In: *Treatise on Adhesion and Adhesives*, Vol. 6, Marcel Dekker, New York, 1989.
9. Eley, D.D., *Adhesion*, Oxford University Press, London, 1961.
10. Kinloch, A.J., *Adhesion and Adhesives*. Chapman and Hall, London, 1987.
11. Pocius, A.V., *Adhesion and Adhesives Technology*. Hanser/Gardner, Cincinnati, 1997.
12. Chaudhury, M.K., *Mut. Sci. Eng. R*, **R16**, 97 (1996).
13. She, H. and Chaudhury, M.K., *Langmuir*, **16**, 622 (2000).
14. Pitkethly, M.J., Favre, J.P., Gaur, U.J.J., Mudrich, S.F., Caldwell, D.L., Drzal, L.T., Nardin, M., Wagner, H.D., Di Landro, L., Hampe, A., Armistead, J.P., Desaegeer, M. and Verpoest, I., *Compos. Sci. Tech.*, **48**, 205 (1993).
15. Fowkes, F.M., *J. Phys. Chem.*, **84**, 510 (1980).
16. Good, R.J., *J. Colloid Interface Sci.*, **52**, 308 (1975).
17. Bellon-Fontaine, M.-N. and Cerf, O., *J. Adhes. Sci. Tech.*, **4**, 475 (1990).
18. Jacob, P.N. and Berg, J.C., *J. Adhes.*, **54**, 115 (1995).
19. Chaudhury, M.K., *J. Adhes. Sci. Tech.*, **7**, 669 (1993).
20. Bangham, D.H., *Trans. Faraday Soc.*, **33**, 805 (1937).
21. Johnson, R.E. Jr. and Dettre, R.H. In: Matijevic, E. (Ed.), *Surface and Colloid Science*, Vol. 2. Wiley-Interscience, New York, 1969, p. 85.
22. Cox, H.L., *Br. J. Appl. Phys.*, **3**, 72 (1952).
23. Gent, A.N. and Petrich, R.P., *Proc. R. Soc. Lond. Ser. A*, **310**, 433 (1969).
24. Gent, A.N. and Kinloch, A.J., *J. Polym. Sci.*, **A2**, 659 (1971).
25. Gent, A.N. and Schulz, J., *J. Adhes.*, **3**, 281 (1972).
26. Andrews, E.H. and Kinloch, A.J., *Proc. R. Soc. Lond. Ser. A*, **332**, 401 (1973).
27. Andrews, E.H. and Kinloch, A.J., *Proc. R. Soc. Lond. Ser. A*, **332**, 385 (1973).
28. Andrews, E.H. and Kinloch, A.J., *J. Polym. Sci. Symp.*, **46**, 1 (1974).
29. Andrews, E.H., *J. Mater. Sci.*, **9**, 887 (1974).
30. Sinicki, R.A. and Berg, J.C., *J. Adhes. Sci. Tech.*, **12**, 1091 (1998).
31. Mittal, K.L. In: Lee, L.-H. (Ed.), *Adhesion Science and Technology*, Plenum Press, New York, 1975, 9A, p. 129.
32. Kim, J.-K. and Mai, Y.-W., *Engineered Interfaces in Fiber Reinforced Composites*. Elsevier, Amsterdam, 1998.
33. Good, R.H. and Chaudhury, M.K. In: Lee, L.-H. (Ed.), *Fundamentals of Adhesion*, Plenum Press, New York, 1991, Chapt. 3.
34. Phillips, M.C., Good, R.J., Cadenhead, D.A. and King, H.F., *J. Colloid Interface Sci.*, **37**, 437 (1971).
35. Berg, J.C. In: Berg, J.C. (Ed.), *Wettability*. Marcel Dekker, New York, 1993, p. 75.
36. Fowkes, F.M., *Ind. Eng. Chem.*, **12**, 40 (1964).
37. Schultz, J., *J. Adhes.*, **37**, 73 (1992).
38. Schonhorn, H. and Hansen, R.H., *J. Appl. Polym. Sci.*, **11**, 1461 (1967).
39. Voyutskii, S.S., *Autoadhesion and Adhesion of High Polymers*. Wiley-Interscience, New York, 1963.
40. Vasinin, R.M., *Adhesion, Fundamentals and Practice*. McLaren and Son, London, 1969.
41. Beuche, F., Cashin, W.M. and Debye, P., *J. Phys. Chem.*, **20**, 1950 (1952).

42. Krotova, N.A. and Morozova, L.P., *Dokl. Akad. Nauk. SSSR*, **127**, 141 (1959).
43. Cazeneuve, C., Castle, J.E. and Watts, J.F., *J. Mater. Sci.*, **25**, 1902 (1990).
44. Chaudhury, M.K., Gentle, T.M. and Plueddemann, E.P., *J. Adhes. Sci. Tech.*, **1**, 29 (1987).
45. Gentle, T.E., Schmidt, R.G., Naasz, B.M., Gellman, A.J. and Gentle, T.M., *J. Adhes. Sci. Tech.*, **6**, 307 (1992).
46. Arrowsmith, D.J., *Trans. Inst. Metal Finish*, **48**, 88 (1970).
47. Derjaguin, B.V. and Smilga, V.P., *Adhesion Fundamentals and Practice*. McLaren and Son, London, 1969.
48. Liston, E.M., *J. Adhes.*, **30**, 199 (1989).
49. Klemberg-Sapieha, J.E., Martinu, L., Sapieha, S. and Wertheimer, M.R. In: Akovali, G. (Ed.), *The Interfacial Interactions in Polymeric Composites*. Kluwer Academic, Dordrecht, 1993, p. 201.
50. Sharpe, L.H. and Schonhorn, H. In: Fowkes, F.M. (Ed.), *Contact Angle, Wettability and Adhesion, Advances in Chemistry*, Series 43. American Chemical Society, Washington, DC, 1964, p. 189.
51. Tabor, D., *Rep. Progr. Appl. Chem.*, **36**, 621 (1951).
52. Baier, R.E., Shafrin, E.G. and Zisman, W.A., *Science*, **162**, 1360 (1968).
53. Connor, M., Harding, P.H., Månson, J.-A.E. and Berg, J.C., *J. Adhes. Sci. Tech.*, **9**, 983 (1995).
54. Zisman, W.A. In: Fowkes, F.M. (Ed.), *Contact Angle, Wettability and Adhesion*. American Chemical Society, Washington DC, 1964, 43, p. 1.
55. Girifalco, L.A. and Good, R.J., *J. Phys. Chem.*, **61**, 904 (1957).
56. Fowkes, F.M., *J. Phys. Chem.*, **66**, 382 (1962).
57. Keller, T.S., Hoffman, A.S., Ratner, B.D. and McElroy, B.J. In: Mittal, K.L. (Ed.), *Physicochemical Aspects of Polymer Surfaces*, Vol. 2. Plenum Press, New York, 1983, p. 861.
58. Bascom, W.D., Cottington, R.L. and Singleterry, C.R. In: Fowkes, F.M. (Ed.), *Contact Angle, Wettability and Adhesion. Advances in Chemistry*, Series 43. American Chemical Society, Washington DC, 1964, p. 355.
59. Kistler, S.F. In: Berg, J.C. (Ed.), *Wettability*. Marcel Dekker, New York, 1993, 49, p. 251.
60. Marmur, A., *Adv. Colloid Interface Sci.*, **19**, 75 (1983).
61. de Gennes, P.G., *Rev. Mod. Phys.*, **57**, 827 (1985).
62. Cazabat, A.-M., *Contemp. Phys.*, **28**, 347 (1987).
63. Tanner, L.H., *J. Phys. D Appl. Phys.*, **12**, 1473 (1979).
64. Hoffman, R.L., *J. Colloid Interface Sci.*, **50**, 228 (1975).
65. de Gennes, P.G. In: Charvolin, J., Joanny, J.F. and Zimm-Justin, J. (Eds.), *Liquids at Interfaces*. Elsevier, Amsterdam, 1990, p. 273.
66. Sauer, B. and Kampert, W.G., *J. Colloid Interface Sci.*, **199**, 28 (1998).
67. Brochard, F. and de Gennes, P.G., *J. Phys. Lett.*, **45**, 597 (1984).
68. Wenzel, R.N., *Ind. Eng. Chem.*, **28**, 988 (1936).
69. Cassie, A.B.D. and Baxter, S., *Trans. Faraday Soc.*, **40**, 546 (1944).
70. Irvine, J.A., Aston, D.E. and Berg, J.C., *Tappi J.*, **82**, 172 (1999).
71. Dyckerhoff, G.A. and Sell, P.J., *Angew. Makromol. Chem.*, **21**, 169 (1972).
72. Iyengar, Y. and Erickson, D.E., *J. Appl. Polym. Sci.*, **11**, 2311 (1967).
73. Mittal, K.L., *Polym. Eng. Sci.*, **17**, 467 (1977).
74. Zosel, A., *Colloid Polym. Sci.*, **263**, 541 (1985).
75. Dann, J.R., *J. Colloid Interface Sci.*, **32**, 302 (1970).
76. Owens, D.K. and Wendt, R.C., *J. Appl. Polymer Sci.*, **13**, 1741 (1969).
77. Kaelble, D.H., *Physical Chemistry of Adhesion*. Wiley-Interscience, New York, 1971.

78. Fowkes, F.M., *J. Adhes. Sci. Tech.*, **1**, 7 (1987).
79. Wu, S., *Polymer Interface and Adhesion*. Marcel Dekker, New York, 1982.
80. de Bruyne, N.A., *Aircraft Eng. (Suppl. Flight)*, **18**, 51 (1939).
81. Fowkes, F.M., Riddle Jr., F.L., Pastore, W.E. and Weber, A.A., *Colloids Surf.*, **43**, 367 (1990).
82. Westerlind, B.S. and Berg, J.C., *J. Appl. Polym. Sci.*, **36**, 523 (1988).
83. Walls, J.M., *Methods of Surface Analysis*. Cambridge University Press, Cambridge, 1989.
84. Wightman, J.P. In: Akovali, G. (Ed.), *The Interfacial Interactions in Polymeric Composites*. Kluwer Academic, Dordrecht, 1993, p. 125.
85. Lloyd, D.R., Ward, T.C., Schreiber, H.P. and Pizaña, C.C. (Eds.), *Inverse Gas Chromatography*. ACS Symposium, Series 391, American Chemical Society, Washington, DC, 1989.
86. Conder, J.R. and Young, C.L., *Physicochemical Measurements by Gas Chromatography*. Wiley, New York, 1979.
87. Dorris, G.M. and Gray, D.G., *J. Colloid Interface Sci.*, **71**, 93 (1979).
88. Page, S.A., Berg, J.C. and Manson, J.-A.E., *J. Adhes. Sci. Tech.*, in press.
89. Jacob, P.N. and Berg, J.C., *Langmuir*, **10**, 3089 (1994).
90. Harding, P.H. and Berg, J.C., *J. Adhes. Sci. Tech.*, **11**, 471 (1997).
91. Fowkes, F.M. and Mostafa, M.A., *I&EC Prod. R&D*, **17**, 3 (1978).
92. Fowkes, F.M., McCarthy, D.C. and Mostafa, M.A., *J. Colloid Interface Sci.*, **78**, 200 (1980).
93. Vrbanc, M.D. and Berg, J.C., *J. Adhes. Sci. Tech.*, **4**, 255 (1990).
94. Vrbanc, M.D., *Acid-Base Interactions in Adhesion and Wetting*, Dissertation Thesis, University of Washington, 1989.
95. Fowkes, F.M. In: Mittal, K.L. (Ed.), *Physicochemical Aspects of Polymer Surfaces*, Vol. 2. Plenum Press, New York, 1983, p. 583.
96. Gutmann, V., *The Donor-Acceptor Approach to Molecular Interactions*. Plenum Press, New York, 1978.
97. Drago, R.S., Vogel, G.C. and Needham, T.E., *J. Am. Chem. Soc.*, **93**, 6014 (1971).
98. Riddle, F.L. and Fowkes, F.M., *J. Am. Chem. Soc.*, **112**, 1235 (1975).
99. Schultz, J. and Lavielle, L. In: Lloyd, D.R., Ward, T.C., Schreiber, H.P. and Pizaña, C.C. (Eds.), *Inverse Gas Chromatography, Advances in Chemistry*, Series 391. American Chemical Society, Washington, DC, 1989, p. 185.
100. Saint-Flour, C. and Papirer, E., *Ind. Eng. Chem. Prod. Res. Dev.*, **21**, 666 (1982).
101. Nardin, M. and Schultz, J. In: Akovali, G. (Ed.), *The Interfacial Interactions in Polymeric Composites*. Kluwer Academic, Dordrecht, 1993, p. 95.
102. Nardin, M. and Schultz, J. In: Akovali, G. (Ed.), *The Interfacial Interactions in Polymeric Composites*. Kluwer Academic, Dordrecht, 1993, 230, p. 81.
103. Mittal, K.L. and Anderson, H.R. Jr. (Eds.), *Acid-Base Interactions: Relevance to Adhesion Science and Technology*. VSP, Utrecht, 1991.
104. Wool, R.P., *Polymer Interfaces, Structure and Strength*. Hanser Publishers, Munich, 1995.
105. Ishida, H. In: Akovali, G. (Ed.), *The Interfacial Interactions in Polymeric Composites*. Kluwer Academic, Dordrecht, 1993, p. 169.
106. Bonnerup, C. and Gatenholm, P., *J. Adhes. Sci. Tech.*, **7**, 247 (1993).
107. Plueddemann, E.P., *Silane Coupling Agents*. Plenum Press, New York, 1982.
108. Mittal, K.L., *Silanes and Other Coupling Agents*, VSP, Utrecht, 1992.
109. Scatchard, G., *Chem. Rev.*, **8**, 321 (1931).
110. Hildebrand, J.H., *J. Am. Chem. Soc.*, **38**, 1462 (1916).

111. Hildebrand, J.H. and Scott, R.L., *Solubility of Nonelectrolytes*. 3rd edn. Dover, New York, 1964.
112. Barton, A.F.M., *Handbook of Solubility Parameters and Other Cohesive Parameters*. CRC Publishers, Boca Raton, FL, 1983.
113. Dunkel, M., *Z. Phys. Chem.*, **A138**, 42 (1928).
114. Van Krevelen, D.W., *Properties of Polymers*. Elsevier, Amsterdam, 1990.
115. Mezzenga, R., Boogh, L. and Månson, J.-A.E., *J. Polym. Sci. B Polym. Phys.*, **38**, 1883 (2000).
116. Page, J.A., Mezzenga, R., Boogh, L., Berg, J.C. and Månson, J.-A.E., *J. Colloid Interface Sci.*, **222**, 55 (2000).
117. Brandup, J. and Immergut, E.M. (Eds.), *Polymer Handbook*, 3rd edn. Wiley-Interscience, New York, 1989.
118. Plueddemann, E.P., *J. Paint Tech.*, **40**, 1 (1968).
119. Knox, B.H., *J. Appl. Polym. Sci.*, **21**, 225 (1977).
120. Ryu, D.Y. and Kim, J.K., *Polymer*, **41**, 5207 (2000).
121. Bowles, C.Q., Miller, R.G., Chappelow, C.C., Pinzino, C.S. and Eick, J.D., *J. Biomed. Mater. Res.*, **48**, 496 (1999).
122. Orafi, H. and Spring, M.S., *Daru J. Sch. Pharm. Tehran Univ. Med. Sci. Health Serv.*, **6**, 6 (1996).
123. Rezaifard, A.H., Hod, K.A., Tod, D.A. and Barton, J.M., *Int. J. Adhes.*, **14**, 153 (1994).
124. White, D.H. and Park, S.C. In: *Mater. Soc. Res. Soc. Symp. Proc.*, Vol. 266. Materials Research Society, Warrendale, PA, 1992.
125. Asmussen, E., Hansen, E.K. and Peutzfeldt, A., *J. Dent. Res.*, **70**, 1290 (1991).
126. Fujimatsu, H., Ogasawara, S., Satoh, N., Komori, K. and Kuroiwa, S., *Colloid Polym. Sci.*, **267**, 500 (1989).
127. Cherry, B.W. and Evelyn, P.B., *J. Adhes.*, **22**, 171 (1987).
128. Asmussen, E. and Peutzfeldt, A., *Eur. J. Oral Sci.*, **108**, 335 (2000).
129. Ansarifard, M.A., Fuller, K.N.G., Lake, G.J. and Raveendran, B., *J. Rubber Res. (Kuala Lumpur)*, **3**, 1 (2000).
130. Clancy, T.C. and Mattice, W.L., *Comput. Theor. Polym. Sci.*, **9**, 261 (1999).
131. Schadelman, J.A. In: TAPPI Hot Melt Symp. Proc. TAPPI Press, Atlanta, GA, 1999.
132. Larsson, A. and Johns, W.E., *J. Adhes.*, **25**, 121 (1988).
133. Ohm, R.F., *Rubber World*, **192**, 34 (1985).
134. Gaylord, N.G., *J. Macromol. Sci. Chem.*, **A26**, 1211 (1989).
135. Barton, A.F.M., *Pure Appl. Chem.*, **57**, 905 (1985).
136. Hansen, C.M. In: Birdi, K.S. (Ed.), *Handbook of Surface and Colloid Chemistry*. CRC Press, Boca Raton, FL, 1997, p. 313.
137. Hansen, C.M., *J. Paint Technol.*, **39**, 104 (1967).
138. Hansen, C.M. and Skaarup, K., *J. Paint Technol.*, **39**, 511 (1967).
139. Hansen, C.M., *J. Paint Technol.*, **39**, 505 (1967).
140. Asmussen, E. and Uno, S., *J. Dent. Res.*, **72**, 558 (1993).
141. Miller, R.G., Bowles, C.Q., Chappelow, C.C. and Eick, J.D., *J. Biomed. Mater. Res.*, **41**, 237 (1998).
142. Prigogine, I. and Defay, R., *Chemical Thermodynamics*. Longmans, London, 1954.
143. Flory, P.J., *J. Chem. Phys.*, **9**, 660 (1941).
144. Huggins, M.L., *J. Phys. Chem.*, **9**, 440 (1941).
145. Price, G.J. In: Lloyd, D.R., Ward, T.C., Schreiber, H.P. and Pizaña, C.C. (Eds.), *Inverse Gas Chromatography*. ACS Symposium, Series 391. American Chemical Society, Washington, DC, 1989, p. 48.

146. Kwei, T.K., Pearce, E.M., Ren, F. and Chen, J.P., *J. Polym. Sci. B Polym. Phys.*, **24**, 1597 (1986).
147. Prausnitz, J.M., Lichtenthaler, R.N. and Gomes de Azevedo, E., *Molecular Thermodynamics of Fluid-Phase Equilibria*. Prentice Hall, Upper Sadle River, NJ, 1999.
148. Wilson, G.M. and Deal, C.H., *Ind. Eng. Chem. Fund.*, **1**, 20 (1962).
149. Fredenslund, A., Jones, R.L. and Prausnitz, J.M., *AIChE J.*, **21**, 1086 (1975).
150. Fredenslund, A., Gmehling, J. and Rasmussen, P., *Vapor-Liquid Equilibria using UNI-FAC*. Elsevier, Amsterdam, 1977.
151. Abrams, D. and Prausnitz, J.M., *AIChE J.*, **21**, 116 (1975).
152. Bondi, A., *Physical Properties of Molecular Crystals, Liquids and Glasses*. Wiley, New York, 1968.
153. Skjold-Joergensen, S., Kolbe, B., Gmehling, J. and Rasmussen, P., *Ind. Eng. Chem. Proc. Des. Dev.*, **18**, 714 (1979).
154. Gmehling, J. and Rasmussen, P., *Ind. Eng. Chem. Proc. Des. Dev.*, **21**, 118 (1982).
155. Macedo, E.A., Weidlich, U., Gmehling, J. and Rasmussen, P., *Ind. Eng. Chem. Proc. Des. Dev.*, **22**, 676 (1983).
156. Tiegs, D., Rasmussen, P., Gmehling, J. and Fredenslund, A., *Ind. Eng. Chem. Res.*, **26**, 159 (1987).
157. Weidlich, U. and Gmehling, J., *Ind. Eng. Chem. Res.*, **27**, 1372 (1987).
158. Hansen, H.K., Rasmussen, P., Fredenslund, A., Schiller, M. and Gmehling, J., *Ind. Eng. Chem. Res.*, **30**, 2352 (1991).
159. Gmehling, J., Fisher, K., Li, J. and Schiller, M., *Pure Appl. Chem.*, **65**, 919 (1993).
160. Gmehling, J., Li, J. and Schiller, M., *Ind. Eng. Chem. Res.*, **32**, 178 (1993).
161. Gmehling, J., *Fluid Phase Equilib.*, **107**, 1 (1995).
162. Lohmann, J., Joh, R., Niehaus, B. and Gmehling, J., *Chem. Eng. Tech.*, **21**, 245 (1998).
163. Gmehling, J., Lohmann, J., Jakob, A., Li, J. and Joh, R., *Ind. Eng. Chem. Res.*, **37**, 4876 (1998).
164. Tseng, C.-H., El-Aasser, M.S. and Vanderhoff, J.W., *J. Appl. Polym. Sci.*, **32**, 5007 (1986).
165. Miller, A.C., Knowlton, M.T. and Berg, J.C., *J. Adhes. Sci. Tech.*, **14**, 1471 (2000).
166. Harding, P.C. and Berg, J.C., *J. Adhes. Sci. Tech.*, **11**, 1063 (1997).
167. Goodier, J.M., *Trans. Am. Soc. Mech. Eng.*, **55**, 39 (1933).
168. Beck, R.H., Gratch, S., Newman, S. and Rusch, K.C., *Polym. Lett.*, **6**, 707 (1968).
169. Harding, P.H. and Berg, J.C., *J. Appl. Polym. Sci.*, **67**, 1025 (1998).
170. Weaver, K., Stoffer, J.O. and Day, E.D., *Polym. Compos.*, **16**, 161 (1995).
171. Raraty, L.E. and Tabor, D., *Proc. R. Soc. Lond. Ser. A*, **245**, 184 (1958).
172. Barbaris, M.J., *Nature*, **215**, 383 (1967).

Direct estimation of the adhesion of solid polymers

V.S. MANGIPUDI^a and AFSHIN FALSAFI^{b,*}

^a 3M Electronic Products Division, 6801 Riverplace Blvd., Austin, TX 78726, USA

^b 3M Dental Products Laboratory, 3M Center, 260-2B-12, St. Paul, MN 55144, USA

1. Introduction

1.1. Contact mechanics

Contact mechanics, in the classical sense, describes the behavior of solids in contact under the action of an external load. The first studies in the area of contact mechanics date back to the seminal publication '*On the contact of elastic solids*' of Heinrich Hertz in 1882 [1]. The original Hertz theory was applied to frictionless non-adhering surfaces of perfectly elastic solids. Lee and Radok [2], Graham [3], and Yang [4] developed the theories of contact mechanics of viscoelastic solids. None of these treatments, however, accounted for the role of interfacial adhesive interactions.

Dutrowski [5] in 1969, and Johnson and coworkers [6] in 1971, independently, observed that relatively small particles, when in contact with each other or with a flat surface, deform, and these deformations are larger than those predicted by the Hertz theory. Johnson and coworkers [6] recognized that the 'excess' deformation was due to the interfacial attractive forces, and modified the original Hertz theory to account for these interfacial forces. This led to the development of a new theory of contact mechanics, widely referred to as the JKR theory. Over the past two decades or so, the contact mechanics principles and the JKR theory have been employed extensively to study the adhesion and friction behavior of a variety of materials.

The JKR theory relates the interfacial-force-induced contact deformation to the thermodynamic work of adhesion between solids, and provides a theoretical

* Corresponding author. E-mail: afalsafi@mmm.com

basis for experiments designed to directly measure the surface and interfacial energies of solids. In recent years, several groups of researchers have studied the interfacial adhesion between polymers using the contact-mechanics-based approach. These studies include the direct measurement of surface and interfacial energies of polymers and self-assembled monolayers; quantitative investigation of the influence of interfacial diffusion and interfacial chemical reaction on adhesion of elastomers; adhesion of microparticles on surfaces; and adhesion of viscoelastic polymers. In the later sections, we review the JKR theory as well as the related theories of contact mechanics, and summarize the results of the above-mentioned experimental studies of adhesion that use the contact mechanics approach. In the following section, we discuss in general terms the phenomenon of adhesion, its molecular basis, and its measurement.

1.2. Adhesion and its molecular basis

The phenomenon of adhesion deals with *attachment or bonding*, which is governed by the interfacial processes occurring between the surfaces forming contact, and *detachment or debonding*, which is influenced by the interfacial and bulk processes occurring in the adhesive and the adherends as they are separated under induced stress. It is important to recognize that the physical processes and material properties involved in *bonding* are separate from those that govern that *debonding*. An understanding of the interfacial processes and measurement of their contribution to the strength of an adhesive bond forms an important fundamental part of the science of adhesion. At this point, it may be necessary to recapitulate the definitions of certain terms that are routinely encountered in the field of adhesion science.

1.2.1. Adhesion

Adhesion is a phenomenon by which two materials form a contact region that is able to sustain or transmit stress. There are a variety of mechanisms or factors that contribute to the adhesion between two materials. These include interfacial van der Waals forces that lead to adsorption; interdiffusion of molecules across the interface; interfacial chemical bonding and/or hydrogen bonding; mechanical interlocking; electrostatic interactions and so on. It should be emphasized that in a given 'engineering' or 'real' situation, one or more of the above-mentioned mechanisms may be operative. It may also be noted that the van der Waals molecular level interactions are universally present in all situations, and that these interactions are usually attractive in nature. The details of the origin and nature of interfacial forces are discussed in several text books and review articles. (See references [7–11], for example.)

1.2.2. Strength of an adhesive bond

Another important term that is often used in the adhesion literature is ‘strength of an adhesive bond’. The strength of an adhesive bond, as can be inferred from the term itself, represents the maximum load or stress that an adhesive joint can withstand before it breaks or debonds. The strength of an adhesive bond is not an intrinsic property of the joint under consideration. This strength, usually measured in a convenient practical method, such as a peel or shear test, includes the contribution of interfacial forces as well as the energy dissipation associated with the bulk deformation of the adhesive and the adherends. This strength, referred to in many cases as the ‘*practical strength of an adhesive bond*’, G , depends on a variety of factors such as geometry of the joint, mechanics of the test method used for debonding, rate and temperature of debonding, and the bulk material properties of the adhesive and the adherends. Different test methods used for debonding differ in their modes of application of stress and the locus of the crack propagation. In a real application, an adhesive bond has to be able to withstand different levels of stress in different modes of failure. Some of the more commonly used test methods are illustrated in Fig. 1. A review of the *practical test methods* may be found elsewhere [7–12].

1.3. Strength of an adhesive bond: role of the interface

As mentioned earlier, adhesive bond formation is governed by interfacial processes occurring between the adhering surfaces. These interfacial processes, as summarized by Brown [13] include: (1) van der Waals or other non-covalent interactions that form bonds across the interface; (2) interdiffusion of polymer chains across the interface and coupling of the interfacial chains with the bulk polymer; and (3) formation of primary chemical bonds between chains or molecules at or across the interface.

The van der Waals and other non-covalent interactions are universally present in any adhesive bond, and the contribution of these forces is quantified in terms of two material properties, namely, the surface and interfacial energies. The surface and interfacial energies are macroscopic intrinsic material properties. The surface energy of a material, γ , is the energy required to create a unit area of the surface of a material in a thermodynamically reversible manner. As per the definition of Dupré [14], the surface and interfacial properties determine the intrinsic or thermodynamic work of adhesion, W , of an interface. For two identical surfaces in contact:

$$W = 2\gamma \quad (1)$$

and, for two dissimilar surfaces in contact:

$$W = \gamma_1 + \gamma_2 - \gamma_{12} \quad (2)$$

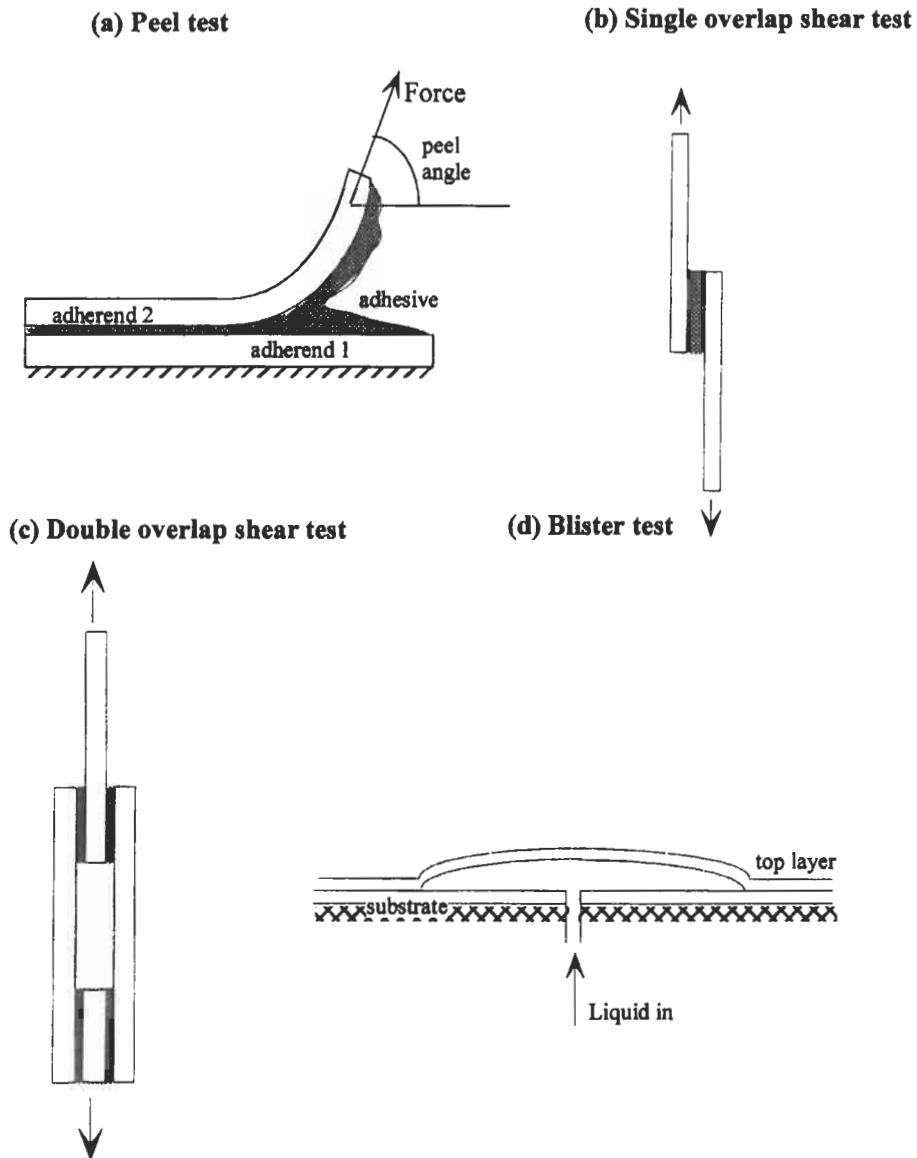


Fig. 1. Schematic of commonly used methods for testing the strength of adhesive joints. (a) Peel test. Note that the peel angle can be changed depending on the test requirements. (b) Double overlap shear test. In this test, the failure is predominantly mode II. (c) Single overlap shear test. In this test the failure mode is mixture of mode I and mode II. (d) Blister test.

where γ_1 , γ_2 are the surface energies of materials 1 and 2, and γ_{12} is the interfacial energy between 1 and 2.

In general, the practical strength of an adhesive bond, sometimes termed the

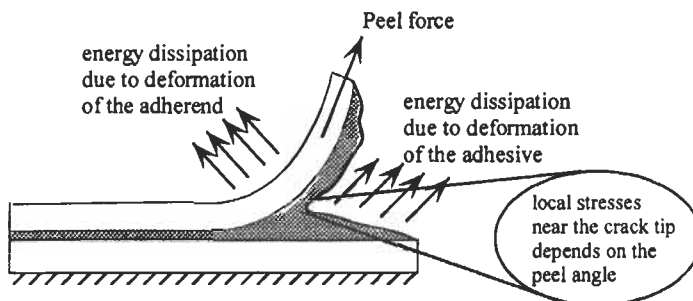


Fig. 2. Schematic of energy dissipation in a commonly used peel test. The energy dissipation can occur in the adhesive and/or the adherends. The extent of energy dissipation depends on the elasto-plastic properties of the adhesive and the adherends under the test conditions as well as the local stresses and strains near the crack tip.

strain energy release rate during debonding, G , is orders of magnitude higher than the thermodynamic work of adhesion, W , of the interface. This is because of energy dissipation associated with the bulk deformations of the adhesive and the adherends that occur during the debonding process in a practical test. This dissipation process is illustrated schematically in Fig. 2. Even though $W \ll G$, it has been demonstrated that the interfacial characteristics play a very important role in determining the strength of an adhesive bond. In their seminal work, Gent and Schultz [15], and Andrews and Kinloch [16], independently, demonstrated that the interfacial strength W , has a multiplicative effect on the practical strength of an adhesive bond, G . Based on the results of their well-conceived experiments, Gent and Schultz, and Andrews and Kinloch suggested the following relation between W and G :

$$G = W [1 + \Phi(v, T)] \quad (3)$$

where Φ is the energy dissipation term that depends on the rate of debonding (v) and the test temperature T . This correlation is only empirical, and is by no means complete. In fact, the functional form of Eq. 3 is yet to be established in a general way. Some of the more recent experimental results suggest a more general form for the correlation between W and G , and the form of this equation will be discussed further later in this chapter.

As demonstrated by the experiments of Gent and Schultz [15], and Andrews and Kinloch [16], and as shown by Eq. 3 and its modifications, the interfacial work of adhesion plays an important role in determining the *practical strength* of an adhesive bond. It has, in general, been a challenging task to design experimental tools to measure the interfacial work of adhesion (W). The recent theoretical and experimental developments in contact mechanics led to a series of new studies aimed at measuring and understanding the role of interfacial work of adhesion of polymeric materials. These developments will be reviewed in this chapter.

2. Outline of this chapter

The Hertz theory of contact mechanics has been extended, as in the JKR theory, to describe the equilibrium contact of adhering elastic solids. The JKR formalism has been generalized and extended by Maugis and coworkers to describe certain dynamic elastic contacts. These theoretical developments in contact mechanics are reviewed and summarized in Section 3. Section 3.1 deals with the equilibrium theories of elastic contacts (e.g. Hertz theory, JKR theory, layered bodies, and so on), and the related developments. In Section 3.2, we review some of the work of Maugis and coworkers.

As mentioned earlier, the contact-mechanics-based experimental studies of interfacial adhesion primarily include: (1) direct measurements of surface and interfacial energies of polymers and self-assembled monolayers; (2) quantitative studies on the role of interfacial coupling agents in the adhesion of elastomers; (3) adhesion of microparticles on surfaces; and (4) adhesion of viscoelastic polymer particles. In these studies, a variety of experimental tools have been employed by different researchers. Each one of these tools offers certain advantages over the others. These experimental studies are reviewed in Section 4.

Section 4.1 briefly describes some of the commonly employed experimental tools and procedures. Chaudhury et al., Israelachvili et al. and Tirrell et al. employed contact mechanics based approach to estimate surface energies of different self-assembled monolayers and polymers. In these studies, the results of these measurements were compared to the results of contact angle measurements. These measurements are reviewed in Section 4.2. The JKR type measurements are discussed in Section 4.2.1, and the measurements done using the surface forces apparatus (SFA) are reviewed in Section 4.2.2.

Elastomer adhesion and the role of interfacial coupling agents has long been studied by several researchers using peel test methods. In certain situations these methods are rather insensitive to the experimental variables. Brown et al. and Tirrell et al. have employed the contact mechanics technique to this problem of adhesion of elastomers in the presence of interfacial coupling agents. These experimental studies have resulted in some very insightful data that verified some of the recent theories, and led to a better understanding of the adhesion of elastomers. These experiments are reviewed in Section 4.3.

Some of the recent work in contact mechanics is focused on understanding the adhesion of viscoelastic polymers and dynamic contributions to the adhesion energy; this work is summarized in Section 5. Sections 6.1 and 6.2 include some of the current applications of contact mechanics in the field of adhesion science. These include possible studies on contact induced interfacial rearrangements and acid–base type of interactions.

3. Contact mechanics of elastic solids

As mentioned earlier, contact mechanics describes the deformation behavior of solids in contact. Heinrich Hertz, in his classical paper '*On the contact of elastic solids*', described the deformation of elastic solid spheres under the action of an external load [1]. The original Hertzian theory was restricted to frictionless, non-adhering surfaces of perfectly elastic bodies. For adhering elastic solids, Johnson et al. developed a new theory of contact mechanics, known as the JKR theory [6]. The JKR theory of contact mechanics is an extension of the Hertzian theory, and accounts for the influence of interfacial forces or adhesion on the contact mechanics of elastic solids. The JKR theory describes the equilibrium situation where the thermodynamic energy of adhesion due to interfacial interactions and the elastic stored energy are balanced. However, in certain elastic situations, the system can be dynamic due to factors such as interfacial diffusion or interfacial rearrangements. Maugis and Barquins extended the JKR treatment to include such dynamic situations [17,18]. In Section 3.1, we briefly outline the equilibrium theories of contact mechanics, in particular the JKR theory, and the related developments. In Section 3.2, we summarize the work of Maugis and coworkers to describe the applicability of contact mechanics to dynamic systems.

3.1. Theories of contact mechanics

Contact mechanics deals with the deformation of solids in contact. Consider two elastic bodies, shown schematically in Fig. 3, of radii of curvature R_1 and R_2 , Young's moduli E_1 and E_2 , and Poisson's ratios ν_1 and ν_2 . Define

$$\frac{1}{R} = \frac{1}{R_1} + \frac{1}{R_2} \quad (4)$$

$$\frac{1}{K} = \frac{3}{4} \left[\frac{1 - \nu_1^2}{E_1} + \frac{1 - \nu_2^2}{E_2} \right] \quad (5)$$

We are particularly interested in the geometry of a sphere in contact with a flat surface since this is the geometry used very commonly in the experimental measurements reviewed in this chapter. The geometry used in the surface forces apparatus (described later) is two orthogonally crossed cylinders. As shown by Derjaguin et al. [19], the geometry of two crossed cylinders is equivalent to the geometry of a sphere in contact with a flat surface. In such a geometry

$$R_1 = R_{\text{sphere}}, \quad R_2 \rightarrow \infty \quad \text{and} \quad R = R_{\text{sphere}} \quad (6)$$

A sphere in contact with a flat surface under the action of an applied load P ($P > 0$ for compression and $P < 0$ for tension) deforms as shown in Fig. 3. Let a be the radius of the contact zone. The center of the sphere is displaced by a

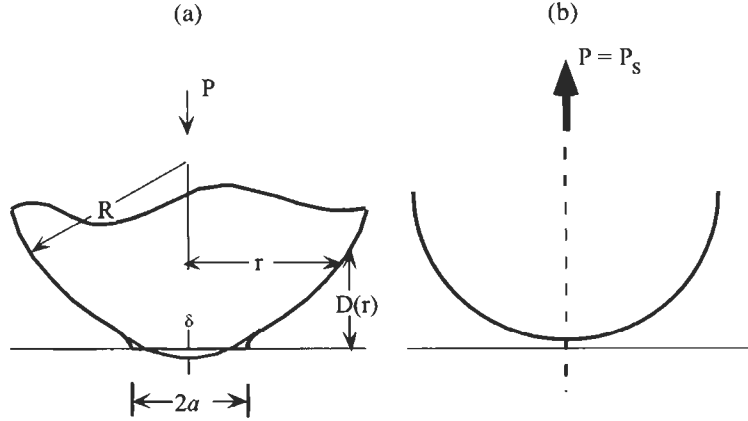


Fig. 3. Schematic of a sphere in contact with a flat surface. (a) The deformation when surfaces are in contact. The radius of the deformed zone is a , and the separation profile is given by D versus r . The central displacement, δ , is shown as the distance between the center of the deformed zone and the tip of the undeformed sphere, represented by the bold line. δ characterizes the displacement of the applied load. (b) When the applied load is $-P_s$, the pull-off force, the surfaces jump out of contact, and the undeformed shape of the surfaces is attained.

distance δ . δ is called the central displacement. r is the radial distance from the center of the contact zone, and D is the separation between the two surfaces at distance r .

3.1.1. Hertz theory

The classical theory of contact mechanics, due to Hertz, treats the bodies in contact with a hard wall repulsive interaction, i.e. there is no attractive interaction whatsoever, and a steep repulsion comes into play when the surfaces of the bodies are in contact. The Hertzian theory assumes that only normal stresses exist, i.e. the shear stress in the contact region is zero. Under these conditions, the contact radius (a), central displacement (δ) and the distribution of normal stress (σ) are given by the following expressions:

$$a^3 = \frac{PR}{K} \quad (7)$$

$$\delta = \frac{P^2 R}{K} = \frac{a^2}{R} \quad (8)$$

$$\sigma(x) = \frac{3Ka}{2\pi R} (1 - x^2)^{1/2} \quad (9)$$

where $x = r/a$ is the normalized radial distance.

The separation profile outside the contact zone, D versus x , is given by

$$D(x) = \frac{a^2}{\pi R} \left[(x^2 - 1) + (x^2 - 2) \tan^{-1} \sqrt{x^2 - 1} \right] \quad (10)$$

The surfaces of all materials interact through van der Waals interactions and other interactions. These interfacial forces, which are attractive in most cases, result in the deformation of the solid bodies in contact. In practice, the radius of the contact zone is higher than the radius predicted by the Hertzian theory (Eq. 7). Johnson et al. [6] modified the Hertzian theory to account for the interfacial interactions, and developed a new theory of contact mechanics, widely known as the JKR theory. In the following section, we discuss the details of the JKR theory. The details of the derivation may be obtained elsewhere [6,20,21].

3.1.2. JKR theory

Roberts, using smooth rubber spheres in contact with a rubber flat, and Kendall, using glass spheres noted that contact area between the sphere and the flat was considerably larger than the area predicted by the Hertzian theory (see Johnson et al. [6]). The difference in contact area was particularly significant under low applied loads. The contact radius was found to be finite even under zero load, i.e. when $P = 0$, and it was necessary to apply a finite tensile load to separate the adhering bodies from contact. A similar observation was made by Dutrowski [5] in his experiments on the contact of a glass sphere with an elastomer. Johnson et al. [6] pointed out that the ‘excess’ deformation was due to the action of attractive forces occurring at the interface, and developed a theory of contact mechanics, known as the JKR theory. The JKR theory is a balance of elastic energy associated with the deformation of the sphere, potential energy associated with the displacement of load, and the surface or interfacial energy associated with the formation of adhesive bond. The incorporation of surface or interfacial energy component into the energy balance results in an equilibrium contact area that is larger than that predicted by the Hertz theory. The contact radius depends on the interfacial work of adhesion (W) and the external applied load (P). The interfacial work of adhesion (W) accounts for the influence of interfacial forces. According to the JKR theory, the contact radius a under an applied load P is given by

$$a^3 = \frac{R}{K} \left[P + 3\pi W R + \sqrt{6\pi W R P + (3\pi W R)^2} \right] \quad (11)$$

where W , R and K are given by Eqs. 2, 4 and 5, respectively. Eq. 11 may be rearranged as

$$W = \frac{\left(P - \frac{a^3 K}{R} \right)^2}{6\pi K a^3} \quad (12)$$

It can be seen from Eq. 11 that the contact radius is finite even at no applied load. The zero load contact radius a_0 is given by

$$a_0^3 = \frac{6\pi W R^2}{K} \quad (13)$$

The separation profile outside the contact zone is given by

$$D(x) = \frac{a^2}{\pi R} \left[(x^2 - 1) + \left\{ x^2 - 2 + \frac{4}{3} \left(\frac{a_0}{a} \right)^{3/2} \right\} \tan^{-1} \sqrt{x^2 - 1} \right] \quad (14)$$

The distribution of the normal stress in the contact circle is given by

$$\sigma(x) = \frac{3Ka}{2\pi R} (1 - x^2)^{1/2} - \left(\frac{3WK}{2\pi a} \right)^{1/2} (1 - x^2)^{-1/2} \quad (15)$$

It can be seen from the above equation that at the edge of the contact circle, i.e. $x = 1$, the stress is tensile and it goes to infinity. This is not physically correct. However, it should be noted that the tensile stresses near the edge of the contact zone are indeed high. In some cases, these stresses could be as high as the yield modulus of the material. The origins of the singularity in stress are discussed later in this section.

When the surfaces are in contact due to the action of the attractive interfacial forces, a finite tensile load is required to separate the bodies from adhesive contact. This tensile load is called the 'pull-off' force (P_s). According to the JKR theory, the pull-off force is related to the thermodynamic work of adhesion (W) and the radius of curvature (R).

$$P_s = \frac{3}{2} \pi W R \quad (16)$$

The ratio of P_s to R is known as the normalized pull-off energy, P_n . The normalized pull-off energy depends only on the surface and interfacial energies.

$$P_n = \frac{3}{2} \pi W = \frac{3}{2} \pi (\gamma_1 + \gamma_2 - \gamma_{12}) \quad (17)$$

The surfaces jump out of contact when the applied load is equal to the pull-off force, i.e. $P = -P_s$. The contact radius at the point of separation, a_s , is given by

$$a_s^3 = \frac{3\pi W R^2}{2K} \quad (18)$$

From Eqs. 13 and 18, it can be seen that the ratio of a_s to a_0 is about 0.63.

In an appropriately designed experiment, it is possible to measure the pull-off force (P_s), contact radius (a versus P , a_0 and a_s), and the separation profile outside the contact zone (D versus x). From these measurements, it is possible to determine the thermodynamic work of adhesion between two surfaces, if the contacting bodies are perfectly elastic.

3.1.3. Origins of stress singularity in JKR analysis

In their analysis, Johnson et al. [6] note that, under an applied load P , the actual contact radius a is higher than the radius predicted by the Hertzian theory. Johnson et al. calculate an equivalent Hertzian load P_1 ($> P$) using Eq. 7, and the corresponding energy (U_1) stored in the system due to elastic deformation of the sphere under Hertzian conditions. U_1 and P_1 are given by

$$P_1 = \frac{a^3 K}{R} \quad (19)$$

$$U_1 = \frac{2}{5} \frac{P_1^{5/3}}{K^{2/3} R^{1/3}} \quad (20)$$

The corresponding normal stress distribution is given by

$$\sigma_1(x) = \frac{3Ka}{2\pi R} (1 - x^2)^{1/2} \quad (21)$$

The JKR treatment further considers that the load on the bodies is reduced from the equivalent Hertzian load P_1 to the actual applied load P , keeping the contact radius constant at a . This is equivalent to reducing the load, from P_1 to P , on a cylindrical punch in contact with a flat surface. This loading–unloading scheme of the JKR analysis is shown schematically in Fig. 4. The elastic energy released during this unloading (U_2), and the corresponding normal stress distribution (σ_2) are calculated using the equations derived by Boussinesq [22]. U_2 and σ_2 are given

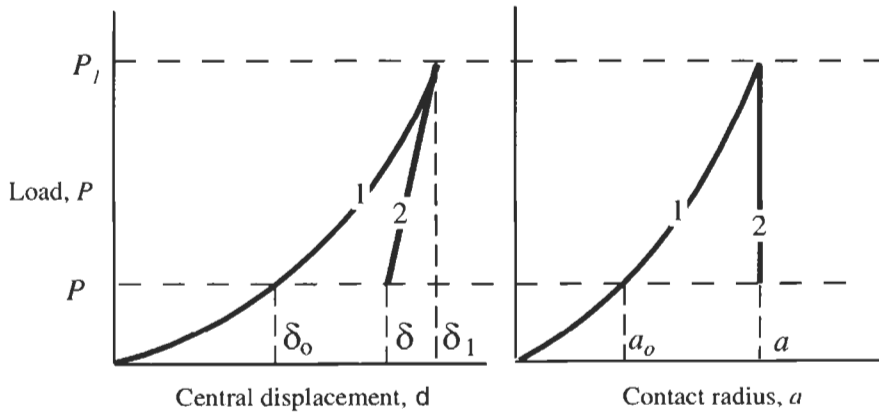


Fig. 4. Schematic of the JKR treatment of contact mechanics calculations. The point (δ, a, P) corresponds to the actual state under the action of interfacial forces and applied load P . P_1 is the equivalent Hertzian load corresponding to contact radius a between the two surfaces. (δ_0, a_0, P) and (δ_1, a, P_1) are the Hertzian contact points. The net stored elastic energy and displacement δ are calculated as the difference of steps 1 and 2.

by the following equations.

$$U_2 = \frac{P_1^2 - P^2}{3P_1^{1/3} K^{2/3} R^{1/3}} \quad (22)$$

$$\sigma_2(x) = \left[\frac{3WK}{2\pi a} \right] (1 - x^2)^{-1/2} \quad (23)$$

The net stored elastic energy is given by $U_E = U_1 - U_2$, and the net normal stress distribution is given by

$$\sigma(x) = \sigma_1(x) - \sigma_2(x) = \frac{3Ka}{2\pi R} (1 - x^2)^{1/2} - \left[\frac{3WK}{2\pi a} \right] (1 - x^2)^{-1/2} \quad (24)$$

In the above analysis, Johnson et al. [6] assume that the interfacial forces act only when the surfaces are in contact, i.e. the attractive forces are considered to be of infinitesimally short range. This analysis ignores the forces acting just outside the edge of the contact circle. Because of this, the theory predicts an infinite tensile stress at the edge of the contact. If the attractive force between the surfaces is allowed to have a finite range, the infinity in the tensile stress disappears. The stress at the edge of the contact circle is still tensile, but it remains finite.

To account for some of the shortcomings of the JKR theory, Derjaguin and coworkers [19] developed an alternative theory, known as the DMT theory. According to the DMT theory, the attractive force between the surfaces has a finite range and acts outside the contact zone, where the surface shape is assumed to be Hertzian and not deformed by the effect of the interfacial forces. The predictions of the DMT theory are significantly different compared to the JKR theory.

There was some argument in the literature over the relative merits and demerits of the JKR and the DMT theories [23–26], but the controversy has now been satisfactorily resolved. A critical comparison of the JKR and DMT theories can be obtained from the literature [23–30]. According to Tabor [23], JKR theory is valid when the dimensionless parameter given by Eq. 25 exceeds a value of about five.

$$\mu = \left(\frac{RW^2}{K^2 z_0^2} \right)^{1/3} \quad (25)$$

where R is given by Eq. 4, K is given by Eq. 5, W is work of adhesion given by Eq. 1 or 2, and z_0 is the equilibrium separation of the surfaces in contact. It is generally agreed that for a hard solid of low surface energy and small radius of curvature the DMT theory would be appropriate, while the JKR theory would be more accurate for soft materials with relatively high surface energy and large radius of curvature. Recently, Maugis [30] demonstrated this JKR–DMT transition using a Dugdale model of fracture mechanics. As far as soft polymeric systems are concerned, it has been found that the JKR theory correctly predicts the contact mechanics. The JKR theory has been widely employed to determine the work

of adhesion W from the measurements of pull-off force P_s and the variation of contact radius as a function of applied load, a versus P .

3.1.4. Contact of layered bodies

Contact mechanics of engineering surfaces, especially layered surfaces has seen significant progress in the last decade [31]. The main achievement has been the removal of the continuum assumptions in the Hertz theory. The application of numerical techniques including finite element methods has successfully solved many contact problems, which are difficult to solve analytically.

The JKR theory, similar to the Hertz theory, is a continuum theory in which two elastic semi-infinite bodies are in a non-conforming contact. Recently, the contact of layered solids has been addressed within the framework of the JKR theory. In a fundamental study, Sridhar et al. [32] analyzed the adhesion of elastic layers used in the SFA and compared it with the JKR analysis for a homogeneous isotropic half-space. As mentioned previously and depicted in Fig. 5, in SFA thin films of mica or polymeric materials (E_1, h_1) are put on an adhesive layer (E_2, h_2) coated onto quartz cylinders (E_3, h_3). Sridhar et al. followed two separate approaches. In the first approach, based on finite element analysis, it is assumed that the thickness of the layers and their individual elastic constants are known in advance, a case which is rare. The adhesion characteristics, including the pull-off force are shown to depend not only on the adhesion energy, but also on the ratios of elastic moduli and the layers thickness. In the second approach, a procedure is proposed for calibrating the apparatus in situ to find the *effective* modulus E_e as a function of contact radius a . In this approach, it is necessary to measure the load, contact area

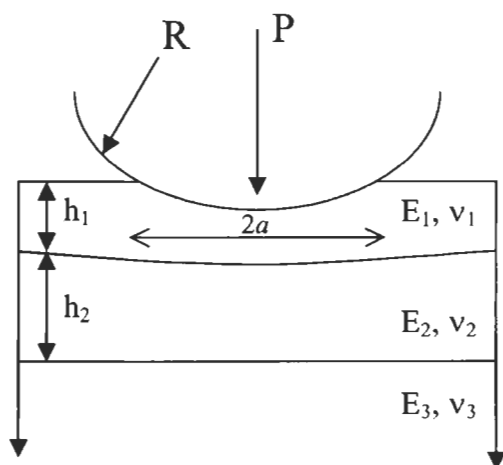


Fig. 5. Deformation of a layered half-space by a smooth and rigid sphere [32].

and compression of the system under condition of zero adhesion

$$E_c(a) = \frac{1}{2a} \frac{dP_H}{d\delta_H} \quad (26)$$

Upon the knowledge of $P_H(a)$ and $E_c(a)$, the following counterpart of Eq. 12 can be used to measure adhesion

$$[P_H(a) - P]^2 = 8\pi W a^3 E_c(a) \left[1 + \frac{a}{E_c(a)} \left(\frac{dE_c(a)}{da} \right) \right]^{-1} \quad (27)$$

Based on the FE analysis and considering the practical range of the moduli and thickness ratios in SFA, the second term in the bracket in the above equation is small for $1 < a/h < 10$. This range corresponds to maximum accuracy of the calibration.

It has been also shown that when a thin polymer film is directly coated onto a substrate with a low modulus ($E < 10$ MPa), if the contact radius to layer thickness ratio is large ($a/h > 20$), the surface layer will make a negligible contribution to the stiffness of the system and the layered solid system acts as a homogeneous half-space of substrate material while the surface and interfacial properties are governed by those of the layer [32,33]. The extension of the JKR theory to such layered bodies has two important implications. Firstly, hard and opaque materials can be coated on soft and clear substrates which deform more readily by small surface forces. Secondly, viscoelastic materials can be coated on soft elastic substrates, thereby reducing their time-dependent effects.

3.1.5. Large deformation contacts and finite size effects

The JKR theory, much like the Hertz theory, assumes a parabolic approximation for the profile of sphere, which is valid for small ratios of contact radii to the sphere's radius. Maugis [34] has shown that for small particles on a soft substrate, this ratio could be so large that such parabolic approximation is no longer valid. Under such conditions, the use of exact expression for the sphere profile is necessary for the applicability of the JKR theory, which is expressed as

$$\delta = \frac{a}{2} \ln \frac{R+a}{R-a} - \sqrt{\frac{8\pi a W}{3K}} \quad (28)$$

$$P = \frac{3aK}{2} \left(\frac{R^2 + a^2}{4a} \ln \frac{R+a}{R-a} - \frac{R}{2} - \sqrt{\frac{8\pi a W}{3K}} \right) \quad (29)$$

A study by Shull et al. [35]. on the adhesion of soft and relatively thin elastomeric lenses to glass substrates shows that the compliance ($C = \delta/P$) predicted by the JKR theory is larger than the actual value by a constant factor.

$$C = C_{\text{thick}} - \Delta C = \frac{2}{3Ka} - \Delta C \quad (30)$$

They argue that the Hertzian load (P_H) is not significantly affected by the finite size effects, therefore the JKR expression relating the load to the contact radius and adhesion energy (Eq. 11) should still be valid. Using a combined analytical and computational approach, Hui et al. [36] found that a correction given by Shull et al. for the compression of such thin lenses was accurate for moderately large contact radius

$$\delta = \delta_{\text{thick}} - P \Delta C = \frac{a^2}{3R} + \frac{2P}{3Ka} - P \Delta C \quad (31)$$

The finite size effects in the contact between a spherical lens of polyurethane and a soft flat sheet of crosslinked poly(dimethyl siloxane) (PDMS) has been addressed by Falsafi et al. [37]. They showed that for deformations corresponding to contact diameters larger than the sheet thickness, the compliance of the system was affected by the glass substrate supporting the soft sheet. In order to minimize the finite size effects in the adhesion measurement of small elastomeric lenses, Falsafi et al. [38] and Deruelle et al. [39] used relatively thick elastic sheets to support their samples.

3.1.6. Contact mechanics of a cylinder and a flat plate

The mechanics of two-dimensional contact between a cylinder and a flat plate has been analyzed by Barquins [40]. For such a contact when the length and the width of the contact area are $2l$ and $2a$, respectively,

$$W = \frac{\left[\frac{3\pi K a^2 l}{8R} - P \right]^2}{6\pi K a l^2} \quad (32)$$

Contrary to spherical contact, the minimum force, or the pull-off force under load-controlled conditions, is dependent on the elastic constant of the system

$$P_{\min} = 3.16 \left(\sqrt[3]{K W^2 R} \right) l \quad (33)$$

For cylindrical contacts, the contact width at separation is 39% of the contact width at zero load, while this value is 63% for spherical contact. The main disadvantage of cylindrical contact is its conformity along the long axis, therefore the alignment between cylinders and flats is very crucial.

3.2. Contact mechanics of elastic solids with interfaces in non-equilibrium

The JKR theory is essentially an equilibrium balance of energy released due to interfacial bond formation and the stored elastic energy. For simple elastic solids the deformation as a function of load, according to the JKR theory is given by

Eq. 34 which is shown below

$$a^3 = \frac{R}{K} \left[P + 3\pi W R + \sqrt{6\pi W R P + (3\pi W R)^2} \right] \quad (34)$$

For simple elastic solids in contact that do not show any time-dependent interfacial or bulk chemical or mechanical changes when in contact, the contact radius versus load (a versus P) behavior is perfectly reversible. In other words, the contact radius remains the same whether it is measured during *compression* (or *loading*) or *decompression* (or *unloading*) cycles. In such a case, the *loading* and *unloading* curves superimpose. That is, there is no *contact adhesion hysteresis*. This kind of behavior is observed in certain elastomeric systems, such as cross-linked poly(dimethyl siloxane). However, if any diffusion driven entanglements across the interface or any interfacial chemical reaction rearrangements occur when the surfaces are in contact under a finite stress, then the contact radius at the given load measured during the *unloading* cycle is higher than that measured during the *loading* cycle. That is, there will be a finite hysteresis. In other words, if the interface or interphase changes with time when solid bodies are in contact without resulting any changes in the bulk elastic properties, then a *contact adhesion hysteresis* is observed. Such systems may be referred to as '*elastic solids with non-equilibrium interfaces*'. The degree of hysteresis may be used as a measure of the extent of rearrangement. It may noted that *contact hysteresis* may be observed when the bulk modulus changes due to applied stresses as in viscoelastic contacts. These contacts are discussed in Section 5. The hysteresis behavior of different systems is illustrated in Fig. 6.

The fracture mechanics treatment of Maugis and Barquins [17], which in a way is an extension of the original JKR theory, can be used to describe the contact mechanics of *elastic solids with non-equilibrium interfaces*. According to Maugis and Barquins, for elastic contacts the edge of the contact surface may be treated as a propagating crack in mode I. Under isothermal conditions, for system under load P , the variation in free energy dF for an infinitesimal change in contact area dA may be written as

$$dF = dU_T = dU_E + dU_P + dU_S \leq 0 \quad (35)$$

where U_E is the elastic energy store in the system; U_P is the potential energy of the applied load P ; and U_S is the interfacial energy. The change in interfacial energy, according to the Dupré equation, is given by

$$dU_S = -(\gamma_1 + \gamma_2 - \gamma_{12})dA = -WdA \quad (36)$$

where W is the Dupré work of adhesion. Using fracture mechanics arguments, Maugis and Barquins [17], defined *strain energy release rate* as

$$G = \frac{dU_E}{dA} + \frac{dU_P}{dA} \quad (37)$$

The change in total energy or free energy, under isothermal conditions, is then given by

$$dF = dU_T = (G - W)dA \quad (38)$$

G is, in this context, called the *strain energy release rate*. GdA is the mechanical energy released when the crack extends by an area dA . The breaking of bonds requires an amount of energy given by WdA , and the excess energy $(G - W)dA$ is changed into kinetic energy if there is no bulk dissipation. The difference $(G - W)$ may be considered as the crack extension force. While the reversible work of adhesion is independent of the loading path, the strain energy release rate is not. The strain energy released due to slip will be partially or totally dissipated as heat [41].

For equilibrium systems with no contact hysteresis $G = W$, which is the classical Griffith criterion in fracture mechanics. For such a system, Eqs. 12 and 37 are the same. That is, the strain energy release rate is given by

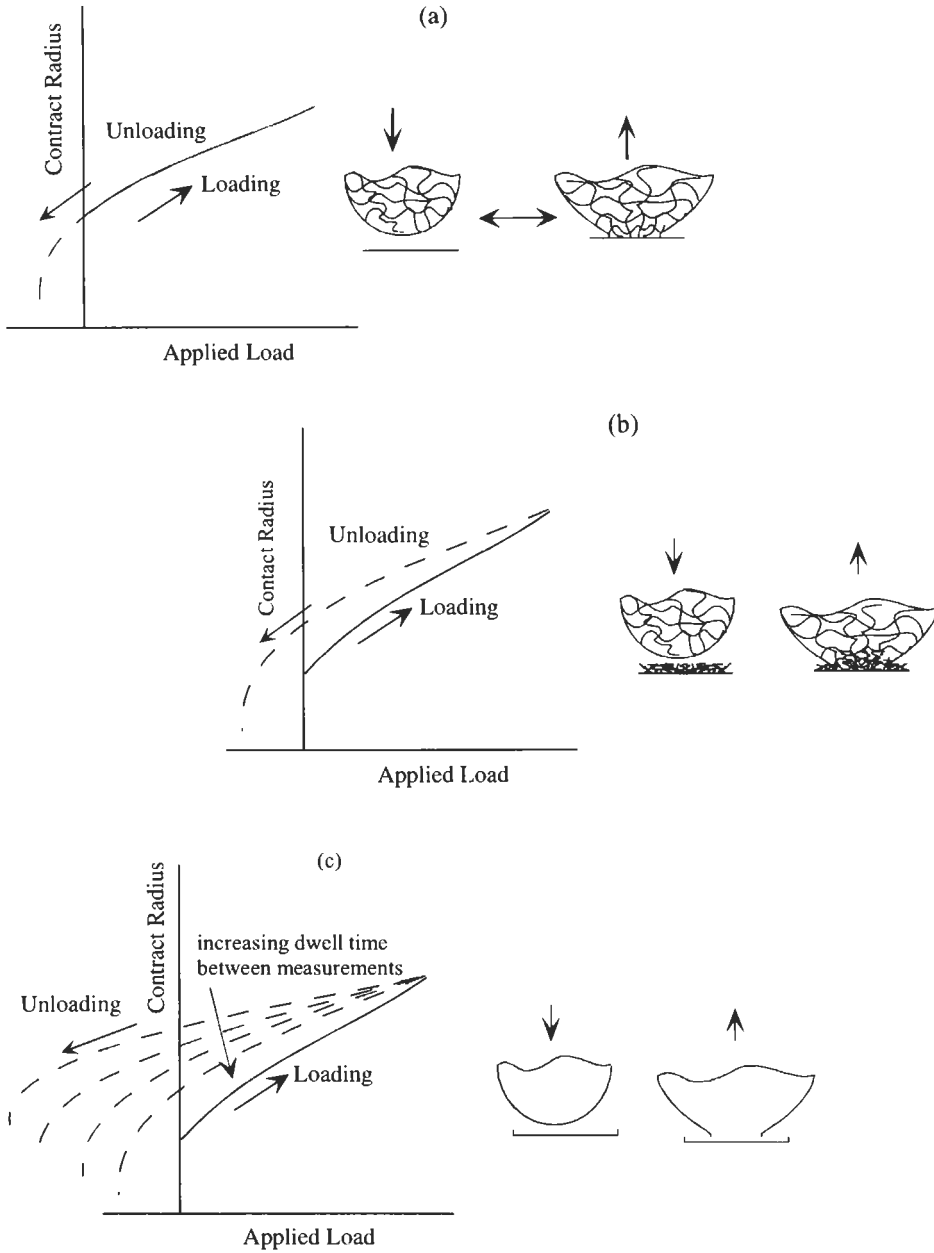
$$G = \frac{\left(P - \frac{a^3 K}{R}\right)^2}{6\pi K a^3} \quad (39)$$

However, in an *elastic system with interfaces in non-equilibrium* the a versus P data correspond to a non-equilibrium value of G which can be written as Eq. 39, except that $G \neq W$. In a typical experiment involving interfaces that change with time when in contact, as mentioned earlier, the a versus P data during *loading* will be different from the *unloading data*. In such a case, the value of W and K are determined from the loading data. Once the value of K is known, G may be calculated using Eq. 39. The difference between G and W signifies the extent of *contact adhesion hysteresis*. This approach has been adopted by Tirrell and coworkers [42–44], and Brown and coworkers [45,46] to study the effect of interfacial coupling agents on the adhesion of elastomers. These measurements are discussed in Section 4.3.

4. Contact-mechanics-based adhesion measurements

As mentioned earlier, the contact-mechanics-based experimental studies on interfacial adhesion primarily include:

- (1) direct measurements of surface and interfacial energies of polymers and self-assembled monolayers;
- (2) quantitative studies on the role of interfacial coupling agents in the adhesion of elastomers;
- (3) adhesion of microparticles on surfaces; and
- (4) adhesion of viscoelastic polymer particles.



In these studies, a variety of experimental tools have been employed by different researchers. These include the JKR apparatus and the SFA. Each one of these tools offers certain advantages over the others. These experimental tools are briefly described in the following section.

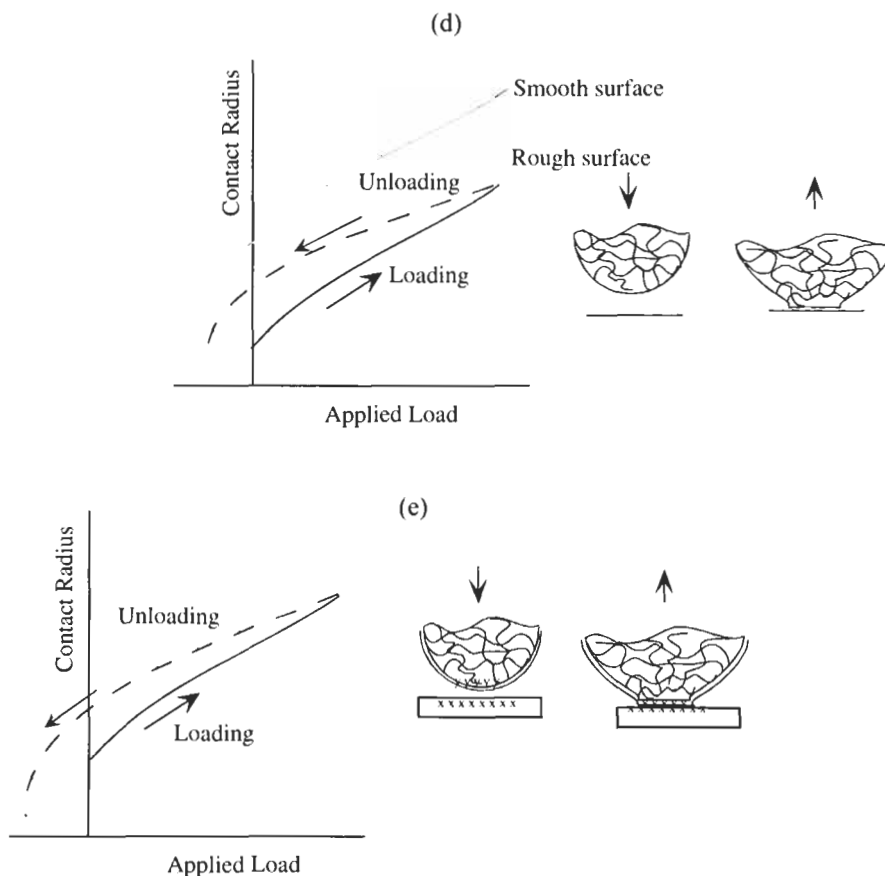


Fig. 6. Contact or adhesion hysteresis in a JKR type adhesion test. As a result of contact hysteresis, the contact radius during *unloading* is higher than that during the *loading* cycle. Hysteresis can be observed in different *nonequilibrium* or *dynamic* systems. Some of these systems are depicted above. In a *real* system, a combination of these factors can cause contact hysteresis. (a) An elastic JKR system with no hysteresis. The loading and unloading curves superimpose. (b) Contact hysteresis due to interfacial coupling agents or diffusion. (c) Contact hysteresis due to viscoelasticity. The extent of hysteresis depends on the viscous (loss) modulus of the material and dwell time between measurements. (d) Rough surfaces in contact: hysteresis due to asperity deformation. The local stresses can exceed the yield strength of the material and cause their plastic deformation. Also, note that the contact area in the case of rough surfaces in contact is lower than that in the case of smooth surfaces in contact. (e) Hysteresis due to rearrangement of interfaces upon contact. Interface rearrangement upon contact would occur in reactive systems or biological systems which adhere through specific interactions. The extent of hysteresis depends on contact time, stress and reactivity of the functional groups.

4.1. Experimental tools for the contact mechanics studies

4.1.1. JKR apparatus

In the JKR experiments, a macroscopic spherical cap of a soft, elastic material is in contact with a planar surface. In these experiments, the contact radius is measured as a function of the applied load (a versus P) using an optical microscope, and the interfacial adhesion (W) is determined using Eqs. 11 and 16. In their original work, Johnson et al. [6] measured a versus P between a rubber–rubber interface, and the interface between crosslinked silicone rubber sphere and poly(methyl methacrylate) flat. The apparatus used for these measurements was fairly simple. The contact radius was measured using a simple optical microscope. This type of measurement is particularly suitable for soft elastic materials.

The JKR apparatus at Minnesota, shown schematically in Fig. 7, was built by Deruelle [43]. Different variations of this type of apparatus have been employed by Brown and coworkers [45,46], Chaudhury and coworkers [47–50], Kramer and coworkers [51,52], Shull and coworkers, [53] Creton and coworkers [54], and Falsafi and coworkers [38]. The apparatus, shown in Fig. 7, consists of a rigid glass support mounted on a translating stage. A spherical cap of a soft material, for example crosslinked polyisoprene (PI) or PDMS, is adhered to the rigid glass support. The flat surface is usually made of a polymer film spin coated or otherwise deposited in a smooth layer on a silicon wafer. These layers need to be smooth with a rms roughness less than a few angstroms. The flat is mounted on a rigid support which is placed firmly on an analytical balance. The spherical

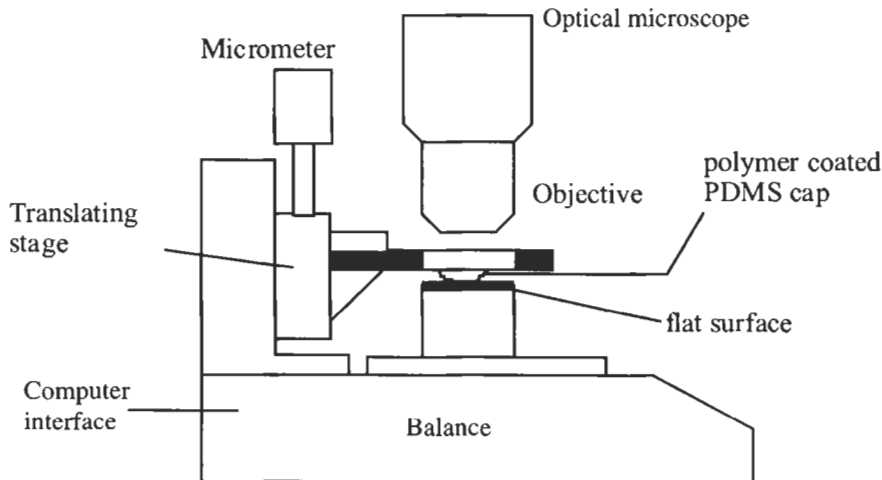


Fig. 7. Schematic of the apparatus used for JKR type adhesion measurements. For a constant applied displacement δ , the contact radius a and the load P are measured.

cap is brought into contact with the flat, and pressed against the flat. This amounts to performing the experiment under an imposed constant central displacement δ . The JKR experiments can be done under conditions of constant load, as in the SFA type instruments. Under an imposed δ , the load P and the contact radius a change, and reach their respective equilibrium values. The load is measured using the analytical balance and the contact radius is measured using the optical microscope. Using the measured values of a and P in Eq. 11 of the JKR theory, we can determine the work of adhesion between surfaces of the flat and the spherical cap. The primary advantage of this apparatus is its simplicity and ease of use. The JKR apparatus has been employed to measure the surface and interfacial energies (reviewed in Section 4.2) as well as to study the adhesion of elastomers in the presence of coupling agents (reviewed in Section 4.3).

In several studies on the adhesion of self-assembled monolayers, Chaudhury modified the surface of a crosslinked PDMS by corona-treatment following self-assembly of monolayers of varying chemistries. In a similar manner, Mangipudi et al. [55] coated thin film of high molecular weight polymer from a solvent on to the oxidized surface of a PDMS cap. These studies are discussed in Section 4.2.

4.1.2. Surface forces apparatus

The SFA, originally developed by Tabor and Winterton [56], and later modified by Israelachvili and coworkers [57,58], is ideally suited for measuring molecular level adhesion and deformations. The SFA, shown schematically in Fig. 8i,ii, has been used extensively to measure forces between a variety of surfaces. The SFA combines a Hookian mechanism for measuring force with an interferometer to measure the distance between surfaces. The experimental surfaces are in the form of thin transparent films, and are mounted on cylindrical glass lenses in the SFA using an appropriate adhesive. SFA has been traditionally employed to measure forces between modified mica surfaces. (For a summary of these measurements, see refs. [59,60].) In recent years, several researchers have developed techniques to measure forces between glassy and semicrystalline polymer films, [61–63] silica [64], and silver surfaces [65,66]. The details on the SFA experimental procedure, and the summary of the SFA measurements may be obtained elsewhere (see refs. [57,58], for example.).

Thin sheets of mica or polymer films, which are coated with silver on the back side, are adhered to two cylindrical quartz lenses using an adhesive. It may be noted that it is necessary to use an adhesive that deforms elastically. One of the lenses, with a polymer film adhered on it, is mounted on a weak cantilever spring, and the other is mounted on a rigid support. The axes of these lenses are aligned perpendicular to each other, and the geometry of two orthogonally crossed cylinders corresponds to a sphere on a flat surface. The back-silvered thin films form an optical interferometer which makes it possible

Mark II Surface Forces Apparatus

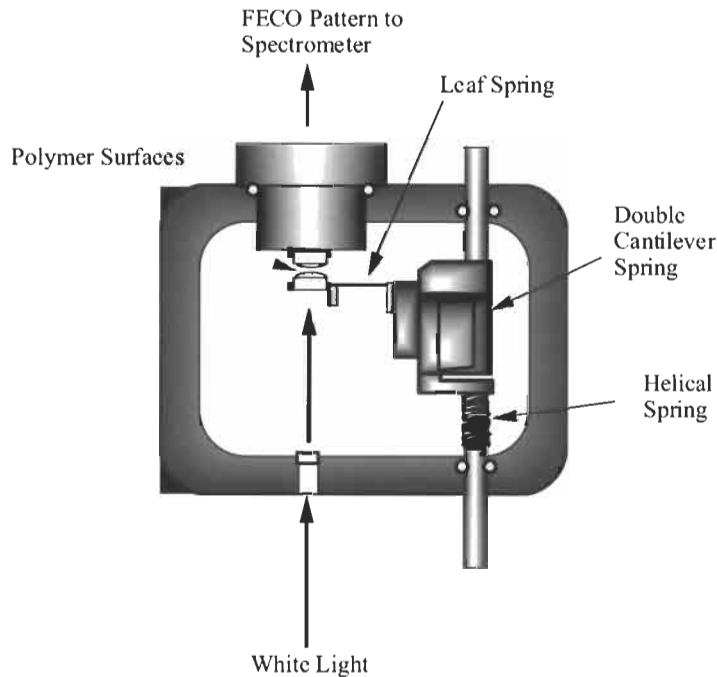


Fig. 8. (i) Surface forces apparatus (SFA). The force between the two surfaces is measured by measuring the deflection of the leaf spring on which one of the surfaces is mounted. The distance between the surfaces is determined by measuring the wavelengths of interference fringes.

to measure the profile of separation outside the contact area as well as the radius of curvature. Since the optical interferometer is an integral part of the SFA, it is necessary to generate thin, smooth and transparent film samples to be used in the SFA. In some of the recent work, Mangipudi et al. [63] prepared thin polymer film samples by coating them on molecularly smooth thin mica sheets. While this procedure made it possible to study the surface energetics of a variety of polymers, it resulted in a complicated 5-layer interferometry. The details of these measurements and the analysis of the associated interferometry may be found in the original papers [63,67]. Finally, the configuration of the samples in the SFA, as mentioned earlier, is of 'multilayer composites', and there is no reported direct analysis of the contact mechanics of these composites. However, the experiments of Horn and coworkers [68] established that the contact mechanics of these layered structures may be described using an *effective elastic modulus* for the composite. In their experiments on non-adhering solids, Horn et al. verified the applicability of the Hertz theory to layered structures. In all the subsequent studies, it has been implicitly assumed that an equivalent elastic modulus would adequately

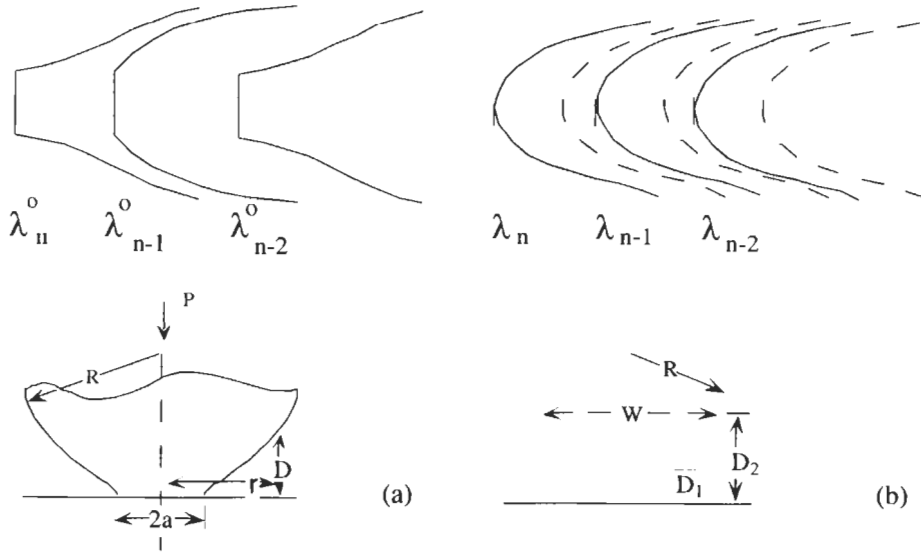


Fig. 8. (ii) Geometry and interferometry in the SFA. The distance between the surfaces is determined from the wavelengths of FECO. (a) The FECO fringes when the surfaces are in contact. The separation profile, D versus r , can be measured from the fringe profile, and compared to that predicted by the JKR theory of contact mechanics. (b) The FECO when the surfaces are separated. By measuring the wavelengths of the fringes when the surfaces are in contact and when they are separated, we can determine the distance between the two surfaces.

describe the contact mechanics of layered structures used in the SFA based contact mechanics studies. More recently, Sridhar et al. [32] used finite element methods to analyze the contact mechanics of layered structures. Using this analysis, Sridhar et al. developed a dimensionless parameter, *adhesion parameter*

$$\alpha = \left(\frac{2WR^2}{E_1 h_1^3} \right)^{1/2}$$

where E_1 and h_1 are the elastic modulus and thickness of the top layer, that characterizes the deviation from the JKR behavior due to layered-structure used in the SFA type experiments. This analysis indicates that the deviation from the JKR theory is significant at low values of α . For details of this analysis, the reader is referred to the original paper.

Israelachvili and coworkers [64,69], Tirrell and coworkers [61–63,70], and other researchers employed the SFA to measure molecular level adhesion and deformation of self-assembled monolayers and polymers. The pull-off force (P_s), and the contact radius (a versus P) are measured. The contact radius, the local radius of curvature, and the distance between the surfaces are measured using the optical interferometer in the SFA. The primary advantage of using the SFA is its ability to study the interfacial adhesion between thin films of relatively high

modulus materials. It should be noted that generating thin, smooth, and optically transparent films suitable for SFA studies has been a challenge in general. The details of these measurements are reviewed in Section 4.2.

4.2. Surface and interfacial energetics of polymers and self-assembled monolayers

As shown by Dupré's equations (Eqs. 1 and 2), the interfacial thermodynamic work of adhesion between two materials depends on the surface and interfacial energetics. The surface energy also determines the adsorption and wetting properties of a solid surface. In the case of a liquid material, it is a rather simple exercise to measure its surface tension. However, measurement of surface energy of a solid has been a non-trivial exercise due the lack of suitable experimental tools. Traditionally, it has been attempted to predict the surface energy of a solid using indirect or extrapolation methods such as wetting (contact angle) measurements, melt surface tension data extrapolation, and so on. A detailed summary of these indirect methods may be found in refs. [8,71]. The fundamentals of the wetting measurements are summarized below.

The phenomenon of wetting of a solid by a liquid depends on the surfaces and interfacial energies. When a liquid droplet is in contact with an ideally smooth solid surface, as shown schematically in Fig. 9, according to the Young's equation [72], the contact angle (θ) of the liquid is given by

$$\gamma_{LV} \cos \theta = \gamma_{SV} - \gamma_{SL} \quad (40)$$

where S, L, V denote the solid, liquid, vapor phases, and γ_{SV} , γ_{LV} , γ_{SL} are the interfacial energies.

The solid–liquid interfacial energy is related to the solid surface energy through

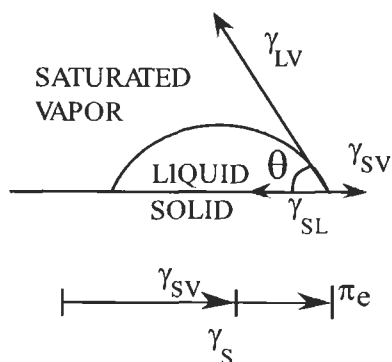


Fig. 9. Schematic of contact angle of a liquid on a solid. By balancing components of interfacial free energies in the horizontal direction, we can obtain the Young's equation.

the following equation:

$$\gamma_{SL} = \gamma_S - \pi_e \quad (41)$$

where π_e is the spreading pressure. Using Eq. 41 in Eq. 40, we get

$$\gamma_{LV} \cos \theta = \gamma_S - \gamma_{SL} - \pi_e \quad (42)$$

Though the above equation looks very simple, it cannot be used readily for determining the solid surface energy from the contact angle data as the solid–liquid interfacial energy (γ_{SL}) may not be known a priori. Further, the surface energy γ_S and the solid–vapor interfacial energy γ_{SV} are not necessarily equal. Over the years, a number of models have been developed to predict the surface energy of a solid from contact angle data. A summary of these models is given in Table 1. It has been argued by several researchers that the solid surface energy estimated from the contact angle data may not be accurate. This is because some of the models used for estimating the surface energy of a solid from the contact angle data do not account for the specific interactions occurring between the solid surface and the probe liquid. Some models, on the other hand, do not distinguish the differences in the interactions of different probe liquids with a given solid. A detailed discussion of these issues can be found elsewhere (see refs. [63,70,86,87], for details.). However, it should be emphasized that the contact angle methods are ideally suited for determining the wetting properties of a surface.

Given the importance of surface and interfacial energies in determining the interfacial adhesion between materials, and the unreliability of the contact angle methods to predict the surface energetics of solids, it has become necessary to develop a new class of theoretical and experimental tools to measure the surface and interfacial energetics of solids. This new class of methods is based on the recent developments in the theories of contact mechanics, particularly the JKR theory.

Johnson and coworkers [6], in their original paper on the JKR theory, reported the measurements of surface energies and interfacial adhesion of soft elastomeric materials. Israelachvili and coworkers [68,69], and Tirrell and coworkers [62, 63,70,88–90] used the SFA to measure the surface energies of self-assembled monolayers and polymer films, respectively. Chaudhury and coworkers [47–50] adapted the JKR technique to measure the surface energies and interfacial adhesion between self-assembled monolayers. More recently, Mangipudi and coworkers [55] modified the JKR technique to measure the surface energies of glassy polymers. All these measurements are reviewed in this section.

4.2.1. Measurements of surface and interfacial energies: JKR apparatus

4.2.1.1. JKR-type measurements on soft elastomers. In their original paper, Johnson and coworkers [6] reported on adhesion measurements between soft materials.

Table 1

Summary of methods for estimating surface energy from the contact angle data

Method	Estimated surface energy	Remarks	Ref.
Zisman's plot	$\cos \theta$ varies linearly with γ_v ; $\gamma_{\text{Zisman}}^c = \gamma_c = \lim_{\theta \rightarrow 0} \gamma_v$	Predicts critical surface tension; linearity does not hold universally; γ_c depends on probe liquids.	[73–76]
Good–Girifalco–Fowkes (GGF) equation	Using $\gamma_{\text{sl}} = \gamma_{\text{sv}} + \gamma_v - 2\phi(\gamma_{\text{sv}}\gamma_v)^{0.5}$ in Young's equation leads to $\frac{1 + \cos \theta}{2} = \left(\frac{\gamma_{\text{sv}}}{\gamma_v}\right)^{0.5}$; γ_{GGF}^c is obtained from a plot $\cos \theta$ versus $\gamma_v^{-0.5}$. ϕ is solid–liquid interaction parameter; $\phi = 1$ if the interactions are purely dispersive.	Based on Berthelot relation for attractive constants; valid only when the solid–liquid interactions are dominantly dispersive.	[77–82]
Wu's equation of state	A series expansion of GGF equation: $\gamma_{c,\phi} = \phi^2 \gamma_s - \pi_c = \frac{(1 + \cos \theta)^2 \gamma_v}{4}$; γ_{Wu}^c is the maximum of the plot of $\gamma_{c,\phi}$ versus γ_v	Accounts for solid liquid interactions, though qualitatively.	[83]
Geometric mean approximation	Dispersive and polar components of solid surface energy are found by solving $\gamma_v(1 + \cos \theta) = 2(\gamma_s^d \gamma_v^d)^{0.5} + 2(\gamma_s^p \gamma_v^p)^{0.5}$	An extension of GGF equation; γ_{sa} predicted is significantly higher than the critical surface tension.	[84]
Harmonic mean approximation	Dispersive and polar components of solid surface energy are found by solving $\gamma_v(1 + \cos \theta) = 4 \frac{\gamma_s^d \gamma_v^d}{\gamma_s^d + \gamma_v^d} + 4 \frac{\gamma_s^p \gamma_v^p}{\gamma_s^p + \gamma_v^p}$	Similar to geometric mean approximation.	[85]

The work of adhesion was determined from the a versus P measurements (see Eq. 11). The work of adhesion between two rubber spheres was found to be 71 ± 4 mJ/m². The work of adhesion reduced to 6.8 ± 0.4 mJ/m² in the presence of 0.01 M solution of dodecyl sulfate. Using these measurements of adhesion between rubber in air and a surfactant solution, Johnson et al. [6] provided the first direct experimental verification of the Young's equation (Eq. 40). They also measured

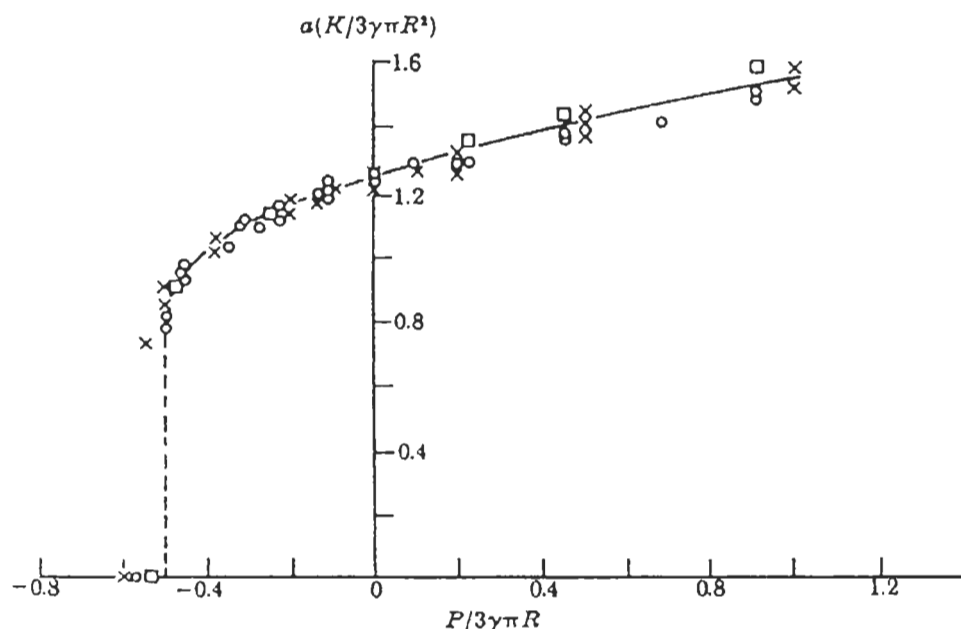


Fig. 10. Normalized contact radius as a function of normalized load for gelatin spheres in contact with poly(methyl methacrylate). Shown here are some of the early data obtained using the JKR method by Johnson and coworkers. (Reproduced with permission from ref. [6].)

the work of adhesion between poly(methyl methacrylate) and gelatin. Based on the data shown in Fig. 10 the work of adhesion between poly(methyl methacrylate) (PMMA) and gelatin was found to be $105 \pm 10 \text{ mJ/m}^2$. In these experiments, Johnson and coworkers [6] verified Eqs. 11 and 16 of the JKR theory.

In an attempt to determine the applicability of JKR and DMT theories, Lee [91] measured the no-load contact radius of crosslinked silicone rubber spheres in contact with a glass slide as a function of their radii of curvature (R) and elastic moduli (K). In these experiments, Lee found that a thin layer of silicone gel transferred onto the glass slide. From a plot of $a_0^3 K$ versus R^2 , using Eq. 13 of the JKR theory, Lee determined that the work of adhesion was about $70 \pm 7 \text{ mJ/m}^2$, a value in close agreement with that determined by Johnson and coworkers [6] using Eqs. 11 and 16.

4.2.1.2. JKR type measurements on monolayers deposited on soft elastomers.

The recent interest in the JKR experiments has been stimulated by the work of Chaudhury and coworkers [47–50]. In a 1991 paper, Chaudhury and Whitesides [47] reported their extensive studies on the measurement of interfacial work of adhesion and surface energies of elastomeric solids. The motivation for this work was to study the physico-organic chemistry of solid surfaces and interfaces.

The primary objective of this work was to correlate the surface thermodynamic parameters obtained from the contact mechanics measurements with the constitutive properties of the interfaces and the chemistry of the solid surfaces. To this end, Chaudhury and Whitesides prepared crosslinked poly(dimethyl siloxane) elastomeric spherical caps and flat sheets, and chemically modified surfaces of these caps and sheets using self-assembled organic monolayers. Using the unmodified PDMS surfaces, Chaudhury and Whitesides verified Eqs. 11, 13 and 16 of the JKR theory, and found that the surface energy of PDMS is about 22 ± 1 mJ/m². These data are shown in Fig. 11a. This value is in agreement with the value calculated from the contact angle data. Using the JKR technique, Chaudhury and Whitesides also found that the work of adhesion between two PDMS surfaces immersed in a mixture of water and methanol decreases as the concentration of methanol increases. These measurements provided yet another direct proof of Young's equation (Eq. 40). For details, see the original paper [47]. Chaudhury and Whitesides also studied the adhesion behavior of modified PDMS surfaces which included oxidized PDMS, and PDMS modified with alkyl siloxane and fluoroalkyl siloxane monolayers. Adhesion or contact hysteresis was observed in all cases. As shown in Fig. 11b,c, the degree of hysteresis in the case of fluoroalkyl siloxane was significantly higher than that in the case of alkyl siloxane. The origin of the contact hysteresis was not clearly understood. One of the important revelations of this work was that, for the systems studied, the works of adhesion between the surfaces obtained from the *loading data* were comparable to the prediction based on advancing contact angles. The work adhesion obtained from the *unloading data* showed little or no correlation with the values predicted from either advancing or receding contact angles.

In a separate study using the JKR technique, Chaudhury and Owen [48,49] attempted to understand the correlation between the *contact adhesion hysteresis* and the phase state of the monolayers films. In these studies, Chaudhury and Owen prepared self-assembled layers of hydrolyzed hexadecyltrichlorosilane (HTS) on oxidized PDMS surfaces at varying degrees of coverage by vapor phase adsorption. The phase state of the monolayers changes from crystalline (solid-like) to amorphous (liquid-like) as the surface coverage (ϕ_s) decreases. It was found that contact adhesion hysteresis was the highest for the most closely packed

Fig. 11. a^3 versus P data and contact hysteresis reported by Chaudhury and Whitesides [47]. (a) The data for unmodified PDMS–PDMS contacts. No contact hysteresis was observed. (b) The data for and PDMS modified with alkyl siloxane monolayers, PDMS^{ox}–O₃Si(CH₂)₉CH₃. A weak contact hysteresis was observed. (c) The data for PDMS modified with fluoroalkyl siloxane monolayers, PDMS^{ox}–O₃Si(CH₂)₂(CF₂)₇CF₃. A large contact hysteresis was observed. In all cases, the open circles represent the *loading data*, and the filled circles represent the *unloading data*.

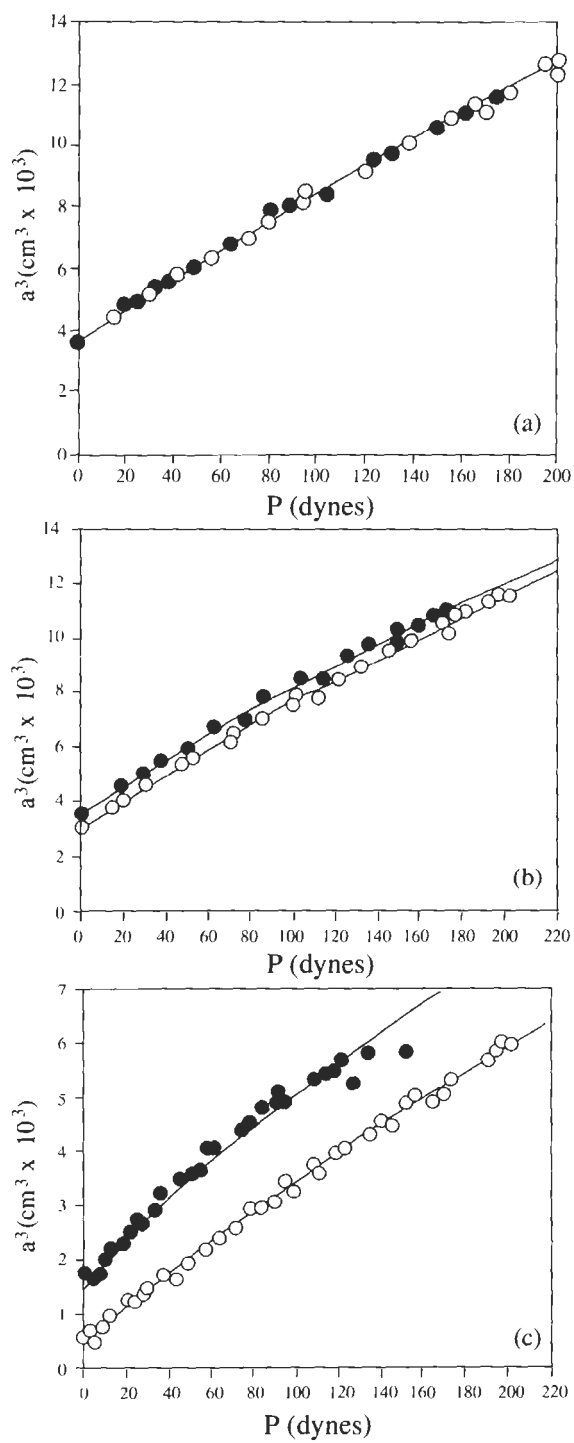


Table 2

Effect of phase state of monolayers of hexadecylsiloxane supported on oxidized PDMS–hysteresis in interfacial energetics as determined by contact mechanics and contact angles

Fractional coverage (%)	Phase state	γ_{sv} by JKR method (mJ/m ²)			Contact angle hysteresis (mJ/m ²)	
		Loading data	Unloading data	Hysteresis, $\Delta\gamma_{JKR}$	ΔW_{water}	$\Delta W_{hexadecane}$
100	solid-like	16.2	24.8	8.6	20	0
80	solid/liquid	21.5	27.6	6.1	18	0
70	liquid	23.3	23.5	0.2	8	0
60	liquid	27	28.3	1.3	12	0
40	liquid	28.5	32.8	4.3	20	0

Data reproduced from ref. [49].

monolayers ($\phi_s \rightarrow 100\%$). The contact adhesion hysteresis seemed to correspond to the contact angle hysteresis when a polar liquid (water) was used. However, no contact angle hysteresis was observed when a non-polar liquid (hexadecane) was used on these surfaces. The results of these studies are shown in Table 2. Interestingly, the *contact adhesion hysteresis* as well as the water *contact angle hysteresis* exhibited a ‘minimum’ at an intermediate coverage of 70%. The authors did not comment on this. The authors attributed the hysteresis in the case of compact monolayers to line defects and point defects formed during the vapor phase adsorption of the monolayers. These defects may act to pin the contact line and deform about the defect sites, causing the adhesion hysteresis. According to the authors, the liquid like monolayers (for $\phi_s < 70\%$) can relax rapidly and thus exhibit no appreciable adhesion. The authors ruled out stress-induced rearrangement or interdigitation as a possible cause of hysteresis in these systems. It should be pointed out that the exact origins of the contact adhesion hysteresis are not well understood.

In his continued studies on surface energetics of self-assembled monolayers, Chaudhury [50] employed contact mechanics (JKR technique) to measure the surface energetics of a variety of surfaces. These monolayers were terminated with $-\text{CF}_3$, $-\text{CH}_3$, $-\text{OCH}_3$, $-\text{COOCH}_3$ and $-\text{Br}$ groups. These surfaces are either dispersive or polar non-associative in nature. The results of the contact mechanics studies were compared to the values of surface energies predicted from contact angle data obtained using water and methylene iodide. The contact angle data were analyzed using the geometric and harmonic mean methods developed by Wu [84,85]. (Also see Table 1.) These data are shown Table 3. For dispersive surfaces ($-\text{CF}_3$ and $-\text{CH}_3$ terminated monolayers), the surface energies obtained from the JKR experiments agreed well with the predictions of the contact angle data. However, in the case of polar non-associative surfaces ($-\text{OCH}_3$, $-\text{COOCH}_3$,

Table 3

Surface energies of different end-functionalized trichlorosilane monolayers self-assembled on oxidized PDMS:

A comparison of contact mechanics and contact angle data

Functional group	γ_{sv}^{JKR}	Contact angle data					
		Geometric mean method			Harmonic mean method		
		$\gamma_{sv}^{dispersive}$	γ_{sv}^{polar}	γ_{sv}^{total}	$\gamma_{sv}^{dispersive}$	γ_{sv}^{polar}	γ_{sv}^{total}
-CF ₃	16.0	15.0	0.8	15.8	15.2	3.6	18.8
-CH ₃	20.8	20.6	0.1	20.7	23.5	0.4	23.9
-OCH ₃	26.8	30.8	6.4	37.2	32.2	10.9	43.1
-CO ₂ CH ₃	33.0	36.0	6.4	42.4	36.7	11.5	48.2
-Br	36.8	37.9	1.7	39.6	38.4	5.6	44.1

and -Br terminated monolayers) the values of surface energies obtained from the JKR measurements were significantly less than the values obtained from the contact angle data. Interestingly, for the above-mentioned polar non-associative surfaces the JKR surface energy values were found to be in rough agreement with the dispersive component of the surface energies obtained from the contact angle data. To explain this, Chaudhury, arguing that the adsorbed monolayers were in a 'liquid-like' state, suggested that the head-group regions of the monolayers were sufficiently disordered. He further suggested that the contribution of the electrostatic interactions to the total surface energy of the monolayers was not significant. Chaudhury also suggested that the above surfaces were polar non-associative, that no H-bonds were formed between these surfaces, and that the energy of cohesion is given by the dispersion forces alone. While this may be so for the disordered 'liquid-like' monolayers in question, if in fact they are disordered, it may not be true with polar surfaces of polymers in which the orientation of the repeat units are more ordered. This issue needs to be examined more thoroughly and systematically. Using the JKR technique, Haidara et al. [92] studied the adsorption of surfactants at the solid-state interface by virtue of surface-induced debonding. Their observations showed that the adsorption of surfactant at solid-liquid interface is slower compared to air-liquid interface.

4.2.1.3. JKR type measurements on glassy polymers. The difference between the JKR contact mechanics and the Hertzian contact mechanics becomes apparent only when the deformation induced by interfacial forces is significant and detectable. Polymers, in general, are low surface energy materials, with their surface energies ranging from 20 to 60 mJ/m². For the surface and interfacial forces to cause significant deformations in the adhering bodies, the materials need to be relatively soft. It has been demonstrated that a material with a bulk modulus of about

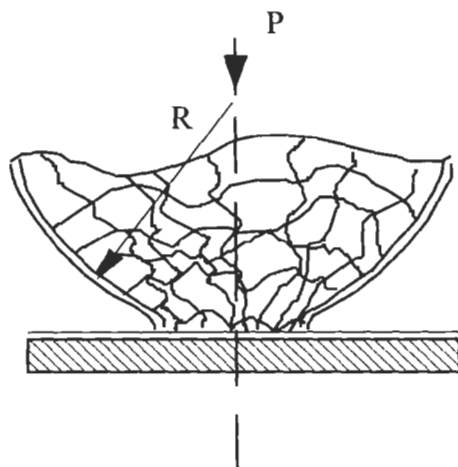


Fig. 12. Schematic of a polymer-coated crosslinked PDMS cap in contact with a polymer-coated flat surface. The PDMS cap is oxidized in O_2 -plasma, and the polymer layer is coated by solvent casting. On flat surface, the polymer layer is spin coated.

10^6 Pa, would deform appreciably under the action of loads comparable to the pull-off force given by Eq. 16. It is for this reason that the JKR type measurements are usually done on soft elastic materials such as crosslinked PI rubber [45,46] or crosslinked PDMS [42–44,47–50]. However glassy polymers such as polystyrene (PS) and PMMA are relatively hard, with bulk moduli of the order of 10^9 Pa. It can be seen from Eq. 11 that a varies as $K^{-1/3}$. Thus, increasing K a factor of 10^3 decreases the contact radius by a factor of 10. For higher values of K , the contact radius a under low applied loads will be very small. It becomes difficult to measure the contact radius using an optical microscope. To get around this limitation, Mangipudi et al. [55,63] developed a novel scheme for the preparation of polymer samples for JKR type adhesion measurements.

To generate samples of glassy polymers for the JKR type experiments, Mangipudi et al. [55,63] coated a thin layer of a polymer on the oxidized surface a spherical cap made of crosslinked PDMS. PDMS caps of 0.1 cm radius of curvature were prepared using a method reported in the literature [42–44,47–50]. The surface energy of a PDMS cap was modified by exposing it to an O_2 -plasma, and thereby increasing its surface energy. The polymer of interest was solvent-cast on the modified PDMS surface. This resulted in a composite which is shown schematically in Fig. 12. The surface of such a composite described above is made of the polymer of our interest and its bulk is soft crosslinked PDMS. Since the polymer layer is relatively thin (thickness ~ 0.1 μm) the effective modulus of the composite is close to that of crosslinked PDMS. The adhesion induced deformation is appreciable, and the radius of the deformed contact zone can be measured using a simple optical microscope.

From the measurements of a versus P , Mangipudi et al. determined the surface energy of the polymers and the bulk modulus of the composite material. The data for PS–PS and PMMA–PMMA contacts are shown in Fig. 13. Shown in Fig. 13a and b are the data for PS–PS contact (PS coated PDMS cap in contact with a PS coated wafer) and PMMA–PMMA contact, respectively. It should be noted that for PS–PS contact as well as PMMA–PMMA contact there is significant contact hysteresis. The loading and the unloading data can be fitted to the JKR models with the same value of bulk modulus, but a different value of surface energy (or work of adhesion). From the receding data, Mangipudi et al. found that the surface energy of PS is about 45 mJ/m^2 . From the advancing data, a value of about 41 mJ/m^2 was found. Similarly, for PMMA, Mangipudi et al. found that the surface energy obtained from the receding data is about $52 \pm 1 \text{ mJ/m}^2$. The value obtained from the advancing data is about $47 \pm 1 \text{ mJ/m}^2$. It may be pointed out that the values of surface energies of PS and PMMA, obtained from the unloading curves, agree well with the values obtained from the SFA measurements. This clearly indicates that the surface energy of solid polymers can be measured accurately in a contact mechanics experiment, and that the JKR type experiments provide an effective alternative to the SFA measurements. Mangipudi et al. also measured the adhesion between PDMS and PS as well as PDMS and PMMA. The a versus P data were fit to the JKR models. These data are shown in Fig. 14. As can be seen from Fig. 14a,b, there is no significant adhesion hysteresis, i.e. there is no difference in the contact radius at a given load obtained during loading and unloading. As can be seen from the data shown in Fig. 14, the work of adhesion between PDMS and PS is about $49 \pm 3 \text{ mJ/m}^2$. Similarly, Mangipudi et al. found that the work of adhesion between PDMS and PMMA is about $57 \pm 1 \text{ mJ/m}^2$.

4.2.2. Measurements of surface and interfacial energies: surface forces apparatus

SFA has been traditionally used to measure the forces between modified mica surfaces. Before the JKR theory was developed, Israelachvili and Tabor [57] measured the *force versus distance* (F vs. d) profile and pull-off force (P_s) between steric acid monolayers assembled on mica surfaces. The authors calculated the surface energy of these monolayers from the Hamaker constant determined from the F versus d data. In a later paper on the measurement of forces between surfaces immersed in a variety of electrolytic solutions, Israelachvili [93] reported that the interfacial energies in aqueous electrolytes varies over a wide range (0.01 – 10 mJ/m^2). In this work Israelachvili found that the adhesion energies depended on pH, type of cation, and the crystallographic orientation of mica.

4.2.2.1. SFA measurements on mica. Horn et al. [68] studied the deformation of mica surfaces in contact. In these studies, Horn et al. established the applicability of Hertz theory of contact mechanics to non-adhering layered solids by measuring

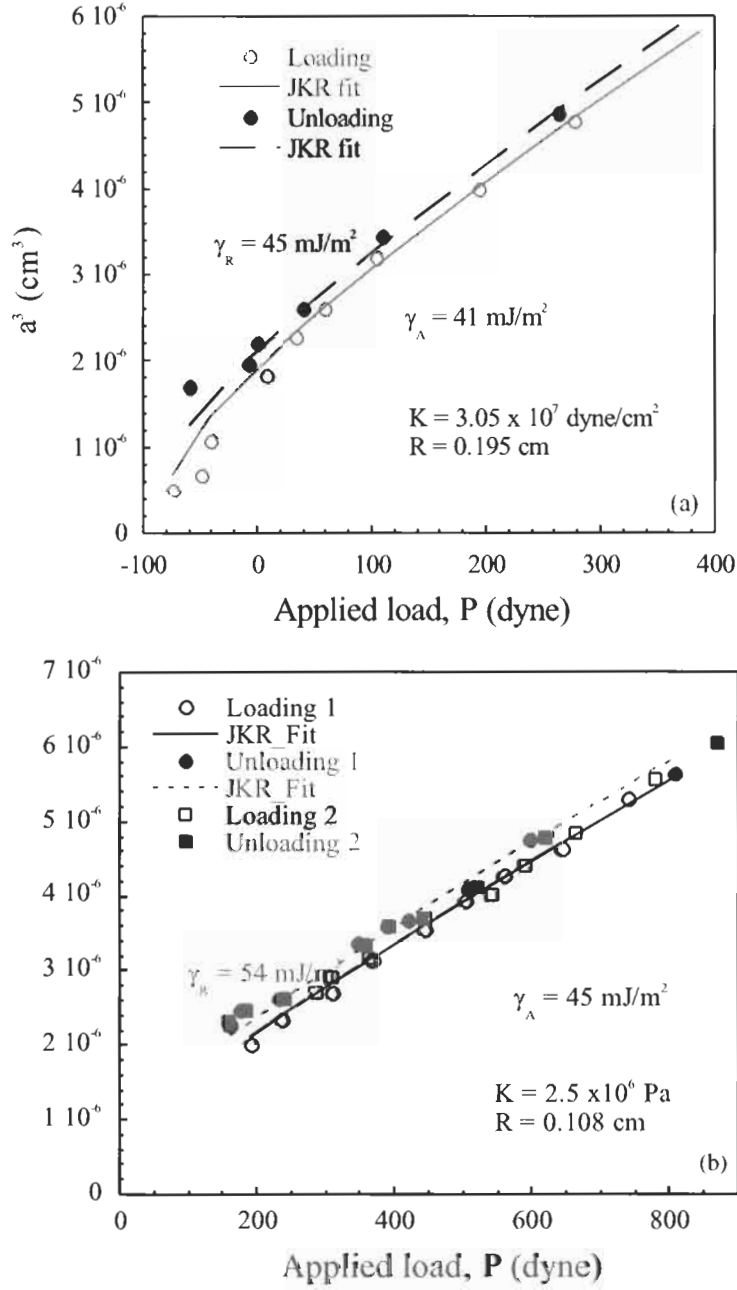


Fig. 13. Measurement of surface energies of PS and PMMA. It can be seen that there was a finite adhesion hysteresis. At a given load, the contact radius during loading was less than the contact radius during unloading. From the unloading data, we get $\gamma_{PS} = 45 \pm 1 \text{ mJ/m}^2$, and $\gamma_{PMMA} = 53 \pm 1 \text{ mJ/m}^2$. These number are in good agreement with the values of surface energies determined from the pull-off force measured using the SFA.

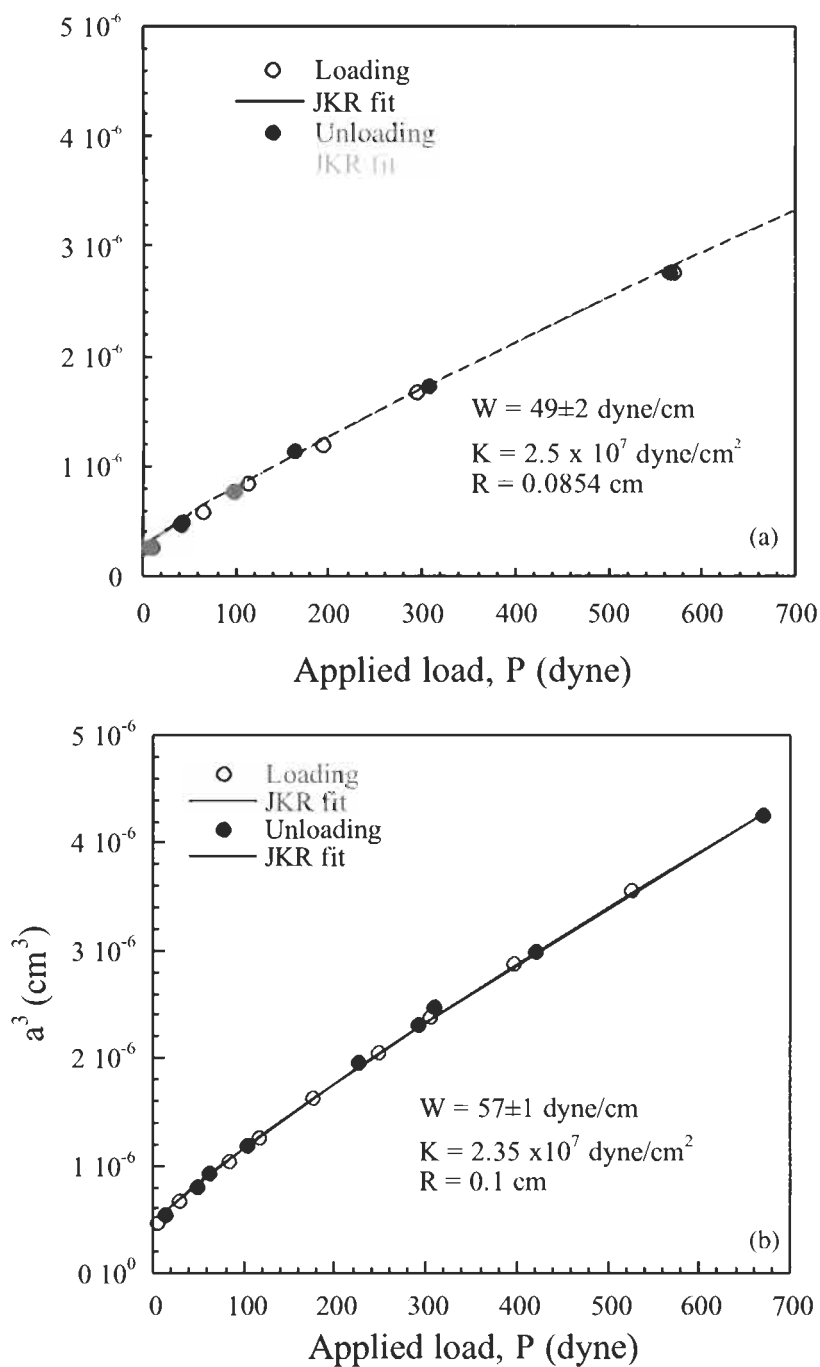


Fig. 14. Measurement of adhesion between PDMS and PS, and PDMS and PMMA. It can be seen that there was no adhesion hysteresis. The contact radius at a given load, during loading and unloading was the same. From these data, we get $W_{\text{PDMS-PS}} = 49 \pm 3$ mJ/m², and $W_{\text{PDMS-PMMA}} = 57 \pm 1$ mJ/m².

the interactions between mica in a potassium chloride solution. In their studies on adhesion between mica in dry air, Horn et al. measured the surface energy of mica. The measured value ($54\text{--}80\text{ mJ/m}^2$) was in rough agreement with the value ($\sim 120\text{ mJ/m}^2$) reported by Bailey and Kay [94]. The separation profile (D versus x , see Eq. 14) outside the contact zone, measured from the fringes of equal chromatic order (FECO), was in agreement with the JKR prediction. The measured contact radius was higher than the JKR prediction, and contact adhesion hysteresis was observed. The authors attributed the hysteresis to the plastic deformation of glue under large stresses in the contact region, and concluded that this inelastic behavior prevented accurate comparison to the JKR theory.

4.2.2.2. SFA measurements on monolayers deposited on mica. Chen and coworkers [69] studied the molecular mechanism associated with contact adhesion and contact angle hysteresis of monolayers adsorbed on mica surfaces. The monolayer was adsorbed on mica either by self-assembly or by the Langmir–Blodgett technique. The phase states of these monolayers were varied systematically. The monolayers studied in this work include: crystalline layers of phospholipids, amorphous solid layers of surfactants; and liquid-like layers of surfactants. In these experiments, Chen et al. found that no contact adhesion hysteresis occurred when the contact was between *crystalline–crystalline* or *crystalline–amorphous* layers. However, significant adhesion hysteresis was observed for *amorphous–amorphous* and *liquid–liquid* contacts. In the case of the amorphous solid, and liquid-like monolayers, the pull-off force increased with time in contact. The extent of increase in pull-off force was about 35% in about 10 min for *amorphous–amorphous* contacts. The rate of increase of pull-off force with time, dP_s/dt_c , decreased with increase in temperature. The rate of increase in pull-off was rather low for *liquid–liquid* like interfaces, and *crystalline–crystalline* contacts. This behavior was attributed to ease of relaxation and interdigitation of the monolayers. The hysteresis disappeared when the monolayers were exposed to vapors of dodecane. This behavior was due to capillary condensation of the hydrocarbon vapors. Based on these studies, Chen et al. concluded that the hysteresis in the above monolayers was associated with chemical non-equilibrium effects associated with approach and separation. The authors argued that chemical non-equilibrium occurred when the surface groups on separation were differently positioned or oriented from those on approach.

According to the authors, hysteresis increases with:

- (1) the ability of the molecular groups at the surface to reorient or interdiffuse across the contact interface which is often determined by the phase state of the surface molecules;
- (2) the time of contact and the magnitude of the externally applied stresses during the dwell time;
- (3) the rate of approach and separation of the surfaces.

Some of these findings are in agreement with the observation of Chaudhury and Whitesides [47]. In an extension of these studies, Tirrell and coworkers [62,63,70,88–90] studied the contact mechanics of polymer surfaces using the SFA.

Ruths and Granick [95] have studied the self-adhesion of several monolayers and adsorbed polymers onto mica. For loose-packed monolayers, the adhesion, in excess of a constant value observed at low rate, increased as a power law with the square root of the separation rate. In the case of adsorbed diblocks, the excess adhesion increased linearly with logarithmic separation rate. The time effects were ascribed to interdigitation and interdiffusion between the contacting layers.

SFA is also used to study the role of sub-boundary lubricants on the deformation and adhesion between rough surfaces. In a series of experiments by Quon et al. [96], different self-assembled monolayers adsorbed onto rough gold were brought into contact with atomically smooth mica. By measuring the deformation-load profiles and pull-off forces, the effect of self-assembled monolayers were assessed. The coated gold showed lower amount of deformation under equal load compared to the uncoated gold. The microdeformation of the coated gold was reversible upon unloading the system. The compressibility of each self-assembled monolayer was estimated using this elastic regime.

4.2.2.3. SFA measurements on polymer films. As mentioned earlier in this section, direct measurement of surface energies of polymers is non-trivial exercise. There are certain disadvantages associated with the interpretation of indirect measurements such as contact angles. Over the years, Tirrell and coworkers [62,63,70,88–90] developed a series of new techniques, based on contact mechanics, to measure the surface and interfacial energies of a variety of polymers. In 1991, Thakkar et al. [61] generated thin films of biaxially stretched poly(ethylene terephthalate) (PET), and measured its surface energy using the SFA. The surface energy was determined from the pull-off force measurements per Eq. 16 of the JKR theory. The value of the surface energy obtained from the SFA measurements was about 60 mJ/m^2 , and this value was significantly higher than the Zisman's critical wetting tension ($\sim 43 \text{ mJ/m}^2$). Thakkar et al. found that the separation profile outside the contact zone (D versus x) is in rough agreement with the prediction of the JKR theory. Thakkar et al. also measured the effect of vapor phase fluorination of PET, and found that the surface energy decreased due to fluorination. The contact angle measurements did not reveal the same. Mangipudi et al. [63,70,88–90] extended these measurements to a variety of polymers. Watanabe et al. [97] studied the adhesion of thin, dry block copolymeric layers adsorbed on mica. They found that the rubbery PI blocks in the dried layers (which were in entropically unfavorable flattened conformations) upon self-contact could interpenetrate each other and increase their conformational entropy. This entropy gain was considered to be responsible for the extra adhesion compared to the contact of adsorbed layers in solvent.

Mangipudi et al. [88–90] in their detailed studies, demonstrated that the *normalized pull-off energy* for PET–PET contact, given by $P_n = P_s/R$, was independent of the rate of crack propagation. P_n was independent of the contact time if an elastomeric hot melt adhesive was used to adhere the PET film to the lenses in the SFA. When a pressure-sensitive adhesive was used, due to its viscoelastic response, the *contact radius* as well as the *pull-off force* increased with contact time. In this work, it was further demonstrated that P_n was independent of the thickness of PET films. Based on these observations, the authors concluded that the SFA measurements on PET were free from dissipative effects. The separation profile outside the contact zone, measured under various loads, agreed well with the JKR profile. The surface energy was determined from the *pull-off force* measurements using Eq. 16 of the JKR theory. Their measurements on PET films agreed with those of Thakkar et al. Mangipudi et al. [88–90] also measured the surface energy of semicrystalline extruded films of polyethylene (PE). In these measurements, it was demonstrated that P_n was independent of the rate of separation. When the surfaces remained in contact over a period of time P_n did not change for shorter times of contact. After about 5 min or so in contact, P_n increased with contact time. The authors argued that the amorphous domains of PE at room temperature, being well above their T_g , would be mobile, and this mobility would lead to interdiffusion of the chains across the interface. The authors used the *pull-off force* measured within a short time (less than 4 min) after contact to determine the surface energy of PE. The value obtained from the SFA measurements ($\sim 33 \text{ mJ/m}^2$) was in good agreement with the value obtained from the Zisman's plot or Good–Girifalco–Fowkes' equation (see Table 1). The primary conclusion of this work was that in the case of PE the SFA measurements agreed with the contact angle measurements, while no such agreement was seen in the case of PET. The authors concluded that this was due to the difference in the nature of specific interactions between PET–PET compared to the PET–probe liquid interactions. In the case of PE, the dispersive interactions between PE and the probe liquid are similar to those between PE and PE surfaces.

In an extension of this work, Mangipudi et al. [89] studied the effect of corona treatment on the surface energetics of PE. As the treatment intensity increased, the surface oxygen concentration increased to about 14–17%. The surface energy of PE increased from 33 to about 58 mJ/m^2 as the surface oxygen concentration increased to about 14%. Once again, these measurements were compared to the values estimated from the contact angle data. In the case of untreated PE, as mentioned above, the SFA and the contact angle measurements were in good agreement. However, the SFA measured surface energies of the corona treated PE samples were significantly higher than the values obtained from the contact angle data. Further, the authors demonstrated that the surface energy predicted from the contact angle data varied depending on the polarity of the probe liquid as well as the method used to analyze the contact angle data. (These different

schemes are listed in Table 1.) The authors attributed this to the variation in the predictions of different methods available to analyze the contact angle data and to the assumptions associated with these methods. To better understand this aspect, Mangipudi et al. [90] measured the adhesion between a variety of polymers with well-controlled backbone chemistry. These polymers include: poly(4-methyl 1-pentene) (TPX), poly(vinyl cyclohexane) (PVCH), PS, PMMA, and poly(2-vinyl pyridine) (PVP). It may be noted that, among the polymers listed above, TPX and PVCH are purely dispersive in nature. PS is predominantly dispersive with some dipole-induced dipole interactions. In the case of PMMA and PVP, just as in the case of PET and corona treated PE surfaces, the non-dispersive interactions are dominant. These polymers essentially form a set with increasing degrees of polar interactions. The values of surface energies of these polymers obtained from the SFA measurements are listed in Table 4.

Examination of the data in Table 4 shows the curious effect that all of the polymers which are dominated by dispersive force intermolecular bonding (PE, TPX, PVCH) show relatively good agreement between the contact mechanics determined surface energy and the contact angle inferred surface energy (depending upon the model chosen for inferring the surface energy). However, the contact mechanics determined surface energy is markedly higher for those polymers which have a substantial component of non-dispersive intermolecular bonding (PET, PVP, PMMA, PS, corona treated PE). The greater the non-dispersive character, the greater the discrepancy between contact angle and contact mechanics determined surface energy. Once again, note that the two different types of contact mechanics measurements of surface energy are in agreement. Mangipudi et al. conjecture that the reason for the discrepancy between these two methods of determination of polymer surface energy is that the intermolecular energetics of the liquids used to determine contact angles are not the same as those in the polymer surfaces. In addition, contact angle liquids can induce changes in the substrate surface (such as rearrangement, crystallization, etc.) which would not occur for a material in contact with itself. In contact mechanics measurements, the probe of surface energy is just the material itself, thus having identical intermolecular bonding on both sides of the interface in question. However, contact mechanics measurements may cause the surface to respond by rearrangement, but possibly in a different fashion from liquid contact.

The Good–Girifalco theory [77–82] was originally formulated to make an attempt to correlate the solid–liquid interfacial tension to the solid surface energy and the liquid surface tension through an interaction parameter, ϕ . The basic formulation of the theory is:

$$\gamma_{SL} = \gamma_S + \gamma_L - 2\phi(\gamma_S\gamma_L)^{1/2} \quad (43)$$

where ϕ is the solid–liquid ‘interaction parameter’. Mangipudi et al. have used literature information to estimate the polarizability, dipole moment, ionization

Table 4

Surface energies determined by SFA and comparison to surface energies inferred from contact angle measurements (in mJ/m²)

	Polymer							
	PE	C-PE ^a	TPX	PVCH	PS	PVP	PMMA	PET
SFA	33 ± 2	52 ± 1	26.5 ± 2	28.2 ± 1	44 ± 2.1	63 ± 4	53 ± 4	61 ± 2
JKR PDMS cap method	–	–	–	–	45 ± 1	–	53 ± 1	–
Zisman's plot	32 ± 2	33.5 ± 1	21.5 ± 1	29 ± 1	30 ± 1	50 ± 2	40 ± 0.2	38 ± 2
Wu's equation of state	34.5 ± 1	45 ± 1	24 ± 1	31 ± 1	42 ± 1	52 ± 1	45 ± 2.1	42 ± 4
Geometric mean	34 ± 2	49 ± 4	25 ± 4	34 ± 6	41 ± 8	53 ± 7	44 ± 5	44 ± 2
Harmonic mean	36 ± 4	53 ± 6	24.5 ± 4	37 ± 7	44 ± 11	52 ± 6	48 ± 7	52 ± 5
Good–Girifalco (using diiodomethane)	33 (0.98)	–	26.5 (0.99)	28 (0.99)	44 (0.99)	60 (0.95)	45 (0.98)	52 (0.99)
Good–Girifalco (using glycerol)	33 (0.8)	–	20 (0.81)	27 (0.81)	44 (0.81)	48 (0.95)	51 (0.84)	58 (0.84)

Values of the interaction parameter, ϕ , are given in brackets.^a C-PE is corona-treated polyethylene.

potential, dielectric constant and molar volume of various liquids and polymers, and calculated the interaction parameter for a series of liquids and polymer pairs. The details can be obtained from ref. [63]. Of the liquids used in contact angle measurements, only diiodomethane, α -bromonaphthalene and glycerol provided reasonable approximations of the contact mechanics measured surface energy. Examples of this data are shown in Table 4. Extraordinary disagreement was obtained when either water or DMSO was used as the contact angle liquid. It may be noted that hydrogen bonding interactions are particularly important in the intermolecular bonding in these liquids.

The results in Table 4 indicate that great care must be taken as it regards inferring surface energies from contact angle data as it depends substantially on the model. According to Mangipudi et al., the source of the discrepancy is likely due to specific interactions between contact angle liquids and surfaces which do not mimic the actual intermolecular bonding in the solid polymer. Mangipudi et al. suggest that some correction can be made for these effects by using contact angle theories which account for specific interactions such as the Good–Girifalco theory. However, even that theory does not do a good job for all liquids. For example, the Good–Girifalco interaction parameter does not account for intermolecular H-bonding in such liquids as water or formamide. Mangipudi et al. observed that the largest disagreement seems to occur for those polymers and liquids which can be considered to be acidic or basic in character or those that exhibit significant H-bonding. According to Mangipudi et al., contact angle methods are well suited for understanding the wetting properties of surfaces. However, calculation of solid surface energy from the wetting measurements requires a constitutive model that accounts for universal (e.g. van der Waals interactions) as well as specific interactions (e.g. H-bonding) occurring between solids and liquids.

4.3. Studies on adhesion of elastomers: role of interfacial chains and coupling agents

Adhesion of elastomers, and in particular, the effect of interfacial coupling agents on the adhesion of elastomers, is a very important topic in adhesion science. A significant amount has been done in this area to understand the effect of interfacial chemical reactions, interdiffusion of polymeric chains across the interface, and the effect of physisorption and chemisorption of moisture at the interface. In most of these studies, the interfacial adhesion has been studied using a peel test (usually a 90° or 180° peel test). Due to the nature of the peel test and its geometry, as well as the energy dissipation associated with these test methods, the measured fracture energies are orders of magnitudes higher than the interfacial adhesion. In addition to the dissipation effects, as pointed out by Brown [13], the other drawbacks of peel test, in the context of studying adhesion of elastomers, include large area and volume of the test specimens, microscopic defects in the test

interface of larger area, relative insensitivity of the test method to minor variation in experimental variables, and so on. The above-mentioned drawbacks of the peel test methods have prompted Brown and coworkers [13,45,46,98], and Tirrell and coworkers [42,43] to employ a variation of the JKR technique to study the effect of interfacial chains and coupling agents on the adhesion of elastomeric polymers. These efforts have resulted in some very useful and insightful experiments. These experiments will be reviewed in this section. As pointed out by Brown [13], the advantages of the JKR technique are that the volume of the material that is under strain is rather very small, and that it is possible to generate smooth surfaces suitable for the adhesion studies.

As mentioned above, the study of the effect of interfacial chains or coupling agents on the adhesion of elastomers is an important problem in adhesion science. As described by Brown [99], the interface between two crosslinked elastomer can be strengthened by the addition of chains that cross the interface and are coupled by entanglement with the bulk elastomer. As a crack grows along the interface, the coupling chains are progressively pulled from the bulk material. This 'pull-out' process is expected to occur in an approximately planar cohesive zone directly ahead of the crack tip. This problem of elastomer adhesion in the presence of coupling chains is illustrated in Fig. 15. The interfacial adhesion is believed to depend on the surface and interfacial energies as well as the molecular characteristics of the chains. These characteristics include chain length,

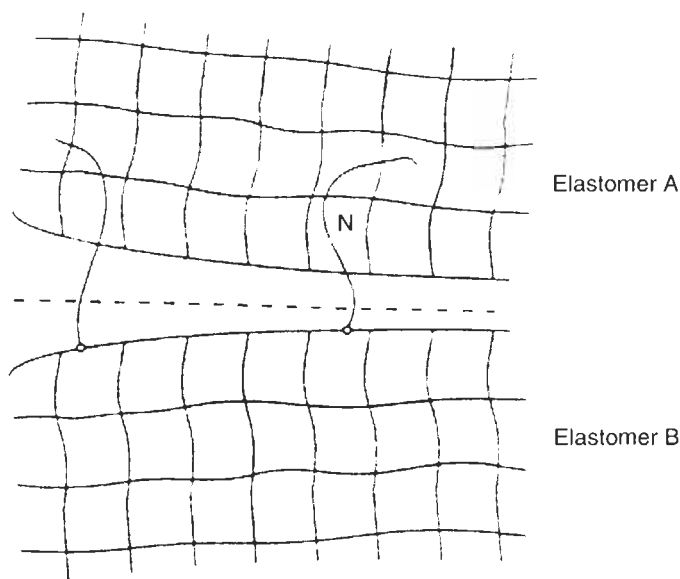


Fig. 15. Schematic of the problem of adhesion of elastomers in the presence of interfacial coupling chains. Reproduced from ref. [98].

area density, friction coefficient, etc. A number of models have been proposed to quantify the effect of each of these variables on the toughness or adhesion strength of the interface. These models describe the process of interfacial chain pull-out, and the relation between chain pull-out and interfacial toughness (see refs. [13,42–46], and the references therein, for details). A summary of the predictions of these models, which are verified by the experiments reviewed in here, is given below.

The models all assume that a threshold stress exists below which chain pull-out does not occur. Corresponding to the threshold stress is a value of *critical speed of crack propagation* (v^*), and the threshold stress depends on *intrinsic adhesion energy* or *threshold toughness*, G_0 . Note that G_0 is independent of the speed of crack propagation, and is larger than the Dupré work of adhesion (see below). The models all predict that the measured toughness of the adhesion increases linearly with the crack speed above the critical speed. That is, for $v < v^*$, $G = G_0$; and for $v > v^*$, $G \propto v$. The critical speed is the speed at which the viscous rate-dependent work of pull-out of the chains becomes comparable to the threshold toughness, and so is related to the number of chains per unit interfacial area (Σ); the number of repeat units in the chain being pulled out (N); and the monomer friction coefficient (ζ_0).

The above-mentioned models differ in the relation that is derived between the rate of pull-out of the individual chain and the crack velocity. These models also differ in their interpretation of the threshold stress and the threshold toughness (G_0). Also, v^* is expected to be dependent on the configuration of the connector chain at the interface. The value of v^* when connector chain crosses the interface just once is higher than the value when the chain forms multiple stitches, even though G_0 is not altered. When the chain forms multiple stitches, the ‘block and tackle’ effect ensures that the viscous processes dominate even at lower velocities, and v^* is reduced by a factor of N from the value obtained from the single crossing case. These models are discussed by Brown and coworkers [45,46].

The most recent model of de Gennes and coworkers [100,101], the threshold toughness is related to the extra surface and elastic energy of the individual chains as they are pulled out. The threshold toughness and the critical crack propagation speed are given by

$$G_0 \approx W + \gamma N \Sigma a^2 \approx W + k T N \Sigma \quad (44)$$

and

$$v^* = \frac{E}{2 \Sigma \zeta_0 N} \quad (45)$$

where W is Dupré work of adhesion; γ is surface energy of the chain; N is number of repeat units in the chain being pulled out; Σ is the area density of the interfacial chains; a is monomer length; k is the Boltzmann constant; ζ_0 is monomer friction coefficient of the chain; E is Young’s modulus of the chain, and T is temperature.

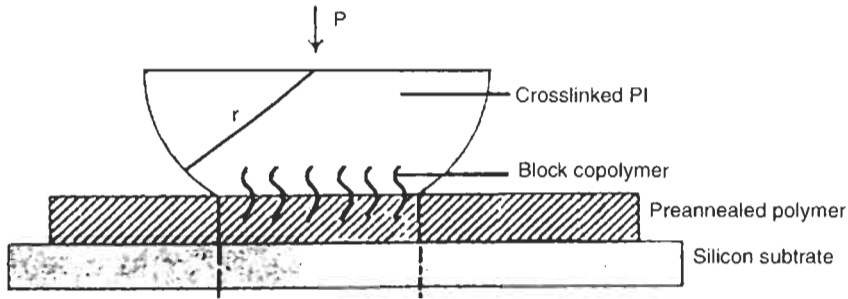


Fig. 16. Schematic of the JKR test specimen used by Brown et al. The crosslinked polyisoprene (PI) lens is first loaded in contact with the substrate with a load P to join the interface. The load is then removed and radius of the contact zone decreases with time. The contact radius $a(t)$ is measured using an optical microscope. Reproduced from ref. [45].

Using the JKR technique in some elegantly designed experiments, Brown and coworkers [13,45,46] and Tirrell and coworkers [42,43] verified the predictions of some of the above-mentioned models. The experimental system used by Brown et al. [13,45,46] consisted of a crosslinked PI spherical cap that was in contact with a thin layer of polystyrene–polyisoprene block copolymer. The block copolymer was coated on a PS-coated silicon wafer, and annealed such that the PI chains were at the air surface. The molecular weight, and hence the chain length, of the polyisoprene was varied systematically, and the area density of the PI chains was controlled by controlling the thickness of the PS–PI layer and annealing conditions. The details of the sample preparation may be obtained from the original papers. The experimental configuration is illustrated in Fig. 16. In these studies, Brown et al. observed the following:

(a) A thin layer of PS–PI block copolymer significantly increased the adhesion between PI-elastomer and PS surface.

(b) The fracture toughness (G , given by Eq. 39) increased with crack speed (v) as well as the area density of the PI chains.

(c) The increase in fracture toughness with crack velocity showed two regimes: a high gradient (dG/dv) regime at low crack velocities; and a low gradient regime at higher crack velocities. This implies that the effective friction was higher at low velocities. The transition seemed to occur at a velocity that independent of Σ . By extrapolating the low crack velocity data to zero, the threshold toughness G_0 was obtained.

(d) While G_0 always increased with Z , its increase with N did not show the linear relationship that would be expected from the models as shown in Eq. 44. A polymer chain with $N = 588$ was found to be less effective than a chain with $N > 882$. This led the authors to conclude that the length of the chain needed to be effective should be higher than a critical value, and this critical value would be

much higher than the average degree of polymerization between the cross links in the network.

(e) Interestingly, the value of fracture toughness (G) at $v > v^*$ (higher crack velocities) indicated that G for higher molecular chains was the same implying that there was little change in the length of penetration per chain when the degree of polymerization was high (for example, $N > 882$). Also, for higher molecular weight chains, a saturation of penetrated length appeared to occur as Σ increased.

Tirrell et al. [42,43] studied the role of interfacial chains in a more detailed fashion. Tirrell et al. [42,43] used a crosslinked PDMS cap in contact with a silicon wafer on to which α,ω -hydroxyl terminated PDMS chains are tethered by adsorption from a solution. The molecular weight of the narrow disperse PDMS samples was in the range of 20,000–700,000. The surface chain density was given by $\Sigma \approx N^{1/2} \Phi^{7/8}$ where Φ is the volume fraction of PDMS in solution. The experimental and theoretical procedure used by Tirrell et al. is similar to that of Brown and coworkers. Tirrell et al. compared their results from the JKR experiments to 90° peel tests. The details of the experiment may be obtained from the original papers. The observations of Tirrell et al. can be summarized as follows:

(a) The fracture toughness increased with crack propagation velocity. However, there was no clear evidence of a transition between a regime in which the adhesion energy (G) becomes independent of the velocity (v) of crack propagation and regime in which G depends strongly on v in the investigated range of velocities (10 – 10^4 nm/s).

(b) Unlike in Brown's work, Tirrell et al. did not observe a linear relation between G and v . The $G(v)$ curves obtained by Tirrell et al. looked like power-law or logarithmic dependence over the investigated range of velocities. Because of this Tirrell et al. considered the fracture toughness at the lowest crack propagation rate (10 nm/s) as the threshold toughness of the interface.

(c) The fracture toughness, at a given velocity, obtained from the 90° peel tests are, in general, higher than the values obtained from the JKR measurements by a factor of 2–4. The difference was attributed to the difference in the mechanics of fracture in the above test methods.

(d) Interestingly, the fracture toughness (G) obtained from the peel tests as well as the JKR experiments as a function of area density of tethered chains (Σ) showed a *maximum*. These data are shown in Fig. 17.

(e) The value of $G(\Sigma)$ increased with increase in the molecular weight (M_0) between the crosslinks in the network. But the position of the *maximum* in $G(\Sigma)$ was not strongly affected by change on M_0 .

When compared to the early models that describe the adhesion of elastomers in the presence of interfacial chains, the central findings of this work, namely, observations b and d above, were quite surprising. In his recent work, de Gennes [102] pointed out that when a surface tethered chain diffuses into an elastomeric

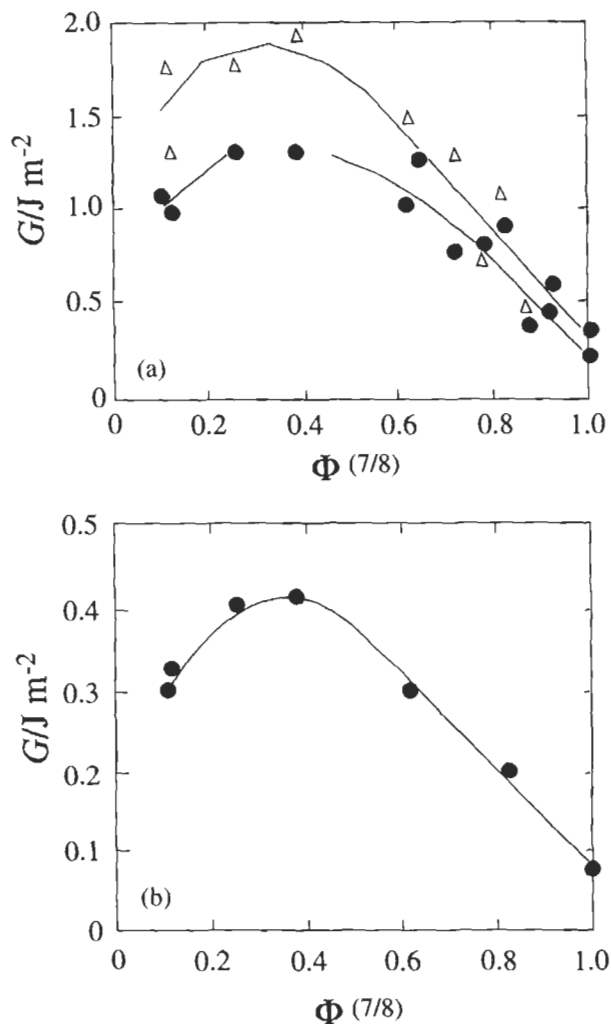


Fig. 17. Adhesion energy G measured as a function of the surface density of the interfacial chains. It may be noted that the strength measured in a peel test (a) is about 5 times larger than that measured using the JKR method (b). Further, a *maximum* exists in the value of G as function of the surface chain density. This is because of swelling effects at larger values of surface chain density. The open symbols represent the data for elastomer molecular weight $M_0 = 24,000$ and the closed symbols represent the data for $M_0 = 10,000$.

network the interdigitation is always accompanied by swelling of the elastomer. This swelling costs energy, and may limit the interdigitation process. More recently, de Gennes and coworkers [103] predict a limiting surface-chain density given by

$$\Sigma_1 = \frac{N_0}{N^{3/2}} \quad (46)$$

where N_0 is the degree of polymerization between the crosslinks in the network; and N is the number of repeat units in the penetrating chain.

If Σ is greater than Σ_1 , the surface chains no longer penetrate into the elastomer over their entire length due to swelling constraints, and these rejected chains form a passive layer on the surface. At a higher value of Σ , the interdigitation is completely forbidden, and the interfacial fracture toughness corresponds to the thermodynamic work of adhesion. For a complete discussion on these arguments, the reader may refer to the original papers.

Brown [46] continued the contact mechanics work on elastomers and interfacial chains in his studies on the effect of interfacial chains on friction. In these studies, Brown used a crosslinked PDMS spherical cap in contact with a layer of PDMS–PS block copolymer. The thickness, and hence the area density, of the PDMS–PS layer was varied. The thickness was varied from 1.2 nm ($\Sigma = 0.007$ chains per nm²) to 9.2 nm ($\Sigma \approx 0.055$ chains per nm²). It was found that the PDMS layer thickness was less than about 2.4 nm, the frictional force between the PDMS network and the flat surface layer was high, and it was also higher than the frictional force between the PDMS network and bare PS. When the PDMS layer thicknesses was 5.6 nm and above, the frictional force decreased dramatically well below the friction between PDMS and PS. Based on these data Brown [46] concluded that:

(a) when the thickness of the PDMS layer was 1.2 nm, i.e. when there are fewer chains on the surface, the PDMS chains expand into the PDMS network. The sliding process involves the frictional energy between PDMS and PS as well as the energy required to pull the PDMS tethered chains from the PDMS network. The latter process causes an increase of friction over that on the bare PS substrate;

(b) when the PDMS thickness is high, all the chains do not penetrate into the network of PDMS as their elastic energy resists swelling of the network by the chains. Because of this a significant portion of the chains remains attached to the surface of PS. In such a case the friction occurs between the PDMS network and the PDMS chains on the surface.

In addition, the PDMS chains on the surface are in a state of higher mobility than the bare PS. (Note that PS is glassy at room temperature, and PDMS chains are mobile.) Even though the nature of interfacial interactions between PDMS–PS and PDMS–PDMS are largely similar (dispersive van der Waals interactions), the additional mobility of the PDMS chains results in much lower friction when the layer thickness is higher. These results are not only novel but also quite revealing. The primary implications of this study are: (1) that a very thin layer of tethered chains can increase interfacial friction; and (2) to reduce friction by using a tethered chain, the layer thickness should be higher than a critical thickness. An

interesting study would be to examine this behavior with materials, for example acrylic elastomers, that have specific interactions over and above van der Waals dispersive interactions.

5. Adhesion of viscoelastic polymers

Viscoelastic polymers essentially dominate the multi-billion dollar adhesives market, therefore an understanding of their adhesion behavior is very important. Adhesion of these materials involves quite a few chemical and physical phenomena. As with elastic materials, the chemical interactions and affinities in the interface provide the fundamental link for transmission of stress between the contacting bodies. This intrinsic resistance to detachment is usually augmented several folds by dissipation processes available to the viscoelastic media. The dissipation processes can have either a thermodynamic origin such as recoiling of the stretched polymeric chains upon detachment, or a dynamic and rate-sensitive nature as in chain pull-out, chain disentanglement and deformation-related rheological losses in the bulk of materials and in the vicinity of interface.

5.1. Contact mechanics of viscoelastic materials

There are two different scales of deformation in any adhesive contact: (1) the bulk scale of deformation which is characterized by the radius a of contact area over which the compressive forces are significant; and (2) the zone of action of surface forces or the cohesive zone at the edge of the contact, characterized by the length d over which the tensile forces are dominant. When the contact boundary is moving with a speed v , the two scales of deformation translate into two time scales, one on the order of (a/v) and the other of the order of (d/v) .

5.1.1. Linear viscoelastic effects in the bulk

Viscoelastic contact problems have drawn the attention of researchers for some time [2,3,104,105]. The mathematical peculiarity of these problems is their time-dependent boundaries. This has limited the ability to quantify the boundary value contact problems by the tools used in elasticity. The normal displacement (u) and pressure (p) fields in the contact region for non-adhesive contact of viscoelastic materials are obtained by a self-consistent solution to the governing singular integral equation given by [106]:

$$u(\bar{x}, t) = \int_0^t c(t-t') \frac{\partial}{\partial t'} \left(\int_{\Omega(t')} K(\bar{x}, \bar{\xi}) p(\bar{\xi}, t') d\Omega \right) dt' \quad (47)$$

where $c(t)$ is closely related to the creep compliance, and the kernel K , containing the strength of stress singularity, is:

$$K(\bar{x}, \bar{\xi}) = \frac{1}{2\pi |\bar{x} - \bar{\xi}|} = \frac{1}{2\pi [(x_1 - \xi_1)^2 + (x_2 - \xi_2)^2]^{1/2}} \quad (48)$$

\bar{x} and $\bar{\xi}$ vectors are the actual and the running coordinates over the planar contact area $\Omega(t)$, respectively. The boundary conditions are:

$$u(\bar{x}, t) = \begin{cases} = \delta(t) - f(\bar{x})H(t) & \text{for } \bar{x} \in \Omega(t) \\ \geq \delta(t) - f(\bar{x})H(t) & \text{for } \bar{x} \notin \Omega(t) \end{cases} \quad (49)$$

$$\int_{\Omega(t)} p(\bar{x}, t) d\Omega = P(t)$$

$f(\bar{x})$ is the profile of separation distances between the two bodies before the contact, and $H(t)$ is the Heaviside step function.

In the absence of moving boundaries, application of the Laplace transform removes the time dependence and the viscoelastic problem will become similar to an elastic one in the new domain; this method is referred to as the Correspondence Principle [2]. If the contact area changes with time, the transformation method cannot be applied directly; the mathematical complexity arises from the presence of the mixed type of boundary conditions. Any point at the surface just outside the contact area, upon being swept through the crack edge during loading will lose its traction-free prescribed boundary condition to a displacement-prescribed one. Moreover, in the case of receding cracks in viscoelastic materials, any point left behind the crack is not stress-free instantaneously; there will be a relaxation associated these points which lie outside the contact area.

Under certain circumstances, there has been success in rendering calculations for some viscoelastic contact problems with moving boundaries. Lee and Radok [2], and later Yang [4], have developed a methodology to extend the elastic solution of the Hertz problem to its viscoelastic counterpart. They show that the contact area at any time t belongs to the one-parameter family of solutions of elastic half-spaces in the parameter t which satisfies the same boundary conditions for the given viscoelastic problem. Their solution consists in replacing the elastic constant in the elastic solution by the corresponding integral operator obtained from the viscoelastic stress-strain relations. Thus, if the deformation history is known, the Young's modulus E can be replaced by the integral operator involving the relaxation modulus $E(t)$. On the other hand, in the case that the stress history is known, $1/E$ is replaced by the creep compliance $J(t)$. Such integral equations are used by Lee and Rogers [107] as a method to calculate the relaxation modulus or the creep compliance of polymers. For validity of the solution, two conditions must be fulfilled: first, stress-strain relationships of the polymer must

be within the limits of linear viscoelasticity; second, the contact area must increase monotonically throughout the experiment. The latter requirement has been relaxed by several authors for linear viscoelastic contacts with any number of maxima and minima for the contact area [3,108]. This particular problem is not inside the scope of this chapter, where only monotonic compressions are considered. The above-mentioned treatment has some inherent limitations. For example, the elastic constants conform to a number of mathematical manipulations which are not necessarily valid for the viscoelastic integral operators, putting a restriction on rearrangement of the employed elastic equation. The following is the linear viscoelastic counterpart of Hertzian contact problem presented by Radok:

$$P(t) = \int_0^t \frac{K(t-t')}{R} da^3(t') \quad (50)$$

The lower bound 0 in the integration refers to the time at which the first contact is made after attaining the fully relaxed state. The upper bound t is the actual time spent in the loading experiment when the load $P(t)$ is recorded.

5.1.2. Viscoelastic effects at the edge of contact

JKR theory consists of a combination of the Hertz and flat punch problems. The flat punch part must be addressed in the context of fracture mechanics describing the viscoelastic stress and displacement near the *crack* tip. Again, with stationary cracks, the elastic solutions can be related to the viscoelastic problems via a classical correspondence principle. However, for the moving cracks only under certain restrictions, similar to those mentioned above for the counterpart of the Hertz problem, an extended correspondence principle proposed by Graham [105] can be used. In the case of a Griffith-type of crack (the JKR theory), Greenwood and Johnson [109] conclude that the apparent adhesion energy for opening cracks is overestimated by a rate-independent factor $k = E(0)/E(\infty)$ where $E(0)$ and $E(\infty)$ are the instantaneous (glassy) and relaxed shear moduli, respectively. This approach is not able to predict the rate dependency of the adhesion energies observed by experimentalists.

By using a Barenblatt-type of crack, Schapery [110] developed a theory for crack growth in viscoelastic materials. Greenwood and Johnson [109] followed Schapery's methodology in order to explain the rate sensitivity of the adhesion energy in view of the rate dependency of the creep compliance. For an opening crack in elastomeric materials, assuming that the viscoelastic crack has the same shape as the elastic one at every growth speed, Greenwood and Johnson [109] have shown that for linear viscoelastic systems the adhesion energy is not constant but is a function of the creep compliance $J(t)$. Instead of a Griffith crack (the JKR theory), Maugis [30] used a Dugdale crack to model the adhesive contact between

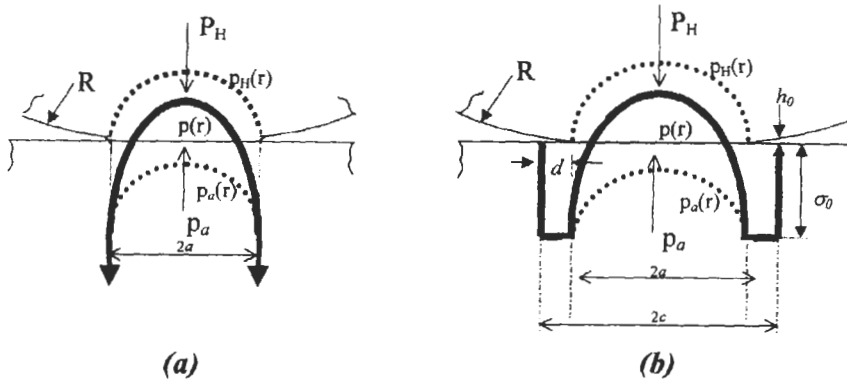


Fig. 18. Adhesive contact of elastic spheres. $p_H(r)$ and $p_a(r)$ are the Hertz pressure and adhesive tension distributions. (a) JKR model uses a Griffith crack with a stress singularity at the edge of contact ($r = a$); (b) Maugis model uses a Dugdale crack with a constant tension σ_0 in $a < r < c$ [111].

elastic bodies. Johnson [111] extended the Maugis' model to linear viscoelastic adhesive contacts and found similar predictions as Schapery's theory. Fig. 18 illustrates the JKR and Maugis models which use Griffith and Dugdale cracks, respectively.

5.1.2.1. Unloading experiments. At least, for opening cracks, or unloading, experiments, it is necessary to differentiate between the rates of deformation experienced in the bulk and in the vicinity of the crack tip. Greenwood and Johnson [109] have shown that

$$\frac{G_{ul}}{W} = \frac{1}{E_{\infty} J(\tau^*)} \quad (51)$$

where

$$\tau^* = t^*/\lambda \quad (52)$$

$$t^* = d/3v \quad (53)$$

E_{∞} is the relaxed value of Young's modulus, d is the length of the cohesive zone, $v = |da/dt|$ is the rate of crack propagation, and λ is the longest relaxation time. For both closing and opening cracks Schapery [110] has shown that the length of cohesive zone varies approximately with the rate of healing or peeling according to

$$d = \frac{d_e}{E_{\infty} J(t^*)} \quad (54)$$

where d_e is the elastic value of the length of the cohesive zone at $v = 0$

$$d_e = \frac{\pi E_{\infty}^* h_0^2}{4W} \quad (55)$$

the crack tip $h_0 = W/\sigma_0$, and σ_0 is the maximum tension in the cohesive zone. From above

$$t^* = \frac{d}{3v} = \frac{d_e}{3vE_\infty J(t^*)} \quad (56)$$

or equivalently,

$$\tau^* E_\infty J(\tau^*) = \frac{d_e}{3\lambda v} \quad (57)$$

the above equation can be solved for τ^* (or t^*). This value of τ^* can be substituted in Eq. 51 to calculate the adhesion energy G_{ul} .

5.1.2.2. Loading experiments. In the case of a closing crack, the residence time of the material flowing through the cohesive zone at the edge of contact area (t^*) and the length of the cohesive zone (d) are still the same as an opening crack while the flow is in reverse direction. Schapery [112] has shown for such cracks the apparent work of adhesion is now given approximately as

$$\frac{G_l}{W} = E_\infty J(\tau^*) \quad (58)$$

where τ^* and d are still given by Eqs. 57 and 54.

Fig. 19 shows that the work of adhesion is augmented when the surfaces are separating (opening crack) and attenuated when they are coming together (closing crack) [111].

One might consider combining the Hertzian linear viscoelastic 'bulk' related phenomenon inside the contact area with the results provided by Greenwood and

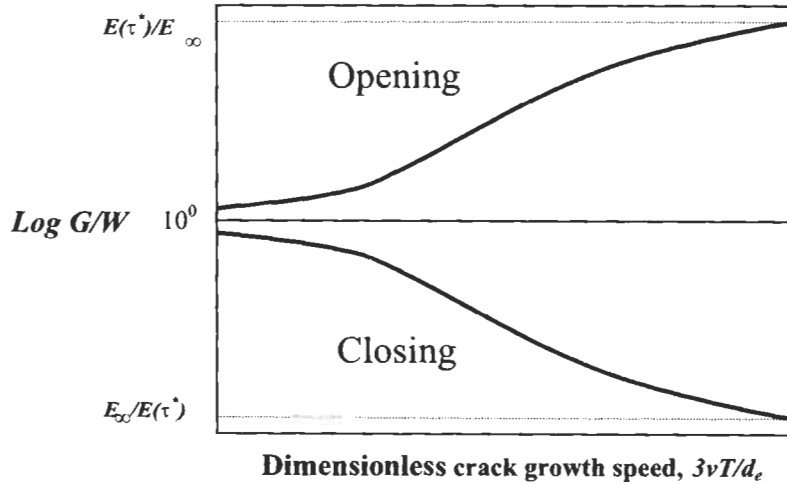


Fig. 19. Variation of strain energy release rate for a moving viscoelastic crack. $G > W$ for an opening crack, and $G < W$ for a closing crack [111].

Johnson [109] for linear viscoelastic effects inside the cohesive zone. For growing cracks

$$P(t) = P_H + P_a = \int_0^t \frac{K(t-t')}{R} da^3(t') - \sqrt{\frac{8\pi a^3 W}{J(\tau^*)}} \quad (59)$$

For closing cracks, the situation is much more complex, especially if the modulus does not show any long-term plateau. Under such conditions, only an approximate solution can be proposed

$$P(t) = P_H + P_a = \int_0^t \frac{K(t-t')}{R} da^3(t') - \frac{J(\tau^*)}{J(t-t_1)} \sqrt{\frac{8\pi a^3 W}{J(\tau^*)}} \quad (60)$$

where τ^* and d are still given by Eqs. 57 and 54, and t_1 is the time at which the last compression was imposed. In order to render the above equations more quantitative in determination of adhesion energy, it is imperative to measure the length of the cohesive zone experimentally.

Via an ad hoc extension of the viscoelastic Hertzian contact problem, Falsafi et al. [38] incorporated linear viscoelastic effects into the JKR formalism by replacing the elastic modulus with a viscoelastic memory function accounting for time and deformation, $K(t)$:

$$\begin{aligned} \text{LHS} &= \int_0^t \frac{K(t-t')}{K(1)} da^3(t') \\ &= \frac{R}{K(1)} [P(t) + 3\pi RG + (6\pi RGP(t) + 9\pi^2 R^2 G)^{1/2}] \end{aligned} \quad (61)$$

where

$$K(t) = \frac{2E(t)}{3(1-\nu^2)} = K(1)t^\beta \quad (62)$$

The premise of the above analysis is the fact that it has treated the interfacial and bulk viscoelasticity equally (linearly viscoelastic; experiencing similar time scales of relaxation). Falsafi et al. make an assumption that the adhesion energy G is constant in the course of loading experiments and its value corresponds to the thermodynamic work of adhesion W . By incorporating the time-dependent part of $K(t)$ into the left-hand side (LHS) of Eq. 61 and convoluting it with the evolution of the cube of the contact radius in the entire course of the contact, one can generate a set of $[\text{LHS}(t), P(t)]$ data. By applying the same procedure described for the elastic case, now the set of $[\text{LHS}(t), P(t)]$ points can be fitted to the Eq. 61 for the best values of $K(1)$ and W .

Fig. 20 demonstrates typical raw experimental data, and the set of points generated according to the procedure described in the previous section, for one of

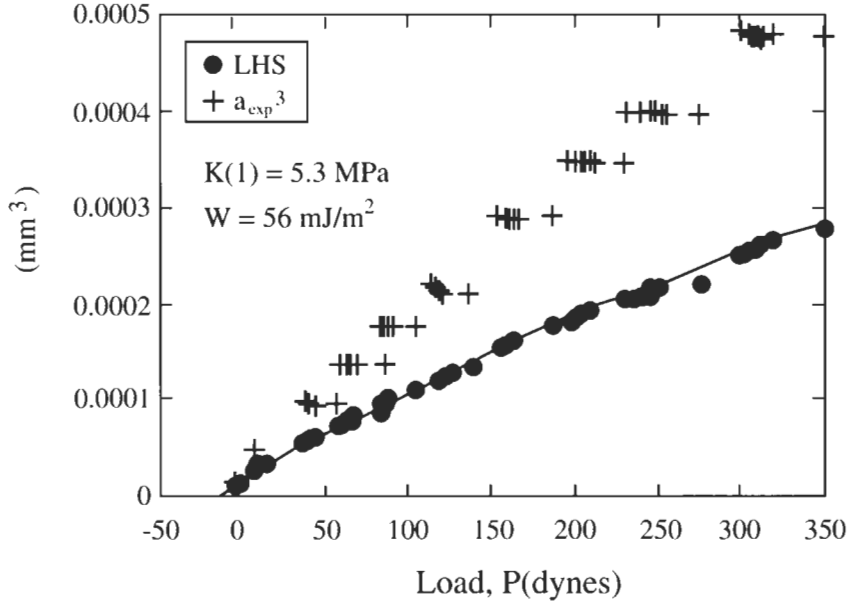


Fig. 20. The JKR representation of loading experimental and modified data for a viscoelastic adhesive contact. Each set of points corresponds to a compression step in which the load P and contact radius a decreases and increases with time, respectively. LHS refers to the term on the left hand side of Eq. 61. It represents the equivalent of a^3 in elastic JKR plot after being weighed by the viscoelastic factor [38].

the studied systems. In obtaining the values for W and $K(1)$, whenever there is an appreciable change in contact radius a during a step of compression, the final value of a is considered for the entire period of that compression. This concerns the lower load region of data in which there is some growth of contact area in each compression. If the actual contact area data for this region are considered, the generated data (LHS) will terminally fall on the curves shown towards the end of these compressions ($G < W$). The application of their analysis to loading experiments on a series of model diblock copolymers enabled them to obtain the surface energies consistent with the reported value from wetting experiments.

Hui et al. [113] also demonstrated that attempts to extend the JKR theory of contact to viscoelastic materials without consideration of the intermolecular forces that act at the edge of contact lead to paradox that is well-known in fracture mechanics. They showed that Schapery's theory, which employs an extremely simple model of cohesive forces, yielded results that agreed reasonably well with Falsafi et al.'s [38] loading experiments. However, they pointed out the difficulty associated with the coupling of surface energy and the model parameters (the elastic length of the cohesive zone d_c) representing the cohesive forces in the theory that prevents deterministic surface energy evaluation. They suggested an

alternative method that would use the relationship between crack propagation speed and the crack tip loading environment (stress intensity factor, K_I) as a basis for describing adhesion.

5.2. Static and dynamic contributions to the adhesion energy

A fundamental issue in analyzing adhesion data is how to de-couple the interfacial contributions from those of the bulk. The bulk effects can be seen as the energy consumed in a volume of material excluding a region in which localized loss processes prevail, i.e. the 'process zone'. The experimental data and the generalized fracture mechanics (GFM) [114] show that bulk effects amplify the thermodynamic work of adhesion in a way that is consistent with the temperature dependency of the loss tangent. The bulk loss function is a function of crack propagation speed v , temperature T and the strain level ε . In the process zone, energy can be further dissipated via a set of processes such as crazing in glassy materials, chain pull-out and disentanglement for inter-diffusing interfaces, and chain recoiling (Lake–Thomas effect [115]) at the edge of the process zone. Even though in the case of low adhesion the level of strain in the bulk is low, the deformations in the process zone could be very high, and thus the potential for further viscoelastic energy losses exists.

Starting with the experimentally found form of the adhesion energy functional given by Gent and Petrich [116], Falsafi et al. [117] have proposed and used the following empirical form to further decouple the bulk and interfacial processes

$$G = W [1 + \phi_{pz}(v, T, M, t_c, n)][1 + \Psi_{VE}(T, v, l)] \quad (63)$$

where

$$\phi_{pz} = \varphi_{CR}(M) + \varphi_i(v, M, t_c, n) \quad (64)$$

φ_{CR} and φ_i are the contributions from chain recoiling and interfacial dynamics (i.e. drag forces and disentanglement), respectively, and Ψ_{VE} is the viscoelastic loss function which has interfacial and bulk parts. l is a characteristic length of the viscoelastic medium, t_c is the contact time and n is the chain architecture factor. Fig. 21 illustrates the proposed rate dependency of adhesion energy.

Ahn and Shull [118] have shown that the relationship between G and v can be adequately described by the following empirical expression:

$$G = G_0 [1 + (v/v^*)^{0.6}] \quad (65)$$

Values of G_0 were within a factor of 2 of the expected W while v^* varied from 5 to 215 nm s⁻¹ in their acrylic elastomeric system. Experiments conducted by Luengo et al. [119] suggest the existence of at least two different dissipation processes: one at the molecular level and the other at the microscopic to macroscopic level.

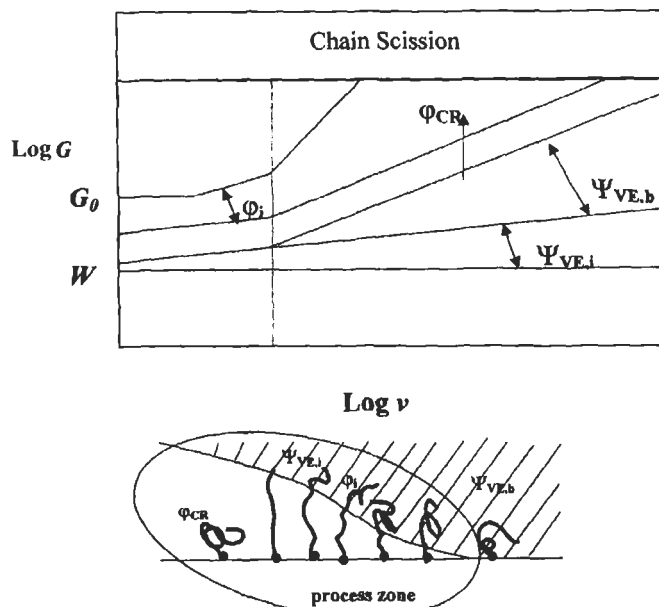


Fig. 21. Patterns of rate dependency of adhesion energy observed in contact mechanical measurements (Eqs. 63 and 64) [117].

Both of these processes appear to be associated with the glass transition and bulk rheological dissipation.

In a study by Falsafi et al. [120] they used the JKR methodology to probe the effect of chain architecture on the adhesion of intrinsically viscoelastic block copolymer mixtures. Polymeric layers were prepared and supported on elastic, surface-treated crosslinked PDMS caps to remove bulk viscoelastic effects, therefore viscoelastic losses, Ψ_{VE} , were limited to the polymeric layers which were fraction of a micron thick. The building blocks of the copolymers had different physical states at room temperature with different dynamic characteristics. They compared the dynamics of disentanglement for diblock 'chains' and triblock 'loops'. Their adhesion results show the influence of chain architecture on the self-adhesion of diblock/triblock mixtures (when $M > 3M_c$) [121] that cannot be merely explained by chain recoiling and/or the layer viscoelasticity. Though the loops were shown to be much more effective than the linear chains in welding the contacting surfaces, they had very slow dynamics of interpenetration which was absent for the diblocks. For contact times shorter than 30 min, the adhesion energy seemed to go through a maximum as the triblock content increased. Consistent with their previous works, the thermodynamic work of adhesion obtained from the loading part of the experiments was shown to depend on the chemistry of

surface-active block and did not vary with chain architecture suggesting the minor role of entropic effects.

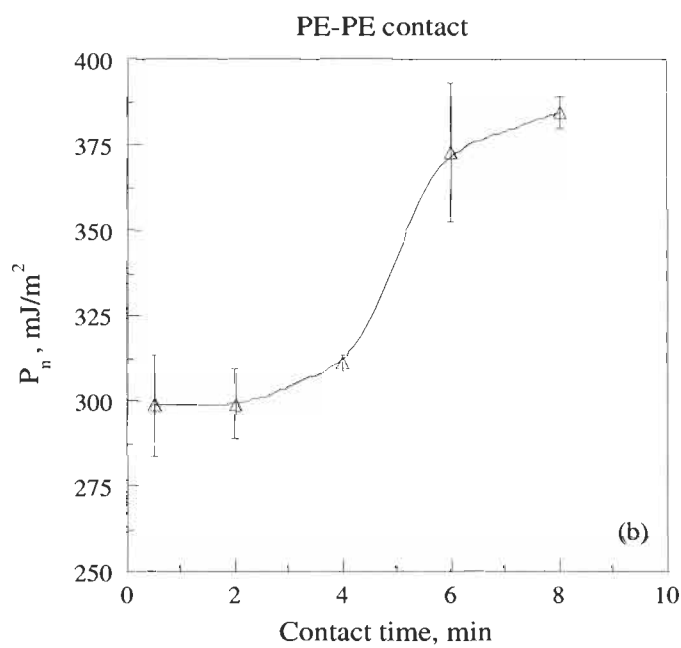
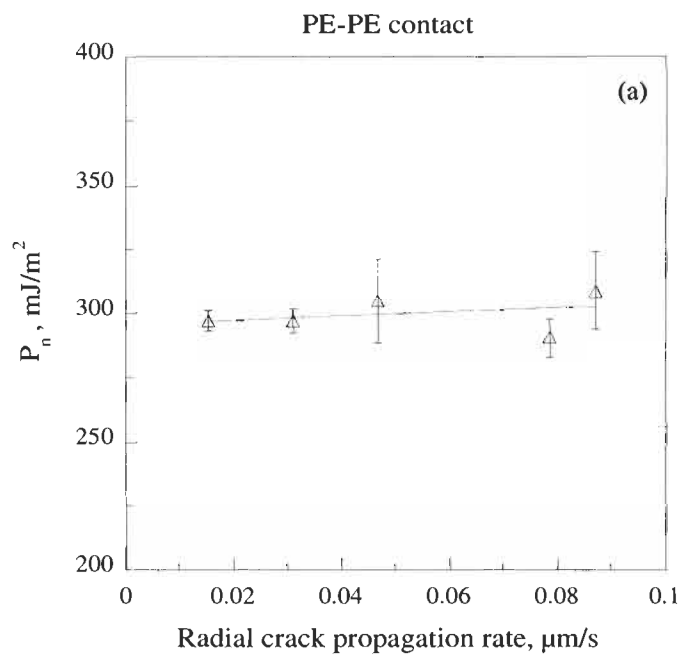
6. Current directions

As reviewed so far, the contact-mechanics-based techniques (JKR and SFA methods) have been effective in the understanding molecular level mechanisms related to the adhesion of elastomers and in measuring the surface and interfacial energies of polymers and self-assembled monolayers. The current work in this area is aimed at understanding contact induced interfacial rearrangements and the role of specific interactions. The recent progress of these studies is discussed in this section.

6.1. Contact induced interfacial rearrangements

Interfacial rearrangements can take place when two surfaces are in contact over a period of time. These rearrangements, which normally occur in H-bonding or acid–base type reactive systems, are usually driven by the tendency of the system to minimize its interfacial free energy. As reported by Silberzan and colleagues [51] and by Kinning [122], in some cases these interfacial rearrangements give rise to an increase in adhesion with contact time. The contact-mechanics-based techniques can be used to study the dynamics of these interfacial rearrangements. In a typical elastic system, the modulus can be determined from the *loading data* using Eq. 11. The stress or contact induced interfacial rearrangements would result in contact hysteresis, and Eq. 39 can be used along with the *unloading data* to determine the effect of interfacial rearrangements on adhesion. Kramer and coworkers [51,52] have employed these methods to study the chemical reaction induced adhesion hysteresis affected by the stress distribution in the contact zone between spheres. Similar experiments led by Chaudhury and coworkers [123] on hydrolyzed PDMS cylinders and flats support that the formation of hydrogen bonds across an interface is dependent on normal stress which increases toward the centerline of contact.

Mangipudi et al. [63,88] reported some initial measurements of adhesion strength between semicrystalline PE surfaces. These measurements were done using the SFA as a function of contact time. Interestingly, these data (see Fig. 22) show that the normalized pull-off energy, a measure of intrinsic adhesion strength is increased with time of contact. They suggested the amorphous domains in PE could interdiffuse across the interface and thereby increase the adhesion of the interface. Falsafi et al. [37] also used the JKR technique to study the effect of composition on the adhesion of elastomeric acrylic pressure-sensitive adhesives. The model PSA they used was a crosslinked network of random copolymers of acrylates and acrylic acid, with an acrylic acid content between 2 and 10%.



The measured surface energies of the model PSA were all approximately 30 mJ m^{-2} , indicating surfaces dominated by methylene groups. Apparently, the system attempts to hide higher energy (carboxyl groups) in the bulk of the material [124,125]. The XPS data also suggested carbon enrichment in the vicinity of the surface, supporting this hypothesis. A surface free energy penalty for carboxyl groups of acrylic acid does not exist in the polymer–polymer interface at the contact area. In the contact region, the carboxyl groups can seek out each other across the interface and form a hydrogen bond. This was suggested to be responsible for the adhesion hysteresis observed in the measurements. Consistent with the observations made by Ahn and Shull [118], they also found that the contact pressure did not affect the extent of hysteresis.

Choi et al. [126] conducted adhesion studies of crosslinked PDMS caps, before and after solvent extraction, using JKR technique. In their experiments, the size of adhesion hysteresis was increased with decreasing values of the crosslinker to PDMS ratio that corresponded to increasing amount of extracted weight. The shorter the extraction process, the smaller the adhesion hysteresis. They concluded that the entanglement of the loose chains with the PDMS network at the interface might be controlling the observed hysteresis. Perutz et al. [127] also studied the role of excess crosslinker and the crosslinking catalyst on the adhesion hysteresis of PDMS networks. They found as excess amounts of crosslinker were added, the adhesion hysteresis increased. They also demonstrated that by poisoning the catalyst with a thiol the hysteresis could be significantly reduced or even removed.

She et al. [128] used rolling contact to estimate the adhesion hysteresis at polymer/oxide interfaces. By plasma oxidation of the cylinders of crosslinked PDMS, silica-like surfaces were generated which could hydrogen bond to PDMS molecules. In contrast to unmodified surfaces, the adhesion hysteresis was shown to be larger and proportional to the molecular weight of grafted polymer on the substrate. The observed hysteresis was interpreted in terms of the orientation and relaxation of polymer chains known as Lake–Thomas effect.

Fig. 22. Normalized pull-off energy measured for polyethylene–polyethylene contact measured using the SFA. (a) P_n versus rate of crack propagation for PE–PE contact. Change in the rate of separation does not seem to affect the measured pull-off force. (b) Normalized pull-off energy, P_n as a function of contact time for PE–PE contact. At shorter contact times, P_n does not significantly depend on contact time. However, as the surfaces remain in contact for long times, the pull-off energy increases with time. In semicrystalline PE, the crystalline domains act as physical crosslinks for the relatively mobile amorphous domains. These amorphous domains can interdiffuse across the interface and thereby increase the adhesion of the interface. This time dependence of the adhesion strength is different from viscoelastic behavior in the sense that it is independent of rate of crack propagation.

6.2. Acid–base interactions with model elastomers

The study of acid–base interaction is an important branch of interfacial science. These interactions are widely exploited in several practical applications such as adhesion and adsorption processes. Most of the current studies in this area are based on calorimetric studies or wetting measurements or peel test measurements. While these studies have been instrumental in the understanding of these interfacial interactions, to a certain extent the interpretation of the results of these studies has been largely empirical. The recent advances in the theory and experiments of contact mechanics could be potentially employed to better understand and measure the molecular level acid–base interactions. One of the following two experimental procedures could be utilized: (1) Polymers with different levels of acidic and basic chemical constitution can be coated on to elastomeric caps, as described in Section 4.2.1, and the adhesion between these layers can be measured using the JKR technique and Eqs. 11 or 30 as appropriate. For example, poly(*p*-amino styrene) and poly(*p*-hydroxy carbonyl styrene) can be coated on to PDMS-ox, and be used as acidic and basic surfaces, respectively, to study the acid–base interactions. (2) Another approach is to graft acidic or basic macromers onto a weakly crosslinked polyisoprene or polybutadiene elastomeric networks, and use these elastomeric networks in the JKR studies as described in Section 4.2.1.

7. Conclusions

As discussed in this chapter, the processes of bonding (or attachment) and debonding (or detachment) are different in their nature. The factors that influence these processes are somewhat different. The traditional adhesion test methods such as peel test or shear test sometimes fail to quantify the factors that influence bonding. The contact mechanics techniques such as the SFA or the JKR method can be used effectively to understand, as well as quantitatively study the molecular level phenomena involved in the bonding and debonding processes. On the other hand, contact mechanics methods may not be quite as versatile with respect to the types of samples as the practical test methods. The wide-ranging application of the SFA and the JKR techniques for adhesion studies is made possible by the development of the JKR theory of contact mechanics. The techniques are employed in such diverse studies as the measurement of surface and interfacial energies of polymer films and self-assembled monolayers, adhesion of elastomers and the influence of interfacial coupling agents on their adhesion, adhesion and deformation of elastic layered bodies, adhesion and deformation of viscoelastic solids. These studies have contributed richly to the science of adhesion. Some of the current studies on viscoelastic systems show the promise in establishing a quantitative relation between the intrinsic adhesion strength and the practical strength thereby coupling

the bonding and debonding processes through a phenomenological description of viscoelasticity.

Acknowledgements

The authors would like to thank Pascal Deprez, Martial Deruelle, David P. Smith, Matthew Tirrell, Alphonsus V. Pocius, and Frank S. Bates for their input on this subject over the course of the last several years. They would also like to thank 3M and the Center for Interfacial Engineering, a National Science Foundation sponsored engineering research center at the University of Minnesota, for financial support.

References

1. Hertz, H. In: *Miscellaneous Papers*. Macmillan, London, 1896, p. 146
2. Lee, E.H. and Radok, J.R.M., *Trans. ASME: J. Appl. Mech.*, **27**, 438 (1960).
3. Graham, G.A.C., *Int. J. Eng. Sci.*, **5**, 495 (1967).
4. Yang, W.H., *Trans. ASME: J. Appl. Mech.*, **33**, 395 (1966).
5. Dutrowski, R.C., *Trans. ASME J. Lubr. Technol.*, **91F**, 732 (1969).
6. Johnson, K.L., Kendall, K. and Roberts, A.D., *Proc. R. Soc. Lond. Ser. A*, **324**, 301 (1971).
7. Israelachvili, J.N., *Intermolecular and Surface Forces*, 2nd edn. Academic Press, San Diego, 1992.
8. Wu, S., *Polymer Interface and Adhesion*. Marcel Dekker, New York, 1982.
9. Kinloch, A.J., *Adhesion and Adhesives — Science and Technology*. Chapman and Hall, London, 1987.
10. Kinloch, A.J., *J. Mat. Sci.*, **15**, 2141 (1980).
11. Pocius, A.V., *Adhesion and Adhesives Technology — An Introduction*. Hanser/Gardner, Cincinnati, OH, 1997.
12. Portelli, G.B. In: Hartshorn, S.R. (Ed.), *Structural Adhesives — Chemistry and Technology*. Plenum Press, New York, 1986.
13. Brown, H.R., *Macromolecules*, **26**, 1666 (1993).
14. Dupré, A., *Théorie Mécanique de la Chaleur*. Paris, 1869.
15. Gent, A.N. and Schultz, J., *J. Adhes.*, **3**, 281 (1972).
16. Andrews, E.H. and Kinloch, A.J., *Proc. R. Soc. Lond. Ser. A*, **332**, 385 (1973).
17. Maugis, D. and Barquins, M., *J. Phys. D.*, **11**, 1989 (1978).
18. Maugis, D. In: Lee, L.H. (Ed.), *Adhesive Bonding*. Plenum Press, New York, 1991.
19. Derjaguin, B.V., Muller, V.M. and Toporov, Y.P., *J. Colloid Interface Sci.*, **53**, 314 (1975).
20. Johnson, K.L., *Br. J. Appl. Phys.*, **9**, 199 (1958).
21. Johnson, K.L., *Contact Mechanics*. Cambridge University Press, Cambridge, 1985.
22. Boussinesq, J., *Theory of Elasticity*. McGraw Hill, New York, 1945, p. 338.
23. Tabor, D., *J. Colloid Interface Sci.*, **58**, 2 (1977).
24. Tabor, D., *J. Colloid Interface Sci.*, **67**, 379 (1978).
25. Tabor, D., *J. Colloid Interface Sci.*, **73**, 294 (1980).
26. Derjaguin, B.V., Muller, V.M. and Toporov, Y.P., *J. Colloid Interface Sci.*, **67**, 378 (1978).

27. Muller, V.M., Yushchenko, V.S. and Derjaguin, B.V., *J. Colloid Interface Sci.*, **77**, 91 (1980).
28. Muller, V.M., Yushchenko, V.S. and Derjaguin, B.V., *J. Colloid Interface Sci.*, **92**, 92 (1983).
29. Horn, R.G., Israelachvili, J.N. and Pribac, F., *J. Colloid Interface Sci.*, **115**, 480 (1987).
30. Maugis, D., *J. Colloid Interface Sci.*, **150**, 243 (1992).
31. Mao, K., Sun, Y. and Bell, T., *Surf. Eng.*, **10**, 297 (1994).
32. Sridhar, I., Johnson, K.L. and Fleck, N.A., *J. Phys. D Appl. Phys.*, **30**, 1710 (1997).
33. Johnson, K.L., Personal communication.
34. Maugis, D., *Langmuir*, **11**, 679 (1995).
35. Shull, K.R., Ahn, D. and Mowery, C.L., *Langmuir*, **13**, 1799 (1997).
36. Hui, C.Y., Lin, Y.Y., Baney, J.M. and Jagota, A., *J. Adhes. Sci. Technol.*, **14**, 1297 (2000).
37. Falsafi, A., Tirrell, M. and Pocius, A.V., *Langmuir*, **16**, 1816 (2000).
38. Falsafi, A., Deprez, P., Bates, F.S. and Tirrell, M., *J. Rheol.*, **41**, 1349 (1997).
39. Deruelle, M., Hervet, H., Jandeau, G. and Leger, L., *J. Adhes. Sci. Technol.*, **12**, 225 (1998).
40. Barquins, M.J., *Adhesion*, **26**, 1 (1988).
41. Kim, K.-S., McMeeking, R.M. and Johnson, K.L., *J. Mech. Phys. Solids*, **46**, 243 (1998).
42. Deruelle, M., Marciano, Y., Tirrell, M., Hervet, H. and Leger, L., *Faraday Discuss. Chem. Soc.*, **98**, 55 (1994).
43. Deruelle, M.L., Leger, L. and Tirrell, M., *Macromolecules*, **28**, 7419 (1995).
44. Leger, L., Hervet, H., Marciano, Y., Deruelle, M. and Massey, G., *Isr. J. Chem.*, **35**, 65 (1995).
45. Creton, C., Brown, H.R. and Shull, K.R., *Macromolecules*, **27**, 3174 (1994).
46. Brown, H.R., *Science*, **263**, 1411 (1994).
47. Chaudhury, M.K. and Whitesides, G.M., *Langmuir*, **7**, 1013 (1991).
48. Chaudhury, M.K. and Owen, M.J., *Langmuir*, **9**, 29 (1993).
49. Chaudhury, M.K. and Owen, M.J., *J. Phys. Chem.*, **97**, 5722 (1993).
50. Chaudhury, M.K., *J. Adhes. Sci. Technol.*, **6**, 669 (1993).
51. Silberzan, P., Perutz, S., Kramer, E.J. and Chaudhury, M.K., *Langmuir*, **10**, 2466 (1994).
52. Perutz, S., Silberzan, P., Kramer, E.J. and Cohen, C., *Proc. Adhes. Soc.*, **116** (1995).
53. Ahn, D. and Shull, K.R., *Macromolecules*, **29**, 4381 (1996).
54. Creton, C. and Leibler, L., *J. Polym. Sci. B Polym. Phys.*, **545** (1996).
55. Mangipudi, V.S., Huang, E., Tirrell, M. and Pocius, A.V., *Macromol. Symp.*, **102**, 131 (1996).
56. Tabor, D. and Winterton, R.H.S., *Proc. R. Soc. Lond. Ser. A*, **312**, 435 (1969).
57. Israelachvili, J.N. and Tabor, D., *Proc. R. Soc. Lond. Ser. A*, **331**, 19 (1972).
58. Israelachvili, J.N. and Adams, G.E., *J. Chem. Soc. Faraday Trans.*, **74**, 975 (1978).
59. Patel, S.S. and Tirrell, M., *Annu. Rev. Phys. Chem.*, **30**, 387 (1989).
60. Israelachvili, J.N., *Surf. Sci. Rep.*, **14**, 109 (1992).
61. Thakkar, B.V., Ph.D. Thesis, University of Minnesota, 1991.
62. Merrill, W.W., Pocius, A.V., Thakkar, B.V. and Tirrell, M., *Langmuir*, **7**, 1975 (1991).
63. Mangipudi, V.S., Ph.D. Thesis, University of Minnesota, 1995.
64. Horn, R.G. and Smith, D.T., *Appl. Optics*, **30**, 59 (1991).
65. Levins, J.M. and Vanderlick, T.K., *J. Colloid Interface Sci.*, **158**, 223 (1993).
66. Levins, J.M. and Vanderlick, T.K., *Langmuir*, **10**, 2389 (1994).
67. Mangipudi, V.S., *J. Colloid Interface Sci.*, **175**, 484 (1995).
68. Horn, R.G., Israelachvili, J.N. and Pribac, F., *J. Colloid Interface Sci.*, **115**, 480 (1987).
69. Chen, Y.L., Helm, C.A. and Israelachvili, J.N., *J. Phys. Chem.*, **95**, 1036 (1991).

70. Mangipudi, V.S., Tirrell, M. and Pocius, A.V., *Proc. Adhes. Soc.*, **7** (1996).
71. Johnson, R.E. and Dettre, R.H. In: Berg, J.C. (Ed.), *Wettability*. Marcel Dekker, New York, 1993.
72. Young, T., *Phil. Trans.*, **95**, 82 (1805).
73. Fox, H.W. and Zisman, W.A., *J. Colloid Interface Sci.*, **5**, 514 (1950).
74. Fox, H.W. and Zisman, W.A., *J. Colloid Interface Sci.*, **7**, 109 (1952).
75. Fox, H.W. and Zisman, W.A., *J. Colloid Interface Sci.*, **7**, 528 (1952).
76. Zisman, W.A. In: Gould, R.A. (Ed.), *Contact Angles, Wettability, and Adhesion*. American Chemical Society, Washington DC.; *ACS Symp. Ser.*, **43**, 1964, p. 1.
77. Girifalco, L.A. and Good, R.J., *J. Phys. Chem.*, **61**, 904 (1957).
78. Good, R.J. and Girifalco, L.A., *J. Phys. Chem.*, **64**, 561 (1960).
79. Berthelot, D., *Compt. Rend.*, **126**, 1703, 1857 (1898).
80. Fowkes, F.M., *J. Phys. Chem.*, **66**, 382 (1962).
81. Fowkes, F.M., *Ind. Eng. Chem.*, **56**, 40 (1964).
82. Good, R.J. and Elbing, E., *Ind. Eng. Chem.*, **62**, 54 (1970).
83. Wu, S., *J. Colloid Interface Sci.*, **71**, 605 (1979).
84. Wu, S., *J. Polym. Sci. C*, **34**, 19 (1971).
85. Wu, S., *J. Adhes.*, **5**, 39 (1973).
86. Dann, J.R., *J. Colloid Interface Sci.*, **32**, 302 (1970).
87. Dann, J.R., *J. Colloid Interface Sci.*, **32**, 321 (1970).
88. Mangipudi, V.S., Tirrell, M. and Pocius, A.V., *J. Adhes. Sci. Technol.*, **8**, 1 (1994).
89. Mangipudi, V.S., Tirrell, M. and Pocius, A.V., *Langmuir*, **11**, 19 (1995).
90. Mangipudi, V.S., Tirrell, M. and Pocius, A.V., unpublished results.
91. Lee, A.E., *J. Colloid Interface Sci.*, **64**, 577 (1978).
92. Haidara, H., Chaudhury, M.K. and Owen, M.J., *J. Phys. Chem.*, **99**, 8681 (1995).
93. Israelachvili, J.N., *Proc. R. Soc. Lond. Ser. A*, **20** (1977).
94. Bailey, A.I. and Kay, S.M., *Proc. R. Soc. Lond. Ser. A*, **301**, 47 (1967).
95. Ruths, M. and Granick, S., *Langmuir*, **14**, 1804 (1998).
96. Quon, R.A., Ulman, A. and Vanderlick, T.K., *Langmuir*, **16**, 3797 (2000).
97. Watanabe, H., Matsuyama, S., Mizutani, Y. and Tadao, K., *Macromolecules*, **28**, 6454 (1995).
98. Brown, H.R., Hui, C.-Y. and Raphael, E., *Macromolecules*, **27**, 608 (1994).
99. Brown, H.R., *Annu. Rev. Mat. Sci.*, **21**, 463 (1991).
100. Raphael, E. and de Gennes, P.G., *J. Phys. Chem.*, **96**, 4002 (1992).
101. de Gennes, P.G., *J. Phys. France*, **50**, 2551 (1989).
102. P.G. de Gennes, *C.R. Acad. Sci. Paris*, **318**(II), 165 (1994).
103. Brochard-Wyart, F., de Gennes, P.G., Leger, L. and Marciano, Y., *J. Phys. Chem.*, **98**, 9405 (1994).
104. Golden, J.M. and Graham, G.A.C., *Boundary Value Problems in Linear Viscoelasticity*. Springer-Verlag, Heidelberg, 1988.
105. Graham, G.A.C., *Q. Appl. Math.*, **26**, 167 (1968).
106. Ting, T.C.T., *J. Appl. Mech.*, **33**, 845 (1966).
107. Lee, E.H. and Rogers, T.J., *J. Appl. Mech. Trans. ASME*, **E30**, 127 (1963).
108. Ting, T.C.T., *J. Appl. Mech.*, **35**, 248 (1968).
109. Greenwood, J.A. and Johnson, K.L., *Philos. Mag. A*, **43**, 697 (1981).
110. Schapery, R.A., *Int. J. Fract.*, **11**, 141 (1975).
111. Johnson, K.L., *Book of Abstracts, 216th ACS National Meeting*, Boston, August 23–27, 1998; POLY-282, American Chemical Society, Washington, DC.
112. Schapery, R.A., *Int. J. Fract.*, **39**, 163 (1989).

113. Hui, C.-Y., Baney, J.M. and Kramer, E.J., *Langmuir*, **14**, 6570 (1998).
114. Kamyab, I. and Andrews, E.H., *J. Adhes.*, **56**, 121 (1996).
115. Lake, G.J. and Thomas, A.G., *Proc. R. Soc. Lond. Ser. A*, **300**, 108 (1967).
116. Gent, A.N. and Petrich, R.P., *Proc. R. Soc. Lond. Ser. A*, **310**, 433 (1969).
117. Falsafi, A., Ph.D. Thesis, University of Minnesota, 1998.
118. Ahn, D. and Shull, K.R., *Langmuir*, **14**, 3646 (1998).
119. Luengo, G., Pan, J., Heuberger, M. and Israelachvili, J.N., *Langmuir*, **14**, 3873 (1998).
120. Falsafi, A., Bates F.S. and Tirrell, M., *Macromolecules*, **34**, 1323 (2001).
121. Brown, H.R. and Russell, T.P., *Macromolecules*, **29**, 798 (1996).
122. Kinning, D.J., *Proc. Adhes. Soc.*, 1995, p. 288.
123. Chaudhury, M.K., Weaver, T., Hui, C.Y. and Kramer, E.J., *J. Appl. Phys.*, **80**, 30 (1996).
124. Elman, J.F., Johs, B.D., Long, T.E. and Koberstein, J.T., *Macromolecules*, **27**, 5341 (1994).
125. Kinning, D.J., *J. Adhes.*, **60**, 249 (1997).
126. Choi, G.Y., Kim, S. and Ulman, A., *Langmuir*, **13**, 6333 (1997).
127. Perutz, S., Kramer, E.J., Baney, J., Hui, C.-Y. and Cohen, C., *J. Polym. Sci. B Polym. Phys.*, **36**, 2129 (1998).
128. She, H., Malotky, D. and Chaudhury, M.K., *Langmuir*, **14**, 3090 (1998).

Chapter 3

Particle adhesion

D.S. RIMAI ^{a,*} and D.J. QUESNEL ^b

^a *NexPress Solutions LLC, Rochester, NY 14653-6402, USA*

^b *University of Rochester, Rochester, NY 14627-0132, USA*

1. Introduction

Particle adhesion is a subject that permeates many aspects of a person's daily life. For example, an individual merely has to think of the plethora of products in their own home that are designed solely for the purpose of removing and collecting dust. Familiar items such as vacuum cleaners and mops to sophisticated dust collection systems, including electrostatic air cleaning and HEPA filtration depend on particle adhesion to function properly. New products on the market range from microfiber cloths that take advantage of van der Waals' interactions to disposable tribocharging cloths that take advantage of electrostatic processes to capture dust without solvents. The expanding knowledge base of particle adhesion is improving our day-to-day quality of life.

Before discussing particle adhesion, it is necessary to define a particle. Webster [1] defines a particle as a "minute quantity or fragment" and as "a relatively small or the smallest possible discrete portion or amount of something". However, such a definition begs the question by substituting the words 'minute' and 'small' for 'particle'. Indeed, a chemist or a condensed matter physicist would define the smallest discrete portion of something as being a molecule. Alternatively, compared to the glaciers that readily pushed them around to form landscapes such as Cape Cod and Long Island, boulders are quite minute.

Fortunately, most people have an intuitive feel by what is meant by the terms 'small' and 'particle'. Certainly, a child's toy marble is small compared to a human, but few people would consider it a particle. Similarly, a pebble is small, but is not generally considered a particle. However, a grain of sand or dust is generally considered a particle. A common similarity is that both sand and dust can readily be made to adhere to a substrate (although perhaps marginally so for the sand) even if the substrate is turned upside down. One needs forces that are

* Corresponding author. E-mail: donald_rimai@nexpress.com

large compared to gravity to remove sand from one's feet after a walk on the beach. This criterion can be used as the basis for operationally distinguishing between a small object and a particle. In other words, a small piece of matter is considered a particle if the gravitational force is less than the force needed to detach that object from a typical substrate. Obviously, this definition still begs the question of just what is a typical substrate. In addition, one could question whether the substrate has an especially low surface energy or is unusually tacky, etc. However, in light of everyday experience, one could say that a particle is a fragment of matter with a 'diameter' less than about 100 μm . Conversely, a single molecule of matter would generally not be considered a particle, except in certain cases such as α -particle scattering experiments. Generally, one must have at least a group of molecules or atoms for a fragment of matter to achieve particulate status. Accordingly, one could consider that nanoclusters would comprise the smallest aggregate of matter that would still be termed particles.

As previously mentioned, particle adhesion permeates many aspects of one's daily life. Obviously, the issue of dust under the refrigerator affects everyone. In more technological areas, toner adhesion in electrophotographic devices, such as laser printers and copiers, plays an exemplary role in the problems encountered in particle adhesion. Consider, for example, how an electrophotographic image is formed [2–4]. In this process, toner particles, all being similarly and highly charged, are deposited image-wise on a photoconductor. The toner is then transferred from the photoconductor to paper, generally upon application of an electrostatic field. The fragile toned image (as is readily acknowledged by anyone who has had to remove a paper jam from a printer and wound up with toner on his hands) must then be transported to a fuser, where the toner is melted and permanently fixed to the paper. Any residual toner must then be removed from the photoconductor by cleaning.

Upon consideration of the electrophotographic process, one is presented with several paradoxes. The toner is highly charged and essentially all the toner particles have the same sign charge. Since like charges repel, why can well defined alphanumeric characters and halftone dots be formed, rather than having the toner particles simply fly apart, becoming uniformly distributed on the photoconductor or paper? Similarly, if there are adhesion forces of such magnitude so as to overcome the electrostatic repulsion, why do the toner particles simply not agglomerate into one giant particle? Conversely, it is obvious that electrostatic forces play a significant role in electrophotography. If that were not correct, how would the toner be initially attracted to the photoconductor to form the toned image? Moreover, how would the application of an electrostatic field allow the toner particles to be transferred from the photoconductor to paper? But that brings us back to the first issue. If electrostatics are so important, how is it that thousands of these highly charged particles can be collected into small densely packed areas, as small as the alphanumeric characters in a typical laser-printed document.

While toner particles were used to exemplify a specific technology and lay the groundwork for discussing the scientific issues surrounding particle adhesion, the topic of particle adhesion extends far beyond copiers. For example, let us consider the fabrication of semiconducting devices.

As is well known, when fabricating a semiconducting device, it is crucial that the surface of the crystal be free of particulate contaminants. What is meant by being free of such contaminants has become more stringent in recent years, as the packing density of circuitry has increased. There are two complementary approaches aimed at keeping the crystals free of such contaminants: (1) fabricating the devices in clean rooms; and (2) removing particles from the surfaces of the crystals. The former approach relies on sophisticated means of controlling contamination and air filtration [5], whereas the latter requires stringent cleaning technologies such as the use of ultrasonics and megasonics [6–9], steam and dry laser methods [10], and momentum transfer cleaning such as with CO₂ snow [11]. An added complication is the necessity of identifying and quantifying the presence of particles on a surface without, in the process, generating additional particles or further contaminating the surface [12].

Another technological area that relies on particle adhesion is pharmacology. Consider, for example, an aerosol-dispensed medication. Here, the active ingredient relies on its adhering to inert carrier particles to be dispensed. However, it is crucial that the carrier particles do not adhere to the container walls, or much of the medication would never reach the patient.

Closely related to pharmacology is the area of medicine. Here, too, particle adhesion is important. Consider, for example, the role of particle adhesion in cancer metastasis. As suggested by Anderson and coworkers [13–15], cancer metastasizes when cancer cells detach from the primary cancer site and travel through the blood stream to a secondary site, where they re-adhere. As a cell is but a sophisticated particle, obeying all the laws of nature, is this not simply a manifestation of particle adhesion? Similarly, as discussed by Baier and coworkers [16,17], the adhesion of foreign particles, such as coal dust, asbestos, etc. (including wear-generated particles from surgical implants) can cause a host of complicated active and passive responses, depending on whether the particles adhere to biological sites or migrate to other locations.

The manufacture of sintered parts such as gears and bushings and that of composite materials are, in a sense, also applications of particle adhesion. After all, a sintered part is simply a part manufactured from a powder that has been subjected to conditions that would encourage the particles to strongly cohere. Similarly, a composite material is one where particles of one or more materials are combined in some fashion so as to adhere within a matrix, thereby imparting certain properties to the composite that none of the materials possess in their own right.

In contrast to processes that rely on adhesion to join particles in the fabrication

of parts and materials, wear and polishing processes depend on the ability to generate particles by overcoming adhesion. Consider, for a moment, the removal of particles from a surface by some means of cleaning. Most such methods actually wear away the surface by the process of material transfer because it is generally easier to generate a cohesive failure within the bulk of a material than it is to create a well-defined adhesional failure along an interface or interphase [18]. Indeed, even the ultrasonic cleaning that is commonly used to remove particles from a substrate generates small defects in the substrate from cavitation [19]. Accordingly, there is little conceptual difference between particles adhering to a surface and a surface possessing a similar level of roughness that can be described as asperities. In that sense, the process of polishing consists of contacting the surface with a polishing pad, including polishing compounds that control physical and chemical interactions, in an effort to generate and manipulate the position of particles in a controlled manner. Particles are often removed from the surface in this process. Similarly, wear occurs because of the relative ease of generating small cohesive failures in a material, thereby generating particles that may or may not adhere to the contacting surfaces. These cohesive failures are far more prevalent than well defined separations at interfaces. Lubricants, by their nature, control wear by coating the two surfaces (hence, the need for oils to have low surface energies), thereby keeping the two surfaces apart. Without direct contact, wear particles due to material transfer are less prevalent. Upon separation, the oil layer shears, at stresses below those associated with cohesive failure of the bulk material.

An example that shows that the cohesive strength of a material is less than that of the adhesional strength of the interface is that of the nominal 50,000 mile steel belted radial tire. It is a simple calculation to show that, on average, a tire leaves a monolayer of rubber particles on the road every time it makes a rotation. In essence, the strength of the adhesional bonding between the road and the tire is greater than that of the rubber within the tire.

The process of wear, or, alternatively, the fracture and separation of contacting materials, often generates electrically charged particles in a process known as 'fracto-emission' [20–25]. These charged particles are often attracted to an oppositely charged substrate and can re-entrain, resulting in problems. For example, dust generated upon grinding precision lenses can become captured by the lens. This can result in optical distortion in the final product. A similar example, where the charged particles are generated during a punching operation, is the manufacture of motion picture film. Here, the process of cutting perforations to allow the film to be driven in a camera can generate small, charged particles that then adhere to the film. These can remain on the film and interfere with the subsequent production of the copies that are distributed to the theaters. Ultimately, they are manifest as the speckle that one sees when watching a movie on a wide screen [26].

Once it is recognized that particles adhere to a substrate so strongly that cohesive fracture often results upon application of a detachment force and that the contact region is better describable as an interphase [18] rather than a sharp demarcation or interface, the concept of treating a particle as an entity that is totally distinct from the substrate vanishes. Rather, one begins to see the substrate–particle structure somewhat as a composite material. To paraphrase this concept, one could, in many instances, treat surface roughness (a.k.a. asperities) as particles appended to the surface of a substrate. These asperities control the adhesion between two macroscopic bodies.

Following through on this thought, let us consider the role of adhesives in bonding materials together. First, it should be recognized that smooth, relatively clean solids bond readily. This is clearly illustrated by the commonly experienced difficulty encountered when trying to separate two glass microscope slides. The apparent adhesion is not an effect of air diffusion in a narrow entry path since its force actually increases when the slides are rotated by 90° , allowing more intimate contact of the flat surfaces, but at a reduced area of contact. Nor is it a kinetic effect, since the adhesion lasts for days without diminishing. However, one encounters no such adhesion effects with etched glass or glass with dust on the surface.

Now, let us consider the role of a bonding agent such as the sticky side of a pressure-sensitive adhesive or glue. For a bonding agent to work, it must first wet both surfaces that are to be bonded together. This requires that the surface energy of the bonding agent be lower than that of either surface in order to encourage wetting. From a surface energy viewpoint, the glue-to-substrate bonding is weaker than that of the substrate-to-substrate bonding. This might seem to suggest that glues cannot work. However, the role of the glue is to fill all voids, thereby negating the separating effects of the asperities. The key question then becomes how do the asperities interact with the viscous medium of the adhesive? Treating the asperities as particles bonded to the surfaces of the two substrates, it is readily recognized that much can be learned about adhesive bonding by studying particles adhesion to materials with the appropriate mechanical properties and surface energetics.

At this point one might ask what are the advantages of using particle adhesion analysis to address issues more relevant to macroscopic systems. The answer is quite simple. By studying particle adhesion, much could be learned about the underlying science of adhesion on a microscopic scale without the complications of the external loads encountered at the macroscopic level. For example, it is necessary for the adhesive material on a pressure-sensitive adhesive (PSA) to engulf the asperities on the substrate for adhesion to occur. The PSA has weight and, in addition, loads are normally applied. The heights of the asperities on the substrate normally vary in size and distribution. If someone wanted to determine the work of adhesion between the PSA and the substrate, it would

be quite difficult. Pull-off force measurements could, of course, be performed. These, however, yield results that are quite difficult to interpret. However, the contact radius between spherical particles and the PSA could be readily measured. In addition known loads could be applied to the particle using nanoindenter or cantilever force microscopy techniques. The work of adhesion could readily be determined under equilibrium conditions in this manner. As can be seen, particle adhesion permeates many aspects of daily life. In addition, the use of particles allows the phenomenon of adhesion to be scientifically studied without the complexities of surface irregularities and asperities. This allows scientists to develop an understanding of adhesive mechanisms, which is vital if adhesion is to be well understood.

2. History of particle adhesion

The foundations for the science of modern particle adhesion were laid in the 19th century with the work of Hertz, Boussinesq, and Cerruti.

Hertz [27] solved the problem of the contact between two elastic elliptical bodies by modeling each body as an infinite half plane which is loaded over a contact area that is small in comparison to the body itself. The requirement of small areas of contact further allowed Hertz to use a parabola to represent the shape of the profile of the ellipses. In essence, Hertz modeled the interaction of elliptical asperities in contact. Fundamental in his solution is the assumption that, when two elliptical objects are compressed against one another, the shape of the deformed mating surface lies between the shape of the two undeformed surfaces but more closely resembles the shape of the surface with the higher elastic modulus. This means the deformed shape after two spheres are pressed against one another is a spherical shape.

Often, Hertz's work [27] is presented in a very simple form as the solution to the problem of a compliant spherical indenter against a rigid planar substrate. The assumption of the modeling make it clear that this solution is the same as the model of a rigid sphere pressed against a compliant planar substrate. In these cases, the contact radius a is related to the radius of the indenter R , the modulus E , and the Poisson's ratio ν of the non-rigid material, and the compressive load P by

$$a^3 = \frac{3(1 - \nu^2)R}{4E} P. \quad (1)$$

Boussinesq and Cerruti made use of potential theory for the solution of contact problems at the surface of an elastic half space. One of the most important results is the solution to the displacement associated with a concentrated normal point load P applied to the surface of an elastic half space. As presented in Johnson [49]

these are:

$$u_x = \frac{P}{4\pi G} \left\{ \frac{xz}{\rho^3} - (1-2\nu) \frac{x}{\rho(\rho+z)} \right\} \quad (2)$$

$$u_y = \frac{P}{4\pi G} \left\{ \frac{yz}{\rho^3} - (1-2\nu) \frac{y}{\rho(\rho+z)} \right\} \quad (3)$$

$$u_z = \frac{P}{4\pi G} \left\{ \frac{z^2}{\rho^3} + \frac{2(1-\nu)}{\rho} \right\} \quad (4)$$

where G is the shear modulus, ν is Poisson's ratio, P is the magnitude of the compressive normal point load, and $\rho = (x^2 + y^2 + z^2)^{1/2}$ is the radial distance of the co-ordinate point x, y, z from the origin. These results are consistent with a similar derivation by Timoshenko and Goodier [28] in cylindrical co-ordinates:

$$u_r = \frac{P}{4\pi G} \left\{ \frac{rz}{\rho^3} - (1-2\nu) \frac{\rho-z}{\rho r} \right\} \quad (5)$$

$$u_z = \frac{P}{4\pi G} \left\{ \frac{z^2}{\rho^3} + \frac{2(1-\nu)}{\rho} \right\} \quad (6)$$

where $r = (x^2 + y^2)^{1/2}$ is the radial co-ordinate and ρ is defined as above, namely, $\rho = (r^2 + z^2)^{1/2}$. For isotropic materials, $G = \frac{E}{2(1+\nu)}$ so that on the $z = 0$ plane representing the free surface, the displacements are:

$$u_x = \frac{-P(1+\nu)}{2\pi E} \left\{ (1-2\nu) \frac{x}{r^2} \right\} \quad (7)$$

$$u_y = \frac{-P(1+\nu)}{2\pi E} \left\{ (1-2\nu) \frac{y}{r^2} \right\} \quad (8)$$

$$u_z = \frac{P}{\pi E} \frac{1-\nu^2}{r} \quad (9)$$

$$u_r = \frac{-P(1+\nu)}{2\pi E} \frac{(1+2\nu)}{r} \quad (10)$$

u_x , u_y , and u_z are the cartesian results; u_r and u_z are the results in cylindrical co-ordinates. Note u_z is in the direction of positive P , pressing into the half plane for compressive loading. The tangential displacements of the free surface are towards the origin in agreement with our intuition.

These important results can be combined by superposition to compute the displacement for any arbitrary normal stress distribution applied to the free surface. Similar approaches can be taken for arbitrary tangential stress distributions.

By assuming a radially symmetric pressure (stress) distribution given by an arbitrary function $p(r)$ over the area of contacts such as would be applied by an

indenter over the contacting surface, we write

$$u_z(R) = \frac{1-\nu^2}{\pi E} \int \frac{p(r)}{s} dA = \frac{1-\nu^2}{\pi E} \iint \frac{p(r)}{s} s d\theta ds \quad (11)$$

where R , r , and s are the magnitudes of vectors in the x - y plane such that

$$\mathbf{r} = \mathbf{R} + \mathbf{s}. \quad (12)$$

The integrations are carried out over all non-zero values of $p(r)$. By judicious choice of $p(r)$, $u_z(R)$ can be made to have particular forms such as constant, representing a flat bottom punch and spherical representing a spherical (Hertzian) punch.

The results obtained in this way are the familiar results found by Hertz. More complete treatments of the contact mechanics of particle adhesion are given in Johnson [49] and in Timoshenko and Goodier [28].

Implicit in all these solutions is the fact that, when two spherical indentors are made to approach one another, the resulting deformed surface is also spherical and is intermediate in curvature between the shape of the two surfaces. Hertz [27] recognized this concept and used it in the development of his theory, yet the concept is a natural consequence of the superposition method based on Boussinesq and Cerutti's formalisms for integration of point loads. A corollary to this concept is that the displacements are additive so that the compliances can be added for materials of differing elastic properties producing the following expressions common to many solutions

$$\frac{1-\nu^2}{E} = \frac{1-\nu_1^2}{E_1} + \frac{1-\nu_2^2}{E_2}. \quad (13)$$

Similarly, the assumption that the contact area is small enough that the particle can be represented by an elastic half space allows the radii of the two contacting particles to be combined into a single effective radius that represents how the contacting shapes interact.

$$R = \frac{R_1 R_2}{R_1 + R_2}. \quad (14)$$

This allows for the equivalence between crossed cylinders and the particle on a plane problem. Likewise, the mechanics of two spheres can be described by an equivalently radiused particle-on-a-plane problem. The combination of moduli and the use of an effective radius greatly simplifies the computational representation and allows all the cases to be represented by the same formula. On the other hand, it opens the possibility of factors of two errors if the formula are used without realizing that such combinations have been made. Readers are cautioned to be aware of these issues in the formulae that follow.

Bradley [29,30] and, independently, Derjaguin [31] were the first to recognize that a particle, under the influence of adhesion forces, could act like a Hertzian

indenter. A mathematical description of P , the attractive force, could be combined with Hertz's theory, Eq. 1, to provide a theory of particle adhesion. The question then became "What was the origin and functional form of P ?"

Hamaker [32] first proposed that surface forces could be attributed to London forces, or the dispersion contribution to van der Waals' interactions. According to his model, P is proportional to the density of atoms n_P and n_S in the particle and substrate, respectively. He then defined a parameter A , subsequently becoming known as the Hamaker constant, such that

$$A = \pi^2 n_P n_S \lambda \quad (15)$$

where λ is the London-van der Waals constant for that particular system. The interaction energy was then calculated by integrating over the volume of the contacting materials and the force determined by differentiating the energy with respect to distance. Accordingly, for two spheres of radii R_1 and R_2

$$P = \frac{A}{6z_0^2} \frac{R_1 R_2}{R_1 + R_2} \quad (16)$$

where z_0 is the separation distance between the two objects. The parameter z_0 is typically assumed to be approximately 4 Å from the interatomic spacings of van der Waals' bonded solids such as argon. For a sphere in contact with a planar substrate, Eq. 3 reduces to

$$P = \frac{AR}{6z_0^2}. \quad (17)$$

This model was later expanded upon by Lifshitz [33], who cast the problem of dispersive forces in terms of the generation of an electromagnetic wave by an instantaneous dipole in one material being absorbed by a neighboring material. In effect, Lifshitz gave the theory of van der Waals' interactions an atomic basis. A detailed description of the Lifshitz model is given by Krupp [34].

By combining Hertz's contact theory (Eq. 1) and with Hamaker's functional form for the attractive force (Eq. 17), the Derjaguin model takes the form

$$a^3 = \frac{A(1-\nu^2)}{8z_0^2 E} R^2. \quad (18)$$

This expression relates the action-at-a-distance forces between atoms to the macroscopic deformations and dominated adhesion theory for the next several decades. The advent of quantum mechanics allowed the interatomic interactions giving rise to particle adhesion to be understood in greater depth.

From a quantum mechanical perspective, an atom or molecule would be considered to have no permanent dipole moment if the probability of finding electrons is symmetric about the nucleus. For example the probability of finding the electron in the ground state of hydrogen is constant with respect to its solid

angle position. As a result, there is no permanent dipole moment. However, an electron can still be localized to a particular position at a given instance, thereby creating an instantaneous dipole. This atom can, then, emit what is referred to as a virtual photon. That photon is then absorbed by a neighboring atom, thereby correlating the positions of the electrons, or instantaneous dipole moment, of that second atom. Details of correlation functions and the generation and absorption of virtual photons comes under the topics of Green's functions and Feynman diagrams and is beyond the scope of this chapter.

With the reader bearing in mind this framework, the Lifshitz theory of van der Waals' interactions can readily be understood. According to the Lifshitz theory, van der Waals' forces arise from the absorption of photons of frequency ω by a material with a complex dielectric constant

$$\varepsilon(\omega) = \varepsilon'(\omega) + i\varepsilon''(\omega) \quad (19)$$

where the $\varepsilon'(\omega)$ is related to the polarizability of the material and $\varepsilon''(\omega)$ is related to the energy dissipation within the material. After some calculation, as presented by Krupp [34], the force of attraction between a particle and a planar substrate is determined to be, according to the Lifshitz model,

$$F = \frac{\hbar \varpi}{8\pi z_0^2} R \quad (20)$$

where

$$\varpi = \int_0^\infty \left[\left(\frac{\varepsilon' - 1}{\varepsilon' + 1} \right) \left(\frac{\varepsilon'' - 1}{\varepsilon'' + 1} \right) \right] d\xi \quad (21)$$

and ξ represents the complex frequency.

By comparing Eqs. 17 and 20, it is clear that the Lifshitz's and Hamaker's treatments of particle adhesion are equivalent if

$$\hbar \varpi = \frac{4\pi}{3} A. \quad (22)$$

By combining Eqs. 1, 20, and 22, the Derjaguin model, once again, takes the form

$$a^3 = \frac{A(1 - \nu^2)}{8z_0^2 E} R^2. \quad (23)$$

but now has a justification rooted in quantum theory.

The detachment of a particle from a surface is accomplished by adding a term corresponding to a negative load to Eq. 17 or its quantum mechanical counterpart, Eq. 20. This load can be due to gravitational effects in the case of sufficiently large particles. Alternatively, it can be due the centrifugal force experience by the particle in an ultracentrifuge, an electrostatic field acting on

a charged particle, etc. As there are no constraints on the values that the total force can have, detachment would occur when the attractive force given by Eq. 17 (or Eq. 20) is balanced by an equal but opposite applied force. Upon application of a negative load, a continually decreases, with detachment occurring when the contact radius vanishes, that is, when there is no net attractive force. In other words, the work needed to create the adhesion-induced deformation is all stored as elastic energy and is all recovered upon separation. Further, the force of attraction is not influenced by the changes in geometry or the particle and substrate during the adhesion-induced deformation. As a result, there is no difference between the size of the attractive force and that needed to detach the particle from the substrate. As will be seen shortly, this is incorrect. Also worth noting is that, according to Eq. 18, the contact radius varies as $R^{2/3}$ and $E^{-1/3}$. As will be seen, these dependencies are characteristics of adhesion theories that assume elastic deformations and, as such, they can be used to differentiate elastically deforming systems from plastically deforming systems.

Krupp [34] was the first to recognize that the stresses arising from surface forces could be sufficiently large to cause the contacting materials to plastically deform. Indeed, Rimai et al. [35] using the analysis of Bowling [36], estimated the adhesion-induced stress of polystyrene particles on a silicon wafer to be approximately a gigapascal. This is close to the Young's modulus of polystyrene and well in excess of its yield strength. Krupp divided the contact zone into two regions: an inner region that was subjected to the highest stresses and, therefore, would deform plastically; and an outer, annular region that, being subjected to lower stresses, would deform elastically. He then calculated the inner and total contact radii by assuming a phenomenologically determined time-dependent hardness. As was the case with the Derjaguin model, only compressive stresses were considered.

3. Current particle adhesion

The era of modern particle adhesion can be thought of commencing with the work of Johnson, Kendall and Roberts [37] (often referred to as the JKR theory), although the mathematical development of the contact mechanics leading up to that theory was done by Johnson [38] much earlier. Experimentally, Roberts [39], using rubber spheres and Kendall [40], using glass spheres observed that the contact areas under low load were considerably larger than those predicted by Hertzian theory and tended towards a finite value as the applied load vanished, suggestive of strong adhesive effects.

Johnson, Kendall and Roberts used an energy-based contact mechanics approach to understand particle adhesion. In their theory, they deviated from the earlier Derjaguin and Krupp models by assuming that tensile stresses are present

near the perimeter of the contact region rather than having only compressive stresses. Furthermore, it was also assumed that all stresses occurred within the contact radius, thereby precluding any long-range interactions.

The so-called 'JKR equation' relates the adhesion-induced contact radius a to the particle radius R and the applied load P by

$$a^3 = \frac{R}{K} \left\{ P + 3w_A\pi R + [6w_A\pi RP + (3w_A\pi R)^2]^{1/2} \right\} \quad (24)$$

where K is given by

$$K = \frac{4}{3\pi(k_1 + k_2)} \quad (25)$$

and

$$k_i = \frac{1 - \nu_i^2}{\pi E_i}. \quad (26)$$

Furthermore, ν_i and E_i refer to the Poisson's ratio and Young's modulus of each of the contacting materials. Finally, w_A represents work of adhesion. It is related to the surface energies γ_1 and γ_2 of the two materials and their interfacial energy γ_{12} by

$$w_1 = \gamma_1 + \gamma_2 - \gamma_{12}. \quad (27)$$

A detailed derivation of the JKR equation is presented in Chapter 2.

There are several distinctive features worth noting about the JKR equation. The first is in the limit of no adhesion (or, equivalently, large applied loads, as commonly occurs with macroscopic particles), Eq. 24 reduces to the Hertz equation

$$a^3 = \frac{RP}{K}. \quad (28)$$

Conversely, in the absence of any applied load, Eq. 24 reduces to

$$a = a(0) = \left(\frac{6\pi w_A}{K} \right)^{1/3} R^{2/3}. \quad (29)$$

The JKR model predicts that the contact radius varies with the reciprocal of the cube root of the Young's modulus. As previously discussed, the $2/3$ and $-1/3$ power-law dependencies of the zero-load contact radius on particle radius and Young's modulus are characteristics of adhesion theories that assume elastic behavior.

The process of exerting a force to detach a particle from a substrate can be considered simply as the application of a negative load. As can be seen from Eq. 24, the effect of such a load is to monotonically decrease the contact radius from its no-load value of $a(0)$ with increasing magnitude of that load. However, the

contact radius predicted by Eq. 24 is real. Therefore all solutions to Eq. 24 must be real. Accordingly, the radical in Eq. 24 cannot be less than zero. Therefore, separation of the particle from the substrate must occur upon application of a load P_S such that

$$P_S = -\frac{3}{2}w_A\pi R. \quad (30)$$

It should be noted that Eq. 30 is independent of the Young's modulus of both the particle and substrate.

It is apparent that, in order to satisfy Eq. 30, the JKR model requires that detachment occurs, not when the contact radius vanishes, as might at first be thought, but rather at a finite value $a_S \approx 0.63a(0)$.

As indicated, an implicit assumption of the JKR theory is that there are no interactions outside the contact radius. More specifically, the energy arguments used in the development of the JKR theory do not allow specific locations of the adhesion forces to be determined except that they must be associated with the contact line where the two surfaces of the particle and substrate become joined. Adhesion-induced stresses act at the surface and not a result of action-at-a-distance interatomic forces. This results in a stress singularity at the circumference of the contact radius [41]. The validity of this assumption was first questioned by Derjaguin et al. [42], who proposed an alternative model of adhesion (commonly referred to as 'the DMT theory'). Needless to say, the predictions of the JKR and DMT models are vastly different, as discussed by Tabor [41].

Whereas the JKR model approached the topic of particle adhesion from a contact mechanics viewpoint, the DMT theory simply assumes that the adhesion-induced contact has the same shape as a Hertzian indenter. The normal pressure distribution $P_H(r)$ for the Hertzian indenter is related to the repulsive force F_e and the distance from the center of the contact circle to the point represented by r according to the relationship [49]

$$P_H(r) = \frac{3F_e}{2\pi a^2} \left(1 - \frac{r^2}{a^2}\right)^{1/2}. \quad (31)$$

Equilibrium is established when the attractive surface forces are balanced by elastic repulsion forces between the materials. The DMT model states that the elastic repulsion force F_e is related to the attractive force within the contact region F_S by

$$F_S = \frac{F_e}{2}. \quad (32)$$

This implies that, according to the DMT model, exactly half of the attractive interactions occur outside the zone of contact and half of the attractive interactions occur inside the zone of contact.

The fundamentally different assumptions between the JKR and DMT theories result in vastly different predictions made by these two theories, even though both models are based on the occurrence of small scale elastic Hertzian deformations resulting from the forces of adhesion. The differences in the theories arise from the means of representing adhesion. The JKR formalism uses changes in surface energy to generate forces while the DMT theory invokes action-at-a-distance interatomic interactions based on the Hamaker approach. For example, since the DMT model assumes that the contact is Hertzian against a rigid substrate, the contact radius a varies with the load P as

$$a = \left[\frac{3}{4} P \left(\frac{1 - \nu_1^2}{E_1} + \frac{1 - \nu_2^2}{E_2} \right) \frac{R_1 R_2}{R_1 + R_2} \right]^{1/3} \quad (33)$$

where the subscripts 1 and 2 designate each of the two materials. $R_2 = \infty$ represents the sphere on plane problem important in adhesion. If there were no adhesion, separation would simply occur whenever there was no applied load. However, since adhesion does occur, a negative load must be applied in order to cause the particle to separate from the substrate. The necessary load to effect detachment, according to the DMT theory as interpreted by Tabor [43], is related to the work needed to create two free surfaces and is given by

$$P_S = -2w_A \pi R \quad (34)$$

As can be seen, the DMT detachment force is greater than that predicted by the JKR theory.

The equilibrium contact radius is determined by substituting the attractive force experienced by the particle into Eq. 33. Accordingly,

$$a_0 = \left\{ \frac{3\pi w_A R^2}{4} \left[\left(\frac{1 - \nu_1^2}{E_1} \right) + \left(\frac{1 - \nu_2^2}{E_2} \right) \right] \right\}^{1/3} \quad (35)$$

Rewriting Eq. 35 in terms of the stiffness K

$$a_0 = \left(\frac{\pi w_A}{K} \right)^{1/3} R^{2/3} \quad (36)$$

Upon comparison of Eqs. 29 and 36, it is readily apparent that both theories predict the same power law dependence of the contact radius on particle radius and elastic moduli. However, the actual value of the contact radius predicted by the JKR theory is $\sqrt[3]{6}$ that predicted by the DMT model. This implies that, for a given contact radius, the work of adhesion would have to be six times as great in the DMT theory than in the JKR model. It should be apparent that it is both necessary and important to establish which theory correctly describes a system.

The discrepancies between the predictions of the JKR and DMT theories were first discussed by Tabor [41]. Tabor's discussion resulted in a rather heated exchange in the literature [42,43]. Subsequently, Muller et al. [44,45] attempted to

resolve these discrepancies by calculating the shape of the contact using numerical simulations and assuming that the particle–substrate interactions can be described using a Lennard-Jones potential using a pair-wise summation between atoms in each material. According to Muller’s model (henceforth referred to as the MYD model) both the JKR and DMT theories have their ranges of validity, with the DMT theory being valid for small, hard particles and the JKR model holding for large particles and more compliant materials. The range of validity for each theory is defined in terms of a dimensionless parameter μ such that

$$\mu = \frac{32}{3\pi} \left[\frac{2Rw_A^2}{\pi E^* z_0^3} \right]^{1/3} \quad (37)$$

where z_0 is the particle–substrate separation distance and E^* is the reduced Young’s modulus and is given by

$$\frac{1}{E^*} = \frac{(1 - \nu_1^2)}{E_1} + \frac{(1 - \nu_2^2)}{E_2}. \quad (38)$$

According to the MYD model, values of $\mu > 1$, corresponding to compliant, higher surface energy materials and relatively large particles, are properly described by the JKR theory. Conversely, for values of $\mu < 1$, corresponding to more rigid, lower surface energy materials and smaller particles, the DMT theory should properly describe the system. These results imply that, if the DMT theory has any actual range where it realistically predicts particle adhesion, it would have to be in the range of very small (submicrometer) particles even for fairly high modulus materials. However, insofar as asperities can also be treated as particles, one can ponder why, in light of the MYD analysis, does not the DMT model accurately describe most particle–substrate contacts. The resolution of this discrepancy will be discussed shortly.

It is somewhat disconcerting that the MYD analysis seems to present a sharp transition between the JKR and DMT regimes. Specifically, in light of the vastly different response predicted by these two theories, one must ponder if there would be a sharp demarcation around $\mu = 1$. This topic was recently explored by Maugis and Gauthier–Manuel [46–48]. Basing their analysis on the Dugdale fracture mechanics model [49], they concluded that the JKR–DMT transition is smooth and continuous.

The MYD analysis assumes that the atoms do not move as a result of the interaction potential. The consequences of this assumption have recently been examined by Quesnel and coworkers [50–55], who used molecular dynamic modeling techniques to simulate the adhesion and release of 2-dimensional particles from 2-D substrates. Specifically, both the Quesnel and MYD models assume that the atoms in the different materials interact via a Lennard-Jones potential ϕ given

by

$$\phi = -4\varepsilon \left[\left(\frac{\sigma}{r} \right)^6 - \left(\frac{\sigma}{r} \right)^{12} \right] \quad (39)$$

where ε is the binding energy between one atom and its nearest neighbor and σ represents the spacing between atoms when the potential is zero. However, whereas the MYD model assumes that the mechanical properties of the materials are independent of their surface energetics and, therefore, the atoms in one material do not relocate as a result of any interactions with the other, the Quesnel model assumes that once the interatomic potential is defined, all interatomic interactions are determined. This allows the atoms in one material to relax under the influence of the stresses generated by the atoms in the second material. According to molecular dynamic modeling by Quesnel et al. [50–55], particle detachment appears to occur at a finite contact radius consistent with the JKR predictions, but inconsistent with those of the DMT theory. These results held independently of the Young's modulus and surface energies of the materials and even for very small particles — conditions that, according to the MYD calculations, should be within the DMT regime. The Quesnel results suggest that the assumptions built into the MYD model may over constrain the system, thereby losing some significant physics. Unfortunately, due to computer limitations (not fundamental limitations of the model), the systems that Quesnel et al. [50–55] were able to examine were limited to hundreds of atoms and, in some cases, to 2-dimensional particles and substrates. Further research is needed to resolve the issues raised by Quesnel and coworkers.

The dependence of the contact radius on particle radius was studied by DeMejo et al. [56] for a quintessential JKR system consisting of soda-lime glass particles, whose radii ranged between approximately 1 and 100 μm , on a polyurethane substrate ($E = 5 \text{ MPa}$). In their study, the authors determined the particle and contact radii using scanning electron microscopy (SEM) and an 88° tilt angle. The power-law dependence of the contact radius on particle radius, determined by linearly regressing $\log(a)$ on $\log(R)$, shown in Fig. 1, was found to be 0.68. This result is in good agreement with both the JKR and DMT models. However, the work of adhesion, as determined from the JKR model, was 0.17 J/m^2 . This value is reasonable for a system consisting of these particles on this type of substrate.

However, if one attempted to determine w_A from the DMT theory, one would get an unrealistically large value. In the same paper, the authors also presented micrographs of particles in contact with the substrate under a negative applied load that was not quite sufficient to effect detachment. It was reported that the observed contact radius under those circumstances was approximately 70% of the expected contact in the absence of the applied load. This observation is in apparent agreement with the JKR prediction that detachment occurs under negative loads that reduce the contact to about 63% of the equilibrium contact radius.

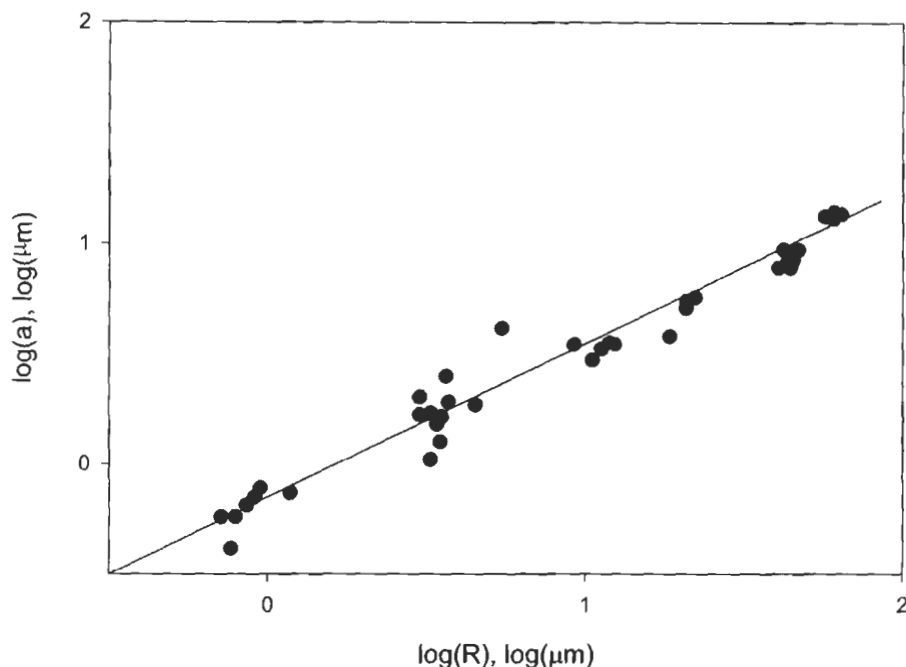


Fig. 1. Log-log plot of the contact radius as a function of particle radius for soda-lime glass particles on polyurethane (from ref. [56]).

Rimai et al. [57] determined the power-law dependence of the contact radius on the substrate's Young's modulus for another quintessential JKR system: that of a soda-lime glass particles on polyurethane substrates. They reported that the contact radius varied as $E^{-1/3}$, with w_A calculated to be 0.12 J/m^2 . The results of these two studies provides strong evidence supporting the JKR theory under certain circumstances.

Lest one be lulled into a false sense that, assuming that the JKR theory properly describes particle adhesion within its regime, DeMejo et al. [56] also reported that, for soda-lime glass particles with radii less than about $5 \mu\text{m}$, the contact radius varied, not as the predicted $R^{2/3}$, but, rather, as $R^{3/4}$. Similar results were reported for other systems including polystyrene spheres on polyurethane [58], as shown in Fig. 2, and for glass particles having radii between about 1 and $100 \mu\text{m}$ on a highly compliant, plasticized polyurethane substrate [59] as illustrated in Fig. 3.

There have been several theories proposed to explain the anomalous $3/4$ power-law dependence of the contact radius on particle radius in what should be simple JKR systems. Maugis [60], proposed that the problem with using the JKR model, per se, is that the JKR model assumes small deformations in order to approximate the shape of the contact as a parabola. In his model, Maugis re-solved the JKR problem using the exact shape of the contact. According to his calculations, a should vary as R^y , where $2/3 \leq y \leq 1$, depending on the ratio a/R .

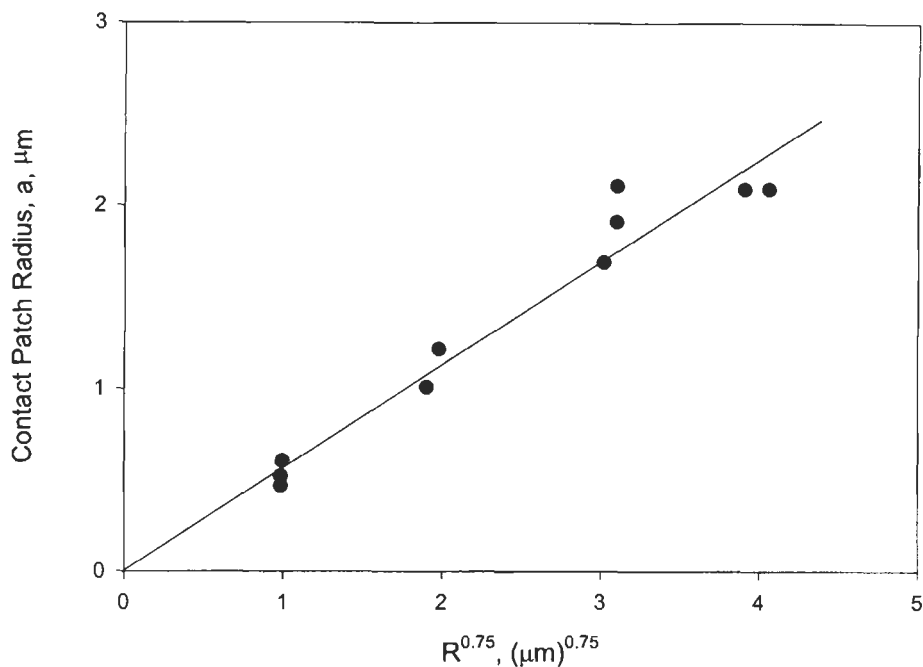


Fig. 2. Contact radius as a function of particle radius to the 3/4 power for polystyrene on polyurethane (from ref. [58]).

Although his approach is logical and Maugis does extend the JKR model to large contact radii, his theory, by itself, does not explain the observed 3/4 power-law dependence. As discussed by Rimai et al. [61], only two values of the exponent have been observed experimentally: 2/3 and 3/4. Maugis' hypothesis calls for a continuous change in exponent with the ratio a/R , a phenomenon that has not been observed experimentally. Moreover, according to Maugis' model, the exponent should only depend on the ratio of a/R . However, as discussed by Rimai et al. [61], the transition point varies with the specific substrate even if the physical properties of the substrate other than Young's modulus are quite similar. Finally, the observed transition between the particle size range where the contact radius varies as $R^{2/3}$ to the range where a varies as $R^{3/4}$ is quite sharp, with no evidence of the curvature that would be expected if there were a continuous range of exponents, as predicted by Maugis.

An alternative explanation has been proposed by Quesnel [62]. Assuming that the adhesion-induced deformation could be treated as a Hertzian indenter, with the load due to the force arising from the surface energy, Quesnel calculated the indentation in a self-consistent manner. That is to say, Quesnel recognized that the attractive force would vary as the particle or substrate deformed, owing to the increased circumference of the contact patch. He also recognized that, due to

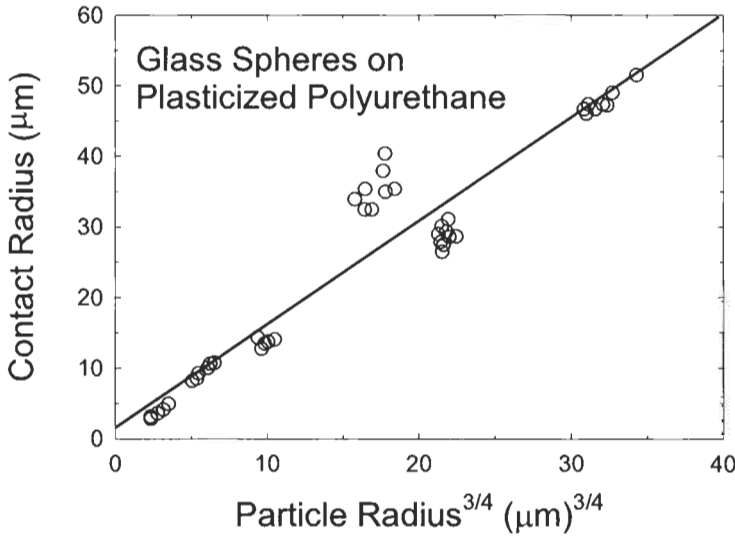


Fig. 3. Plot of the a for glass particles as a function of $R^{3/4}$ on a highly compliant polyurethane substrate (from ref. [59]).

geometric considerations, the contact area would be different for a rigid particle indenting a compliant substrate than for a compliant particle flattening against a rigid substrate. Specifically, Quesnel related the load P to the interaction potential ϕ by

$$P = -\frac{d\phi}{d\Delta} = -w_A \frac{dA}{d\Delta} \approx -w_A \frac{\delta A}{\delta \Delta} \quad (40)$$

where Δ represents the shift in the center of mass of the particle relative to the plane, δA is a variation in A , and variation $\delta \Delta$ is a variation in Δ . By the ratio of similar triangles, this is found to be

$$\Delta = \frac{a^2}{R} \quad (41)$$

so

$$\delta \Delta = 2a\delta a/R \quad (42)$$

where δa is a variation in the contact patch radius. This relationship holds for both the compliant sphere on a rigid substrate and a rigid sphere on a compliant substrate.

For the compliant sphere against a rigid substrate, the contact area is a flat circle of radius a so that

$$A = \pi a^2 \quad (43)$$

or

$$\delta A = 2\pi a \delta a. \quad (44)$$

For the case where the substrate is rigid compared to the particle, substitution of Eqs. 40–44 into the Hertz equation (Eq. 1) gives

$$a = \sqrt[3]{\frac{3}{4} w_A \pi \left(\frac{1 - \nu_S^2}{E_S} + \frac{1 - \nu_P^2}{E_P} \right)} R^{2/3} \quad (45)$$

which is the familiar dependence of the contact radius on the particle radius to the 2/3 power and is identical to the DMT expression, Eq. 35.

However, for the case of the rigid particle indenting a compliant substrate, the change in area, which arises from the stretching of the surface of the substrate, is given by the expansion in size of a spherical cap.

$$\delta A = 2\pi \sqrt{\frac{R^2}{R^2 - a^2}} a \delta a. \quad (46)$$

Upon substituting this relationship into the Hertz equation and solving numerically, Quesnel found that a varied as $R^{0.771}$. For situations of intermediate compliance ratios, it is logical to expect the dependence on R to be bounded by these extremes.

Thus the Quesnel model predicts a range of power law values from 2/3 to 0.771 depending on the ratio of the elastic modulus of the particle and the substrate. The 2/3 behavior is for a compliant particle and the 0.771 is for a compliant substrate. The transition should be smooth with changes in modulus, but does not depend on the size of the particle.

Other ideas proposed to explain the 3/4 power-law dependence include effects due to viscoelasticity, non-linear elasticity, partial plasticity or yielding, and additional interactions beyond simply surface forces. However, none of these ideas have been sufficiently developed to enable predictions to be made at this time. An understanding of this anomalous power-law dependence is not yet present.

Up to this point, the discussion has been limited to cases where the adhesion-induced stresses result in elastic deformation. However, as previously discussed, this need not be the case. Indeed, these stresses can be, in many instances, comparable to the Young's moduli of the contacting materials, often resulting in plastic deformations. This area has been most notably explored by Maugis and Pollock [63].

According to the theory proposed by Maugis and Pollock, hereafter referred to as the MP model, if the adhesion induced stresses cause at least one of the contacting materials to yield and undergo a totally plastic response, the contact region formed will increase in size until the force causing the yielding is balanced

by the force needed to further expand the contact. In essence, the applied load P and the adhesion-induced attractive force is balanced by the hardness H of the material so that

$$P + 2\pi w_A R = \pi a^2 H. \quad (47)$$

As also discussed by Maugis and Pollock, the hardness of the material is related to its yield strength Y by $H = 3Y$. The factor of 3 is a consequence of the deformation constraints of the indenter geometry used in hardness measurements.

In the absence of an applied load, the MP theory predicts that

$$a = \sqrt{\frac{2w_A}{3Y}} R^{1/2}. \quad (48)$$

As is evident, there are several distinctive characteristics of adhesion-induced plastic deformations, compared to elastic ones. Perhaps the most obvious distinction is the power-law dependence of the contact radius on particle radius. Specifically, the MP model predicts an exponent of $1/2$, compared to the $2/3$ predicted by either the JKR or DMT models.

An example of a Maugis–Pollock system is polystyrene particles having radii between about 1 and 6 μm on a polished silicon substrate, as studied by Rimai et al. [64]. As shown in Fig. 4, the contact radius was found to vary as the square root of the particle radius. Similar results were reported for crosslinked polystyrene spheres on SiO_2 /silicon substrates [65] and micrometer-size glass particles on silicon substrates [66].

Recently, Rimai et al. [67] determined the power-law dependence of glass particles to a thermoplastic substrate containing between 0 and 20% plasticizer. They found that, when the levels of plasticizer were low so that the ambient temperature T was less than the glass transition temperature T_g of the substrate so that the substrate was in the glassy state, the contact radius varied as the particle radius to the $1/2$ power. Alternatively, when $T > T_g$, so that the substrate was in the rubbery state, a varied as $R^{2/3}$. In general, experimental results obtained to date show behavior consistent with adhesion theories that assume elastic response only when one of the materials is elastomeric. In those instances when the contacting materials have higher Young's moduli (≥ 3 GPa), the power-law dependence of the contact radius on particle radius is consistent with plastic, rather than elastic, response. In other words, the present results might seem to suggest that there are two distinct regions of adhesion-induced deformations: the JKR regime, in which at least one of the materials is elastomeric; and the MP regime, for higher modulus materials.

Detachment of a particle from a substrate when plastic deformations have occurred is somewhat a more complicated problem than in the case of simple elasticity. Essentially, one has to first determine if the detachment occurs because of a cohesive or interfacial failure and whether the failure is ductile or brittle. For

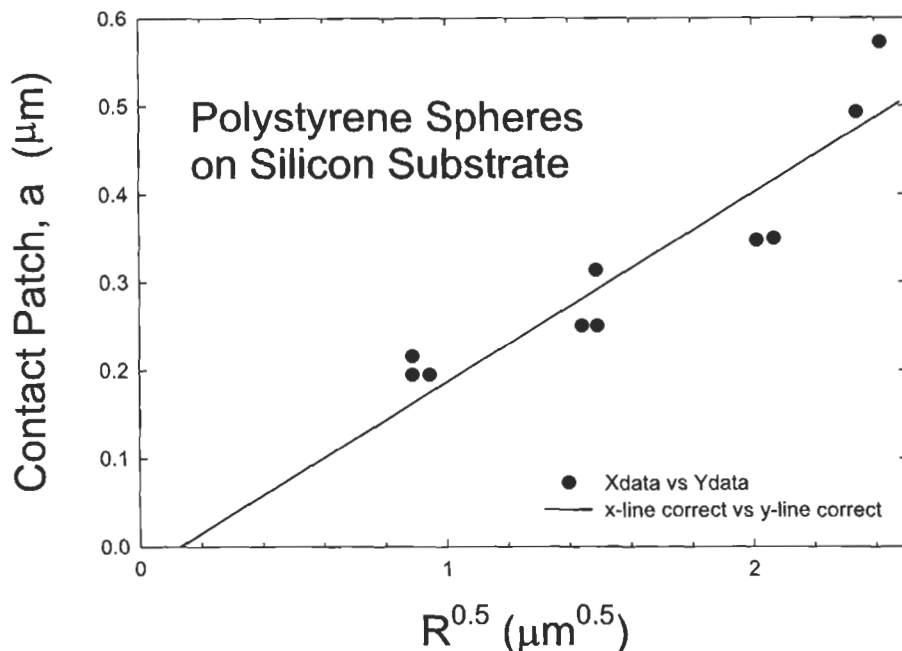


Fig. 4. The contact radius as a function of the square root of the particle radius for polystyrene spheres on a silicon substrate (from ref. [64]).

the case of a ductile failure, the detachment force will depend upon the contact radius when detachment occurs. In the simple case where detachment occurs in a ductile manner from the equilibrium contact radius, Eq. 47 can be used to show that

$$P_s = -\pi a(0)^2 H. \quad (49)$$

Alternatively, if detachment is associated with a brittle failure, then one must first determine if the fracture followed an elastic loading where an elastic model such as the JKR theory is appropriate or if it follows a plastic or elastic-plastic loading. In this latter case, the force needed to detach the particle from the substrate depends on the specific properties of the materials and the details of the deformations [63].

4. Origins of adhesion forces

Let us now turn our attention to understanding the nature of the interactions giving rise to the adhesion of particles to surfaces. First, one should recognize that most particles commonly encountered have been exposed to ambient conditions for lengthy times. As a result, any functionally reactive groups on the particles

have probably reacted, resulting in, in general, fairly inert particles. This is not always true, of course. Lee [68], for example, studied the adhesion of particles of lunar dust. The atmospheric pressure on the moon is between 10^{-12} and 10^{-16} Torr. In addition, the daytime temperature reaches 400 K [68]. As a result, the particles have not interacted with the ambient and can be considered to have clean surfaces. In his studies, Lee concluded that the adhesion of the lunar dust particles is governed by Lewis acid–base interaction.

Another exception to the rule of contaminated surfaces involves very small particles, generally referred to as nanoclusters. These are generally formed and the adhesion of these particles to substrates studied in situ, under ultrahigh vacuum conditions. Owing to the vacuum and the short existence of these particles prior to deposition, it is possible for chemistry to occur.

Still another area where chemical and physical interactions can occur involves the enhancement of particle adhesion due to capillary condensation [69]. However, for the purposes of the present discussion, let us limit ourselves to dry particles.

With these caveats, it is clear that, in general, particle adhesion is governed by physical, rather than chemical, interactions. Therefore, let us turn our attention to understanding the nature of the physical interactions that lead to the adhesion of particles to substrates.

Of the four types of forces generally referred to in physics texts — the strong and weak nuclear interactions, electromagnetic interactions, and gravitational forces, it is quite clear that the size scale of particle interactions is sufficiently large so as to preclude either of the nuclear interactions. Gravitational forces are important in understanding the deposition of particles on surfaces. Indeed, for a sufficiently large particle — say greater than about 100 μm in radius, the largest force attracting a particle to a surface may be gravity. However, as discussed in the introduction, one generally limits the concept of a particle to smaller structures. Therefore, we can ignore gravity for the purposes of the present discussion. That limits the source of particle adhesion to electromagnetic interactions.

Magnetic interactions are important for certain classes of particles. Everyone, for example, is familiar with iron filings adhering to various steel objects. Perhaps less familiar, but at least equally important, is the adhesive properties of magnetic carrier particles in electrophotographic engines [2–4]. However, the extent to which magnetic interactions are important is limited by the relatively small number of particles which interact magnetically. Perhaps because of this reason, research in this area has also been limited. For those reasons, as well as space constraints, a discussion of magnetic interactions will not be pursued here.

The majority of particles adhere to surfaces, as well as to each other, through electrical interactions. These can be either electrostatic, due to the presence of a static charge on the particle, or electrodynamic, as might be the case for London or van der Waals forces. Indeed the relative roles of both of these types of interactions has been the subject of much debate for many years [70–78].

Complicating the problem [34,79,80] of determining whether particle adhesion is dominated by electrostatics or by electrodynamics is that particles rarely are simple, homogeneous, spherical particles. Rather, they tend to be irregular in shape. As previously discussed in this article, since van der Waals' forces are short ranged compared to electrostatic forces, such irregularities or asperities tend to reduce such forces. Moreover, the charge, rather than being uniformly distributed on the particles, may lie predominantly on those same asperities, thereby increasing the effect of the electric charge [81]. Further complicating this situation is the fact that the charge on the particle may vary due to contact electrification, thereby affecting adhesion. While studying the adhesion between two smooth silica surfaces, one of which was coated with an amine terminated monolayer of dimethylethoxysilane, Horn et al. [82,83] and Smith [84] reported an increase in the force needed to separate the materials, measured using an atomic force apparatus [85], as a result of their contact. The surfaces were uncharged prior to contact and possessed a charge of -2 to -3 mC/m² on the bare silica after contact with an equal and opposite charge on the coated substrate. More recently, Gady et al. [86] reported an increase in the attraction of a polystyrene particle to a graphite substrate after each contact, corresponding to a transfer of electrons. These are examples of contact electrification which produce measurable changes in apparent adhesion.

5. Electrostatic forces

Let us first consider the role of electrostatic forces. To do this, we will start with the simplest case of a spherical, uniformly charged, dielectric particle on a grounded, conducting planar substrate.

As is well known, an electrically charged particle will experience a force of attraction to a grounded conducting substrate. This force arises from the fact that the charged particle will generate an electric field. However, charge within a conducting body flows so as to exclude any electric field from within that material. The material becomes polarized, with the charge in the substrate arranging itself so that the charge opposite of that on the particle is located closer to the particle. This results in a net attractive force. However, it must be remembered that, because the substrate is grounded, its potential must be zero everywhere. This can only be accomplished if the charge distribution within the substrate is mathematically equivalent to a point charge located an equal distance into the substrate as the center of the particle is above the surface of the substrate. With this realization, the attractive force can readily be calculated. Because of its similarity to a reflected image in a mirror, this is generally referred to as the 'method of images' [87,88], and is illustrated in Fig. 5a. To illustrate this concept, let us first consider a spherical particle of radius R having a uniform, fixed charge density ρ . Separated

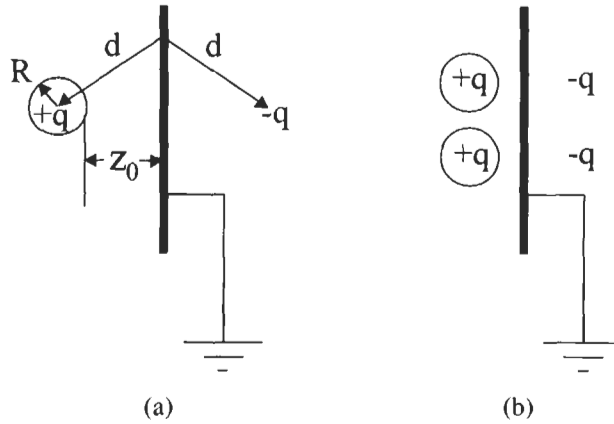


Fig. 5. Electrostatic image charges induced in a grounded, conducting substrate due to the presence of 1 (a) and 2 (b) charged spherical particles.

from the surface of this particle by some distance z_0 is the planar surface of an electrically conducting, grounded plane. This is shown in Fig. 5a.

The force of attraction, calculated from Coulomb's law, for a uniformly charged, spherical, particle in contact with a grounded, conducting substrate is simply

$$F = \frac{1}{4\pi\epsilon_0} \frac{q^2}{[2(R + z_0)]^2}, \quad (50)$$

where z_0 is the separation distance and the factor of 2 comes from the fact that the image charge is located an equivalent distance into the substrate as the center of the particle is from the surface of the substrate.

Now assume that a second particle is brought into close proximity with both the first particle and the substrate. The second particle will also generate an image charge in the substrate, as shown in Fig. 5b. Naturally, the first particle will be attracted to that image charge, as well as its own. Accordingly, there is an increase in the net electrostatic force of attraction between the first particle the substrate. due to the presence of a second particle. It is also apparent that, as the number of particles increases, the electrostatic force of attraction between a single particle and the substrate also increases.

The effect of varying densities of charged particles on the electrostatic image force was studied by Goel and Spencer [89]. According to them, the maximum image force occurs when the particles are arranged in a hexagonally close packed array. Under these conditions, the net image force experience by a single charged particle in contact with the substrate is 6.95 times the force experienced by an isolated particle. Goel and Spencer also report that the maximum image force

generated by a square array of particles is 6.28 times greater than the force felt by a single particle.

It is intuitively obvious that multiple layers of charged particles would also cause an increase in the number of image charges. However, because these particles are further away from the plane, their effect on the layer of particles in direct contact with the plane would be correspondingly smaller. For example, a particle spaced a distance $2R$ from the substrate would experience an image force of only $1/9$ that of a particle in direct contact. The image force experienced by a particle in contact with the plane, but located directly below this second particle would be 1.25 times the image force if the second particle were not present. Finally, the upper layers of particles would also experience image forces. However, offsetting these forces is the Coulombic repulsion between particles. Goel and Spencer estimated that, for three layers of particles, the uppermost layer would experience a net electrostatic attractive force of 36–44% of that experienced by the lowermost layer.

Thus far in this discussion it has been assumed that the charge in a dielectric particle is totally immobile. However, this is not quite correct. Although the electric charges in a dielectric material cannot move over macroscopic distances under the influence of an electric field, as they can with a conductor, they do undergo microscopic displacements so that the charges align with the field when an electric field is applied. This separation and alignment of charge is generally referred to as polarization and is crucial to understanding particle adhesion. Indeed, as will be discussed, the major component to van der Waals' interactions comes from the tendency of a material to become polarized due to the presence of instantaneous dipoles present in neighboring materials.

Whether or not polarization effects results in a net force on a dielectric material depends on the uniformity of the field. Consider, for example, a polarizable dielectric particle with a charge q in a uniform field E . In this case, there would be a force equal to qE . However, there would be no net force arising from the polarization of the particle. This can be understood simply in terms of the displacement of the charge. The applied field would separate the positive and negative charges slightly, thereby creating a dipole. Each of these charges would 'pull' equally on the particle, but in opposite directions. This would result in no net force exerted by the uniform field on the particle. Now let us assume that the field is spatially non-uniform. The dielectric particle would still become polarized. However, since one side of the particle would experience a slightly weaker force than the other side would, there would be a net force resulting from the interaction of the dipole with the gradient of the field. Similarly, higher order multipoles would interact with higher derivatives of the field.

The electric field that generates the multipoles does not have to be externally applied. Rather, the image charge generated by the particle causes a non-uniform electric field that, not only polarizes the particle, but can result in attractive forces.

Mathematically, this can be expressed as

$$P = \epsilon_0 \kappa E \quad (51)$$

where P , E , and κ are the polarization, electric field, and electric susceptibility of the particle.

It can be shown that the electric susceptibility is related to the relative permittivity or dielectric constant ϵ of the particle by the relationship [88]

$$\kappa = \epsilon - 1. \quad (52)$$

By combining these concepts it can be seen that the electric charge q on an insulating particle induces an image charge in a grounded, electrically conducting plane. The image charge, then, polarizes the particle according to Eq. 51, thereby creating a dipole. That dipole creates additional image charges in the substrate, ad infinitum. While the contributions of the multipoles falls rapidly with separation distance and are infinitesimal at large separation distances, they may be significant for a particle 'in contact' with a substrate.

Fowlkes and Robinson [90] calculated the effects of the multipoles on the force of attraction by defining an interaction potential $\varphi(r, \theta)$ and expanding that potential in terms of the Legendre polynomials

$$\varphi(r, \theta) = \sum_{n=0}^{\infty} \frac{p^{(n)} p_n(\cos \theta)}{4\pi \epsilon_m r^{n+1}} \quad (53)$$

where ϵ_m is the dielectric constant of the media surrounding the particle ($= \epsilon_0$ for particles in vacuum) and $p^{(n)}$ are the multipole moments. For a spherical dielectric particle of radius R , these are given by [91,92]

$$p_i^{(n)} = \frac{4\pi \epsilon_m (\epsilon_p - \epsilon_m) R^{2n+1}}{(n-1)! [n\epsilon_p + (n+1)\epsilon_m]} \frac{\partial^{n-1} E_z}{\partial z^{n-1}}, \quad n = 1, 2, 3 \dots \quad (54)$$

where E_z is the z -component of the axially symmetric field. The first multipole (i.e. the monopole) is simply that charge on the particle

$$p^{(0)} = q. \quad (55)$$

Now let us consider a spherical particle of radius R that has a charge q uniformly distributed either on its surface or within its volume. The field produced by its image charge at some distance z above the surface of the substrate is given simply by

$$E_z^{(0)} = \frac{1}{4\pi \epsilon_m} \frac{-q}{(z+R)^2}. \quad (56)$$

The resulting dipole moment arising from the polarization of the particle can be found by substituting Eq. 56 into Eq. 54. The potential due to the dipole is then calculated by substituting that result into Eq. 53.

Now, the quadrupole moment can next be calculated by differentiating the potential to get the electric field due to the dipole moment. The reader can now see that an infinite series can be thus generated. The total electric field is simply the sum of all the individual multipole contributions, given by

$$E_z = \sum_{n=0}^{\infty} \frac{((n+1)!p^{(n)})}{4\pi\epsilon_m(z+R)^{n+2} + E_0} \quad (57)$$

where E_0 is the additional contribution arising from any externally applied field.

The total electrostatic force of attraction F_e on a dielectric is then given by

$$F_e = \sum_{n=0}^{\infty} \frac{p^{(n)}}{n!} \frac{\partial^n E_z}{\partial z^n} \quad (58)$$

or, upon substitution of Eq. 57 into Eq. 58,

$$F_e = p^{(0)}E_z^{(0)} + \frac{1}{4\pi\epsilon_m} \sum_{n=0}^{\infty} \sum_{k=0}^{\infty} \frac{(-1)^{n+k+1}(n+k+1)!p^{(n)}p^{(k)}}{n!k!(z+R)^{n+k+2}}. \quad (59)$$

Any effects due to the presence of multipoles have not been observed experimentally [86]. This may be due, in part, to the fact that multipole effects rapidly become insignificant with increasing separation. However, they do not appear to affect the size of the detachment force either. As Gady et al. [86] have shown, the measured attractive force appears to be consistent with the experimentally determined detachment force without considering the role of multipoles. Although the reasons for this are not fully understood, there are several factors that may contribute to this effect. First, when a particle is in contact with a substrate, the materials deform. Furthermore, as discussed in the introductory section of this paper, the particle and substrate bond and form an interphase. Both of these conditions preclude the ability to construct the Gaussian surface that was needed by Fowlkes and Robinson in their calculations. Moreover, as can be seen from Eqs. 54 and 59, the multipole terms also vanish when $\epsilon_p = \epsilon_m$. Although this would not alter the results for a dielectric particle ($\epsilon_p \approx 3$) in contact with a conducting substrate (no intervening media for that part of the particle in contact with the substrate and $\epsilon_s \approx \infty$), it would suggest that multipole effects for most materials would be negligible. Finally, it should be noted that Gady's results [86] were for an insulating particle and a conducting substrate. It should be obvious that there are still issues to be resolved with respect to the role of multipoles in particle adhesion.

So far the discussion has been limited to the case where the particle's charge is uniformly distributed. However, as discussed by researchers such as Goel and Spencer [89], and Hays [76,81], this might not be the case, especially if the particle is irregularly shaped. This can occur, as argued by Hays, if asperities on the particle prevent much of the surface area from contacting a neighboring

material, thereby impeding tribocharging. Under this scenario, as advanced by Hays, all charge would rely only on the asperities. The localization of charge has been referred to as 'charged patches' by Hays.

The localization of charge into a patch can increase the attractive force exerted on the particle. Presumably, the particle would rotate so as to align with the field. This would allow more charge to come into closer proximity to the substrate than would be possible with a uniformly charged particle, thereby increasing the attractive force. It should be noted that the strength of the field resulting from the concentration of the charge is limited by the dielectric strength of the surrounding medium. This limitation is often referred to as the Paschen limit and, for air, is of the order of 10^7 V/m.

Hays measured the current associated with electrically charged $99\text{ }\mu\text{m}$ diameter particles of styrene divinylbenzene particles as these particles traversed gaps of 520 and $137\text{ }\mu\text{m}$ separating two parallel electrodes. Based on these results, Hays [81] argued for the existence of locally charged patches on the particles.

In Hays' experiment, sinusoidal currents were observed as a function of time. In the case of the large separation, the current was ascribed to the particle moving from one electrode to the other. From this current, the traversal time and charge on the particle were determined. In the case of the smaller separation distance, there was an additional sinusoidal component to the current that had a longer period than that due to the particle moving between the two electrodes. This was to a rocking motion of the particle in the applied field as the dipole moment on the particle, caused by a charged patch, aligned with the field.

In order to calculate the force of attraction between the particle and surface, Hays had to estimate the dipole and quadrupole moments on the particle. He did this by assuming that the charge distribution $\sigma(\theta)$ around the surface of the particle was given by

$$\sigma(\theta) = \sigma_U + \sigma_D \cos\theta + \sigma_Q \frac{(3 \cos^2\theta - 1)}{2} \quad (60)$$

where the terms σ_U , σ_D , and σ_Q are the first three terms of a spherical harmonic expansion of an axially symmetric arbitrary charge distribution. The monopole term is simply the charge q on the particle and is given by

$$q = \sigma_U 4\pi R^2. \quad (61)$$

Hays further assumed that the dipole and quadrupole moments are given by

$$p^{(1)} = \frac{\sigma_D 4\pi R^3}{\epsilon_p + 2} \quad (62)$$

and

$$p^{(2)} = \frac{\sigma_Q 4\pi R^4}{2\epsilon_p + 3}. \quad (63)$$

The electrostatic contribution to the force of attraction can be approximated by substituting Eqs. 61–63 into Eq. 60. The result is given by

$$F_e = \frac{-\alpha q^2}{16\pi\epsilon_0 R^2} + \beta q E - \gamma \pi \epsilon_0 R^2 E^2 - \frac{\eta 3 p^{(1)2}}{32\pi\epsilon_0 R^4} + \frac{\lambda q p^{(1)}}{8\pi\epsilon_0 R^3} - \frac{\mu p^{(1)} E}{R} \\ - \frac{15\nu p^{(2)2}}{128\pi\epsilon_0 R^6} - \frac{3\xi q p^{(2)}}{32\pi\epsilon_0 R^4} + \frac{\rho p^{(2)} E}{R^2} + \frac{3\chi p^{(1)} p^{(2)}}{16\pi\epsilon_0 R^5} \quad (64)$$

where the coefficients α, \dots, χ depend on the dielectric constant of the particle.

For a relative permittivity of 2.5, $\alpha = 1.45$, $\beta = 1.29$, $\gamma = 0.298$, $\eta = 1.79$, $\lambda = 1.71$, $\mu = 0.446$, $\nu = 1.96$, $\xi = 2.10$, $\rho = 0.487$, and $\chi = 1.95$. Upon substitution of these values into Eq. 64, it is easy to see that the existence of localized charged patches can result in a substantial increase in the attractive force. An assumption made in Hays' analysis is that, although the occurrence of charged patches is a direct result of the highly irregular shape of the particles, the charge distribution can be inferred by assuming spherical symmetry of the particle. In fact, the observed dipole moment may not be a result of a charged patch at all, but, rather, due to variations in the distance of the surface of the particle at a given location from the center of mass. Real particles are likely to involve both of these effects.

As is well known, the force needed to detach a particle from a substrate is highly dependent on a number of factors aside from the size of the force of attraction. These factors include the charge on the particle, as well as the size and shape of the particle. As discussed by Hays [93] and by Gady et al. [94], the force needed to detach an irregularly shaped electrophotographic toner particle (typical size range: 8–20 μm) has been reported in the range of 50–4000 nN, with an average value of about 1000 nN. Moreover, as also discussed by Gady et al. [94] because of limitations resulting from the Paschen discharge limit, the electrostatic contribution to the force of attraction is limited to about 50 nN. Accordingly, for this type of particle, electrostatics contributes, but does not appear to be a major factor. However, as the surface of the particle is roughened and the detachment force decreases, electrostatics would be expected to play a more significant role [94].

Another limitation of the charged-patch model is that it totally ignores non-electrostatic forces such as van der Waals' interactions. In addition, deformations of the contacting materials are ignored in the charged-patch model. This has two consequences. First, such deformations would serve to average out charge density fluctuations, as well as increase the role of van der Waals' forces. Second, the charged patch model equates the attractive and detachment forces. However, once it is allowed that material deformations also occur, this cannot be done. Rather, in order to determine the detachment force, the work needed to create the deformations must be taken into account. Therefore, the detachment force must be calculated in a way that includes the deformed geometry, favoring energy considerations over simple force balance approaches.

It is clear that the presence of electrostatic charges, whether due to contact charging, fractoemissions, or some other mechanism, will affect particle adhesion. However, to date there has been no satisfactory attempt made at properly integrating electrostatic forces into particle adhesion theory.

6. Electrodynamic forces

As previously mentioned, electrodynamic interactions, such as those arising from London forces, can also contribute to the adhesion of particles. These forces are dominated by dipole interactions and are broadly lumped into the classification known as 'van der Waals' interactions. A more detailed description of van der Waals interactions than can be presented in this article is given in books by Israelachvili [95] and by Rimai and Quesnel [96].

There are three types of interactions that contribute to van der Waals forces. These are interactions between freely rotating permanent dipoles (Keesom interactions), dipole-induced dipole interaction (Debye interactions), and instantaneous dipole-induced dipole (London dispersion interactions), with the total van der Waals force arising from the sum. The total van der Waals interaction between materials arise from the sum of all three of these contributions.

Let us now calculate the three components of the van der Waals attraction by first calculating these interactions between two molecules. Subsequently, the total van der Waals potential between bodies will be determined by assuming that the molecules belong to two different materials and integrating the molecular interactions over the volumes of the materials.

6.1. Freely rotating permanent dipoles

Let us first consider the case where a molecule has no net charge, but the spatial distribution of the positive and negative charges is such that a permanent dipole moment exists. Highly polar molecules such as water, HCl, HF, and NH_3 are examples of such molecules.

Although the details of the charge distributions at the molecular level can be quite complex, the far-field behavior of a molecule with a spatially non-uniform charge distribution is often represented by a simpler model system. In this instance, the model system is composed of two charges of equal and opposite sign, $+q$ and $-q$, separated by a vector displacement \mathbf{d} . This idealized model system has a behavior characterized by a dipole vector $\mathbf{u} = q\mathbf{d}$. Molecules, such as H_2O and NH_3 often contain more than one covalent bond. Accordingly, they can have several bonds with the associated charge separations. The net dipole moment of the molecule, in such cases, is calculated by vectorially adding the individual dipole moments of each covalent bond.

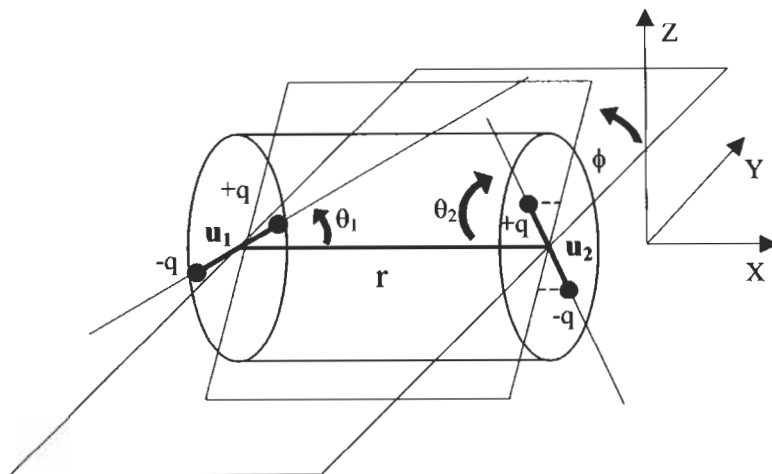


Fig. 6. The orientation of two dipoles in space.

The dipole–dipole (Keesom) interaction comes about from the fact that on the average, two freely rotating dipoles will align themselves so as to result in an attractive force, similar to that commonly observed with bar magnets. In order to calculate the net dipole–dipole interaction, it is necessary to examine all the possible orientations of the dipoles with respect to one another. It is also necessary to determine any $1/r^2$ effects due to the field associated with a point charge, in order to determine the net effect when amorphous solids are placed side by side. We also need to consider what happens if the dipoles can reorient in each other's fields.

To begin, let us consider two electric dipoles, dipole moments u_1 and u_2 , respectively, separated by some distance r , but fixed in space with respect to orientation. Let us further assume that each dipole is oriented along some angle θ_1 and θ_2 with respect to the axis separating the two dipoles as shown in Fig. 6. In addition, let us also assume that there is some angle ϕ representing the angular orientation of one dipole with respect to the other about that axis. The interaction energy, $w(r, \theta_1, \theta_2, \phi)$, for fixed magnitudes of the dipole moments u_1 and u_2 , is given by [88]

$$w(r, \theta_1, \theta_2, \phi) = \frac{-u_1 u_2 (2 \cos \theta_1 \cos \theta_2 - \sin \theta_1 \sin \theta_2 \cos \phi)}{4\pi \epsilon_0 r^3}. \quad (65)$$

Now allow the dipoles to freely rotate in space. This can occur, for example, when the thermal energy is greater than the interaction energy, as would occur at large separations or high dielectric constant materials. The interaction energy, averaged over all orientations, can be calculated using the Boltzmann distribution

$$e^{-w(r)/kT} = \frac{\int e^{-w(r, \theta, \phi)} \sin \theta d\theta d\phi}{\int \sin \theta d\theta d\phi} \quad (66)$$

where θ and ϕ vary between 0 and π and 0 and 2π , respectively, T is the absolute temperature and k is the Boltzmann constant. For $w(r, \theta, \phi)$ less than kT , Eq. 66 can be expanded in terms of $1/T$ according to

$$e^{-w(r)} \approx 1 - \frac{w(r)}{kT} + \dots \quad (67)$$

Upon averaging over θ_1 , θ_2 , and ϕ , it can be shown that $w(r)$ is given by

$$w(r) = -\frac{u_1^2 u_2^2}{3(4\pi\epsilon_0)^2 kT r^6}. \quad (68)$$

It should be noted that, if the medium between the particle and substrate is something other than vacuum and possesses a dielectric constant ϵ , the interaction energy in Eq. 68 is reduced by a factor of ϵ^2 . Eq. 68, which relates the interaction energy between permanent electric dipoles and their separation distances is known as the Keesom effect.

6.2. Permanent-induced dipole interactions

In the second type of interaction contributing to van der Waals forces, a molecule with a permanent dipole moment polarizes a neighboring non-polar molecule. The two molecules then align with each other. To calculate the van der Waals interaction between the two molecules, let us first assume that the first molecule has a permanent dipole with a moment u and is separated from a polarizable molecule (dielectric constant ϵ) by a distance r and oriented at some angle θ to the axis of separation. The dipole is also oriented at some angle from the axis defining the separation between the two molecules. Overall, the picture would be very similar to Fig. 6 used for dipole–dipole interaction except that the interaction is induced as opposed to permanent.

The magnitude of the electric field E caused by the dipole in the vicinity of the molecule is given by

$$E = u(1 + 3\cos^2\theta)^{1/2}/4\pi\epsilon r^3. \quad (69)$$

The interaction energy of a material having a polarizability α and an applied electric field is given by [97]

$$w(r, \theta) = -\frac{1}{2}\alpha E^2 \quad (70)$$

where α is given by

$$u = \alpha E. \quad (71)$$

By substituting Eq. 69 into Eq. 70 it is readily found that

$$w(r, \theta) = \frac{-u^2\alpha(1 + 3\cos^2\theta)}{2(4\pi\epsilon)^2 r^6}. \quad (72)$$

The effective interaction potential, found by averaging $\cos^2 \theta$ over all angles, is then equal to

$$w(r) = -\frac{\alpha u^2}{(4\pi\epsilon)^2 r^6}. \quad (73)$$

6.3. Dispersion forces

The third type of interaction that contributes to van der Waals interactions arises from the formation of an instantaneous dipole in one molecule inducing an instantaneous dipole in a neighboring molecule. Often referred to as ‘London’ or ‘dispersion’ forces, this type of interaction is frequently the most significant contributor to van der Waals forces and it is often assumed that van der Waals forces arise solely from these interactions. As an example of this type of interaction, consider a metal that has a clean surface and lacks permanent dipole moments. As a result of its high polarizability, such a material typically has a very high surface energy. Similarly, semiconductors, which are still fairly polarizable, also tend to have high surface energies, although not as high as metals. Even for many polymers, the surface energy is dominated by dispersion forces, as estimated by measuring the contact angle made with polar and non-polar liquids such as water and diiodomethane, respectively [98,99].

To understand the origins of dispersion forces, let us consider two Bohr atoms, each of which consists of an electron orbiting around a nucleus comprised of a proton, having a radius a_0 , often referred to as ‘the first Bohr radius’. It is obvious that a Bohr atom has no permanent dipole moment. However, the Bohr atom can be considered to have an instantaneous dipole moment given by

$$u = ea_0 \quad (74)$$

where e is the electron charge. Recognizing that, for a Bohr atom to be stable, the electrostatic attractive force between the electron and the nucleus must equal the centrifugal force, it is required that

$$\frac{m_e v^2}{a_0} = \frac{e^2}{4\pi\epsilon_0 a_0^2} \quad (75)$$

where m_e is the electron mass and v is its velocity. It is further required by quantum mechanics that the angular momentum is proportional to an integer times Planck’s constant, or

$$\oint L d\theta = nh \quad (76)$$

where $L = m_e a_0 v$ is the angular momentum of the electron, n is an integer ($= 1$ for the first Bohr radius), and h is Planck’s constant. Upon some algebraic

manipulation, it is readily found that

$$a_0 = \frac{h^2 \epsilon_0}{\pi m_e e^2} \approx 0.53 \times 10^{-10} \text{ m.} \quad (77)$$

Moreover, it is also found that the total energy E (potential plus kinetic) of the electron is given by

$$E = -\frac{e^2}{4\pi \epsilon_0 (2a_0)}. \quad (78)$$

The frequency of oscillation ν of an electron in the first Bohr orbit is approximately $3.3 \times 10^{15} \text{ s}^{-1}$. This corresponds to an energy of approximately $2.2 \times 10^{-18} \text{ J}$. This is the energy needed to ionize the atom and is often referred to as the first ionization potential I . It should be noted that this frequency is in the *UV* part of the spectra and has a corresponding wavelength of approximately 90 nm. By the time an electromagnetic wave originating at one atom reaches another atom located this distance away from the first, the position of the electron would have measurably changed. The resulting interaction between the two atoms would not be between dipoles as they presently exist, but, rather, as they previously existed. As a result, the interactions would have to be calculated assuming retardation effects, when the distances are comparable or larger than the wavelength. This would result in the interaction potential falling as $1/r^7$ [95,96], rather than as $1/r^6$, as occurs in the non-retarded case for atoms very close to one another.

Returning now to the previous discussion, the (non-retarded) interaction potential $w(r)$ can now be calculated by Eqs. 77, 74, and 73. For dissimilar atoms, as designated by the subscripts 1 and 2, this is given by

$$w(r) = -\frac{3}{2} \frac{\alpha_1 \alpha_2}{(4\pi \epsilon_0)^2 r^6} \frac{h \nu_1 \nu_2}{\nu_1 + \nu_2}. \quad (79)$$

Eq. 79 can be expressed in terms of the ionization potentials I_1 and I_2 of the two atoms as

$$w(r) = -\frac{3}{2} \frac{\alpha_1 \alpha_2}{(4\pi \epsilon_0)^2 r^6} \frac{I_1 I_2}{I_1 + I_2}. \quad (80)$$

It is interesting to note that all three mechanisms contributing to the attractive van der Waals interactions vary as the reciprocal of the separation distance to the sixth power. It is for this reason that the Lennard-Jones potential has been extensively used to model van der Waals forces.

The total van der Waals interaction potential is obtained by simply adding the individual contributions arising from the Keesom, Debye, and London interactions. Because the radial power-law dependencies of all these interactions vary as $1/r^6$, the total van der Waals interaction can be expressed simply as

$$w(r) = -\left[(u_1^2 \alpha_2 + u_2^2 \alpha_1) + \frac{u_1 u_2}{3kT} + \frac{3\alpha_1 \alpha_2 h \nu_1 \nu_2}{2(\nu_1 + \nu_2)} \right] \frac{1}{(4\pi \epsilon_0)^2} \frac{1}{r^6}. \quad (81)$$

Table 1

The relative contributions to van der Waals interactions arising from the Debye, Keesom, and London effects

	Debye (%)	Keesom (%)	London (%)
Ne-Ne	0	0	100
CH ₄ -CH ₄	0	0	100
HCl-HCl	4.9	8.9	86.2
HBr-HBr	2.1	1.6	96.3
HI-HI	0.5	0.1	99.4
CH ₃ Cl-CH ₃ Cl	7.7	24.3	68.0
NH ₃ -NH ₃	9.0	34.2	56.8
H ₂ O-H ₂ O	7.2	69.1	23.7
Ne-CH ₄	0	0	100
HCl-HI	3.4	0.5	96.1
H ₂ O-Ne	8.3	0	91.7
H ₂ O-CH ₄	13.4	0	86.6

6.4. Comparisons of the relative contributions to the van der Waals interactions

The relative contributions of each type of interaction to the total van der Waals interaction has been determined by Israelachvili [95] for pairs of similar and dissimilar molecules theoretically by comparing the magnitudes of the terms within the square brackets, using reported values for the polarizability and the ionization potential of these molecules. These results are summarized in Table 1.

It is clear from Table 1 that, for a few highly polar molecules such as water, the Keesom effect (i.e. freely rotating permanent dipoles) dominates over either the Debye or London effects. However, even for ammonia, dispersion forces account for almost 57% of the van der Waals interactions, compared to approximately 34% arising from dipole-dipole interactions. The contribution arising from dispersion forces increases to over 86% for hydrogen chloride and rapidly goes to over 90% as the polarity of the molecules decrease. Debye forces generally make up less than about 10% of the total van der Waals interaction.

It is worthwhile to highlight an inconsistency in the literature. Specifically, one often finds that authors attribute the origins of van der Waals forces solely to dispersion forces. Although this is not strictly correct, in light of the present discussion, one can see that assuming that London and van der Waals forces are synonymous is often not a bad approximation. However, the reader is cautioned that this is not quite correct and can lead to erroneous conclusions under some circumstances.

It should also be noted that contributions to van der Waals interactions from the Keesom effect are likely to be decreased in solids due to the locking in of the

molecules in most lattices. However, as had been discussed, in most materials van der Waals interactions are dominated by London forces in any event so corrections to the van der Waals interactions due to the constraints on the rotational degrees of freedom of atoms in a solid lattice are likely to be small.

7. Comparison of electrostatic and electrodynamic forces

As previously discussed, there has been much debate as to whether electrostatic or electrodynamic interactions dominate particle adhesion. There is one school of thought that argues strongly that electrostatically charged patches on the surface of a particle can account for the measured detachment force. There is the other school of thought that argues that van der Waals interactions accurately predict the detachment force and those advocating the presence of the charged patch model must first discount the role of van der Waals forces and then propose charge distributions that result in unrealistically high electrostatic fields. Alternatively, those who espouse van der Waals forces as the mode of adhesion tend to ignore electrostatic contributions. Suffice to say, the argument will not be resolved in this paper. However, sources for the discrepancies, which are, unfortunately, often neglected by advocates of both sides, will be presented.

Let us first assume that we have a spherical particle with a radius of 5 μm similar to an idealized toner particle, which is comprised of polystyrene, in contact with an electrically conducting substrate. A typical electric charge on a toner particle of that size is of the order of 10^{-14} C. The Hamaker coefficient (Eq. 15) for such a system would be about 1.5 eV.

In the case of a toner particle, the charge q on the particle was produced by triboelectrification. As such, it is fair to assume that the charge is uniformly distributed and proportional to the surface area, with a proportionality constant σ . The force of attraction between the particle and the substrate is obtained using the method of images, discussed previously. Accordingly,

$$F_q = \frac{1}{4\pi\epsilon_0} \frac{q^2}{(2R)^2} \quad (82)$$

where ϵ_0 is the permittivity of free space. However, since the charge is proportional to the surface area of the particle,

$$q = 4\pi R^2 \sigma \quad (83)$$

which gives, upon substitution of Eq. 83 into Eq. 82,

$$F_q = \frac{\sigma^2 \pi R^2}{\epsilon_0}. \quad (84)$$

By comparing Eq. 17 with Eq. 84, it is clear that, whereas van der Waals forces vary linearly with the particle radius, the electrostatic forces vary quadratically.

This means that the relative importance of the electrostatic and van der Waals forces will vary with the size of the particle, with electrostatic forces more important for larger particles and van der Waals forces dominant for smaller particles.

Assuming a separation distance of 4 Å and equating the force in Eq. 17 to that in Eq. 84, it is easy to show that the critical radius above which electrostatics dominates is about 280 μm. However, if the separation distance is 6 Å rather than 4 Å, the critical radius decreases to about 124 μm. Similarly, doubling the charge would result in quartering the critical radius. Moreover, any effect due to a locally charged patch would also affect the critical radius. As can be seen, many factors determine whether particle adhesion is dominated by electrostatic or electrodynamic forces. The reader is also reminded that the present discussion is limited to an electrically conducting substrate. As discussed by Jones [100], the problem of the attraction of an electrostatically charged particle to a dielectric substrate has not yet been solved.

Another issue that complicates discussions of what type of force dominates attraction is the separation of the particle from the substrate. It should be clear from the discussion thus far presented that the range of electrostatic forces is far greater than that of van der Waals forces. Accordingly, it is conceivable, and probably common, that electrostatic forces are more important than van der Waals forces at relatively large separations, whereas, once the particle has actually 'contacted' the substrate, van der Waals forces might dominate. As examples, one could consider a laser printer and an electrostatic dust collector. In the former, toner is attracted to appropriately charged regions of a photoconductor. However, once in close proximity, the mechanism of the dominant attractive force can change to a van der Waals interaction. This can explain why toner is only deposited in the image areas of the photoconductor but is difficult to transfer upon application of an electric field and why the toner particles, despite being similarly charged, are sufficiently cohesive so as to allow alphanumerics and halftones to be faithfully reproduced. Similarly, electrostatic dust collectors rely on the relatively long range of the electrostatic interactions to attract dust. However, once the dust is on the filter, van der Waals forces often play the dominant role to ensure that the dust does not become redispersed.

All this being said, perhaps the most definitive study of the relative roles of electrostatic and van der Waals forces was performed by Gady et al. [86,101,102]. In their studies, they attached a spherical polystyrene particle, having a radius between 3 and 6 μm, to the cantilever of an atomic force microscope. They then conducted three distinct measurements that allowed them to distinguish between electrostatic and van der Waals forces that attracted the particle to various conducting, smooth substrates.

In the first experiment, Gady measured the bend of the cantilever as a function of particle-to-substrate displacement. This allowed him to determine the power-

law dependence of the attractive force as a function of particle-to-substrate displacement. In the second experiment, the cantilever was vibrated and the resonance frequency determined as a function of the separation distance between the particle and substrate. These measurements allowed the force gradient to be measured. Finally, in the third experiment, the distance at which the particle snaps into contact with the substrate was measured as a function of the radius of the sphere. The snap-together phenomenon occurs when both the total force acting on the particle (the attractive force plus the restoring force due to the bent cantilever) as well as the total force gradient equal zero. This measurement allows one to estimate the size of both the attractive force and force gradient and compare them to the electrostatic and van der Waals forces.

In addition to simply measuring the attractive force *per se*, the charge on the particle was also controlled by allowing the particle to contact the substrate varying numbers of times. In addition, charge transfer was controlled by choosing particles and substrates with varying triboelectric properties. Finally, the charge on the particle was decreased by washing the particle with alcohol. This allowed the experiment to be run reversibly by increasing the charge with multiple contacts, then decreasing it by washing.

Gady found that, depending on the charge of the particle, van der Waals forces dominated over the forces associated with electrostatically charged patches when the particle-to-substrate separation was between 3 and 10 nm, depending on the particle charge. In addition, he found that the distance at which the snap-together occurred required that van der Waals forces dominate over electrostatic. In all his measurements, however, a component of the total attractive force, even at close separations, was observed to be electrostatic in nature.

Gady's results might seem to resolve the issue of electrostatic versus electrodynamic interactions. However, they are limited to the ideal case of an insulating, spherical particle in the micrometer-size range, and their conclusions must necessarily be restricted to that case. In contrast, DeMejo et al. [103] published an SEM micrograph of a micrometer-size nickel particle on a silicon substrate that showed the particle resting on one asperity. Similar micrographs of gold particles on silicon substrates have been published by Rimai et al. [104]. Considering the small radius of the asperity in contact with the substrate in each case, it is hard to imagine that the dominant mode of attraction arise from van der Waals interactions. However, considering the conductive nature of both the particle and substrate and the fact that the micrographs were taken in a scanning electron microscope, it seems quite plausible that, in these instances, the attraction could be due to the establishment of an image charge. Obviously, further research is needed to more fully understand the respective roles of electrostatic and electrodynamic interactions in particle adhesion.

8. Acid–base interactions

For the sake of completeness, it is worthwhile to briefly discuss role of acid–base interactions in adhesion. In this context, the term acid refers to a Lewis acid (an electron acceptor) and a Lewis base (electron donor), rather than the more conventional acid and base definitions. The role of acid–base interactions in adhesion is discussed in detail by Lee [105].

As derived from quantum mechanics, electrons in atoms orbit the nuclei in discrete energy levels, often referred to as shells. Each shell can hold up to a fixed number of electrons, depending on the energy level of that shell. Moreover, it is energetically favorable for an atom to have completely filled shells. Thus, atoms such as fluorine and oxygen, which need one or two electrons, respectively, to fill their outermost shells, tend to attract electrons strongly and are, therefore, electronegative (Lewis acid). Conversely, the alkali and alkali earths can minimize their energy levels most efficiently by emptying their outermost shells and are, therefore, electron donors or Lewis bases. Depending on the electronegativities of the atoms, the resulting bonds that are formed between the contacting materials will have varying degrees of ionic and covalent character.

Drago et al. [106] proposed the use of four parameters, E_A , E_B , C_A , and C_B to describe the ionic (E) and covalent (C) nature of the Lewis acid (A) and base (B). He then related these parameters to the change in enthalpy ΔH^{A-B} of the acid–base interaction. The acid–base interaction contribution to the work of adhesion w_A^{A-B} is then given by

$$w_A^{A-B} = -fn^{A-B}\Delta H^{A-B} \quad (85)$$

where f represents a free energy to enthalpy correction factor and n is the surface area fraction, in terms of moles per unit area, involved in the contact.

Fowkes [107] has argued that the van der Waals contribution to the work of adhesion w_A^{vdW} in solids arises mainly from the dispersion forces. Moreover, the work of adhesion can be approximated by the geometric mean of the dispersion contributions to the surface energies γ_1^d and γ_2^d according to

$$w_A^{vdW} = \sqrt{\gamma_1^d \gamma_2^d}. \quad (86)$$

It should be intuitively obvious that the contribution to the work of adhesion arising from acid–base interactions cannot be expressed in terms of the geometric mean of the surface energies. Therefore, the entire work of adhesion would be

$$w_A = w_A^{vdW} + w_A^{A-B} \quad (87)$$

or

$$w_A = \sqrt{\gamma_1^d \gamma_2^d} + w_A^{A-B}. \quad (88)$$

Upon combining Eqs. 88 and 85, one finds that the total work of adhesion is related to the surface energies of the contacting materials as well as the enthalpy associated with acid–base interactions by

$$w_A = \sqrt{\gamma_1^d \gamma_2^d} - f n^{A-B} \Delta H^{A-B}. \quad (89)$$

As discussed earlier in this paper, acid–base interactions generally do not significantly contribute to the adhesion of particles. This is because, in general, the surfaces of particles have been allowed to react with the ambient and there are no free sites left that can undergo acid–base interactions. This is not always the case, however, as exemplified by Lee's study of the cohesive interactions between lunar dust particles. Other examples where acid–base interactions may be significant include the formation and deposition of nanoclusters under ultrahigh vacuum (UHV) conditions and the generation of particles upon the cleavage of surfaces, also performed under UHV conditions.

9. Time dependence of particle adhesion

As previously discussed, many, if not most, cases of particles adhering to substrates involve at least one of the contacting materials deforming plastically, rather than elastically. Under such circumstances, it would be expected that the extent of the contact should increase with time and, with it, the force needed to detach a particle from a substrate. Moreover, material flow can occur, resulting in the engulfment or encapsulation of the particles.

The relationship between the increase in contact radius due to plastic deformation and the corresponding increase in the force required to detach submicrometer polystyrene latex particles from a silicon substrate was determined by Krishnan et al. [108]. In that study, Krishnan measured the increase in the contact area of the particles over a period of time (Fig. 7a) and the corresponding decrease in the percentage of particles that could be removed using a force that was sufficient to remove virtually all the particles initially (Fig. 7b).

Krishnan found that both the contact area and removal efficiency curves could be fitted by logarithmic equations with approximately the same time constants (148 and 164 h for the contact area and removal efficiency curves, respectively). Although the precise time constants would be expected to vary with the specific contacting materials, Krishnan's results to establish a clear correlation between plastic flow and particle adhesion.

Further evidence of the occurrence of adhesion-induced plastic flow was supplied by Vrtis et al. [109]. In this study, Vrtis removed gold and tin micrometer-size particles from an alternating block copolymer of polyester and polydimethylsiloxane (PDMS) by amalgamating with mercury. SEM micrographs of the sub-

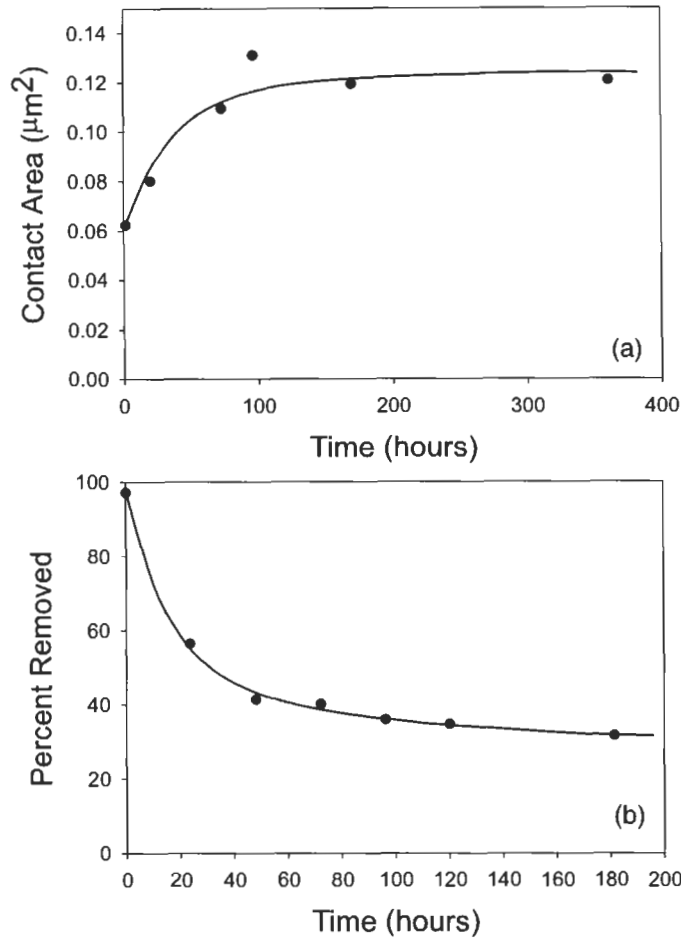


Fig. 7. The increase in contact area (a) and corresponding decrease in detachment efficiency (b) as a function of time (from ref. [108]).

strate both before and after amalgamation clearly showed the presence of craters corresponding to the particles after the particles had been removed.

Another example of time-dependent adhesion has been reported by Rimai et al. [110]. In this study, adhesion-induced stresses were found to cause an alternating block polyester/PDMS copolymer was found to flow over stacks of particles during a 2-week-long interval, suggestive of the occurrence of viscoelastic flow.

Johnson [111] addressed the problem of viscoelastic flow by attempting to modify the JKR equation. In his approach, he postulated a creep compliance function

$$\Phi(t) = \frac{\phi(t)}{E_{\infty}} \quad (90)$$

where E_∞ is the Young's modulus at very low rates of strain and $\phi(t)$ is defined by

$$\phi(t) = [1 - (1 - k)e^{t/T}] \quad (91)$$

where T is the characteristic time constant of the system. The constant k is defined as the proportionality constant relating the Young's modulus E at high strain rates to that at low strain rates, or $E = E_\infty/k$. The JKR equation for viscoelastic materials is then written as

$$a^3(t) = \frac{3R}{4} \int_0^t \Phi(t-t') \frac{d}{dt'} P(t') dt'. \quad (92)$$

Upon integrating and expressing time in terms of the reduced time $\tau = t/T$, one finds

$$a^3(\tau) = \frac{3RP}{4E_\infty^* \tau} [\tau - (1 - k)(1 - e^{-\tau})] \quad (93)$$

where E_∞^* represents the reduced modulus at slow strain rates. In essence, Eq. 93 represents a phenomenological, time-dependent JKR equation relating the contact and particle radii in a viscoelastic system.

Another manifestation of a time dependence to particle adhesion involves the phenomenon of total engulfment of the particle by the substrate. It is recognized that both the JKR and MP theories of adhesion assume that the contact radius a is small compared to the particle radius R . Realistically, however, that may not be the case. Rather, the contact radius depends on the work of adhesion between the two materials, as well as their mechanical properties such as the Young's modulus E or yield strength Y . Accordingly, there is no fundamental reason why the contact radius cannot be the same size as the particle radius. For the sake of the present discussion, let us ignore some mathematical complexities and simply assume that both the JKR and MP theories can be simply expanded to include large contact radii. Let us further assume that, under conditions of no externally applied load, the contact and particle radii are equal, that is $a(0) = R$. Under these conditions, Eq. 29 reduces to

$$a = \frac{9\pi w_A(1 - \nu^2)}{2E} \quad (94)$$

for elastic deformations, whereas, for the case of plastic deformations, Eq. 47 reduces to

$$a = \frac{2w_A}{3Y}. \quad (95)$$

It is obvious that, as the Young's modulus, or yield strength in the case of plastic deformations decreases, or as w_A increases, the value of the contact

radius a should increase in magnitude. It is also intuitive that the contact radius cannot exceed the particle radius. Let us assume that conditions are such that the computed value of a is equal to the particle radius. According to JKR, DMT, or MP theory, a has a dependence on R that is weaker than linear. This means that an increase in R , with all other parameters held constant, would result in a correspondingly smaller increase in a . Conversely, a decrease in R suggests a correspondingly smaller decrease in a , producing the non-physical situation of the contact radius being larger than the particle radius. This, then, raises the question of what actually happens when these situations are realized. Suppose the particle *were* a little smaller or, equivalently, if the material were a bit more compliant or the work of adhesion were a little higher. What would happen?

One could obviously get the substrate to engulf the particle by applying an external load. However, in the absence of an external load, can the substrate engulf the particle. For purposes of this discussion, let us assume that the particle is rigid compared to the substrate. If one thinks of simple wetting, a surface is wet by a liquid if the decrease in the Gibb's free energy resulting from the decrease in surface area is sufficient to offset the energy expended to create the liquid–solid interface. A similar effect can be proposed for that allows a particle to be engulfed by a substrate due to surface forces. Specifically, a critical radius R_C can be defined as [112]

$$R_C \approx 7(\gamma_{12}/E) \quad (96)$$

for elastically deforming substrates and

$$R_C \approx 2(\gamma_{12}/3Y) \quad (97)$$

for plastically deforming substrates. If $R < R_C$ the particle will become significantly embedded into the substrate.

The existence of the critical radius and substantial engulfment was shown by Rimai et al. [112]. In that study, 4 and 11 μm radius glass particles were deposited onto a plasticized polystyrene substrate. After a lengthy period of time, SEM micrographs showed that the contact radius for the larger particles was just a trifle less than the particle radius. In contrast, the smaller particles were about 80% embedded into the substrate. Subsequently, Rimai et al. [113] reported that the engulfment process was not linear and that, even after a period of months, the crowns of the particles were still visible. The authors suggested that the non-linearity and the failure to submerge the crowns of the particles might be due to the z -component of the force associated with the surface energy might not be sufficient to overcome the drag on the particle.

As should be evident, time dependencies of particle adhesion are commonly observed. However, there is still much room for both experimental and theoretical advances before this area can be classified as well understood.

10. Adhesion of non-ideal particles

Thus far, the discussion of particle adhesion has been mainly limited to ideal spherical particles. This idealization has been employed to simplify the analysis and allow one to better understand the underlying science governing this topic. However, it is clear that most particles normally encountered are highly irregular.

The role of particle irregularities has already been discussed with respect to the distribution of electrical charge on the surface of a particle and its impact on the attractive force. However, irregularities also are significant in determining the role of van der Waals interactions. Specifically, as determined by Gady et al. [114] van der Waals forces are significant at ranges up to a few nanometers. Thus, if asperities separate the bulk of a particle from a substrate by more than a few nanometers, the particle is, in essence, located at infinity and only the radius of curvature of the asperity and the molecules that comprise that asperity significantly contribute to the van der Waals interactions. It should be noted that the asperities can exist on either the particle or the substrate with, essentially, the same effect.

The role of asperities on adhesion was demonstrated by Gane et al. [115] using clean, crossed cylinders of hard, elastic materials such as titanium carbide, sapphire, and diamond. They reported that the measured force needed to separate these cylinders was between two and three orders of magnitude smaller than predicted and attributed this observation to the role of surface roughness. Schaefer et al. [116] attached micrometer-size particles of glass, tin, and gold to the cantilever of an atomic force microscope (AFM) and measured the detachment force of those particles from atomically smooth highly oriented pyrolytic graphite (HOPG) and mica. They found that, although the detachment force scaled appropriately with the surface energies of the particles and substrates, the actual magnitude of the force was between a factor of 50 and 200 lower than predicted from the JKR model, assuming spherical particles. Using the AFM as a profilometer, they showed that a large fraction of the discrepancy arose from the roughness of the particles. Asperities on particles were found to reduce the apparent adhesion.

As previously discussed, the JKR theory predicts that the detachment force is independent of the Young's modulus. Yet despite that, when Gady et al. [117] measured the detachment force of polystyrene particles from two elastomeric substrates having Young's moduli of 3.8 and 320 MPa, respectively, they found that the detachment force from only the more compliant substrate agreed with the predicted value. The force needed to separate the particle from the more rigid substrate was about a factor of 20 lower. Estimates of the penetration depth revealed that the particles would penetrate into the more compliant substrate more deeply than the heights of the asperities. Thus, in that case, the spherical particle approximation would be reasonable. On the other hand, the penetration depth

would be less than the asperity height for the more rigid substrate, thereby limiting van der Waals interactions to those between the asperities and the substrate.

At first, it might seem as if the problem of treating asperities would be quite straightforward. One should simply substitute the radius of curvature of the asperities for the particle radius and multiply by the number of asperities contacting the substrate to calculate the detachment force. However, this is not the case. Rather, both the radius of curvature of the particle and the varying heights of the asperities make the actual estimate of the detachment force much more complicated. This can be understood by considering the following example. Assume two planar surfaces are brought into contact with one another. At first only the largest of the asperities actually contact. However, with increasing load, smaller asperities come into contact with the opposing surface as the larger asperities deform under the stress. Upon separation, the smaller asperities initially detach, followed by the larger. The contacts between the asperities and the surface are not all broken simultaneously. There is a zippering effect with the asperities last to contact on approach releasing first on removal of the particle.

A similar analysis can be done for the curved surface of an essentially spherical particle that contains asperities. Let us assume that all the asperities are the same size. Initially, no more than three asperities on the particle can contact the presumably smooth surface. As the asperities compress under the applied load, more asperities, that are situated further away from the substrate due to the curvature of the particle's surface, come into contact. These are the first to separate from the substrate upon application of a detachment force. In essence, detachment occurs by breaking the contacts between the asperities and the contacting surface, one at a time.

As of this time, no one has solved the problem of the effect of asperities on a curved surface nor has anyone addressed the issue of crystalline facets. Needless to say, the problem of asperities on an irregular surface has not been addressed. However, Fuller and Tabor [118] have proposed a model that addresses the effects of variations of asperity size on adhesion for the case of planar surfaces. Assuming elastic response to the adhesion-induced stresses, they treated surface roughness as a random series of asperities having a Gaussian height distribution $\varphi(z)$ and standard deviation σ . Accordingly,

$$\varphi(z) = \frac{1}{(2\pi)^{1/2}} \exp\left(-\frac{z^2}{2\sigma^2}\right). \quad (98)$$

The force p needed to compress a single asperity and the displacement δ of its tip relative to the undeformed region of the substrate was calculated using JKR theory and determined to be related to the radius of curvature of the asperity β and the contact radius a by

$$\delta = \frac{(Ka^3 + 2p\beta)}{3\beta Ka} \quad (99)$$

where K is related to the Young's moduli $E_{P(S)}$ and Poisson's ratio $\nu_{P(S)}$ of the particle and substrate by

$$K = \frac{4}{3} \left[\frac{1 - \nu_P^2}{E_P} + \frac{1 - \nu_S^2}{E_S} \right]^{-1}. \quad (100)$$

Treating an asperity as an independent particle, JKR theory states that the force p_S needed to effect detachment of a spherical asperity from a planar substrate is given by

$$p_S = \frac{3}{2} \pi w_A \beta. \quad (101)$$

Fuller and Tabor then defined the term δ_S

$$\delta_S = \frac{1}{3\beta} \left(\frac{3\beta p_S}{K} \right)^{2/3}. \quad (102)$$

Physically, p_S and δ_S represent the applied force and displacement of the asperity when detachment occurs.

The pressure p was then calculated as a function of the displacement δ , or

$$\frac{p}{p_S} = F \left(\frac{\delta}{\delta_S} \right). \quad (103)$$

Eq. 103 was solved numerically by Fuller and Tabor and the results have been tabulated [118]. If $w_A = 0$, Eq. 103 simplifies to the Hertz relationship

$$\frac{p}{p_S} = \frac{1}{\sqrt{3}} \left(\frac{\delta}{\delta_S} \right)^{3/2}.$$

As previously proposed, $\varphi(z)$ is defined as the probability of an asperity having a height z above a reference plane. Assuming the presence of N asperities per unit area, the probability that n of these would contact a smooth surface having a separation distance d is given by

$$n = N \int_d^\infty \varphi(z) dz. \quad (104)$$

The total force per unit area P' between the two planes is given by the sum of all the forces that are exerted by the asperities whose heights exceed d . This is given by the relation

$$P' = N \int_d^\infty p(z) dz = \frac{N p_S}{(2\pi)^{1/2} \sigma} \int F \left(\frac{\delta}{\delta_S} \right) \exp \left(-\frac{z^2}{2\sigma^2} \right) dz. \quad (105)$$

By changing the variable of integration to $\delta = z - d$ from z and expressing the displacements in terms of the standard deviation so that $\Delta = \delta/\sigma$, $\Delta_S = \delta_S/\sigma$, and $h = d/\sigma$, one can express Eq. 105 as

$$P' = \frac{Np_S}{(2\pi)^{1/2}} \int_0^{\infty} F\left(\frac{\Delta}{\Delta_S}\right) \exp\left[-\frac{1}{2}(h + \Delta)^2\right] d\Delta. \quad (106)$$

Eq. 106 describes the force as the separation between the surfaces is decreased. Let us now assume that, after reaching some minimum separation distance d_0 , a force is applied to separate the surfaces. In this case, the force will differ slightly from that given in Eq. 106, as the asperities are extended above their original height up to a maximum extension δ_S , at which point the asperity will separate from the substrate. In order to calculate the separation force P_S , one must change the lower limit of integration in Eq. 106 to

$$P = \frac{Np_S}{(2\pi)^{1/2}} \int_{-L}^{\infty} F\left(\frac{\Delta}{\Delta_S}\right) \exp\left[-\frac{1}{2}(h + \Delta)^2\right] d\Delta \quad (107)$$

where $L = \Delta_S$ or $L = h - h_0$, whichever is less. When the separation distance $d = d_0$, $P = P'$ and the force is compressive. However, upon application of a negative or tensile force, the separation distance increases. If this were a spherical particle without asperities in contact with a smooth, planar substrate, the magnitude or absolute value of the separation force would increase (i.e. the applied force would decrease, owing to its sign) until the JKR limit were reached. At that point, the particle would detach from the substrate. However, due to the presence of asperities, detachment does not simply take place with one catastrophic occurrence. Rather, as the size of the tensile force increases to some value P_S , contact with the highest asperities are first broken. The magnitude of the force now needed to break the remaining contacts decreases. As the asperity contacts are broken, the magnitude of the separation force will asymptotically approach zero. In essence, particle–substrate separation, in the presence of asperities, can be thought of as an unzipping mechanism as the individual contacts break. The ratio P_S/Np_S represents a measure of the reduction of the force of adhesion due to the variations in the heights of the asperities. In other words, asperities would not only reduce the force needed to remove a particle from a substrate due their smaller effective radius, as per the Krupp model, but would actually further reduce the magnitude of maximum total applied force needed as the contact ‘unzipped’.

It can be argued that the asperities themselves are relatively smooth, as asperities are generally small. Moreover, if they are not totally flattened during the adhesion-induced deformation process, thereby allowing the bulk of the particle to come into contact with the substrate, they must be relatively hard. As such, it has

been proposed [119] that perhaps it would be more appropriate to describe their contribution to adhesion using the DMT model [120]. This problem has recently been addressed by Maugis [121], who found that the resulting differences would be quite small.

11. Conclusions

The field of particle adhesion is, in many ways, a mature field. Certainly, many aspects of adhesion in general, and particle adhesion in specific, can be understood in terms of the basic theories that presently exist. However, there remain many questions that have yet to be answered. Effects of humidity and capillary action, contact charging, yielding phenomena and partial plasticity, and time-dependent effects are but a few of the topics that need to be better understood. In addition, recent advances in computing technology opens the door to molecular dynamic modeling that can take realistic potentials and derive the entire spectra of physical properties, from their Young's moduli, Poisson's ratios, and yield strengths to their surface energies and works of adhesion. The potentials, themselves, can be studied using new techniques such as force-probe microscopy. Such novel computational and experimental methods allow particle adhesion interactions to be studied in detail that probably could not even be envisioned a decade ago.

A scientific discipline may be important in its own right. However, it is perhaps even more significant if that discipline provides a novel approach towards solving problems in related areas. This is the case with particle adhesion. For example, as discussed in the introduction, researchers in the area of bioadhesion and medicine are beginning to analyze their results in terms of particle adhesion effects. There are indications that the area of pressure-sensitive adhesives is also beginning to borrow concepts from particle adhesion. The general understanding of the compliant adhesive interactions between curved surfaces that is central to particle adhesion will, undoubtedly, find use in a wide range of related fields.

Another measure of the importance of a scientific discipline is its contributions to technology. In this arena, the study of particle adhesion has a long list of accomplishments and is expected to continue to add value in a variety of industries.

All things considered, the study of the adhesion of particles will likely remain a vibrant field for years to come, offering challenges and opportunities to those who seek them in this field.

References

1. Webster's New Collegiate Dictionary, G&C Merriam Company, Springfield, 1981.
2. Schein, L.B., *Electrophotography and Development Physics*, 2nd edn. Laplacian Press,

- Morgan Hill, 1996.
3. Schaffert, R.M., *Electrophotography*, Focal Press, London, 1980.
 4. Brown, R.C., *Air Filtration*, Pergamon Press, Oxford, 1993.
 5. Busnaina, A.A., Kashkoush, I.I. and Gale, G.W., *J. Electrochem. Soc.*, **142**, 2812 (1995).
 6. Berg, D.M., Grimsley, T., Hammond, P. and Sorenson, C.T. In: Mittal, K.L. (Ed.), *Particles on Surfaces 2: Detection, Adhesion, and Removal*. Plenum, New York, 1989, pp. 307–316.
 7. Gale, G.W. and Busnaina, A.A., *J. Particul. Sci. Technol.*, **13**, 249 (1995).
 8. Menon, V.B., Michaels, L.D., Donovan, R.P. and Ensor, D.S. In: Mittal, K.L. (Ed.), *Particles on Surfaces 2: Detection, Adhesion, and Removal*. Plenum, New York, 1989, pp. 297–306.
 9. Berg, D.M., Grimsley, T., Hammond P. and Sorenson, C.T. In: Mittal, K.L. (Ed.), *Particles on Surfaces 2: Detection, Adhesion, and Removal*. Plenum, New York, 1989, pp. 307–316.
 10. Wu, X., Sacher, E. and Meunier, M., *J. Adhes.*, **70**, 167 (1999).
 11. Jackson, D. and Carver, B., *Precis. Clean.*, **7**, 16 (1999).
 12. Fein, M. In: Mittal, K.L. (Ed.), *Particles on Surfaces 2: Detection, Adhesion, and Removal*. Plenum, New York, 1989, pp. 189–200.
 13. Summers Moss, M.A., Siskin, B., Zimmer, S. and Ward Anderson, K., *Biorheology*, **36**, 359 (1999).
 14. M.A. Summers Moss, B.S. Zimmer and K. Ward Anderson, *Anticancer Res.*, in press.
 15. Santos, C., Chandler, K., Zimmer, S., Fisher, P., Gunthert, U. and Ward Anderson, K., *Cell Biophys.*, **26**, 1 (1995).
 16. Baier, R.E. In: Anderson, G.L. (Ed.), *Proceedings of the 23rd Annual Meeting of the Adhesion Society*, Adhesion Society, Blacksburg, 2000, pp. 57–58.
 17. Baier, R., Meyer, A. and Glaves-Rapp, D. In: Anderson, G.L. (Ed.), *Proceedings of the 23rd Annual Meeting of the Adhesion Society*, Adhesion Society, Blacksburg, 2000, pp. 69–70.
 18. Sharpe, L.H. In: DeMejo, L.P., Rimai, D.S. and Sharpe, L.H. (Eds.), *Fundamentals of Adhesion and Interfaces*. Gordon and Breach, Amsterdam, 1999, pp. 277–290.
 19. Busnaina, A.A., Private communication.
 20. Dickenson, J.T., Jensen, L.C., Langford, S.C. and Hirth, J.P., *J. Mater. Res.*, **6**, 112 (1991).
 21. Doering, D.L., Dickenson, J.T., Langford, S.C. and Xiong-Skiba, P., *J. Vac. Sci. Technol. A*, **8**, 2401 (1990).
 22. Dickenson, J.T. In: Lee, L.-H. (Ed.), *Adhesive Bonding*, Plenum, New York, 1991, pp. 395–423.
 23. Dickenson, J.T., Jensen, L.C., Langford, S.C. and Dion, R.P., *J. Poly. Sci. Part B: Poly. Phys.*, **31**, 1441 (1993).
 24. Dickenson, J.T., Jensen, L.C. and Dion, R.P., *J. Appl. Phys.*, **73**, 3047 (1993).
 25. Dickenson, J.T. In: Lee, L.-H. (Ed.), *Adhesive Bonding*, Plenum, New York, 1991, pp. 395–423.
 26. R. Bouvy, private communication.
 27. Hertz, H., *Miscellaneous Papers*. Macmillan, London, 1896, p. 196.
 28. Timoshenko, S.P. and Goodier, J.N., *Theory of Elasticity*. McGraw Hill, New York, 1970, p. 402.
 29. Bradley, R.S., *Philos. Mag.*, **13**, 853 (1932).
 30. Bradley, R.S., *Trans. Faraday Soc.*, **32**, 1088 (1936).
 31. Derjaguin, B.V., *Kolloid Z.*, **69**, 155 (1934).
 32. Hamaker, H.C., *Physica*, **4**, 1058 (1937).

33. Lifshitz, E.M., *Soviet Phys. JETP*, **2**, 73 (1956).
34. Krupp, H., *Adv. Colloid Interface Sci.*, **1**, 111 (1967).
35. Rimai, D.S., DeMejo, L.P. and Bowen, R.C., *J. Adhes. Sci. Technol.*, **8**, 1333 (1994).
36. Bowling, R.A. In: Mittal, K.L. (Ed.), *Particles on Surfaces I: Detection, Adhesion, and Removal*. Plenum, New York, 1988, pp. 129–142.
37. Johnson, K.L., Kendall, K. and Roberts, A.D., *Proc. R. Soc. Lond. Ser. A*, **324**, 301 (1971).
38. Johnson, K.L., *Br. J. Appl. Phys.*, **9**, 199 (1958).
39. Roberts, A.D., Ph.D. Thesis, Cambridge University, 1968.
40. Kendall, K., Ph.D. Thesis, Cambridge University, 1969.
41. Tabor, D., *J. Colloid Interface Sci.*, **58**, 2 (1977).
42. Derjaguin, B.V., Muller, V.M. and Toporov, Yu.P., *J. Colloid Interface Sci.*, **67**, 378 (1978).
43. Tabor, D., *J. Colloid Interface Sci.*, **67**, 380 (1978).
44. Muller, V.M., Yushchenko, V.S. and Derjaguin, B.V., *J. Colloid Interface Sci.*, **77**, 91 (1980).
45. Muller, V.M., Derjaguin, B.V. and Toporov, Yu.P., *Colloids Surf.*, **7**, 251 (1983).
46. Maugis, D., *J. Colloid Interface Sci.*, **150**, 243 (1992).
47. Maugis, D. and Gauthier-Manuel, B., *J. Adhes. Sci. Technol.*, **8**, 1311 (1994).
48. Maugis, D. and Gauthier-Manuel, B. In: Rimai, D.S. and Mittal, K.L. (Eds.), *Fundamentals of Adhesion and Interfaces*. VSP Press, Utrecht, 1995, pp. 49–60.
49. K.L. Johnson, *Contact Mechanics*, Cambridge Press, Cambridge, 1985, p. 171 (see discussion and references cited therein).
50. Quesnel, D.J., Rimai, D.S. and DeMejo, L.P., *Phys. Rev. B*, **48**, 6795 (1993).
51. Quesnel, D.J., Rimai, D.S. and DeMejo, L.P., *J. Adhes. Sci. Technol.*, **9**, 1015 (1994).
52. Quesnel, D.J., Rimai, D.S. and DeMejo, L.P. In: Rimai, D.S., DeMejo, L.P. and Mittal, K.L. (Eds.), *Fundamentals of Adhesion and Interfaces*. VSP, Utrecht, 1994, pp. 281–296.
53. Quesnel, D.J., Rimai, D.S. and DeMejo, L.P., *J. Adhes.*, **51**, 49 (1995).
54. Quesnel, D.J., Rimai, D.S. and DeMejo, L.P., *Sol. State Commun.*, **85**, 171 (1993).
55. Quesnel, D.J., Rimai, D.S. and DeMejo, L.P., *J. Adhes.*, **67**, 235 (1998).
56. DeMejo, L.P., Rimai, D.S. and Bowen, R.C., *J. Adhes. Sci. Technol.*, **5**, 959 (1991).
57. Rimai, D.S., DeMejo, L.P., Vreeland, W., Bowen, R., Gaboury, S.R. and Urban, M.W., *J. Appl. Phys.*, **71**, 2253 (1992).
58. Rimai, D.S., DeMejo, L.P. and Bowen, R.C., *J. Appl. Phys.*, **66**, 3574 (1989).
59. Rimai, D.S., DeMejo, L.P., Vreeland, W.B. and Bowen, R.C., *Langmuir*, **10**, 4361 (1994).
60. Maugis, D., *Langmuir*, **11**, 679 (1995).
61. D.S. Rimai, D.J. Quesnel and R.C. Bowen, to be published.
62. D.J. Quesnel, unpublished. See, also, ref. [61].
63. Maugis, D. and Pollock, H.M., *Acta Metall.*, **32**, 1323 (1984).
64. Rimai, D.S., DeMejo, L.P. and Bowen, R.C., *J. Appl. Phys.*, **68**, 6234 (1990).
65. Rimai, D.S., Moore, R.S., Bowen, R.C., Smith, V.K. and Woodgate, P.E., *J. Mat. Res.*, **8**, 662 (1993).
66. Bowen, R.C., DeMejo, L.P. and Rimai, D.S., *J. Adhes.*, **51**, 201 (1995).
67. Rimai, D.S., DeMejo, L.P. and Bowen, R.C., *J. Adhes.*, **51**, 139 (1995).
68. Lee, L.-H. In: Rimai, D.S., DeMejo, L.P. and Mittal, K.L. (Eds.), *Fundamentals of Adhesion and Interfaces*. VSP, Utrecht, 1995, pp. 73–94.
69. Tang, J. and Busnaina, A.A. In: Anderson, G.L. (Ed.), *Proceedings of the 23rd Annual Meeting of the Adhesion Society*. Adhesion Society, Blacksburg, 2000, pp. 367–369.
70. Lee, M.H. and Jaffe, A.B. In: Mittal, K.L. (Ed.), *Particles on Surfaces I: Detection, Adhesion, and Removal*. Plenum Press, New York, 1988, pp. 169–178.

71. Hays, D.A. In: Mittal, K.L. (Ed.), *Particles on Surfaces I: Detection, Adhesion, and Removal*. Plenum Press, New York, 1988, pp. 351–360.
72. Fowlkes, W.Y. and Robinson, K.S. In: Mittal, K.L. (Ed.), *Particles on Surfaces I: Detection, Adhesion, and Removal*. Plenum Press, New York, 1988, pp. 143–155.
73. Mastrangelo, C.J., *Photogr. Sci. Eng.*, **26**, 194 (1982).
74. Cross, J., *Inst. Phys. Conf. Ser.*, **27**, 202 (1975).
75. Donald, D.K., *J. Adhes.*, **4**, 233 (1972).
76. Hays, D.A., *Photogr. Sci. Eng.*, **22**, 232 (1978).
77. Lee, M.H. and Ayala, J., *J. Imag. Technol.*, **11**, 279 (1985).
78. Nebenzahl, L., Borgioli, J., De Palma, V., Gong, K., Mastrangelo, C. and Pourroy, F., *Photogr. Sci. Eng.*, **24**, 293 (1980).
79. Schaefer, D.M., Carpenter, M., Gady, B., Reifenberger, R., DeMejo, L.P. and Rimai, D.S. In: Rimai, D.S., DeMejo, L.P. and Mittal, K.L. (Eds.), *Fundamentals of Adhesion and Interfaces*. VSP, Utrecht, 1995, pp. 35–48.
80. Mizes, H. In: Rimai, D.S. and Sharpe L.H. (Eds.), *Advances in Particle Adhesion*. Gordon and Breach Publishers, Amsterdam, 1996, pp. 155–166.
81. Hays, D.A. In: Rimai, D.S., DeMejo, L.P. and Mittal, K.L. (Eds.), *Fundamentals of Adhesion and Interfaces*. VSP, Utrecht, 1995, pp. 61–71.
82. Horn, R.G., Smith, D.T. and Grabbe, A., *Nature*, **366**, 442 (1993).
83. Horn, R.G. and Smith, D.T., *Science*, **256**, 362 (1992).
84. Smith, D.T., *J. Electrostat.*, **26**, 291 (1991).
85. Israelachvili, J.N. and Adams, G.E., *J. Chem. Soc. Faraday Trans. 1*, **74**, 975 (1978).
86. Gady, B., Reifenberger, R., Rimai, D.S. and DeMejo, L.P., *Langmuir*, **13**, 2533 (1997).
87. Lorrain, P. and Corson, D., *Electromagnetic Fields and Waves*, 2nd edn. Freeman Press, San Francisco, 1970.
88. Smythe, W.R., *Static and Dynamic Electricity*, 3rd edn. Hemisphere Publishing Company, New York, 1989.
89. Goel, N.S. and Spencer, P.R. In: Lee, L.H. (Ed.), *Adhesion Science and Technology, Part B*, Plenum Press, New York, 1975, pp. 763–829.
90. Fowlkes, W.Y. and Robinson, K.S. In: Mittal, K.L. (Ed.), *Particles on Surfaces I: Detection, Adhesion, and Removal*. Plenum Press, New York, 1988, pp. 143–155.
91. Jones, T.B. In: *Proceedings of the IEEE-IAS 1984 Annual Meeting*, 1984, p. 1136.
92. Jones, T.B., *J. Electrostat.*, **18**, 55 (1986).
93. Hays, D.A. In: Rimai, D.S. and Sharpe, L.H. (Eds.), *Advances in Particle Adhesion*. Gordon and Breach Publishers, Amsterdam, 1996, pp. 41–48.
94. Gady, B., Quesnel, D.J., Rimai, D.S., Leone, S. and Alexandrovich, P., *J. Imag. Sci. Technol.*, **43**, 288 (1999).
95. Israelachvili, J., *Intermolecular and Surface Forces*. Academic Press, San Diego, 1992.
96. Rimai, D.S. and Quesnel, D.J., *Fundamentals of Particle Adhesion*. Global Press, Moorhead, in press.
97. Lorrain, P. and Corson, D., *Electromagnetic Fields and Waves*, 2nd edn. W.H. Freeman, San Francisco, 1970.
98. Adamson, A.W., *Physical Chemistry of Surfaces*, 4th edn. Wiley, New York, 1982.
99. Jaycock, M.J. and Parfitt, G.D., *Chemistry of Interfaces*. Ellis Horwood, West Sussex, 1981.
100. Jones, T.B., *Electromechanics of Particles*. Cambridge University Press, Cambridge, 1995.
101. Gady, B., Reifenberger, R. and Rimai, D.S., *J. Appl. Phys.*, **84**, 319 (1998).
102. Gady, B., Schleef, D., Reifenberger, R. and Rimai, D.S., *J. Adhes.*, **67**, 291 (1998).

103. DeMejo, L.P., Rimai, D.S. and Bowen, R.C., *J. Adhes. Sci. Technol.*, **2**, 331 (1988).
104. Rimai, D.S., DeMejo, L.P. and Bowen, R.C., *J. Appl. Phys.*, **65**, 755 (1989).
105. Lee, L.H. In: Lee, L.-H. (Ed.), *Fundamentals of Adhesion*. Plenum, New York, 1991, pp. 1–86.
106. Drago, R.S., Vogel, G.C. and Needham, T.E., *J. Am. Chem. Soc.*, **93**, 6014 (1971).
107. Fowkes, F.M., *J. Adhes. Sci. Technol.*, **1**, 7 (1987).
108. Krishnan, S., Busnaina, A.A., Rimai, D.S. and DeMejo, L.P., *J. Adhes. Sci. Technol.*, **8**, 1357 (1994).
109. Vrtis, J.K., Athanasiou, C.D., Farris, R.J., DeMejo, L.P. and Rimai, D.S., *J. Adhes. Sci. Technol.*, **8**, 929 (1994).
110. Rimai, D.S., DeMejo, L.P., Chen, J., Bowen, R.C. and Mourey, T.H., *J. Adhes.*, **62**, 151 (1997).
111. Johnson, K.L., Presented at the ACS meeting in Boston, August, 1998.
112. Rimai, D.S., DeMejo, L.P. and Bowen, R.C., *J. Adhes.*, **51**, 139 (1995).
113. Rimai, D.S., Quesnel, D.J., DeMejo, L.P. and Bowen, R.C. In: Dickie, R.A. (Ed.), *Proceedings of the 21st Annual Meeting of the Adhesion Society*. Adhesion Society, Blacksburg, 1998, pp. 266–268.
114. Gady, B., Schleef, D., Reifenberger, R., Rimai, D. and DeMejo, L.P., *Phys. Rev. B*, **53**, 8065 (1996).
115. Gane, N., Pfaelzer, P.F. and Tabor, D., *Proc. R. Soc. Lond. Ser. A*, **340**, 495 (1974).
116. Schaefer, D.M., Carpenter, M., Gady, B., Reifenberger, R., DeMejo, L.P. and Rimai, D.S., *J. Adhes. Sci. Technol.*, **9**, 1049 (1995).
117. Gady, B., Reifenberger, R., Schaefer, D.M., Bowen, R.C., Rimai, D.S., DeMejo, L.P. and Vreeland, W., *J. Adhes.*, **67**, 19 (1998).
118. Fuller, K.N.G. and Tabor, D., *Proc. R. Soc. Lond. Ser. A*, **345**, 327 (1975).
119. Rimai, D.S., Quesnel, D.J. and Busnaina, A.A., *Colloids Surf. A*, **165**, 3 (2000).
120. Derjaguin, B.V., Toporov, V.M. and Toporov, Yu.P., *J. Colloid Interface Sci.*, **53**, 314 (1975).
121. Maugis, D., *J. Adhes. Sci. Technol.*, **10**, 161 (1996).

Surface mechanical measurements at the nanoscale

K.J. WAHL ^{a,*} and S.A. SYED ASIF ^b

^a *Naval Research Laboratory, Code 6176, Washington, DC 20375-5342, USA*

^b *Hysitron Inc., Minneapolis, MN 55439, USA*

1. Introduction

Recently, a number of instruments have been developed that allow researchers to probe adhesive interactions and mechanical properties of surfaces with nanoscale force, displacement, and spatial resolution. These instruments fall into two general categories, atomic force microscopy (AFM) [1] and depth-sensing nanoindentation [2]. Both techniques employ spring-based systems to evaluate force–displacement relationships between a probe (tip) and a sample surface; AFM and some nanoindenters provide imaging through topographic mapping of the sample with nanometer-scale resolution. Over the past decade, experimental capabilities provided by AFM and nanoindentation (e.g. nanoscale adhesion, hardness, and modulus measurements) have become widely available to researchers through various commercial instruments. Both AFM and nanoindentation instruments have significantly enhanced nanoscale adhesion and mechanics studies of thin films, composites, polymers, biological materials, and colloidal particles.

As is true for macroscopic adhesion and mechanical testing experiments, nanoscale measurements do not a priori sense the intrinsic properties of surfaces or adhesive junctions. Instead, the measurements reflect a combination of interfacial chemistry (surface energy, covalent bonding), mechanics (elastic modulus, Poisson's ratio), and contact geometry (probe shape, radius). Furthermore, the probe/sample interaction may not only consist of elastic deformations, but may also include energy dissipation at the surface and/or in the bulk of the sample (or even within the measurement apparatus). Study of rate-dependent adhesion and mechanical properties is possible with both nanoindentation and

* Corresponding author. E-mail: wahl@stm2.nrl.navy.mil

AFM through force or displacement modulation techniques. Numerous methods have evolved that take advantage of the greater sensitivity modulation techniques provide, allowing dissipative processes to be examined. However, evaluation of the probe/sample response requires care with test protocols and instrument calibration, as well as application of appropriate contact mechanics models; only a few of these techniques have evolved into quantitative methods.

Perhaps the most significant complication in the interpretation of nanoscale adhesion and mechanical properties measurements is the fact that the contact sizes are below the optical limit ($\sim 1\ \mu\text{m}$). Macroscopic adhesion studies and mechanical property measurements often rely on optical observations of the contact, and many of the contact mechanics models are formulated around direct measurement of the contact area or radius as a function of experimentally controlled parameters, such as load or displacement. In studies of colloids, scanning electron microscopy (SEM) has been used to view particle/surface contact sizes from the side to measure contact radius [3]. However, such a configuration is not easily employed in AFM and nanoindentation studies, and undesirable surface interactions from charging or contamination may arise. For adhesion studies (e.g. Johnson–Kendall–Roberts (JKR) [4] and probe-tack tests [5,6]), the probe/sample contact area is monitored as a function of load or displacement. This allows evaluation of load/area or even stress/strain response [7] as well as comparison to and development of contact mechanics theories. Area measurements are also important in traditional indentation experiments, where hardness is determined by measuring the residual contact area of the deformation optically [8]. For micro- and nanoscale studies, the dimensions of both the contact and residual deformation (if any) are below the optical limit.

Consequently, for studies at the nanoscale to go beyond simple measurements of force and displacement requires a different approach, namely an indirect measurement of the contact area. For hardness measurements in indentation, the size of the permanently deformed region can be obtained *ex situ* with SEM or topographical imaging using AFM. *In situ*, contact areas can be inferred indirectly from depth-sensing nanoindentation experiments by careful calibration of the indenter geometry to obtain a depth–area relationship [9]. Finally, contact stiffness measurements, made using a small force or displacement perturbation, can also be used with AFM or indentation to infer the contact area during an experiment. All of these techniques provide necessary methods to obtain valuable information about the adhesion and mechanical response, despite the small scale of these contacts.

In this chapter, we overview basic techniques for making nanoscale adhesion and mechanical property measurements. Both quasi-static and dynamic measurements are addressed. In Section 2 of this chapter, we overview basic AFM instrumentation and techniques, while depth-sensing nanoindentation is overviewed in Section 3. Section 4 addresses recent advances in instrumentation and techniques

combining both depth-sensing nanoindentation and scanning capabilities ('hybrid' nanoindenter).

2. Atomic force microscopy

Following development of the scanning tunneling microscope (STM), which required conducting surfaces, Binnig and co-workers [1] realized that by employing a small gold cantilever with a diamond tip, forces between the tip and sample could be measured if the cantilever's deflection and spring constant were known. They used the tunneling between the STM tip and the cantilever to detect the displacement, and the force, F , was determined using Hooke's law, $F = -kz$, where z is the cantilever's vertical displacement and k is the spring constant. Today, the optical lever technique (employing a focused laser beam [10] deflected off the cantilever onto a photodetector [11]), is most commonly used to detect the cantilever's motion, although various techniques such as interferometry [12–14] and embedded piezoelectric films [15] have also been used. The sample x – y – z motion and position, controlled by piezoelectric ceramics that expand and contract with applied voltage, can be used for either imaging [1] (using feedback techniques to keep the cantilever deflection constant) or force–displacement (force curve) measurements [16]. The cantilevers, with pyramidal or conical shaped tips, are typically manufactured from silicon nitride or silicon; early studies used etched tungsten wire. The ends of the tips are blunted, and their radii can vary from less than 10 nm to hundreds of nanometers. Micron-scale spheres can also be attached to the levers to vary tip material and contact geometry [17].

2.1. *Quasi-static measurements: force–distance curves and adhesion*

Numerous AFM imaging techniques have been developed and commercialized to monitor topography, friction, mechanical response, capacitance, magnetic properties, etc. However, adhesion measurements require the tip to come into, and out of, contact to measure attractive and adhesion forces. Therefore, other than to select an analysis region, most imaging techniques are not useful for adhesion studies. Instead, measurements are necessarily based on force–displacement curve approaches.

In a force–displacement curve, the tip and sample surfaces are brought close to one another, and interact via an attractive potential. This potential is governed by intermolecular and surface forces [18] and contains both attractive and repulsive terms. How well the shape of the measured force–displacement curve reproduces the true potential depends largely on the cantilever spring constant and tip radius. If the spring constant is very low (typical), the tip will experience a mechanical instability when the interaction force gradient (dF/dD) exceeds the

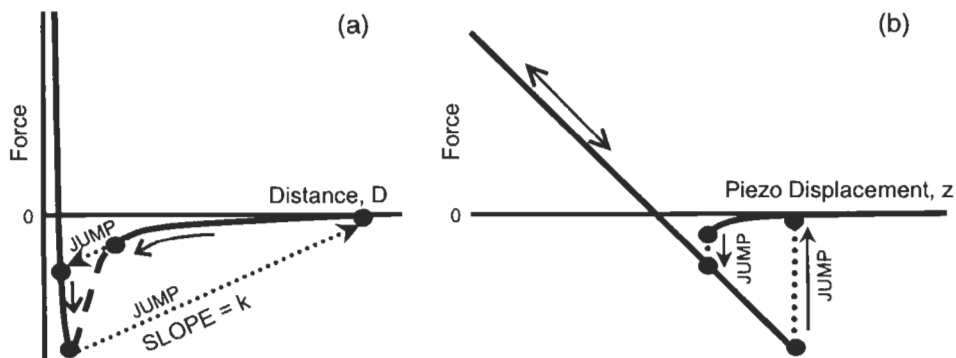


Fig. 1. Schematic diagram illustrating the mechanical instability for (a) a weak spring (spring constant k) a distance D from the surface, experiencing an arbitrary surface force (after [19]) and (b) the experimentally observed force–distance curve relative to the AFM sample position (piezo displacement) for the same interaction.

spring stiffness and suddenly snap into contact with the surface (see Fig. 1a) [19]. A similar jump will occur when the sample is retracted and the tip separates from the sample, often at a different location due to the shape of the potential. It is important to realize that hysteresis, between the attractive and adhesion forces, is often observed under these conditions and is due to mechanical instability and not chemical interactions. The force curve data obtained by the experimenter will be a function of sample position (z piezo displacement) and cantilever deflection, from which force can be calculated (Fig. 1b shows an example for a weak spring). Increasing the cantilever stiffness will increase the fraction of the interaction probed; however, if the cantilever is too stiff the deflection may be so small that the forces cannot be detected. It is also important to note that if the sample stiffness is lower than the cantilever stiffness (as might be the case for low modulus polymers), the sample surface itself may instead jump into contact with the tip when the contact is formed [19].

Hertzian mechanics alone cannot be used to evaluate the force–distance curves, since adhesive contributions to the contact are not considered. Several theories, namely the JKR [4] model and the Derjaguin, Muller and Torporov (DMT) model [20], can be used to describe adhesion between a sphere and a flat. Briefly, the JKR model balances the elastic Hertzian pressure with attractive forces acting only within the contact area; in the DMT theory attractive interactions are assumed to act outside the contact area. In both theories, the adhesive force is predicted to be a linear function of probe radius, R , and the work of adhesion, W_A , and is given by Eqs. 1 and 2 below.

$$F_{\text{JKR}} = -1.5\pi R W_A \quad (1)$$

$$F_{\text{DMT}} = -2\pi R W_A \quad (2)$$

For a tip/sample interaction, the work of adhesion can be estimated by the Dupré equation, $W_A = \gamma_t + \gamma_s - \gamma_{ts}$, where γ_t and γ_s are the surface energies of the tip and of the sample, and γ_{ts} is the interfacial free energy. These two models represent limiting cases, the former for materials with low elastic modulus, large radius, and small surface energy, and the latter with high modulus, small radius and large surface energy. The transition between the models has been compared by Tabor [21] and evaluated by Muller et al. [22,23] and later generalized by Maugis [24].

The first force curve studies by Burnham et al. [25] measured attractive forces and adhesion between a tungsten tip and various samples as a function of sample surface energy in dry nitrogen. They found that these forces, normalized to the tip radius, strongly depended on sample surface energy. Capillary forces (e.g. from condensation of water vapor [14] or liquid films [26]) can strongly affect adhesion. To eliminate the effects of capillary forces and limit surface contamination, one can work in liquids [27–30] or ultra-high vacuum (UHV) [31,32]. For example, by working in ethanol and functionalizing both tip and surface with covalently bonded self-assembled monolayers (SAMs), Frisbie et al. [28] were able to rank the adhesion between various combinations of hydrophilic (–COOH), and hydrophobic (–CH₃) surfaces. They found that tip/sample interactions ranked, in decreasing order, COOH/COOH > CH₃/CH₃ > CH₃/COOH, which qualitatively agreed with expectations from calculations based on surface energies obtained through contact angle measurements [33]. The sensitivity of the AFM allows many other types of measurements, including single-molecule interactions [34], protein unfolding [35], and measurements of polymer chain pullout [36]. There are numerous examples in the literature exploring surface forces measurements with AFM; thorough reviews have recently been given by Cappella and Dietler [37] and Janshoff et al. [38] and hence will not be attempted here. Further discussions of force curve interpretation are also available elsewhere [39,40].

The scanning capabilities of the AFM can also be used to compare and map tip/sample adhesion over a surface by making a series of force curves while rastering the sample under the tip.¹ Two methods have been used and involve making multiple contacts to either a preset maximum force (see e.g. [41,42]) or over a preset displacement range [43–45]. The spatial variation in adhesion, topography or elastic properties can be plotted as an image using the force curve techniques (see e.g. Fig. 2) [46]. Finally, combinatorial approaches to studying adhesion can be explored by using tipless cantilevers and substrates with multiple tips [47].

¹ The force–curve mapping technique is often referred to as force–volume mapping commercially, although sample volume is not probed unless stiff levers or compliant surfaces are used.

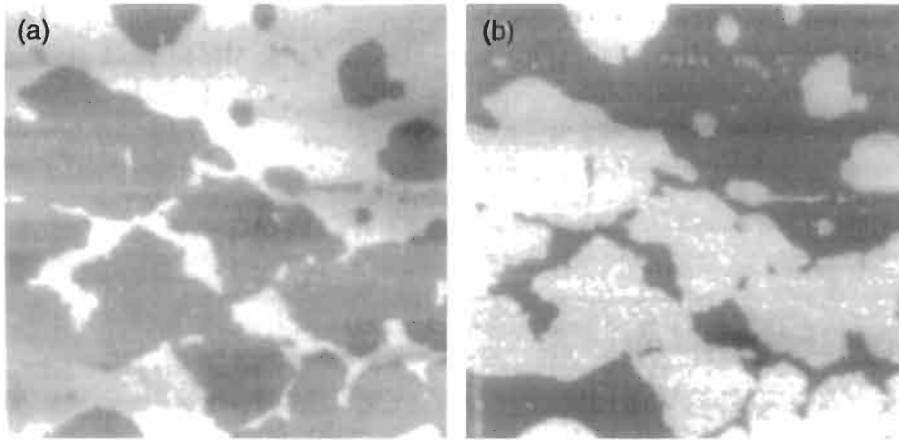


Fig. 2. Maps ($2 \times 2 \mu\text{m}$) of sample topography (height variation) and pull-off adhesive force for a Langmuir–Blodgett film on mica consisting of a 1 : 1 mixture of palmitic (C16) and lignoceric (C24) fatty acids [46].

2.2. *Quasi-static measurements: force–distance curves and mechanical properties*

Mechanical properties of materials can also be obtained through analyses of force–distance curves generated with an AFM. In the AFM, it is important to understand that measurements are usually displacement controlled — the sample is displaced against a cantilever indenter via a piezoelectric actuator — and forces are inferred from the measured deflection of the cantilever and its (nominally) known spring constant. Several different cantilever configurations and displacement detection schemes have been used for these measurements (Fig. 3a) [40]. Early studies by Burnham and Colton [16] employed double beam and crossed beam spring configurations, with spring deflection measured via STM tunneling current. More recently, simple diving-board cantilevers and optical detection are being used [48–50]. Because the AFM uses a displacement based configuration, the simple mechanical model is that of two springs in series (Fig. 3b) and the contact stiffness given by [51]

$$k_{\text{contact}} = 2E^*a \quad (3)$$

where E^* is the reduced modulus calculated from the Poisson's ratios, ν , and elastic moduli, E , of the two contacting materials ($E^* = [(1 - \nu_1^2)/E_1 + (1 - \nu_2^2)/E_2]^{-1}$), and a is the contact radius. This configuration has several ramifications for indentation via AFM. First, the indenter spring stiffness must be matched to the contact stiffness in order to get a measurable deformation in the sample itself, rather than simple deflection of the cantilever spring. Secondly, depth of

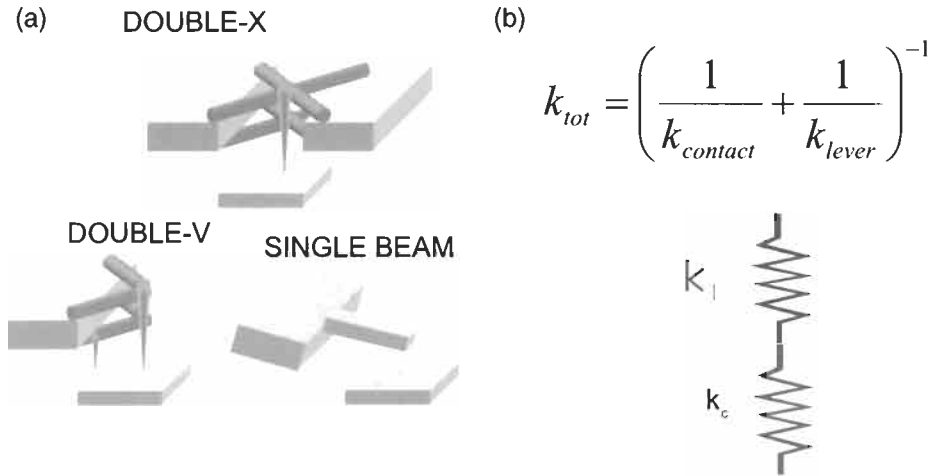


Fig. 3. (a) Illustration of various AFM cantilever configurations for indentation experiments and (b) simple mechanical model for AFM-based indentation (by sample displacement).

penetration (and projected contact area), for all but the most compliant materials, is difficult to determine due to piezo creep and hysteresis effects [52].

A series of force–distance curves for various materials pairs examined (gold/nickel, diamond/graphite, diamond/diamond) are shown in Fig. 4 [39]. For an indentation, the unloading slope (dF/dx) of the force–displacement curve is a measure of the contact stiffness and can be used to determine the modulus if the contact area (A) is known using a variant of Eq. 3 below.

$$E^* = \frac{\sqrt{\pi} \cdot \text{slope}}{2\sqrt{A}} \quad (4)$$

Trends in the unloading slopes of force–distance curves in Fig. 4 were consistent with expected relative reduced moduli. However, because of the difficulty in determining indenter penetration relative to the sample surface for these relatively stiff materials, A was unknown and only qualitative results could be obtained. Semi-quantitative measurements are possible under certain circumstances (e.g. compliant elastomers) [50] where tip penetration into the sample is significant. However, the indentation geometries involving non-perpendicular tip-sample approach result in significant lateral force contributions during indentation (evidenced by asymmetrical indents) [48]. Additionally, the compliant materials systems accessible with this approach often have significant time-dependent materials properties (e.g. creep relaxation and viscoelastic behavior) that complicate (and even prevent) analyses of mechanical properties from simple force–displacement curves [53].

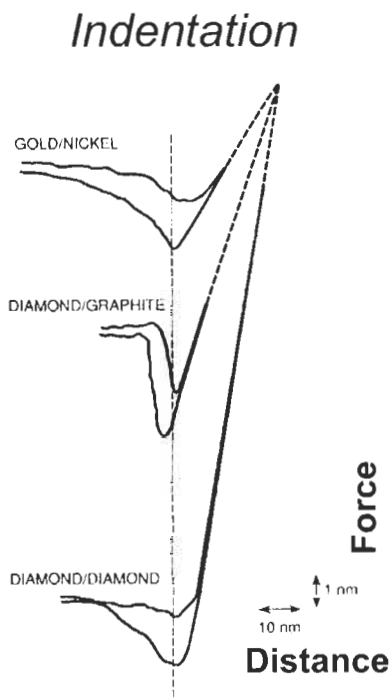


Fig. 4. AFM force curves (using double-cross configuration) showing unloading slope differences for various material pairs. Reprinted with permission from ref. [39]. Copyright 1994 Institute of Physics.

2.3. Dynamic measurements via cantilever oscillation

Another force curve technique involves applying an oscillation to the base of the cantilever support, causing the tip end of the cantilever to oscillate [54]. The amplitude or phase of the oscillation can be monitored using a lock-in amplifier, and the changes in amplitude or phase due to tip/sample interactions can be used to produce images (using feedback techniques) or enhance force curves. This technique is often referred to as intermittent contact or tapping mode in the literature, and can be used to produce high-resolution images of compliant, sticky materials. In general, oscillation frequencies near the cantilever resonance are used (typically tens to hundreds of kiloHertz for very stiff cantilevers). Quantitative interpretation of phase or amplitude images and force curves obtained with this method can be difficult, due in part to the non-linearity of the tip sample response when large oscillation amplitudes are used (see e.g. [55–60] for further discussion of interpretation). As a recent example, Bar and coworkers [61] have used tapping mode force curves to investigate stiffness changes of polydimethylsiloxane (PDMS) surfaces that were plasma oxidized. The results of

their experiments compared favorably with models of tip-surface interaction and qualitatively demonstrated that the PDMS modulus was increased by oxidation.

2.4. Dynamic measurements: inferring the contact area

The above measurements all rely on force and displacement data to evaluate adhesion and mechanical properties. As mentioned in the introduction, a very useful piece of information to have about a nanoscale contact would be its area (or radius). Since the scale of the contacts is below the optical limit, the techniques available are somewhat limited. Electrical resistance has been used in early contact studies on clean metal surfaces [62], but is limited to conducting interfaces. Recently, Enachescu et al. [63] used conductance measurements to examine adhesion in an ideally hard contact (diamond vs. tungsten carbide). In the limit of contact size below the electronic mean free path, but above that of quantized conductance, the contact area scales linearly with contact conductance. They used these measurements to demonstrate that friction was proportional to contact area, and the area vs. load data were best-fit to a DMT model.

A very useful way to infer the contact area in a nanoscale measurement is by monitoring the contact interaction stiffness, in either the normal or lateral direction. In AFM, Jarvis and coworkers [64] were first to implement this technique by directly oscillating the tip perpendicular to the sample using magnetic forces applied via a small magnet glued to the end of a cantilever. This provided interaction stiffness information along with the force-displacement curves and greatly increased measurement sensitivity. Additionally, since the force is applied directly to the end of the cantilever, the experiment is force-controlled and removes problems associated with cantilever instabilities.

2.4.1. Lateral contact stiffness and elastic contacts

A very practical way to infer the contact area was later developed by Carpick et al. [65] and Lantz et al. [66]. In these experiments, a small (up to nanometer) lateral modulation, dx , is applied to the sample, and torsion² of the cantilever is monitored with a lock-in amplifier to detect the lateral force response, dF (Fig. 5). In this way, the lateral stiffness, k_{tot} [51], given by

$$\frac{dF}{dx} = k_{\text{tot}} = \left[\frac{1}{k_{\text{lever(lateral)}}} + \frac{1}{k_{\text{contact}}} \right]^{-1} \quad (5)$$

² The shape of AFM cantilevers (much thinner than the width) results in torsional deflection when forces push the tip laterally as in friction measurements (when the tip is sliding) or lateral stiffness measurements (when the tip is stuck).

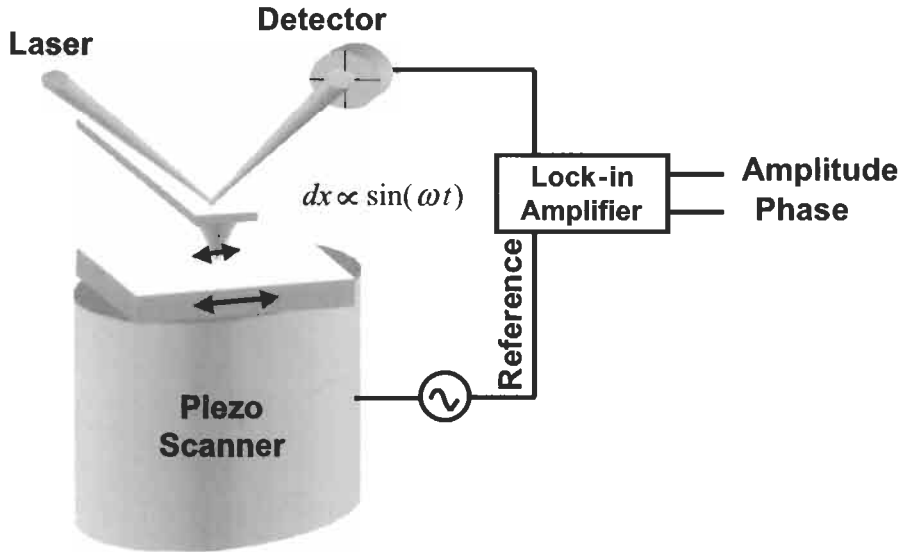


Fig. 5. Schematic diagram of AFM setup for shear modulation measurement.

can be measured as a function of load. The mechanical response of Eq. 5 is a convolution of the cantilever's lateral spring stiffness, $k_{\text{lever(lateral)}}$, and the contact lateral stiffness, k_{contact} , evaluated for a perfectly elastic contact as two springs in series, the same as shown in Fig. 3b for the normal contact stiffness. The lateral contact stiffness for a sphere/plane contact is given by [65]

$$k_{\text{contact}} = 8G^*a \quad (6)$$

where G^* is the reduced shear modulus calculated from the tip and sample shear moduli, and a is the contact radius. By measuring the lateral contact stiffness as a function of load during a force–displacement curve (Fig. 6 [67]), the contact radius can be inferred if G^* is assumed to be constant. Both groups used this measure of the contact area, combined with friction data over an equivalent load range, to determine the shear strength of silicon nitride vs. mica [65] and silicon vs. NbSe₂ interfaces [66]. This technique was extended by Mazeran and Loubet [68] to determine the sample modulus during imaging of an elastic contact assuming DMT theory applied.

The measurements of inferred contact area (from lateral stiffness or conductance data) as a function of load (e.g. during a force curve) can be compared to the continuum mechanics adhesion models (e.g. JKR, DMT, Maugis transition regime). Ranges of behaviors spanning DMT and JKR have been observed in nanoscale contacts. While the diamond/tungsten contact described above had DMT-like behavior, the silicon nitride/mica interface was best fit by the JKR model [69], and the silicon vs. NbSe₂ interfaces fell within the Maugis transition regime. To simplify the fitting of contact area–load data obtained in these experi-

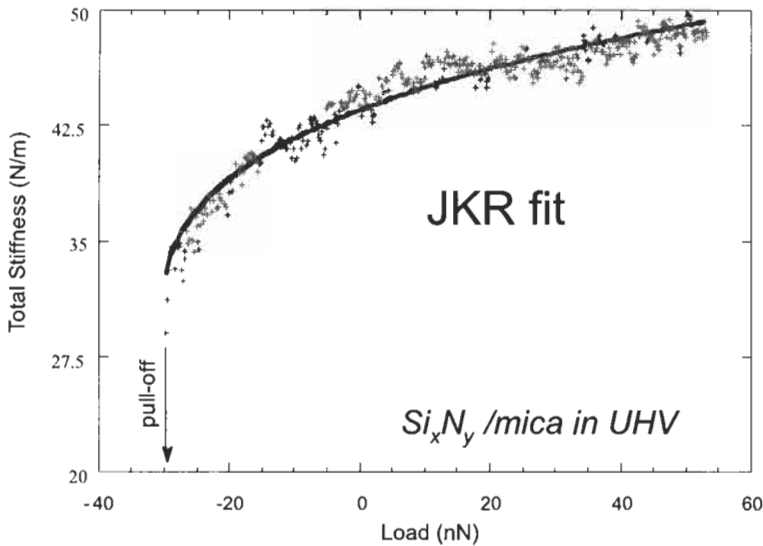


Fig. 6. Lateral stiffness vs. load data for a silicon nitride tip vs. mica surface in ultra-high vacuum. Solid line is fit of the JKR model to the data. Reprinted with permission from ref. [67].

ments, Carpick et al. [70] devised a general equation allowing use of conventional curve fitting software. This method provides a fast way to determine where the contact behavior lies (JKR, DMT or transition) using an empirical relationship rather than the more cumbersome analytic relationship provided by Maugis. One can also determine Maugis' 'transition parameter' λ (or equivalently Tabor's parameter μ) with this method (see earlier chapters in this volume).

2.4.2. Lateral contact stiffness and viscoelastic contacts

If the sample surface mechanical response is not perfectly elastic, the above stiffness analysis is inappropriate, as the dissipation will result in a phase shift of the tip-sample response with respect to the drive oscillation. Wahl et al. [71] extended the use of lateral contact stiffness measurements with AFM to viscoelastic polymers by modeling the sample as a Voigt element (spring and dashpot in parallel). In these experiments, the viscoelastic shear response was investigated by monitoring both the lateral amplitude and phase response of the tip with respect to the drive signal during a force-distance curve or at fixed loads. Frequency dependence (between 100 and 1000 Hz) of the contact stiffness and relaxation times at a fixed load are shown in Fig. 7. By varying the load (e.g. during a force curve measurement), both the quasi-static (force curve indentation rate) and dynamic (frequency) dependent properties of the contact could be studied simultaneously. The lateral modulation technique has been further extended by

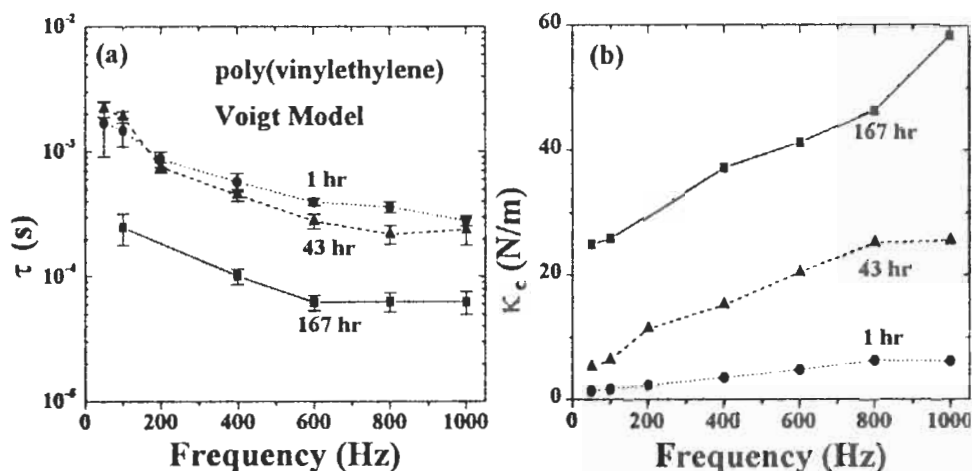


Fig. 7. Voigt model analysis of (a) lateral contact stiffness and (b) the response time, τ , for a silicon nitride tip vs. poly(vinylethylene) as a function of frequency and polymer aging times. Reprinted with permission from ref. [71].

Basire and Fretigny [72] to determine the sample modulus quasi-statically for viscous contacts.

2.4.3. Lateral contact stiffness and glass transition temperature

Recently, Overney and coworkers [73] have used lateral stiffness measurements to measure glass transition temperatures, T_g , of polymer thin films of varying thickness and molecular weight (Fig. 8). They observe a sharp increase in the slope of the tip amplitude response (related to contact stiffness) as function of sample temperature. The T_g values measured compared favorably with the bulk for polystyrene films as thin as 17 nm. Somewhat surprisingly, the strong increase in stiffness response at T_g coincides with a large drop in modulus polymers experience at T_g . From Eq. 6 one would expect a drop in stiffness if the contact area remained constant; however, the AFM cannot keep the tip-sample penetration depth constant during the measurement. The resulting increase in measured stiffness is a convolution of the increased contact radius as the tip sinks into the sample and the decreased shear modulus, and in these measurements, the contact radius dominated the stiffness response. The T_g behavior of heterogeneous films have also been examined with this technique [74].

2.5. Summary

Overall, the AFM is a powerful tool that can provide very high force and spatial resolution measurements of adhesion and mechanical properties. The reader is

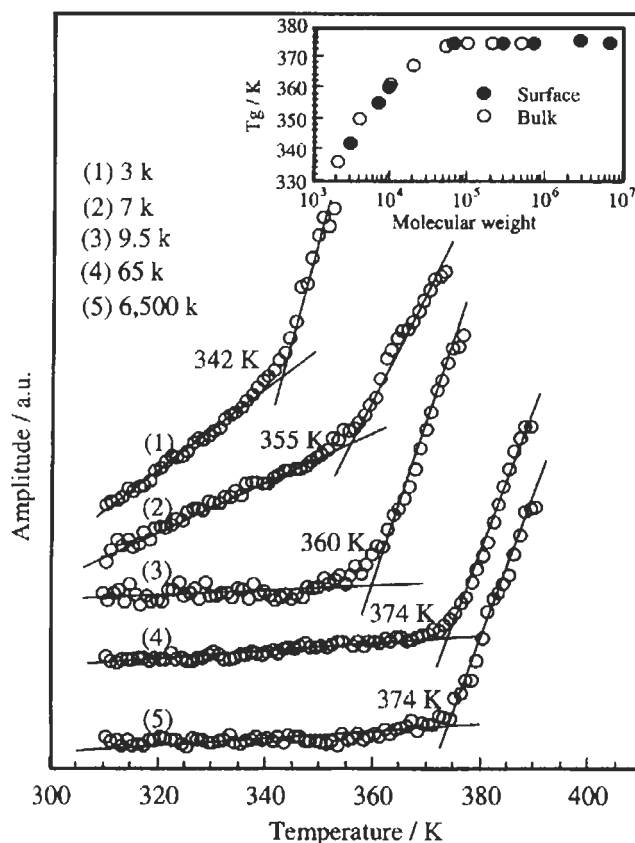


Fig. 8. Lateral tip amplitude response vs. temperature curves for PS films 200–300 nm thick of molecular weights between 3 and 6500 kg/mol. Reprinted with permission from ref. [73].

cautioned that drawbacks (challenges!!) of the AFM, however, can include significant calibration, geometric and mechanical issues [75]. Calibration of normal spring constants is reasonably well established using a variety of techniques [76–78]. Accurate calibration of the lateral spring constants of cantilevers is more difficult (although certainly not impossible [79]), and can affect quantification of lateral forces for friction or contact stiffness measurements. Additionally, the almost universal use of micromachined cantilevers having short tips has necessitated in an off-normal (10–15°) tip-sample approach (which differs from the early use of crossed or bent wires with long tips that allowed perpendicular tip/sample orientation, as shown in Fig. 3a). This results in the tip often sliding along the sample during adhesion or indentation measurements [48]. Finally, it is important to note that the dynamic response of the mechanical system (cantilever/tip/sample) is highly dependent on the choice of oscillation frequency, where the oscillation is applied (e.g. to cantilever base or the sample), and how the oscillation is applied

(displacement or force modulation) [80]. For example, another variation of the modulation method uses vertical (z) oscillation of the sample above cantilever resonance frequency and can be used to produce local maps of sample elasticity [81].

Additional suggested resources for the reader include introductory articles on scanning probe techniques for materials properties measurement [82,83]. A comprehensive manual describing various surface preparation techniques, experimental procedures and instrumentation is also a good resource [84], although the more recent modulation based techniques are not covered. Key textbooks include Johnson's on contact mechanics [51] and Israelachvili's on surface forces [18], as well as a treatment of JKR/DMT issues by Maugis [85].

3. Depth-sensing nanoindentation

Indentation has been used for over 100 years to determine hardness of materials [8]. For a given indenter geometry (e.g. spherical or pyramidal), hardness is determined by the ratio of the applied load to the projected area of contact, which was determined optically after indentation. For low loads and contacts with small dimensionality (e.g. when indenting thin films or composites), a new way to determine the contact size was needed. Depth-sensing nanoindentation [2] was developed to eliminate the need to visualize the indents, and resulted in the added capability of measuring properties like elastic modulus and creep.

In depth-sensing nanoindentation, a controlled, variable force is applied to a sample through an indenter, and the resulting displacement of the indenter is measured. The resulting 'load vs. displacement' data, together with the indenter geometry, can be analyzed to obtain hardness and elastic modulus using well-established mechanical models [9]. In general, the most common instrument configuration uses a parallel plate geometry, where a center plate is held by leaf springs between two rigid parallel plates (Fig. 9a). A diamond indenter tip

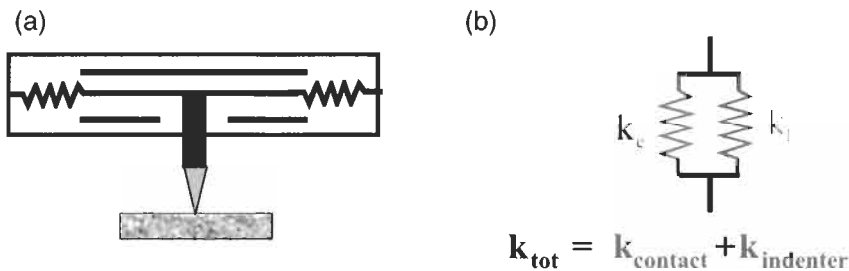


Fig. 9. (a) Depth-sensing nanoindenter model and (b) simple mechanical model for force controlled indentation assuming purely elastic contact mechanics.

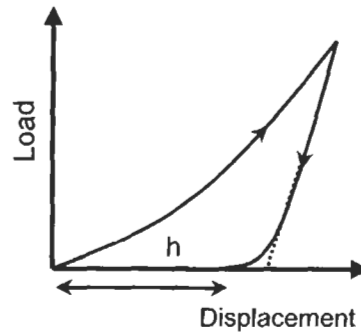


Fig. 10. Typical load–displacement graph for elasto-plastic indentation.

is mounted to the center plate via a shaft and accommodated by a small hole in the center of the lowest plate. A force is generated by applying a voltage between the center plate and one of the fixed plates through electrostatic means. The resulting displacement actuation of the middle plate can be measured by the change in capacitance between the middle and outer plates. An advantage of force-controlled operation is that indentation is not limited to contacts with lower stiffness than the indenter spring stiffness (typically 100 N/m or greater). Because the force is applied to the indenter against the spring by electrostatics, the applicable simple mechanical model is two springs in parallel, shown in Fig. 9b.

3.1. *Quasi-static measurements: mechanical properties*

A typical load–displacement curve is shown in Fig. 10. The loading portion of the curve results from both plastic and elastic deformation response of the contact, while the unloading portion of the curve is related to the elastic recovery of the contact. If the indenter geometry and materials properties are known, the modulus can be obtained by fitting the unloading curve to determine the contact stiffness at maximum load [9,86]. In this case, Eqs. 3 and 4 apply, where the unloading slope is determined from the load–displacement curve and the projected contact area, A , determined from indenter geometry and penetration depth. Generally, the hardness can be determined by measuring the residual contact depth, h , to determine A [9]. For more information, the reader is directed to a good overview of indentation practice written by Hay and Pharr [87].

3.2. *Quasi-static measurements: adhesion*

Like the AFM, load–displacement curves from nanoindentation can also be used to measure tip-sample adhesion. However, because the force resolution of nanoindentation is typically of order tens to hundreds of nanoNewtons, such experiments

are generally limited to cases where adhesion is high (e.g. large contact areas, high surface energy, low modulus). In some cases, tip-sample adhesion can be high enough to distort modulus values determined from indentation, as recently demonstrated by Grunlan et al. [88]. In this work, two tip materials (diamond and tungsten) and two substrates (low-density polyethylene, LDPE, and polystyrene, PS) were examined. The adhesion between the polymers and diamond was an order of magnitude higher than with tungsten, increasing the contact area and resulting in overestimates of the elastic moduli; the contact area increase can be corrected by using JKR analyses. Adhesion and creep of nanoscale spherical contacts to viscoelastic materials is also being studied (see e.g. [89,90]) and modeled [91,92].

While the force resolution of nanoindentation is not as good as AFM, the higher spring stiffness typical of the indenter provides the advantage of greatly reducing the tendency of the tip to jump into contact with the specimen. Joyce and Houston [93] have developed a capacitance based nanoindenter, called the interfacial force microscope (IFM), based on a 'teeter-totter' design. The instrument uses capacitance to sense displacement of the tip, and self-balancing fast feedback electronics to increase the effective indenter stiffness. Using this instrument, surface sensitive measurements of the adhesion between SAMs with various endgroup terminations ($-\text{CH}_3$, $-\text{NH}_2$, and $-\text{COOH}$) were measured and ranked in a study similar to that of Frisbie et al. [28] discussed earlier.

Interfacial adhesion between coating and substrate has also been studied by indentation methods. Marshall and Evans [94,95] examined blisters formed by buckling of a residually stressed coating induced by indentation. Fracture mechanics modeling of the interface crack enables determination of interface toughness and strain energy release rate (see also [96,97]). Pharr and colleagues [98] showed that by using sharp indenters to produce radial cracks on uncoated substrates, the interfacial fracture toughness, K_{Ic} , could be measured.

3.3. Dynamic measurements: inferring the contact area

3.3.1. Normal contact stiffness and mechanical properties

By adding a small AC modulation to the force during experiments, and monitoring displacement with a lock-in amplifier, Pethica and Oliver [99] demonstrated they could obtain normal contact stiffness ($\partial F/\partial z$) continuously throughout the indentation. From this stiffness measurement, the effective contact radius (and then area, A) can be directly determined using Eq. 3 and known geometric properties of the indenter. Previously, this contact area information was obtained by analyzing unloading slopes at various contact depths from multiple indents as described above in Section 2.2. and Section 3.1. Importantly, hardness and modulus vs. depth information, as well as tip characterization, can be performed

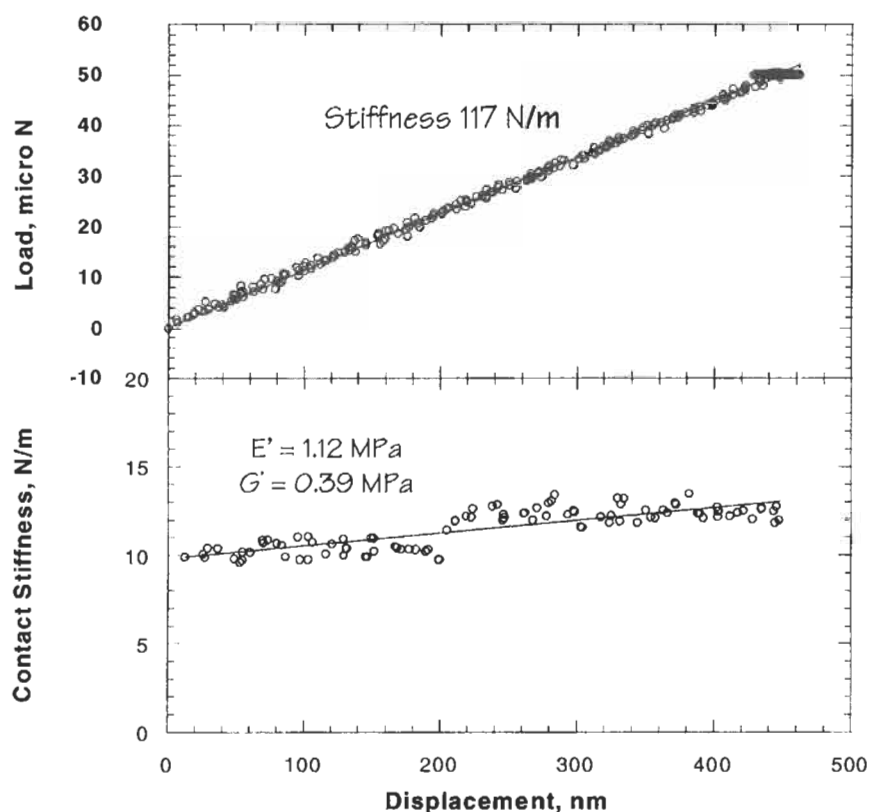


Fig. 11. Load–displacement data and contact stiffness for poly-isoprene. Reprinted with permission from ref. [102].

in one single experiment. Quantification of the data depends on obtaining accurate dynamic characterization of the instrument (dynamic response vs. frequency), and applying an appropriate dynamic mechanical model [99]. The addition of AC force modulation to the nanoindentation measurements increases sensitivity to elasto-plastic deformation and creep, as well as enables examination of damping or loss properties of materials, critical for determining mechanical properties of polymers [100,101].

Measuring the mechanical properties of very compliant materials by indentation is difficult because the indenter springs are generally several orders of magnitude stiffer than the contact stiffness. Larger contact areas (e.g. spherical indenters) can be used, but that may defeat the purpose by reducing lateral resolution significantly. An example demonstrating the increased sensitivity of the AC technique over standard load–displacement methods is shown in Fig. 11 [102]. The upper plot shows the load–displacement curve for an indentation against poly-isoprene. The data are linear, demonstrating elastic behavior of the contact

with a slope of 117 ± 1 N/m. However, the stiffness of the indenter itself is 116 N/m, and subtracting this value to obtain the contact stiffness leaves a value within the uncertainty of the measurement. The same measurement made using AC force modulation (AC force of 300 nN at 40 Hz), is shown in Fig. 11, lower plot. From these data, the elastic modulus of the poly-isoprene sample was found to be 1.1 ± 0.4 MPa.

3.3.2. Normal contact stiffness and surface detection

One of the challenges in nanoindentation involves detecting the sample surface (before indentation): specimens may undergo damage on approach, and very compliant samples might not be sensed at all (as in the case shown in Fig. 11). Monitoring the dynamic response of the nanoindenter during tip-sample approach provides a very sensitive way to determine the location of the surface prior to indentation and provides a mode of force–distance curve acquisition [103,104]. This surface detection scheme is similar to that described for intermittent contact AFM studies in Section 2.3. In this case, the indenter is oscillated at a frequency near its resonance. As the tip approaches the sample surface, any change in dynamic compliance due to tip-surface interaction results in a large phase shift sensed by the indenter and allows examination of adhesive and repulsive interactions. By using a small oscillation force, the tip oscillation amplitude is greatly reduced, minimizing intermittent contact during force–distance curve acquisition. Importantly, the resulting measurement may best termed an ‘interaction stiffness curve’ as what is measured is really a convolution of tip–surface interaction potential and true contact stiffness.

3.3.3. Normal contact stiffness and adhesion

An example of interaction stiffness and force curves for a Si surface with a native oxide at $\sim 60\%$ relative humidity (RH) is shown in Fig. 12 [104]. The stiffness and force data show an adhesive interaction between the tip and substrate. The hysteresis on retraction is due to a real change in contact area from surface oxide deformation and is not an experimental artifact. The adhesive force observed during retraction was consistent with capillary condensation and the surface energy measured from the adhesive force was close to that of water.

We have recently been exploring this technique to evaluate the adhesive and mechanical properties of compliant polymers in the form of a nanoscale JKR test. The force and stiffness data from a force–displacement curve can be plotted simultaneously (Fig. 13). For these contacts, the stiffness response appears to follow the true contact stiffness, and the curve was fit (see [70]) to a JKR model. Both the surface energy and modulus can be determined from the curve. Using JKR analyses, the maximum pull off force, surface energy and tip radius are

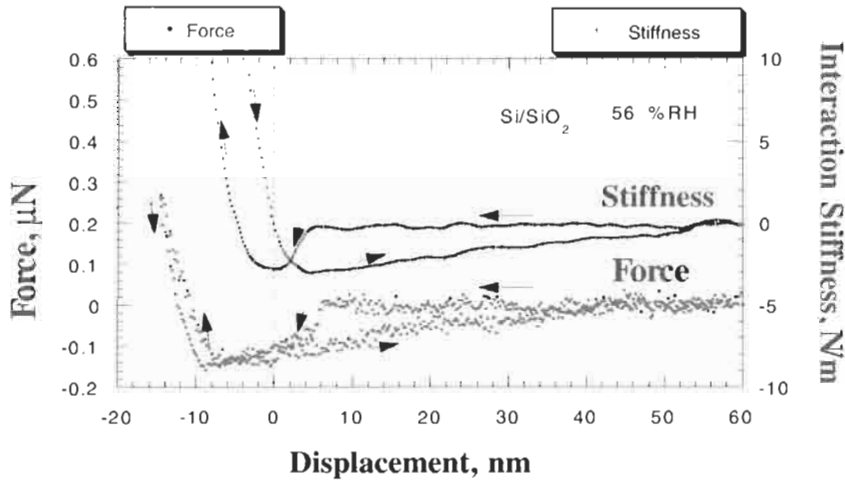


Fig. 12. Force and interaction stiffness curves during approach (←) and retraction (→) [104].

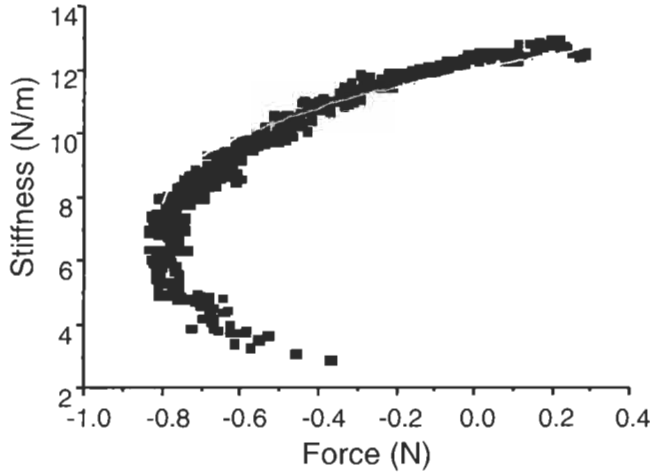


Fig. 13. Load vs. stiffness response for diamond hemisphere ($R = 5.3 \mu\text{m}$) vs. silicone polymer. Solid line is JKR fit.

related by Eq. 1. At zero applied load, the elastic modulus can be determined if the contact stiffness at zero load, S_0 , tip radius and surface energy are known from the following equation

$$E^* = \sqrt{\frac{S_0^3}{36\pi W_A R}} \quad (7)$$

In Fig. 13, using $R = 5.3 \mu\text{m}$, surface energy was found to be 24 mJ/m^2 , and E of the sample to be 3.5 MPa for a PDMS polymer, slightly higher than the modulus

measured by other means (1.5–2 MPa). This technique is quite promising, and additional testing and modeling are ongoing. Like the lateral stiffness technique for AFM (Section 2.4), the dynamic nature of these experiments allows multiple frequencies to be examined and hence opening up the ability to do dynamic mechanical properties probing during the adhesion test.

3.4. Summary

Depth-sensing nanoindentation is one of the primary tools for nanomechanical mechanical properties measurements. Major advantages to this technique over AFM include: (1) simultaneous measurement of force and displacement; (2) perpendicular tip-sample approach; and (3) well-modeled mechanics for dynamic measurements. Also, the ability to quantitatively infer contact area during force–displacement measurements provides a very useful approach to explore adhesion mechanics and models. Disadvantages relative to AFM include lower force resolution, as well as far lower spatial resolution, both from the larger tip radii employed and a lack of sample positioning and imaging capabilities provided by piezoelectric scanners.

4. ‘Hybrid’ indentation

Some of the best capabilities of both the AFM and depth-sensing nanoindentation can be realized simultaneously by combining the instruments. High resolution, quantitative mapping of mechanical properties is possible through the use of a ‘hybrid’ nanoindenter, combining depth-sensing nanoindentation with an AFM scanner [105,106]. This combination enables quantitative nanomechanical properties analyses (difficult with AFM) with nanometer-scale positioning and topographical mapping (impossible without scanned probe positioning capabilities).

Recently, we have improved the sensitivity of the hybrid nanoindenter by introducing a small sinusoidal component to the indentation force and detecting the displacement signal with a lock-in amplifier [103]. By scanning the sample under the oscillating probe at low loads (elastically), a 2-dimensional map of the dynamic stiffness of the sample can be obtained [107], and storage and loss stiffnesses can be determined using an appropriate dynamic model [99,103]. When the probe radius, R , applied load, P , and measured contact stiffness, k_{contact} , are known, and if adhesive forces are negligible, the reduced elastic modulus, E^* , can be directly calculated, pixel by pixel, from the contact stiffness image data obtained during scanning from the Hertz equation,

$$E^* = \sqrt{\frac{k_{\text{contact}}^3}{6PR}} \quad (8)$$

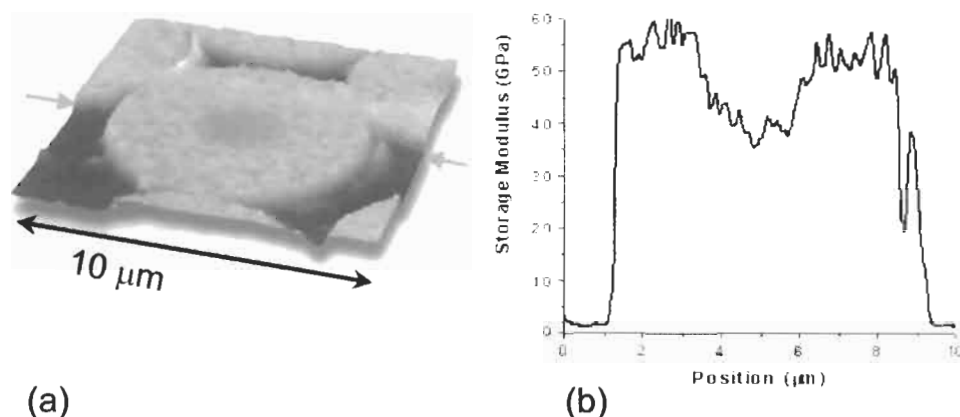


Fig. 14. (a) Two dimensional map of the elastic modulus of a carbon fiber-epoxy composite material. Brighter regions of the image correspond to higher modulus. (b) Cross section line scan through the center of the image (marked by arrows in a) shows the storage modulus in the epoxy and the modulus gradient at the center of the fiber [107].

Fig. 14a shows a $10 \times 10 \mu\text{m}$ image mapping the elastic (storage) modulus of a carbon fiber-epoxy composite. Contrast in the image, as well as the rendered height, corresponds directly to modulus with lighter regions having higher modulus. A cross-section through the center of the image of the elastic modulus is shown in Fig. 14b. The image shows that the center of the carbon fiber has a lower modulus than the periphery, while the epoxy has a substantially lower modulus than the fiber. The elastic modulus values obtained during the modulus mapping experiment were consistent with measured values from standard indentation experiments.

With this instrument, stiffness images can be acquired over a range of frequencies up to $\sim 250 \text{ Hz}$, allowing investigation of dynamic mechanical properties of viscoelastic materials. Fig. 15a and b show two contact stiffness images of a cross section of a layered polyethylene (PE) sample, with alternating low (PE1) and high (PE2) molecular weight. The lighter regions in the images correspond to higher contact stiffness. The two images were taken from the same region of the sample while oscillating the probe at 105 and 200 Hz, respectively. At 200 Hz, the image contrast is reversed from that observed at 105 Hz and is simply related to the tip-sample interaction.

This image contrast reversal reflects a change in contact compliance ($1/\text{'interaction stiffness'}$) of the nanoindenter probe in contact with the two polymers. At the imaging load of $\sim 2 \mu\text{N}$, the stiffness of PE2 is greater, shifting the compliance curve farther to the right (Fig. 15c). Thus the contrast in the two images results from the relative position of the contact resonances at the imaging frequencies chosen. When the tip-sample interaction is deconvoluted to provide values for

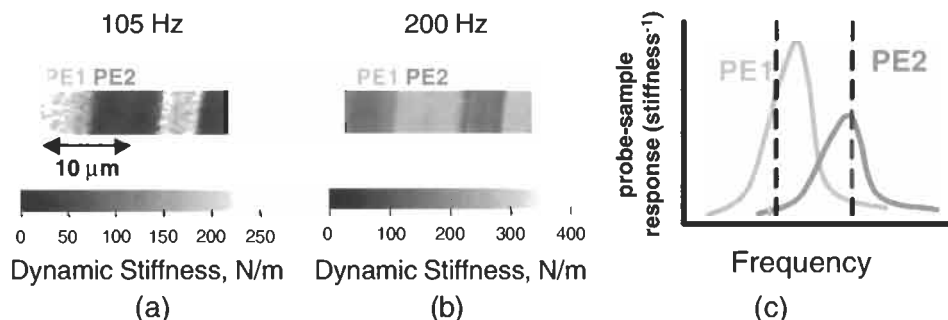


Fig. 15. Dynamic stiffness images of alternating layers of polyethylene (PE) of two molecular weights at (a) 105 Hz and (b) 200 Hz. The contrast is due to changes in contact compliance ($1/\text{stiffness}$) of the nanoindenter probe in contact with each of the two polymers. The probe-sample response ($1/\text{stiffness}$) as a function of frequency shown in (c) is consistent with the dynamic stiffness images.

storage and loss stiffness (not shown), the stiffness of PE2 was greater than PE1 over the range of frequencies examined (1 Hz to 250 Hz).

5. Conclusions

This chapter summarizes adhesion and mechanics tools, techniques and measurements possible at the micro- to nanoscale. Both AFM and depth-sensing nanoindentation instruments provide researchers with many capabilities for studying materials and interfacial properties using both quasi-static and dynamic testing. While these tools are relatively mature (one to two decades), techniques and applications are still rapidly evolving as their usage by scientists in different disciplines widens. Similar techniques have evolved enabling both types of instruments to measure contact stiffness, providing a way to monitor the size of these sub-optical limit contacts during the experiments. Evolution also continues through the new capabilities offered by combining instrumentation for depth-sensing indentation, scanning probe microscopy and/or dynamic measurements, which can provide powerful new capabilities to quantitatively map dynamic mechanical properties and adhesion.

Acknowledgements

The authors are grateful for the contributions of our colleagues Rich Colton, Oden Warren, Bill Unertl, Stan Stepnowski, Ken Lee, Brian Cassella and T.J. Mullen. This work was supported by ONR and AFOSR.

References

1. Binnig, G., Quate, C.F. and Gerber, Ch., Atomic force microscope. *Phys. Rev. Lett.*, **56**, 930–933 (1986).
2. Pethica, J.B., Hutchings, R. and Oliver, W.C., Hardness measurement at penetration depths as small as 20 nm. *Philos. Mag. A-Phys. Condens. Matter Struct. Defects Mech. Prop.*, **48**, 593–606 (1983).
3. Rimai, D.S., Demejo, L.P. and Bowen, R.C., Mechanics of particle adhesion. *J. Adhes. Sci. Technol.*, **8**, 1333–1355 (1994).
4. Johnson, K.L., Kendall, K. and Roberts, A.D., Surface energy and contact of elastic solids. *Proc. R. Soc. Lond. Ser. A Math. Phys. Eng. Sci.*, **324**, 301–313 (1971).
5. Barquins, M. and Maugis, D., Influence of dwell time on the adherence of elastomers. *J. Adhes.*, **14**, 63–82 (1982).
6. Barquins, M. and Maugis, D., Tackiness of elastomers. *J. Adhes.*, **13**, 53–65 (1981).
7. Creton, C. and Lakrout, H., Micromechanics of flat-probe adhesion tests of soft viscoelastic polymer films. *J. Polym. Sci. B Polym. Phys.*, **38**(7), 965–979 (2000).
8. Tabor, D., *The Hardness of Metals*. Clarendon Press, Oxford, 1951.
9. Oliver, W.C. and Pharr, G.M., An improved technique for determining hardness and elastic-modulus using load and displacement sensing indentation experiments. *J. Mater. Res.*, **7**, 1564–1583 (1992).
10. Sarid, D., Iams, D., Weissenberger, V. and Bell, L.S., Compact scanning-force microscope using a laser diode. *Opt. Lett.*, **13**(12), 1057–1059 (1988).
11. Meyer, G. and Amer, N.M., Novel optical approach to atomic force microscopy. *Appl. Phys. Lett.*, **53**(12), 1045–1047 (1988).
12. Rugar, D., Mamin, H.J., Erlandsson, R., Stern, J.E. and Terris, B.D., Force microscope using a fiber-optic displacement sensor. *Rev. Sci. Instrum.*, **59**(11), 2337–2340 (1988).
13. Martin, Y., Williams, C.C. and Wickramasinghe, H.K., Atomic force microscope force mapping and profiling on a sub 100-Å scale. *J. Appl. Phys.*, **61**(10), 4723–4729 (1987).
14. Erlandsson, R., McClelland, G.M., Mate, C.M. and Chiang, S., Atomic force microscopy using optical interferometry. *J. Vac. Sci. Technol. A Vac. Surf. Films*, **6**(2), 266–270 (1988).
15. Chui, B.W., Stowe, T.D., Kenny, T.W., Mamin, H.J., Terris, B.D. and Rugar, D., Low-stiffness silicon cantilevers for thermal writing and piezoresistive readback with the atomic force microscope. *Appl. Phys. Lett.*, **69**(18), 2767–2769 (1996).
16. Burnham, N.A. and Colton, R.J., Measuring the nanomechanical properties and surface forces of materials using an atomic force microscope. *J. Vac. Sci. Technol. A Vac. Surf. Films*, **7**(4), 2906–2913 (1989).
17. Ducker, W.A., Senden, T.J. and Pashley, R.M., Direct measurement of colloidal forces using an atomic force microscope. *Nature*, **353**(6341), 239–241 (1991).
18. Israelachvili, J.N., *Intermolecular and Surface Forces*. Academic Press, San Diego, 1992.
19. Landman, U., Luedtke, W.D., Burnham, N.A. and Colton, R.J., Atomistic mechanisms and dynamics of adhesion, nanoindentation, and fracture. *Science*, **248**(4954), 454–461 (1990).
20. Derjaguin, B.V., Muller, V.M. and Toporov, Y.P., Effect of contact deformation on adhesion of particles. *J. Colloid Interface Sci.*, **53**, 314–326 (1975).
21. Tabor, D., Surface forces and surface interaction. *J. Colloid Interface Sci.*, **58**, 2–13 (1977).
22. Muller, V.M., Yushchenko, V.S. and Derjaguin, B.V., General theoretical consideration of

- the influence of surface forces on contact deformations and the reciprocal adhesion of elastic spherical-particles. *J. Colloid Interface Sci.*, **92**(1), 92–101 (1983).
23. Muller, V.M., Yushchenko, V.S. and Derjaguin, B.V., On the influence of molecular forces on the deformation of an elastic sphere and its sticking to a rigid plane. *J. Colloid Interface Sci.*, **77**(1), 91–101 (1980).
 24. Maugis, D., Adhesion of spheres — the JKR–DMT transition using a Dugdale model. *J. Colloid Interface Sci.*, **150**(1), 243–269 (1992).
 25. Burnham, N.A., Dominguez, D.D., Mowery, R.L. and Colton, R.J., Probing the surface forces of monolayer films with an atomic force microscope. *Phys. Rev. Lett.*, **64**, 1931–1934 (1990).
 26. Mate, C.M., Lorenz, M.R. and Novotny, V.J., Atomic force microscopy of polymeric liquid-films. *J. Chem. Phys.*, **90**(12), 7550–7555 (1989).
 27. Weisenhorn, A.L., Hansma, P.K., Albrecht, T.R. and Quate, C.F., Forces in atomic force microscopy in air and water. *Appl. Phys. Lett.*, **54**(26), 2651–2653 (1989).
 28. Frisbie, C.D., Rozsnyai, L.F., Noy, A., Wrighton, M.S. and Lieber, C.M., Functional-group imaging by chemical force microscopy. *Science*, **265**(5181), 2071–2074 (1994).
 29. Weisenhorn, A.L., Maivald, P., Butt, H.J. and Hansma, P.K., Measuring adhesion, attraction, and repulsion between surfaces in liquids with an atomic-force microscope. *Phys. Rev. B Condens. Matter*, **45**(19), 11226–11232 (1992).
 30. Butt, H.J., Measuring electrostatic, Van der waals, and hydration forces in electrolyte-solutions with an atomic force microscope. *Biophys. J.*, **60**(6), 1438–1444 (1991).
 31. Giessibl, F.J., Atomic-force microscopy in ultrahigh-vacuum. *Jpn. J. Appl. Phys. Part 1 Reg. Pap. Short Notes Rev. Pap.*, **33**(6B), 3726–3734 (1994).
 32. Dai, Q., Vollmer, R., Carpick, R.W., Ogletree, D.F. and Salmeron, M., Variable-temperature ultrahigh-vacuum atomic-force microscope. *Rev. Sci. Instrum.*, **66**(11), 5266–5271 (1995).
 33. Noy, A., Frisbie, C.D., Rozsnyai, L.F., Wrighton, M.S. and Lieber, C.M., Chemical force microscopy — exploiting chemically modified tips to quantify adhesion, friction, and functional-group distributions in molecular assemblies. *J. Am. Chem. Soc.*, **117**(30), 7943–7951 (1995).
 34. Lee, G.U., Kidwell, D.A. and Colton, R.J., Sensing discrete streptavidin biotin interactions with atomic – force microscopy. *Langmuir*, **10**(2), 354–357 (1994).
 35. Rief, M., Gautel, M., Oesterhelt, F., Fernandez, J.M. and Gaub, H.E., Reversible unfolding of individual titin immunoglobulin domains by AFM. *Science*, **276**(5315), 1109–1112 (1997).
 36. Rief, M., Oesterhelt, F., Heymann, B. and Gaub, H.E., Single molecule force spectroscopy on polysaccharides by atomic force microscopy. *Science*, **275**(5304), 1295–1297 (1997).
 37. Cappella, B. and Dietler, G., Force–distance curves by atomic force microscopy. *Surf. Sci. Rep.*, **34**(1–3), 1 (1999).
 38. Janshoff, A., Neitzert, M., Oberdorfer, Y. and Fuchs, H., Force spectroscopy of molecular systems – single molecule spectroscopy of polymers and biomolecules. *Angew. Chem. Int. Edn.*, **39**(18), 3213–3237 (2000).
 39. Burnham, N.A., Colton, R.J. and Pollock, H.M., Interpretation of force curves in force microscopy. *Nanotechnology*, **4**, 64–80 (1993).
 40. Burnham, N.A. and Colton, R.J., Force microscopy. In: Bonnell, D.A. (Ed.), *Scanning Tunneling Microscopy and Spectroscopy: Theory, Techniques and Applications*, 2nd ed. Wiley-VCH, New York, NY, 2001, Chapt. 10, pp. 337–370.
 41. Koleske, D.D., Lee, G.U., Gans, B.I., Lee, K.P., DiLella, D.P., Wahl, K.J., Barger, W.R.,

- Whitman, L.J. and Colton, R.J., Design and calibration of a scanning force microscope for friction, adhesion, and contact potential studies. *Rev. Sci. Instrum.*, **66**, 1 (1995).
42. Baselt, D.R. and Baldeschwieler, J.D., Imaging spectroscopy with the atomic-force microscope. *J. Appl. Phys.*, **76**(1), 33–38 (1994).
43. Krotil, H.U., Stifter, T., Waschipky, H., Weishaupt, K., Hild, S. and Marti, O., Pulsed force mode: a new method for the investigation of surface properties. *Surf. Interface Anal.*, **27**(5-6), 336–340 (1999).
44. RosaZeiser, A., Weilandt, E., Hild, S. and Marti, O., The simultaneous measurement of elastic, electrostatic and adhesive properties by scanning force microscopy: pulsed-force mode operation. *Measur. Sci. Technol.*, **8**(11), 1333–1338 (1997).
45. Radmacher, M., Cleveland, J.P., Fritz, M., Hansma, H.G. and Hansma, P.K., Mapping interaction forces with the atomic-force microscope. *Biophys. J.*, **66**(6), 2159–2165 (1994).
46. Colton, R.J., Barger, W.R., Baselt, D.R., Corcoran, S.G., Koleske, D.D. and Lee, G.U. In: Van Ooij, W.J. and Anderson, H.R., Jr. (Eds.), *Atomic Force Microscopy: Surface Forces, Adhesion and Nanomechanics Measurements*. Mittal Festschrift, VSP, 1998.
47. Green, J.B.D. and Lee, G.U., Atomic force microscopy with patterned cantilevers and tip arrays: force measurements with chemical arrays. *Langmuir*, **16**(8), 4009–4015 (2000).
48. VanLandingham, M.R., McKnight, S.H., Palmese, G.R., Eduljee, R.F., Gillespie, J.W. and McCulough, R.L., Relating elastic modulus to indentation response using atomic force microscopy. *J. Mater. Sci. Lett.*, **16**(2), 117–119 (1997).
49. VanLandingham, M.R., The effect of instrumental uncertainties on AFM indentation measurements. *Microsc. Today*, **97**, 12–15 (1997).
50. VanLandingham, M.R., McKnight, S.H., Palmese, G.R., Elings, J.R., Huang, X., Bogetti, T.A., Eduljee, R.F. and Gillespie, J.W., Nanoscale indentation of polymer systems using the atomic force microscope. *J. Adhes.*, **64**(1-4), 31–59 (1997).
51. Johnson, K.L., *Contact Mechanics*. Cambridge University Press, Cambridge, 1985.
52. Hues, S.M., Draper, C.F., Lee, K.P. and Colton, R.J., Effect of PZT and PMN actuator hysteresis and creep on nanoindentation measurements using force microscopy. *Rev. Sci. Instrum.*, **65**(5), 1561–1565 (1994).
53. Briscoe, B.J., Fiori, L. and Pelillo, E., Nano-indentation of polymeric surfaces. *J. Phys. D Appl. Phys.*, **31**(19), 2395–2405 (1998).
54. Maivald, P., Butt, H.J., Gould, S.A., Prater, C.B., Drake, B., Gurley, J.A., Elings, V.B. and Hansma, P.K., Using force modulation to image surface elasticities with the atomic force microscope. *Nanotechnology*, **2**, 103–106 (1991).
55. Burnham, N.A., Behrend, O.P., Oulevey, F., Gremaud, G., Gallo, P.-J., Gourdon, D., Dupas, E., Kulik, A.J., Pollock, H.M. and Briggs, G.A.D., How does a tip tap? *Nanotechnology*, **8**, 67–75 (1997).
56. Tamayo, J. and Garcia, R., Effects of elastic and inelastic interactions on phase contrast images in tapping-mode scanning force microscopy. *Appl. Phys. Lett.*, **71**(16), 2394–2396 (1997).
57. Tamayo, J. and Garcia, R., Relationship between phase shift and energy dissipation in tapping-mode scanning force microscopy. *Appl. Phys. Lett.*, **73**(20), 2926–2928 (1998).
58. Gotsmann, B., Seidel, C., Anczykowski, B. and Fuchs, H., Conservative and dissipative tip-sample interaction forces probed with dynamic AFM. *Phys. Rev. B Condens. Matter*, **60**, 11051–11061 (1999).
59. Anczykowski, B., Gotsmann, B., Fuchs, H., Cleveland, J.P. and Elings, V.B., How to measure energy dissipation in dynamic mode atomic force microscopy. *Appl. Surf. Sci.*, **140**, 376–382 (1999).

60. Cleveland, J.P., Anczykowski, B., Schmid, A.E. and Elings, V.B., Energy dissipation in tapping-mode atomic force microscopy. *Appl. Phys. Lett.*, **72**(20), 2613–2615 (1998).
61. Bar, G., Delineau, L., Hafele, A. and Whangbo, M.H., Investigation of the stiffness change in, the indentation force and the hydrophobic recovery of plasma-oxidized polydimethylsiloxane surfaces by tapping mode atomic force microscopy. *Polymer*, **42**(8), 3627–3632 (2001).
62. Pashley, M.D. and Tabor, D., Adhesion and deformation properties of clean and characterized metal micro-contacts. *Vacuum*, **31**(10-1), 619–623 (1981).
63. Enachescu, M., van den Oetelaar, R.J.A., Carpick, R.W., Ogletree, D.F., Flipse, C.F.J. and Salmeron, M., Atomic force microscopy study of an ideally hard contact: the diamond(111) tungsten carbide interface. *Phys. Rev. Lett.*, **81**(9), 1877–1880 (1998).
64. Jarvis, S.P., Oral, A., Weihs, T.P. and Pethica, J.B., A novel force microscope and point-contact probe. *Rev. Sci. Instrum.*, **64**(12), 3515–3520 (1993).
65. Carpick, R.W., Ogletree, D.F. and Salmeron, M., Lateral stiffness: A new nanomechanical measurement for the determination of shear strengths with friction force microscopy. *Appl. Phys. Lett.*, **70**(12), 1548–1550 (1997).
66. Lantz, M.A., O'Shea, S.J., Welland, M.E. and Johnson, K.L., Atomic-force-microscope study of contact area and friction on NbSe₂. *Phys. Rev. B Condens. Matter*, **55**(16), 10776–10785 (1997).
67. Carpick, R.W., Enachescu, M., Ogletree, D.F. and Salmeron, M., Making, breaking, and sliding of nanometer-scale contacts. In: Beltz, G.E., Selinger, R.L.B., Kim, K.-S. and Marder, M.P., (Eds.), *Fracture and Ductile vs. Brittle Behavior-Theory, Modeling and Experiment*. Materials Research Society, Warrendale, PA, 1999, pp. 93–103.
68. Mazeran, P.E. and Loubet, J.L., Normal and lateral modulation with a scanning force microscope, an analysis: implication in quantitative elastic and friction imaging. *Tribol. Lett.*, **7**(4), 199–212 (1999).
69. Carpick, R.W., The study of contact, adhesion, and friction at the atomic scale by atomic force microscopy. University of California-Berkeley, Berkeley, CA, 1997.
70. Carpick, R.W., Ogletree, D.F. and Salmeron, M., A general equation for fitting contact area and friction vs. load measurements. *J. Colloid Interface Sci.*, **211**(2), 395–400 (1999).
71. Wahl, K.J., Stepnowski, S.V. and Unertl, W.N., Viscoelastic effects in nanometer-scale contacts under shear. *Tribol. Lett.*, **5**, 103–107 (1998).
72. Basire, C. and Fretigny, C., Determination of viscoelastic moduli at a submicrometric scale. *Eur. Phys. J. Appl. Phys.*, **6**(3), 323–329 (1999).
73. Ge, S., Pu, Y., Zhang, W., Rafailovich, M., Sokolov, J., Buenviaje, C., Buckmaster, R. and Overney, R.M., Shear modulation force microscopy study of near surface glass transition temperatures. *Phys. Rev. Lett.*, **85**(11), 2340–2343 (2000).
74. Dinelli, F., Buenviaje, C. and Overney, R.M., Glass transition measurements on heterogeneous surfaces. *Thin Solid Films*, **396**(1-2), 138–144 (2001).
75. Unertl, W.N., Implications of contact mechanics models for mechanical properties measurements using scanning force microscopy. *J. Vac. Sci. Technol. A Vac. Surf. Films*, **17**(4), 1779–1786 (1999).
76. Sader, J.E., Larson, I., Mulvaney, P. and White, L., Method for the calibration of atomic force microscope cantilevers. *Rev. Sci. Instrum.*, **66**(7), 3789–3798 (1995).
77. Cleveland, J.P., Manne, S., Bocek, D. and Hansma, P.K., Nondestructive method for determining the spring constant of cantilevers for scanning force microscopy. *Rev. Sci. Instrum.*, **64**(2), 403–405 (1993).
78. Tortonese, M. and Kirk, M., Characterization of application specific probes for SPMs. *SPIE*, **3009**, 53–60 (1997).

79. Ogletree, D.F., Carpick, R.W. and Salmeron, M., Calibration of frictional forces in atomic force microscopy. *Rev. Sci. Instrum.*, **67**(9), 3298–3306 (1996).
80. Burnham, N.A., Gremaud, G., Kulik, A.J., Gallo, P.-J. and Oulevey, F., Materials' properties measurements: choosing the optimal scanning probe microscope configuration. *J. Vac. Sci. Technol. B*, **14**, 1308–1312 (1996).
81. Oulevey, F., Burnham, N.A., Kulik, A.J., Gallo, P.-J., Gremaud, G. and Benoit, W., Mechanical properties studied at the nanoscale using scanning local-acceleration microscopy (SLAM). *J. Phys. IV*, **6**, 731–734 (1996).
82. Burnham, N.A., Kulik, A.J., Oulevey, F., Mayencourt, C., Gourdon, D., Dupas, E. and Gremaud, G., A beginner's guide to LPM materials properties measurements. Part I: Conceptual aspects. In: Bhushan, B. (Ed.), *NATO ASI*. Kluwer Academic Publishers, Portugal, 1997, pp. 421–438.
83. Burnham, N.A., Kulik, A.J., Oulevey, F., Mayencourt, C., Gourdon, D., Dupas, E. and Gremaud, G., A beginner's guide to LPM materials properties measurements. Part II: Materials properties measurements. In: Bhushan, B. (Ed.), *NATO ASI*. Kluwer Academic Publishers, Portugal, 1997, pp. 439–454.
84. Colton, R.J., Engel, A., Frommer, J.E., Gaub, H.E., Gewirth, A.A., Guckenberger, R., Rabe, J., Heckl, W.M. and Parkinson, B., (Eds.), *Procedures in Scanning Probe Microscopies*. Wiley, Chichester, 1998.
85. Maugis, D., *Contact, Adhesion and Rupture of Elastic Solids*. Solid State Sciences. Springer, Berlin, 2000.
86. Doerner, M.F. and Nix, W.D., Stresses and deformation processes in thin-films on substrates. *CRC Crit. Rev. Solid State Mater. Sci.*, **14**(3), 225–268 (1988).
87. Hay, J.L. and Pharr, G.M., Instrumented indentation testing. In: *ASM Handbook: Mechanical Testing and Evaluation*. ASM International, Materials Park, OH, 2000.
88. Grunlan, J.C., Xia, X.Y., Rowenhorst, D. and Gerberich, W.W., Preparation and evaluation of tungsten tips relative to diamond for nanoindentation of soft materials. *Rev. Sci. Instrum.*, **72**(6), 2804–2810 (2001).
89. Giri, M., Bousfield, D. and Unertl, W.N., Stress intensity in viscoelastic contacts. *Tribol. Lett.*, **9**(1–2), 33–39 (2000).
90. Giri, M., Bousfield, D.B. and Unertl, W.N., Dynamic contacts on viscoelastic films: work of adhesion. *Langmuir*, **17**(10), 2973–2981 (2001).
91. Johnson, K.L., Contact mechanics and adhesion of viscoelastic solids. In: Tsukruk, V.V. and Wahl, K.J. (Eds.), *Microstructure and Microtribology of Polymer Surfaces*. ACS, Washington, DC, 1998, pp. 24–41.
92. Baney, J.M., Hui, C.Y. and Cohen, C., Experimental investigations of a stress intensity factor based description of the adhesion of viscoelastic materials. *Langmuir*, **17**(3), 681–687 (2001).
93. Joyce, S.A. and Houston, J.E., A new force sensor incorporating force-feedback control for interfacial force microscopy. *Rev. Sci. Instrum.*, **62**(3), 710–715 (1991).
94. Marshall, D.B. and Evans, A.G., Measurement of adherence of residually stressed thin-films by indentation. 1. Mechanics of interface delamination. *J. Appl. Phys.*, **56**(10), 2632–2638 (1984).
95. Rossington, C., Evans, A.G., Marshall, D.B. and Khuriyakub, B.T., Measurements of adherence of residually stressed thin-films by indentation. 2. Experiments with ZnO/Si. *J. Appl. Phys.*, **56**(10), 2639–2644 (1984).
96. Rosenfeld, L.G., Ritter, J.E., Lardner, T.J. and Lin, M.R., Use of the microindentation technique for determining interfacial fracture energy. *J. Appl. Phys.*, **67**(7), 3291–3296 (1990).

97. Kriese, M.D., Gerberich, W.W. and Moody, N.R., Quantitative adhesion measures of multilayer films: Part I. Indentation mechanics. *J. Mater. Res.*, **14**(7), 3007–3018 (1999).
98. Pharr, G.M., Harding, D.S. and Oliver, W.C., Measurement of fracture toughness in thin films and small volumes using nanoindentation methods. *MRS*, 1995, pp. 663–675.
99. Pethica, J.B. and Oliver, W.C., Tip surface interactions in STM and AFM. *Phys. Scripta*, **T19A**, 61–66 (1987).
100. Asif, S.A.S., *Time Dependent Microdeformation of Materials*. Oxford, 1997.
101. Loubet, J.L., Oliver, W.C. and Lucas, B.N., Measurement of the loss tangent of low-density polyethylene with a nanoindentation technique. *J. Mater. Res.*, **15**, 1195–1198 (2000).
102. Asif, S.A.S., Colton, R.J. and Wahl, K.J., Nanoscale surface mechanical property measurements: Force modulation techniques applied to nanoindentation. In: Overney, R.M. and Frommer, J.E. (Eds.), *Interfacial Properties on the Submicron Scale*. ACS/Oxford Press, Oxford, 2001.
103. Asif, S.A.S., Wahl, K.J. and Colton, R.J., Nanoindentation and contact stiffness measurement using force modulation with a capacitive load–displacement transducer. *Rev. Sci. Instrum.*, **70**, 2408–2413 (1999).
104. Asif, S.A.S., Wahl, K.J. and Colton, R.J., The influence of oxide and adsorbates on the nanomechanical response of silicon surfaces. *J. Mater. Res.*, **15**, 546–553 (2000).
105. Bhushan, B., Kulkarni, A.V., Bonin, W. and Wyrobek, J.T., Nanoindentation and picoindentation measurements using a capacitive transducer system in atomic force microscopy. *Philos. Mag. A Phys. Condens. Matter Struct. Defects Mech. Prop.*, **74**(5), 1117–1128 (1996).
106. Joyce, S.A., Houston, J.E. and Michalske, T.A., Differentiation of topographical and chemical structures using an interfacial force microscope. *Appl. Phys. Lett.*, **60**(10), 1175–1177 (1992).
107. Asif, S.A.S., Wahl, K.J., Colton, R.J. and Warren, O.L., Quantitative imaging of nanoscale mechanical properties using hybrid nanoindentation and force modulation. *J. Appl. Phys.*, **90**(3), 1192–1200 (2001).

Micro-mechanical processes in adhesion and fracture

HUGH R. BROWN *

*BHP Institute of Steel Processing and Products, University of Wollongong,
Wollongong, NSW 2522, Australia*

1. Introduction

The aim of this chapter is to describe the micro-mechanical processes that occur close to an interface during adhesive or cohesive failure of polymers. Emphasis will be placed on both the nature of the processes that occur and the micro-mechanical models that have been proposed to describe these processes. The main concern will be processes that occur at size scales ranging from nanometres (molecular dimensions) to a few micrometres. Failure is most commonly controlled by mechanical process that occur within this size range as it is these small scale processes that apply stress on the chain and cause the chain scission or pull-out that is often the basic process of fracture. The situation for elastomeric adhesives on substrates such as skin, glassy polymers or steel is different and will not be considered here but is described in a chapter on 'tack'. Multiphase materials, such as rubber-toughened or semi-crystalline polymers, will not be considered much here as they show a whole range of different micro-mechanical processes initiated by the modulus mismatch between the phases.

It is necessary to consider the micro-mechanical processes of polymer glasses and elastomers separately as their mechanical properties are so different. In addition, cross-linking profoundly affects the deformation processes in glasses but very little is known about the micro-mechanical processes that occur in single phase cross-linked glasses so the latter materials will not be discussed further.

* E-mail: Hugh_Brown@uow.edu.au

2. Glassy polymers

2.1. Overview

The mode of failure of a glassy polymer depends strongly on its molecular weight. At low molecular weights the material fails by chain pull-out with little deformation round the crack tip. As the molecular weight is increased, the force required to pull-out chains that cross the crack path from the matrix increases, causing initially some form of local yield. As the chain length continues to increase, the stress borne by the chains across the crack path becomes high enough to cause a local yield and voiding process called crazing. At this point, the material obtains some useful toughness. Increasing chain length to significantly above the entanglement molecular weight changes the chain failure mode from pull-out to scission and continues to increase the energy dissipated in the craze, and hence the toughness. Eventually the toughness saturates at high molecular weight as the chain sections that cross the interface all fail by scission. In this latter context, the relevant chain section is a chain length between entanglements.

The processes that occur during adhesive failure are similar to those described above for cohesive failure. There are two basic situations: (1) when specific coupling chains are placed or formed at the interface, and (2) when two pieces of the same or different polymers are welded together. The main differences originate in the fact that, for case (1) both the areal density Σ (at the interface) and the length of coupling chains can be altered independently of the molecular weight and nature of the materials being coupled. There is, however, a maximum areal density of the coupling chains Σ_{sat} that can be accommodated at the interface. The situation is more complex for case (2) as the chains diffuse across the interface during the welding process so the time dependence of the interface structure is important.

Consider first the case of specific coupling chains. If the coupling chains are very short the failure is by simple chain pull-out with little deformation round the crack tip and low toughness. As the coupling chain length increases the pull-out force increases and the failure mode can change to crazing and chain pull-out with a significant increase in toughness. This change occurs when the stress at the interface, controlled by coupling chain length and Σ , becomes greater than the stress to cause crazing. This transition is only observed at high Σ . As the length of the coupling chains is increased more the pull-out force becomes greater than the force to cause chain scission, so the chains fail by scission. When Σ is low, the stress at the interface can be too low to cause much deformation, even when the chains break, and so the toughness is low. As Σ is increased then yielding and crazing start to occur round the crack tip, the toughness increases and in favourable circumstances the interface toughness can become almost as large as the bulk toughness of the material being joined.

Understanding of the joining of glassy polymers by welding requires both a knowledge of the development of the chain topology across the interface during the welding process and the relationships between this topology and the micro-mechanical processes that can occur during interface failure. There is understanding of the interdiffusion processes that occur when two pieces of the same polymer are joined, and knowledge of the equilibrium interface thickness that occurs when two dissimilar polymers are joined. But the relationships between the interface structures and the micro-mechanical failure processes are not very clear.

The micro-mechanical processes will be presented next, followed by the models used to describe them. The predictions of the models will then be compared with results obtained using well-defined coupling chains. Application of the models to the joining of dissimilar polymers will then be described. Finally welding of glassy polymers will be considered.

2.2. Experimental studies of micro-mechanical processes

The main experimental techniques used to study the failure processes at the scale of a chain have involved the use of deuterated polymers, particularly copolymers, at the interface and the measurement of the amounts of the deuterated copolymers at each of the fracture surfaces. The presence and quantity of the deuterated copolymer has typically been measured using forward recoil ion scattering (FRES) or secondary ion mass spectroscopy (SIMS). The technique was originally used in a study of the effects of placing polystyrene–polymethyl methacrylate (PS–PMMA) block copolymers of total molecular weight of $\sim 200,000$ Da at an interface between polyphenylene ether (PPE or PPO) and PMMA copolymers [1]. The PS block is miscible in the PPE. The use of copolymers where just the PS block was deuterated and copolymers where just the PMMA block was deuterated showed that, when the interface was fractured, the copolymer molecules all broke close to their junction points. The basic idea of this technique is shown in Fig. 1.

The techniques described above have been used to demonstrate that failure can occur by (1) simple chain pull-out, (2) chain scission close to the interface, or (3) chain scission within one of the blocks (typically PS). The transition from chain pull-out to scission is essentially controlled by molecular weight whilst the location of the scission seems to depend on the entanglement density. Fig. 2 shows the transition between (2) and (3) as Σ is increased.

Processes that occur at a size scale larger than the individual chain have been studied using microscopy, mainly transmission electron microscopy (TEM), but optical microscopy has been useful to examine craze shapes. The knowledge of the crazing process obtained by TEM has been ably summarised by Kramer and will not be repeated here [2,3]. At an interface between two polymers a craze often forms within one of the materials, typically the one with lower crazing stress.

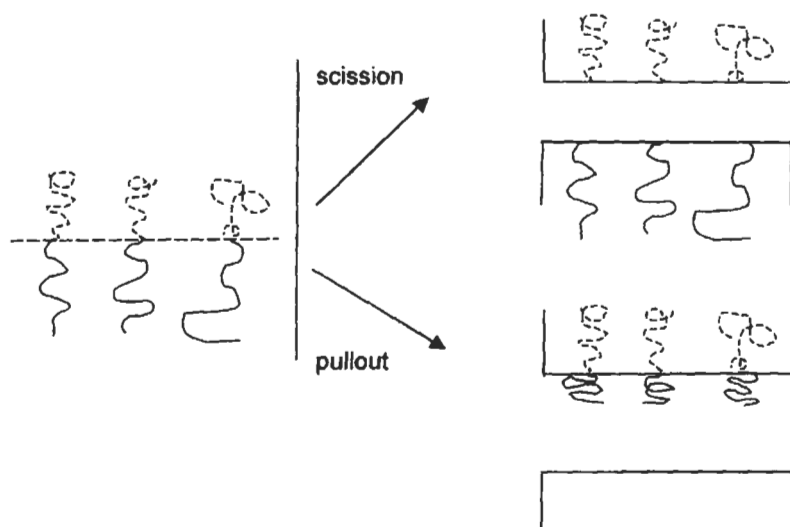


Fig. 1. Block copolymers tend to organise at an interface so that the two blocks, shown here as solid and dashed lines, are on either side of the interface. If one of the blocks is deuterated then chain pull-out can be distinguished from chain scission by the location of the deuterium on the fracture surface.

TEM has been used to demonstrate that the craze normally fails at the material interface [4–6]. In addition the fracture energy calculated from the craze shape tends to agree well with the macroscopic measure of toughness.

2.3. Models of chain pull-out in glassy polymers without crazing

Xu et al. developed a model of chain pull-out in glassy polymers [7] shown in Fig. 3. The chain, embedded in the polymer, is pulled at one end with a force f which is larger than the critical value $f = Nf_{\text{mono}}$ below which chain pull-out cannot occur, where f_{mono} is a static monomer friction coefficient and N is the number of monomers in the chain. If the length of the connector chain pulled out by the force f is given by δ , when $\delta = \Delta$, where Δ is the total connector chain length, the chain is completely pulled out and the force vanishes. Assuming that the chains are pulled out normal to the interface then σ , the stress normal to the planar interface, is related to the force f and Σ , by $\sigma = f\Sigma$. The stress σ is related to the rate of chain pull-out $\dot{\delta}$ and the remaining chain length $\Delta - \delta$ by:

$$\sigma = b(\Delta - \delta)(\dot{\delta} + \dot{\delta}^*) \quad \dot{\delta} > 0 \quad (1)$$

where b and $\dot{\delta}^*$ are material constants. In this model, when the normal stress on the interface is less than $\sigma^* = b\dot{\delta}^* \equiv f_{\text{mono}}N\Sigma$, chain pull-out cannot occur. For such a model f_{mono} can be considered to be a monomer static friction coefficient.

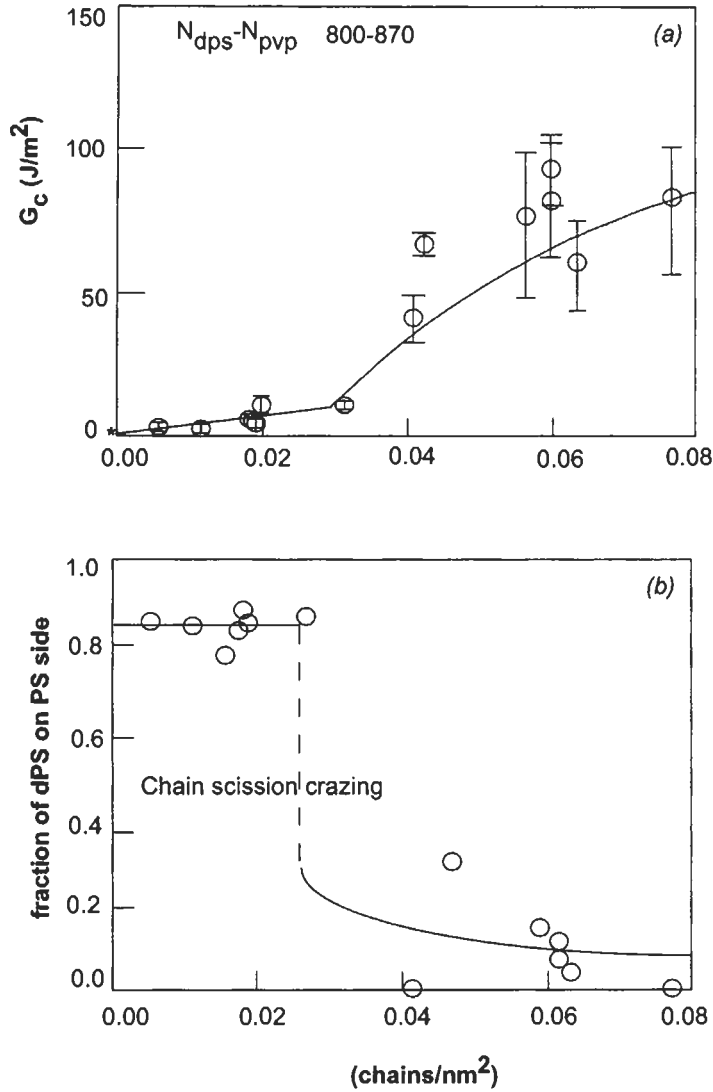


Fig. 2. This figure illustrates the transition from failure by simple chain scission to failure by crazing with chain scission. In PS crazes the scission tends to occur not at the junction point but in the PS copolymer block.

Using this model, Xu et al. have demonstrated that for sufficiently slow crack growth rate, i.e., $\dot{a} \rightarrow 0$, the fracture toughness $G_c(\dot{a})$ is given by:

$$G_c(\dot{a}) = G_c^0 = \frac{\sigma^* l}{2} = \frac{f_{\text{mono}} \Sigma N^2 l_0}{2} \quad \text{for} \quad \dot{a} \ll 0.36 \frac{\pi E^* \delta^*}{\sigma^*} \quad (2)$$

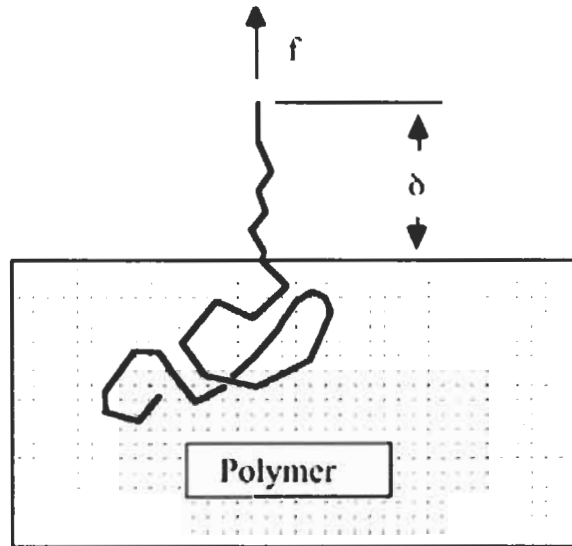


Fig. 3. The basic geometry of chain pull-out.

where $E^* = E/4(1 - \nu^2)$, E being Young's modulus and ν Poisson's ratio and a is a monomer length, so that $\Delta = Na$.

The main results of this micro-mechanical model in the quasi-static regime have been compared with experimental results obtained by placing polystyrene (PS)–polyvinyl pyridine (PVP) diblock copolymers with a short PVP block between PS and PVP homopolymers. The fracture toughness was found to increase linearly with Σ from that of the bare PS/PVP interface, while the slope of the line increased with the degree of polymerization of the block being pulled out. If the data for the different copolymers were plotted as ΔG_c vs. $(N_{\text{PVP}})^2 \Sigma$ (where $\Delta G_c = G_c(\Sigma) - G_c(0)$), they fall on a single line consistent with a single value of the monomer friction coefficient, as shown in Fig. 4. This value can be estimated by assuming that the only dissipative process is the frictional extraction of the PVP block where $\Delta G_c = f_{\text{mono}} N_{\text{PVP}}^2 \Sigma (a/2)$ taking a , the PVP monomer length, to be 0.23 nm. The value obtained for f_{mono} , 2.5×10^{-11} N/monomer is, however, an overestimate as it does not take into account any viscoelastic dissipation near the interface. The most important point to emphasize is that the maximum ΔG_c that can be obtained from this pull-out mechanism is very low, less than 5 J/m². The reason for this low maximum toughness is that the maximum displacement of the pull-out zone at the crack tip is only of order 40 nm, the length of an un-entangled connector chain.

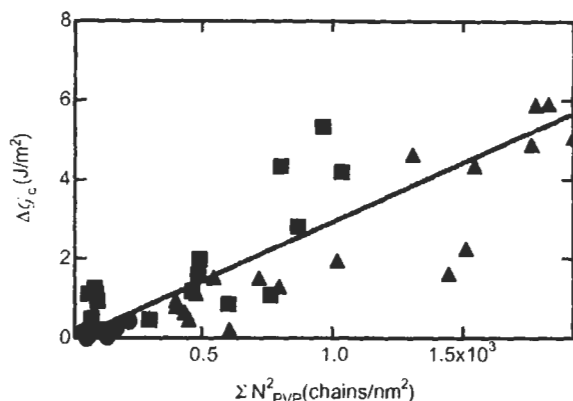


Fig. 4. The effect of chain pull-out of PVP on G_c for three PS-PVP diblocks whose PVP block varied from degree of polymerisation 49 to 220 [4].

2.4. Models of crazing failure for glassy polymers

2.4.1. The models

When the stress that can be born at the interface between two glassy polymers increases to the point that a craze can form then the toughness increases considerably as energy is now dissipated in forming and extending the craze structure. The most used model that describes the micro-mechanics of crazing failure was proposed by Brown [8] in a fairly simple and approximate form. This model has since been improved and extended by a number of authors. As the original form of the model is simple and physically intuitive it will be described first and then the improvements will be discussed.

A craze is a planar (crack-like) deformation zone that can form normal to the maximum principle stress in a glassy polymer. The two sides of the craze are joined by an array of fine interconnected fibrils that together hold the craze stress σ_c . The toughness of a polymer material that fails by a crazing mechanism is essentially the energy required to grow the crack tip craze(s) to their maximum width. The maximum craze width occurs at the crack tip. The model of failure by crazing is concerned with situations where there is one crack tip craze in which most of the fracture energy is dissipated (see Fig. 5). As the craze fibrils are interconnected with cross-tie fibrils, a stress concentration can occur within the craze. Therefore, even if the stress at the craze-matrix interfaces is approximately constant, the stress at the crack tip (within the craze) can be high enough to cause chain scission or pull-out, and hence fibril failure.

The aim of the model is to find the relation between the energy dissipated in growing the crack tip craze, as that is the macroscopic toughness and the local force at the fibril closest to the crack tip which controls the molecular level failure

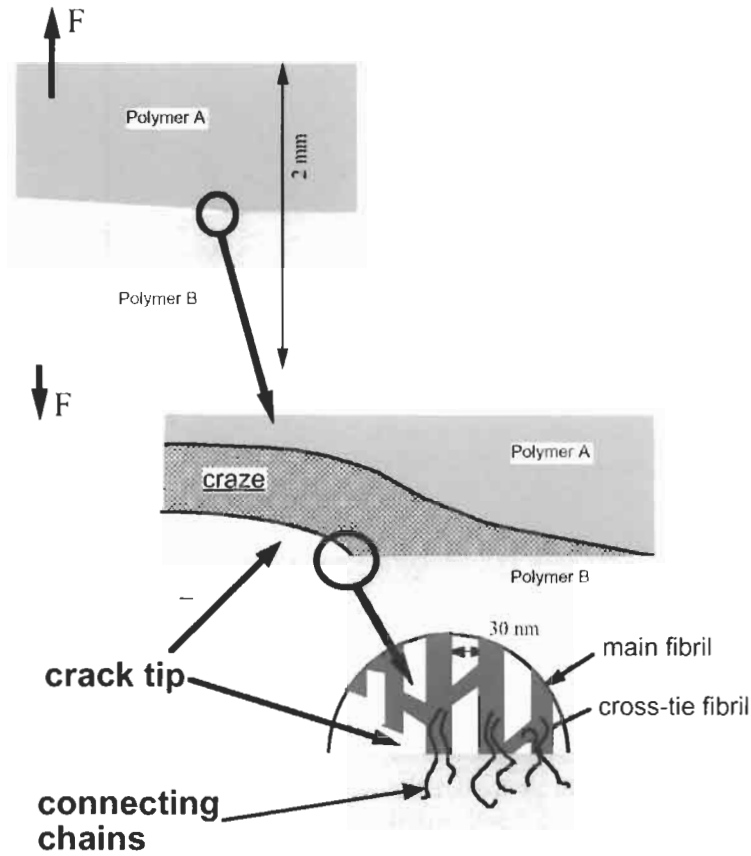


Fig. 5. An illustration of the basic idea of the model of failure by crazing showing the different relevant length scales.

process. In the original model the craze was modelled as a highly anisotropic continuum with a longitudinal modulus C_{22} and shear modulus C_{66} , between rigid clamps. The stress intensity at the crack tip (K_{tip}) was estimated from relations derived for elastomer failure. The craze is assumed to be a parallel-sided elastic strip of material between rigid clamps. The tensile stress σ_{22} directly ahead of the crack tip which is located at the origin ($x = 0$, $y = 0$) has an inverse square root singularity as $x \rightarrow 0$, i.e.:

$$\sigma_{22} \cong K_{tip}(2\pi x)^{-1/2} \quad (3)$$

K_{tip} is found to be

$$K_{tip} = A\sigma_c(C_{66}/C_{22})^{1/4}\sqrt{h} \quad (4)$$

where σ_c is the crazing stress, h is the half width of the craze at the crack tip and A is a constant of order one. The important issue here is that the crack tip stress increases with the width of the craze.

The stress on the craze fibril directly ahead of the crack tip was assumed to be

$$\sigma_{\text{fibril}} = K_{\text{tip}}(\pi d)^{-1/2} \quad (5)$$

where d is a fibril diameter

To obtain G_c , σ_{fibril} is set equal to the failure stress $\sigma_{\text{fibril}} = \Sigma f_c$, where f_c is the force to break or pull-out a chain, f_b or f_p

The toughness G_c is the energy per unit area to grow the craze to its maximum width so assuming that the stress σ_c along the craze is constant

$$G_c = \sigma_c(1 - v_f)h \quad (6)$$

where v_f is volume fraction of the fibrils in the craze.

By combining Eqs. 4–6 one obtains the basic relation between interface toughness and the force required to break or pull-out a chain

$$G_c = \frac{\pi d(1 - v_f)}{A^2} \sqrt{\frac{C_{22}}{C_{66}}} \frac{\Sigma^2 f_c^2}{\sigma_c} \quad (7)$$

The constant A was assumed equal to 1 in the original work.

The model has been improved by Hui et al. [9–11] in three distinct ways. Firstly they obtained a more accurate relation for the stress within the craze still assuming the displacement boundary conditions. They find that for broad crazes the best value for A^2 is 2.88. Secondly the simple model is bound to fail for weak crazes (low Σ) where the craze opening is narrow, the same order as the distance between the craze fibrils, and so the continuum solution cannot be valid. Discrete models have been constructed for this case [10–12]. Thirdly they relaxed the displacement boundary conditions for the strip and studied models, consisting of arrays of springs, where craze shape and craze/matrix stress are determined self-consistently. The craze shapes were found to be similar to the predictions of the Dugdale model assumed in the early work. They find that the following relation is an excellent approximation over the whole range from narrow to very wide crazes. The \ln factor agrees with the square law of Eq. 7 for wide crazes and the factor of 1.2 was found empirically to make the strip model results agree with those from the anisotropic self-consistent model spring model [11].

$$G_c = \frac{\pi d \sigma_c(1 - v_f) \sqrt{C_{22}/C_{66}}}{2 \ln \left(\left\{ 1 - \left[\frac{1.2 \sigma_c}{\Sigma f_c} \right]^2 \right\}^{-1} \right)} \quad (8)$$

In order to use this model it is necessary to estimate the ratio of the longitudinal to shear elastic constants, C_{22}/C_{66} . In the original model this quantity was

estimated crudely from typical distribution of the fibril directions of a craze from the tensile stress direction obtained experimentally by transmission electron microscopy and low angle electron diffraction. A more sophisticated mechanical modelling approach was used by Hui et al. [9], who considered the mechanics of a couple of possible microstructural models for the craze matter and obtained estimates of 0.02–0.03 for the modulus ratio. Very recently M.O. Robbins et al. (private communication, 2001) have used coarse-grained molecular simulation to grow a craze, obtaining a structure similar to those typically seen by transmission electron microscopy. They then deformed the simulated structure to directly find the relevant moduli.

In the discussion so far it has been assumed that Σ , the areal density of chains connecting across the interface, is the same as the density of such chains before the craze forms. However, it has been argued that a considerable number of chains are broken during the crazing process and so the number of effective chains, Σ_{eff} is less than the number of chains before crazing. If the surviving fraction of load bearing chain strands is given by q then $\Sigma_{\text{eff}} = q\Sigma$ if specific coupling chains are placed at the interface [13]. Alternatively if bulk polymer failure is the main concern then [3]

$$\Sigma_{\text{eff}} = q\Sigma [1 - (M_e/qM_n)] \quad (9)$$

where M_e is the molecular weight between entanglements and M_n is the number average molecular weight of the polymer.

2.4.2. Comparison with experiments using defined coupling chains

The model of crazing failure has been compared with experimental results obtained in a number of systems. The most direct tests have been obtained by measurement of the fracture toughness of interfaces between immiscible polymers that have been toughened by placing a known amount of diblock copolymer at the interface. The immiscible polymers were chosen so that the interface had low toughness without diblock and the diblock chosen so that each molecule could be expected to act as a single stitch between the bulk polymers, so one block was miscible in each of the homopolymers. The main systems studied have been (1) polystyrene (PS)–polymethylmethacrylate (PMMA) diblock copolymers joining PS and PMMA homopolymers or polyphenylene ether (PPE) and PMMA homopolymers, and (2) PS-PVP (polyvinyl pyridine) copolymers joining PS and PVP homopolymers. Typical results, shown in Figs. 6 and 7, agree well with the predictions of Eq. 8 (and often the simpler Eq. 7) over a wide range of Σ and toughness. It is clear that the model works well when the molecular level failure process is chain scission, but not enough experimental data exist to be confident of its applicability when the failure is by chain pull-out. The chain scission force f_b has been estimated to be in the range of 1.2–4 nN, where the main uncertainty

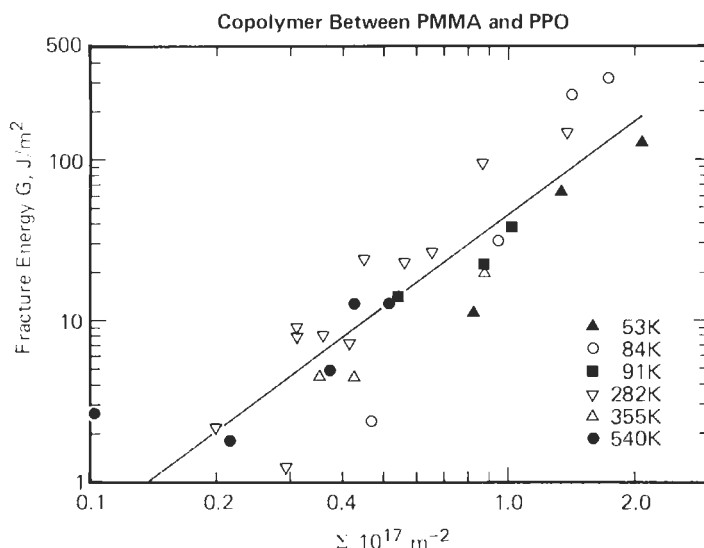


Fig. 6. Variation of interface toughness with area density of copolymer for a range of different molecular weight PS-PMMA copolymers between PMMA and PPO (or PPE) [39].

comes from the uncertainty in the craze modulus ratio. In principle the chain scission force would be expected to be time dependent. However, the time dependencies of the other parameters in Eq. 8 are unknown so it would not be possible to estimate the time dependence of f_b .

The model has also been found to work well in describing the mechanics of the interface between the semicrystalline polymers polyamide 6 and polypropylene coupled by the in-situ formation of a diblock copolymer at the interface. The toughness in this system was found to vary as Σ^2 where Σ was measured after the sample was fractured (see Fig. 8). The model probably applied to this system because the failure occurred by the formation and breakdown of a primary craze in the polypropylene [14].

2.5. Joining immiscible glassy polymers

The main difficulty in application of the simple chain pull-out model and the crazing failure model to the interfaces between immiscible polymers without coupling chains has been in estimating the effective value of Σ from the interface width and the known chain topologies. Brown [15] has proposed a simple technique to calculate the relation between interface width and Σ , based on the idea that the important molecular failure processes is scission of entangled strands (the strands are really loops). The polymers are assumed to be of high molecular weight (ignoring the effect of chain ends), and Σ is taken as a measure of the number of

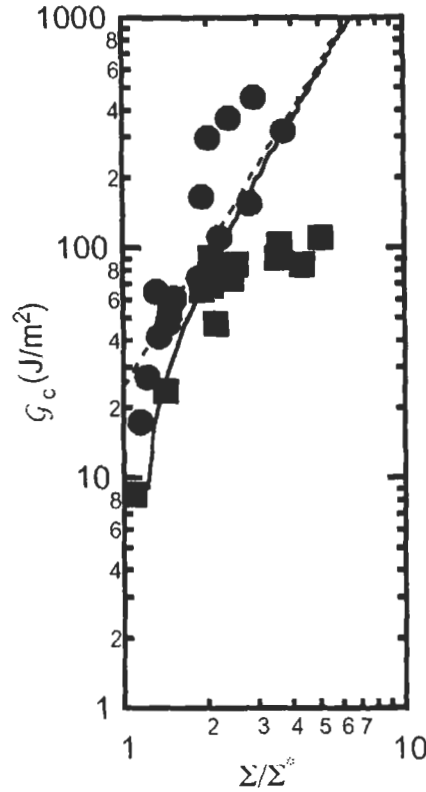


Fig. 7. Variation of G_c with Σ for both PS-PMMA diblocks between PPE and PMMA (●) and PS-PVP diblocks between PS and PVP (■) [13]. The solid line is a fit to Eq. 8 and the dashed line to Eq. 7.

polymer strands that have consecutive entanglements on each side of the interface. The probability of a chain of material A crossing the interface from a position z to a position z' is assumed to be proportional to the volume fractions of the material A at z and z' . The volume fractions are assumed to follow the normal hyperbolic tangent law. The calculated values of Σ were used in Eq. 8 to find the expected toughness.

A second model was proposed by Benkoski et al. [16] based on the idea that chain friction and pull-out, rather than chain scission are the important molecular scale failure processes. It is assumed that the chain failure force is given by $f_c = Nf_{\text{mono}}$, where N is the number of monomers in a loop that crosses the interface, and that

$$N\Sigma = \rho_{\text{mer}}w/2$$

where ρ_{mer} is the number density of monomers in the material and w is the

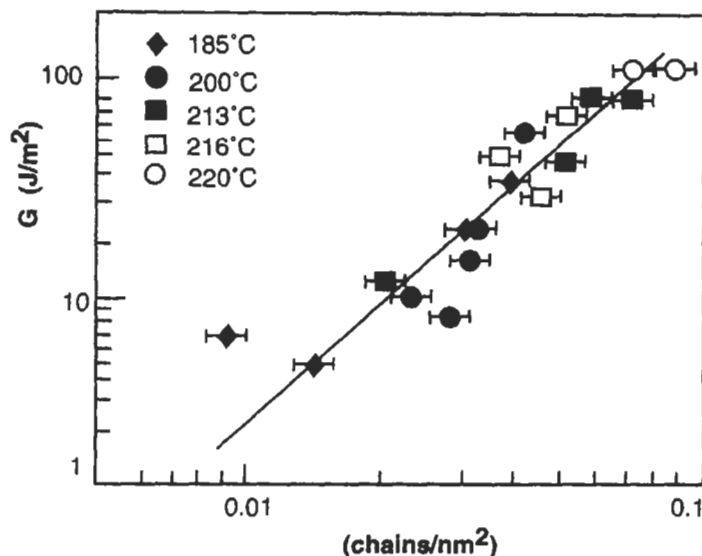


Fig. 8. Variation of G_c with Σ for polypropylene-polyamide 6 joints reinforced with PP-PA-6-grafted chains [14].

interface width. The important parameter that is required for use in Eqs. 7 or 8 is the product Σf_c , which in this model equals $\rho_{\text{mer}} w f_{\text{mono}}/2$.

The toughness of interfaces between immiscible amorphous polymers without any coupling agent has been the subject of a number of recent studies [15–18]. The width of a polymer/polymer interface is known to be controlled by the Flory–Huggins interaction parameter χ between the two polymers. The value of χ between a random copolymer and a homopolymer can be adjusted by changing the copolymer composition, so the main experimental protocol has been to measure the interface toughness between a copolymer and a homopolymer as a function of copolymer composition. In addition, the interface width has been measured by neutron reflection. Four different experimental systems have been used, all containing styrene. Schnell et al. studied PS joined to random copolymers of styrene with bromostyrene and styrene with paramethyl styrene [17,18]. Benkoski et al. joined polystyrene to a random copolymer of styrene with vinyl pyridine (PS/PS-r-PVP) [16], whilst Brown joined PMMA to a random copolymer of styrene with methacrylate (PMMA/PS-r-PMMA) [15]. The results of the latter study are shown in Fig. 9.

The different experimental systems all yield a similar pattern of variation of toughness with interface width. The toughness initially increases slowly with width at low interface width, and then increases rapidly with width and saturates at high width at a value close to the bulk toughness. If the density of entangled strands controlled the toughness, then the interface width at which the toughness

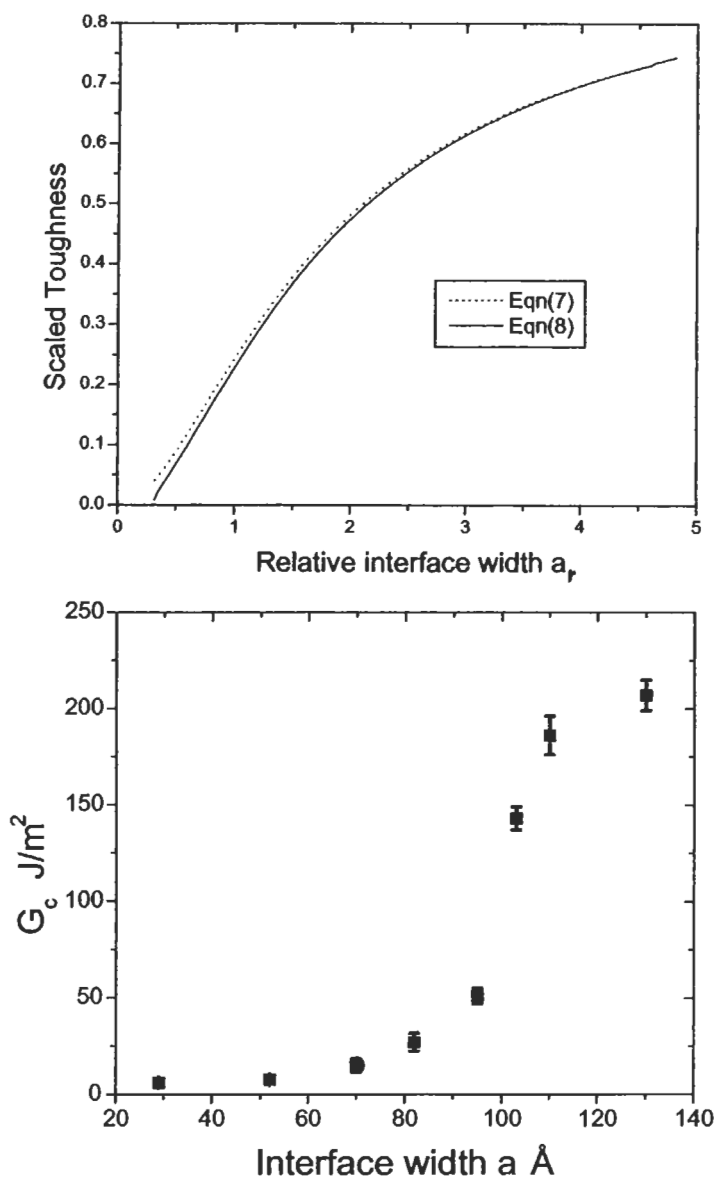


Fig. 9. The upper panel shows the predictions of Brown's [15] model for the coupling of an immiscible polymer interface. Clearly the predictions do not agree with his experimental results on PMMA joined to PS-r-PMMA shown in the lower panel.

rapidly increases would be related to the mean distance between entanglements. However, that is not observed. In addition the toughness increases much more rapidly with interface width than the predictions of Brown's model. The data

obtained on the PS/PS-*r*-PVP were shown by Benkoski et al. to be consistent with their pull-out model and they suggested that chain friction increases with the χ value between the units of the copolymer. Hence they suggested that chain friction might be dominant in PS/PS-*r*-PVP while entanglement and scission are dominant in PMMA/PS-*r*-PMMA. This explanation can qualitatively explain the differences between the different polymer systems studied and is consistent with the shape of the toughness vs. interface width curve seen with PS/PS-*r*-PVP but does not explain the rapid increase of toughness with interface width seen in PMMA/PS-*r*-PMMA. The latter observation could perhaps be explained by the effect of interface width on entanglement density.

2.6. Welding of glassy polymers

A good understanding of the welding of glassy polymers would require a combination of the understanding of three separate processes. (1) The understanding of the interdiffusion process needs to be at a level that gives reliable information on the number and length of chains or chain loops that cross the interface. (2) Knowledge of the relationships between the molecular structure of the interface caused by interdiffusion and the likely molecular level failure processes, chain pull-out and scission, is required to give a good estimate of the interfacial failure stresses. (3) The basic failure micro-mechanical failure processes, such as those described by Eqs. 2 or 8, need to be understood well. Although there has been much work on polymer interdiffusion and welding [19], in the author's opinion this combination still does not exist.

The interdiffusion of polymer chains occurs by two basic processes. When the joint is first made chain loops between entanglements cross the interface but this motion is restricted by the entanglements and independent of molecular weight. Whole chains also start to cross the interface by reptation, but this is a rather slower process and requires that the diffusion of the chain across the interface is led by a chain end. The initial rate of this process is thus strongly influenced by the distribution of the chain ends close to the interface. Although these diffusion processes are fairly well understood, it is clear from the discussion above on immiscible polymers that the relationships between the failure stress of the interface and the interface structure are less understood. The most common assumptions used have been that the interface can bear a stress that is either proportional to the length of chain that has reptated across the interface or proportional to some measure of the density of cross interface entanglements or loops. Each of these criteria can be used with the micro-mechanical models but it is unclear which, if either, assumption is correct.

3. Elastomeric polymers

Micro-mechanical processes that control the adhesion and fracture of elastomeric polymers occur at two different size scales. On the size scale of the chain the failure is by breakage of Van der Waals attraction, chain pull-out or by chain scission. The viscoelastic deformation in which most of the energy is dissipated occurs at a larger size scale but is controlled by the processes that occur on the scale of a chain. The situation is, in principle, very similar to that of glassy polymers except that crack growth rate and temperature dependence of the micro-mechanical processes are very important.

3.1. Chain pull-out

The main difference between chain pull-out processes in glassy polymers and in elastomers is that the friction per monomer in the latter is expected to be very much lower and to be essentially viscous. The friction at zero rate is thus expected to be zero. However, as pointed out by Raphaël and de Gennes [20], it does not follow that the toughness contribution from pull-out should tend to zero as the crack velocity tends to zero. They considered a situation where connector molecules, chemically identical to a cross-linked network, were grafted to a rigid substrate. The network was left in contact with the substrate so that the connector molecules diffused into it. They pointed out that single or multiple chain fibrils would be expected to form in a craze-like zone at the crack tip when a crack propagates along the interface. The dimensions (diameter) of these fibrils would be controlled by equilibrium between the fibril surface energy, tending to make them narrow, and the stretching energy of the chain. They predicted that the connector chains became highly stretched in these fibrils and when eventually the connector chain is pulled out the surface the stretching energy was dissipated. At zero crack growth rate they predicted a toughness G_0 given by

$$G_0 - W_A \approx \gamma N \Sigma a^2 \approx k T N \Sigma \quad (9)$$

where W_A is the work of adhesion of the interface, γ is the surface energy of the polymer whose monomer dimension is a . N is the degree of polymerisation of a connector chain. This threshold toughness is relevant when the crack speed is below a critical value V^* where

$$V^* \approx \frac{E}{3 \Sigma \zeta_0 N}$$

and ζ_0 is a monomer friction coefficient. Above the crack velocity V^* the toughness is predicted to increase linearly with V as

$$\frac{dG}{dV} \approx \frac{G_0}{V^*}$$

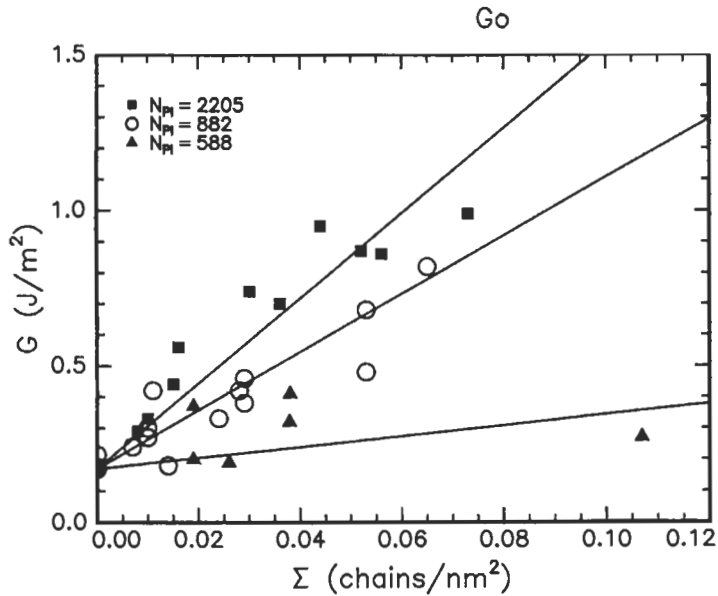


Fig. 10. The variation of G_0 with Σ for three different molecular weight polyisoprene tethered chains in a cross-linked polyisoprene lens [23].

The effects of connector chain aggregation have been examined theoretically and found to modify the predictions at high values of Σ [21].

The actual toughness values predicted by this model are very small, typically of the same order as the work of adhesion. The model's predictions have been compared with experiment by a number of authors [22–25] using the JKR technique. In this test an elastomer lens is pressed against a flat substrate and the contact area studied as a function of the load. Using polyisoprene [22,23], G_0 was found to vary with both the density and length of the connector chains as predicted (see Fig. 10). The values of $G_0 - W_A$ obtained were consistent with the model but the value of critical velocity V^* was found to be very low. More recently $G_0 - W_A$ has been measured using polydimethylsiloxane (PDMS) lenses and results obtained are again consistent with Eq. 9 (L. Léger, private communication, 2001).

3.2. Chain scission

The classic model that describes chain scission in elastomers was proposed many years ago by Lake and Thomas [26]. The aim of the model is to calculate the energy dissipated in breaking all the polymer strands that have adjacent cross-links on either side of the crack plane. The basic assumption of this model is that all the main chain bonds in any strand that breaks must be strained to the dissociation

energy of a main chain bond. It is assumed that this energy in the strand is dissipated when the chain fractures. If a strand has a degree of polymerisation N and each monomer unit contains n main chain bonds then

$$G_0 = \Sigma NnU \quad (10)$$

where U is the dissociation energy of a main chain bond. For cohesive failure

$$\Sigma = \nu_x d/2 = A\nu_x N^{0.5} = BN^{-0.5} \quad (11)$$

where d is the mean distance between adjacent cross-links on a strand and ν_x is the number of cross-links per unit volume and A and B are known constants depending on the flexibility of the polymer chain and its density. Combining these two equations demonstrates immediately that G_0 is predicted to vary as $N^{0.5}$.

The Lake–Thomas model is specifically for the threshold toughness, that is to say the toughness as the crack speed tends to zero, as there are expected to be viscoelastic contributions to the toughness at finite crack growth rates. However, Ghatak et al. [27] has argued that the model cannot be correct because chain scission is a thermally activated process and so, as the crack speed tends to zero, strands at the crack tip will undergo scission when the average energy per main chain bond is much less than the dissociation energy. In principle, this argument is correct, but in reality the Lake–Thomas model works rather well. Probably there is a range of slow crack rates where the viscoelastic dissipation is small but in thermally activated terms, scission is fairly fast so a constant chain breakage force (or energy per main chain bond) is a reasonable approximation.

The predictions of the Lake–Thomas model have been compared with measurements of cohesive toughness obtained at high temperatures and low crack growth rates, often in materials swollen in a solvent. Good agreement between experiment and the model is normally found [28]. The model has also been found to be consistent with the use of an end-linkable siloxane connector chain between a PDMS lens and a substrate [29] (see Fig. 11). In this work the length of the strand between cross-links was much greater than the length between entanglements and the relevant strand length was $\sim 2N_e$.

3.3. Viscoelastic energy dissipation in elastomers

The toughness of elastomers in both adhesion and cohesion is profoundly influenced by viscoelastic deformation in the region round the crack tip in most systems. The vast majority of the energy to propagate a crack is dissipated viscoelastically rather than in the actual process to break or pull-out chains. In many systems the following simple relationship, first proposed by Andrews and Kinloch [30,31], and Gent and Schultz [32] has been found to give a good description of the effects of W_A , crack speed (V) and temperature on the failure process.

$$G_c = G_0(1 + \phi(a_T V)) \quad (12)$$

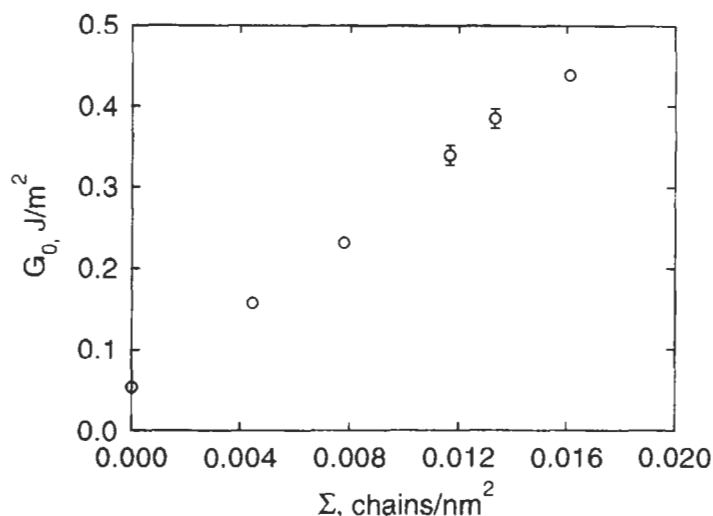


Fig. 11. The variation of the threshold toughness G_0 with Σ when an end-reactive PDMS chain was coupled into a PDMS network (H.R. Brown, W. Hu, J. Koberstein, unpublished work).

where G_0 describes the molecular failure energy including the work of adhesion W_A , and the viscoelastic shift factor a_T is the same relation that describes the time-temperature relationship for elastic modulus.

De Gennes [33,34] proposed a model for failure in lightly cross-linked or soft adhesives that gives a qualitative picture of the viscoelastic deformation. He proposed that one should consider four regions round a crack tip. Very close to the tip is the process zone where the actual chain pull-out, scission or dewetting occurs. Round that is a hard region in which the effective modulus is the unrelaxed modulus of the elastomer. Further out again is the viscous region where the dissipation occurs, and finally there is a region characterised by the relaxed elastic modulus. If the material shows just a single relaxation time τ , then the liquid-like zone extends from a distance $V\tau$ to a distance $\lambda V\tau$ from the crack tip, where λ is the ratio of the relaxed to the unrelaxed modulus. G is predicted to increase rapidly with V and then reach a constant value of λG_0 until the viscous region starts to be restricted by the size of the sample. At high crack speed G is then predicted to decrease with crack speed. The mechanics of this model was examined in more detail by Hui and co-workers [35,36] who obtained results that broadly agree with those of de Gennes. For finite size specimens they find that their results can be closely approximated by Eq. 12 as long as a specimen size parameter is also included.

The question of the actual form of the relation between toughness and crack speed is still rather unclear. It is tempting to relate $\phi(V)$ to the imaginary part of the elastic modulus, but the size parameter required to relate V to a time or

frequency scale does not seem very physical. De Gennes [34] suggests that, if the material can be described by a range of relaxation times then the crack velocity dependence of G may be related to the frequency dependence of the lower size cut-off of the viscous zone at the edge of the process zone. However, this idea has never been tested experimentally.

3.4. Interface slip

When an elastomeric material adheres to a rigid substrate the huge elastic mismatch causes considerable shear stresses to occur at the interface. Chaudhury and co-workers [37,38] have demonstrated that these shear stresses can cause failure mediated by interfacial slip. The toughness of the interface was shown to be controlled, not by the work of adhesion but by the shear stress that the interface could withstand. The existence of the slip was demonstrated explicitly by placing fluorescent beads in the material close to the interface and observing their motion. In the original work the process was modelled as a dewetting and the energy assumed to be dissipated within a wetting wedge. However, recent experiments where the distortions of the elastomeric film have been observed in more detail, have shown that the energy dissipation can be explained by simple viscoelastic distortion within the elastomeric adhesive [40].

4. Conclusions

At the scale of polymer repeat unit or chain, failure tends to occur by the detachment of simple Van der Waals bonds, by chain pull-out or by chain scission. All these processes can be found at both glassy and elastomeric polymer interfaces. The energy dissipated by these processes is very small, so toughness, either of a material or at an interface, requires that the chain scale processes couple into processes that occur in a larger volume and so dissipate more energy. For a glassy polymer this process is normally crazing, whilst in an elastomer it is viscoelastic deformation. A quantitative understanding of failure and toughness hence requires an understanding of coupling between the processes that occur at different length scales. The understanding is good for simple coupling chains at glassy polymer interfaces but more work is required to obtain a quantitative understanding of other situations in glassy polymers or failure in elastomeric or many semi-crystalline systems.

Acknowledgements

The author would like to thank C. Creton for permission to reproduce a number of figures from his work.

References

1. Brown, H.R., Deline, V.R. and Green, P.F., Evidence for cleavage of polymer chains by crack propagation. *Nature*, **341**, 221 (1989).
2. Kramer, E.J., Microscopic and molecular fundamentals of crazing. *Adv. Polym. Sci.*, **52**, 1–56 (1983).
3. Kramer, E.J. and Berger, L.L., Fundamental processes of craze growth and fracture. *Adv. Polym. Sci.*, **91**, 1–68 (1991).
4. Washiyama, J., Kramer, E.J., Creton, C. and Hui, C.Y., Chain pull-out fracture of polymer interfaces. *Macromolecules*, **27**, 2019–2024 (1994).
5. Washiyama, J., Creton, C. and Kramer, E.J., TEM fracture studies of polymer interfaces. *Macromolecules*, **25**, 4751–4758 (1992).
6. Plummer et al., C.J.G., Structure and microdeformation of (iPP/iPP-g-MA)-PA reaction bonded interfaces. *Macromolecules*, **31**(18), 6164–6176 (1998).
7. Xu, D.-B., Hui, C.-Y., Kramer, E.J. and Creton, C., A micromechanical model of crack growth along polymer interfaces. *Mech. Mater.*, **11**, 257–268 (1991).
8. Brown, H.R., A molecular interpretation of the toughness of glassy polymers. *Macromolecules*, **24**, 2752 (1991).
9. Hui, C.Y., Ruina, A., Creton, C. and Kramer, E.J., Micromechanics of crack growth into a craze in a polymer glass. *Macromolecules*, **25**, 3949–3955 (1992).
10. Sha, Y., Hui, C.Y., Ruina, A. and Kramer, E.J., Continuum and discrete modelling of craze failure at a crack tip in a glassy polymer. *Macromolecules*, **28**, 2450–2459 (1995).
11. Sha, Y., Hui, C.Y., Ruina, A. and Kramer, E.J., Detailed simulation of craze fibril failure at a crack tip in a glassy polymer. *Acta Mater.*, **45**, 3555–3563 (1997).
12. Xiao, F. and Curtin, W.A., Numerical investigation of polymer craze growth and fracture. *Macromolecules*, **28**, 1654–1660 (1995).
13. Creton, C., Kramer, E.J., Hui, C.-Y. and Brown, H.R., Failure mechanisms of polymer interfaces reinforced with block copolymers. *Macromolecules*, **25**, 3075–3088 (1992).
14. Boucher et al., E., Effects of the formation of copolymer on the interfacial adhesion between semicrystalline polymers. *Macromolecules*, **29**, 774–782 (1996).
15. Brown, H.R., The relation between the width of an interface between two polymers and its toughness. *Macromolecules* (2001, in press).
16. Benkoski, J.J., Fredrickson, G.H. and Kramer, E.J., The effect of composition drift on the effectiveness of random copolymer reinforcement at polymer–polymer interfaces. *Macromolecules* (2001, in press).
17. Schnell, R., Stamm, M. and Creton, C., Direct correlation between interfacial width and adhesion in glassy polymers. *Macromolecules*, **31**, 2284–2292 (1998).
18. Schnell, R., Stamm, M. and Creton, C., Mechanical properties of homopolymer interfaces: transition from simple pullout to crazing with increasing interfacial width. *Macromolecules*, **32**(10), 3420–3425 (1999).
19. Wool, R.P., *Polymer Interfaces: Structure and Strength*. Hanser Gardner, Cincinnati, OH, 1995.

20. Raphaël, E. and de Gennes, P.G., Rubber–rubber adhesion with connector molecules. *J. Phys. Chem.*, **96**, 4002–4007 (1992).
21. Ligoure, C. and Harden, J.L., Connector chain aggregation effects in elastomer–elastomer adhesion promotion. *J. Phys. Chem. B*, **101**, 4613–4619 (1997).
22. Brown, H.R., Effects of chain pull-out on the adhesion of elastomers. *Macromolecules*, **23**, 1666–1670 (1993).
23. Creton, C., Brown, H.R. and Shull, K.R., Molecular weight effects in chain pull-out. *Macromolecules*, **27**, 3174–3183 (1994).
24. Deruelle, M., Léger, L. and Tirrell, M., Adhesion at the solid–elastomer interface: influence of the interfacial chains. *Macromolecules*, **28**(22), 7419–7428 (1995).
25. Léger, L., Raphaël, E. and Hervet, H., Surface-anchored polymer chains: their role in adhesion and friction. *Adv. Polym. Sci.*, **138**, 185–225 (1999).
26. Lake, G.J. and Thomas, A.G., The strength of highly elastic materials. *Proc. R. Soc.*, **300**, 108–119 (1967).
27. Ghatak et al., A., Interfacial rate processes in adhesion and friction. *J. Phys. Chem. B*, **17**, 4018–4030 (2000).
28. Bhowmick, A.K., Threshold fracture of elastomers. *J. Macromol. Sci., Rev. Macromol. Chem. Phys.*, **C28**, 339–370 (1988).
29. Koberstein et al., J.T., Creating smart polymer surfaces with selective adhesion properties. *J. Adhes.*, **66**, 229–245 (1998).
30. Andrews, E.H. and Kinloch, A.J., The mechanics of adhesive failure, I. *Proc. R. Soc.*, **332**, 385–399 (1973).
31. Andrews, E.H. and Kinloch, A.J., The mechanics of adhesive failure, II. *Proc. R. Soc.*, **332**, 401–414 (1973).
32. Gent, A.N. and Schultz, J., Effect of wetting liquids on the strength of adhesion of viscoelastic materials. *J. Adhes.*, **3**, 281–294 (1972).
33. de Gennes, P.G., Fracture of a weakly crosslinked adhesive. *Compt. Rend.*, **307**, 1949–1953 (1988).
34. de Gennes, P.G., Soft adhesives. *Langmuir*, **12**, 4497–4500 (1996).
35. Hui, C.Y., Xu, D.B. and Kramer, E.J., A fracture model for a weak interface in a viscoelastic material (small scale yielding analysis). *J. Appl. Phys.*, **72**(8), 3294–3304 (1992).
36. Xu, D.-B., Hui, C.-Y. and Kramer, E.J., Interface fracture and viscoelastic deformation in finite size specimens. *J. Appl. Phys.*, **72**(8), 3305–3316 (1992).
37. Zhang Newby, B.-M., Chaudhury, M.K. and Brown, H.R., Macroscopic evidence of the effect of interfacial slippage on adhesion. *Science*, **269**, 1407–1409 (1995).
38. Zhang Newby, B.M. and Chaudhury, M.K., Effect of interfacial slippage on viscoelastic adhesion. *Langmuir*, **13**(6), 1805–1809 (1997).
39. Char, K., Brown, H.R. and Deline, V.R., Effects of a diblock copolymer on adhesion between immiscible polymers, 2. PS-PMMA copolymer between PPO and PMMA. *Macromolecules*, **26**(16), 4164–4171 (1993).
40. Amauroux, N., Petit, J. and Léger, L., Role of interfacial resistance to shear stress on adhesive peel strength. *Langmuir*, **17**(21), 6510–6517 (2001).

Chapter 6

Surface analysis in adhesion science

F. JAMES BOERIO *

University of Cincinnati, Cincinnati, OH 45221-0166, USA

1. Introduction

Surface analysis has made enormous contributions to the field of adhesion science. It enabled investigators to probe fundamental aspects of adhesion such as the composition of anodic oxides on metals, the surface composition of polymers that have been pretreated by etching, the nature of reactions occurring at the interface between a primer and a substrate or between a primer and an adhesive, and the orientation of molecules adsorbed onto substrates. Surface analysis has also enabled adhesion scientists to determine the mechanisms responsible for failure of adhesive bonds, especially after exposure to aggressive environments. The objective of this chapter is to review the principals of surface analysis techniques including attenuated total reflection (ATR) and reflection-absorption (RAIR) infrared spectroscopy, X-ray photoelectron spectroscopy (XPS), Auger electron spectroscopy (AES), and secondary ion mass spectrometry (SIMS) and to present examples of the application of each technique to important problems in adhesion science.

2. Infrared spectroscopy

Infrared spectroscopy, including Fourier-transform infrared (FTIR) spectroscopy, is one of the oldest techniques used for surface analysis. ATR has been used for many years to probe the surface composition of polymers that have been surface-modified by an etching process or by deposition of a film. RAIR has been widely used to characterize thin films on the surfaces of specular reflecting substrates.

FTIR has numerous characteristics that make it an appropriate technique for

* E-mail: f.james.boerio@uc.edu

investigations related to adhesion science. Most importantly, infrared spectroscopy is primarily sensitive to functional groups whereas other techniques are mostly sensitive to elements. Therefore, the technique can provide a great deal of information about curing reactions of adhesives and about other chemical reactions that are relevant to adhesion. The technique is also non-destructive since virtually no sample degradation occurs when a specimen is illuminated with infrared radiation. Using the ATR technique, maps and depth profiles can be constructed showing the distribution of functional groups across the surface of a sample or with distance away from the surface of the sample and into the bulk. In RAIR, monolayer or even sub-monolayer sensitivity is almost routine, making the technique extremely useful for investigating surface processes on metals, such as corrosion or adsorption of components of adhesive systems. The cost of an FTIR system is low, especially when compared to that of instruments needed for surface characterization by vacuum techniques.

FTIR also has several disadvantages. For example, depth profiling is not possible in RAIR. In ATR, surface sensitivity is limited to approximately the wavelength of infrared radiation or about one micrometer (see below). The spatial resolution of conventional infrared techniques is limited by diffraction effects and is only approximately a few tens of micrometers.

In an FTIR spectrometer, a source (usually a resistively heated ceramic rod) emits infrared radiation that is focused onto an interferometer whose main components consist of a beamsplitter, fixed mirror, movable mirror, and detector. The beamsplitter divides the beam into two beams. One beam is reflected off the beamsplitter toward the fixed mirror and is then reflected back through the beamsplitter to the detector. The other beam is transmitted through the beamsplitter toward the movable mirror and is then reflected off of the beamsplitter and to the detector [1].

The intensity measured by the detector depends on the difference in path length that the two beams travel to reach the detector. Since one of the mirrors can be moved or scanned, the intensity reaching the detector can be measured as a function of retardation (δ) or the difference in path length between the two beams. The output of the detector can be displayed as an interferogram consisting of a plot of intensity versus retardation. If an absorbing sample is placed between the beamsplitter and the detector, then the appearance of the interferogram is modified somewhat. The Fourier transform of the interferogram can be calculated to obtain the infrared absorption spectrum of the sample [1].

2.1. Attenuated total reflection (ATR)

In order to characterize the surface regions of a sample that has been modified in some way, as is usually the case in adhesion-related investigations, some sort of a reflection experiment is required. Two types of experiments, attenuated total reflection (ATR) and reflection-absorption infrared spectroscopy (RAIR),

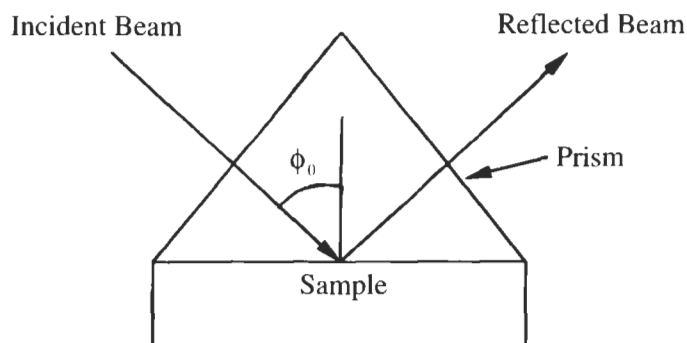


Fig. 1. Schematic drawing of an attenuated total reflection (ATR) experiment.

are commonly used. ATR is used when the substrate is a relatively soft material with *low* refractive index. In this case, a prism of a material with a relatively *high* refractive index is placed in intimate contact with the sample and the infrared radiation is reflected off the prism/sample interface (see Fig. 1). The angle of incidence is related to the angle of refraction (the angle that the beam transmitted into the sample makes with the normal to the interface) by Snell's law:

$$n_1 \sin(\theta_1) = n_2 \sin(\theta_2) \quad (1)$$

In this expression, n_1 is the refractive index of the prism, θ_1 is the angle of incidence, n_2 is the refractive index of the sample, and θ_2 is the angle of refraction. Since n_1 is greater than n_2 , θ_2 is greater than θ_1 . That means that for some value of θ_1 , called the critical angle θ_c , the angle of refraction is greater than 90° and there is no traveling wave transmitted into the sample. Instead, an 'evanescent' wave having an amplitude that decreases exponentially as a function of distance away from the prism/sample interface exists in the sample. The 'penetration depth' (δ) is the distance that it takes for the wave in the sample to decrease to $1/e$ times its value at the interface and is given by the expression:

$$\delta = \lambda_0 / 2\pi n_1 [\sin^2(\theta_1) - (n_2/n_1)^2]^{1/2} \quad (2)$$

where λ_0 is the wavelength of the infrared radiation [2]. From Eq. 2, it is evident that the depth of penetration is closely related to the refractive index of the prism and to the wavelength of the radiation. Also, δ increases as wavelength increases. For a typical prism material (germanium, $n_1 = 4.0$), the depth of penetration is on the order of one micrometer.

As long as $\theta_1 > \theta_c$ and the sample is not absorbing, the reflectivity of the prism/sample interface will be complete. However, at any wavelength where the sample is absorbing, the reflectivity will be 'attenuated' or less than complete. Thus, an absorption spectrum that is similar to that obtained in transmission can be produced in ATR.

The refractive index of the sample can be written as a complex number $n_2 = n_2 - ik_2$. At wavelengths where the sample is not absorbing, k_2 , the absorption constant, equals zero. However, k_2 is non-zero at wavelengths where the sample is absorbing. In transmission spectroscopy, the intensity of an absorption band depends almost entirely on k_2 while in ATR the intensity of the same band is a complex function of n_2 and k_2 . Nevertheless, the statement made previously still holds. There will be absorption bands in ATR at wavelengths where $k_2 \neq 0$. Thus, bands are expected at the same wavelengths in transmission and in ATR but their intensities may be dissimilar.

As indicated above, the penetration depth is on the order of a micrometer. That means that in ATR, absorption of infrared radiation mostly occurs within a distance δ of the surface and ATR is not as surface sensitive as some other surface analysis techniques. However, ATR, like all forms of infrared spectroscopy, is very sensitive to functional groups and is a powerful technique for characterizing the surface regions of polymers.

ATR infrared spectroscopy can be used to construct a depth profile showing the way in which the surface composition of a polymer changes as a function of distance away from the surface and into the polymer [3]. As long as the polymer is not a very strong absorber, the absorbance of an infrared band in ATR is:

$$A(\delta) = \int \alpha(z) \exp(-\delta z) dz \quad (3)$$

In this expression, z is the distance from the surface into the sample, $\alpha(z)$ is the absorption coefficient, and δ , the depth of penetration, is given by Eq. 2. A depth profile can be obtained for a given functional group by determining $\alpha(z)$, which is the inverse Laplace transform of $A(\delta)$, for an absorption band characteristic of that functional group.

Experimentally, the absorbance $A(\delta)$ of a band is measured as a function of the angle of incidence θ and thus of δ . Two techniques can be used to determine $\alpha(z)$. A functional form can be assumed for $\alpha(z)$ and Eqs. 2 and 3 used to calculate the Laplace transform $A(\delta)$ as a function of δ [4]. Variable parameters in the assumed form of $\alpha(z)$ are adjusted to obtain the best fit of $A(\delta)$ to the experimental data. Another approach is to directly compute the inverse Laplace transform of $A(\delta)$ [3,5]. Programs to compute inverse Laplace transforms are available [6].

Fig. 2 shows one application of ATR depth profiling. In this case, ATR spectra were obtained as a function of angle of incidence from a polymethylmethacrylate (PMMA) film of thickness $0.5 \mu\text{m}$ that was deposited onto a germanium hemicylinder [4]. The solid line represents the ATR spectrum of PMMA while the squares represent the film thickness that was recovered from the infrared spectra using four different bands. It can be observed that the recovered film thickness was very close to the measured thickness.

Blais et al. used ATR to investigate etching of high-density polyethylene

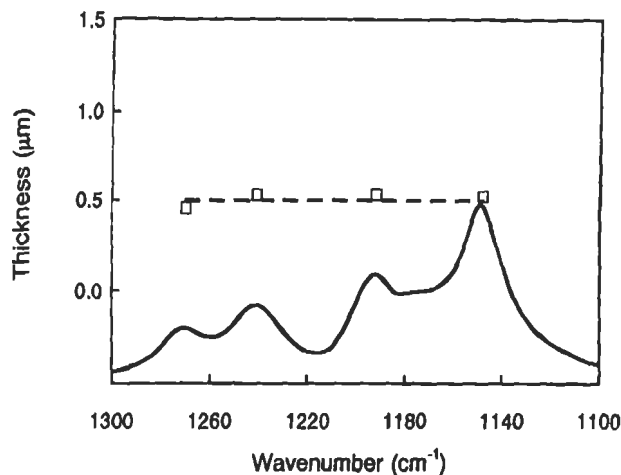


Fig. 2. ATR spectra obtained as a function of angle of incidence from a polymethylmethacrylate (PMMA) film of thickness $0.5\ \mu\text{m}$ that was deposited onto a germanium hemi-cylinder. The solid line represents the ATR spectrum of PMMA while the squares represent the film thickness that was recovered from the infrared spectra using four different bands. Reprinted by permission of Society for Applied Spectroscopy from Ref. [4].

(hd-PE), low-density polyethylene (ld-PE), and isotactic polypropylene (i-PP) in chromic acid solutions ($\text{K}_2\text{Cr}_2\text{O}_7 : \text{H}_2\text{O} : \text{H}_2\text{SO}_4 = 4.4 : 7.1 : 88.5$) at 70°C [7]. High-density and low-density polyethylene had about 3–4 and 50 branches per methylene group, respectively. They observed the appearance of bands near $3300\ \text{cm}^{-1}$ ($-\text{OH}$), $1710\ \text{cm}^{-1}$ ($>\text{C}=\text{O}$), and possibly $-\text{SO}_3\text{H}$ at 1200 and $1030\ \text{cm}^{-1}$ in ATR spectra of ld-PE (see Fig. 3). No changes in the spectra were observed for high-density polyethylene or polypropylene.

Peel test specimens were prepared by adhering etched polymer films to stainless steel supports using double-sided tape and then bonding a nylon fabric onto the film using an adhesive. The force required to peel the nylon fabric from the polymer film was determined as a function of etching time. Peel strength increased with etch time for all of the polymer samples before leveling off at etch times of about 100 s. This effect was observed even for high-density polyethylene and polypropylene when no new functional groups were detected using ATR. It was suggested that functional groups were inserted into the surfaces of hd-PE and i-PP but the concentrations were too small to be observed by ATR.

Papirer et al. used ATR, XPS, and SIMS to determine the effect of flame treatment on adhesion of polyethylene and polypropylene to styrene/butadiene (SBR) rubber [8]. Each flame treatment consisted of a 75-ms pass over a circular burner. The distance between the upper flame front and the polymer was kept fixed at 8 mm. A band was observed near $1720\ \text{cm}^{-1}$ in the ATR spectra and assigned to carbonyl groups; this band increased in intensity as the number of flame

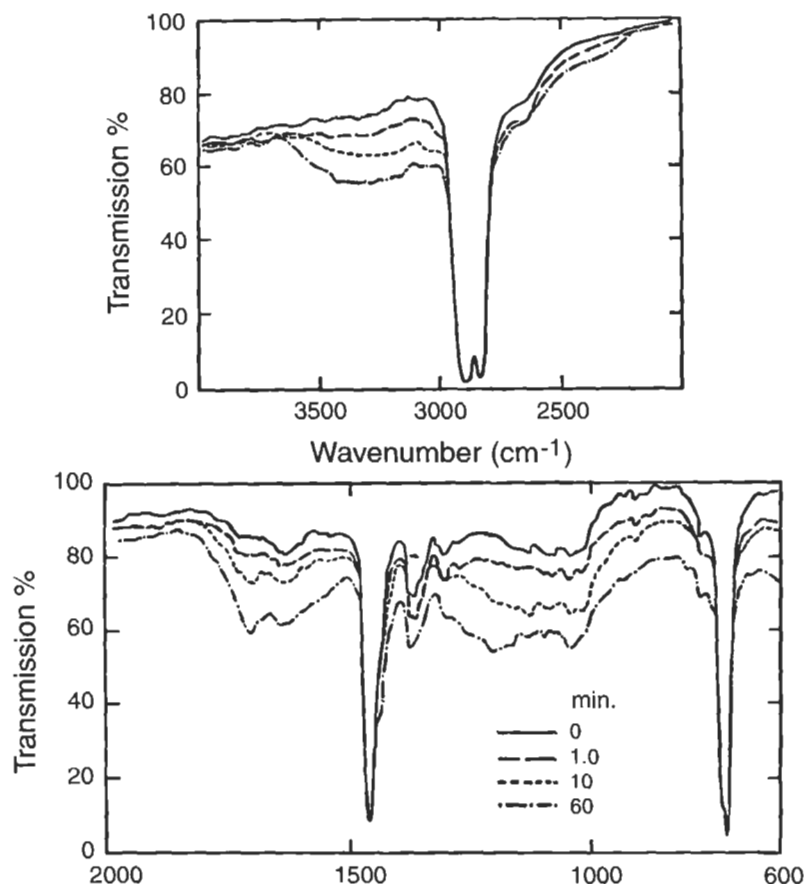


Fig. 3. ATR infrared spectra obtained from low-density polyethylene after exposure to chromic acid for times between 0 and 60 min. Reprinted by permission of Academic Press from Ref. [7].

treatments of polyethylene increased. Another band near 1630 cm^{-1} that was tentatively assigned to unsaturation also increased in intensity with the number of flame treatments. Peel strength was negligible for test specimens prepared from SBR and PE or PP that was not flame treated. However, peel strength increased dramatically with the number of flame treatments before leveling off at about two treatments.

2.2. Reflection-absorption infrared spectroscopy (RAIR)

In order to obtain the infrared spectrum of a thin film on a reflecting substrate, a transmission experiment is out of the question since infrared radiation cannot be transmitted through any significant thickness of a reflecting material. Instead,

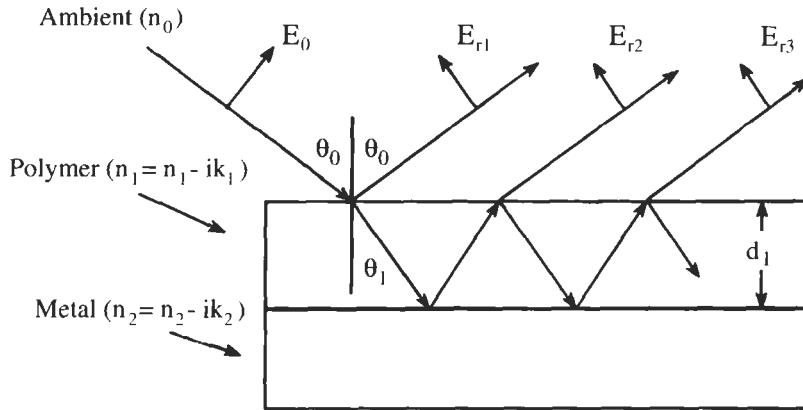


Fig. 4. Schematic drawing of a reflection-absorption infrared (RAIR) spectroscopy experiment.

a reflection experiment is required. Reflection-absorption infrared spectroscopy (RAIR) is a powerful technique for characterizing thin films on reflecting substrates by reflecting parallel-polarized infrared radiation off the substrates at large, almost grazing angles of incidence.

In order to understand RAIR spectroscopy, it is convenient to model the experiment (see Fig. 4). Consider a thin film with refractive index $n_1 = n_1 - ik_1$ and thickness d_1 supported by a reflecting substrate with refractive index $n_2 = n_2 - ik_2$. The refractive index of the ambient atmosphere is n_0 . Infrared radiation impinges on the film at an angle of incidence of θ_0 . The incident radiation can be polarized parallel to or perpendicular to the plane of incidence.

When infrared radiation with electric field amplitude E_0 impinges on the film-covered substrate, some is reflected from the ambient/film interface while some is transmitted into the film and then reflected at the film/substrate interface. Some of the radiation reflected at the film/substrate interface is reflected back into the film at the film/ambient interface. However, some is transmitted into the ambient (see Fig. 4). The reflection coefficient (r) for the film/substrate system is calculated by summing the electric field amplitudes for all of the waves reflected into the ambient and then dividing by the electric field amplitude (E_0) of the incident radiation.

$$r = (E_{r1} + E_{r2}e^{2i\delta} + E_{r3}e^{4i\delta} + \dots) / E_0 \quad (4)$$

2δ is the phase difference between successive reflected waves and is given by:

$$\delta = 2\pi n_1 d_1 \cos(\phi_1) / \lambda_0 \quad (5)$$

Eq. 4 can ultimately be written as:

$$r = (r_1 + r_2 e^{-2i\delta}) / (1 + r_1 r_2 e^{-2i\delta}) \quad (6)$$

where r_1 and r_2 are the reflection (Fresnel) coefficients for the ambient/film and film/substrate interfaces, respectively. For parallel polarized radiation, r_1 and r_2 are given by:

$$r_1 = [n_o \cos(\phi_1) - n_1 \cos(\phi_o)] / [n_o \cos(\phi_1) + n_1 \cos(\phi_o)] \quad (7)$$

$$r_2 = [n_1 \cos(\phi_2) - n_2 \cos(\phi_1)] / [n_1 \cos(\phi_2) + n_2 \cos(\phi_1)] \quad (8)$$

For perpendicular polarized radiation, the reflection (Fresnel) coefficients are given by the expressions:

$$r_1 = [n_o \cos(\phi_o) - n_1 \cos(\phi_1)] / [n_o \cos(\phi_o) + n_1 \cos(\phi_1)] \quad (9)$$

$$r_2 = [n_1 \cos(\phi_1) - n_2 \cos(\phi_2)] / [n_1 \cos(\phi_1) + n_2 \cos(\phi_2)] \quad (10)$$

The reflectivity of the film/substrate system can be calculated from Eq. 6 as:

$$R = rr^* \quad (11)$$

where r^* is the complex conjugate of r . The size (intensity) of a band in the RAIR spectrum can be calculated as:

$$A = -\log(R/R_o) \quad (12)$$

where R_o and R represent the reflectivity of the film/substrate system when the film is ($k_1 \neq 0$) or is not ($k_1 = 0$) absorbing [9].

Eq. 12 can be used in various ways. If the refractive index ($\mathbf{n}_1 = n_1 - ik_1$) of the film is known at one wavelength where the film is absorbing (i.e., at the position of an absorption band of the film), the intensity of an absorption band in the RAIR spectrum can be calculated. This can be done as a function of the angle of incidence and of the polarization (parallel to or perpendicular to the plane of incidence). If $\mathbf{n}_1 = n_1 - ik_1$ and $\mathbf{n}_2 = n_2 - ik_2$ are known as a function of wavelength, the entire RAIR spectrum can be calculated. As before, this can be done as a function of the angle of incidence and of the polarization.

Fig. 5 shows a plot of RAIR band intensity versus angle of incidence (θ_o) for a typical polymer film with a carbonyl absorption band at approximately 1740 cm^{-1} . In this case, it was assumed that $\mathbf{n}_1 = n_1 - ik_1$, $\mathbf{n}_2 = n_2 - ik_2$, $d_1/\lambda = 0.0003$, and that the infrared radiation was polarized parallel to the plane of incidence [9]. From Fig. 5, it is evident that band size is negligible for small values of θ_o but increases significantly at larger angles and reaches a maximum near $\theta_o = 85^\circ$. When the infrared radiation is polarized perpendicular to the plane of incidence, band size is always negligible. It can be concluded that in order to obtain the RAIR spectrum of a thin film on a reflecting substrate, it is necessary to use parallel polarized radiation and large, almost grazing angles of incidence. From a practical perspective, the largest angle of incidence that can be used conveniently is about 85° . However, using an angle of incidence near this value, it is possible to obtain RAIR spectra of films as thin as a monomolecular layer.

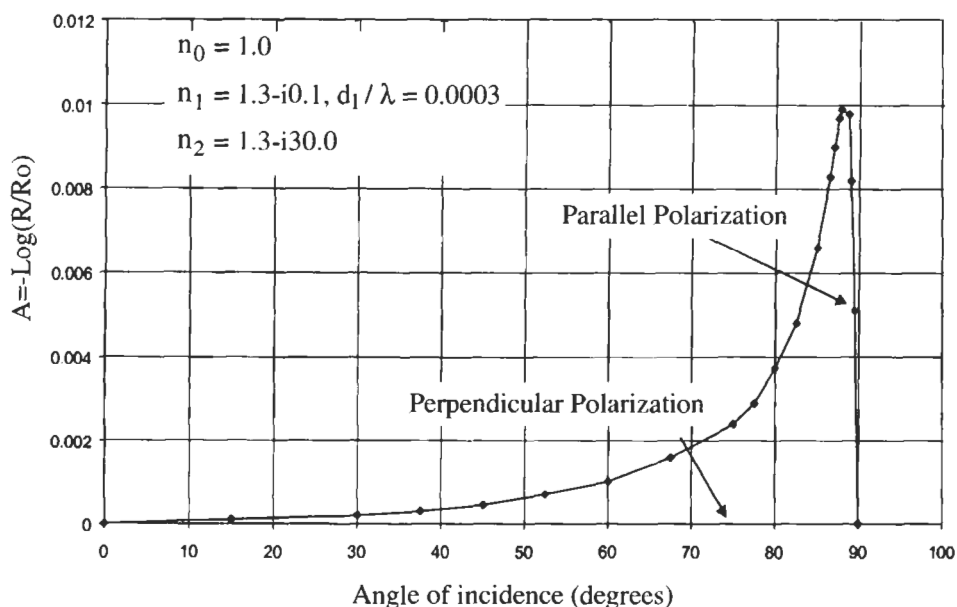


Fig. 5. A plot of RAIR band size as a function of angle of incidence.

A powerful characteristic of RAIR spectroscopy is that the technique can be used to determine the orientation of surface species. The reason for this is as follows. When parallel polarized infrared radiation is specularly reflected off of a substrate at a large angle of incidence, the incident and reflected waves combine to form a standing wave that has its electric field vector (E) perpendicular to the substrate surface. Since the intensity of an infrared absorption band is proportional to $I \sim (E \cdot M)^2$, where M is the 'transition moment', it can be seen that the intensity of a band is maximum when E and M are parallel (i.e., both perpendicular to the surface). I is a minimum when M is parallel to the surface (as stated above, E is always perpendicular to the surface in RAIR spectroscopy).

If $n_1 = n_1 - ik_1$ and $n_2 = n_2 - ik_2$ are known as a function of wavelength, Eq. 12 can be used to calculate the entire RAIR spectrum of a surface film. Since transmission infrared spectroscopy mostly measures k_1 , differences between transmission and RAIR spectra can be identified. Fig. 6 shows a k_1 spectrum that was synthesized assuming two Lorentzian-shaped absorption bands of the same intensity but separated by 25 cm^{-1} . The corresponding spectrum of n_1 values was calculated from the k_1 spectrum using the Kramers-Kronig transformation and is also shown in Fig. 6. The RAIR spectrum was calculated from the n_1 and k_1 spectra using Eqs. 11 and 12 and is shown in Fig. 7.

Two important features of RAIR spectroscopy can be observed by comparing the RAIR spectrum in Fig. 7 with the k_1 spectrum in Fig. 6, remembering that the

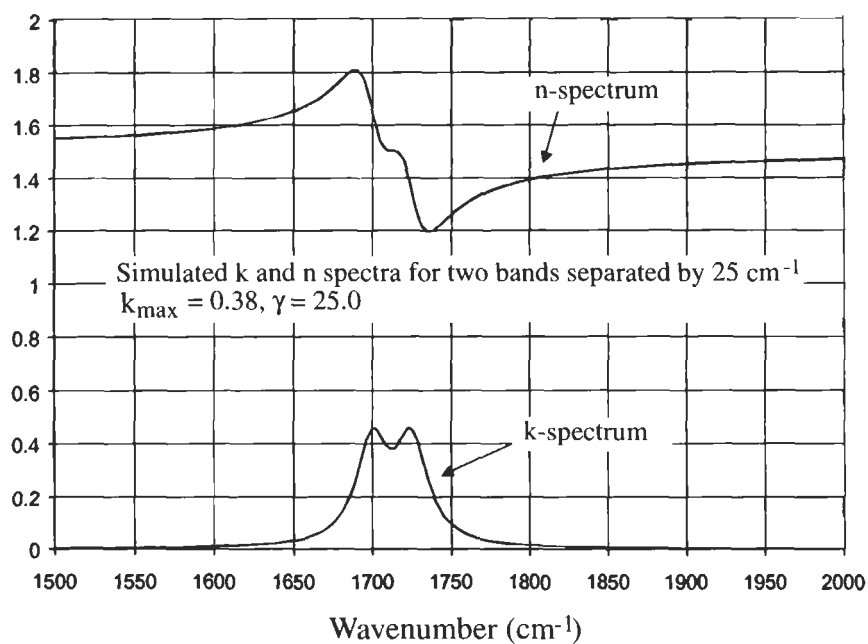


Fig. 6. Spectra of calculated k_1 and n_1 values as a function of wavenumber.

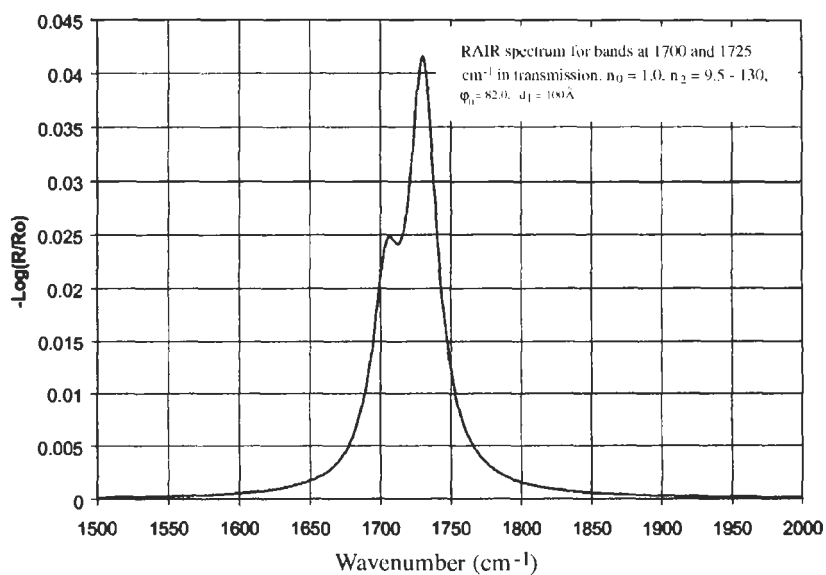


Fig. 7. RAIR spectrum calculated from the n_1 and k_1 spectra shown in Fig. 6.

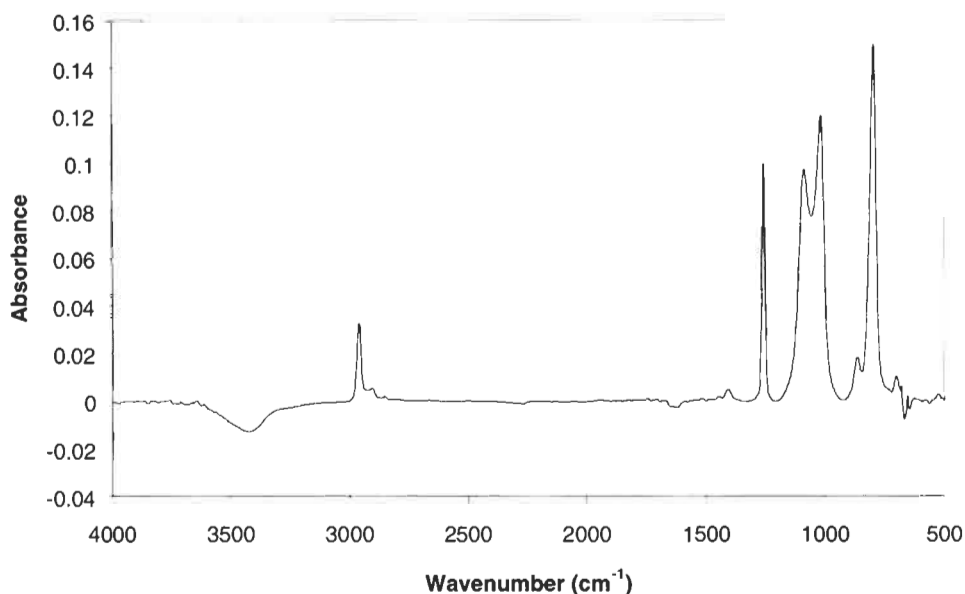


Fig. 8. Transmission infrared spectrum of PDMS.

transmission spectrum resembles the k_1 spectrum. The first is that bands in RAIR spectra do not necessarily appear at the same wavenumbers as the corresponding bands in transmission spectra. In Fig. 6, the bands in the k_1 spectra are at 1700 and 1725 cm⁻¹. However, in Fig. 7, the corresponding bands appear at 1708 and 1735 cm⁻¹. Thus, it can be concluded that bands in RAIR spectra are sometimes shifted toward higher wavenumbers when compared to their counterparts in transmission spectra. The second important feature of RAIR spectroscopy is that bands sometimes appear with different relative intensities than in transmission spectra. This is clearly seen by comparing the k_1 spectrum in Fig. 6 with the RAIR spectrum in Fig. 7. Whereas the two bands in the k_1 spectrum had the same intensity, the corresponding bands in the RAIR spectrum have significantly different intensities. This is a general feature of RAIR spectroscopy. When there are two nearby bands of similar intensity in the transmission spectrum, the band at higher frequency will have greater relative intensity in the RAIR spectrum.

This characteristic of RAIR can be observed experimentally. Fig. 8 shows the transmission spectrum of polydimethylsiloxane (PDMS) while Fig. 9 shows the RAIR spectrum of a thin film of PDMS spin-coated onto a chromium substrate. It can be observed that the bands near 1024 and 1095 cm⁻¹ have similar intensities in the transmission spectra but the band at higher frequencies is clearly much more intense in the RAIR spectrum. This change in relative intensity when PDMS is deposited onto a reflecting substrate is related to optical effects and is not related to orientation effects.

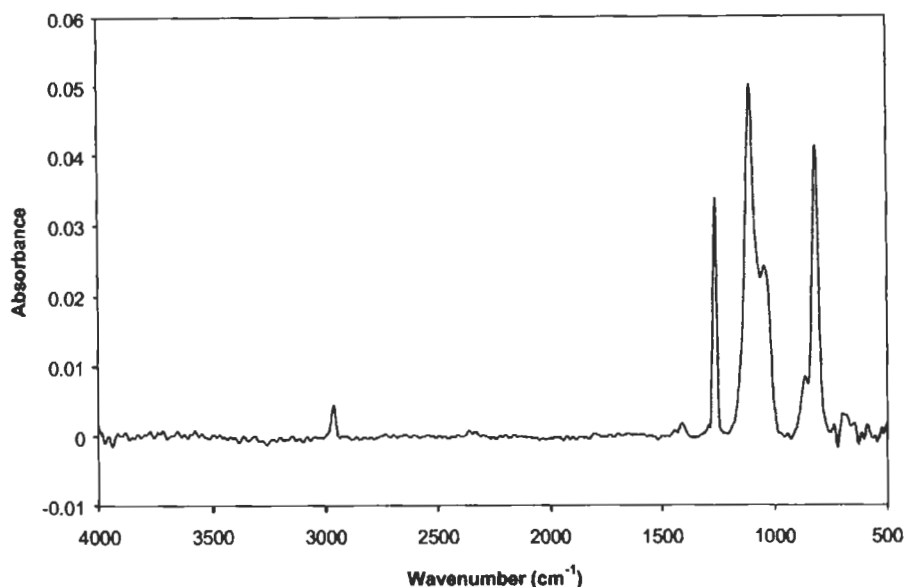


Fig. 9. RAIR spectrum of PDMS spin-coated onto a chromium substrate.

There have been many applications of reflection-absorption infrared spectroscopy that are relevant to adhesion science. Young et al. [10] investigated the adsorption of 4-mercaptophenylphthalimide (4-MPP) from solution onto gold substrates. The objective was to determine the mechanism of bonding between 4-MPP and the substrate and to determine the orientation of the adsorbed compound. Fig. 10 shows the transmission FTIR spectrum of 4-MPP. Bands near 1782, 1710, 1388, 1121, and 717 cm^{-1} were assigned to the symmetric C=O stretching, asymmetric stretching, CNC axial stretching, CNC transverse stretching, and CNC out-of-plane bending modes, respectively. Fig. 11 shows the RAIR spectrum of a 4-MPP monolayer adsorbed onto a gold substrate from a dilute solution in chloroform. The intense band near 1710 cm^{-1} in the transmission spectrum is relatively weak in the RAIR spectrum while the band near 1388 cm^{-1} , which had medium intensity in the transmission spectrum is the strongest band in the RAIR spectrum.

The relative intensities of the bands in the transmission and RAIR spectra were used to determine the orientation of the long axis of the 4-MPP molecules with respect to the normal to the gold surface. It was found that this 'tilt angle' was about 21° , a value that was similar to that obtained from molecular dynamics simulations [11].

Tsai et al. have used RAIR extensively in investigations of plasma polymerized acetylene films as primers for rubber-to-metal bonding [12]. Fig. 12 shows RAIR spectra of films having a thickness between about 5.7 and 90.0 nm. A strong band

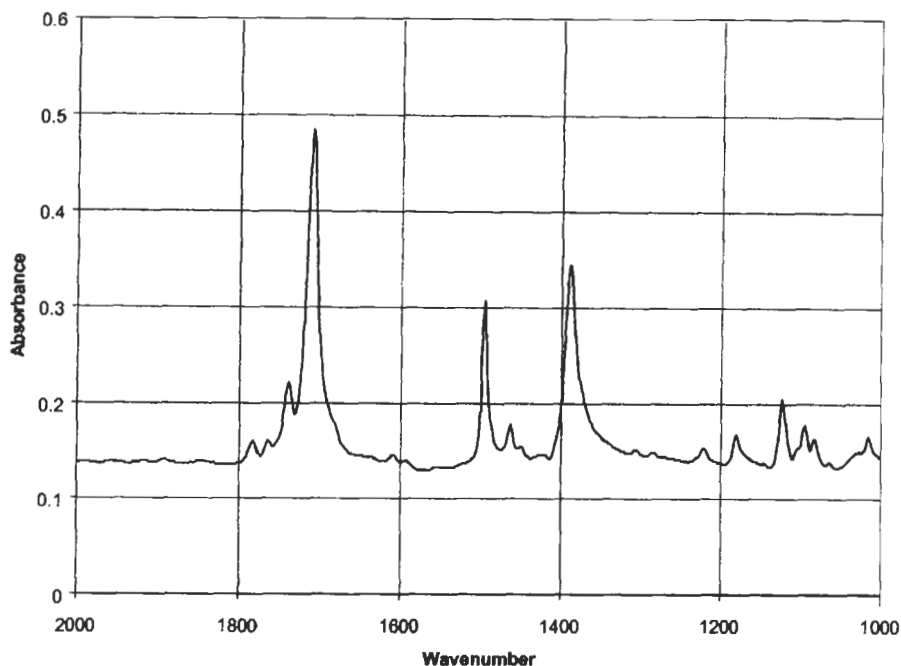


Fig. 10. Transmission infrared spectrum of 4-mercaptophenylphthalimide (4-MPP). Reproduced by permission of the American Chemical Society from Ref. [9].

was observed near 3295 cm^{-1} in the spectra and attributed to the C–H stretching vibration of mono-substituted acetylene groups. Other bands were observed near 3027 , 2960 , 2928 , 2870 , and 2853 cm^{-1} . The band near 3027 cm^{-1} was assigned to C–H stretching in vinyl ($\text{RHC}=\text{CH}_2$) groups while the bands near 2960 , 2928 , 2870 , and 2853 cm^{-1} were assigned to C–H vibrations in methyl and methylene groups. The band near 916 cm^{-1} was related to vinyl groups while the band near 758 cm^{-1} was characteristic of mono-substituted acetylene. Considering that bands characteristic of mono-substituted acetylene, vinyl, methyl and methylene groups were observed, it was evident that considerable rearrangement of the acetylene molecules occurred in the plasma. The strong bands between 1600 and 1700 cm^{-1} were assigned to $>\text{C}=\text{C}<$ stretching vibrations of vinyl groups and to $>\text{C}=\text{O}$ stretching vibrations of carbonyl groups that resulted from oxidation of the films after exposure to the atmosphere.

Tsai et al. have also used RAIR to investigate reactions occurring between rubber compounds and plasma polymerized acetylene primers deposited onto steel substrates [12]. Because of the complexities involved in using actual rubber formulations, RAIR was used to examine primed steel substrates after reaction with a 'model' rubber compound consisting of *squalene* (100 parts per hundred or phr), zinc oxide (10 phr), carbon black (10 phr), sulfur (5 phr), stearic acid (2 phr),

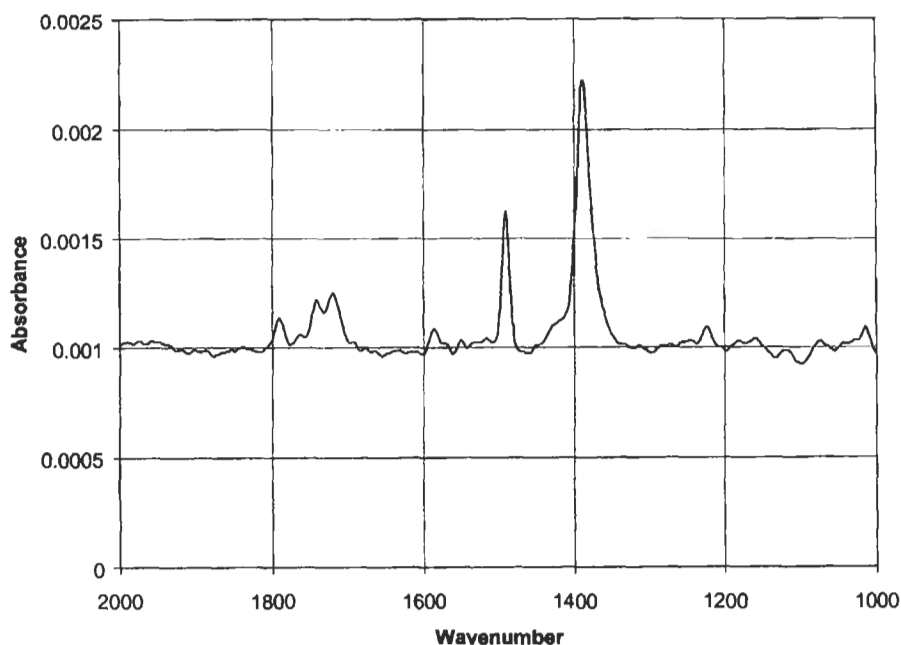


Fig. 11. RAIR spectrum of 4-MPP adsorbed onto a gold substrate. Reproduced by permission of the American Chemical Society from Ref. [9].

N,N-dicyclohexyl-benzothiazole-sulfenamide (DCBS), cobalt naphthenate, and diaryl-*p*-diphenylene-amine (each 1 phr).

Polished steel substrates primed with plasma polymerized acetylene films were immersed into a stirred mixture of these materials at a temperature of $155 \pm 5^\circ\text{C}$ to simulate the curing of rubber against a primed steel substrate. During the reaction, the mixture was continuously purged with nitrogen to reduce oxidation. At appropriate times between 1 and 100 min, substrates were removed from the mixture, rinsed with hexane ultrasonically for 5 min to remove materials that had not reacted, dried, and examined using RAIR. The RAIR spectra obtained after reaction times of 0, 15, 30, and 45 min are shown in Fig. 13.

After reaction for 15 min, the band near 3295 cm^{-1} (not shown in Fig. 13) decreased significantly in intensity, indicating that the mono-substituted acetylene groups were reacting. New bands also appeared near 1539 and 1512 cm^{-1} . After reaction for 30 min, several additional bands appeared near 1011 , 1030 , 1085 , 1232 , 1320 , 1430 , and 1515 cm^{-1} . The bands near 1011 , 1030 , 1085 , 1232 , 1320 , and 1430 cm^{-1} were clearly related to the benzothiazole sulfenamide fragment of DCBS while the band near 1539 cm^{-1} was related to zinc stearate.

When a plasma polymerized acetylene film on a steel substrate was reacted with the squalene-containing model rubber compound at 155°C for 15 min, a new band assigned to zinc stearate appeared near 1539 cm^{-1} in the RAIR spectra

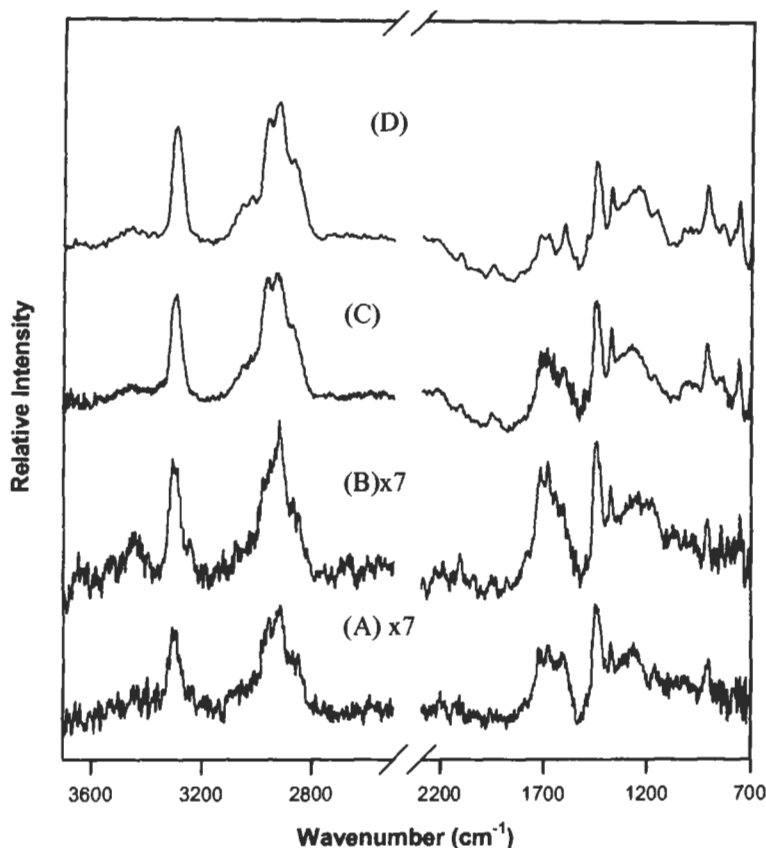


Fig. 12. RAIR spectra obtained from plasma polymerized acetylene films on polished steel substrates. The film thickness was (A) 5.7, (B) 9.0, (C) 63.5 and (D) 90.0 nm. Reprinted by permission of Gordon and Breach Science Publishers from Ref. [12].

of the film. Another band that was clearly related to the $>C=C<$ stretching mode in squalene appeared near 1667 cm^{-1} while a band that was most likely related to conjugated double bonds formed in squalene during the 'crosslinking' reaction appeared near 1649 cm^{-1} [12]. After reaction for 30 min, additional bands appeared near 1011 , 1030 , 1085 , 1232 , 1320 , 1430 , and 1551 cm^{-1} that were related to the benzothiazole sulfenamide fragment of DCBS.

RAIR spectra indicated that there was little reaction between a similar model rubber compound containing squalane, the saturated analog of squalene, and the plasma polymerized acetylene primer. It was concluded that an important product was formed by reaction of components of the curing system with squalene and that product reacted with the plasma polymer film, eventually leading to crosslinking between squalene and the film [13]. This reaction product was not formed in the presence of squalane.

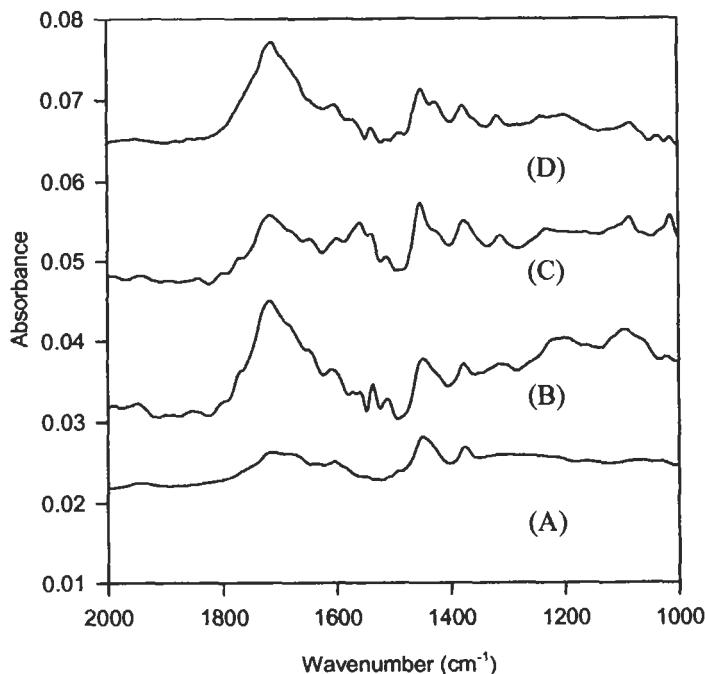
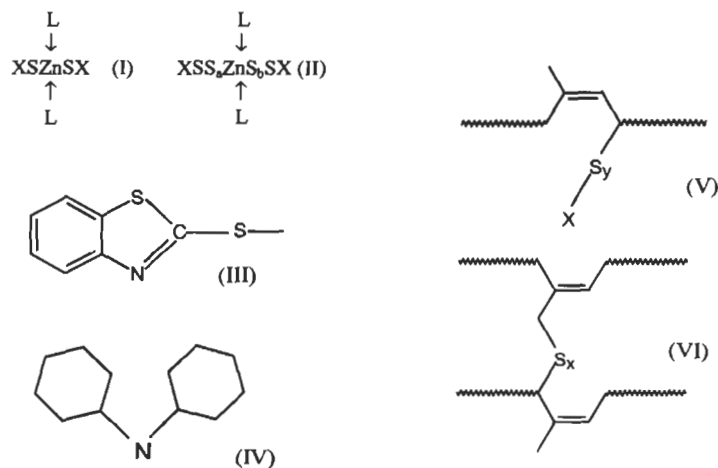


Fig. 13. RAIR spectra of model rubber compound reacted with plasma polymerized acetylene films on steel substrates for (A) 0, (B) 15, (C) 0 and (D) 45 min. Adapted by permission of Gordon and Breach Science Publishers from Ref. [12].

Results from RAIR, XPS, AES, and SIMS were combined to develop a model for the reaction between squalene (and, by inference, natural rubber or NR) and plasma polymerized acetylene primers. According to this model, the early stages of curing NR with sulfur, an accelerator (DCBS), and an activator (ZnO) involve formation of zinc stearate and then zinc/accelerator or zinc/accelerator/perthiomercaptide complexes [14]. The zinc/accelerator and zinc/accelerator/perthiomercaptide complexes have structures (I) and (II), respectively, where X is an accelerator fragment and L is a ligand. Since the accelerator used here was DCBS, X has structure (III) and the ligand L has structure (IV). The complexes react with NR to form rubber-bound pendant groups such as (V). Eventually, pendant groups disproportionate, forming crosslinks (VI) between NR molecules and between NR molecules and the plasma polymer.

Another illustrative example of the application of FTIR spectroscopy to problems of interest in adhesion science is provided by the work of Taylor and Boerio on plasma polymerized silica-like films as primers for structural adhesive bonding [15]. Mostly these films have been deposited in a microwave reactor using hexamethyldisiloxane (HMDSO) as monomer and oxygen as the carrier gas. Transmission FTIR spectra of HMDSO *monomer* were characterized by strong



Structures I to VI

bands near 1058 , 1260 , and 844 cm^{-1} and medium bands near 2959 , 2901 , and 756 cm^{-1} . The band near 1058 cm^{-1} was assigned to an Si-O-Si stretching mode. Bands near 2959 and 2901 , 1260 , and 844 and 756 cm^{-1} were attributed to CH stretching, bending, and rocking modes, respectively, in the methyl groups [15].

As shown in Fig. 14, RAIR spectra of plasma polymerized films deposited onto polished aluminum (6111 alloy) substrates using HMDSO as the monomer and oxygen as the carrier gas were characterized by a very strong band near 1225 cm^{-1} . Broad bands were observed near 3650 and 3360 cm^{-1} while weaker bands appeared near 940 , 810 , and 490 cm^{-1} [15]. The bands near 1225 , 810 , and 490 cm^{-1} were related to longitudinal optical (LO) phonons in silica-like structures. Observation of a silica-like structure in the films indicated that most methyl groups had been removed from the monomers during polymerization. This conclusion was supported by the lack of bands related to methyl groups. The bands near 3360 and 940 cm^{-1} were attributed to O-H and Si-O stretching modes of silanol groups having hydrogen atoms hydrogen-bonded to oxygen atoms of adjacent silanol groups. Similarly, the band near 3650 cm^{-1} was assigned to O-H stretching in isolated silanol groups having hydrogen atoms that were hydrogen-bonded to oxygen atoms of Si-O-Si groups [16]. Most silanol groups probably resulted from reaction of free radicals in the films with water molecules formed by decomposition products of HMDSO in the plasma. However, some silanol groups probably formed by reaction of free radicals in the films with water in the atmosphere after the film-covered substrates were removed from the reactor.

When films were deposited on aluminum substrates and then annealed at 180°C for 30 min, the bands near 3360 and 940 cm^{-1} decreased significantly in intensity, indicating that adjacent hydroxyl groups condensed to form Si-O-Si linkages, increasing 'crosslinking' in the films [15]. The band near 3650 cm^{-1} did not

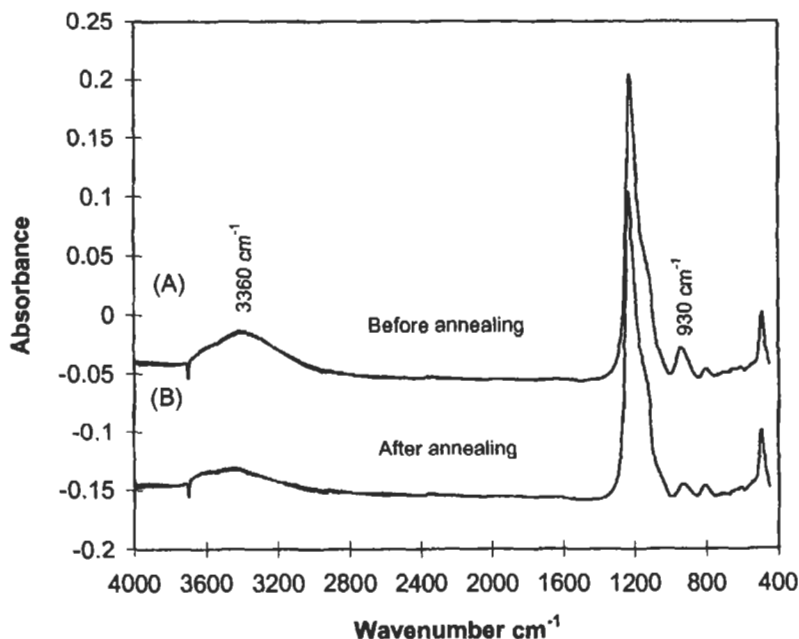


Fig. 14. RAIR spectra of a plasma polymerized silica-like film deposited onto a polished aluminum substrate (A) before and (B) after annealing at 180°C for 30 min. Film thickness was about 735 Å. Reprinted by permission of Gordon and Breach Science Publishers from Ref. [15].

decrease significantly in intensity, indicating that the isolated silanol groups were relatively stable at this temperature (see Fig. 14).

Observation of absorption bands due to LO phonons in RAIR spectra of thin, silica-like films deposited onto reflecting substrates demonstrates an important difference between RAIR and transmission spectra. Berreman has shown that absorption bands related to transverse optical (TO) phonons are observed in transmission infrared spectra of thin films obtained at normal incidence [17]. However, bands related to LO phonons are observed in transmission spectra of the same films obtained at non-normal incidence and in RAIR spectra. Thus, it is possible for RAIR and transmission spectra of thin films of some materials to appear very different for reasons that are purely optical in nature. For example, when the transmission infrared spectrum of a thin, silica-like film on a KBr disc was obtained at normal incidence, bands due to TO phonons were observed near 1060, 790, and 450 cm⁻¹ [18].

As discussed above, it is desirable to use large, almost grazing angles of incidence in RAIR spectroscopy in order to maximize the sensitivity of the technique to ultra-thin films. Using such large angles of incidence usually requires the substrates to be at least a few centimeters in length. This severely limits the spatial

resolution of RAIR spectroscopy and its use for analyzing the failure surfaces of adhesive joints. However, several manufacturers have developed objective lenses that permits RAIR spectra to be obtained from areas as small as $100\text{ }\mu\text{m}$ in diameter using an FTIR microscope. The use of 'RAIR microscopy' should expand the application of infrared spectroscopy to problems in adhesion science.

Gaillard et al. applied RAIR microscopy to the failure analysis of polymer/metal peel test specimens [19]. In one example, polypropylene was grafted with glycidyl methacrylate and then laminated against aluminum. The polymer was then peeled from the metal substrate and RAIR microscopy was used to examine the metal failure surface. Several strong bands were observed in the CH stretching region of the spectrum using RAIR microscopy. By comparison, only two weak bands were observed using micro-FTIR at a near-normal 29° angle of incidence. In another example, a polyester film was peeled from a steel substrate and RAIR microscopy was used to characterize the substrate failure surface. The bands near 1710 cm^{-1} and 1240 cm^{-1} due to the ester groups were easily observed using RAIR microscopy; the same bands were barely visible above the noise level when using micro-FTIR at 29° incidence.

3. X-ray photoelectron spectroscopy (XPS)

In X-ray photoelectron spectroscopy (XPS), a beam of soft X-rays with energy $h\nu$ is focused onto the surface of a solid that is held under an ultra-high vacuum, resulting in the ejection of photoelectrons from core levels of the atoms in the solid [20]. Fig. 15 shows an energy level diagram for an atom and illustrates the processes involved in X-ray-induced photoelectron emission from a solid.

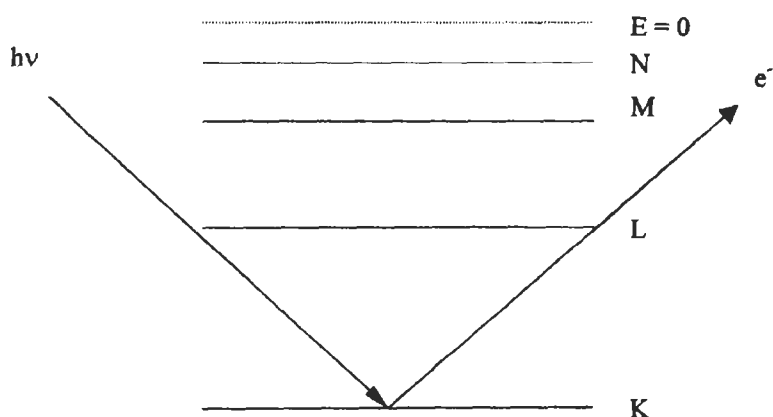


Fig. 15. Energy level diagram for an atom near the surface of a solid, showing the processes involved in XPS.

Photoelectrons can be ejected from any level of the atom for which $h\nu > E$. If the energy of the X-rays is known and the kinetic energy (T) of the electrons is measured, the binding energy (E) of the photoelectrons can be calculated from the expression:

$$h\nu = T + E \quad (13)$$

An XPS spectrum consists of a plot of $N(E)/E$, the number of photoelectrons in a fixed small interval of binding energies, versus E . Peaks appear in the spectra at the binding energies of photoelectrons that are ejected from atoms in the solid. Since each photoemission process has a different probability, the peaks characteristic of a particular element can have significantly different intensities.

XPS has many characteristics that make it a powerful tool for research in adhesion science. Since the only electrons that escape from the solid into the surrounding vacuum are those that are emitted from atoms within a few multiples of the electron mean free path (λ_o) of the surface, XPS is very surface sensitive and can be used to probe the *surface* regions of the solid to a depth of approximately 10 nm. Another important characteristic of XPS is that the binding energies of every element in the periodic table are unique. Thus, it is possible to determine the surface *composition* of the solid from knowledge of the binding energies of the photoelectrons ejected from the solid. The binding energies of the photoelectrons depend slightly on the oxidation state of the atoms from which they were ejected. As a result, XPS provides information about the elements present on the surface of the solid and on their *chemical environments*. Maps showing the distribution of an element or even an oxidation state of an element across a surface can be constructed. Depth profiles showing the way in which the concentration of chemical species changes as a function of distance away from the surface and into the bulk of the solid can also be constructed. Finally, the XPS technique is quantitative and can be used to determine the atomic concentrations of all elements detected.

The primary drawback to the application of XPS in adhesion science is associated with the limited spatial resolution of the technique. This can make it difficult to study processes that are highly localized, such as corrosion, or to accurately characterize certain types of failure surfaces where, for example, the locus of failure may pass back and forth between two phases.

Although the main peaks in the XPS spectrum of a solid correspond to photoelectrons ejected from an atom on the surface, several other types of peaks can also occur. Peaks due to 'Auger electrons' emitted from the surface represent one example. Fig. 16 shows an energy level diagram for an atom and depicts the processes involved in Auger emission. If a photoelectron is ejected from the K shell, an electron from a higher energy level can fall down into the K shell, losing energy in the process. This energy can be used to eject an electron from a higher energy level into the vacuum. This process is known as Auger electron

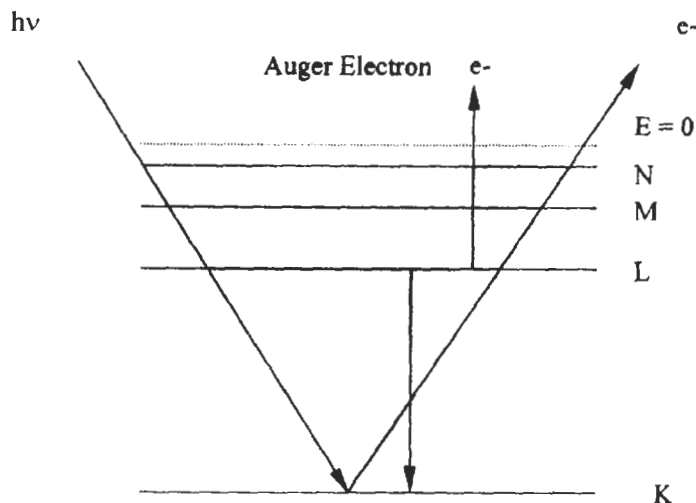


Fig. 16. Processes involved in Auger electron emission during X-ray photoelectron spectroscopy.

emission and is explained in greater detail below in the section dealing with Auger electron spectroscopy. Auger processes are labeled according to the initial and final vacancies in the energy levels. Thus, the process depicted in Fig. 16 is referred to as a KLL Auger process since the initial vacancy is in the K shell, that vacancy is filled by creating a vacancy in the L shell, and the energy evolved is used to eject an Auger electron from the L shell.

Peaks in the XPS spectrum due to Auger electrons and photoelectrons are easily distinguished. The kinetic energy of a photoelectron ejected from the surface of a solid obviously depends on the energy ($h\nu$) of the X-ray photon according to Eq. 13. If the energy of the X-ray photons is changed, the kinetic energy of the photoelectron will change by the same amount but the binding energy will stay the same. However, the kinetic energy of an Auger electron does not depend on the energy of the X-ray photons. It depends only on the difference in energy between the energy level from which the photoelectron was ejected and the energy level from which an electron fell down to fill the vacancy. Therefore, the kinetic energy of an Auger electron will not change when the energy of the X-ray photons is changed but, according to Eq. 13, the apparent binding energy of the Auger electron will change. As a result, peaks in the XPS spectrum due to photoelectrons and Auger electrons can easily be distinguished. When the energy of the X-ray photons is changed, the apparent binding energy of the Auger electrons will change but that of the photoelectrons will remain the same.

Two other types of peaks that can be observed in the XPS spectrum of solid materials are referred to as a 'shake-up' and 'shake-off' satellites. When a core-level electron is ejected from an atom by photoemission, the valence

level electrons experience an apparent increase in nuclear charge. This results in reorganization of the valence electrons and may include excitation of a valence electron to an unfilled level at higher energy. The excitation energy is obtained from the ejected photoelectron and results in the photoelectron having somewhat lower kinetic energy and higher binding energy than it would have otherwise. Thus, a weak peak referred to as a 'shake-up' satellite appears at a binding energy that is a few electron volts greater than that of the photoelectron peak. Shake-up satellites are very common in the C(1s) spectra of conjugated and aromatic polymers where they are associated with the $\pi \rightarrow \pi^*$ transition.

In some cases, a valence electron can be completely ionized, resulting in vacancies in both the core and valence levels. In those cases, weak peaks referred to as 'shake-off' satellites are also observed at binding energies a few electron volts higher than the photoelectron peak. Such cases are, however, not very common.

There are several considerations that go into selecting an X-ray line to excite XPS spectra. Included are the energy of the X-rays and the width of the line. If the energy is too low, the number of photoelectron lines that will be excited will be too small for general use. If the line width is too large, the resolution in the XPS spectrum will also be too small. Therefore, it is useful to consider the processes involved in X-ray generation.

In an X-ray tube, electrons are emitted from a heated filament and accelerated toward an anode. When the electrons strike the anode, they lose energy, emitting X-rays with a continuous range of wavelengths in the process. If they are energetic enough, electrons that impinge on the anode may also cause ejection of electrons from core levels of atoms in the anode. When electrons in higher energy levels make transitions to lower levels to fill these vacancies, they emit what are referred to as 'characteristic' X-rays. When an electron makes a transition from the L level to fill a vacancy in the K level, the X-rays emitted are referred to as K_α X-rays. If an electron in the M level fills a vacancy in the K level, the radiation emitted is referred to as K_β radiation. Similarly, if an electron from the M level fills a vacancy in the L level, the radiation emitted is referred to as L_α X-rays.

When all of the considerations for selecting an X-ray line are taken into account, the K_α lines from magnesium and aluminum are most appropriate for general XPS analysis. These lines have acceptable energies (1253.6 and 1483.6 eV, respectively), line widths (0.7 and 0.85 eV, respectively), and intensities for widespread applications. However, X-rays with higher energies, such as Zr L_α (2042.4 eV), are sometimes used. Using higher-energy X-rays permits some new photoelectron lines, such as Si(1s), to be observed. However, spectral resolution will usually be lower than with Mg or Al K_α radiation (the width of the Zr L_α line is about 1.7 eV).

The L energy level of an atom actually consists of several closely spaced energy levels. As a result, the K_α line consists of several lines with very similar

Table 1

Relative intensities and displacement of the various lines in the K_{α} X-ray spectrum of magnesium relative to the $K_{\alpha 1,2}$ line (adapted by permission of Physical Electronics Corp. from Ref. [21])

Line	Displacement (eV)	Relative intensity
$K_{\alpha 1,2}$	0.0	100
$K_{\alpha 3}$	8.4	8.0
$K_{\alpha 4}$	10.2	4.1
$K_{\alpha 5}$	17.5	0.55
$K_{\alpha 6}$	20.0	0.50

wavelengths. These lines are referred to as $K_{\alpha 1}$, $K_{\alpha 2}$, $K_{\alpha 3}$, etc. For magnesium and aluminum, the $K_{\alpha 1}$ and $K_{\alpha 2}$ lines are so close that they are not usually resolved and are referred to as the $K_{\alpha 1,2}$ line. Table 1 gives the relative intensities of the various K_{α} X-rays emitted from a magnesium anode and their displacement in electron volts from the $K_{\alpha 1,2}$ line [21].

Since the K_{α} radiation emitted from a magnesium anode consists of the intense $K_{\alpha 1,2}$ line plus the much weaker $K_{\alpha 3}$, $K_{\alpha 4}$, etc. lines, strong lines in the XPS spectrum of a material that are excited by Mg K_{α} radiation will be accompanied by weak peaks called 'X-ray satellites' that are shifted toward lower binding energies by 8.0 and 10.2 eV [20]. The satellites excited by the $K_{\alpha 5}$ and $K_{\alpha 6}$ lines are usually too weak to be observed. Similar features can be observed in XPS spectra excited using K_{α} X-rays from aluminum.

Some X-ray photoelectron spectrometers are equipped with monochromators that can be used to remove unwanted radiation, such as the continuous radiation and even some of the weaker characteristic X-rays such as $K_{\alpha 3}$, $K_{\alpha 4}$, $K_{\alpha 5}$, and $K_{\alpha 6}$, from the emission spectrum of the anode. A monochromator can also be used to resolve the $K_{\alpha 1,2}$ line into its two components $K_{\alpha 1}$ and $K_{\alpha 2}$. Using a monochromator has at least two beneficial effects. It enables the narrow, intense $K_{\alpha 1}$ line to be used to excite spectra at very high resolution. A monochromator also prevents unnecessary radiation (continuous, $K_{\alpha 2}$, $K_{\alpha 3}$, $K_{\alpha 4}$, $K_{\alpha 5}$, and $K_{\alpha 6}$) that might contribute to thermal or photochemical degradation from impinging on the sample.

As indicated above, one of the most important characteristics of XPS is that the binding energies characteristic of an atom depend somewhat on the chemical environment of the atom. In particular, the binding energy of an electron will be increased if the atom is bonded to a highly electron-withdrawing element such as oxygen or fluorine. Similarly, the binding energy of an electron will be decreased if the atom is bonded to a highly electron-donating element, such as a metal. This characteristic of XPS makes it possible to identify the elements that are present on the surface of a solid and to obtain information about the chemical state of the atom.

When an element is present on the surface of a sample in several different oxidation states, the peak characteristic of that element will usually consist of a number of components spaced close together. In such cases, it is desirable to separate the peak into its components so that the various oxidation states can be identified. Curve-fitting techniques can be used to synthesize a spectrum and to determine the number of components under a peak, their positions, and their relative intensities. Each component can be characterized by a number of parameters, including position, shape (Gaussian, Lorentzian, or a combination), height, and width. The various components can be summed up and the synthesized spectrum compared to the experimental spectrum to determine the quality of the fit. Obviously, the synthesized spectrum should closely reproduce the experimental spectrum. Mathematically, the quality of the fit will improve as the number of components in a peak is increased. Therefore, it is important to include in a curve fit only those components whose existence can be supported by additional information.

In most cases, information about the chemical environment of an atom is obtained from the binding energies of the photoelectrons. However, in some cases, the chemical environment of an atom may have a stronger effect on the apparent binding energy of the Auger electrons than it has on the binding energy of the photoelectrons. In such cases, it may be possible to obtain more information about the chemical environment from the Auger lines than from the photoelectron lines. A quantity (α) referred to as the 'modified Auger parameter' can be defined as:

$$\alpha = h\nu + E - A \quad (14)$$

In this expression, $h\nu$ is the energy of the X-rays, E is the binding energy of an electron, and A is the apparent binding energy of the Auger electron. Since the calculation of α involves subtraction of A from E , the modified Auger parameter is not affected by any sample charging (see below) that may occur. An 'Auger map' can be prepared by plotting the modified Auger parameter on the vertical axis and the binding energy of the photoelectron on the horizontal axis. This map can be used to identify chemical species even when the binding energies of the photoelectrons do not change appreciably with chemical environment.

XPS can be used to determine the composition of a solid as a function of distance away from the surface and into the bulk of the solid. Such a 'depth profile' can be constructed in two ways. One way in which a depth profile can be constructed is by using a beam of inert gas ions to sputter away material from the surface of the sample and to then record the XPS spectrum. If this procedure is repeated several times, a 'profile' showing the composition of the material as a function of sputtering time and thus of depth into the sample can be constructed. Another way to construct a depth profile involves tilting the sample with respect to the X-ray beam. In Fig. 17A, the 'take-off' angle or the angle between the sample surface and the direction of propagation of the ejected photoelectrons is 90° . In

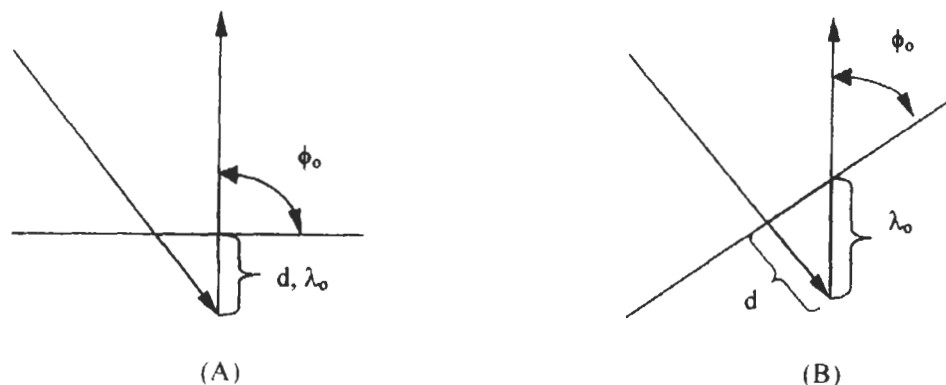


Fig. 17. The analysis depth in XPS varies as a function of the take-off angle or the angle between the sample surface and the direction in which the ejected electrons are propagating.

that case, the 'analysis depth' and the mean free path of the electrons in the solid are the same. In Fig. 17B, the sample surface has been tilted with respect to the incident of X-rays. In that case, the 'analysis depth' and the mean free path of the electrons are related by the expression:

$$d/\lambda_0 = \sin(\phi_0) \quad (15)$$

It can be seen that varying the take-off angle will change the depth of analysis. Thus, a depth profile can also be constructed by obtaining XPS spectra as a function of take-off angle.

XPS can also be used to construct maps showing the distribution of some chemical species across the surface of a sample. The species in question can be elements or even a particular oxidation state of an element. This can be done by dividing the sample surface into a number of small area elements and recording the XPS spectrum from each element. The intensity of the peak corresponding to some particular element or oxidation state of an element can then be displayed for each area element to obtain a two-dimensional representation of the distribution of that element or oxidation state across the surface. The accuracy of such a map is obviously related to the spatial resolution of the spectrometer. Older instruments had spatial resolutions on the order of millimeters and could not be used to construct meaningful maps. Newer instruments have spatial resolution on the order of a few tens of micrometers and can be used for mapping the composition of a surface. However, as discussed below, Auger electron spectrometers and secondary ion mass spectrometers have even greater spatial resolution and are preferred for mapping, as long as sample damage in the case of AES is not a factor.

Another important characteristic of XPS is that relatively little damage occurs when samples are illuminated with X-rays, especially from a non-monochromatic

source. Photo-induced reactions, such as the disproportionation of copper, can occur:



Thermal effects, including the dehydrohalogenation of polymers such as polyvinylchloride (PVC) can also occur. However, these effects are the exception and for the most part, XPS can be considered a non-destructive technique for surface characterization.

When photoelectrons are ejected from the surface of an insulating sample during an XPS experiment, the surface of the sample becomes positively charged. As a result, a photoelectron that is ejected from the surface of the solid into the surrounding vacuum will experience a weak attraction back toward the sample. This will result in the kinetic energy of the electron being less than and the binding energy being greater than in the absence of sample charging. This effect can be eliminated in two ways. One is to simply shift the measured binding energies toward lower binding energies. The amount of the shift can be determined by comparing the measured binding energy of some element to its known value. For organic compounds, the binding energy for C(1s) electrons in hydrocarbons is about 284.6 eV and represents a convenient standard for eliminating charging effects. Another technique for eliminating charging effects is to 'spray' the sample with electrons from a filament to replace those lost by photoemission.

As discussed earlier, the XPS technique is quantitative. If A_i is the area under the peak in the spectrum that is characteristic of element i , then the atomic concentration of element i on the surface of the sample is given by the expression:

$$C_i (\%) = 100 \times \frac{A_i/S_i}{\sum(A_i/S_i)} \quad (17)$$

In this expression, S_i is the 'sensitivity factor' for element i and the sum in the denominator is taken over all elements that are detected [21].

Many applications of XPS to problems in adhesion science have been reported in the literature. One interesting example is provided by the work of Tsai et al. on the use of XPS to investigate reactions between model rubber compound and plasma polymerized acetylene films that was discussed above [22,23]. Consideration of that system permits some interesting comparisons to be made regarding the type of information that can be obtained from RAIR and XPS.

The XPS survey spectrum of a 75 nm thick film of plasma polymerized acetylene that was deposited onto a polished steel substrate is shown in Fig. 18 [22]. This film consisted mostly of carbon and a small amount of oxygen. Thus, the main peaks in the spectrum were attributed to C(1s) electrons near 284.6 eV and O(1s) electrons near 533.2 eV. Additional weak peaks due to X-ray-induced O(KVV) and C(KLL) Auger electrons were also observed. High-resolution C(1s) and O(1s) spectra are shown in Fig. 19. The C(1s) peak was highly symmetric,

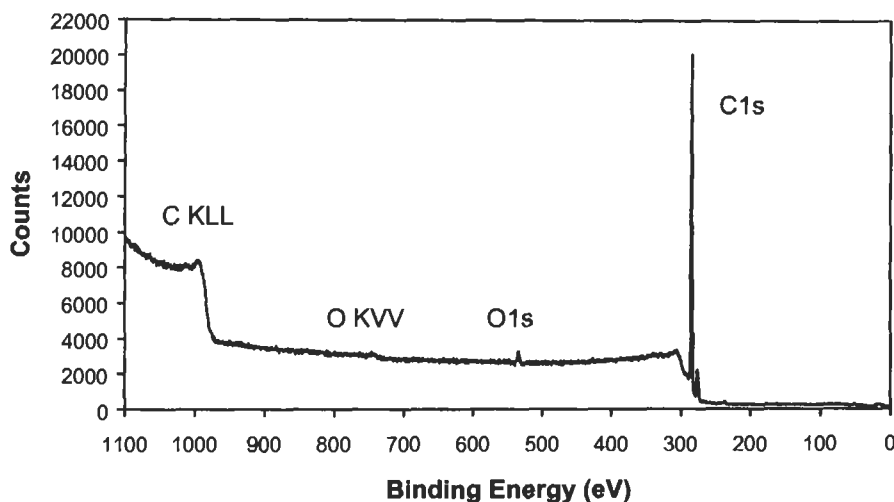


Fig. 18. XPS survey spectrum of a plasma-polymerized acetylene film with a thickness of 75 nm that was deposited onto a polished steel substrate. Reproduced by permission of John Wiley and Sons from Ref. [22].

indicating that most carbon atoms were bonded to other carbon atoms or to hydrogen atoms. However, a weak peak shifted upward in binding energy from the main C(1s) peak by about 1.5 eV was observed and was assigned to C–O bonds. A shake-up satellite was also observed near 291.2 eV, at a shift of about 6.6 eV from the main C(1s) peak. The O(1s) spectrum was also very symmetric and was fit with a single peak.

XPS survey spectra of plasma polymerized acetylene films reacted with the model rubber compound described earlier for various times are shown in Fig. 20 [23]. Only two peaks were observed in spectra of the as-deposited films, corresponding to carbon and oxygen. After reaction for 15 min, peaks due to carbon and oxygen were still observed but new peaks related to zinc, sulfur, and nitrogen were also observed. For a reaction time of 35 and 65 min, the spectra were similar but weak peaks attributed to cobalt were also seen. The results obtained from XPS were complementary to those obtained from FTIR since infrared spectroscopy does not provide any direct information about metal ions and is not especially sensitive to bonds involving sulfur. Observation of peaks attributed to zinc and sulfur in the spectra shown in Fig. 20 provided strong support for the formation of zinc/accelerator/perthiomercaptide complexes having structures (I) and (II), respectively, and for the formation of rubber-bound pendant groups such as (V).

Leadley and Watts used monochromatized AlK_α radiation to investigate the interactions that were responsible for adhesion between polymers and substrates [24]. When polymethylmethacrylate (PMMA) was adsorbed onto silicon substrates, the C(1s) spectrum shown in Fig. 21a was obtained. Originally, it was

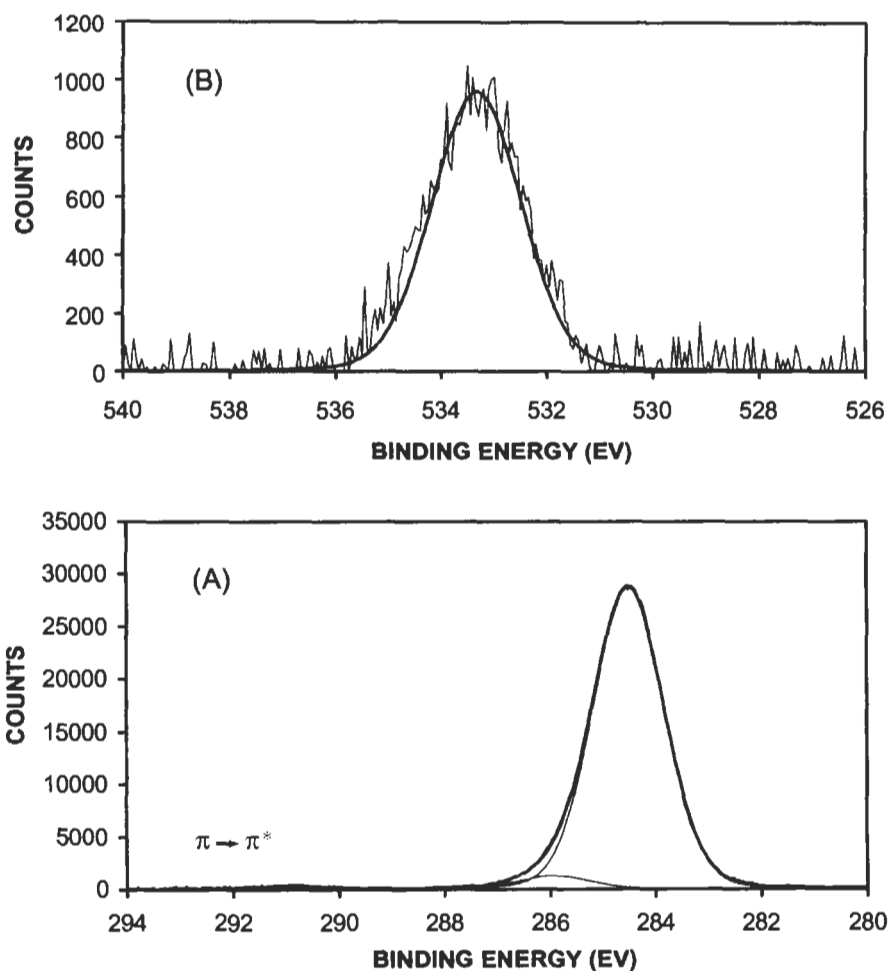


Fig. 19. High-resolution (A) C(1s) and (B) O(1s) XPS spectra of a plasma polymerized acetylene film with a thickness of 75 nm that was deposited onto a polished steel substrate. Reproduced by permission of John Wiley and Sons from Ref. [22].

thought that this spectrum consisted of just three components assigned to aliphatic, ester, and methyl carbon atoms. However, Pjipers and Donners suggested that a fourth component attributed to a secondary effect caused by electron withdrawal from aliphatic carbon by the ester group was needed [25]. Thus, the C(1s) spectrum of PMMA adsorbed onto silicon consisted of four components that were located at 285.0, 285.7, 286.8, and 289.1 eV (see Fig. 21a). These components were assigned to aliphatic hydrocarbon, the secondary effect caused by electron withdrawal from aliphatic carbon, methyl carbon making one bond with oxygen, and ester carbon making three bonds with oxygen, respectively. It was noted that

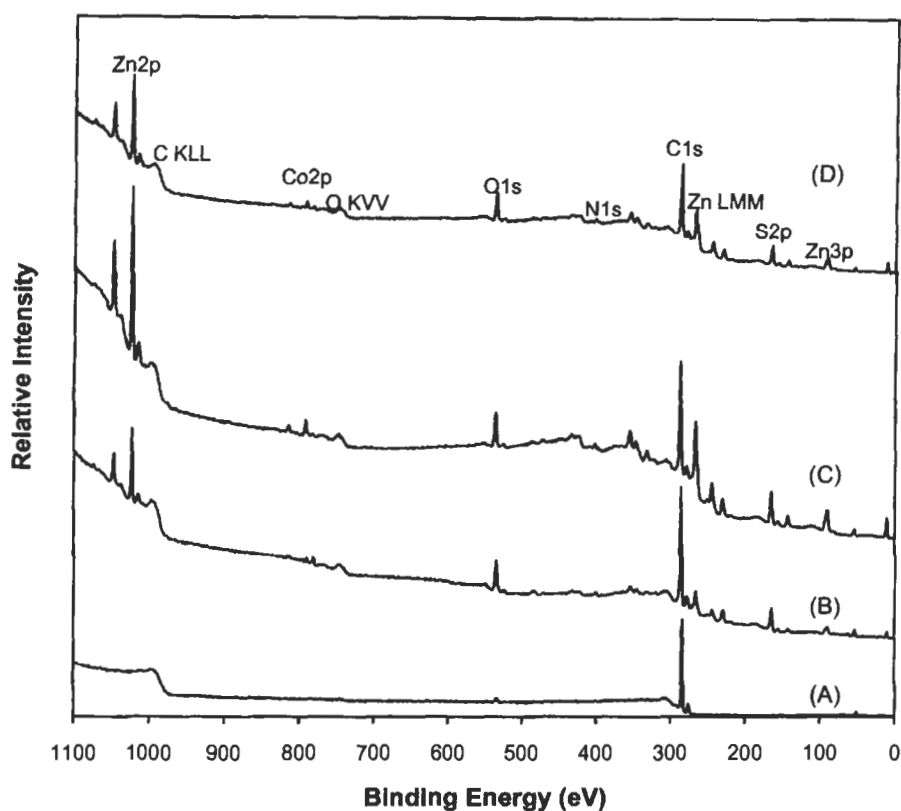


Fig. 20. XPS survey spectra of plasma polymerized acetylene films as a function of reaction time with a model rubber compound. The reaction times were (A) 0, (B) 15, (C) 35, and (D) 65 min. Reprinted by permission of Gordon and Breach Science Publishers from Ref. [23].

the C(1s) binding energy of the ester carbon was about 0.1 eV greater for PMMA adsorbed onto silicon than for bulk PMMA. This small increase in the binding energy of the ester carbon atom was attributed to hydrogen bonding between hydroxyl groups on the silicon surface and the carbonyl oxygen atoms.

When PMMA was adsorbed onto an iron substrate, four components were not sufficient to explain the C(1s) spectrum (see Fig. 21b) and a fifth component had to be added at 288.1 eV as shown in Fig. 21c. This component was attributed to carboxyl groups, indicating that the ester groups were partially hydrolyzed. Similarly, Leadley and Watts found that there were five components in the C(1s) spectrum of PMMA spin-coated onto aluminum, copper, and nickel substrates [24].

Leadley and Watts also investigated the interaction of polyacrylic acid (PAA) with oxidized metal substrates [26]. Through careful curve fitting of the C(1s) spectra, three specific types of interaction between PAA and the oxidized metal

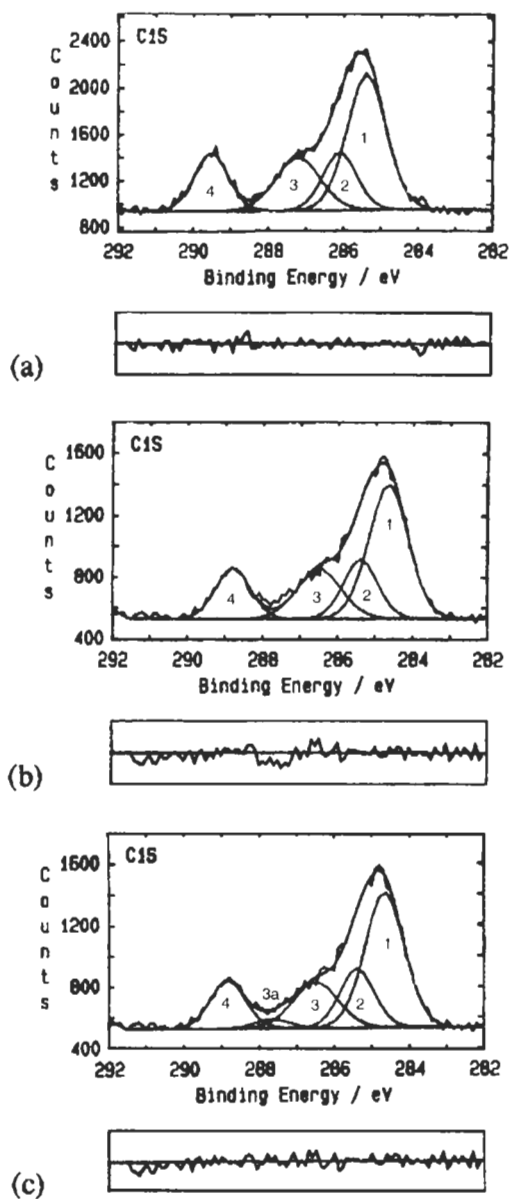


Fig. 21. High-resolution XPS spectra of PMMA spin-coated onto (a) silicon and (b,c) iron. The C(1s) spectrum of PMMA on silicon was explained by four components but an additional component was needed to explain the C(1s) spectrum of PMMA on iron. Reproduced by permission of Gordon and Breach Science Publishers from Ref. [24].

substrates were identified. The first involved hydrogen bonding of PAA with strongly acidic surface sites. Formation of these bonds resulted in a shift of the C(1s) binding energy of the acid group to higher values by about 0.1 eV compared to its value for bulk PAA. The second type of bond between PAA and oxidized metal substrates involved interaction of PAA molecules with weakly basic surface sites and resulted in formation of carboxylate anions that necessitated adding a component with a binding energy of 3.4 eV to the C(1s) spectra of PAA. Finally, nucleophilic attack of the acyl carbon in PAA by strongly basic surface sites was also observed. This made it necessary to add a component to the C(1s) spectrum that was shifted upwards in binding energy by about 5.0 eV.

Many investigators have used XPS to investigate reactions occurring at the interface when metals are vapor deposited onto polymers. Burkstrand [27] used XPS to investigate the factors responsible for increased adhesion of vapor-deposited copper on polystyrene after exposure of the polystyrene to atomic oxygen in an oxygen plasma. The main peak in the C(1s) spectrum of neat polystyrene was located at 285.0 eV. After treatment of PS with an oxygen plasma, a weak shoulder was observed near 286.5 eV in the C(1s) spectra and attributed to formation of a C–O single bond. After vapor deposition of 0.5 monolayers of copper onto plasma etched PS, two significant changes were observed in the XPS spectra. The peak in the O(1s) spectrum became broader and shifted toward lower binding energies. In addition, the weak peak characteristic of the simple C–O bond disappeared from the C(1s) spectrum. These changes in the XPS spectra after deposition of copper onto plasma etched PS indicated formation of a copper–oxygen–polymer complex.

A very simple tape test was used to demonstrate that a significant increase in adhesion of copper to PS accompanied formation of this complex. Copper films applied to clean PS were easily removed when a tape was pressed against the copper films and then peeled away. However, copper films applied to PS that was treated with an oxygen plasma were never removed by the tape, indicating significantly increased adhesion.

Friedrich et al. also used XPS to investigate the mechanisms responsible for adhesion between evaporated metal films and polymer substrates [28]. They suggested that the products formed at the metal/polymer interface were determined by redox reactions occurring between the metal and polymer. In particular, it was shown that carbonyl groups in polymers could react with chromium. Thus, a layer of chromium that was 0.4 nm in thickness decreased the carbonyl content on the surface of polyethylene terephthalate (PET) or polymethylmethacrylate (PMMA) by about 8% but decreased the carbonyl content on the surface of polycarbonate (PC) by 77%. The C(1s) and O(1s) spectra of PC before and after evaporation of chromium onto the surface are shown in Fig. 22. Before evaporation of chromium, the C(1s) spectra consisted of two components near 284.6 eV that were assigned to carbon atoms in the benzene rings and in the methyl groups. Two additional

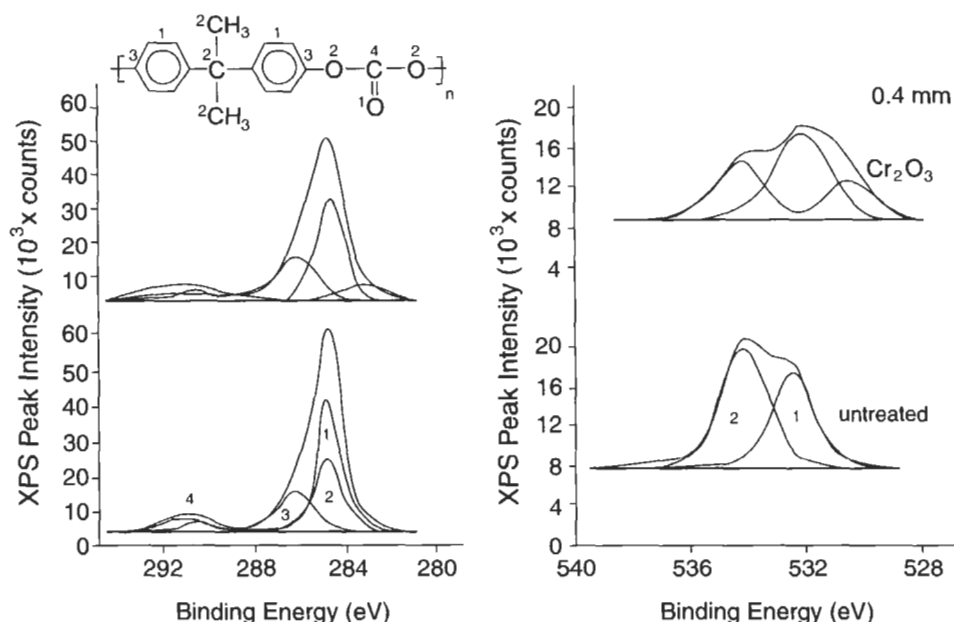


Fig. 22. C(1s) and O(1s) spectra of polycarbonate before (bottom) and after (top) deposition of 0.4 nm of chromium. Reproduced by permission of Gordon and Breach Science Publishers from Ref. [28].

components were observed near 286.2 eV and 290.8 eV and assigned to carbon atoms making one (1) and four (4) bonds to oxygen, respectively. An additional weak component near 291.3 eV was related to the $\pi \rightarrow \pi^*$ satellite. After evaporation of chromium onto the surface, a new peak appeared near 283.5 eV and was attributed to formation of chromium carbide. The O(1s) spectra of neat PC consisted of components near 532.5 and 534.2 eV that were assigned to oxygen in the carbonyl and ether groups, respectively. After evaporation of chromium, a new component appeared near 530.7 and was attributed to Cr_2O_3 .

The C(1s) and O(1s) spectra of polyphenylene ether (PPE) before and after evaporation of chromium onto the surface are shown in Fig. 23. C(1s) spectra of neat PPE consisted of two components, near 284.6 and 286.0 eV, that were assigned to carbon atoms in the benzene and methyl groups and in the ether groups, respectively. The O(1s) spectrum consisted of a single peak, near 533.4 eV, that was assigned to the ether oxygen atoms. After evaporation of chromium, a new peak related to formation of Cr_2O_3 was observed near 531.0 eV.

Many authors have used XPS to investigate the mechanisms by which vapor-deposited metals such as copper interact with the surfaces of polyimides. Chou and Tang [29] observed that only small changes occurred in the XPS line shapes after vapor deposition of copper on polyimide; they suggested that no

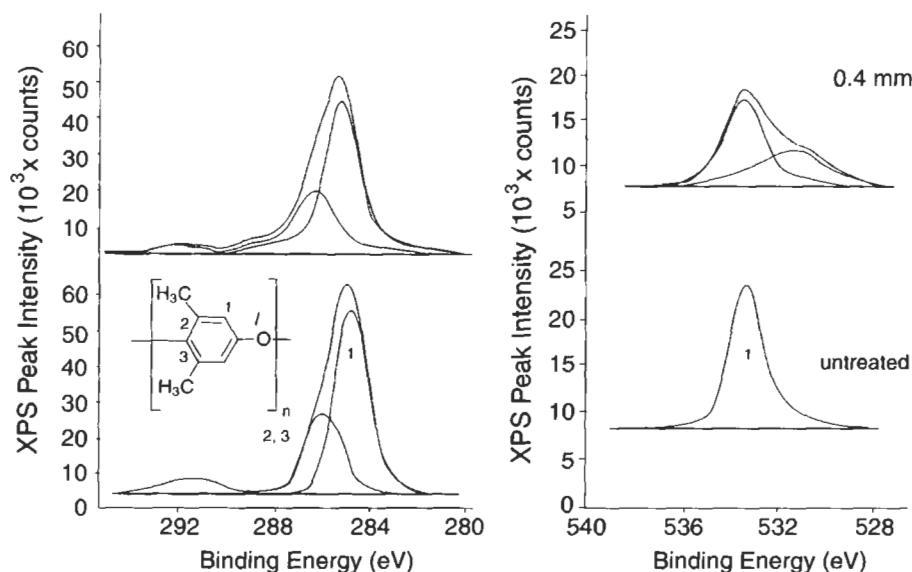


Fig. 23. C(1s) and O(1s) spectra of polyphenylene ether before (bottom) and after (top) deposition of 0.4 nm of chromium. Reproduced by permission of Gordon and Breach Science Publishers from Ref. [28].

chemical reaction took place. Sanda et al. investigated model polyimides [30] and suggested that copper interacted with the ether groups. Haight et al. reported that a complex formed between copper and the delocalized π -electrons of polyimide; they excluded the possibility of interaction between copper and the ether groups [31]. Pertsin and Pashunin suggested that copper reacts with the carbonyl groups of polyimide at low coverages [32].

Wolany et al. recently used XPS and TOF-SIMS to investigate the interaction of copper with polyimide before and after pretreatment of the polyimide with oxygen plasmas [33]. Their XPS results will be discussed here whereas their TOF-SIMS results will be discussed below, in the section on SIMS. Wolany et al. investigated the polyimide from pyromellitic dianhydride (PMDA) and oxydianiline (ODA) and numbered the carbon and oxygen atoms as shown in Fig. 24. Other investigators have fitted as many as six components to the C(1s) spectra of PMDA/ODA polyimide but Wolany used only three, arguing that the resolution in the spectra was not sufficient to justify using more components. As shown in Fig. 25, the three components in the C(1s) spectra of untreated polyimide were located at 284.75, 285.64, and 288.60 eV and were assigned to carbon atoms C1, C2–C5, and C6. Weak peaks assigned to $\pi \rightarrow \pi^*$ satellites are also shown in Fig. 25 as dotted lines. The O(1s) spectra consisted of two components, near 531.99 and 533.26 eV, that were assigned to oxygen atoms O1 and O2.

Exposure of the polyimide to an oxygen plasma for times as short as 1 s

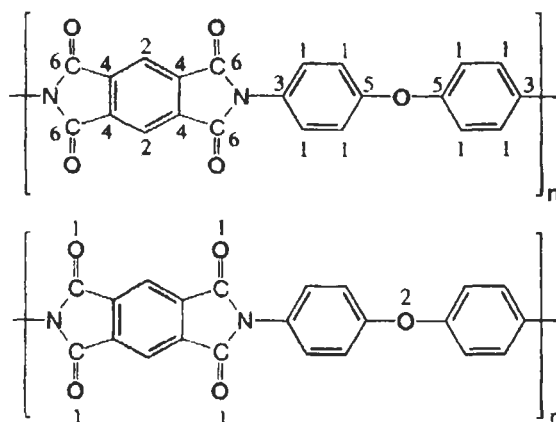


Fig. 24. Numbering of the carbon and oxygen atoms in the repeat unit of PMDA/ODA polyimide. Reproduced by permission of John Wiley and Sons from Ref. [33].

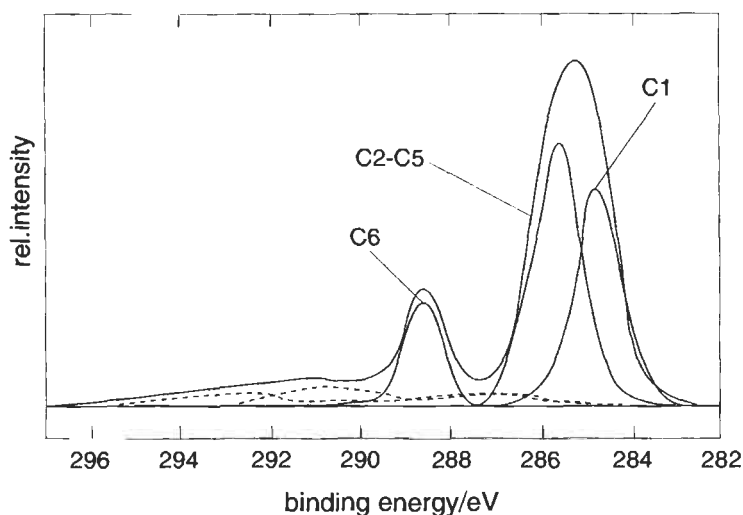


Fig. 25. C(1s) XPS spectra of PMDA/ODA before treatment with an oxygen plasma. Reproduced by permission of John Wiley and Sons from Ref. [33].

resulted in substantial uptake of oxygen and in a significant change in the C(1s) and O(1s) spectra (see Fig. 26). New peaks that were assigned to carbon atoms making one, two, or four bonds to oxygen were observed. These peaks were characteristic of carbon atoms in ether (C7), carbonyl (C8), or carbonate groups (C9). Correspondingly, two new peaks were observed in the O(1s) spectra and assigned to O3 and O4.

Deposition of 0.5 nm of copper (approximately one monolayer) onto untreated

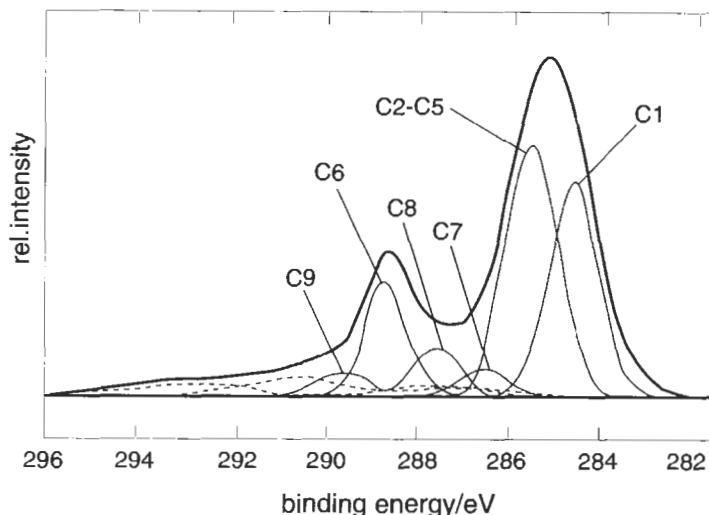


Fig. 26. C(1s) XPS spectra of PMDA/ODA after treatment with an oxygen plasma for 1 s. Reproduced by permission of John Wiley and Sons from Ref. [33].

polyimide resulted in significant changes in the C(1s) spectra. The most obvious effect was the appearance of a peak related to a new binding state of carbon, designated as C*, and a decrease in the intensity and the binding energy of the peak due to C6 in the imide carbonyl groups. This result indicated that interaction between copper and untreated polyimide involved the imide carbonyl groups. The decrease in the binding energy of C6 was the result of charge transfer from copper to the carbonyl groups that weakened the imide carbonyl bonds. After deposition of 0.5 nm of copper, the O(1s) spectra were dominated by the appearance of a new component referred to as O* and by a decrease in the intensity of the component due to O1, indicating interaction between copper and the imide carbonyl groups to form a Cu–O–C complex. The proposed reaction mechanism of copper with untreated polyimide is shown in Fig. 27.

After deposition of 0.5 nm of copper onto plasma modified polyimide, the peaks due to carbon atoms C8 and C9 and the oxygen atoms O3 and O4 were reduced in intensity, indicating that new states formed by the plasma treatment were involved in formation of copper–polyimide bonds instead of the remaining intact carbonyl groups. Fig. 28 shows the proposed reaction mechanism between copper and polyimide after mild plasma treatment.

Adhesion of copper films to PMDA/ODA polyimide was determined by peel tests conducted on samples that were prepared by vapor-depositing a thin layer of copper onto the polyimide and then building the thickness of the metal layer to about 18 μm by electrodeposition of copper. Results of the adhesion measurements correlated well with substrate pretreatment. When the substrate

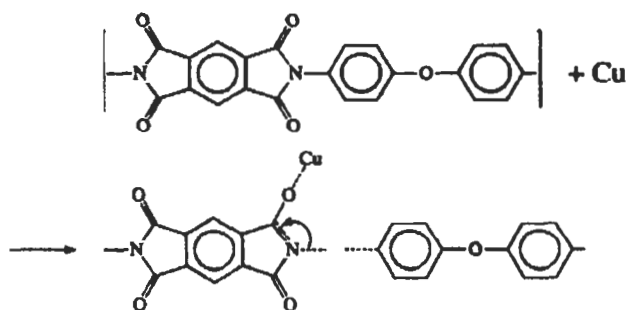


Fig. 27. Proposed mechanism for reaction of copper with untreated PMDA/ODA polyimide. Reproduced by permission of John Wiley and Sons from Ref. [33].

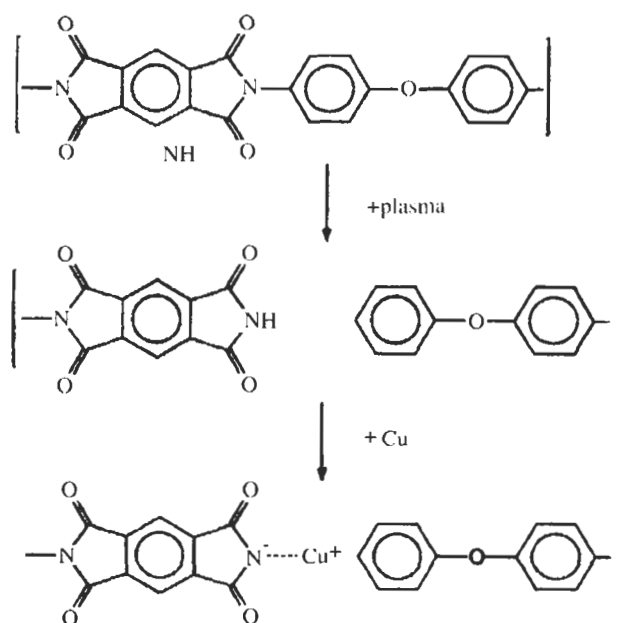


Fig. 28. Proposed mechanism for reaction of copper with PMDA/ODA polyimide that was treated in an oxygen plasma for 1 s. Reproduced by permission of John Wiley and Sons from Ref. [33].

was not pretreated, the peel force was low, about 0.9 N/cm. However, when the substrate was etched in an oxygen plasma before deposition of copper, it was found that the peel force depended on the length of the plasma treatment. For treatment times of 1, 10, and 60 s, the peel force was 4.7, 3.0, and 1.6 N/cm, respectively. It was suggested that the molecular structure of the polyimide surface was destroyed at longer etching times, resulting in the formation of a layer with poor cohesion.

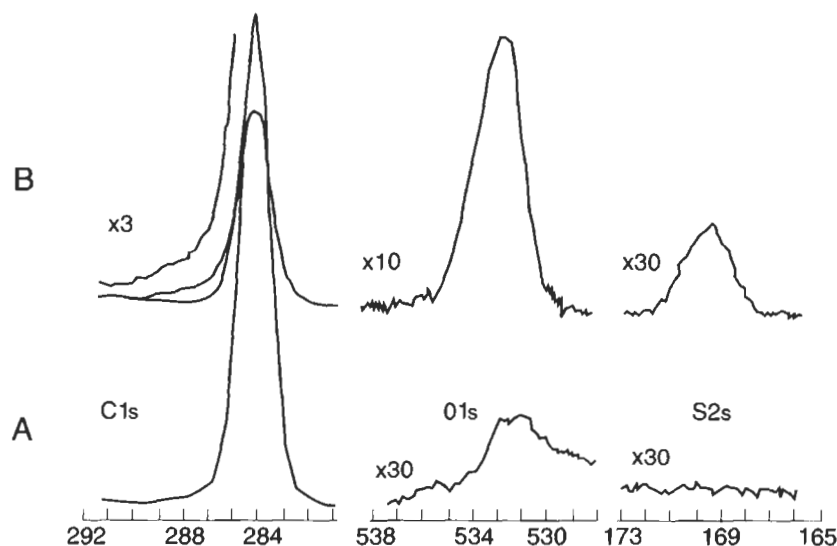


Fig. 29. XPS spectra obtained from low-density polyethylene (A) as received and (B) after etching in chromic acid for 30 min at 70°C. Reproduced by permission of Chapman and Hall Ltd. from Ref. [34].

Briggs et al. used XPS to investigate the effect of chromic acid etching on the surface composition of ld-PE and polypropylene [34]. Films were immersed in a solution of chromic acid ($\text{K}_2\text{Cr}_2\text{O}_7 : \text{H}_2\text{O} : \text{H}_2\text{SO}_4 = 7 : 12 : 150$ by weight) for times between 1 min and 6 h and temperatures between 20 and 70°C. After removal from the acid solutions, the films were rinsed in distilled water for 15 min or overnight. The surface composition of untreated polyethylene was mostly carbon although traces of oxygen were detected. After exposure to chromic acid for 1 min at 20°C, the surface composition was 94.4% carbon, 5.2% oxygen, and 0.4% sulfur and 0.37% of the carbon atoms had $-\text{SO}_3\text{H}$ groups attached. After exposure to chromic acid for 30 min at 70°C, the surface composition was 86.4% carbon, 13.2% oxygen, and 0.4% sulfur and 1.25% of the carbon atoms had $-\text{SO}_3\text{H}$ groups attached (see Fig. 29). Based on the shape of the $\text{C}(1s)$ spectrum, it was inferred that other oxygenated functional groups such as carbonyl and hydroxyl groups were also formed. The increase in oxygen and sulfur in the surface regions was related to an increase in lap joint strength. Joints prepared from unetched PE substrates had a strength of 0.55 MPa whereas joints prepared from PE substrates that were etched in chromic acid for 1 min at 20°C or 30 min at 70°C had strengths of 7.45 and 7.58 MPa, respectively. Somewhat similar results were obtained for polypropylene. However, it was found that polypropylene reached its maximum state of oxidation more quickly than did polyethylene.

Briggs et al. also used XPS to investigate flame treatment of low-density polyethylene [35]. They found that a normal flame treatment of PE resulted in

a high level of oxidation. Normal flame treatment was for 1.2 s with flow rates of natural gas and air equal to 37 and 150 cm³/s, respectively. Addition of an anti-oxidant to PE did not result in any significant decrease in oxidation. The depth of oxidation was between 4.0 and 9.0 nm and was much smaller than that obtained when etching the same material in chromic acid. Before etching, only carbon and traces of oxygen were detected on the PE surface. After flame treatment, carbon, oxygen and nitrogen were all detected. The C(1s) spectra consisted of the main peak at 285.0 eV plus three weaker peaks that were assigned to carbon making one bond with oxygen in hydroxyl, ether, or ester groups, carbon making two bonds with oxygen in ketone groups, and carbon making three bonds with oxygen in ester or carboxyl groups. After oxidation, the N(1s) spectrum consisted of two components, one near 399.7 eV that was assigned to amine or nitrile groups and an additional component at slightly higher bonding energies that was assigned to primary or secondary amides. The extent of oxidation correlated well with the strength of lap joints prepared from pre-treated PE substrates.

As discussed earlier, Papirer et al. [8] also used XPS to investigate the effect of flame treatment on the surface composition of high-density polyethylene (hd-PE). They found that as-received hd-PE contained a small amount of oxygen (5.5%) but no detectable nitrogen. hd-PE contained 25% oxygen and 1.7% nitrogen after four 75-ms passes over a flame. Additional passes over the flame resulted in a decrease in the amount of oxygen and a slight increase in the amount of nitrogen on the surface. The C(1s) spectra of flame treated hd-PE increased in complexity as the number of flame treatments increased (see Fig. 30). These spectra were fitted with four peaks. A peak at 285.1 eV was attributed to non-functionalized carbon. Peaks shifted upward in binding energy by 1.6 and 2.9 eV were assigned to hydroxyl and carbonyl groups, respectively, while a peak shifted upward by 4.1 eV was assigned to carboxyl groups. Peel test specimens were prepared by compression molding hd-PE against sheets of SBR rubber. The peel strength of as-molded specimens was negligible but it increased to about 1800 J/m² after one flame treatment and then leveled off.

One of the most important problems in adhesion science involves environmental stability of adhesive bonds to metal substrates. The oxide on the surface of as-fabricated metal parts frequently does not have the morphology or the chemical stability required to produce bonds that are strong and durable during exposure to the service environment. Surface modification is usually necessary to produce an oxide that has the desired characteristics. A typical case in point is aluminum. During exposure to warm, moist environments, the air-formed oxide on most as-fabricated aluminum parts hydrolyzes to form boehmite, a hydrated oxide with the composition Al₂O₃·H₂O [36]. Boehmite spalls from the surface of aluminum very easily. If the oxide on the surface of an aluminum substrate transforms to boehmite during service, the strength of an adhesive bond to the substrate will degrade very quickly. In order to prevent this transformation and to obtain

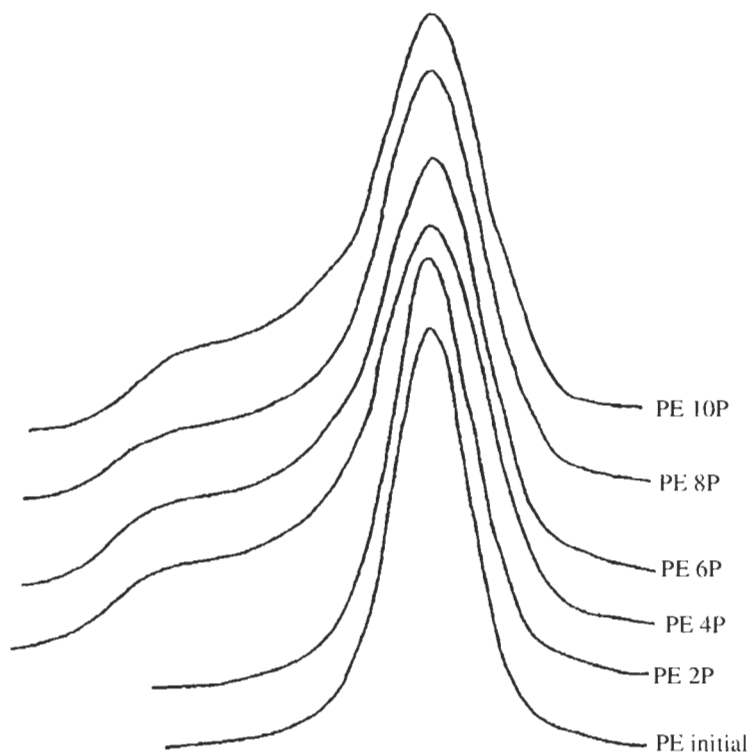


Fig. 30. C(1s) XPS spectra of high-density polyethylene before and after flame treatment. Reproduced by permission of VNU Science Press B.V. from Ref. [8].

bonds that are environmentally stable, it is necessary to produce an oxide on the aluminum surface that is stable during exposure to warm, moist environments.

The most successful surface pretreatment process for aluminum is currently phosphoric acid anodization (PAA) [37]. XPS has made significant contributions to our understanding of the PAA process. Fig. 31 shows the XPS survey spectrum of an 2024-T3 aluminum substrate immediately after anodizing in phosphoric acid [38]. The only elements detected on the surface of the anodized aluminum were Al, P, O, and C. The minor alloying elements Mg, Cu, and Mn were not observed. The C observed on the surface was attributed to adsorbed hydrocarbon contaminants. Based on the binding energies, it was determined that the surface consisted of Al_2O_3 terminated in a monolayer of AlPO_4 .

XPS was used to determine the surface composition of the anodized aluminum substrate during exposure to warm, moist environments. The information obtained was used to construct surface behavior diagrams that showed that hydration of the surface involved three steps [38]. Step one, which was reversible, consisted of adsorption of water onto the AlPO_4 monolayer. The second step, which was rate-controlling, involves dissolution of the phosphate followed by rapid hydration

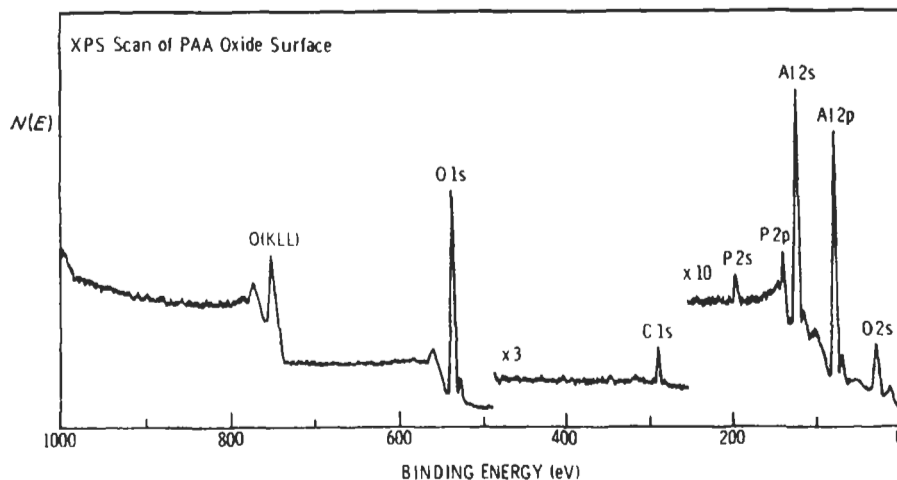


Fig. 31. XPS spectrum of a freshly prepared PAA/Al oxide surface. Reproduced by permission of Chapman and Hall Ltd. from Ref. [38].

of the anodic oxide to form boehmite. Step three involved the growth of bayerite, $\text{Al}_2\text{O}_3 \cdot 3\text{H}_2\text{O}$, on top of the layer of boehmite. It was suggested that the slow dissolution of the AlPO_4 layer was responsible for the superior resistance to hydration and for the long-term durability of adhesive bonds to aluminum that was anodized in phosphoric acid.

Another very important application of XPS involves failure analysis of adhesive bonds. Tsai et al. [39] used XPS to determine the mechanisms involved when the polyimide formed from the polyamic acid of pyromellitic dianhydride (PMDA) and 2,2-bis[4-(4-aminophenoxy)phenyl]hexafluoropropane (4-BDAF) was debonded from a silver substrate. Initially, Tsai investigated the XPS spectra of the neat polyamic acid and polyimide of PMDA/4-BDAF (see Fig. 32) and showed that the $\text{C}(1s)$ spectra of the polyamic acid and polyimide consisted of eight (8) and seven (7) components, respectively (see Table 2). There were two significant differences in the $\text{C}(1s)$ spectra of the polyamic acid and polyimide. In spectra of the polyamic acid, there were peaks near 287.9 and 288.8 eV that were attributed to the $\text{C}=\text{O}$ bonds in the amide and acid groups, respectively. These two peaks merged into a single peak near 286.6 eV that was assigned to $\text{C}=\text{O}$ bonds in spectra of the polyimide. In addition, a large peak appeared near 285.7 eV in spectra of the polyimide. This peak was partly due to carbon atoms making a single bond to nitrogen atoms. However, most of the intensity of the peak was due to the electron-withdrawing effect of the imide groups that shifted the $\text{C}(1s)$ binding energy of carbon atoms in the benzene ring of the PMDA moieties toward higher binding energies by about 1.1 eV from its position in spectra of the polyamic acid.

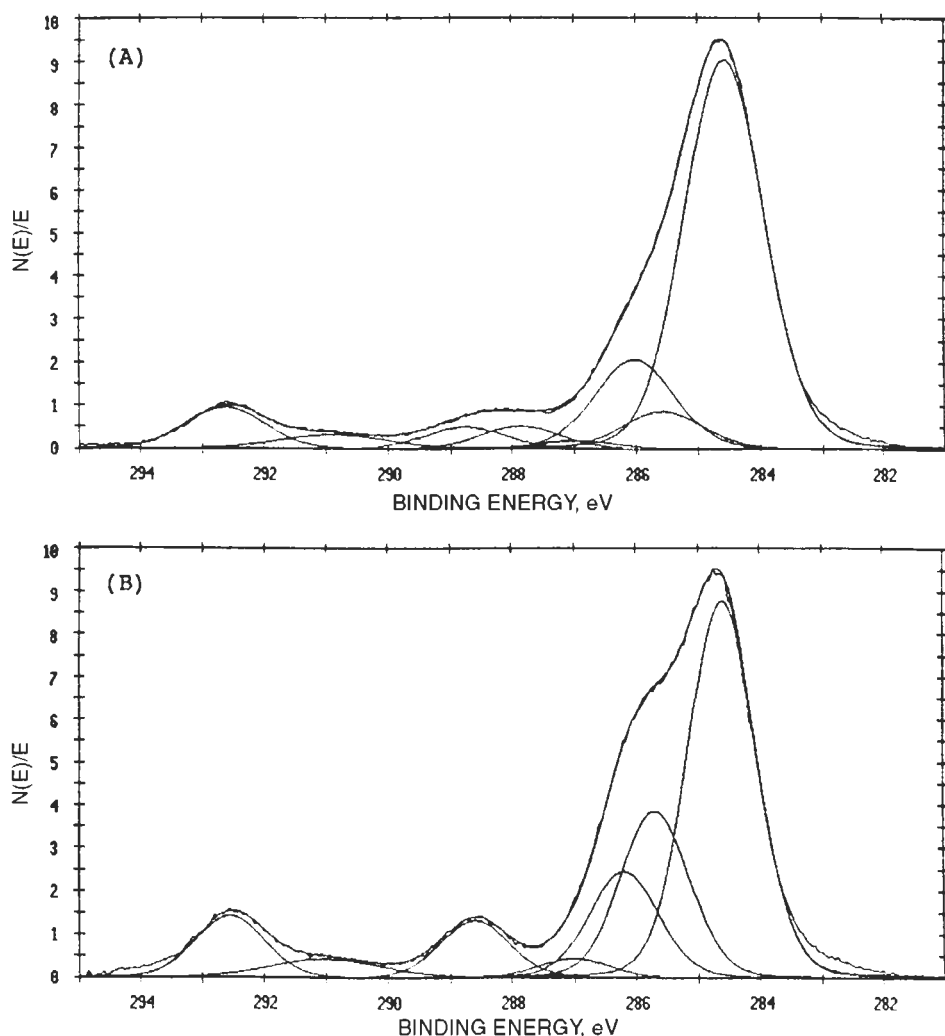


Fig. 32. High resolution C(1s) XPS spectra obtained from the bulk (A) polyamic acid and (B) polyimide of PMDA/4-BDAF. Reproduced by permission of the American Chemical Society from Ref. [39].

Tsai then applied thick films of the polyamic acid of PMDA and 4-BDAF to polished silver substrates and thermally imidized the films. The substrates were immersed into liquid nitrogen, causing the films to delaminate and XPS was used to examine the polyimide and silver fracture surfaces (see Fig. 33). The C(1s) spectra of the silver fracture surface were very similar to those of neat polyamic acid, indicating that imidization was inhibited by interaction of the polyamic acid with the silver substrate. This was evident from the observation of two peaks near

Table 2

Peaks fitted in the C(1s) spectra of the bulk polyamic acid and polyimide of PMDA/4-BDAF (adapted by permission of the American Chemical Society from Ref. [39])

Peak position (eV)	Shift from main peak (eV)	Percentage of total C(1s) area	Assignment
<i>Polyamic acid</i>			
284.6		62.1	C–C, C–H
285.6	1.0	6.0	C–N
286.1	1.5	14.2	C–O–C
287.0	2.4	1.3	C–(CF ₃) ₂
287.9	3.3	3.5	amide C=O
288.8	4.2	3.4	acid C=O
290.9	6.3	3.0	$\pi \rightarrow \pi^*$
292.6	8.0	6.5	CF ₃
<i>Polyimide</i>			
284.6		46.3	C–C, C–H
285.7	1.1	20.3	C–N + C–imide
286.2	1.6	12.9	C–O–C
287.0	2.4	2.3	C–(CF ₃) ₂
288.6	4.0	7.0	imide C=O
291.0	6.4	3.6	$\pi \rightarrow \pi^*$
292.6	8.0	7.6	CF ₃

287.8 eV that were assigned to C=O bonds in amide and carboxylate groups. However, the C(1s) spectra of the polyimide fracture surface were very similar to those of the neat polyimide and were characterized by peaks near 285.7 and 288.6 eV that were related to the imide groups. It was thus concluded that a very thin layer of poorly imidized polymer was formed between the silver surface and the bulk of the well imidized film and that failure occurred at the interface between this layer and the bulk of the polyimide film. Buchwalter and Greenblatt obtained similar results [40] using XPS to examine the locus of failure between the polyimide of PMDA and oxydianiline (ODA) and SiO₂ substrates.

Fitzpatrick et al. [41] used small-spot XPS to determine the failure mechanism of adhesively bonded, phosphated hot-dipped galvanized steel (HDGS) upon exposure to a humid environment. Substrates were prepared by applying a phosphate conversion coating and then a chromate rinse to HDGS. Lap joints were prepared from substrates having dimensions of 110 × 20 × 1.2 mm using a polybutadiene (PBD) adhesive with a bond line thickness of 250 μm. The joints were exposed to 95% RH at 35°C for 12 months and then pulled to failure.

Visually, the failed specimens appeared as shown in Fig. 34. Failure was mostly cohesive within the adhesive. However, there was a small region of apparent interfacial failure at one end of each substrate that was referred to as the 'metal

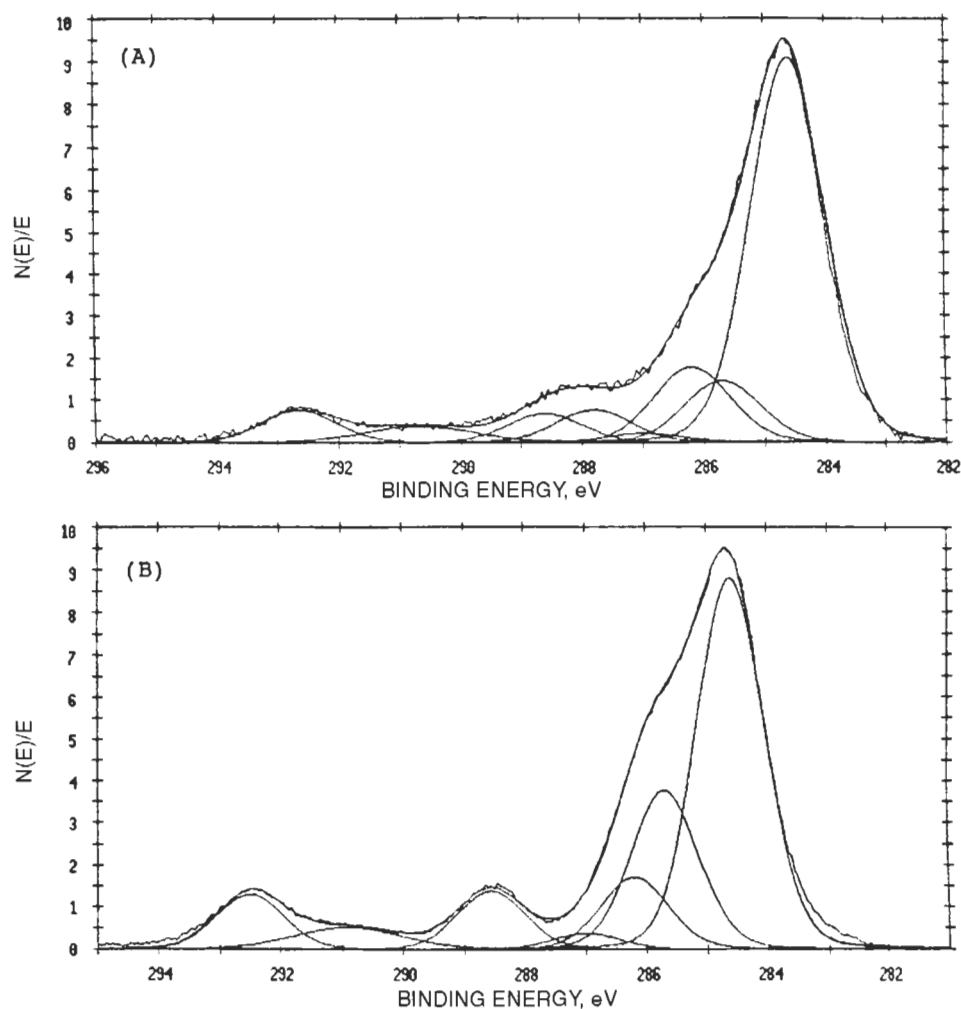


Fig. 33. High resolution C(1s) XPS spectra obtained from (A) silver and (B) polymer fracture surfaces of specimens prepared by curing the polyamic acid of PMDA/4-BDAF against polished silver substrates. Reproduced by permission of the American Chemical Society from Ref. [39].

initiation zone'. Areas that appeared bright and dark were observed in the metal initiation zone using optical microscopy (see Fig. 35). Small-spot XPS (20 μm spot size) showed that the bright areas corresponded to clean, polymer-free zinc substrate; dark areas corresponded to areas where only a trace of polymer was left on the substrate upon failure. High-resolution (50 μm spot size) XPS line scans were obtained from six spots across the metal initiation zone, ranging from the region of cohesive polymer formation to the edge of the substrate as shown in Fig. 36. Profiles showing the distribution of various elements across the

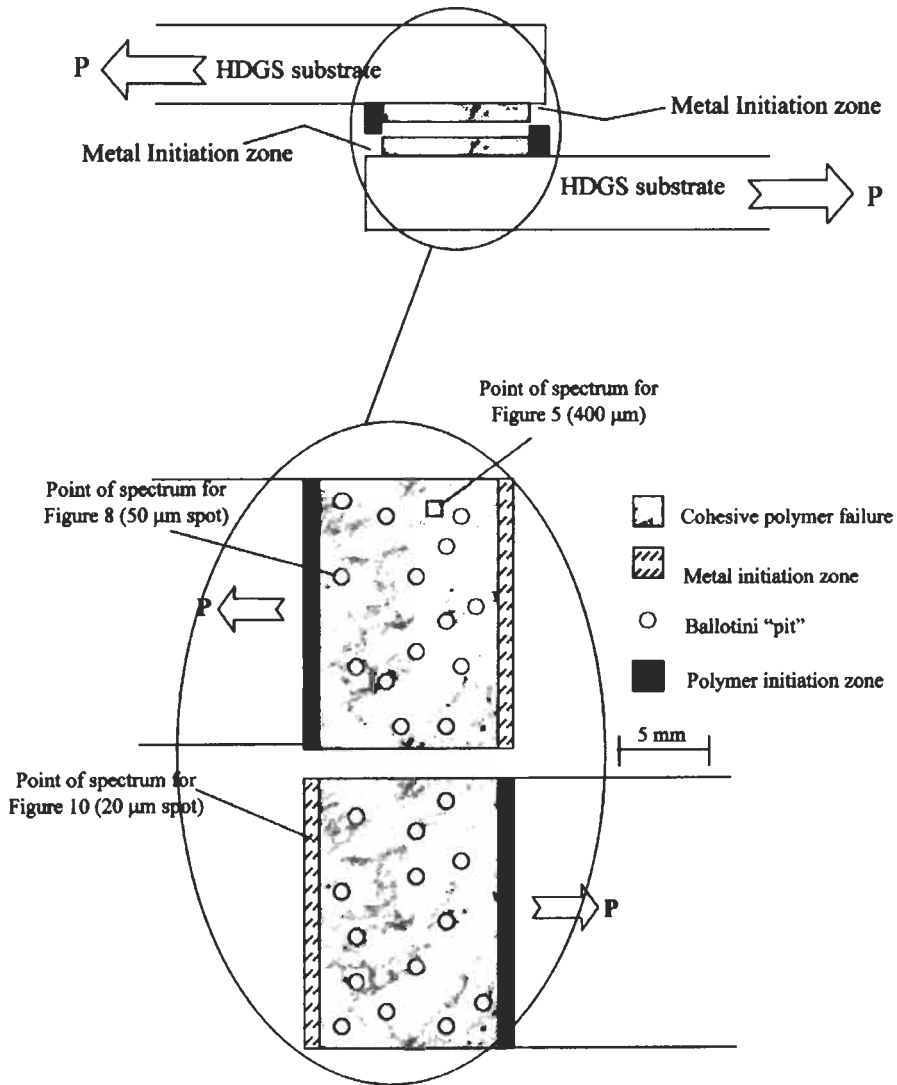


Fig. 34. Schematic drawing of the visual appearance of the failure surfaces of lap joints prepared from hot-dipped galvanized steel substrates. Reproduced by permission of John Wiley and Sons from Ref. [41].

metal initiation zone were constructed from the line scans. From these profiles, it was concluded that the carbon concentration was low enough to correspond to interfacial failure only for spots 5 and 6, implying that the interfacial failure zone was only approximately $100\ \mu\text{m}$ in width (see Fig. 37). Interestingly, there was a measurable concentration of phosphorus only at spot 3, implying that the remaining phosphate layer was patchy. It was concluded that hydroxyl ions

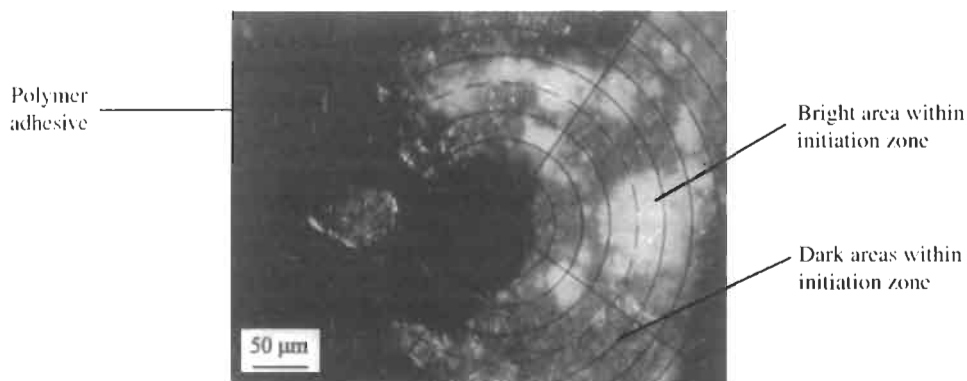


Fig. 35. Optical micrograph showing the bright and dark areas observed within the initiation zone of a lap joint prepared from hot-dipped galvanized steel substrates. Reproduced by permission of John Wiley and Sons from Ref. [41].

resulting from cathodic activity resulted in dissolution of the phosphate crystals from the pretreatment. However, the presence of at least some polymer within the initiation zone indicated that failure involved 'weakening' of the PBD as well as cathodic dissolution of the phosphate.

Many authors have used XPS to characterize thin films formed by silane 'coupling agents' deposited onto various substrates from dilute aqueous solutions. Domingue et al. investigated films formed by γ -aminopropyltriethoxysilane (γ -APS) spin-coated onto c-Si(100) from 0.05% (w/w) solutions in 95% (v/v) methanol–water [42]. The as-deposited films were washed extensively in deionized water to ensure that only chemisorbed materials remained on the surface. Results obtained from XPS showed that the resulting films had a thickness of approximately 0.35 nm. When the atomic concentrations were obtained from the films as a function of take-off angle, some surprising results were obtained. Regardless of the angle, the silicon concentration was always about 10%. However, the nitrogen concentration was always much less than the silicon concentration even though the atomic ratio of Si to N in neat γ -APS was 1 : 1. These results indicated that fragmentation and rearrangement of the γ -APS molecules occurred during deposition. Domingue et al. suggested that the amino groups of γ -APS were adsorbed onto the silicon substrate through the lone pair of electrons. This resulted in a loss of electron density and in homolytic scission of the C–N bond, leaving $-C^{\bullet}$ groups. These groups could react with similar groups to produce crosslinks. Reactions with water would form hydroxyl groups while intermolecular chain transfer would form vinyl groups.

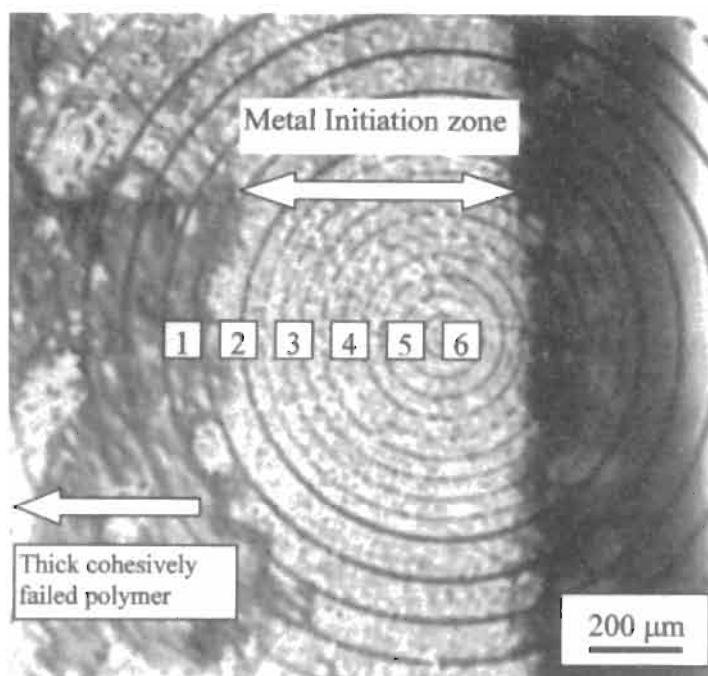


Fig. 36. Photograph of the metal initiation zone of a lap joint prepared from hot-dipped galvanized steel substrates showing the six locations where small-area XPS spectra were acquired. Reproduced by permission of John Wiley and Sons from Ref. [41].

4. Auger electron spectroscopy (AES)

Processes involving emission of Auger electrons have already been discussed in connection with XPS (see above). In Auger electron spectroscopy (AES), a solid sample is illuminated with electrons having energies in the range of 1–10 eV, resulting in ejection of electrons from core electron energy levels of atoms in the solid. Electrons that make transitions from higher levels fill the vacancies in the core levels. Some of the energy released in the process is used to eject an Auger electron from a higher level. Although Auger electrons are ejected from atoms as far as a few micrometers below the surface of the sample, only those electrons that are ejected from atoms within a few mean free paths of the surface escape into the vacuum with suffering collisions and contribute to the signal of interest. As discussed previously, Auger processes are labeled according to the initial and final energy levels where vacancies occur. Thus, a KLL Auger process involves an initial vacancy in the K shell that is filled by an electron from the L shell and ejection of an Auger electron from the L shell.

AES has several characteristics that make it a valuable tool for research related to adhesion phenomena. The surface sensitivity of AES is similar to that of XPS.

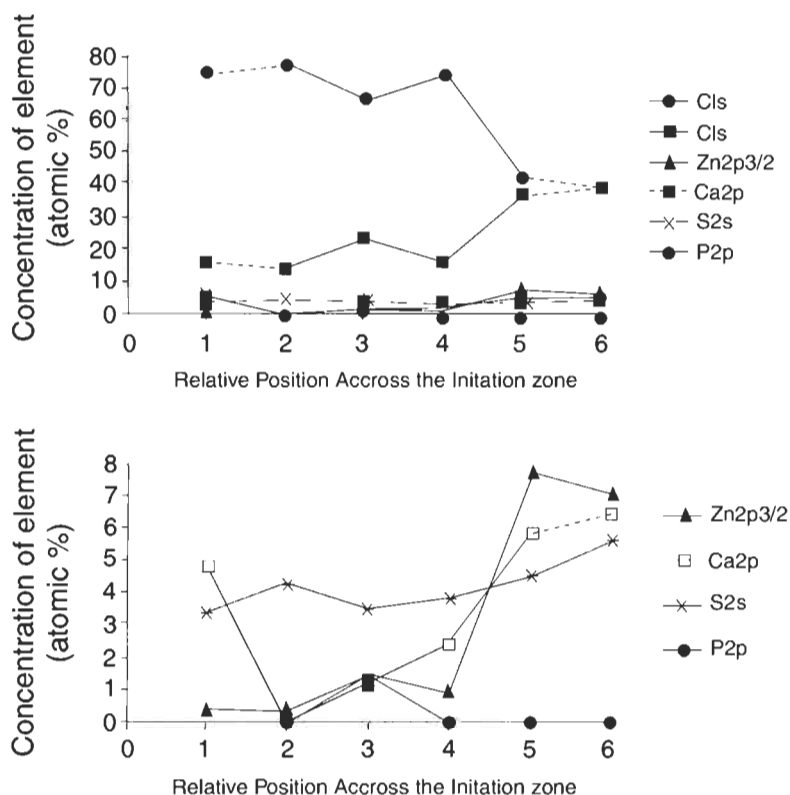


Fig. 37. Atomic concentrations for various elements at the six locations shown in Fig. 36. Reproduced by permission of John Wiley and Sons from Ref. [41].

However, the spatial resolution of AES is much greater than that of XPS and can approach approximately 25 nm. This makes AES a powerful technique for constructing high-resolution maps showing the distribution of chemical species across a surface. Because of the small analysis area, it is an easy matter to combine AES with inert gas sputtering to construct depth profiles showing the distribution of chemical species as a function of distance away from the surface and into the bulk of the solid. Quantitative analysis can be done using sensitivity factors and an equation similar to Eq. 17.

In order to carry out depth profiling with AES, the sputtering rate must be determined. The sputtering rate is usually measured by determining the time required to sputter through a layer of known thickness. Anodized tantalum foils are convenient for this purpose since the oxide thickness can easily be controlled and since the interface between the metal and the oxide is relatively sharp [43].

There are two drawbacks to the application of AES in adhesion science. One is associated with degradation that occurs when an organic compound is illuminated

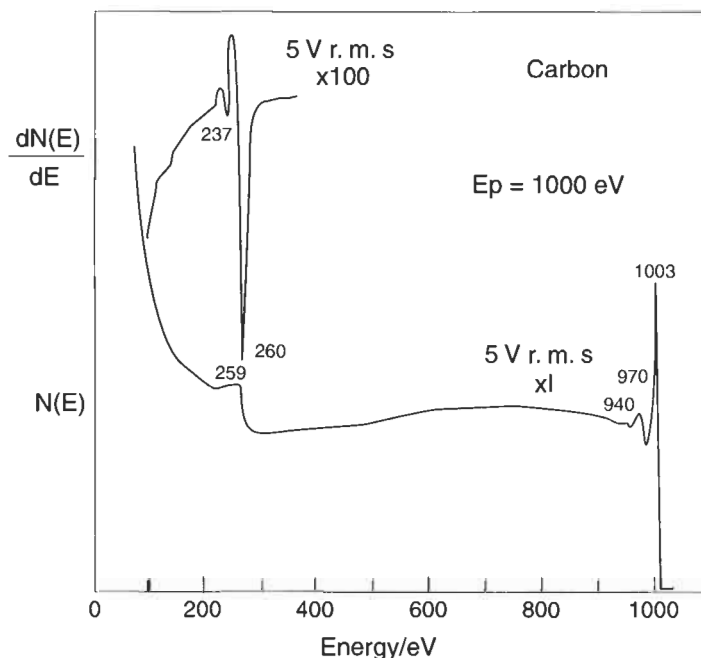


Fig. 38. Plots of (A) $N(E)$ versus E and (B) $dN(E)/dE$ versus E for an AES experiment on graphite. Reproduced by permission of John Wiley and Sons from Ref. [44].

under an electron beam. This means that AES is most appropriate for the analysis of materials such as metal substrates and inorganic conversion coatings. Another drawback is that AES provides only a limited amount of information about chemical states.

The processes involved in AES are similar to those shown in Fig. 16. However, electrons rather than X-ray photons are used to excite AES spectra. The data obtained in an AES experiment are sometimes presented as a plot of the number of electrons $N(T)$ ejected from the surface of a solid versus the kinetic energy T of the electrons. A typical plot of this type is shown for graphite in Fig. 38 [44].

In Fig. 38A, the intense, sharp peak near 1000 eV is due to elastically scattered primary electrons (electrons with a kinetic energy of 1000 eV were used to excite the spectrum). Also, in Fig. 38A, there are two weak peaks at kinetic energies of 970 and 940 eV. These peaks are associated with plasmons. There is a strong, broad peak at low values of the kinetic energy. This peak is associated with 'true' secondary electrons that have suffered collisions in escaping from the solid and thus have low kinetic energies. The medium-intensity peak at about 258 eV is associated with the emission of Auger electrons from graphite.

Although the results of an AES experiment can be plotted as shown in Fig. 38A, it is much more common to plot the derivative of $N(E)$ with respect to E , i.e.,

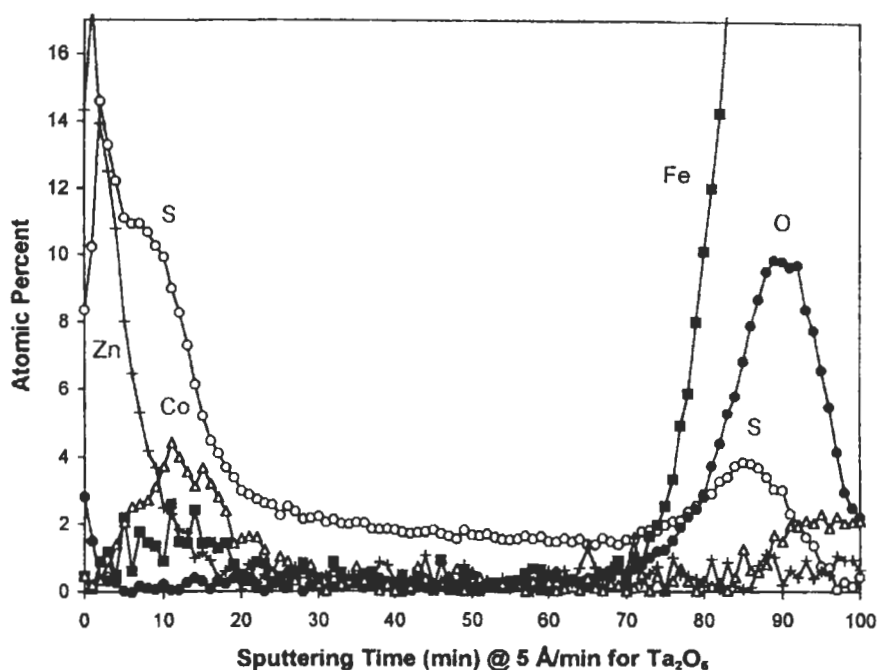


Fig. 39. Auger depth profile obtained from a plasma-polymerized film on a polished steel substrate after the film was reacted with a model rubber compound for 65 min. Reproduced by permission of Gordon and Breach Science Publishers from Ref. [45].

$dN(E)/dE$ versus E as shown in Fig. 38B [44]. This way of plotting the results makes it possible to detect weak peaks and greatly reduces the background due to inelastically scattered electrons. By convention, peak positions in AES are taken as the position of the minimum in the plot of $dN(E)/dE$ versus E and are not necessarily the same as peak positions in the plot of $N(E)$ versus E .

The Auger depth profile obtained from a plasma polymerized acetylene film that was reacted with the same model rubber compound referred to earlier for 65 min is shown in Fig. 39 [45]. The sulfur profile is especially interesting, demonstrating a peak very near the surface, another peak just below the surface, and a third peak near the interface between the primer film and the substrate. Interestingly, the peak at the surface seems to be related to a peak in the zinc concentration while the peak just below the surface seems to be related to a peak in the cobalt concentration. These observations probably indicate the formation of zinc and cobalt complexes that are responsible for the insertion of polysulfidic pendant groups into the model rubber compound and the plasma polymer. Since zinc is located on the surface while cobalt is somewhat below the surface, it is likely that the cobalt complexes were formed first and zinc complexes were mostly formed in the later stages of the reaction, after the cobalt had been consumed.

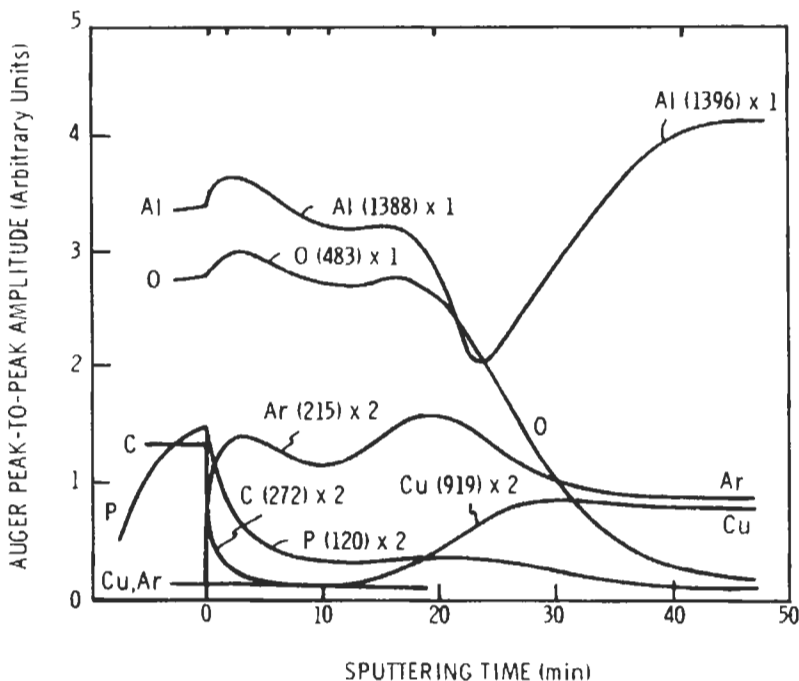


Fig. 40. Auger depth profile of an as-prepared oxide obtained by anodizing 2024 aluminum alloy in phosphoric acid. Reproduced by permission of Chapman and Hall Ltd. from Ref. [38].

The presence of a third peak in the sulfur profile, near the film/substrate interface, indicates that some sulfur diffused through the plasma polymer films and reacted with iron, probably forming FeS at the interface.

An Auger depth profile for a 2024-T3 aluminum alloy specimen that had been anodized in phosphoric acid is shown in Fig. 40 [38]. As discussed above, the surface regions of the specimen consisted mostly of aluminum and oxygen. Small amounts of carbon and phosphorus were also detected but no evidence of the alloying elements Al, Mn, and Mg was observed. The carbon was attributed to adsorbed hydrocarbon contaminants but phosphorus was related to formation of a monolayer of AlPO_4 at the surface of the anodic oxide. After a sputtering time of approximately 25 min, the concentration of oxygen decreased significantly and that of aluminum increased, indicating that the interface between the oxide and the metal had been reached. The carbon concentration rapidly dropped to zero as a function of sputtering time. Although the concentration of phosphorus also decreased rapidly in the early stages of sputtering, some phosphorus was detected until the oxide/metal was approached.

The Auger depth profile of an aluminum substrate that was anodized in phosphoric acid and then exposed to 100% relative humidity at 50°C for 73 h is

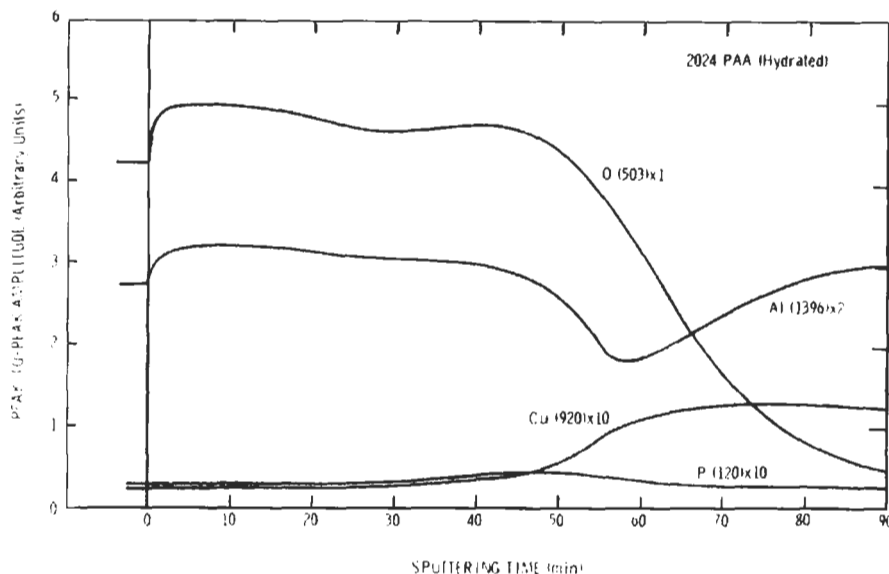


Fig. 41. AES depth profile of the anodic oxide on 2024 aluminum after hydration in 100% RH at 50°C for 73 h. Reproduced by permission of Chapman and Hall Ltd. from Ref. [38].

shown in Fig. 41. In this case, the phosphorus concentration was always low, even at the surface of the oxide, and the oxygen concentration within the oxide was always higher than that of aluminum. These results were attributed to dissolution of AlPO_4 and to hydration of the anodic oxide [38].

Very recently Jeon and Seo used AES depth profiling to determine the effect of curing temperature on adhesion of natural rubber to brass [46]. In their investigation, natural rubber was vulcanized against a thin brass film that was sputtered onto a glass plate. After vulcanization, the rubber was removed from the glass and AES was used to construct depth profiles starting from the brass and proceeding toward the brass/rubber interphase. Fig. 42 shows the copper and sulfur profiles (top) and the zinc and oxygen profiles (bottom) that were obtained for various vulcanization temperatures between 130°C and 190°C. For the samples vulcanized at 130°C, a shoulder appeared near the end of the copper peak. This shoulder coincided with a peak in the sulfur profile, suggesting that a copper sulfide was formed. There was also a peak at the end of the zinc profile that coincided with a peak in the oxygen profile, suggesting formation of zinc oxide. Considering the atomic concentrations detected for the various elements, it was suggested that there was too much sulfur and too much zinc for only copper sulfide and zinc oxide to form. Therefore, it was also suggested that some zinc sulfide also formed at lower temperatures.

The depth profiles were similar for temperatures of 145°, 160°, and 175°C.

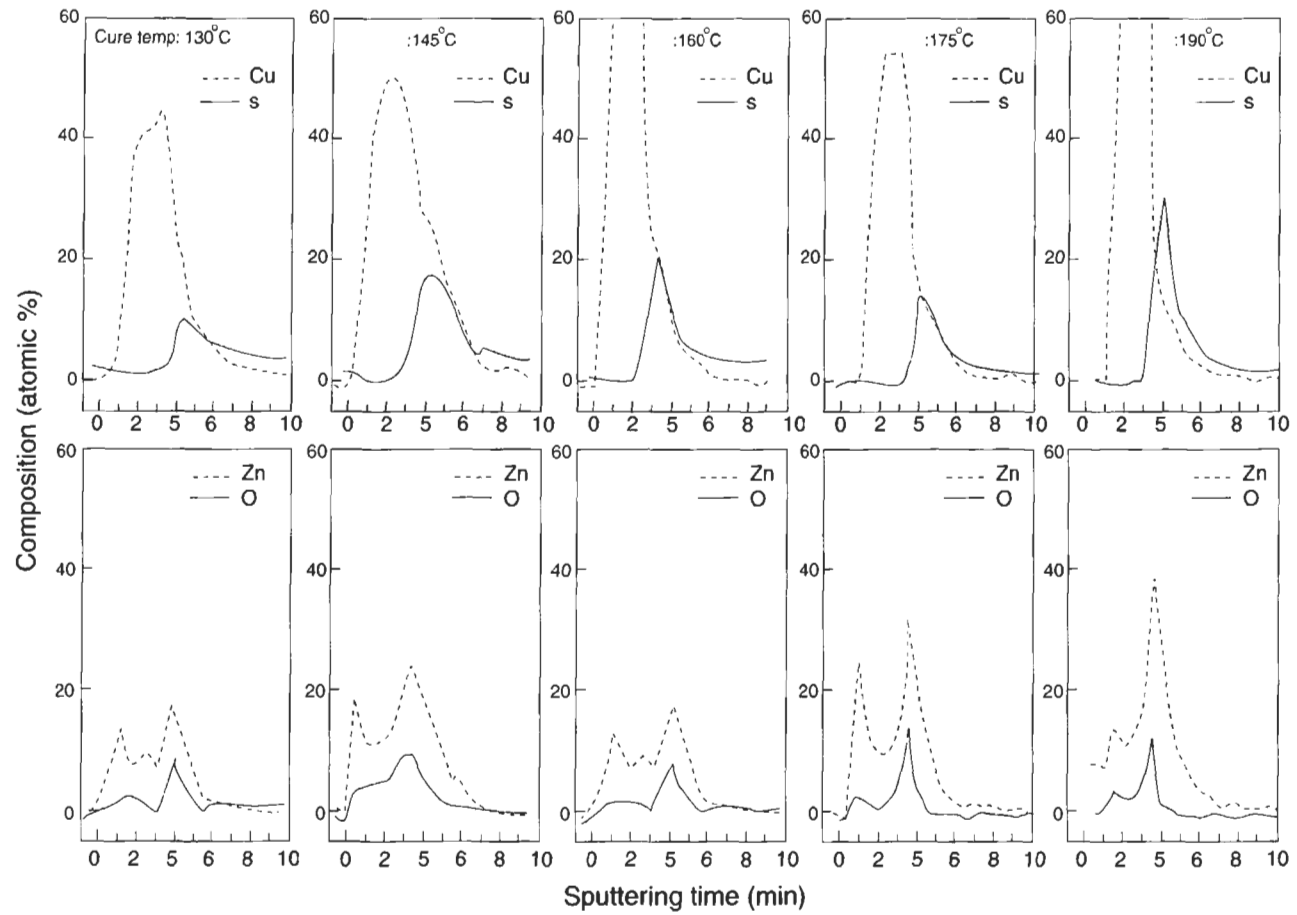


Fig. 42. AES depth profiles of copper and sulfur (top) and zinc and oxygen (bottom) for the brass-on-glass adhesion specimens as a function of curing temperature. Reproduced by permission of Gordon and Breach Science Publishers from Ref. [46].

However, when the vulcanization temperature was increased to 190°C, it was observed that the peaks in the copper and sulfur profiles no longer coincided. Instead, the peak in the sulfur profile coincided with the peaks in the zinc and oxygen profiles. These results indicated that at higher vulcanizing temperatures, zinc sulfide formed in abundance while formation of copper sulfide decreased.

Changes observed in the composition of the rubber/brass interphase correlated well with results of adhesion tests carried out on brass-plated steel wires embedded in blocks of rubber [46]. The force required to pull the wires out of the blocks decreased steadily as vulcanization temperature increased. This effect was especially pronounced when the specimens were aged at elevated temperature and humidity for several days before the wires were pulled out of the rubber blocks.

Geon and Seo [47] also determined the effect of vulcanization time on the adhesion of natural rubber to brass-plated steel. For relatively short times, there was a peak at the end of the copper profile that corresponded well with a peak in the sulfur profile. Similarly, peaks in the zinc and oxygen profiles corresponded well. These results showed that copper sulfide and zinc oxide mostly formed at short times but some evidence for formation of zinc sulfide was also obtained. For long times, the peak in the sulfur profile no longer corresponded with that in the copper profile. Instead, the peak in the sulfur profile corresponded to the peak in the zinc profile. It was concluded that the formation of zinc sulfide increased substantially at long times. An increase in vulcanization time correlated well with a decrease in the force required to pull brass-plated steel wires out of rubber blocks.

5. Secondary ion mass spectrometry (SIMS)

In secondary ion mass spectrometry (SIMS), a beam of energetic primary ions is focused onto the surface of a solid. Some of the ions are reflected but most of the energy of the primary ions is dissipated in the surface by binary collisions that cause neutrals, excited neutrals, and ions (positive and negative) to be ejected or sputtered from the surface. The secondary ions can be analyzed by a mass spectrometer to provide information about the surface composition of the solid.

SIMS has superb surface sensitivity since most of the secondary ions originate within a few nanometers of the surface and since high detection efficiency enables as little as 10^{-4} of a monolayer to be detected for most elements. Because of its very high surface sensitivity, SIMS can be used to obtain depth profiles with exceptionally high depth resolution (<5 nm). Since the beam of primary ions can be focused to a small spot, SIMS can be used to characterize the surface of a sample with lateral resolution that is on the order of micrometers. Elements with low atomic numbers, such as H and He, can be detected, isotope analysis can be conducted, and images showing the distribution of chemical species across

the surface can be constructed. When mass analysis is carried out using a time-of-flight mass spectrometer (TOF-SIMS), very high mass resolution is possible, making unambiguous identification of sputtered particles possible. The most significant disadvantage of the technique concerns quantitative analysis. Matrix effects and effects induced by the primary ion beam strongly affect the yield of secondary ions, making quantitative analysis difficult.

In TOF-SIMS, the source of primary ions is pulsed at a rate of a few kHz. The pulse width is on the order of ~ 1 ns. Secondary ions ejected from the sample surface are accelerated through a potential V and then drift through a field-free TOF analyzer with different velocities, depending on their masses. The drift velocity of an ion with charge-to-mass ratio z/m can be determined from the expression:

$$zeV = \frac{1}{2}mv^2 \quad (18)$$

For a simple linear TOF analyzer of length d , the arrival time at the detector is

$$t = d(2zeV/m)^{-1/2} \quad (19)$$

A mass spectrum is obtained for each pulse by determining the arrival times of the secondary ions at the detector and converting the arrival times to masses using Eq. 19 [48].

Various ion sources are available commercially. These include noble gas ion sources that range from moderate focus, low cost guns to fine focus guns that are useful for rastering and mapping. Liquid metal ion guns are also available. The advantages of these sources include fine focusing for imaging, the addition of a low gas load to the vacuum system, a large depth of focus, and greater secondary ion yield from organics when compared to noble gas ion sources. Disadvantages include the relatively high initial cost and a potentially shorter lifetime. The most commonly used metal in these sources is gallium because of its low melting point ($\sim 30^\circ\text{C}$). Typically a gallium gun will focus about 0.3 nA of ion current into a spot of about 200 nm when operated at 25 keV. This results in a large ion current density that is very useful for fast surface mapping or fast depth profiling but is too great for organic analysis. Thus, for characterization of polymers and other organics, the spot is defocused and the ion current density is limited to a much smaller value [48].

SIMS is inherently damaging to the sample since ion bombardment removes some material from the surface. However, other forms of damage may also occur. These include surface roughening, knock-on effects, preferential sputtering, decomposition, and implantation of source ions [49].

Charging can be a significant problem when the sample is an insulator. Bombarding the sample with positive ions can lead to implantation of positive ions as well as the emission of electrons. One way that this problem can be overcome is by flooding the sample surface with a beam of low-energy electrons [50].

Table 3

Typical ion formation processes in SIMS

Ion formation process ^a	Description
$M^0(s) \longrightarrow M^0(g)$ $M^0(g) + e^- \longrightarrow M^\pm(g)$	Electron ionization
$C^+(s) \longrightarrow C^+(g)$	Direct desorption
$M^0(s) \longrightarrow M^0(g)$ $M^0(g) + C^+ \longrightarrow (M + C)^+(g)$	Cationization
$M^0(s) \longrightarrow M^0(g)$ $M^0(g) + A^- \longrightarrow (M + A)^-(g)$	Anionization
$M^0(s) \longrightarrow M^0(g)$ $M^0(g) + H^+ \longrightarrow (M + H)^+(g)$	Cationization by protonation
$(C_m A_n)^\pm(s) \longrightarrow (C_m A_n)^\pm(g)$	Direct cluster desorption

^a M = molecule; C⁺ = cation; A⁻ = anion.

If it is required that the surface of the sample remains undisturbed during analysis, SIMS must be carried out at very low surface removal rates, typically about 10^{-4} monolayer/s. The terms 'static' and 'dynamic' are used to divide the sputtering rate of the sample into regimes where only surface species are observed (static SIMS) or where surface and bulk species are observed (dynamic SIMS). The static limit is usually considered to be $<10^{12}$ ions/cm² impinging on the sample surface. Under these conditions, only about 1/1000 atoms on the surface of the sample are struck by a primary ion.

The predominant species observed in SIMS spectra are singly charged atomic and molecular ions [51]. However, inorganic and organic cluster ions can also be formed. If the sample consists of a simple single-component metal, then clusters such as M_2^+ , M_3^+ , etc., are observed in addition to M^+ [52]. Oxidation of the metal results in formation of MO^+ , MO_2^+ , $M_xO_y^\pm$, etc. The relative yield of MO^+ to M^+ depends on the bond dissociation energy of the oxide [52]. For a two-component, oxidized metal, clusters of the type M_x^\pm , $M_xN_y^\pm$, $M_xO_y^\pm$, and $M_xN_yO_z^\pm$ are observed [51].

Cluster ions are also emitted from organic materials; their identity and yield depend on the chemical structure of the materials. Molecular or quasi-molecular ions may be observed as well as other ions that are formed by fragmentation, rearrangement, decomposition, or reaction [52]. Several typical ion formation processes are summarized in Table 3 [40].

Quantitative analysis by SIMS is difficult because of matrix effects. The yield of secondary ions depends strongly on the chemical and electronic characteristics of the sample. For example, the yield of Al, Cr, and V are about 10^3 greater for

clean metal surfaces than for fully oxidized surfaces [51]. Moreover, the relative ion yields for different elements in the same matrix can exceed 10^4 but this effect diminishes in importance as the sample changes from a metal to an oxide or insulator [51].

Certain characteristics of the primary ions, such as energy, mass, and chemical nature, strongly influence the yield of secondary ions. For example, the yield of secondary ions increases strongly as the energy of the primary ions increases from a fraction of an eV up to about 6–8 eV and then levels off. The chemical nature of the primary ions is not a significant factor when the ion dosage is kept $< 10^{14}/\text{cm}^2$. However, at higher dosages, sufficient implantation may occur to affect the matrix and, as indicated above, the yield of secondary ions depends strongly on matrix effects [51].

Depth profiles can be obtained by using an ion gun in DC mode for sputtering and in pulsed mode for data acquisition. Alternatively, two guns can be used; one can be operated in DC mode for sputtering while the other is operated in pulsed mode for data acquisition. SIMS imaging can be accomplished in two ways. One is to raster a highly focused primary beam across the sample and to acquire a complete mass spectrum at each spot on the sample surface that is illuminated. The data acquired can then be rearranged to produce maps showing the distribution of particular mass numbers across the surface of the sample. Another technique is to use a much broader primary beam to illuminate the sample and to retain the spatial distribution of the secondary ions through the use of a parallel detection scheme. In this approach, a complete mass spectrum is obtained at each pixel of the detector [53].

Many applications of SIMS to problems in adhesion science have been reported. Papirer et al. used static SIMS to investigate flame treatment of hd-PE [8]. Peaks at $m/z = 31$, 43, and 45 were detected on flame-treated hd-PE and assigned to the oxidized surface species COH_3^+ , C_3H_7^+ or C_2OH_3^+ , and C_2OH_5^+ or CO_2H^+ , respectively. Peaks due to nitrogen species were also observed after flame treatment of hd-PE, as were peaks at $m/z = 77$, 91, 115, and 128 that were attributed to unsaturated species. As discussed previously, the peel strength of compression-molded laminates of hd-PE and SBR rubber increased greatly after brief flame treatment.

Abel et al. investigated the adsorption of γ -glycidoxypolytrimethoxysilane (γ -GPS) onto grit-blasted aluminum from aqueous solutions [54]. One of the objectives of their investigation was to determine if evidence for the formation of Al–O–Si bonds between γ -GPS and the aluminum substrate could be obtained. This would be difficult to do without the high mass resolution provided by a time-of-flight mass spectrometer because several other fragments, including $\text{C}_5\text{H}_{11}^+$, have the same nominal mass-to-charge ratio (71). Fragments with a nominal mass of $m/z = 71$ were examined very carefully for evidence of Al–O–Si⁺ formation. A fragment with an exact mass of 70.9534 was detected and attributed to formation

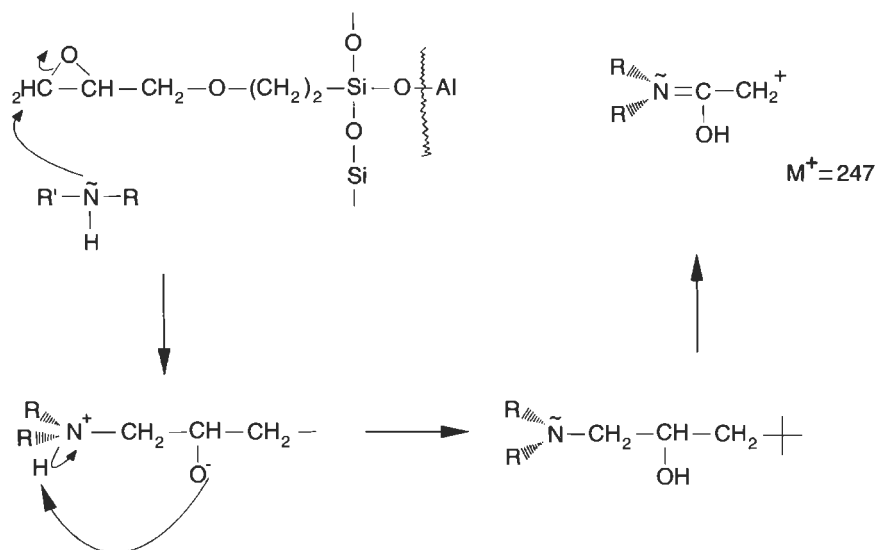
of Al-O-Si^+ , providing strong support to the theory that silanes form covalent bonds with the oxidized surfaces of at least some metals. Another fragment with nominal mass $m/z = 85$ was detected and attributed to $\text{Al-O-Si}^+=\text{CH}_2$, providing additional support for the formation of covalent bonds between γ -GPS and aluminum. This is perhaps the most unambiguous evidence for the existence of Si-O-M bonds between a silane coupling agent and a metal (oxide) substrate.

Abel and et al. also used TOF-SIMS to investigate the adsorption of diethanolamine (DEA) onto grit-blasted aluminum and onto grit-blasted aluminum that was coated with a thin film of γ -GPS [55]. DEA was selected for this investigation because its molecular structure is similar to that of an amine-cured epoxide adhesive. Adsorption was carried out from 0.01 and 0.5 M solutions in absolute ethanol. A fragment with a nominal mass of 106 was assigned to protonated DEA. The intensity of the peak corresponding to this fragment was very strong, especially when compared to that due to the molecular fragment of DEA at $m/z = 105$. Observation of a fragment at mass greater than that of DEA showed that the model epoxide compound adsorbed intact onto the aluminum and γ -GPS-treated aluminum substrates.

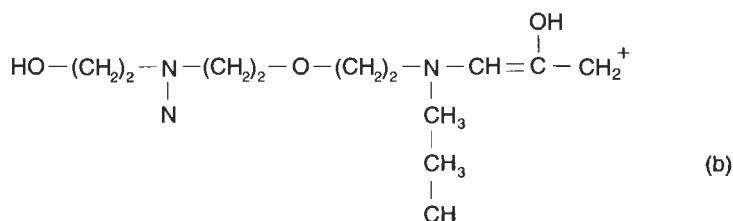
An interesting observation in this work was that a fragment with $m/z = 247$ was observed for DEA adsorbed onto aluminum coated with γ -GPS. This demonstrated the interaction of DEA dimer rather than DEA with γ -GPS as shown in Scheme 1.

Tsai et al. made extensive use of SIMS in their work on plasma polymerized acetylene films as primers for rubber-to-metal bonding [56]. The positive and negative SIMS spectra obtained from a plasma-polymerized acetylene film deposited onto a polished steel substrate are shown in Fig. 43. Peaks observed in the positive spectrum at mass numbers 15, 27, 41, 55, 77, and 91 were assigned to CH_3^+ , C_2H_3^+ , C_3H_5^+ , C_4H_7^+ , C_6H_9^+ , and C_7H_7^+ , respectively. Negative spectra had peaks at mass numbers 12, 13, 16, 17, 24, 25, 49, and 62 were attributed to C^- , CH^- , O^- , OH^- , C_2^- , C_2H^- , C_4H^- , and C_5H_2^- , respectively. As expected for plasma polymerized acetylene, most of the ions detected consisted only of carbon and hydrogen. However, a few ions were detected that contained oxygen, probably indicating post-deposition reaction of the films with oxygen and water vapor in the atmosphere.

Positive SIMS spectra obtained from plasma polymerized acetylene films on polished steel substrates after reaction with the model rubber compound for times between zero and 65 min are shown in Fig. 44. The positive spectrum obtained after zero reaction time was characteristic of an as-deposited film of plasma polymerized acetylene. However, as reaction time increased, new peaks appeared in the positive SIMS spectrum, including $m/z = 59$, 64, and 182. The peaks at 59 and 64 were attributed to Co^+ and Zn^+ , respectively, while the peak at 182 was assigned to $\text{NH}_2^+(\text{C}_6\text{H}_{11})_2$, a fragment from the DCBS accelerator. The peak at 59 was much stronger than that at 64 for a reaction time of 15 min. However,



Where R is $\text{HO-CH}_2\text{-CH}_2\text{-}$ and R' is $\text{HO-(CH}_2\text{)}_2\text{-NH-(CH}_2\text{)}_2\text{-O-(CH}_2\text{)}_2\text{-}$ (a)



Scheme 1. (a) Formation of a fragment with $m/z = 247$ from a covalent bond between γ -GPS and DEA dimer. (b) Final structure of the cation with $m/z = 247$. Reproduced by permission of the American Chemical Society from Ref. [55].

for reaction times of 35 and 65 min, the peak at 64 was stronger. These results were consistent with cobalt entering into crosslinking reactions between squalene molecules and between squalene molecules and the plasma polymerized films before zinc entered into similar reactions. As indicated earlier, similar conclusions were obtained from XPS analysis. The peak at 182 was strong for reaction times of 15, 35, and 65 min, indicating the presence of complexes such as I and II at those reaction times. Additional evidence for crosslinking between squalene and plasma polymerized acetylene films was provided by peaks near 55 and 69 that increased in intensity as a function of reaction time. These peaks were assigned to C_4H_7^+ and C_5H_9^+ , respectively.

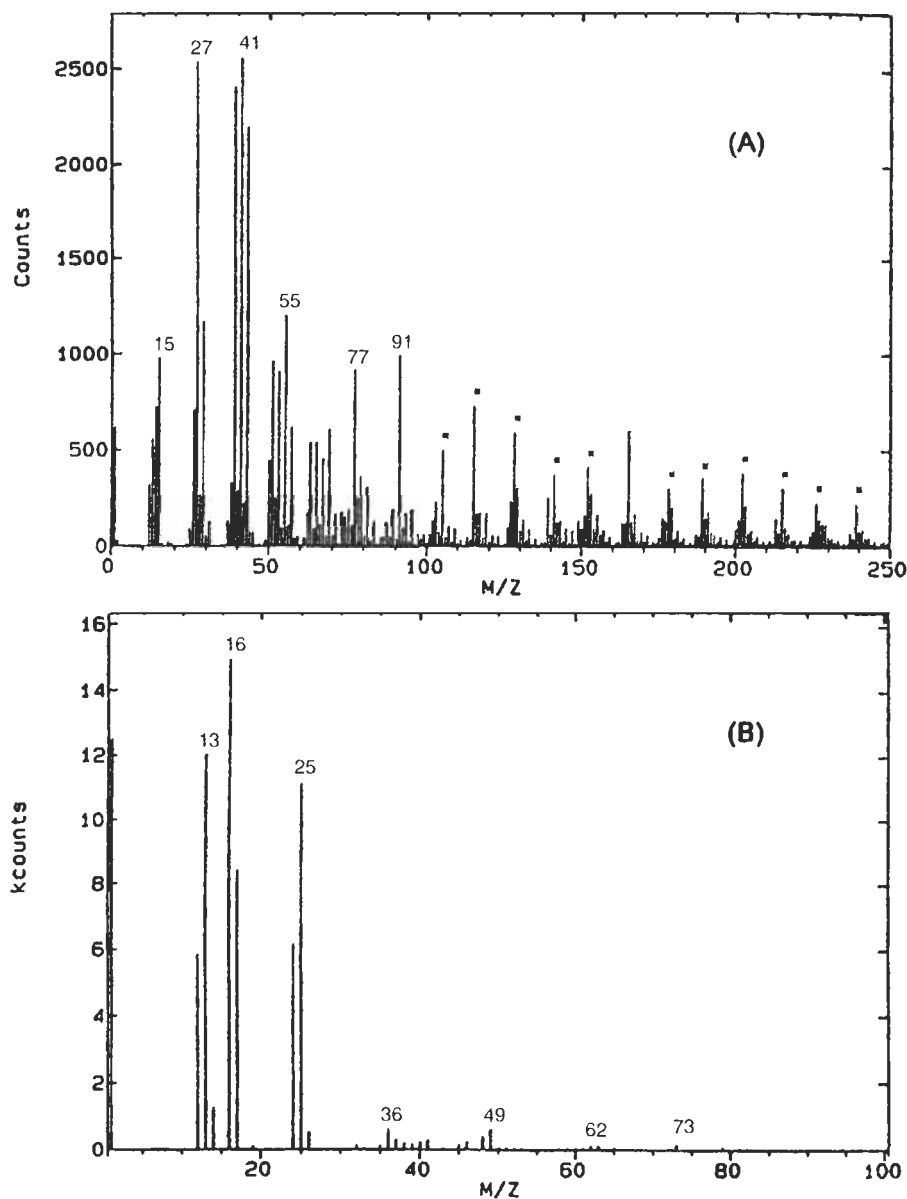
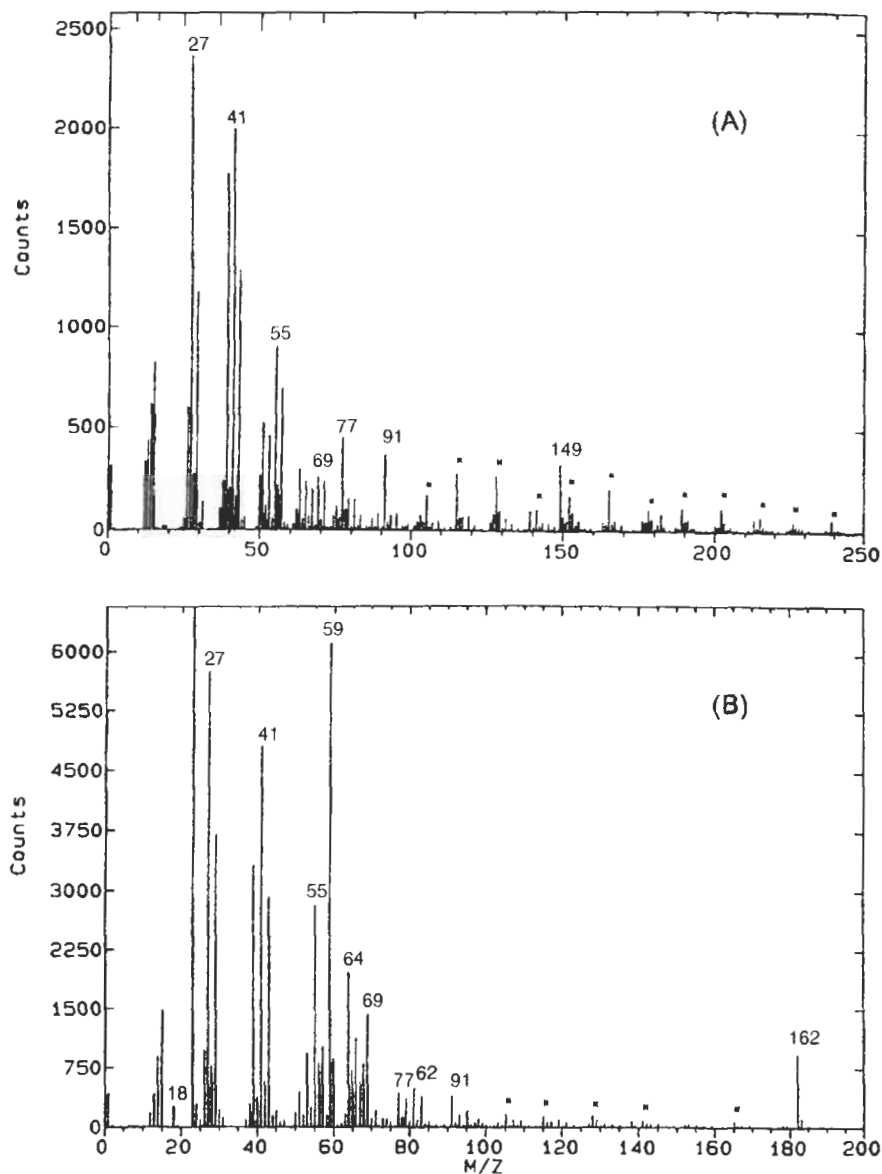


Fig. 43. (A) Positive and (B) negative SIMS spectra of a plasma-polymerized acetylene film on a polished steel substrate. Reproduced by permission of Gordon and Breach Science Publishers from Ref. [56].

Negative SIMS spectra obtained from plasma polymerized acetylene films on polished steel substrates as a function of reaction time with the model rubber compound are shown in Fig. 45. The most important changes observed in the



negative spectra as a function of reaction time involved the appearance of peaks at 32, 64, and 96 that were assigned to S^- , S_2^- , and S_3^- ions, respectively, that were characteristic of polysulfidic crosslinks or pendant groups of different lengths. Peaks were also observed at 134 and 166 and were assigned to fragments such as III that were characteristic of the sulfenamide part of the accelerator. Observation

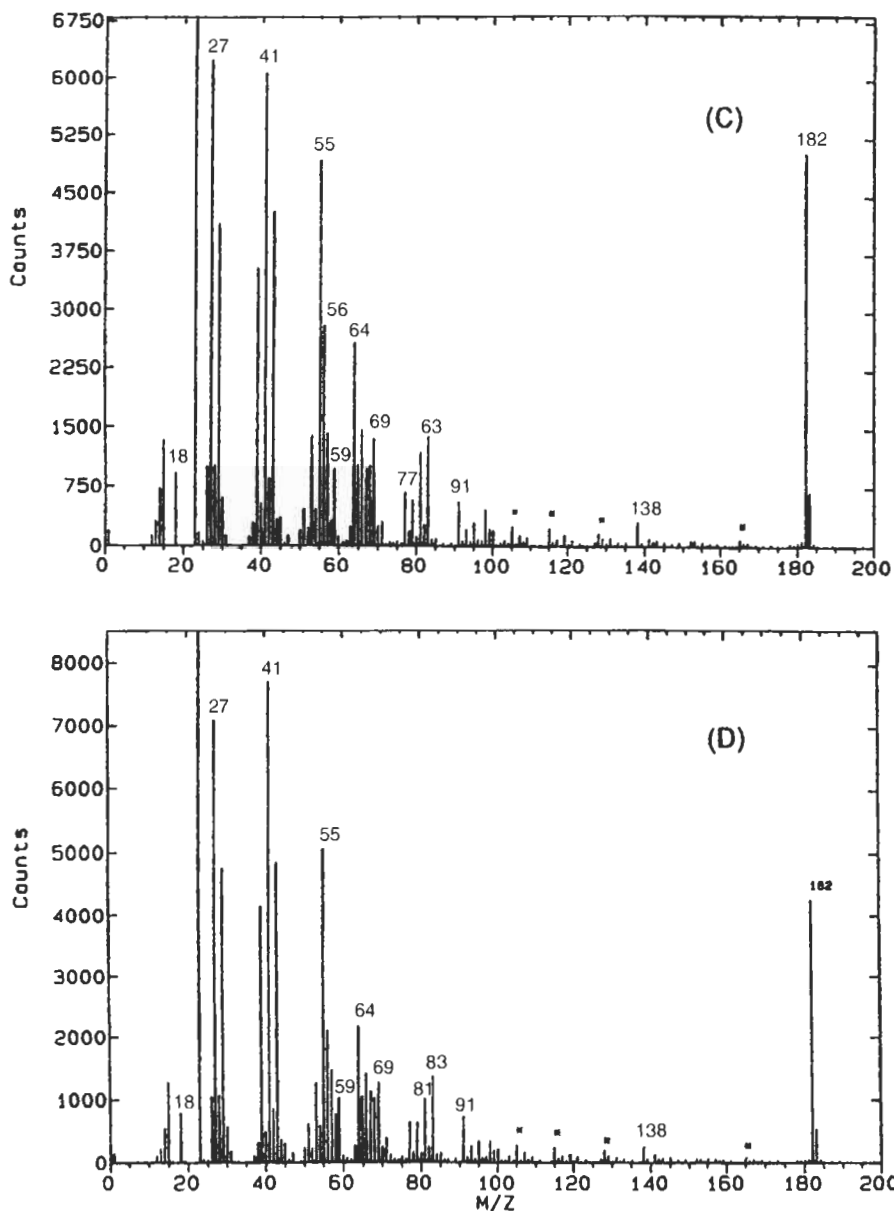
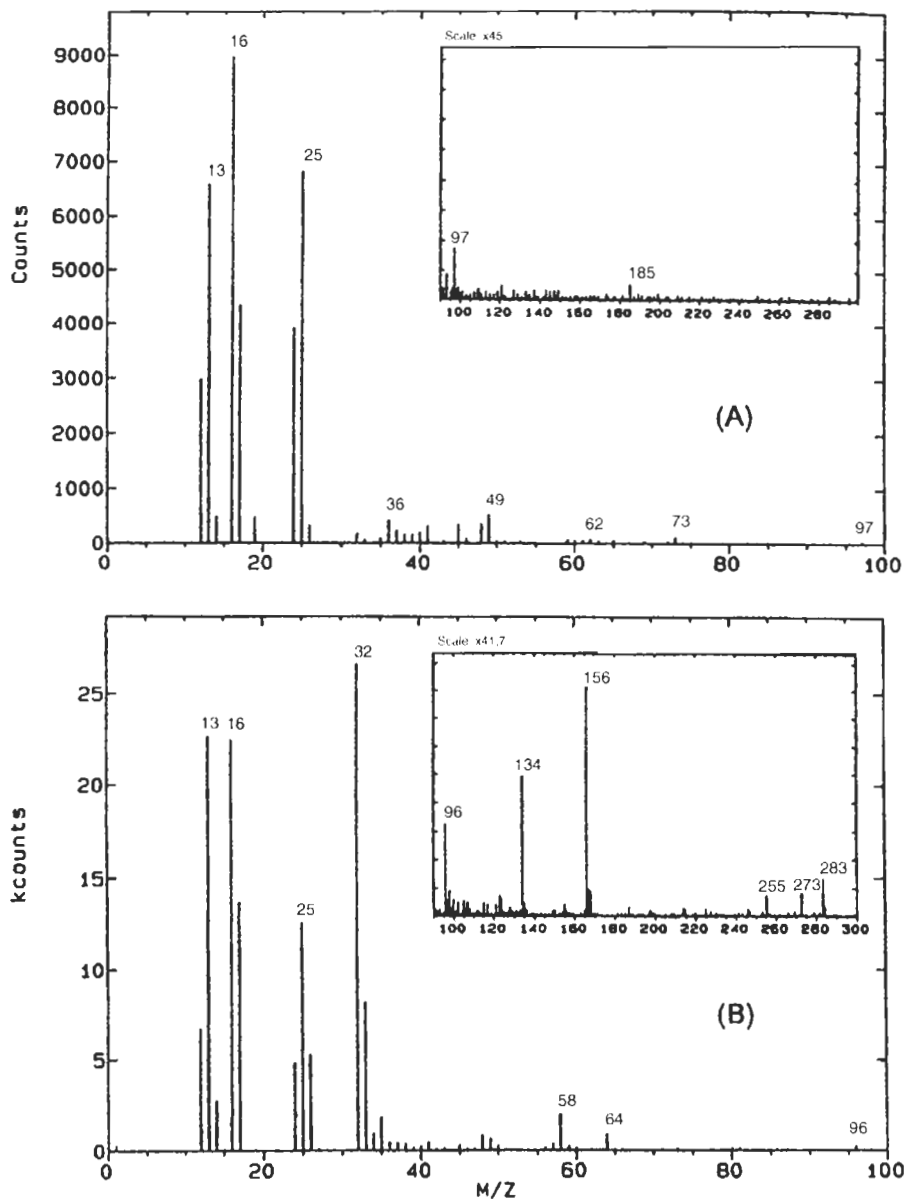


Fig. 44. Positive TOF-SIMS spectra of plasma polymerized acetylene film after reaction with a model rubber compound for (A) 0 and (B) 15 min. Positive TOF-SIMS spectra of plasma polymerized acetylene film after reaction with a model rubber compound for (C) 35 and (D) 65 min. Reproduced by permission of Gordon and Breach Science Publishers from Ref. [56].



of these peaks indicated the presence of accelerator-terminated pendant groups such as VI.

Fitzpatrick and Watts [57] also applied imaging TOF-SIMS to determine the failure mechanisms of adhesively bonded, phosphated hot-dipped galvanized steel

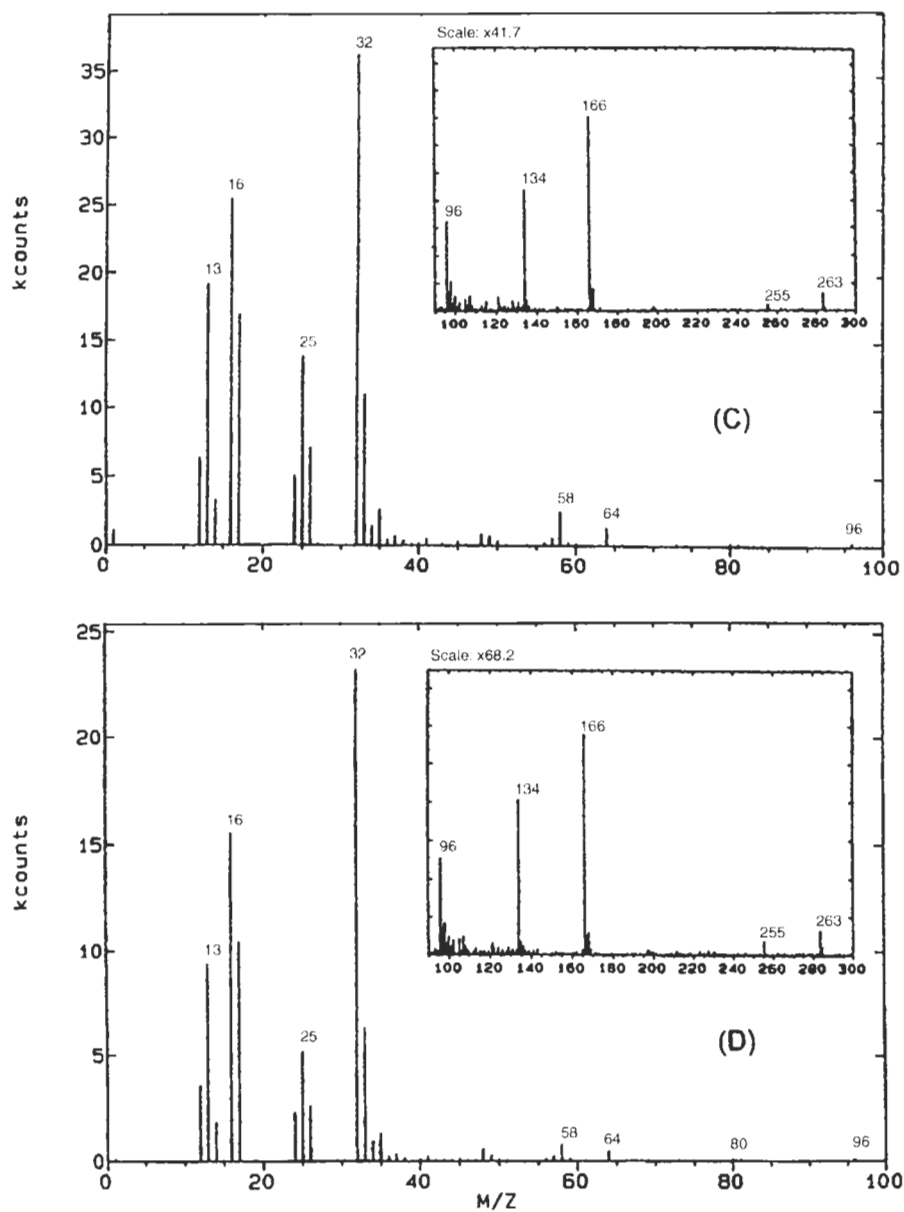


Fig. 45. Negative TOF-SIMS spectra of a plasma-polymerized acetylene film after reaction with a model rubber compound for (A) 0 and (B) 15 min. Negative TOF-SIMS spectra of a plasma-polymerized acetylene film after reaction with a model rubber compound for (C) 35 and (D) 65 min. Reproduced by permission of Gordon and Breach Science Publishers from Ref. [56].

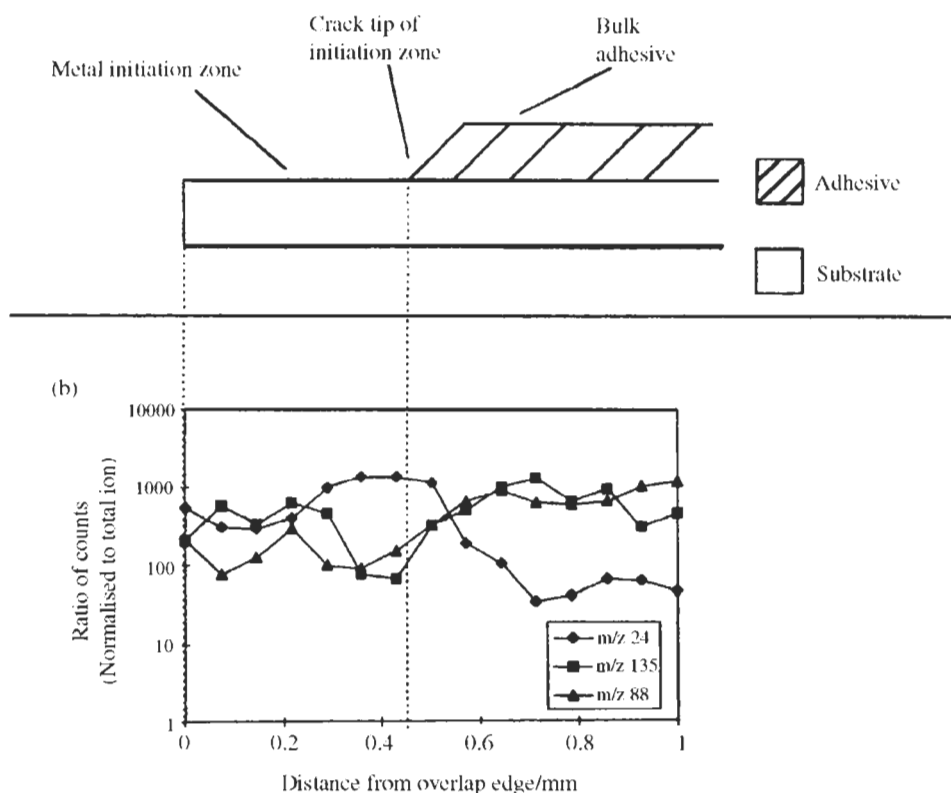


Fig. 46. Schematic drawing of the failure surface of a lap joint prepared from hot-dipped galvanized steel substrates (top) and TOF-SIMS line scans showing the distribution of several mass numbers as a function of distance from the edge of the overlap (bottom). Reproduced by permission of John Wiley and Sons from Ref. [57].

(HDGS) upon exposure to a humid environment. As described above, substrates were prepared by applying a phosphate conversion coating and then a chromate rinse to HDGS. Lap joints were prepared from substrates having dimensions of $110 \times 20 \times 1.2$ mm using a commercial epoxide adhesive with a bond line thickness of $250 \mu\text{m}$. The joints were exposed to 95% RH at 35°C for 12 months and then pulled to failure.

Visually, failure was mostly cohesive within the adhesive (see Figs. 34 and 46). However, there was a small area of apparent interfacial failure ('initiation zone') located at one end of each substrate. Line scans were conducted across the initiation zone, from the edge of the substrate to the area of cohesive failure within the adhesive. From the line scans, it was apparent that there were patches of polymer present in the initiation zone, even when failure appeared to be interfacial (see Fig. 46). SIMS images of the initiation zone were constructed for various mass numbers (see Figs. 47–49). The images showed well-defined cation-rich

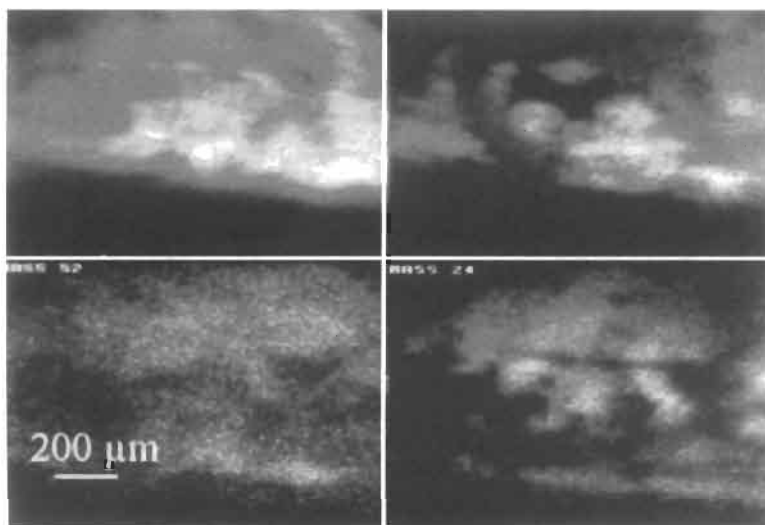


Fig. 47. TOF-SIMS image highlighting cation-rich areas, indicating that local cathodic cells occur within the initiation zone. Image shows (A) total counts, (B) $m/z = 40$, (C) $m/z = 52$ and (D) $m/z = 24$. Reproduced by permission of John Wiley and Sons from Ref. [57].

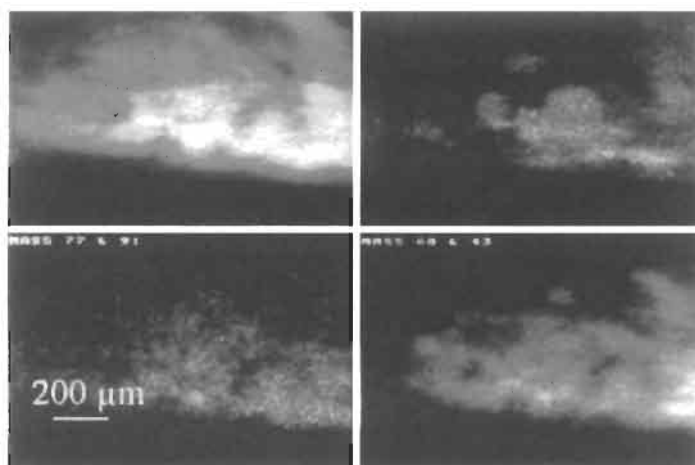


Fig. 48. TOF-SIMS image showing that ions characteristic of the polymer are also found in some areas within the initiation zone. Image shows (A) total counts, (B) $m/z = 88$, (C) $m/z = 77 + 91$ and (D) $m/z = 60 + 43$. Reproduced by permission of John Wiley and Sons from Ref. [57].

areas, suggesting local cathodic cells within the initiation zone (Fig. 47). Images also confirmed that the distribution of polymer within the initiation zone was patchy (Fig. 48). These observations lead to the conclusion that water ingress may have weakened the adhesive so that there were small areas of 'cohesive' failure within the polymer even in the initiation zone. Finally, the images confirmed that

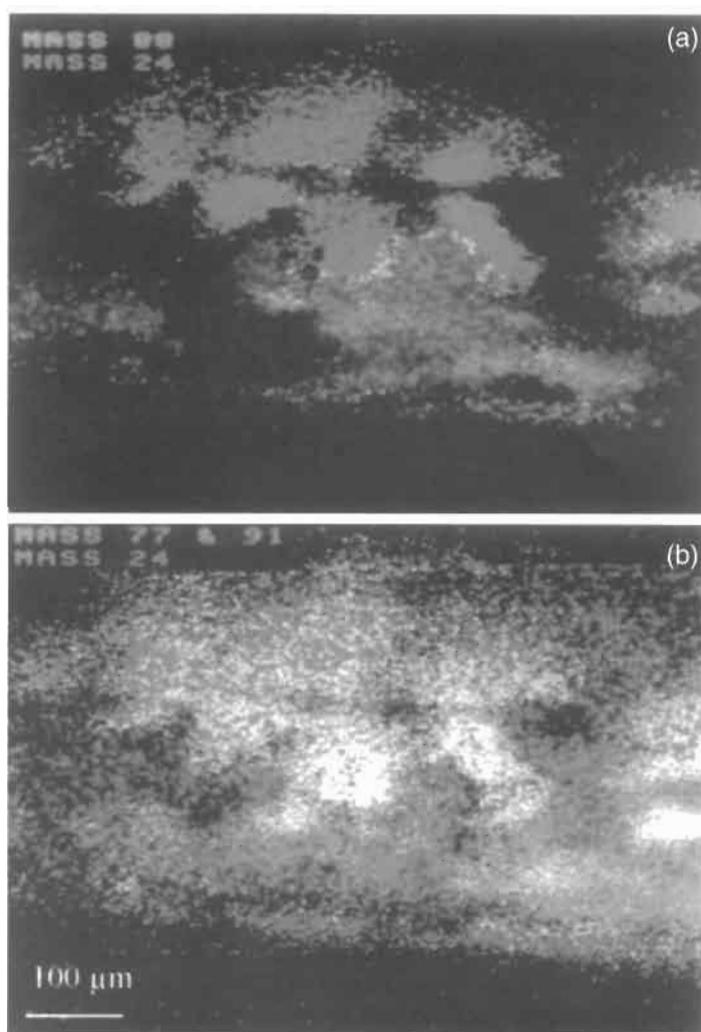


Fig. 49. TOF-SIMS images showing that the cation-rich areas in the initiation zone do not correspond to polymer-rich areas: (A) $m/z = 88$ on 24; (B) $m/z = 77 + 91$ on 24. Reproduced by permission of John Wiley and Sons from Ref. [57].

there were areas within the initiation zone that were cation-rich and adhesive-deficient and others that were adhesive-rich and cation-deficient. The SIMS imaging approach thus demonstrated that different failure mechanisms (adhesive weakening, cathodic activity) dominated in different areas of the initiation zone.

Brewis et al. used TOF-SIMS to determine the surface composition of hydrocarbon polymers after electrochemical pretreatment with nitric acid alone or in the presence of silver ions [58]. AgNO_3^+ was generated by electrolysis of a 0.1 M solution of silver nitrate in 3.25 M nitric acid in the anode compartment of a

standard two-compartment 'H' cell. The catholyte consisted of 3.25 M nitric acid and was separated by a medium-porosity sintered glass frit. Experiments were also carried out to determine if surface oxidation of hydrocarbon polymers could be obtained in an electrolyte consisting only of nitric acid.

Introduction of oxygen-containing functional groups into the surface of high-density polyethylene (hd-PE) during electrochemical treatment with nitric acid at 60°C in the presence of silver ions was easily observed from the negative ion spectra where peaks appeared at $m/z = 16$ and 17 (O^- , OH^-). Peaks were also observed in the negative ion spectra at 46 and 62 and were assigned to NO_3^- and/or nitrate ester groups on the surface. Additional peaks characteristic of CN^- and CNO^- were observed at $m/z = 26$ and 42 , respectively. Peaks characteristic of F^- ($m/z = 19$), Cl^- ($m/z = 35, 37$), and SO_4^-/HSO_4^- ($m/z = 80, 96, 97$) were also observed but their origin was not clear.

The overall appearance of the positive ion spectra did not change after treatment with nitric acid in the presence of silver ions. However, at high mass resolution it was observed that many of the peaks related to hydrocarbon fragments ($C_xH_y^+$) had one or two additional components at lower masses (see Fig. 50). These peaks were attributed to fragments containing one or two oxygen atoms and having the general formula $C_{x-1}H_{y-4}O^+$ or $C_{x-2}H_{y-8}O_2^+$. Positive ion spectra obtained from samples treated for 1 min and 5 min at 60°C were virtually identical but in the negative ion spectra, the ratios OH^-/O^- and NO_3^-/NO_2^- increased as treatment time increased.

Oxidation of polypropylene (PP) increased about 30% when the treatment time was increased from 1 min to 5 min at 60°C but was much lower than for hd-PE under similar conditions. The extent of oxidation for polystyrene (PS) at 60°C was much greater than for hd-PE. However, the NO_2^-/NO_3^- peaks were usually weaker than for the hydrocarbons. Numerous peaks with high mass numbers but low intensity were observed in the negative ion spectra, including those characteristic of $C_6H_5O^-$ and $C_8H_7O^-$ ($m/z = 93$ and 119 , respectively). In the positive spectra, the peak due to the protonated repeating unit ($m/z = 105$) was split into two components; the component at lowest mass number was assigned to $C_7H_5O^+$.

Electrochemical treatment of the polymers in nitric acid in the absence of silver ions was carried out at room temperature. Extent of oxidation was low for hd-PE and PP. It was not possible to directly compare the results with those obtained for oxidation in the presence of silver ions since different temperatures were used (room temperature versus 60°C). However, the spectra obtained after treatment indicated similar chemical effects for the two cases. For PS, it was possible to make direct comparisons because the same temperature was used for treatment in the presence and absence of silver ions. In that case, the overall degree of oxidation was lower.

Two explanations were suggested for the great intensity of the peaks due to oxygen-containing positive ion fragments relative to the original hydrocarbon

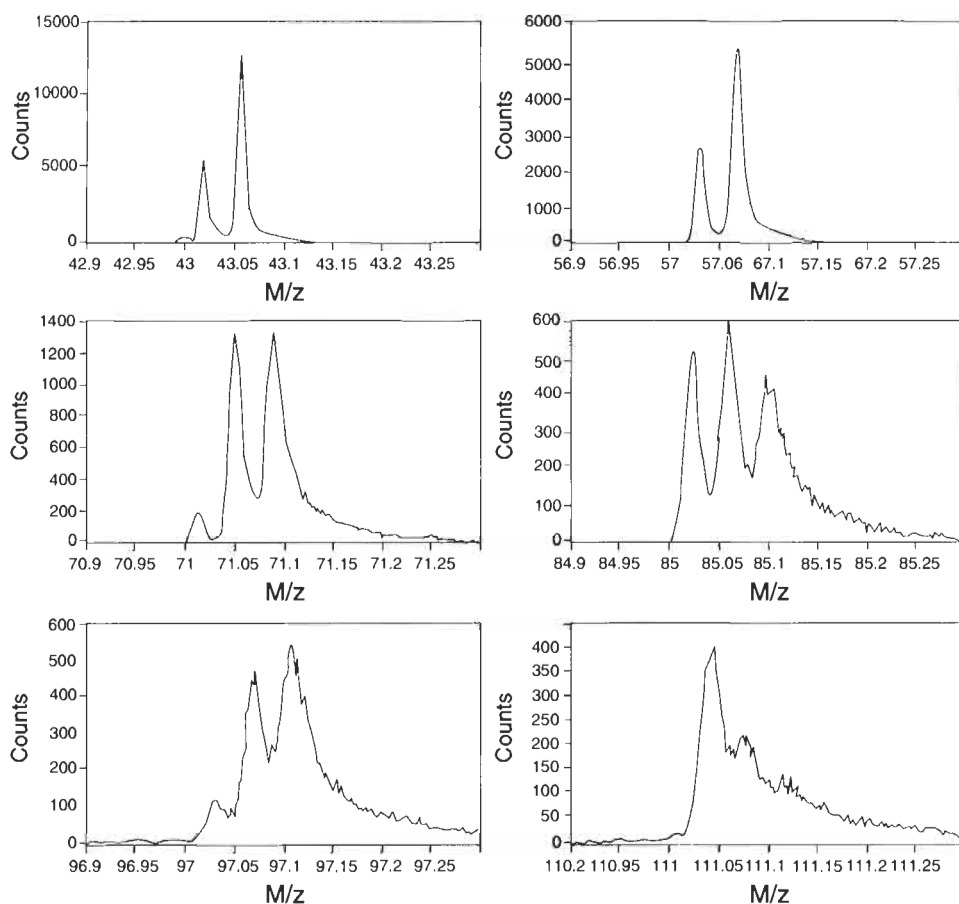

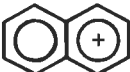

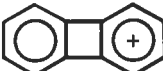
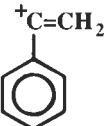
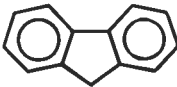




Fig. 50. High-resolution positive ion spectra of hd-PE after electrochemical treatment with nitric acid for 1 min at 60°C in the presence of silver ions. Peak components in order of increasing mass: $m/z = 43 - \text{C}_2\text{H}_3\text{O}^+$, C_3H_7^+ ; $m/z = 57 - \text{C}_3\text{H}_5\text{O}^+$, C_4H_9^+ ; $m/z = 71 - \text{C}_3\text{H}_3\text{O}_2^+$, $\text{C}_4\text{H}_7\text{O}^+$, $\text{C}_5\text{H}_{11}^+$; $m/z = 85 - \text{C}_4\text{H}_5\text{O}_2^+$, $\text{C}_5\text{H}_9\text{O}^+$, $\text{C}_6\text{H}_{13}^+$; $m/z = 97 - \text{C}_5\text{H}_2\text{O}_2^+$, $\text{C}_7\text{H}_{13}^+$; $m/z = 111 - \text{C}_6\text{H}_7\text{O}_2^+$, $\text{C}_7\text{H}_{11}\text{O}^+$, $\text{C}_8\text{H}_{15}^+$. Reprinted by permission of John Wiley and Sons from Ref. [58].

fragments. One was that these fragments were inherently more stable than the hydrocarbon fragments. The other was that the peaks due to oxygen-containing positive ion fragments represented new end-groups. It has been established that the yield of ions derived from end-groups is generally much higher than the yield of ions from the polymer backbone. It was suggested that the latter explanation was most likely responsible for the relatively great intensity of the oxygen-containing peaks in the positive spectra and that new end-groups resulted from chain scission and formation of hydroxyl groups and carbonyl groups. In the case of PS, the new peak at $m/z = 105$ ($\text{C}_7\text{H}_5\text{O}^+$) was almost surely due to the benzoyl cation ($\text{C}_6\text{H}_5\text{CO}^+$), indicating attack at the phenyl-substituted position as well as chain

Table 4

Fragments and masses observed in positive TOF-SIMS spectra of PMDA/ODA polyimide (reproduced by permission of John Wiley and Sons from Ref. [33])

78		128	
91		152	
103		165	
115		178	

scission to produce an alkyl aryl ketone. Brewis et al. suggested mechanisms for the oxidation of the polymers that they investigated.

The results obtained by Brewis et al. demonstrate an important feature of TOF-SIMS and that is the ultra-high mass resolution of the technique. Without such high spectral resolution, it would be impossible to resolve peaks such as those shown in Fig. 50 into components and a great deal of information about the oxidation process would be unavailable.

As discussed previously, Wolany et al. [33] have used TOF-SIMS as well as XPS to investigate reactions occurring when copper was vapor-deposited onto PMDA/ODA polyimide that was untreated or briefly treated in an oxygen plasma. The positive and negative TOF-SIMS spectra of untreated PMDA/ODA polyimide are shown in Fig. 51. The positive spectra consisted of a number of fragments that occur frequently in spectra of aromatic compounds and were thus not very characteristic of the polyimide. Some of these fragments are summarized in Table 4. Several peaks in the negative spectra were interpreted as direct fragmentation products of the repeating unit of the polyimide plus a hydrogen atom. These fragments are summarized in Fig. 52. Several other lines from the negative spectra and their interpretations are listed in Table 5.

Negative TOF-SIMS spectra of PMDA/ODA polyimide before and after plasma treatment are shown in Fig. 53. The spectra generally show increasing fragmentation as a function of plasma treatment time. This tendency was especially evident for the peak at $m/z = 215$ (PMDA + H⁻).

TOF-SIMS spectra supported the suggestion that copper interacted with untreated polyimide through the imide carbonyl group as shown in Fig. 27. Numer-

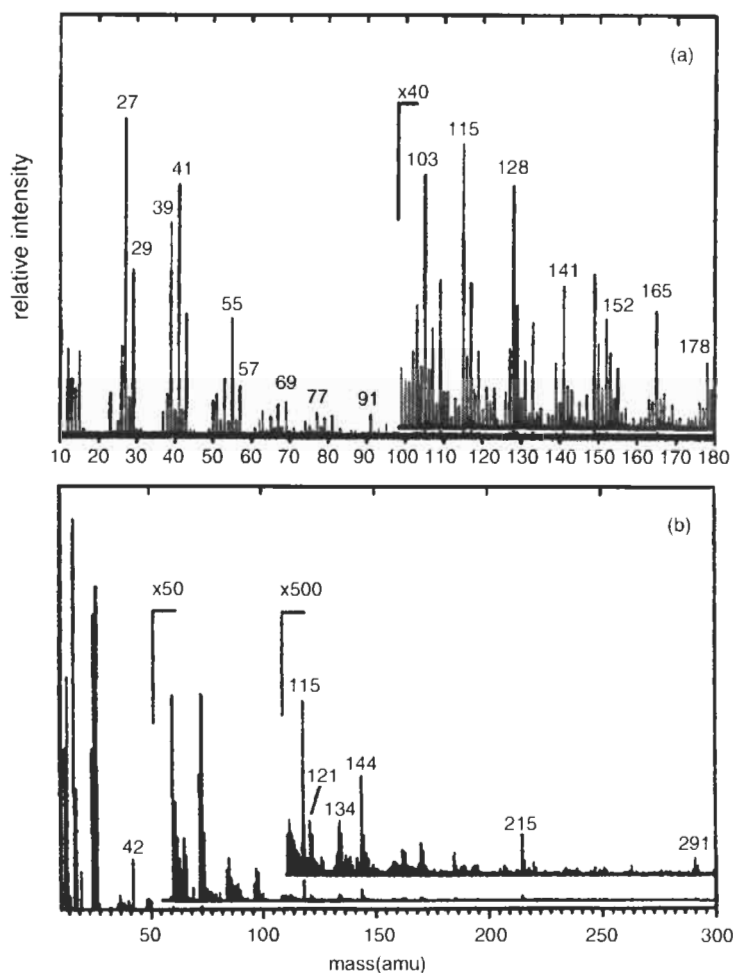


Fig. 51. Positive (a) and negative (b) TOF-SIMS spectra obtained from untreated PMDA/ODA polyimide. Reproduced by permission of John Wiley and Sons from Ref. [33].

ous peaks were observed in the positive ion spectra that were related to reaction of copper with PMDA/ODA polyimide. These included peaks characteristic of CuH^+ , CuH_2^+ , CuCH_x^+ ($x = 0-3$), CuNH_3^+ , CuO^+ , CuOH^+ , CuOH_2^+ , CuC_2H_x^+ ($x = 0-6$), CuO_2^+ , and CuO_2H^+ . Especially important was the observation of a peak attributed to CuOC^+ since the proposed mechanism for reaction between copper and untreated PMDA/ODA polyimide suggested formation of Cu–O–C complexes.

After metallization of the plasma-modified polyimide, there were a number of peaks in the TOF-SIMS spectra that confirmed the existence of Cu–N bonds as required by the proposed reaction mechanism (see Fig. 28). The most significant

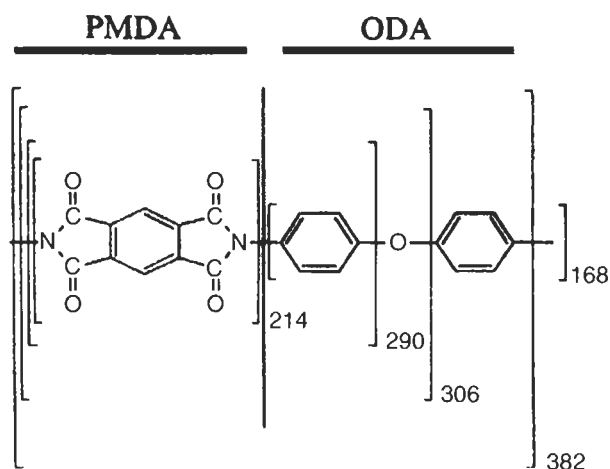


Fig. 52. Characteristic fragments for the repeating unit of PMDA/ODA polyimide. Reproduced by permission of John Wiley and Sons from Ref. [33].

Table 5

Structure and mass numbers for some fragments observed in negative TOF-SIMS spectra of PMDA/ODA (reproduced by permission of John Wiley and Sons from Ref. [33])

118	
134	
144	

of these peaks corresponded to the CuNH_3^+ ion. The intensity of this peak was a maximum for a copper film thickness of 0.5 nm (monolayer of copper), as expected for a signal that was characteristic of the metal/polymer interface.

6. Conclusion

From the preceding discussion, it is evident that surface analysis techniques have contributed greatly to the understanding of adhesion related phenomena. Surface analysis has made it possible for adhesion scientists to determine the composition

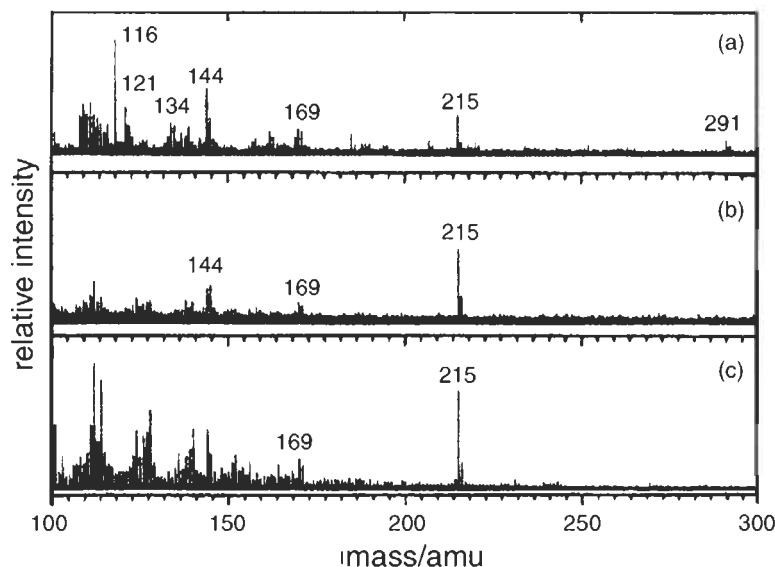


Fig. 53. Negative TOF-SIMS spectra of PMDA/ODA polyimide (a) before plasma treatment and after plasma treatment for (b) 1 s and (c) 60 s. Reproduced by permission of John Wiley and Sons from Ref. [33].

of anodic oxides on metals, the surface composition of polymers that have been pretreated by techniques such as acid-etching and exposure to flames, the nature of reactions occurring at the interface between a primer and a substrate or between a primer and an adhesive, and the orientation of molecules adsorbed onto substrates. Surface analysis has also enabled adhesion scientists to determine the mechanisms responsible for failure of adhesive bonds, especially after exposure to aggressive environments.

Continued improvements in areas such as spectral resolution and spatial resolution will make it possible for surface analysis to make even greater contributions to adhesion science in the future. Improved spectral resolution will enable adhesion scientists to distinguish bonding states that have similar energies and will greatly enhance understanding of pretreatment processes, chemical reactions at interfaces, and chemical reactions occurring during the environmental degradation of adhesive bonds. Enhanced spatial resolution will lead to more widespread applications of imaging techniques and to improved understanding of adhesion-related phenomena, such as corrosion-induced debonding, on a spatially resolved basis.

References

1. Griffiths, P.R., *Chemical Infrared Fourier Transform Spectroscopy*. John Wiley and Sons, New York, NY, 1975.

2. Harrick, N.J., *Internal Reflection Spectroscopy*. Interscience Publishers, New York, NY, 1967, p. 30.
3. Hirschfeld, T., *Appl. Spectrosc.*, **31**, 289 (1977).
4. Schick, R.A., Koenig, J.L. and Ishida, H., *Appl. Spectrosc.*, **47**, 1237 (1993).
5. Reichert, W.M., Suci, P.A., Ives, J.T. and Andrade, J.D., *Appl. Spectrosc.*, **41**, 503 (1987).
6. Davies, D. and Martin, B., *J. Comput. Methods*, **33**, 1 (1979).
7. Blais, P., Carlsson, D.J., Sullog, G.W. and Wiles, D.M., *J. Colloid Interface Sci.*, **47**, 636 (1974).
8. Papirer, E., Wu, D.Y. and Schultz, J., *J. Adhes. Sci. Technol.*, **7**, 343 (1993).
9. Boerio, F.J., Zhao, W.W. and Young, J.T., In: *Multidimensional Spectroscopy of Polymers*. ACS Symposium Series #598, American Chemical Society, Washington, DC, 1995, p. 8.
10. Young, J.T., Boerio, F.J., Zhang, Z. and Beck, T.L., *Langmuir*, **12**, 1219 (1996).
11. Zhang, Z., Beck, T.L., Young, J.T. and Boerio, F.J., *Langmuir*, **12**, 1227 (1996).
12. Tsai, Y.M., Boerio, F.J. and Kim, D.K., *J. Adhes.*, **55**, 151 (1995).
13. Boerio, F.J., Tsai, Y.M. and Kim, D.K., *Rubber Chem. Tech.*, **72**, 199 (1999).
14. Chapman, A.V. and Porter, M., In: Roberts, A.D. (Ed.), *Natural Rubber: Science and Technology*. Oxford University Press, Oxford, ch. 12, 1988.
15. Taylor, C.E. and Boerio, F.J., *J. Adhes.*, **69**, 217 (1999).
16. Parada, E.G., Gonzalez, P., Pou, J., Serra, J., Fernandez, D., Leon, B. and Perez-Amor, M., *J. Vac. Sci. Technol.*, **A14**, 436 (1996).
17. Berreman, D.W., *Phys. Rev.*, **130**, 2193 (1963).
18. H.S. Nikolic, M.S. Thesis, University of Cincinnati, Cincinnati, OH, 1999.
19. Gaillard, F., Linossier, I., Sweeney, M., Reffner, J.A. and Romand, M., *Surf. Interface Anal.*, **27**, 865 (1999).
20. Briggs, D. and Riviere, J.C., In: Briggs, D. and Seah, M.P. (Eds.), *Practical Surface Analysis by Auger and X-ray Photoelectron Spectroscopy*. John Wiley and Sons, Chichester, 1983, ch. 3.
21. Wagner, C.D., Riggs, W.M., Davis, L.E., Moulder, J.F. and Muilenberg, G.E., *Handbook of X-ray Photoelectron Spectroscopy*. Perkin-Elmer Corporation, Physical Electronics Division, Eden Prairie, MN, 1979.
22. Tsai, Y.M., Boerio, F.J., van Ooij, W.J., Kim, D.K. and Rau, T., *Surf. Interface Anal.*, **23**, 261 (1995).
23. Tsai, Y.M., Boerio, F.J., van Ooij, W.J. and Kim, D.K., *J. Adhes.*, **62**, 127 (1997).
24. Leadley, S.R. and Watts, J.F., *J. Adhes.*, **60**, 175 (1997).
25. Pijpers, A.P. and Donners, W.A.B., *J. Polym. Sci., Polym. Chem. Ed.*, **23**, 453 (1985).
26. Leadley, S.R. and Watts, J.F., *J. Electron. Spectrosc. Rel. Phenom.*, **85**, 107 (1997).
27. Burkstrand, J.M., *Appl. Phys. Lett.*, **33**, 387 (1978).
28. Friedrich, J.F., Koprinarov, I., Giebler, R., Lippitz, A. and Unger, W.E.S., *J. Adhes.*, **71**, 297 (1999).
29. Chou, N.J. and Tang, C.H., *J. Vac. Sci. Technol.*, **A3**, 739 (1984).
30. Sanda, P.N., Bartha, J.W., Clabes, J.G., Jordan, J.L., Feger, C., Silverman, B.D. and Ho, P.S., *J. Vac. Sci. Technol.*, **A4**, 1035 (1986).
31. Haight, R., White, R.C., Silverman, B.D. and Ho, P.S., *J. Vac. Sci. Technol.*, **A6**, 2188 (1988).
32. Pertsin, A.J. and Pashunin, Y.M., *Appl. Surf. Sci.*, **47**, 115 (1991).
33. Wolany, D., Fladung, T., Duda, L., Lee, J.W., Gatenfort, T., Wiedemann, L. and Benninghoven, A., *Surf. Interface Anal.*, **27**, 609 (1999).
34. Briggs, D., Brewis, D.M. and Konieczko, M.B., *J. Mater. Sci.*, **11**, 1270 (1976).
35. Briggs, D., Brewis, D.M. and Konieczko, M.B., *J. Mater. Sci.*, **14**, 1344 (1979).

36. Alwitt, R.S., In: Diggle, J.W. and Vijn, A.K. (Eds.), *Oxides and Oxide Films*, Vol. 4. Marcel Dekker, New York, 1976, Ch. 3.
37. Marceau, J.A., Moji, Y. and McMillan, J.C., In: *Proceedings of the 21st National SAMPE Symposium*, SAMPE, Covina, CA, 1976.
38. Davis, G.D., Sun, T.S., Ahearn, J.S. and Venables, J.D., *J. Mater. Sci.*, **17**, 1807 (1982).
39. Tsai, W.H., Cave, N.G. and Boerio, F.J., *Langmuir*, **8**, 927 (1992).
40. Buchwalter, L.P. and Greenblatt, J., *J. Adhes.*, **19**, 257 (1986).
41. Fitzpatrick, M.F., Ling, J.S.G. and Watts, J.F., *Surf. Interface Anal.*, **29**, 131 (2000).
42. Domingue, A., Piyakis, K., Sacher, E., DiRenzo, M., Denommee, S. and Ellis, T.H., *J. Adhes.*, **40**, 151 (1993).
43. Briggs, D. and Riviere, J.C., In: Briggs, D. and Seah, M.P. (Eds.), *Practical Surface Analysis by Auger and X-ray Photoelectron Spectroscopy*. John Wiley and Sons, Chichester, 1983, p. 147.
44. Briggs, D. and Riviere, J.C. In: Briggs, D. and Seah, M.P. (Eds.), *Practical Surface Analysis by Auger and X-ray Photoelectron Spectroscopy*. John Wiley and Sons, Chichester, 1983, p. 92.
45. Tsai, Y.M., Boerio, F.J., van Ooij, W.J. and Kim, D.K., *J. Adhes.*, **62**, 127 (1997).
46. Geon, G.S. and Seo, G., *J. Adhes.*, **76**, 201 (2001).
47. Geon, G.S. and Seo, G., *J. Adhes.*, **76**, 223 (2001).
48. Busch, K.L., In: *Ion Spectroscopies for Surface Analysis*. Plenum Press, New York, NY, 1991, ch. 3.
49. Powell, C.J., Hercules, D.M. and Czanderna, A.W., In: *Ion Spectroscopies for Surface Analysis*. Plenum Press, New York, NY, 1991, ch. 7.
50. Briggs, D., Brown, A. and Vickerman, J.C., *Handbook of Static Secondary Ion Mass Spectrometry (SIMS)*. John Wiley and Sons, Chichester, 1989.
51. McHugh, J.A., In: Czanderna, A.W. (Ed.), *Methods of Surface Analysis*. Elsevier Scientific Publishing Co., Amsterdam, 1975, ch. 6.
52. Vickerman, J.C., In: Vickerman, J.C., Brown, A. and Reed, N.M. (Eds.), *Secondary Ion Mass Spectrometry: Principals and Applications*. Oxford University Press, Oxford, 1989, ch. 2.
53. Eccles, A.J., In: Vickerman, J.C., Brown, A. and Reed, N.M. (Eds.), *Secondary Ion Mass Spectrometry: Principals and Applications*. Oxford University Press, Oxford, 1989, ch. 4.
54. Abel, M.-L., Digby, R.P., Fletcher, I.W. and Watts, J.F., *Surf. Interface Anal.*, **29**, 115 (2000).
55. Abel, M.-L., Rattana, A. and Watts, J.F., *Langmuir*, **16**, 6510 (2000).
56. Tsai, Y.M., Boerio, F.J., van Ooij, W.J. and Kim, D.K., *J. Adhes.*, **62**, 127 (1997).
57. Fitzpatrick, M.F. and Watts, J.F., *Surf. Interface Anal.*, **27**, 705 (1999).
58. Brewis, D.M., Briggs, D., Dahm, R.H. and Fletcher, I., *Surf. Interface Anal.*, **29**, 572 (2000).

Chapter 7

Surface roughness and adhesion

DAVID E. PACKHAM *

Centre for Materials Research, University of Bath, Claverton Down, Bath, BA2 7AY, UK

1. Introduction

Almost every tube of adhesive to be seen in a hardware store carries the advice “roughen surfaces before applying glue”. The relevance of surface roughness to adhesion has been long recognised. Galileo discussed adhesion to rough surfaces in different terms from that to smooth surfaces [1]. Over 75 years ago when a modern scientific analysis was first applied to the phenomenon of adhesion, McBain and Hopkins considered that there were two kinds of adhesion, specific and mechanical [2]. The former was concerned with adsorption, the latter with porous and rough surfaces. The author has reviewed elsewhere the development of the mechanical theory of adhesion [3–5]: this chapter is concerned more generally with the question of surface roughness and how it is related to adhesion. It seeks to place this subject within a broader account of adhesion, by which observations concerned with the practical strength of adhesive joints are related to theoretical concepts of physics and chemistry.

The chapter then starts with a discussion of surfaces and of how surface energy is defined and related to the fundamental and practical adhesion to ideal smooth surfaces. After some comments on the measurement of surface energies of solids, attention is turned to ways in which surface roughness can be accommodated within this general framework. It is argued that many of the surfaces encountered in adhesion are very rough, and cannot be regarded simply as smooth surfaces with a higher surface area. Indeed some of these surfaces are fractal in nature and so the concept of ‘surface area’ is strictly without meaning. Consideration is given to simple thermodynamic and kinetic principles which enable the extent of penetration of an adhesive into idealised pores of a surface to be gauged.

Attention is then directed towards an examination of literature reports of

* E-mail: d.e.packham@bath.ac.uk

adhesion to rough surfaces. Examples are discussed where the roughness ranges from the macroscopic to the molecular scale. Finally mechanisms by which roughness affects practical adhesion are discussed in terms of its effects on both fundamental and practical adhesion.

2. Surface energy

2.1. Definitions

It is common to regard a surface as a smooth plane dividing two homogeneous phases. Although for many purposes such a model is adequate, it is desirable to remember that it is an *idealisation*. Because of the asymmetry of the intermolecular force field as an interface is approached, the density of molecules in the surface regions differs from that in the bulk. This perturbation, which may extend over many atomic spacings, is a consequence of the system's adjusting to reduce the excess energy associated with an interface. Thus an interface is never sharp: there is always a finite and varying concentration gradient (Fig. 1b, cf. 1a). Further, where a multicomponent phase is concerned, there is in general no reason to suppose that the concentration profile of each component will be the same (Fig. 1c). Some of these features are illustrated in Fig. 2 which gives the structure predicted by atomistic simulation techniques for a calcite (CaCO_3) surface, and shows rotation of surface groups and adsorbed water [6].

The excess energy associated with an interface is formally defined in terms of a surface energy. This may be expressed in terms either of Gibbs, G^E , or Helmholtz, A^H , free energies. In order to circumvent difficulties associated with the unavoidably arbitrary position of the 'surface' plane, the surface energy is defined as the surface excess [7,8], i.e. the excess (per unit area) of the property concerned consequent upon the presence of the surface. Thus Gibbs surface free energy is defined by

$$G^S = \frac{G - G^b}{A} \quad (1)$$

where A is the area of the surface, G is the total value of the Gibbs free energy in the system and G^b is the value the total Gibbs free energy would have if all the constituent particles (atoms, molecules etc.) were in the same state as they are in the bulk of the phase.

A related energy term is γ which is defined as

$$\gamma = \left(\frac{\partial G}{\partial A} \right)_{P, V, n_i} \quad (2)$$

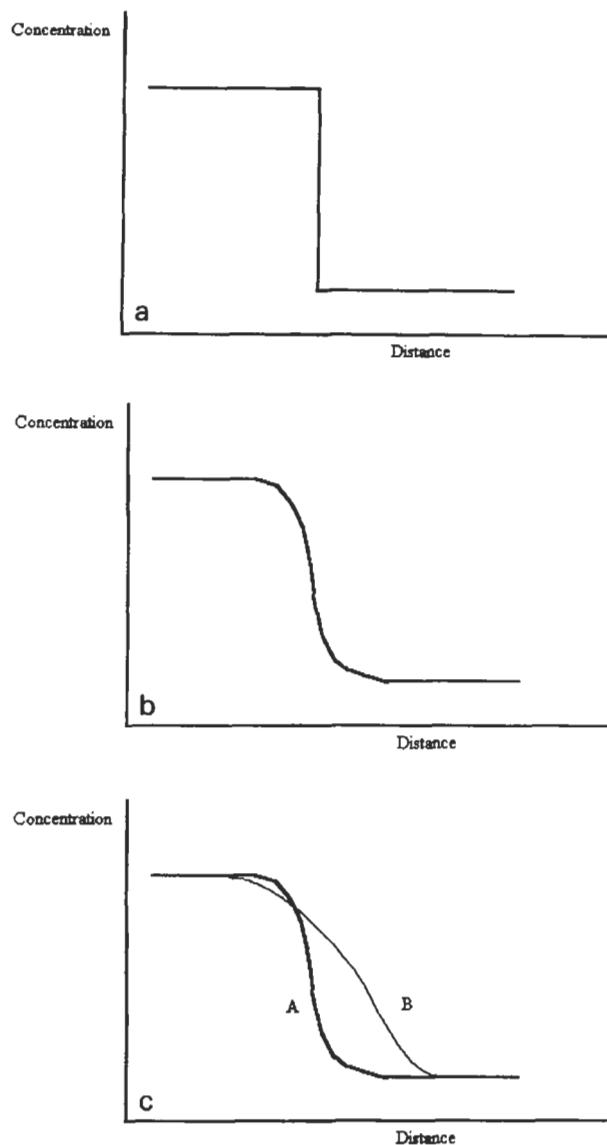


Fig. 1. Concentration profiles at an interface (a) sharp (not realistic), (b) typical profile, (c) with two components A and B.

In most cases γ and G^S are taken as being the same and are both loosely referred to as 'surface energy':

$$G^S = \gamma \quad (3)$$

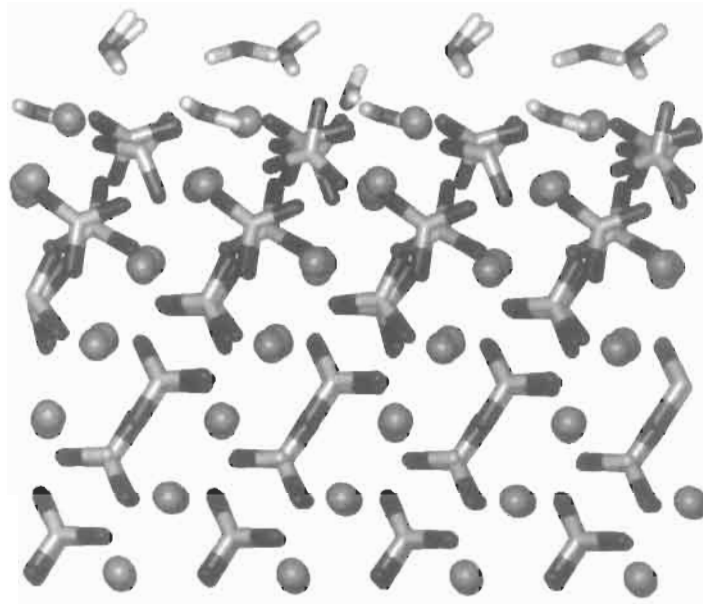


Fig. 2. Fully hydrated calcite $\{10\bar{1}1\}$ surface showing rotation of surface carbonate groups with bulk ordering below (after [6]).

2.2. Surface energy and adhesion

Surface energies are associated with *formation* of the adhesive bond because they determine the extent to which, at equilibrium, a liquid adhesive will come into contact with a solid surface. This is reflected in the value of the contact angle, θ , which is related to the surface energies (written, following common usage, as γ) by Young's equation [9]

$$\gamma_{sv} = \gamma_{sl} + \gamma_v \cos \theta \quad (4)$$

where v refers to the vapour in equilibrium with the solid (s) and liquid (l).

This equation may be derived by considering the small displacement from equilibrium of a sessile drop on a plane surface, Fig. 3. If a small length, w , of the edge of the drop (assumed straight) advances by a distance dx , such that the drop takes up a new contact angle $(\theta - d\theta)$, the energy change will be:

$$dE = \gamma_{sl}w dx - \gamma_{sv}w dx + \gamma_v \cos(\theta - d\theta)w dx \quad (5)$$

Because θ is, *ex hypothesi*, the equilibrium contact angle, dE/dx is zero, giving Eq. 2.

Another useful relationship concerns the energy change (per unit area) when liquid l spreads over the surface of solid s. This is called the spreading coefficient

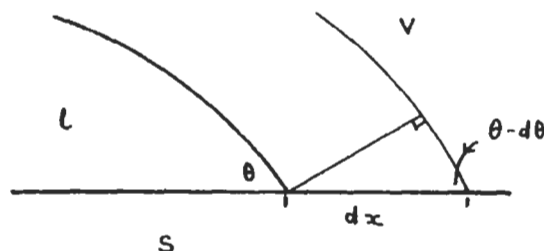


Fig. 3. Sessile drop with equilibrium contact angle θ : displacement of edge a distance dx (s = solid; l = liquid; v = vapour).

Table 1

Contact angle, θ , and spreading coefficient for a liquid on a solid surface; comparison of spreading coefficient S for a smooth surface with S' for a surface of roughness factor r

		Smooth surfaces	Rough surfaces
' $\theta < 0^\circ$ ' ^a	Spontaneous spreading	$S > 0$	$S' > S$
$90^\circ > \theta > 0^\circ$	Finite contact angle	$0 > S/\gamma_v > -1$	$S' > S$
$180^\circ > \theta > 90^\circ$	Finite contact angle	$-1 > S/\gamma_v > -2$	$S' < S$
' $\theta > 180^\circ$ ' ^a	Spontaneous dewetting	$S/\gamma_v < -2$	$S' < S$

^a The quotation marks are used because strictly $0^\circ < \theta < 180^\circ$.

or spreading energy, S , [9] and is necessarily related to the surface energies:

$$S = \gamma_{sv} - \gamma_{sl} - \gamma_v \quad (6)$$

Eqs. 4 and 6 enable the extent of contact between a liquid adhesive and a solid substrate to be gauged. Some consequences are shown in Table 1 where the concept of the 'reduced spreading coefficient' S/γ_v , employed by Padday [10], was used to clarify the situation. As is readily seen, if S is positive, the liquid at equilibrium will be spread completely over the solid, but if S/γ_v is less than -2 , spontaneous dewetting will occur.

Surface energies are also associated with *failure* of an adhesive bond, because failure involves forming new surfaces and the appropriate surface energies have to be provided. The surface energy term may be the work of adhesion, W_A , or the work of cohesion, W_{coh} , depending on whether the failure is adhesive or cohesive. For phases 1 and 2, these are defined as follows [10]:

$$W_A = \gamma_1 + \gamma_2 - \gamma_{12} \quad (7)$$

$$W_{coh} = 2\gamma_1 \quad (8)$$

The practical adhesion, for example fracture energy Γ , will comprise a surface energy term Γ_0 (W_A or W_{coh}) to which must be added a term ψ representing other

energy absorbing processes — for example plastic deformation — which occur during fracture:

$$\Gamma = \Gamma_0 + \psi \quad (9)$$

Usually ψ is very much larger than Γ_0 . This is why practical fracture energies for adhesive joints are almost always orders of magnitude greater than works of adhesion or cohesion. However, a modest increase in Γ_0 may result in a large increase in adhesion as ψ and Γ_0 are usually coupled. For some mechanically simple systems where ψ is largely associated with viscoelastic loss, a multiplicative relation has been found:

$$\Gamma = \Gamma_0\{1 + \phi(c, T)\} \approx \Gamma_0 \times \phi(c, T) \quad (10)$$

where $\phi(c, T)$ is a temperature- and rate-dependent viscoelastic term [11,12]. In simple terms, stronger bonds (increased Γ_0) may lead to much larger increases in fracture energy because they allow much more bulk energy dissipation (increased ψ) during fracture.

2.3. Surface energy measurement

Before equations such as Eqs. 6, 7 and 8 can be used, values for the surface energies have to be obtained. While surface energies of liquids may be measured relatively easily by methods such as the du Nouy ring and Wilhelmy plate, those of solids present more problems. Three approaches will be briefly described. Two involve probing the solid surface with a liquid or a gas, the third relies on very sensitive measurement of the force required to separate two surfaces of defined geometry. All involve applying judicious assumptions to the experimental results.

2.3.1. Contact angles

Many of the most widely used methods are based on measuring the contact angles of a series of test liquids on the solid surface, and evaluating the surface energies via Young's equation, Eq. 4 above.

The surface energy of the solid γ_s can be obtained from equilibrium contact angle measurements of a series of test liquids on the solid surface, providing the relationship between γ_{sl} and the solid γ_s (in vacuo) and liquid γ_l surface energies is known. The exact relationship is given by the Good and Girifalco equation [13,14]:

$$\gamma_{sl} = \gamma_s + \gamma_l - 2\phi\sqrt{\gamma_s\gamma_l} \quad (11)$$

$$\gamma_s - \gamma_{sv} = \pi_e \quad (12)$$

where ϕ is the Good–Girifalco interaction parameter and π_e is called the spreading pressure. The spreading pressure is difficult to measure, and it is common to

neglect it. This may be justifiable for a non-polar solid (e.g. an alkane), but is difficult to justify where a high surface energy solid is involved. In principle the solid surface energy is calculated by eliminating γ_{sl} between Eqs. 4 and 11 giving:

$$\gamma_v(1 + \cos \theta) = 2\phi\sqrt{(\gamma_s\gamma_v)} \quad (13)$$

The difficulty with Eq. 13 is that ϕ is not generally known. Over past decades enormous intellectual effort has been put into devising ways of circumventing the problem of not knowing ϕ , and much controversy has been generated in the process. Three of the resulting relationships are:

$$\gamma_v(1 + \cos \theta) = 2\sqrt{(\gamma_s^d\gamma_v^d)} + 2\sqrt{(\gamma_s^p\gamma_v^p)} \quad (14)$$

$$\gamma_v(1 + \cos \theta) = 4\frac{\gamma_s^d\gamma_v^d}{\gamma_s^d + \gamma_v^d} + 4\frac{\gamma_s^p\gamma_v^p}{\gamma_s^p + \gamma_v^p} \quad (15)$$

$$\gamma_v(1 + \cos \theta) = 2\sqrt{(\gamma_s^{LW}\gamma_v^{LW})} + 2\sqrt{(\gamma_s^+\gamma_v^+)} + 2\sqrt{(\gamma_s^-\gamma_v^-)} \quad (16)$$

The first was proposed by Owens and Wendt [15] and Kaelble and Uy [16], the last two by Wu [17] and by Good and van Oss [18], respectively. All imply that the spreading pressure may be neglected.

These equations result from assuming that the total surface energy can be split into the sum of components associated with different types of bonding, for example dispersion γ^d plus polar γ^p (Eqs. 14 and 15), or Lifshitz–van der Waals γ^{LW} plus acid–base γ^{AB} (Eq. 16). The γ^+ and γ^- terms are respectively the Lewis acid and Lewis base component of surface interaction. The acid–base component γ^{AB} is given by:

$$\gamma^{AB} = 2\sqrt{(\gamma^+\gamma^-)} \quad (17)$$

2.3.2. Gas adsorption

The adsorption of gas onto a solid surface can also be used to estimate surface energy. Both inverse gas chromatography (IGC) and isotherm measurement using the BET method [19] have been used. Further discussion and detailed references are given by Lucic et al. [20] who compare the application of IGC, BET and contact angle methods for characterising the surface energies of stearate-coated calcium carbonate fillers.

2.3.3. Surface forces apparatus

An alternative approach to measuring surface energies is provided by the surface forces apparatus, SFA [21]. The apparatus uses surfaces of defined geometry, such

as crossed cylinders of molecularly smooth, cleaved mica, between which forces may be measured with a sensitivity of 10^{-8} N (10^{-6} gf). The basic experiment by which the surface forces apparatus is used to deduce surface energy values involves bringing the two surfaces concerned into contact and observing either the load necessary to cause them to separate, or the relationship between the radius of the contact zone and the applied load.

The results are most commonly analysed by the Johnson, Kendall and Roberts (JKR) equation [22]. For two elastic spheres, of radii R_1 and R_2 , in contact this takes the form:

$$a^3 = \left[F + 3\pi R W_{12} + \sqrt{6\pi R W_{12} F + (3\pi R W_{12})^2} \right] R / K \quad (18)$$

where a is the radius of the area of contact, $R = R_1 R_2 / (R_1 + R_2)$, F is the normal load, K is an elastic constant. The term W_{12} is a surface energy term which is obtained via Eq. 18 from a plot of a^3 vs. load F . If it is assumed that the spreading pressure is zero (Eq. 12), surface energy term W_{12} may be interpreted as the work of adhesion (Eq. 7) where surfaces 1 and 2 are different, and work of cohesion (Eq. 8) where they are the same. However, assertions that the JKR surface energy is a 'true' thermodynamic quantity should not be accepted uncritically [23].

An issue, at present unresolved, is that Derjaguin, Muller and Toporov [24,25] have put forward a different analysis of the contact mechanics from JKR. Maugis has described a theory which comprehends both the theories as special cases [26].

3. Roughness of surfaces

We have seen how the concept of surface energy in principle relates to adhesion. The surface energy terms discussed (e.g. Eqs. 1–8) are all energies per unit area. We now need to consider carefully what we mean by the interfacial area.

If the interface between phases 1 and 2 is 'perfectly' flat, there is no problem in defining the interfacial area, A . However, this chapter is particularly concerned with rough surfaces: indeed almost all practical surfaces of are to a degree rough. We first consider modest degrees of roughness, where a simple geometric factor may be applied. It is argued, however, that the complexity of many rough surfaces makes them different in kind from a flat surface. Ultimately the ascription of a numerical value to quantify roughness itself may be arbitrary, depending on the size of the probe chosen to measure it. It is concluded that the only practicable interpretation of 'unit area' is the nominal geometric area. The consequence is that the production of a rough surface per se increases surface energy (Eq. 1), and from this, work of adhesion and fracture energy of the joint (Eqs. 7 and 10).

3.1. Roughness factor

Where the surface roughness is not very great it might be adequately expressed by a simple Wenzel roughness factor [27,28],

$$r = \frac{A}{A_0} \quad (19)$$

where A is the 'true' surface area, A_0 the nominal area. For simple ideal surfaces, r can be calculated from elementary geometric formulae. Thus a surface consisting of a hemisphere would have a roughness factor of 2, one consisting of square pyramids with all sides of equal length, a roughness factor of $\sqrt{3}$. For simple real surfaces the roughness factor can be calculated from straight forward measurements, such as profilometry. In such cases we could substitute a corrected area into the definition of surface energy (Eq. 1) and thence via Eqs. 3 and 4 evaluate the spreading coefficient and work of adhesion. Thus the spreading coefficient S' for a rough surface becomes:

$$S' = r(\gamma_{sv} - \gamma_{sl}) - \gamma_{lv} \quad (20)$$

Some of the effects of roughness on the spreading of a liquid may be predicted from Eqs. 4, 6 and 20, providing the liquid does not trap air as it moves over the surface. These are summarised in Table 1.

It is important to appreciate the assumption implicit in the concept of roughness factor: chemical nature and local environment of surface molecules on the rough surface and on smooth surface are the same.

3.2. Further conceptual development

Can the simple roughness factor approach (Eq. 19) be applied if the surface is very much rougher? Many of the surfaces encountered in adhesion technology are very rough indeed. Consider Fig. 4a which shows a microfibrinous oxide on copper [29] and the dendritic zinc surface [30] in Fig. 4b. As the scale of roughness becomes finer, the application of a simple roughness factor becomes increasingly unrealistic and unconvincing. It becomes unconvincing not just because of increasing practical difficulty in measuring the 'true' area of such surfaces, it becomes conceptually unconvincing. The roughness itself is an essential characteristic of the surfaces. As we approach molecular scale roughness, indeed long before we get there, the energy of the surface molecules is modified as a consequence of the topological configurations they take up. It is unjustifiable to regard these surfaces as essentially the same as smooth surfaces which happen to be rough!

Moreover, roughness at an interface may actually develop as a result of bringing the two phases together. They will take up these configurations as a consequence of the molecular interactions at the interface: they are an essential feature of

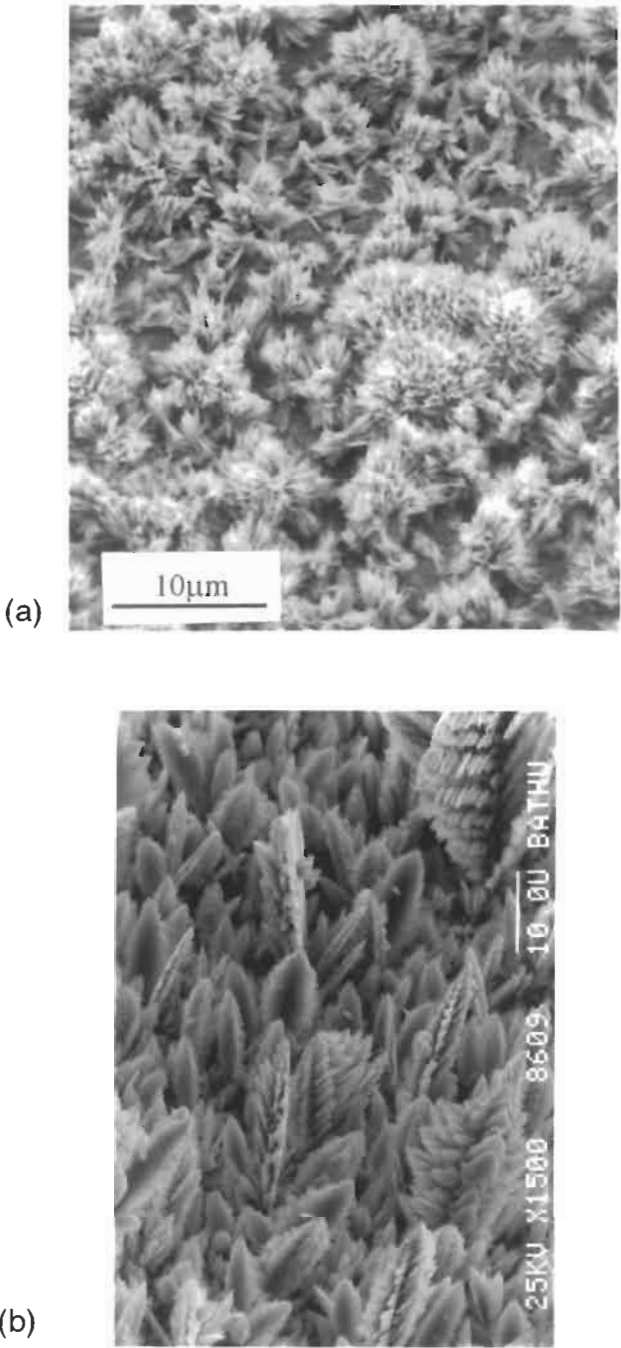


Fig. 4. Examples of rough surfaces pretreated for adhesive bonding: (a) microfibrinous oxide on copper (cf. [29]); (b) a dendritic zinc surface (cf. [30]).

bringing together the two phases 1 and 2. Such roughening can be seen as an increasing of the low surface entropy implied by a smooth surface [24,31–33].

3.2.1. Fractal surfaces

It may not be possible, even in principle, to ascribe an unique ‘surface area’ to a surface. It has long been recognised from work on gas adsorption on porous solids (e.g. using the BET technique) that the surface area measured depends on the size of the probe molecule. A smaller probe can enter finer surface features and therefore may give a larger value. The surface area is, as Rideal [34] recognised in 1930, in a sense arbitrary, not absolute. More recently, evidence has been produced suggesting that many engineering surfaces and many fracture surfaces are fractal in nature [35,36]. For a fractal surface, the area depends on the size of the ‘tile’ used to measure it, the actual relationship depending on the fractal dimension of the surface. The area of such a surface tends to infinity as the tile size tends to zero.

The concept of fractals has often been illustrated by considering the ‘length’ of a coastline. The perimeter of Britain (say), measured from a map in an atlas will be much shorter than that taken from a series of large-scale hiking maps which reveal much finer detail of the various coves and inlets. With the large-scale map a much shorter measuring rod is in effect being used. The process can, in principle, be repeated indefinitely. Using a large scale architects’ plan, a smaller rod size would be appropriate; an observer on the ground might use a 12-inch school ruler, or even a magnifying glass allowing a rod size of less than a millimetre. So how long is the coastline of Britain? In terms of fractal geometry, the answer is that it is indeterminate: the length depends on the size of the rod used, the length tending to infinity as the rod size tends to zero.

The situation for a fractal surface is analogous to that for a fractal line. The rod is replaced by a ‘measuring tile’. As magnification increases, more and more surface features are revealed and so the apparent surface area increases. A cauliflower provides a mundane example of a fractal surface, and, as was pointed out above, many engineering surfaces are fractal in nature: their surface area tends to infinity as the tile size tends to zero.

3.3. Roughness factor for a fractal surface

The roughness factor may be calculated for a fractal surface. As demonstrated below, its value varies according to the probe size and the fractal dimension.

Consider the adsorption of probe molecules of various sizes ¹ (cross-sectional

¹ σ must be in dimensionless form, as a ratio to some large, fixed area, such as the sample area.

area σ) on a fractal surface [37,38]. Let n be the number of molecules required to form a monolayer. If $\log n(\sigma)$ is plotted against $\log \sigma$, a straight line with negative slope is obtained which can be represented as:

$$\log n(\sigma) = (-D/2)\log \sigma + C \quad (21)$$

where D is the fractal dimension of the surface and C is a constant.

$$\therefore n(\sigma) = \beta \sigma^{-D/2} \quad (22)$$

where β is another constant. (For an ideal plane surface ($D = 2$), this equation reduces to the trivial relationship that the number of probes required to cover a given surface is inversely proportional to the probe area.)

The area (in dimensionless form) can be expressed as:

$$A = n(\sigma)\sigma \quad (23)$$

$$\therefore A(\sigma) = \beta \sigma^{1-D/2} \quad (24)$$

Consider the roughness factor, r (Eq. 19), for such a fractal surface:

$$r = \frac{A}{A_0}$$

where A is the 'true' surface area, A_0 the nominal area, i.e. the area of a plane surface. For a plane surface $D = 2$, so:

$$r = \frac{A}{A_0} = \frac{\beta \sigma^{1-D/2}}{\beta} = \sigma^{1-D/2} \quad (25)$$

For a fractal surface $D > 2$, and usually $D < 3$. In simple terms the larger D , the rougher the surface. The intuitive concept of surface area has no meaning when applied to a fractal surface. An 'area' can be computed, but its value depends on both the fractal dimension and the size of the probe used to measure it. The area of such a surface tends to infinity, as the probe size tends to zero.

Obviously the roughness factor is similarly arbitrary, but it is of interest to use Eq. 25 to compute its value for some trial values of D and σ . This is done in Table 2. In order to map the surface features even crudely, the probe needs to be small. It can be seen that high apparent roughness factors are readily obtained once the fractal dimension exceeds 2, its value for an ideal plane.

The roughness factor concept may be useful for surfaces which exhibit modest departures from flatness. Beyond this, it is misleading as changes in the local molecular environment make the rough surface qualitatively different from a flat one. In many cases it is not meaningful to talk of *the* area of a rough surface as if it had, in principle, a unique value. What area, then, should be used for a rough surface in the context of surface energy and work of adhesion, Eqs. 1 to 10? It seems inescapable when we refer to the surface area A that we must use the ideal,

Table 2

'Roughness factor' calculated for a fractal surface, according to the fractal dimension D and probe area σ

D	Roughness factor for $\sigma =$			
	10^{-4}	10^{-8}	10^{-12}	10^{-18}
2	1	1	1	1
2.1	1.6	2.5	4	7.9
2.5	10	100	1,000	32,000
2.8	40	1,600	63,000	16,000,000

formal area, i.e. macroscopic area of the interface. This has important implications for the effect of surface roughness on adhesive joint strength. The production of a rough surface per se increases surface energy (per unit nominal area, Eq. 1), and consequently increases the work of adhesion and fracture energy of the joint (Eqs. 7 and 10).

4. Surface roughness and wetting

In Section 2.2 relationships between surface energies, wetting and adhesion were explored in the context of smooth surfaces. This was followed above (in Section 3) by a discussion of some characteristics of rough surfaces. It is now appropriate to link these two topics by considering how substrate roughness affects the wetting by an adhesive. Attention will first be focused on the effect on contact angles, and will then move to consider the penetration of an adhesive into pores on a rough surface. Both thermodynamic and kinetic aspects of this problem will be considered as it is always possible that an adhesive will set before equilibrium penetration has been achieved.

4.1. Contact angles on rough surfaces

As was shown above (Section 2.2, Eq. 5), Young's equation (Eq. 4) may be derived by considering the small displacement from equilibrium of a sessile drop on a plane surface. If the same derivation is applied to the situation where the solid surface has a roughness factor (Eq. 19) of r , it is readily seen that Eq. 5 becomes [28]

$$dE = [\gamma_{sl}w \, dx - \gamma_{sv}w \, dx]r + \gamma_{lv} \cos(\theta - d\theta)w \, dx \quad (26)$$

from which it follows that

$$\cos \theta_{\text{rough}} = r \cos \theta_{\text{smooth}} \quad (27)$$

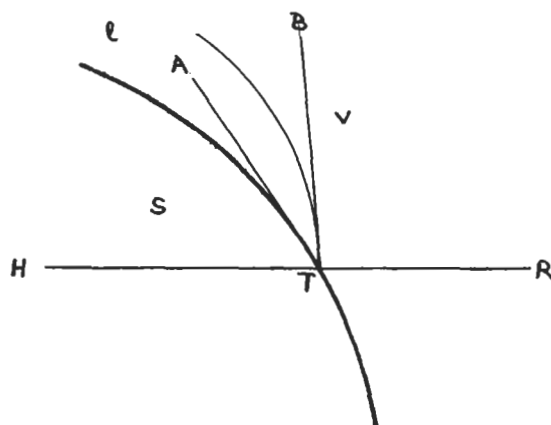


Fig. 5. Sessile drop on a rough surface: 'true' contact angle BTA and apparent contact angle BTH. Thick curve = surface of solid (s); thin curve = surface of liquid (l); v = vapour. T is the triple point; HTR a horizontal; AT a tangent to the solid surface; BT a tangent to the liquid surface.

This much-quoted equation immediately suggests that

if $\theta_{\text{smooth}} < \pi/2$ then $\theta_{\text{rough}} < \theta_{\text{smooth}}$

but if $\theta_{\text{smooth}} > \pi/2$ then $\theta_{\text{rough}} > \theta_{\text{smooth}}$

There would seem to be some problems with Eq. 27 and the predictions which stem from it. First, θ_{rough} is treated as an equilibrium angle, yet the observed contact angle on a rough surface is related to an assumed horizontal. It would be expected that the equilibrium value would be manifest at the edge of the drop between the local gradient of the rough surface and the surface of the liquid (Fig. 5). Moreover the derivation of Eq. 27 relies on examining the limit of Eq. 26 as x tends to zero. Eq. 27 is only obtained with the assumption that the roughness factor, r , remains constant, i.e. is independent of x . This is conceptually flawed because for Eq. 19, defining the roughness factor, to be valid, the area A must be sufficiently large for the roughness within it to be typical of the surface as a whole.

As long as the liquid actually wets the rough surface, a less contentious approach linking the roughness factor to the extent of contact would seem to be via the spreading coefficient as shown in Eq. 20 and summarised in Table 1. If air is trapped within pits by the liquid, a composite surface is produced.

Cassie [39] extended Wenzel's treatment to composite surfaces. His treatment can be applied to a rough surface incompletely wetted by a liquid so that it consists of an area fraction f_1 wetted and f_2 unwetted surface. Then:

$$\cos\theta_{\text{rough}} = rf_1 \cos\theta_{\text{smooth}} - f_2 \quad (28)$$

where r is the roughness factor. $\theta_{\text{rough}} > \theta_{\text{smooth}}$ unless the roughness factor is

relatively large. The two contact angles are obviously equal where:

$$\cos\theta = f_2/(rf_1 - 1) \quad (29)$$

4.2. Equilibrium penetration into pores

If the contact angle is known, insight into the extent of wetting to be expected at equilibrium can be obtained from calculations for idealised rough surfaces. The conclusions may require modification when kinetic effects, such as setting of the adhesive, are taken into account.

Consider first penetration into a cylindrical pore. An estimate of the extent of penetration can be obtained by equating the back pressure of trapped air to the capillary driving pressure. Then the distance x penetrated into a pore of length l and radius r is then:

$$x = l(1 - \{P_a r / [2\gamma_v \cos\theta + P_a r]\}) \quad (30)$$

where P_a is atmospheric pressure and γ_v and θ respectively the surface energy and contact angle of the adhesive. Clearly the smaller the pore the greater the proportion of its length filled at equilibrium [40].

De Bruyne [41] has applied the same principles to other idealised shapes for pores. As would be expected, penetration into a re-entrant 'ink bottle' pore is much less than for cylinders (Fig. 6). The critical importance of contact angle in determining the extent of penetration should be noted.

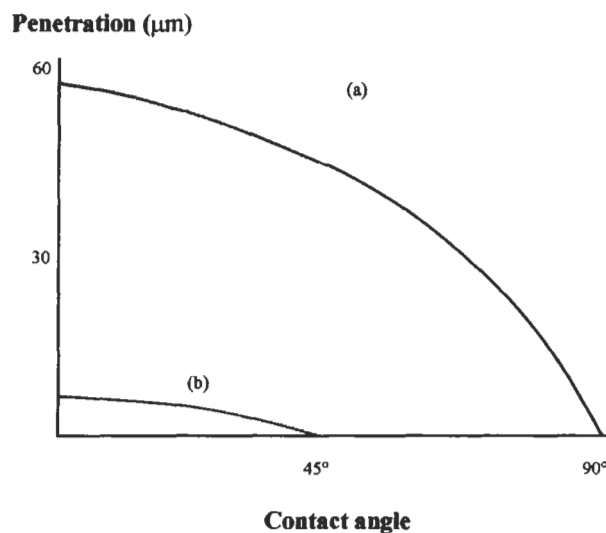


Fig. 6. Penetration of a liquid into (a) a cylindrical and (b) a re-entrant pit (after de Bruyne [41]). Pit depth 100 μm, diameter at mouth 1 μm, re-entrant angle 45°.

4.3. Kinetics of pore penetration

The discussion above assumes that equilibrium contact between liquid adhesive and rough substrate is achieved. However, adhesives set in what may be quite a short time, and so may never reach equilibrium contact. It is therefore relevant to consider the kinetics of penetration of the adhesive into a pore.

A simple starting point for such a discussion is Poiseuille's law [42] for the flow of a Newtonian liquid of viscosity η in a tube of radius r under the influence of a pressure P :

$$x \frac{dx}{dt} = \frac{r^2 P}{8\eta} \quad (31)$$

If the driving pressure is taken to be the capillary pressure, $2\gamma_v \cos \theta / r$, Eq. 23 may be integrated, assuming θ and η are constant to give the Washburn equation [43] which shows the penetration x_t is proportional to the square root of time:

$$x_t^2 = r \gamma_v \cos \theta \frac{t}{2\eta} \quad (32)$$

4.3.1. Increased of viscosity with time

The viscosity of most adhesives increases with time as they set by cross-linking, cooling from the melt or loss of solvent. The cross-linking of a phenolic-polyvinyl formal adhesive and of cold-setting epoxies was found by de Bruyne [41] to be represented adequately by an exponential relationship:

$$\eta = \eta_0 e^{bt} \quad (33)$$

Thus he modified Poiseuille's equation (Eq. 23) to describe the penetration of such a liquid into a closed pore of length L :

$$x \frac{dx}{dt} = r^2 e^{-bt} \frac{P_1 - P_a L / (L - x)}{8\eta_0} \quad (34)$$

P_1 is the driving pressure and the second term in the brackets represents the back pressure of trapped air. The back pressure can be neglected when the driving pressure is appreciable. With this simplification, integration of Eq. 28 gives the limiting distance of penetration x_{\max} as

$$x_{\max} = \frac{r}{2} \sqrt{\frac{P_1}{\eta_0 b}} \quad (35)$$

With typical values of $\eta_0 = 6 \times 10^4 \text{ N s/m}^2$ and $b = 0.01 \text{ s}^{-1}$, penetration will be about ten diameters under a driving pressure of 1 N/mm^2 (ca. 10 atmospheres). With a higher initial viscosity of $6 \times 10^5 \text{ N s/m}^2$ — perhaps as a result of delay in applying the same adhesive — penetration would only be 3.2 diameters.

5. Roughness and adhesion: a résumé

A principal aim of the discussion thus far has been to set out a theoretical framework within which it is possible to rationalise the effects of surface roughness on adhesion. It may be useful to summarise this framework before examining practical examples taken from the literature.

Clearly contact between adhesive and substrate is essential for the *formation* of an adhesive bond. The values of surface energy of the components determine the extent of contact which may be judged through such quantities as contact angle and spreading coefficient (Eqs. 4 and 6 and Table 1). Low contact angle and high spreading coefficient favour bond formation.

Surface energies are again important in determining the practical adhesion, Γ , in the *breaking* of an adhesive bond. Eqs. 7 to 10 show how the two are related. Emphasis was placed on the important contribution to fracture energy of ψ , which represents energy absorbing processes other than those (W_A and W_{coh}) directly associated with the actual formation of new surfaces. It must be remembered that ψ is often linked to the surface energy terms (Eq. 10).

Where a substrate surface is *rough*, contact with the adhesive may be inhibited. Both thermodynamic (equilibrium) and kinetic principles have to be considered. The discussion given of pore penetration is in terms of empirical or simplified relationships, did serve to give an indication of the influence of relevant factors, and enables rough calculations at least to be made. Clearly good penetration of an adhesive into the interstices of a rough surface is favoured by a low viscosity, a long setting time, and, of particular importance, low contact angle. Roughness may seriously limit the extent of contact, but this is not necessarily so. Under favourable circumstances good penetration of the adhesive should be achieved into the topographical features of the substrate surface.

If contact with a rough surface is *poor*, whether as a result of thermodynamic or kinetic factors, voids at the interface are likely to mean that practical adhesion is low. Voids can act as stress concentrators which, especially with a brittle adhesive, lead to low energy dissipation, ψ , and low fracture energy, Γ . However, it must be recognised that there are circumstances where the stress concentrations resulting from interfacial voids can lead to enhanced plastic deformation of a ductile adhesive and increase fracture energy by an increase in ψ [44].

Under other circumstances, surface roughness can lead to increased spreading coefficient and thus to *good* contact. The rough surface essentially increases the work of adhesion and thus (Eq. 10) the fracture energy of the joint. With very rough surfaces, very high values of work of adhesion are predicted; indeed with fractal surfaces, the value will tend to infinity! A very high work of adhesion will often mean that the bond fails cohesively within the polymeric adhesive. So long as the polymer is tough (high ψ), high practical adhesion can result from a rough substrate surface.

6. Surface roughness and joint strength

In this section some examples will be discussed where surface roughness has an influence on adhesion. It is very difficult indeed to alter the topography of a surface without altering its surface chemistry in some way. Conversely, many surface treatments which are seen as primarily changing the surface chemistry of a substrate will also bring about topographical changes. Thus it is difficult — and probably ultimately futile — to try to draw an absolute line between ‘chemical’ and ‘mechanical’ effects in adhesion. Nevertheless there are cases where roughness can be said with some confidence to exert a decisive effect. The scale of roughness involved may range from the macro- down to the molecular scale. As previously discussed, there are many cases where the roughening of a substrate leads to poor adhesion, often because of inhibiting wetting. Generally of more interest are examples where roughness is associated with some unambiguously desired effect, such as enhanced strength or durability in a hostile environment. It is mostly examples of this latter category which have been chosen for discussion below.

6.1. Metal deposition onto polymers: microfibrinous metal surfaces

The important beneficial effects that substrate roughness can bring were firmly established in the late sixties and early seventies, principally as a result of work in two areas. The first was associated with the electroless deposition of metals onto plastics such as ABS and polypropylene. In the process the plastics must be etched in a way which produces pits on a micrometre scale. Such a topography had been shown to be a necessary, but not sufficient condition for adequate adhesion [40].

The second category was concerned with adhesion to porous or microfibrinous surfaces on metals. Aluminium may be anodised to form an oxide surface comprising pores of diameter of tens of nanometers. Electroforming and chemical oxidation can be used to produce microfibrinous or needle-like coatings on metals, including copper, steel and titanium. The substrate topography was demonstrated to play an vital part in adhesion to these surfaces [45–48].

The increasing need of the aerospace industry for strong, consistent and durable adhesive bonds was among the factors that stimulated considerable development of pore-forming surface treatments for aluminium and titanium. The American aerospace companies were particularly active in this field [49–57]. The broad consensus of work published during the late seventies and into the early years of the eighties is that strong bonds, and more particularly bonds of high durability, tend to be associated with a highly porous surface oxide, providing, of course, that the values of viscosity and surface tension of the adhesive are such as to allow it to penetrate the pores (see discussion in Sections 4.2 and 4.3 above). The importance of porosity was brought out strongly in a 1984 review by Venables

[58]. He concluded that for aluminium and titanium: "certain etching or anodization pretreatment processes produce oxide films on the metal surfaces, which because of their porosity and microscopic roughness, mechanically interlock with the polymer forming much stronger bonds than if the surface were smooth".

Much work since this period [4] has reinforced the importance of surface topography in these areas of adhesion. Two recent examples will be cited.

The electroless deposition of copper onto an inorganic rather than a polymer surface was investigated by Sun et al. [59]. They used spray pyrolysis to deposit thin zinc oxide films of different morphologies on glass surfaces, and then deposited the copper. The adhesion of the copper was greatly affected by the zinc oxide morphology, greatest adhesion being obtained with a rough, porous structure comprising balls about 0.6 μm in diameter between which the copper penetrated, giving a strong mechanical anchoring effect.

Microporous and microfibrinous surfaces on metals are increasingly used in biomedical applications. A recent review by Wen et al. [60] identified advantages over metals with smooth surfaces which included early better adhesion of biomolecules and cells and firmer fixation of bone or connective tissue.

6.2. Some macroscale effects

In recent years there has been a renewed appreciation of potential beneficial effects of roughness on a macroscale. For example Morris and Shanahan worked with sintered steel substrates bonded with a polyurethane adhesive [61]. They observed much higher fracture energy for joints with sintered steel compared with those with fully dense steel, and ascribed this to the mechanical interlocking of polymer within the pores. Extra energy was required to extend and break these polymer fibrils.

Plasma spraying [62] provides a method of producing a porous surface layer without the use of chemical solutions. The porosity is much coarser than that associated with anodising, being of the order of micrometres rather than tens of nanometres. Clearfield et al. [63] at Martin Marietta Laboratories compared anodising treatments for titanium alloy [Ti-6Al-4V] with plasma-sprayed coating of the alloy. Durability results showed comparable performance. Alumina powder has been used on aluminium, titanium and steel [64]. More recent work from Martin Marietta by Davis et al. have reported on the potential of plasma-sprayed coating as pretreatments for aluminium and titanium [65,66]. The best performance on aluminium which they report is for a 40- μm -thick coating of aluminium-silicon alloy mixed with polyester.

Janarthanan et al. [67] have employed roughness on a micron scale to enhance the adhesion between two immiscible polymers, polycarbonate and styrene-acrylonitrile copolymer, SAN. Grooves of depths between 5 and 35 μm were scribed in the polycarbonate surface before laminating the two polymers. The

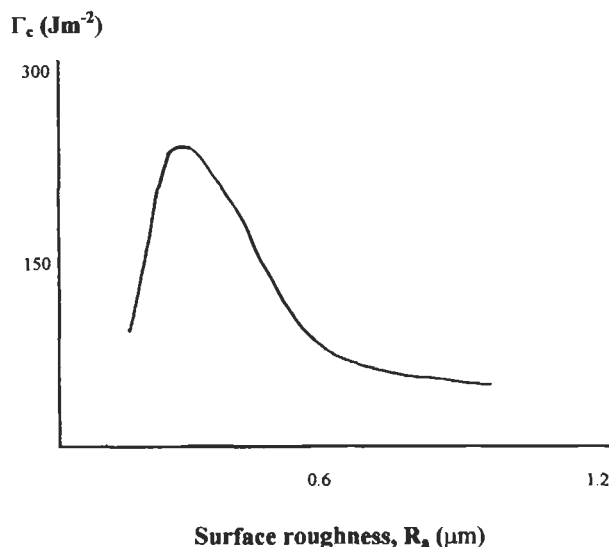


Fig. 7. Adhesion (critical energy release rate, Γ_c) of zinc coatings to steel substrates: effect of steel surface roughness (after Ye et al. [68]).

fracture toughness of the laminate, which was determined using a double cantilever beam test specimen, increased from 8 J/m^2 for the ungrooved specimen to 170 J/m^2 for the specimen with $35 \mu\text{m}$ grooves. The crack propagated by a stick-slip mechanism, slowing considerably at each groove. The increased toughness was associated with extensive deformation of both polymers in the vicinity of the grooves.

Ye et al. [68] identified substrate topography as a crucial parameter in their study of the adhesion of zinc coatings electrodeposited onto steel substrates. The steel surfaces were mechanically polished to give different degrees of roughness. The adhesion passed through a maximum with a surface roughness (R_a) of about $0.3 \mu\text{m}$ (Fig. 7). They argued that the surface profile was of more significance than the roughness value per se, as the $0.3 \mu\text{m}$ surface provided the maximum density of interlocking sites.

6.3. Results for fractal surfaces

The seemingly simple question of the relation the characteristics of a mechanically prepared metal surface and adhesion to that surface has sporadically occupied attention for many decades without any very general conclusion being reached [69]. In some recent work, Amada et al. [70,71] grit-blasted a steel substrate, varying the angle between the gun and the specimen surface, and measured the adhesion of a plasma-sprayed alumina coating. They examined profiles of the

grit-blasted surfaces and argued that their form was that of a self-affine fractal of dimension which depended on the blasting angle. The highest fractal dimension (1.07) is reported to correspond with the blasting angle which gave maximum adhesion. The fractal dimension correlated better with adhesion than did surface roughness measurements. It may be doubted whether this is the last word on this complex subject.

Wool [32] has considered the fractal nature of polymer-metal and of polymer-polymer surfaces. He argues that diffusion processes often lead to fractal interfaces. Although the concentration profile varies smoothly with the dimension of depth, the interface, considered in two or three dimensions is extremely rough [72]. Theoretical predictions, supported by practical measurements, suggest that the two-dimensional profile through such a surface is a self-similar fractal, that is one which appears similar at all scales of magnification. Interfaces of this kind can occur in polymer-polymer and in polymer-metal systems.

Polymer-polymer fractal interfaces may result from the interdiffusion of monomers or of polymers themselves. Koizumi et al. [31] annealed the interface between polystyrene and a styrene-isoprene diblock polymer at 150°C and showed extensive roughening of the interface by mutual interdiffusion on a micron scale (Fig. 8).

Polymer-metal fractal interfaces may result from processes such as vacuum deposition and chemical vapour deposition where metal atoms can diffuse con-

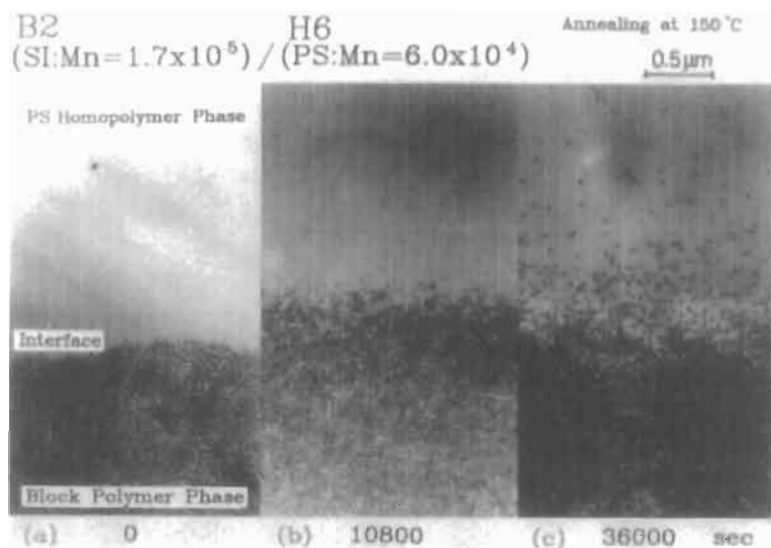


Fig. 8. Electron micrographs showing the interface between polystyrene (top) and a styrene-isoprene diblock polymer (bottom), annealed at 150°C for the times shown. Isoprene units are stained and appear black) (reproduced from [31], copyright American Chemical Society).

siderable distances into the polymer. Mazur et al. [73,74] electrodeposited silver within a polyimide film. The silver(I) solution was able to diffuse into the polymer film where it was subsequently reduced to the metal. The adhesion was excellent: the only way that Mazur could remove the silver was by abrasion. Examination of a section through the interface by transmission electron microscopy shows an extremely rough interfacial region on sub-micron scale. Wool [32] analysed the profile and showed the interface to be fractal with a dimension of around 1.6.

6.4. Development roughness on a nanoscale

Most polymer pairs are thermodynamically incompatible, in the sense that their free energy of mixing is positive. This does not mean that there is absolutely no interdiffusion at all at the interface between them: adjacent to the interface limited interdiffusion occurs, which can be seen as an increasing of the low surface entropy implied by a smooth surface [30–33]. This nanoscale roughening of an interface can increase the adhesion between the polymers.

Helfand and Tagami [75,76] introduced a model which considered the probability that a chain of polymer 1 has diffused a given distance into polymer 2 when the interactions are characterised by the Flory–Huggins interaction parameter χ . They predicted that at equilibrium the ‘thickness’, d_∞ , of the interface would depend upon the interaction parameter and the mean statistical segment length, b , as follows:

$$d_\infty = \frac{2b}{(6\chi)^{1/2}} \quad (36)$$

They further suggest that the thickness is related to the interfacial tension, γ , and the mean density in terms of number of monomer units per unit volume, ρ_o , thus:

$$d_\infty = \frac{b^2 \rho_o k T}{3\gamma} \quad (37)$$

where k is Boltzmann’s constant and T absolute temperature.

Intuitively the toughness of an interface would be expected to be related to the depth of interpenetration of the chains. Wool [32] argues that the fracture energy, Γ , for chain disentanglement at least, is proportional to the square of the interface thickness, which, via Eqs. 36 and 37, gives:

$$\Gamma \propto d_\infty^2 \propto \frac{1}{\chi} \propto \left(\frac{T}{\gamma}\right)^2 \quad (38)$$

Godail and Packham [77,78] have applied these ideas to the adhesion of ethylene–octene copolymers laminated to polypropylene. Variations in adhesion energy found with different laminating temperatures were interpreted in terms of

the temperature variation of interface thickness given in the proportionality (Eq. 38) above.

More extensive roughening of an interface between incompatible polymers can be obtained by use of various types of copolymer, introduced at the interface as putative compatibilisers. The interface may be strengthened, as a result of interdiffusion and roughening on a nanoscale. Many elegant experiments have been done in this area.

With suitable copolymers, roughening of the interface between two incompatible polymers by interdiffusion can lead to a range of values for fracture toughness Γ . For diblock copolymers both surface density (Σ) and degree of polymerisation (N) of the blocks are important. If the blocks are shorter than the entanglement length N_e of the corresponding homopolymer, failure occurs by chain pull-out and Γ is low. If $N > N_e$ chain scission will occur at low surface density (Σ), but as Σ is increased the fracture energy Γ rises steeply and plastic deformation, for example crazing, occurs in the polymer followed by chain scission or pull-out.

These effects have been found by Creton et al. [79] who laminated sheets of incompatible polymers, PMMA and PPO, and studied the adhesion using a double cantilever beam test to evaluate fracture toughness Γ_c . For the original laminate Γ_c was only 2 J/m², but when interface reinforced with increasing amounts of a symmetrical P.M.M.A.–P.S. diblock copolymer of high degree of polymerisation ($N > N_e$), the fracture toughness increased to around 170 J/m², and then fell to a steady value of 70 J/m² (Fig. 9).

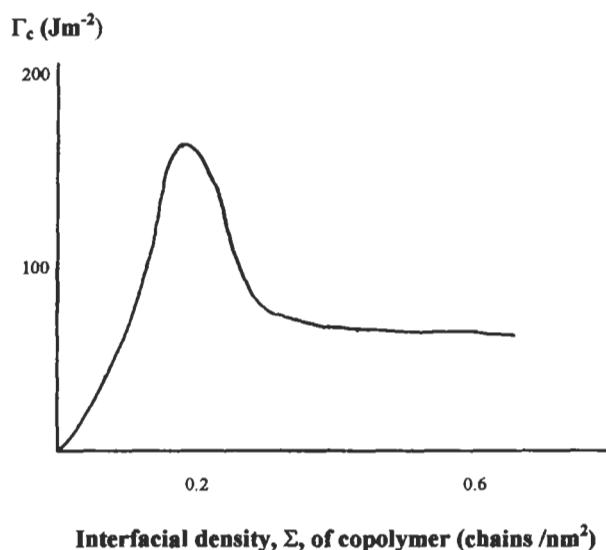


Fig. 9. Adhesion of P.M.M.A. to P.P.O. Effect on fracture toughness, Γ_c , of interfacial density, Σ , of a reinforcing diblock copolymer (after Creton et al. [80]).

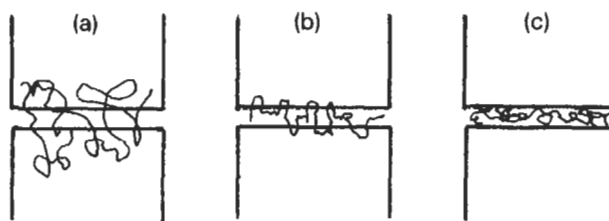


Fig. 10. Schematic representation of a random copolymer at the interface between two incompatible homopolymers. Incompatibility increases in the order (a), (b), (c).

At low surface coverage fracture occurs close to the junction point of the diblock, with each fragment remaining on the 'correct' side of the interface. At higher values of Σ the surface saturates, crazing occurs during fracture and Γ_c reaches a maximum. With further increase in surface density of the copolymer a weak layer forms at the interface and the fracture toughness falls to a limiting value.

Toughening of a polymer–polymer interface with random copolymers can sometimes be more effective than with diblocks, providing the polymers are not too incompatible [80]. This is of industrial, as well as of scientific, interest as random copolymers are usually cheaper to produce.

Diblock copolymers will form a single, strong chemical linkage across the interface. However, if the incompatibility between the homopolymers is not too large, a random copolymer will form Gaussian coils wandering many times across interface. The many 'stitches' formed are shown schematically in Fig. 10a. At larger incompatibilities, the random copolymer will no longer describe Gaussian coils, but the homopolymers will still be linked by 'loops' (Fig. 10b). If the incompatibility is too large the copolymer will simply form a collapsed globule at interface, a weak boundary layer giving no enhancement of adhesion (Fig. 10c).

As with block copolymers, the important parameters are the surface density and length of the copolymer chains. Toughening of the interface may occur as a result of pull-out or scission of the connector chains, or of fibril or craze formation in matrix. This last mechanism gives the highest fracture toughness, Γ , and tends to occur at high surface density of chains.

6.5. Results from the surface forces apparatus

The surface forces apparatus (Section 2.3) enables the estimation of a surface energy term, Γ_0 (Eq. 9), providing sufficiently smooth surfaces can be produced. In recent years Chaudhury, Pocius and colleagues have made a valuable contribution to the field of adhesion by developing the technique to study energies of adhesion and of surface energies of polymers [81–85]. These SFA results provide alternatives to values based on traditional destructive tests or contact angle measurements.

In studying contact between films of polyethylene (PE) and polyethylene terephthalate (PET) bonded to quartz cylinders, they observed an increase in adhesion energy with contact time for a PE/PE pair, but not for PE/PET or PET/PET combinations. They interpreted this as evidence for the development of nanoscale roughness due to the interdiffusion of chains across the PE/PE interface [84].

Israelachvili and his colleagues have used the SFA to study the interactions between surface layers of surfactant and of other molecules representing functionalised polymer chains, adhesion promoters or additives. Typically a monolayer of the molecule concerned is deposited onto cleaved mica sheets. The values of surface energies obtained from the JKR equation (Eq. 18) throw some interesting light on the nature and roughness of surface layers in contact.

The JKR equation enables values for surface energy to be obtained both when the surfaces are advancing into closer contact, γ_A , and when they are receding further apart, γ_R . These two values would be expected to be the same, as indeed they some times are. In many cases, however, there is hysteresis with $\gamma_R > \gamma_A$. Israelachvili and his colleagues have studied this phenomenon in some detail [23,24,86,87].

In a typical experiment, Israelachvili deposited monolayers of surfactants onto cleaved mica sheets, and evaluated the surface energies using the JKR equation. Fig. 11 contrasts results for mica coated with monolayers of (a) L- α -dipalmitoyl-phosphatidylethanolamine (DMPE) where $\gamma_A = \gamma_R = 27 \text{ mJ/m}^2$ and (b) hexadecyltrimethylammonium bromide (CTAB) where $\gamma_A = 20 \text{ mJ/m}^2$ and $\gamma_R = 50 \text{ mJ/m}^2$.

Israelachvili argues that the hysteresis is a result of reorganisation of the surfaces after they are brought into contact. This may occur at a macroscopic, microscopic or molecular level. Here he argues that interdigitation or interpenetration occurs, roughening the interface at the molecular level. He has classified his surface layers as crystalline (solid-like), amorphous solid and liquid-like (Fig. 12). The first tend not to reorganise, so hysteresis is low. The liquid-like surfaces reorganise very quickly both on loading and unloading, so again hysteresis tends to be low. It is the solid amorphous surfaces, where reorganisation may take place over a significant time scale, that hysteresis is generally greatest. On a simplistic level, the analogy with viscoelastic loss is obvious, and it is not surprising to find that adhesional hysteresis is considered to have a temperature/rate dependence (Fig. 13). Under the experimental conditions employed DMPE forms a crystalline ordered layer, but the CTAB layer is amorphous.

Thus this adhesion hysteresis is a result of a time-dependent roughening of the interface. It shows that roughness at an interface may actually develop as a result of bringing the two phases together as a result of the intrinsic properties of the surface molecules.

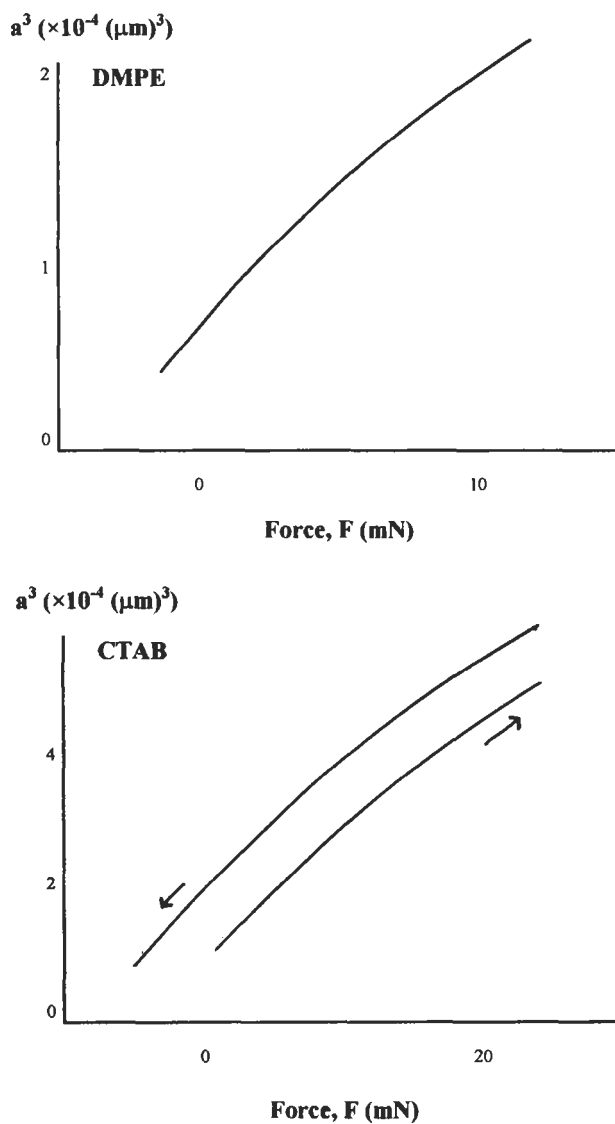


Fig. 11. Use of the JKR equation (Eq. 18) relating applied force, F , to radius of contact, a , to analyse results from the surface forces apparatus. Surface energy, γ , of surfactant layers (DMPE), cf. (CTAB) (after Chen et al. [24]).

7. Discussion

McBain and Hopkins [2], in their classical scientific study, argued that the surface roughness of a porous material was the basis of 'mechanical adhesion', its being

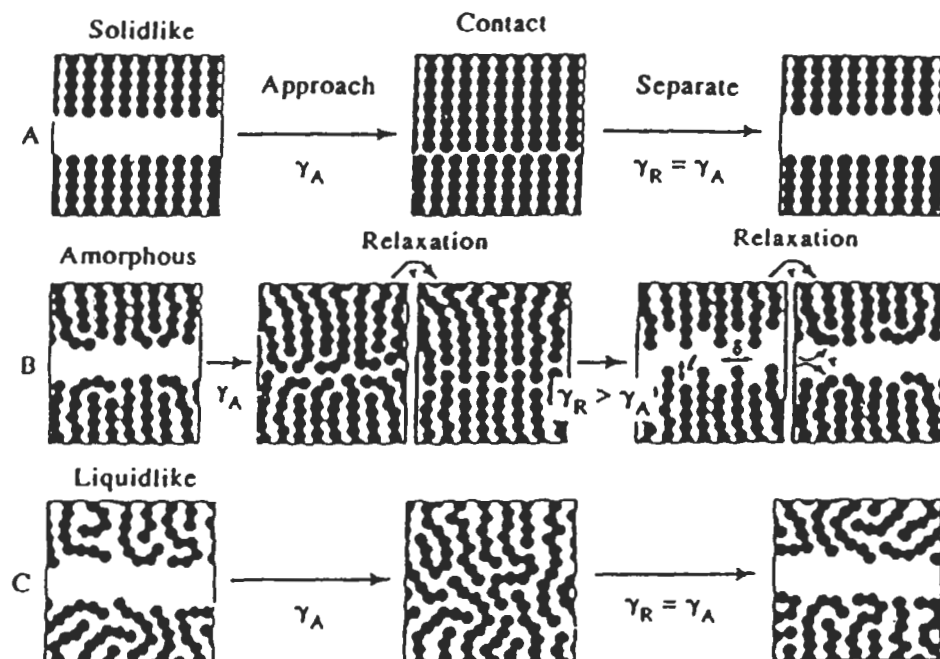


Fig. 12. Schematic representation of solid-like (crystalline), amorphous solid, and liquid-like surface layers (reproduced from [87], copyright American Chemical Society).

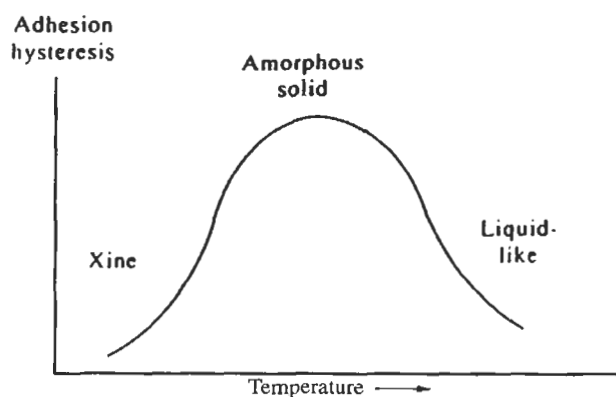


Fig. 13. Effect of temperature on adhesion hysteresis [23].

“obvious that a good joint must result whenever a strong continuous film of partly embedded adhesive is formed in situ”. That was the position in 1925; what account can be given today of the effect of surface roughness on adhesion? We can return

to Eq. 9 to provide a focus for answering this question.

$$\Gamma = \Gamma_0 + \psi$$

This equation shows that the fracture energy Γ of the adhesive joint is made up of a fundamental surface energy term, Γ_0 , and a term ψ , usually much larger, which represents the other energy absorbing processes which occur during fracture — for example plastic deformation. It is important to remember that Γ_0 and ψ are coupled (cf. Eq. 10), so that a small absolute increase in Γ_0 can lead to much greater energy dissipation away from the fracture surface, and so cause a much larger absolute increase in fracture energy. Let us examine each term in turn, considering how it might contribute to the hypothetical fracture energy.

The *surface energy term* Γ_0 is of the form ‘surface excess energy’ per unit area of surface (cf. Eq. 1), so may be expressed as:

$$\Gamma_0 = \frac{\Delta G}{A} \quad (39)$$

It is readily appreciated that some surface treatments are selected to increase ΔG by introducing more chemically active groups into the substrate surface. However, other treatments which are regarded primarily as roughening a surface, will bring about cognate chemical change, raising ΔG . Over and above this, ΔG will also be increased as a result of roughening the surface per se. An atom near an asperity peak or fine fractal feature will clearly have a much greater ‘atomic’ surface energy than a chemically similar atom in a plane crystal surface.

Turning attention to the area A in Eq. 39, it is important to remember that A refers to the formal area, the macroscopic area of the interface. For a rough surface the ‘true’ area will be greater. Of course, if the rough surface is not well wetted by the adhesive (cf. Table 1 and Sections 4.2 and 4.3), the effective surface area will be smaller, and the fracture energy reduced. However, where wetting does occur, an increase in surface area, for moderately rough surfaces, may well lead to a proportionate increase in adhesion. Gent and Lai have convincingly demonstrated this effect in careful experiments comparing adhesion of rubber to smooth and to grit-blasted steel [88].

As the scale of roughness becomes finer, the effective increase in A can become enormous. Consequently Γ_0 may be raised to very high value. Indeed, as many engineering surfaces are fractal in nature [36], we can only retain the concept of ‘area’ at all, if we accept that it can be considered as indefinitely large. The practical adhesion does not become infinite, because the joint with a strong interfacial region will fail (cohesively) in some other region where Γ_0 is smaller [89].

The coupling of Γ_0 with the ‘other’ loss terms ψ (cf. Eq. 10) means that even a modest absolute increase in Γ_0 may lead to a much larger increase in fracture energy Γ .

Returning to Eq. 9, let us now consider explicitly the *other energy absorbing processes* ψ which occur during fracture. These often make the dominant contribution to Γ . As we have seen, where interdigitation of polymer chains is involved, these losses may include energy involved in chain pull-out or scission. It is notable that the highest fracture energy, in these cases, occurs where the interdigitation is sufficiently extensive to initiate crazing or other plastic dissipation processes.

For many adhesive bonds, there is a very large difference in elastic modulus between the two phases joined. This has the effect of concentrating applied stresses at the interface, leading to smooth crack propagation close to the interface, often giving a low fracture energy. A rough surface, especially a microfibrinous or microporous one, can be seen as causing irregular stress concentrations on a local scale which, Evans and Packham [90] argue, interfere with this smooth crack propagation and can lead to the deformation of larger volumes of material leading to increased energy loss. Gent and Lin [91] have clearly demonstrated this effect using model porous surfaces. Creton and his colleagues [92–94] have shown how differences in surface roughness of a steel probe can produce differences in the cavitation behaviour in pressure-sensitive adhesives and thus in the fracture energy Γ , as the probe is withdrawn from a film of the adhesive. The effect of surface roughness on fracture energy depended on the mechanical properties (ψ) of the adhesive which in turn depended on the test temperature. For example, with a styrene–isoprene–styrene adhesive the rough, compared to the smooth probe gave a lower fracture energy at 20°C but a higher value at 60°C.

A high modulus gradient at the interface is also to be avoided in materials joined as a result of the interdiffusion of materials to form a fractal surface [32]. The effect is to produce an interfacial composite region. This strengthens the interface and leads to a more gradual change in modulus and avoids the sharp concentrations of stress which would occur at a smooth interface.

Let us finally consider the implications of the roughness of the *fracture surface*. It is significant that the fracture surfaces produced when strong adhesive bonds are broken are often extremely rough. (This, of course, holds for strong bonds irrespective of the roughness of the substrate surface.) Eq. 9 gives the fracture energy in terms of the different energies which contribute to it. For the sake of being specific, suppose the failure mode is cohesive. Should the surface energy term be W_{coh} , given by Eq. 8? This would not take into account the very rough surfaces produced in the fracture. The surface energy term needs to be increased by two factors, the first, r , taking into account the larger surface area, the second, s , allowing for the increased ‘atomic’ surface energy on the rough surface:

$$W_{\text{coh}}^* = 2rs\gamma = W_{\text{coh}} + (2rs - 2)\gamma \quad (40)$$

If the roughness of the fracture surface is large this may be written:

$$W_{\text{coh}}^* = 2rs\gamma = W_{\text{coh}} + 2rs\gamma \quad (41)$$

and Eq. 9 is now:

$$\Gamma = \Gamma_0 + 2rs\gamma + \psi \quad (42)$$

The term r might be the roughness factor, but as argued above, it should often be a factor involving the fractal dimension of the fracture surfaces, which, as Table 1 shows, may be extremely large.

$$\Gamma = \Gamma_0 + 2s\gamma\sigma^{1-D/2} + \psi \quad (43)$$

Mecholsky [95] has proposed an equation of this sort to represent the brittle fracture of ceramics: it would be of interest to investigate its applicability to the fracture of adhesive bonds.

8. Conclusions

It has long been recognised that surface roughness was an important factor in adhesive bonding. Pretreatments which produce rough surfaces are widely used to give particular properties desired in bonded components. Such properties include controlled (usually high) strength and durability in hostile environments. It is now possible broadly to account for these effects within a broader account of adhesion, which relates the practical strength of adhesive joints to fundamental concepts of surface science.

References

1. Galilei, Galileo, *Discorsi e dimostrazioni matematiche intorno a due nuove scienze*. Elzevir in Leida, 1638 Gionata Prima, p. 59. Pagination as *Edizione nazionale delle Opere di Galileo Galilei*. Barbera, Firenze, 1890–1909.
2. McBain, J.W. and Hopkins, D.G., *J. Phys. Chem.*, **29**, 188 (1925).
3. Packham, D.E., *J. Adhes.*, **39**, 137 (1992).
4. Packham, D.E., The mechanical theory of adhesion — a seventy year perspective and its current status. In: van Ooij, W.J. and Anderson, H.R., Jr. (Eds.), *1st International Congress on Adhesion Science and Technology: Invited Papers*. VSP Publishers, Utrecht, 1998, pp. 81–108.
5. Packham, D.E. The mechanical theory of adhesion. In: Pizzi, A. and Mittal, K.L. (Eds.), *Handbook of Adhesives Technology*, 2nd edn. Marcel Dekker, New York, NY, 2002.
6. de Leeuw, N.H. and Parker, S.C., *J. Chem. Soc., Faraday Trans.*, **93**, 467 (1997).
7. Lewis, G.N. and Randall, M., *Thermodynamics*, 2nd edn. Revised by Pitzer, K.S. and Brewer, L. McGraw-Hill, 1961, p. 472.
8. Somorjai, G.A., *Principles of Surface Chemistry*. Prentice-Hall, Englewood Cliffs, NJ, 1972.
9. Adamson, A.W., *Physical Chemistry of Surfaces*, 5th edn. Wiley, New York, NY, 1990.
10. Padday, J.F., In: Packham, D.E. (Ed.), *Handbook of Adhesion*. Longman, London, 1992, p. 509.

11. Gent, A.N. and Kinloch, A.J., *J. Polym. Sci. A2*, **9**, 659 (1971).
12. Andrews, E.H. and Kinloch, A.J., *Proc. R. Soc. A*, **332**, 385 (1973).
13. Girifalco, L.A. and Good, R.J., *J. Phys. Chem.*, **61**, 904 (1957).
14. Girifalco, L.A. and Good, R.J., *J. Phys. Chem.*, **64**, 561 (1960).
15. Owens, D.K. and Wendt, R.C., *J. Appl. Polym. Sci.*, **13**, 1741 (1969).
16. Kaelble, D.H. and Uy, K.C., *J. Adhes.*, **2**, 50 (1970).
17. Wu, S., *J. Adhes.*, **5**, 39 (1973).
18. Good R.J. and van Oss C.J., In: Schrader M.E. and Loeb, G.I. (Eds.), *Modern Approaches to Wettability*. Plenum, New York, NY, 1992, p.12.
19. Brunauer, S., Emmett, P.H. and Teller, E., *J. Am. Chem. Soc.*, **60**, 309 (1937).
20. Lucic, S., Kovacevic, V., Packham, D.E., Bogner, A., Gerzina, A., Stearate-modified calcium carbonate fillers and their effect on the properties of polyvinyl acetate composites. *Proc. 2nd Int. Symp. Polymer Surface Modification: Relevance to Adhesion*, Newark, NJ, 24–26 May, 1999.
21. Israelachvili, J.N., *Intermolecular and Surface Forces*, 2nd edn. Academic Press, London, 1992.
22. Johnson, K.L., Kendall, K. and Roberts, A.D., *Proc. R. Soc. A*, **324**, 301 (1971).
23. Packham, D.E., *Int. J. Adhes. Adhes.*, **16**, 121–128 (1996).
24. Chen, Y.L., Helm, C.A. and Israelachvili, J.N., *J. Phys. Chem.*, **95**, 10736 (1991).
25. Derjaguin, B.V., Muller, V.M. and Toporov, Yu.P., *J. Colloid Interface Sci.*, **53**, 314 (1975).
26. Maugis, D.J., *Colloid Interface Sci.*, **150**, 243 (1992).
27. Wenzel, R.N., *Ind. Eng. Chem.*, **28**, 988 (1936).
28. Cherry, B.W., *Polymer Surfaces*. Cambridge University Press, Cambridge, 1981.
29. Evans, J.R.G. and Packham, D.E., *J. Adhes.*, **10**, 39 (1979).
30. Hine, P.J., El Muddarris, S. and Packham, D.E., *J. Adhes.*, **17**, 207 (1984).
31. Koizumi, S., Hasegawa, H. and Hashimoto, T., *Macromolecules*, **24**, 2467 (1990).
32. Wool, R.P., *Polymer Interfaces: Structure and Strength*. Hanser, Munich, 1995, p. 112 et seq.
33. Creton, C., Brown, H.R. and Shull, K.R., *Macromolecules*, **27**, 3174 (1994).
34. Rideal, E.K., *Introduction to Surface Chemistry*. Cambridge University Press, Cambridge, 1930, pp. 175, 179.
35. Meakin, P., *Phys. Rep. Rev. Sect. Phys. Lett.*, **235**, 189 (1993).
36. Bhushan, B., Israelachvili, J.N. and Landman, U., *Nature*, **374**, 607 (1995).
37. Harrison, A., *Fractals in Chemistry*. Oxford University Press, Oxford, 1995, p. 6.
38. Farin D. and Avnir, D., In: Avnir, D. (Ed.), *Fractal Approach to Heterogeneous Chemistry*. Wiley, New York, NY, 1989, p. 272.
39. Cassie, A.B.D., *Disc Faraday Soc.*, **3**, 11 (1948).
40. Packham, D.E., The adhesion of polymers to metals the role of surface topography. In: Mittal, K.L. (Ed.), *Adhesion Aspects of Polymeric Coatings*. Plenum, London, 1983, p. 19.
41. de Bruyne, N.A., *Aero Res. Tech. Notes Bull.*, 168 (1956).
42. Massey, B.S., *Mechanics of Fluids*, 4th edn. Van Nostrand Reinhold, New York, NY, 1979, p. 146.
43. Washburn, E.D., *Phys. Rev.*, **17**, 374 (1921).
44. Evans, J.R.G., Packham, D.E. and Adam, T., *J. Adhes.*, **10**, 279 (1980).
45. Bright, K., Malpass, B.W. and Packham, D.E., *Nature*, **223**, 1360 (1969).
46. Arrowsmith, D.J., *Trans. Inst. Metal Finishing*, **48**, 88 (1970).
47. Bright, K., Malpass, B.W. and Packham, D.E., *Br. Polym. J.*, **3**, 205 (1971).
48. Allen, K.W., Alsallim, H.S. and Wake, W.C., *Faraday Special Disc. Chem. Soc. No. 2 Solid/Solid Interfaces*. Chemical Society, London, 1972, p. 38.

49. Farkas, G., *Surfaces*, **14**(93), 37 (1975).
50. Bethune, A.W., *SAMPE J.*, **11**, 4 (1975).
51. McMillan, J.C., Quinlivan, J.T. and Davis, R.A., *SAMPE Q.*, **7**, 13 (1976).
52. Marceau, J.A., *SAMPE Q.*, **9**, 1 (1978).
53. Venables, J.D., *J. Adhes.*, **39**, 79 (1992).
54. Chen, J.M., Sun, T.S., Venables J.D. and Hopping, R., *Proc. 22nd SAMPE Symp.*, April 1997, p. 25.
55. Sun, T.S., Chen, J.M. and Venables, J.D., *Appl. Surf. Sci.*, **1**, 202 (1978).
56. Venables, J.D., McNamara, D.K., Chen, J.M., Sun, T.S. and Hopping, R.L., *Appl. Surf. Sci.*, **3**, 88 (1979).
57. Sun, T.S., McNamara, D.K., Ahearn, J.S., Chen, J.M., Ditchek, D. and Venables, J.D., *Appl. Surf. Sci.*, **5**, 406 (1980).
58. Venables, J.D., *J. Mater. Sci.*, **19**, 2431 (1984).
59. Sun, R.-D., Tryk, D.A., Hashimoto, K. and Fujishima, A., *J. Electrochem. Soc.*, **146**, 2117 (1999).
60. Wen, X., Wang, X. and Zhang, N., *Bio.-Med. Mater. Eng.*, **6**, 173 (1996).
61. Morris, A.E.P. and Shanahan, M.E.R., *Int. J. Adhes. Adhes.*, **14**, 145 (1994).
62. Reiter, H., In: Packham, D.E. (Ed.), *Handbook of Adhesion*. Longman, 1992, p. 192.
63. Clearfield, H.M., Shaffer, D.K., Vandoren, S.L. and Ahearn, J.S., *J. Adhes.*, **29**, 81 (1989).
64. Pike, R.A., Patarini, V.H., Zatoski, R. and Lamm, F.P., *Int. J. Adhes. Adhes.*, **12**, 227 (1992).
65. Davis, G.D., Shaffer D.K., Whisnant, P.L., Groff G.B. and Venables, J.D., *3rd Int. Conf. Adhesion and Surface Analysis*, Loughborough, April 1994, paper L13.
66. Davis, G.D., Whisnant, P.L., Shaffer, D.K., Groff, G.B. and Venables, J.D., *J. Adhes. Sci Technol.*, **9**, 527 (1995).
67. Janarthanan, V., Garrett, P.D., Stein, R.S. and Srinivasarao, M., *Polymer*, **38**, 105–111 (1997).
68. Ye, M., Deplancke, J.L., Berton, G., Segers, L. and Winand, R., *Surf. Coatings Technol.*, **105**, 184 (1998).
69. Taylor, D. and Rutzler, J.E., *Ind. Eng. Chem.*, **50**, 928 (1958).
70. Amada, S. and Satoh, A., *J. Adhes. Sci. Technol.*, **14**, 27–41 (2000).
71. Amada, S. and Hirose, T., *Surf. Coatings Technol.*, **102**, 132 (1998).
72. Wool, R.P. and Long, J.M., *Macromolecules*, **26**, 5227 (1993).
73. Mazur, S. and Reich, S., *J. Phys. Chem.*, **90**, 1365 (1986).
74. Mazur, S., Lugg, P.S. and Yarnitzky, C., *J. Electrochem. Soc.*, **134**, 346 (1987).
75. Helfand, E. and Tagami, Y.J., *Chem. Phys.*, **56**, 3592 (1972).
76. Helfand, E., *Macromolecules*, **25**, 1676 (1992).
77. Godail, L. and Packham, D.E., *Le Vide: Sci., Tech. Appl.*, **296**, 403–407 (2000).
78. Godail, L. and Packham, D.E., Adhesion of ethylene–octene copolymers to polypropylene: interfacial structure and mechanical properties. *J. Adhes. Sci. Technol.*, **15**, 1285–1304 (2001).
79. Creton, C., Brown, H.R. and Deline, V.R., *Macromolecules*, **27**, 1774 (1994).
80. Pickett, G.T., Balazs, A.C. and Jasnow, D., *Trends Pol. Sci.*, **5**, 128 (1997).
81. Merrill, W.M., Pocius, A.V., Thakker, B.V. and Tirrell, M., *Langmuir*, **7**, 1975 (1991).
82. Chaudhury, M.K., *J. Adhes. Sci. Technol.*, **7**, 669 (1993).
83. Silberzan, P., Perutz, S., Kramer, E.J. and Chaudhury, M.K., *Langmuir*, **10**, 2466 (1994).
84. Mangipudi, V., Tirrell, M. and Pocius, A.V., *J. Adhes. Sci. Technol.*, **8**, 1251 (1994).
85. Mangipudi, V., Tirrell, M. and Pocius, A.V., *Langmuir*, **11**, 19 (1995).
86. Yoshizawa, H., Chen, Y.L. and Israelachvili, J.N., *J. Phys. Chem.*, **97**, 4128 (1993).

87. Yamada, S., Chen, Y.L. and Israelachvili, J.N., *J. Phys. Chem. B*, **102**, 234 (1998).
88. Gent, A.N. and Lai, S.M., *Rubber Chem. Technol.*, **68**, 13 (1995).
89. Good, R.J., *J. Adhes.*, **4**, 133 (1972).
90. Evans, J.R.G. and Packham, D.E., *J. Adhes.*, **10**, 177 (1979).
91. Gent, A.N. and Lin, C.W., *J. Adhes.*, **32**, 113 (1990).
92. Hooker, J.C., Creton, C., Tordjeman, P. and Schull, K.R., *Proc. 22nd Annu. Meet. Adhes. Soc.*, Panama City Beach, 21–24 Feb., 1999, pp. 415–417.
93. Chiche, A., Pareige, P. and Creton, C., *Le Vide: Sci., Tech. Appl.*, **296**, 419–423 (2000).
94. Chiche, A., Pareige, P. and Creton, C., *C.R. Acad. Sci. IV-Phys.*, **1**, 1197–1204 (2000).
95. Mecholsky, J.J., *Proceedings of the XVII International Congress on Glass*, Vol. 5. Chinese Ceramic Society, Beijing, 1995, p. 473.

Chapter 8

Diffusion and autohesion

RICHARD P. WOOL *

Department of Chemical Engineering, University of Delaware, Newark, DE 19716-3110, USA

1. Diffusion and autohesion

1.1. Introduction

Polymer interfaces are ubiquitous. They play a critical role in determining the properties, reliability and function of a broad range of materials. For example, polymer melt processing via injection molding (for plastic auto parts) and extrusion (for plastic pipe) create many interfaces in the form of internal weldlines where the fluid fronts coalesce and weld. Compression molding and sintering (of artificial hip joints) requires the coalescence of pellets or powder when their surfaces contact in the mold. Drying of latex paints and coatings entails a very large number of interfaces per unit volume, as the relatively tiny (ca. 1000 Å) latex particles interdiffuse together to form a continuous film. Construction of composites with thermoplastic matrices (aircraft bodies) requires the fiber filled laminates to weld by an interdiffusion process at the interface. Welding of two pieces of polymer by thermal or solvent bonding is a commonly encountered example of strength development at a polymer–polymer interface; tack between uncured rubber sheets during auto tire manufacture is an important example of this kind of welding.

Numerous examples of ‘symmetric interfaces’ exist where the same polymer occurs on both sides of the interface. In contrast, rubber toughening of glassy polymers (bullet-proof glass) requires that the interface formed by the rubber particle with the glass (Plexiglas™) matrix be sufficiently strong to promote stable energy dissipation. The rubber/Plexiglas is an example of an ‘asymmetric interface’ where two different polymers are joined. Asymmetric or dissimilar interfaces come about when polymer are blended, when dissimilar materials are

* E-mail: wool@ccm.udel.edu

laminated (in electronic materials applications), when coupling agents are used in composites, when plastic mixtures from municipal waste are recycled, when different materials are coextruded and when photographs are developed. As our knowledge of material interfaces expands, so does our ability to fabricate more sophisticated material systems, be they artificial organs, biomedical implants, rocket motors, high speed integrated circuits, the Super Auto of 2000, advanced composite space vehicles, more effective drug delivery molecules for cells, new chewing gum, plastic bridges, tractors from soybeans, or perhaps, a better paint [1].

We find the subject of interfaces is very rich if we consider the wide variety of possible pairs involving polymers and materials with different chemical composition, crystalline and amorphous content, compatibility, incompatibility, molecular weight distributions, additives, surface chemistry, etc. In this chapter, we examine how interfaces form, describe their structure and provide an understanding of the relationship between structure and strength. We first examine the structure of these interfaces and then relate the structure to fracture strength through microscopic deformation mechanisms involving chain disentanglement and bond rupture. The evolution of structure at diffuse interfaces is controlled by the dynamics of the chains and the thermodynamics of chemically interacting species. Once the structure is known, a 'connectivity relation', is required to relate the structure to mechanical properties. The connectivity relation for amorphous polymers is developed in terms of an entanglement percolation model [1–4]. We can then understand what is required to break the connectivity at the interface by disentanglement and/or bond rupture. The latter microscopic deformation mechanisms consume a known amount of energy from which the strength of the interface can be determined.

1.2. Defining the problem

The problem of evaluating the fracture energy G_{1c} of polymer interfaces is represented in Fig. 1. Material A is brought into contact with material B to form an A/B interface, the weld is fractured and the strength is related to the structure of the interface through microscopic deformation mechanisms. Typically, a crack propagates through the interface region preceded by a deformation zone at the crack tip. For cohesive failure, the fracture energy is determined by the J-integral method [5], where G_{1c} is the integral of the traction stresses with draw displacements δ , in the cohesive zone following yielding at a local yield or craze stress σ_Y . The cohesive zone at the crack tip breaks down by a vector percolation process (dependent on $H(t)$) at a maximum stress value, $\sigma_m > \sigma_Y$. Typical ratios of σ_m/σ_Y are about 4–10. Both σ_m and δ are rate dependent and in the simplest case, the fracture energy is determined by $G_{1c} = \sigma_m \delta_m$, where δ_m is the critical crack opening displacement. Both σ_m and δ_m depend on the interface structure

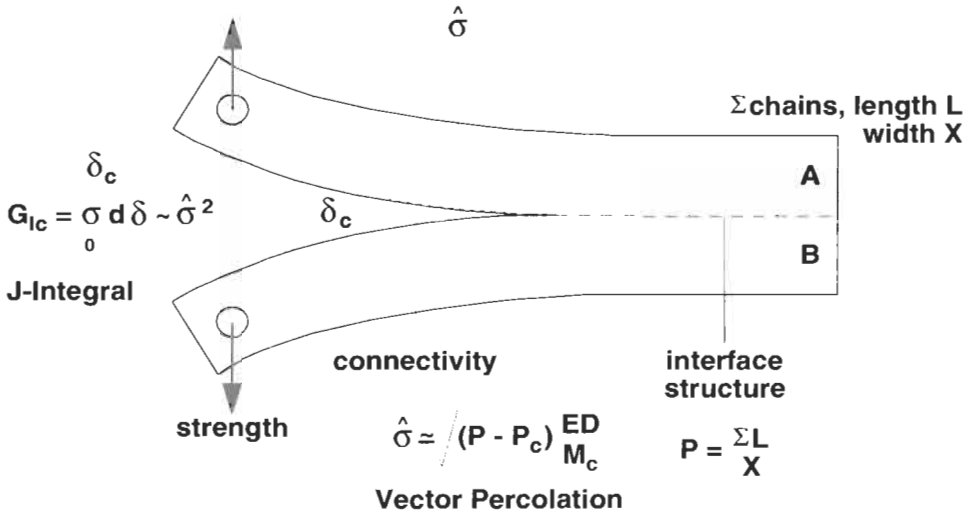


Fig. 1. The microscopic entanglement structure, e.g. at an interface or in the bulk, is related to the measured macroscopic fracture energy G_{Ic} via the VP theory of breaking connectivity in the embedded plastic zone (EPZ) at the crack tip. The VP theory determines σ_{max} in the EPZ, which is related to G_{Ic} via Hutchinson's J-integral theory.

and the microscopic deformation mechanisms controlling the percolation fracture process via disentanglement and bond rupture. The stress field at the crack tip in Fig. 1 can be quite complex for dissimilar materials and may produce crack propagation which significantly deviates from the simple Mode I tensile fracture which we commonly encounter. Instead, differences in moduli, Poisson ratio, sample thickness, material anisotropy and yield stress can result in mode mixing, where the interaction of shear, tension and torsion can result in propagation away from the interface plane. Most of the discussion in this chapter pertains to the simple Mode I fracture case.

The development of the relation between interface structure and strength is suggested to proceed as follows:

Step 1. The time dependent structure of the interface is determined. Relevant properties may be characterized by a general function $H(t)$, which for the case of polymer melts can usually be described in terms of the static and dynamic properties of the polymer chains. For example, with symmetric ($A = B$) amorphous melt interfaces, $H(t)$ describes the average molecular properties developed at the interface by the interdiffusion of random coil chains as [1,6]

$$H(t) = H_{\infty}(t/\tau)^{r/4} \quad (1.1)$$

where

$$H_{\infty} \sim M^{(3r-s)/4}, \quad r, s = 1, 2, 3 \quad (1.2)$$

in which τ is a characteristic relaxation time and H_∞ is the equilibrium value of the property $H(t)$ at $t = \tau$. $H(t)$ can be measured from the concentration depth profile $C(x, t)$ for symmetric interfaces. This function could be a measure of the extent of diffusion across the interface, e.g., the average monomer interpenetration distance, the number of chains crossing the interface plane, etc. With incompatible amorphous interfaces, limited interdiffusion occurs up to an equilibrium depth d_∞ , which becomes the important descriptor of the interface structure.

In the case of polymer-metal interfaces, the function $H(t)$ could be a measure of the interface roughness, diffusion depth, time dependent surface rearrangement, entanglement topology, fractal properties, etc. For example, when metal atoms are vapor deposited on polymers during electronic material fabrication, a diffuse polymer-metal interface can form which is highly ramified. [6,7] The time dependent roughness $N_f(t)$, of the interface depends on the average diffusion depth $\langle X \rangle$, according to [1,6]

$$N_f(t) \sim \langle X(t) \rangle^{1-1/d_f} \quad (1.3)$$

where d_f is the fractal dimension [8] of the interface [7,9].

Similarly, when polymer chains with sticker groups adhere to a solid substrate [10] such as glass, metal, etc., the strength is determined by the near polymer/solid interface connectivity, which in turn, affects the chain conformation, entanglement density and long range interphase connectivity coupling the polymer bulk to the solid substrate. Many polymer-solid interfaces break cohesively in the weak boundary layer adjacent to the solid surface. This occurs when the first layer of chains strongly adsorbs to the solid substrate but disconnects from the chains in the bulk adjacent to the substrate [10–12]. This effectively moves the interface of interest away from the plane of contact at the solid surface to a nearby polymer-polymer interface, comprising the weak boundary layer. Thus, for each interface we examine the structure in terms of relevant descriptors, which could affect the mechanical, thermal, optical, or electrical properties.

The interface properties can usually be independently measured by a number of spectroscopic and surface analysis techniques such as secondary ion mass spectroscopy (SIMS), X-ray photoelectron spectroscopy (XPS), specular neutron reflection (SNR), forward recoil spectroscopy (FRES), scanning electron microscopy (SEM) and transmission electron microscopy (TEM), infrared (IR) and several other methods. Theoretical and computer simulation methods can also be used to evaluate $H(t)$. Thus, we assume for each interface that we have the ability to measure $H(t)$ at different times and that the function is well defined in terms of microscopic properties.

Step 2. After a contact time t , the material is fractured or fatigued and the mechanical properties determined. The measured properties will be a function of the test configuration, rate of testing, temperature, etc., and include the critical strain energy release rate G_{IC} , the critical stress intensity factor K_{IC} , the critical

crack opening displacement δ_c , the critical fracture stress σ_c , the fatigue crack propagation rate da/dN , and other properties. Related properties can be measured when other modes of fracture (torsion and shear) are used.

Step 3. The set of fracture properties $G(t)$ are related to the interface structure $H(t)$ through suitable deformation mechanisms deduced from the micromechanics of fracture. This is the most difficult part of the problem but the analysis of the fracture process in situ can lead to valuable information on the microscopic deformation mechanisms. SEM, optical and XPS analysis of the fractured interface usually determine the mode of fracture (cohesive, adhesive or mixed) and details of the fracture micromechanics. However, considerable modeling may be required with entanglement and chain fracture mechanisms to realize useful solutions since most of the important events occur within the deformation zone before new fracture surfaces are created. We then obtain a solution to the problem,

$$G(t) = f\{H(t)\} \quad (1.4)$$

where f is a known function of $H(t)$ at constant temperature and pressure. In the simplest case, $G(t)$ is proportional to $H(t)$, as found for many polymer welding problems, or it may be obtained in the form of a scaling law with known constants and exponents [1].

2. Welding and crack healing

Welding and crack healing in polymers has been the subject of many investigations in recent decades [13–46]. When two similar pieces of bulk polymer are brought into contact at a temperature above the glass transition temperature T_g , the interface gradually disappears and mechanical strength develops as the crack or weld heals. Crack healing and welding are related problems but basically very different. In crack healing we are concerned with healing of two fractured surfaces, which contain the remnants of the deformation zone through which the crack had propagated. The molecular weight distribution is expected to be altered depending on the microscopic deformation mechanisms leading to fracture. If chain disentanglement occurs as with uncured linear elastomers, then the molecular weight distribution will be relatively unaffected. However, the location of the chain ends may be preferentially biased towards the surface. If significant chain fracture occurs, as during the fracture of high molecular weight glasses, then the molecular weight will be significantly changed in the surface layer. We have made estimates of the molecular weight change using GPC methods [19]. Welding involves the contact of two melt surfaces, which previously had not been in contact, and the molecular weight at the surface is expected to be the same as the bulk. Allowances for molecular weight segregation can be made for polydisperse molecular weight distributions.

Healing, implying the recovery of mechanical strength with time, is primarily due to the diffusion of chains across the interface. The chain diffusion is a special type of mass transfer, which cannot be described by the conventional diffusion equation. Wool and O'Connor [13] studied healing of interfaces in terms of the following stages: (1) surface rearrangement; (2) surface approach; (3) wetting; (4) diffusion; and (5) randomization. By the end of the wetting stage, potential barriers associated with inhomogeneities in the interface disappear and chains are free to move across the interface in the following stages of diffusion and randomization. The latter stages of diffusion and randomization are the most important because the characteristic strength of the polymer material appears in these stages.

2.1. Surface rearrangement

Before bringing the surfaces together, one should consider the roughness or topography of the surface and how it changes with time, temperature, and pressure following contact. In fractured polymers, rearrangement of fibrillar morphology, etc., can affect the rate of crack healing. Chain end distributions near the surface can change as molecules diffuse back into the bulk polymer. Spatial changes of the molecular weight distribution may also occur, e.g., where the low molecular weight species preferentially migrate to, or away from the surface. Chemical reactions, e.g., oxidation and crosslinking can occur on the surface and complicate the molecular dynamics of diffusion. Many other processes, e.g., molecular orientation changes, can contribute to the stage of surface rearrangement. Each material and experimental technique usually possesses unique surface rearrangement processes, which may need to be quantified.

Wool and O'Connor [13,14] found significant effects of surface rearrangement on the healing rate of lightly cross-linked polybutadiene such that the fracture energy at constant healing time decreased with increasing surface rearrangement time (prior to contact). This effect can be explained by the chain ends diffusing back into the bulk such that they were not as readily available for diffusion during healing.

Surface rearrangement plays a dominant role in the adhesion of chains with sticker groups to solid substrates (metal, wood, glass, ceramics, fibers). The dynamics and conformation of chains partly adhered to a substrate is a very strong function of the sticker group spacing, as observed by Gong and Wool [10], and the time dependence of adhesion may be several orders of magnitude greater than the characteristic relaxation time of a chain in the bulk.

2.2. Surface approach

Surface approach takes into consideration time-dependent contact of the different parts of the surfaces to create the interface. For example, in crack, craze, and

void healing, contact may be achieved at different locations at different times in the interface depending on the closure mode [1]. For example, slow closure of a double cantilever beam crack would result in different extents of healing along the closed crack. Consolidation between thermoplastic composite laminates, tows and tapes, involving time dependent flow between the fibers and wetting of the interface is another example of surface approach. This stage typically contributes as a boundary value problem to the other stages of wetting and diffusion. While it seems trivial, surfaces which cannot approach, will not weld or heal and this may be a very important issue in designing smart, self-healing composites, for example, where damage in the interface potentially prevents surface approach.

2.3. Wetting

Wetting, which is the establishment of molecular contact at the Van der Waals level, can occur in a time-dependent fashion at the interface. This is usually treated in terms of the 'spreading coefficient' $F_{ij} = \Gamma_j - \Gamma_i - \Gamma_{ij}$, which is used to estimate the wettability of phase i spreading on phase j , with component surface tensions Γ_i , Γ_j and interfacial surface energy, Γ_{ij} . When F_{ij} is positive, spreading occurs and good molecular contact is achieved between the surfaces. The dynamics of wetting and de-wetting has received considerable attention from Brochard et al and an excellent molecular understanding is developing for many polymer systems. For our purposes, we provide a brief phenomenological description of wetting to illustrate potential problems in evaluating the time-dependence of welding. Fig. 2 shows a schematic region of the plane of contact of a polymer interface [13]. Due to surface roughness, etc., good contact and wetting are not achieved instantaneously at all locations. Typically, wetted 'pools' are nucleated at random locations at the interface and propagate radially until coalescence and complete wetting are obtained. This problem can be treated phenomenologically as a two-dimensional nucleation and growth process such that the fractional wetted area, $\phi(t)$, is given as [13]

$$\phi(t) = 1 - \exp(-kt^m) \quad (2.1)$$

where k and m are constants depending on the nucleation function and radial spreading rates. The nucleation function is strongly dependent on surface roughness at the moment of contact and the spreading function is influenced both by surface topography and the molecular aspects of the interfacial tension. Françoise Brochard has developed detailed molecular pictures of wetting dynamics in recent years and the topic of polymer thin films de-wetting from solid substrates has also received considerable attention.

Contact theories suggest that complete strength may be obtained when the interface has wetted at $\phi = 1$. Wetting is a prerequisite for strength development but does not imply that the maximum strength has developed when molecular

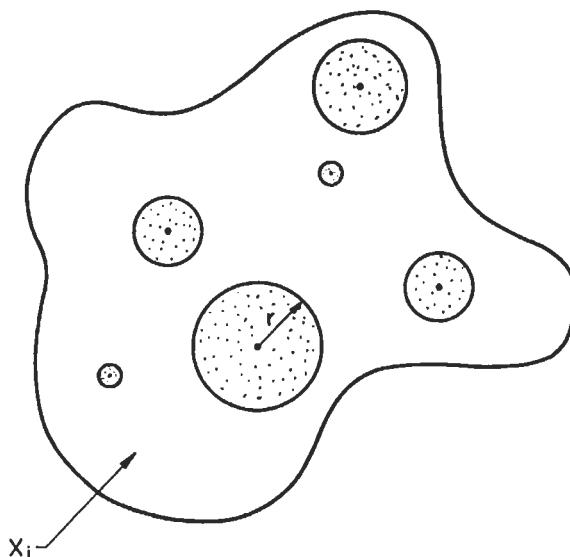


Fig. 2. Partially wetted domain in a crack interface.

contact has been achieved. Even for polymer–solid interfaces, where no interdiffusion occurs, surface rearrangement of sticker groups occurs over very long times after wetting has been achieved [10]. Others argue that interdiffusion is necessary for strength development and for polymer–polymer interfaces, the evidence is significant [1]. The time dependence of viscous flow to promote contact and that of interdiffusion may be comparable since they are subject to the same molecular dynamic processes. Wetting of high molecular weight ($M > M_c$) amorphous symmetric interfaces will involve segmental interdiffusion depths of about 30 Å, before significant diffusion of order R_g occurs, as discussed in the next section.

2.4. Diffusion

The diffusion stage, characterized by $H(t)$, will be discussed in detail with respect to the instantaneous wetting condition. However, in the presence of a time dependent wetting function $\phi(t)$, Eq. 2.1, we see from Fig. 2 that diffusion will have progressed to different extents in different areas of the interface. If the intrinsic diffusion function, $H(t)$ as given by Eq. 1.1 does not change its nature with time due to the other stages, then the net diffusion, $H''(t)$ can be expressed as the convolution product

$$H^1(t) = \int_{-\infty}^t H(t-\tau) \frac{\partial \phi}{\partial \tau} \partial \tau \quad (2.2)$$

where τ is a 'dummy' variable on the time axis. The convolution process for typical $\phi(t)$ functions may mask the time-dependence of the intrinsic diffusion function $H(t)$ and related mechanical properties. This part of the problem can be solved mathematically by letting the wetting function be a Dirac delta function

$$\frac{d\phi}{dt} = \delta(t) \quad (2.3)$$

such that Eq. 2.2 reduces to $H''(t) = H(t)$. This can be attempted experimentally by obtaining near-instantaneous wetting of atomically smooth surfaces under moderate contact pressure at temperatures above T_g . However, we have found that the wetting stage can result in difficulty with the analysis of most short time welding data. Useful information can be obtained under conditions where the time range of diffusion greatly exceeds that for wetting.

2.5. Randomization

The randomization stage refers to the equilibration of the nonequilibrium conformations of the chains near the surfaces and in the case of crack healing and processing, the restoration of the molecular weight distribution and random orientation of chain segments near the interface. The conformational relaxation is of particular importance in the strength development at incompatible interfaces and affects molecular connectivity at polymer–solid interfaces.

The stages of crack healing can have interactive time-dependent functions such that the welding problem can consist of processes involving five-way convoluted functions resulting in mechanical properties whose time dependence may not be readily interpretable. Thus, we must take great care in conducting welding experiments designed to critically explore molecular level theories of strength development.

3. Structure of diffuse amorphous interfaces

The strength of a symmetric amorphous polymer–polymer interface (A/A) depends on the structure which develops during welding. The average structure is related in a unique manner to the dynamics and shape (statics) of the chains attempting to diffuse across the interface. The detailed ramified structure of diffuse interfaces with fractal characteristics can be described by gradient percolation, following the work of Sapoal et al. [9]. When two amorphous polymers are brought into good contact above T_g , the chain conformations at the interface tend to relax towards those in the bulk because of Brownian motion. Five different time regions can be identified [17,18] involving:

- (1) short range Fickian diffusion of monomers;

- (2) Rouse relaxation of entanglements;
- (3) Rouse relaxation of the whole chain,
- (4) reptation diffusion to R_g ;
- (5) Fickian long-range diffusion.

The five time regions are based on the reptation theory proposed by De Gennes [46,47] and Doi and Edwards [48,49] for bulk dynamics of polymer melts and concentrated polymer solutions, and are discussed in detail in Chapter 3 of Ref. [1].

For the purposes of evaluating strength development during welding of A/A interfaces, the reptation region involving diffusion of chain segments to depths of order R_g is the most important. In this section we first elucidate the structure development due to the reptation dynamics. Secondary contributions from segmental motion and Rouse dynamics are treated briefly herein, based on studies by Zhang [18]. The average structure of the interface can be expressed through the concentration profile $C(x, t)$, as derived by Kim and Wool [16] and Zhang and Wool [17,18] from which a set of molecular properties, $H(t)$ can be deduced. The latter are important in developing microscopic deformation models for strength of interfaces.

3.1. Minor chain reptation model

The reptation model proposed by DeGennes [46,47] and Edwards [48,49] describes the dynamics of chains in the melt as a chain moving within a tube, where the tube represents the topological constraints imposed by entanglements with other chains. The reptation model has recently been elucidated by the ripple experiments (Section 3.3) and is the correct model to describe interdiffusion at polymer–polymer interfaces [50–53]. In order to see how a chain disengages itself from the initial tube, chain conformations at different times are shown in Fig. 3 [16]. Here, the tube defined at time $t = 0$ (i.e., the initial tube) is shown as two dotted lines at various times. At $t = t_1$, some end portions of the chain have already ‘escaped’ from the initial tube. The portions of the chains that are no longer in the initial tube increase with time and are called the ‘minor chains’ (Kim and Wool [16]). The random coil (most probable) spherical envelopes enclosing the minor chains at different times are shown as circles in Fig. 4. A minor chain has length $l(t)$, which is an increasing function of time and has the conformation of a random Gaussian chain. We will see later that $l(t)$ is the most important molecular property controlling strength development.

There are three basic time scales in the reptation model [49]. The first time $\tau_e \sim M_e^2$, describes the Rouse relaxation time between entanglements of molecular weight M_e and is a local characteristic of the wriggling motion. The second time $\tau_{RO} \sim M^2$, describes the propagation of wriggle motions along the contour of the chain and is related to the Rouse relaxation time of the whole chain. The important

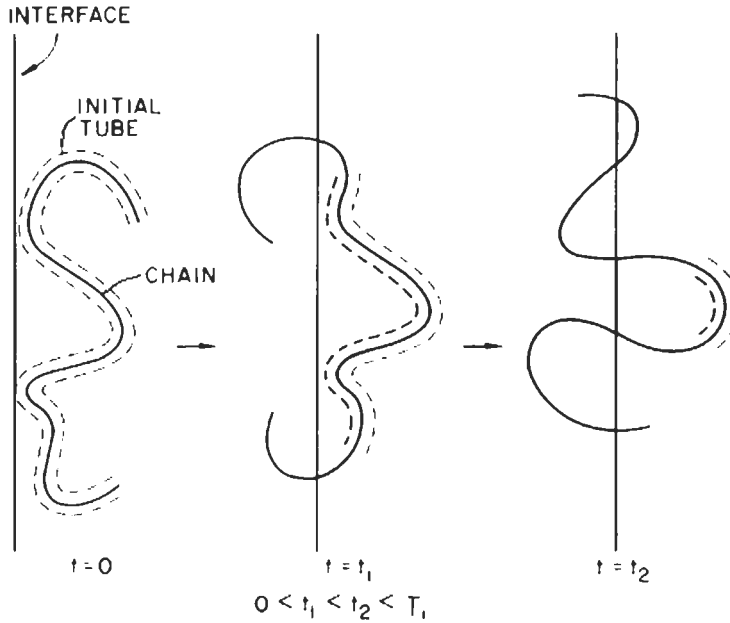


Fig. 3. Disengagement of a chain from its tube near the interface. Only the portion of the initial tube still confines the part of the chain is shown.

time for the welding problem is the reptation time $T_\gamma \sim M^3$, which describes the time required for the chain to escape from its initial tube. T_γ is often referred as the tube renewal time. It is the characteristic relaxation time for the chain and properly refers to the time when about 70% of the chain has escaped from the tube. The 'complete escape time' T_d , is related to T_γ by $T_d = 1.94T_\gamma$ [54,55], or is about twice T_γ . Since the molecular weight M of the linear chains is typically large, the reptation time T_γ is much larger than the Rouse relaxation time, τ_{RO} .

Example: consider polystyrene with $M = 245,000$ and welded to itself at 118°C , the characteristic relaxation times are $\tau_e \sim 10$ s, $\tau_{RO} \sim 21$ min and $T_\gamma \sim 1860$ min [15]. At these relaxation times, the respective average monomer interdiffusion distance is as follows [1]:

$$X(\tau_e) = 0.8R_{ge} \quad (3.1)$$

where R_{ge} is the radius of gyration of the entanglement length. Since $M_e = 18,000$, $R_{ge} = 37$ Å and hence $X(\tau_e) \approx 30$ Å. At the Rouse relaxation time, we have

$$X(\tau_{RO}) = 0.8R_{ge}(M/M_e)^{1/4} \quad (3.2)$$

and hence $X(\tau_{RO}) \approx 60$ Å. At the reptation time,

$$X(T_r) = 0.8R_g \quad (3.3)$$

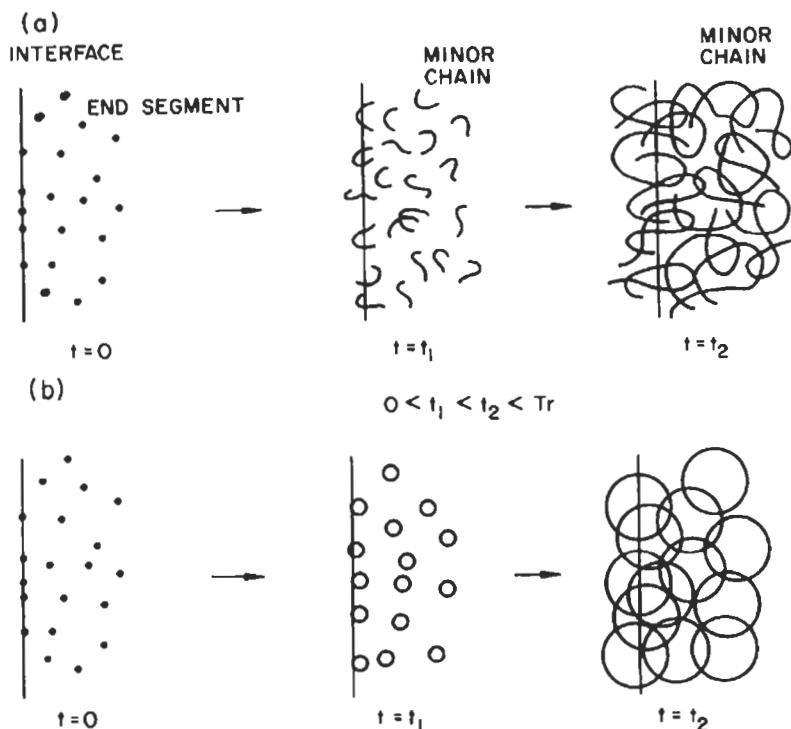


Fig. 4. (a) Motion of minor chains that have poked through from one side of the interface. (b) Growth of the minor chain spherical envelopes that have emerged from side of the interface.

and since $R_g = 136 \text{ \AA}$, we obtain $X(T_r) \approx 110 \text{ \AA}$. We will see later that the weld strength reaches its maximum value at interdiffusion distances $X^* \approx 110 \text{ \AA}$, corresponding to the radius of gyration of polymer with molecular weight $M^* \approx 8M_c \approx 250,000$. Thus, for very high molecular weight polymers, e.g. $M \approx 3 \times 10^6$, X^* can be achieved at the Rouse relaxation time, i.e. when $X^* \approx X(\tau_{RO})$.

The time scale of importance in welding of polymers with molecular weights in the range $M_c \ll M \leq M^*$, is in the region $\tau_{RO} < t \leq T_g$. Welding at times less than τ_{RO} is of importance for high rate fracture processes and for incompatible interfaces. Thus for now, we will ignore times less than τ_{RO} with the understanding that t is always greater than τ_{RO} . The concept of the minor chain turns out to be very useful when evaluating molecular properties at an interface.

3.2. Scaling laws for interdiffusion

The molecular properties $H(t)$, determined by the minor chain model (Table 1), are interrelated and have a convenient common scaling law. The dynamic proper-

Table 1

Molecular aspects of interdiffusion at a polymer–polymer interface

Molecular aspect	Symbol	Dynamic relation ($t < T_r$)	Static relation H ($t = T_r$)	r, s
General property	$H(t)$	$t^{r/4} M^{-s/4}$	$M^{(3r-s)/4}$	r, s
Average contour length	$l(t)$	$t^{1/2} M^{-1/2}$	M	2,2
Number of chains	$n(t)$	$t^{1/4} M^{-5/4}$	$M^{-1/2}$	1,5
Number of bridges	$P(t)$	$t^{1/2} M^{-3/2}$	M^0	2,6
Average monomer diffusion depth	$X(t)$	$t^{1/4} M^{-1/4}$	$M^{1/2}$	1,1
Total number of monomers diffused	$N(t)$	$t^{3/4} M^{-7/4}$	$M^{1/2}$	3,7
Center of mass diffusion	X_{cm}	$t^{1/2} M^{-1}$	$M^{1/2}$	2,4
Fractal diffusion front length	N_f	$t^{1/2} M^{-3/2}$	M^0	2,6

ties, $H(t)$, for the symmetric interface are related to the static properties, H_∞ and the reduced time, t/T_r , by [1]

$$H(t) = H_\infty (t/T_r)^{r/4} \quad (3.4)$$

where

$$H_\infty \sim M^{(3r-s)/4} \quad (3.5)$$

where $r, s = 1, 2, 3, \dots$

If the chain ends are segregated on the surface at the start of the welding, then the same general scaling law applies but with different values of r and s for some of the ‘number’ properties. The average properties remain unaffected [1].

Significant experimental support for these relations and the minor chain reptation model has been obtained from neutron reflection and SIMS experiments using specially deuterated polymers

3.3. Do polymers really move like snakes?

3.3.1. The ripple experiment

We present here a simple experiment, conceived to test both the reptation model and the minor chain model, by Welp et al. [50] and Agrawal et al. [51–53]. Consider the HDH/DHD interface formed with two layers of polystyrene with chain architectures shown in Fig. 5. In one of the layers, the central 50% of the chain is deuterated. This constitutes a triblock copolymer of labeled and normal polystyrene, which is, denoted HDH. In the second layer, the labeling has been reversed so that the two end fractions of the chain are deuterated, denoted by DHD. At temperatures above the glass transition temperature of the polystyrene ($\sim 100^\circ\text{C}$), the polymer chains begin to interdiffuse across the

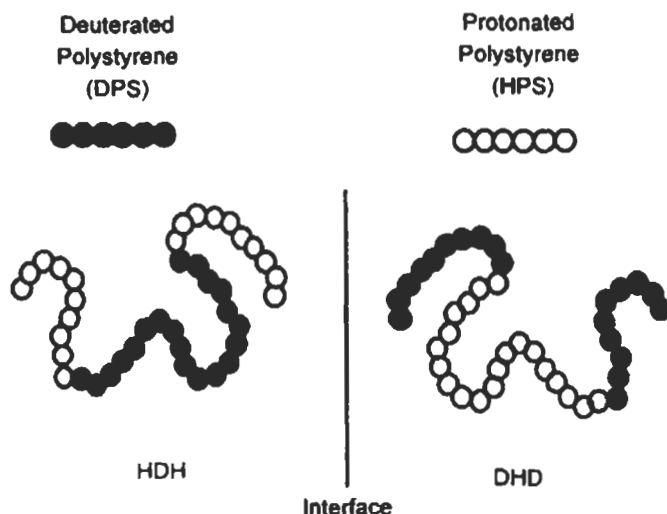


Fig. 5. Labeled triblocks used in the HDH + DHD experiments. The HDH chains have their centers deuterated 50% and the DHD chains have their ends deuterated 25% on each end for a total of 50%.

HDH/DHD interface. If the motion of the polymer was the same for each portion of the molecule, i.e., isotropic, the concentration of deuterium across the interface would remain constant. However, if the monomer motion is anisotropic, such as with reptation, where the chain ends lead the centers, a high amplitude ripple in the concentration profile, as described below will be displayed. For a reptating chain, lateral motion of the central segment of the chain is permitted up to depths approximating the tube diameter, after which the central segments must follow the chain ends in a snake-like fashion.

The ripple experiment works as follows: In Fig. 6, HDH and DHD are depicted by open and filled circles where the filled circles represent the deuterium labeled portions of the molecule and the open circles are the normal (protonated) portions of the chains. Initially, the average concentration vs. depth of the labeled portions of the molecules is 0.5, as seen along the normal to the interface, unless chain-end segregation exists at $t = 0$. If the chains reptate, the chain ends diffuse across the interface before the chain centers. This will lead to a 'ripple' or an excess of deuterium on the HDH side and a depletion on the DHD side of the interface as indicated in the concentration profile shown at the right in Fig. 6. However, when the molecules have diffused distances comparable to R_g , the ripple will vanish and a constant concentration profile at 0.5 will again be found.

Figs. 7 and 8 respectively show the ripples obtained by SIMS and neutron reflection during welding of HDH/DHD interfaces. Its interesting to note that all dynamics models predict ripples since in general, the chain ends move faster than the chain centers. However, their shape, amplitude and time dependence provide a

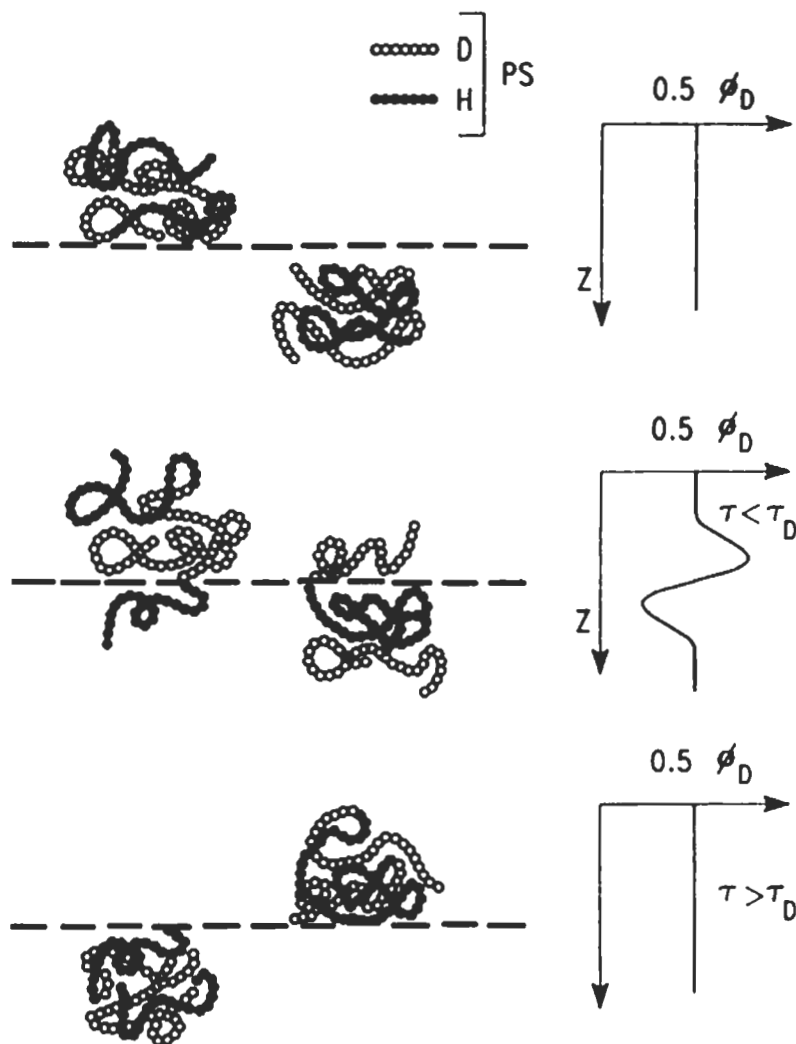


Fig. 6. The ripple experiment at the interface between a bilayer of HDH- and DHD-labeled polystyrene, showing the interdiffusion behavior of matching chains. The protonated sections of the chain are marked by filled circles. The D concentration profiles are shown on the right. Top: the initial interface at $t = 0$. The D concentration profile is flat, since there is 50% deuteration on each side of the interface. Middle: the interface after the chain ends have diffused across ($\tau < \tau_D$). The deuterated chains from Que side enrich the deuterated centers on the other side, vice versa for the protonated sections, and the ripple in the depth profile of D results. A ripple of opposite sign occurs for the H profile. Bottom: the interface when the molecules have fully diffused across. The D profile becomes flat [20,56].

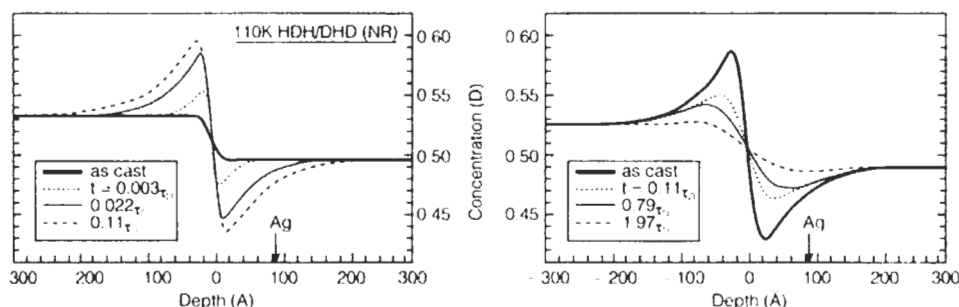


Fig. 7. Concentration profiles of deuterium at the 110 K HDH + DHD interface at the indicated welding times. Left: from 0 to $0.11 \tau_D$. Right: from 0.11 to $1.97 \tau_D$.

unique fingerprint of the dynamics and the observed experimental ripples cannot be explained by models other than reptation [50]. The ripple experiments with polystyrene samples of different molecular weights provide compelling evidence for the validity of the reptation model and the minor chain relations in Table 1. Fig. 9 summarizes and correlates predicted and observed key ripple features for the reptation, mode coupling (PMC) and Rouse dynamics models. It is clear that the reptation model provides a near-perfect correlation with the experimental data while the PMC and Rouse models exhibit substantial deviations. We conclude from this and related studies that the reptation model is the correct model to describe the dynamics of welding at polymer–polymer interfaces.

4. Interface structure vs. strength

4.1. Physics of fracture

We introduce a new vector percolation (VP) model of fracture of polymers in the bulk [1,2] and apply here to examine strength development during autohesion at polymer–polymer and adhesion at polymer–solid interfaces. The model is intended to bridge the gap between interface structure and strength of entangled polymer networks. We clearly distinguish between adhesion at weak interfaces using the nail solution [58] where fracture occurs on a 2D plane, and strong interfaces, where fracture occurs in a 3D network, e.g. via a craze at a crack tip. The VP model addresses the breaking/formation of molecular connectivity in entangled nets and we show how this model can be used to describe the cohesive nature of failure at polymer–solid interfaces. The approach to analyzing the strength of Polymer interfaces is divided into three interdependent parts, as presented in Fig. 2 and discussed in terms of structure, strength and connectivity. We first determine the structure of the A/B interface. This involves a precise description

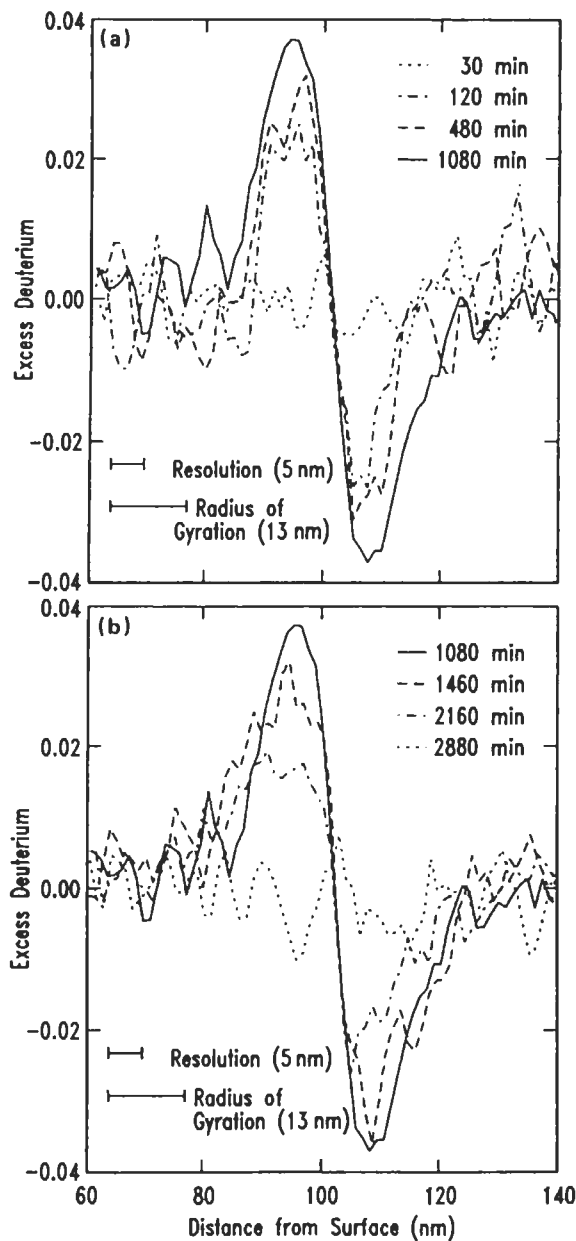


Fig. 8. SIMS analysis of the ripple experiment. Excess deuterium depth profiles for the HDH + DHD bilayer annealed at 118°C; (a) The ripple increasing from 30 to 1080 min. (b) The ripple amplitude decreasing with increasing time from 1080 to 2880 min [20,57].

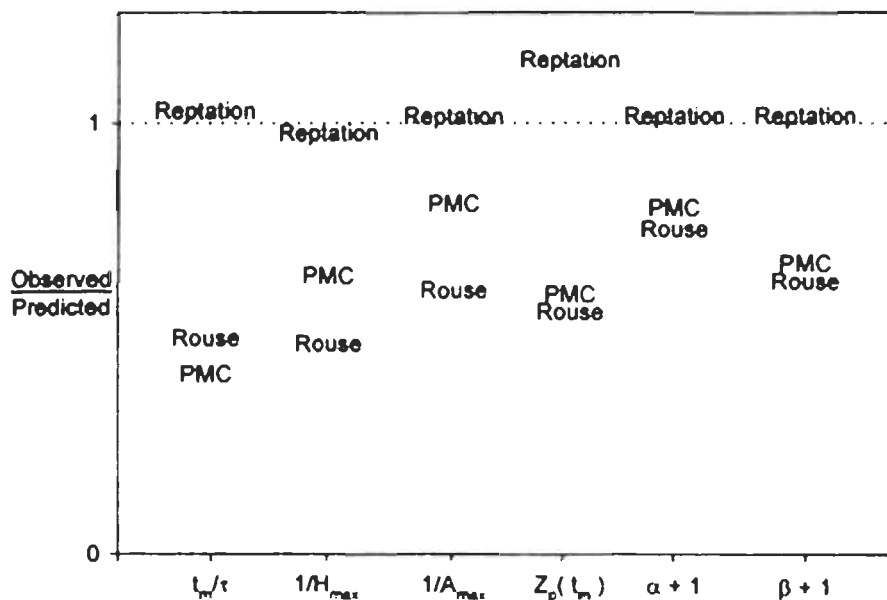


Fig. 9. A correlation chart for the observed/predicted ripple characteristics for the reptation, Rouse and polymer mode coupling models. The reptation model gives the best correlation (~ 1) between theory and experiment.

of the solid substrate and polymer interface at the molecular (5 \AA) and mesophase level ($50\text{--}1000 \text{ \AA}$). Variables include the number of chains Σ , in contact with unit area of the substrate, the molecular length L , the thickness of the interface layer X , the number of sticker groups on the polymer chains $\phi(X)$ and the number of receptor sites $\phi(Y)$ on the solid substrate, the strength of the $X\text{--}Y$ interaction, etc. For an interface with a known structure, we measure the strength G_{lc} or durability da/dN using fracture mechanics. The fracture stress σ , in the deformation zone in Fig. 2 is related to the interface structure through molecular connectivity arguments expressed via vector percolation relations p and related to the externally measured fracture energy G_{lc} through Hutchinson's J-integral theory [5] for an embedded plastic zone (EPZ). P represents the normalized entanglement density ($p = 1$ for a perfect net) in the interface which can be expressed in terms of molecular parameters, Σ , L , $\phi(X)$, $\phi(Y)$, as presented herein.

Using this integrated approach ranging from microscopic to macroscopic, we obtain a relationship between the structure of the interface and its strength for a broad range of interfaces. In this section, we develop the vector percolation theory of fracture and apply it to several cases involving: (1) bulk fracture; (2) fracture by disentanglement; (3) polymer welding and healing; (4) copolymer reinforcement of incompatible polymer interfaces; (5) polymer–solid adhesion; and (6) thermosets.

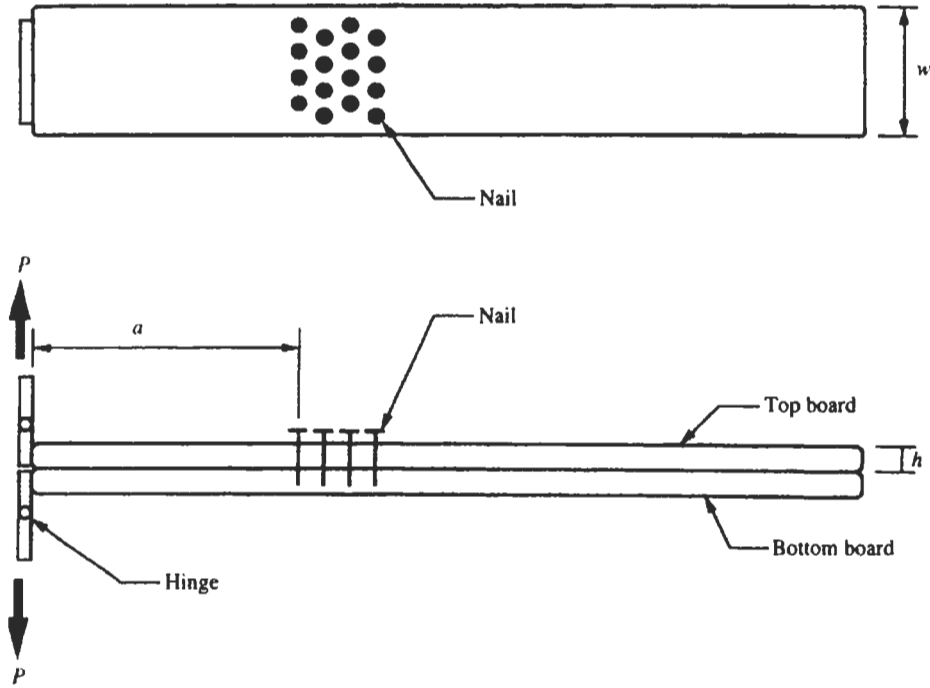


Fig. 10. Cantilever beams used to measure the fracture energy of nail pullout from wood. Top: plan of beam showing nail heads. Bottom: method of loading beams with a load P ; after [58].

4.2. The nail solution: weak interfaces

When relating interface structure to strength, the literature is replete with analyses, which are based on the nail solution [1,58], as shown in Fig. 10. This model is excellent when applied to very weak interfaces ($G_{lc} \sim 1 \text{ J/m}^2$) where most of the fracture events in the interface occur on a well-defined 2D plane. However, the nail solution is not applicable to strong interfaces ($G_{lc} \sim 100\text{--}1000 \text{ J/m}^2$), where the fracture events occur in a 3D deformation zone, at the crack tip. In Fig. 10, two beams are bonded by Σ nails per unit area of penetration length L . The fracture energy G_{lc} , to pull the beams apart at velocity V is determined by

$$G_{lc} = 1/2 \mu_0 \Sigma L^2 V^a \quad (4.1)$$

such that the critical force behaves as $P_{cr} \sim \Sigma^{1/2}$, the fracture energy is linearly proportional to the number of nails per unit area, $G_{lc} \sim \Sigma$ and since energy is force times distance, $f \times L$ with $f \sim L$, then $G_{lc} \sim L^2$. These relations were confirmed by experiments with wooden beams nailed together by Σ nails per unit area [58]. In the special case when the force to pullout the nails exceeds their

fracture force (weak nails), then we obtain

$$G_{lc} = D_o \Sigma \quad (4.2)$$

where D_o is the energy to break a nail.

When comparing the nail solution with molecular systems, an additional surface energy term G_o , term needs to be added to the fracture energy [1]

$$G_{lc} = G_o(\text{surface}) + G_{lc}(\text{friction}) \quad (4.3)$$

in which $G_{lc}(\text{friction}) \sim \Sigma L^2$, as described by Eq. 4.1; $G_o P(\text{surface})$ is the modified Griffith surface tension term [1]

$$G_o \approx 2S\Gamma \quad (4.4)$$

where Γ is the usual surface energy of the debonded beams and S is the Sapoval number describing surface roughness ($S = 1$ for a perfectly flat fracture surface and $\Gamma \approx 0.1 \text{ J/m}^2$). For diffuse interfaces with diffusion length X , the surface roughness S is obtained from gradient percolation theory by [1,9]

$$S = (X/b)^{v(D-1)/(v+1)} \quad (4.5)$$

where b is a characteristic bond length, D is the fractal dimension of the fractal clusters and v is the critical exponent. For example, in two dimensions, $D = 7/4$, $v = 4/3$ and $S \sim X^{0.43}$; in 3D, $v = 0.8$ and $D \approx 2.5$ such that $S \sim (X/b)^{2/3}$. For random walk chains consisting of N steps of length b , $X \approx N^{1/2}b$, and hence $S \sim N^{1/3}$.

The nail solution can be applied to understand the behavior of real molecules at interfaces, provided they behave like nails in simple friction pullout and fracture events are generally associated with a single plane. A useful example is the strength of incompatible A/B interfaces reinforced with A–B diblocks in which one end A, of the diblock is below its entanglement molecular weight and the other end B is highly entangled. In that case, Creton et al. [59,60] have shown that the short A-end pulls out cleanly from the A-side while the long B-end remains anchored on the B-side. Their data provide support for $G_{lc} \sim \Sigma L^2$ up to a critical length L_c . In this case, we expect contributions from both friction and the surface interfacial energy term, Γ_{AB} , such that

$$G_{lc} = 2S\Gamma_{AB} + 1/2\mu_o L^2 \Sigma \quad (4.6)$$

in which Σ is the areal density of diblock chains.

For weak interfaces formed with low molecular weight chains (less than the critical entanglement molecular weight M_c), chain segment pullout dominates the fracture process. However, the whole chain does not pullout, but rather bridge segments of length $L \sim M^{1/2}$. The number of bridges per unit area Σ , is

independent of molecular weight. Thus, the friction term $G \sim \Sigma L^2 \sim M$, and we expect the fracture energy to be determined by an expression of the form

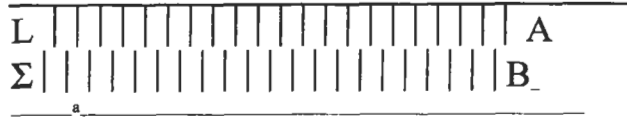
$$G_{lc} = G_0 + kM \quad (4.7)$$

where the constant k is proportional to the monomer friction coefficient. Analysis of wedge-cleavage fracture experiments with low molecular weight ($M < M_c$) polystyrene indicate that $G_0 = 0.24 \text{ J/m}^2$ and $k = 3.4 \times 10^{-5} \text{ J/m}^2 \text{ Da}$. In this case, $2\Gamma = 0.08$ such that the Sapoval number in Eq. 4.4 is $S \approx 3$, which represents an average value over the molecular weight range from M_0 to M_c , where X varies from $X \approx b \approx 1 \text{ nm}$ to about 5 nm .

As shown in Fig. 10, the nail solution applies to relatively weak interfaces, $G_{lc} \sim 1 \text{ J/m}^2$, where all the fracture events occur on one plane and the matrix holding the molecular nails does not deform but offers frictional resistance. In the next section, we explore how the fracture energy can increase by several orders of magnitude as we proceed from nails to nets.

4.3. Bi-material interfaces and viscoelastic deformation

Consider an incompatible semicrystalline A/B interface, where for example material A is a soft viscoelastic thermoplastic (e.g., polybutadiene or polyurethane) and B is a rigid semicrystalline polymer (e.g., PET or ethylene vinyl alcohol). The strength that develops at the A/B interface following contact in the melt, is largely determined by crystalline influxes (Chapt. 10, [1]) from one or both sides, which can be either inter-spherulitic, or intra-spherulitic. The origin of influxes derives from differences in crystallization rates, melting points, and they occur during initial crystallization from the extruded melt and during annealing [1]. Influxes occur due to local volumetric shrinkage induced by first order phase transitions from liquid to solid, and due to entrapment of one material in the other during lamellar growth and twisting of ribbon-like lamella bundles in the spherulite morphology. The influxes provide mechanical connectivity and strength across the A/B interface. Although typically weak, with low intrinsic fracture energy at the interface, the influxes generate sufficient stresses to activate significant energy dissipative processes in the A layer. The external peel forces are resisted by the influxes which transmit initial elastic energy into the body of A, most of which becomes dissipated by visco-plastic processes. The external peel force necessary to store elastic energy in the layers and overcome the visco-plastic processes in the interface can appear to be quite large. Overall, these processes are exceedingly complex, both from a basic understanding of the influx mechanism (interface structure) coupled with an understanding of the visco-plastic deformation processes controlling interface strength. In this section, we will simplify matters considerably by: (a) assuming an interface influx structure; (b) develop an expression for the intrinsic interface strength due to influxes; and (c) couple the interface structure with a



Scheme 1. Schematic of influxes of length L , spacing a , and areal density Σ .

primitive visco-plastic fracture model. We will see that major trends are predicted in terms of composite design and interface structure.

4.4. Interface strength with influxes

The influxes behave as nails at the interface, bonding A and B together (Scheme 1). They have an average length L , spacing a , and an areal density Σ , which is the number of influxes per unit area. Typically, there will be a maximum number of influxes that can be generated, $\Sigma_0 \sim 1/a^2$ and the influx areal coverage index I , is given by

$$I = \frac{\Sigma}{\Sigma_0} \quad (4.8)$$

This influx coverage parameter I , can be used to characterize both intra and inter-spherulitic influxes and combinations of the two. The maximum force F_i , required to cohesively break an influx is determined by

$$F_i = \sigma_0 a^2 \quad (4.9)$$

where σ_0 is the fracture stress of the influx, which can be determined from the bulk fracture properties of material A or B. The force F to pull out an influx will be less than F_i , if it does not break. The fracture energy of the interface is determined by the nail solution, Eq. 4.1, where we have the simple predictions, $G_{lc} \sim \Sigma$ and $G_{lc} \sim L^2$ (up to some maximum value L_c when the pullout forces exceed the cohesive fracture forces of the influx).

To evaluate the influx solution experimentally for an A/B cantilever beam configuration as shown in Fig. 1, we apply Griffith's theory at the critical moment of fracture, such that the incremental change in stored elastic energy U , with change in crack length a , is just sufficient to overcome the fracture surface energy S

$$\frac{\partial U}{\partial c} \geq \frac{\partial S}{\partial c} \quad (4.10)$$

in which the surface energy term $S = cwG_{lc}$, such that $\partial S/\partial c = wG_{lc}$. The strain energy in the beams U , is determined from simple beam theory by

$$U = \frac{P^2 c^3}{3EI} \quad (4.11)$$

in which E is the modulus and $I = wh^3/12$ is the moment of inertia. Since

$$\frac{\partial U}{\partial c} = \frac{P^2 c^2}{EI} \quad (4.12)$$

we obtain the fracture energy in terms of the critical force P_{cr} and dimension of the beams as

$$G_{lc} = \frac{12P_{cr}^2 c^2}{Ewh^3} \quad (4.13)$$

This solution assumes that the beams behave elastically and that all the energy dissipation is associated with the pullout process. Typically for rigid incompatible interfaces, this fracture energy is quite low, ca. 1–5 J/m² [1,20,21,61,59].

In a peeling mode, the critical peel force F_c is determined by the resistance of the influxes on the first row across the ‘peel front’, such that the critical peel force F_c , depends on the square root of the number of influxes per unit area, as

$$F_c = F_1 w \Sigma^{1/2} \quad (4.14)$$

Here, F_1 is the force required to pullout or break one influx. The stress σ_c associated with the critical peel force F_c is determined by

$$\sigma_c = \frac{F_c}{wa} = \frac{F_1 \Sigma^{1/2}}{a} \quad (4.15)$$

To make an approximate estimate of G_{lc} for influxes in terms of known properties, we substitute F_1 for F_1 in Eq. 4.15 and obtain the maximum critical stress for any influx index I as

$$\sigma_c = \sigma_0 a \Sigma^{1/2} \quad (4.16)$$

Since $\Sigma = I/a^2$, we obtain

$$\sigma_c = \sigma_0 I^{1/2} \quad (4.17)$$

The fracture energy for influxes with a maximum fracture force F_i is determined by

$$G_{lc} = \frac{1}{2} F_i L_c \Sigma \quad (4.18)$$

where L_c is the critical length at which the influx breaks. From the latter three equations, it is apparent that the maximum intrinsic fracture energy for influxes at the A/B interface is obtained as

$$G_{lc} = \frac{1}{2} \sigma_0 L_c I \quad (4.19)$$

Example: Let us assume for an A–B bilayer in peel that we have the following: $\sigma_0 = 4000$ psi, (fracture or yield strength of A); $I = 1$ (complete influx coverage);

$L_c = 4 \times 10^{-5}$ in (about 1 μm , which is generous). This would give the maximum intrinsic fracture energy of the A/B interface $G_{lc} \sim 0.1$ pli. This would be at least an order of magnitude less than would be observed experimentally. This important discrepancy is addressed in the next section.

4.5. Visco-plastic peel of A–B bilayers with influxes

Peel energies of viscoelastic polymers are typically an order of magnitude greater than the intrinsic fracture energy of the interface, as discussed above. The influxes provide sufficient connectivity at the A/B interface to generate a visco-plastic deformation zone at the crack tip. Solutions to this problem are exceedingly complex and usually done on supercomputers when sufficient information is known about the constitutive properties of both materials and the nature of the deformation zone and interface. The J-integral theory is used to determine the fracture energy and this approach accounts for all the energy dissipated in the deformation zone. Detailed studies of bi-material interfaces normally consider differences in moduli, sample thickness, Poisson ratios, yield points, deformation zone evolution, tri-axial stresses, and fracture mode mixing (tensile, shear and twist). Let us assume that the yield strength of the A material is less than B, and that most of the visco-plastic processes occur in the A layer. The traction stresses σ , in the deformation zone will cause either fracture of the influxes at the interface, or cohesive fracture in the zone itself by the vector percolation process (Section 5). To simplify matters further, we can safely assume that the influxes control the evolution of the traction stresses.

The peel energy G , of the A–B interface can be determined by

$$G = P/2w \quad (4.20)$$

where P is the measured peel force and w is the width. The work W , to debond a new crack of length c , is determined by

$$W = Pc = U_v + 2G_{lc}wc \quad (4.21)$$

in which U_v is the visco-plastic energy dissipation, and G_{lc} is the true interface strength (Eq. 4.19) due to the influxes. Note that when $U_v = 0$, $G_{lc} = P/2w$, as in Eq. 4.20. We now make a useful approximation for U_v , which allows us to couple the volumetric energy dissipation to the true interface strength described in the last section. We let U_v be described by

$$U_v = \beta \frac{\sigma_c^2}{2E} hwc \quad (4.22)$$

where h is the effective layer thickness, E is the rate sensitive tensile modulus of the A layer, σ_c is the critical peel stress developed at the interface due to the influxes (Eq. 4.17), hwc is the volume where the energy is being dissipated at

the crack tip, and β is the fraction of the stored elastic energy density which is dissipated by visco-plastic processes. Note that the term $\sigma^2/2E$ is the normal stored energy density term for elastic bodies subjected to a uniaxial stress σ . Triaxial stresses for bi-material interfaces are exceedingly complex and can be used in a more detailed study, but which we will neglect for now in this approximation.

Differentiating Eq. 4.21 with respect to crack length c , we obtain the critical forces and energy as

$$G = \frac{P}{2w} = \beta \frac{\sigma_c^2}{2E} h w + G_{lc} \quad (4.23)$$

Since $\sigma_c = \sigma_o I^{1/2}$ and the strength due to influxes is $G_{lc} = 1/2 \sigma_o L_c I$, we obtain the final coupled visco-plastic fracture equation for the A–B interface as

$$G = \beta \frac{\sigma_o^2}{2E} I h + \frac{1}{2} \sigma_o L_c I \quad (4.24)$$

Basically, the term $[\beta(\sigma_o^2/2E)Ih]$ is the visco-plastic dissipation term and the term $[1/2 \sigma_o L_c I]$ is the intrinsic interface strength term. This equation can be further rearranged to

$$G = \frac{1}{2} \sigma_o I \left[\frac{\sigma_o}{E} h + L_c \right] \quad (4.25)$$

In which we summarize the terms as: σ_o = cohesive fracture strength of A; E = modulus of A; h = thickness of A layer; L = influx length to a maximum length L_c ; I = influx coverage of the A–B interface ($I < 1$); β = fraction of elastic energy dissipated in the A layer ($\beta < 1$).

A few useful predictions are evident from the above relations as follows:

- (1) Influxes: when $I = 0$, no influxes, the peel strength goes to zero. We also have $G \sim I$, such that G increases linearly with I .
- (2) Elastic vs. viscoelastic: when $\beta = 0$, no visco-plastic deformation occurs, Eq. 4.25 gives the intrinsic strength of the interface.
- (3) Thickness effect h : since $h \gg L_c$, Eq. 4.25 predicts that $G \sim h$.
- (4) Influxes length L : as the influx length increases, the influx strength σ increases from zero to its maximum value σ_o according to $\sigma(L) = \sigma_o(L/L_c)$. Since the first term (in Eq. 4.25) dominates the peel energy, we see that $G \sim L^2$.
- (5) True vs. apparent strength: the visco-plastic energy dissipation dominated the magnitude of the peel strength. However, little dissipation occurs if the interface becomes very weak. In other words, some influxes are necessary to produce sufficient stress to activate the viscoelastic deformation in the body of the A.

Example: the peel energy G is given by

$$G = \beta \frac{\sigma_o^2}{2E} I h + \frac{1}{2} \sigma_o L_c I.$$

Let us examine this relation for typical values of the A/B interface: $\beta = 1$ (max energy dissipation in the A layer); $I = 1$ (max strength of interface with influxes); $E = 12,000$ psi; $\sigma_o = 4000$ psi; $h = 30$ mils (10^{-3} in); $L_c = 4 \times 10^{-5}$ in. We obtain for both terms: $G = 20$ pli (energy dissipated) + 0.08 pli (true interface strength with max influxes), or $G \sim 20$ pli, which says that the measured peel strength is dominated by visco-plastic deformation processes.

Note that for autohesion of viscoelastic layers in contact above T_g , that the above equations can be utilized by substituting for I with the molecular structure factor $H(t)$ (and appropriate ratios) from Table 1 such that

$$I(t) = H(t)/H_\infty \quad (4.26)$$

In the next section, we will see that for the commonly encountered symmetric amorphous interface that

$$I \sim \frac{n(t)L(t)X_\infty}{X(t)n_\infty L_\infty} \quad (4.27)$$

In which X is the average monomer interpenetration distance, L is the contour length of interdiffused chains and $n(t)$ is the number of chains diffused at time t . The time and molecular weight dependence of these molecular properties are given in Table 1.

5. The net solution: strong interfaces

Strong interfaces develop when the energy is dissipated in a large volume containing the interface, e.g., at crazes and deformation zones at crack tips, as described in Fig. 2. During welding of linear polymer chains in the melt, as interdiffusion proceeds across the polymer-polymer interface, we need to consider fracture events occurring on many planes away from the interface plane defined at the moment of contact. The long chains diffusing across the interface create fractal connectivity between the planes (ala gradient percolation) and this connectivity is broken by deformation mechanisms involving chain disentanglement or bond rupture. In this section, we use a percolation model to describe connectivity between chains and relate the interface structure to the breakdown process of the deformation zone at a crack tip. Scalar percolation theory concerns the connectivity of one component randomly dispersed in another. Examples include gelation during polymerization of monomers with multifunctional linkages, conduction of electricity through metal particles randomly dispersed in an insulator and microbial

invasion on randomly distributed biodegradable particles in a non-biodegradable matrix [62]. Vector percolation [57,63–73] involves the transmission of forces or vectors through a lattice (2D or 3D) where a certain fraction of the bonds are broken or missing. Thus, we can examine how the stiffness and strength of the lattice changes with bond fracture or disentanglement. Vector percolation has many potential applications in molecular fracture, craze fibril breakdown, network relaxation in the terminal zone of polymer melts, and melting of thin films.

5.1. Vector percolation model of fracture in nets

The transmission of forces through a lattice as a function of the fraction p , of bonds in the lattice has been analyzed by Kantor and Webman [63], Feng and colleagues [64–66], Thorpe et al. [68–72] and others [73]. The normalized elastic modulus E/E_0 , of the lattice as a function of p was found to obey relations similar to scalar percolation

$$E/E_0 = (p - p_c)^v \quad (5.1)$$

where p_c is the percolation threshold and v is the critical exponent. For example, in 2D, the exponent for scalar percolation is about 1.3, which compares with exponents in the range of 3–5 for vector percolation. Vector percolation is considered to belong to a different universality class than scalar percolation.

We examined the role of vector percolation in the fracture of model nets at constant strain and subjected to random bond scission, as shown in Fig. 11 [1,2]. In this experiment, a metal net of modulus E_0 containing $N_0 = 10^4$ bonds was stressed and held at constant strain (ca. 2%) on a tensile tester. A computer randomly selected a bond, which was manually cut, and the relaxation of the net modulus was measured. The initial relaxation process as a function of the number of bonds cut N , could be well described by the effective medium theory (EMT) via

$$E/E_0 = 1 - 3N/N_0 \quad (5.2)$$

The fraction of bonds p remaining in the lattice is related to the number cut N by

$$p = 1 - N/N_0 \quad (5.3)$$

and the relaxation equation is derived as

$$E/E_0 = 3p - 2 \quad (5.4)$$

The EMT analysis indicated that the stress relaxes in proportion to the number of bonds removed. The initial linear decrease of E/E_0 with is intuitively appealing and is the basis for many linear constitutive theories of polymers. An example is the Doi–Edwards theory of viscoelasticity of linear polymer melts [49] in which

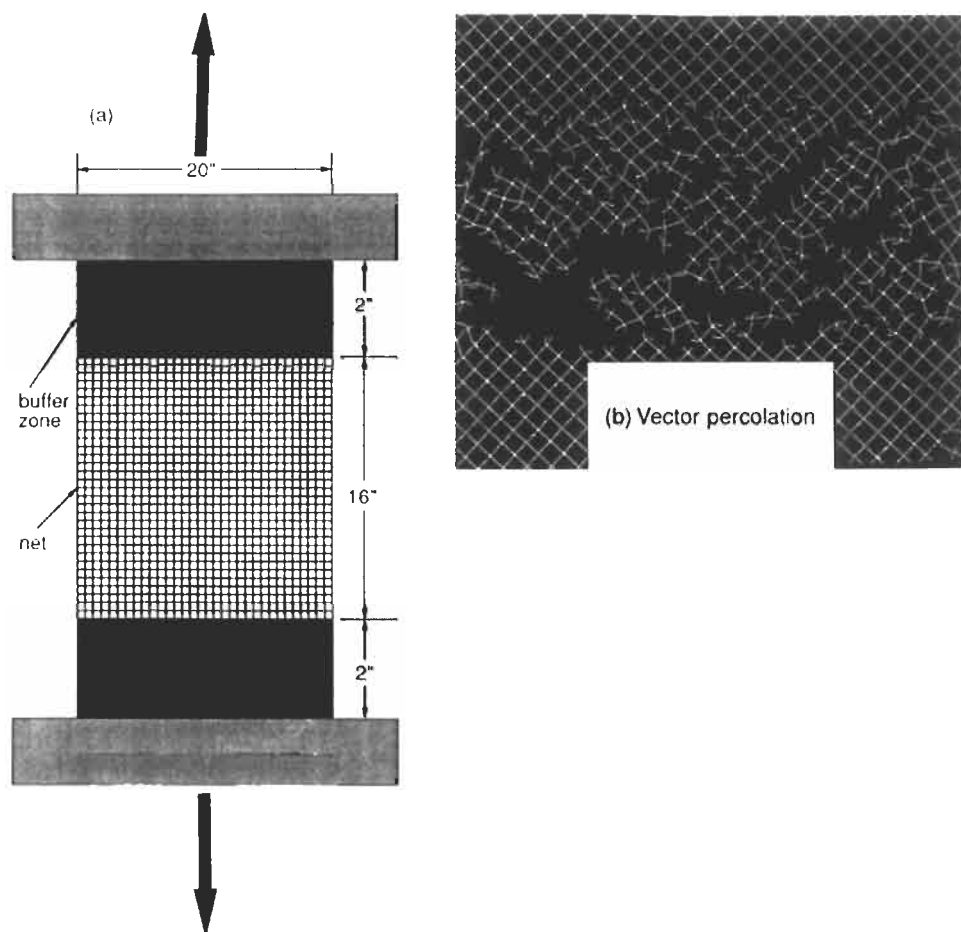


Fig. 11. The role of vector percolation in the fracture of model nets at constant strain and subjected to random bond scission.

the stress relaxation modulus is proportional to the number of entanglements remaining in the relaxing rubbery network. In our studies of model nets, we find that the EMT analysis is excellent for lattices of finite size containing fewer than 2000 bonds. For such small lattices, the modulus ratio E/E_0 relaxes with a slope given by $3/N_0$ and an intercept on the N -axis of $N_0/3$, in accord with Eq. 5.2.

However, for larger lattices, $N_0 \sim 10^4$, percolation develops after about 80% relaxation occurs; such a lattice near percolation is shown in Fig. 11. For vector percolation to be observable, the lattice size must be large enough so that as percolation is approached near p_c , finite sized clusters of fractured bonds do not completely relax the lattice by bridging the mechanical grips holding the lattice. In percolation language, this means that the lattice length L must be greater than

the cluster correlation length and obey the relationship

$$L > (p - p_c)^{-\nu} \quad (5.5)$$

where $(p - p_c) \approx 0.05$ (within 5% of percolation) and ν is the critical exponent for the correlation length. Lobb and Forester demonstrated this relation for torsional rigidity relaxation of cylindrical nets subjected to random bond scission [57]. For most molecular systems, especially entanglement networks, the lattice size is effectively infinite compared to the above macroscopic experiment and we expect vector percolation to play an important role in the final stages of stress relaxation and fracture. As the initial fraction of bonds ($p = 1$) decays to the percolation threshold p_c , the stored strain energy U in the net similarly decays to zero. Thus, to fracture or stress relax a lattice, it is not necessary to break all the bonds, but only a percolation fraction $(p - p_c)$. In relaxation of linear polymer entangled nets, we have hypothesized that the term $(p - p_c)$ gives rise to the controversial $\eta \sim M^{3.4}$ law for the molecular weight dependence of the zero-shear viscosity [1].

Several interesting points are presented by the vector percolation process. As deduced from Fig. 11, the stress distribution in the lattice bonds becomes highly non-uniform such that some bonds are highly stressed and others bear little stress. The existence of highly stressed bonds is a prelude to molecular fracture and parallels the 'hot bonds' in conductivity percolation. In electrical circuits, hot bonds arise from high current density in single bonds in a tortuously connected network near the percolation threshold. The hot bond overheats in the high current density. The concept of mechanical hot bonds is relevant to fracture of polymers in general. When polymers such as polypropylene and polyethylene are subjected to uniform tensile stresses, we and others have shown using infrared and Raman spectroscopy that the molecular stress distribution can be quite broad, even though the applied stress is well below the macroscopic fracture stress [1,2]. The development of the molecular stress distribution $\phi(\sigma)$ is due to the inherent sloppiness of the lattice.

Another point of interest is that only a fraction of the bonds must be fractured before complete failure occurs. Thus, in a deformation zone at a crack tip, the crack advances through the zone by breaking a fraction $p - p_c$ of bonds or fibrils in parts of a craze network. The broken bonds do not lie on the same plane, as often assumed, but are distributed over the deformation zone volume. An important corollary of the existence of the threshold p_c is that when $p < p_c$, no strength exists (above that of the nail solution). Thus, the molecular lengths M must be long enough, the number of chains Σ at the interface must be great enough and the number of entanglements in the lattice has to exceed the percolation threshold before strength develops. In each case the normalized entanglement density p , will result in critical molecular parameters such as M_c and Σ_c .

Consider the vector percolation experiment shown in Fig. 11 applied to any 3D lattice in general. The stored strain energy density U in the lattice due to an

applied stress σ is determined in the uniaxial approximation by

$$U = \frac{\sigma^2}{2E} \quad (5.6)$$

The stored strain energy can also be determined for the general case of multiaxial stresses [1] and lattices of varying crystal structure and anisotropy. The latter could be important at interfaces where mode mixing can occur, or for fracture of rubber, where U is a function of the three stretch ratios λ_1 , λ_2 and λ_3 , for example, via the Mooney–Rivlin equation, or suitable finite deformation strain energy functional.

The energy dissipation per unit volume to fracture a network consisting of a bond density $N_{ev} = \rho/M_e$ bonds per unit volume is

$$U_f = D_o(p - p_c) \frac{\rho}{M_e} \quad (5.7)$$

where D_o is the bond fracture energy, ρ is the density and $(p - p_c)$ is the percolation fraction of bonds which must be broken to cause fracture in the network. In this approach, the strain energy U is first stored in the net and we inquire if this energy is sufficient to break $(p - p_c)\rho/M_e$ bonds per unit volume when it releases at a critical strain energy density $U^* = \sigma^{2*}/2E$, such that at the critical condition,

$$U^* \geq U_f \quad (5.8)$$

It is important to note that we assume the random fracture approximation (RPA) is applicable. This assumption has certain implications, the most important of which is that it bypasses the real evolutionary details of the highly complex process of the lattice bond stress distribution $\phi(\sigma)$ creating bond rupture events, which influence other bond rupture events, redistribution of $\phi(\sigma)$, microvoid formation, propagation, coalescence, etc., and finally, macroscopic failure. We have made real lattice fracture calculations by computer simulations but typically, the lattice size is not large enough to be within percolation criteria before the calculations become excessive. However, the fractal nature of the distributed damage clusters is always evident and the RPA, while providing an easy solution to an extremely complex process, remains physically realistic.

Substituting for U^* and U_f in Eq. 5.8 and solving for the critical stress σ^* , we obtain the 'net solution' as

$$\sigma^* = \left[2(p - p_c)E_c D_o \frac{\rho}{M_e} \right]^{1/2} \quad (5.9)$$

This equation predicts that the fracture stress increases with the square root of the number of bonds to be broken and is inversely proportional to M_e . The percolation parameter p is in effect, the normalized bond density such that for a perfect net without defects, $p = 1$ and for a net that is damaged or contains missing bonds,

then $p < 1$. Obviously, as p approaches p_c , the fracture stress decreases and we have a very fragile material. This relation could therefore be used to evaluate durability, or retention strength of a material by tracking damage accumulation through a single parameter p . Note that the net solution refers to the stress required to fracture a unit volume of the net in uniaxial tension. When applied to interfaces, we let the volume of material or net, contain the interface such that we can calculate σ^* with a knowledge of p based on a local normalized entanglement density. In all applications of the VP model, the stressed state is the reference state to assess percolation and connectivity. This will become more apparent when we examine disentanglement for example, where an unraveling, or disentanglement process in the stretched state breaks connectivity.

When fracture is confined to a single plane of the lattice, the net solution collapses to the nail solution. Consider an atomically thin slab of dimension $v = AL$, where A is unit area and L is a bond length, the strain energy stored is $U = \sigma^2 AL/2E$ and the energy dissipated is $U_f = D_0 \Sigma(p - p_c)$. The VP model then predicts that $G_{lc} \sim \sigma^{*2}$ such that

$$G_{lc} \sim D_0 \Sigma \quad (5.10)$$

where Σ is the number of bonds to be broken per unit area and D_0 is the energy to break a single bond. In this case, we see that the net solution returns to the nail solution as the 3D fracture process becomes confined to a single plane. In the following sections, we explore applications of the net solution.

6. Fracture of entangled polymer nets

Entangled linear polymers form 'sloppy' nets of irregular entanglement lengths whose average length is determined by the familiar entanglement molecular weight, M_e . When a stress σ is applied to the polymer, hot bonds break at molecular stresses, which are typically two orders of magnitude greater than the applied macroscopic stress σ . Rupture of the hot bonds occurs randomly in the net and they accumulate and connect in a percolation fashion, as discussed in the last section. As the bonds break (1 per entanglement length), the stored energy U in the net is consumed and approaches zero at the vector percolation threshold, p_c . Macroscopic fracture occurs when the stored energy is released by percolating random microscopic fracture events, implied schematically in Fig. 11.

The net solution for fracture stress (Eq. 5.9) can be further simplified by the following assumptions: (a) for very high molecular weights, $p \approx 1$ (no chain end effects on the entanglement density), $p_c \approx 1/2$ and hence $2(p - p_c) \approx 1$; (b) the stress in the craze is higher than the macroscopic stress due to the area reduction at high draw ratio λ , which gives $\sigma^* = \sigma_c/\lambda$, where σ^* is the applied stress at the craze/glass fibril interface and λ is the fibril draw ratio; (c) for most drawing

processes, $\lambda \approx 4$. Making these substitutions in Eq. 5.9, the fracture stress of high molecular weight polymers undergoing vector percolation via random bond fracture is

$$\sigma^* \approx \left(\frac{E D_o \rho}{16 M_e} \right)^{1/2} \quad (6.1)$$

The latter equation contains constants with well-known values and can therefore be used to predict the fracture stress of most polymers. For example, the bond dissociation energy D_o , is about 80 kcal/mol for a C–C bond. For polystyrene, the modulus $E \approx 2$ GPa, $\lambda \approx 4$, $\rho = 1.2$ g/cm³, $M_e = 18,000$, and we obtain the fracture stress, $\sigma^* \approx 47$ MPa, which compares well with reported values. Polycarbonate, with similar modulus but a lower $M_e = 2,400$ is expected to have a fracture stress of about 100 MPa. In general, letting $E \sim 1$ GPa, $\rho = 1.0$ g/cm³, and $D_o = 335$ kJ/mol, the tensile strength is well approximated by

$$\sigma = K / M_e^{1/2} \quad (6.2)$$

where the constant $K \sim 4.6$ GPa (Da)^{1/2} for unit density and modulus ($E = 1$ GPa)

Vincent analyzed the tensile fracture stress σ , of a broad range of polymers as a function of the number of backbone bonds per cross sectional area (Ω) and found a nearly linear relation, $\sigma \sim \Omega$, as shown in Fig. 12. Ω is related to M_e via the theory of entanglements for random walk chains as [74]

$$\Omega = \frac{3.93 (C_{oo} j / M_o)^{1/2} b \rho N_a}{M_e^{1/2}} \quad (6.3)$$

or

$$\Omega = \beta / M_e^{1/2} \quad (6.4)$$

where the parameter $\beta = \{3.93 (C_{oo} j / M_o)^{1/2} b \rho N_a\}$ in which C_{oo} , j , M_o , b and N_a are the characteristic ratio, number of backbone bonds per monomer, monomer molecular weight, bond length and Avogadro's number, respectively. Combining Eq. 6.4 with Eq. 6.2, we obtain the relation

$$\sigma = (K / \beta) \Omega \quad (6.5)$$

Thus, if the ratio K / β is constant, then the behavior shown in Fig. 12 could be described by the net solution. For many polymers, the characteristic ratio is around 7–10, the ratio M_o / j is the molecular weight per backbone bond (ca. 30–50) and will not vary extensively, $b = 1.54$ Å and the density is about 1 g/cm³ such that the parameter β is nearly constant. Since K is not very sensitive to the polymer properties, Eq. 6.5 is considered to describe the observed fracture behavior shown in Fig. 12. However, the data are not expected to fall on the straight line due to differences in K and β for each polymer. As a specific test case, consider

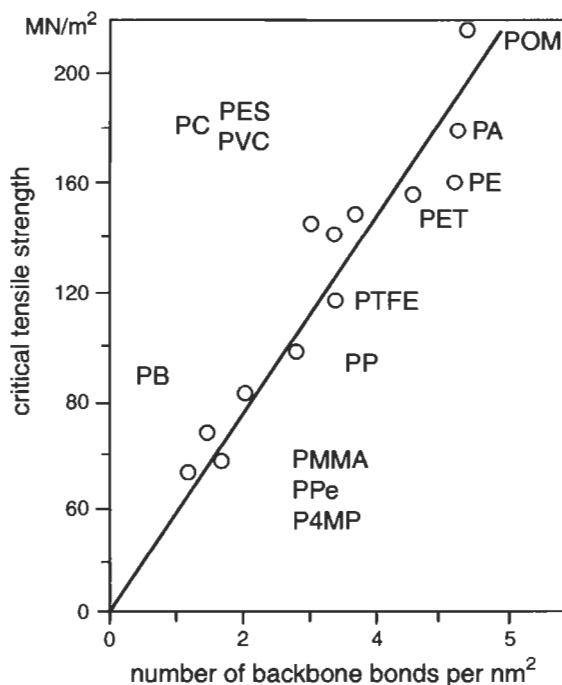


Fig. 12. Tensile strength σ , vs. number of backbone bonds per monomer $1/a$, reported for a range of polymers by Vincent [75]. The solid line is the theoretical line for vector percolation analysis of strength discussed herein.

polypropylene (PP), where from Fig. 12, $\sigma = 95$ MPa and $\Omega = 3$. Since $C_{00} = 5.8$, $j = 2$, $M_0 = 42$ g/mol, $b = 1.54$ Å, $\rho = 1.0$ g/cm³ and $M_e = 3500$ g/mol, hence from Eq. 6.4 we obtain $\beta = 191$ Da^{1/2}/nm² and $\Omega = 3.2$, which is reasonable. The fracture stress for PP as predicted from Eq. 6.5 is expected to be 77 MPa, which is lower than reported by Vincent (ca. 95 MPa). The slope of the line in Fig. 12 is 35 MPa/nm², which compares with $K/\beta = 24$ for PP and 41 MPa/nm² for PS.

6.1. Hot bond fracture stress

The 'hot bond' fracture stress σ_h , is determined from the anharmonic nature of the C–C bond using the Morse potential energy function by [1]

$$\sigma_h = \frac{D_0 a_m}{2a \cos \theta} \quad (6.6)$$

where $a_m = 1.99$ Å⁻¹ is the Morse parameter, a is the cross-sectional area of the molecule and $\cos \theta$ is the angle between the bond and the applied stress (typically, $\cos \theta \approx 1$). Using values for polystyrene with $a = 111$ Å² and $D_0 = 80$ kcal/mol, we obtain $\sigma_h \approx 5$ GPa. Thus, the applied macroscopic stress creates a broad

stress distribution with molecular stresses that are up to 100 times greater. As bonds break, the stress distribution $\phi(\sigma)$ rearranges, the strain energy decreases and moves around, vectors propagate along remaining connected pathways, microvoids form, coalesce and eventually lead to microscopic crack propagation through the fractal percolation clusters.

7. Relation to J-integral fracture mechanics

Using the Hutchinson [5] theory of fracture for EPZ, such as crazes at crack tips, the fracture energy is approximated using the J-integral approach as shown in Fig. 13. The EPZ model addresses small scale yielding at the crack tip and describes the work of separation as a function of rate, yield stress and the stress as a function of displacement δ in the zone. The vector percolation model describes the maximum stresses attainable in the deformation zone. However, the crack opening displacements δ are determined by the drawability or ductility of the matrix. This process is exceedingly complex and for polymers involves the non-Newtonian flow and plastic deformation of the strain hardened craze-like material in the zone. The craze fibrillar structure evolves from a combination of Saffmann–Taylor meniscus instability combined with cavitation processes, depending on rate and molecular weight [1]. Thus, the deformation zone initiates when the stress field at the crack tip exceeds the yield stress σ_y and propagates with increasing traction stresses σ up to the maximum stress σ^* . As the zone breaks down, the stresses decrease but the displacements continue to increase and finally the crack advances at δ_c . The traction stresses have a displacement function $\sigma(\delta)$ as shown in Fig. 13 such that the fracture energy G_{Ic} is the integral of $\sigma(\delta)$ over the displacement range $\delta = 0$ to $\delta = \delta_c$. Solutions to the EPZ integrals are complex

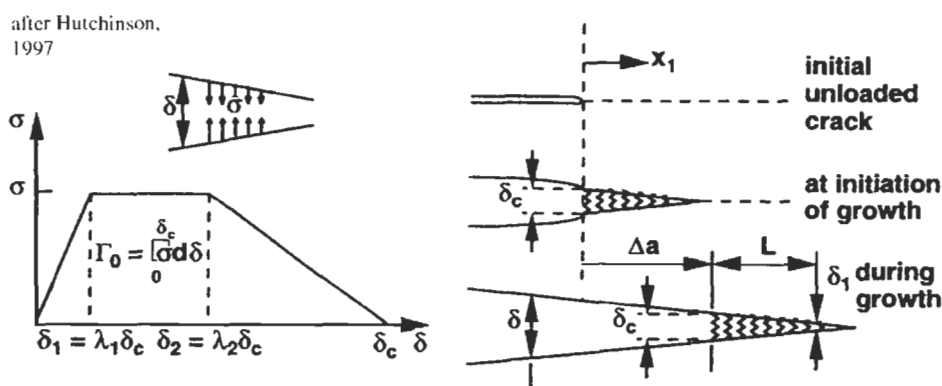


Fig. 13. The fracture energy using the J-integral approach.

with regard to rate and the non-linear constitutive character of the drawing process and are usually obtained by computer simulation [5]. To provide comparison of the vector percolation theory with fracture experiments, we approximate $\sigma(\delta)$ as a box function with maximum value σ^* , such that G_{lc} is obtained as

$$G_{lc} = \sigma^* \delta_c \quad (7.1)$$

In the traditional Dugdale model [56], $\sigma^* = \sigma_y$ and the familiar result is obtained, $G_{lc} = \sigma_y \delta_c$. In the EPZ model, σ^* exceeds σ_y and typically σ^*/σ_y is in the range 4–8. We make the assumption that the critical crack opening displacement δ_c is proportional to the maximum stresses σ^* in the deformation zone

$$\delta_c = \psi \sigma^* \quad (7.2)$$

where ψ is a constant associated with the plastic drawing process. In effect, the highly complex non-Newtonian plastic zone drawing process is viewed as a pseudo elastic (non-reversible) process, such that the higher the σ^* value, the higher will be δ_c . There is considerable evidence for this behavior for linear polymers [1], but we can expect different results for highly crosslinked thermosets, as discussed in Section 7.1. Substituting for δ_c in Eq. 7.1, we obtain

$$G_{lc} = \sigma^{*2} \psi \quad (7.3)$$

where σ^* is given by the VP model via Eq. 6.1 and ψ is a constant to be determined. Thus, the final equation for the fracture energy of polymers with craze deformation zones is given by

$$G_{lc} = 2\psi(p - p_c)E_c D_o \frac{\rho}{\lambda^2 M_c} \quad (7.4)$$

Since $G_{lc} \sim \sigma^{*2}$, the VP model gives for high molecular weight ($M > 8M_c$) glassy polymers

$$G_{lc}^* \sim G_o/M_c \quad (7.5)$$

where $G_o \sim 3 \times 10^4 \text{ J/m}^2 \text{ Da}$ and is essentially constant for linear glassy polymers with comparable modulus and density. The latter relation highlights the role of M_c in fracture processes, where the tighter entanglement nets require larger fracture energies. Thus, we would expect polycarbonate to have a fracture energy about 6 times that of polystyrene, or $G_{lc} \sim 6 \text{ kJ/m}^2$.

7.1. Fracture of thermosets

For thermosets with molecular weight between crosslinks M_x , the crosslink density ρ_x , is described by $\rho_x \sim N_a/M_x$. As ρ_x increases, the nets become tighter and stiffer, and thus require more stress to break via

$$\sigma^* \sim \rho_x^{1/2} \quad (7.6)$$

However, the ability of the matrix to flow and provide high displacements δ , in the deformation zone diminishes and the resulting fracture energy $G_{lc} \sim \sigma^* \delta_c$ involves a competition between an increasing σ^* value coupled with a decreasing δ_c value. We can approximate the displacement δ in the deformation zone as $\delta_c \sim \lambda R$, where λ is the draw ratio and R is the end-to-end vector of the crosslinked structure. Since $\lambda \sim M_x^{1/2}$ and $R \sim M_x^{1/2}$, this gives $\delta_c \sim M_x$. From the net solution, $\sigma^* \sim M_x^{-1/2}$, it follows that

$$G_{lc} \sim M_x^{1/2} \quad (7.7)$$

or

$$G_{lc} \sim \rho_x^{-1/2}$$

There is considerable evidence in the thermoset literature that the fracture energy decreases with increasing crosslink density, consistent with the intuitive result that crosslinking inhibits flow. In the limit of very high crosslink density, where for example we approach the structure of diamond, fracture can occur on a single crystal plane such that

$$G_{lc} \sim \sigma_h b \quad (7.8)$$

where σ_h is the atomic hot bond stress (Eq. 6.6) and b is the strained bond length. Thus, σ^* and δ_c have approached their ultimate limits, σ_h and b , respectively. Even though $\sigma_h \sim 5$ GPa and $b \sim 0.4$ nm, we see that $G_{lc} \sim 2$ J/m², which could be considered a very weak system, once the very high stress required to commence the fracture stress has been reached.

8. Fracture by disentanglement

How do highly interpenetrated random coil chains disentangle to cause fracture? Disentanglement is considered to occur as shown in Fig. 14, where we depict the response of an entangled chain to a constant (step function) draw ratio λ as follows:

(a) The average entangled chain with $M/M_c > 1$ is uniaxially deformed to a constant draw ratio λ . The extension is accommodated by extending the random walk (slack) between entanglements such that the end-to-end vector between entanglement behaves as $R_e(\lambda) = \lambda R_e$. The end-to-end vector R of the whole chain behaves similarly, $R(\lambda) = \lambda R$. The entanglement points deform affinely and the chain stores elastic strain energy. The primitive contour path length L , behaves as $L(\lambda) = \lambda L_0$, where $L_0 = MR_e/M_e$ is the non-strained primitive path at $\lambda = 1$. When the stretched path relaxes to the critical length $L_c \approx 2\lambda R_e$, the chains become critically connected and disentangle.

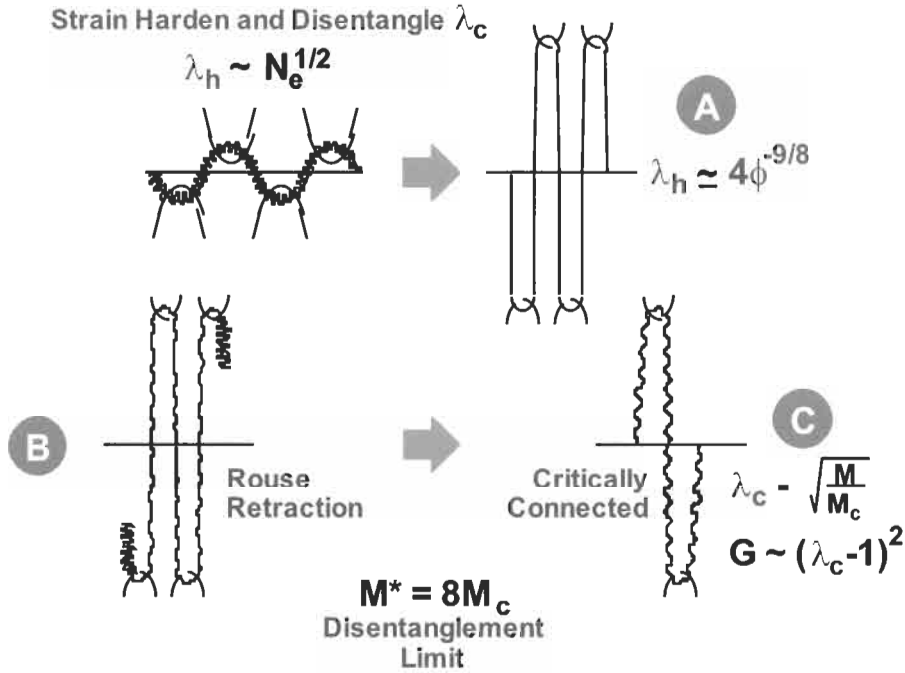


Fig. 14. Disentanglement mechanism: (A) Tightened slack between entanglements. (B) Retraction and disentanglement by Rouse relaxation. (C) Critically connected state.

(b) Rouse-like dynamics causes a retraction of the extended chain primitive path length $L(\lambda)$ and the stored strain energy begins to release. The retraction process will be rate sensitive. As the chain shortens towards its equilibrium path length, it begins to lose entanglements and becomes critically connected at $L_c \approx 2\lambda R_e$. The time dependence of the retraction process can be approximated as a simple exponential such that the stressed fraction of the primitive path $L(t)$ as a function of time is $L(t)/L(\lambda) \approx \exp(-t/\tau_{RO})$, where τ_{RO} is the Rouse relaxation time of the chain or minor chain segment (during welding).

(c) When the chain retracts to a critical length $L_c = 2R_e\lambda$, then each chain possesses one bridge and the network becomes critically connected. This state corresponds to the failure time of the entanglement network, τ_f , and is determined by

$$\tau_f \sim \tau_{RO} \ln \frac{M}{M_c} \quad (8.1)$$

When $M \approx M_c$, disentanglement is nearly instantaneous but approaches τ_{RO} when $M \approx 8M_c$, which is the strain hardened ($\lambda \sim 4$) upper bound for chain pullout without bond rupture. For welding, the relaxation times τ_{RO} refer to the minor chains of length $l(t)$ such that the retraction time is approximated by $\tau_{RO} \sim l(t)^2$. When $M > 8M_c$, the chains cannot disentangle completely at the Rouse time and

begin to re-entangle due to reptation. Thus, bond rupture would be necessary to complete the fracture process and the value of $M^* \approx 8M_c$ sets an upper limit for fracture by disentanglement or chain pullout.

The percolation parameters ($p - p_c$) associated with the disentanglement process are derived as follows; p is the normalized entanglement density defined as

$$p = \frac{g(\lambda)N_v}{\rho_e} \quad (8.2)$$

where $g(\lambda)$ is the number of entanglements per chain, N_v is the number of chains per unit volume and ρ_e is the entanglement density of the perfect net. We define $g(\lambda)$ as

$$g(\lambda) = \frac{M}{M_e(\lambda)} - 1 \quad (8.3)$$

Since $N_v = \rho N_a/M$ and $\rho_e = \rho N_a/M_c$ then we have

$$p = \frac{[M/M_e(\lambda) - 1] \rho N_a/M}{\rho N_a/M_c(\lambda)} \quad (8.4)$$

where $M_e(\lambda)$ is the stretch dependent M_e value after it has relaxed to position C, as shown in Fig. 14. $M_e(\lambda)$ is given by the following approximation

$$M_e(\lambda) = \lambda^2 M_e \quad (8.5)$$

$M_e(\lambda)$ increases between entanglement points due to the retraction process at constant λ . A more detailed treatment of disentanglement would account for the orientation function of the entanglements and lateral contraction, as discussed elsewhere [1]. Eq. 8.4 becomes

$$p = 1 - \lambda^2 M_e/M \quad (8.6)$$

A very important consequence of the latter equation is that when $\lambda = 1$, there exists a critical value of molecular weight $M = M_c$ for which $p = p_c$ and we obtain the relation between M_e and M_c as

$$M_c = \frac{M_e}{1 - p_c} \quad (8.7)$$

Since $p_c \approx 1/2$, we observe that $M_c \approx 2M_e$, as commonly observed. M_e is determined from the onset of the rubbery plateau by dynamic mechanical spectroscopy and M_c is determined at the onset of the highly entangled zero-shear viscosity law, $\eta \sim M^{3.4}$. This provides a new interpretation of the critical entanglement molecular weight M_c , as the molecular weight at which entanglement percolation occurs while the dynamics changes from Rouse to reptation. It also represents the

transition from the nail to the net solution and the onset of significant strength development via the formation of stable oriented fibrillar material in the deformation zones preceding the crack advance.

When $M > M_c$, we obtain the critical draw ratio for fracture λ_c from Eqs. 8.6 and 8.7 as

$$\lambda_c \approx (M/M_c)^{1/2} \quad (8.8)$$

The maximum molecular weight M^* at which disentanglement can occur is determined when strain hardening occurs at $\lambda_c \approx 4$ such that

$$M^* \approx 8M_c \quad (8.9)$$

Thus, fracture occurs by first straining the chains to a critical draw ratio λ_c and storing mechanical energy $G \sim (\lambda_c - 1)^2$. The chains relax by Rouse retraction and disentangle if the energy released is sufficient to relax them to the critically connected state corresponding to the percolation threshold. Since $\lambda_c \sim (M/M_c)^{1/2}$, we expect the molecular weight dependence of fracture to behave approximately as

$$G_{lc} \sim \left[\left(\frac{M}{M_c} \right)^{1/2} - 1 \right]^2 \quad (8.10)$$

or

$$G_{lc} \sim M \left[1 - \left(\frac{M_c}{M} \right)^{1/2} \right]^2 \quad (8.11)$$

when M is in the range $M_c \leq M \leq 8M_c$. The critical stress intensity factor $K_{lc} \sim G_{lc}^{1/2}$ and is derived from Eq. 8.11 as

$$K_{lc} \sim (M^{1/2} - M_c^{1/2}) \quad (8.12)$$

which has been demonstrated by Wool and O'Connor [13].

8.1. Fracture by bond rupture

At high rates of strain, or when complete disentanglement cannot occur when $M > M^*$, bond rupture occurs randomly in the network and the percolation parameter p becomes dominated by chain ends such that

$$p = 1 - M_c/M \quad (8.13)$$

Since $G_{lc} \sim p - p_c$, we obtain

$$G_{lc} = G_{lc}^* [1 - M_c/M] \quad (8.14)$$

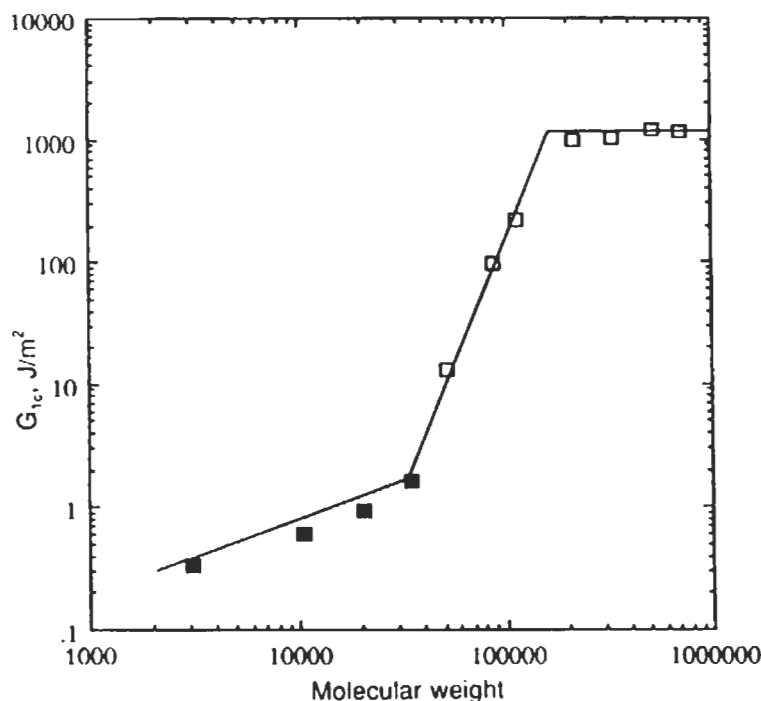


Fig. 15. G_{1c} versus weight for polystyrene in the virgin state. Data of Robertson [76] (M less than 40,000, ■) and Wool and O'Connor [13] (□).

where G_{1c}^* is the plateau fracture energy at high molecular weight. The latter equation is identical to the empirical relation for the molecular weight dependence of fracture suggested by P.J. Flory, who coincidentally developed the first percolation theory of polymer gelation.

In summary, Fig. 15 shows the molecular weight dependence of the fracture energy for polystyrene in which the three solutions are graphed for the three pertinent regions. (1) When $M < M_c$, the nail solution (Eq. 4.1) applies to very fragile glasses. (2) When $M_c < M < M^*$, disentanglement predominates and Eq. 8.9 applies such that little bond rupture occurs. (3) When $M > M^*$, bond rupture dominates and Eq. 8.14 applies.

9. Polymer-polymer welding

The molecular aspects of interdiffusion of linear entangled polymers ($M > M_c$) during welding of polymer interfaces are summarized in Table 1 [1]. The reptation dynamics and the interface structure relations in Table 1 have been

verified experimentally by a series of interdiffusion experiments with selectively deuterated polymers using dynamic secondary ion mass spectroscopy (DSIMS) and neutron reflectivity [50–53]. Initially as the interface wets by local Rouse segmental dynamics, we find that rapid interdiffusion occurs to distances of the order of the radius of gyration of the entanglement molecular weight, ca. 30 Å. However, the interface is very weak and fracture could be described by the nail solution. At the wetting stage, the frictional pullout of intermeshed chain segments, which have ‘elbowed’ their way across the interface, determines fracture. As welding proceeds, Σ minor chains of length L diffuse via reptation dynamics into an interface of width X . The diffusing chains are fractal random walks and interpenetrate with chains, which are fully entangled (ignoring surface reflection configuration effects on entanglement density).

The structure of the interface resembles a box of width X with fractal edges containing a gradient of interdiffused chains. Gradient percolation theory [6,9] requires that chains which contribute to the interface strength straddle the interface plane during welding; chains in the concentration gradient which have diffused further than their radius of gyration cease to be involved. We have shown that this amounts to a very small number [1]. When the stress exceeds the yield stress, the deformation zone forms and the oriented craze fibrils consist of mixtures of fully entangled matrix chains and partially interpenetrated minor chains. Fracture of the weld can occur by disentanglement of the minor chains, or bond rupture. It is interesting to note that if the stress rises to the point where random bond rupture in the network begins to dominate the deformation mechanism, instead of disentanglement, then the weld will appear to be fully healed, regardless of the extent of interdiffusion. This can occur at high rates of testing when the minor chains cannot disentangle and bond rupture pervades the interface breaking both the minor chains and the matrix chains.

The percolation term $[p - p_c]$ determines the number of bonds to be broken, or disentangled such that when Σ chains, each with L/L_c entanglements per chain, interdiffuse in an interface of width X , we obtain

$$[p - p_c] \sim \Sigma L / X \quad (9.1)$$

The stored strain energy in the interface of volume proportional to X is consumed in disentangling the minor chains and we obtain

$$G_{1c} \sim \Sigma L / X \quad (9.2)$$

Since $\Sigma \sim X/M$ (Table 1) and $L \sim t/\tau^{1/2}$, we obtain

$$G_{1c}(t) = G_{1c}^*(t/\tau^*)^{1/2} \quad (9.3)$$

where G_{1c}^* is the maximum strength obtained at $M^* = 8M_c$ and is independent of molecular weight. The average contour length $\langle L \rangle$ controls the disentanglement

process via $\lambda_c \approx [(L)/L_c]^{1/2}$. The welding time τ , to achieve complete strength behaves as

$$\tau \sim M^3 \quad (9.4)$$

in which $M < M^*$. When $M > M^*$, the welding time is determined by the time required to diffuse a distance of order of the radius of gyration of M^* , such that $\tau^* \sim M^{*2} M$. Even though the welding time $\tau^* \sim M$ is shorter than $T_r \sim M^3$, the molecular weight dependence of the welding rate remains unaffected and we have for all molecular weights

$$G_{1c}(t) \sim t^{1/2} M^{-1/2} \quad (9.5)$$

As the interdiffusion distance approaches R_g , the welding state becomes indistinguishable from the virgin state and Eq. 9.3 converges to Eq. 8.11, when $M < M^*$, or Eq. 8.14, when $M > M^*$.

Total interpenetration of chains (X approaches R_g) is not necessary to achieve complete strength when $M > M^*$ and $\tau^* < T_r$. However, a word of caution: while complete strength may be obtained in terms of critical fracture measures such as G_{1c} and K_{1c} , the durability, measured in sub-critical fracture terms, such as the fatigue crack propagation rate da/dN , may be very far from its fully healed state at τ^* . We have shown that while the weld toughness K_{1c} increases linearly with interdiffusion depth X as $K_{1c} \sim X$, the fatigue crack propagation behavior of partially healed welds behaves as [1]

$$\frac{da}{dN} \sim X^{-5} \quad (9.6)$$

which is a very strong function of interdiffusion and underscores the penalty to pay for partial welding. Thus, the weld strength may be near, or at the virgin strength but the fatigue strength may be dramatically reduced below its maximum value. Thus, one should always design a welding time with respect to T_r to achieve maximum durability of welds and interfaces. The time to achieve complete strength is related to the reptation time by

$$\tau^* = 64 \left(\frac{M_c}{M} \right)^2 T_r \quad (9.7)$$

such that when $M = 8M_c$, $\tau^* = T_r$. The reptation time T_r is determined from the self-diffusion coefficient D and the end-to-end vector R , by

$$T_r = \frac{R^2}{3\pi^2 D} \quad (9.8)$$

Example: consider welding polystyrene at 125°C, $D \approx 4 \times 10^{-6}/M^2$ (cm²/s) [77–80], $R^2 = 0.45 \times 10^{-16}M$ (cm²) such that $T_r = 4 \times 10^{-13}M^3$ (s) and $\tau^* =$

0.0234M (s). For the case where $M = 400,000$ and $M_c = 30,000$, from Eq. 9.7, we have $\tau^*/T_r = 0.36$, where $T_r = 435$ min and $\tau^* = 156$ min. In this example, if the maximum weld strength were obtained at an allowed welding time of 156 min, the durability as measured by da/dN , would only be about 1/5 of its virgin value compared to complete welding at $T_r = 435$ min. When plastic parts are being injection molded, laminated, sintered or co-extruded, many internal weld lines are encountered and this aspect of welding needs to be considered in designing materials with optimal durability.

10. Reinforcement of incompatible interfaces

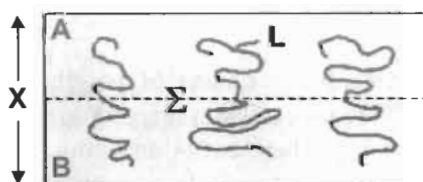
Consider the incompatible A/B polymer interface shown in Fig. 16. In the absence of compatibilizers, the interface is very weak such that the strength can be described by the nail solution as [1]

$$G_{lc}(\text{friction}) \sim d^2 M^0 \quad (10.1)$$

Here, d is the interface width, which according to Helfand [12] is determined by

$$d \sim 1/\chi^{1/2} \quad (10.2)$$

in which χ is the Flory–Huggins interaction parameter. The equilibrium interface thickness d , derives from a minimum in the free energy of mixing F , associated with the positive relief of entropy S , of surface confined chain segments of length L ($S \sim k \ln L$) as they blossom forth across the interface, counterbalanced by the negative enthalpy of mixing H of incompatible A–B segments ($H \sim \chi L$). Letting $F = H - TS$ and evaluating the free energy minimum $dF/dL = 0$, we obtain the



$$P = \Sigma L/X \quad \left(\frac{\text{Number of Chains} \times \text{Length}}{\text{Width}} \right)$$

$$P_c = \Sigma_c L/X$$

$$G_{lc} \sim P - P_c$$

$$G_{lc} \sim \frac{L}{X} (\Sigma - \Sigma_c)$$

Fig. 16. A/B incompatible interface of width X , with Σ di-block compatibilizers of length L .

equilibrium mixing length $L \sim kT/\chi$. Since $d \sim L^{1/2}$, the equilibrium incompatible interface thickness is derived as $d \sim 1/\chi^{1/2}$, as expressed in Eq. 10.2. This analysis assumes that d is less than the radius of gyration R_{ge} of the entanglement molecular M_e , typically around 2–3 nm. With increasing compatibility, or as χ approaches zero, d approaches the normal interface width $X \sim Rg$ and the intermeshing segments becomes highly entangled, thereby producing a much higher fracture energy comparable to the virgin state [1].

By placing diblocks or random copolymers of aerial density Σ , at incompatible interfaces (Fig. 16), following the work of Creton, Brown and Kramer et al. [59,60,81–83], the percolation model predicts that

$$G_{lc} \sim \frac{\Sigma L}{X} - P_c \quad (10.3)$$

Since L and X are constant, in the absence of brush-like ordering, $P_c \sim \Sigma_c$, which represents a critical number of chains required to build up the network above the percolation level. Hence we have

$$G_{lc} \sim \Sigma - \Sigma_c \quad (10.4)$$

The latter function, when examined on a $\log G_{lc}$ vs. $\log \Sigma$ plot will have an apparent slope of about 2 over much of the data range, which suggests the empirical relation, $G_{lc} \sim \Sigma^2$. Essentially, all mechanical properties dependent on percolation phenomena via $(P - P_c)^v$ terms, such as adhesion strength, viscosity, fracture energy etc., give incorrect exponents $v' \neq v$ when analyzed on \log Property vs. $\log p$ plots. The zero shear melt viscosity dependence on molecular weight, $\eta \sim M^{3.4}$ is a unique example of a property subject to percolation that has prompted many to seek a fundamental meaning in the empirical 3.4 exponent.

11. Adhesion at polymer–solid interfaces

When using sticker groups X to adhere linear chains of length M to solid substrates such as glass, or metal and which may contain receptor groups Y , some very interesting effects occur [10,62,84,11]. There exists an optimal number of both receptor X -groups and acceptor Y -groups to obtain maximum adhesion at the polymer–solid interface. The optimal number of X -groups is only about 3% while the optimal number of Y -groups on the solid is closer to 50%. We believe these results are a balance between the connectivity of the first layer of chains to the substrate and the ability of this layer to be connected to the polymer bulk above the substrate. If the polymer is too well adhered to the substrate and adopts a flat conformation, it may not be well connected to the polymer layer above, with a resultant loss of interface strength. This leads to many new concepts of adhesion design, which can be understood in terms of molecular connectivity, and percolation concepts.

Table 2

Experimental results of cPBD adhesion: stick and receptor concentration effects

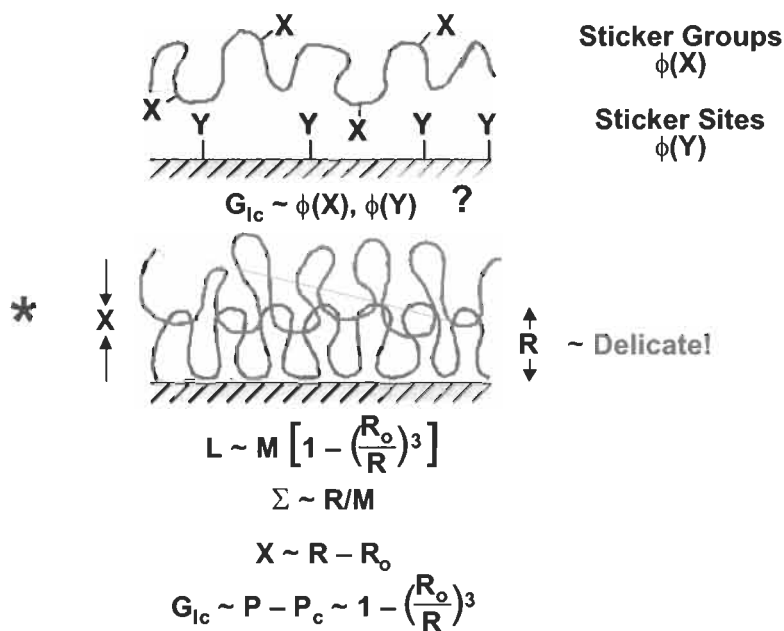
Case	χ_{X-Y} (cal/mol)	Optimum ϕ_X^* or ϕ_Y^*	Optimum $(\chi\phi_X\phi_Y)^*$ (cal/mol)	Maximum G_{IC}^* (J/m ²)
1. cPBD–Al	3,000–7,000 (–COOH vs. –OH)	$\phi_X^* = 3$ mol% at constant $\phi_Y = 100$ mol%	90–210	300±25
2. cPBD–AlS	16,000–25,000 (–COOH vs. –NH ₂)	$\phi_X^* = 0.5$ mol% at constant $\phi_Y = 100$ mol%	80–125	600±50
3. cPBD–AlS	16,000–25,000 (–COOH vs. –NH ₂)	$\phi_Y^* = 30$ mol% at constant $\phi_X = 3$ mol%	144–225	600±60

cPBD, Al and AlS are carboxylated polybutadiene, aluminum oxide surface, and mixed silane modified aluminum oxide surface, respectively.

Gong, Lee and Wool [54,55,62,84,11] conducted experiments to investigate the influence of a small amount of sticker groups ($-X$) distributed randomly along the polymer chains, adhering with receptor groups ($-Y$) distributed on the solid surface, and the X – Y interaction parameter χ , as summarized in Table 2. The problem was defined as the ‘ X – Y problem’ at the polymer–solid interface (see Fig. 17), where one queried how the fracture energy G_{IC} depended on the number of sticker $\phi(X)$ and receptor groups $\phi(Y)$. In this polymer–solid interface study, G_{IC} was explored as a function of: (a) interface structure; (b) surface restructuring time and temperature; (c) deformation rate in terms of polymer viscosity and non-Newtonian rheology; (d) Saffman–Taylor meniscus instability phenomena and cavitation effects in the deformation zone; (e) microscopic deformation mechanisms involving disentanglement and bond rupture; and (f) interrelationships between structure and strength of polymer–solid interfaces.

11.1. Role of sticker groups $\phi(X)$ on adhesion

In the first experiment by Gong and Fiend [12], the influence of $\phi(X)$ on G_{IC} at constant $\phi(Y) \sim 1$ was investigated. Carboxyl sticker groups were placed randomly on linear polybutadiene (PBD) chains and the polymer melt was adhered to aluminum (Al) foil surfaces. Pure PBD chains adhere very weakly to Al surfaces. The X – Y interaction was determined by the hydrogen bonding acid–base interaction between $-\text{COOH}$ and aluminum oxide. It was found for this cPBD–AL interface that with increasing sticker group concentration $\phi(X)$, the fracture energy G_{IC} , increased and then decreased as shown in Fig. 18. An optimal sticker group concentration $\phi^*(X) = 3$ mol%, gave a maximum fracture energy of about 300 J/m². The trend shown in Fig. 18 seemed counterintuitive in terms



* Gong and Wool, *Macromolecules* **31**, 3706 (1998)

Fig. 17. A polymer–solid interface with X sticker groups on the polymer and Y -receptor groups on the solid. As the chain adsorbs strongly on the solid, it tends to disentangle from the other chains in the polymer.

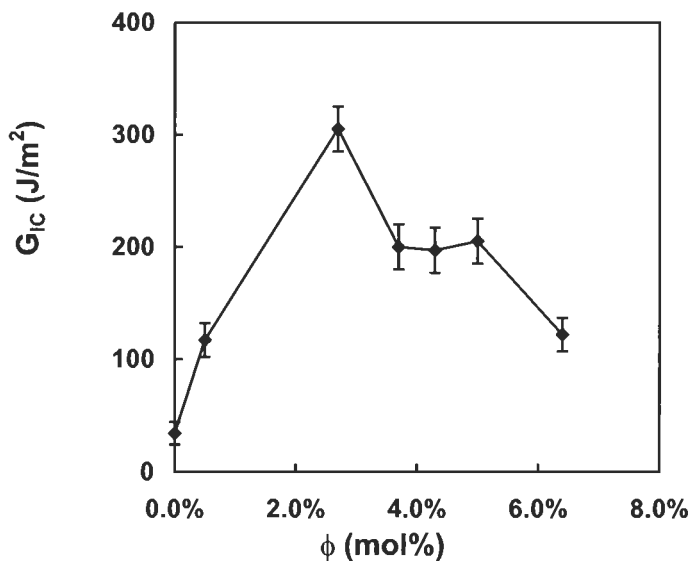


Fig. 18. Fracture energy of carboxylated PB on aluminum as a function of the number of carboxyl sticker groups ϕ_X . (Gong and Wool [10]).

of current wisdom of adhesion, but was reproduced several times using different synthetic techniques and testing methods at several locations.

There were significant effects of surface rearrangement times which varied with $\phi(X)$ such that the maximum fracture energy was obtained in the shortest time at the optimal sticker group concentration $\phi(X) \sim 3$ mol%. Surface restructuring occurred at times several orders of magnitude longer than characteristic single chain relaxation times, e.g., the reptation time. Furthermore, it was found that non-Newtonian viscoelastic effects dominated the deformation zone evolution and breakdown. A microscopic analysis of the mode of failure (AFM, XPS, SEM) indicated that cohesive failure was occurring predominantly in a layer immediately adjacent to the metal surface. At low G_{IC} and $\phi(X)$ values, simple adhesive or mixed adhesive-cohesive failure occurred.

In the second experiment by Gong, the influence of χ was examined using aluminum oxide surfaces treated with amine terminated silanes, creating $-\text{NH}_2$ substrate receptor groups with a much stronger $X-Y$ interaction. Then, the sticker concentration effect on the cPBD-AIS interface was investigated at constant $\phi(Y) \sim 1$. It was found that similar trends to that shown in Fig. 18 occurred, but the maximum G_{IC} doubled to 600 J/m^2 and the optimal sticker concentration decreased to $\phi^*(X) \sim 0.5$ mol%. Again, the failure mode was cohesive at high G_{IC} values and adhesive near $\phi(x) \sim 0$.

11.2. Role of receptor groups $\phi(Y)$ on adhesion

Finally, the third experiment by Lee and Wool varied the coverage of active amine receptor groups $\phi(Y)$ in the range 0–100% on the Aluminum surface using mixed silanes ($-\text{CH}_3$ and $-\text{NH}_2$ terminated). A cPBD polymer with a constant sticker group concentration $\phi(X) \sim 3$ mol%, corresponding to $\phi^*(X)$ in Fig. 18, was used in the peel experiments. The results of G_{IC} vs. $\phi(Y)$ are shown in Fig. 19 for surface restructuring times of 10, 100 and 1000 min. Significantly, G_{IC} reaches its maximum value of about 600 J/m^2 at an optimal partial coverage of $\phi^*(Y) \sim 30\%$. In the above experiments, the bonding dynamics were several orders of magnitude longer (up to 1000 min) than the characteristic relaxation time of the PBD bulk (~ 1 min). Additionally, the adhesion dynamics were strongly dependent on the concentrations of the sticker and receptor groups. The trend with $\phi(Y)$ was similar to that of $\phi(X)$ and suggests that there exists design rules for optimizing polymer–solid interface strength.

An entanglement sink probability (ESP) model motivated by vector percolation explains the non-monotonic influences of sticker concentration (ϕ_X), receptor concentration (ϕ_Y), and their interaction strength (χ) on the adhesion strength G_{IC} of the polymer–solid interface. The ESP model quantifies the degree of interdigitation between adsorbed and neighboring chains based on the adsorbed chain domain using an extension of the scaling treatment of de Gennes. Here, the

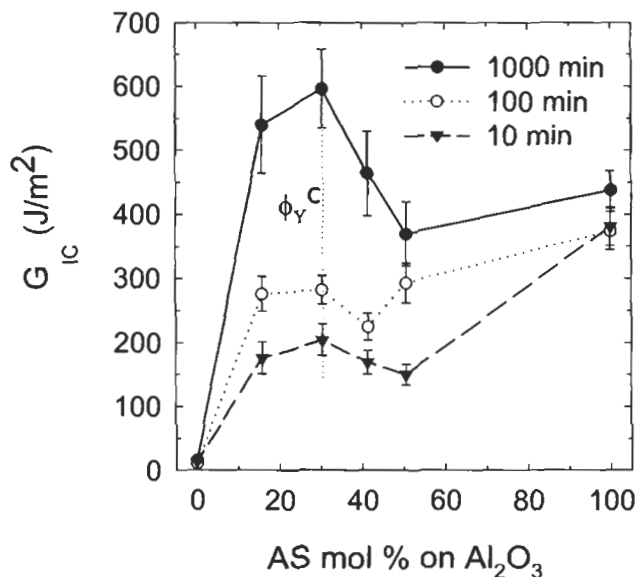


Fig. 19. Fracture energy of CPB ($\phi_X = 3\%$) vs. the fraction of NH_2 receptor groups ϕ_Y on an Al_2O_3 substrate at different contact times (Lee and Wool [84,85]).

adsorbed chain domain changes thermodynamically with respect to the energy of interaction parameter, $r = \chi\phi_X\phi_Y$. Basically, this model considers the situation of a blend consisting of a small volume fraction of adhesive molecules as a compatibilizer at the interface, where these molecules promote adhesion by adsorbing to the surface via sticker–receptor interactions. The ESP model scales solely with $r = \chi\phi_X\phi_Y$, and this parameter can be related to both the adhesive potential (G_A) and the cohesive potential (G_C). G_A describes adhesive failure between adsorbed chains and the solid surface and linearly behaves as $G_A \sim r = \chi\phi_X\phi_Y$. The cohesive strength between adsorbed and neighboring chains corresponds to $G_C \sim r^{-0.5 \sim -1.0} = (\chi\phi_X\phi_Y)^{-0.5 \sim -1.0}$. When the fracture stresses for cohesive and adhesive failure are equal, the model predicts maximum adhesion strength at an optimal value of $r^* = (\chi\phi_X\phi_Y)^*$. Thus, for a given χ value, there exists optimal values ϕ_X^* and ϕ_Y^* for the sticker and receptor groups, above or below which the fracture energy will not be optimized. Alternatively, if the X – Y interaction strength χ increases, then, the number of sticker groups required to achieve the optimum strength decreases. Significantly, the optimum strength is not obtained when the surface is completely covered with receptor groups ($\phi_Y = 1$) and is closer to 30%. For polybutadiene, the optimum value of r^* was determined experimentally, and typically $\phi_X^* \sim 1$ –3%, $\phi_Y^* \sim 25$ –30%.

Many of the important results for diffusion and adhesion at interfaces discussed in this chapter are summarized in Table 3.

Table 3

Summary relations for strength of interfaces

Property	Relation	Comment/application
Percolation	$G_{1c} \sim P - P_c$ $P_c = 1 - M_c/M_c$	$P \sim$ entangle density $P \sim 1/M_c$
Interface structure	$H(t) = H_\infty(t/T)^{r/4}$	Dynamics of welding
Virgin state	$H_\infty = M^{(3r-s)/4}$	$r, s = 1, 2, \text{ or } 3$
Fracture energy	$G_{1c} = G_\infty(t/\tau)^{1/2}$	$\tau \sim M^3$ if $M < M^*$
Symmetric welds	$G_{1c} \sim \Sigma L/X$	$(M^* = 8M_c)$ $\tau \sim M$ if $M > M^*$
Bond rupture	$G_{1c} \sim G^*[1 - (M_c/M)]$	$M > M^*$
Disentanglement	$G_\infty \sim G^*M[1 - (M_c/M)^{1/2}]^2$	$M_c < M < M^*$
Virgin toughness	$K_{1c} \sim M^{1/2} - M_c^{1/2}$	$M_c < M < M^*$
Nail solution	$G_{1c} = 2SI^* + 1/2\mu_0 L^2 \Sigma V^a$	Weak interfaces
Net solution	$\sigma = [ED_0(p - p_c)\rho/8M_c]^{1/2}$	Strong interfaces
Fatigue of welds	$da/dN \sim M^{-5/2}(t/T_r)^{-5/4}$	Penalty for poor weld
Weld time	$\tau = 64(M_c/M)^2 T_r$	$M \geq M^*$
Autohesion tack	$\sigma \sim (t/M)^{1/4}$	Linear elastomers
Compatibilizers	$G_{1c} \sim \Sigma - \Sigma_c$ $P \sim \Sigma L/R$	Incompatible strong interface
Fractal roughness	$N_f = H^{d/4}/M$	Gradient percolation

Acknowledgements

The author is grateful to the National Science Foundation, Department of Energy, Environmental Protection Agency, the Army Research Office, Hercules and Cara Plastics for their generous support of this research. Particular thanks are extended to my graduate students and research associates for shouldering the brunt of the research.

References

1. Wool, R.P., *Polymer Interfaces: Structure and Strength*. Hanser Press, New York, 1995.
2. Wool, R.P., *Interfaces and adhesion*. In: Brostow, W. (Ed.), *Performance of Plastics*. Hanser/Gardner Publishers, Munich, 2000, chapter 15.
3. Wool, R.P., *Rubber Chem. Technol.*, **57**, 307 (1984).
4. Wool, R.P., *J. Elast. Plast.*, **17**, 107 (1985).
5. Hutchinson, J.J., Liking scales in fracture mechanics. Plenary Address, Proceedings of the Ninth International Conference on Fracture, Sydney Australia, April 1997.
6. Wool, R.P. and Long, J.M., *Macromolecules*, **26**, 5227 (1993).
7. Wool, R.P., Dynamics and fractal structure of polymer interfaces. In: Lee, L.-H. (Ed.), *New Trends in Physics and Physical Chemistry of Polymers*. Plenum Press, New York, 1989, p. 129.

8. Mandelbrot, B.B., *The Fractal Geometry of Nature*. Freeman, New York, 1982.
9. Sapoval, B., Rosso, M. and Gouyet, J.F.J., *Phys. Lett.*, **46**, L149 (1985).
10. Gong, L. and Wool, R.P., *Macromolecules*, **31**(11), 3706 (1998).
11. Lee, I. and Wool, R.P., Thermodynamic analysis of polymer adhesion: sticker and receptor group effects. *J. Polym. Sci. Phys. Ed.*, submitted.
12. Lee, I. and Wool, R.P., *J. Adhes.*, **75**, 299 (2001).
13. Wool, R.P. and O'Connor, K.M., *J. Appl. Phys.*, **52**, 5953 (1981).
14. Wool, R.P. and O'Connor, K.M., *J. Polym. Sci. Polym. Lett. Ed.*, **20**, 7 (1982).
15. Wool, R.P., Yuan, B.-L. and McGarel, O.J., *Polym. Eng. Sci.*, **29**, 1340 (1989).
16. Kim, Y.H. and Wool, R.P., *Macromolecules*, **16**, 1121 (1983).
17. Zhang, H. and Wool, R.P., *Macromolecules*, **22**, 3018 (1989).
18. Zhang, H. and Wool, R.P., *Am. Chem. Soc. Polym. Prepr.*, Washington, DC, August, 1990.
19. Willett, J.L., O'Connor, K.M. and Wool, R.P., *J. Polym. Sci. Polym. Phys. Ed.*, **24**, 2583 (1986).
20. Foster, K. and Wool, R.P., *Macromolecules*, **24**, 1397 (1991).
21. Willett, J.L. and Wool, R.P., *Macromolecules*, **26**, 5336 (1993).
22. Voyutskii, S.S., *Rubber Chem. Tech.*, **33**, 748 (1960).
23. Voyutskii, S.S., *Autohesion and Adhesion of High Polymers*. John Wiley and Sons, New York, 1963.
24. Voyutskii, S.S. and Vakula, V.L., *J. Appl. Polym. Sci.*, **7**, 475 (1963).
25. Voyutskii, S.S., Yagnyatinskaya, S.M., Kaplunova, L. and Garetskaya, N.L., *Rubber Age*, 1973, p. 37.
26. Kausch, H.H. and Jud, K., *Plastics Rubber Proc. Appl.*, **2**, 265 (1982).
27. Jud, K. and Kausch, H.H., *Polym. Bull.*, **1**, 697 (1979).
28. Kausch, H.H., *Polymer Fracture*, 2nd edn. Springer-Verlag, Berlin, 1981.
29. Kausch, H.H., *Pure Appl. Chem.*, **55**, 833 (1983).
30. Kausch, H.H. and Tirrell, M., *Annu. Rev. Mater. Sci.*, **19**, 341 (1989).
31. Jud, K., Williams, J.G. and Kausch, H.H., *J. Mater. Sci.*, **16**, 204 (1982).
32. Kausch, H.H., *Pure Appl. Chem.*, **55**, 833 (1983).
33. de Gennes, P.-G., *J. Chem. Phys.*, **72**, 4756 (1980).
34. de Gennes, P.-G., *C.R. Acad. Sci. Paris*, **307**, 1841 (1988).
35. de Gennes, P.-G., *C.R. Acad. Sci. Ser. B*, **291**, 219-221 (1980).
36. de Gennes, P.-G., *C.R. Acad. Sci. Paris*, **292**(2), 1505 (1981).
37. de Gennes, P.G. and Leger, L., *Annu. Rev. Phys. Chem.*, **33**, 49 (1982).
38. de Gennes, P.-G., *Europhys. Lett.*, **15**(2), 191 (1991).
39. de Gennes, P.-G., *J. Phys. France*, **50**, 2551 (1989).
40. de Gennes, P.-G., *C.R. Acad. Sci. Paris*, **308**, 13 (1989).
41. Brochard-Wyart, F., de Gennes, P.G. and Troian, S., *C.R. Acad. Sci. Paris*, **310**(II), 1169 (1990).
42. Raphael, E. and de Gennes, P.-G., *J. Chem. Phys.*, **96**, 4002 (1992).
43. Prager, S. and Tirrell, M., *J. Chem. Phys.*, **75**, 5194 (1981).
44. Adolf, D., Tirrell, M. and Prager, S., *J. Polym. Sci. Polym. Phys. Ed.*, **23**, 413 (1985).
45. Mikos, A.G. and Pappas, N.A., *J. Chem. Phys.*, **88**, 1337 (1988).
46. de Gennes, P.-G., *J. Chem. Phys.*, **55**, 572 (1971).
47. de Gennes, P.-G., *Scaling Concepts in Polymer Physics*. Cornell University Press, Ithaca, NY, 1979.
48. Edwards, S.F., *J. Chem. Soc. Lond.*, **92**, 9 (1967).
49. Doi, M. and Edwards, S.F., *The Theory of Polymer Dynamics*. Clarendon Press, Oxford, 1986.

50. Welp, K.A., Wool, R.P., Mays, J., Pispas, A. and Satija, S., *Macromolecules*, **31**(15), 4921 (1998).
51. Agrawal, G., Wool, R.P., Dozier, W.D., Felcher, G.Z.P., Zhou, J., Mays, J.W. and Russell, T.P., *J. Polym. Sci. Part B*, **34**, 2919 (1996).
52. Russell, T.P., Deline, V.R., Dozier, W.D., Felcher, G.P., Agrawal, G., Wool, R.P. and Mays, J.W., *Nature*, **365**, 235 (1993).
53. Agrawal, G., Wool, R.P., Dozier, W.D., Felcher, G.P., Russell, T.P. and Mays, J.W., *Macromolecules*, **27**, 4407 (1994).
54. Lee, A.Y. and Wool, R.P., *Macromolecules*, **19**, 1063 (1986).
55. Lee, A.Y. and Wool, R.P., *Macromolecules*, **20**, 1924 (1987).
56. Dugdale, D.S., *J. Mech. Phys. Solids*, **8**, 100 (1960).
57. Feng, S., Thorpe, M.F. and Garboczi, E., *Phys. Rev. B*, **31**(1), 276 (1985).
58. Wool, R.P., Bailey, D. and Friend, A., *J. Adhes. Sci. Technol.*, **10**, 305 (1996).
59. Creton, C., Kramer, E.J., Hui, C.-Y. and Brown, H.R., *Macromolecules*, **25**, 3075 (1992).
60. Creton, C. and Kramer, E.J., *Macromolecules*, **24**, 1846 (1991).
61. Brown, H.R., *J. Mater. Sci.*, **25**, 2791 (1990).
62. Helfand, E., *Macromolecules*, **25**, 1676 (1992).
63. Kantor, Y. and Webman, I., *Phys. Rev. Lett.*, **52**, 1891 (1984).
64. Feng, S., Sen, P.N., Halperin, B.I. and Lobb, C.J., *Phys. Rev. B*, **30**(9), 5386 (1984).
65. Feng, S., Halperin, B.I. and Sen, P.N., *Phys. Rev. B*, **35**(9), 197 (1987).
66. Feng, S. and Sen, P.N., *Phys. Rev. Lett.*, **52**(3), 216 (1984).
67. He, H. and Thorpe, M.F., *Phys. Rev. Lett.*, **54**(19), 2107 (1985).
68. Garboczi, E.J. and Thorpe, M.F., *Phys. Rev. B*, **31**(11), 7276 (1985).
69. Thorpe, M.F. and Garboczi, E.J., *Phys. Rev. B*, **35**(16), 8579 (1987).
70. Tang, W. and Thorpe, M.F., *Phys. Rev. B*, **36**(7), 3798 (1987).
71. Tang, W. and Thorpe, M.F., *Phys. Rev. B*, **37**(10), 5539 (1988).
72. Yan, H., Day, A.R. and Thorpe, M.F., *Phys. Rev. B*, **38**(10), 6876 (1988).
73. Wool, R.P., Bernaert, Y., Daley, M.A. and Agrawal, G., *Bull. Am. Phys. Soc.*, **36**, 792 (1991).
74. Wool, R.P., *Macromolecules*, **26**, 1564 (1993).
75. Vincent, P.I., *Polymer*, **13**, 557 (1972).
76. Robertson, R.E., In: *Toughness and Brittleness of Plastics*, *Adv. Chem. Ser.*, **154**, Am. Chem. Soc., Washington, DC, 1976.
77. Green, P. and Kramer, E.J., *J. Mater. Res.*, **1**(1), 202 (1986).
78. Green, P. and Kramer, E.J., *Macromolecules*, **19**, 1108 (1986).
79. Whitlow, S.J. and Wool, R.P., *Macromolecules*, **22**, 2648 (1989).
80. Whitlow, S.J. and Wool, R.P., *Macromolecules*, **24**, 5926 (1991).
81. Cho, K., Brown, H.R. and Miller, D.C., *J. Polym. Sci. Polym. Phys.*, **28**, 1699 (1990).
82. Brown, H.R., Char, K., Deline, V.R. and Green, P.F., *Macromolecules*, **26**, 4155 (1993).
83. Char, K., Brown, H.R. and Deline, V.R., *Macromolecules*, **26**, 4164 (1993).
84. Lee, I. and Wool, R.P., Controlling amine receptor group density on aluminum oxide surfaces by mixed silane self-assembly. *J. Thin Solid Films*, **379**, 94 (2000).
85. Lee, I. and Wool, R.P., Thermodynamic analysis of polymer–solid adhesion: Sticker and receptor group effects. *J. Polym. Sci. Polym. Phys. Ed.*, **40**(19), October (2002).

Coupling agents: chemical bonding at interfaces

MICHAEL JAMES OWEN

Dow Corning Corporation, Midland, MI, USA

1. Introduction

The best prescription for good adhesion between two phases would seem to be the provision of multiple, strong linkages across the interface between two materials. This can be most readily achieved by utilizing bifunctional molecules where one functionality can bond with one phase and the other functionality with the other phase. If placed at the interface, or capable of migrating to that interface, such a molecule could effectively ‘couple’ the two phases and is accordingly known as a coupling agent. Coupling agents placed at the interface are a type of primer treatment; those that are incorporated in the bulk of one of the phases and migrate to the interface, are usually termed adhesion promoters.

The most familiar of these agents are the silane coupling agents $\text{XRSi}(\text{OR}^1)_3$ where the X moiety is designed to react with an organic phase such as a polymer and the OR^1 with an inorganic phase such as glass or a metal oxide [1]. Groups that react readily with organic polymers usually cause the silane molecule to be too unstable if directly attached to the silicon atom. Consequently a bridging group R, often $(\text{CH}_2)_n$ where n is 2 or 3 is necessary. The OR^1 groups directly substituted on silicon, where R^1 is typically either methyl or ethyl, can hydrolyze and condense to form $\text{Si}-\text{O}-\text{Si}$ siloxane linkages with silanol groups on the inorganic substrate surfaces. Other hydroxylated inorganic surfaces can form $\text{Si}-\text{O}-\text{M}$ oxane linkages in similar fashion. Essentially, these hybrid silane molecules combine dual organic and inorganic chemical reactivity in the same molecule. Note that in principle, XRSiCl_3 molecules should be just as effective as both these and the corresponding alkoxy compounds first react to give equivalent silanol compounds. Normally, the trialkoxysilane is used in preference to the trichlorosilane because the former is easier to handle and does not form the corrosive HCl by-product on hydrolysis.

Clearly, there is more to these molecules than simple bifunctionality. Most noticeably there are three hydrolyzable groups per molecule, which can condense with each other as well as with hydroxylated surfaces. The siloxane network that forms is an important aspect of the coupling mechanism in many cases. Although there is some evidence that good adhesion can sometimes be attained with monolayers of $\text{XRSi}(\text{R}^2)_2(\text{OR}^1)$ (where R^2 is a non-reactive group, usually methyl), it is also abundantly evident that development of an interfacial network phase more extensive than a single monolayer can be very beneficial to adhesion enhancement by silane coupling agents. Several investigators have concluded that there is an optimum thickness of this coupling agent region or interphase, significant deviation from which results in substantial declines in performance. Naturally, this optimum thickness is highly system-dependent. For example, Schmidt and Bell [2] have reported an optimum coupling agent layer thickness for ethylene–mercaptoester copolymer coupling agents used in a polyamide-cured epoxy resin/steel system. They determined that a thickness of 14 nm was the optimum over a range of 2.5 to 35 nm. The peel strength at 14 nm was over 200% greater than that obtained at 5 nm thickness. An explanation of this phenomenon was offered based on weak boundary layer and chemical bonding theories. In another example, Plueddemann [3] has reported optimum adhesion of polypropylene to aluminum with silane primer layers between 0.5 and 10 μm thick, with adhesion dropping off with thicker or thinner layers.

Another advantage of this molecular architecture lies in the fact that silanol condensation becomes easier as the number of silanols per silicon atom increases. Reaction will occur under milder conditions for the $\text{XRSi}(\text{OR}^1)_3$ species than it will for the $\text{XRSi}(\text{R}^2)_2(\text{OR}^1)$ species. $\text{Si}(\text{OR}^1)_4$, exemplified by tetraethoxysilane (TEOS), offers the most facile reactivity and can be incorporated in primer and adhesion promoter formulations to enhance network formation. Fully hydrolyzed TEOS results in the SiO_2 silica structure. This is often the inorganic phase to which a polymer needs to be coupled. This provides another perspective on the role of the organosilicon interphase in that it provides a region of intermediate cross-link density between the relatively lightly cross-linked organic phase and the highly condensed siliceous phase. Such an intermediate density interphase can usefully absorb stresses that might cause interfacial failure if the interfacial phase were not present.

2. Types of coupling agent

Conceivably, many compounds of inorganic elements have chemical reactivity that could contribute to improved adhesion to mineral surfaces. A fairly wide range of compounds, not restricted to any particular group in the periodic table, have been proposed as coupling agents as is shown in the following list:

- Silanes
- Orthosilicates
- Other orthoesters
- Chromium complexes
- Thiols and related compounds
- Copolymers
- Other compounds

Despite this variety, silicon-containing materials dominate the application. This is to be expected as silicon makes up 25.7% of the earth's crust, second only to oxygen in its abundance. Consequently, it is no surprise, as Arkles points out [4], that a great number of encounters between dissimilar materials will involve at least one member that is siliceous or has surface chemistry with siliceous properties. Representative commercial coupling agents [5] are shown in Table 1. Table 2 [1] shows the degree of improvement in adhesion that various additives can produce. The additives used are various methacrylate derivatives. They embrace several of the coupling agent classes listed above; the sixth in the list is a conventional silane coupling agent, the seventh is a chromium complex, and the eighth and ninth are orthosilicates (both providing on hydrolysis a $\text{XROSiO}_{3/2}$ structure). The table is given to illustrate the magnitude of the effect involved. Evidently, the conventional silane, the chromium complex, and one of the orthosilicates, provide significant improvement in flexural strength of the resultant composite with good resistance to boiling-water exposure.

Table 1
Representative commercial coupling agents

Organofunctional group	Chemical structure
Vinyl	$\text{CH}_2=\text{CHSi}(\text{OMe})_3$
Chloropropyl	$\text{Cl}(\text{CH}_2)_3\text{Si}(\text{OMe})_3$
Epoxy	$\text{CH}_2\text{CH}(\text{O})\text{CH}_2\text{O}(\text{CH}_2)_3\text{Si}(\text{OMe})_3$
Methacrylate	$\text{CH}_2=\text{C}(\text{Me})\text{COO}(\text{CH}_2)_3\text{Si}(\text{OMe})_3$
Primary amine	$\text{H}_2\text{N}(\text{CH}_2)_3\text{Si}(\text{OEt})_3$
Diamine	$\text{H}_2\text{N}(\text{CH}_2)_2\text{NH}(\text{CH}_2)_3\text{Si}(\text{OMe})_3$
Mercapto	$\text{HS}(\text{CH}_2)_3\text{Si}(\text{OMe})_3$
Cationic styryl	$\text{CH}_2=\text{CHC}_6\text{H}_4\text{CH}_2\text{NH}(\text{CH}_2)_2\text{NH}(\text{CH}_2)_3\text{Si}(\text{OMe})_3 \cdot \text{HCl}$
Cationic methacrylate	$\text{CH}_2=\text{C}(\text{Me})\text{COO}(\text{CH}_2)_2\text{N}^+(\text{Me})_2\text{CH}_2)_3\text{Si}(\text{OMe})_3 \cdot \text{Cl}^-$
Chrome complex	$\{\text{CH}_2=\text{C}(\text{Me})\text{COO}\}\text{Cr}(\text{OH})\text{Cl}_2 \cdot \text{H}_2\text{O} \cdot \text{ROH}^a$
Titanate	$\{\text{CH}_2=\text{C}(\text{Me})\text{COO}\}_3\text{TiOCH}(\text{Me})_2$
Zirconaluminate	$\text{HO}(\text{Al}/\text{Zr})\text{RCOOH}$
Cross-linker	$(\text{MeO})_3\text{Si}(\text{CH}_2)_2\text{Si}(\text{OMe})_3$
Mixed silanes	$\text{C}_6\text{H}_5\text{Si}(\text{OMe})_3 + \text{diamine-functional silane}$
Formulated	Melamine resin + epoxy-functional silane

^a Very simplified structure of these Werner-type complexes of Cr(III) is shown.

Table 2

Polyester glass laminates (with 2% methacrylate monomer)

Functional group of methacrylate additive	Flexural strength of composite (Mpa)	
	dry	wet, 2 h boil.
No additive	386	240
-COOH	457	296
-CH ₂ CH ₂ OH	440	285
-CONH ₂	408	268
-CH ₂ CH(O)CH ₂	408	281
-CH ₂ CH(OH)CH ₂ OPO(OH) ₂	438	307
-(CH ₂) ₃ Si(OMe) ₃	633	588
-Chrome complex ^a	502	427
-CH ₂ CHClCH ₂ OSiCl ₃	622	539
-CH ₂ CH ₂ OSi(OMe) ₃	347	232

^a Du Pont Volan™, pre-applied to glass from water.

2.1. Silanes

The advent of fiberglass-reinforced organic resins in 1940 produced a need for new bonding technology [6]. Although the glass-filled composites had good strength, properties deteriorated after prolonged exposure to atmospheric moisture, indicating loss of bonding between the glass and the resin. This problem was effectively solved in the mid-1950s when the plastics industry began using small amounts of silane coupling agents to improve composite properties. These adhesion promoters, defined above as molecules of the structure $\text{XRSi}(\text{OR})_3$, are now used in many systems, including urethane, epoxy, PVC plastisol, acrylic and latex coatings. Tables 3 and 4 are an example of the effect of silane addition on adhesion of epoxy and urethane coatings to mild steel and aluminum taken from the work of Walker [7]. The silanes used in this study are the same ones listed in Table 1. The adhesion was measured by direct pull-off in an Instron Universal Testing Machine. The data shown were obtained by applying the silanes as a primer pre-treatment, but Walker also evaluates their effectiveness as additives in the coatings and explores other variables, such as humidity and water immersion. He concludes that silanes have a wide potential application in polymer technologies where improved dry bond strength is desirable or bond strength under water-soaked conditions is important. He also notes that careful attention to detail is required if optimum effects on bond strength are to be obtained. One such critical detail is the state of cleanliness of the substrate. Note the effect of the two different cleaning regimens in Tables 3 and 4. Coupling agents can compensate for the presence of certain contaminants but it is always advisable to begin with substrates as clean as possible. Naturally, the degree of cleanliness necessary is

Table 3
Effect of silanes on bond strength of epoxide coatings

Silane	Substrate	Cleaning technique	Bond strength (Mpa)	Area detached (%)
None	Mild steel	Degrease	21	30–40
Epoxy	Mild steel	Degrease	25	0–40
Methacrylate	Mild steel	Degrease	28	20
Primary amine	Mild steel	Degrease	30	10–20
Diamine	Mild steel	Degrease	32	0
Mercapto	Mild steel	Degrease	24	10–40
None	Mild steel	Grit blast	28	20
Epoxy	Mild steel	Grit blast	29	10–20
Methacrylate	Mild steel	Grit blast	32	10
Primary amine	Mild steel	Grit blast	35	0
Diamine	Mild steel	Grit blast	36	0
Mercapto	Mild steel	Grit blast	34	0
None	Aluminum	Degrease	23	40–60
Epoxy	Aluminum	Degrease	27	10–40
Methacrylate	Aluminum	Degrease	31	20
Primary amine	Aluminum	Degrease	29	5–20
Diamine	Aluminum	Degrease	29	5–20
Mercapto	Aluminum	Degrease	26	10–30
None	Aluminum	Grit blast	33	20
Epoxy	Aluminum	Grit blast	38	0
Methacrylate	Aluminum	Grit blast	36	10
Primary amine	Aluminum	Grit blast	36	0
Diamine	Aluminum	Grit blast	37	0
Mercapto	Aluminum	Grit blast	36	0

very dependent on the particular system in question. Should the oxide layer on the metal, for example, be the weakest link in a system, then it should be removed, usually by etching and regenerating in a thinner, stronger form before coupling agents can be effective. In other cases removal of air-borne organic contamination by solvent degreasing may be sufficient.

This improvement in adhesion is generally believed to depend on interaction both with the inorganic (mineral) surface and the organic polymer (resin). 'Receptive' inorganic surfaces are characterized by the presence of hydroxyl groups attached to certain elements such as Si, Al, Ti, and Fe, capable of forming oxane bonds with adequate resistance to subsequent hydrolysis, whereas 'non-receptive' surfaces such as graphite, boron, and alkali metals and oxides do not form sufficiently hydrolytically stable covalent bonds with silanols. Generally, to interact, the silane coupling agent's OR^1 groups must first be converted to a reactive silanol (SiOH) form by hydrolysis. This can be accomplished by pre-treatment of the

Table 4

Effect of silanes on bond strength of polyurethane coatings

Silane	Substrate	Cleaning technique	Bond strength (Mpa)	Area detached (%)
None	Mild steel	Degrease	18	100
Epoxy	Mild steel	Degrease	27	40–100
Methacrylate	Mild steel	Degrease	29	10–20
Primary amine	Mild steel	Degrease	28	10
Diamine	Mild steel	Degrease	34	0–5
Mercapto	Mild steel	Degrease	24	20–40
None	Mild steel	Grit blast	34	10–40
Epoxy	Mild steel	Grit blast	31	50–90
Methacrylate	Mild steel	Grit blast	36	0–20
Primary amine	Mild steel	Grit blast	38	0
Diamine	Mild steel	Grit blast	39	0
Mercapto	Mild steel	Grit blast	35	0–30
None	Aluminum	Degrease	13	100
Epoxy	Aluminum	Degrease	11	100
Methacrylate	Aluminum	Degrease	31	0–60
Primary amine	Aluminum	Degrease	22	10–30
Diamine	Aluminum	Degrease	25	5–50
Mercapto	Aluminum	Degrease	19	100
None	Aluminum	Grit blast	28	10–30
Epoxy	Aluminum	Grit blast	26	10–50
Methacrylate	Aluminum	Grit blast	34	10
Primary amine	Aluminum	Grit blast	37	0
Diamine	Aluminum	Grit blast	33	0
Mercapto	Aluminum	Grit blast	36	0

substrate with an aqueous solution of the silane, addition of the silane to a latex water-based polymer system, or hydrolysis by absorbed or adsorbed moisture when applied in an organic solvent. Good interfacial bonding requires that the siloxane/silanol equilibrium favors siloxane formation over silanol formation. An important side reaction, particularly when applied in aqueous solution, is self-condensation of the coupling agent to form siloxane polymers. The coupling agent remains somewhat effective if the polymer formed is water-soluble, as in the case with aminosilanes, but if polymer precipitation occurs coupling activity will be lost.

On the organic side of the interface, chemical bonds are formed between the organofunctional R group of the silane and the reactive species in the polymer matrix. For example, a methacrylate- or styryl-functional silane reacts with polyesters copolymerized with styrene or similar monomers, while amino- or chloroalkyl-functional silanes are unsuitable in this particular case. Polybutadiene

resins, which have pendent vinyl groups, work well with vinyl silanes. Amino- and epoxy-functional silanes are suitable for use with epoxy resins. Controlled compatibility with the organic phase is crucial. This is markedly affected not only by the chemical constitution of the silane but also its degree of cure. Overcured layers may be too rigid and incompatible, while undercured layers may dissolve in the resin and not be available for bonding at the interface. Optimum curing can develop beneficial interpenetrating networks and this topic will be dealt with further in the later section on adhesion mechanisms. The reactivity rate of the silane organofunctionality is also critically important. The rate must be similar to that occurring in the matrix polymer so that it will bond to the polymer before the latter's reactive groups are consumed or immobilized. The close link between the reactivities of cross-linker and adhesion promoter is very familiar to adhesion technologists.

Notwithstanding the potential benefits of developing an interpenetrated inter-phase at the interface, there is currently great scientific and technological interest in self-assembled monolayers (SAMs) [8]. This subject is raised here because silanes are one of the two most important SAM classes (alkyl thiols and related compounds are the other). The term 'self-assembled monolayer' has variations in meaning depending on the scientific discipline in which it is used, so an explanation here of its usage in adhesion science is necessary. Self-assembly implies a high degree of order in the assembled monolayer and a considerable degree of permanence to that assembly. The capability of packing laterally into a highly ordered monolayer is usually conferred by the alignment of relatively long alkyl or fluoroalkyl chains. The permanence issue is usually interpreted to mean chemisorption involving covalent bond formation rather than strong physical adsorption. Thus conventional silane coupling agents, although capable of chemisorption, cannot be considered SAMs because they lack the required degree of ordered structure and normally form multilayers rather than monolayers. Reactive chloro- and alkoxy-functional silanes with longer alkyl or fluoroalkyl chains are capable of packing well together to form self-assembled monolayers on hydroxylated metal, oxide and glass surfaces. Conditions must be carefully controlled to avoid multilayer formation with di- or tri-alkoxy functional silanes. Obviously, this is not a problem with mono-alkoxy functional silanes although the other non-reactive groups on the silane, usually methyl groups, may disrupt the packing of the monolayer.

2.2. Orthosilicates

Orthosilicates are derivatives of orthosilicic acid $\text{Si}(\text{OH})_4$. The most common is tetraethyl orthosilicate $\text{Si}(\text{OC}_2\text{H}_5)_4$, often called TEOS, an acronym that also fits the alternative way of naming such a compound, tetraethoxysilane. Thus orthosilicates are actually a sub-set of the larger class of $\text{XRSi}(\text{OR}^1)_3$ silanes, where the XR group is also an alkoxy group. The XR and OR^1 groups do not have to be the

same, for example the compound $\text{CH}_2=\text{CH}(\text{CH}_2)_9\text{OSi}(\text{OEt})_3$, undecenyl oxytriethoxysilane (UTES) is a useful coupling agent for improving adhesion between polymers containing reactive SiH groups, which will react with the terminal olefin moiety, and hydroxylated inorganic substrates [9]. This SiH/SiVinyl reaction, known as hydrosilylation, offers a convenient, low-temperature, addition curing system that is widely exploited in silicone sealants, adhesives and elastomers and increasingly so in other polymer systems such as polyisobutylene. One significant drawback of this cure system is the absence of polar groups, such as silanols, for reaction with hydroxylated oxide surfaces, which can result in poor adhesion. The tetraalkoxy substitution provides the most reactive silanol functionality as the equilibrium constant of hydrolysis of orthosilicates to metals and glasses is even more favorable than those of conventional organofunctional silane coupling agents. As a practical benefit they are effective at lower cure temperatures. Since these unsaturated tetraalkoxysilane adducts are based on a Si–O–C linkage which is less hydrolytically stable than the Si–C linkage, there is a need to evaluate this aspect of adhesion performance. On some substrates adhesion may not be compromised by water exposure, but if it should be, mixtures of UTES and conventional silanes can be used to retain the rapid adhesion benefit of incorporating the former and benefit from the robust, hydrolytically stable adhesion contributed by the latter.

TEOS and similar materials are often added to silane coupling agent formulations. Their reaction in situ with other silanes helps develop reactivity with the inorganic substrate and facilitates network formation. Plueddemann [1] has reported that orthosilicates can be effective adhesion promoters when used alone. Presumably, they function by partial hydrolysis to oligomers that interdiffuse with liquid polymers and then cross-link to form interpenetrating networks at the interface. On the positive side, such a primer ultimately cross-links to silica, which has outstanding thermal and hydrolytic stability. A drawback is the rather narrow ‘window’ of time during which this type of primer film is soluble and compatible with matrix polymers. They must be applied within a few minutes or hours, depending on ambient temperature and humidity conditions, and hence are not suitable as coupling agents for pre-treated fillers or fiberglass that are to be stored for several months before incorporation into resins.

2.3. Other orthoesters

Various inorganic esters have been claimed as coupling agents for reinforced plastics, including aminobenzyl phosphonates, dicetyl isopropylborate, alkoxy compounds of aluminum, zirconium and titanium, zircoaluminates, and numerous substituted titanates [1]. These metal alkoxides could function in a similar manner to the orthosilicates by reacting with hydroxylated substrates. Like the simple orthosilicates such as tetraethyl orthosilicate (TEOS), it is less evident how an-

chorage to the organic phase is achieved, although there are many examples of the effectiveness of these compounds. For example, aluminum tri-*sec*-butoxide and aluminum tri-*tert*-butoxide primers significantly enhance the durability of bonds between mild steel and both a thermoplastic polyethersulfone and a thermoset epoxy adhesive [10]. In this instance, the improvement in adhesion was greater than that achieved with tetrabutyl orthosilicate, while titanium(IV) butoxide showed no improvement. The failure plane in these adhesively bonded samples varied with the relative humidity during the priming process. These metal alkoxides react rapidly with water, suggesting that degrees of hydrolysis/polymerization are important, a factor that is consistent with the hypothesis of an interpenetrating network formation with the organic polymer.

The oxane bonds that are formed between silanols and these metal alkoxides are less hydrolytically stable than those formed with silane coupling agents. Thus they do not compete strongly with silanes in the fiberglass reinforcement arena but are useful with other substrates. For example, Cohen [11] has reported that zircoaluminates are effective with substrates such as alumina trihydrate, calcium carbonate, and titanium dioxide, while Moles [12] suggests corona discharge-treated plastics and anodized aluminum as good substrates for zirconium-based adhesion promoters. The chemistry of zirconium has some similarities to silicon. It has a normal oxidation state of 4, its solution chemistry is dominated by the tendency to form polymeric species, and it has a marked preference for the formation of bonds with oxygenated species [12]. All aqueous zirconium compounds have polymeric structures, sometimes with ligands bonded to the zirconium-based polymer. The polymeric nature of zirconium in aqueous systems is similar to that of titanium compounds. However, zirconium compounds tend to be significantly more stable towards hydrolytic polymerization. These zirconium polymers react most readily with carboxyl groups to form strong covalent bonds; weaker bonds are formed with other oxygenated functional groups such as esters or ethers. Hydrogen bonds are formed with hydroxyl groups. Monte [13] has reviewed current developments and applications of titanate, zirconate and aluminate coupling agent additive technology in various thermoset and thermoplastic waterborne, high-solids, and powder coatings. He concludes that they act according to proton-coordination coupling mechanisms to form organofunctional monolayers on a wider variety of substrates than silanes and then bond or catalyze via various mechanisms such as catalysis, cross-linking, metallocene-like catalysis, repolymerization, or copolymerization to most polymer matrixes.

2.4. Chromium complexes

At one time these were the only commercially important non-silane coupling agents. Supplied by du Pont under the VolanTM tradename, they are coordination complexes of carboxylic acids with chromium(III) chlorides. Hydrolysis of the

chlorides produces oligomeric salts with hydroxyl groups that can hydrogen bond with surface silanol groups and possibly form covalent oxane bonds. The organic acid group is complexed with the chromium and carries other functionality for reaction with suitable polymers. For example, the chromium complex with methacrylic acid has been used for many years as a standard finish on glass for reinforcement of polyesters and epoxies. Interest continues in this material. See, for example, a recent patent [14] describing an adhesion promoter consisting of a methacrylate–chromium complex and poly(vinyl alcohol) (PVA) for bonding metals and thermoset resins. For one specific metal/resin combination, average tensile bond strength was 500 g/cm compared to 371 g/cm for samples without the PVA and 105 g/cm for samples without PVA or chromium complex.

2.5. Thiols and related compounds

Thiols with long alkyl or fluoralkyl entities are the other principal class of compounds used to form self-assembled monolayers (SAMs). As with silanes, much of the scientific and technological interest has been in materials that are inert, particularly compounds bearing aliphatic alkyl or fluoroalkyl groups. It is not necessary for a thiol or related compound to carry a functionality capable of bonding to an organic phase in order to qualify as a SAM. However, such functionality is clearly necessary for a ‘coupling’ SAM. There is a substantial literature concerning such organofunctional SAMs where the functionality, often an olefin, resides at the terminus of the alkyl chain away from the thiol or silane entity, in order to maximize reactivity with the organic phase and disrupt the alkyl chain packing the least. Such materials are used to construct two-dimensional composites where the regularity afforded by the monolayer is more valuable than any enhancement of adhesion that might accrue from a more disordered, thicker interphase region. Thiols are particularly useful for enhancing adhesion to noble metals such as silver or gold, which are inert to most other chemical functionalities.

For example, mercaptoesters are effective coupling agents for bonding metals using epoxy two-component adhesives with enhanced bonding strength and improved durability. Using grazing angle Fourier transform infrared (FT-IR) spectroscopy, Yang and Wakamatsu [15] have shown that the key mode of interaction of thioesters (octylthioglycolate, dodecylthioglycolate and stearylthioglycolate) and gold is strong chemical bonding, rather than wetting or hydrogen bonding. Only the longer two alkyl chains form densely packed regular orientations. The shorter octyl group does not self-assemble or orient on the gold surface. Van Velzen [16] has described a thiol functional silane coupling agent 3-(trimethoxysilyl)propanethiol that obviously fits both the silane and thiol classification categories.

2.6. Copolymers

Block copolymers are often used to promote dispersion of one polymer in another. Such compatibilizers or polymer-in-polymer emulsifiers constitute a particular aspect of coupling behavior that is only of peripheral interest to our focus on adhesion promotion in composites. However, there are some applications of copolymers that are more germane to our subject, such as the already mentioned use of ethylene–mercaptoester copolymers to couple epoxy resin to steel [2], the thiol functionality being able to react with both the epoxy and the steel (Fe^{3+}). In another example, Park [17,18] has reported the use of polyacrylamide–polycarbonate and polyacrylamide–polypropylene copolymers as coupling agents in carbon fiber-reinforced composites with polycarbonate and polypropylene, respectively. Interest has also developed in phenolic and quinoid compounds because of their ability to chelate metals like iron and copper. Vaccaro and co-workers [19] report that amino-*p*-benzoquinone polymers, poly{(2,5-hexamethylenediamino)-1,4-benzoquinone} and poly{(2,5-(2,2'-bistrifluoromethyl)-4,4'-biphenylenediamino)-1,4-benzoquinone}, improve torsional shear strength when used as adhesion promoters for steel/epoxy joints. The improvement in adhesion could be attributed to the formation of a chelate between the polyaminoquinone and the iron surface and a chemical reaction with the epoxy resin, based on electron spin resonance (ESR) studies of a low molecular weight model compound, *bis*{2,5-(4-methylanilido)1,4-benzoquinone}.

Not surprisingly, copolymers containing alkoxy silane functionality are also useful adhesion promoters. For example, copolymers of vinyl imidazole and vinyltrimethoxysilane, used as a primer, can improve the adhesion between polyimides and copper at elevated temperatures [20]. The copolymer also provided beneficial corrosion protection to the copper. Britcher and co-workers [21] have described the synthesis and characterization of some polymeric siloxane coupling agents. Given that silanes could be pre-reacted at least to the oligomeric state, this might not seem at first glance to be particularly advantageous. However, several of the polymers investigated are copolymers that offer attractive features. For example, the copolymers of methyltrialkoxysilane and dimethylsiloxane offer control of silane layer wettability, whereas those with residual methylhydrogensiloxane character have the potential to react with both hydroxylated, inorganic substrates and with hydrocarbon unsaturation in organic polymers. The synthetic approaches of Britcher et al. encompass a variety of molecular weights, extent of coupling functionality, and the distribution of coupling groups on the siloxane backbone. They offer a distinct alternative to conventional silane coupling agents; industry has yet to take up the challenge but it will be interesting to see how effective they can be in composite applications compared to their silane counterparts.

Should it be capable of reacting with both phases, there is nothing to preclude a functional homopolymer from being an effective coupling agent. For example,

Hirayama et al. [22] have shown that polyhydrogenmethylsiloxane can bind to aluminum, copper and steel surfaces via activation with a suitable platinum complex. The attached polymer promotes the adhesion of silicone materials whose cure involves SiH/SiVinyl hydrosilylation. Presumably, it would also be effective with other unsaturated organic polymer phases.

A particular class of polymers that would seem predestined to play a significant role in coupling technology are dendritic polymers, i.e. hyperbranched polymers and dendrimers. They are characterized by a high density of functional end groups; in the case of dendrimers these are favorably exo-presented and their number increases in a geometrically progressive manner with each generation. Very few block or graft dendritic copolymers have yet been prepared so their main present role is more to aid development of a cross-linked interphase than to directly couple dissimilar phases. A number of dendritic polymers have been claimed as coupling agents in patents. For example alkyl-terminated, multi-amine compounds with a cascade, dendrimer, hyperbranched or comb-like structure, when used as primers, substantially improve bond strength to cyanoacrylate adhesive bonded assemblies with a polyolefin substrate such as HDPE, LDPE or polypropylene [23]. There is as yet no widespread use of such materials to enhance adhesion.

2.7. Other compounds

Human ingenuity being what it is, a considerable range of materials and techniques have been evaluated as adhesion promoters. Many of these are more properly the subject of other chapters in this volume and will not be surveyed here. For example, triphenylphosphine and cobalt acetylacetonate are effective primers for ethyl cyanoacrylate adhesive bonding to polyolefins [24]. These chemicals function by dissolving in the polymer surface and facilitating interpenetration of the polyolefin and the adhesive. Although no covalent bonds are formed between the adhesive and adherend, this interpenetrating network formation has much in common with the mode of action of certain more conventional coupling agents. Another related approach is to activate a polymer surface in some way, for example, by plasma or corona pre-treatment, and then polymerize a reactive monomer in situ with simultaneous lamination to a metal substrate. Kang et al. [25] have described such an approach for bonding PTFE to copper foil using vinyl monomers such as 4-vinyl pyridine. These topics fit better in the following chapters on priming to improve adhesion, and surface modification of plastics to improve adhesion, and will not be pursued here.

3. Coupling agent adhesion mechanisms

The considerations raised in the introduction suggest a variety of mechanistic possibilities whereby silane and other coupling agents might operate. These

mechanisms are summarized in the following list:

- Chemical bonding theory
- Reversible hydrolysis theory
- Wetting and surface energy effects
- Interpenetrating network hypothesis
- Compatibility/penetration theory
- Restrained layer theory
- Deformable layer theory
- Morphology modification effects

It is not necessary to seek any one ‘best’ mechanism. All will play a greater or lesser role depending on the nature of a specific interface. That “adhesion is a very complex field beyond the reach of any single model or theory” as Schulz and Nardin [26] put it, is abundantly so for coupling agents when one considers the diversity of bonding conditions experienced, the variety of materials to be bonded and the multiplicity of bulk and surface effects involved. Accordingly, each of these theories will be briefly reviewed with little prejudice with the proviso, explicit in the title of this chapter, that if there is a dominant mechanism operative in many interfacial coupling instances, it is the chemical bonding theory.

3.1. Chemical bonding theory

This is the oldest and in many ways the most fundamental of the coupling agent adhesion mechanism theories. Much of the preceding section (Section 2) was necessarily framed primarily in terms of different chemical bonding possibilities. Almost all coupling agents are deliberately designed to contain chemical functional groups that can react with hydroxylated inorganic surfaces such as glass, producing covalent bond linkages. Additionally, most coupling agents contain at least one other, different functional group that could co-react with the organic polymer phase, usually during cure of that phase. The coupling agent then acts as a bridge to bond the glass to the cross-linked polymer or resin with a chain of primary bonds that, in principle, could be expected to lead to the strongest interfacial bond. Progress in the studies of molecular and microstructure of interfaces in composites, coatings, and adhesive joints was reviewed by Ishida [27] in 1984. He presented considerable evidence of the occurrence of chemical bonding at a variety of coupling agent interfaces. The following discussion is a far from comprehensive selection of both more recent and ‘classic’ studies, chosen to illustrate the main analytical techniques found to be particularly useful in establishing experimental evidence for bonding at the interface. These have proved to be X-ray photoelectron spectroscopy (XPS), secondary ion mass spectrometry (SIMS) — particularly time-of-flight SIMS (ToF-SIMS), inelastic tunneling spectroscopy (ITES), FTIR (e.g. FTIR diffusion–reflectance analysis), and solid-state, multi-nuclear, nuclear magnetic resonance (NMR). Scanning electron microscopy (SEM) (for examining

surface morphology) and ellipsometry (for layer thickness determination) have also been very useful techniques. Clearly, atomic force microscopy (AFM) will be a strongly contributing technique in the future.

That coupling agents react with the inorganic substrate is really not in doubt. In the case of alkoxy functional silanes there is convincing evidence that interfacial Si-O-M oxane bonds are formed with Fe, Cr, Al, Pb, Ti, and, of course, Si. Specific, convincing examples of the reaction with Si have been available for over three decades. For example, Johansson et al. [28] studied the physicochemical role of radioactively labeled silane coupling agents by determining their adsorption on E-glass and Aerosil surfaces. 3-(methacryloxy)propyltrimethoxysilane and 3-(2,3-epoxypropoxy)propyltrimethoxysilane were investigated. The results of tracer studies and electron photomicrographic examination of fiber surfaces indicated that the coupling agents form continuous films on E-glass surfaces with covalent bonding occurring at the interface. Failure of the glass-coupling agent interface in the presence of boiling water occurs by attack on the glass substrate itself, with relatively large amounts of coupling agent being removed by the mechanical action of the boiling water. The tracer studies also show that copolymerization occurs at the coupling agent/(methyl methacrylate)-styrene resin interface during free radical initiated polymerization, and can be accompanied by monomer solubilization in the partially cured coupling agent films.

Chemical bond formation between chemically etched stainless steel and 3-glycidoxypropyltrimethoxysilane was reported by Gettings and Kinloch [29]. They applied the silane coupling agent as a primer using an amine curing agent to catalyze the primer outside of the joint environment so that it could be directly analyzed by the static SIMS (SSIMS) and XPS techniques. Fig. 1 is the SSIMS spectrum taken at a depth of circa 12 nm for one of the silane-treated stainless steels. Fragments attributable to FeSiO^+ and CrSiO^+ ions were detected, indicative of chemical reaction between Fe and Cr in the steel surface and the silane coupling agent.

Another metal to which silanes covalently bond is Pb. Miller and Ishida [30] presented diffuse reflectance FTIR evidence for the occurrence of chemical bonding between 3-methacryloxypropyltrimethoxysilane and the surface of low surface area lead oxide. An infrared adsorption band near 965 cm^{-1} was detected near monolayer coverage of the adsorbate and assigned as the antisymmetric stretching vibration of the Pb-O-Si bond. Fig. 2 (spectrum A) is from the surface of the lead oxide at a coverage of two molecular layers and is dominated by this 965 cm^{-1} plumbosiloxane bond. Spectrum B is at much higher silane concentrations where the surface component is no longer visible, the spectrum being dominated by methacrylate modes. Spectra C and D are transmission spectra of the unhydrolyzed and hydrolyzed silane, respectively. Similar diffuse reflectance FTIR evidence has been presented for the existence of Al-O-Si and Ti-O-Si bonds at metal oxide/3-aminopropyldimethylethoxysilane interfaces

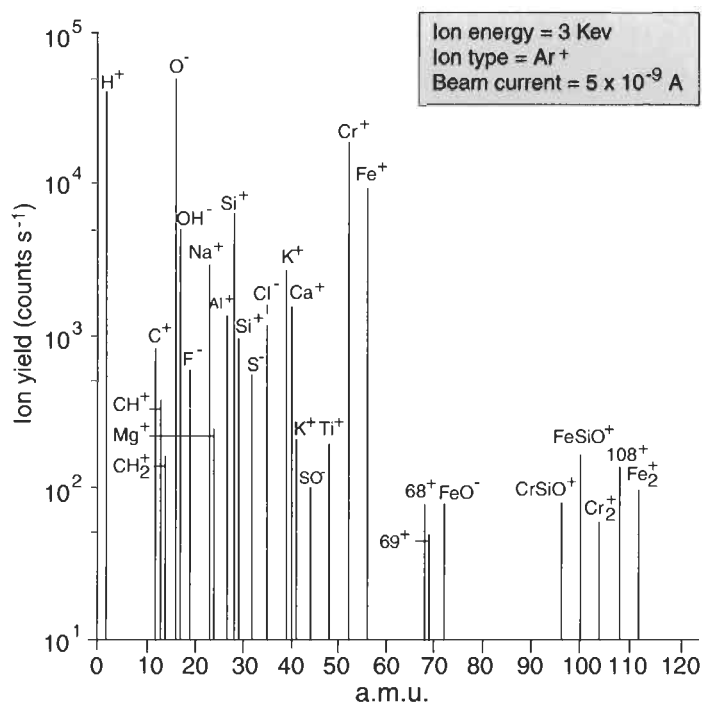


Fig. 1. SSIMS spectrum showing evidence of Fe–O–Si and Cr–O–Si bonding at a silane/steel interface (from Ref. [29]).

[31]. The amino group of the silane was also shown to hydrogen bond with silica surfaces.

Ishida and Koenig [32] used FTIR to study the 3-methacryloxypropyltrimethoxysilane/polyester system. A high surface-area silica was treated with vinyltrimethoxysilane and 3-methacryloxypropyltrimethoxysilane and mixed with styrene. After polymerization of the styrene, both coupling agents had lost their C=C groups indicating copolymerization and establishing that the coupling agent/matrix interface is covalently bonded. Note, however, that when E-glass fibers are used, only the methacryloxy silane interphase undergoes complete polymerization with styrene. The vinyl silane interphase remains mostly unreacted, accounting for the known difference in mechanical performance of these two coupling agents when used with E-glass fiber.

Another technique that has proved useful in establishing chemical bonding of coupling agents at interfaces is inelastic electron tunneling spectroscopy (ITES). For example, Van Velzen [16] examined 3-(trimethoxysilyl)propanethiol by this technique. Approximately monolayer quantities of this silane were adsorbed on the barrier oxide of an aluminum–aluminum oxide–metal tunneling junction; two metals were investigated, lead and silver. It was concluded that the silane is

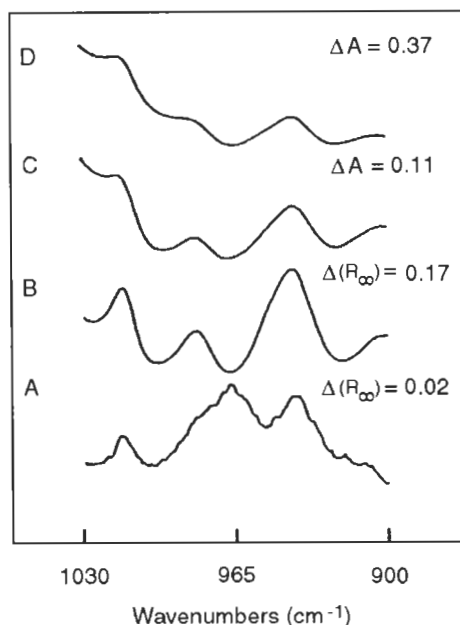


Fig. 2. Diffuse reflectance FTIR spectra showing evidence of Pb–O–Si bonding at a silane/lead oxide interface (from Ref. [30]).

chemically bonded by condensation of the methoxy groups with hydroxyl groups on the aluminum oxide surface. No interaction with the lead surface is observed, the SH and SiOH groups of the molecule probably interacting with each other in this case. However, there was clear evidence of interaction with the silver surface, since the thiol stretching vibration was absent in the spectra, the corresponding silver thiolate being most likely formed.

Caravajal et al. [33] have used solid-state NMR techniques to obtain detailed information about the structure of the reaction product of 3-aminopropyltriethoxysilane with silica gel. ^{13}C cross-polarization/magic-angle spinning (CP/MAS) NMR provides useful information about chemical interactions of the amino group and can quantify the number of residual ethoxy groups after reaction. ^{29}Si CP/MAS NMR also determines this latter number but additionally provides direct information about molecular bonding between silane molecules and silica silanols. In another example, Huijgen and co-workers [34] used solid-state NMR techniques to study a ^{13}C labeled version of the same amino silane in micro-composite samples composed of polyamide-6 and glass microspheres. Covalent bonding between the amino group of the silane and the polyamide-6 matrix could not be conclusively established directly; however, the motional dynamics of the amino group in situ provide support for both the covalent bonding and

interpenetrating network mechanisms. Solid-state ^{13}C NMR has been used by Parker and MacLachlan [35] to follow the hydrolysis of ^{13}C methoxy labeled phenylaminopropyltrimethoxysilane in a poly(vinyl chloride) (PVC) polymer film as a function of process history. Adhesion of the polymer to glass increased with the in-situ hydrolysis of the silane, monitored by the disappearance of the ^{13}C labeled methoxy group from the solid polymer matrix. Silane hydrolysis depended on relative humidity and exposure to heat during processing.

One should not necessarily assume that it is only the silanols in a hydrolyzed silane coupling agent that are capable of interacting with metal oxide substrates. For example, Horner et al. [36] have used N (1s) high-resolution XPS spectra to show that some fraction of the amino groups of 3-aminopropyltriethoxysilane is irreversibly protonated by interaction with hydroxyl groups on the surfaces of silicon, nickel, chromium, iron, titanium, aluminum and magnesium. The extent of protonation is greatest on Si, Al and Ti, intermediate on Fe, Cr and Ni, and least on Mg, which correlates well with the predicted isoelectric points of the oxides. Note the related earlier work of Naviroj et al. [31] previously discussed.

3.2. Reversible hydrolysis theory

This mechanism is a modification of the chemical bonding theory that views the reversibility of oxane bond formation as a contributory factor. It was first proposed by Plueddemann [1] who postulated that the formation and hydrolysis of stressed bonds between the coupling agent and the inorganic substrate in the presence of water might offer a beneficial stress-relaxation mechanism enabling the coupling agent layer to adjust to the stress without critically fracturing. Such a mechanism requires that the resin at the interface be rigid not rubbery because elastic recovery would separate the phases and reduce the likelihood of reformation of siloxane or oxane bonds. As Marsden and Sterman point out [37], the requirement of a rigid interface may be true for reinforced resins; however, the excellent reinforcement obtained by the use of silane coupling agents in mineral-filled rubbers raises some interesting questions. Do the reinforced resin and the reinforced rubber function by the same mechanism? Does the interaction of silane/rubber/filler result in a rigid interface in an overall elastic system? Detailed answers to these questions remain to be found; however, this provides a good example of our contention that it is futile to expect any one theory to explain all coupling agent adhesion phenomena.

3.3. Wetting and surface energy effects

Interfacial contact and development of attractive forces across the interface are prerequisites for subsequent interlocking, interdiffusion, or chemical bonding so the surfaces of the materials in question and the effect on those surfaces of any

Table 5

Surface energies of silane coupling agents on glass surfaces at 20°C

Functional group	σ_C (mN/m)	σ_S (mN/m)
CF ₃ (CF ₂) ₆ CH ₂ O(CH ₂) ₃ –	14	–
(CF ₃) ₂ CFO(CH ₂) ₃ –	18	–
	15–16	–
CH ₃ –	22.5	24.0
CH ₂ =CH–	25–26	27.2–31.5
CH ₂ =C(Me)COO(CH ₂) ₃ –	28.0	36.7
	38.9	–
Me(CH ₂) ₂ –	28.5	31.7
CF ₃ (CH ₂) ₂ –	33.5	34.7
H ₂ N(CH ₂) ₂ NH(CH ₂) ₃ –	33.5	30.8
	36.0	42.4
CN(CH ₂) ₂ –	34.0	35.5
MeC ₆ H ₄ – (mixed)	34.0	–
H ₂ N(CH ₂) ₃ –	35.0	34.2
	37.5	42.8
MeCOO(CH ₂) ₃ –	37.5	33.6
H ₂ N(CH ₂) ₂ NH(CH ₂) ₂ NH(CH ₂) ₃ –	37.5	38.4
(O)C ₆ H ₃ (CH ₂) ₂ –	39.5	36.5–52.8
C ₆ H ₅ –	40.0	33.2
CH ₂ (O)CH(CH ₂) ₃ –	40.0	48.8
(O)C ₆ H ₉ (CH ₂) ₂ –	40.0	53.7
Cl(CH ₂) ₃ –	40.5	33.0
	43	–
	41.0	37.7–40.3
HS(CH ₂) ₃ –	41.0	43.0
	33.6	40.2
(Me) ₂ CHC ₆ H ₄ – (mixed)	41.5	–
BrCH ₂ C ₆ H ₄ – (mixed)	42.0	–
Br ₂ C ₆ H ₃ – (mixed)	42.0	–
CH ₂ (O)CHCH ₂ O(CH ₂) ₃ –	42.5	–
BrC ₆ H ₄ – (mixed)	43.5	–
HOCH ₂ CH(OH)CH ₂ O(CH ₂) ₃ –	44.6	55.3
ClC ₆ H ₄ (CH ₂) ₂ –	45–47	–

applied coupling agent will play a crucial role in the adhesion at that interface. Because of the polar nature of most inorganic substrates, wetting of glasses, metal oxides, etc. is not usually a problem for aqueous or alcoholic solutions of coupling agents. What can sometimes present a problem is the wetting of such treated surfaces by the organic matrix, as the organic component of the coupling agent can contribute to relatively low-surface-energy, difficult-to-wet surfaces. Table 5, compiled by Owen [38], illustrates the range of surface energies provided by

diverse silane coupling agents. This table lists critical surface tensions of wetting, σ_C , and solid surface tension, σ_S , obtained in a manner similar to that of Owens and Wendt [39] but with a series of hydroxy-containing liquids rather than just water and methylene iodide. The data come from various sources and must be compared with caution; substrate type and treatment, deposition procedure, use and type of catalyst, relative humidity, nature of reactive alkoxy functionality, contact angle test liquids etc., all vary. Despite the differing conditions, the information provides a useful approximate ranking of the surface energies of silane coupling agent films that broadly parallels expectations from Zisman's studies [40] of the effect of various surface constituents on polymer wettability. When wetting difficulties are experienced, low levels of conventional surfactant wetting agents can be advantageous but the appropriate use-level must be carefully determined as excess surfactant is a potential source of weak boundary layer complications.

One way to improve the durability of M–O–Si oxane bonds is to simply prevent water from reaching the interface. Hydrophobic silanes are often used in combination with conventional silanes to reduce the wettability of the interface. For example, Jang et al. [41] reacted long hydrocarbon chains of varying length onto an acrylic-based trimethoxysilane. Improvements in initial adhesion and durability of glass-reinforced polyester laminates and castings were noted although no clear correlation between durability and length of hydrocarbon chain was evident. The potential for a non-wettable layer produced by the ordered packing of hydrocarbon chains was a significant motivation for Cave and Kinloch's exploration of self-assembled monolayer coupling agents [42] (see Section 4).

3.4. *Interpenetrating network hypothesis*

Despite the continuing advances in improving sensitivity and depth and lateral resolution of modern surface science characterization techniques, it is still a considerable challenge to use them to unequivocally prove whether a particular mechanism is operative in any given situation. The coupling agent layer is a classic example of a long-established problem in surface characterization, the 'buried interface' problem. Should the coupling agent be effective, it is virtually certain that failure will not be at the interface. The investigator then has to devise physical or chemical strategies to remove cohesively failed material without destroying the interfacial region. Depth profiling by ion sputtering with techniques such as SIMS and XPS is subject to problems of differential sputtering and scrambling of the information which gets worse the greater the depth to be sputtered. Moreover, the coupling agent is usually present at rather low levels and, consequently, only carefully planned model studies have the potential to contribute meaningful information. Attempts to depth profile through actual joints using 'real' substrates and formulations typically fail to detect evidence of coupling agent presence at all.

The first convincing evidence of interdiffusion between a silane coupling agent film and a polymer was provided by Sung and co-workers [43]. They used sapphire ($\alpha\text{-Al}_2\text{O}_3$) single-crystal plates as the model substrate. Aqueous 3-aminopropyltriethoxysilane (APS) solutions were spray-coated onto this substrate and laminated to polyethylene film, chosen because chemical reaction with the silane is unlikely. As only the silane contains silicon, a concentration profile of this element across the interface can provide evidence of interdiffusion should it be occurring. SEM-EDS (electron dispersion spectroscopy, also known as EDX, or X-ray fluorescence energy dispersive analysis) of a vertical cross-section through the interface was used to obtain this information. As the spatial resolution of SEM-EDS is of the same order as the typical thickness of a coupling agent layer (ca. 100 nm), a much thicker layer ($>50\text{ }\mu\text{m}$) than usual was selected for this model system study. Evidence was obtained of interdiffusion between the silane and polyethylene at 149°C , a temperature chosen to be above the melting point of polyethylene and the T_g of the silane film. Diffusion constants of the order of $10^{-12}\text{ cm}^2/\text{s}$ were obtained, with a tendency toward reduced diffusion as a consequence of extensive drying of the silane film, an expected trend as drying progressively increases the degree of cure of the silane film. This was proven by infrared spectroscopy and thermal analysis.

That similar effects occur with realistically thin silane layers of the order of 50 nm was established by Chaudhury et al. [44,45] who utilized a similar model system to Sung together with the more depth-sensitive XPS and secondary neutral mass spectrometry (SNMS) techniques. Using a different aminosilane, *N*-(2-aminoethyl)-3-aminopropyltrimethoxysilane, and polymers such as polystyrene and poly(vinyl chloride) (PVC), they similarly showed that heat treatment of the deposited silane layer greatly reduces the interdiffusion of the silane and polymer. They were careful to select components that contained unique 'tag' atoms that would clearly signal the arrival of the analytical probe at a particular interface. They used a fluorocarbon release layer (F marker atom), germanium as the inorganic, metallic phase, organosilicon coupling agent (Si marker atom, plus others such as N when aminofunctional materials were being investigated), and various polymers, some of which also had unique elemental tags, e.g. PVC (Cl marker atom). By paying particular attention to creating layers as thin as possible, for example by sputter coating a ca. 100 nm metal coating onto the release layer, depth profiling artifacts were minimized. On removing the release layer, a short depth profile through the germanium soon came to the coupling agent region and the organic polymer. Fig. 3 [45] shows the atomic concentration of Si from such a XPS depth profile study for the system Ge/aminofunctional silane/PVC. Since the primer is the only phase that contains Si, an estimate of the diffusion of primer into PVC can be made. The concentration profiles of Si corresponding to two drying temperatures indicate that the primer dried at 25°C (less cured) penetrated into the polymer more than did the primer dried at

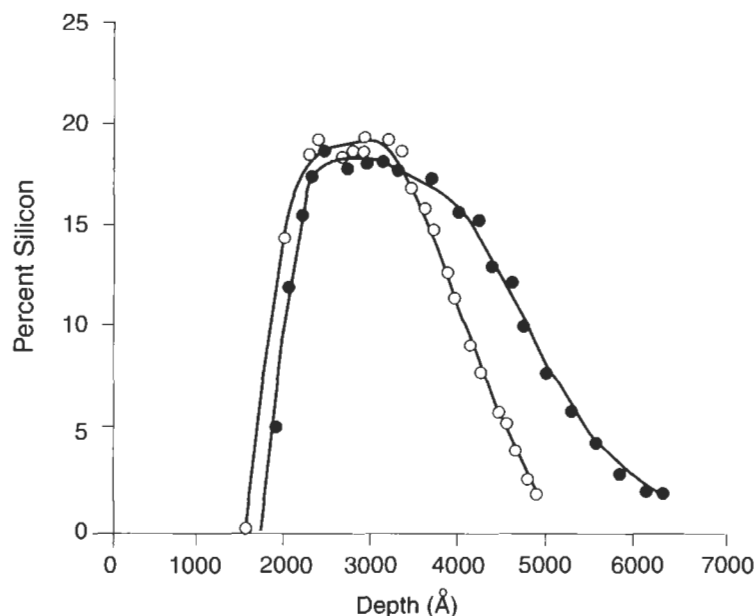


Fig. 3. XPS evidence of interpenetration at a silane/PVC interface (from Ref. [45]). Open circles: primer dried at 175°C; filled circles: primer dried at 25°C.

175°C (more cured). Similar SNMS studies utilizing an epoxy-functional silane and polyacrylamide [44] also suggest that coupling agent/polymer interdiffusion occurs. However, for this system the extent of interdiffusion was independent of the heat-treatment conditions used for the coupling agents. Evidently, other variables such as solubility parameters of the coupling agent, polymer, and solvent influence the outcome and, as with most aspects of complex, inter-related adhesion phenomena, generalization is unwarranted.

Mention has already been made of Parker and MacLachlan's solid-state NMR study [35] of methoxysilyl hydrolysis. They also concluded that the hydrolysis was accompanied by an increase in the fraction of silane with solid-like rigidity, most likely as a result of silane self-condensation within the polymer matrix. This is suggestive of an interpenetration mechanism but the ^{13}C label provides no insight into the degree of silane condensation that might have occurred after hydrolysis; these 'rigid' silane species could be monomeric, oligomeric, or polymeric. Bertelsen and Boerio [46] have used solution ^1H and ^{29}Si NMR to shed more light on this hydrolysis versus oligomerization question. They investigated aqueous solutions of 3-glycidoxypolytrimethoxysilane. By comparing the ^{29}Si NMR results with the wedge test adhesion data of Kuhbander and Mazza [47] on an aluminum/3-glycidoxypolytrimethoxysilane/epoxy system, they showed that the adhesion performance of the silane pre-treatments in the wedge tests

decreased as the oligomer concentrations in solution increased. One possible interpretation of this observation is that it is related to poorer interdiffusion of the oligomeric species.

Another interesting aspect of this study is the insight gained into the effectiveness 'window' of aqueous silane solutions. Kuhbander and Mazza [47] showed that 1% 3-glycidoxypropyltrimethoxysilane solutions were most effective when the hydrolysis time was about 1 h. Bertelsen and Boerio [46] showed that hydrolysis was complete in 1% heavy water solution after about 34 min. However, condensation took considerably longer. Clearly, in this case, the familiar aging period specified in practical recipes for aqueous silane coupling agent solution application is related more to ensuring hydrolysis to silanol than it is to subsequent condensation.

3.5. Compatibility/penetration theory

This proposed mechanism can be seen as a shorter-length-scale molecular variant of the interpenetrating network hypothesis. In this view, the compatibility afforded by the organofunctional group permits advantageous penetration of that group into the organic polymer but does not require the bulk silane film to penetrate. It was proposed by Harding and Berg [48] who systematically varied both interfacial bond formation conditions and the size and functionality of the silane organofunctional group. They used a series of aminofunctional silanes with constant C : N ratio and identical surface energies to couple poly(vinyl butyral) to spherical glass particles and were able to show a relationship between the length of the aminofunctional group and interfacial strength. Direct interfacial strength measurements using single-particle composites showed that variation in the time-temperature profile of bond formation did not significantly affect interfacial strength as would have been expected had interpenetrating network formation prevailed. Also related to such compatibility concepts is the general correlation between enhanced interfacial strength and more favorable thermodynamic mixing suggested for silane coupling agents by Miller and Knowlton [49]. They used the group contribution method of UNIFAC (universal functional activity coefficients) to calculate the free energy of mixing.

3.6. Restrained layer theory

Kumins and Roteman [50] have proposed that the resin in the region of mineral filler should have a modulus somewhere between that of the mineral and the matrix resin. The restrained layer theory suggests that coupling agents function by 'tightening up' the polymer structure in the interphase region. This concept has much in common with the interpenetrating network formation idea, providing one explanation of why an interfacial interpenetrating network might be beneficial.

Stein and co-workers [51] have suggested mechanisms where the polymer cross-linking catalyst associates itself with the adhesion promoter that is incorporated in the polymer phase in some formulations. These associated catalyst/coupling agent molecules then migrate to the interface and react to produce a more highly cross-linked region at the interface. They have shown that the platinum hydrosilylation catalyst is more soluble in the adhesion promoter/inhibitor phase than in the silicone. NMR imaging results support this concept.

Such migration requires only partial miscibility in the polymer matrix, silicone in the particular case studied by Stein et al. Owen and co-workers [9] have suggested that solubility parameter calculations can be useful in designing suitable compositions with partial miscibility. These ideas appear superficially to be at odds with compatibility/penetration and interpenetrating network concepts. However, these contrary solubility requirements are a consequence of the initial placement of the adhesion promoter. When used as a primer, it is already placed at the interface so needs no partial solubility characteristic to drive it there, as is needed when it is initially dispersed throughout the polymer matrix. In both cases it is the development of a strengthening interfacial phase that accounts for the enhancement in adhesion that is sought by the user.

The system described by Stein et al. [51] employed a novel class of bifunctional adhesion promoters for self-priming addition cure siloxane systems. Additives such as *bis*(trimethoxysilylpropyl)fumarate, $[(\text{CH}_3\text{O})_3\text{Si}(\text{CH}_2)_3\text{OCO}]_2\text{CH}=\text{CH}$, migrate to surfaces such as aluminum during the curing process. This results in an entanglement of the promoter at the interface and also changes the cure profile such that the material cures more rapidly at the interface. The adhesion promoter reacts rapidly with any accessible surface hydroxyls as well as undergoing self-condensation reactions. The interfacial layer is a random organosilicate thermoset bonded tightly to adventitious sites on the hydrated aluminum surface. The silicone elastomer is most likely entangled with the organosilicate thermoset in the interfacial layer. Note that the interfacial enrichment of these fumarate adhesion promoters was proven by XPS studies. Similar studies with conventional silane coupling agents such as 3-aminopropyltrimethoxysilane showed them to be uniformly distributed in the siloxane matrix [52].

3.7. Deformable layer theory

At the other extreme to the restrained layer theory is the deformable layer theory where a flexible, deformable phase seems desirable to accommodate stresses set up at the interface due to differential thermal shrinkage between resin and filler when the composite is cooled. There is still considerable confusion and debate over what morphology might be desirable in resin adjacent to treated mineral and metal substrates. The amount of coupling agent in a typical finish is probably insufficient to provide a low-modulus layer at the interface. However, Erickson

et al. [53] have proposed that the silane coupling agent treated surfaces might allow preferential adsorption of one ingredient in the resin. Unbalanced cure in the polymer part of the interphase could provide a flexible resin much thicker than the coupling agent layer. An extreme version of the deformable layer theory is the suggestion that it provides lubrication to protect the mineral against abrasion during fabrication [54]. Such protection is especially important with glass fibers but this attribute is best viewed as a desirable added benefit rather than a significant adhesion-enhancement mechanism.

Clearly, the restrained layer and deformable layer mechanisms are directly at odds with each other. There may be cases where the deformable layer theory is operative but most researchers in the field believe the restrained layer theory to be more general. For example, Plueddemann [1] believed that performance data of silanes in reinforced composites suggest that a restrained layer is required at the interface for maximum bonding and resistance to hydrolytic cleavage. He noted that in both polyesters and epoxies, silane treatments of fillers often overcome cure inhibition as measured by cure exotherms. Silanes that allowed maximum exotherms, i.e. those most effective in overcoming surface inhibition, were generally the most effective coupling agents as indicated by mechanical properties and chemical resistance of composites. He concluded that a restrained layer rather than a deformable layer is the best morphology in the interphase region for optimum properties of composites.

3.8. Morphology modification effects

Obviously, differences in surface topography and morphology will affect the performance of all adhesive joints including those modified by the presence of coupling agents. For example, we have already discussed in Section 3.1 the use of SSIMS by Gettings and Kinloch [29] to establish chemical reaction between a silane coupling agent and stainless steel. These authors used steels of similar bulk composition but manufactured in different ways. They also carried out joint durability studies and were able to demonstrate clear improvements in durability that could be ascribed to chemical reaction between the primer and metal surface for two of the steels (200 and 300). However, for one of the steels (100) little evidence for primer/substrate bonding was found and only a small improvement in durability on application of the silane primer was detected. Surface analysis revealed that the distribution of adventitious contamination in the surface region of all three etched steels was similar, so this could not account for the variation in behavior. The 100 steel was known from earlier studies [55] to have a significantly rougher surface as a result of a pickling process in its manufacture. Moreover, its surface structure was a mixture of austenite and martensite compared with the pure austenite on the 200 and 300 steels. It is reasonable to ascribe the performance differences to these differences in surface morphology.

It has also been suggested that silane treatments on reinforcements and fillers may in some way modify the morphology of adjacent polymer to improve adhesion. For example, the probability that orientation may extend beyond the silane finish into the resin phase is suggested by the work of Kahn [56] with orientation of liquid crystals on mineral surfaces treated with silane coupling agents. A methylaminopropylsilane on oxide surfaces caused parallel alignment, whereas an octadecylaminopropylsilane caused perpendicular alignment of liquid crystals in contact with the surface.

4. Other interfacial studies

Because of the numerous ways in which coupling agents can affect behavior of the interfacial region in composites, and the wide variation in composite composition, it is usually necessary to conduct designed experiments to optimize coupling agent type and use-level. There are a growing number of such studies where the practical results are correlated with surface characterization studies to shed light on the operative mechanisms of adhesion in specific instances. For example, Rider and Arnott [57] have described various combinations of grit blasting, boiling, and silane treatments, and investigated the resultant surface effects using XPS. Their chosen system was aluminum alloy/epoxy structural adhesive/3-glycidoxypopyltrimethoxysilane. The effect of grit blasting is self-evident; boiling is a familiar feature of aluminum treatments to encourage formation of porous oxide films conducive to mechanical interlocking.

Rider and Arnott were able to produce notable improvements in bond durability in comparison with simple abrasion pre-treatments. In some cases, the pre-treatment improved joint durability to the level observed with the phosphoric acid anodizing process. The development of aluminum platelet structure in the outer film region combined with the hydrolytic stability of adhesive bonds made to the epoxy silane appear to be critical in developing the bond durability observed. XPS was particularly useful in determining the composition of fracture surfaces after failure as a function of boiling-water treatment time. A key feature of the treatment is that the adherend surface prepared in the boiling water be treated by the silane solution directly afterwards. Given the adherend is still wet before immersion in silane solution, the potential for atmospheric contamination is avoided. Rider and Arnott have previously shown that such exposure is detrimental to bond durability.

3-Aminopropyltriethoxysilane is widely used as a coupling agent in glass-fiber-reinforced plastics. It has proved difficult to exploit the XPS technique for the study of glass fibers but in combination with the extremely surface-sensitive time-of-flight secondary ion mass spectrometry (ToF-SIMS) technique, significant progress has been made. Wang et al. [58] have confirmed the formation of chem-

ical bonds between E-glass fiber surfaces and the aminosilane layer. They have also demonstrated the formation of distinct chemical bonds between the silane and a diglycidyl ether epoxy resin. This work adds to the experimental evidence for bonding reviewed in the preceding section. However, it adds complexity to the mechanisms involved in the development of the interfacial phase by showing that aluminum ions from the glass surface are incorporated uniformly and integrally into the interphase between the fiber surface and the silane. Thus not only can monomer from the organic phase be incorporated in the silane layer as shown by Johansson et al. [28], but now it appears that components of the inorganic phase can likewise be incorporated. For the aluminum to be chemically incorporated into the silane layer it may have dissolved into the aqueous solution and co-deposited with the silane as an aluminosilane link. Clearly further work is needed to fully understand the detailed mechanisms, but in this specific example there appears to be a combination of chemical reactivity to both phases and penetration of components of both phases into the coupling agent interfacial region. Doubtless, further striking revelations yet await us as a wider arsenal of surface-sensitive techniques are brought to bear on a wider variety of coupling-agent-modified interphases.

Although experience has shown that a monolayer of coupling agent usually does not yield an optimum mechanical strength, there are specific instances where monolayers are effective and provide a clear example of coupling via the chemical bonding mechanism. Highly ordered, self-assembled monolayers (SAMs) expectedly provide a good example of this concept. Cave and Kinloch [42] have evaluated long-chain, vinylic terminated trichlorosilanes, adsorbed on aluminum mirrors, as adhesion promoters. They determined the structure of the monolayers by XPS, SIMS, ellipsometry and reflection high-energy electron diffraction. The structure of the adsorbed films is dependent on alkyl chain length in line with other SAM structure studies. Highly ordered monolayer films are obtained with C_{18} atoms and longer; as the hydrocarbon chain length is reduced the films become progressively more disoriented. The terminal vinyl groups were converted into hydroxyl groups for reaction with isocyanate-cured polyurethane resin adhesive. Adhesion was evaluated by a blister test. It was found that both a C_{18} and a C_{10} silane produced higher adhesive fracture energies under dry conditions than can be obtained with conventional silane coupling agents. When water was present only the C_{18} silane exhibited a high resistance to moisture attack. The rapid failure of the C_{10} silane is attributed to facile diffusion of water to the interface through the disorganized, less densely packed monolayer that is produced compared to the C_{18} silane situation. The authors' overall assessment is that the performance of the C_{18} SAM as an adhesion promoter is comparable to the best performance achieved using commercially available 3-aminopropyl functional silanes.

5. Summary

The purpose of this chapter was to review the range of materials used to enhance adhesion between dissimilar phases and to explore the variety of mechanisms that have been proposed to account for their behavior. These coupling agents or adhesion promoters are of great technological importance in adhesive bonding, reinforced composites, and various coating technologies. We have seen that organic polymer/inorganic glass and metal oxide interfaces are of greatest interest and that silanes are the most widely used class of coupling agent. Their mechanism of action is as varied as any other aspect of the multidisciplinary subject of adhesion. It is abundantly evident that covalent bonding to hydroxyl groups on the glass or metal oxide surface is one of the keys to their effectiveness. Reactivity and controlled compatibility with the organic phase are also vital, with many situations being explained by some combination of the chemical bonding and interpenetrating network adhesion mechanism theories.

The application of modern surface analysis techniques such as XPS and ToF-SIMS, and molecular-level chemistry probes such as solid-state, multinuclear NMR, has elucidated the bonding mechanism in a growing number of specific polymer/coupling agent/metal oxide combinations. We can anticipate a further broadening of understanding of technologically important interphases not yet examined in detail to be forthcoming. This new understanding will permit better optimization of existing coupling agents and will be the basis for the development of new types of adhesion promoter. There is no reason to suppose that the novelty and ingenuity shown in the past in the adhesion promotion field will not continue in the future. Although our focus in this chapter has been on interfacial reactivity, considerable insight has been gained in recent years regarding the solution reactivity of coupling agents. The hydrolysis and condensation of silanes, particularly in aqueous solution, is now well-understood and similar advances for other coupling agents are expected.

Although the historical development of the field has rightly focused on organic/inorganic coupling, researchers involved in coupling agent technology will be aware of the growing need to improve the adhesion between different polymers, for example silicones and fluoropolymers. The surface modification of plastics to improve adhesion is the subject of a separate chapter in this volume. However, combination of such chemistry with novel coupling agents is an easy prediction to make.

References

1. Plueddemann, E.P., *Silane Coupling Agents*, 2nd edn. Plenum Press, New York, NY, 1991.
2. Schmidt, R.G. and Bell, J.P., *J. Adhes.*, **27**, 135 (1989).

3. Plueddemann, E.P., *Appl. Polym. Symp.*, **19**, 75 (1972).
4. Arkles, B., *CHEMTECH*, 766 (1977).
5. Plueddemann, E.P., In: Mittal, K. (Ed.), *Silanes and Other Coupling Agents*. VSP, Utrecht, 1992.
6. Collins, W.T., In: Calbo, L.J. (Ed.), *Handbook of Coatings Additives*. Marcel Dekker, New York, NY, 1987.
7. Walker, P., In: Mittal, K.L. (Ed.), *Silanes and Other Coupling Agents*. VSP, Utrecht, 1992.
8. Ulman, A., *Chem. Rev.*, **96**, 1533 (1996).
9. Lutz, M.A., Gentle, T.E., Perz, S.V. and Owen, M.J., In: Mittal, K. (Ed.), *Silanes and Other Coupling Agents*, Vol. 2. VSP, Utrecht, 2000, p. 3.
10. Menon, B., Pike R.A. and Wightman, J.P., In: Mittal, K. (Ed.), *Silanes and Other Coupling Agents*. VSP, Utrecht, 1992.
11. Cohen, L.B., In: Mittal, K.L. (Ed.), *Silanes and Other Coupling Agents*. VSP, Utrecht, 1992.
12. Moles, P.J. In: Mittal, K.L. (Ed.), *Silanes and Other Coupling Agents*. Utrecht, 1992.
13. Monte, S.J., *Proc. 25th Int. Symp. Waterborne, High-Solids, Powder Coating*, 190 (1998).
14. Kwei, J.Z., U.S. Patent 5,904,797, 18 May 1999 (assigned to E.I. du Pont de Nemours and Co.).
15. Yang, D.B. and Wakamatsu, T., *Surf. Interface Anal.*, **24**, 803 (1996).
16. Van Velzen, P.N.T., *Surface Sci.*, **140**, 437 (1984).
17. Park, J.-M., *Korea Polym. J.*, **7**, 46 (1999).
18. Park, J.-M., *Pollimo*, **18**, 783 (1994).
19. Vaccaro, E., Simone, C.D. and Scola, D.A., *J. Adhes.*, **72**, 157 (2000).
20. Kim, H. and Jang, J., *Polymer*, **41**, 6553 (2000).
21. Britcher, L.G., Kehoe, D.C., Matisons, J.G. and Swincer, A.G., *Macromolecules*, **28**, 3110 (1995).
22. Hirayama, M., Soares, M.C., Caseri, W.R., Suter, U.W. and Goussev, O., *J. Adhes.*, **72**, 51 (2000).
23. Woods J.G. and Frechet, J.M.J., PCT Int. Appl. (1999), WO 98-US19783 (assigned to Loctite Corporation).
24. Yang, J. and Garton, A., *J. Appl. Polym. Sci.*, **48**, 359 (1993).
25. Kang, E.T., Zhang, J.F., Cui, C.Q. and Lim, T.B., In: Mittal, K. (Ed.), *Silanes and Other Coupling Agents*, Vol. 2. VSP, Utrecht, 2000.
26. Schultz, J. and Nardin, M., In: Pizzi, A. and Mittal, K.L. (Eds.), *Handbook of Adhesive Technology*. Marcel Dekker, New York, NY, 1994.
27. Ishida, H., *Polym. Comp.*, **5**, 101 (1984).
28. Johansson, O.K., Stark, F.O., Vogel, G.E. and Fleischmann, R.M., *J. Compos. Mater.*, **1**, 278 (1967).
29. Gettings, M. and Kinloch, A.J., *Surf. Interface Anal.*, **1**, 89 (1979).
30. Miller, J.D. and Ishida, H., In: Leyden, D.E. (Ed.), *Chemically Modified Surfaces*, Vol. 1. Gordon and Breach, New York, NY, 1986.
31. Naviroj, S., Koenig, J.L. and Ishida, H., *J. Adhes.*, **18**, 93 (1985).
32. Ishida, H. and Koenig, J.L., *J. Polym. Sci., Polym. Chem. Ed.*, **17**, 615 (1979).
33. Caravajal, G.S., Leyden, D.E. and Maciel, G.E., In: Leyden, D.E. (Ed.), *Chemically Modified Surfaces*, Vol. 1. Gordon and Breach, New York, NY, 1986, p. 283.
34. Huijgen, T.P., Angad Guar, H., Weeding, T.L., Jenneskens, L.W., Schuurs, H.E.C., Huysmans, W.G.B. and Veeman, W.S., *Macromolecules*, **32**, 3063 (1990).
35. Parker, A.A. and MacLachlan, J., In: Mittal, K.L. (Ed.), *Silanes and Other Coupling Agents*, Vol. 2. VSP, Utrecht, 2000, p. 27.

36. Horner, M.R., Bocrio, F.J. and Clearfield, H.M., In: Mittal, K.L. (Ed.), *Silanes and Other Coupling Agents*, Vol. 2. VSP, Utrecht, 2000, p. 241.
37. Marsden, J.G. and Sterman, S., In: Skeist, I. (Ed.), *Handbook of Adhesives*, 2nd edn. Van Nostrand Reinhold, New York, NY, 1977, p. 640.
38. Owen, M.J., In: Zeigler, J.M. and Fearon, F.W.G. (Eds.), *Silicon-Based Polymer Science*. Adv. Chem. Ser., **224**, ACS, Washington, DC, 1990, p. 705.
39. Owens, D.K. and Wendt, R.C., *J. Appl. Polym. Sci.*, **13**, 1741 (1969).
40. Zisman, W.A., In: Fowkes, F.M. (Ed.), *Contact Angle, Wettability, and Adhesion*. Adv. Chem. Ser., **43**, ACS, Washington, DC, 1964, p. 1.
41. Jang, J., Ishida, H. and Plueddemann, E.P., *25th Annu. Tech. Conf. Reinf. Plast. Div. SPI*, 2-C, 1986.
42. Cave, N.G. and Kinloch, A.J., *Polymer*, **33**, 1162 (1992).
43. Sung, N.H., Kaul, A., Chin, I. and Sung, C.S.P., *Polym. Eng. Sci.*, **22**, 637 (1982).
44. Gellman, A.J., Naasz, B.M., Schmidt, R.G., Chaudhury, M.K. and Gentle, T.M., *J. Adhes. Sci. Technol.*, **4**, 597 (1990).
45. Chaudhury, M.K., Gentle, T.M. and Plueddemann, E.P. *J. Adhes. Sci. Technol.*, **1**, 29 (1987).
46. Bertelsen, C.M. and Boerio, F.J., In: Mittal, K. (Ed.), *Silanes and Other Coupling Agents*, Vol. 2. VSP, Utrecht, 2000, p. 41.
47. Kuhbander, R.J. and Mazza, J.J., *Proc. SAMPE Symp.*, **38**, 1225 (1993).
48. Harding, P.H. and Berg, J.C., *J. Appl. Polym. Sci.*, **67**, 1025 (1998).
49. Miller, A.C. and Knowlton, M.T., *74th Colloid and Surface Science Symposium*, Paper 248, Lehigh University, Bethlehem, PA, June 19–21, 2000.
50. Kumins, C.A. and Roteman, J., *J. Polym. Sci., Part A*, **1**, 527 (1963).
51. Stein, J., Eichinger, B.E. and Early, T., *2nd Int. Symp. Adhesive Joints: Formation, Characteristics and Testing*, Newark, NJ, May 22–24, 2000.
52. Stein, J., Valenty, S.J., Smith, G.A., Bresniak, D.V. and Prutzman, L.C., *Macromolecules*, **19**, 2291 (1986).
53. Erickson, P.W., Volpe, A.A. and Cooper, E.R., *SPI, 19th Annual Tech. Conf. Reinf. Plast.*, 24-A (1974).
54. Outwater, J.O., *SPI, 11th Annu. Tech. Conf. Reinf. Plast.*, 9-B (1956).
55. Gettings, M. and Kinloch, A.J., *J. Mater. Sci.*, **12**, 2511 (1977).
56. Kahn, F.J., *Appl. Phys. Lett.*, **22**, 386 (1973).
57. Rider, A.N. and Arnott, D.R., *Int. J. Adhes. Adhes.*, **20**, 209 (2000).
58. Wang, D., Jones, F.R. and Denison, P., *Catal. Today*, **12**, 375 (1992).

Priming to improve adhesion

GILES DILLINGHAM *

Brighton Technologies Group, Cincinnati, OH, USA

1. Introduction

The joining of materials through adhesive bonding, the encapsulation of materials with a protective coating of paint, or the modification of material characteristics through incorporation of a distinct phase with complimentary properties are all processes that produce composite materials or structures. The presence of interfaces with properties that determine to a large extent the overall performance of a material or structure is one of the defining characteristics of a composite material.

The interface that is created between the two dissimilar phases in a composite structure is both a chemical and physical discontinuity. Even though it may be many molecular layers removed from a free surface, an interface retains the important surface characteristic of an increased chemical potential over the bulk phase due to a non-equilibrium intermolecular force field. This increased interfacial chemical potential is further augmented by the presence of residual stresses resulting from unequal dimensional changes in the constituent phases during processing, and stress concentrations that occur during loading due to the discontinuity in moduli of the constituent phases. These all contribute to the non-equilibrium state of an interface and represent destabilizing influences that contribute to the tendency of composite materials or structures to fail in a manner controlled by the interfacial properties.

The volume of substance in a composite material that exists in a non-equilibrium state due to its proximity to an interface has been termed an *interphase* [1]. The interphase is a zone of distinct composition and properties formed by chemical or physical processes such as interdiffusion of mutually soluble components or chemical interaction between reactive species.

* Corresponding author. E-mail: gdillingham@fuse.net

Improving the properties of composites frequently requires addressing the issues of interfacial strength and stability. One approach to improving these characteristics is to intentionally introduce an interphase region to improve initial adhesion, provide chemical stabilization against degradation in aggressive environments, and perhaps provide for a broad transitional zone in mechanical properties between the phases. An interphase engineered to accomplish these goals that is applied as a separate manufacturing step is referred to as a primer.

Primers belong to a class of surface engineering distinct from surface pretreatments such as the electrochemical etching or anodization of metal surfaces, and surface functionalization processes for plastics such as flame treatment, corona discharge or plasma treatment. Such treatments focus on either improving the stability of one of the phases against degradation through corrosion or hydration [2], increasing the chemical compatibility of the two phases at the interface by providing specific chemical functionality, or providing a surface morphology optimized for mechanical interlocking of the constituent phases [3,4]. With surface pretreatments such as these, the effects generally extend only a few molecular layers at most from the interface into either bulk phase. While an interphase may be created in situ through the interaction between the surfaces, the dimensions are generally on a molecular level.

In addition to providing a means for engineering an interphase for improved material performance, primers can be employed to facilitate a manufacturing process. In the case of metals prepared for painting or adhesive bonding by cleaning and etching processes, the clean oxide surfaces are highly reactive and subject to rapid contamination through handling or simply through exposure to atmospheric moisture and airborne contaminants. Application of an appropriate primer to these surfaces effectively passivates the surface against oxidation and contamination prior to final adhesive bonding or painting. In these situations, an excellent primer may be nothing more than a solution of an appropriate polymer that is soluble in the final coating or adhesive.

Primers may be divided into several broad categories based upon the type of interface they are designed to improve. Table 1 shows one such classification. Further discussion in this chapter is based upon this classification scheme.

2. Primers for structural adhesive bonding of metals

2.1. Coupling agents

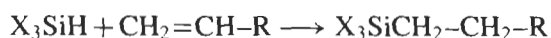
Coupling agents are multifunctional compounds designed to provide a means for chemically coupling to both the inorganic surface and to the organic adhesive or coating. The most widely used coupling agents are based on organosilicon chemistry, although titanates and zirconates have also enjoyed modest technical

Table 1
Classification scheme for adhesive and coating primers

Metal-polymer, structural adhesive bonding	Coupling agents
	Non-corrosion-inhibiting primers
	Corrosion-inhibiting primers
	Inorganic barrier primers
	Rubber to metal primers
Metal-polymer, protective or decorative coating	Galvanic systems
	Barrier systems
	Inhibiting systems
Adhesive bonding and painting of polymers	Primers for cyanoacrylate adhesives, chlorinated polyolefin primers

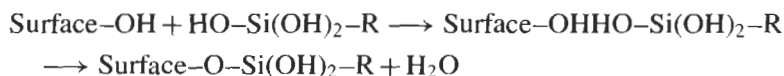
and commercial success. These compounds may be applied directly to the substrate surface from dilute solution or may be compounded into an adhesive or coating to generate a self-priming formulation. The technology is very rich and has stimulated a tremendous volume of research over the last 3 decades, which has resulted in a good understanding of the mechanisms of adhesion promotion through organosilanes. On a larger scale, this work has resulted in a much greater understanding of the phenomenon of adhesion in general. It is entirely possible that the widespread adoption of fiber-reinforced plastics would not have occurred without the development of organosilane coupling agent technology to provide moisture resistance to the glass/polymer interface in these materials. An excellent (though slightly dated) review of coupling agent technology may be found in [5].

Silane coupling agents are generally synthesized through addition of silicon hydrides to unsaturated organic molecules:



where X is a hydrolyzable group such as Cl, $-\text{OCH}_2\text{CH}_3$, or $-\text{OCH}_3$. In practice, organosilanes are frequently synthesized from the chlorosilane precursor which is subsequently hydrolyzed in the appropriate alcohol to form the ethoxy or methoxy analogue. This avoids the generation of HCl (the byproduct of Si-Cl hydrolysis) in the end user's manufacturing process. Ethoxysilanes are gaining favor over methoxy versions due to toxicity considerations of the methanol generated during hydrolysis.

Coupling to a mineral surface requires the presence of active hydroxyls on the substrate. The coupling reaction is a multi-step process that proceeds from a state of physisorption through hydrogen bond formation to actual covalent bond formation through condensation of surface hydroxyls with silanols:



The formation of actual covalent bonds between the mineral surface and the silanol would certainly help explain the resistance of organosilane-modified interfaces to degradation in the presence of moisture, but the detection of such bonds is extremely difficult. The challenge is detection and structural analysis of what is essentially a monomolecular layer buried between two bulk phases. The presence of covalent bond formation is widely accepted in the case of glass and silica substrates where the chemistry of silanol condensation is well understood. Similarly, condensation of silanols with metal hydroxides to form low concentrations of M–O–Si species has been demonstrated in several instances using techniques such as static secondary mass spectrometry (SSIMS) [6–9]. However, the significance of these occurrences to the observed adhesion enhancement in adhesive joints primed with organosilanes is not clear. There are well-developed arguments that covalent bond formation is not necessary for obtaining a strong, water-resistant interface.

Steric considerations limit the ability of more than one silanol per organosilane to interact with surface hydroxyls. The remaining silanols readily condense with neighboring silanols to form polysiloxane networks whose degree of crosslinking and three dimensional structure largely determines the film properties. Films of coupling agents are generally a fraction of a micron in thickness, so it becomes necessary to consider the bulk structure of the coupling agent in order to understand its properties and interactions with the organic overlayer. Due to the size scale of this aspect of the coupling agent film, the bulk film structure is somewhat more accessible to analysis than the mineral surface–organosilane interface and consequently is a little better understood.

As primers for adhesive bonding, organosilanes are typically hydrolyzed in solution to the corresponding silanol prior to application. In most cases, these silanols begin to homopolymerize in solution and therefore have a limited shelf life. One result of this condensation is that the structure of the final film has its origins in the solution history prior to film deposition. Hence knowledge of solution properties can be critical to primer performance. As the film dries and the water of condensation is removed through evaporation, the rate of polymerization greatly increases and a polysiloxane network is formed on the surface. The structure of this network determines not only the mechanical properties of the polysiloxane film, but its ability to interact with the organic overlayer through interpenetration and interdiffusion. Critical parameters that determine the film structure include type of solvent and concentration, pH of the solution, solution structure (e.g. the amount of condensation that has occurred prior to film deposition), film thickness, and drying conditions.

Organosilanes are available with a wide variety of organofunctional substituents, and coupling agent formulation generally starts with a screening of potential substituents based on potential reactivity or solubility with the organic coating or adhesive. Table 2 shows a list of some representative commercial silanes.

Table 2

Representative commercial silane coupling agents

Organofunctional group	Chemical structure
Vinyl	$\text{CH}_2=\text{CHSi}(\text{OCH}_3)_3$
Chloropropyl	$\text{ClCH}_2\text{CH}_2\text{CH}_2\text{Si}(\text{OCH}_3)_3$
Epoxy	$\begin{array}{c} \text{O} \\ \\ \text{CH}_2\text{CHCH}_2\text{OCH}_2\text{CH}_2\text{CH}_2\text{Si}(\text{OCH}_3)_3 \end{array}$
Methacrylate	$\begin{array}{c} \text{CH}_3 \\ \\ \text{CH}_2=\text{C}-\text{COOCH}_2\text{CH}_2\text{CH}_2\text{Si}(\text{OCH}_3)_3 \end{array}$
Primary amine	$\text{NH}_2\text{CH}_2\text{CH}_2\text{CH}_2\text{Si}(\text{OCH}_3)_3$
Diamine	$\text{NH}_2\text{CH}_2\text{CH}_2\text{NHCH}_2\text{CH}_2\text{CH}_2\text{Si}(\text{OCH}_3)_3$
Mercapto	$\text{HSCH}_2\text{CH}_2\text{CH}_2\text{Si}(\text{OCH}_3)_3$
Cationic styryl	$\text{CH}_2=\text{CHC}_6\text{H}_4\text{CH}_2\text{NHCH}_2\text{CH}_2\text{NH}(\text{CH}_2)_3\text{Si}(\text{OCH}_3)_3=\text{HCl}$

In primer formulations for adhesive bonding of metals, the coupling agents that are most frequently used are those based on epoxy and amine functionalities. Aqueous solutions of aminosilanes have been successfully used for obtaining stable adhesive bonds between epoxy and steel [10] and epoxy and titanium [11,12], while epoxy functional silanes are preferable for applications involving aluminum substrates [13,14]. A simple solution of 1% epoxy functional silane in water is currently used for field repairs of military aircraft [15] where phosphoric acid anodization would be extremely difficult to carry out, and performance is deemed quite acceptable.

While both amino- and epoxy-functional silanes are capable of chemically reacting with thermosetting adhesives, such as epoxies and urethanes, such chemical reaction may not be a prerequisite for excellent adhesion. In a classic paper, Sung and coworkers [16] demonstrated that aminosilanes provided significant reinforcement for polyethylene/sapphire (Al_2O_3) adhesive joints as long as the degree of silane crosslinking was not excessive and the film thickness was about 1000 Å, conditions shown to be necessary for interdiffusion. Because the aminosilane was believed incapable of reacting with the polyethylene at the lamination temperature (149°C), the mutual solubility of aminosilane and polyethylene was used to explain the adhesion enhancement. In later work, Chaudhury and coworkers [17] showed that a combination of interdiffusion and chemical crosslinking was responsible for adhesion enhancement in aminosilane-primed aluminum/PVC adhesive joints.

2.2. Resin-based primers for aerospace adhesives

The most common aerospace adhesives include nitrile epoxy systems, epoxy polyamides, epoxy phenolics, and various unmodified epoxies [18]. Polyimides

have seen some application in high temperature applications as well. While all of these adhesives generally adhere quite well to properly prepared unprimed surfaces, the use of primers can provide distinct advantages in mechanical and physical properties. Of equal importance is the protection from contamination and physical damage that a primer film provides to a delicate prepared oxide surface during handling and storage prior to bonding. Application standards require that pretreated aluminum surfaces must be bonded within 2 and 16 h of treatment [19,20], in some cases within 72 h [21].

Commercial primers for structural adhesive bonding of aircraft are generally formulated to match a given adhesive and marketed as part of a packaged adhesive/primer system. Primers in this class are frequently prepared by diluting the adhesive polymers in a suitable solvent and applying to the prepared substrate as a film between about 0.0001 and 0.0025 inch thick. Frequently, an inert dye will be included in the product to help identify a surface that has been primed with a uniform film. The addition to these formulations of corrosion inhibitors is almost universal, and the result has been a significant improvement in long-term durability. In the past decade, environmental considerations have resulted in a trend towards water-borne primers for these applications, and performance of these systems can be excellent as well [22].

As long as the primer and adhesive have similar moduli, the improvements in mechanical properties of adhesive joints prepared from primed adherends are derived largely from the improvement in substrate wetting of the primer. A properly prepared metallic substrate will have a clean, high energy surface. If the surface is relatively smooth, then complete wetting by a viscous adhesive is readily achievable. However, the best pretreatments for aluminum also provide a microscopically rough morphology that is believed to aid in mechanical interlocking with the adhesive [23]. Grit blasting is frequently recommended for steel surfaces as a method for cleaning and removal of scale and weak oxide. It is difficult for a viscous adhesive to completely wet these microscopic features to obtain a void-free bond line. A low viscosity primer based on a solvent-diluted adhesive or an adhesive latex dispersed in water can readily flow into these asperities and planarize the adherend surface with a thin protective film that the adhesive resin can wet and interdiffuse with during cure.

While primers are believed to improve the performance of adhesively bonded aluminum structures primarily through improved corrosion resistance and improved wetting of the microscopically rough adherend surface by the adhesive, modification of the mechanical properties of the adhesive near the substrate can have a large effect on both the stress distribution and total strain energy. Finite element analysis has shown [24] that a deformable primer layer (i.e. one that is more compliant than the adhesive) has the effect of reducing both the stress concentration and the magnitude of the maximum stresses through the thickness of the adhesive layer in a loaded single lap shear joint. Perhaps more significantly, although

the presence of a more compliant primer layer does not significantly alter the total strain energy release rate ($G_T = G_I + G_{II}$), it increases the mode mixity (G_I/G_{II}). The crack-opening mode strain energy release rate is enhanced at the expense of the shear mode. This is the mode responsible for failure in single lap-shear joints.

High-strength aluminum such as the 2000 series alloys are susceptible to pitting corrosion due to the galvanic couples formed between the matrix metal and the strengthening precipitates. These alloys will sometimes be clad with pure aluminum (alclad) to protect the surface from corrosion. Interestingly, problems were noted obtaining reproducibly durable adhesive bonds to these substrates using the sodium dichromate/sulfuric acid etch (FPL process) that was standard in the 1960s [25,26]. As a result, clad alloys garnered a reputation for being poor materials for adhesively bonded structures. It was subsequently shown that the irreproducibility was due to differences in oxide morphology between the edges and center of FPL-treated panels unless the etching solutions were seeded with copper [27]. For this reason, although properly etched or anodized clad alloys may be readily primed and adhesively bonded, these materials have fallen from favor for these applications.

2.3. Corrosion-inhibiting primers

Several studies have established a general relation between the corrosion resistance of metals and durability of adhesive bonds [28]. One approach to controlling this corrosion in adhesive bonds to aluminum is through the inclusion in the primer of a carefully controlled quantity of finely ground corrosion inhibitor, usually a chromate salt (based on zinc, strontium, or barium) [29] at a loading that is on the order of 10% of the solution by weight. This concept represents one of the most significant advances in the history of primer technology. Table 3 shows the type of improvement in salt spray resistance afforded by a corrosion-inhibiting primer.

Corrosion-inhibiting primers based on this technology have been in continuous service since they were first utilized with nitrile epoxies in the late 1960s. These inhibitors function by passivating the aluminum. In this process, water permeating the adhesive bondline carries a certain amount of inhibitor to the oxide surface.

Table 3

Effect of corrosion inhibiting primer on strength retention after exposure to salt spray [29]

Exposure time (days)	Lap shear, psi	
	Non-corrosion inhibiting (BR 123)	Corrosion inhibiting (BR 127)
Initial	5875	5680
30	3490	5890
90	1460	4970
120	0	4480

Because of the high oxidizing potential of Cr^{6+} , the cathodic reaction becomes reduction of the hexavalent chrome to the corresponding trivalent state, instead of reduction of water to form hydroxide ions and hydrogen [30–32].

To be effective, there must be a certain minimum concentration of inhibitor at the interface to be protected. Therefore, there must be sufficient inhibitor in the primer, and these inhibitors need to be soluble enough in water to enable transport of inhibitor to the oxide surface as water permeates the adhesive joint. However, too high of a solubility will rapidly deplete the primer layer of inhibitor resulting in a loss of protection. One of the fortuitous properties of zinc and strontium chromates is the limited solubility of these compounds in water (about 1.2 g/l at 15°C [33]).

The substitution of water-borne versions of these primers is increasing as environmental restrictions on the use of organic solvents become stricter. These are generally aqueous emulsions of epoxy novolac or phenolic based resins stabilized by surfactants [34]. Non-ionic surfactants are preferred, as they are non-hygroscopic in the dried primer films. Hygroscopic ionic surfactants could result in excessive water absorption by the primer film in service.

Formulation of water-based primers is significantly more complex than the solvent-borne versions. Rather than simple solutions of resins, curing agents, and corrosion inhibitors in suitable solvents, the presence of water makes necessary the inclusion of many other ingredients such as pH buffers, anti-foaming agents, surfactants, and fungicides [35]. Frequently, a small quantity of an organic solvent, such as an alcohol, is still required, so that water borne primers are generally not completely free of volatile organic compounds (VOCs).

Water-borne primers may or may not contain chromate-based corrosion inhibitors. The limited solubility of chromate salts in water makes them less than ideal for use in water-based primers, and much work has gone into developing alternatives [36], but the performance of recently developed water based primers using strontium chromate as the corrosion inhibitor is excellent, however, and appears equivalent to the solvent-borne analogues [37].

Although chromate-based corrosion inhibitors work extremely well, their use has been increasingly limited since 1982 due to their potential carcinogenicity. The most common reported adverse health effect due to exposure to Cr^{6+} is lung cancer, although other ailments may result from exposure as well [38]. There is speculation that chromates will be completely banned, but it is likely that they will merely continue to come under increasingly stringent legislative control rather than be banned entirely, similar to the situation with VOCs [39]. This situation has spawned a large amount of research to identify and develop replacements for chromate-based corrosion-inhibiting pigments that are potentially less toxic. Zinc phosphates are one example. They provide some corrosion protection to aluminum alloys and are non-toxic. One of the best in a recent comparative study [40] of zinc phosphate corrosion-inhibitor performance on chromate-conversion coated

Table 4

Comparison of tensile lap shear strengths: solvent-based chromate-inhibited primers versus non-chromate and low VOC primers [42]

Primer (source)	Adhesive	Tensile lap shear strength (psi)				
		RT (73°F)	180°F	180°F wet	30 day salt fog	60 day salt fog
BR 127 (cyanamid)	FM 73	6005	4312	2622	6105	5846
	AF 163-2K	6421	4617	3499	6505	6400
BR 250 (cyanamid)	FM 73	5685	3498	2162	5479	—
	AF 163-2K	6420	4636	3234	6393	—
BR 250-2 (cyanamid)	FM 73	7980	4145	2614	5853	5722
	AF 163-2K	6564	4358	3304	6465	6366
BR-X250-NC (cyanamid)	FM 73	6163	4186	2722	6062	5927
	AF 163-2K	6564	4358	3304	6465	6366
EC 3982 (3M)	FM 73	6182	4395	2891	6427	6051
	AF 163-2K	6733	4271	3633	6711	6573
XEA 9290 (Hysol)	FM 73	5255	—	—	4791	—
	AF 163-2K	6217	—	—	6079	—

2024-T3 aluminum was calcium strontium zinc phosphosilicate. Other potential non-chromate corrosion-inhibiting pigments include cerium and molybdenum salts or organic inhibitors. A recent review of these compounds can be found in [41]. Another interesting non-chromate inhibitor that is currently marketed in a water-based primer for structural adhesive bonding is ion exchanged silica. This inhibitor is completely insoluble in water and only releases active inhibiting Ca^{2+} ions when potentially corrosive electrolyte species are present.

Non-chromate and low-VOC containing primers are capable of excellent performance. Table 4 shows the results of a comparison of various environmentally acceptable primers with 250°F curing adhesive with the 'standard' BR 127 solvent-based chromate inhibited primer [42].

The need to identify replacements for chromate-based technologies has also resulted in the development of alternatives to resin-based corrosion-inhibiting primers. These are primarily inorganic barrier coating techniques, such as sol-gel processes, which may or may not include corrosion inhibitors. These are discussed in a later section.

2.4. Structural adhesive bonding of steel

Large-scale adhesive bonding of steel is of great interest to the automotive and appliance industries because of the opportunities it provides for design flexibility, weight savings, and manufacturing economy. Because of its economic importance,

the needs of the automotive industry have especially dictated development of adhesive and primer technology for steel.

Primer technology seems to play a much less important role in the adhesive bonding of steel than in aluminum, however, and the adhesive resin-based corrosion-inhibiting primers that are an integral part of the adhesive bonding of aluminum are not used as frequently in these applications. This may stem from the fundamental differences in the aerospace versus consumer products industries. The expense of aircraft dictates that the airframes must have a long service life, at least twice the projected lifetime of about 10 years for an automobile. The low volume production of aircraft allows the use of multistep manufacturing procedures that are more difficult to automate. Furthermore, the service environment for aircraft is more severe than for automobiles, and reliability issues have potentially more devastating consequences.

As discussed above, silane primers have been investigated extensively for adhesive bonding of steel substrates and have been shown to be quite effective, but the extent to which these are in current commercial use is not known.

2.5. Bonding to electroprimed steel

Much of the steel used in automobile manufacture is electroprimed prior to fabrication and painting. In this process, a thin layer of zinc phosphate crystals (ca. 0.6 μm) is deposited onto a clean steel surface, and then overcoated with an electrodeposited organic primer (10–40 μm). The zinc phosphate provides corrosion inhibition during service while the organic primer improves the quality of the subsequent paint finish by functioning as a primer–surfacer, filling sanding marks and other small surface imperfections.

While these primers were not developed specifically for preparing surfaces for adhesive bonding, the ability to obtain strong and durable adhesive bonds to electroprimed steel is important if manufacturing operations require components to be bonded to previously primed structures. They appear to perform the function of adhesive primers very well. With properly formulated adhesives, bonds to electroprimed substrates were actually *stronger* than to the unprimed substrates by as much as 30% [43]. In this case, ‘properly formulated’ referred to adhesives that did not contain compounds capable of chemically degrading the primer, causing voids in the primer phase due to gas evolution. Fig. 1 shows the results of tensile testing of single lap shear joints constructed of solvent-cleaned, grit-blasted steel bonded with an imidazole-cured epoxy novolac.

2.6. Primerless adhesive bonding of steel

Issues with adhesive bonding of steel frequently hinge on surface cleaning and deoxidation, and preventing oxide growth during storage and handling prior to

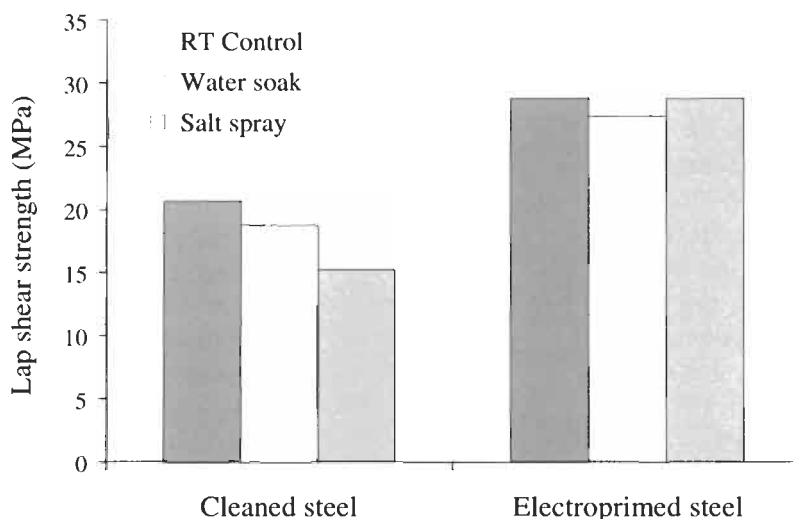


Fig. 1. Comparison of unprimed and electroprimed single lap-shear adhesive joint strengths for steel coupons bonded with imidazole-cured epoxy [43].

bonding. During shipping, storage, and manufacturing, steel is generally coated with a film of oil to protect against the otherwise rapid formation of ferric hydroxide (rust). One approach for obtaining strong, durable bonds to this steel requires removal of the oils immediately prior to coating the exposed surface with a protective primer, paint, or adhesive. This involves in-line cleaning systems with their attendant maintenance and waste disposal issues. An alternative approach that has met with considerable success has been the development of adhesives and coatings capable of absorbing and/or displacing the protective oil. For epoxies, DGEBA resin by itself is not capable of absorbing contaminating oils to a significant extent [44], but certain curing agents or phase-segregated tougheners can accomplish this goal. Polyamide curing agents with oleophilic fatty acid moieties can absorb significant amounts of oil and provide strong and durable adhesive bonds to oily steel surfaces. Furthermore, the amount of oil displacement by a particular formulation can be related to the amine number of the curing agent [45]. Oil displacement or absorption can also be accomplished through inclusion of liquid carboxy-terminated butadiene acrylonitrile (CTBN) rubber in dicyandiamide-cured DGEBA epoxy adhesives as long as a high curing temperature is used [46].

2.7. Inorganic primers

Inorganic coatings as primers for adhesive bonding and painting have been investigated for almost two decades. The basic mechanism by which they en-

hance adhesion and protect an adhesive/substrate interface against deterioration is different from organic primers discussed above. Organic primers depend upon corrosion-inhibiting pigments to electrochemically protect the substrate from corrosion. They are poor barriers to diffusion, and the inhibitors are actually inert until water saturates the interface region. In this sense, water ingress activates the corrosion-inhibition process in these materials. In contrast, inorganic primers probably do not electrochemically inhibit corrosion, but rather function as barriers to diffusion of electrolyte to the primer/substrate interface.

Inorganic primers are generally based on either aqueous sol-gel coatings or plasma polymerized coatings. Both produce highly crosslinked amorphous oxide films that are rough on a microscopic scale. This roughness has been implicated in the excellent adhesion enhancement provided by these films [47] and may be the source of what is potentially the most significant economic and environmental advantage: excellent performance can be obtained without oxide conversion processes. This eliminates one of the most costly and environmentally damaging aspects of preparing metals such as aluminum for adhesive bonding.

Sol-gel primers use inorganic or metal-organic precursors (generally aluminum, silicon or titanium alkoxides) whose chemistry is closely related to the silane coupling agents discussed previously. These precursors are dissolved in alcohol, then hydrolyzed by the addition of water:



Each alkoxy group hydrolyzes with a distinct rate constant, with the first hydrolysis proceeding much faster than subsequent ones [48].

Film formation proceeds through condensation of hydroxyls to create a three-dimensional oxide network:

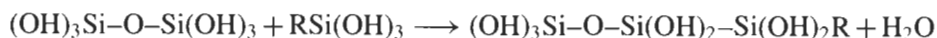


Elevated temperature drying accelerates this process.

A simple embodiment of this concept [49] involves dissolving 1% sec-butyl aluminum alkoxide in toluene, applying to an acid-etched and anodized aluminum surface, and drying at 75°C. Atmospheric moisture accomplishes hydrolysis after solvent evaporation, and the films are believed to be a stable form of amorphous Boehmite (AlOOH). Crack propagation rates in wedge test specimens prepared with adherends treated in this manner were improved over the organic-primed controls, and furthermore substrates prepared using a chromic acid etch (FPL process) prior to the inorganic primer application provided performance essentially equivalent to a phosphoric acid anodized (PAA) surface [50].

These inorganic polymers can be copolymerized with organofunctional silanes to modify the physical properties or to include specific reactive functionalities to

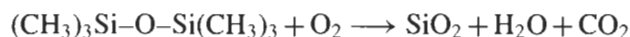
improve coupling to an adhesive or coating:



A typical comonomer could be a polydimethylsilane to increase the toughness of the polymerized film, or an amine functional silane for chemical coupling with an epoxy adhesive.

Inorganic or hybrid inorganic–organic films suitable for primers can also be synthesized using plasma polymerization. The plasmas used in these processes are low pressure gases subjected to an electric field. Cascading collisions between neutral gas molecules and the electrons and ions accelerated by the field generate a gas rich in active species, including electrons, ions, electrically excited species, and free radicals. Because the gas in a plasma is low pressure, however, gas phase collisions are infrequent and the degree of ionization of the gas is low. The fraction of gas molecules that are activated is typically only around 10^{-10} . Because of their low mass, electrons in the plasma have much higher average velocities than the relatively massive ions and therefore the flux of electrons striking a surface in the plasma is much higher than the flux of ions. This causes surfaces in contact with a plasma to charge negatively with respect to the plasma. This negative charge accelerates ions from the gas to the surface with sufficient energy (several eV) to rapidly clean and dehydrate metal surfaces. The resulting surface is extremely clean and in an active state due to the absence of adsorbed contaminants. After this initial cleaning, monomer is introduced into the plasma. This rapidly chemisorbs onto the clean metal surface. Subsequent ion flux to the surface creates free radicals that are the source of film growth.

Molecules that are normally unreactive can be readily polymerized in such a process. Examples include organic gases such as ethane and various organosilanes. Monomers such as hexamethyldisiloxane can be readily polymerized to form tightly adherent films having a silica-like structure:



The outer surfaces of these plasma polymers are terminated with hydroxyl groups and have high surface energies. They are readily wet by adhesives and form strong and durable adhesive bonds [51].

The basic mechanism of adhesion between an inorganic primer and a substrate is distinct from that of an organic primer. Organic primers adhere to an oxide substrate through a combination of mechanical interlocking with the textured oxide and secondary atomic interactions, probably through surface hydroxyls. As the surface energy of a clean oxide is largely polar, the polar–polar (or acid–base) interactions are the predominant intermolecular interactions at the primer–oxide interface. These linkages are susceptible to hydrolysis upon exposure to water, and corrosion and attendant failure at the primer–oxide interface is the common failure mode. With inorganic primers, however, there is an increasing body of

evidence that these materials are capable of condensing with surface hydroxyls to bond with the oxide through primary chemical linkages. Corrosion and failure at this primer–oxide interface is very uncommon.

The adhesive–primer interface is distinct for inorganic primers as well. Organic primers depend upon formation of a diffuse interface with the primer through interdiffusion, and overcuring of the primer film can result in poorer performance due to reduced interpenetration. Inorganic primers, however, present a rough, hydroxylated oxide surface for mechanical interlocking with the adhesive. A crucial difference between this oxide surface and that on prepared metal surfaces such as aluminum is that the sol-gel or plasma polymerized oxide is stable and does not corrode during exposure to electrolyte. As long as the interactions responsible for adhesion between the adhesive and the inorganic primer are stable to the environment, the adhesive joint will maintain its integrity. Improved durability at the interface between inorganic primers and organic adhesives can be obtained through modifying the structure of the primers for specific, higher-energy interactions with the adhesive.

2.8. Surface roughness effects in inorganic primer films

Surface roughness has been implicated in many studies as being a critical factor in obtaining strong, durable adhesive bonds, and the microscopically rough surface presented by properly etched or anodized aluminum or grit-blasted steel is an important factor in the adhesion enhancement afforded by these processes. Inorganic primer films, whether derived from sol-gel or plasma polymerization routes, have surface morphologies similar in many ways to that of anodized aluminum, and may owe a significant fraction of their effects to this morphology.

Quantifying the effect of surface roughness or morphology is difficult, however. Surface preparations that provide different degrees of surface roughness also usually produce surfaces that have different oxide thicknesses and mechanical properties, different compositions, or different contaminant levels. The problem of separation of these variables was circumvented in a recent study [52] by using a modified microtome as a micro milling machine to produce repeatable, well-characterized micron-sized patterns on clad 2024-T3 aluminum adherends. Fig. 2 shows the sawtooth profile created by this process.

Adherends textured in this fashion were used as substrates for wedge tests, with the furrows running perpendicular to the direction of crack propagation. Surface analysis indicated a consistent surface composition regardless of the profile. The performance of wedge test specimens prepared using this technique were compared to similar samples prepared by grit-blasting, which produced a surface with a thicker oxide and more hydrocarbon contamination than the micro milled surfaces. Failure in all samples after exposure to 50°C/95% RH was interfacial, but the fracture energies showed an exponential dependence on the

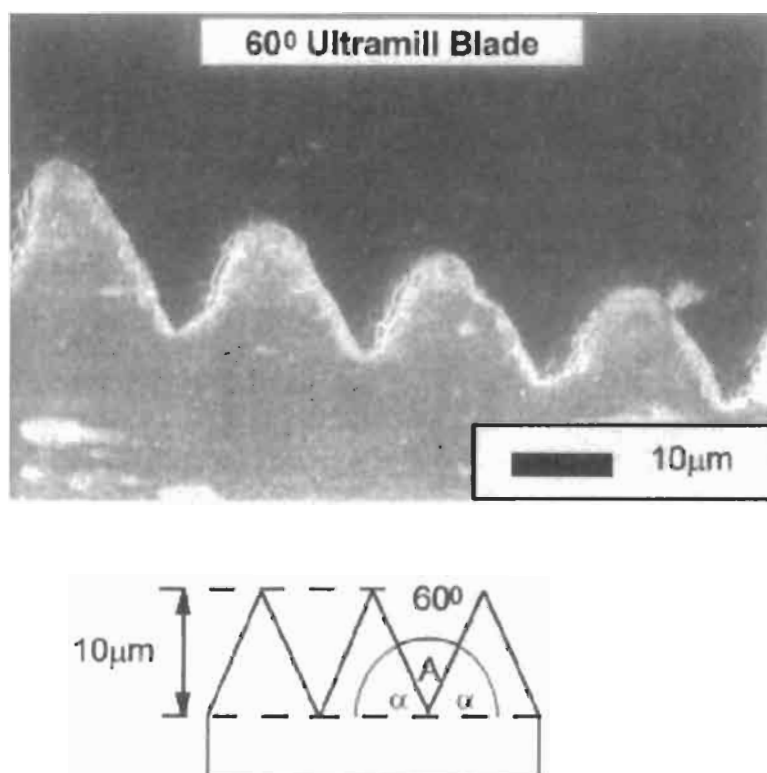


Fig. 2. SEM cross-section of a 60° ultramilled aluminum bonded to epoxy resin. Also indicated is a diagrammatic representation of the ultramill profile showing the base angle [52].

surface morphology. Fig. 3 shows a linear relationship on a semilog plot between the fracture energy after 150 h aging and $\tan \alpha$ (α is defined in Fig. 2). This figure shows that surface texture alone can provide a 100× increase in the fracture energy of an adhesive joint aged in a humid environment.

A mechanical analysis of the near surface stresses in a wedge test as a function of surface geometry shows that $\tan \alpha$ is equal to the ratio of the shear stress to the peel stresses (Fig. 4).

Fig. 3 suggests that surface textures that enhance the surface peel component can promote bond degradation under aggressive aging conditions. The authors suggested that interfacial voids generated by peel stresses ahead of the crack tip facilitated moisture ingress and accelerated bond degradation.

2.9. Attachment site density effects in inorganic primer films

In addition to the beneficial effects of creating a textured surface, inorganic primers can provide a very high density of specific chemical attachment sites for

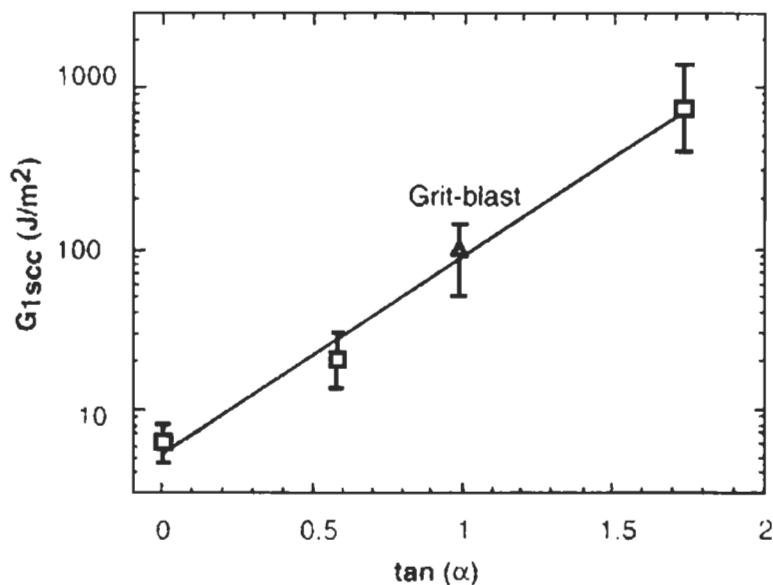


Fig. 3. $G_{I_{scc}}$ determined from crack-length data at 150 h as a function of resolved vertical and horizontal component of the surface profile angle [52].

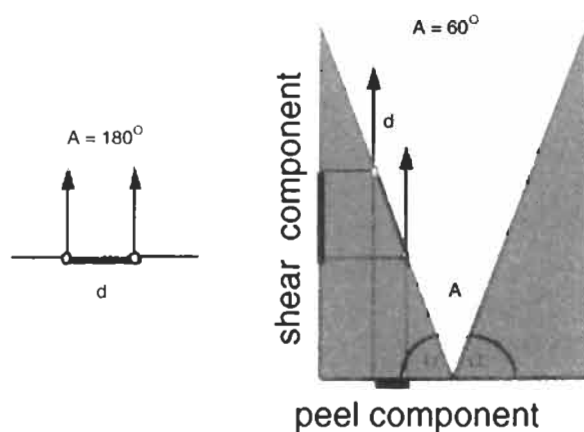


Fig. 4. The forces at the epoxy–aluminum interface resolved into shear and peel components. Shear component/peel component = $\tan(\alpha)$ [52].

an organic overlayer such as a paint or an adhesive. At one level, this increases the reversible work of adhesion (W_a) between the coating or adhesive and the substrate. However, the enhancement in fracture energy of the adhesive joint that results from an increase in W_a stems from the long-range influence that the interfacial bonds exert on the adhesive fracture energy G_I of the adhesive far from the interface.

Cognard showed that the fracture energy of an adhesive joint is a function of crack velocity. In the range of crack velocities between 10^{-7} and 10^{-1} ms^{-1} , the relationship can be expressed by:

$$G = G_0 + \alpha K_2 v^n \quad (1)$$

The term $\alpha K_2 v^n$, derived from reptation theory, describes the velocity-dependent energy necessary to fracture the bulk adhesive. K_2 is the 'consistency' which relates the viscosity to the shear rate for a non-newtonian fluid. $\alpha = \pi r a L^2 / h^n$, with r being the chain radius, L the chain length, a the density of chains crossing over the fracture plane, and h is the distance between the chain and reptation tube.

G_0 is the 'static toughness', or fracture energy at zero crack velocity. This number can be obtained through wedge test measurements. The crack length in a wedge test is inversely proportional to the strain energy release rate through the following equation:

$$G_1 = \frac{E d^2 h^3}{16} \frac{3(a + 0.6h)^2 + h^2}{[(a + 0.6h)^3 + ah^2]^2} \quad (2)$$

where h is the adherend thickness; E is the adherend Young's modulus; d is the crack opening displacement by wedge insertion; and a is the crack length measured from point of wedge contact.

Eq. 2 shows that the elastic strain energy decreases with the inverse fourth power of the crack length. When a wedge is driven into the specimen, the crack grows at a velocity defined by Eq. 1 until the strain energy has decreased to G_0 . Crack growth ceases at this point until some change in the system reduces G below that defined by the crack length. Changes that could bring about further crack growth include substrate corrosion at the interface or plasticization of the adhesive by moisture.

G_0 is related to the reversible work of adhesion W_a obtained using contact angle measurements, but in general is greater than W_a . This is because once an interface is formed and the adhesive solidifies, strain energy is required to mechanically disrupt the interface. This strain energy arises because of the physical connection between the attachment sites between the adhesive and the substrate and the connectivity between this interface and the adhesive bulk.

W_a quantifies the specific, discrete interactions that exist between a wetting liquid and a substrate. These interactions may be Van der Waals, acid-base, or covalent. The reversible work of adhesion is the product of the areal density of these interaction sites (or attachment points) and the energy per attachment point:

$$W_a = \nu U_c \quad (3)$$

where ν is the areal density of attachment sites; and U_c is the energy per interfacial attachment point.

Table 5

Wedge test fracture energy (from Eqs. 1 and 2) vs. adherend surface treatment (from ref. [3])

Surface treatment	G_0 (J m ⁻¹)
None	900
Solvent wipe	1000
Alkaline clean	2000
Asuclean ^a	6000

All failures were cohesive within the adhesive. Adhesive: E610 nylon epoxy (Asulab SA).

^a Asuclean is a proprietary formulation of Asulab SA.

This interaction energy is reversible because removal of the wetting liquid from the surface only requires the disruption of these interaction sites. Solidification of the liquid into an adhesive changes the requirements for dewetting, however.

When an adhesive solidifies and the joint is loaded through such an interface, stress is transferred from the substrate to the adhesive through these attachment points, and the adhesive resin adjacent to these attachment points is loaded. The strain energy in this system is expressed by the following equation [53]:

$$G = \nu N U_x \quad (4)$$

where N is the number of stressed network links in the adhesive per interfacial attachment point; U_x is the energy per stressed network link. And by combining Eqs. 3 and 4:

$$G = N W_a U_x / U_c \quad (5)$$

when crack growth just stops in a wedge test, $G = G_0$.

Eqs. 1–5 hold whether failure is interfacial or cohesive within the adhesive. Furthermore, Eq. 5 shows that the reversible work of adhesion directly controls the fracture energy of an adhesive joint, even if failure occurs far from the interface. This is demonstrated in Table 5, which shows the static toughness of a series of wedge test specimens with a range of adherend surface treatments. All of these samples failed cohesively within the resin, yet show a range of static toughness values of over 600%.

3. Primers for rubber to metal bonding

The applications of rubber as an engineering material almost invariably involve bonding to a rigid substrate or reinforcement. In some instances these bonds need to be established to a fully cured thermoset rubber or a molded thermoplastic rubber, and a wide variety of adhesives suitable for this purpose are available. In

some instances, surface treatment (such as oxidation or chlorination of natural or NBR rubbers) or primers (in the case of olefin-based thermoplastic rubbers) are necessary.

Many applications of thermoset rubbers require them to be processed in an uncrosslinked state, for example by injection molding, compression molding, or transfer molding. In these processes, bonds between the rubber and a rigid substrate must be established during vulcanization. Establishing a suitably strong and durable bond between a thermoset rubber and a substrate during vulcanization almost invariably requires an adhesive or primer. This has primarily been attributed to the absence of polarity in the rubber [54].

This is not an issue when vulcanizing certain sulfur-cured natural rubbers against brass, however. It was known as early as 1862 that coating metal with a layer of electrodeposited brass created strong bonds to rubber vulcanized in contact with the surface [55]. The mechanisms of adhesion are still being actively researched and debated in the literature, but appears related to both chemical bonding due to formation of $\text{Cu}_x\text{S}-\text{S}_y-\text{NR}$ bridges [56] and mechanical interlocking with a porous, dendritic sulfide film formed in situ during the vulcanization process [57]. More recent work emphasizes the potential importance of both mechanisms [58]. This process is extremely important in the tire industry for obtaining adhesion of natural rubber compounds to steel tire cords. The brass plating plays a dual role in this instance. The steel in brass plated prior to drawing into wires, and the lubricious nature of the brass surface improves the drawing process considerably. However, adhesion is very sensitive to rubber formulation and the plating process generates large volumes of hazardous waste. These factors limit the utility of brass interlayers for rubber-metal adhesion, and in many applications solvent or water-borne organic primers and adhesives are used.

Systems for bonding rubber to a substrate during vulcanization that do not exploit the reactivity of sulfur and brass are generally two layer primer/adhesive systems. The bond to the substrate results from strong interactions between a polar and/or reactive polymeric primer and the surface. This primer is then coated with a less polar adhesive or cover cement that can interdiffuse and perhaps crosslink with both the primer and the rubber stock during vulcanization. The graded structure that results provides a smooth transition between the rigid, polar metal and the compliant, non polar rubber. One of the earliest embodiments of this concept was in a patent to Hugh Lord (founder of the Lord Corporation) in 1930 [59]. In this system, the primer and cover cement contained the same ingredients but in different proportions (Table 6).

Solutions of the two recipes were blended in varying proportions to provide tie coats of continuously varying composition. The patent shows an example of eight plies or layers of graded composition between the rubber and the metal substrate. Because of the high fraction of reactive filler, the material closest to the metal substrate would be the most rigid and polar. The stiffness and polarity

Table 6

An early primer and stock formula for rubber-metal bonding [59]

Component	Primer recipe	Stock recipe
Raw rubber	30	100
Zinc oxide	50	3
Iron oxide	15	—
Sulfur	5	5
Hexamethylene tetramine	—	1
Lime	1.25	—

would progressively decrease over the thickness of the adhesive layer to provide a smooth transition in polarity and modulus. This was claimed to prevent stress concentration near the interface.

The concept of graded layers transitioning from a rigid, polar primer to a compliant, non-polar adhesive is still employed in most primer/adhesive systems for rubber to metal bonding, although the number of layers is generally only two. Since the mid 1900s, the primer coats have been generally based on phenolic or epoxy resins with chlorinated rubber and metal oxides (zinc or titanium), while the adhesives (or cover cements) have been based on halogenated rubber with a crosslinking agent [60,61].

The phenolic resins used in primer layers for rubber adhesion are usually based on the condensation products of aromatic alcohols (such as phenol, cresol, or resorcinol) and hexamethylene tetramine. They can be applied as a separate primer layer or in some applications blended in the rubber stock. These resins function as adhesion promoters for a wide range of substrates, including steel, brass-plated steel, various polymers, and natural cellulosic fibers. The mechanisms of adhesion promotion have not been well documented. The polymerization mechanism is complex and the resulting polymers are highly functional. The excellent adhesion that results may be related to the ability of the phenolics to condense with hydroxyl groups during polymerization and/or the ability of the hexamethylene tetramine to inhibit corrosion of steel and chelate copper in the brass. The strong interface between the primer and halogenated cover cement is certainly related to interdiffusion of these layers, and perhaps co-polymerization with the reactive halogenated rubber.

The reactivity of the halogenated rubber in cover cements was shown in an investigation that demonstrated that halogenated polymers are labile and capable of reacting with unsaturated rubber under vulcanizing conditions, even without crosslinking agents [62]. Infrared spectra of solution cast films of natural rubber and chlorinated natural rubber show little change after heating to 170°C for 30 min. Fig. 5 shows the spectra of the natural rubber before and after heating. Appearance of bands above 1700 and near 1150 cm^{-1} with heating is due to

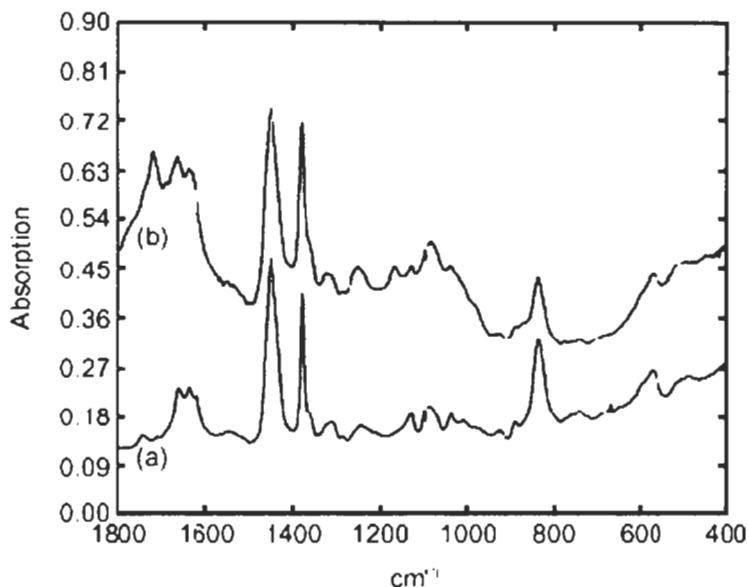


Fig. 5. Transmission IR spectra of natural rubber, solvent cast from xylene. (a) Before heating, and (b) after heating at 170°C for 30 min [62].

carbonyl products of oxidation, but the effect is relatively slight. Fig. 6 shows the results of heating chlorinated rubber under identical conditions. This material shows even less oxidation than the unchlorinated rubber.

But heating of a mixed film produced dramatic results. The two polymers are not miscible, and solution cast films phase separate. But heating a solution cast film of a 1:1 wt% blend of natural rubber and chlorinated natural rubber results in a homogeneous film that is oxidized to a much greater extent than either of the components. Fig. 7 shows the infrared spectra before and after heating. The spectrum of the mixed film before heating appears to be a linear combination of the spectra of the chlorinated and unchlorinated rubber. Heating resulted in extensive oxidation, and, furthermore, the films became single phase. This suggests that it is not merely the polarity of chlorinated rubber that is responsible for its utility as a primer component in rubber to metal bonding agents, but its ability to chemically react with natural rubber. The miscibility that results may be a byproduct of this reaction.

There have been other approaches to obtaining rubber/metal adhesion besides primers or additives consisting of phenolics or epoxies plus halogenated elastomers. For example, carboxylated polymers (olefins and diolefins copolymerized with acrylic acid monomers) have shown excellent adhesion to metals. Very little carboxyl is necessary, and polymers with carboxyl contents as low as 0.1% show good adhesion when laminated to bare steel. When these materials possess

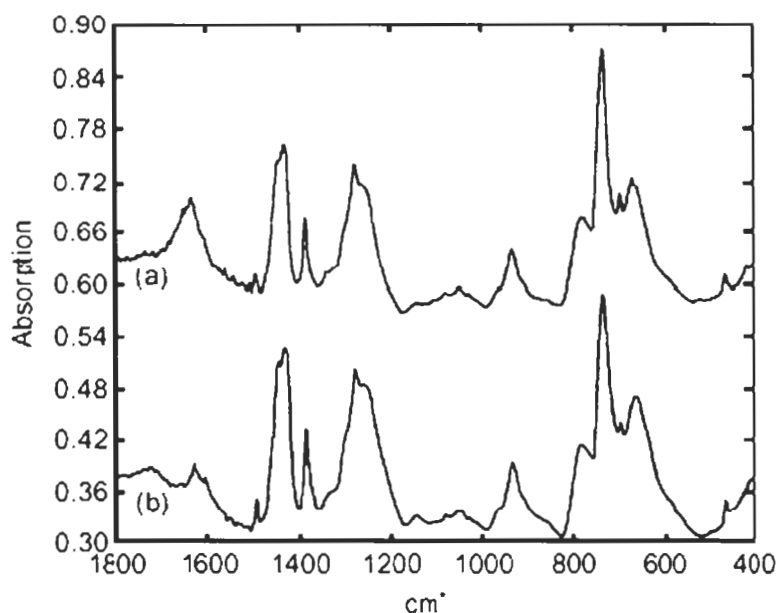


Fig. 6. Transmission IR spectra of chlorinated natural rubber, solvent cast from xylene. (a) Before heating, and (b) after heating at 170°C for 30 min [62].

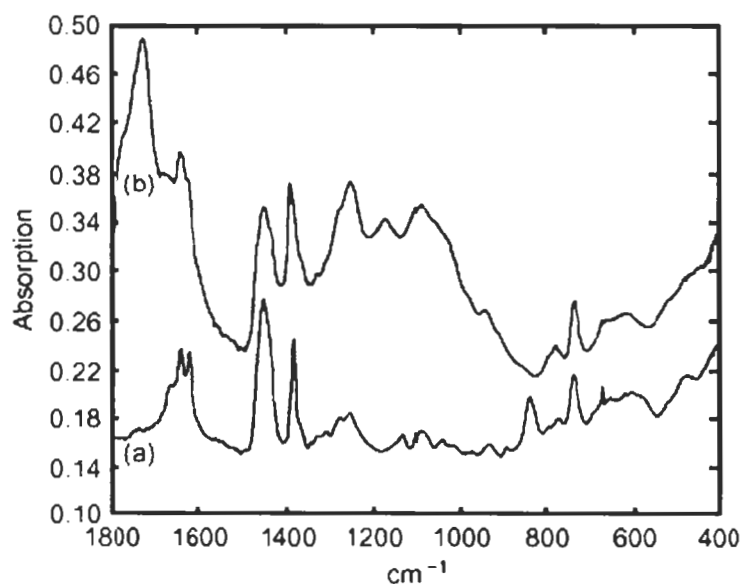


Fig. 7. Transmission IR spectra of a 1:1 wt% blend of natural rubber and chlorinated natural rubber, solvent cast from xylene. (a) Before heating, and (b) after heating at 170°C for 30 min [62].

sufficient diene content for vulcanization to rubber along with sufficient carboxyl content, solution-deposited coatings are suitable primers for bonding rubber to grit blasted steel [63,64]. These materials may be blended with phenolic/halogenated rubber primer systems to improve adhesion of rubbers to metals and various natural and synthetic fibers [65]. More recently, it has been shown that plasma polymerized olefins deposited onto steel under conditions that retain significant residual unsaturation can provide tremendous adhesion between natural rubber and steel [66]. These systems have some potential for replacing both solvent and water-borne primer/adhesive systems with a more environmentally benign process. Other recent work also indicates that mixtures of appropriate organosilane coupling agents can provide significant adhesion of sulfur cured rubber to a variety of metal substrates [67].

4. Primers for protective and decorative coatings on metals

Encasing metals such as steel and aluminum in protective or decorative organic coatings requires addressing many of the same technological problems of structural adhesive bonding. The coatings must demonstrate good initial adhesion and good durability under adverse environmental conditions. Because the requirements for the outer coating surface properties are very different from those of the film near the substrate/film interface, coating systems frequently include a separate primer layer.

While the *mechanical* challenges faced by a coating system are generally less demanding than those faced by an adhesive, the *environmental* challenges can be significantly greater. An adhesive bond is protected from the elements by the adherends except at the perimeter of the joint. For adhesive joints, the rate-controlling step in the degradation of bond strength is the rate of moisture diffusion through the bondline edge, and at least in the case of epoxy/steel adhesive joints, debonding can be accurately predicted to occur when the local concentration of water exceeds a critical level [68,69]. With coating systems, because the relative amount of exposed surface is so much greater than for an adhesive, the rate-limiting step in degradation becomes the rate of reactions (such as substrate corrosion) occurring at the interface. These rates are determined by the intrinsic reaction rates and the relative rate of transport of corrosive species and inhibitors through the film to the interface.

With the exception of coupling agent technology, primers for structural adhesive bonding have received little theoretical treatment in the literature beyond a discussion of mechanisms of corrosion inhibition by primer additives and limited discussion about statistical techniques for primer formulation. Perhaps because of the much more widespread use and greater economic importance of corrosion-protective coatings, the design and function of primers for these systems have

been thoroughly discussed in the literature and placed on firm theoretical footing. A consideration of the principles developed in paint technology could potentially aid in the advancement of primer technology for structural adhesive bonding.

Primers for protective coatings may be divided into three broad classes based on the mechanism of substrate protection: barrier primers that function by preventing the ingress of moisture and electrolytes, primers that protect the substrate galvanically in the presence of electrolytes, and primers that contain electrochemical inhibitors to passivate the substrate. Each of these approaches requires a distinct primer film structure due to the different mechanisms of protection.

A primer film consists of an organic binder and dispersed filler particles. In the terminology of paint formulators, the fillers are generally referred to as pigments. The pigment volume concentration (PVC) determines the structure of the primer film in the following manner. At low PVC, there is no connectivity between the pigment particles and the substrate, and the film is void-free. The PVC can be adjusted over a wide range without substantially increasing particle-particle or particle-substrate contact. However, when the PVC reaches a percolation threshold, particle-particle and particle-substrate contact increases dramatically. At this point the binder is still void-free, and the pigment volume concentration is labeled the critical pigment volume concentration (CPVC). At PVC higher than the CPVC, interstitial voids appear because of a lack of sufficient binder. While PVC is a formulating variable, the CPVC is a constant for any given binder/pigment combination.

The PVC can be readily expressed mathematically as follows. The dry film volume consists of the sum of the individual volume elements of the film components. The total volume of the film (V_f) may be represented by the following expression:

$$V_f = P_v + V_a + V_b + V_c + V_v$$

where P_v is pigment volume; V_b is binder volume between filler particles; V_a is binder volume adsorbed to filler; V_c is binder volume adsorbed to substrate; and V_v is void volume.

The PVC is simply P_v/V_f and is determined by the volume of filler added to the formulation. The CPVC occurs when the binder particles are close packed and $V_v = 0$. At the CPVC, there is just enough binder to coat all of the filler particles and the substrate with at least monomolecular layer of binder, and fill the interstices between particles.

The ratio PVC/CPVC (or reduced CPVC) is a simple but profound index of primer film structure that is perhaps the most important parameter in all of paint technology [70]. The relationship of the reduced CPVC to film structure can be appreciated by reference to Fig. 8. This figure shows a representation of a dry primer film with a range of pigment volume fraction that increases from left to right.

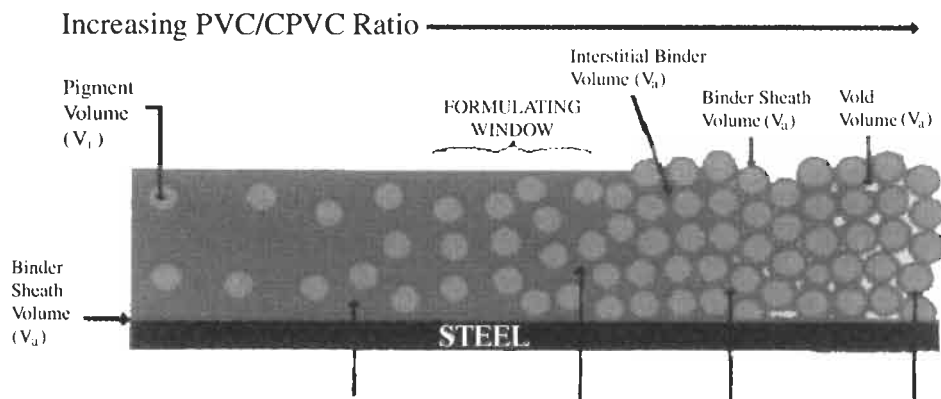


Fig. 8. Structure of dry primer film with inhibiting pigment showing range of filler volume fractions. From ref. [70].

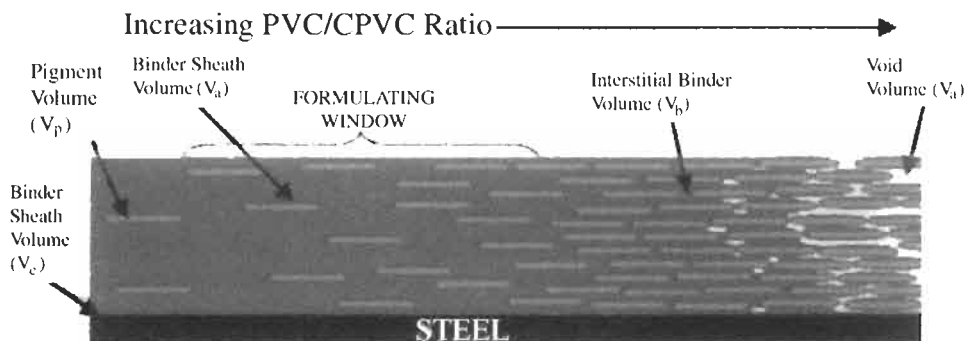


Fig. 9. Barrier primer film structure as a function of PVC. From ref. [70].

The CPVC can be readily identified in Fig. 8 as the point where the filler particles are close packed with just sufficient binder to coat the filler and substrate leaving no interstitial voids. At this point, $PVC/CPVC = 1$. Below the CPVC, there is excess binder and the filler particles are not close packed. Above the CPVC, interstitial voids exist due to insufficient binder.

The optimum PVC that provides the best corrosion protection for the substrate is a strong function of the corrosion protecting mechanism. Figs. 8–10 represent primer films based on three different protection mechanisms, and indicate the appropriate formulating windows for each type of primer.

Fig. 8 shows a primer formulated with a corrosion-inhibiting pigment such as a chromate. As discussed previously, some permeability to moisture is necessary for these pigments to dissolve and be transported to the interface where passivation of the substrate can occur. Optimum performance is generally found at $PVC/CPVC$ just below 1 [71].

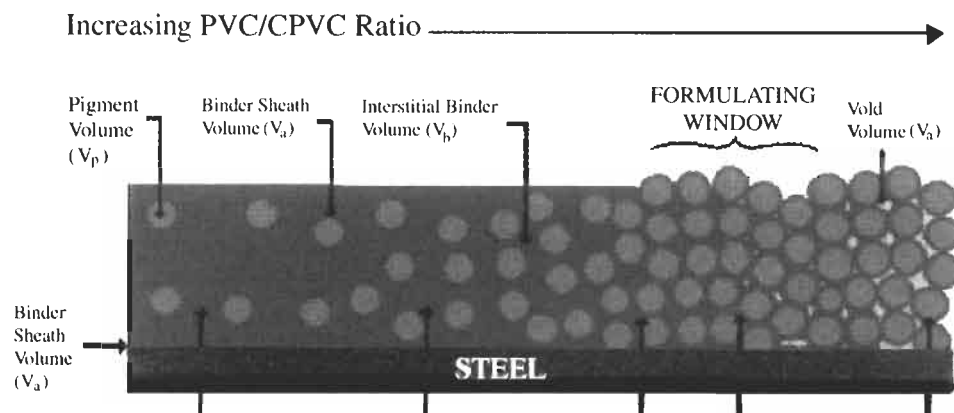


Fig. 10. Galvanic primer film structure as a function of PVC. From ref. [70].

Barrier primers are represented in Fig. 9. These systems require thick, impermeable films based on binders such as epoxies with platy pigments such as stainless steel flake or aluminum flake. These pigments provide a tortuous path that increases the diffusion length from the surface to the substrate. Because many of the pigments utilized in barrier primers can be galvanically more noble than the substrate, it is generally important to maintain electrical isolation of the particles from each other and from the substrate. The requirements for pigment isolation and low void fraction dictates that while the PVC must be high enough to provide substantial barrier to diffusion, the $PVC/CPVC \ll 1$ to maintain low void volume and electrical isolation of the pigment.

Galvanic systems are represented in Fig. 10. In primers of this type, the pigment must anodically corrode to protect the substrate, which requires the passage of current between the pigment particles and the substrate. While true contact is not possible because of the presence of a thin binder sheath on the substrate and pigment particles (V_b and V_s), the contact must be as close as possible. This corresponds to a $PVC/CPVC = 1$. For zinc dust, a common anodic pigment, the theoretical CPVC is 65.6% [70]. Lower PVC than this results in excessive electrical resistance of the films and poor protection. Higher PVCs result in interstitial void volume, which is necessary for protection. When the voids fill with electrolyte, the galvanic cells that result allow sacrificial corrosion of the zinc and protect the substrate. Therefore, these pigments work best at $PVC/CPVC > 1$.

5. Primers for adhesive bonding of plastics

Polymeric surfaces are fundamentally different from metal oxide surfaces, and consequently the technical challenges to obtaining strong and durable adhesive

Table 7
Surface energies of polymeric and metal oxide surfaces

Surface	Surface energy (dynes/cm)
PMDA/ODA polyimide	50
ABS	42
Polycarbonate	42
Polystyrene	36
Polyethylene	31
Polypropylene	29
Polytetrafluoroethylene	18
Glass	250–500
Aluminum	840
Copper	1100

Table 8
Comparison of polymeric and metal oxide surfaces

	Metals	Polymers
Surface energy	High	Low
Corrosion resistance	Low	High
Initial bond strength	High	Low
Bond durability	Low	High
Function of primers:	– Protect treated surface – Provide corrosion resistance	– Protect treated surface – Provide high initial bond strength

bonds to polymers are very different. Table 7 compares the surface energy for several polymers and metals; Table 8 contrasts a few of the differences that affect the strength and durability of adhesive bonds to these surfaces. The high surface energy of a clean metal oxide ensures strong intermolecular interactions with liquid adhesives, resulting in complete wetting and good initial bond strength. It also makes the surfaces susceptible to rapid contamination after cleaning, and absorption of water to the adhesive/oxide interface is an unavoidable thermodynamic consequence. Debonding and corrosion frequently ensue. Primer technology for adhesive bonding of metals addresses these issues: metal primers provide protection for a clean oxide surface prior to adhesive bonding and corrosion protection for the adhesive/oxide interface during use.

The primary challenge facing adhesive bonding of metals is to obtain sufficient *durability* of a bonded structure. Initial bond strength in metal–polymer adhesive joints is almost invariably excellent. Challenging the application of adhesives in polymer–polymer joining, however, is the problem of obtaining a joint that is

sufficiently strong from the outset. This requires sufficient *wetting* followed by the establishment of strong *adhesion* across the adhesive–adherend interface.

While polymeric surfaces with relatively high surface energies (e.g. polyimides, ABS, polycarbonate, polyamides) can be adhered to readily without surface treatment, low surface energy polymers such as olefins, silicones, and fluoropolymers require surface treatments to increase the surface energy. Various oxidation techniques (such as flame, corona, plasma treatment, or chromic acid etching) allow strong bonds to be obtained to such polymers.

Adhesive bonding of polymers is a case of polymer–polymer bonding. The strength of a polymer–polymer interface is developed from one of two mechanisms. If molecular mobility is sufficient, a diffuse interface is created through interdiffusion and entanglement, and the strength of the structure depends on the cohesive strength of the interpenetrated interphase region. If interdiffusion sufficient to produce entanglement is not possible, however, adhesion results from similar mechanisms to those in polymer–metal adhesive bonding: specific intermolecular interactions acting across a well-defined interface.

Interdiffusion is the dominant mechanism in adhesive bonding of polymers, such as polyolefins, which have significant molecular mobility but lack the high-energy functional groups necessary for establishing strong chemical interactions across an interface. Adhesive bonding of many engineering thermoplastics as well as surface-treated polyolefins results from specific molecular interactions between the adhesive and polar functional groups on the polymer surface.

Because of these characteristics of polymer–polymer interfaces, primers employed for adhesive bonding of these materials have very different properties from those used for adhesive bonding and painting of metals. Low surface energy and lack of reactive surface functionality in many polymers necessitates some sort of surface treatment in order to obtain wetting and adhesion. Two types of primers are generally used in these cases: surface ‘activators’ for bonding with cyanoacrylate adhesives, and chlorinated polyolefin adhesion promoters for use with other adhesives and paints such as are commonly used in the United States for obtaining adhesion to toughened polypropylenes (TPOs). In both cases, a solvent carrier which permits penetration of the substrate by the active primer components is critical. In this manner, these primers act to functionalize the polymer surface and provide specific attachment sites for the adhesive.

Cyanoacrylate adhesives cure by anionic polymerization. This reaction is catalyzed by weak bases (such as water), so the adhesives are generally stabilized by the inclusion of a weak acid in the formulation. While adhesion of cyanoacrylates to bare metals and many polymers is excellent, bonding to polyolefins requires a surface modifying primer. Solutions of chlorinated polyolefin oligomers, transition metal complexes, and organic bases such as tertiary amines can greatly enhance cyanoacrylate adhesion to these surfaces [72]. The solvent is a critical component of these primers, as solvent swelling of the surface facilitates inter-

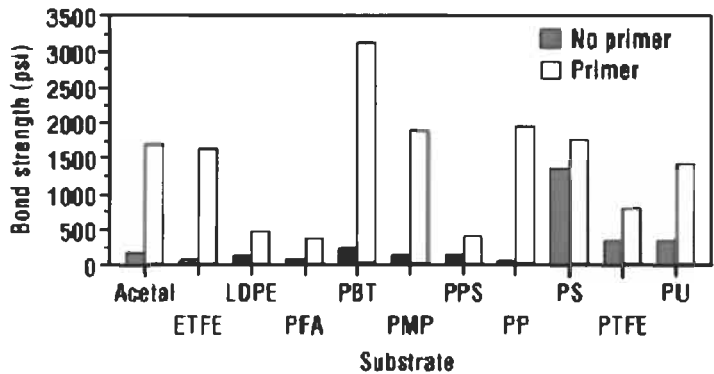


Fig. 11. Effect of polyolefin primers on bond strength of ethyl cyanoacrylate to plastics. All assemblies tested in accordance with ASTM D 4501 (block shear method). ETFE = ethylene tetrafluoroethylene copolymer; LDPE = low-density polyethylene; PFA = polyperfluoroalkoxyethylene; PBT = polybutylene terephthalate, PMP = polymethylpentene; PPS = polyphenylene sulfide; PP = polypropylene; PS = polystyrene; PTFE = polytetrafluoroethylene; PU = polyurethane. From ref. [73].

penetration of the primer and substrate. The effectiveness of polyolefin primers increases as the crystallinity of the plastic they are used on decreases, since the more amorphous substrates facilitate interdiffusion. Fig. 11 shows the effect of primer on ethyl cyanoacrylate/polymer adhesion for various plastics [73].

Adhesion of paints and adhesives to TPOs is especially problematical due to the aliphatic nature of the substrate material. In Europe, plasma and corona treatment is employed to render these surfaces wettable and obtain strong adhesion by adhesives and paints in automotive manufacture. In the United States, however, primers based on solvent-borne chlorinated polyolefin oligomers (CPOs) have become the treatment of choice for these substrate materials. The VOC emissions from these primers are considerable (as in all solvent-borne adhesives), but the less

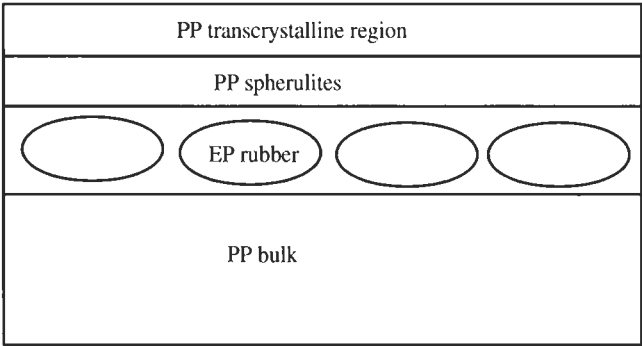


Fig. 12. Schematic of TPO surface regions.

capital intensive and more easily controllable nature of a sprayable liquid primer system is seen as a major advantage. These primers may be water or solvent borne and composed of chlorinated polyolefins plus tackifying resins, solvents, and fillers. They are typically applied to a dried film thickness of 2.5–7.5 μm [74].

Similar to the primers developed for cyanoacrylate resins, the solvent carrier plays an important role in facilitating interdiffusion of the primer and the substrate. Fig. 12 shows a schematic view of the top few microns of an injection molded TPO surface.

Adhesion development depends on diffusion of the CPO component of the primer through the crystalline boundary layers followed by swelling and entanglement with the rubber rich layer [75].

References

1. Adhesion International 1993. In: Sharpe, L.H. (Ed.), Proceedings of the 16th Annual Meeting of The Adhesion Society, Inc., Williamsburg, VA, Feb. 21–26, 1993. Gordon and Breach, 1996.
2. Pocius, A.V., *J. Adhes.*, **39**, 101 (1992).
3. Venables, J.D., *J. Mater. Sci.*, **19**, 2431 (1984).
4. Clearfield, H.M., McNamara, D.K. and Davis, G.D. In: Lee, L.H. (Ed.), *Adhesive Bonding*. Plenum Press, New York, 1991, p. 203.
5. Pleuddemann, E.P., *Silane Coupling Agents*. Plenum Press, New York, 1982.
6. Gettings, M. and Kinloch, A.J., *J. Mater. Sci.*, **12**, 2511 (1977).
7. Davis, S.J. and Watts, J.F., *Int. J. Adhes. Adhes.*, **16**, 5 (1996).
8. Abel, M.-L., Digby, R.P., Fletcher, I.W. and Watts, J.F., *Surf. Interface Anal.*, **29**(2), 115–125 (2000).
9. Reichlmaier, S., Hammond, J.S., Hearn, M.J. and Briggs, D., *Surf. Interface Anal.*, **21**, 739 (1994).
10. Boerio, F.J. and Williams, J.W., *Appl. Surf. Sci.*, **7**, 19 (1981).
11. Schrader, M.E. and Cardamone, J.A., *J. Adhes.*, **9**, 305 (1978).
12. Boerio, F.J. and Dillingham, R.G. In: Mittal, K. (Ed.), *Adhesive Joints: Formation, Characteristics, and Testing*. Plenum Press, New York, 1984.
13. Boerio, F.J. In: Patrick, R.L. (Ed.), *Treatise on Adhesion and Adhesives*, Vol. 6. Marcel Dekker, New York, 1989.
14. Theidman, W., Tolan, F.C., Pearce, P.J. and Morris, C.E.M., *J. Adhes.*, **22**, 197 (1987).
15. Kuhlbander, R.J. and Mazza, J.J., *SAMPE Symposium Series*, **38** (1993).
16. Sung, N.H., Kaul, A., Chin, I. and Sung, C.S.P., *Polym. Eng. Sci.*, **22**(10), 637 (1982).
17. Chaudhury, M.K., Gentle, T.M. and Pleuddemann, E.P., *J. Adhes. Sci. Technol.*, **1**(1), 29 (1987).
18. Millard, E.C. In: Thrall, E.W. and Shannon, R.W. (Eds.), *Adhesive Bonding of Aluminum Alloys*. Marcel Dekker, 1985, p. 99.
19. Defence Standard 03-2/Issue 3. Cleaning and preparation of metal surfaces, British Ministry of Defence, March 1995.
20. British Standard Aerospace Series, BS EN 2334. Chromic–sulphuric acid pickle of aluminum and aluminum alloys. BSi, 1977.

21. Boeing Process Specification, BAC 5555 Issue M. Phosphoric acid anodizing of aluminum for structural bonding. Boeing Airplane Company, 1995.
22. Lindner Meyler, K.L. and Brescia, J.A., *J. Adhes. Sci. Technol.*, **9**(1), 81 (1995).
23. Rider, A.N. and Arnott, D.R., *J. Adhes.*, **75**, 203 (2001).
24. Schmueser, D.W., *J. Eng. Mater. Technol.*, **112**, 321 (1990).
25. Sharpe, L.H., *Apply. Polym. Symp.*, **3**, 353 (1966).
26. Bethune, A.W., *SAMPE J.*, **Aug.**, 4–10 (1975).
27. Pocius, A.V., *J. Adhes.*, **39**(2–3), 101 (1992).
28. Minford, J.D. In: Patrick, R.L. (Ed.), *Treatise on Adhesion and Adhesives*, Vol. 5. Marcel Dekker, New York, 1981, p. 45.
29. Politi, R.E. In: Skeist, I. (Ed.), *Handbook of Adhesives*, 3rd edn. Van Nostrand Reinhold, New York, 1990, p. 713.
30. Boises, D.B., Northern, B.J. and McDonald, W.P., *Corrosion Inhibitors in Primers for Aluminum*, Paper 31, National Association of Corrosion Engineering, Houston, TX, 1969.
31. Davis, G.D. and Shaffer, D.K. In: Pizzi, A. and Mittal, K.L. (Eds.), *Handbook of Adhesive Technology*. Marcel Dekker, NY, 1994, p. 113.
32. Kendig, M.W., Davenport, A.J. and Isaacs, H.S., *Corros. Sci.*, **34**, 1 (1993).
33. *Handbook of Chemistry and Physics*, Vol. 69, CRC Press, Boca Raton, FL, 1988–1989.
34. Bascom, W.D. In: *Engineered Materials Handbook, Adhesives and Sealants*, Vol. 3, ASM International, 1990.
35. Bishopp, J.A., Parker, M.J. and O'Reilly, T.A., *Int. J. Adhes. Adhes.*, **21**, 473–480 (2001).
36. Reinhart, T.J. In: Allen, K.W. (Ed.), *Adhesion 2, Novel Concepts for Priming Metallic Adherends for Structural Adhesive Bonding*. Applied Science Publishers, Barking, 1987, p. 87.
37. Kohli, D.K. and Sitt, H.W., *Proc. Int. SAMPE Symp. Exh.*, **42**(2), 1225 (1997).
38. EPA Federal Register, National Emission Standards for Hazardous Air Pollutants for Source Categories: Aerospace Manufacturing and Rework Facilities 60, 170 p. 45947, 1995.
39. Twite, R.L. and Bierwagen, G.P., *Prog. Org. Coat.*, **33**, 99–100 (1998).
40. MacQueen, R.C., Miron, R.R. and Granata, R.D., *J. Coat. Technol.*, **68**, 857 (1996).
41. Twite, R.L. and Bierwagen, G.P., *Prog. Org. Coat.*, **33**, 99–100 (1998).
42. Kuhbander, R.J. and Mazza, J.J. In: *Proceedings of the 38th Annual SAMPE Symposium*, May 1993, pp. 785–795.
43. Foister, R.T., Gray, R.K. and Madsen, P.A., *J. Adhes.*, **24**, 17–46 (1987).
44. Hong, S.G. and Boerio, F.J., *J. Appl. Polym. Sci.*, **55**, 437 (1995).
45. Hong, S.G., Cave, N.G. and Boerio, F.J., *J. Adhes.*, **36**, 265 (1992).
46. Siebert, A.R., Tolle, L.L. and Drake, R.S., CTBN-modified epoxies work in poor bonding conditions. *Adhes. Age*, **29**, 19 (1986).
47. Zheng, H., Du, Y., Damron, M., Wright, J. and Tang, M., *Metal Finishing*, 1998, pp. 35–38.
48. Leyden, D.E. and Atwater, J.B., *J. Adhes. Sci. Technol.*, **5**(10), 815–829 (1991).
49. Pike, R.A. and Lamm, F.P., *J. Adhes.*, **26**, 171–179 (1988).
50. Pike, R.A., *Int. J. Adhes. Adhes.*, **6**, 21 (1986).
51. Turner, R.H., Segall, I., Boerio, F.J. and Davis, G.D., *J. Adhes.*, **62**(1), 1–21 (1997).
52. Rider, A.N. and Arnott, D.R., *J. Adhes.*, **75**, 203–208 (2001).
53. Cognard, J., *J. Adhes.*, **57**, 31–43 (1996).
54. Alstadt, D.M., *Rubber World*, **133**, 221 (1955).
55. Buchan, S., *Rubber to Metal Bonding*. Crosby Lockwood and Son, London, 1948.
56. Haemers, G., *Adhesion*, 4th edn. Barking, London, 1980, p. 175.
57. Van Ooij, W.J., *Rubber Chem. Technol.*, **57**, 421 (1984).

58. Popatov, E.E., Salych, G.G. and Sakharova, E.V., *Int. Polym. Sci. Technol.*, **17**(6), T/6 (1990).
59. U.S. Patent 1,749,824, 1930.
60. Cook, J.W., Edge, S. and Packham, D.E., *Int. J. Adhes. Adhes.*, **17**, 333–337 (1997).
61. Lindsay, J., *Materials World*, **May**, 266–268 (1999).
62. Cook, J.W., Edge, S. and Packham, D.E., *J. Mat. Sci. Lett.*, **16**, 445–447 (1997).
63. Frank, C.E., Kraus, G. and Haefner, A.J., *Ind. Eng. Chem.*, **44**, 1600–1603 (1952).
64. Frank, C.E., Kraus, G. and Haefner, A.J., *J. Polym. Sci.*, **10**, 441 (1953).
65. Weber, C.D., Fox, L.A. and Gross, M.E. In: Skeist, I. (Ed.), *Handbook of Adhesives*, 3rd edn. Van Nostrand Reinhold, 1990, pp. 270–283.
66. Tsai, Y.M., Boerio, F.J. and Kim, D.K., *J. Adhes.*, **61**, 247 (1997).
67. Jayaseelan, S.K. and Van Oij, W.J., In: *Rubber Bonding 2000 Conference Proceedings*, Rapra Technology Ltd., UK, p. 1.
68. Gledhill, R.A., Kinloch, A.J. and Shaw, S.W., *J. Adhes.*, **11**, 3 (1980).
69. Boerio, F.J. and Williams, J.W., In: *Proceedings of the 37th Annual Conference*. SPI Rein. Plastics/Composites Inst., Sec. 2D, 1982.
70. Hare, C.H., *J. Coat. Technol.*, **72**(910), 21–27 (2000).
71. LeBlanc, O., *Surf. Coat. Int.*, **Aug.**, 288 (1991).
72. Yang, J. and Garton, A., *J. Appl. Polym. Sci.*, **48**, 359–370 (1993).
73. Courtney, P.J. and Verosky, C., Medical Device and Diagnostic Industry, Sept. 1999.
74. Ryntz, R.A., *Automot. Eng.*, **101**(5), 37–40 (1993).
75. Prater, T.J., Kaberline, S.L., Holubka, J.W. and Ryntz, R.A., *J. Coat. Technol.*, **68**(857), 83–91 (1996).

Chapter 11

Pressure sensitive adhesives

ALBERT I. EVERAERTS* and L.M. CLEMENS

3M Company, St. Paul, MN, USA

1. History of pressure sensitive adhesives

Products adhered with pressure sensitive adhesives (PSAs) are found nearly everywhere in modern society. The following is a partial listing of these products:

Duct tapes	Traffic control reflective products
Masking tapes	Decals and commercial graphics
Electrical tapes	Drug delivery tapes (e.g. nitroglycerine patches)
Foil, film, and general industrial tapes	Office tapes and Post-it™ Notes
Carton and box sealing tapes	Label and identification products
Medical dressings and bandages	Disposable diaper closures
Surgical drapes	Mounting foam tapes
Diagnostic electrodes	Postage stamps
Optical display films	

These products provide utility and convenience for the consumer and high reliability and low-cost manufacturing in the industrial sector. The infusion of new products based on PSA technology has led to a growth rate of about 8% per year for the last 25 years. The US market [1] for pressure sensitive tapes alone has been estimated at greater than five billion dollars in 2000.

The earliest references to pressure sensitive adhesive materials probably date to the medical plasters (i.e. single dressings) first devised in the early decades of the 1800s. These dressings were often a combination of a natural rubber PSA and a medication impregnated onto a bandage material.

The earliest PSA tapes began to make their appearance at the turn of the century. Most popular were the cloth tapes used in medical applications, holding bandages and appliances in place. All these were based on natural rubber/tackifier formulations reinforced with zinc oxide [2,3].

* Corresponding author. E-mail: aieveraerts@mmm.com

The era of modern pressure sensitive adhesive technology was ushered in during the 1930s with the development of masking tapes for automotive paint applications. Clear cellophane tapes used for office applications followed shortly after the introduction of masking tapes. More film and foil tapes soon followed for electrical and many other industrial applications. World War II brought new polymers, including acrylates to the PSA platform, largely in response to the allocation of natural rubber to defense applications. These acrylate PSAs brought about a further product expansion in medical, graphic, and new and improved office products. The major PSA polymer classes were rounded out in the mid-1960s with the introduction of the styrene/rubber block copolymers.

It is the intent of the present chapter to review the chemistry of the significant PSA polymer classes and discuss their application to tape and related products.

2. Definition of a pressure sensitive adhesive

The following points are abstracted from the definition of the Pressure Sensitive Tape Council [4]. A pressure sensitive adhesive is:

- (1) Aggressive and permanently tacky.
- (2) Adheres without the need of more than finger or hand pressure.
- (3) Requires no activation by water, solvent, or heat.
- (4) Exerts a strong holding force.
- (5) Has sufficient cohesiveness and elasticity that it can be removed from smooth surfaces without leaving a residue.

The definition is intended to differentiate these adhesives from merely sticky materials like flypaper or materials that may have only substrate specific adhesion.

3. Criteria for pressure sensitivity

After some early uncertainty in the literature about the nature of the pressure sensitive bond, Dahlquist [5,6] related modulus data to tack–temperature studies and observed that the compression modulus of the adhesive had to be less than about 3×10^6 dyne/cm² (3×10^5 Pa) before any adhesive tack was observed. This was explained as the highest modulus that still allowed the adhesive to be sufficiently compliant to wet out or come into molecular contact with the substrate and form dispersive bonds. As other investigators [7–9] accepted this requirement it was termed the ‘Dahlquist Criterion’.

A second general criterion for pressure sensitivity is that the glass transition temperature of the adhesive be below the use temperature, which is usually room temperature. Broadly speaking, the T_g will be about 30–70°C below room temperature, depending on the base polymer and any added modifiers.

Table 1
Common PSA polymer classes

Inherently tacky	Need tackification
Polyalkylacrylate and copolymers	Natural rubber
Polyvinylethers	Styrene isoprene block copolymers
Polyalphaolefins	Styrene butadiene block copolymers
	Styrene butadiene random copolymers
	Polyisobutylene
	Polysiloxanes

With these criteria, Chu [10] has suggested that the first step in designing a PSA is to formulate the adhesive to a predetermined target T_g and modulus window. This is discussed further in Section 7.1.5.

4. PSA polymer classes

While there are a large number of elastomers that can be formulated into pressure sensitive adhesives, the following list is intended to focus on commercially significant materials. Two subsets are differentiated in Table 1: those polymers that can be inherently tacky, and those that require modification with tackifiers to meet the T_g and modulus criteria to become pressure sensitive.

5. PSAs in perspective

Comparatively speaking, PSAs fall on the weak end of the adhesive scale. Sometimes this is by design: a Post-it™ Note ought not adhere to the point of tearing the paper substrate on removal. An office tape does not have to be designed to hold large loads. When high holding power is required, a larger area of attachment must be used with a PSA, relative to a thermoset adhesive. But even here the industrial process and cost benefits may favor the PSA approach over a conventional adhesive, since no mixing or heat is required and a uniform bond line is always achieved. When acrylic foam tape is used to adhere the heavy body side molding extrusions that protect car doors and panels, a further benefit results: no rivets penetrate the panel (the older method of attachment) eliminating a point of corrosion and a point of stress concentration. In Table 2, a performance comparison of some common adhesives and PSAs is made. Since the test methods used for PSAs are somewhat different than for conventional adhesives, the comparisons are only approximate, but the sense of order is correct.

Table 2

A comparison of PSA bonds and conventional adhesives

Type	Load bearing/holding power (kPa)	Peel strength (N/m)
Structural epoxy	14,000–40,000	650–750
Semi-structural adhesive	7,000	
Hot-melt adhesive	3,500–7000	
Acrylic foam tape	1,400	275
Office tape	35–70	25–35
Post-it™ note	0	1

Table 2 indicates that only the acrylic foam tapes compete in adhesive strength comparison in any realistic sense with the conventional adhesives.

6. Pressure sensitive tape testing

6.1. General

With such a wide variety of products using PSAs as the attachment mechanism, it is not surprising to learn that a large number of specific tests exist in the industry. These tests are usually focused on critical aspects of product performance: Is the automotive masking tape adhesive strong enough to hold the masking apron in place during the vehicle's trip through the paint bake oven? Does the medical tape adhere effectively to the skin and yet remove without causing much discomfort? Will the truck graphic stay in place for the life of the product despite varying environmental conditions? To answer these questions one needs a battery of specially designed tests, often run in parallel with more fundamental adhesion tests. Only these latter tests will be addressed here.

The fundamental tests would ordinarily consist of peel adhesion tests, shear holding power tests, and one or more tack tests. Often these adhesion tests will be carried out on 25.4 mm (1.0 inch) wide tapes prepared by accurately coating a 0.025–0.050 mm thick adhesive (dry) on a standard backing, such as a 0.025–0.050 mm thick polyester film. A flexible, but relatively inextensible film like polyester eliminates possible backing contributions to adhesive measurements. Pressure sensitive adhesive testing requires the same protocol common to all adhesive testing — careful preparation of samples, clean reproducible substrates, knowledge that the proper failure mode has been achieved, and the like. PSAs are viscoelastic materials, so test results will be very sensitive to test rate and temperature. To reduce temperature and humidity effects, both ASTM and PSTC standards require tape conditioning and testing at 23°C and 50% relative humidity.

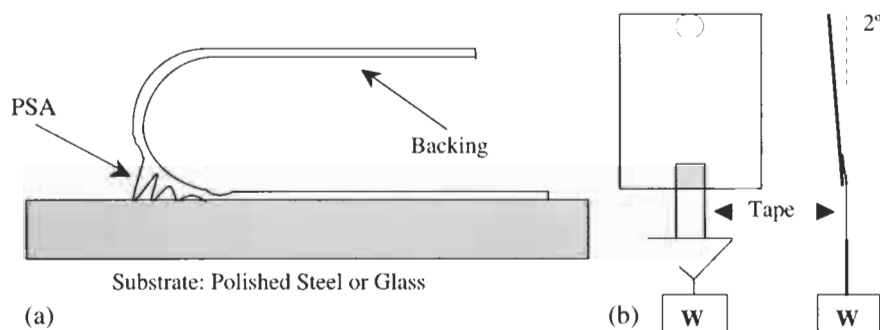


Fig. 1. PSA testing. (a) 180° Peel test (radius exaggerated). (b) Shear holding power test, front and side view.

The humidity requirement is probably most significant for polar or hydrophilic adhesives, for example, some of the acrylate adhesives.

It is the intent of the present section to outline these fundamental tests to provide the reader sufficient background relative to the central theme of the chapter. A more detailed understanding of the dynamics and modeling of PSA testing is discussed in Chapter 13, Volume 1 of this series.

6.2. Peel adhesion testing

The peel adhesion test is basic to PSA characterization. Fig. 1a shows the configuration of a 180° peel test with an exaggerated curvature radius. The test may be run with a variety of general purpose mechanical testing devices such as an Instron™ tester, or with testing equipment specifically designed for tape testing, as for example, the IMASS™ Slip/Peel Tester. Both 90° and 180° testing is commonplace, although the 90° tests require a jig to maintain the peel angle while moving the peel front. Test data at these two peel angles are not equivalent. Experimental data in the literature usually show the 90° peel force value often exceeds the 180° value, with the shape of the peel force–peel angle curve either smoothly increasing as the angle changes from 180° to low angles, [11] or passing through a minimum [12–14] and then to higher values. Backings that undergo extensive stretching or plastic deformation, behave less predictably. It is also should be noted that at constant test machine speed, the peel front in a 180° test moves at one half the rate of that of the 90° test.

While detail may be found in the ASTM D-3330 or PSTC-1 and PSTC-2 standards, the peel test is typically carried out as follows: The tape is conditioned at 23°C and 50% relative humidity for 1 day. Next, the tape is rolled down with a weighted standard roller onto a clean test substrate (usually polished 302 stainless steel), allowed to dwell for a specified time (usually 1 min), and then clamped with the testing fixture in the test machine and peeled at a specified rate.

Peel tests are commonly carried out at rates of 5 mm s^{-1} (12 in. min^{-1}) in standardized testing, but depending on the intent of the testing (i.e. meeting requirements of a test standard, or obtaining fundamental understanding) it is prudent to run a series of tests from very slow to high rates where the adhesive starts to exhibit stick-slip failure. Since PSAs are viscoelastic materials the force will vary with rate, increasing with rate when starting from very low rates. The peel force–rate plot can give a measure of the robustness of the tape. Only data in the desired mode of failure should be considered, i.e. adhesive failure with clean removal from the substrate and no failure from the backing.

PSA peel testing is sensitive to a variety of factors and careful testing is necessary to get reproducible results. Critical variables include the following:

- Peel rate and angle.
- Temperature of the test specimen.
- Roll down pressure and speed, and number of passes.
- Time of tape dwell on the substrate before testing.
- Adhesive thickness (peel force increases with increasing thickness.)
- Backing thickness, modulus, and stretchiness.
- Substrate texture, surface energy, and cleanliness.

6.3. Shear adhesion or holding power

This test measures the ability of a tape to resist creep under applied load. The test is covered in ASTM D-3654 and PSTC-7. A specified area (typically $12.7 \text{ mm} \times 12.7 \text{ mm}$) of conditioned tape is rolled down with a specified pressure on the substrate of choice, such as polished 302 stainless steel. The panel is fixed in the vertical position or up to 2° tilted back so that there is no element of low angle peel in the test (Fig. 1b). A weight (often 1000 g) is fixed to the end of the tape and the time to failure, i.e. complete detachment from the plate, is measured. Infrequently, the time required for the tape to creep a given distance is measured and reported.

In uncrosslinked, or very lightly crosslinked adhesives an actual shearing process takes place, resulting in viscous flow and cohesive failure of the adhesive. This leaves adhesive residue on both the panel and the tape backing as the tape creeps off the panel. This is the most predictable or reproducible failure mode in this test. More extensively crosslinked adhesives and some high modulus adhesives fail by an adhesive failure ('pop-off') mechanism, leaving no residue on the panel and no evidence of a shearing mechanism on the tape. Here the failed adhesive surface is shiny and untextured. Although the time of failure may be on the order of hours or days, this is a catastrophic failure and the standard deviation for several tests will be large. Another undesirable failure mode would be a primer failure, evidenced by an absence of adhesive on the tape backing at the end of the test. Many factors that are important for peel testing apply to shear adhesion testing as well, especially temperature, adhesive thickness, and backing effects.

There is second shear adhesion test that is now being reported with increasing frequency, the so-called SAFT, or shear adhesion failure temperature test. It is particularly popular among block copolymer PSA developers. In this test [15], a shear specimen with an overlap area of $2.54\text{ cm} \times 2.54\text{ cm}$ is prepared and suspended in a circulating air oven. A 1-kg weight is attached to the tape and the oven temperature is raised continuously 5.5°C per 15 min until failure. An industry wide standard has not yet been written for this test.

6.4. Tack testing

There are several tests for measuring the quick stick of PSAs. The most fundamental is the *probe tack* test, ASTM D-2975, illustrated in Fig. 2a. The conditioned adhesive tape is taped over a cylindrical weight with an annular opening. A probe with a flat or slightly curved face passes thorough the annular opening and contacts the tape with sufficient extension to lift the weight, bonding the probe to the tape during the very brief contact time (usually 1 s). The probe is then withdrawn at a specified rate, typically 1 cm s^{-1} , and the force of removal is measured. The test is the mechanical equivalent of a 'thumb appeal' examination, in which one fingers a tape for an estimate of tack level. A newer testing device [16,17] measures the entire force curve of attachment and detachment. This allows the development of comparative data for families of adhesives that may be examined for characteristic response patterns. Rate of contact and removal, force of contact, temperature, adhesive thickness, contact time, and probe texture and composition are all important test factors in the probe tack tests. A representative tack-temperature response curve for a natural rubber PSA is shown in Fig. 2b. It is instructive to note the adhesive has little tack at either very cold or very warm temperatures.

A *loop tack* (Fig. 2c) test consists of allowing a tear-shaped loop of conditioned tape to drape into contact with a test surface of specified area (usually $25.4 \times 25.4\text{ mm}$), with the force of contact limited to the weight of the tape itself (ASTM Ref. D-6195). The ends of the loop are held in a tensile tester. After a momentary contact time the tester is engaged and the tape is removed at a specified speed. The maximum in the removal force is ordinarily observed just at the point where the two peel fronts join. The value is reported in a force per area of tape width, or lb in.^{-2} . While this tack test has some popularity, it is perhaps more of a very short dwell time peel test, and it has variables more associated with that test, especially backing effects, since heavier backings lead to higher tack values.

In another tack test, a steel ball of specified diameter is rolled down a grooved incline onto a conditioned surface area of pressure sensitive adhesive (ASTM D 3121, PSTC-6). The length of travel before it stops is the '*rolling ball tack*' (Fig. 2d) reported in millimeters. It is relatively inexpensive and simple to set up. Similar test variables to the probe tack test apply.

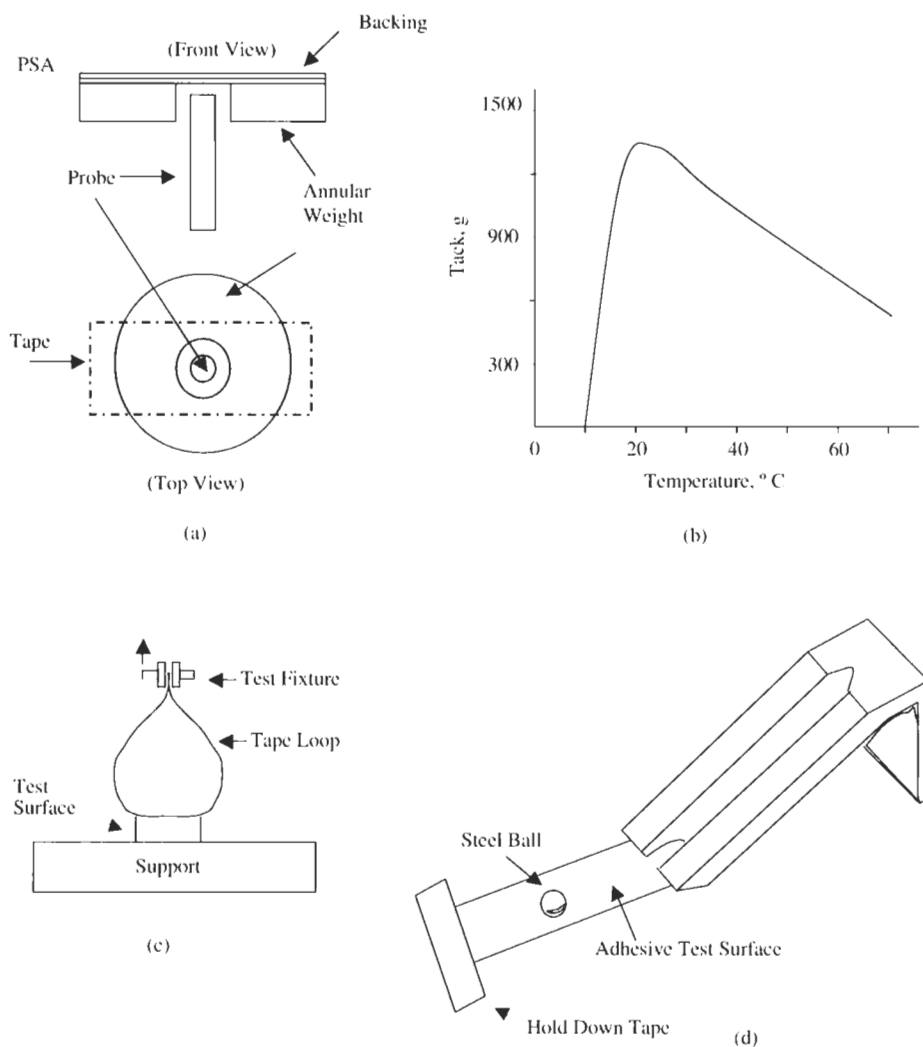


Fig. 2. Tack tests and results. (a) Probe tack. (b) Probe tack vs. temperature for a natural rubber PSA. (c) Loop tack. (d) Rolling ball.

7. PSA polymer classes

7.1. Natural rubber-based PSAs

7.1.1. Historical

Natural rubber was the first polymer base for the early pressure sensitive adhesives. Their origin may be traced to the early medical plasters formulated in

pharmacies in the mid-1800s. Two pharmacists, William Shecut and Horace Day obtained US Patent 3956 in 1845, titled 'Improvements in Adhesive Plasters'. They compounded the following formulation with turpentine solvent and coated it onto a bandage dressing:

India rubber	5 lb.
Southern pine gum	1 lb.
Balsam of Peru	6 oz.
Litharge	1 lb.
Capsicum annum	4 oz

After drying, the adhesive was activated by adding further balsam of Peru, before application. The balsam of Peru and gum of Southern pine are tackifiers (see Section 7.1.5) while the capsicum annum acts as a plasticizer to further soften the formulation. The latter is an extract of cayenne or red pepper and also acts as the medicament that warms the portion of the body to which the plaster is applied. Litharge (lead monoxide) acts as filler, reinforcing the adhesive. It is unclear if the construction would meet the precise definition of a PSA relative to the requirement for clean removability (see Section 2, above), but it provided direction for early formulators. Later plaster patents incorporated other medications, such as mercury salts to treat fungal infections, and opiates [18] to relieve pain. Johnston [19] has recently reviewed natural rubber pressure sensitive adhesives, including the origins of the technology.

7.1.2. Natural rubber as a raw material

Raw natural rubber is obtained as latex from the rubber tree, *Hevea brasiliensis*. The latex is neutralized and stabilized, and then dried and baled for shipping. The resulting rubber has a broad molecular weight distribution with the high-end molecular weight fraction exceeding the 10^7 Da range [20]. The raw rubber has about a 2% bound protein content, which acts as a crosslinker and makes the rubber difficult to process. There is also some level of gel content in the rubber introduced through the drying process. The preferred rubber for most PSAs is either the light colored rubber 'pale crepe' that results from air drying, or the less expensive, darker colored 'smoked sheet' that results from drying at elevated temperature. To render the rubber more processible it is usually milled or subjected to some other hot shearing process, which reduces the rubber molecular weight, denatures the bound protein, and destroys the crosslinking. This milled rubber is the first step to preparing a rubber-based PSA.

7.1.3. Rubber/resin adhesives

Two processes to natural rubber PSA tapes are outlined in Fig. 3, starting from the mechanically broken down rubber. The first route compounds the rubber with

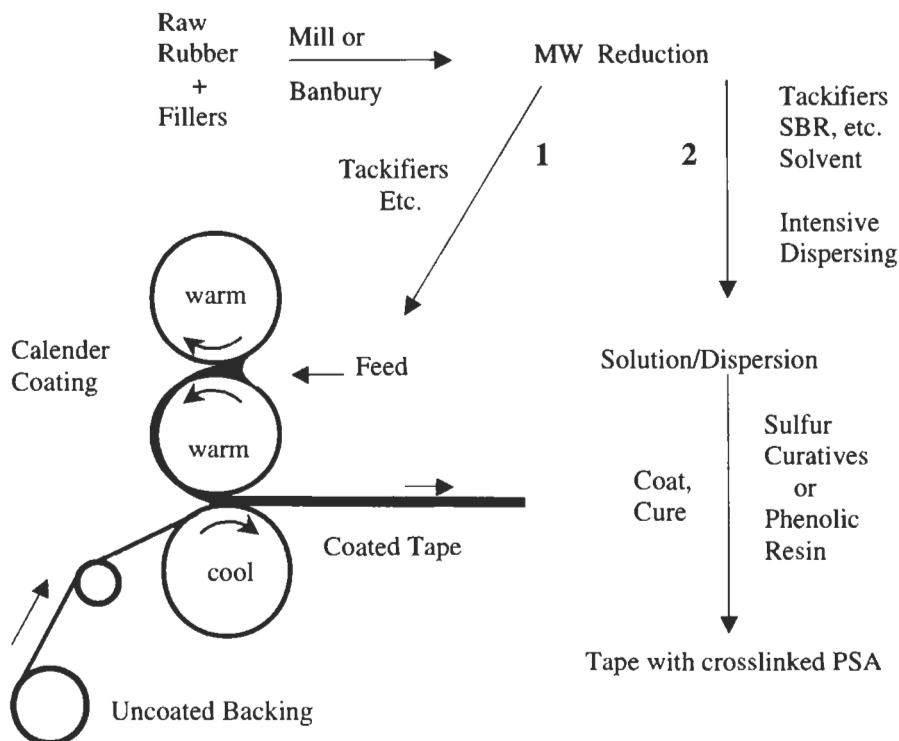


Fig. 3. Two routes to rubber/resin tapes: 1, Traditional calender-mill; and 2, solution polymer method for high performance tape.

tackifiers, fillers, etc. on a three-roll calender mill or equivalent equipment. The resultant PSA is then coated onto a fabric to provide a PSA tape. The earliest tapes made by this process included the white cotton cloth tapes used in surgical bandaging. Today's familiar, general-purpose 'duct' tapes are often made by this process. The early medical tapes had poor temperature performance and low creep resistance when subjected to stress, since the adhesive was not crosslinked and had a greatly reduced molecular weight due to milling. Despite these drawbacks, these tapes and the older water activated paper glue tapes were the only choice for masking the new 'two tone' cars that suddenly came into vogue in the 1920s.

The second path in Fig. 3 outlines the approach to a more robust tape designed by Drew [21]. Here the milled rubber and filler are combined with tackifiers and other additives/stabilizers in an intensive dispersing step, such as a Mogul or Banbury mixer. Next, a phenolic resin or an alternative crosslinker is added and allowed to react with the rubber crosslinker to a point somewhat short of crosslinking. The compounded mixture is then charged to a heavy duty churn and dissolved in a suitable solvent like mineral spirits. To prepare a masking tape,

the solution is coated on a paper substrate and oven dried. The oven step also crosslinks the adhesive through further phenolic resin reaction with the rubber. The final product is wound up and slit to the desired width.

Drew employed this process for the production of a crepe paper automotive masking tape with a crosslinked rubber/resin PSA. The light crosslinking imparts creep resistance and cohesive integrity to the adhesive so that the tape and attached paper aprons remain in place in the paint oven (ca. 350°F), and can be rapidly stripped from the hot vehicle on exiting the oven. The creped paper allowed the tape to be stretched to fit curves in the paint design and the body panels, while still providing a sharp edge for paint demarcation. (The name 'Scotch' is said to have first been applied to these tapes because of a painter's complaint that the tape had too little adhesive.)

It should be pointed out that earlier Drew patents [22,23] concentrated on uncrosslinked rubber/resin PSA coated on creped paper for auto masking. Even with uncrosslinked adhesive, the crepe paper product provided a significant advantage over the ragged-edged and dimensionally unstable cloth tapes. Solvent processing also allowed a higher molecular weight rubber (less breakdown, better cohesive strength) to be processed than the calender mill method. This contributed to the performance of these early tapes.

7.1.4. Crosslinking rubber/resin PSA

The overall effect of light crosslinking in a PSA is to increase the shear holding power (creep resistance) of the adhesive, while only minimally reducing the peel strength. When a phenolic crosslinking resin is employed, it is a thermosetting, oil soluble type [24], compatible with the rubber. It has been postulated that the crosslinking reaction involves the 1,4 addition of a quinone methide intermediate of the phenolic resin reacting with the unsaturated double bonds in the rubber to form a chroman ring [25]. Usually the reaction is catalyzed with a Lewis acid, such as compatible zinc soap. The early phenolic resins used in rubber/resin PSAs were based on alkylphenols such as *t*-butylphenol and *t*-amylphenol [21,24,26]. Later patents included higher alkylphenols [27] for better compatibility and reported improved tape properties and brominated phenolic resins [28] with higher reactivity.

Sulfur chemistry [29] has also been used to crosslink rubber/resin PSAs, although the use of elemental sulfur itself yields tapes that can stain substrates. Other patents exemplify the use of typical rubber vulcanizing chemistry such as 'Tetrone A', dipentamethylenethiuramtetrasulfide, and 'Tuads', tetramethylthiuram disulfide [30], or zinc butyl xanthate [31] for this purpose. Early art [32] also claimed electron beam curing of both natural rubber and other adhesives that were solvent coated on tape backings. Later references to electron beam curing

of natural rubber and other PSAs have included solventless, extruder/die coated products and adhesive films on various backings [33].

7.1.5. Tackification and PSA formulation

Since most elastomeric materials are not pressure sensitive, their rheological properties need modification to move them into the PSA range. This is the case for several common polymers including natural rubber and styrene isoprene block copolymers that are used for preparing pressure sensitive adhesives. For example from the graphical data of Class and Chu [34], milled natural rubber has a $\tan \delta$ derived T_g of about -56°C , and a low-frequency storage modulus, G' , at room temperature of about 4.5×10^6 Pa. To be formulated to a PSA, the T_g must be increased and the storage modulus must be decreased per the earlier discussion in Section 3. Compatible, low molecular weight resins (ca. 300–2000 Da) with T_g greater than the elastomers are used for this purpose. Such materials are termed tackifiers. It should be noted that the tackifier industry often uses softening point instead of T_g to define the physical properties of the tackifier. This softening point is more a measure of flow and its value is normally significantly higher (approximately 40°C) than the T_g .

Class and Chu [34] have studied the tackification of natural rubber and SBR over a wide range of resin concentrations for several tackifiers. From their graphical data it can be estimated that 1 : 1 tackification (by weight) with a poly(*t*-butyl styrene) resin, MW 850 and $T_g = 59^\circ\text{C}$, gives a PSA with T_g about -13°C , and storage modulus, G' about 8.8×10^5 Pa, well within the PSA window.

These researchers have pointed out that the basic principles of polymer physics apply to tackified elastomers, such as natural rubber. Thus the T_g relationship provided by the Fox–Flory equation applies:

$$\frac{1}{T_{g\text{PSA}}} = \frac{W_1}{T_{g1}} + \frac{W_2}{T_{g2}} + \frac{W_3}{T_{g3}} + \dots \quad (1)$$

W_1 is the weight fraction of the elastomer, W_2 the tackifier, W_3 a further compatible additive, such as an oil, and so forth, for the remaining components in the formulated PSA. Application of the Fox equation to the poly(*t*-butylstyrene) tackified natural rubber adhesive (cited above) gives a value of -11°C , in good agreement with the interpolated value of -13°C .

The modulus relationship may be related as follows:

$$G'_{\text{PSA}} = V_{\text{Elast}}^{2.3} \times G'_{\text{Elast}} \quad (2)$$

where G' is the plateau storage modulus and V_{Elast} is the volume fraction of the elastomer. The exponent of the volume term in Eq. 2 may vary from 2.2 to 2.6, depending on the elastomer, but the equation remains directive (see comments on formulating below). The shear storage modulus of the adhesive and elastomer

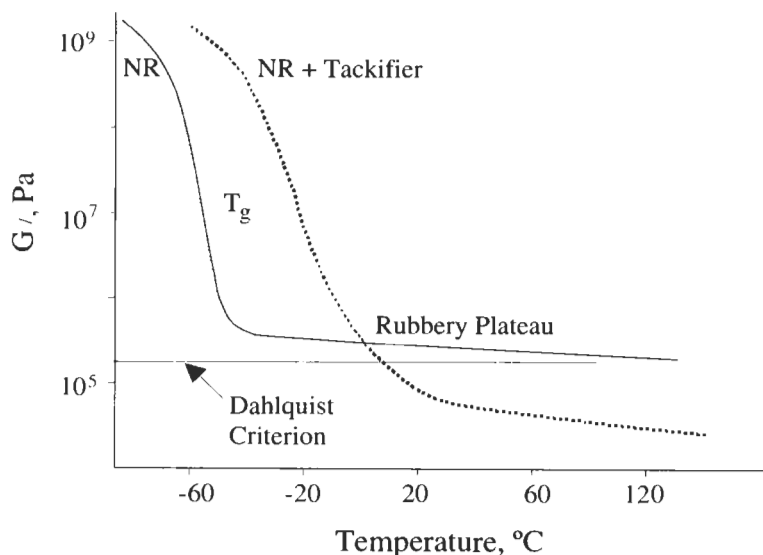


Fig. 4. Modulus-temperature relationship for milled natural rubber and 1:1 tackified natural rubber.

are ordinarily measured in a rheometer employing parallel plate geometry. The plateau modulus value is taken at the point where $\tan \delta$ is at a minimum.

The net effect is that tackifiers raise the T_g of the blend, but because they are very low molecular weight, their only contribution to the modulus is to dilute the elastic network, thereby reducing the modulus. It is worth noting that if the rheological modifier had a T_g less than the elastomer (as for example, an added compatible oil), the blend would be plasticized, i.e. while the modulus would be reduced due to network dilution, the T_g also would be reduced and a PSA would not result. This general effect of tackification of an elastomer is shown in the modulus-temperature plot in Fig. 4, after the manner of Class and Chu. Chu [10] points out that the first step in formulating a PSA would be to use Eqs. 1 and 2 to formulate to a T_g /modulus window that approximates the desired PSA characteristics. Windows of T_g /modulus for a variety of PSA applications have been put forward by Carper [35].

Class and Chu demonstrated that if a tackifier is chosen that is largely incompatible with the elastomer, a modulus increase due to the filler effect is observed and little change in T_g results, and once again a PSA would not be obtained. This was observed for mixtures of low molecular weight polystyrene resin and natural rubber. The same polystyrene resin did tackify SBR, a more polar elastomer that is compatible with the resin. Hydrogenating the polystyrene to the cycloaliphatic polyvinylcyclohexane changed the resin to one now compatible with the less polar natural rubber and no longer compatible with SBR. These authors also provide

evidence that molecular weight is also a criterion for tackifier compatibility with too high a resin molecular weight (or presumably a resin with a fraction of high molecular weight) changing a resin from compatible to incompatible. Lowerey [36] has reviewed synthetic tackifiers and observes that the tackifier M_z , as measured by GPC, offers a better measure for compatibility with an elastomer.

7.1.6. Choosing tackifiers for natural rubber

The earliest tackifiers used for natural rubber PSAs were the synthetic cumarone–indene resins (low MW acid polymerized oligomers of a petroleum fraction rich in indene and benzofuran), and Burgundy pitch or colophony. The latter are both conifer tree extracts rich in sesquiterpene acids, principally abietic acid. Wood rosin, a purified sesquiterpene fraction was also used. These low molecular weight resins appear not to have conferred sufficient stability on the compounded adhesive. Wood rosin esters of polyhydric alcohols like glycerol and pentaerythritol, the so-called ester gums, and Pentalyn™ A, gradually became preferred, along with their partially hydrogenated counterparts, the Staybelite™ and Foral™ esters. The latter have better oxidative resistance and show better long-term aging characteristics in adhesives.

Other natural product-based resins also became widely used, such as the light colored Lewis acid oligomerized products of terpenes such as α -pinene, β -pinene, and limonene. These natural product resins are relatively expensive, however, and formulators now often use the newer, less expensive synthetic resins in present day natural rubber PSAs. These are termed the aliphatic or C-5 resins and are Lewis acid oligomerized streams of predominately C-5 unsaturated monomers like *cis*- and *trans*-piperylene and 2-methyl-2-butene [37]. These resins are generally low color products with compatibility and softening points similar to the natural product resins. Representative products in the marketplace would be Escorez™ 1304 and Wingtack™ 95. In most natural rubber PSA formulations, rubber constitutes about 100 parts and the tackifier about 75–150 parts.

In the earlier art, there was some consideration that partial incompatibility of the tackifier resin with the rubber was responsible for the appearance of tack, but this no longer is seriously held in light of continuing studies by many investigators. Aubrey [38] has addressed this in his review of the mechanism of tackification and the viscoelastic nature of pressure sensitive adhesives. Chu [39] uses the extent of modulus depression with added tackifier as a measure of compatibility. Thus in a plot of modulus vs. tackifier concentration, the resin that produces the deepest minimum is the most compatible. On this basis, Chu rates the following resins in order of compatibility for natural rubber: rosin ester > C-5 resin > α -pinene resin > β -pinene resin > aromatic resin.

In general, single tackifiers or blends of tackifiers may be used to formulate to optimum product performance, following the modulus/ T_g criteria outlined

earlier. Chu shows a blend of solid and liquid (i.e. low T_g) tackifiers moving a block copolymer composition to a predetermined T_g and modulus window corresponding to a 'good' PSA.

7.2. Block copolymer PSAs

7.2.1. Introduction

First introduced to the marketplace in the mid-1960s, these materials now constitute the base for the largest volume of PSAs in the industry. Extruder compounding and hot-melt die coating of these adhesives lead to the efficient manufacture of commodity products such as the oriented polypropylene carton sealing tapes. These tapes are widely used in automated packaging lines equipped with automated tape dispensing devices, and constitute the largest single use for PSAs. The base elastomers were initially commercialized under the name Kraton™ by Shell Chemical (now Ripplewood Holdings, LLC). Subsequently, a number of other suppliers have joined the market, including Dexco (Vector™), Enichem (Europrene™), and Nippon-Zeon (Quintac™).

Block copolymer chemistry and architecture is well described in polymer textbooks and monographs [40]. The block copolymers of PSA interest consist of anionically polymerized styrene–isoprene or styrene–butadiene diblocks usually terminating with a second styrene block to form an SIS or SBS triblock, or terminating at a central nucleus to form a radial or star polymer (SI)_n. Representative structures are shown in Fig. 5. For most PSA formulations the softer SIS is preferred over SBS. In many respects, SIS may be treated as a thermoplastic, thermoprocessible 'natural rubber' with a somewhat higher modulus due to filler effect of the polystyrene fraction. Two longer reviews [41,42] of styrenic block copolymer PSAs have been published.

The very regular physical network of the block copolymer allows the higher loading of tackifier required to achieve optimum PSA properties relative to natural rubber adhesives. A loading level of tackifier at 1.5 times the level of elastomer is not uncommon. For the PSA designer, the T_g and modulus equations given in Section 7.1.5 may still be used as a starting formulation point, although only the weight or volume fraction of rubber should be used, i.e. the polystyrene fraction of the elastomer should be factored out. Sometimes the reduction of modulus and increase in the T_g that is required to move the elastomer into the PSA property window is accomplished with a combination of both tackifier and low-cost plasticizing hydrocarbon oils or low molecular weight, liquid polymers like polybutene. While the tackifiers may have a T_g ranging from -30 to 80°C , these oils or polymers have a T_g close to that of the elastomers. The oil loading often is on the order of 10–30% of the weight of the elastomer.

The block copolymer architectures are all designed to provide elastomers that

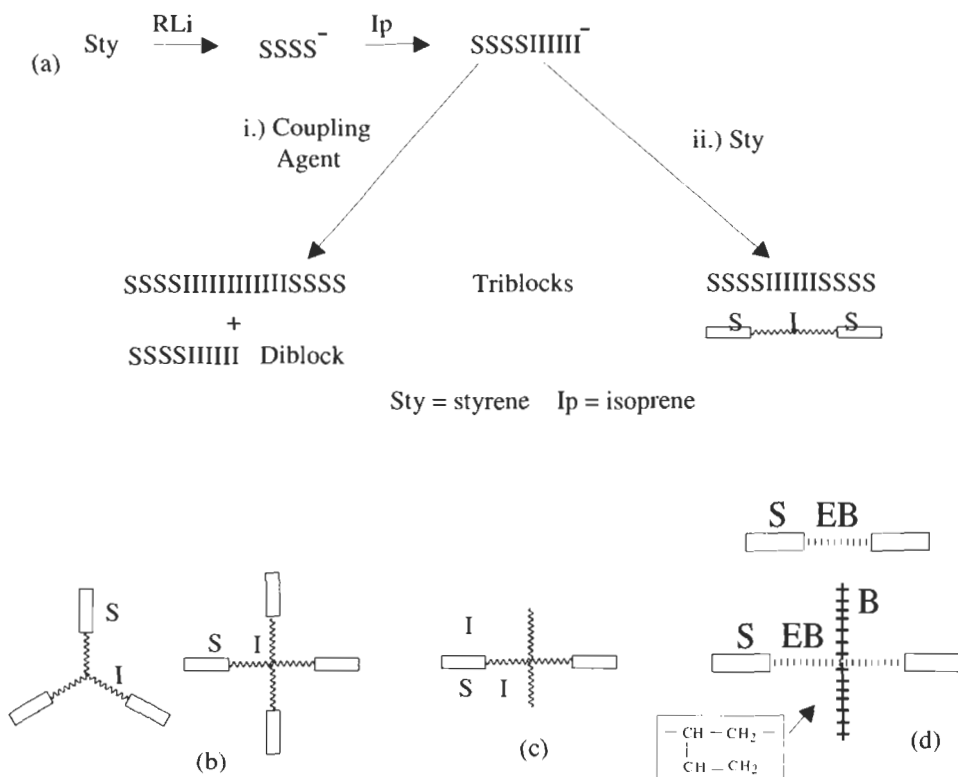


Fig. 5. Representative block copolymer structures. (a) Routes to SIS: i, coupling reaction; ii, sequential. (b) Three and four-arm SI stars. (c) $(\text{SI})_2\text{I}_2$ radial. (d) $(\text{SEB})_2\text{B}_2$ radial.

are physically crosslinked at room temperature due to the phase separation that takes place between the rubbery block and the aromatic block. Phase separation occurs because of the dissimilarity of the polydiene and the polystyrene segments. Individual polystyrene segments from many chains organize into a discontinuous polystyrene phase that effectively acts as a crosslink site. With heat, the polystyrene phase loses its glassy state, undergoes some dissociation and the elastomer becomes thermally processible. A fully formulated block copolymer PSA can be extruder processed in the temperature range of 275–350°F.

The earliest SIS block copolymers used in PSAs were nominally 15 wt% styrene, with an overall molecular weight on the order of 200,000 Da. The preparation by living anionic polymerization starts with the formation of polystyryl lithium, followed by isoprene addition to form the diblock anion, which is then coupled with a difunctional agent, such as 1,2-dibromoethane to form the triblock (Fig. 5a, path i). Some diblock material is inherently present in the final polymer due to inefficient coupling. The diblock is compatible with the triblock and acts

as a diluent for the elastic network, reducing the crosslink density and increasing energy dissipation characteristics due to the increased number of free chain ends. Properly formulated, a styrene–isoprene–styrene triblock polymer alone, or with additional diblock can be tackified to a useful PSA [43,44].

7.2.2. Diblock levels in block copolymers

Since about 1990, some SIS polymers without diblock content [45,46] have been commercialized as part of the Vector™ polymers marketed by Dexco. This triblock synthesis proceeds in an alternative polymerization route (Fig. 5a, path ii) in which a second charge of styrene is added directly to the diblock anion. Because the additions of monomers are sequential, there is no coupling agent employed and little likelihood of forming diblock. The availability of pure triblocks widens the formulating possibilities available to the adhesive designer, especially for very high shear strength adhesives. Like other suppliers, the Dexco product line also provides triblock SIS with diblock present. Dilman [47] explored adhesive properties of pure triblocks and blends of triblocks and diblocks in representative formulations containing tackifier and oil. Properties such as peel and holding power to steel, as well as SAFT to steel and fiberboard were measured. A variety of design experiments were undertaken and the results show the complexity facing the formulator even when specific adhesive properties are deemed ‘good’ or significantly more important than others. The case is made that diblock content is frequently very helpful, and if, for example, a balance of properties including high shear holding power and high peel strength is required, diblock content would be necessary. Other investigators [48] have noted the benefits of increasing the level of diblock content in similar triblock polymer formulations in a carton sealing application. Here the ability of tape to prevent carton flaps from springing open was correlated with increasing diblock level. It was not predicted by the shear holding power, which was inversely correlated with diblock level. Nevertheless, formulating with or without diblock may depend on factors that include cost, ease of processing, and tape performance. For example, replacing diblock with oil could result in a lower cost adhesive, and lower melt viscosity.

The last decade has also seen the advent of commercial SIS polymers with 15–18% styrene content, but with higher diblock content (typically 30–55%). These are available from many of the major suppliers. The higher diblock content makes them ideal for label applications where low modulus PSAs provide easy die cuttability in processing, and rapid wet out and bonding to the substrate in the label application. The shear holding power characteristic would be reduced, but this would not be a critical factor for many label applications.

7.2.3. *High styrene polymers*

During this same period several suppliers [49–51] entered the market place with somewhat lower molecular weight SIS block copolymers with styrene contents ranging from about 20 to 35%. Polymers on the low end of this styrene range can be formulated to PSAs with good tape properties, while the higher styrene levels are designed for hot-melt formulations that are air sprayable and used in disposable diaper and other disposable item manufacturing. For some of these PSA applications, more low-cost oil can be loaded into the formulation. Similarly, the high styrene hot-melt formulations may contain as little as 20–22% block copolymer, with the remainder tackifier and oil. To get air sprayability, the tackifier package may even have an aromatic–aliphatic component, since an all-aliphatic tackifier may border on incompatible at these high styrene levels. Adding even more aromatic content to the tackifier may lead to some softening of the styrene phase, but this may be required to reduce the melt viscosity for the air assisted spraying. This also leads to some reduction in high-temperature shear-holding power, an acceptable trade-off for this type of application.

7.2.4. *New radial polymers*

Until recently, most commercial radial block copolymers had been limited to styrene–butadiene polymers, although some styrene–isoprene radial polymers had been available in the United States until their manufacture was discontinued by Phillips Petroleum. Now there has been a new emphasis on radial block copolymer for use in both PSA and hot-melt adhesive development. All the major manufacturers supply them, usually as a radial with a small amount (ca. 20–30%) of added diblock or triblock for optimal compounding characteristics. Formulas b, c, and d in Fig. 5 exemplify this type of architecture. Komatsuzaki [52] points out that a radial polymer has a lower hydrodynamic volume than a corresponding linear polymer of the same molecular weight. Consequently, the melt flow viscosity will be less for the radial polymer at a given molecular weight than for a linear polymer. This again is observed experimentally [52] for radial and linear SIS. It is also well known that the zero shear viscosity of a polymer is proportional to the 3.4 power of the average molecular weight. Since shear holding power is related to zero shear viscosity one can effectively get a higher shear holding from a radial polymer with the same melt viscosity as a linear polymer (Chapter 13, Volume 1 of this series). Komatsuzaki again provides tape data on compounded block copolymer PSAs supporting this point. Finally, chain scission events, such as those that occur during high-temperature extruder processing, will have less effect on a radial polymer, since with one chain-breaking event, a four-arm star is only reduced to a still physically crosslinked three-arm star (see Fig. 5b). In contrast, a linear triblock would be reduced to a diblock,

with a corresponding considerable drop in crosslinking and shear holding power. The author supports this conclusion with GPC analysis of radial and linear SIS polymers subjected to kneading at 180°C.

The four-arm radial polymer in Fig. 5b, (SI)₄, is a 20% styrene block copolymer that is the major component (70%) in Dexco DPX-551, with the remainder SI diblock. The four-arm architecture is achieved by tipping the SI anion with a small amount of butadiene [53] before coupling with an agent like SiCl₄. Ordinary coupling reactions of the polyisoprenyl anion would lead to predominately three-arm stars due to steric hindrance. The data [54] for the compounded adhesive again support the position that higher tackifier and oil levels, and lower melt viscosities and lower melt processing temperatures, are possible relative to 3-arm star or triblock polymers. The high styrene content and added diblock polymer make this a candidate for label applications. The architecturally similar DPX-552 is a higher styrene radial (30%), designed for air sprayed disposable product applications. Like other high styrene polymers, this material may be highly diluted for spray application and still retain useful adhesive properties. Model hot-melt adhesives [55] formulated with as little as 15% polymer showed good shear holding power and very low melt viscosities.

KratonTM GRP-6919 is a radial polymer with the formula (SEB)₂(I₂) (Fig. 5c) devised by Shell Chemical [56]. The load-bearing portion of the polymer is the SEB-BES segment, while the two polyisoprene arms are intended as tackifier 'sinks'. The weight ratio of components in the polymer is 18% polystyrene, 46% polyethylenebutylene, and 36% polyisoprene. The design is intended to address some of the shortcomings of block copolymer adhesive performance in the areas of long-term aging in air, UV resistance, and heat and mechanical stability. By way of background, linear triblock polymers with the block sequence *p*-styrene-*p*-ethylenebutylene-*p*-styrene, or 'SEBS', have been available as elastomers that provide good aging and UV resistance since the 1970s. They are prepared by hydrogenating SBS triblock copolymer that has a high 1,2-vinyl addition content. The saturated rubbery midblock is inherently more stable than an isoprene or butadiene midblock, even when the latter are protected with antioxidants and UV stabilizers. For PSA applications, however, the SEBS polymer has a relatively high modulus and its non-polar character is such that when it is softened and tackified, the resulting PSA does not have good tack and peel characteristics. The GRP-6919 design is intended to keep the best of all worlds by maintaining a saturated 'working' chain of the polymer for stability, while providing the pendant polyisoprene arms to provide more polarity for tackification. Formulated PSAs of the new radial [57] polymer show it to have better tack, peel, and shear adhesion characteristics relative to SEBS PSAs. Additionally, the melt viscosity of the radial PSA is intermediate between SEBS and SIS PSA and it shows much better long-term melt stability than SIS, approaching the SEBS system.

The final radial polymer [58] recently introduced is Kraton D-KX222C, rep-

resented by the formula $(\text{SEB})_2\text{B}_2$ and is shown as structure d in Fig. 5. This polymer is intended to answer the need for block copolymer adhesives that can be crosslinked with radiation. Without actual covalent bond crosslinks, the high-temperature performance of block copolymer adhesives is limited to temperatures approaching the onset of the T_g of the hard segment. This is about 90°C for a polystyrene block. Like natural rubber adhesives, it is possible to crosslink the isoprene midblock with agents like sulfur derivatives, or oil soluble phenolic resins, but these chemical approaches cannot be implemented in a hot-melt extrusion process. While there have been past reports of block copolymer systems compounded with multifunctional acrylates [59] and photoinitiator, these UV curable formulations do not appear to be widely used. Likewise, an electron-beam curable multi-arm SI star, Kraton 1320D, is no longer available.

The KX222C architecture has a load-bearing SEB–BES segment with pendant polybutadiene arms. The polybutadiene segments have a high pendant vinyl content, which makes the polymer relatively susceptible to crosslinking with electron-beam, or UV when photocatalyzed [60]. This high vinyl content also raises the rubbery block T_g , which must be taken into account by the PSA formulator. The relatively low styrene level (18%), coupled with the pendant butadiene arms makes the polymer soft enough for PSA formulations. When tapes based on tackified formulations containing about 35% polymer were electron-beam cured (60 kGy/6 Mrad) there was little change in tack and peel, but SAFT moved from 93°C to greater than 150°C. UV curing gave similar results with photocatalyzed formulations.

7.2.5. Tackification of block copolymer PSAs

In formulating PSAs, the rubbery midblock is the phase to be tackified. With a polyisoprene rubbery phase, the situation is very much like tackifying natural rubber, so the tackifiers of choice are also similar. On a cost basis, the aliphatic C-5 resins or the hydrogenated cyclopentadiene resins are generally preferred for low styrene content block copolymers. Aliphatic resins with a low level of aromatic content would probably provide the closest compatibility with the somewhat polar polyisoprene phase, but care would have to be taken that the aromatic level is not so high as to significantly partition the tackifier into the polystyrene phase. Any significant level of partitioning would soften the hard segment and impair the shear holding power and high-temperature resistance of the adhesive. Consequently the aromatic–aliphatic tackifiers like the C5–C9 resins would ordinarily be avoided (however, see earlier comments on high styrene content block copolymer tackification in Section 7.2.3).

It is worth noting that occasionally high T_g compatible additives are incorporated into the polystyrene phase, when the PSA requires higher temperature performance. These additives are usually based on poly- α -methylstyrene,

polyphenylene oxide, or high T_g cumarone–indene resins. Recently, a more compatible, low molecular weight polyphenylene oxide resin has become available [61] for end-block reinforcement.

7.3. Acrylic PSAs

7.3.1. Introduction

Acrylics are some of the most common and most versatile materials used in the PSA industry. Although the basic monomers and some of the acrylic polymers have been known for about a century, their commercial application as pressure sensitive adhesives did not happen until after the Second World War.

Acrylic acid, the main precursor to acrylic adhesives had been synthesized in the mid 1800s and the first acrylic acid esters were made and characterized at the turn of the century [62]. The first commercial launch of acrylic polymers in the form of poly(methylmethacrylate) took place in 1927 when the German company Rohm and Haas AG introduced this new plastic to the market. Soon after, other companies such as BASF introduced acrylic dispersions.

Despite these early successes in the commercialization of acrylic polymers, no acrylic PSAs were manufactured on a larger scale until many years later. One of the primary reasons for the initial commercial failure of the acrylic PSAs was their lack of cohesive strength. Unlike the higher T_g , plastic-like polymers obtained from monomers like methylmethacrylate, polymers synthesized from alkyl acrylates typically formed sticky, cold-flowing materials with little if any utility.

A significant step towards commercial success came with a discovery in the late 1950s by E. Ulrich at 3M when he found that copolymerization of hydrogen bonding monomers, like acrylic acid with alkyl acrylates resulted in cohesively strong, yet tacky materials [63]. Since then, newer developments in such areas as polymer crosslinking, and the synthesis and copolymerization of new monomers, have led to a rapid penetration of acrylics throughout the PSA industry.

Among the different pressure sensitive adhesives, acrylates are unique because they are one of the few materials that can be synthesized to be inherently tacky. Indeed, polyvinylethers, some amorphous polyolefins, and some ethylene–vinyl acetate copolymers are the only other polymers that share this unique property. Because of the access to a wide range of commercial monomers, their relatively low cost, and their ease of polymerization, acrylates have become the dominant single component pressure sensitive adhesive materials used in the industry. Other PSAs, such as those based on natural rubber or synthetic block copolymers with rubbery midblock require compounding of the elastomer with low molecular weight additives such as tackifiers, oils, and/or plasticizers. The absence of these low molecular weight additives can have some desirable advantages, such as:

- The elimination of possible bleeding or migration of these materials.
- The increased probability of maintaining high cohesive strength at elevated temperatures because the polymer is not in a diluted state.
- A completely polymeric adhesive minimizes the risk of skin irritation or sensitization by the lower molecular weight additives.

Acrylate polymers also have fully saturated polymer backbones free of any heteroatoms in the main chain. This makes the polymers highly resistant to oxidation, photo-degradation and chemical attack. The acrylate groups are esters, which could be hydrolyzed under severe conditions. However, the hydrophobic nature of most acrylic polymers minimizes the risk for hydrolysis and, even if this reaction happened to some extent, the polymer backbone would still be intact.

Other desirable acrylate properties include the following:

- They are typically clear and non-yellowing.
- They show low allergenic response when in contact with skin.
- They can be made plasticizer and/or gasoline resistant.
- They can be breathable with high moisture vapor transmission.
- When properly formulated, they will adhere well to low surface energy substrates.

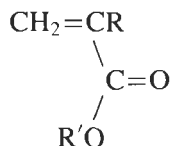
Acrylate polymerization is also relatively simple, requiring typical free-radical initiators to start the reaction and minimal, if any, heat to run the actual polymerization. This has allowed both larger chemical companies to supply these adhesives at moderate cost, and some of the larger PSA article manufacturers to make the adhesives in house for captive use. The first acrylic PSAs were polymerized in solvent but this was quickly followed by the synthesis in emulsion. Today, acrylic PSAs are available as solution, emulsion, radiation curable, and hot-melt materials. This wide range of formats also allows coating to be done using a number of methods, including processes such as knife coating, curtain coating, gravure coating, slide coating, extrusion, and the like.

The ease of synthesis and coating, the favorable economics, and the versatility of the different polymers have resulted in acrylate PSAs being utilized in a wide variety of products. Examples include graphic applications for advertising but also for decoration of vehicles, retroreflective sheeting, labels, double-coated tapes, medical electrodes, medical tapes and wound dressings, removable notes, foam attachment tapes, thermally or electrically conductive tapes, optical adhesives, transdermal drug delivery patches, repulpable splicing tapes, and the like.

As indicated above, one of the main attributes of acrylic PSAs is their broad formulation and processing latitude. While this is an important benefit to the end user, it also poses a significant challenge to the adhesive developer not only to understand what each component can do for the performance of the adhesive, but also on how to combine these components to get the best balance of properties. To help understand acrylic PSA formulation, one needs to know the major components and their impact on the PSA properties.

7.3.2. Alkyl acrylate and polar monomers

Acrylic PSAs are obtained by polymerizing acrylate monomers having the following general structure:



When R is a hydrogen atom, the monomer is referred to as an acrylate. If R is a methyl group, the monomer is called a methacrylate. The acrylate or methacrylate monomers are derived from the corresponding acrylic or methacrylic acids (where R' = hydrogen) by a simple esterification reaction with an alcohol. Although almost any alcohol can be used, primary or secondary are preferred because the tertiary alcohols yield esters with limited stability. Because of the variety of alcohols available, a wide range of (meth)acrylate monomers is also manufactured on a commercial scale. Homopolymers of these monomers are very easily obtained by free-radical polymerization. In general, acrylates yield polymers with lower glass transition temperature (T_g) and lower rubbery plateau modulus than the corresponding methacrylates. Since soft and tacky polymers are desired for PSA application, acrylate monomers are most commonly used as the main constituent of the PSA polymer.

As shown in Table 3, the glass transition temperature of the acrylate homopolymers is very much dependent on the nature of the alcohol that was used to make the acrylate ester. Typically, the T_g is the lowest when the number of carbons in the alkyl group (R' in the formula above) is about 8–12.

Note that polymethylacrylate and polyethylacrylate have glass transition temperatures, which are close to room temperature. These polymers also have fairly

Table 3
 T_g as a function of the alkyl group (R') in the acrylate

Alkyl group	Number of carbons	T_g (K)
Methyl	1	283
Ethyl	2	249
Propyl	3	236
<i>n</i> -Butyl	4	210
<i>s</i> -Butyl	4	251
2-Ethyl hexyl	8	206
Isodecyl	10	210
Isotridecyl	13	214

T_g measured by differential scanning calorimetry.

high rubbery plateau modulus values making them less useful for PSA application. Indeed, in common practice, these monomers are often used as significant components in acrylic rubbers and sealants, but only as minor components in PSA formulation.

With the exception of the monomers with long, linear alkyl groups such as octadecyl (18 carbons), most of the acrylate monomers are liquids, which makes them easy to handle. The long, linear alkyl substituted monomers are waxy solids that can be easily melted and dissolved prior to polymerization. When these monomers are copolymerized at sufficiently high levels, they may also crystallize in the polymer form resulting in tack-free acrylates. For example, stearyl acrylate copolymers rich in the linear, high alkyl acrylate have melting points slightly below skin temperature. When in contact with the human body, the crystallites melt and the polymer softens making it into a pressure sensitive adhesive. The process is completely and repeatedly reversible, requiring nothing else but cooling below the crystallization temperature of the long alkyl side chains. This crystallization causes an increase in the modulus and a loss of tack. This type of property has been used for the development of medical tapes, which are easily removed by simple chilling of the tape [64].

In general, homo- and copolymers of acrylate monomers show desirable pressure sensitive tack, but their cohesive strength is limited because of the weak interaction between polymer chains. These polymers have an inherently high entanglement molecular weight so that even the highest molecular weight materials are less entangled and less cohesive than a typical rubber. In the absence of other reinforcing mechanisms, crosslinking of the adhesive can be used to increase the cohesive strength of these alkylacrylate homo- and copolymers.

A good PSA will have a low rubbery plateau modulus to facilitate wet-out of a surface and a glassy to rubbery state transition temperature (called the T_g) within a certain range because of its significant effect on the peel behavior of the material. Whereas in rubber-based PSAs, the compounding with tackifiers and oils controls the rubbery plateau modulus and the T_g ; in the case of the inherently tacky acrylates, it is not always desirable or necessary to go by this route. Actually, the addition of these additives will dilute the polymer more, making it difficult to control cohesiveness. Consequently in the early art, combining different alkyl acrylates into the polymer backbone controlled the T_g of the PSA. However, since most alkylacrylate monomers yield polymers with low T_g , the choices were very limited leaving little room to tailor the rheology and adhesive properties of the material.

It is for this reason that the discovery by Ulrich was of significant importance to the successful development of acrylic PSAs. He found that by copolymerizing polar monomers, such as acrylic acid, one could greatly increase the cohesive strength of the polymer allowing PSA articles coated with this type of material to sustain a load without premature shear failure. These polar monomers commonly

yield high T_g polymers and they allow the adhesive formulator to adjust the rheological characteristics of the material.

Some of the more common polar monomers are:

acrylic acid:	$\text{CH}_2=\text{CH}-\text{COOH}$
acrylamide:	$\text{CH}_2=\text{CH}-\text{CONH}_2$
2-hydroxyethylacrylate:	$\text{CH}_2=\text{CH}-\text{COO}-\text{CH}_2-\text{CH}_2-\text{OH}$
acrylonitrile:	$\text{CH}_2=\text{CH}-\text{CN}$

These types of polar monomer provide sites for hydrogen bonding which increase the cohesive strength of the PSA because of strong inter-chain interaction, and they can also allow for hydrogen bonding or other polar interactions with some substrates.

The ability to incorporate a variety of polar monomers is one of the important differentiating factors between acrylics and other PSAs. Properly formulated acrylic PSAs can build strong interactions with a polar substrate by taking advantage of such properties as hydrogen bonding, acid/base interaction, or dipole/dipole interaction. By contrast, rubber-based adhesives obtain their properties mainly by controlling their bulk rheology, and little can be done to enhance their interfacial adhesion because the non-polar backbone provides at best only weak dispersive interaction with the substrate.

An example of the contribution of polar interactions between an acrylic PSA and a substrate is shown in Fig. 6. By copolymerizing iso-octylacrylate and acrylic acid, using a monomer ratio of, respectively, 95/5 and 90/10, two otherwise identical PSAs were made. The PSAs were laminated to both sides of a foam core to make an attachment tape as used in the automotive industry for the application of body side moldings to a car. One side of the foam tape was laminated against an aluminum foil backing. The other side was laminated against an automotive paint-coated panel to make the final test sample. The test sample was allowed to

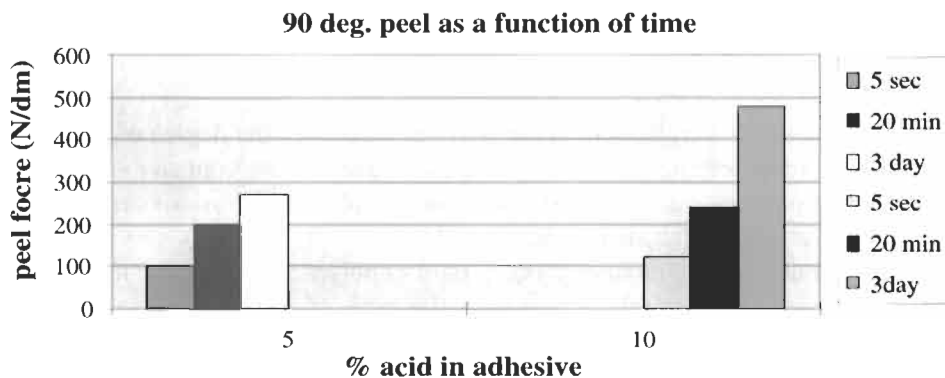


Fig. 6. 90° peel as a function of dwell time.

dwelt for different times (5 s, 20 min and 3 days) against the paint under room temperature conditions. After the specified time, the tape sample was pulled at a 90° angle and a speed of 30 cm min⁻¹ from the panel and the peel force was recorded. The adhesive always failed cleanly from the paint surface in this test, making the PSA/paint interface the weak link. In both cases, the peel force build with the dwell time but the increase was more dramatic for the PSA containing 10% acid. Although part of the peel difference can be attributed to the slightly different bulk rheology of the two PSAs, the main difference in performance results from the strong interfacial interaction between the acrylic acid groups in the adhesive and the polar functionalities in the paint surface.

One should also note that the interaction across the interface between the PSA and the paint takes time to build. Both continued wet-out of the adhesive and the interfacial rearrangements of the functional groups are contributing factors to this time delayed adhesion build.

Very similar observations can be made on other polar surfaces such as glass, metals, wall paints, paper and the like. Again strong hydrogen bonding or acid/base interactions can develop between the polar groups in the PSA and the more polar sites in the substrates. Examples of these polar sites include silanol groups (glass), melamines (common crosslinkers in paints), hydroxy groups (cellulose used in papers), urethanes (paints), acids (paints), basic oxides (for example resulting from metal oxidation), and the like. Polar groups with a high dipole moment, such as acrylonitrile may also contribute to the cohesive strength of the polymer by dipole–dipole coupling between these groups. In addition to the internal reinforcement of the adhesive, they may also add to the interfacial bond strength between the PSA and a substrate with dipolar character or easy polarizability.

One of the other benefits of incorporating polar monomers in the PSA is the enhancement in cohesive strength. This can be observed in the form of higher shear holding in a static shear test and/or better creep resistance of the adhesive when subject to a constant load.

Fig. 7 shows the effect of an increasing amount of polar monomer on static shear holding tested at room temperature in a non-crosslinked iso-octylacrylate/acrylic acid copolymer PSA.

As the amount of acrylic acid in the polymer increases, the degree of hydrogen bonding between polymer chains also increases causing the cohesive strength to improve without the need for crosslinking. Very similar observations can be made for other polar monomers, such as acrylamide.

The amount of polar monomer one would copolymerize with the alkyl acrylate monomer(s) very much depends on the type of polar monomer and the desired change in rheological properties one would like to achieve. Strong hydrogen bonding monomers, such as acrylic acid, methacrylic acid, acrylamide, or methacrylamide are typically used at levels of 12% or less of the total monomers.

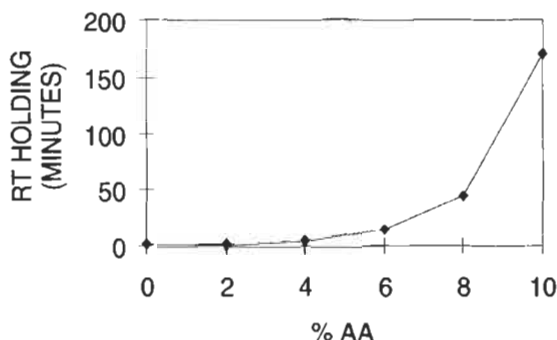


Fig. 7. Room temperature adhesive holding power as a function of acrylic acid content.

Weaker polar monomers like, vinylacetate, *N*-vinyl pyrrolidone, *N*-vinyl caprolactam or *N,N*-dimethyl acrylamide may be used at levels as high as 30–40% of the total monomers. Combinations of polar monomers [65–67] can also be used to formulate acrylic PSAs with a good balance of properties.

While polar monomers are usually beneficial in acrylic PSA formulations, there are times when their presence is deleterious. Examples of this may be the use of acrylic acid containing adhesives for electronic applications, for adhering to some metallic surfaces, or for application to paper used in books. Higher levels of acrylic acid not only increase the acidity of the PSA but they also increase the moisture uptake in the adhesive making dissociation of the acid easier. This can increase corrosion problems in the electronic or metal applications, or severe discoloration and degradation of paper with time. The latter is often a significant concern to librarians who deal with repair and archival restoration of books. In applications such as these, acid-free adhesives are more desirable, or at the very least the amount of acid has to be low and caution has to be taken to fully incorporate the monomer into the PSA.

For some applications, such as for repulpable type PSAs, it may be advantageous to incorporate high levels of acrylic acid because this makes the polymer more hydrophilic. At the same time, high levels of acid also improve the water-dispersibility of the adhesive, especially at higher pH where the acid groups are converted to the more water-soluble neutralized salt form. Since the high level of acid increases the T_g of the resulting polymer, a non-tacky material results. To make the adhesive pressure sensitive, the polymer can be softened with water-dispersible or soluble plasticizers, such as polyethers [68].

Polar monomers may also be introduced into the PSA because they provide a simple way to incorporate functional groups into the polymer backbone that are available for further chemical reaction. For example, monomers like 2-hydroxyethyl acrylate or 3-hydroxypropylacrylamide will introduce hydroxy functionality in the polymer. These hydroxy groups can be used for chemical

crosslinking of the PSA with the help of multifunctional isocyanates. Similarly, copolymerizing carboxylic or sulfonic acid monomers will yield acid functional polymers. These acid groups can be used for ionic crosslinking with multivalent metal ions or they can be used for chemical reactions such as for example the covalent crosslinking with the help of multifunctional melamine resins [69,70].

In summary, the most common acrylic PSAs in their simplest form will consist of a copolymer of the following components:

- About 60–99 parts of one or more alkyl acrylate monomer. This can also include lower levels of one or more methacrylate monomer.
- About 40–1 part of one or more polar monomer. The higher polar monomer concentrations are typically used for the less reinforcing monomers, like *N*-vinyl pyrrolidone.

7.3.3. Polymerization and coating

The monomeric components are copolymerized using free-radical mechanisms under a variety of conditions, including solution, emulsion, suspension, and bulk. Depending on the type of reaction, it may be necessary to include a solvent or water as the reaction medium, in which case the polymers are typically also coated from this medium. The type of reaction and reaction conditions will also affect the molecular weight of the polymers used for PSA application. In general, acrylic PSAs have high molecular weights with MW values (as determined by gel permeation chromatography) on the order of several 100,000 Da to perhaps a million or higher. The highest molecular weight polymers are typically obtained in emulsion polymerizations, which have the additional advantage that they can yield low viscosity materials coatable from the aqueous phase. This property and the significant environmental advantage they offer has led to the increasing displacement of the original high molecular weight, low solids solution polymers with emulsion PSAs. Another environmentally advantageous approach might be the direct polymerization of the acrylic PSA on the backing using UV curing, which allows the manufacturer to also circumvent the coating viscosity limitations while still making a high molecular weight or even crosslinked PSA. High solids solution polymers and hot melts provide another alternative to the older, solvent intensive methods. Here lower molecular weight polymers provide manageable viscosities for coating.

7.3.4. Crosslinking

7.3.4.1. Introduction. Crosslinking of the acrylic polymer can be a very important factor in formulating a PSA. As can be expected, for a given PSA composition, it is typically observed that the cohesive strength of a non-crosslinked polymer decreases with the decreasing molecular weight. This drop in performance can be

explained by the decrease in the degree of polymer chain entanglement, which together with the polar group interaction between chains is the main reinforcing mechanism for the PSA. Chain entanglement can be controlled by such factors as the chemical composition of the adhesive and its molecular weight. Selecting the right amount and type of monomer can allow the PSA formulator to optimize polar or dipole interaction. However, these specific interactions cannot always be maximized because of their effect on the T_g and modulus of the polymer, sometimes pushing both out of the window where a useful PSA can be obtained. The strength of these specific interactions is also very much dependent on factors such as temperature and the presence of moisture in the adhesive. Typically, as the temperature increases, the strength of the specific interactions decreases. Similarly, polymers reinforced by hydrogen bonding sites in their backbone, become weaker as the moisture content in the adhesive increases and the water starts to compete for interaction with these sites. Both factors may limit the performance of an acrylic PSA so it may be necessary to crosslink the polymer in order to maintain good cohesive strength at high temperature and/or high humidity. Crosslinking may result in a slight drop in tack and possibly some drop in peel adhesion, but generally crosslinking improves performance.

Crosslinking the PSA will increase the solvent resistance of the material and it will also have a significant effect on the rubbery plateau modulus of the polymer. Fig. 8 shows the effect of increasing amounts of a multifunctional aziridine crosslinker, such as CX-100 (available from AVECIA, Blackley, Manchester, UK) on the rheology of an acrylic polymer containing 10% acrylic acid. The amounts of crosslinker are based by weight on the dry weight of the PSA polymer.

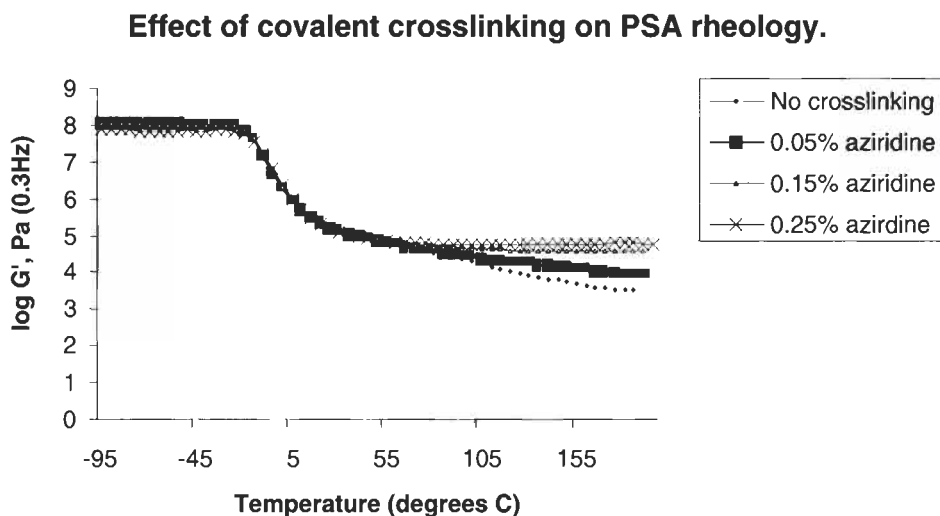


Fig. 8. Effect of covalent crosslinking on PSA rheology.

Increasing the amount of crosslinker extends the plateau modulus to higher and higher temperatures, eventually eliminating the flow of the polymer. The effect on the glass transition is minimal.

Acrylics can be crosslinked by several mechanisms including:

- Direct reaction with the polymer backbone.
- Reaction with the polar monomers.
- Reaction between crosslinking monomers already incorporated in the backbone.
- Phase-separation between incompatible polymer segments.

For this discussion, we will classify the crosslinking based on the type, which we can describe as follows:

- Covalent crosslinking between polymer chains.
- Ionic crosslinking between polymer chains.
- Physical crosslinking of the adhesive.

Covalent crosslinking results in a permanent network structure, which at or beyond the gel point makes the polymer insoluble and non-meltable. Even at crosslink densities below the gel point, coating problems may arise if the reaction starts too soon causing viscosity changes and heterogeneities in the fluid. For this reason, hot-melt or solution coating of the PSA has to be done before the covalent crosslinking process starts or proceeds too far. An exception to this is the coating of crosslinked polymer from emulsion, dispersion, or suspension polymerizations.

In these cases, the polymer remains processible in the gelled state, because it is in the form of discrete PSA particles dispersed in the reaction medium. However, once the particles are dried, redispersion may be difficult if strong interactions develop between the particle surfaces. Polymerization of the acrylic PSA directly on the substrate, as in the case of UV polymerization, can also yield a covalently crosslinked polymer that does not require any further coating steps [71].

In contrast with covalent crosslinking, ionic or physical crosslinking may be thermally reversible. This may be advantageous in cases where a polymer may have to be reprocessed after manufacturing, such as for example in hot-melt coating. The choice of ionic crosslinking agent can allow the PSA formulator to select the temperature at which the crosslinking breaks up, or the reagent may also be chosen to make a permanent ionomeric structure. Similarly, physical crosslinking can be tailored by the proper selection of the immiscible polymer segments.

Further details of each crosslinking mechanism will be discussed below.

7.3.4.2. Covalent crosslinking. Acrylic polymers can be covalently crosslinked through direct reaction between functional monomers in the polymer itself or by the addition of a crosslinking reagent, which typically reacts with the functional groups or polymer backbone in the PSA. In general, acrylic polymers are very

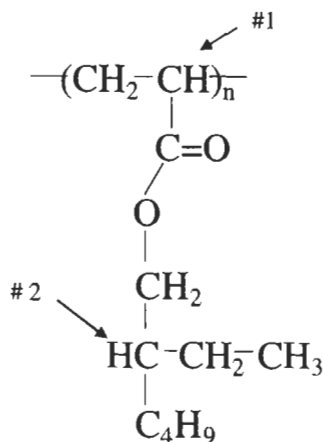


Fig. 9. Active hydrogen sites on acrylic polymer.

stable under a variety of conditions; however, a closer look at the polymer structure reveals some sites that are potentially reactive under more extreme circumstances. In the absence of functional monomers, the two most reactive sites in an acrylic polymer are the α -hydrogen (position 1) and the tertiary hydrogen (position 2) shown in the structure in Fig. 9. These two hydrogen atoms can be easily abstracted in the presence of free-radical sources such as electron-beam irradiation, or strong free-radical generators, such as peroxides. Abstraction of these hydrogens generates carbon-centered free radicals, which have long enough life times to eventually allow them to recombine with other radicals generated along the polymer backbone and create a carbon-carbon covalent bond.

Free-radical initiators, such as peroxides, may induce the hydrogen abstraction reaction [72,73]. Typically the initiator is added to the dissolved polymer and as the PSA is being dried, the coating eventually reaches a sufficiently high temperature to decompose the initiator and trigger the hydrogen abstraction reaction. Since the polymer is normally completely dry at that stage, the crosslinking reaction happens in the bulk state. An important requirement for this reaction to be successful is that the amount of free radicals generated by the initiator is sufficiently high and the energy of these free radicals is high enough to be able to abstract the active hydrogens on the polymer. In general practice, care is taken to completely consume the free-radical source during the drying step so that the crosslinked PSA is both storage and end-use stable.

Instead of using thermal energy to trigger the hydrogen abstraction mechanism, photo-induced reactions can be also be used to successfully crosslink acrylic PSAs [74-76]. In this case, photoactive compounds, such as for example those containing benzophenone, anthraquinone or triazine nuclei are compounded with the polymer or copolymerized as one of the monomers. After drying, the adhesive

coating is exposed to the proper dose and source of UV light to trigger the reaction. Typical UV sources are of high intensity, such as medium pressure mercury lamps or Fusion™ type bulbs [77]. These UV sources emit in overlapping ranges with the absorption spectrum of photochemically active compound. When the reagent absorbs the light, it reaches an energy state where it can easily abstract active hydrogens from a polymer. Similar to the peroxide triggered reaction, this may lead to free radicals along the polymer backbone which couple to form the covalent link between polymer chains.

Alternatively, the photosensitive unit may abstract active hydrogens from the polymer and through some intermediate reactions couple itself with the newly formed polymer radical to form a covalent link. If the photochemical reagent has multifunctionality or is already linked to a polymer chain, covalent crosslinking will result. An example of the latter is shown in the reaction of an acrylic polymer containing a copolymerized benzophenone compound (Fig. 10). Polymer pendant benzophenone groups are shown in the polymer drawing as BP, with the crosslinking reaction and the general chemical structure depicted for one of these groups.

Another free-radically induced crosslinking method involves the use of electron-beam irradiation [78–81]. Unlike methacrylates, acrylates tend to crosslink when exposed to this type of high-energy irradiation. To crosslink the acrylate PSA, a dried sample of the material is passed under the electron-beam unit to generate free radicals along the polymer chain by a similar hydrogen abstraction mechanism as outlined above for the peroxide cure. Typical irradiation dosages are on the order of 20–80 Kgy (2–8 Mrad), depending on the desired degree of crosslinking and the thickness of the sample. Electron beam irradiation has the benefit that it can penetrate the PSA under most conditions, even when the samples are filled, pigmented or colored. To facilitate the electron beam crosslinking reaction, acrylic polymers with pendant ethylenically unsaturated groups have also been described.

Instead of covalently crosslinking the polymer through its backbone, it is also possible to create the crosslinking through reaction with the polar groups along the polymer chain. Numerous such reactions have been described in the literature [82–85]. Most of these reactions involve the use of a multi-functional reagent for the polar groups and possibly some heat or catalyst to facilitate or trigger the crosslinking. Examples include reactions such as those between:

- Carboxylic acids and multi-functional melamines.
- Carboxylic acids or hydroxy groups with multi-functional isocyanates.
- Carboxylic acids with multifunctional aziridines.
- Carboxylic acids with multifunctional epoxides or epoxy functional monomers already incorporated in the same polymer backbone. An example of the latter would be the use of glycidyl (meth)acrylate as a comonomer with an alkyl acrylate and a carboxylic acid.
- Amides with formaldehyde or melamine reagents.

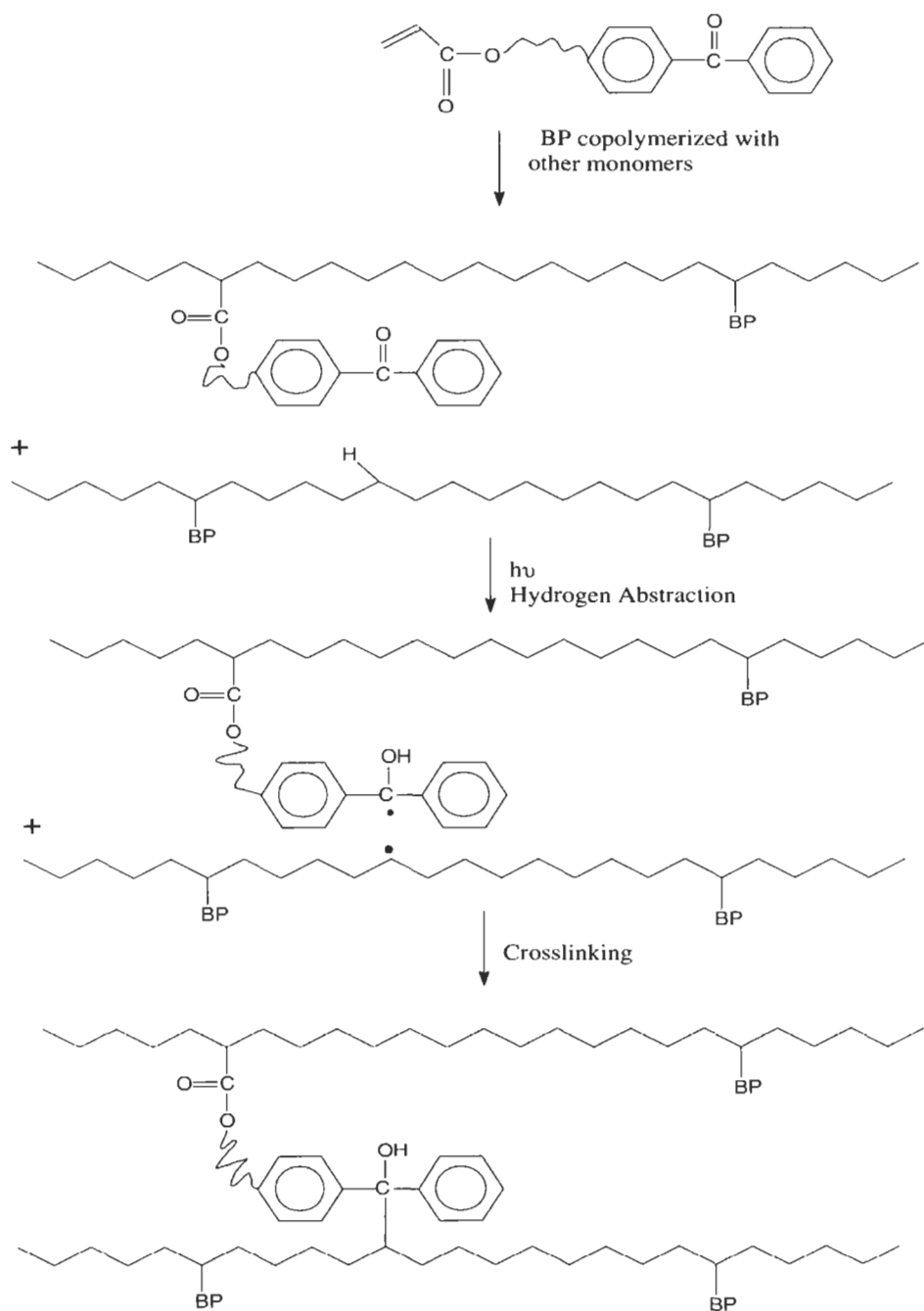


Fig. 10. Crosslinking through UV-mediated hydrogen abstraction.

Other crosslinking reactions may be triggered by a catalyzed reaction between different units of a copolymerized functional monomer, such as *N*-methylol acrylamide or a copolymerized silane compound [86].

It may also be possible to crosslink the acrylic PSA with the help of multifunctional acrylates or methacrylates [87]. These monomers can simply be copolymerized with the balance of the other monomers to form a covalently crosslinked network in one step. Since the resulting polymer is no longer soluble, this type of crosslinking is typically limited to bulk reactions carried out as an adhesive coating directly on the article or in emulsion polymerizations where the crosslinked particles can be dried to a PSA film.

One of the main challenges in the covalent and other types of crosslinking of acrylic PSAs is to maintain the balance between cohesive strength and peel/tack of the product. Unlike acrylics used in paints, pressure sensitive adhesives cannot be crosslinked too much or the properties may be lost. In the absence of any crosslinking the polymer may be relatively weak, but also aggressively tacky. As crosslinking increases, solvent resistance improves, cohesive strength and tensile properties improve, and elongation slowly diminishes. By the same token, the uncrosslinked polymer may have a significant viscous flow component, but as the crosslinking increases, the elastic nature of the material becomes more significant. This change in crosslink density will also be reflected in the shear holding power of the PSA. For instance, in the uncrosslinked state the PSA typically fails cohesively, leaving residue on both the test panel and the tape backing. As the crosslink density increases, failure becomes more adhesive (no residue left on the test panel) maximizing the holding power of the adhesive. As one continues to add crosslinker, the polymer slowly loses its viscoelastic character, the holding power drops and the adhesion properties will eventually no longer be present.

7.3.4.3. Ionic crosslinking. Ionic crosslinking can be used with acrylic polymers containing copolymerizable acid groups, such as those derived from carboxylic, phosphonic or sulfonic acid type monomers. These acids groups can be crosslinked with the help of multivalent metal ions, such as those based on zinc, chromium, titanium, zirconium, aluminum, and the like [88–90]. Some ionic bonds, such as zinc carboxylates, may be susceptible to heat, allowing the crosslinking reaction to be reversed and the polymer to be melt-processed [91,92].

Typically, the metal ions are not introduced in the unprotected form because the polymer may start to gel prematurely, making coating difficult, if not impossible. Instead, the metal ions are introduced in the form of salts such as zirconium acetate, or in the form of a chelate or an ortho ester, such as aluminum acetylacetonate or an ortho-alkyl titanate. As the polymer dries during coating, the metal ion is slowly liberated and the crosslinking reaction will start. Since the metal ion is diffusion limited, it may take several hours or days before the crosslinking reaches completion.

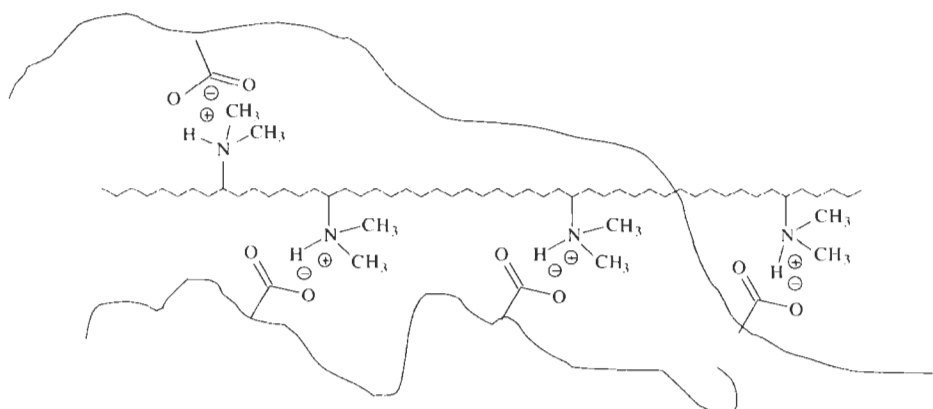
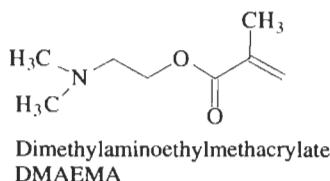


Fig. 11. Acid/base ionic crosslinking.

Multifunctional amines, either in small molecule or polymeric form may also be used for crosslinking with acid groups [93]. In the case of repulpable adhesives, it may be advantageous to use this type of crosslinking because the acid/base salts facilitate the dispersing of the adhesive in water. An example of a polymeric ionic crosslinking reaction is shown in Fig. 11 as the interaction between a carboxylic acid containing adhesive and a crosslinking polymer having *N,N*-dimethyl aminoethyl methacrylate units.

The acid/base interaction between the two polymers significantly increases the cohesive strength of the polymer blend at normal use temperatures but at elevated temperature the interaction can be interrupted and the polymer can still be melt processed. Other examples of basic polymers use for crosslinking include polyethylenimines, vinyl pyridine copolymers, and the like.

7.3.4.4. Physical crosslinking. Another method of crosslinking a PSA relies on the phase separation of high T_g , glassy polymer segments from low T_g , rubbery segments. The high T_g segments are typically the minor, discontinuous phase, which associates in crosslinking domains. The low T_g segments are typically the major phase and they form the continuous rubbery part of the polymer. If the rheology of the rubbery phase meets the Dahlquist criterion for tack, these types of materials can indeed act as crosslinked, pressure sensitive adhesives.

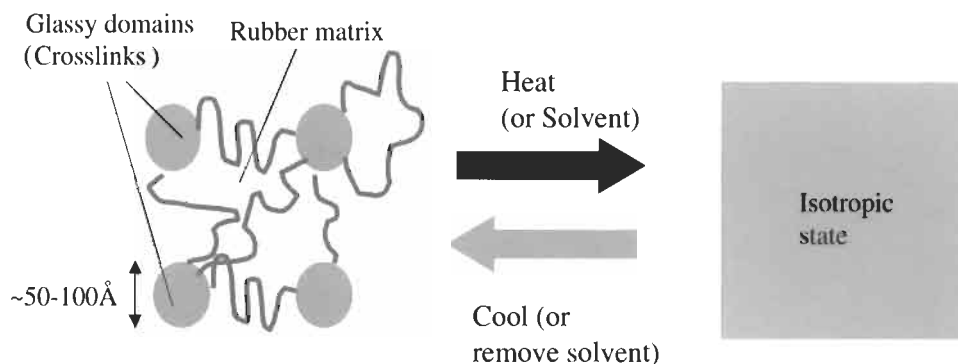


Fig. 12. Physical crosslinking in a phase separated polymer.

As long as the polymer temperature remains below the T_g of the glassy domains, the physical crosslinking will significantly increase the cohesive strength of the PSA. However, once the PSA temperature is near or exceeds the T_g of the glassy domains, the crosslinking phases slowly lose their reinforcing character and the cohesive strength of the PSA will start to suffer. At sufficiently high temperatures, the phase segregation between the glassy and rubbery domains may disappear and the organized, physically crosslinked structure may be lost. Once the polymer reaches this isotropic state, the PSA will lose its cohesive strength and the material becomes flowable, making melt processing possible. Solvent can also be used to dissolve the whole polymer which upon drying phase separates to form the physically crosslinked PSA. Fig. 12 demonstrates this reversible form of crosslinking.

This type of physical crosslinking is well-known in the form of block copolymer PSAs, such as those based on rubbery ABA triblocks, wherein A is a high T_g block, such as polystyrene, and B is a low T_g block, such as polybutadiene or polyisoprene. These types of block copolymers are commonly synthesized using anionic polymerization mechanisms. Unfortunately, until recently, anionic polymerization of (meth)acrylic monomers has been impossible and other living or controlled polymerization methods were unknown. With the development of new polymerization techniques, such as those using atom-transfer polymerization (ATRP), anionic polymerization, TEMPO mediated reactions, or radical addition-fragmentation (RAFT), block copolymers with acrylic segments have been disclosed in the literature. These new block copolymers are claimed to be good elastomers with potential utility in adhesives [94–97].

Earlier, successful attempts at physically crosslinking acrylic PSAs have been disclosed in the work of Husman et al. [98], Mancinelli and colleagues [99,100] and others. Instead of making ABA type structures, these authors studied and developed the use of high T_g macromers in acrylic copolymers. Macromers are

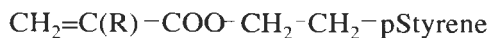


Fig. 13. Polystyrene macromer.

nothing else but lower molecular weight polymers (typical MW values on the order of a few thousand to about 20,000 Da) with a copolymerizable group on one end of the macromolecule. By copolymerizing these macromers with other acrylic monomers, comb-like structures or graft copolymers result. The macromers chosen for this type of reaction were typically high in T_g and immiscible with the rest of the polymer once it had been dried. Very similar to the block copolymers, phase segregation of the high T_g , grafted polymer segments into glassy domains provided for physical crosslinking and cohesive reinforcement of the PSA. The rest of the polymer formed the continuous, rubbery phase, which also gave the material its tack and adhesion properties.

The morphology of the dried, or hot-melt-coated adhesive looks essentially the same as pictured above for the block copolymers. Instead of having high T_g blocks on both ends of the rubbery part of the polymer, now we have high T_g polymer pendant from the rubbery acrylic polymer backbone. As long as the acrylic polymer chain has at least one high T_g graft, it can be attached to the network. Those chains having at least two grafts per backbone will form the physical network.

Common examples of the high T_g macromers are based on polystyrene or polymethylmethacrylate (PMMA) polymers of sufficiently high molecular weight to have a high T_g (typically on the order of 70–100°C as measured by differential scanning calorimetry) and also to make them immiscible with the acrylic polymer backbone once the solvent or heat has been removed. Typical molecular weight of the polystyrene or PMMA macromers is on the order of 5000–10,000 Da. Their generic structure can be pictured as in Fig. 13 (shown there for polystyrene).

A copolymerizable group, such as an acrylate ($\text{R} = \text{H}$) or methacrylate ($\text{R} = \text{methyl}$), on one end of the molecule, and the high T_g polymer on the other end characterize the macromer. A chemically inert group, such as oxyethylene may be present to connect the two parts of the macromer. Macromers have been synthesized by different methods and some are commercially available.

7.3.5. Tackification and plasticization

Acrylic polymers have the advantage that they can be formulated to be inherently tacky. However, for certain applications it may be desirable to adjust the rheological properties of the PSA beyond what can be obtained by selecting the right polymer composition and crosslink density.

Examples where the acrylic polymer may be compounded with tackifiers or plasticizers include:

- Repulpable adhesives.
- PSAs for low surface energy plastics.
- Plasticizer resistant PSAs.
- Drug-delivery patches.
- Low-temperature applicable PSAs.

Plasticizers and tackifiers are lower molecular weight additives that are at least partially miscible with the acrylic polymer. Both act as a permanent diluent for the polymer decreasing the entanglement and rubbery plateau modulus of the material. Tackifiers are glassy materials, which have softening points above the glass transition temperature of the acrylic polymer. As a result, the addition of a tackifier typically increases the glass transition of the compounded PSA, while at the same time decreasing its rubbery plateau modulus. Unlike tackifiers, plasticizers typically have very low softening points. Therefore, compounding of plasticizers with an acrylic polymer typically results in a blended polymer with both a reduced T_g and reduced rubbery plateau modulus value versus the neat starting polymer.

Lowering of the rubbery plateau modulus increases the compliance of the polymer making faster wet-out of a substrate possible. As a result, the PSAs show more aggressive tack properties. Provided the surface energy of the substrate allows for complete polymer wetting, a PSA with improved quick-stick and faster adhesion build will be obtained.

The change in rheological behavior will also be reflected in the peel performance of the PSA. Depending on the performance of the starting polymer, peel can either be increased or decreased. For example, repulpable polymers may be too high in T_g and modulus to be pressure sensitive. The addition of a plasticizer to this polymer allows the PSA formulator to soften the polymer to the point where it becomes aggressively tacky making bonding to paper possible, for example as a splicing tape.

In some cases, plasticization of a PSA may be detrimental to its performance. A well-known example is the deterioration of the performance of an adhesive applied to plasticized PVC. Migration of the plasticizer from the flexible vinyl into the PSA often softens the adhesive to the point where it fails cohesively from the vinyl, leaving sticky residue behind during removal of the adhesive-coated article from the substrate. One way to address this detrimental effect of plasticizer migration is to formulate an already plasticized PSA, perhaps because a better balance exists between the plasticizer in the PVC substrate and the PSA in contact with it [101].

The presence of these low molecular weight tackifiers and plasticizers may also have other negative effects on the PSA performance. For example, the reduced entanglement of the polymer typically reduces the cohesive strength of the PSA, although crosslinking may be used to compensate for this loss in property. Plasticizers and tackifiers may also be susceptible to migration and/or oxidation, both

of which can change the PSA properties with time. Careful selection of the type and amount of these additives is indeed necessary to insure stable PSA properties.

Since most acrylic polymers for PSA use are synthesized with the adhesive properties already in mind, the rheologically modifying additives are typically used for performance fine-tuning only. For this reason, the amounts of tackifier or plasticizer needed in acrylic PSA formulation are normally lower than those used for rubber PSA compounding. Indeed, for rubber-based PSAs, the amount of additive used is often 100 parts by weight or more based on 100 parts by weight of the polymer. For acrylic PSAs this amount is seldom used, with tackifier and/or plasticizer levels of about 5–60 parts by weight being the most common.

As pointed out earlier, acrylics differ from the commonly used rubber precursors for PSA formulation in the fact that they often incorporate polar monomers, such as acrylic acid, *N*-vinyl pyrrolidone, vinyl acetate, or acrylamide. As a result, the solubility parameters of acrylic polymers are typically higher than those of rubbers, like polyisoprenes or polybutadienes.

The increased polarity of the acrylic polymers puts more stringent requirements on the properties of the tackifiers or plasticizers that can be used. The very low polarity additives commonly found in rubber based PSAs are not useful in most acrylic PSA formulations. For example, materials like paraffin waxes, mineral oils, and synthetic hydrocarbon tackifiers have little or no value in most acrylic PSAs.

Tackifiers based on rosin feedstock, tall oil, or terpenes are typically much more polar than synthetic hydrocarbon-based tackifiers, which makes them the most widely used in acrylic PSA formulation. These tackifiers are typically high in color, which can cause the otherwise clear acrylic PSAs to become colored as well. Some of the early commercial tackifiers were also vulnerable to oxidation, making the compounded acrylic PSA also less durable. Fortunately, the tackifier industry has addressed this shortcoming by providing tackifiers with significantly reduced color and improved aging stability. This has been achieved by purification of the tackifier feedstock, hydrogenation of the final product, the use of stabilizer packages, and the like.

Rosin and tall oil-based tackifiers are derived from feedstock, which is typically obtained by extraction and distillation of the materials from shredded tree stumps or wood chips. A typical structure of one of the different products obtained through this process is this abietic acid structure shown in Fig. 14 as a representative of the rosin acid family.

This type of raw material can be chemically modified to make a variety of rosin derivatives having different degrees of compatibility and softening points. Common chemical reactions include:

- Esterification of the acid groups with alcohols like glycerol or pentaerythritol.
- Hydrogenation of the conjugated C=C bonds to increase oxidative stability and reduce color.
- Condensation into dimers to change solubility and softening points.

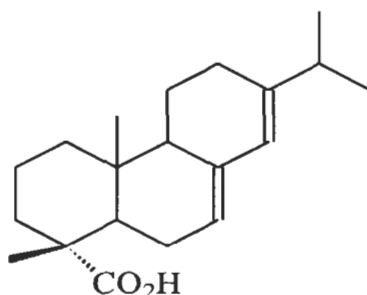


Fig. 14. Abietic acid.

Rosin and its derivatives have shown wide compatibility with a broad range of acrylics and other PSA polymer precursors. This property has made them one of the most common tackifiers in the industry.

The other class of acrylic compatible tackifiers includes those based on terpenes. Terpenes are monomers obtained by wood extraction or directly from pine tree sap. To make the polyterpene tackifiers, the monomers have to be polymerized under cationic conditions, typically with Lewis acid catalysis. To adjust properties such as solubility parameter and softening point, other materials such as styrene, phenol, limonene (derived from citrus peels), and others may be copolymerized with the terpenes.

Common rosin and polyterpene tackifiers typically are fairly low in molecular weight (commonly in the neighborhood of 1000–2000 Da) and they have softening points in the range of 60–120°C.

Plasticizers used in acrylic adhesives can be selected from many different classes, including polyethers, phenol modified polyethers, phthalates and the like. The higher polarity of these plasticizers and their low molecular weight favors miscibility with acrylate PSAs. However, their low molecular weight and low softening point can also make them very migratory. As indicated earlier, this may be a concern if one is applying acrylic PSAs against surfaces that contain these types of plasticizers, such as PVC canvasses and awnings. In these cases, special care has to be taken to prevent the plasticizers from migrating, something that has been addressed by using polymeric plasticizers in the vinyl.

The PSA formulator can also take advantage of plasticizers. For example, polyether-based plasticizers have both good low-temperature flexibility and good hydrophilicity. Using these properties, acrylic PSAs have been formulated with these types of plasticizers to obtain high adhesion to food packages stored under refrigerated conditions [102]. Similarly, polyether plasticized acrylics have been used to make repulpable PSAs [103].

Perhaps a more specialized case of using plasticizers in acrylic formulations can be found in drug delivery patches. Here, plasticizing additives called excipients

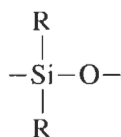
are compounded with the acrylic polymer to help solubilize the drugs and to facilitate their penetration through the skin barrier [104]. These excipients are typically fatty acid esters, such as oleates and myristates. Due to their high solubility in the acrylic matrix and their low softening points, esters like these also have a plasticizing effect on the adhesive for which the PSA formulator has to compensate.

Similar to the tackifiers discussed earlier, plasticizers have a very dramatic softening effect on the rubbery plateau modulus of the PSA. For this reason, high levels of plasticizers have to be avoided to maintain good cohesive strength in the adhesive, especially at elevated temperatures. Indeed, if high cohesive strength is desired, the amount of plasticizer used in a PSA is typically kept to a minimum, if used at all.

A unique case of plasticizing a polymer to make a PSA is the recent development of semi-structural adhesives. These new materials behave like pressure sensitive adhesives but when triggered with heat or UV light, they cure to semi-structural properties [105,106]. As such, they combine the simple handling of a PSA in the form of a tape or coated article with the high bond strength of curing, liquid systems. A typical example of this type of semi-structural adhesive is the combination of epoxy monomers with an acrylic polymer. To make these types of adhesives, the acrylic monomers and the epoxies are mixed together with initiators that can independently activate the polymerization of each component. In this case, the acrylic polymer may be polymerized with heat or UV irradiation, leaving the epoxies in their uncured stated as a plasticizer for the formulation. If desired, epoxy monomers can also be compounded with an already existing acrylic polymer and an initiator for the epoxy. In a secondary step, the epoxy monomer cure is triggered, typically just prior or after application of the PSA to a substrate. Dependent on the desired cure mechanism, the epoxy will be compounded with a thermal or UV initiator. Once the epoxies polymerize, the PSA character of the material is lost and semi-structural to structural bond strength is obtained.

7.4. Silicone PSAs

Silicones are probably best known for their application as sealants and as release materials for pressure sensitive adhesives [107]. The silicone polymer combines an inorganic backbone made from silicon–oxygen bonds with organic substitution on the silicon atom. This repeating unit, shown below is called a siloxane.



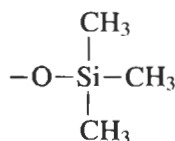
where R = alkyl, aryl, alkenyl, etc.

The most common silicones have either dimethyl substitution on each of the silicon atoms (called polydimethylsiloxanes) or they combine repeating units, one having dimethyl, the other having diphenyl substitution on the silicon (called polydimethyldiphenylsiloxanes). Other siloxane substitutions, such a combination of one vinyl group and one methyl group, or one phenyl and one methyl group, also exist. The bulkier diphenyl siloxane unit can be used to replace up to 12–15 mol% of the dimethylsiloxane in the polymer backbone with higher substitution resulting in a higher T_g for the polymer. Despite this increase in T_g , this substitution imparts better low-temperature performance to the polymer because the larger group prevents crystallization of the backbone at about -40°C , typical for pure polydimethylsiloxanes.

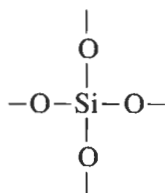
The unique properties of silicones are derived from the high flexibility and rotational freedom of the $-\text{Si}-\text{O}-$ bond. This bond is also very oxidatively stable leaving only its substituents vulnerable to degradation at higher temperatures. As a result of the highly flexible backbone, silicones show a very low glass transition temperature of about -120°C , a high free-volume allowing vapors to very readily permeate through the polymer, and a low modulus. Silicones also are known for their low surface energy characteristics resulting from the surface-active nature of the methyl groups. This low surface energy property greatly facilitates wetting of a surface they come in contact with, making bonding possible to difficult to adhere to surfaces, like silicone rubbers, wet substrates, polyolefins and some fluoropolymers.

The low modulus and desirable wetting properties of the silicones make them very attractive candidates for PSA formulation; however, the high material cost has limited their use to specialized applications. A typical silicone PSA is made from a silicone polymer (the gum) with a molecular weight of 100,000–500,000 Da and a specialized tackifying resin (MQ resin). The gum is typically derived from the ring-opening reaction of the cyclic dimethylsiloxane tetramer (called D_4), yielding a silanol ($-\text{Si}-\text{OH}$) terminated polymer. The tackifying resins are glassy materials made from two main repeating units: the tetrafunctional group also known as Q and the monofunctional trimethylsilyloxy group known as M. In addition to these two main parts, the MQ resin may also contain about 2% of a silanol group [108]. The structure of the M and Q resin parts is shown below:

M unit:



Q unit:



As a model would show, inter-connecting several of the M and Q units with

an occasional silanol functional end group makes the MQ resin a very rigid molecule with methyl groups and, if present, a few silanol groups exposed at its surface. Typical MQ resins would have molecular weights of several thousands with variations possible in the M to Q ratio, the absolute molecular weight, and the amount of silanol functionality. The very rigid MQ molecules do not melt without degrading first. This characteristic and the hybrid inorganic/organic nature of the material make it very different from the organic tackifiers used in the formulation of hydrocarbon PSAs.

Typically, to prepare the PSAs, the gum and MQ tackifier are dissolved in a common solvent such as toluene. In a so-called bodying step, this solvent mixture is commonly processed in such a way as to facilitate some condensation between the silanol groups of the gum and the resin. This condensation results in some chain-extension of the gum and some of the MQ resin becoming covalently attached to the siloxane backbone. To increase solvent resistance and cohesive strength of the PSA, crosslinking between polymer chains is introduced. To crosslink the silicone PSAs they are commonly coated and dried in the presence of organic peroxides at temperatures in excess of 130°C. The peroxide radicals can abstract hydrogens from the dimethylsiloxane units leaving methylene radicals available for crosslinking with radicals formed on different polymer backbones. As such, a typical silicone PSA is a covalently crosslinked network of siloxane polymer with some of the MQ tackifier covalently attached to it as a result of the bodying step. These typical silicones are coated from solvents at 30–50% solids level. Some of the major shortcomings of these peroxide cured silicones is their high solvent content and the need to run the drying ovens at high temperature to trigger the peroxide reaction, making coating on heat-sensitive substrates difficult, if not impossible.

Newer silicone adhesives having solids levels up to 97% are also commercially available [109]. Instead of using silanol condensation reactions, they rely on addition chemistry between vinyl functional silicone oligomers and silicon hydride terminated silicones. This addition reaction is typically facilitated with platinum derived catalysts. This hydrosilation process can be run at reduced oven temperatures, but the finished products typically do not yield the same balance of properties as seen for condensation cure materials.

Instead of these covalently crosslinked silicones, the industry has also explored the use of physically crosslinked silicone materials. One such example is the chain-extension of α,ω -bis (aminopropyl) polydimethylsiloxanes with diisocyanates to make a chain-extended silicone with the urea groups providing the physical crosslinking [110]. These elastomers can also be tackified with MQ resins to make a silicone PSA, which maintains some of the desirable properties of a conventional silicone. However, the introduction of an organic urea group limits the high-temperature service temperature of the polymer due to the break-up of the physical crosslinking and eventual degradation of the organic polymer segment.

The rheological characteristics of the adhesives with an all siloxane backbone depend on such factors as the type of MQ resin used, the molecular weight and type of the gum, the ratio of the gum to the tackifier, the degree of 'bodying', and the degree of crosslinking. Perhaps the most significant variable is the tackifier to gum ratio. For conventional silicone PSAs (those based on gum and resin) increasing tackifier loadings typically result in better shear holding power and higher temperature performance. Peel resistance and tack also increase to a certain level, but they abruptly drop at too high a MQ loading. The tack of many silicone PSAs is rather low, resulting in a 'dry' feel. Most commercial silicone PSAs will have 50–60 wt% MQ resin, the balance being the gum. At higher MQ loadings, the pressure sensitive tack of the adhesive is lost.

Continued speculation exists about the exact interaction of the MQ tackifier with the polysiloxane gum. Dynamic mechanical thermal analysis of a typical silicone PSA commonly shows two major transitions: a T_g at low temperatures close to that of the pure gum, and a second T_g at higher temperature. Increasing tackifier loadings have little effect on the first transition but, as shown in Fig. 15, they shift the second transition to increasingly higher temperature [111]. By using

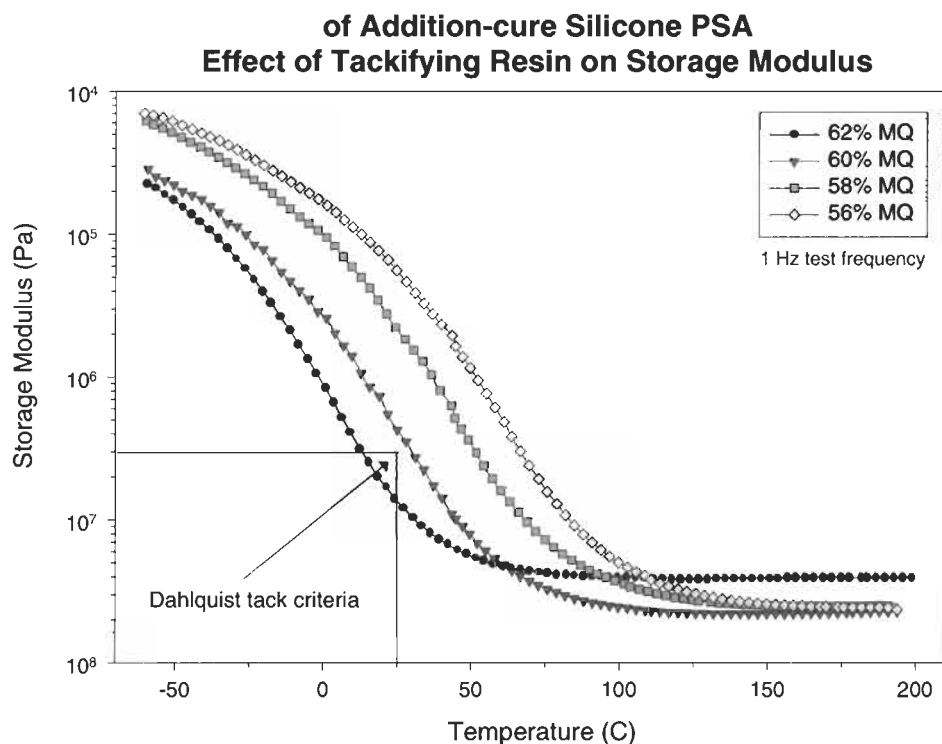


Fig. 15. Effect of tackifying resin on storage modulus of addition-cured silicone PSA.

the Dahlquist criteria for pressure sensitive adhesive tack, it becomes clear that at MQ loadings near or above 60 wt%, the formulated adhesive becomes very dry to tack-free. However, it may still show some peel after prolonged dwelling on the substrate.

It has been suggested that this rheological behavior is the result of a two-phase morphology with the lowest transition corresponding to the silicone polymer having little or no MQ dissolved in it (gum rich phase), and the second transition resulting from a resin rich phase [112,113]. A recent study suggests that the MQ resin actually forms as thermodynamically stable solid state solution with the polysiloxane backbone [114]. As expected, the interaction between the silicone polymer and the MQ resin is also dependent on the type of silicone and type of resin used. For example, it has been shown that the amount of diphenylsiloxane in the polymer backbone also influences the amount of MQ resin that can be retained in the resin-rich phase [115]. Similarly, it was found that the glass transition and molecular weight of the MQ resin could have significant effects on the peel and tack of the formulated adhesives.

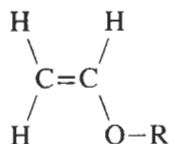
One of the important breakthroughs in the silicone PSA industry has been the development of new release liners based on fluorosilicones [116]. These new materials significantly improve the release characteristics of the silicone PSAs, something that has been difficult to achieve because of the high adhesion silicone PSAs show to low energy substrates, including silicone rubbers and liners.

The suppliers typically offer coater-ready adhesives thus leaving little freedom for formulation and performance adjustment by the end user. However, they have also developed a significant knowledge basis, which has allowed them to make silicones into a very versatile, yet specialized class of PSAs.

7.5. Other PSAs

Besides the higher volume pressure sensitive adhesives discussed above, the industry also uses other synthetic elastomers as the base component for PSA formulation. Most of these elastomers require some form of tackification to make the materials tacky. However, a few materials are low enough in T_g and sufficiently compliant to be useful without requiring compounding with tackifiers.

One class of materials with some inherent PSA properties includes *polyvinyl-ethers*. Vinyl ether monomers are industrially derived from the reaction of acetylene with alcohols [117]. The most common alcohols used are methanol, ethanol or isobutanol. A generic structure of the vinyl ether is shown below:



The monomers derived from these alcohols are cationically polymerized yielding products ranging from viscous, tacky oils for the lowest molecular weight materials to tacky rubbers for the higher molecular weight versions. All have glass transition temperatures below 0°C. The monomers can also be copolymerized with acrylic monomers using free-radically initiated reactions. Polyvinylethers are susceptible to oxidation, which results in discoloration and degradation of the mechanical properties. To avoid this problem, commercial PSAs are typically compounded with anti-oxidants. Polyvinylethers are also often mixed with other polyvinylethers or other elastomers, such as acrylates, to obtain the desired PSA properties. Commercial applications of polyvinyl ethers include labels, medical tapes, and some sheeting products.

Another class of elastomers, which includes some inherently tacky materials, is the so-called *polyalphaolefins* [118]. These materials are derived from monomers such as propylene, 1-hexene and 1-octene. Homopolymers of the higher alkene monomers (i.e. those having six to eight carbons) are more or less tacky dependent on the molecular weight of the polymer. Copolymers of the higher olefins with propylene are typically rubbery and they require tackification to make them into pressure sensitive materials. These polymers have a fully saturated polymer backbone, which makes them oxidatively more stable than PSAs derived from polyisoprene or polybutadiene. Common tackifiers include those based on hydrocarbon monomers also known as aliphatic or aromatic petroleum feedstock. These tackifiers are often hydrogenated to make them more stable and lighter in color. Since they are all hydrocarbon, the surface energy of these adhesives is low allowing them to wet and adhere to other low surface energy substrates. In order to increase cohesive strength of the adhesive, covalent crosslinking using photoactive groups or moisture curing silanes incorporated in the polymer backbone has been reported [119,120].

Other polymers used in the PSA industry include synthetic polyisoprenes and polybutadienes, styrene-butadiene rubbers, butadiene-acrylonitrile rubbers, polychloroprenes, and some polyisobutylenes. With the exception of pure polyisobutylenes, these polymer backbones retain some unsaturation, which makes them susceptible to oxidation and UV degradation. The rubbers require compounding with tackifiers and, if desired, plasticizers or oils to make them tacky. To improve performance and to make them more processible, diene-based polymers are typically compounded with additional stabilizers, chemical crosslinkers, and solvents for coating. Emulsion polymerized *styrene butadiene rubbers* (SBRs) are a common basis for PSA formulation [121]. The tackified SBR PSAs show improved cohesive strength as the Mooney viscosity and percent bound styrene in the rubber increases. The peel performance typically is best with 24–40% bound styrene in the rubber. To increase adhesion to polar surfaces, carboxylated SBRs have been used for PSA formulation. Blends of SBR and natural rubber are commonly used to improve long-term stability of the adhesives.

If *polychloroprene* is the base polymer for the adhesive, special grades have to be selected to avoid detackification of the PSA with time due to the strong tendency of the polymer to crystallize. When properly blended a mixture of *polyisobutylenes* can be inherently tacky; however, in many cases compounding with tackifiers is preferred. To allow for easier curing, polyisobutylenes commonly contain a small amount of isoprene. As a low surface energy polymer free of polar groups, PSAs derived from this material adhere well to a variety of surfaces without building significant adhesion with time. This property has made these types of adhesive useful in medical, transdermal, label, and recently automotive transit tape type applications [122,123]. A more specialized class of PSAs has also been derived from polymers having a high affinity for moisture. For example, homo- and copolymers derived from *N*-vinyl-pyrrolidone have been formulated with water, plasticizers and other additives to make glue sticks, splicing tapes for the paper industry and sticky adhesives or gels for medical use. Copolymers of water soluble monomers with hydrophilic macromers have also been described as adhesives for moist skin environments [124].

8. PSA applications

8.1. Introduction

Because of their ease of use and their cost-effectiveness relative to other methods of assembly, pressure sensitive adhesives continue to penetrate all kinds of industrial applications. Some of the main reasons PSAs and PSA coated articles are prime candidates for industrial applications include the following:

- Ready to use, simply requiring pressure to make the bond.
- Typically already coated, providing for uniform thickness.
- Can bond dissimilar materials together without special preparations or substrate incompatibility concerns.
- Provide damping and help accommodate differences in thermal expansion coefficient of the substrates.
- Allow for clean application without the need for specialty dispensing equipment or special cure/drying cycles.
- Aesthetically more pleasing than screws and bolts, while also introducing less localized stress on the substrates.
- Can seal out dust, moisture and environmental contaminants.

Pressure sensitive adhesives can be coated on a substrate such as a polyester or paper backing to make a tape or label, or on a release liner to make a transfer adhesive, or a special substrate to make a graphic film or retro-reflective sheeting product. In some cases, where precision placement of the PSA is required, one may also coat directly on the substrate using techniques such as screen-printing.

When a PSA is coated on a flexible substrate, such as a film, a cloth, a non-woven or paper backing, the flexibility and elongational characteristics of this substrate will have an impact on the adhesion performance of the total construction. For example, a thick foam-like backing can significantly boost the adhesion to a substrate without necessarily requiring a thicker PSA coating. In addition to the impact on the peel mechanics of a given construction, the backing may also protect the PSA from UV exposure or fluids that can solvate the PSA. For these reasons, the PSA selection will have to be made in view of the performance requirements of the construction as a whole.

8.2. Single- and double-coated industrial tapes

8.2.1. General overview

Some of the biggest applications for PSAs include single and double-coated tapes, where the adhesive is applied to, respectively, one or both sides of a backing. The backing materials include polymeric films, papers, woven and non-woven substrates, metal foils, foams and the like. These backings are often chemically primed, corona-treated and/or physically altered to insure permanent bonding of the PSA to the substrate. In the case of single-coated tapes, the substrate is often treated on its non-PSA-coated side with a coating providing release from the PSA, making unwinding of a roll of tape possible. For double-coated tapes, a release liner is often inserted to facilitate unwinding of a roll of material. Double-coated tapes offer the possibility to coat dissimilar adhesives on both sides of the backing. In doing so, tapes can be made with different performance characteristics on each side of the backing. For example tapes combining such properties as permanency/removability, or high tack/low tack are easy to manufacture using this construction. The backing in double sided tape may also facilitate handling and dispensing of the tape, or it can provide barrier properties effectively eliminating migration of materials, such as moisture or plasticizers from one substrate to the other.

Both types of tapes have found broad applicability throughout the industry. Some of the major uses for single-coated tapes include packaging, masking, electrical, office and medical related applications. Double-coated tapes are quite commonly used in assembly type of operations.

8.2.2. Packaging and masking tapes

The largest volume use for PSA coated backings is packaging related. Packaging tapes are applied in the assembly of cardboard boxes, for sealing packages, for securing boxes on a shipping pallet, for extra protection of shipping labels, or for the protection of surfaces susceptible to scratching during shipment. A more

specialized use for packaging tapes may be for sealing food packages or metal juice cans. These applications require that the PSA be approved for food contact.

Depending on the desired strength of the tape, different backings can be used. These backings include polyester, which has high tear strength and high puncture resistance, vinyl, papers, filament reinforced backings and some fabrics. For sealing applications, such as the tabs for juice cans, aluminum foils are used. Due to its low-cost, biaxially oriented polypropylene is the most popular backing in the packaging tape industry. It is commonly used for cardboard box closures, label protection and securing of stacked boxes. Light-duty polypropylene is typically manufactured using a blowing tower process. Heavy-duty polypropylene is extruded as a thick film and oriented in a so-called tentering operation to improve the strength of the product.

To construct packaging tapes, these films are typically coated with block copolymer PSAs using a solvent or hot-melt casting process. These adhesives provide high shear holding power, high tack, and good cardboard fiber pull resulting in substrate failure at high peel force. The tackified polystyrene–polydiene–polystyrene block copolymers are known to adhere well to polyolefins; so simple corona treatment of the backings is sufficient to provide permanent anchorage of the adhesive to the backing. For the same reasons, the face side of the tape is typically coated with a release coating for the adhesive in order to facilitate unwind of the tape. Note that these release coatings often have additional functions, such as ink-receptivity for printed advertising on the tape. Tamper evident packaging tapes have also been constructed to address a growing customer need to secure their goods during shipment.

Instead of the block copolymer-based adhesives, natural rubber-based PSAs and acrylics are also being used for packaging tapes. These adhesives are typically coated from solvent or, in the case of acrylics, also from water. Due to the low surface tension of the polypropylene backing, surface treatment and the use of special wetting agents for the emulsion acrylics is necessary to make adhesion of the PSA to the backing and high-speed coating possible.

Vinyl backed packaging tapes are quite popular in Europe. The vinyl backing is commonly manufactured using a calendering process. Printability and smooth unwind of the tape rolls are amongst the desirable features of these tapes.

Some of the strongest packaging tapes are made from filament-reinforced backings. These tapes are used for more demanding applications such as strapping and bundling of goods. Filaments selected from glass or polymeric fibers are typically applied in the machine direction of the tape. Depending on the process used, the filaments may be embedded in the backing itself or they can be laid on top of the film or paper backing for subsequent over-coating with the PSA. Again, solvent-coated or hot-melt extruded block copolymer based PSAs, natural rubber PSAs, and acrylics are used for this application.

Another important application for single-coated tapes relates to the masking

of substrates during paint jobs. Due to the exposure to the wet paint and the drying conditions required, the PSAs used for this type of application require fluid and high-temperature resistance. Indeed, the masking tapes are supposed to keep the paint edge clean and well defined, allowing no adhesive to transfer and no adhesive swelling by the wet paint. Due to the physical crosslinking sensitivity to high temperatures, block copolymer adhesives are only used for general purpose masking applications that do not require any oven drying of the paint. Acrylics can be used for masking tape applications, but their higher cost and tendency to build adhesion against a substrate has kept their use to a minimum. Covalently crosslinked natural rubber-based PSAs continue to be the most popular for this type of application. Not only do they have good solvent resistance, but they also show minimal adhesion build against the substrate after exposure to the conditions used to dry and cure the paints. The natural rubber adhesives are typically compounded with tackifiers and curatives, followed by solvent coating. Blends of natural rubber and synthetic rubbers such as styrene–butadiene copolymer have also been tackified to make PSAs for masking application [125]. In order to minimize adhesion build-up and to increase the high temperature and solvent resistance of the tape, moderate tackification levels are used. For similar reasons, coating thicknesses for the PSAs are kept to a minimum.

The backings used for masking tape applications include papers and some vinyls. Vinyl backings will not stand up to high-temperature bake cycles but they can provide very clean, defined edges and good conformability to the substrates. Paper backings are chosen for their high-temperature resistance required to withstand oven baking of paints used in the marine, aviation and automotive industries. These backings are typically derived from raw paper with good elongation and tear properties, and a significant amount of open volume between the paper fibers. This raw paper is not very strong by itself so it is normally treated with solution-based or latex saturants, such as styrene–butadiene rubber, to fill the voids and reinforce the paper. This process also yields a backing with better solvent holdout than plain paper. These saturated crepe papers continue to be very popular in the masking tape industry. An important performance factor for some masking applications is the anchorage of the dry paint to the backing. Indeed, flaking of the paint upon removal of the masking tape can result in contamination of the freshly coated surface. In order to eliminate the flaking issue, release coatings have to be chosen which provide good anchorage of the paint, yet make unwinding of the tape roll possible.

8.2.3. Transportation and appliance industry

Pressure sensitive adhesives and adhesive-coated articles have found a growing list of applications in the automotive, marine, airplane and appliance industries. The main uses are in assembly and decoration, but applications in the areas of

protection and sound deadening also exist. Examples of assembly and decorative applications include the use of PSAs for the attachment of body-side moldings and cladding, attachment of emblems, panel stiffening, and panel attachment in trailers, airplane wings or fuselage parts. Protective applications include tapes and sheets, which are typically made from tough, impact resistant polymer films such as polyurethanes, to shield the vehicle body from abrasion, gravel impact or scratching. Due to their viscoelastic character, PSAs have also been used for damping applications in areas prone to vibration, such as car door panels.

One of the biggest challenges in this industry is the wide variety of substrates that can be encountered for any given application. Not only can the materials be substantially different in their chemical make up, but they may also be quite different in surface roughness, surface curvature and thermal expansion behavior. To help adhesion to these substrates, preparation of the surface to be bonded may be critical. This preparation may be as simple as a cleaning step, but may also include chemical priming and sanding of the surface.

Common substrates include metal surfaces with or without corrosion protection treatment, paints, glass and plastics. The capability of PSAs to bond dissimilar surfaces has been a significant factor in allowing the industry to combine several of these substrates in one vehicle or appliance without the need for drilling, rivets, or fasteners. PSAs used in these types of applications also need to perform for many years while being exposed to significant environmental changes. For example, the PSAs applied to vehicles may need to stand up to fuel spills, detergents, oils, water, salt spray, impact and thermal cycling. Appliance applications may expose the adhesive to steam, vibrations, water, and temperature extremes. Clearly, both the bulk properties and the interfacial interaction of a PSA with its substrate will be challenged in these types of applications.

The bulk properties of PSAs are of significant importance to the adhesion but they also are often the limiting factor in making the final adhesive selection. Long-term durability requirements limit the adhesive choices to acrylates, stabilized rubber-based adhesives, and some silicones. However, due to concerns about silicone contamination in a paint environment, and their higher cost, silicone adhesives have seen limited acceptance on the production floor of the assembly plants. Stabilized rubber-based adhesives, in particular block copolymer adhesives, are used for their excellent adhesion to most plastics. In order to increase their high-temperature performance they are often covalently crosslinked using electron beam or UV irradiation [126]. In the case of block copolymers, high T_g resins or high T_g polymers, such as polyphenyleneoxides, are often mixed into the hard block to push their softening towards higher temperatures.

Hybrids of block copolymer rubbers and acrylics have also been used to increase the low-temperature impact resistance of the adhesive used for body-side molding attachment [127]. To further enhance performance, a new type of hybrid adhesive has been developed, which combines an adhesive polymer, like an

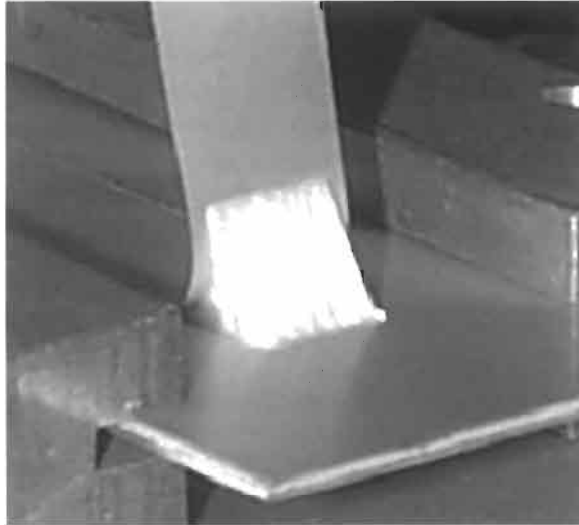


Fig. 16. Extensive deformation of foam core during debonding.

acrylic or polyester, with curable epoxy monomers to make a PSA for coating on a backing. Upon exposure to heat or light, this tape can be cured to semi-structural performance levels. These tapes offer the advantage that they can be applied without expensive dispensing equipment or the clamping often required with fluid curing systems, but can be trigger cured to build to semi-structural adhesion levels [128].

Acrylic adhesives have been widely used in this industry because of their durability, high cohesive strength and strong interfacial adhesion build-up against paint substrates. The latter is of particular importance in the transportation industry because interfacial adhesive failures are generally not accepted. For example, when body-side moldings and cladding is applied to a car body, the typical performance specifications require that these parts cannot be removed from the car body without cohesive failure of the adhesive. Acrylic adhesive-coated foam backings such as those made from neoprene, polyethylene, polyurethane and acrylic polymers are very popular for this type of application. The foam can be coated with the same or different types of adhesive on each of its surfaces. The foam core of the tape is an important part of the attachment tape for the following reasons:

- The deformation of the core significantly increases the peel force during debonding (see Fig. 16).
- The thickness of the foam helps in the wet-out of uneven body parts.
- The foam relieves some of the stresses resulting from body curvature and thermal expansion differential between the car body and the attached parts.
- The foam typically becomes the locus for failure during debonding.

Since cohesive failure of the foam at high peel strengths is desired, good interfacial adhesion of the tape to the body parts is critical. As indicated earlier, a wide range of automotive paints exist in the industry. Traditional paints have been enamel based, but newer paints use a base coat/clear coat dual layer construction. The base coat provides the color and metallic appearance while the clear coat provides protection to the automotive finish. These paints have also been moving more and more towards high solids, requiring them to be extensively crosslinked to get the mechanical performance. Most common crosslinkers include melamines and isocyanates, which are typically used in slight excess. Interfacial bond strength between the PSA and the substrate typically builds as a result of polar group interactions, which may require that the groups rearrange during the process. The high crosslink density of the paint surface makes interfacial rearrangements difficult, but fortunately the surfaces are quite polar making adhesion and adhesion build against polar acrylics still possible. The newest automotive paints continue to move towards higher solids, and include application as powders and powder slurries. Some of these newer formulations include paint leveling and wetting agents that can be migratory, making PSA adhesion more challenging. To increase the paint resistance against environmental factors, such as acidic rain, different curing mechanisms have been incorporated in the formulation. This has resulted in paints, which can be difficult to adhere to, requiring the development of new adhesives [129].

8.2.4. Electrical and electronic tapes

PSA coated tapes are used for a variety of applications in the electrical industry, but they have to meet additional requirements to be accepted in this industry. The adhesive are typically expected to be non-corrosive, they need to have good dielectric properties, they need to hold out moisture, and they need to show good flame retardancy. Especially for electronic applications, little or no outgassing is acceptable, and the adhesive should not introduce migratory contaminants resulting from exposure to release coatings or the presence of additives.

Examples of some of the most important applications for electrical and electronic tapes include the following:

- Construction of electrical transformers and motors.
- Electrical insulation of cables, wires and electrical splices.
- Silicon wafer grinding and dicing tapes used in electronic chip manufacturing.
- Carrier tapes for electronic components.
- Protective tapes used during solder reflow processing.
- z-Axis conductive adhesives and thermally conductive tapes used for controlling the heat build up in electronic components.

For electrical applications, dielectric strength of the tape is critical because it provides a good indication of how the tape will hold up against strong electrical

fields. The dielectric strength of the tape is the ratio of the breakdown voltage (the voltage where the insulative tape properties are lost) divided by the thickness of the tape.

Another important factor is the corrosiveness of the adhesive. This may be especially important in those cases where the PSA has direct contact with the bare wire, the electronic component, or the silicon wafer in a dicing operation. In those cases where an electrical current is running through the device, electrolytic corrosion processes may occur, especially if moisture can penetrate into the adhesive or bond line.

Some of the other critical properties defined by the industry include volume resistivity, dielectric dissipation factor, insulative resistance and the like.

Environmental factors can also be very demanding on the PSAs used for these types of tapes. Electrical tapes used in some devices will have to function for many years under adverse weather conditions, and they may be exposed to fluids or encapsulating gels. For wafer grinding applications, the adhesive is often exposed to lubricating fluids and cleansing agents. Materials that migrate from the backing may also affect the adhesives. For example, plasticizers often migrate from the PVC backing which is commonly used for electrical tapes because of good flame retardancy and high flexibility. Flame retardancy of the electrical tape depends on both the backing and the adhesive used. Backing selection is very important for these electrical applications because they help control some of the critical performance requirements of the tape. Besides the PVC backing already mentioned, other halogenated polymers such as polyperfluoroethylene, polysulfones, aromatic polyimides and glass fiber fabrics are used. The pressure sensitive adhesives used in the tape construction are typically the most combustible. Except for silicone adhesives, which inherently have good flame-retardant properties, typical PSAs require special additives for them to resist combustion. Common flame-retardant additives include organic halogen compounds, which release halogen radicals at high temperatures, interfering with the combustion process. Because of its synergistic effect, antimony trioxide is often used in combination with these halogenated compounds. One of the main concerns with these compounds is their toxic outgassing, an important consideration for the aviation industry. Another concern is the fact that these compounds are not soluble in the adhesives, making them in essence fillers, which have a negative impact on PSA performance when used at higher loading levels. Other flame-retardant agents including organic phosphorus compounds like triphenylphosphate, and inorganic flame-retardants like magnesium carbonate or aluminum hydroxide which are also insoluble. One of the limiting factors in choosing a PSA for an electrical application is the often-required higher temperature performance. Extended operation at elevated temperatures on the order of 150°C is relatively common, with some applications requiring temperature resistance well above that. For continued operation at temperatures in excess of 150°C, crosslinked silicone PSAs are often the only

choice. They are typically combined with high-temperature-resistant backings like polyimides to make the high-temperature-resistant tapes. For more moderate temperatures, covalently crosslinked natural rubber and acrylic adhesives are used.

In recent years, PSA coated tapes have also found an increasing number of applications in the electronic industry. Some of the same product requirements seen in the electrical applications apply here as well. However, because of some unique applications, new tape constructions have been developed. Examples of these new applications include tapes to protect circuitry from electronic interference, tapes to provide magnetic shielding, conductive tapes to either transport electricity or to remove heat from sensitive components, anti-static protective tapes, wafer grinding and dicing tapes, and tapes used to protect conductive lead wires during solder reflow processing. For shielding and anti-static applications, the industry has used tape backings filled with conductive particles and fibers, vapor-coated backings with metallic properties, and backings compounded with conductive polymers. Both conductive particles and fibers have also been used to make the adhesives conductive [130,131]. The main limitations are the cost of some of the conductive additives and their often detrimental effects on the PSA properties.

Instead of electrically conductive additives, thermally conductive additives have also been used to construct thermally conductive tapes used for heat management [132]. A particular example of an electrical conductive tape is a z-axis conductive construction shown in Fig. 17. In this case, the conductive particles make contact in the z-direction of the tape without doing so with neighboring particles in the

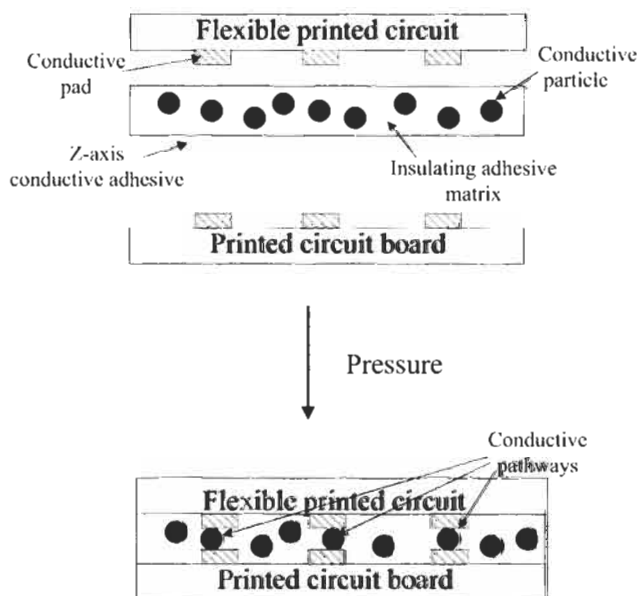


Fig. 17. Schematic of a z-axis conductive PSA bonding elements in an electronic circuit board.

x - y direction. The net result is that the tape conducts only through its thickness but remains insulative in the x - y direction. This has allowed the end user to make electrical connections between two parts by simply sticking them together, eliminating the need for soldering.

Another important application area for PSAs in the electronic industry focuses on the manufacturing, transport and assembly of electronic components into larger devices, such as computer disk drives. Due to the sensitivity of these components, contamination with adhesive residue, its outgassing products, or residue transferred from any liners used, needs to be avoided. Cleanliness of the whole tape construction becomes very critical, because residuals like metal ions, surfactants, halogens, silicones, and the like can cause product failures of the electronic component or product. Due to their inherent tackiness, acrylic PSAs are very attractive for this type of application. Other PSAs can be used as well, but particular attention has to be given to the choice of tackifier or other additives needed in the PSA formulation. The choice of release liner also becomes very critical because of the concern about silicone transfer to the adhesive, which may eventually contaminate the electronic part.

8.3. Adhesive transfer tapes

'Adhesive transfer tape' refers to an adhesive that has been coated on a release liner for easy application to a first substrate. Upon removal of the liner, the adhesive is effectively transferred to this substrate and ready for adhesion to a second substrate. The adhesives used in this type of application mainly include block copolymer and acrylic-based PSAs. If a single-layer adhesive is used, the adhesive may be coated directly on the release liner and crosslinked to increase the cohesive strength. Additionally, to increase the tensile strength or to facilitate dispensing, materials such as glass or polymeric fibers may be mixed in with the adhesive. Other reinforcing agents, such as a thin tissue, or a non-woven or woven fabric have also been included.

Instead of using a single layer of adhesive, tapes with two layers of adhesive, which can be of the same or different type, have also been constructed. Here, a thin film backing may be used as the central layer of the tape, with the adhesives coated on each side of the backing. This type of tape construction is commonly referred to as a double-stick or double-faced tape.

Single adhesive layer constructions are known as transfer tapes because they truly allow the user to transfer a thin layer of adhesive to a substrate. High-performance transfer tapes, also known as laminating adhesives, are used to assemble multi-layer constructions, such as membrane switches. These single-layer adhesives need to hold the laminate together under sometimes very demanding environmental conditions (heat and/or high humidity, repeated flexing, sunlight exposure, among others). Transfer or laminating tapes offer significant benefits to

Membrane Switch Assembly Laminating Adhesive Films



Fig. 18. Transfer tape use in membrane switch assembly. (On right: liner is removed, leaving die cut PSA ready for placement of laminate on the left.)

the end user, including the following:

- Adhesive is ready for use. No coating or drying is required.
- Adhesive is applied in a uniform thickness (typically from about 30 to about 250 μm).
- Adhesive is clean because of the protection by the liner.
- Adhesive layer can be die-cut to allow for precision placement of the PSA.
- Adhesive can be clear, allowing for the assembly of laminates used in optical or backlit applications.

Common applications for transfer tapes include the assembly of membrane switches used in the electronic industry, the attachment of face plates to appliances and other equipment, the assembly of automotive displays in the instrument cluster, and the assembly of displays, such as touch screens for computers and teller machines. Fig. 18 pictures the use of a transfer tape adhesive in the assembly of a membrane switch.

The demands on the PSA performance for these types of applications can be very high, especially in the areas of creep, shear resistance and long-term durability. For these reasons, crosslinked acrylics and stabilized block copolymer adhesives have become the main PSA material choices.

Release liners also play an important role in these applications. Most of these liners are very high-quality siliconized films and polycoated papers. The silicone release coating is chosen to provide easy release from the liner, with liner removal forces only being on the order of a few hundred grams per decimeter width. These liners are also chosen to prevent contamination of the adhesive, either by the releasing material itself or environmental contaminants like dust. Transfer tapes often go through significant converting operations and the liner has to stand up to them without allowing the transfer tape performance to deteriorate. Especially for die-cut parts, the liner plays a critical role in the successful application of the

adhesive. Not only does the liner have to support the adhesive during transfer, but it also has to release reliably from any adhesive weed prior to application, and from the applied adhesive once on the substrate.

8.4. Pressure sensitive labels and office products

Pressure sensitive labels and tapes for the consumer markets form a very significant portion of the PSA industry. Whereas the original products were rather simple in construction and use, today's products often perform unique functions that result from more sophisticated assembly of a label or tape product. Examples of these unique functions include the monitoring of food or drug storage conditions, or the ability to monitor the charge status of a battery.

The products may have to adhere permanently or may have to remain removable for long periods of time. They can also be applied to a wide variety of surfaces and can be exposed to a range of environmental conditions. Examples of these substrates and their environments include the following:

- Labels for soft drink bottles, shampoo bottles, plastic food containers and the like, require high adhesion to materials like polyester and polyolefins. Once applied, the adhesive may have to withstand repeated flexing, freezing, water and other fluid spillage, while maintaining aesthetic appearance.
- Labels may be applied to surfaces that are often contaminated, such as those used for the tracking of tires and metals parts in the factory.
- Labels used in the engine compartment of a car are often exposed to oils and heat. They may also be subject to spillage of coolant or be exposed to the corrosive environment of a battery.
- Labels and tapes may also be applied to a variety of papers or cardboard, some being printed with inks or protective coatings.

Office tapes have been used for many different applications, a significant portion of which is against paper surfaces. Uses include gift-wrapping, assembly of collages, attachment of photos, and book repair. Traditional tapes used tackified natural rubber-based adhesives. Applications requiring non-yellowing, clear adhesives now make acrylics the primary choice for these products. For specialty type of applications, such as archiving of library books or for the overtaping of photographic pictures, PSAs need to be non-staining and they should not deteriorate the paper. Acid-free acrylic PSAs typically address this need.

Tape backings can be selected from both polymeric films and papers. Dispensability of the backing is often an important performance factor limiting the choice of polymeric backings. To facilitate tape unwind, the tape backing may be coated with a tight release agent, also known as a low-adhesion backsize. These specialized coatings provide tight enough release from the PSA to make a stable roll of tape possible, while at the same time being low enough to enable the unwinding.

Labels can be applied under very different circumstances, ranging from manual application in the well-controlled environment of an office, to those that are machine applied at very high speed in a non-conditioned warehouse or factory.

As discussed earlier in this chapter, PSA performance is very much dependent on temperature, speed of application or removal, and surface contamination.

From the above discussion, it is clear that label adhesives have to perform well under a broad range of conditions both during the actual application and after attachment to the substrate.

Peel adhesion and tack are the most important PSA properties controlling the label performance, due to the very limited load a label has to support. However, cohesive strength of the adhesive cannot be ignored because of its importance during the label converting operation, its storage, and the actual use of the product. For example, an adhesive with poor cohesive strength may have high tack but the adhesive will also have the tendency to creep and ooze, resulting in contamination of the converting equipment and problems like welding of the adhesive exposed at the label edges.

Most types of PSAs have found some application in the label industry. Block copolymer-based adhesives are perhaps the most popular because of their high adhesion to a variety of surfaces, their low cost, their good performance over a range of temperatures and peel rates, and their ease of processing. For applications where high temperature performance is required, block copolymers have been formulated with high T_g end block associating resins or polymers.

Acrylic adhesives are also quite commonly used, especially where long-term durability or secure attachment in hot environments is required. For applications requiring good repositionability and permanent removability without damaging the substrate, acrylic adhesives in particulate format offer very desirable properties. As shown in the microphotographs in Fig. 19, the particulate adhesives provide some unique topology to the PSA coating. In addition, the particles elongate significantly during the peeling of the product without failing cohesively, but they recover to their original shape once the adhesive releases from the substrate. This behavior makes them both cleanly removable and re-attachable for repeated use. A well-known example of a product using this type of adhesive is the Post-it™ note [133].

The backing the adhesive is coated upon controls a significant part of the label performance. Backings include papers, polymeric films, metallized films and metal foils. Since a label is typically used to deliver a message, printability or writability of the backing is of major importance. For these reasons, ink receptive and protective coatings are often applied to the non-adhesive side of the substrate. Paper backings are very common, but in cases where the substrate undergoes a lot of flexing or where the PSA needs protection from fluids, film backings are preferred.

Like transfer tapes, reliable label performance will very much depend on the

Particulate PSAs

- This picture of a fresh particle coating shows the characteristic topology of the PSA.
- Upon peeling, each particle dissipates energy by stretching to several times its diameter before debonding from the surface.
- After debonding, each particle recovers its shape, thus being able to bond again.

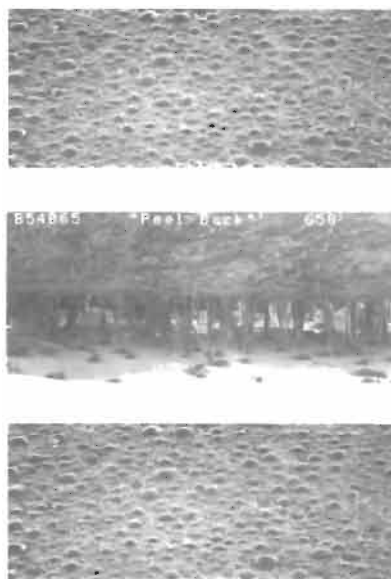


Fig. 19. Topology and peel removal of discrete PSA particles from a substrate.

adhesive, but also on the release liner used. In order for a label to work, the release liner has to function properly at both low and high peel rates. For example, for hand-applied labels a customer will use low peel rates, but for automated equipment labels will have to release reliably at high rates. At the same time, the label has to remain well attached to the liner during shipment and storage. When wound in rolls, the labels should adhere well enough to the liner to avoid premature release and flagging of the label. However, in automated label applicators, the label will actually be released from the liner by running it over a sharp bend of a peeling blade. For this process to work, the release level of the liner and the stiffness of total label construction have to be carefully controlled.

To avoid the need for a liner, the industry has also developed linerless labels that have the release coating on the face of the labels allowing them to be stacked without liner and to be peeled one at a time. The release coatings for these types of application are often quite different from those used on a conventional liner. Since the label is typically printed or written upon, ink-receptivity of the release coating becomes critical. As the industry identifies more and more applications requiring this type of performance, specialized release coatings have also been developed.

While not exactly labels, repositionable paper notes, such as Post-it™ Notes, and tape flags (used to call a reader's attention to certain pages in a document) have to meet similar types of release requirements. Like linerless labels, reliable

release from the note pad or other tape flags is required while maintaining good writability of the product.

8.5. PSA coated articles for skin application

Recently, several independent authors have reviewed the application of PSAs in the medical field [134–136]. PSA coated tapes and articles are common in first aid and hospital applications, but also in areas like sports, recreation, and even cosmetics. Tapes may be used to secure dressings and tubing, to immobilize or limit movement of soft tissue, to help the closing of wounds, to attach surgical drapes to the body, to seal surgical instrument pouches during autoclaving, and the like. Other examples of PSA coated products include anti-bacterial surgical incise drapes, medical electrodes used during electro-surgery or used for patient monitoring (see Fig. 20), drug-delivery patches, absorbent and burn dressings. Athletes and people involved in recreational activities often use self-adhering bandages and wraps to support limbs and limb joints. PSA coated



Fig. 20. Medical electrodes for monitoring of patients.

tapes have recently also penetrated the cosmetic industry for uses like the removal of blackheads from skin.

PSAs used against skin are often very different from those used against other substrates. Unlike other substrates, skin is both very flexible and very variable in nature. The latter can result from a person's condition when the tape is applied, but it also changes person to person as a result of age or origin, or the position on the body where the PSA needs to be applied. For example, skin can be dry and flaky for a person in rest in a low-humidity environment. This same skin can become very wet when this same person has been active or hyperventilates because of a medical condition. Skin may also be saturated with natural skin lipids or be oily because of conditioners applied to it for treatment. Age and race may also change the nature of the skin. For example, babies and elderly people often have more fragile skin than healthy people in the balance of the general population. Finally, since skin is a live tissue it is constantly subject to breathing and the shedding of dead skin cells.

A common requirement for the PSAs used in all these applications is that they should not irritate or compromise the skin. Unlike typical PSAs, which can be approved for application based on their composition, medical adhesives have to go through rigorous testing against animal skin and eventually human skin. The PSA has to be checked for possible triggering of allergic reactions or simple skin irritation. The PSA coated article will also have to undergo thorough testing for the same properties, but also for irritation of the skin due to mechanical effects or occlusivity of the construction. Mechanical irritation may result when a tape or medical device restricts the flexing and movement of the skin. Occlusivity may cause the skin to become highly hydrated making it susceptible to laceration or creating an environment for excessive bacteria growth.

Typical medical adhesives are highly compliant in order to minimize the risk for mechanical skin irritation and to maximize wet-out. At the same time, the materials are chosen to be cleanly removable from the skin surface even after extended wear. Traditional medical tapes used cloth backings with natural rubber-based adhesives. Due to limited breathability, and especially the irritation of certain skin types, these rubber-based adhesives have been increasingly replaced with synthetic adhesives. Since natural rubber is not tacky by itself, adhesives have to be compounded with anti-oxidants and tackifiers. Natural rubber also contains a protein, which can trigger severe allergenic response in certain people. The presence of small molecules like stabilizers, curatives, plasticizers and tackifiers has been of significant concern in the formulation of a PSA for skin contact. For this reason, inherently tacky polymers like silicones, polyisobutylenes, polyvinylethers and especially acrylics have become the standard PSAs used against skin. Acrylic PSAs have the additional benefit that they can be formulated to obtain a wide range of properties without compromising their excellent skin adhesion. For example, by choosing more hydrophilic formulations, the moisture vapor transmission rate of

an adhesive can be significantly improved. Other approaches, such as the blending of PSAs with hydrophilic non-PSA polymers or the introduction of porosity in the PSA coating have also been used. To obtain optimum performance, these PSAs are typically coated on breathable backings like a microporous film, a tissue or fabric, a non-woven, and polymers that have inherent breathability. In areas exposed to fluids, adhesives with good adhesion to both dry and wet skin are often required. Again, blending of hydrophilic components with moisture tolerant PSA allows the adhesive formulator to meet these requirements.

Some applications, such as incise drapes require loading of the PSA matrix with anti-bacterial agents. Proper selection of the monomers allows the PSA to be compatible with compounds like iodine, while maintaining the adhesion to the skin.

Although not considered PSAs per se, tacky gels with good skin adhesion are used in medical electrode type applications. These gels are typically electrically conductive and they need to maintain good skin contact to insure proper transmission of the monitoring signal or to transport current from the body in electro-surgical applications. To provide secure adhesion for extended periods of time or in more demanding applications, adhesion of the electrode may be assisted with the help of a PSA applied as a border around the actual conductive gel.

Perhaps one of the most desirable features in a PSA for skin application is the possibility to remove it without trauma. Being inherently tacky limits the possibility to minimize the peel force during removal of the tape. An elegant approach takes advantage of a melting point transition in the adhesive, where the tape only becomes tacky when exposed to the heat of the body [137]. To facilitate removal, the tape is simply chilled causing the adhesive polymer to crystallize so it loses much of its peel force. Another approach has been to cover a light sensitive tape with a non-transparent overlay. Upon removal of the overlay, the adhesive crosslinks decreasing the adhesion and facilitating removal [138].

8.6. PSA coated graphic, optical and protective films

Besides the typical tape and label products discussed earlier, larger sheeting products are often applied using pressure sensitive adhesives. Examples of these sheeting products include:

- Optically active films used to polarize light or enhance brightness in a liquid crystal display.
- Graphic and decorative products used in advertising and the decoration of vehicles.
- Retroreflective sheeting products used on traffic control signs and retro-reflective license plates for vehicles.
- Tinting films used to filter out light for house and office windows, or for vehicles.

- Protective films applied to vehicles during transit from the manufacturing plant to the dealers.

The film that is selected for the application mainly controls the properties these products deliver to the customer. However, in the case of optical applications where transmission of the light is needed, the choice of pressure sensitive adhesive and the quality of the application to the substrate become very critical. Even for the non-optical uses, the PSAs have to perform reliably under sometimes very demanding circumstances.

Without going into much detail on each specific application, we will describe some of the general guidelines used in the selection of PSAs for these sheeting product applications. In general, most of these products will use a low adhesive thickness on the order of about 20–50 μm . Cohesive strength of the adhesive is important, especially if long-term bond strength has to be maintained or the product needs to be cleanly removable for months or years after application. In the latter case, it may also be desirable that the adhesion does not build excessively with time, so the removal remains easy. Shear strength of the adhesive is less critical than in conventional tape applications, especially because the area of contact with the substrate is large and typically flat. However, cohesive strength of the adhesive is still important because of the clean removal requirements often encountered for these products and the holding power, which is necessary around rivets or any curvature in the substrate.

Some applications, such as vehicle graphics, license plates, retro-reflective traffic signs, retroreflective conspicuity markings on vehicles and buoys, and the like, require that the articles adhere securely for several years under outdoor exposure. This can include exposure to temperature extremes, salt water spray and wave impact, rain, wind shear, pressure washing, detergents, and gasoline. Due to these very demanding conditions, acrylic adhesives are often the materials of choice. Other adhesives, such as those based on tackified block copolymers or natural rubber may be used for some of these applications, especially for shorter-term use. However, this requires that the adhesives be well protected with anti-oxidants and light stabilizers.

The pictures in Fig. 21 demonstrate retroreflective film applications on a truck. The retroreflective part of the graphic in the daylight picture is still visible at night when the headlights of an approaching vehicle hit the surface. This makes it also an important safety feature by improving nighttime visibility.

One of the shorter-term applications is the use of protective films on vehicles for shipment from the manufacturer to the dealers. These protective films are typically polyolefins coated with a removable adhesive for easy application and removal without leaving hard to clean adhesive residue on the vehicle. Several adhesives have been reported for this type of application, including the less common polyisobutylene-based PSAs [139]. A possible advantage of combining a polyolefin backing with a polyisobutylene-based adhesive is that the protective



Fig. 21. Retroreflective sheeting in a transportation application. (Left, in daylight. Right, illuminated by headlight at night).

sheet is now an all-olefin type material, which may facilitate recycling of the sheet.

The optical applications briefly discussed above often require that the PSAs allow the light to pass through the substrate to the outside (for example in a liquid crystal display) or from the outside through the PSA coated film (for example in a window tinting application). Since the PSA coated article is used for light management with the end user viewing the light traveling through the article, optical defects and distortions are typically not acceptable. This not only requires that the PSAs have optical quality (i.e. right refractive index, minimum yellowness, among others) but that they also have been coated on the sheeting with great care (i.e. no herringbone patterns, streaks, among others). Most applications cannot tolerate any visible defects requiring that the coating be done in a clean room environment so no dirt gets entrained in the finished product. Because of the ease of filtration and coating, solution, radiation-cured and emulsion-based adhesives dominate this type of application. Since durability and optical clarity are typically required, adhesives with oxidative and/or light sensitivity, yellowness (for example resulting from tackification) and/or haziness (for example resulting from phase separation in the adhesive) are normally not acceptable. Due to their inherent tackiness, optical clarity and durability, acrylic adhesives currently dominate this type of application.

9. Summary and conclusion

Significant advances in the synthesis, design and fundamental understanding of these viscoelastic materials have fueled the tremendous growth of the PSA product industry and opened up a variety of often demanding new product applications. There is every reason to believe this growth will continue since these products provide convenience and versatility for both the industrial and consumer market.

The earliest PSAs were based on tackified natural rubber, and these materials still command a significant volume in the marketplace, particularly in the areas of masking tapes and duct tapes. Block copolymers offer a good balance of cohesive strength and adhesion to a variety of surfaces. They constitute the largest volume polymer class for both label and tape applications, since they provide low-cost, hot-melt processible adhesives for some large commodity applications, like box sealing tapes and shipping labels. Acrylic copolymers represent the third major PSA polymer class, mostly derived from inherently tacky polymers with excellent durability. A variety of specific polymers have been designed for specialty applications for use in medical, industrial, graphic, optical, and office products.

Acknowledgements

The authors are grateful to 3M for its support in preparing this review and to their many colleagues who have contributed their knowledge over the years. Special thanks are due to C.A. Dahlquist for his many contributions and his unflagging enthusiasm for the field.

References

1. *Adhes. Age*, **Dec.**, 10 (2000).
2. Zoellner, S., *Adhes. Tech.*, **April**, 21 (2000).
3. *The Therapeutic Uses of Tape*, Vol. 1. Johnson and Johnson, 1972.
4. Glossary of Terms. *Test Methods for Pressure Sensitive Adhesive Tapes*, Pressure Sensitive Tape Council, 1996.
5. Dahlquist, C.A., Tack. In: *Adhesion: Fundamentals and Practice*. Elsevier, Amsterdam, 1970, pp. 143–152.
6. Dahlquist, C.A., Creep. In: Satas, D. (Ed.), *Handbook of Pressure Sensitive Adhesive Technology*. Van Nostrand Reinhold, New York, 1989, p. 97.
7. Kraus, G., Jones, F.B., Mars, O.L. and Rollman, K.W., *J. Adhes.*, **8**(3), 235 (1977).
8. Tse, M.F., *J. Adhes. Sci. Technol.*, **3**, 551 (1989).
9. Yang, H.W.H. and Chang, E.-P., *Trends Poly. Res.*, **5**, 380 (1997).
10. Chu, S.G., Viscoelastic properties of pressure sensitive adhesives. In: Satas, D. (Ed.), *Handbook of Pressure Sensitive Adhesive Technology*. Van Nostrand Reinhold, New York, 1989, p. 191.
11. Fukuzawa, K. and Uekita, T. In: *Proceedings of the Adhesion Society*, 1999, p. 69.
12. Gent, A.N. and Kaang, S.Y., *J. Adhes.*, **24**, 173 (1987).
13. Kaelble, D.A., *Trans. Soc. Rheol.*, **4**, 45 (1960).
14. Dahlquist, C.A., Pressure sensitive adhesives. In: Patrick, R.L. (Ed.), *Adhesion and Adhesives*, Vol. 2. Marcel Dekker, 1969, p. 250.
15. Jagisch, F.C., Novel radial styrene-isoprene polymers for pressure sensitive adhesives. In: *Proceedings of the European Tape and Label Conference*, Antwerp, Belgium, April 18, 1997.

16. Chuang, H.C., Chiu, C. and Paniagua, R., *Adhes. Age*, **Sept.**, 18 (1997).
17. Johnson, B., *Adhes. Age*, **July**, 40 (2000).
18. Richards, A.D. (Tufts, Grosvenor and Co.), US Patent 111,682, Feb. 7, 1871.
19. Johnston, J., *Pressure Sensitive Adhesive Tapes*, published by the Pressure Sensitive Tape Council, 2000.
20. Lee, S. and Molnar, A., *Macromolecules*, **28**, 6354 (1996).
21. Drew R.G. (3M), US Patent 2,410,053. Oct. 29, 1946.
22. Drew, R.G. (3M), US Patent 1,760,820, May 27, 1930.
23. Drew, R.G. (3M), US Patent 1,814,132, July 14, 1931.
24. Ebel, C.J. (3M), Canadian Patent, 437338, Oct. 8, 1946.
25. Lattimer, R.P., Kinsey, R.A., Layer, R.W. and Rhee, C.K., *Rubber Chem. Technol.*, **62**, 107 (1989).
26. Ebel, C.J. (3M), US Patent 2,553,816, Feb. 16, 1948.
27. Bemmels, C.W. and Gagliardi, D.D. (Johnson and Johnson), US Patent 2,987,420, June 6, 1961.
28. Korpman, R. (Johnson and Johnson), US Patent 3,535,152, Oct. 20, 1970.
29. Pendelton, J.L. (J. Mandelberg and Co.), US Patent 2,386,696, Oct. 9, 1941.
30. Kellgren, W. (3M), US Patent 2,410,079, Oct. 29, 1946.
31. Kisbany, F.N. (American Tape Co.), US Patent 2,881,096, April 7, 1959.
32. Hendricks, J.O. (3M), US Patent 2,956,904, Oct. 18, 1960.
33. Bredahl, T.D., Levery, H.W., Smith, R.L., Bennett, R.E., Yarusso, D.J., Munson, D.C. and Cox, G.E. (3M), US Patent RE 36,855, Sept. 5, 2000.
34. Class, J.B. and Chu, S.G., *J. Appl. Poly. Sci.*, **30**, 805–814, 815–824 and 825–842 (1985).
35. Carper, J.D., *Adhes. Age*, **Aug.**, 35 (1989).
36. Lowerey, R.D., Synthetic resins. In: *Kirk–Orthmer Encyclopedia of Chemical Technology*, 4th edn. Wiley and Sons, New York, 1995, Vol. 13, 717.
37. Pace, H.A. and Anhorn, V.J. (Goodyear Tire and Rubber Co.), US Patent 3,577,398, May 4, 1971.
38. Aubrey, D.W., *Rubber Chem. Tech. Rubber Rev.*, **61(3)**, 448 (1988).
39. Chu, S.G., Viscoelastic properties of pressure sensitive adhesives. In: Satas, D. (Ed.), *Handbook of Pressure Sensitive Adhesive Technology*. Van Nostrand Reinhold, New York, 1989, p. 179.
40. Legge, N.R., Holden, G. and Schroeder, H.E., Thermoplastic elastomers based on polystyrene–polydiene block copolymers. *Thermoplastic Elastomers*, Hanser Publishers, New York, 1987.
41. Erwins, E.E., St. Clair, D.J., Erickson, J.E. and Korcz, W.H., Thermoplastic rubbers: ABA block copolymers. In: Satas, D. (Ed.), *Handbook of Pressure Sensitive Adhesive Technology*. Van Nostrand Reinhold, New York, 1989, pp. 317–373.
42. Jagisch, F.C. and Tancrede, J.M., Styrenic block copolymers. In: Satas, D. (Ed.), *Handbook of Pressure Sensitive Adhesive Technology*, 3rd edn. Satas and Associates, Warwick, RI, 1999.
43. Dahlquist, C.A. and Kolpe, V.V. (3M), US Patent 3,787,531, Jan. 22, 1974.
44. Korpman, R. (Johnson and Johnson), US Patent 4,136,071, Jan. 23, 1979.
45. Jagish, F.C. and Tancrede, J.M., *Adhes. Age*, **Sept.**, 24 (1990).
46. Jagish, F.C., *Adhes. Age*, **Sept.**, 17 (1991).
47. Dillman, S.H., *Pressure Sensitive Tape Council Technical Seminar*, May, 119 (1991).
48. Matsubara, T. and Ishiguro, M., *ACS Polym. Preprints*, **37(2)**, 720 (1996).
49. Chin, S., *Adhes. Age*, **July**, 26 (1991).
50. Giordano, S., Parodi, C., Riva, A. and Sacconi, L.V., *Adhes. Age*, **Nov.**, 32 (1994).

51. Georjon, O., Faissat, M., Chambon, F., *Adhes. Age*, **Feb.**, 44 (1999).
52. Komatsuzaki, S., *TAPPI Hot Melt Symposium*, 171 (1999).
53. Diehl, C.F., Tancrede, J.M. and Marchand, G.R. (Dow Chemical Company and Exxon Chemical Patents, Inc.), US Patent 5,399,627, March 21, 1995.
54. Jagisch, F.C., Novel radial styrene-isoprene polymers for pressure sensitive adhesives. In: *Proceedings of the European Tape and Label Conference*. Antwerp, Belgium, April 18, 1997.
55. Tancrede, J.M., Diehl, C.F., *Adhes. Age*, **Nov.**, 36–39; and **Dec.**, 34–39 (1996).
56. Himes, G.R., Spence, B.A., Hoxmeier, R.J. and Chin, S.S. (Shell Chemical), US Patent 5,393,841 (Feb. 28, 1995) and US Patent 5,486,574 (Jan. 23, 1996).
57. Himes, G.R. and Oliveri, L.H., *Adhesives Age*, **Feb.**, 41 (1998).
58. Dupont, M., Masse, M. and Schneider, J. In: *RadTech '99 Proceedings*, Berlin, November, 1999, p. 551.
59. Erwins, E.E., St. Clair, D.J., Erickson, J.E. and Korcz, W.H. In: Satas, D. (Ed.), *Handbook of Pressure Sensitive Adhesive Technology*. Van Nostrand Reinhold, New York, 1989, pp. 363–365.
60. Dupont, M. and Mayenez, C., *Adhes. Tech.*, **March**, 24 (1999).
61. Le Du, C., *Adhes. Tech.*, **Dec.**, 18 (1999).
62. Peckmann, H.V. and Rohm, O., *Ber. Deutsch. Chem. Ges.*, **34**, 429 (1901).
63. Ulrich, E.W., Re 24,906, Dec. 13, 1960, assigned to 3M.
64. Stewart, R.F., (Landec Corp.), US Patents 5,156, 911, Oct. 20, 1992 and 5,387,450, Feb. 7, 1995.
65. Pietsch, H. and Curtis, J., US Patent 3,728,148, Apr. 17, 1973, assigned to Beiersdorf, AG.
66. Wiest, H., Weissberger, R. and Lieb, E. (Wacker Chemie, GmbH), US Patent 4,322,516, Mar. 30, 1982.
67. Ando, M., Yamanaka, T., Moroishi, Y., Tokunaga, Y. and Kitamura, Y. (Nitto Denko Corp.), US Patent 5,334,686, Aug. 2, 1994.
68. Blake, F.D. (3M), US Patent 4,569,960, Feb. 11, 1986.
69. Bauer, D.R. and Dickie, R.A., *J. Pol. Sci. Pol. Phys. Ed.*, **18**, 1997 (1980).
70. McKenna, L.W., Jr., Finkelstein, R.S., Haynes, J.K., Jr. (Monsanto Co.), US Patent 4,234,660, Nov. 18, 1980.
71. Quirk, B., *Adhes. Age*, **Oct.**, 33 (1999).
72. Ulrich E.W. (3M). US Patent 2,973,286, Feb. 28, 1961.
73. Mendelsohn, M.A., *Ind. Eng. Chem. Prod. Res. Dev.*, **3**, 67 (1964).
74. Kellen, J.N. and Taylor, C.W. (3M), US Patent 4,737,559, Apr. 12, 1988.
75. Rehmer, G., Boettcher, A. and Portugall, M. (BASF), US patent 5,264,533, Nov. 23, 1993.
76. Auchter, G., Barwich, J. and Jager, H., *Adhes. Age*, **July**, 20 (1994).
77. Fisher, R., *Adhes. Age*, **Oct.**, 40 (2000).
78. Bordoloi, B.K., Plamthottam, S.S. and Van Ham, R. (Avery Dennison Corp.), US Patent 5,187,235, Feb. 16, 1993.
79. Ramharack, R. and Chandran, R. (National Starch and Chemical Investment Holding Corp.) US Patent 5,536,759, July 16, 1996.
80. Mallya, P., Plamthottam, S.S. and Ozari, Y. (Avery International Corp.), US Patent 5,011,867, Apr. 30, 1991.
81. Chandran, R., Ramharack, R., Davis, I.J. and Leighton, J.C. (National Starch and Chemical Investment Holding Corp.), US Patent 5,416,127, May 16, 1995.
82. Sanderson, F.T. and Zdanowski, R.E. (Rohm and Haas Co.), US Patent 3,740,366, June 19, 1973.
83. Guse, G. and Pietsch, H.G. (Beiersdorf, AG), US Patent 3,923,752, Dec. 2, 1975.

84. Knapp, E.C. (Monsanto Corp.), US Patent 3,284,423, Nov. 8, 1966.
85. Lehmann, G.W.H. and Curtis, H.A.J. (Beiersdorf, AG), US Patent 4,038,454 July 26, 1977.
86. Li, X. and Berner, B. (Ciba-Geigy Corp.), US Patent 5,288,827, Feb. 22, 1994.
87. Heilmann, S.M. and Moon, J.D. (3M), US Patent 4,379,201, Apr. 5, 1983.
88. Knoepfel, H. and Silver, S.F. (3M), US Patent 3,770,708, Nov. 6, 1973.
89. Samour, C.M. (Kendall Corp.), US Patent 3,790,533, Feb. 5, 1974.
90. Gabriel, H.R.L., Post, L.K., Culbertson, B.M. and Graham, C.M. (Ashland Oil Corp.), US Patent 4,292,231, Sept. 29, 1981.
91. Su, S., Ozari, Y., Vargas, R.R. and Lum, H., Jr. (Avery Dennison Corp.), US Patent 5,252,662, Oct. 12, 1993.
92. Sanderson, F.T. and Zdanowski, R.E. (Rohm and Haas Co.), US Patent 3,740,366, June 19, 1973.
93. Guerin, J.D., Hutton, T.W., Miller, J.J. and Zdanowski, R.E. (Rohm and Haas Co.), US Patent 4,152,189, May 1, 1979.
94. Mancinelli, P.A., *Materiaux et Techniques*, **March/April**, 41 (1990).
95. Heim, P., Lutz, P., Nicol, P., Rein, D., Rempp, P. and Vuillemin, B. (Elf Atochem SA), US Patents 5,708,091 and 5,837,778, Jan. 13 and Nov. 17, 1998.
96. Matyjazewski, K. and Wang J. (Carnegie-Mellon U.), US Patent 5,763,548, June 9, 1998.
97. Corpart, P., Charmot, D., Zard, S.Z., Biaditti, T. and Michelet, D. (Rhodia Chimie), US Patent 6,153,705, Nov. 28, 2000.
98. Husman, J.R., Kellen, J.N., McCluney, R.E. and Tumey, M.L. (3M), US Patent 5,057,366, Oct. 15, 1991.
99. Mancinelli, P.A. and Norris, S.O., *Adhes. Age*, **Sept.**, 37 (1985).
100. Mancinelli, P.A. (Monsanto Co. and E.I. Du Pont de Nemours and Co. Inc.), US Patent 5,006,582, Apr. 9, 1991.
101. Landin, D.T. (3M), US Patent 4,946,742, Aug. 7, 1990.
102. Medina, S.W. (Air Products Corp.), US Patent 5,049,608, Sept. 17, 1991.
103. Blake, F.D. (3M), US Patent 4,569,960, Feb. 11, 1986.
104. Moore, C.L., Nelson, G.R., Wick, S.M. and Zerbe, H. (3M), US Patent 5,223,261, June 29, 1993.
105. Everaerts, A.I., Halm, L.W., Karim, N., Keipert, S.J., Kinzer, K.E. and Williams, J.W. (3M), US Patent 5,721,289, Feb. 24, 1998.
106. Bennett, G., Klingen, J., Geiss, P.L. and Thorsten, N., *Adhes. Age*, **Sept.**, 19 (1996).
107. Kerr, S.R., III and Lin, S.B., *Adhes. Age*, **Sept.**, 36 (1994).
108. Wengrovius, J.H., Burnell, T.B., Zumburum, M.A. and Bendler, J.T. In: *Proceedings of the 12th Organosilicon Symposium*, Troy, NY, March, 1994.
109. Lin, S.B., *Int. J. Adhes. Adhes.*, **14**(3), 185 (1994).
110. Hoffman, J.J., Leir, C.M., Tushaus, L.A. and Wiederholt, G. (3M), US Patent 5,214,119, May 25, 1993.
111. Melancon, K.C., Unpublished results (3M).
112. Wengrovius, J.H., Burnell, T.B. and Zumburum, M.A. In: *Proceedings of the 10th Organosilicon Symposium*, Poznan, Poland, August, 1993.
113. Copley, B.C., *Org. Coat. Appl. Poly. Sci. Proc.*, **48**, 121 (1983).
114. Mazurek, M. and Kinning, D.J. In: *Proceedings of the 12th International Symposium on Organosilicon Chemistry*, Sendai, Japan, May, 1999.
115. Lin, S.B. and Krencseski, M.A., *Proc. Adhes. Soc.*, 363 (1996).
116. Tangney, T.J., *Adhes. Age*, **Dec.**, 17 (1991).

117. Hofmann, E., Vinylethers. In: *Ullmann's Encyclopaedie der Technischen Chemie*, 3rd edn. Vol. 18. 1963.
118. Robe, G., *Adhes. Age*, **Feb.**, 25 (1993).
119. Babu, G.N., Nam, S., Peterson, J.R. and Peterson, F.R. (3M), US Patent 5,227,442, July 13, 1993.
120. Babu, G.N., Christopher, S.S., Copley, B.C. and Overstreet, T.S. (3M), US Patent 5,112,882, May 12, 1992.
121. Kord, J.M. and Wykoff, A.E. In: *Pressure Sensitive Tape Council Proceedings*, May 3–5, Orlando, FL, 1995, pp. 35–45.
122. Komaharu, M., Eda, H., Ueda, H., Shibata, K., Suzuki, T., Onishi, H., Okada, K., Inoue, T., Horada, M., Sano, K. and Hayashi, K. (Kansai Paint Co. Ltd. and Nitto Denko Corp.), US Patent 5,601,917, Feb. 11, 1997.
123. Stucker, N.E. and Higgins, J.J., Butyl rubber and polyisobutylene in adhesives and sealants. In: Skeist, I. (Ed.), *Handbook of Adhesives*. Van Nostrand Reinhold, New York, 1977, p. 225.
124. Zajackowski, M.J. (Adhesives Research, Inc.), US Patent 5,726,250, Mar. 10, 1998.
125. British Patent 694,190, July 15, 1953 (3M).
126. Erickson, J.R., *Adhes. Age*, **April**, 22 (1986).
127. Bogaert, Y.A., Everaerts, A.I., Kinning, D.J., Purgett, M.D. and Smolders, R.R.L. (3M), European Patent 352,901, Jan. 31, 1990.
128. Bennett, G., Kligen, J., Geiss, P.L. and Thorsten, N., *Adhes. Age*, **Sept.**, 19 (1996).
129. Everaerts, A.I., Stark, P.A. and Takeda, S. (3M), US Patent 5,612,136, Mar. 18, 1997.
130. Angelopoulos, M., Gelormc, D. and Kuczynski, J.P. (IBM), US Patent 5,645,764, July 8, 1997.
131. Glackin, R.T. (Adhesives Research, Inc.), US Patent 5,082,595, Jan. 31, 1992.
132. Muta, S., Ohura, M. and Yoshikawa, T. (Nitto Denko Corp.), US Patent 6,162,319, Dec. 19, 2000.
133. Silver, S.F., Creative Invention Award Address (for Post-it™), ACS Meeting, May 1998, Dallas, TX.
134. Webster, I., *Int. J. Adhes. Adhes.*, **17(1)**, 69 (1997).
135. Lucast, D.H., *Adhes. Age*, **Oct.**, 36 (2000).
136. Kummer, A.B., *Adhes. Age*, **Dec.**, 40 (2000).
137. Stewart, R.F. (Landec Corp.), US Patents 5,156,911, Oct. 20, 1992, and 5,387,450, Feb. 7, 1995.
138. Webster, I. (Smith and Nephew, PLC). WO9918136, Apr. 15, 1999.
139. Komaharu, M., Eda, H., Ueda, H., Shibata, K., Suzuki, T., Onishi, H., Okada, K., Inoue, T., Horada, M., Sano, K. and Hayashi, K. (Kansai Paint Co. Ltd. and Nitto Denko Corp.), US Patent 5,601,917, Feb. 11, 1997.

Release coatings for pressure sensitive adhesives

DAVID J. KINNING * and HILDEGARD M. SCHNEIDER

3M Company, St. Paul, MN, USA

1. Introduction

Release coatings are important components of pressure sensitive adhesive (PSA) products such as tapes and labels [1]. Release materials are coated onto the backside of PSA tape backings (often called low adhesion backsizes or LABs in this form) to provide the desired tape roll unwind force. They are also coated onto various substrates to form release liners for PSA products such as labels and transfer tapes. Typically the thickness of the release coating is less than 1 μm , and often times less than 0.1 μm . Release coatings can be thought of as the PSA delivery system, providing a controlled unwind or release force and protecting the adhesive from contamination and unintentional contact until it is applied.

The requirements for a release coating include:

(1) Providing a release force desired for the intended application. The release forces provided by a release coating are often categorized as premium, between about 1 and 10 g/cm, modified, between about 10 and 50 g/cm, or tight, between about 50 and 500 g/cm. Release materials for liners are generally formulated to provide premium to modified release, while release materials for low adhesion backsizes are usually in the tight range.

(2) The release force must be stable under whatever environmental (e.g., temperature and humidity) conditions the PSA product will experience.

(3) The release material should be well anchored to the backing so that it does not transfer to the PSA, thereby decreasing the subsequent PSA adhesion (herein referred to as readhesion). Similarly, the release material should not contain labile components that could transfer to the PSA and decrease the readhesion by an unacceptable amount.

* Corresponding author. E-mail: djkinning1@mmm.com

Some additional requirements of the release coating may include the ability to write, print, or paint onto it, to provide quiet or smooth unwind, or to exhibit low coefficient of friction. There is also a trend towards the use of solventless release materials in the form of waterbased or 100% solids coatings.

The types of polymers that are used as release coatings include silicone networks, silicone containing copolymers, polymers with long alkyl or fluoroalkyl side chains, fluoropolymers, and polyolefins. These polymers have surface energies that are less than the surface energies of commonly used PSAs, an important feature of release materials.

2. Release mechanisms

2.1. Surface energy and work of adhesion

The release of a pressure sensitive adhesive from a release coating is a complex phenomenon [1]. Many factors can play a role in determining the force necessary to peel a PSA from a release coating other than just the choice of the release material, including the PSA rheology, PSA chemical composition, PSA surface energy, potential chemical interactions at the PSA/release coating interface, the rheology and topology of the backing, the processing conditions used to coat or cure the release material, and the testing conditions. In this chapter, the effect of the release material chemistry, surface and interfacial composition, and rheology on release performance will be emphasized, in addition to the potential chemical interactions between the PSA and release coating. Consider the situation of a PSA tape being peeled from a release coated substrate. According to the conventional theories of adhesion [2,3], the work required to peel the tape can be written in the form

$$\text{Work to peel} = W_a \times f(\nu, T)$$

where W_a is the thermodynamic work of adhesion, determined by the strength of the chemical interactions at the PSA/release coating interface, and is given by the equation

$$W_a = \gamma_a + \gamma_r - \gamma_{ar}$$

Where γ_a is the surface energy of the adhesive, γ_r is the surface energy of the release coating, and γ_{ar} is the interfacial energy between the adhesive and release coating. $f(\nu, T)$ is a function which describes the energy dissipated during the peeling, for example in the form of irreversible deformation of the PSA, release coating, or backing. The amount of energy dissipation, and thus the peel force, will depend on the peeling rate, ν , and temperature, T . As the PSA is peeled from the release coating the PSA will deform, and the deformation will have both an

elastic non-dissipative component and a viscous flow dissipative component. It has been proposed [4–6] that when the stored elastic strain energy in the PSA exceeds the work of adhesion the PSA will separate from the release coating at the peel front. A PSA which can flow more and dissipate more energy will then exhibit a higher peel force (of course if the PSA flows too easily, then it would fail cohesively, which is usually not desired). Similarly, a higher work of adhesion will allow for more dissipation within the PSA before the PSA is released, and thus a higher peel force is obtained.

Studies by Owen [7] have shown that a negative spreading coefficient, S , defined as

$$S = W_a - W_{\text{coh}} = \gamma_r - \gamma_{\text{ar}} - \gamma_a$$

where W_{coh} is the work of cohesion of the PSA (given by $2\gamma_a$), is generally required in order for a material to function as a release coating (failure at the PSA/release coating interface and not within the PSA). However, the magnitude of the spreading coefficient is not a good predictor of the PSA release force.

The work of adhesion between a PSA and a release coating can be expressed in terms of the dispersive and polar components of the surface energies of the PSA and release coating [8].

$$W_a = 2(\gamma_a^d \gamma_r^d)^{1/2} + 2(\gamma_a^p \gamma_r^p)^{1/2}$$

where the superscripts d and p refer to the dispersive and polar components respectively. Except in the case of pure silicone networks, release materials are generally multicomponent or multisegmented polymers. Their release feature is imparted by the low surface energy components, which preferentially accumulate at the release coating surface, thereby reducing the release coating surface energy, and thus the work of adhesion. The surface energies of some of the chemical constituents commonly found in release coatings, including hydrocarbon, fluorocarbon, and polydimethylsiloxane segments, are listed in Table 1 [9]. In most cases, these constituents have surface energies less than about 23 mJ/m². In comparison, the surface energies of rubber-resin and alkyl acrylate based PSAs are typically in the 30–40 mJ/m² range [10–13].

Typically, the polar surface energy component of polymers used for release coatings is relatively small and the work of adhesion can be written simply as

$$W_a = 2(\gamma_a^d \gamma_r^d)^{1/2}$$

Based on the arguments presented thus far, it would seem that, for a given PSA, the work of adhesion, and thus the peel force, should decrease systematically as the surface energy of the release coating is decreased. Therefore, fluorochemical containing polymers should provide the lowest release forces. In practice, these generalities often do not hold, due to other factors, such as interfacial dynamics and rheological considerations.

Table 1

Surface energies of the chemical constituents commonly found in PSA release coatings

Constituent	Surface energy, γ (mJ/m ²)
Hydrocarbon segments	
$-\text{CH}_3$	23.0
$-\text{CH}_2-$	35.9
Fluorocarbon segments	
$-\text{CF}_3$	14.5
$-\text{CF}_2-$	22.6
Polydimethylsiloxane	
$-\text{Si}(\text{CH}_3)_2\text{O}-$	19.8

Several authors have examined the effect of substrate surface energy on the tack or peel force of pressure sensitive adhesives. For example, Dahlquist [14,15] found that the peel forces for a rubber-resin type PSA peeled from various polymer substrates generally increased with increasing surface energy of the substrate, although there was considerable scatter in the data. Toyama and coworkers [10,11] measured the tack and peel force of rubber-resin and acrylate based PSAs for polymer surfaces having critical surface tensions between 18 and 43 mJ/m². They found that, for substrate surface tensions less than that of the PSAs (35–36 mJ/m²), both the peel and tack force increased with increasing substrate surface tension. At higher substrate surface tensions a decrease in the peel and tack force was seen. In contrast, Sherriff et al. [12] observed a monotonic increase in the tack of rubber-resin PSAs as the probe surface energy was increased from 18 to 42 mJ/m². Zosel [13] found that the adhesive failure energy of polyisobutylene PSAs, peeled from substrates with surface tensions between 19 and 44 mJ/m², increased with increasing substrate surface tension until the substrate surface tension reached that of the PSA. At higher substrate surface tensions the adhesive failure energy remained fairly constant. The common finding in these studies is that the PSA adhesion generally decreases at the lower substrate surface energy, consistent with the thought that a release material needs to have low surface energy. However several authors have pointed out that there is often a lack of correlation between the magnitude of the PSA release force and the release material surface energy [7,16–19]. While a low surface energy is a prerequisite for a polymer to be a good PSA release material, it alone does not guarantee good performance under all aging conditions [19,20]. The surface energy of the release coating is an important contributing factor in determining the release force of a PSA, but it is clear that other phenomena can also play important roles.

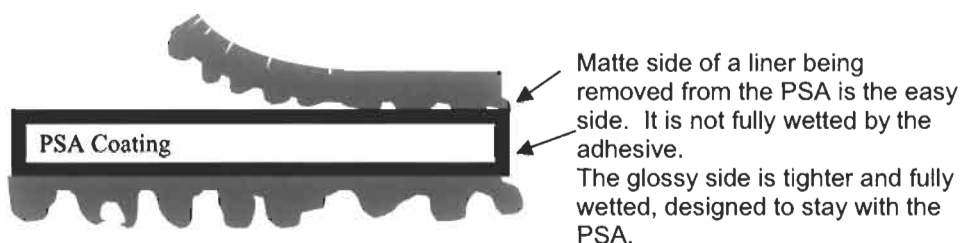


Fig. 1. PSA coating example.

2.2. Topological considerations

When considering release mechanisms, the physical and chemical heterogeneity of the adhesive/release interface cannot be ignored. At its most basic level, roughness of the release and PSA surface, the stiffness of the PSA and the method in which the PSA and release surface are brought together define the contact area of the interface. The area of contact between the PSA and release material defines not only the area over which chemical interactions are possible, but also potential mechanical obstacles to release. In practice, a differential liner for a transfer adhesive can be made to depend in part on the substrate roughness for the differences in release properties [21].

In the example illustrated in Fig. 1, the PSA is coated from solution onto the glossy side of the liner, which is the tight release side. After drying the adhesive solution, the PSA and liner are wound into a roll and in winding the rough matte side is brought into contact with the adhesive. Since the PSA was solution coated onto the smooth side of the liner, the more intimate contact offers slightly higher release force than the matte side of the liner, which is just wound in place. The roughness scale of the matte patterning and the stiffness of the PSA are sufficient to avoid PSA penetration even when being aged in roll form. One must, however, also recognize that (with different coating methods or PSA stiffness) the opposite is possible and that penetration of PSA into micro or macrostructured liners will increase contact, possibly increasing surface interactions as well as mechanical energy dissipation during peel. Finally, a patterned release coating may make an impression on the PSA that can alter its subsequent adhesion. This property can be beneficial or detrimental to the PSA performance, and should be carefully controlled. Utilization of substrate roughness is one route to modifying release properties, but is not commonly used without also modifying the surface with particular release chemistries.

2.3. Chemical patterning

Heterogeneity extends beyond the geometric, and chemical patterning can also be critical. Chemically patterned release surfaces can result in various levels of

regularity, from microphase separating blends of release polymers [22], unintentional artifacts of coating [23], intentionally pattern coated release systems [24], or subsequent purposeful 'damage' of release coatings [25,26]. Typically, the size scale of microphase separation is small enough that the system presents a uniform release level over measurable length scales which is an average of the composition of the release systems employed. One must realize that surface energetics will influence the composition presented to the PSA relative to that in the bulk, and that subsequent restructuring is possible. Phase separation is most commonly used in silicone acrylates or epoxysilicones when blending polymers of varying levels of functionality. Manipulating release values by intentionally damaging certain parts of a release surface, like those partially exposed to corona, can produce differential release levels. Intentionally pattern coated surfaces employing either differential chemistries or differential coat weights have measurable variation in release comparable to the length scale of the pattern, however if the system is appropriately chosen, the desired peel level and character can be controlled and maintained [24].

2.4. Interdiffusion

Another important adhesion mechanism between polymers is that of interdiffusion. However, most pairs of high polymers are incompatible, and a narrow interface (interphase) is expected to form between them. Since most release coatings have a significantly lower surface energy than that of the PSAs, they will have a high degree of incompatibility with the PSA, and interdiffusion would not be expected to contribute significantly to the adhesion level. An exception to this generality is the specific combination of silicone release coatings and silicone PSAs. Unless the silicone release coating is highly crosslinked [27], interdiffusion can occur leading to increasing release forces with time. Usually silicone PSAs require the use of fluorochemical containing release materials [28]. The fluorochemical component lowers the surface energy of the release coating, but it also increases the incompatibility between the silicone PSA and the release coating, thereby reducing interdiffusion across the release coating/PSA interface. Alternatively, phenyl groups have been incorporated into the siloxane used in the PSA to provide incompatibility between the silicone PSA and the silicone liner [29]. PSAs often times contain low molecular weight additives such as liquid tackifiers, oils, or surfactants. Depending on the chemical nature of the PSA additives and release coating, these low molecular weight additives may diffuse to the PSA/release coating interface and affect the interfacial adhesion. For example, it has been shown that surfactants used to prepare acrylic emulsions can migrate towards surfaces and interfaces upon aging, thereby changing the adhesion properties of coatings made from the emulsions [30,31].

2.5. Chemical interactions at the PSA/release coating interface

In order to minimize the force necessary to peel a PSA from a release coating, the chemical attractive forces at the PSA/release coating interface must be minimized. The attractive dispersion type forces will always be present; however, other attractive interactions such as polar, acid–base, or hydrogen bonding interactions can be minimized through proper design of the release material and selection of the particular PSA/release material pair. Most polymeric materials used for release coatings are multicomponent or multisegment, with one segment (typically alkyl, fluoroalkyl, or silicone) having low polarity and low surface energy. The low surface energy components accumulate at the coating surface to provide the low adhesion feature. Typically, the other components present in the release material, which have higher surface energy and may have significant polar or acid–base character, are buried underneath the coating surface. These components are often needed to enhance the mechanical strength of the coatings, to ensure anchorage of the coating to the backing, to provide a chemical linking of the release moiety to the polymer backbone, to provide an additional feature such as printability, or to provide reactive sites in the case of materials to be cured on web. In order to achieve a stable release force between the PSA and the release coating, a stable interfacial structure is required so that the higher energy polar segments in the release coating and PSA are kept separated from each other. However, upon contact between the PSA and release coating, restructuring can occur within the PSA and release material near the PSA/release material interface, provided that there is sufficient segmental mobility and that there are specific favorable chemical interactions between the chemical groups in the PSA and the release material to drive the restructuring. Many studies have demonstrated that polymer surfaces can restructure upon contact with another medium [32–38]. In the case of a PSA/release coating interface, such interfacial restructuring can result in a marked increase in the release force with increasing aging time or temperature [19,20,39].

2.6. Weak boundary layers

Another factor that can contribute to the low release force provided by a release material is the presence of a mechanically weak boundary layer at the surface of the release coating [40,41]. Upon peeling the PSA from the release coating, the locus of failure is within this mechanically weak layer, resulting in transfer of material to the adhesive and a subsequent loss in adhesion of the PSA. Although the use of a weak boundary layer may not be the preferred method of achieving low adhesion for PSA release coatings, it can be useful if the amount of transfer is consistent and kept to a minimum [42]. However, in many cases the unintentional or uncontrolled transfer of a weak boundary layer to a PSA results in an undesirable loss in readhesion.

2.7. *Rheological contributions*

Assuming a PSA/release system in which no weak boundary layer exists, prediction of release force and peel character are difficult even if one has knowledge of the chemistry and contact area, the surface energies of both the release and PSA surface, and the interfacial energy of the system. In addition to the rheology of the PSA, the rheology of the release system can play an important role. To illustrate this point, comparison can be drawn between a silicone surface and a well-crystallized alkyl side chain polymer (or self-assembled monolayer), in which only methyl groups are presented at the surface. While the surface energies of these systems are identical at room temperature, and both are non-interacting with the PSA, release from the silicone layer is likely to be smoother and easier than that from the side chain polymer at most peel rates [17,18]. The operative difference between the two release systems considered is flexibility. Alkyl side chain polymers depend on side chain crystallinity to remain non-interacting with the adhesives. PDMS, on the other hand, is a very flexible molecule with a very low T_g , still fluid though viscous at very high molecular weights. It is the flexibility of the crosslinked PDMS network that makes it a superior release system [17,18]. Work with fluorinated materials also dramatically underscores the importance of rheology or flexibility to release. Many comparisons have been made between PDMS and fluorinated release surfaces that show that even though the fluorinated surfaces present lower surface energies, their release is tighter and more likely to be raspy. In comparing PDMS and Teflon, the rougher texture of the Teflon surface is assumed to contribute to the higher release force; however, the dominant contributor is speculated to be the difference in system rheology and interfacial slippage [43,40].

Visual observations by Newby and colleagues [17,18] and others show that the peel front of transparent commercial tapes being removed from PDMS, hydrocarbon and fluorocarbon monolayers is dramatically different. While surface free energies and the spreading coefficient described previously [7], would predict that the release force should be lowest for the fluorinated system, PDMS gives the easiest release. Observational experiments include those in which fluorescent molecules were placed at the adhesive release interface, or within the bulk of the adhesive. During peel from fluorinated layers, particles at the interface did not move appreciably as the peel front approached, but those in the bulk showed large displacements. This indicates friction at the interface and shear dissipation within the bulk, both of which result in high release forces. In contrast, the same PSA on PDMS showed equivalently large displacements of particles ahead of the crack tip, whether at the interface or in the bulk. This implies that interfacial slippage can occur which minimizes shear dissipation within the system. The observations show that on the more flexible PDMS layer, slip is allowed, preventing profound fingering of the PSA and high shear deformation in the region above the crack tip.

The dependence of release force on the flexibility of the release layers is noted in systems other than silicones. Recent work in olefin release shows that release is a strong function of the density or crystallinity of the layer [44]. At a density above 0.9 g/cm^3 , release for an acrylate PSA is greater than 270 g/cm . However, when the density of PE is dropped to 0.865 g/cm^3 , the release force of the same adhesive construction drops to 35 g/cm . An investigation of interfacial friction and slip in these systems has not yet been reported, but again the manipulation of release rheology greatly impacts the measured peel force.

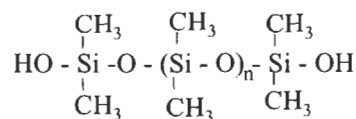
3. Release material chemistries

3.1. Silicone networks

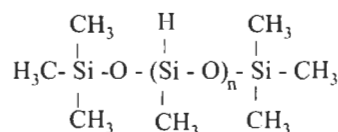
The goal of silicone release liner chemistry is to provide a silicone (polydimethylsiloxane, PDMS) system which can be delivered to a substrate to form a complete thin film, anchored to the backing, and cured such that the PSA can be removed with minimal contamination. Further required is that the release chemistry be tailorable to provide a predictable level of release force for a given adhesive chemistry, with stable release forces over a range of storage time and temperature conditions. From these basic release needs, four major classes of silicone chemistries have evolved, each offering a unique balance of economic and performance advantages. Economic considerations include cure time and energy input, substrate compatibility, processing equipment, raw material costs, environmental concerns, etc. Technological advancements center on tailoring release, release stability, contamination, processing advancements and added functionality.

The oldest of the silicone liner cure chemistries, initially produced in 1955, is the condensation cure system. This system continues to be used and developed, although for environmental reasons is losing favor [23,45,46]. In its most basic form, the release chemistry includes a silanol functional high molecular weight silicone base polymer, a hydride functional crosslinker and a condensation catalyst (i.e. dibutyl tin dilaurate). Additional components can include fast cure additives, bath life extenders, and anchorage additives. The primary components and reaction schemes are shown in Fig. 2. Condensation cure encompasses two basic reactions. The most dominant reaction is that between the silanol and the silyl hydride, forming the siloxane bond and liberating hydrogen. Secondly, silanol ends can react to form the siloxane bond, with water being liberated.

Although waterborne systems were developed in the 1960s, the form of this chemistry that dominates the industry utilizes end-functional, high molecular weight base polymers dissolved in organic solvents. Work on solventless condensation systems continues, but has not yet become commonplace [45,47]. Solvent-borne condensation cure systems are convenient for their ease of pro-



Base Polymer – $n > 500$



Crosslinker: $n = 10-50$



Fig. 2. Primary components and reaction schemes.

cessing, thermal cure during solvent drying, good anchorage to substrate and slippery feel. The major drawbacks are handling of solvent and the pronounced post cure phenomenon, wherein the release chemistry continues to react for hours to days after becoming 'smear free'. (Post cure and vitrification will be more fully discussed in the section on epoxy silicones.) Cure chemistries developed more recently, discussed in the following paragraphs, eliminate the need for solvent, and increase the cure speed.

Hydrosilation silicones or 'addition cure' systems utilize a hydride functional crosslinker with a vinyl functional base polymer and a noble metal catalyst. While the cure can be initiated with UV [48,49], thermal cure versions dominate the commercial market [23,50]. In thermal cure systems, inhibitors are necessary for processing and anchorage additives are common.

Addition cure silicones can be delivered from solvent, waterborne emulsions, or 100% solids systems. The solvent free versions employ base polymers of intermediate molecular weight to achieve processable viscosity. These base polymers can have reactive moieties in terminal and/or pendant positions. These lower molecular weight, more functional systems result in a tighter crosslink network which feels 'rubbery' to the hand. Low amounts of high molecular weight additives are included in some formulations to provide a more slippery feel [51,52].

Advantages of the hydrosilation system (Fig. 3) include the elimination of solvent, improved cure speed, and potential for UV or thermal cure. Drawbacks to the system include more expensive multiroll coating methods, potential poisoning of the Pt catalyst (with Sn, S, Cr, amines, etc.), poor anchorage to some films, and a need to carefully balance the hydride to vinyl ratio employed for cure to avoid detrimental interactions with acid containing adhesives [23,53].

Epoxy cured silicones were developed to be photo initiated rather than thermally cured [54]. The chain length of these materials ranges to 200 monomer repeat units, but the majority component of most formulations is significantly shorter. The structure of a typical base polymer is shown in Fig. 4. The chain can be terminal and/or pendant functional, with degree and type of epoxy function-

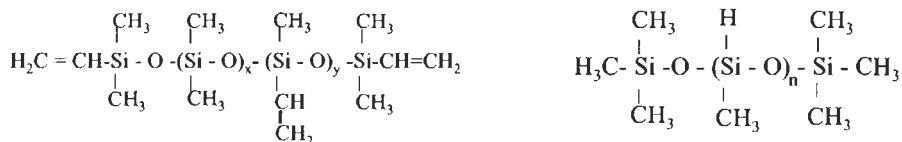
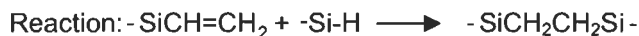
Base polymer: $x + y = 50-400$ Crosslinker: $n = 10-50$ 

Fig. 3. Hydrosilation system.

ality varying by vendor source [54–56]. The release formulations contain one or more types of base polymer, a cationic photoinitiator and a ‘reactive diluent’ chain transfer agent. The formulations while deliverable from solvent or aqueous emulsion [57], are typically coated at 100% solids, eliminating the need for solvent drying. UV irradiation is thus the only energetic cost requirement and the photoinitiator absorbs and reacts during this exposure. The photolysis of the catalyst (several are available [56,58–61]) results in the formation of a sulfur or iodine centered radical, which abstracts a hydrogen to become a strong acid. The cure results from homopolymerization of the epoxy system initiated by protonation of the oxirane ring.

As the system continues to crosslink, ‘vitrification’ occurs which can result

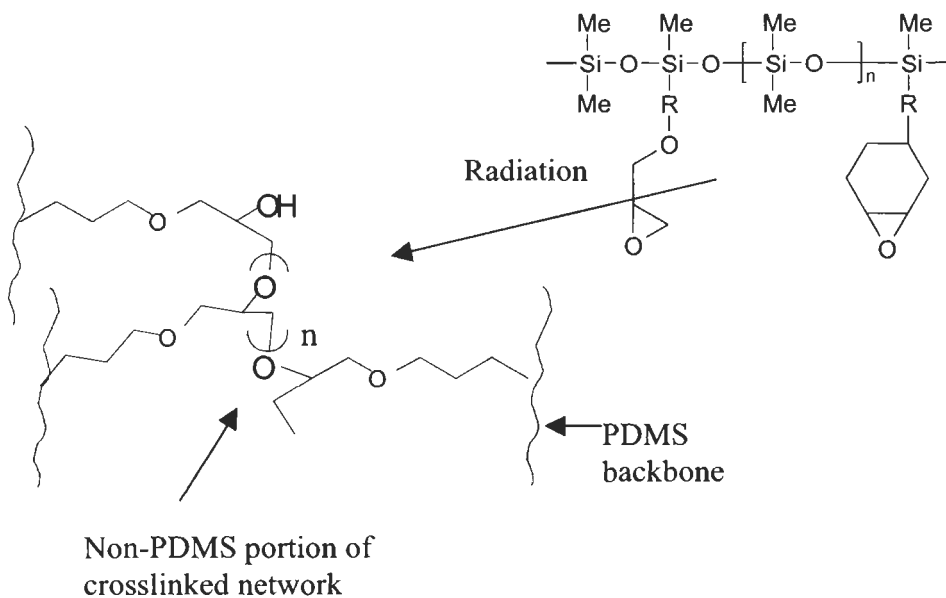


Fig. 4. Epoxy cured silicones.

in an extended post-cure similar to that described in the condensation system [23,56]. At this point, the system is sufficiently gelled to drastically constrain mobility. Polymer diffusion to active radical sites is suppressed, leaving unreacted functional groups to interact with subsequent acid containing adhesive coatings. In epoxy systems, alcohols are added as chain transfer agents. Reaction of an alcohol with the oxirane ring converts the immobile oxonium ion to a mobile proton, initiating a new polymer chain. External heat can also aid in driving the reaction to completion. By the proper utilization of chain transfer agent and optional heating, the post cure phenomenon can be minimized in this system.

Epoxy silicones also differentiate themselves from the previous two classes discussed in that variations of the base polymer structure (% PDMS vs. % epoxy) can yield a broad range of release values. Highly functional base polymers exhibit tighter release, more robust anchorage to substrates, and lower Si transfer levels [62,63]. Base polymers that contain more PDMS, and are preferably only terminal functional, are added at low levels to give premium release and smooth peel [56,64,65]. These additives can increase cure times and silicone transfer. Very tight release is possible by blending epoxy silicones with epoxy terminated organic monomers or polymers [66,67].

Advantages of the epoxy systems are the absence of solvent, UV initiated cure that does not require inerting, a wide range of release levels possible and excellent anchorage to film. Disadvantages include cure inhibition on basic substrates and the need to carefully balance formulation cure speed and completeness with release properties.

Silicone acrylate technology, while known since the 1970s [68], has been applied to release coatings more recently [69]. Both homopolymerization of multifunctional silicone acrylates and copolymerization with organic acrylates is practiced [22,70]. Examples of blended systems will be deferred to the next section, understanding that an increase in the non-silicone component acts to increase the release level, analogous to the epoxy system described above.

Silicone acrylates (Fig. 5) are again lower molecular weight base polymers that contain multiple functional groups. As in epoxy systems, the ratio of PDMS to functional material governs properties of release, anchorage, transfer, cure speed, etc. Radiation induced radical cure can be initiated with either exposure of photo initiators and sensitizers to UV light [22,46,71] or by electron beam irradiation of the sample.

Advantages are similar to the epoxy system, in that these can be solventless and do not require thermal energy. Disadvantages unique to this system, however, include the need to inert the cure chamber to avoid air-inhibition of cure as well as some release instability with acrylate adhesives [72].

Silicone release coatings are the workhorses of the easy release industry because the very nature of the molecule fulfills most requirements for low adhesion. When well cured, silicone networks are fairly inert and present a very low sur-

favorable interactions with epoxy or acrylate containing silicones. Increase in release force with aging is thus possible.

A word should be said about the 'weak boundary layer' effect and silicone release [40,41]. Studies have shown that having loose silicone oil that can transfer to the PSA will lower release, however subsequent adhesion will likely suffer as well. In most commercial instances using silicone liners, a weak boundary layer is not intentionally employed. Additionally, many 'low transfer' silicone liners are commercially available which provide premium release and show low to no PDMS transfer to PSAs, indicating that PDMS transfer is not a necessary condition for easy release.

With proper processing and curing conditions, silicones are fairly easy to coat and provide smooth uniform surfaces. Molecularly, silicones are very flexible, providing low friction and the interfacial slippage discussed previously. It is by this molecular flexibility that silicones distinguish themselves, allowing easier release than their similarly low energy, non-interacting organic release counterparts. The flexibility of silicones is curtailed by the addition of organic molecules or silicate resins to provide release tailoring.

Modifying the rheology of silicones is the dominant method of tailoring the release force of silicone liners, again supporting the importance of the rheology of the release system. Controlled release additives are very high T_g methyl-treated silicate resins, also called MQ resins (Fig. 6). Their molecular weight is usually a few thousand, and the resin may be partially functional (OH, vinyl, etc.). In most cases, the resins are dissolved for ease of blending with the silicone formulation before coating. At low concentrations of MQ solution in the formulation, little effect is seen; however, release forces usually increase sharply with MQ level above about 30 wt%. The MQ resins act on the release layer in several ways. To some degree, interactions with the adhesive can be affected, but the effect on the surface energy is not large. Studies have shown that the MQ resin can reduce the segmental mobility of the PDMS chain [73], but that overall effect

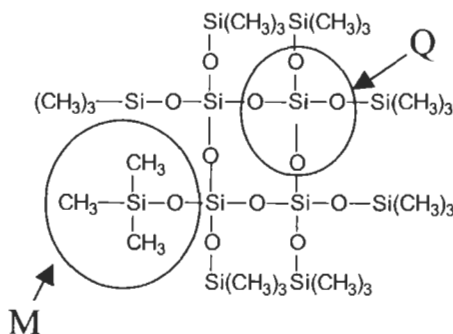


Fig. 6. MQ resin.

should be similar to increasing the crosslink density of the cured network, which is minor. Adding MQ to the silicone network greatly increases the T_g of the release system, which has been shown to correlate with tighter peel and more raspy peel at given peel rates. Studies have shown that both the storage and loss modulus increase, with the greater effect in loss modulus [74]. In addition to the bulk rheological effect, MQ inclusion affects the release surface dynamics as well. The most compelling explanation offered so far again ties back to interfacial mobility and slip. Measurements of slippage for silicone networks containing various amounts of controlled release additive show that adding MQ resin can reduce or even eliminate slip. Interfacial shear measurements also increase markedly with incorporation of MQ resin [75]. Again the argument is that the reduction in flexibility of the silicone network results in increased friction, and a rigid surface which sustains higher stress levels.

3.2. Fluoropolymers

Fluoropolymers are theoretically interesting release systems since very low surface energies can be obtained. Release layers of Teflon[®], fluorinated waxes, self assembled monolayers and high molecular weight curable polymers have been evaluated and find very limited success as release for PSAs [18,76]. Fluoropolymers, as mentioned previously, provide low surface energy coatings, but may not be flexible molecules. The lack of flexibility leads to raspy, tighter peel when compared to silicone coatings [17,18]. Fluoropolymer coatings are very expensive, and are therefore usually coated quite thin. These systems tend to be very application dependent, used in markets like healthcare and electronics which can support custom tailoring of adhesive and release formulations.

Several systems comprised of curable perfluoropolyethers [42,77] have been reported. An example of a perfluoropolyether molecule is shown in Fig. 7, with the level of ether linkage, type of curable functional group and overall molecular weight being variable. The curing of the functional groups proceeds as is typical for those chemistries; for example the acrylate functional fluorinated polyether can be cured by UV irradiation as is discussed in the section on silicones. To some extent, the degree of cure completeness is manipulated to control the release level, and an example of using a weak boundary to achieve low release was given previously [42].

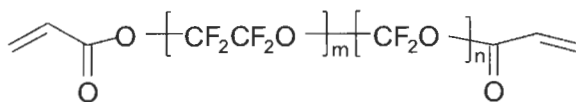


Fig. 7. A perfluoropolyether molecule.

3.3. Fluorosilicones

Fluorosilicones consist of PDMS backbones with some degree of fluoro-aliphatic side chains. The fluorinated group can be trifluoropropyl, nonafluorohexylmethyl, or fluorinated ether side group [78,28,79]. These polymers differ not only in substituent group, but also in the amount of fluoro-substitution relative to PDMS, the overall molecular weight and crosslink density, and the amount of branching. In most commercially available cases, these polymers are addition cure systems and the reactions are those discussed previously for silicone networks.

The mechanisms employed for release in silicones are similar for fluorosilicones. A well crosslinked network provides a very low surface energy and few opportunities for direct chemical interaction between it and the PSA. Fluorosilicones are generally employed with silicone PSAs, in which case the fluorinated side groups act to help make the release polymer immiscible with the PSA. The amount of fluoro-substitution and the length of the fluorinated side group also impact the physical interdiffusion of the release and PSA molecules. To a point, increasing the amount of fluoro-substitution lowers mixing of the molecules and leads to lower peel forces. Restructuring of these networks is possible with time and temperature in the presence of the PSA, and aging can be difficult [80,81].

3.4. Alkyl side chain polymers

Polymers containing long alkyl side chains, typically between 16 and 22 carbon atoms in length, have been used extensively as low adhesion backsizes for PSA tape products for many years. The general structure of such polymers is shown schematically in Fig. 8. The alkyl side chains are attached through a bridging group, R_1 , to the polymer backbone, and the backbone may contain comonomers, R_2 .

In 1950, Dahlquist et al. [82] reported the use of polyvinyl *N*-alkyl carbamates as PSA release materials. Since then, many other types of alkyl side chain polymers have been patented for use as release coatings, including copolymers based on higher alkyl acrylates or methacrylates [83–86], polyvinyl esters of higher aliphatic fatty acids [87], higher alkyl vinyl esters or ethers and a maleic

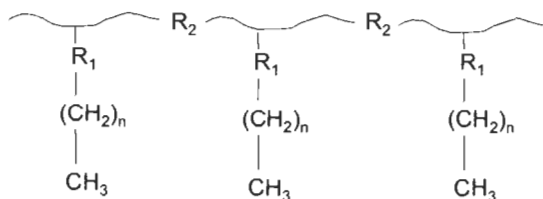


Fig. 8. Alkyl side chain polymers.

acid [88], *N*-alkyl polyacrylamides [89], the reaction product of ethylene–maleic anhydride and higher alkyl amines [90], octadecyl maleamic acid [91], fatty acid itaconates [92], poly-*N*-acyl-imines [93], and polyethylene imines acylated with higher fatty acids [94]. These types of release materials are typically coated from dilute solutions in organic solvents, although those containing acid groups can be dispersed in water by treating with a base, such as morpholine, followed by stripping of the solvents [83,85,88]. Alternatively, certain versions can be made directly in water via an emulsion polymerization process [86]. The alkyl side chain polymers generally provide release forces between about 50 and 500 g/cm, depending on the particular release material chemistry, PSA composition, tape backing, aging condition, etc. Therefore, they are most often used as LABs for PSA tape rolls, rather than for liners. The nonpolar alkyl side chains are attached to the polymer backbone through a bridging group, which is typically a polar group. In addition, the polymer backbone may contain polar segments or comonomers. The nonpolar alkyl groups, in particular the methyl groups on the ends of the alkyl side chains, provide a low energy surface in order to reduce the adhesion, while the polar groups provide mechanical strength and anchorage to backings. In order for such materials to be useful as release coatings, they need to provide stable unwind forces under whatever temperature and humidity conditions the PSA product will experience. In addition, they should ideally provide stable release forces for a variety of different PSA chemistries. While most, if not all, of the previously mentioned patented release materials can provide stable release under room temperature aging conditions, many of these release materials exhibit a significant increase in release force when aged at higher temperatures. For example, Williams et al. [87] reported that the low adhesion properties of polyvinyl stearate based copolymers were lost when aged against rubber-resin PSAs at temperatures above their melting points (35–43°C). Smith [92] reported that the release force of a rubber-resin based PSA tape, peeled from a poly stearyl itaconate release coating, increased from 60 g/cm when aged at room temperature to over 530 g/cm when aged at 65°C. In order to overcome this type of aging instability, Grossman et al. [91] developed release materials having melting points much higher than any aging temperature the tape might experience. For example, a copolymer of octadecyl maleamic acid with methyl acrylate, which had a melting point of 105–110°C, gave an initial release force of 75 g/cm and a 1 week 65°C aged release force of only 100 g/cm for a rubber-resin type PSA. In addition, Dahlquist et al. [82] mention that polyvinyl carbamates containing residual hydroxyl groups can be chemically crosslinked with a small proportion of a diisocyanate, thereby increasing their heat resistance (softening points).

X-ray scattering studies have shown that polymers containing long alkyl side chains typically form alternating layered structures in the bulk, with the polymer backbone forming one layer and the alkyl side chains forming the other layer [95–97], as shown schematically in Fig. 9. Generally, for side chain lengths

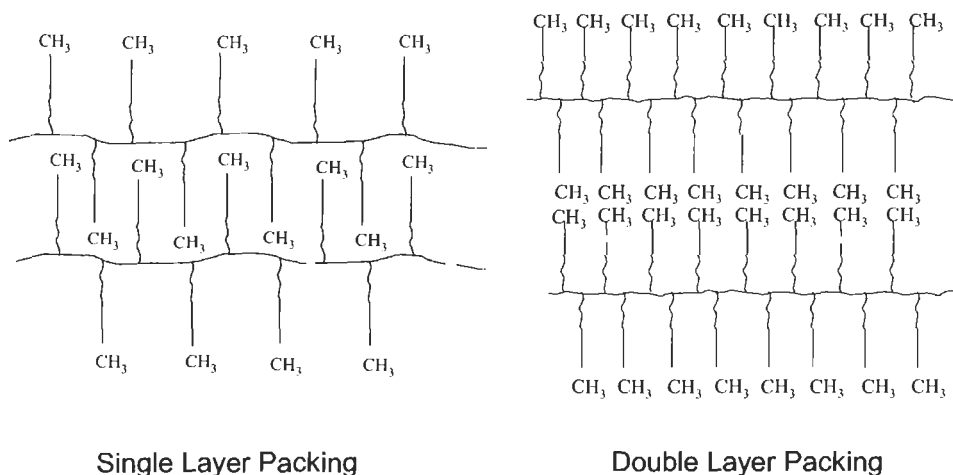


Fig. 9. Polymers containing long alkyl side chains typically form alternating layered structures.

greater than about 10–12 carbon atoms, the side chains will crystallize with hexagonal packing and be oriented, more or less, perpendicular to the backbone layer [95–97]. As would be expected, increasing the length of the alkyl side chain results in an increase in the layer spacing. Thermal studies have shown that only the portion of the side chain beyond the first 10–12 carbon atoms is involved in the hexagonal packing [98]. Typically, alkyl side chain polymers used for release coatings contain side chains of about 18 carbon atoms in length, in order to have sufficiently high melting points. As shown schematically in Fig. 9, both one-layer and two-layer packing have been observed depending on the specific chemical structure and the thermal history of the material [97], with the two-layer packing exhibiting slightly higher melting temperatures. Generally, decreasing the distance between the side chains along the backbone or increasing the flexibility of the polymer backbone favor two-layer packing. The melting point of these side chain polymers usually increases with increasing side chain length [95,96]. For example, the melting points of poly (*n*-alkyl acrylates) are about 32°C, 43°C, and 56°C for alkyl side chains having 14, 16, and 18 carbon atoms, respectively [96]. The melting point also tends to increase with increasing side chain content [97,99,100], increasing flexibility of the backbone [99,101,102], or annealing [96].

Polymers with long (e.g., 18 carbons) alkyl side chains have often been shown to possess surface energies that are similar to that of a monolayer of methyl groups (23 mJ/m²), indicating that the methyl groups on the ends of the side chains can pack effectively at the polymer surface [19,103,104]. The surface energy has been found to decrease steadily as the length of the side chain is increased, at least up to a side chain length of 10–12 carbons [103,104] where the side chains start

to crystallize. At the higher side chain lengths, lower surface energies have been reported in the cases of higher side chain content and higher backbone flexibility [103]. Note that these are the same factors that promote higher melting points in the bulk, indicating a correlation between the surface and bulk packing of the side chains. It is evident that the layered structure present in the bulk can persist at the polymer surface, with the alkyl side chains oriented nearly perpendicular to the surface.

In order for release materials to provide stable release forces for pressure sensitive adhesives, a stable interfacial structure is required so that the higher energy or polar segments in the release coating and PSA are separated from each other. However, upon contact between the PSA and the release coating, restructuring can occur within the PSA and release material near the PSA/release material interface, provided that there is sufficient segmental mobility and that there are specific favorable chemical interactions between the chemical groups in the PSA and the release material to drive the restructuring. The crystallization of the alkyl side chains provides a means by which the segmental mobility of the side chain release polymer can be greatly reduced [19,105]. The initial low surface energy structure of the release coating can then be preserved upon contact with the PSA, leading to stable release forces. Therefore, the melting point of the alkyl side chain polymer can play an important role in determining the release performance as a function of aging temperature.

Kasemura et al. [106] studied the surface dynamics, at room temperature, of the alkyl side chains in poly(vinyl alkylate)s using dynamic contact angle methods. In the case of alkyl side chains having 6 to 12 carbon atoms, the surface mobility is quite high and a large hysteresis between the advancing and receding water contact angle is seen. However, for higher side chain lengths, between 14 and 18 carbons in length, where the side chains crystallize, the hysteresis was greatly reduced due to a lower segmental mobility.

Kinning [19] studied the bulk, surface and interfacial structure of copolymers of polyvinyl *N*-alkyl carbamates and vinyl acetate (1 : 1 molar ratio), having either 10 or 18 carbons in the alkyl side chains, using thermal analysis, X-ray scattering, contact angle analysis, X-ray photoelectron spectroscopy (XPS), and static secondary ion mass spectrometry (SSIMS). While both polymers exhibited an overlayer of the alkyl side chains at the polymer surface and a surface energy typical of a monolayer of methyl groups, the release force profiles for the two polymers were quite different. The decyl version was unable to maintain a stable release force against an acidic acrylate PSA at any aging temperature, while the octadecyl version was able to provide stable release at aging temperatures less than about 50°C. The increase in release force was shown to be a result of interfacial restructuring, whereby the concentration of basic urethane and vinyl acetate groups in the release coating increased at the interface with the acidic PSA, leading to increased acid–base interactions and higher adhesion. In the case of

octadecyl side chains, side chain crystallization was apparent with a melting range of about 45–65°C, resulting in reduced segmental mobility and stable release forces at temperatures at least as high as 50°C. In contrast, the decyl version did not exhibit side chain crystallinity, only a glass transition centered at about 48°C. It is interesting to note that stable aging was not obtained for the decyl version at a temperature nearly 30°C less than the backbone glass transition temperature. Crystallization proved much more effective at locking the original surface structure in place, upon contact with the PSA, than having a high glass transition temperature.

Cai et al. [105] studied the surface and adhesion properties of undecyl oxazoline homopolymers as well as undecyl/phenyl oxazoline copolymers. Such polymers had relatively high melting points of between 135°C and 145°C, due to the fact that the polymer crystallizes into a triclinic unit cell involving both the backbone and side chain segments [107]. Contact angle and XPS analyses indicated that the undecyl side chains were oriented towards the surface, with the methyl endgroups covering the surface. In Cai's study, the peel forces of Scotch™ Brand Magic tape from coatings of the undecyl oxazoline polymers were quite low, increasing from an initial value of about 5 to about 12 g/cm after aging for 2 days at room temperature. The low peel forces could be maintained at aging temperatures approaching the melting point of the undecyl oxazolines. The increase in peel strength at aging temperatures near, or above, the melting point was attributed to the undecyl oxazoline coating dissolving into the PSA, once it melted. Alternatively, the melting of the undecyl oxazoline, and the concomitant increase in segmental mobility, could have resulted in an interfacial restructuring at the PSA interface, leading to attractive acid–base interactions between the basic amide groups in the release coating and the acidic groups in the PSA. Block copolymers of undecyl/phenyl oxazoline exhibited much higher peel forces than the undecyl oxazoline homopolymer. In addition, the peel forces increased significantly with aging time, even at low aging temperatures. The authors attributed this behavior to an incomplete coverage of the block copolymer surface with the undecyl groups.

Cai and Litt [108–110] also studied the surface and adhesion properties of random copolymers made from pentamethyl disiloxanyl decyl oxazoline and undecyl oxazoline. For these copolymers the melting point and crystalline content decreased steadily as the content of pentamethyldisiloxanyl groups increased. The critical surface tensions of the copolymers were measured to be 21 mJ/m² for all the copolymers, indicating that the amide groups in the polymer backbones were buried and the methyl groups covered the surface. The copolymers with less than 50 mol% pentamethyl disiloxanyl decyl oxazoline showed good release properties towards Scotch™ Brand Magic tape at aging temperatures of 50°C or less. However, the peel strengths increased dramatically as the aging temperature approached the melting points of the copolymers. Again, the melting of the release

polymer, and the concomitant increase in segmental mobility, likely resulted in an interfacial restructuring at the PSA interface, leading to attractive acid–base interactions between the basic amide groups in the release coating and the acidic groups in the PSA.

As mentioned previously, alkyl side chain polymers typically do not provide low enough release forces for most liner applications, in spite of having surface energies similar to the siloxane coatings that can provide very low release forces. This difference may be due, in part, to differences in bulk and surface rheology. Because the alkyl side chain polymers usually rely on crystallinity to provide stable release properties, they are typically high modulus materials. In contrast, polydimethylsiloxanes have a much lower modulus and a lower coefficient of friction which have been shown to be important factors in determining release force [17,18]. In general, the type of polymers which provide the easiest release tend to have low modulus.

3.5. Fluoroalkyl side chain polymers

Polymers containing fluoroalkyl type side chains have also been used as release coatings for PSAs, though not as extensively as alkyl side chain polymers. Such polymers can form ordered layered structures in the bulk similar to those seen for alkyl side chain polymers [111]. Volkov et al. [112] studied the structure of perfluoroalkyl side chain polymers having $-\text{C}_8\text{F}_{17}$ endgroups on the side chains, and found that increasing the main chain flexibility, on going from polyfumurate to polymethacrylate to polyacrylate enhanced the ability to form an ordered structure. The polyfumurate was amorphous, the polymethacrylate showed an ordered layered structure of the backbone without hexagonal packing of the side chains (Smectic A type liquid crystalline structure), and the polyacrylate showed both an ordered layering of the backbone and a hexagonal packing of the side chains (Smectic B type liquid crystalline structure). X-ray scattering studies indicated that a transition from the Smectic B liquid crystalline structure to the isotropic state occurred at a temperature of 77°C.

It has long been known that polymers containing fluorinated side chains can exhibit extremely low surface energies. For example, Bernett and Zisman [113] showed that polymers having $-\text{C}_7\text{F}_{15}$ and $-\text{C}_8\text{F}_{17}$ containing side groups had critical surface tensions of 10–11 mJ/m², nearly as low as the critical surface tensions of perfluoroalkanoic acid close packed monolayer [114]. It was proposed, therefore, that the fluorinated side chains were oriented nearly normal to the surface and nearly close packed, with the $-\text{CF}_3$ groups covering the surface.

Pittman and Ludwig [115] studied the wetting properties of a series of fluoroalkyl acrylates having $-\text{CH}_2(\text{CF}_2)_n\text{CF}_2\text{H}$ side chains, where n was 1, 3, 5, 7, or 9. The acrylates with $n = 7$ and 9 were partially crystalline (attributed to packing of the fluorochemical side chains) with melting points of about 56°C and

113°C, as determined by DSC. These polymers exhibited surface tensions of 13 and 15 mJ/m², respectively, similar to that of the corresponding acid monolayer. It was also shown that these polymers exhibited a sudden change in wetting behavior (decrease in hexadecane contact angle) near their melting points, which was attributed to a transition from a surface dominated by -CF₂H groups below the melting point to a surface dominated by -CF₂- groups above the melting point. Pittman et al. [116] later studied the wetting properties of polymers with -CH₂(CF₂)₆CF₃ containing side chains on one or three out of every four carbon atoms along the backbone. Critical surface tensions as low as 7.5 mJ/m² were reported.

Yokota and Hirabayashi [117] studied the structure of fluoroalkyl methacrylate homopolymer having -CH₂CH₂(CF₂)₇CF₃ side chains as well as alternating copolymers with butadiene. Even with a fluoroalkyl side chain on only every sixth carbon atom along the backbone these copolymers had a critical surface tension of 10.6 mJ/m², similar to the earlier results of Burnett and Zisman. Evidently, the fluoroalkyl side groups were able to pack effectively at the surface even though they were fairly widely spaced along the backbone.

In spite of their very low surface energies, fluoroalkyl side chain polymers are not used as extensively as alkyl side chain polymers for PSA release coatings since they often have a tendency to exhibit unstable release forces upon aging. For example, Dixon [118] reported the use of terpolymers of *N*-ethyl perfluorooctyl sulfonamido ethyl methacrylate, acrylic acid, and alkyl acrylates or methacrylates as low adhesion backsize coatings for paper backed (masking) tapes with various types of PSAs. In these terpolymers the fluorochemical monomer provides the low surface energy and release feature, the acrylic acid provides polarity for anchorage to the tape backing, and the alkyl (meth)acrylate provides solubility in organic solvents. It was reported that a high softening point, preferably greater than 100°C, was needed in order to obtain good release performance. In one example (55/40/5 weight ratio of *N*-ethyl perfluorooctyl sulfonamido ethyl methacrylate/acrylic acid/octadecyl acrylate), the release force for a tackified natural rubber type PSA was 180 g/cm initially and built to 445 g/cm after 7 months of natural aging. This same polymer provided a relatively high release force of 290 g/cm for an isooctyl acrylate/acrylic acid PSA after aging at 50°C for 11 days, the only aging condition tested. In spite of the very low surface energy of coatings made with this terpolymer, the coatings do not provide either low or stable peel forces. It was reported by Ramharack and Nguyen [119] that the homopolymer of *N*-ethyl perfluorooctyl sulfonamido ethyl methacrylate does not exhibit crystallinity, rather a glass transition centered at about 75°C was observed by DSC. Therefore, the terpolymer discussed by Dixon is not expected to exhibit side chain crystallinity either. This lack of side chain crystallinity probably accounts for the lack of release force aging stability, as the original near surface structure of the release coating is not effectively locked in place upon contact with the PSA. Rather, some degree of

interfacial restructuring likely occurs leading to increased chemical interactions at the PSA/release coating interface.

As discussed by Wang et al. [120], fluorinated block and segmented copolymers typically exhibit surface restructuring upon contact with a polar medium, whereby the amorphous fluorinated surface groups move away from the interface and the polar groups move towards the interface. This interfacial restructuring has limited the practical applications of such copolymers; however, recent studies have suggested methods to provide stable interfacial structures. For example, Maekawa et al. [121] reported that stable low energy surface structures could be obtained for perfluoroalkyl alkyl acrylates having high melting points. Such polymers had $-(CF_2)_nCF_3$ endgroups on the side chains with $n \geq 8$, and could maintain a high water receding contact angle. Wang et al. [120] demonstrated that stable low energy surface structures could be obtained for certain poly (styrene-*b*-semifluorinated side chain) block copolymers. By controlling the block copolymer composition and the relative lengths of the fluorocarbon and alkyl units in the side chain, the effect of chemical structure on the surface properties and the influence of liquid crystalline structure of the semifluorinated side chains on the surface behavior were evaluated. In the case of shorter fluorocarbon units in the side chains (i.e., $-(CF_2)_6-$), a Smectic A phase formed with a critical surface tension of 10.8 mJ/m^2 , and the polymer surface could undergo significant restructuring when immersed in water. In contrast, when the side chains contained $-(CF_2)_n-$ units with $n > 8$, a more highly ordered Smectic B phase was formed having lower critical surface tension (8 mJ/m^2) and a much more stable surface structure. Morita et al. [122] studied the surface properties of perfluoroalkylethyl acrylate/*n*-alkyl acrylate copolymers having about 60 wt% perfluoroalkylethyl acrylate. The perfluoroalkylethyl acrylate had a $-(CF_2)_8CF_3$ endgroup and the length of the alkyl group in the *n*-alkyl acrylate was varied from one carbon (methyl acrylate) through 18 carbons (octadecyl acrylate). Copolymers prepared with *n*-alkyl groups containing less than 12 carbon atoms exhibited a large hysteresis in water contact angle; however, in the case of 16 or 18 carbon atoms in the *n*-alkyl group a high receding contact angle could be maintained due to the crystallization of both the perfluoroalkyl and alkyl side chains. XPS on freeze dried surfaces showed that the contact angle hysteresis, in the case of the shorter alkyl acrylates, was due to a reorientation of the fluorochemical side chains when the surface was exposed to water. The crystallization of the side chains greatly decreased the segmental mobility in the near surface region of the coatings, resulting in a more stable surface structure. For the copolymer based on stearyl acrylate, a sudden decrease in the receding water contact angle was observed to occur as the temperature was raised beyond the copolymer's melting point (48°C), indicating that the surface molecular mobility reflects the bulk molecular mobility.

Dabroski [123] reported the use of waterbased release coatings based on blends of a small amount of a perfluoroalkyl-alkyl acrylate polymer with a film forming

polymer emulsion. For example, a blend of only 0.8% perfluorinated ester polymer (Scotchban™ FC-824) with an acid modified EVA emulsion provided a 10 day room temperature aged unwind of 160 g/cm for a masking tape based on tackified natural rubber PSA. After 10 days aging at 50°C, the unwind only increased to 180 g/cm. The mechanism by which a stable release force was obtained was not discussed.

3.6. Silicone–organic copolymers and networks

As discussed previously, crosslinked silicone networks are widely used as release coatings for liner applications where premium release (1–10 g/cm) is required. Such release coatings typically provide release forces which are too low for tapes in roll form, however. If the unwind forces are too low, telescoping, flagging, or premature unwinding of the tape roll can occur. For many aggressive PSAs, alkyl and fluoroalkyl side chain polymers typically have difficulty providing unwind forces less than about 80 g/cm. In order to bridge the gap between the release forces obtained with pure, or nearly pure, silicone networks and the side chain polymers, various silicone containing copolymers and networks have been developed. By adjusting such parameters as the silicone content, the silicone block or segment length, as well as the chemical composition of the non-silicone components, the release force can be adjusted as desired for a particular PSA or application. In addition, the wide range of compositions and molecular architectures that can be obtained with these silicone containing polymers allows other functionalities such as printability, writeability, and smooth unwind to be attained.

Various patents discuss the use of vinyl–silicone copolymers, and blends thereof, as PSA release coatings [124–127]. For example, Clemens et al. [124] discloses silicone grafted copolymers prepared from polydimethylsiloxane macromonomers (molecular weights between 1000 and 50,000) having vinyl endgroups and various vinyl monomers such as butyl methacrylate and acrylic acid. The polar comonomer provides anchorage to tape backings. A high degree of incorporation of the silicone grafts is needed to ensure a low level of silicone transfer to the PSA and good readhesion. Controlled and predictable release force is achieved through variation of the number and length, e.g., the molecular weight, of the polysiloxane grafts in the copolymer, as well as the composition of the vinyl backbone. Relatively small concentrations of silicone, usually less than 10%, are required to obtain efficient release since the low energy siloxane segments are highly surface active. Both solvent based and water based versions of vinyl–siloxane copolymers have been described. In addition, some of these compositions are reported to be writable [127].

The use of small amounts (0.5–3%) of polyethylene–polydimethylsiloxane or polystyrene–polydimethylsiloxane block copolymers in blends with a host

polymer have also been disclosed as PSA release coatings [128]. These blends can be extruded as a single layer or coextruded with a backing polymer to form, for example, a backing for PSA tapes. Relatively low copolymer molecular weights (e.g., between 2000 and 10,000) are preferred so that the copolymer can diffuse efficiently to the blend surface upon extrusion. A wide range of release forces can be obtained, depending on the amount and composition of the block copolymer. In the case of copolymers containing polyethylene blended into a polyethylene host matrix it is proposed that the polyethylene block in the copolymer can cocrystallize with the polyethylene matrix, thereby locking the copolymer onto the blend surface and decreasing the extent of silicone transfer to the PSA. However, the readhesion values reported are only between 48% and 73% of the control, consistent with a relatively high level of silicone transfer.

Various types of polyurea or polyurea/urethane segmented copolymers containing silicone segments have also been described as PSA release coatings [129–132]. Again, by adjusting the silicone content, silicone block length, and composition of the non-silicone segments the release force can be tailored for a specific PSA. The polar hard segments in these materials provide anchorage to backings, improved mechanical properties of the coatings, and modification of the release force, while the siloxane segments provide the low energy surface needed for release.

Silicone containing copolymeric networks, wherein a mixture of a functional silicone and copolymerizable monomers or oligomers are coated onto a web and cured, have also been used as PSA release coatings. Various chemistries, including polyurethane/urea–silicone networks [133], (meth)acrylate functional silicones coreacted with other vinyl monomers [134–136], and epoxyfunctional silicones coreacted with vinyl, epoxy, or hydroxy functional monomers [66,137,138] have been disclosed. Again, depending on the silicone content, silicone segment molecular weight, and composition of the non-silicone component, the release force can be tailored for a specific PSA. Usually, only small amounts of silicone are needed in the case of release coatings for tape rolls. A high degree of incorporation of the silicone segments into the network is required for good readhesion.

There have been many studies concerning the surface structure of various silicone containing copolymers and networks, including polydimethylsiloxane–polystyrene diblock and triblock copolymers [139,140], polydimethylsiloxane–polyvinyl alcohol graft copolymers [141], multiblock copolymers of bisphenol A polycarbonate and polydimethylsiloxane [142], diblock copolymers of polydimethylsiloxane and Nylon 6 [143], polydimethylsiloxane–polyamide multiblock copolymers [144], polydimethylsiloxane grafted polyurethanes [145], polydimethylsiloxane grafted acrylate copolymers [146], polydimethylsiloxane–polyethyleneoxide networks [147], and polydimethylsiloxane containing polyurethane, polyurea, or polyurethane–urea segmented copolymers [20,148–152]. It has been consistently

found that the surfaces of films prepared from such materials are dominated by the polydimethylsiloxane blocks or segments even at only a few percent siloxane, due to the low surface energy of the siloxane segments. Often times the polydimethylsiloxane segments form a thin overlayer (10–100 Å) on the surface, with the thickness of the overlayer increasing with increasing silicone content and increasing silicone segment molecular weight. Other factors can also play a role in determining the surface silicone concentration or silicone overlayer thickness including the molecular architecture, the degree of incompatibility, and processing conditions (e.g., choice of casting solvents and thermal history). Like other types of copolymers, silicone containing copolymers have also been shown to undergo interfacial restructuring upon contact with a polar medium such as water [20,141,145,148,152], whereby the silicone segments migrate away from the interface and the more polar or hydrophilic segments migrate towards the interface.

Hsu et al. [146] studied the effect of siloxane content (0.1–10 wt%) and siloxane molecular weight (500–25,000) on the surface composition and PSA release characteristics of a series of siloxane grafted butyl methacrylate/acrylic acid copolymers. Surface analysis by XPS showed that the amount of silicone in the near surface region increased with increasing bulk silicone concentration, leading to decreased peel forces for both rubber based and acrylic based PSA tapes. The release force was also found to decrease with increasing siloxane graft molecular weight, especially at graft molecular weights between 500 and 5000. By changing the silicone content and molecular weight, the silicone concentration near the surface could be easily adjusted, leading to tailored release forces for a variety of PSAs.

Kasemura et al. [153] studied blends of siloxane grafted methylmethacrylate/glycidylmethacrylate copolymer additives coreacted with epoxy resin. The relatively low molecular weight copolymer additives contained 15% of a 5000 molecular weight siloxane macromonomer and various glycidylmethacrylate contents. It was expected that the low surface energy siloxane segments would cover the surface of the blend and the glycidyl groups would coreact with the epoxy resin during curing. Only small amounts (about 1%) of the siloxane additive were needed to obtain a highly siliconized surface and low peel forces for a PSA tape. While the surface concentration of silicone was not affected by the glycidyl methacrylate content in the additive, the peel forces increased systematically with increasing glycidyl methacrylate content. Since no readhesion measurements or surface analysis of the PSA and release coatings were made after peeling them apart, it is difficult to determine the exact mechanism for the observed increase in peel force.

Kinning [20] studied the bulk, surface, and interfacial structures of a series of polyureas containing polydimethylsiloxane segments. In this study, the siloxane segment molecular weight (5000) and content (25 wt%) were kept constant, while

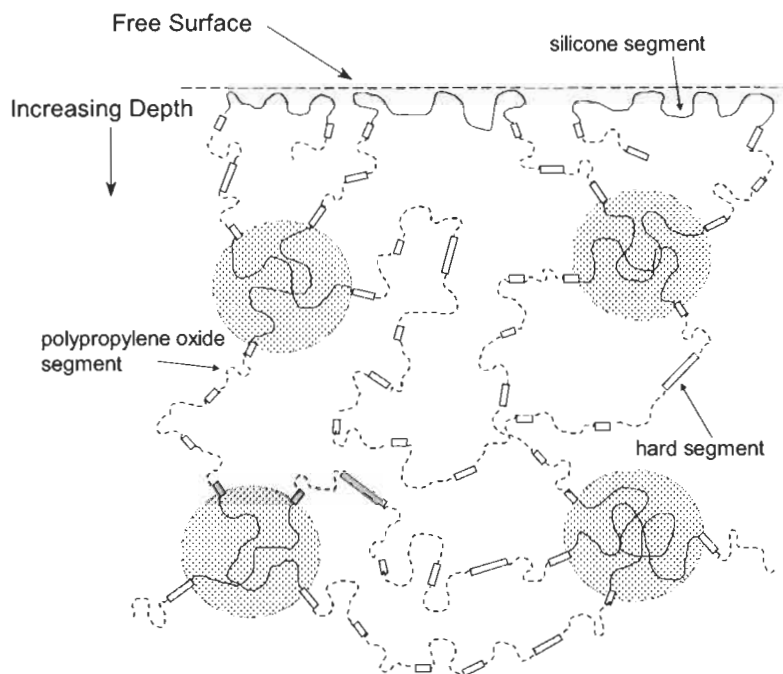


Fig. 10. Silicone polyurea near-surface structure prior to PSA contact. (From Ref. [20], copyright ownership by Overseas Publishers Association, reprinted with permission from Gordon and Breach Publishers.)

the non-silicone segment composition was adjusted in order to obtain a series of materials having a range of glass transition temperatures (between -1 and 170°C) for the non-silicone matrix phase. Surface analysis by XPS, SSIMS, and contact angle analysis showed that all of the silicone polyureas exhibited a thin overlayer, $15\text{--}20\text{ \AA}$ thick, of the siloxane segments at the coating surfaces, consistent with other studies of siloxane containing copolymers. The release force of a PSA tape containing an alkyl acrylate/acrylic acid copolymer PSA was measured as a function of aging time and temperature. Initially, the release forces provided by the various silicone polyureas were quite low, similar to that provided by silicone based liners. However, the release forces were observed to increase with increasing aging time and/or increasing aging temperature. Silicone polyureas with higher non-silicone matrix phase glass transition temperatures exhibited a slower rate of adhesion build. The build in adhesion was shown to be due to an interfacial restructuring at the PSA/silicone polyurea interface, whereby the non-silicone segments in the silicone polyurea (e.g., the urea groups) migrated towards the interface and the silicone segments migrated away from the interface, as shown schematically in Figs. 10 and 11.

In the case of an acrylate PSA containing an acidic comonomer, there is the

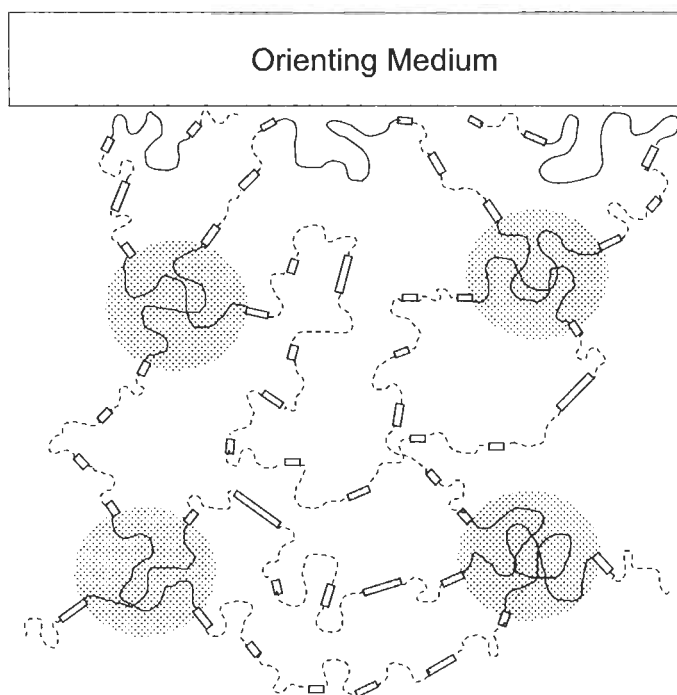


Fig. 11. Silicone polyurea interfacial structure against orienting medium (PSA). (From Ref. [20], copyright ownership by Overseas Publishers Association, reprinted with permission from Gordon and Breach Publishers.)

potential for acid–base interactions between the acrylic acid in the PSA and the basic urea groups in the polyurea, and these favorable chemical interactions provide the driving force for the interfacial restructuring. The rate of increase in peel force upon aging, and the rate of interfacial restructuring, is dependent on the degree of segmental mobility in the polyurea near the interface with the PSA. Polyureas having lower non-silicone matrix phase T_g values have a higher degree of segmental mobility and therefore exhibit higher rates of adhesion build. For example, for the polyurea with a matrix T_g of -1°C , the peel force built to over 650 g/cm within 15 min contact time. In contrast, the polyurea with a matrix T_g of 170°C exhibited a peel force of only 175 g/cm after aging for 1 week at room temperature. Aging at elevated temperatures induces more segmental mobility within the silicone polyurea which also increases the rate of adhesion build. It is interesting to note that a significant build in adhesion was observed even when the non-silicone matrix phase T_g was over 100°C higher than the aging temperature, indicating that the segmental mobility near the interface is higher than it is in the bulk. Similar trends, in terms of the ability of the silicone containing polyureas to restructure, were seen when the orienting medium was water instead of the PSA.

Thanawala and Chaudhury [39] studied polydimethylsiloxane elastomers modified by reacting allyl amide functional perfluorinated ether segments to the siloxane network by a hydrosilation reaction. Only 1–2 wt% of the surface active perfluorinated ether was needed to reduce the surface energy of the elastomer from 22 to 8 mJ/m². However, the addition of the perfluorinated ether to the siloxane network actually resulted in a significant increase in the peel force of an acrylic PSA tape, measured after a short contact time at room temperature. It was also found that the water contact angle hysteresis increased markedly with increasing amount of the perfluorinated ether. These results were attributed to an interfacial reconstruction, whereby the high energy amide functionalities of the perfluorinated ether (originally buried beneath the surface) were attracted to the interface where they could interact with the water or the PSA. The addition of the perfluorinated ether to the siloxane network was therefore proposed as a way of tailoring the PSA release force. No measurements of the effect of aging time or temperature on the release force were reported, however.

3.7. Polyolefins

The use of polyolefins as release materials evolves naturally from the inherent difficulty most PSAs have in adhering to them [154]. Polyethylene (PE) and polypropylene (PP) substrates, when not surface treated (i.e. by corona or flame, etc.) present low energy surfaces, that for some PSAs result in low enough adhesion values to become their means of delivery. Olefin release materials also present fairly non-interacting surfaces. Again, release is only stable where interdiffusion with the PSA is avoided, making olefin release materials inappropriate for most olefin PSAs. Polyethylene used as release materials can be of the high, medium, low or ultra low-density variety. Most current commercial uses of olefins as release components target higher release levels. However, as mentioned previously, manipulation of resin density can lower the release of some PSAs by an order of magnitude. In general, branching of the polyethylene molecule can be used to control the crystalline content or density of the PE film. Additionally, copolymerization with an α -olefin like propylene, butene, pentene, hexene, methyl-pentene or octene via metallocene or traditional catalysis is possible [44,155–157]. In some more recent developments, acrylates copolymerized in the system act to lower the density and also provide reasonable release [158].

Olefins when used as release materials are commonly extruded either as the complete release film or as a skin layer on a multi-layer system. Processing effects can impact the release force in as much as temperatures and orientation can effect crystallinity and density. The polymers are of high enough molecular weight to be sufficiently entangled, and curing is not required. In multi layer systems it is often important that there be tie layers or some priming technique involved to ensure adequate anchorage between the releasing system and the bulk of the substrate.

4. Additional functionalities

As mentioned in the introduction, release coatings are often required to perform other functions besides providing an appropriate release level for the PSA. For example, a tape user may want to write on the release coated tape backing with a pencil or pen. It may also be desirable to be able to print a logo or message directly onto the release coated backing of a tape or a label. In the case of a masking tape used to paint an automobile, the paint needs to adhere to the tape backing when the tape is removed so that the paint does not flake off onto the freshly painted surface. In some cases, for example a tape used to attach a baby's diaper, quiet or smooth release is a desirable feature. In other cases, such as a liner for a transfer PSA, a low coefficient of friction of the release coating can make the PSA application easier.

Typically, writeability, printability, or paintability can be obtained by blending or coreacting a release component with an ink or paint receptive component that can be swollen by, or be dissolved into, the carrier for the ink or paint. Such coatings should not exhibit any dewetting of the ink or paint, and the ink or paint should adhere well enough to the release coating such that it cannot be smeared, rubbed, or flaked off. Mertens et al. [127] disclose the use of siloxane grafted release materials comprising free radically polymerizable vinyl monomers, hydrophilic comonomers, and a siloxane macromonomer for PSA release coatings that can be written on with pens containing either solvent or water based inks. Mertens et al. teach that the incorporation of a hydrophilic comonomer, such as acrylic acid, methacrylic acid, hydroxyethylacrylate, or *N*-vinyl pyrrolidone, results in coatings that can be written on with pens using water based inks due to the water being absorbed into the coating, which facilitates a rapid restructuring of the release coating surface. Initially, the surface is covered with the siloxane segments, but after contact with the water based ink, the hydrophobic siloxane segments migrate away from the interface with the ink, and the more hydrophilic segments come into contact with the ink. The interfacial restructuring reduces the interfacial tension, and thus, the tendency for dewetting of the ink, and must take place quite quickly, in a matter of seconds. Silicone copolymers which exhibit a lower rate of interfacial restructuring in contact with water [145,148,152] are not expected to be very writeable with waterbased inks. The requirements stated by Mertens et al. for an acceptable combination of writeability and stability in the release force included a receding water contact angle less than 25° (i.e., a large hysteresis in water contact angle), a difference in the hydrated and dry T_g of the non-silicone matrix being greater than 20°C (i.e., the water needs to plasticize the coating sufficiently to facilitate restructuring), and a hydrated T_g between -15°C and 35°C . Hydrated T_g values less than -15°C tended to result in unstable PSA release forces, while hydrated T_g values greater than 35°C did not provide rapid enough restructuring. It is also stated that fillers (e.g., silica or calcium carbonate)

may be added to create a surface texture that is more receptive to marking with a pencil or with roller ball pens due to the additional friction that the fillers provide.

Yamamoto and Minamizaki [159] disclose the use of a curable silicone based release agent blended with resin particles which swell or are soluble in organic solvent. Coatings made with such blends can be written on with solvent based inks. For example, an addition cure silicone network containing 20 wt% 0.1 μm diameter PMMA particles exhibited both good writeability (no ink dewetting and smear free) and a low release force of 10 g/cm for a PSA tape.

Several patents discuss the use of alkyl side chain type LABs, blended with various film forming resins, to provide release coatings that can be printed with solvent based flexographic inks [160–162]. For example, Truskolaski and Pohl [162] disclose a blend of polyvinyl *N*-octadecyl carbamate [82] and chlorinated polyolefin resin. They teach that heating the tapes coated with this release blend above the melting point of the polyvinyl *N*-octadecyl carbamate softens the release coating making the resulting printed image adhere better to the tape backing. Blends of a film forming polymer and a silicone containing release material have also been disclosed as release coatings that can be printed with flexographic inks [163].

Several approaches have been disclosed to make release coatings that can be printed with ink jet or laser jet printers (e.g., to make linerless labels). For example, Khatib and Langan [164] disclose a blend of two different acrylate functional silicones, one with a high level of acrylate functionality to provide the printability and one with a low level of acrylate functionality to provide easy PSA release. Lievre and Mirou [165] describe an aqueous blend of a crosslinkable silicone and poly(vinyl alcohol–vinyl acetate) resins while Shipston and Rice describe a blend of acrylic resin and a surfactant [166].

Another example of an application requiring a printable release coating is a linerless roll of postage stamps. The release coating must be able to accept the cancellation inks used by the post office, which are typically glycol based. In order for the cancellation mark to be smear free in a short period of time, the release coating must be able to absorb the ink quickly. One approach that has been disclosed to accomplish this is to blend a silicone containing polyurea, such as those taught in Tushaus and Weiderholt [129], with calcium carbonate and polyvinyl pyrrolidone [167]. Another approach is to blend a condensation or addition curable silicone with polyurethane, polyamide, or polyurea resin particles [168].

As discussed by Yarusso [6], as the rate at which a PSA tape is peeled from a release coated backing increases, a transition from smooth peel to shocky or raspy peel is often encountered. This shocky peel is typically accompanied by an undesirably high noise level, particularly for large jumbos of tape in a factory setting. Therefore, there has been an effort to develop tapes which exhibit quiet and smooth unwind characteristics. Some of the factors which can affect the shockiness include the stiffness and surface topology of the backing, the

rheology of the PSA and release coating, and the level of the release force. Stiffer backings, PSAs, and release coatings tend to promote shocky unwind. Several patents have discussed approaches for reducing the PSA stiffness in order to promote smooth unwind, including the addition of oil to the PSA [169], and the use of styrene–diene block copolymer PSAs having specific levels of diblock and tackifier content, as well as a glass transition temperature within a certain range [170]. Backings with microtopographical features have also been disclosed as a way of reducing shockiness at higher peel rates [171]. The shockiness can also be affected by the choice of the release coating, with stiffer release coatings, such as the crystalline alkyl side chain type polymers, tending to provide more shocky peel. Elastomeric silicone networks with low crosslink density can provide smooth peel, but the peel forces may be too low for the intended application (e.g., tape rolls or liners with modified release level). Higher peel forces can be obtained, for example, with epoxy or acrylate functional silicones having a higher level of epoxy or acrylate functionality; however, this also results in a higher crosslink density and a greater tendency for shocky or raspy release. A blend of two silicones, one having a high level of functionality, and the other having a low level of functionality, has been proposed to obtain simultaneously a modified release level and smooth release for epoxy [172] or acrylate [173] functional silicones. Alternatively, Kessel et al. [174] have proposed using an epoxysilicone having both a low level of epoxy groups, to reduce the crosslink density and shockiness, as well as a high level of alkyl, aryl, or alkyl aryl substitution (e.g., styryl groups), to increase the release force. Lu [175] disclosed the addition of higher alkyl acrylate comonomers (e.g., octyl or decyl acrylate) to a blend of acrylate functional silicones in order to simultaneously increase the release force and maintain smooth peel. The higher alkyl acrylates copolymerize with the silicone acrylates, reducing the crosslink density and forming low T_g acrylate polymer, which help to maintain a low coating modulus. In contrast, the addition of MQ resins as a release modifier led to a stiffer coating promoting raspy or shocky peel.

Another property that can be desired of release materials is ‘slippery feel’ or low coefficient of friction. This is of particular concern in applications where the liner is smoothed over a part by hand, as when transfer tape is adhered to a substrate. Rubbery feel (high friction) occurs in liners in which the silicone network is highly crosslinked, like the solvent free addition cure, or highly functional radiation cure materials. Related to the discussion above on the modification of raspy peel, the coefficient of friction can be modified by the addition of higher molecular weight, less functional silicones. Lowering the crosslink density of a silicone network will lead to lower friction. In practical application to solvent free silicone systems, only a small amount of high molecular weight material must be added to obtain the slippery feel, and processing viscosity need not be detrimentally effected [51,52].

References

1. Satas, D., *Handbook of Pressure Sensitive Adhesive Technology*, 2nd edition. Van Nostrand Reinhold, New York, 1989.
2. Gent, A.N. and Schultz, J., *J. Adhes.*, **3**, 281 (1972).
3. Andrews, E.H. and Kinloch, A.J., *Proc. R. Soc. Lond. Ser. A*, **332**, 385 (1973).
4. Mizumachi, H. and Hatano, Y., *J. Appl. Polym. Sci.*, **37**, 3097 (1989).
5. Hata, T., *J. Adhes. Soc. Jpn.*, **8**, 64 (1972).
6. Yarusso, D.J., *J. Adhes.*, **70**, 299 (1999).
7. Owen, M.J., *Proc. Adhes. Soc.*, **19**, 367 (1996).
8. Owens, D.K. and Wendt, R.C., *J. Appl. Polym. Sci.*, **13**, 1740 (1969).
9. Wu, S., *Polymer Interface and Adhesion*. Marcel Dekker, New York, 1982.
10. Toyama, M., Ito, T. and Moriguchi, H., *J. Appl. Polym. Sci.*, **14**, 2039 (1970).
11. Toyama, M. and Ito, T., *Polym. Plast. Technol. Eng.*, **2**, 161 (1973).
12. Sherriff, M., Knibbs, R.W. and Langley, P.G., *J. Appl. Polym. Sci.*, **17**, 3423 (1973).
13. Zosel, A., *Colloid Polym. Sci.*, **263**, 553 (1985).
14. Dahlquist, C.A., *ASTM Special Technical Publication*, **360**, 46 (1963).
15. Dahlquist, C.A., In: Alner, D.J. (Ed.), *Aspects of Adhesion-5*. University of London Press, London, 1969, p. 183.
16. Duel, L.A. and Owen, M.J., *J. Adhes.*, **16**, 49 (1983).
17. Newby, B.Z., Chaudhury, M.K. and Brown, H.R., *Science*, **269**, 1407 (1995).
18. Newby, B.Z. and Chaudhury, M.K., *Langmuir*, **13**, 1805 (1997).
19. Kinning, D.J., *J. Adhes.*, **60**, 249 (1997).
20. Kinning, D.J., *J. Adhes.*, **75**, 1 (2001).
21. Coughlan, R.T. and Bojarski, S.M., U.S. Patent 4,454,266, assigned to Daubert Coated Products, 1984.
22. Radiation curing silicones, Goldschmidt Informiert #65, January 1987.
23. Jones, D.J., Factors Affecting the Selection and Performance of Silicone Release Coatings. Dow Corning Corp., 1997.
24. Kreckel, K.W., U.S. Patent 5,061,535, assigned to 3M, 1991.
25. Nippon, K., JP Patent 62209183, 1987.
26. Kogyo, F., JP Patent 58015537, 1981.
27. Pennace, J.R. and Quinn, S.A., U.S. Patents 4,614,677 and 4,684,557, both assigned to Flexcon Company, 1986 and 1987.
28. Brown, P.L. and Stickles, D.L., U.S. Patent 4,736,048, assigned to Dow Corning Corp., 1988.
29. O'Malley, W.J., U.S. Patent 4,039,707, assigned to General Electric, 1977.
30. Zhao, C.L., Dobler, F., Pith, T., Holl, Y. and Lambla, M., *J. Colloid Interface Sci.*, **128**, 437 (1989).
31. Zhao, C.L., Holl, Y., Pith, T. and Lambla, M., *Br. Polym. J.*, **21**, 155 (1989).
32. Lavielle, L. and Schultz, J., *J. Colloid Interface Sci.*, **106**, 438 (1985).
33. Holmes-Farley, S.R., Reamey, R.H., Nuzzo, R., McCarthy, T.J. and Whitesides, G.M., *Langmuir*, **3**, 799 (1987).
34. Lee, S.H. and Ruckenstein, E., *J. Colloid Interface Sci.*, **120**, 529 (1987).
35. Deng, Z. and Schreiber, H.P., *J. Adhes.*, **36**, 71 (1991).
36. Lewis, K.B. and Ratner, B.D., *J. Colloid Interface Sci.*, **159**, 77 (1993).
37. Tezuka, Y. and Araki, A., *Langmuir*, **10**, 1865 (1994).
38. Senshu, K., Kobayashi, M., Ikawa, N., Yamashita, S., Hirao, A. and Nakahama, S., *Langmuir*, **15**, 1763 (1999).

39. Thanawala, S.K. and Chaudhury, M.K., *Langmuir*, **16**, 1256 (2000).
40. Owen, M.J., *Surf. Coat. Int.*, **9**, 400 (1996).
41. Nakao, K. and Nishimura, Y., *J. Adhes.*, **46**, 117 (1994).
42. Pellerite, M.J., U.S. Patent 5,306,758, assigned to 3M, 1994.
43. Owen, M.J., *1st International Congress on Adhesion Science and Technology*, 1998, p. 255.
44. Adamko, M., U.S. Patent 5,948,517, assigned to Norton Performance Plastics, 1999.
45. Clarson, S.J., *Siloxane Polymers*. PTR Prentice Hall, Englewood Cliffs, NJ, 1993.
46. Ansel, D.S., *PSTC Tech XVI Conf. Proc.*, Ed. Pressure Sensitive Tape Council, Schaumburg, IL, 1993.
47. Dallavia, A.J., EP Patent 216376, assigned to General Electric, 1987.
48. Drahnak, T.J., U.S. Patent 4,530,879, assigned to 3M, 1985.
49. Butts, M.D. and Szary, A.C., EP Patent Application 1050538 A2, assigned to General Electric Company, 2000.
50. Traver, F.J. and Cietek, T.J., U.S. Patent 4,190,688, assigned to General Electric Company, 1980.
51. Hara, Y. and Momii, K., JP Patent 61264052, assigned to Shin Etsu, 1986.
52. Kessel, C.R. and Melancon, K.C., U.S. Patent 5,432,006, assigned to 3M, 1995.
53. Garden, W.D., GB Patent 1518371, assigned to Imperial Chemical, 1978.
54. Eckberg, R.P., *Radcure 88 Conf. Proc.*, 1988, p. 576.
55. Kessel, C.R. and Nelson, M.C., U.S. Patent 5,332,797, assigned to 3M, 1994.
56. Kerr, S.R., *Adhes. Age*, **Aug.**, 26 (1996).
57. Johnson, G.C. and Metzler, R.B., U.S. Patent 4,046,930, assigned to Union Carbide, 1977.
58. Desorcie, J.L. and O'Brien, M.J., U.S. Patent 5,010,118, assigned to General Electric, 1991.
59. Nitto Electric, JP Patent 61120879, 1986.
60. Crivello, J.V. and Lam, J.H.W., *J. Polym. Sci. Polym. Chem. Ed.*, **17**, 977 (1979).
61. Crivello, J.V. and Lam, J.H.W., *Macromolecules*, **10**, 1307 (1977).
62. Kessel, C.R. and Bany, S.W., U.S. Patent 4,822,687, assigned to 3M, 1989.
63. Riding, K.D., U.S. Patent 5,158,991, assigned to General Electric, 1992.
64. Eckberg, R.P. and LaRochelle, R.W., U.S. Patent 4,279,717, assigned to General Electric, 1981.
65. Eckberg, R.P., U.S. Patent 4,576,999, Assigned to General Electric, 1986.
66. Eckberg, R.P., CA Patent 1218494, assigned to General Electric, 1987.
67. Koshar, R. and Bany, S.W., U.S. Patent 4,313,988, assigned to 3M, 1982.
68. Norstrom, T. and Zelek, C., U.S. Patent 3,650,813, assigned to Ford Motor, 1972.
69. Gornowicz, G.A., U.S. Patent 4,563,539, assigned to Dow Corning Corp., 1986.
70. Cyterski, D.J., *Radcure '84 Conf. Proc.*, 1984.
71. Lin, S.Q.S. and Jacobine, A.F., U.S. Patent 4,534,838, assigned to Locktite, 1985.
72. Jones, D.J., *Tech. XIII, Proc. Of PSTC*, Itasca, IL, May 1990, p. 155.
73. Cosgrove, T., Weatherhead, I., Turner, M.J., Schmidt, R.G., Gordon, G.V. and Hannington, J.P., *Polym. Preprints*, (1998).
74. Gordon, G.V., Perz, S.V., Tabler, R.L., Stasser, J.L., Owen, M.J. and Tonge, J.S., *Adhes. Age*, **41(11)**, 35 (1998).
75. Gordon, G.V., Leaym, T.M., Owen, M.J., Owens, M.S., Perz, S.V., Stasser, J.L., Tonge, J.S., Chaudhury, M.K. and Vorvolakos, K.A., *Adh. Soc.*, 39 (2000), taken from the 23rd annual meeting of the Adhesion Society.
76. Ditoot, S.M. and Thompson, D.C., EP Patent Application 1034198, assigned to Rexam, 1999.

77. Larson, J.M., U.S. Patent 4,830,910, assigned to 3M, 1989.
78. Griswold, R.M. and O'Brien, M.J., EP 0903388 A2, assigned to General Electric, 1999.
79. Shunji, A., JP Patent 09176491, assigned to Shin Etsu Chem. Co., 1997.
80. Owen, M.J., *Fluoropolymers Conf.*, 1992. RAPRA Technology, Ltd.
81. Owen, M.J. and Kobayashi, H., *Surf. Coat. Int.*, **78**(2), 52 (1995).
82. Dahlquist, C.A., Hendricks, J.O. and Sohl, W.E., U.S. Patent 2,532,011, assigned to 3M, 1950.
83. Hendricks, J.O., U.S. Patent 2,607,711, assigned to 3M, 1952.
84. Crocker, G.J., U.S. Patent 3,502,497, assigned to Johnson and Johnson, 1970.
85. Doehnert, D.F., U.S. Patent 4,299,741, assigned to Permacel, 1981.
86. Urquiola, M.B., U.S. Patent 5,516,865, assigned to 3M, 1996.
87. Williams, P.L., U.S. Patent 2,829,073, assigned to Adhesives Tapes Limited, 1958.
88. Dahlquist, C.A., Ahlbrecht, A.H. and Dixon, G.M., U.S. Patent 2,876,894, assigned to 3M, 1959.
89. Lavanchy, P., U.S. Patent 3,051,588, assigned to Johnson and Johnson, 1962.
90. Christmas, H.F., U.S. Patent 3,240,330, assigned to Adhesives Tapes Ltd., 1966.
91. Grossman, R.F. and Webber, C.S., U.S. Patent 3,342,625, assigned to Norton Company, 1967.
92. Smith, R.M., U.S. Patent 3,052,566, assigned to Johnson and Johnson, 1962.
93. Bartell, C., Milutin, I.C., Porsche, J.D. and Rolih, R.J., U.S. Patent 3,475,196, assigned to Borden, Inc., 1969.
94. Demmig, H.W. and Rehnelt, K., U.S. 3,510,342, assigned to Henkel and Cie G.m.b.H., 1970.
95. Greenberg, S.A. and Alfrey, T., *J. Am. Chem. Soc.*, **76**, 6280 (1954).
96. Plate', N.A. and Shibaev, V.P., *Macromol. Rev.*, **8**, 117 (1974).
97. Hseih, H.W.S., Post, B. and Morawetz, H., *J. Polym. Sci. Polym. Phys. Ed.*, **14**, 1241 (1976).
98. Jordan Jr., E.F., Feldeisen, D.W. and Wrigley, A.N., *J. Polym. Sci. Part A-1*, **9**, 1835 (1971).
99. Jordan Jr., E.F., Artymyshyn, B., Specca, A. and Wrigley, A.N., *J. Polym. Sci.*, **9**, 3349 (1971).
100. Yokota, K. and Hirabayashi, T., *Polym. J.*, **17**, 991 (1985).
101. Plate', N.A., Shibaev, V.P., Petrukhin, B.S., Zubov, Y.A. and Kargin, V.A., *J. Polym. Sci. Part A-1*, **9**, 2291 (1971).
102. Mathias, L.J., *Polym. Commun.*, **29**, 352 (1988).
103. Schwarcz, A. and Farinato, R.S., *J. Polym. Sci. Polym. Phys. Ed.*, **10**, 2025 (1972).
104. Kamagata, K. and Toyama, M., *J. Appl. Polym. Sci.*, **18**, 167 (1974).
105. Cai, G., Litt, M.H. and Krieger, I.M., *J. Polym. Sci. Polym. Phys.*, **29**, 773 (1991).
106. Kasemura, T., Takahashi, S., Nakane, N. and Maegawa, T., *Polymer*, **37**, 3659 (1996).
107. Litt, M., Rahl, F. and Roldan, L.G., *J. Polym. Sci. A-2*, **7**, 463 (1969).
108. Cai, G. and Litt, M.H., *J. Polym. Sci. Polym. Chem.*, **30**, 649 (1992).
109. Cai, G. and Litt, M.H., *J. Polym. Sci. Polym. Chem.*, **30**, 659 (1992).
110. Cai, G. and Litt, M.H., *J. Polym. Sci. Polym. Chem.*, **30**, 671 (1992).
111. Shimizu, T., Tanaka, Y., Kutsumizi, S. and Yano, S., *Macromolecules*, **29**, 156 (1996).
112. Volkov, V.V., Plate', N.A., Takahara, A., Kajiyama, T., Amaya, N. and Murata, Y., *Polymer*, **33**, 1316 (1992).
113. Bennett, M.K. and Zisman, W.A., *J. Phys. Chem.*, **66**, 1207 (1962).
114. Hare, E.F., Shafirin, E.G. and Zisman, W.A., *J. Phys. Chem.*, **58**, 236 (1954).
115. Pittman, A.G. and Ludwig, B.A., *J. Polym. Sci. Part A-1*, **7**, 3053 (1969).

116. Pittman, A.G., Wasley, W.L. and Sharp, D., *J. Polym. Sci. Polym. Chem. Ed.*, **12**, 521 (1974).
117. Yokota, K. and Hirabayashi, T., *Polym. J.*, **17**, 991 (1985).
118. Dixon, G.M., U.S. Patent 3,318,852, assigned to 3M, 1967.
119. Ramharack, R. and Nguyen, T.H., *J. Polym. Sci. Polym. Lett.*, **25**, 93 (1987).
120. Wang, J., Mao, G., Ober, C.K. and Kramer, E.J., *Macromolecules*, **30**, 1906 (1997).
121. Maekawa, T., Kamata, S. and Matsuo, M., *J. Fluor. Chem.*, **54**, 84 (1991).
122. Morita, M., Ogisu, H. and Kubo, M., *J. Appl. Polym. Sci.*, **73**, 1741 (1999).
123. Dabroski, W.C., U.S. Patent 4,513,059, assigned to Permacel, 1985.
124. Clemens, L.M., Kantner, S.S. and Mazurek, M., U.S. Patent 4,728,571, assigned to 3M, 1988.
125. Kantner, S.S., Kumar, R.C. and Eian, G.L., U.S. Patent 5,032,460, assigned to 3M, 1991.
126. Kumar, R.C. and Kantner, S.S., U.S. Patent 5,229,179, assigned to 3M, 1993.
127. Mertens, T.A., Kantner, S.S. and Melancon, K.C., U.S. Patent 5,154,962, assigned to 3M, 1992.
128. Mann, R.H., Sun, E.I., Plamthottam, S.S. and Newing, C.W., U.S. Patent 5,728,469, assigned to Avery Dennison Corp., 1998.
129. Tushaus, L.A. and Weiderholt, G.T., U.S. Patent 5,290,615, assigned to 3M, 1994.
130. Shores, A.A., U.S. Patent 5,356,706, 1994.
131. Larson, W.K., Bennett, R.E. and Franchina, N.L. U.S. Patent 5,679,754, assigned to 3M, 1997.
132. Sengupta, A., U.S. Patent 5,750,630, assigned to 3M, 1998.
133. Schurb, F.A. and Evans, J.L., U.S. Patent 3,997,702, assigned to 3M, 1976.
134. Mazurek, M.H., Kantner, S.S. and Everaerts, A.I., U.S. Patent 5,527,578, assigned to 3M, 1996.
135. Nguyen, T.V., Allen, J. and Lu, Q., U.S. Patent 5,616,629, assigned to Avery Dennison Corp., 1997.
136. Curatolo, B.S. and Fox, T.J., U.S. Patent 5,888,649, assigned to Avery Dennison Corp., 1999.
137. Manzouji, R. and Okawa, T., U.S. Patent 5,750,587, assigned to Dow Corning Toray Silicone Co., 1998.
138. Kline, J.R., U.S. Patent 6,022,050, assigned to Monarch Marking Systems, 2000.
139. Clark, D.T. and Peeling, J., *J. Polym. Sci. Polym. Chem. Ed.*, **14**, 543 (1976).
140. Chen, X., Gardella Jr., J.A. and Kumler, P.L., *Macromolecules*, **25**, 6621 (1992).
141. Tezuka, Y., Fukushima, A., Matsui, S. and Imai, K., *J. Colloid Interface Sci.*, **114**, 16 (1986).
142. Chen, X., Lee, H.F. and Gardella Jr., J.A., *Macromolecules*, **26**, 4601 (1993).
143. Chen, X., Gardella Jr., J.A. and Cohen, R.E., *Macromolecules*, **27**, 2206 (1994).
144. Senshu, K., Furuzono, T., Koshizaki, N., Yamashita, S., Matsumoto, T., Kishida, A. and Akashi, M., *Macromolecules*, **30**, 4421 (1997).
145. Tezuka, Y., Ono, T. and Imai, K., *J. Colloid Interface Sci.*, **136**, 408 (1990).
146. Hsu, T., Kantner, S.S. and Mazurek, M., *Polym. Mater. Sci. Eng.*, **55**, 562 (1986).
147. Chaikof, E.L. and Merrill, E.W., *J. Colloid Interface Sci.*, **137**, 340 (1990).
148. Tezuka, Y., Kazama, H. and Imai, K., *J. Chem. Soc. Faraday Trans.*, **87**, 147 (1991).
149. Benrashid, R., Nelson, G.L., Linn, J.H., Hanley, K.H. and Wade, W.R., *J. Appl. Polym. Sci.*, **49**, 523 (1993).
150. Yoon, S.C., Ratner, B.D., Ivan, B. and Kennedy, J.P., *Macromolecules*, **27**, 1548 (1994).
151. Chen, X., Gardella Jr., J.A., Ho, T. and Wynne, K.J., *Macromolecules*, **28**, 1635 (1995).
152. Pike, J.K., Ho, T. and Wynne, K.J., *Chem. Mat.*, **8**, 856 (1996).

153. Kasemura, T., Komatu, C., Nishihara, H., Takahashi, S., Oshibe, Y., Ohmura, H. and Yamamoto, T., *J. Adhes.*, **47**, 17 (1994).
154. Bently, D.J., *Paper Film Foil Converter*, 20 (1997).
155. Nishiyama, N., Ohura, M., Takahiro, H. and Yamamoto, H., JP Patent Application 2000239624, assigned to Nitto Denko Corp., 2000.
156. Shibano, T., Maruchi, S., Yakan, K., Kobayashi, T. and Akimoto, S., U.S. Patent 4,339,485, assigned to Sanyo-Kokussaku Pulp Co., 1982.
157. Shibano, T., Maruchi, S., Yakan, K., Kobayashi, T. and Akimoto, S., U.S. Patent 4,425,176, assigned to Sanyo-Kokussaku Pulp Co., 1984.
158. OuYang, D.T., WO Patent Application 2000 44845A1, assigned to 3M, 2000.
159. Yamamoto, T. and Minamizaki, Y., U.S. Patent 5,376,420, assigned to Nitto Denko Corp., 1994.
160. Blum, A. and Bartell, C., U.S. Patent 4,070,523, assigned to Borden, 1978.
161. Puskadi, F., U.S. Patent 4,424,244, assigned to Permacel, 1984.
162. Truskolaski, B. and Pohl, D.P., U.S. Patent 4,599,260, assigned to 3M, 1986.
163. Maietti, A., U.S. Patent 5,168,002, assigned to Vibac S.p.A., 1992.
164. Khatib, K. and Langan, J.W., U.S. Patent 5,621,020, assigned to Moore Business Forms, 1997.
165. Lievre, A. and Mirou, C., U.S. Patent 5,817,717, assigned to Rhone-Poulenc Chimie, 1998.
166. Shipston, A.C. and Rice, D.K., U.S. Patent 5,985,982, 1999.
167. Birkholz, R.B. and Schwartz, M.E., U.S. Patent 5,663,227, assigned to United States Postal Service, 1997.
168. Scholz, W.F., Meader, C.D., Su, W.C. and Hseih, D.T., U.S. Patent 6,074,747, assigned to Avery Dennison Corp., 2000.
169. Galli, G., U.S. Patent 4,699,816, assigned to Manuli Autoadhesivi S.p.A., 1987.
170. Miller, J.A., Tate, E., Jr., Velasquez Urey, R.E., Kono, Y., Akiyama, Y. and Mulder, R.S., U.S. Patent 5,300,057, assigned to 3M, 1994.
171. Carpenter, T.L., Sipinen, A.J. and Bany, S.W., U.S. Patent 5,342,339, assigned to 3M, 1994.
172. Kerr, S.R., *Adhes. Age*, **Aug.**, 26 (1996).
173. Irifune, S. and Ohba, T., U.S. Patent 5,436,281, assigned to Shin-Etsu, 1995.
174. Kessel, C.R., Lockwood, R.G., Woodward, T.R. and Wu, M.S., International Patent Application WO 94/28080, 1994.
175. Lu, P.C. *U.S. Patent 5,425,991*, assigned to Mobil Oil Corp., (1995).

Chapter 13

Rubber base adhesives

JOSÉ MIGUEL MARTÍN-MARTÍNEZ *

Adhesion and Adhesives Laboratory, University of Alicante, 03080 Alicante, Spain

1. Introduction

Rubber base adhesives, also called elastomeric adhesives, are widely used in industrial and household applications. In fact, about one-third of the adhesives used in the World are made from natural or synthetic rubbers. Some of the elastomeric adhesive systems showing industrial importance in recent years are the following:

- (1) pressure-sensitive tapes and labels;
- (2) construction adhesives;
- (3) contact adhesives;
- (4) hot-melts packaging and bookbinding adhesives;
- (5) high-strength structural applications for aircraft, automotive and construction.

Some rubber base adhesives need vulcanization to produce adequate ultimate strength. The adhesion is mainly due to chemical interactions at the interface. Other rubber base adhesives (contact adhesives) do not necessarily need vulcanization but rather adequate formulation to produce adhesive joints, mainly with porous substrates. In this case, the mechanism of diffusion dominates their adhesion properties. Consequently, the properties of the elastomeric adhesives depend on both the variety of intrinsic properties in natural and synthetic elastomers, and the modifying additives which may be incorporated into the adhesive formulation (tackifiers, reinforcing resins, fillers, plasticizers, curing agents, etc.).

1.1. Brief history of rubber base adhesives

The first elastomeric adhesive was prepared at the end of the 18th Century and consisted of naphtha solutions of natural rubber. This kind of adhesive is currently

* E-mail: jm.martin@ua.es

still in use to produce temporary joints in textile, art material and footwear (where they are specifically called cement adhesives). One of the early applications of the natural rubber adhesives was lamination of textile products to impart waterproof resistance. For this application, cross-linking (vulcanization) after application of adhesive was necessary. Adhesives made with natural rubber latex were first prepared in the middle of the 19th Century. Organic solvents were used to prepare these adhesives which generally contained rosins (also a natural product derived from pine sap). However, the strength provided by these formulations was poor and, in general, porous substrates (e.g. paper, leather, textiles) were necessary to produce acceptable joints.

During World War II, several new synthetic elastomers were produced and new types of adhesives (mainly styrene-butadiene and acrylonitrile copolymers) were manufactured to produce adequate performance in joints produced with new difficult-to-bond substrates. Furthermore, formulations to work under extreme environmental conditions (high temperature, resistance to chemicals, improved resistance to ageing) were obtained using polychloroprene (*Neoprene*) adhesives. Most of those adhesives need vulcanization to perform properly.

Structural applications of rubber base adhesives were also obtained using rubber-thermosetting resin blends, which provided high strength and low creep. The most common formulations contain phenolic resins and polychloroprene or nitrile rubber, and always need vulcanization.

Thermoplastic block copolymers were used for pressure-sensitive and hot-melt rubber adhesives as from the middle sixties. These adhesives found application in packaging, disposable diapers, labels and tapes, among other industrial markets. The formulation of these adhesives generally includes an elastomer (generally containing styrene endblocks and either isoprene, butadiene or ethylene-butylene midblocks) and a tackifier (mainly a rosin derivative or hydrocarbon resin).

2. Contact adhesives

One of the most common rubber adhesives are the contact adhesives. These adhesives are bonded by a diffusion process in which the adhesive is applied to both surfaces to be joined. To achieve optimum diffusion of polymer chains, two requirements are necessary: (1) a high wettability of the adhesive by the smooth or rough substrate surfaces; (2) adequate viscosity (in general rheological properties) of the adhesive to penetrate into the voids and roughness of the substrate surfaces. Both requirements can be easily achieved in liquid adhesives. Once the adhesive solution is applied on the surface of the substrate, spontaneous or forced evaporation of the solvent or water must be produced to obtain a dry adhesive film. In most cases, the dry-contact adhesive film contains residual solvent (about 5–10 wt%), which usually acts as a plasticizer. The time necessary

to produce evaporation is called *drying time*, and it can be easily measured by touching the adhesive surface with a finger under light pressure; the drying time will be obtained when the adhesive does not stick to the finger.

Environmental conditions under which solvent release from the adhesive on the substrate is produced must be carefully controlled. Humidity is critical because loss of heat due to solvent evaporation may allow attainment of the dew point (the evaporation of the solvent is an endothermic process), and then condensation of water on the adhesive can result. This phenomenon is often called *moisture blooming*. The presence of water on the adhesive film causes a detrimental effect because the autoadhesion of rubber chains is greatly inhibited. Therefore, humidity must be controlled and avoided by increasing the temperature during solvent evaporation.

The dry adhesive films on the two substrates to be joined must be placed in contact to develop adequate autoadhesion, i.e. diffusion of polymer rubber chains must be achieved across the interface between the two films to produce intimate adhesion at molecular level. The application of pressure and/or temperature for a given time allows the desired level of intimate contact (coalescence) between the two adhesive film surfaces. Obviously, the rheological and mechanical properties of the rubber adhesives will determine the degree of intimacy at the interface. These properties can be optimized by selecting the adequate rubber grade, the nature and amount of tackifier and the amount of filler, among other factors.

The diffusion process in natural and polychloroprene rubber adhesives can be explained by Campion's approach [1] which considers the concept of molecular free volume. This free volume is mainly affected by the solvent mixture of the adhesive (which will determine the degree of uncoiling of rubber chains) and by the ingredients in the formulation (mainly the amount and type of tackifier).

The *open time* is the time at which the coalescence between two identical adhesive films drops to an unacceptable level, i.e. the time after which autoadhesion and diffusion cannot be adequately produced. During the open time several changes in the adhesive films are produced due to the loss of residual solvent which affect the viscoelastic properties of the film (loss of plasticization) and the crystallization of the rubber chains. The open time can be measured by applying a thin layer of adhesive on Kraft paper by means of a doctor blade. After various time intervals the thin adhesive films are brought together under a given pressure and time, assessing the degree of coalescence obtained. The open time is obtained when there is a lack of coalescence between the adhesive films.

Natural rubber adhesives were traditionally used as contact adhesives. However, synthetic polymers are more generally used today. Polychloroprene adhesives are the most common contact adhesives based on synthetic rubber, although recently some have been displaced by polyurethane and acrylic polymers [2].

3. Specific features of rubber base adhesives

The chemical nature and molecular weight of the rubber will greatly determine the properties of elastomeric adhesives. However, some common characteristics can be found in most of the rubber base adhesives. The elastomeric adhesives show the following specific features in assembly operations.

(a) *Broad range of substrates for assembly.* Elastomeric adhesives can be used to join several substrates in a temporary or permanent way. For many applications curing (i.e. cross-linking or vulcanization) is not necessary. To provide high strength and, mainly, heat and chemical resistance to the joints produced with these adhesives, vulcanization is mandatory.

(b) *Flexibility.* The resilience of rubber helps to absorb the stresses applied to the joints. Therefore, these adhesives properly resist impact, shear, elongation, vibration and peel stresses.

(c) *High peel strength.* The intrinsic properties of rubbers (high ability to produce high elongation under stress) impart adequate strength to the joints under peeling forces. However, rubber polymers show poor resistance to shear stresses.

(d) *Versatility of formulation.* Several types of elastomers can be used in elastomeric adhesives. For each family of rubber, several grades and different chemical modifications (e.g. grafting of polymers) can be achieved to impart specific properties to the joints. Furthermore, specific elastomeric adhesive formulations for particular end-uses can be easily achieved by adding several ingredients (fillers, reinforcing agents, etc.). However, the basic properties of the formulations are provided by the nature of the rubber.

(e) *High green strength.* This is one of the most important properties of the elastomeric adhesives. The *green* (immediate) *strength* can be defined as the ability to hold two surfaces together when first contacted and before the adhesive develops its ultimate bonding properties when fully cured. In other words, the green strength is the intrinsic capacity of elastomeric adhesives to strongly adhere to the substrates immediately after application. This unique property justifies the term 'contact adhesive', generally used to name elastomeric adhesives. The green strength can be modified by changing the solvent composition (for solvent-borne adhesives) and/or by incorporating ingredients in the formulations (mainly tackifiers). Green strength is essential in pressure-sensitive rubber adhesives (PSA) and in some polychloroprene rubber–phenolic resin blends.

(f) *Variety of form.* Rubber base adhesives can be supplied for assembly operations as solvent or water-borne dispersions, hot melts, precast films, extruded tapes or reinforced films. In addition solvent and water-borne dispersions can be supplied as single or two-components systems.

Rubber base adhesives develop strength faster than most other polymeric types. Fig. 1 [3] shows the differences in the development of peel strength for several rubber polymers (without additional additives, except an antioxidant). Natural

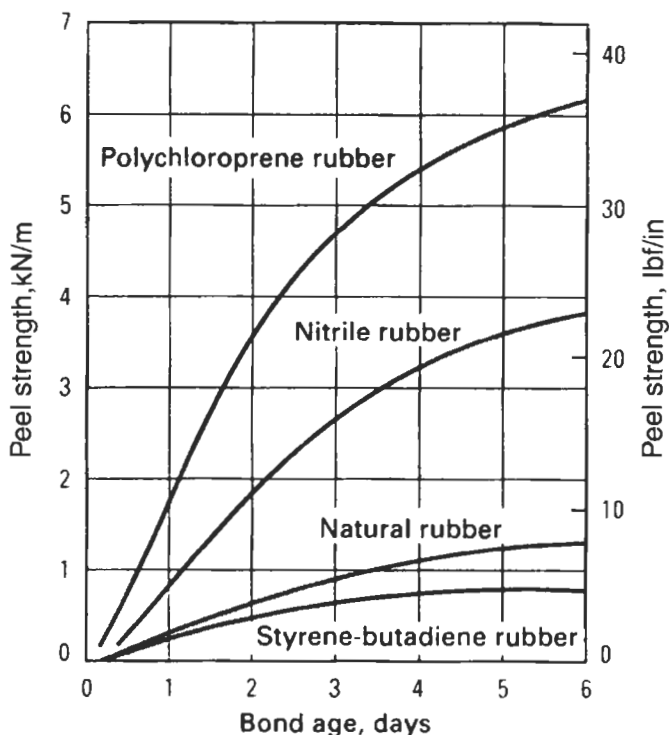


Fig. 1. Bond strength development at room temperature as a function of time for different rubbers [3].

rubber and styrene-butadiene rubber provide higher initial peel strength values. As time after joint formation progresses, polychloroprene and nitrile rubber develop much higher peel strength, particularly after a few hours.

The viscosity of elastomeric adhesives determines their method of application. Typically, solvent-borne rubber compounds require low viscosities for application. Thus, viscosities lower than 0.6 Pa s for spray, curtain or dip applications are required, whereas for brush application viscosities lower than 5 Pa s are generally used. Roll-coating technology requires viscosities between 5 and 15 Pa s.

In recent years, the use of solvent-borne adhesives has been seriously restricted. Solvents are, in general, volatile, flammable and toxic. Further, solvent may react with other airborne contaminants contributing to smog formation and workplace exposure. These arguments have limited the use of solvent-borne adhesives by different national and European regulations. Although solvent recovery systems and afterburners can be effectively attached to ventilation equipment, many factories are switching to the use of water-borne rubber adhesives, hot melts or 100% solids reactive systems, often at the expense of product performance or labour efficiency.

Because most latices have low viscosities by compounding, most of the water-borne rubber adhesives are sprayable. Thickeners such as fumed silicas can be added to increase viscosity and thixotropy. This means that even at relatively large viscosities (over 10 Pa s) many water-based rubber adhesives can be sprayed. Dip and curtain applications require viscosities between 0.05 and 0.3 Pa s, whereas brush application works with viscosities between 1 and 50 Pa s.

4. Ingredients of the rubber base adhesives

Elastomeric adhesives typically contain an elastomer and a tackifying or modifying resin as key components, but in general other ingredients are also included. The formulation of rubber base adhesives may contain up to nine different components: elastomer; resins; plasticizer or softener; fillers; pigments; curing agents; antioxidants; solvents; and other additives, such as emulsifiers, coagulant, biocides, etc.

In general, most of the rubber base adhesive formulations do not contain all the previous ingredients. As typical examples, compositions of solvent-borne, water-borne, pressure-sensitive and hot-melt rubber base adhesives are given in Table 1. The amounts of the different ingredients are given only as examples. The composition of rubber base adhesives can be expressed as percentages in weight percent or, more commonly, as phr (parts of one component in respect to 100 parts elastomer) (Table 1). Compositions in phr will be generally used in this chapter.

There are some general aspects related to the formulation of rubber base adhesives. In solvent-borne rubber adhesives, a variety of *solvents* can be chosen to control drying rate, adjust viscosity and dissolve important ingredients. *Resins* can be added to improve tack, wetting properties, heat resistance, bond strength and oxidation resistance. The most common resins used in rubber base adhesives are rosins, rosin esters, and terpene, coumarone–indene, hydrocarbon and phenolic resins. *Plasticizers and softeners* reduce hardness, enhance tack and decrease cost of rubber adhesive formulations. Paraffinic oils, phthalate esters and polybutenes are typical plasticizers. *Fillers* are not commonly added to rubber adhesive formulations because they reduce adhesion, but they do decrease cost and increase solution viscosity. Excess filler in a low-viscosity solution may sediment because of differences in the densities (fillers are generally more dense than the other ingredients in rubber adhesives). Carbon black and titanium dioxide are also used to provide colour to the adhesive. Clays, calcium carbonate and silicates are also common fillers in rubber adhesive formulations. For water-borne adhesives, typically protective colloid, preservative, defoamers, wetting agents and emulsifiers are included in the formulations.

In the next sections, the manufacture, chemistry and properties of the main ingredients of the rubber base adhesives will be considered.

Table 1

Composition of rubber base adhesives

Typical composition of a <i>solvent-borne rubber adhesive</i>	
Elastomer	100 phr
Tackifying resin	30 phr
Magnesium oxide	4 phr
Zinc oxide	5 phr
Water	1 phr
Antioxidant	2 phr
Solvent mixture	500 phr
Typical composition of a <i>water-borne rubber adhesive</i>	
Latex polymer	100 phr
Surfactant	As required
Antifoam	As required
Tackifying resin	50 phr
Thickener	As required
Zinc oxide	5 phr
Antioxidant	2 phr
Typical formulation of a <i>pressure-sensitive rubber adhesive</i>	
Elastomer	100 phr
Tackifier	150 phr
Lanolin	25 phr
Zinc oxide	50 phr
Antioxidant	1 phr
Solvent mixture	400 phr
Typical formulation of <i>hot-melt rubber adhesive</i>	
Thermoplastic elastomer	100 phr
Endblock resin	150 phr
Midblock resin	50 phr
Plasticizing oil	50 phr
Antioxidant (stabilizer)	2 phr

4.1. Elastomer

Rubber is composed of very large molecules containing thousands of atoms arranged one after another in a string-like manner. The arrangement of the atoms repeats in a regular cycle, so the structure can be considered as a certain segment which is repeated ' n ' times. The polymerization of the monomers with one double carbon-carbon bond proceeds by opening up to form links between the repeating segments. As molecular weight increases, the density, melting point, and boiling point increase, the last property increases to the point where the material decomposes before it evaporates. High molecular weight is necessary for strong,

load-bearing rubbers. Viscosity is roughly proportional to the molecular weight of the rubbers.

The least complicated repeating unit in a polymer corresponds to ethylene. The regular, repeating structure of polyethylene allows neighbouring segments to align in perfect order to form crystals. To make a rubbery polymer, it is necessary to minimize crystallization by breaking up the structural regularity of the repeating $-\text{CH}_2-$ segments. There are two ways to prevent regular alignment in polymers.

(1) Add side groups such as methyl or chlorine. The methyl group (for instance in ethylene-propylene rubber) prevents neighbouring chain segments from aligning perfectly.

(2) Include unsaturation or carbon-carbon double bonds in the polymer chain. Diene monomers have two carbon-carbon double bonds and polymerize in such a way that the repeating segments are joined at the extreme carbon atoms with the other double bond remaining in each segment. These remaining carbon-carbon double bonds prevent rotation, hindering the alignment of the molecular segments and disturb crystallization. Styrene-butadiene and nitrile rubbers are non-crystallizing polymers containing unsaturation.

Both side groups and carbon-carbon double bonds can be incorporated into the polymer structure to produce highly resilient rubbers. Two typical examples are polyisoprene and polychloroprene rubbers. On the other hand, the incorporation of polar side groups into the rubber structure imparts a dipolar nature which provides oil resistance to these rubbers. Oil resistance is not found in rubber containing only carbon and hydrogen atoms (e.g. natural rubber). Increasing the number of polar substituents in the rubber usually increases density, reduces gas permeability, increases oil resistance and gives poorer low-temperature properties.

When the temperature is lowered, rubbers become stiff and brittle. All rubbers eventually stiffen to a rigid, amorphous glass at the glass transition temperature (T_g). This temperature also indicates the low-temperature service limit of the rubber. T_g values are dependent on the structure, degree of cross-linking (vulcanization) and isomeric composition of the rubber.

The physical properties of rubber are mainly determined by the molecular weight and the structure of the repeating units. By making branched chains rather than linear ones, low-viscosity polymers for solution applications are obtained. By lightly cross-linking to form insoluble or gel polymers, better extruding polymers can be obtained. By broadening the molecular weight distribution, easier mixing polymers can be obtained.

In some cases, diene polymers (for instance polychloroprene rubbers) can add to the growing polymer chain by 1,2 addition (also called vinyl addition). This creates labile hydrogen or reactive halogen on tertiary carbon atoms. A few percent of this type of structure in the rubber will assist cross-linking reactions.

Several elastomers can be used in rubber base adhesives. The elastomer used is the backbone of the adhesive, so the performance of the adhesive is provided

Table 2

Some properties of elastomers used in rubber base adhesives

Elastomer	Abbr.	Density (g/cm ³)	T_g (°C)	Max. service T (°C)
Natural rubber	NR	0.91	-75	70
Butyl rubber	BR	0.92	-65	100
Styrene-butadiene rubber	SBR	0.93	-55	70
Nitrile rubber	NBR	0.98	-40	100
Polychloroprene rubber	CR	1.23	-50	100

by the rubber properties. However, several specific properties for application are imparted by adding other ingredients in the formulation.

The elastomers considered in this section have been selected considering the most commonly used in rubber base adhesives: natural rubber; butyl rubber and polyisobutylenes; styrene-butadiene rubber; nitrile rubber; polychloroprene rubber (neoprene). Typical properties of these rubbers are shown in Table 2.

4.1.1. Natural rubber (NR)

Natural rubber can be obtained from the sap of a number of plants and trees, the most common source is the *Hevea brasiliensis* tree. Although natural rubber was known in Central and South America before the arrival of Christopher Columbus in 1492, the first use as an adhesive was established in a patent dated in 1891. As rubber became an important part of the industrial revolution, the rubber adhesives market grew in importance. To comply with the increasing demand on natural rubber materials, plantations of *Hevea brasiliensis* trees were established in southeast Asia in the early 20th Century, mainly to supply the demand from the automobile industry.

Natural rubber is harvested as latex by tapping trees in a manner similar to maple syrup. Tree latex contains about 35 wt% rubber solids, as well as small quantities of carbohydrates, resins, mineral salts and fatty acids. Ammonia should be immediately added to the latex to avoid coagulation by these other ingredients and to prevent bacterial degradation. After collection, the latex can be concentrated to 60–70% solids if the latex product is required for end-use. Otherwise, the latex is coagulated, washed, dried, and pressed into bales for use as dry rubber.

NR latex grades are described by the method of concentration used. Evaporation, creaming and centrifuging are the most common methods used in the industry.

(a) *Evaporated latex* is produced by heating at a reduced pressure, and the ammonia is replaced by potassium hydroxide containing a small amount of soap

to assist stabilization. It has a solid content of about 73%. This NR latex grade shows improved resistance to ageing and is adequate when high level of fillers have to be added during formulation.

(b) *Creamed latex* is obtained by adding fatty acid soap and a creaming agent (e.g. an alginate) in a tank; separation of the creamed layer from the serum must be completed. The solids content in the creamed rubber is 66–69%. This grade of NR is not interesting for adhesive manufacturers.

(c) *Centrifuged latex* is the most important and common type of NR (about 95% of latex production). Water-soluble non-rubber components are removed by centrifuging. The solids content ranges from 50 to 67%. This NR latex grade is preserved by adding 0.7% ammonia.

In solid form, the natural rubber is graded according to the content of dirt remaining from the precipitation of latex at the plantation. Eight basic NR types have been traditionally recognized internationally. Only the so-called ribbed smoked sheets and the pale crepes are normally used for adhesives. The predominant grade system, the Standard Malaysian Rubber system, has been used since 1965.

There are some aspects in the raw dry NR grades for adhesive manufacturing to be considered. NR tends to suffer oxidative degradation catalyzed by metals (mainly copper). The susceptibility of NR to oxidation can be measured using the plasticity retention index. The better grades of rubber have the higher plasticity retention index.

On the other hand, an increase in viscosity and gel content of NR latex can be produced during storage (*storage hardening*). The presence of aldehyde groups on the rubber chain may produce cross-linking reactions, which are responsible for the formation of gel. Addition of small amounts of hydroxylamine to the latex before coagulation helps to prevent storage hardening.

For use in solution adhesives, NR must be masticated sufficiently to break down gel and reduce viscosity for dissolution in suitable solvents. When low gel content is achieved, viscosity-stabilized rubbers dissolve without the need for mastication. It is usual to form the rubber into a thin layer to present a large surface to the solvent for rapid swelling. This can be easily achieved by using particulate NR forms which are produced by mechanical grinding of dry rubber. To avoid agglomeration of dry rubber particles during storage and manipulation, an anti-tack agent (calcium stearate for example) is added.

4.1.1.1. Chemistry of NR. The chemical composition of NR mainly corresponds to *cis*-1,4-polyisoprene (Fig. 2).

Natural latex is polydisperse (size of individual particles may vary from 0.01 to 5 μm). However, synthetic latex has a relatively narrow particle size, and therefore the viscosity at a given rubber content is higher in synthetic rubber (polyisoprene) solutions. The average molecular weight is typically about 1 million g/mol, although it depends on the gel content.

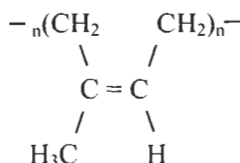


Fig. 2. Chemical structure of the *cis*-1,4-polyisoprene.

The main characteristics of NR latex are as follows: high gel content; high molecular weight; high cohesive strength; high self tack; and high rubber content.

4.1.1.2. Forms of NR. Chemically modified NR grades are available in the market. The most common grade is a *methyl methacrylate graft polymer* called *Heveaplus MG*, in which the natural rubber backbone contains polymethyl methacrylate side chains. Heveaplus latex is about 50% solids. Although there is always some methyl methacrylate homopolymer in the latex, at least 50% is grafted. For use in solution adhesives, the solid Heveaplus MG should be milled in a two-roll mill to remove the gel material. The degree of milling must be carefully controlled to avoid the elimination of the grafted material. Equal amounts of toluene and methyl-ethyl ketone is a good solvent mixture for Heveaplus MG.

Depolymerized liquid natural rubber is prepared by extensive mastication of NR in air at 250°C in the presence of a peptizing agent. Depending on the time of treatment, several viscosities can be obtained. This material is soluble in many organic solvents but not alcohols or ketones, and is compatible with many drying oils and ester-type plasticizers. It has been shown [4] that chemically depolymerized latex exhibits good peel strength without addition of resin, and because the glass transition temperature of natural rubber is not affected by the reaction, these materials can be used in low-temperature applications.

The increasing demand on natural rubber for several applications and the increase in production cost (labour, transportation, relatively low added value of NR in the market) allows the manufacture of *synthetic polyisoprene* as an alternative to NR. Although polyisoprene should replace NR in adhesive formulations, there are some differences in molecular weight and gel content, and in the content in *trans* isomer. Therefore, the gel-free nature of polyisoprene gives solubility in organic solvents without mastication, but relatively poorer tack and green strength are obtained compared with NR. With respect to the vulcanizing adhesives, formulations containing polyisoprene tend to cure more slowly and need the addition of higher amounts of tackifier than NR formulations.

Many grades of *recycled rubber* produced from grinding and heating of vulcanized rubber products such as tyres, baby bottle nipples and other goods are also available. Although reclaimed rubber offers some processing advantages, its use has declined in recent years because of the extensive use of blended polymers.

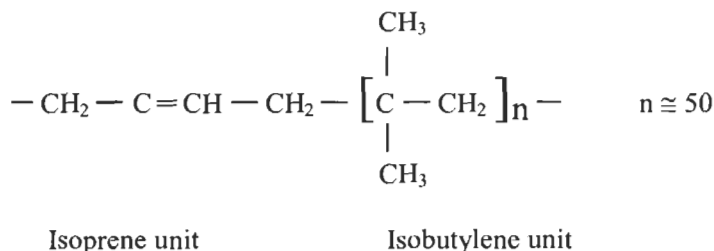


Fig. 3. Chemical structure of butyl rubber.

4.1.2. Butyl rubber (BR) and polyisobutylenes (PIB)

Butyl rubber (BR) and polyisobutylene (PIB) are widely used in adhesives as primary elastomeric binders and as tackifiers and modifiers. The main difference between these polymers is that butyl is a copolymer of isobutylene with a minor amount of isoprene (which introduces unsaturation due to carbon–carbon double bonds), while polyisobutylene is a homopolymer.

4.1.2.1. Chemistry of butyl rubber and polyisobutylene. The chemical structure of butyl rubber (Fig. 3) is mainly composed of long and straight carbon–hydrogen backbone, containing between 47,000 and 60,000 units. The small percentage of isobutylene provides some degree of unsaturation (generally lower than 2% of that found in natural rubber) to allow curing, but at the same time renders butyl rubber very stable and inert to weathering, ageing and heating. BR has good resistance to oils and to chemicals, and has very low water absorption [5]. On the other hand, the many side groups attached to the main polymer chain are not large in size and are regularly spaced, leading to BR being a unique low air, moisture and gas permeability rubber.

Polyisobutylene has a similar chemical backbone to butyl rubber, but does not contain double carbon–carbon bonds (only terminal unsaturation). Many of its characteristics are similar to butyl rubber (ageing and chemical resistance, low water absorption, low permeability). The polymers of the isobutylene family have very little tendency to crystallize. Their strength is reached by cross-linking instead of crystallization. The amorphous structure of these polymers is responsible for their flexibility, permanent tack and resistance to shock. Because the glass transition temperature is low (about -60°C), flexibility is maintained even at temperatures well below ambient temperature.

The structure of the isobutylene-derived polymers is hydrocarbonaceous and is non-polar, so poor adhesion to many surfaces is obtained. The addition of polar resins may improve adhesion.

4.1.2.2. Forms of BR and polyisobutylene. The properties of butyl rubber and polyisobutylene depend on their molecular weight, degree of unsaturation, nature of the stabilizer incorporated during manufacture and, in some cases, chemical modification. It is common to produce halogenated forms of butyl rubber to increase polarity and to provide a reactive site for alternate cure mechanisms [6].

Chlorobutyl rubber is prepared by chlorination of butyl rubber (chlorine content is about 1 wt%). This is a substitution reaction produced at the allylic position, so little carbon–carbon double unsaturation is lost. Therefore, chlorobutyl rubber has enhanced reactivity of the carbon–carbon double bonds and supplies additional reactive sites for cross-linking. Furthermore, enhanced adhesion is obtained to polar substrates and it can be blended with other, more unsaturated elastomers.

Several partially cross-linked butyl rubbers are commercially available. The more tightly cross-linked grades are designed for butyl tapes. On the other hand, various depolymerized butyl rubbers and butyl/plasticizers blends are also available.

Butyl latices are prepared by emulsification of butyl rubber. Butyl latex has excellent mechanical, chemical and freeze–thaw stability, and when dried it shows the typical properties of butyl rubber [7].

4.1.3. Styrene–butadiene rubber (SBR)

Styrene–butadiene rubber (SBR) is mainly used for tyre manufacturing and only a small amount is consumed in adhesives. SBR was developed during World War II in Germany and the USA as a substitute for natural rubber which was in short supply. This SBR was produced by the emulsion copolymerization of butadiene and styrene, and was called synthetic natural rubber. After the war, when natural rubber became available, the use of SBR declined because, albeit its low cost, this rubber lacks building tack, has poor cohesive and tensile strength, reduced hot tear strength, lower elongation and resilience than natural rubber. However, in the 1950s new polymerization procedures at low temperature using redox catalysts and the development of solution polymerization using organolithium catalysts began to overcome those deficiencies, and SBR found application in numerous adhesive formulations [8]. Currently, SBR adhesives are used as latices or as solid rubbers.

4.1.3.1. Chemistry of SBR. There are three steps in the manufacturing of SBR: polymerization, monomer recovery and finishing. The polymerization step determines the basic characteristics of SBR, whereas the product form (latex or dry rubber, oil extended or not) depends on the finishing step.

SBR is produced by addition copolymerization of styrene and butadiene monomers in either emulsion or solution process. The styrene/butadiene ratio controls the glass transition temperature (T_g) of the copolymer and thus its stiffness. T_g

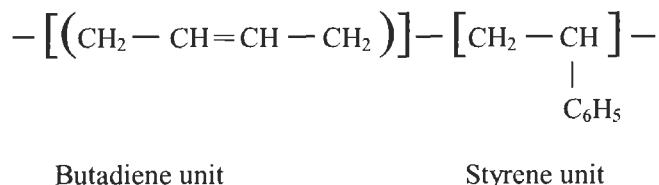


Fig. 4. Chemical structure of styrene–butadiene rubber.

can be varied from -80°C (butadiene) to 100°C (styrene), and thus the higher the styrene content, the higher the stiffness of the copolymer.

The chemical structure of SBR is given in Fig. 4. Because butadiene has two carbon–carbon double bonds, 1,2 and 1,4 addition reactions can be produced. The 1,2 addition provides a pendant vinyl group on the copolymer chain, leading to an increase in T_g . The 1,4 addition may occur in *cis* or *trans*. In free radical *emulsion polymerization*, the *cis* to *trans* ratio can be varied by changing the temperature (at low temperature, the *trans* form is favoured), and about 20% of the vinyl pendant group remains in both isomers. In *solution polymerization* the pendant vinyl group can be varied from 10 to 90% by choosing the adequate solvent and catalyst system.

Formation of gel generally must be avoided. Gel formation is due to cross-linking of polymer chains during the growing step in the emulsion polymerization. Gel content can be controlled by changing the temperature, adjusting the monomer to polymer conversion and by adding chain transfer agents. However, the gel portion in SBR polymers is often sufficient to give good strength and creep resistance properties without cure.

4.1.3.2. Forms of SBR. SBR is sold for adhesive manufacturing as latices or in solid form.

SBR latices are high-solids dispersions of rubber particles in water, the viscosity and rheology of which are, in general, independent of the polymer properties, unlike solutions. They offer a wide range of molecular weight and glass transition temperature. Three classes of SBR latices are available in the market.

(a) *Cold latex*. It is a cold-polymerized and high solid content latex, with a styrene content of 20–35 wt%. This latex is produced by emulsion polymerization below 15°C , and because of the low polymerization temperature, fairly linear and high molecular weight copolymers are obtained. A soap-type surfactant (fatty acid) is generally used and the particle size of the latex after polymerization is quite small (100 nm). A further agglomeration of particles is generally carried out to obtain a latex with 60–70% solids content, and pH of 10–11. Films made from these latexes have low modulus and high elongation. To obtain improved physical properties curing with sulphur/accelerator system is necessary.

(b) *Hot latex*. It is a medium-solid latex with a styrene content of about 45%. This latex is produced by emulsion polymerization at temperatures higher than

30°C, and because the relatively high polymerization temperature, less linear and lower molecular weight copolymers than those of the cold latex SBRs are obtained. Hot latex generally contains a higher gel content than cold latex. Except for the lower solids content (40–50%), hot latices are similar to cold latices. Films made from these latices have higher modulus and lower elongation than the cold latices. To obtain improved physical properties, curing with a sulphur/accelerator system is necessary.

(c) *Carboxylated latex*. Carboxylated latex is a hot-polymerized, medium-solid latex which contains small amounts of an unsaturated carboxylic acid. The styrene content varies over a wide range and the content of unsaturated carboxylic acid is lower than 10 wt% of total monomers. This latex tends to have a relatively high gel content. It is obtained by hot polymerization at acid pH. Therefore, the surfactant is generally dodecylbenzene sulphonic acid. The chemical and mechanical stability of the carboxylated latex is higher than for the other two SBR latices. Films made from these latices have higher modulus and lower elongation than the other two types of latices. To obtain improved physical properties, cure systems are not necessary.

Solid SBR is often preferred to natural rubber because of its better thermal oxidative stability, higher abrasion resistance and easier processability. Solid SBRs are generally grouped into three families according to the production method.

(a) *Emulsion SBR*. The solid rubber is obtained by coagulation of cold or hot latices. Hot SBRs are more common in adhesive formulations.

(b) *Solution SBR*. It is obtained by solution polymerization and generates a product without surfactants. These rubbers are gel-free and have a more narrow molecular weight distribution than those obtained by emulsion polymerization.

(c) *Oil and carbon black master-batches*. These rubbers are mainly used in the tyre industry.

4.1.4. Nitrile rubber (NBR)

Acrylonitrile–butadiene rubber (also called nitrile or nitrile butadiene rubber) was commercially available in 1936 under the name Buna-N. It was obtained by emulsion polymerization of acrylonitrile and butadiene. During World War II, NBR was used to replace natural rubber. After World War II, NBR was still used due to its excellent properties, such as high oil and plasticizer resistance, excellent heat resistance, good adhesion to metallic substrates, and good compatibility with several compounding ingredients.

Several excellent review articles describe NBR in detail [9–12].

4.1.4.1. *Chemistry of NBR*. Nitrile rubbers are copolymers of a diene and a vinyl-unsaturated nitrile. The chemical structure of NBR is given in Fig. 5.

The NBR used in adhesive formulations is obtained by emulsion polymeriza-

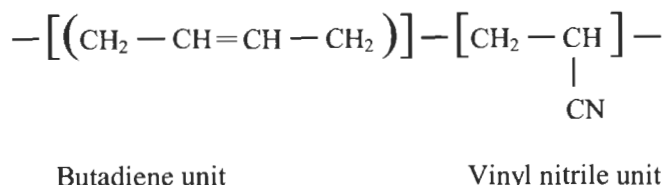


Fig. 5. Chemical structure of nitrile rubber.

tion of 1,3-butadiene and acrylonitrile or by solution-polymerized functionally terminated telechelic liquid copolymers of butadiene and acrylonitrile.

In *emulsion polymerization*, NBR with acrylonitrile content between 15 and 50% can be obtained. The increase in the acrylonitrile content in the NBR produces an increase in the polar nature and solubility parameter in the copolymer [12]. Furthermore, the increase in acrylonitrile content improves the resistance to oils and also increases the glass transition temperature of the copolymers from -60 to -10°C .

The diene commonly used is 1,3-butadiene, although isoprene, 2-ethyl butadiene and other substituted dienes can be used. Acrylonitrile is the usual nitrile compound. Small amounts of a third monomer, such as methacrylic acid, ethyl acrylate, styrene or vinyl acetate, can also be added to adjust the adhesive and elastomeric properties. Most commercial NBR production is conducted at a polymerization temperature of 5°C and the resulting product is called cold rubber. In adhesive applications, hot NBR is generally used (polymerization temperature is 25 – 50°C). Hot NBR exhibits a higher degree of branching and slightly higher *cis*-1,4 butadiene segments than cold NBR [13].

Several variables in the emulsion polymerization affect the adhesive properties of the resulting copolymers.

(a) Emulsifier type/level. NBR is polymerized with anionic emulsifiers. The emulsifier remains after the latex is coagulated and dried, the type and level of emulsifier may affect the adhesive properties.

(b) Molecular weight modifier. Aliphatic mercaptans are generally used to control the molecular weight of NBR. Without a modifier, undesirable branching may occur and poor properties are obtained. For adhesives, low molecular weight NBR is desired.

(c) Conversion. As conversion of monomer to polymer increases, highly branched and cross-linked copolymers are obtained. This leads to gel formation which affects the solubility of the NBR. Therefore, low conversions need to be employed.

(d) Coagulation and drying. Residual non-polymer components (emulsifier, antioxidant, etc.) affect the adhesive properties of NBR. The method of coagulation (aluminium sulphate or calcium chloride can be generally used), washing and drying is therefore important.

(e) Some NBR is ground to produce larger surface area products which are more readily soluble, mainly for cement applications. To prevent re-agglomeration, anti-cake additives (talc, resins) are added which may affect the performance of the adhesive.

Functionally terminated telechelic liquid NBRs are obtained by solution polymerization with a suitable initiator/chain transfer agent that results in a nearly difunctional molecule. These liquid copolymers have a low molecular weight (about 3500 g/mol) and acrylonitrile contents between 10 and 27%. Although the acrylonitrile content is lower than for the emulsion copolymers, a combination with monomers containing carboxylic groups imparts higher reactivity. The difunctional character of these reactive NBR liquids facilitates the reaction with other polymers or prepolymers (epoxies, polyesters, polyurethanes) to give high molecular weight materials containing short nitrile rubber block in the backbone. Furthermore, to avoid the use of solvents, the liquid NBRs can be mixed with epoxies.

4.1.5. Polychloroprene (neoprene) rubber (CR)

Polychloroprene rubber (CR) is the most popular and versatile of the elastomers used in adhesives. In the early 1920s, Dr. Nieuwland of the University of Notre Dame synthesized divinyl acetylene from acetylene using copper(I) chloride as catalyst. A few years later, Du Pont scientists joined Dr. Nieuwland's research and prepared monovinyl acetylene, from which, by controlled reaction with hydrochloric acid, the chloroprene monomer (2-chloro-1,3-butadiene) was obtained. Upon polymerization of chloroprene a rubber-like polymer was obtained. In 1932 it was commercialized under the tradename 'DuPrene' which was changed to 'Neoprene' by DuPont de Nemours in 1936.

Prior to World War II, natural rubber adhesives were the only ones widely used in the industry, mainly for tyre building, joining of sponge in automobile doors and temporary attachment of shoe soles. Although those adhesives have low cohesive strength and poor ageing (when uncured), substitution by polychloroprene adhesives were not produced due to their higher cost, the need of using more expensive aromatic solvents, and the lower viscosities obtained for a similar solids content.

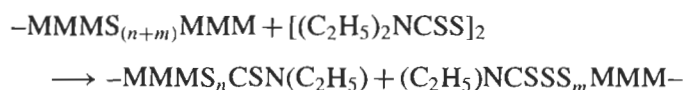
During World War II, polychloroprene was chosen as a replacement for natural rubber because of its availability. Two copolymers of chloroprene and sulphur which contain thiuram disulphide were available (Neoprene GN and CG). One of the first successful applications of these polychloroprene adhesives was for temporary and permanent sole attachment in the shoe industry. However, these polychloroprene cements show a decrease in viscosity on ageing and a black discolouration appears during storage in steel drums. Discolouration was produced by trace amounts of hydrochloric acid produced by oxidation of polychloroprene

on ageing. This acid reacts with iron to form iron chloride which also reacts with thiuram disulphide to produce black iron sulphide. Addition of acid acceptors (magnesium oxide and zinc oxide) prevented discolouration but a decrease in the viscosity stability of adhesive solutions was produced. Addition of hydrated calcium silicate or a terpene phenolic resin improved the stability of polychloroprene adhesives and increased cohesive strength. However, to avoid most of the inconveniences of Neoprenes GN and CG, new polychloroprene grades adhesives were developed.

4.1.5.1. Chemistry of polychloroprene rubber. Polychloroprene elastomers are produced by free-radical emulsion polymerization of the 2-chloro-1,3-butadiene monomer. The monomer is prepared by either addition of hydrogen chloride to monovinyl acetylene or by the vapour phase chlorination of butadiene at 290–300°C. This latter process was developed in 1960 and produces a mixture of 3,4-dichlorobut-1-ene and 1,4-dichlorobut-2-ene, which has to be dehydrochlorinated with alkali to produce chloroprene.

The emulsion polymerization of chloroprene involves the dispersing of monomer droplets in an aqueous phase by means of suitable surface-active agents, generally at a pH of 10–12. Polymerization is initiated by addition of a free-radical catalyst at 20–50°C. The polymerization is terminated by destroying the remaining free radicals with the addition of antioxidants and stabilizing agents. After removal of the monomer, the solid elastomer is isolated by destabilizing the colloidal system (by freeze coagulation), separating the aqueous phase and drying the polymer.

During emulsion polymerization, a high conversion of monomer to polymer produces cross-linked rubber which is insoluble. To obtain a high conversion in the polymerization reaction and a processable polymer, suitable polymer modification should be made. The use of sulphur moieties allows this goal to be reached [2]. Sulphur-modified polychloroprenes contain di- and polysulphide sequences in the polymer chains. After the polymerization reaches the desired degree, reaction is stopped by adding thiuram disulphide:



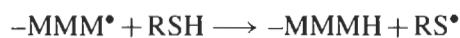
These polymers are very sensitive to mastication. Mastication decreases the solution viscosity and increases the ease of solution. Because the reactive sulphur linkages, rapid vulcanizing properties are obtained. On the other hand, the presence of thiuram disulphide improves the resistance of CR to dehydrochlorination.

Mercaptan-modified polychloroprenes only contain sulphur at the ends of the polymer chain. Polymerization is carried out in the presence of a mercaptan to act

Type of Addition	Formula
<i>trans</i> -1,4	
<i>cis</i> -1,4	
1,2	
3,4	

Fig. 6. Molecular structure of polychloroprene [14].

as a chain transfer agent which controls the molecular weight:



Mercaptan-modified polychloroprenes provide lighter colour to solutions and are more resistant to discolouration than sulphur-modified polychloroprenes. Also mercaptan-modified polychloroprenes exhibit better ageing, and improved thermal and solution stability.

The properties of polychloroprene can be altered by modification of the conditions and experimental variables during polymerization. During the polymerization, the monomer can be added in a number of ways, the *trans*-1,4 addition is the most common (Fig. 6). The proportion of each configuration determines the degree of crystallinity in the polymer and its reactivity. Crystallinity in polychloroprene is produced by the *trans*-1,4 addition and reaction conditions are usually selected to maximize this. In crystallizing polychloroprene grades there is more than 90% *trans*-1,4 addition whereas non-crystallizing grades generally contain 80–85% *trans*-1,4 addition. The control of the *trans*-1,4 addition is often obtained by selecting monomers other than 2-chloro-1,3-butadiene and identifying chain-branching sites.

The ability of polychloroprene adhesives to crystallize is unique as compared to other elastomers. Crystallization is the tendency of polymer chains to order themselves in a three-dimensional array. As a result of crystallization, the cohesive strength of polychloroprene is much greater than that of the amorphous polymers. Crystallization is reversible under temperature or dynamic stresses. Thus, for a temperature higher than 50°C uncured polychloroprene adhesives lose their crystallinity and upon cooling the film re-crystallizes and cohesive strength is regained. The increase in crystallinity improves the modulus, hardness and cohesive strength of polychloroprene adhesives, but decreases their flexibility, their resistance to oil swelling, and their resistance to permanent set. In general, the raw polychloroprene polymers crystallize ten times faster than vulcanized, plasticizer-free compounds.

Polychloroprene polymers also vary in the degree of branching in the polymer. Polychloroprenes with little or no branching are called *sol polymers*, whereas those with considerable branching are referred to as *gel polymers*. Sol polymers are soluble in aromatic solvents. All of the solvent-grade polychloroprene polymers (except Neoprene AG) are sol polymers. The gel content in the polychloroprene affects the cohesive strength, resilience, elongation, open tack time, resistance to permanent set, and oil swell.

Summarizing, the variations in the microstructure are responsible for significant changes in the polychloroprene properties. The main modifications produced in the polychloroprene chains affect its properties as follows:

- (1) Increase in the *trans* content of the polychloroprene, increasing its crystallization tendency.
- (2) Increase in the 1,2- and *cis*-1,4-additions in the polychloroprene, reducing the degree of crystallization, and faster curing is necessary.
- (3) Increase in the chain branching in the polychloroprene, reducing the stability in polymer viscosity and deteriorating the processing properties.
- (4) Reactive end groups, reducing branching of the polychloroprene and facilitating processing.
- (5) Polymer chains with sulphur atoms, improving breakdown of polychloroprene during mastication, increasing tear resistance and dynamic behaviour.
- (6) Reduction in the stereo-regularity by adding co-monomers, reducing the crystallization tendency of the polychloroprene.
- (7) Increase in the molecular weight of the polychloroprene, increasing viscosity and tensile strength of vulcanizates.
- (8) Increase in the molecular weight distribution, improving processability and reducing tensile strength of the polychloroprene.

Although there are several manufacturers of polychloroprene elastomers, Du Pont probably has the broader range of polychloroprene grades on the market. As an example in Table 3, the equivalencies between the peptizable sulphur-modified and stabilized with thiuram disulphide polychloroprenes are given

Table 3

Peptizables grade polychloroprenes, sulphur-modified and stabilized with thiuram disulphide

Grade	<i>Neoprene</i>	<i>Baypren</i>	<i>Butachlor</i>	<i>Denka</i>	<i>Skyprene</i>
General	GN	710	SC20	PM40NS	R22
Staining	GNA	–	SC21	PM40	–
Antioxidant	GS	–	SC22	–	–
Nonstaining	GT	–	SC11	PT60	R11
Low crystallizing	GRT	610	SC10	PS40	R10

Comparison between polychloroprenes provided by different suppliers: Du Pont (*Neoprene*), Bayer (*Baypren*), BP-Distugil (*Butachlor*), Denki-Kagaku (*Denka*) and Toyo-Soda (*Skyprene*) [2].

[14]. In this section the polychloroprenes manufactured by Du Pont are described.

Several types of polychloroprene elastomers have been commercialized. The most important polymers used in solvent-borne adhesives are the following.

– *Neoprene GN* (1942). It is a general-purpose sulphur-modified polychloroprene used in the shoe industry. This polychloroprene has two limitations: the viscosity decreases on ageing and a black discolouration appears during storage.

– *Neoprene AC* (1947). This polychloroprene was developed to provide better viscosity stability and resistance to discolouration, but it cures much more slowly at room temperature. It is a fast crystallizing grade and contains about 90% *trans*-1,4 structure.

– *Neoprene AD* (1958). This is more stable than *Neoprene AC*. This polychloroprene does not change colour in contact with iron and viscosities of the solutions are maintained stable over long periods of time. They are fast crystallizing grades and contain about 90% *trans*-1,4 structure.

– *Neoprene AD-G*. It is a *Neoprene AD* grafted with methyl methacrylate. It provides longer *pot life* (i.e. the time after which a mixture of two components in an adhesive maintains its properties) in two-part adhesives systems.

– *Neoprene AF* (1963). It is a polychloroprene modified with methacrylic acid. Although it is a slow-crystallizing elastomer, the cohesive strength develops very rapidly and it has improved creep resistance at high temperature compared with *Neoprene AC* or *AD*. The improved properties of *Neoprene AF* are derived from the interaction between the carboxyl functionality with the metal oxides added in the solvent-borne polychloroprene adhesives.

– *Neoprene AG* (1967). It is a high-gel polymer which exhibits a high degree of thixotropy. It is specially designed for spraying applications.

– *Neoprene AH* (1975). It is a methylacrylate-modified elastomer which is non-crystallizing and is chemically peptizable in aliphatic solvents. However, it is generally prepared as a dispersion in hexane, and has balanced properties between conventional solvent-borne adhesives and aqueous systems.

Table 4

Solution and peel properties of polychloroprenes with fast crystallizing characteristics but different molecular weight

	<i>Neoprene grade</i>		
	WM-1	W	WHV
Mooney viscosity	39	48	118
Molar mass (intrinsic viscosity in toluene)	230,000	370,000	820,000
Solution viscosity ^a (mPa s)	8,700	18,400	57,000
Peel strength canvas–canvas (kN/m):			
25°C	48	55	80
50°C	17	20	40
70°C	5	6	18

CR adhesives contain 20 wt% solids content. Formulation: 100 phr elastomer; 4 phr MgO; 5 phr ZnO; 2 phr hindered phenolic antioxidant; 500 phr solvents mixture [2].

^a Brookfield RVT. Spindle 7 at 20 rpm. 25°C.

– *Neoprene WHV-A*. It is a non-peptizable and mercaptan-modified polychloroprene elastomer. It is a slow-crystallizing, high molecular weight type and contains only 85% *trans*-1,4 structure. It is generally used in blends with low molecular weight crystallizing polychloroprene types to increase solution viscosity.

– *Neoprene XD*. Developed in the 1980s, this polychloroprene family was prepared using special xanthogendisulphides as chain modifiers, offering improved processability and vulcanizate properties. In solution, these polychloroprenes show slow crystallization and high temperature resistance.

– *New Neoprene M- and XD grades*. These polychloroprenes were developed in the 1990s and combine low temperature flexibility, improved heat resistance and dynamic properties.

The polymer type influences several properties of solvent-borne CR adhesives, mainly the molecular weight and rate of crystallization.

(a) The increase in the molecular weight of the polychloroprene increases its solution viscosity, adhesive strength and heat resistance (Table 4) [2].

(b) The rate of crystallization of polychloroprene elastomers can be obtained using DSC (differential scanning calorimetry) and TMA (thermal mechanical analysis). On the other hand, the increase in the crystallization rate of the polychloroprene improves the rate of development of bond strength and the ultimate strength at high temperature, but a reduction in open time (*tack*) is obtained (Table 5) [2]. However, the tack can be varied by changing the pressure during joint formation (Table 6) and by an adequate selection of the solvent [2]: the lower the volatility of the solvent, the longer the open time of the solvent-borne CR adhesive. Correspondingly, a blend of volatile solvents (e.g. acetone + hexane) will significantly reduce the open time of the solvent-borne CR adhesives (Table 7).

About one dozen *polychloroprene latices* have been developed for adhesive

Table 5

Solution and peel properties of polychloroprenes with different crystallizing characteristics^a

	<i>Neoprene</i> grade			
	AD30	WHV	W	WRT
Solution viscosity – 25°C (mPa s)	4460	5720	1860	1740
Peel strength at 23°C (kN/m):				
Initial	4.1	4.0	3.6	3.1
1 day	7.9	4.8	4.4	4.2
3 days	8.2	5.6	5.5	4.7
7 days	8.4	7.9	5.5	4.6
7 days at 23°C, tested 60°C	2.7	2.1	0.1	0.15
Tack retention ^b (min)	30–40	~900	~1700	>2500

CR adhesives contain 20 wt% solids content. Formulation: 100 phr elastomer; 4 phr MgO; 5 phr ZnO; 2 phr hindered phenolic antioxidant; 500 phr solvents mixture [2].

^a *Neoprene WRT*, extremely low rate of crystallization; *Neoprene W*, medium rate of crystallization; *Neoprene WHV*, fast rate of crystallization; *Neoprene AD30*, extremely fast rate of crystallization.

^b Laminating pressure = 0.4 MPa, 1 min.

Table 6

Effect of laminating pressure (during 1 min) on tack retention of a CR adhesive

Laminating pressure	Tack retention for <i>Neoprene AD30</i> (min)
0.4 MPa	50
0.2 MPa	30
0.1 MPa	26
70 kPa	20
30 kPa	12
10 kPa	8

Formulation: 100 phr elastomer; 4 phr MgO; 5 phr ZnO; 2 phr hindered phenolic antioxidant; 500 phr solvents mixture [2].

applications. Polychloroprene latices differ from their solid elastomer counterparts (used in solvent-borne CR adhesives) in that they are gel polymers (e.g. insoluble in organic solvents). Latex systems derive their strength characteristics from the gel structure rather than crystallinity as in solvent solution systems.

There is only one non-ionic latex (*Neoprene latex 115*); all other polychloroprene latices are anionic and are emulsified with rosin soaps.

Neoprene latex 115 contains a copolymer of chloroprene and methacrylic acid, stabilized with polyvinyl alcohol [15]. With respect to other polychloroprene latices, this latex has two major advantages: (1) excellent colloidal stability, which gives high resistance to shear and a broad tolerance to several materials;

Table 7

Influence of solvent on viscosity and tack of polychloroprene adhesives

Solvent	Mixing ratio	Solution viscosity – 20°C (mPa s)	Tack time (min)
Toluene	–	4460	35
Toluene/ <i>n</i> -hexane/MEK	35/5/15	3500	25
<i>n</i> -Hexane/MEK	55/45	1520	15
Cyclohexane/acetone	80/20	3700	18
MEK/acetone	75/25	2100	15
Toluene/ <i>n</i> -hexane/ethyl acetate	34/33/33	3600	30
Toluene/MEK/acetone	34/33/33	3400	22
<i>n</i> -Hexane/acetone	50/50	1140	7
Dichloromethane	–	4670	30
1,1,1-Trichloroethane	–	4600	38

Formulation: 100 phr elastomer; 4 phr MgO; 5 phr ZnO; 2 phr hindered phenolic antioxidant; 500 phr solvents mixture [2].

(2) carboxyl functionality, which imparts specific adhesion to many nonporous substrates and allows curing with metal oxides at room temperature.

Among the anionic polychloroprene latices, the following grades are the most common.

- *Neoprene 400*. It contains a fast-crystallizing polymer with the highest chlorine content and the highest uncured cohesive strength among all anionic latexes. However, this latex has a relatively short open time and requires high lamination pressures to achieve coalescence.

- *Neoprene 571*. It contains a very high-gel polymer which allows to produce high-strength films with low permanent set.

- *Neoprene 654*. It is a high-solids, low-viscosity latex containing a very low gel polymer. It offers good tack and flexibility.

- *Neoprene 671A*. It is a high-solids, low-viscosity latex containing a medium-high gel polymer. It combines a high uncured cohesive strength and good open tack time.

- *Neoprene 750A*. It is a medium-gel, slow-crystallizing polymer. It combines flexibility, dry tack, heat-reactivity and cohesive strength.

- *Neoprene 735A*. It is a sol polymer which gives the longest dry open tack time of all latices.

4.2. Resins

Tackifiers and modifiers are generally added to improve the adhesive performance of synthetic elastomers. All resins added to an adhesive formulation modify their properties (viscosity, open time, tack) and therefore these resins are also called

modifiers. If the main aim of the addition of a resin is the increase of tack and adhesion properties, the resin acts as a tackifier. The term resin will be used in this chapter for both tackifiers and modifiers.

Resins used in rubber base adhesive formulations have the following characteristics [16]:

- (1) low molecular weight ($M_w = 200\text{--}2000$ g/mol), thermoplastic resins;
- (2) viscous liquids to hard, brittle glasses at room temperature;
- (3) they are obtained from the derivatization of rosin or by polymerization of petroleum distillates, turpentine fractions, coal tar and pure monomers;
- (4) ranging from water-clear to dark brown or black colour;
- (5) are soluble in aliphatic and aromatic hydrocarbons, as well as in many common organic solvents.

t-Butyl phenolic resin is a typical tackifier for solvent-borne polychloroprene adhesives. For these adhesives, rosin esters and coumarone–indene resins can also be used. For nitrile rubber adhesives, hydrogenated rosins and coumarone–indene resins can be used. For particular applications of both polychloroprene and nitrile rubber adhesives, chlorinated rubber can be added. Styrene–butadiene rubber adhesives use rosins, coumarone–indene, pinene-based resins and other aromatic resins.

In this section the rosins and rosin derivative resins, coumarone–indene and hydrocarbon resins, polyterpene resins and phenolic resins will be considered. The manufacture and structural characteristics of natural and synthetic resins will be first considered. In a second part of this section, the characterization and main properties of the resins will be described. Finally, the tackifier function of resins in rubbers will be considered.

4.2.1. General aspects of resins

The term resin is not well-defined. Originally, it was applied to low molecular weight natural products, usually yellowish to brown in colour, transparent to opaque, soft to brittle, easily fusible, tacky, amorphous material, soluble in most common organic solvents and insoluble in water. With the development of the chemical industry, the term resin has also been applied to synthetic materials used as substitutes for natural resins, or to materials with similar physical properties. According to the international standards ISO 472 and ISO 4618/3, resins are defined as ‘solid, semisolid, or pseudosolid organic materials that have an indefinite and often high relative molecular mass, and generally soften or melt over a range of temperatures’. The resins have the following characteristics:

- (1) a medium molecular weight (lower than 10,000 g/mol);
- (2) an amorphous and complex structure;
- (3) they do not exhibit a sharp melting point, but have a glass transition temperature;

- (4) they have a softening point (transition temperature from a pseudosolid to plastic state).

Resins can be divided into natural and synthetic types. *Natural resins* have a vegetable or animal origin. Typical examples are rosins. *Synthetic resins* result from controlled chemical reactions, and can be divided into two subgroups.

(a) Hydrocarbon resins produced by polymerization. These resins are derived from coal tar, petroleum and turpentine feedstock. Like natural resins, these resins are added to polymers to impart tack, flow and hardness.

(b) Synthetic resins obtained by addition polymerization and polycondensation, which are intermediates in the synthesis of higher molecular weight plastics.

4.2.2. *Manufacture and structural characteristics of resins*

4.2.2.1. *Rosins and rosin derivatives.* The resins more commonly used in rubber base adhesives are rosin esters, particularly glycerol and pentaerythritol esters, as well as rosins modified by disproportionation and hydrogenation. The glycerol ester of hydrogenated rosin has been reported to be an excellent tackifier for polychloroprene adhesives (see pp. 344–357 in [17]).

Extraction of rosin. Rosin resins are produced from three types of rosin, i.e. gum, tall oil, and wood. Extensive details about rosin resins extraction and derivatization can be found on page 269 in the book edited by Zinkel and Russell [18].

Extraction of *gum rosin* from exudation of living pines was America's first widespread industry, which started in Nova Scotia in 1606. Normal resin ducts are found in the genera *Pinus*, *Picea*, *Pseudotsuga*, and *Larix*. They arise by producing vertical (longitudinal) and radial (horizontal) wounds in the log using a special tool called a hack. From the wounds, a slow flow of resin arises (which is greater in the first few hours after wounding a pine) and ceases after a few days. Resin flow stops because of tylosoid formation, crystallization of resin acids and/or solidification of the resin [19]. Resin flow can be forced by spraying the wound with a diluted sulphuric acid solution containing 5–8 wt% of 2-chloroethylphosphonic acid. The resin flows through a plastic or aluminium cup (iron cups cause oxidative darkening of the resin). The resin collected in the cups is transferred to a barrel for further processing. Before processing, the crude pine gum is cleaned by adding small amounts of oxalic acid to remove water-soluble impurities, iron contamination and solid impurities (chips, bark). The resulting purified crude pine gum is distilled using a continuous stream of water to separate the turpentine (volatile essential oil in the gum) from the rosin (the non-volatile resinous material which remains at the bottom of the distillation unit). The rosin is discharged and passed over cotton batting to remove unwanted solid material.

Wood rosin is obtained by solvent extraction of stumps obtained from lumbering operations of pine trees. Stumps are first cleaned to remove sand, dirt, rocks and other contaminants. Then, the stumps are reduced to relatively uniform-size chips using mechanical cutting devices. The chips are transported to the extraction equipment where they are steamed to recover volatile terpene oils before solvent extraction begins. Several solvents can be used for rosin extraction but aliphatic petroleum hydrocarbon fractions with higher and narrower boiling ranges or methyl isobutyl ketones are generally used [20]. Extraction is generally carried out at elevated temperature and under pressure (7–10 atm) for some hours. The extract solution is separated in continuous evaporators into three fractions: recovered solvent (which is reused in the extraction process), volatile terpenes, and rosin. Rosin obtained from this extraction operation can be used without further operation, but very often colour refining is done by adsorption or by using two immiscible solvents of different polarity. A typical yield of wood rosin in this process is about 70%.

Tall oil rosin is obtained from crude tall oil obtained from the Kraft (sulphate) pulping of various coniferous trees in the paper manufacturing industry. During the Kraft pulping process the fatty acids and the resin acids from the coniferous wood are saponified by the alkaline medium. On concentration of the resulting pulping liquor, the sodium soap of these mixed acids rises to the surface from where they are skimmed out. By acidification of this material with sulphuric acid, the crude tall oil is obtained. Fractional steam distillation of the crude tall oil allows the separation of the tall oil fatty acids and the tall oil rosins [21].

Chemistry of rosin. All three types of rosin consist primarily of C_{20} monocarboxylic diterpene resin acids, the most common of which have the molecular formula $C_{20}H_{30}O_2$. In addition, rosins contain small amounts of neutral and other acidic components (e.g. fatty acids in tall oil rosin). The neutral components of rosins are diterpene alcohols, hydrocarbons and aldehydes, and their contents generally vary between 5 and 15 wt%.

With very few exceptions, the pine resin acids belong to four basic skeletal classes: abietane, pimarane, isopimarane, and labdane (Fig. 7). The acids of the abietane, pimarane and isopimarane series have a isopropyl or methyl/ethyl group in the carbon-13 position and a single carboxyl group in the carbon-18 position, and differ only in the number and location of the carbon–carbon double bonds (the most common have two carbon–carbon double bonds). The acids of labdane series are less common and contain one carboxyl group in the carbon-19 position.

The structures and nomenclature for the common pine resin acids based on the abietane skeleton (abietic-type acids) are given in Fig. 8. The abietic, neoabietic, palustric and levopimaric acids differ only in the location of their two double bonds. All double bonds are endocyclic, except in the neoabietic acid in which one is exocyclic.

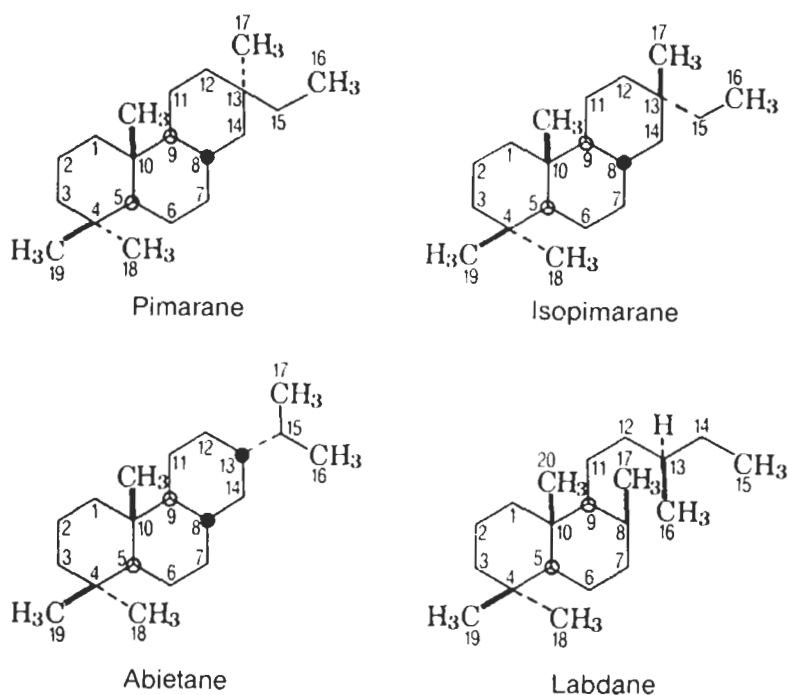


Fig. 7. Principal monocarboxylic diterpene acids skeletons in rosins. Dotted line indicates that the chemical group is located below plane (see p. 266 in [18]).

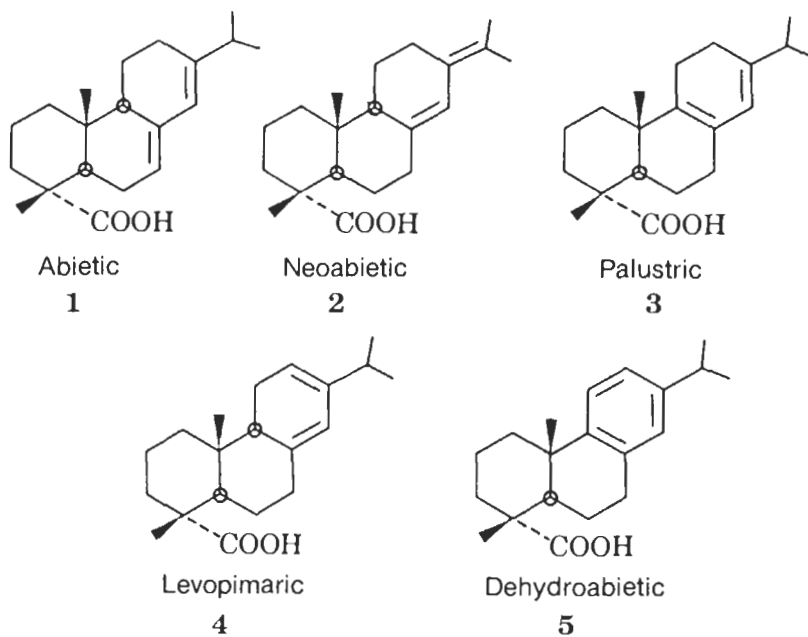


Fig. 8. Common acids of the abietane skeletal class (abietic-type acids) (see p. 268 in [18]).

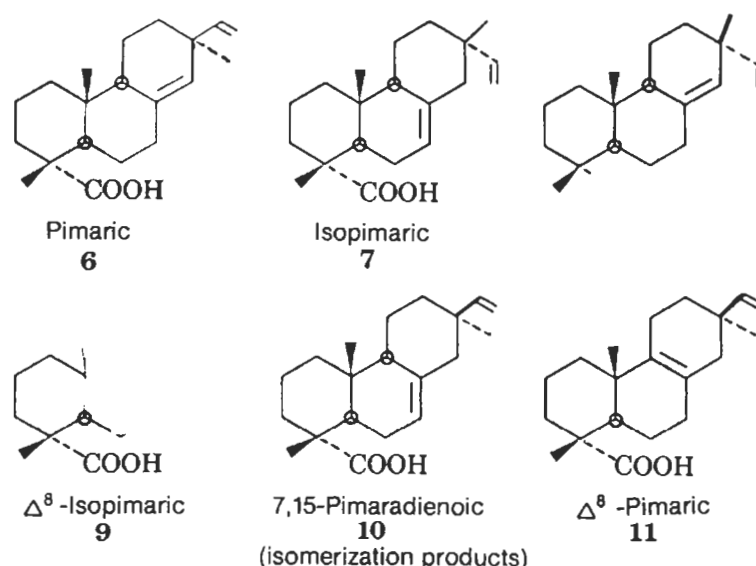


Fig. 9. Common acids of the pimarane and isopimarane skeletal class (pimaric-type acids) (see p. 269 in [18]).

The common pine resin acids based on the pimarane and isopimarane skeletal (pimaric-type acids) are shown in Fig. 9. The pimarane and isopimarane acids series differ only in the methyl group position in the carbon-13 position. Isopimaric and sandaracopimaric acids differ in the location of the carbon-carbon double bond.

The resin acids found in rosins are generally of the abietic- and pimaric-type. Rosins of various pine species differ in their content of abietic vs. pimaric-type acids. Rosins from species exhibiting high abietic-type acid compositions are preferred for production of rosin derivatives. However, the differences in properties of rosins are often associated with their non-resin acid content instead of their chemical compositions. On the other hand, the compositions of rosins from different sources greatly differ [22]. Table 8 shows a typical distribution of resin acids in rosins obtained from gum, tall oil and wood sources.

Most rosin utilization takes advantage of the carboxyl and olefinic functionalities of the resin acids.

The *olefinic functionality* produces instability of rosin to oxidation which causes an undesirable yellowish colour. The conjugated carbon-carbon double bonds of the abietic acids leads to oxygen addition reactions and isomerization reactions. Rosin can be stabilized by removal of this conjugated unsaturation through hydrogenation and dehydrogenation reactions. Hydrogenation of the first conjugated carbon-carbon double bond is quite easy by catalytic reaction with

Table 8

Typical composition (in per cent of acid fraction) of the common resin acids in rosins obtained from different sources [22]

Resin acid	Tall oil rosin	Wood rosin	Gum rosin
Pimaric	4.4	7.1	4.5
Sandarcopimaric	3.9	2.0	1.3
Communic	1.0	–	3.1
Levopimaric	–	–	1.8
Paulstric	8.2	8.2	21.2
Isopimaric	11.4	15.5	17.4
Abietic	37.8	50.8	23.7
Dehydroabietic	18.2	7.9	5.3
Neoabietic	3.3	4.7	19.1

palladium or Raney nickel. After hydrogenation of the first carbon–carbon double bond, the residual carbon–carbon bond is hindered by steric effects and is more resistant to further hydrogenation. The hydrogenation at high pressure in the presence of noble metal catalysts produces a fully hydrogenated product. Rosins can also be stabilized by heating at 200–300°C for several hours.

The most important single reactions produced in the *carboxyl functionality* of the resin acids are salt formation, Diels–Alder additions, and esterification. Other reactions, such as disproportionation and polymerization, are less important. For some specific applications, rosins are subjected to a combination of these reactions.

Salt formation. The resin acids have a low acid strength. The pK_s (ionization constants) values of resin acids are difficult to obtain, and values of 6.4 and 5.7 have been reported [23] for abietic and dehydroabietic acids, respectively. Resin acids form salts with sodium and aluminium. These salts can be used in detergents because of micelle formation at low concentrations. Other metal salts (resinates) of magnesium, barium, calcium, lead, zinc and cobalt are used in inks and adhesive formulations. These resinates are prepared by precipitation (addition of the heavy metal salt to a solution of sodium resinate) or fusion (rosin is fused with the heavy metal compound).

Esterification. The esterification of rosin provides important commercial products for the adhesive industry. Rosin esters are formed by the reaction of rosins with alcohols at elevated temperatures. Because the carboxyl group of the resin acids is hindered by attachment to a tertiary carbon, esterification with an alcohol can only be accomplished at elevated temperatures. This hindrance is in turn responsible for the high resistance of the resin acid ester linkage to cleavage by water, acid and alkali.

Rosins are commonly combined with alcohols with more than one hydroxyl group such as ethylene glycol and diethylene glycol (two hydroxyl groups),

glycerol (three hydroxyl groups) and pentaerythritol (four hydroxyl groups). The reaction is carried out under inert gas atmosphere (to prevent oxidation) at 260–280°C with or without a catalyst (boric acid, zinc oxide, lactic acid, etc.); about 15–20% excess of alcohol with respect to the rosin is generally added. Water is a byproduct of the reaction and its removal allows the reaction to be completed. Catalysts are generally used to speed-up the reaction and mainly to improve colour and heat stability of the resulting rosin ester. Upon completion of esterification, some undesirable compounds (unreacted alcohol, traces of water, rosin oils) are removed under reduced pressure or steam sparging. In 1982, a new method to produce rosin esters at 30–40°C was established [24]. The method consists of allowing a quaternary ammonium salt of resin acids to react with a polychloro organic chemical, which also acts as solvent.

The rosin esters are clear and light in colour. They are soluble in hydrocarbon solvents (solubility parameters of 8.4 to 9.0). They contain reduced acid numbers (about 10 for the glycerol ester and about 15 for the pentaerythritol ester) and are free of unsaturated alcohols (which would lower the softening point and decrease the water resistance of the rosin ester). The glycerol ester (usually called ester gum) remains one of the most important rosin esters which find use in several adhesive formulations. The use of pentaerythritol esters imparts improved properties for varnishes because they have higher softening points and greater molecular weight than those of analog glycerol esters.

Reduction to alcohols. Copper chromite-catalytic hydrogenation of the methyl ester of rosin at 300°C under high pressure produced a hydroabietyl alcohol. During hydrogenation, the carboxyl acid group is converted to a primary alcohol group, and the carbon-carbon double bonds of the parent resin acids are altered. The product is light in colour and very resistant to air oxidation, and finds application in adhesives as well as wetting agents and plasticizers.

4.2.2.2. Coumarone-indene resins. The first commercial coumarone-indene resin was manufactured in 1910. The basic material for the production of coumarone-indene resins is high-temperature coal tar. Coal tar is one of the byproducts of coal carbonization. In the coking process, hard coal undergoes a pyrolytic conversion at temperatures of 1000–2000°C. The main product is coke but there are several byproducts partly recoverable by condensation and extraction from the gases liberated during carbonization. Crude tar accounts for 3 wt% of the coal carbonization process. Distillation of coal tar renders less than 3 wt% coal-tar light oil, which is the main source for manufacturing of coumarone-indene resins. This light oil fraction boils at 70–200°C and contains 10–40% of unsaturated aromatics (Fig. 10).

A typical composition of a coumarone-indene feedstream is:

- 2 wt% styrene
- 1 wt% α -methylstyrene

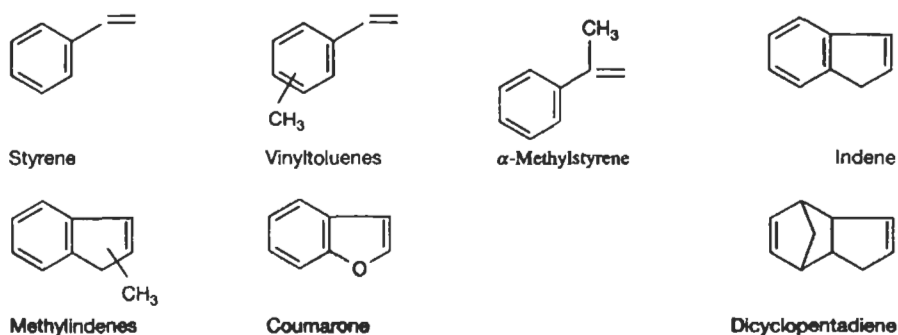


Fig. 10. Chemical structure of components in coumarone-indene resins.

- 30 wt% alkylbenzenes
- 4 wt% vinyltoluenes
- 5 wt% dicyclopentadiene
- 7 wt% coumarone
- 48 wt% indene
- 3 wt% methylindenes and methylcoumarones.

According to the typical chemical composition of these resins, the coumarone content in the feedstock (and in the final resin) is very low compared to that for indene. Therefore, the use of the term polyindene resins would be more appropriate than coumarone-indene resins; however, this is not a common practice.

During the high-temperature operations, intermolecular hydrogen transfer reactions occur, transforming some indene to indane. The high indane concentration in the resin feedstock causes low yield and poor quality in the polymerization process. The indene loss can be reduced by decreasing the temperature and the residence time during distillation.

The raw material has to be washed to remove impurities. Diluted sodium hydroxide allows the removal of phenols and benzonitrile, and diluted sulphuric acid reacts with pyridine bases. The resulting material is distilled to concentrate the unsaturated compounds (raw feedstock for coumarone-indene resin production), and separate and recover interesting non-polymerizable compounds (naphthalene, benzene, toluene, xylenes). Once the unsaturated compounds are distilled, they are treated with small amounts of sulphuric acid to improve their colour; activated carbons or clays can be also used. The resulting material is subjected to polymerization. It is important to avoid long storage time of the feedstock because oxidation processes can easily occur, affecting the polymerization reaction and the colour of the coumarone-indene resins.

Coumarone-indene resins were produced by adding sulphuric acid to the stirred feedstock at 20–35°C, taking care to produce a good dispersion of the sulphuric acid to avoid scorching (dark-coloured resins are obtained), and to con-

trol the temperature (it is a strongly exothermic reaction). Today, the coumarone–indene resins are obtained using a BF_3 /phenol mixture as initiator (see below).

The polymerization process of coal tar and petroleum fraction (from which aromatic hydrocarbon resins are obtained) are similar. The process is extensively described in the book by Mildenberg et al. [25]. There are three basic steps in the polymerization of coumarone–indene and hydrocarbon resins.

- (1) Initiation. A Friedel–Craft acid (hydrochloric acid, water, phenol) is used as initiator together with a proton source ('co-initiator', BF_3 or AlCl_3 are the most common). The mixture produces a cation which is the true initiating species.
- (2) Propagation.
- (3) Termination. It can be achieved using nucleophiles (alcohols, ammonia, amines, alkalis, water).

Several reaction parameters affect the composition of the coumarone–indene resins. In the presence of AlCl_3 , the resins have higher molecular weight than those produced in the presence of BF_3 . The high initial concentration of the initiator gives coumarone–indene resins with lower molecular weight. Finally, the molecular weight and the yield of the resin increase by increasing the temperature of the reaction.

After deactivation and removal of the initiating system, the coumarone–indene resin is separated from solvent and low molecular weight materials by vacuum distillation. The removal of the low molecular weight materials is important because they produce strong odour, they act as softeners and they cause an undesirable decrease in softening point. Therefore, at this stage the softening point of the coumarone–indene resins is adjusted. Finally, stabilizers are added to the liquid resin while it is still hot to inhibit further oxidation (which causes discolouration and odour).

One of the key properties of coumarone–indene resins is the softening point. This is determined by careful selection of the feedstock, manufacturing process, level of constancy in temperature during reaction and concentration of initiating system. Coumarone–indene resins which are obtained using this procedure have softening points from liquid to 170°C and Gardner colour of 5 to 9.

The structural element of a coumarone–indene resin is relatively similar to that for aromatic hydrocarbon resins, as they differ only in the proportion of indene-type structures which are present in higher concentration in the coumarone–indene resins. The main monomers in the aromatic resins are styrene and indene. Styrene produces the atactic conformation of the resins, whereas indene introduces rigidity into the polymer chain. A typical structural element of an aromatic resin is given in Fig. 11.

Coumarone–indene resins can be modified to match specific properties. Some of the most common modifications in those resins are the following.

- (a) *Styrene-modified coumarone–indene resins*. It is intended for formulating

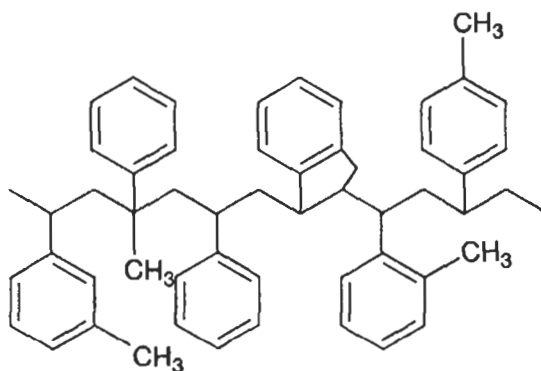


Fig. 11. Structural element of an aromatic hydrocarbon resin.

floor tiles to avoid indentations produced by the pressure of women's heels footwear. The modification is produced by copolymerization of the coumarone–indene resin with 15 wt% styrene using the normal polymerization conditions. The resulting resin has higher solution and melt viscosity than the unmodified coumarone–indene resin.

(b) *Phenol-modified aromatic resins.* Coumarone–indene resins are essentially non-polar in nature. The reaction with phenol allows the introduction of hydroxyl groups which provide polarity. About 10–15 wt% phenol is incorporated in the resin and it is completely reacted (e.g. there is no free phenol). These phenol-modified resins can be used in adhesive formulations (e.g. floor coverings) because the adequate solubility (in alcohols, glycols, esters and ketones) and compatibility. The most common grade has a softening point of 90°C.

4.2.2.3. *Hydrocarbon resins.* There is not much literature concerning the manufacturing, chemistry and properties of hydrocarbon resins. One of the few contributions in this area is the recent book by Mildenberg et al. [25], p. 43.

Separation of raw feedstock. The pyrolysis of petroleum feedstream is carried out at 650–900°C at normal pressure in the presence of steam. The so-called steam-cracking process involves carbon–carbon splitting of saturated, unsaturated and aromatic molecules. The following steam-cracker fractions are used as raw materials to produce hydrocarbon resins.

(a) *C₅ streams.* They contain linear and cyclic olefins, such as isoamylene, isoprene, piperylene, C₅ paraffins and cyclopentadiene (Fig. 12). *Aliphatic hydrocarbon resins* can be obtained from the unsaturated components of this fraction. Cyclopentadiene tends to dimerize during operation and is deposited at the bottom of the reactor (heat-soaking favours deposition). The dicyclopentadiene is removed from the reactor and used to produce the DCPD resins. Finally, isoprene

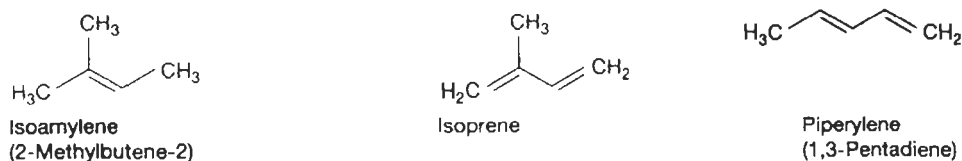


Fig. 12. Chemical structure of components in aliphatic hydrocarbon resins.

is separated from piberylene concentrate, which is the feedstock to manufacture aliphatic hydrocarbon resins.

(b) *C₈/C₉ streams.* They contain unsaturated aromatics (e.g. styrene, indenenes). *Aromatic hydrocarbon resins* can be obtained from these streams. Benzene, toluene and xylene are drawn off from the stream and a C₉ material containing unsaturated compounds with a boiling range 160–200°C is obtained. This C₉ resin material has the following composition:

- 2 wt% styrene
- 4 wt% α -methylstyrene
- 20 wt% vinyltoluene
- 6 wt% dicyclopentadiene and co-dimers
- 20 wt% indene
- 5 wt% methylindenenes
- 5 wt% naphthalene
- 38 wt% other nonreactive aromatics

A further source of C₉ material is coal tar. Structures of the two resins precursors are roughly similar, except the presence of small quantities of coumarone in coal tar feedstream. There is a significant difference in the concentrations of individual monomers: coal-tar-based raw material is richer in indene (styrene/indene ratio = 1 : 7) than the petroleum-based feedstream (styrene/indene ratio = 1 : 1).

(c) *C₄ streams.* They contain olefins, mainly isobutenes, which by cationic polymerization produce polybutene oligomers. Low molecular weight *polybutene resins* are mainly composed of isobutene (15–30 wt%), 1-butene (10 wt%) and *cis* and *trans* 2-butenes (10–15 wt%) (Fig. 13).

(d) *Dicyclopentadiene streams.* Dicyclopentadiene concentrates are generated by dimerization of cyclopentadiene (Fig. 14) in the heat soaking process of the

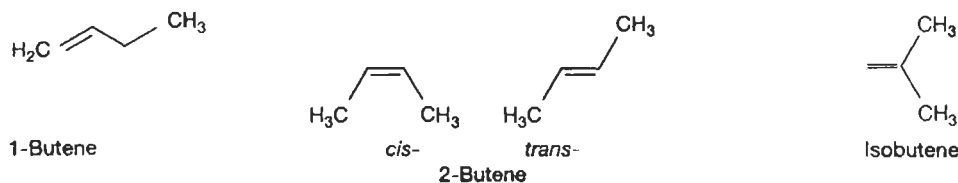


Fig. 13. Chemical structure of components in polybutene resins.

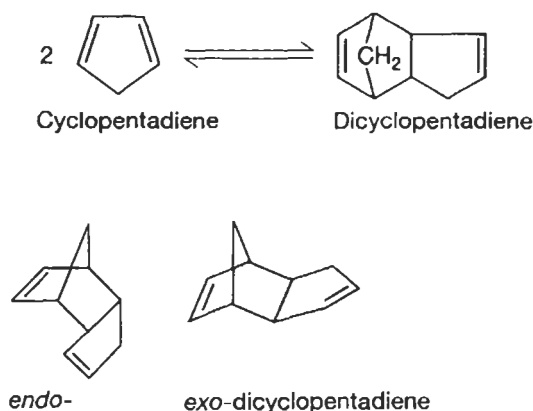


Fig. 14. Chemical structure of components in dicyclopentadiene resins.

effluents in the C_8/C_9 stream-cracking of petroleum feedstock. *Dicyclopentadiene resins* can be obtained from these streams.

Polymerization of raw feedstock. Aliphatic hydrocarbon resins. Raw feedstock contains straight-chain and cyclic molecules and mono- and diolefins. The most common initiator in the polymerization reaction is $AlCl_3/HCl$ in xylene. The resinification consists of a two-stage polymerization in a reactor at $45^\circ C$ and high pressure (10 MPa) for several hours. The resulting solution is treated with water and passed to distillation to obtain the aliphatic hydrocarbon resins. Several aliphatic hydrocarbon resins with different softening points can be adjusted.

- Unmodified aliphatic hydrocarbon resins: softening point = $80\text{--}100^\circ C$, Gardner colour = 3.5–7.
- Modified aliphatic hydrocarbon resins:
 - cyclic-modified: softening point = $115^\circ C$, Gardner colour = 5.
 - aromatic-modified: softening point = liquid to $90^\circ C$, Gardner colour = 5–9.
 - cyclic/aromatic-modified: softening point = $95^\circ C$, Gardner colour = 3.

The structure of aliphatic resins is difficult to determine as they contain straight-chain and cyclic structures. A possible structural element is given in Fig. 15 [25].

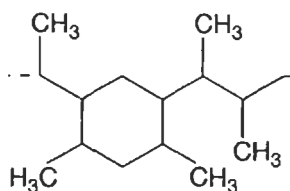


Fig. 15. Structural element of an aliphatic hydrocarbon resin (see p. 43 in [25]).

Aromatic hydrocarbon resins. The polymerization procedure and variables in the reactions of the aromatic hydrocarbon resins are similar to those for the coumarone–indene resins. However, the C_9 feedstreams used in the polymerization of the aromatic hydrocarbon resins do not contain significant amounts of phenols or pyridine bases, so they are submitted directly to fractional distillation. Distillation produced more byproducts than light coal-tar oils. The aromatic hydrocarbon resins obtained have softening points between liquid and 125°C and Gardner colour of 6 to 11. By changing distillation conditions, aromatic hydrocarbon resins with softening points between 65 and 170°C and Gardner colour of 5 to 10 can also be obtained.

Dicyclopentadiene (DCPD) resins. In contrast with the polymerization process to produce aliphatic and aromatic resins, the polymerization of DCPD is carried out by heating (it is a very exothermic reaction, so temperature must be carefully controlled). Addition of aromatic unsaturated species (e.g. styrene, vinyltoluene) to DCPD is usual, because the heat of the reaction is reduced and allows appropriate modification of the properties in the final resins. The polymerization of DCPD streams is a pressure/temperature reaction which does not require a catalyst. After blending the DCPD stream with a high flash point solvent diluent (xylene, mineral spirits 140/160, naphtha), pressure is applied with preheating at about 60°C . The polymerization is produced in 15 h by increasing the temperature in two or three steps until a temperature between 200 and 280°C is obtained. The resulting material is distilled and DCPD resins with softening points between 30 and 120°C , Gardner colours of 5 to 6, and iodine numbers from 95 to 175 are obtained. The basic structure of the DCPD resins is given in Fig. 16 [25].

The highly unsaturated DCPD resins are generally modified to improve their performance in adhesives and printing ink industry. Three modifications are generally produced.

(1) **Hydrogenated DCPD resins.** Hydrogenation of resins leads to very light-coloured products and also produces remarkable stability to light and heat. Hydrogenation of DCPD resins is generally carried out under pressure and high

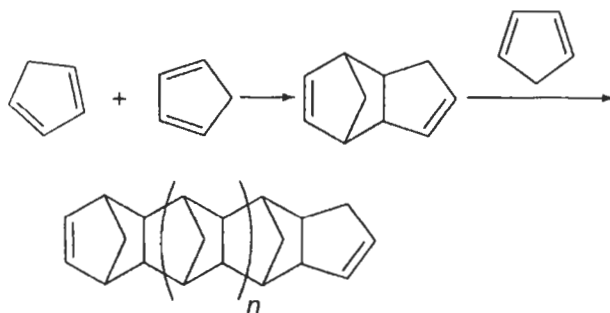


Fig. 16. Structural element of a dicyclopentadiene resin (see p. 45 in [25]).

temperature in the presence of a nickel catalyst for about 3 h. The resulting hydrogenated DCPD resins have softening points of 80–130°C and Gardner colour below 1.

(2) *Maleic anhydride-modified DCPD resins*. Heating of the DCPD resin with 10 wt% maleic anhydride for 3 h at 200°C produces a resin with a softening point of 180°C and an acid number of 53.

(3) *Rosin-modified DCPD resins*. The DCPD resin is heated with 30 wt% rosin ester.

Polybutene resins. These liquid resins are obtained by cationic polymerization of petroleum C₄ streams in the presence of AlCl₃ at relatively low temperature. Temperature and AlCl₃ concentration are important factors as they influence the molecular weight and viscosity of the final resin. After reaction, the mixture is deactivated with water, methanol, ammonia or aqueous sodium hydroxide. The organic layer is separated and distilled to remove solvent and unconverted material.

4.2.2.4. Polyterpene resins. Terpene resins are obtained from natural terpene monomers obtained from naval stores, paper pulp production, and citrus juice production. Terpenes are found in almost all living plants, and the turpentine oil from pine trees is the most important source.

Gum turpentine is obtained from wounding living trees to get an exudate containing turpentine and rosin. Turpentine is separated from the rosin by continuous steam distillation and further fractionation. Wood turpentine comes from the extraction of stumps of pine trees using naphtha, and subsequent separation of rosin and turpentine by fractional distillation. Tall-oil turpentine is a byproduct of the Kraft sulphate paper manufacture. Terpenes are isolated from the sulphate terpentine and separated from the black digestion liquor. The composition of turpentine oils depends on its source, although α -pinene and β -pinene are the major components.

Crude turpentine is distilled to obtain refined products used in the fragrance and flavour industry. Only the unsaturated mono- and bicyclic terpenes are of interest for resin production. These are mainly α -pinene, β -pinene and dipentene (D,L-limonene) (Fig. 17). D-Limonene is obtained by extraction of orange peel in citrus fruits.

Polymerization of terpene monomers is carried out at 30–50°C using AlCl₃ as initiator and xylene or toluene as diluting solvent. The reaction must be carried out under inert gas atmosphere to avoid oxidation of the polyterpenes. The initiating system is deactivated by adding water under vigorous stirring. After phase separation, the organic layer is separated and submitted to vacuum distillation to take off the diluent. At this stage the softening point of the resin can be adjusted by removal of the low molecular weight dimers and trimers. Finally, antioxidants must be added for protection against oxidation. The typical structure of the polyterpene resins is given in Fig. 18 [25].

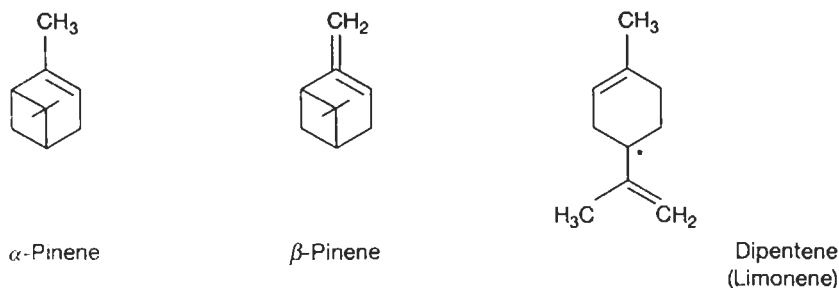


Fig. 17. Chemical structure of components in polyterpene resins.

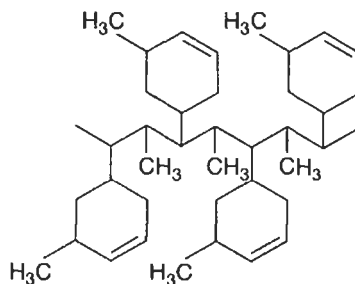


Fig. 18. Structural element of a polyterpene resin (see p. 47 in [25]).

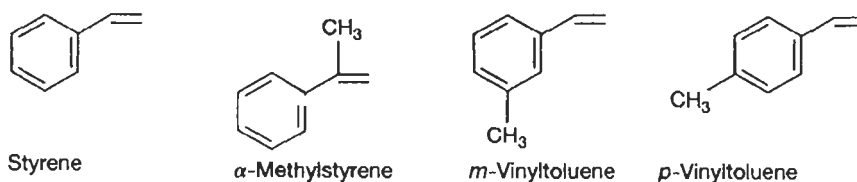


Fig. 19. Chemical structure of components in resins obtained from pure monomers.

4.2.2.5. Resins from pure monomers. Some colourless resins can be produced from pure unsaturated monomers, such as styrene, α -methylstyrene and vinyltoluenes (Fig. 19). These monomers are used individually or as blends with terpenes or unsaturated aliphatics.

The raw feedstock used to produce these resins are obtained using synthetic routes:

- styrene is obtained by alkylation of benzene with ethylene in the presence of aluminium chloride as catalyst, followed by dehydrogenation;
- α -methylstyrene is obtained as a byproduct in the production of phenol by oxidation of cumene to the hydroperoxide and subsequent splitting by acids;
- vinyltoluenes are manufactured by alkylation of toluene followed by dehydrogenation.

Production of these resins is similar to that for the coumarone–indene resins. As the raw material does not contain impurities, a small amount of the initiating system can be used.

4.2.3. Characterization and main properties of resins

The properties of the resins provide information about their suitability for specific applications and may also help to predict some characteristics as aliphatic/aromatic character, unsaturation degree, etc.

Commercial data sheets generally provide the following properties for the resins: softening point; colour; degree of unsaturation; acid number; saponification number; density; ash content; odour.

However, other properties are very important in adhesive performance, such as the solubility, the compatibility, the chemical and thermal stability, the viscosity, and the molecular weight and molecular weight distribution.

4.2.3.1. Softening point. The resins are non-crystalline amorphous materials which soften gradually over a range of temperatures. Therefore, the softening point is controlled by the average molecular weight of the resin. The softening point is also related to the intrinsic viscosity, hardness and brittleness of resins.

The softening point is defined as the temperature at which the resin flows under a given load on heating. Several standard methods have been proposed to determine the softening point of resins.

(1) *Ring and Ball method (R&B)* — *ASTM D 3461-76, DIN ISO 4625*. This method is the most frequently used to determine the softening point of resins. Fig. 20 shows the experimental device used for determination of R&B softening point. The resin is melted into a metal ring and left to cool. The ring is placed in a special metallic device which is placed into a water or glycerol bath. A steel ball of a given diameter and mass is placed on the ring and the bath is heated at a given rate. The temperature at which the ball forces the softening resin downward is noted as the softening point.

(2) *Krämer–Sarnow method (KS)* — *DIN 53 180*. This is the oldest method used to determine the softening point of resins, and is relatively similar to the Ring and Ball method. Instead of a ring, a small glass tube open at both ends is used and the load is a small mercury drop. The softening point is obtained as the temperature at which the mercury drop breaks through the softening resin and falls.

(3) *Mettler softening point method* — *ASTM D 3461-76*. This is the most recent method. This automatic method measures the temperature at which the resin flows out of a sample cup under its own weight. The temperature is recorded when the first drop crosses the light path of a photocell (Fig. 21). This method is quite accurate and reproducible.

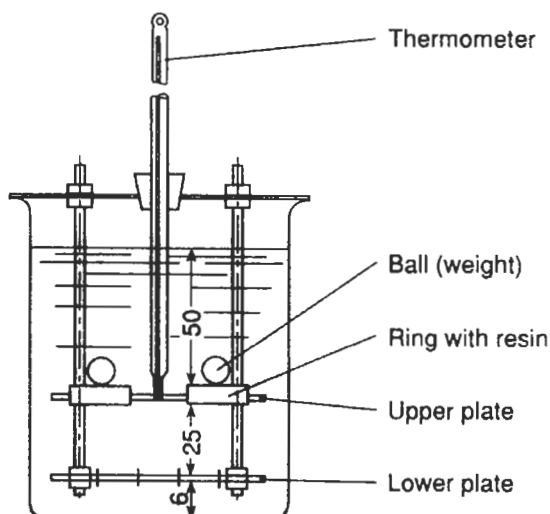


Fig. 20. Determination of Ring and Ball softening point (numbers in mm) (see p. 47 in [25]).

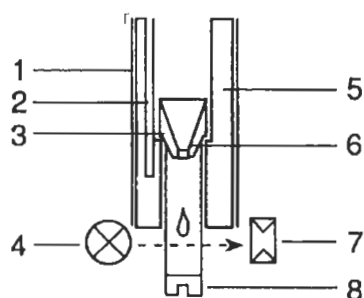


Fig. 21. Determination of the Mettler softening point. 1, heating element; 2, platinum resistance thermometer; 3, sample; 4, light source; 5, furnace; 6, sample cup; 7, photo cell; 8, collector sleeve (see p. 48 in [25]).

(4) *Plate-plate stress rheometer test.* The resin is placed between the two steel plates of a stress-controlled rheometer, maintaining a gap larger than 0.5 cm. The upper plate oscillates at a given frequency whereas the lower plate is heated. The variation of the storage and loss moduli as a function of the temperature is monitored. Softening temperature can be estimated from the temperature at cross-over between the two moduli [26].

Although not widely used, there are other methods to determine the softening point, such as the capillary method, the flow point, the drop point, and the Kofler method. The different methods provide different values of the softening point. In general, the Ring and Ball method provides the highest softening point while the

Mettler softening point provides the lowest for a given resin. Therefore, both the softening point value and the method used for its determination should be given. In general, manufacturers supply the resins with a tolerance of about 3°C in the Ring and Ball (R&B) softening point.

Rubber-grade resins are mostly in the softening point range 70–100°C R&B. A deviation of 5–10°C in softening point may cause problems. The softening point of a resin affects the properties of adhesives. Hence, for pressure-sensitive rubber adhesives the decrease in the softening point of the resin produces a more tacky adhesive with less cohesive strength.

4.2.3.2. Colour. The colour of resins ranges from water-white to dark brown. Colour may be an important factor in resin choice depending on end use. Pale colours are necessary in some types of adhesives, whereas darker colours may be tolerated in rubber formulations, especially where carbon black filler is incorporated. Medium-coloured resins can be used in most adhesive formulations.

The colour can be determined by various methods such as the Gardner, Barrett, iodine colour number or US Colophonium standard methods. Usually, the Gardner or the Barrett standards are used. A comparison between the different methods to determine the colour of resins is given in Table 9. In both methods, the colour is evaluated in resin solutions. A 50 wt% resin solution in toluene is used as the Gardner standard, and a solution of 2 g resin in 25 ml toluene is used in the Barrett

Table 9

Comparison of colour standard for resins (p. 49 in [25])

Barrett	Gardner	Iodine number	US Colophonium standard
0.5	6	10	X
	7	12	WW
	8	15	WG
	8.5		N
1	9	20	M
	10	25	K
	11	40	I
	12	70	H
	12.5		G
1.5	13	105	
	14	145	F
	15	190	
	16	245	E
2	17	300	
2.5	18	445	D
3		2000	

standard. These solution are made in calibrated tubes, and are compared with a set of standard colour disks.

On the other hand, not only initial colour but colour change (discolouration) of the resin under UV light and heat is important. Colour retention of a resin is related to the chemical stability and increases as the degree of non-aromatic conjugated unsaturation of the resin molecule decreases. Thus, for rosins a high level of abietic-type resin acids lead to relatively unstable resins. Hydrogenation and disproportionation as well as esterification provide improved stability and colour retention to rosins.

4.2.3.3. Odour. This aspect is important in resins derived from natural sources. Rosins based on wood and gum rosin retain trace quantities of terpenes and have a 'piney' odour. Tall oil rosins retain the typical sour odour of the rosin. Odour can be removed by steam sparging under vacuum before or during esterification of rosins. Addition of odour masks can also be done.

4.2.3.4. Degree of unsaturation. Unsaturation accounts for the existence of carbon-carbon double bonds in resins. It is generally indicated by the bromine or iodine number. Both methods are based on the halogen addition to the double carbon-carbon bonds. Because the different reactivity of bromine and iodine, both numbers cannot be compared. The bromine or iodine number does not necessarily correlate with the reactivity of the resin, for instance in the ageing process. However, within a given resin series of the same structure, relative comparisons can be made.

- **Bromine number ASTM D 1159-84.** The bromine number is defined as the amount of bromine in grams accepted by 100 grams of resin. Typical values are:
 - non-reactive resins: 10–45 g Br₂/100 g resin;
 - reactive resins: 55–75 g Br₂/100 g resin;
 - highly reactive resins: 65–100 g Br₂/100 g resin.
- **Iodine number ASTM 1959-69.** The iodine number is defined as the amount of iodine in grams accepted by 100 g of resin.

4.2.3.5. Acid number (ASTM D 974-80, DIN 51 558). The acid number is defined as the amount of potassium hydroxide in milligrams required to neutralize 1 g of resin under fixed conditions.

The acid number is mainly defined for rosins and rosin-derived resins and for phenol-modified resins. Standard hydrocarbon resins have zero acid number because the absence of functional groups. However, the acid number allows one to control deterioration by oxidation with formation of carbonyl and carboxyl groups in hydrocarbon resins. Typical acid number values of different resin types are:

- hydrocarbon resins: 0.1 mg KOH/g resin;

- phenol-modified resins: 0.3–0.5 mg KOH/g resin;
- rosins: 150–175 mg KOH/g resin;
- rosin esters: 50–15 mg KOH/g resin.

For rosins and rosin esters, the products having high acid numbers are the most susceptible to oxidation and have inferior viscosity stability and colour stability in adhesive formulations. Thus, when stability properties are essential in adhesives, rosin esters rather than high acid number rosins are used. However, the high acid number resins are polar and display better adhesion to polar elastomers and polymeric surfaces.

4.2.3.6. Saponification number (DIN 51 559). The saponification number is indicative of the presence of ester groups in a resin. The saponification number is defined as the consumption of potassium hydroxide in milligrams by one gram of resin under standardized conditions.

Saponification number is important for rosin derivatives.

4.2.3.7. Density. Density is the mass of unit volume at a given temperature. For solid resins, density is evaluated according to DIN 51 757 at 20°C, whereas for liquid resins DIN 1995 U2 at 20°C is more appropriate. Densities of resins usually are in the range 0.88 to 1.15 g/cm³.

4.2.3.8. Ash content (DIN 52 005). Unwanted presence of inorganic impurities due to incorrect filtration of neutralization residues and rust contaminants is undesirable because may contribute to premature ageing. Ash determination provides some interesting information. In general, most resins have ash content lower than 0.1%.

4.2.3.9. Glass transition temperature (T_g). Resins are amorphous polymers exhibiting a glass transition due to the reduction of molecular mobility by the collapse of free volume with falling temperature. DSC is an appropriate technique to obtain T_g values of resins. In general, resins exhibit a relaxation process near the glass transition which makes it difficult to quantify the T_g value [27]. It is recommended to remove the thermal history of the resin during a first heating run in the DSC equipment. Followed by a sudden cooling down of the melted resin to low temperatures, a second run is carried out, from which the T_g value can be easily obtained.

T_g values of resins (30–90°C) are higher than those of rubbers (–70 to –30°C), so the addition of resin can be used to raise the average T_g of the rubber base formulations.

4.2.3.10. Solubility. Generally, resins are soluble in most common organic solvents, especially aromatics, esters, and chlorinated solvents. They are insoluble in

water. Solubility depends on resin type, its average molecular weight and distribution. In general, higher softening point resins are less soluble than lower softening point types.

Solubility of resins can be predicted in a similar way as for the solubility of polychloroprene rubbers in a solvent mixture (see Section 5.5) by means of solubility diagrams (plots of the hydrogen bonding index (γ) against the solubility parameter (δ)). Another more simple way to determine the solubility of resins is the determination of the cloud point, the aniline and the mixed aniline points.

(1) *Cloud point*. Measures the solubility/compatibility of a resin with solvents. The value reported is the temperature at which a specific mixture of a resin and a solvent or solvents blend gives a cloudy appearance, having been cooled from a temperature at which the mixture was clear. Commonly, a test tube of a given diameter is used and the temperature is noted when the lower end of the thermometer, placed at the bottom of the tube, disappears. Resins with cloud points below 0°C are commonly regarded as soluble and cloud points greater than 70°C indicate poor solubility/compatibility. White spirit with various aromatic contents is a widely used solvent in the determination of cloud point, but other solvents or solvents mixtures are also used.

(2) *Aniline and mixed aniline point (DIN 51 775 modified)*. It is similar to the cloud point test except that the solvent is aniline, a very polar liquid. The aniline point is defined as the temperature at which a mixture of equal parts of aniline and the resin show the beginning of phase separation (i.e. the onset of clouding). Phase separation for aromatic resins occurs between 15°C and below zero; for resins with intermediate aromaticity, it lies between 30 and 50°C; and for non-aromatic resins, it is 50 to 100°C. Sometimes the mixed aniline point is used. It is similar to the aniline point except that the solvent is a mixture of one part of aniline and one part of *n*-heptane. The problem of both procedures is that precipitation of resins can be produced before the cloud is generated.

One important factor influencing the solubility of rosin derivatives is its tendency to crystallize. Initially, a rosin product may appear to be soluble in a given solvent, but on standing, the rosin will crystallize out of soluble solution. This tendency of rosin to crystallize can be overcome by derivatization, mainly esterification.

4.2.3.11. Compatibility. Clear definition of compatibility is rather difficult. Compatibility has been defined as the ability of two or more materials to exist in close and permanent association for an indefinite period without phase separation and without adverse effect of one on the other [28]. On the other hand, compatibility is easily recognized in solvent-borne adhesives as a homogeneous blend of materials without phase separation. Normally, compatibility is understood as a clear transparent mixture of a resin with a given polymer. But, compatibility is a more complex thermodynamic phenomenon which can be evaluated from specific

physical properties, such as the glass transition temperature. For instance T_g measurements allow the determination of the compatibility of blends in rubber–resin blends [29]. A compatible blend will exhibit only one T_g with an intermediate value between the T_g values of the rubber and the resin, whereas an incompatible blend will exhibit two T_g values.

In general, resins are compatible with a large number of materials (oils, plasticizers, polyethylene waxes, rubbers). Compatibility depends on resin type, molecular weight and its distribution, resin structure and configuration, and finally on application requirements.

The most common method to measure the compatibility of resins with other substances is to dissolve both materials in a mutually compatible solvent, and to cast a film on a glass slide. After solvent evaporation, a compatible system gives a clear film, while incompatibility results in an opaque film. A more accurate procedure is to melt the resin and the substance under a phase microscope, and compatibility is observed on the film after cooling.

A more quantitative estimation of compatibility can be obtained with the solvent cloud point test. The solvent cloud point is based on the idea that resins will be compatible with elastomers of similar chemical nature. Thus aliphatic resins will be effective tackifiers for aliphatic elastomers, such as natural rubber, while aromatic solvents are needed for aromatic elastomers, such as SBR. Solvent cloud point tests are carried out in three solvent systems which represent aliphatic, aromatic, or polar systems [16]:

- aliphatic system: odourless mineral spirit (OMS);
- aromatic system: methylcyclohexanone/aniline (MMA);
- polar system: diacetone alcohol/xylene (DACP).

Rosin esters show low cloud points and would have wide compatibility with most elastomers. Aliphatic hydrocarbon resins, however, will only be compatible with aliphatic elastomers (e.g. natural rubber).

In general, fully compatible resin are desirable. However, there are many applications where borderline compatibility is tolerated, and even in some cases, borderline compatibility or controlled incompatibility may enhance tack in adhesive systems. On the other hand, a resin with a borderline compatibility in combination with an oil or plasticizer in an adhesive formulation, will result in phase separation and therefore the migration of the oil or plasticizer to the adhesive surface is favoured.

4.2.3.12. Viscosity. Solvent viscosity of resins is influenced by the concentration of resin, the softening point, the molecular weight distribution, the chemical composition of the resin, and the type of solvent. The higher the resin concentration, the higher the viscosity. For a given concentration, solution viscosity depends on the softening point of the resin (Fig. 22).

The softening point is related to the average molecular weight of a given

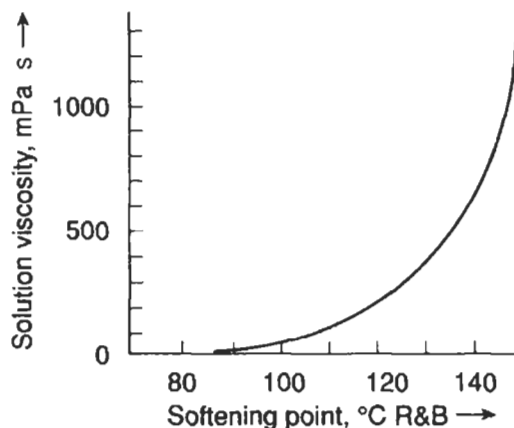


Fig. 22. Solution viscosity of an aromatic C₉ resin as a function of softening point. 50 wt% resin in white spirit with 5 wt% aromatics (see p. 63 in [25]).

resin, but resins with similar softening point may have different molecular weight distributions and hence different viscosity in solution. The molecular weight distribution has a tremendous influence on resin solution viscosity. The narrower the molecular weight distribution, the higher the viscosity of the resin solution.

4.2.4. Tackifier function of the resins

To produce a suitable rubber base adhesive, three key aspects are required: (1) tack and wetting properties; (2) adhesive strength; (3) cohesive strength.

Adhesive strength refers to the bond produced by contact of an adhesive to a surface. It used to be measured by peeling tests. This ultimate strength depends on temperature, applied pressure and time of contact.

Cohesive strength is the internal strength of an adhesive or the ability of the adhesive to resist splitting. Unlike tack and adhesion strength, cohesive strength is not influenced by the substrate.

Tack is difficult to define. In adhesives technology, tack can be defined as the property of a material which enables it to form a bond of measurable strength immediately upon contact with another surface, usually with little or no applied pressure. Therefore, tack is associated with instantaneous adhesion and differs from final strength which requires longer time to develop. Tack is a function of the rheological properties of the adhesive and of the surface energies of the adhesive and the bonded substrate surface. Tack is sensitive to variations in temperature, pressure, rate of application and removal pressure, and contact time. Measurement of tack is difficult and several procedures have been suggested [16]. However, none of them are completely satisfactory, although it seems that the probe tack is the most widely accepted.

- Finger test. This is the most simple test. A small amount of adhesive is placed on a finger and pressed against the thumb. The difficulty to separate the finger and thumb provides a rough estimation of tack.

- Rolling ball. A small steel ball with specific weight and diameter is rolled down an inclined plane onto a thin film of adhesive placed at the bottom. The distance the ball rolls on the adhesive film before stopping is a measure of the tack (the longer the distance, the lower the tack).

- Probe tack. A probe (flat or not) is contacted with an adhesive film at a given pressure and dwell time. The force required to remove the probe from the adhesive is a measure of tack [30].

In contact adhesives, the so-called *tack open time* is important. This can be defined as the time available after the adhesive is applied during which the surface remains tacky enough for the application of the adherend. It can be easily measured by applying a thin layer of fresh adhesive on Kraft paper and making a bond at different times until no bond is obtained.

Tackifying resins enhance the adhesion of non-polar elastomers by improving wettability, increasing polarity and altering the viscoelastic properties. Dahlquist [31] established the first evidence of the modification of the viscoelastic properties of an elastomer by adding resins, and demonstrated that the performance of pressure-sensitive adhesives was related to the creep compliance. Later, Aubrey and Sherriff [32] demonstrated that a relationship between peel strength and viscoelasticity in natural rubber–low molecular resins blends existed. Class and Chu [33] used the dynamic mechanical measurements to demonstrate that compatible resins with an elastomer produced a decrease in the elastic modulus at room temperature and an increase in the $\tan \delta$ peak (which indicated the glass transition temperature of the resin–elastomer blend). Resins which are incompatible with an elastomer caused an increase in the elastic modulus at room temperature and showed two distinct maxima in the $\tan \delta$ curve.

The modification of an elastomer by a low molecular weight resin is determined by the compatibility (or solubility) of the resin in the elastomer. Compatibility is necessary to generate tack, but it does not assure that desired adhesive properties will be obtained. The adhesive performance of a resin–elastomer blend is mainly determined by the elastic modulus at the application temperature and the glass transition temperature of the blend. The glass transitions of the resins are higher than those of the elastomers, so the glass transition temperature of a resin–elastomer blend will increase by increasing the resin content [34] (Fig. 23). The addition of resin decreases the elastic modulus of an elastomer, so the elastic modulus of a resin–elastomer blend will decrease by increasing the resin content. Fig. 24 shows the increase in $\tan \delta (= E''/E')$ (obtained from DMTA experiments), e.g. a decrease in the elastic modulus, E' , by increasing the aromatic hydrocarbon resin content in a polychloroprene–hydrocarbon resin blend [34].

All resin–elastomer blends show a similar variation in tack as a function

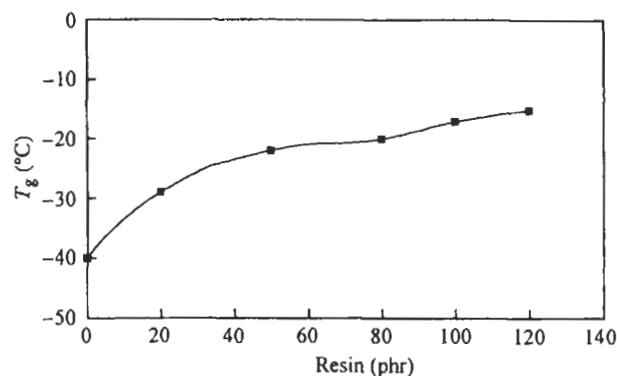


Fig. 23. Evolution of the glass transition temperature of polychloroprene-aromatic hydrocarbon resin blends as a function of the resin content. T_g values were obtained from DSC experiments.

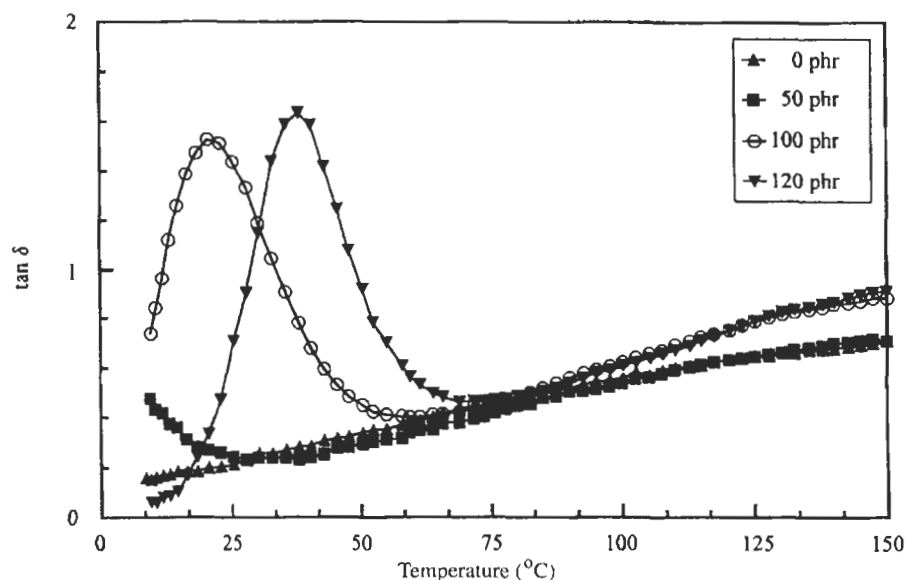


Fig. 24. Variation in $\tan \delta$ as a function of the temperature of polychloroprene-aromatic hydrocarbon resin blends containing different resin content. Frequency = 1 Hz. Target strain = 0.005. DMA experiments.

of the resin content (Fig. 25) [34]. Little enhancement of tack is produced for resin contents lower than 50 phr (33 wt% resin). Between 50 and 80 phr resin contents (33 to 45 wt%) a sudden increase in tack is produced, and a rapid drop off in tack for resin contents above 80 phr is produced. Above 45 wt%, the aromatic hydrocarbon resin-polychloroprene system becomes overloaded in resin, incompatibility develops, and tack drops. Although the resin loadings may change

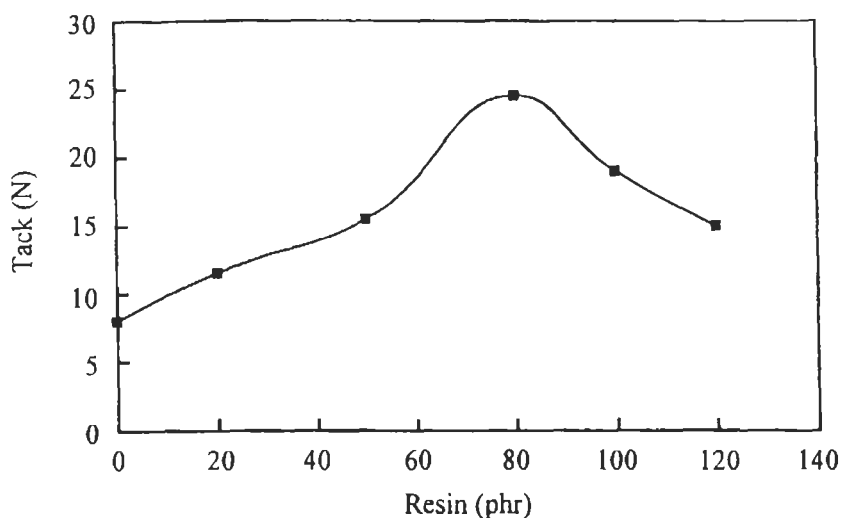


Fig. 25. Evolution of the tack of polychloroprene–aromatic hydrocarbon resin blends as a function of the resin content. Tack was obtained as the immediate T-peel strength of joints produced with 0.6 mm thick styrene–butadiene rubber strips placed in contact without application of pressure. Peeling rate = 10 cm/min.

depending on the elastomer and resin characteristics, the above trend is found in most resin–elastomer systems. The maximum tack in the resin–polychloroprene blend will be determined by the general compatibility of the resin with the polychloroprene. Typically, the lower softening point of chemically similar resins will develop maximum tack at higher resin loadings than the higher softening point resins.

Adhesion of the resin–elastomer blends is generally enhanced for low resin loadings, decreasing by increasing the resin content [34]. Fig. 26 shows the variation in T-peel strength of joints produced with polychloroprene–aromatic hydrocarbon resin blends, the same system for which tack is given in Fig. 25. The maximum in adhesion corresponds to resin loading of 50 phr (33 wt%), decreasing suddenly for higher aromatic resin loading. A comparison of Figs. 25 and 26 evidences that the start of tack development in polychloroprene–hydrocarbon resin blends corresponds to the decrease in peel strength.

The chemical nature of the tackifier also affects the compatibility of resin–elastomer blends. For polychloroprene (a polar elastomer) higher tack is obtained with a polar resin (PF blend in Fig. 27) than with a non-polar resin (PA blend in Fig. 27). Further, the adhesion of resin–elastomer blends also decreases by increasing the aromatic content of the resin [29]. Fig. 28 shows a decrease in T-peel strength of styrene–butadiene rubber/polychloroprene–hydrocarbon resin blends by increasing the MMAP cloud point. Because the higher the MMAP

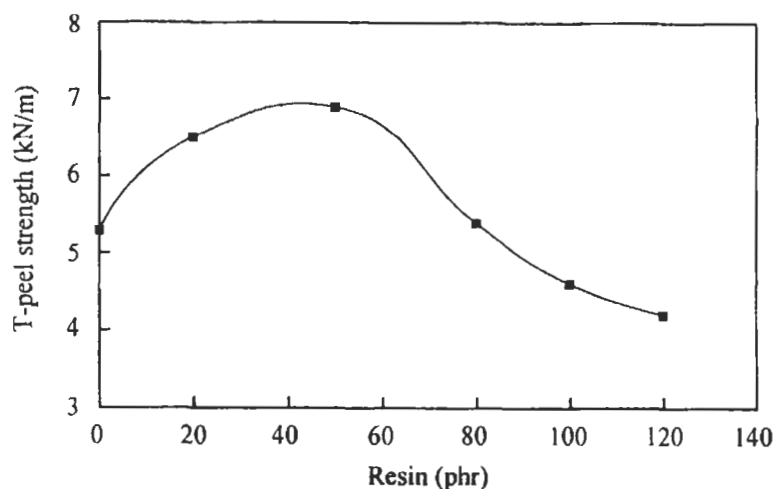


Fig. 26. Evolution of the T-peel strength of roughened styrene-butadiene rubber/polychloroprene-aromatic hydrocarbon resin blends as a function of the resin content. Peeling rate = 10 cm/min.

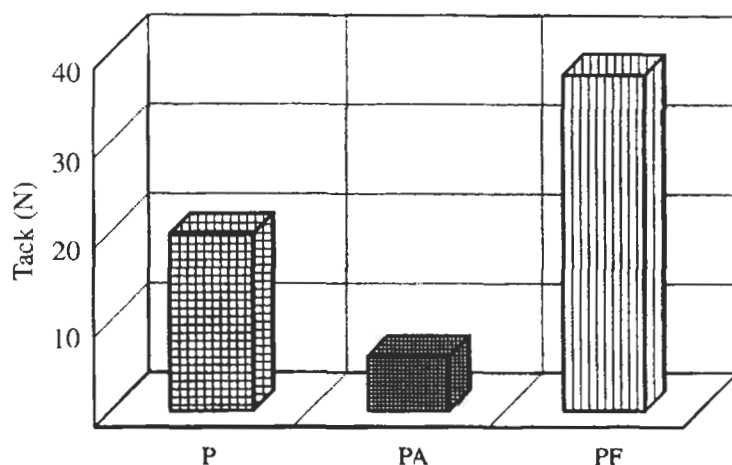


Fig. 27. Tack of polychloroprene-hydrocarbon resin blends (33 wt% resin content) as a function of the nature of the hydrocarbon resin. Tack was obtained as the immediate T-peel strength of joints produced with 0.6 mm thick styrene-butadiene rubber strips placed in contact without application of pressure. Peeling rate = 10 cm/min.

cloud point value, the lower the aromatic nature of the resin, the aliphatic aromatic resin-polychloroprene blends exhibit poor adhesion.

Addition of low molecular weight resins with narrow molecular weight distribution produces compatible resin-elastomer blends, while incompatible blends are obtained with resins having a wide molecular weight distribution. In a recent study

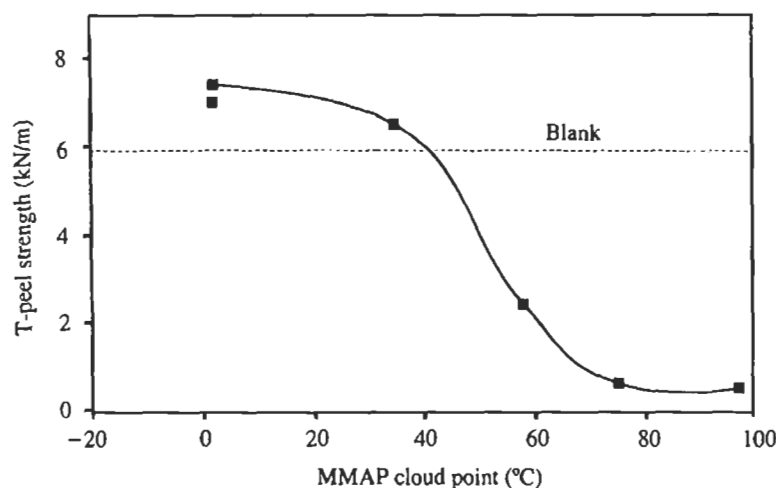


Fig. 28. Evolution of the T-peel strength of roughened styrene–butadiene rubber/polychloroprene–aromatic hydrocarbon resin blends as a function of the MMAP cloud point. Peeling rate = 10 cm/min.

[27] different aromatic hydrocarbon resins with different molecular weights and molecular weight distributions were added to a polychloroprene elastomer. Blends contained 17 wt% aromatic hydrocarbon resins. The polydispersity of one of the resins (*Piccolastic DI25* from Hercules) was extremely high ($M_w/M_n = 32.5$). For the blend produced with this resin a noticeable decrease in tack was found (PD blend in Fig. 29) because incompatibility with the polychloroprene was produced. Incompatibility was evidenced using DSC (Fig. 30) which shows that the increase in the glass transition temperature in the *Piccolastic DI25*–polychloroprene blend was much lower than for the blend produced with an aromatic hydrocarbon resin (*Kristalex 5140* from Hercules) with similar M_n value but smaller polydispersity ($M_w/M_n = 3.3$). Furthermore, the adhesion properties of the joint produced with the *Piccolastic DI25*–polychloroprene blend was much lower than for the joints produced with blends containing resins with narrower molecular weight distribution (Fig. 31). On the other hand, whereas tack of aromatic hydrocarbon resin–polychloroprene blends was not affected by the increasing molecular weight of the aromatic hydrocarbon resin (Fig. 29), an increase in T-peel strength was obtained (Fig. 31).

4.3. Plasticizers

Plasticizers are substances (usually low molecular weight diluents) that are incorporated into polymeric materials to improve their workability and increase flexibility. Polymeric plasticizers are low glass transition temperature (T_g) poly-

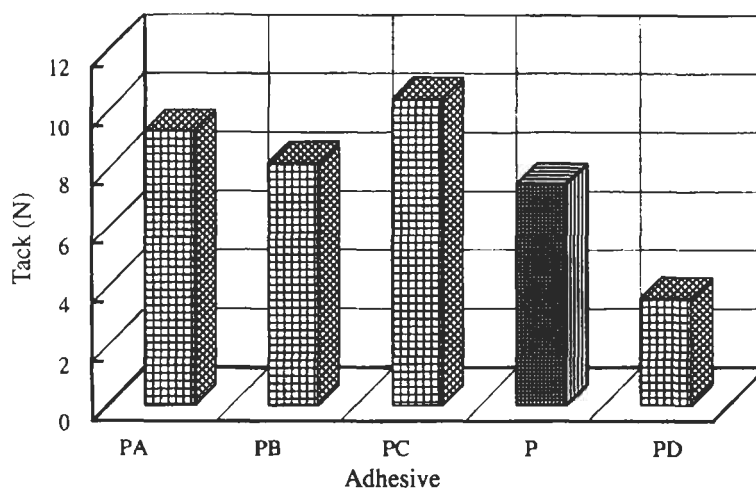


Fig. 29. Tack of polychloroprene-aromatic hydrocarbon resin blends (17 wt% resin content) as a function of the molecular weight of the hydrocarbon resin. Tack was obtained as the immediate T-peel strength of joints produced with 0.6 mm thick styrene-butadiene rubber strips placed in contact without application of pressure. Peeling rate = 10 cm/min.

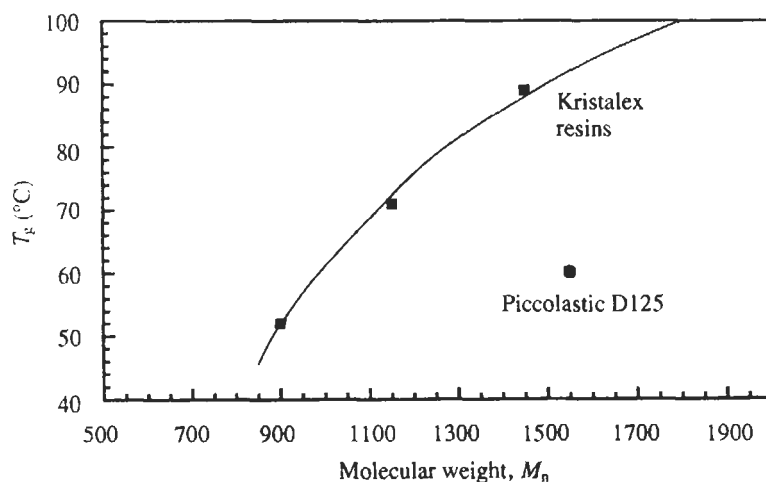


Fig. 30. Evolution of the glass transition temperature of polychloroprene-aromatic hydrocarbon resin blends (17 wt% resin content) as a function of the number average molecular weight of the hydrocarbon resin. T_g values obtained from DSC experiments.

mers that form homogeneous mixtures when blended with a polymer with higher T_g .

Primary and secondary plasticizers can be distinguished. Primary plasticizers are compatible with the polymer, while secondary plasticizers are less compatible

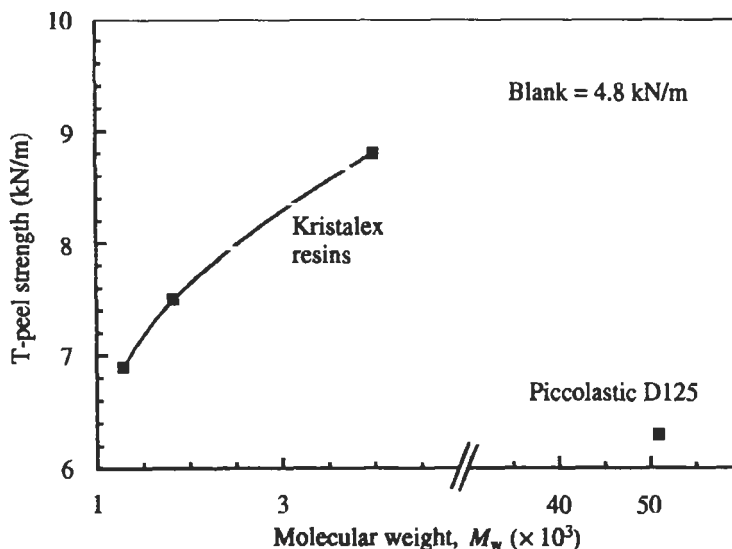


Fig. 31. Evolution of the T-peel strength of roughened styrene-butadiene rubber/polychloroprene-aromatic hydrocarbon resin blends as a function of the weight average molecular weight of the hydrocarbon resin. Peeling rate = 10 cm/min.

and are generally used in mixtures with the primary plasticizers to confer adequate balance of properties. About two-thirds of the plasticizers used today are diesters of phthalic anhydride with C_4 – C_8 alcohols. The C_8 alcohols offer the best balance of properties for general-purpose plasticizers, DOP (dioctyl phthalate) being the most common. Other classes of plasticizers are triaryl phosphates, alkyl esters of dibasic alkyl acids, alkyl trimellitate esters, high molecular weight polyesters, and epoxies.

Plasticizers can be classified according to their chemical nature. The most important classes of plasticizers used in rubber adhesives are phthalates, polymeric plasticizers, and esters. The group *phthalate plasticizers* constitutes the biggest and most widely used plasticizers. The linear alkyl phthalates impart improved low-temperature performance and have reduced volatility. Most of the *polymeric plasticizers* are saturated polyesters obtained by reaction of a diol with a dicarboxylic acid. The most common diols are propanediol, 1,3- and 1,4-butanediol, and 1,6-hexanediol. Adipic, phthalic and sebacic acids are common carboxylic acids used in the manufacture of polymeric plasticizers. Some polyhydroxybutyrates are used in rubber adhesive formulations. Both the molecular weight and the chemical nature determine the performance of the polymeric plasticizers. Increasing the molecular weight reduces the volatility of the plasticizer but reduces the plasticizing efficiency and low-temperature properties. Typical esters used as plasticizers are *n*-butyl acetate and cellulose acetobutyrate.

The mode of action of plasticizers can be explained using the Gel theory [35]. According to this theory, the deformation resistance of amorphous polymers can be ascribed to the cross-links between active centres which are continuously formed and destroyed. The cross-links are constituted by micro-aggregates or crystallites of small size. When a plasticizer is added, its molecules also participate in the breaking down and re-forming of these cross-links. As a consequence, a proportion of the active centres of the polymer are 'solvated' and do not become available for polymer-to-polymer links, the polymer structure being correspondingly loosened.

The chemical structures of the plasticizers are related to the properties they impart to polymers.

- *Molecular weight*. The increase in the molecular weight of the plasticizer decreases its volatility, migration and softening efficiency.

- *Polarity*. The increase in the polarity of the plasticizer (e.g. existence of polar groups, substitution of aryl groups by alkyl ones) reduces softening efficiency, worsens low-temperature properties of the plasticized polymers, improves solvation, and reduces extractability by aliphatic solvents.

- *Alkyl chain*. The increase in the alkyl chain length and linearity improves the efficiency of the plasticizer and the low-temperature flexibility of the plasticized polymers.

- *Separation of ester groups*. Increasing the distance between ester groups increases solvation and softening efficiency.

- *A_p/P_o ratio*. The A_p/P_o ratio is calculated by dividing the numbers of carbon atoms in aliphatic chains in a plasticizer molecule by the number of ester groups present. The A_p/P_o ratio correlates well with several properties of the plasticizers such as melting point, density, modulus and water absorption.

Addition of a plasticizer decreases the T_g of the polymer and, in partially crystalline polymers, also influences both crystallization and melting. The amount of plasticizer affects its effectiveness. Thus, while the T_g of the polymer is strongly depressed by small plasticizer additions, the increase in the plasticizer content leads to lower decrease in T_g and in several systems two T_g values can be found [36]. Therefore, the increase in the plasticizer content in polymers does not show a monotonic decrease in T_g .

Plasticizers reduce hardness, enhance tack and reduce cost in rubber base adhesive formulations. A plasticizer must be easily miscible and highly compatible with other ingredients in the formulations and with the surfaces to which the adhesive is applied. The compatibility and miscibility of plasticizers can be estimated from the solubility parameter values. Most of plasticizers have solubility parameters ranging between 8.5 and 10.5 hildebrands. However, the high miscibility and compatibility also lead to easier diffusion of the plasticizer to the surface, decreasing the adhesion properties. Therefore, plasticizers should be carefully selected and generally combinations of two or more of them are used.

It is desirable that the plasticizer compounded with a polymer be permanently retained. Loss of plasticizer changes the properties of a given formulation, and can be produced by volatilization, extraction or migration. The volatility of a plasticizer in a formulation can be related to the surface area, thickness of the polymeric material, and viscosity (e.g. molecular weight) of the plasticizer itself.

4.4. Fillers and pigments

Fillers may be broadly defined as solid particulates or fibrous materials, substantially inert chemically, incorporated in polymer compositions to modify the properties and/or to reduce cost. Cost reduction is not the primary reason to incorporate fillers in adhesives but they are used to impart specific properties such as flow, improved adhesion, mechanical, thermal, electrical and optical properties, chemical and weather resistance, and rheological behaviour.

Fillers may also act as inorganic pigments, because they impart colour to the rubber formulations. Carbon blacks, titanium dioxide and iron oxides are typical examples of pigments used in rubber base adhesives. The pigments are fine-particle materials, intimately dispersible (but not soluble) in the polymer formulations, which even at low concentrations impart colour. Generally, pigments are stable, they have high colour value and are relatively inexpensive. The stability of colour to environmental influences as heat, photochemical action, and weathering, is a key aspect in the use and selection of pigments. On the other hand, the pigments must be resistant to migration and should not have adverse interactions with plasticizers or other components in the formulation.

There are a few excellent books dealing with the characteristics and properties of fillers. Two of the most interesting are *Handbook of Fillers and Reinforcements for Plastics* [37] and *Handbook of Fillers* [38].

In adhesives, the balance between tensile properties and adhesion is important. Fillers frequently increase hardness and reinforce adhesives, so the choice of the filler and its concentration are often critical. In addition, adhesion may also be affected by the filler's presence either due to absorption of coupling agents, change in the rheological properties (reducing mechanical adhesion), or changing moisture permeability which affects hydrolytic changes at the interphase. In some formulations, addition of fillers also assists in the reduction of shrinkage during curing.

In rubber base adhesives, fillers may affect properties such as cohesion, cold flow, rheology and peel adhesion. Most fillers increase cohesion and reduce cold flow. In some formulations, even a small addition of filler dramatically reduces peel strength either because of interactions with the tackifier or because filler particles at the surface reduce the area of contact between the adhesive and the substrate.

Pigments and fillers are added to rubber base adhesives for various purposes:

(1) To reduce cost. Clay and talc are the most common fillers in rubber adhesives.

(2) To opacify the adhesives. Opacity is required for aesthetic reasons or as an indication of how uniformly the adhesive is applied. Titanium dioxide is used to make the adhesive opaque.

(3) For viscosity or sag control. When the rubber base adhesive is applied on a vertical surface, addition of a filler prevents the adhesive from running down the wall. In solvent-borne formulations, fumed silica can be used as anti-sag filler. In water-borne systems, clays impart yield stress and excellent sag control.

(4) Resistance to weathering. Zinc oxide and magnesium oxide stabilize polychloroprene against dehydrochlorination. Further, zinc oxide helps vulcanize the rubber, and magnesium oxide reacts with *t*-butyl phenolic resin to produce a resinate which improves heat resistance of solvent-borne polychloroprene adhesives.

In general, carbon black, clay, calcium carbonate and talc are the most common fillers added to rubbers. Some rubbers are less demanding of fillers (e.g. nitrile rubber, butyl rubber, polybutadienes) than others.

Several properties of fillers are important in their use as additives in polymer formulations. An extensive list of these properties includes the absorption coefficient, the acidity or alkalinity of water extract, ash content and volatile matter, brightness, colour and tinting strength, specific surface area, density and tamped volume, electrical properties, extractables and soluble matter, heating loss and heat stability, hiding power, iodine absorption number, loss on ignition, mechanical properties, oil absorption, particle size and particle size distribution, pH, and resistance to light [38]. Among them, the key properties of fillers used in rubber adhesive formulations are the following.

(1) *Density*. Most fillers added in rubber base formulation have a density between 2 and 2.7 g/cm³, except barium sulphate (4–4.9 g/cm³) and zinc oxide (5.6 g/cm³). Addition of filler increases the free volume of the polymer and, in general, there is a critical concentration of filler at which the density of the formulation increases. The method of incorporation of filler in the adhesive formulation is important because air voids may appear when a poor dispersion is produced.

(2) *Particle shape and roughness*. The shape of filler particles is determined by their crystal structure and cleavage. The surface area of the crystal increases by milling, but it retains the original feature. The interactions between the filler surface and the polymer depend on the crystal structure (which dictates the chemical organization) and on the functional groups (which may react with the polymer). In synthetic fillers, the surface organization also depends on the internal structure of the particles. On the other hand, the surface roughness is determined by the shape of filler particles and it is important in the development of adhesion

forces between the filler and the polymer. Platelets particles (i.e. clay) usually interact better with polymers than spherical particles do.

(3) *Particle size*. In general, fillers used in rubber adhesive formulations should have particle sizes lower than 5 μm to avoid settlement from solutions. Fumed and precipitated silicas, and ultra-fine titanium dioxide particles are produced in primary particle sizes lower than 10 nm. Most of the mineral fillers of the smallest particle sizes have a size above 100 nm. All pigments also belong to the same group (0.1–0.5 μm). The synthetic fillers with a particle size of a few nanometres usually tend to aggregate and to agglomerate in their powder forms. Thus, for the dispersion of fillers, agglomerate and aggregate size is usually as relevant as the primary particle size. The lower the primary particle size of the filler, the higher the tendency to agglomerate. The small particle size filler is difficult to disperse (although it gives more transparency and better reinforcement). Fillers with particle size about 0.1 μm show an adequate balance between performance and dispersion in adhesive formulations [39].

(4) *Particle size distribution*. Although almost all fillers are fractionated to remove the coarser particles, a distribution of particles is generally found. The particle size distribution may affect the viscosity, rheological properties and the amount of filler to be incorporated in a formulation. In general, narrow particle size distributions are recommended in fillers to obtain the best performance in rheological, mechanical and optical properties. Further, the tint strength and opacity of pigments is also affected by the particle size distribution. In this case a narrower distribution is preferred to avoid the undertone of pigments.

(5) *Specific surface area*. Surface area is one of the most important properties of fillers. The specific surface area comprises the total surface of particles including its pores and at least part of the free volume of the aggregates. Larger, nonporous particles such as talc have the lowest specific surface areas. Fillers with small particle size and not very porous such as calcium carbonate and clay, occupy the middle range of specific surface area. Very small particles (precipitated silicas), formation of aggregates (fumed silica, furnace carbon blacks) and minerals with high porosity (sepiolite, attapulgite) give fillers having the highest surface areas. Specific surface area is related to the particle size in nonporous or poorly porous fillers. Further, the specific surface area depends on the filler treatment. Fillers with moderate surface areas are recommended in adhesive formulations [40].

(6) *Degree of agglomeration*. Some fillers such as clay, carbon blacks and fumed silicas have a natural tendency to agglomerate. Van der Waals forces are primarily responsible for agglomeration of fillers during production and storage. However, agglomeration of filler particles is complex as it can be also influenced by the particle size, chemical groups on the filler surface, moisture level, and the method of filler production. For instance, water adsorption is mainly responsible for the agglomeration of titanium dioxide, while interactions between silanol groups on the filler surface are responsible for the agglomeration of fumed silicas.

The degree of agglomeration of fillers affects the dispersion and the rheological properties of adhesives [41], and disagglomeration of fillers during adhesives manufacturing should be produced to obtain acceptable properties.

(7) *pH*. The majority of fillers have a neutral pH, but many fillers have a broad range of pH either due to their origin, manufacturing technology, or surface treatment. The pH of a filler may affect the interaction with other components in a polymer formulation. Some typical pH values of some fillers are the following: (a) $\text{pH} < 3$ — antimony trioxide, carbon blacks; (b) pH between 3 and 7 — kaolin, fumed silica, titanium dioxide, precipitated silica; (c) $\text{pH} > 7$ — aluminium trihydrate, calcium carbonate, talc.

(8) *Aspect ratio*. Aspect ratio is the length of the particle divided by its diameter. A high aspect ratio (typically provided by fibres) provides reinforcement of polymers. The majority of fillers have a low aspect ratio (below 10).

(9) *Surface energy*. The surface energy of a filler determines its wettability and adhesion properties. The dispersive non-polar component of the surface energy of a filler can be associated with polymer–filler interactions, while the polar component of the surface energy is associated with the filler networking and agglomeration. Calcium carbonates, zinc oxide and most carbon blacks have dispersive components of about 50 mJ/m^2 [42,43], while titanium dioxide and fumed silica have 80 mJ/m^2 [42]. Talc has the highest dispersive component of the surface energy (130 mJ/m^2 [42]).

(10) *Moisture*. The presence of water in a filler is not usually beneficial. Most fillers added to adhesives have a moisture content lower than 1 wt%. Only precipitated silicas and sepiolite contain about 5–10 wt% moisture. For some applications, fillers must be completely dried to exhibit adequate performance. Moisture absorbed on the surface of fillers impacts the rate and extent of curing of rubber base adhesives.

(11) *Oil absorption*. Oil absorption is a parameter used to characterize the effect of filler on the rheological properties of filled polymers. If oil absorption is low, the filler (barium sulphate, calcium carbonate, titanium dioxide) does not greatly affect the rheological properties of polymers. Fillers which have medium oil absorption (talc, bentonite, carbon black) are useful co-thickeners. Fillers having very high oil absorption (precipitated and fumed silicas) are used as thickeners and absorbents. If filler particles are highly porous, high oil absorption is obtained. (Oil absorption can also be related to the degree of reinforcement in polymers. The reinforcement of polymers by fillers increases as the filler content increases, but this increase is limited by the effect a filler has on the rheological properties of filler–polymer mixtures. Therefore, there is a certain filler loading above which the reinforcing effect of the filler is lost.)

(12) *Hydrophilic/hydrophobic properties*. In water-based systems, the filler should be compatible with water because filler dispersion occurs in an aqueous medium before a polymer emulsion is added. In general, most fillers are hydropho-

bic, as they tend to float on water. Grafting and surface coating are two procedures commonly used to impart hydrophilic properties to the fillers. Grafting with silanes and titanates may give also improved compatibility of the filler and water. Surface coating with polyethylene glycol is also effective to increase the hydrophilic surface of fillers. For kaolin, surface coating with fatty acids (stearic acid, oleic acid) and derivatives (magnesium stearate, calcium stearate) also impart hydrophilic properties. However, the hydrophilic surface of fillers is often a disadvantage because the majority of the polymers are hydrophobic. Hydrophobic properties are also important to avoid the agglomeration of particles during storage. Surfactants (tetrabutylammonium chloride, sodium dodecylsulphate) and fatty acid derivatives give improved hydrophobic properties to calcium carbonate [44]. Incorporation of 7,10,13,16-tetrathiadocosane and 9-butyl-3,6-dioxa-azatridecanol is effective to produce hydrophobic precipitated silicas [45].

The most common fillers used in rubber base formulations will be briefly described. On the basis of their chemical structure, these fillers may be classified in five broad groups: silicates, silicas, metal oxides, calcium carbonate, and carbon blacks.

4.4.1. Silicates

Clay and talc are the most common fillers in rubber base adhesive formulations. Both have platy shapes favouring the interactions with elastomers.

Clay ($\text{Al}_2\text{O}_3 \cdot 2\text{SiO}_2 \cdot 2\text{H}_2\text{O}$). Kaolin clay, China clay, bentonite, Fuller's earth, and vermiculite are clay minerals which are used as fillers. Kaolin is the most common clay used as filler in rubber base adhesives. Kaolin is a product of the hydrothermal decomposition under acid conditions of granite and white feldspar. Some typical properties are: density 2.6 g/cm^3 ; pH of water suspension 3.5–11; particle size $0.2\text{--}7 \text{ }\mu\text{m}$; oil absorption $45\text{--}120 \text{ g/100 g}$; specific surface area $8\text{--}65 \text{ m}^2/\text{g}$. The mined clay mineral needs refining to impart good properties as filler and a grinding process is used to reduce the size and delaminates the stacks of the mineral. Further, the calcination of kaolin above 450°C alters the clay structure and improves electrical resistance and brightness.

Talc ($\text{Mg}_3\text{Si}_4\text{O}_{10}(\text{OH})_2$). Talc is the major constituent of soapstone rocks and has a plate-like structure with a relatively important aspect ratio. Some typical properties are: density $2.7\text{--}2.85 \text{ g/cm}^3$; pH of water suspension 8.7–10.6; particle size $1.4\text{--}19 \text{ }\mu\text{m}$; particle thickness $0.2\text{--}6 \text{ }\mu\text{m}$; aspect ratio 5–20; oil absorption $22\text{--}57 \text{ g/100 g}$; specific surface area $2.6\text{--}35 \text{ m}^2/\text{g}$. The composition of talc varies depending on its source and depending on the tremolite content. Talc processing is done using dry and wet processes. The dry process consists in selective mining (mainly by colour and mineralogy) followed by grinding. The finest grades ($3\text{--}10 \text{ }\mu\text{m}$) are obtained by micronization of ground particles in jet mills. The wet process separates contaminations by flotation, so more pure talc materials are

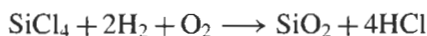
obtained. After flotation, the talc is filtered, dried and milled by impact mills or jet mill micronization. Some grades of wet-processed talcs have silane surface treatment.

The layers in the plate-like structure of talc are joined by very weak van der Waals forces, and therefore delamination at low shear stress is produced. The plate-like structure provides high resistivity, and low gas permeability to talc-filled polymers. Furthermore, talc has several other structure-related unique properties: low abrasiveness, lubricating effect, and hydrophobic character. Hydrophobicity can be increased by surface coating with zinc stearate.

4.4.2. Silicas

Although natural quartz, cristobalite and opal are used as fillers, only synthetic products (fumed and precipitated silicas) find use as fillers in rubber base adhesives.

Fumed silicas (SiO_2). Fumed silicas are common fillers in polychloroprene [40], natural rubber and styrene-butadiene rubber base adhesives. Fumed silicas are widely used as filler in several polymeric systems to which it confers thixotropy, sag resistance, particle suspension, reinforcement, gloss reduction and flow enhancement. Fumed silica is obtained by gas reaction between metallic silicon and dry HCl to form silica tetrachloride (SiCl_4). SiCl_4 is mixed with hydrogen and air in a burner (1800°C) where fumed silica is formed:



The primary particles of fumed silica leaving the burner are in a molten state; therefore, on collision they are able to coalesce, forming bigger particles (aggregates). During cooling down and collection, these aggregates produce agglomerates. These agglomerates can be disintegrated on mixing during the adhesive manufacturing process. Some typical properties of the fumed silicas are: density $2.0\text{--}2.2\text{ g/cm}^3$; pH of water suspension $3.6\text{--}4.5$; primary particle size $5\text{--}40\text{ nm}$; aggregate size $0.2\text{--}15\text{ }\mu\text{m}$; density of silanol groups $1.5\text{--}4.5\text{ groups/nm}^2$; oil absorption $100\text{--}330\text{ g/100 g}$; specific surface area $50\text{--}400\text{ m}^2/\text{g}$. Fumed silicas are characterized by several interesting properties which makes them a quite suitable additive in adhesives.

(1) Fumed silicas have an amorphous nature probably caused by the fast cooling during the manufacturing process. It is an important benefit because it does not cause silicosis.

(2) The surface of fumed silica is highly hydrophilic. Several kinds of silanol groups are produced during manufacturing (about $3\text{--}4.5\text{ OH groups per square nanometre}$) which are essential to impart rheological properties. The mechanism of thickening liquids by fumed silica is explained by hydrogen bond formation between neighbouring aggregates of silica, leading to the formation of a regular

network [46]. On the application of shear some of these bonds are broken which reduces viscosity. The initial stage is regained when material is left to stand. For some applications, hydrophobic properties of fumed silicas are important. By treatment with appropriate silanes, the concentration of silanol groups can be reduced to about 1.5 OH groups per square nanometre.

(3) The morphology of fumed silica is spherical and is composed of grain-like agglomerates. The mixing process of fumed silicas should produce the formation of small aggregates which form a network of chains interconnected throughout the polymer–filler mixture. Overmixing reduces the size of aggregates too much and only a partial network is created.

Precipitated silicas (SiO_2). Precipitated silicas are common fillers in natural rubber and styrene–butadiene rubber base formulation. Precipitated silicas impart thixotropy to several adhesives, paints and coatings. Precipitated silicas are produced by reaction of sodium silicate ($3\text{SiO}_2 \cdot \text{Na}_2\text{O}$) with sulphuric or hydrochloric acid. The concentration of reactants, rates of addition, temperature and drying are process variables determining the properties of the precipitated silica, such as oil absorption, specific surface area, porosity, primary particle and agglomerate size and shape. Moisture content in precipitated silicas is high (3–7%) and three types of water are available: free water (easily removed by heating at 105°C), adsorbed water (removed on heating at 200°C), and constitutional water (removed at 700 – 900°C). Some typical properties of the precipitated silicas are: density 1.9 – 2.1 g/cm^3 ; pH of water suspension 3.5 – 9 ; primary particle size 5 – 100 nm ; aggregate size 1 – $40 \mu\text{m}$; density of silanol groups 5 – 12 groups/nm^2 ; oil absorption 60 – 320 g/100 g ; specific surface area 12 – $800 \text{ m}^2/\text{g}$.

The thickening mechanism of precipitated silicas is similar to that of the fumed silicas. Precipitated silicas have more silanol groups than fumed silicas, but they have a lower concentration of silica (precipitated silicas generally contain some sodium sulphate).

4.4.3. Metal oxides

Titanium dioxide is a common pigment, and zinc oxide and magnesium oxide are common fillers in rubber base adhesives.

Titanium dioxide (TiO_2). Titanium dioxide is the most common white pigment used today. As a pigment, titanium dioxide is unique because it combines both high colouring and high opacifying capacity. This is mainly due to its high refractive index (2.7). Furthermore, titanium dioxide is an excellent UV absorber (it is used in sun protective creams). Some typical properties are: density 3.3 – 4.25 g/cm^3 ; pH of water suspension 3.5 – 10.5 ; particle size 8 – 300 nm ; oil absorption 10 – 45 g/100 g ; specific surface area 7 – $160 \text{ m}^2/\text{g}$. Most titanium dioxide is produced from the rutile (TiO_2) or ilmenite (titanate of ferrous iron). Titanium dioxide can be obtained using different processes.

(1) Sulphate process. The ilmenite is reacted with sulphuric acid giving titanium sulphate and ferric oxide. After separation of ferric oxide, addition of alkali allows precipitation of hydrous titanium dioxide. The washed precipitate is calcined in a rotary kiln to render titanium dioxide. The nucleation and calcination conditions determine the crystalline structure of titanium dioxide (e.g. rutile or anatase).

(2) Chloride process. This process requires a high titanium feedstock. Rutile is reacted with hydrochloric acid to produce titanium tetrachloride, which can be hydrolyzed with steam or oxidized with air to render the dioxide. A rutile form of titanium dioxide is obtained.

(3) Tioxide process. This process is similar to that used to produce fumed silicas. Ultra-low particle size titanium dioxide (15–35 nm) is obtained for use as photocatalyst or UV absorber (for instance in sun protective creams).

Titanium dioxide used for adhesive applications should contain an inorganic coating to control polarity, improve its ease of dispersion, and improve its weather resistance. The inorganic coating (zirconium dioxide, silica, alumina) is applied in the aqueous slurry by precipitation of one or more hydrated metal oxides and by neutralization of acidic and alkaline compounds.

Three aspects determine the performance of titanium dioxide as pigment and UV absorber.

(1) Particle size: optimum particle size to produce maximum opacity is 200–300 nm.

(2) Amount: if too little titanium dioxide is added, the distance between particles is too large and there is not enough opacity, while if the titanium content is too high, the particles interfere with each other and poor efficiency is obtained.

(3) Dispersion in the polymer: optimum dispersion should produce a good distribution and separation of titanium dioxide particles in the formulation.

Zinc oxide. Zinc oxide is a popular cross-linking agent for rubber and for various resins. It is essential in the formulation of solvent-borne polychloroprene adhesives. Furthermore, zinc oxide is a good UV stabilizer, has biocidal activity and has a relatively high refractive index (2.0) which makes it an efficient white pigment. Some typical properties are: density 5.6 g/cm³; particle size 0.036–3 µm; oil absorption 10–20 g/100 g; specific surface area 10–45 m²/g. Zinc oxide is produced by reaction of the metal in the vapour state with oxygen. Zinc oxide is nonporous and is quite pure. Thus, the high surface area of some grades is due to the small particle size of zinc oxide. Some grades, especially for use in the rubber industry, are surface modified by deposition of 0.2–0.4% of stearic acid, propionic acid, or light oil [47].

Magnesium oxide (MgO). It is used as a curing agent and an acid scavenger in solvent-borne polychloroprene adhesives. It is a white powder with a high melting point. It has a greater ability to reflect visible light more efficiently than titanium dioxide

4.4.4. Calcium carbonate

Calcium carbonate (CaCO_3) is the most widely used filler in polymer formulations. As a filler, calcium carbonate allows cost reduction and improved mechanical properties. It is found in sedimentary rocks (chalk, limestone), marbles and minerals (dolomite). Some typical properties are: density 2.7–2.9 g/cm³; pH of water suspension 9; particle size 0.2–30 µm; oil absorption 13–21 g/100 g; specific surface area 5–24 m²/g. Depending on their origin and history of formation, and their impurities, the calcium carbonates have different properties. Three major technological processes are used in the production of calcium carbonate fillers: milling, precipitation, and coating. However, most calcium carbonate fillers are processed by milling using a dry or wet method. Dry milling provides ultra-fine calcium carbonate grades (particle size about 0.6 µm). Natural milled calcium carbonates are added to decrease cost in rubber base adhesives.

4.4.5. Carbon blacks

Carbon blacks are typical fillers for reinforcing rubber. An extensive literature has been devoted to the manufacture, structure, and characterization of carbon blacks, as well to their effects as fillers in polymers. Some specific and more detailed information can be found in Refs. [38,48].

Carbon blacks are synthetic materials which essentially contain carbon as the main element. The structure of carbon black is similar to graphite (hexagonal rings of carbon forming large sheets), but its structure is tridimensional and less ordered. The layers of carbon blacks are parallel to each other but not arranged in order, usually forming concentric inner layers (turbostratic structure). Some typical properties are: density 1.7–1.9 g/cm³; pH of water suspension 2–8; primary particle size 14–250 nm; oil absorption 50–300 g/100 g; specific surface area 7–560 m²/g.

Carbon blacks are obtained by pyrolysis or combustion of hydrocarbon-containing materials (hydrocarbon gases, viscous residual aromatic hydrocarbons). Thermal and furnace carbon blacks are used in rubber base adhesives. In the thermal decomposition process, natural gas is fed in absence of air into a generator at a temperature of 1300°C, where it undergoes cracking. The thermal carbon blacks are obtained from the stream of products gases. The oil-furnace process is the most prevalent method of carbon black production. A reactor is fed by liquid hydrocarbon feedstock which is mixed with preheated air and natural gas. The furnace carbon black is obtained from the combustion gases. In general, the furnace carbon blacks have lower particle size and higher specific surface area than thermal carbon blacks.

Particle and aggregate size are the most important factors in carbon blacks. During the manufacture of carbon blacks, primary particles are obtained in the

gas or liquid states. As the formation of primary particles at high temperature is produced, they tend to adhere to each other and partial fusion may occur producing aggregates. The aggregates can also be joined to produce agglomerates. The aggregates determine the properties of the carbon blacks because they cannot break even under very abrasive processing methods. On the other hand, depending on the manufacturing process, different active groups are exposed on the surface of carbon black; these groups affect wetting, dispersion, adsorption of moisture and reinforcing of polymers by carbon blacks.

4.4.6. Flame retardants

Some inorganic fillers are used as flame retardants in rubber base formulations. Flame retardants act in two ways: (1) limiting or reducing access of oxygen to the combustion zone; (2) reacting with free radicals (especially HO^\bullet), thus acting as terminator for combustion-propagation reaction. The additives most widely used as flame retardants for polymers are antimony oxides and alumina trihydrate.

Antimony trioxide (Sb_2O_3). It is produced from stibnite (antimony sulphide). Some typical properties are: density 5.2–5.67 g/cm³; pH of water suspension 2–6.5; particle size 0.2–3 μm ; specific surface area 2–13 m²/g. Antimony trioxide has been the oxide universally employed as flame retardant, but recently antimony pentoxide (Sb_2O_5) has also been used. Antimony oxides require the presence of a halogen compound to exert their fire-retardant effect. The flame-retarding action is produced in the vapour phase above the burning surface. The halogen and the antimony oxide in a vapour phase (above 315°C) react to form halides and oxyhalides which act as extinguishing moieties. Combination with zinc borate, zinc stannate and ammonium octamolybdate enhances the flame-retarding properties of antimony trioxide.

Alumina trihydrate ($\text{Al}_2\text{O}_3 \cdot 3\text{H}_2\text{O}$). It is obtained as a byproduct in the aluminium metal production. Some typical properties are: density 2.4 g/cm³; pH of water suspension 8–10.5; particle size 0.7–55 μm ; oil absorption 12–41 g/100 g; specific surface area 0.1–12 m²/g. The flame-retardant and smoke-suppressing action of alumina trihydrate is due to several effects. The water of hydration in the compound rapidly splits off at temperatures higher than 300°C (upon burning), and the steam evolved obstructs the access of oxygen to the polymer, thus hindering the combustion process. On the other hand, the decomposition reaction of $\text{Al}_2\text{O}_3 \cdot 3\text{H}_2\text{O}$ in Al_2O_3 and H_2O is endothermic; the heat absorption lowers the temperature and suppresses pyrolysis, thus reducing smoke generation. Further, the alumina (Al_2O_3) formed in the reaction has a very small particle size and thus may also act as a heat barrier and even absorb some of the smoke constituents. Large quantities of filler must be used to obtain flame-retarding properties, and as a consequence the mechanical and rheological properties of the polymers are

reduced. Additives such as compounds of zinc are used to reduce the alumina trihydrate concentration.

Other flame retardants and/or smoke suppressants can also be used such as magnesium hydroxide, magnesium carbonate, magnesium–zinc complexes and some tin–zinc compositions. Zinc oxide is a common ingredient in many rubber base formulations used as part of the curing system. At the same time, the action of zinc oxide is similar to that of antimony trioxide, but less effective.

4.5. Curing agents

Raw rubber is an entanglement of high molecular weight hydrocarbon chains. Consequently, rubber flows on standing and does not retain its shape. For rubber to become useful, its chains must be permanently linked together to increase its strength. Rubber can be cross-linked (i.e. vulcanized) by heating with sulphur and lead oxide. During vulcanization, sulphur linkages form bridges between rubber chains.

The vulcanization process established by Goodyear in 1839 is still currently in use. Sulphur vulcanization takes place in three stages.

(1) Induction period. The curatives react with themselves in preparation for the cross-linking reaction. This period allows the ingredients to be safely mixed avoiding premature curing ('scorch').

(2) Vulcanization of the rubber. Sulphur bridges between rubber chains are actually produced.

(3) Reversion. This is undesirable and is produced when heating is continued beyond the time needed to develop an optimum cure.

The Goodyear vulcanization process takes hours or even days to be produced. Accelerators can be added to reduce the vulcanization time. Accelerators are derived from aniline and other amines, and the most efficient are the mercaptobenzothiazoles, guanidines, dithiocarbamates, and thiurams (Fig. 32). Sulphenamides can also be used as accelerators for rubber vulcanization. A major change in the sulphur vulcanization was the substitution of lead oxide by zinc oxide. Zinc oxide is an activator of the accelerator system, and the amount generally added in rubber formulations is 3 to 5 phr. Fatty acids (mainly stearic acid) are also added to avoid low curing rates. Today, the cross-linking of any unsaturated rubber can be accomplished in minutes by heating rubber with sulphur, zinc oxide, a fatty acid and the appropriate accelerator.

Vulcanization changes the physical properties of rubbers. It increases viscosity, hardness, modulus, tensile strength, abrasion resistance, and decreases elongation at break, compression set and solubility in solvents. All those changes, except tensile strength, are proportional to the degree of cross-linking (number of cross-links) in the rubber network. On the other hand, rubbers differ in their ease of vulcanization. Since cross-links form next to carbon–carbon double bonds,

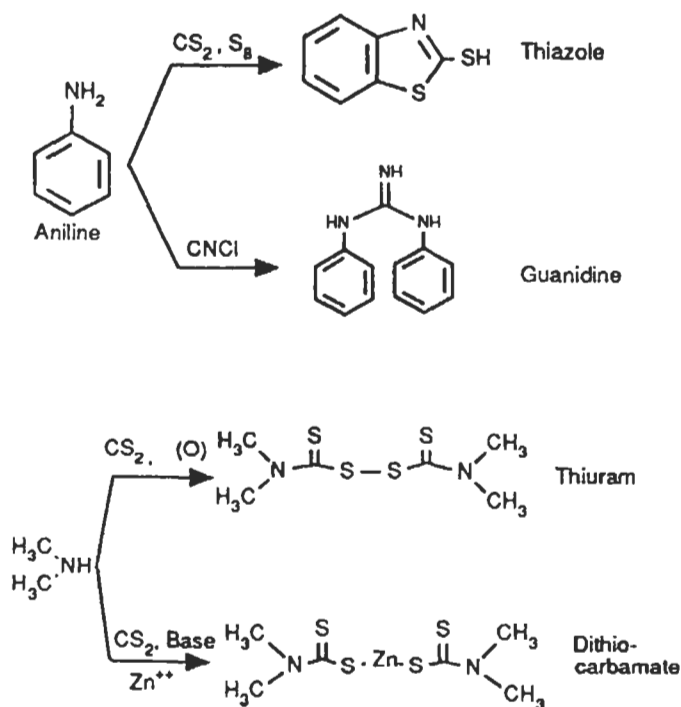


Fig. 32. Classes of accelerators in rubber vulcanization.

rubbers which are highly unsaturated are the most easily cured (for instance natural rubber is easier vulcanized than styrene-butadiene rubber).

Rubber cross-linking can also be produced with curing agents different than sulphur.

(1) Peroxides. Peroxides cure by decomposing on heating into peroxy radicals which abstract a hydrogen from the elastomer and generate a polymer radical. Most of these radicals immediately combine to form cross-links. Peroxides offer the advantage of curing both saturated and unsaturated rubbers and produce quite thermally stable carbon-carbon cross-links. However, the peroxide curing has some disadvantages; because of the poor tensile and tear strengths obtained, many antioxidants cannot be used, and it has higher cost than sulphur vulcanization.

(2) Metal oxides. Magnesium oxide is used to cure polychloroprene by converting its few active allylic chloride from 1,2 addition into ether cross-links. There is a synergistic effect when magnesium oxide is used in combination with *t*-butyl phenolic resins in solvent-borne polychloroprene adhesives. When solvent is removed, the phenolic group in the resin reacts with the magnesium oxide to cross-link [49].

(3) Phenol-formaldehyde resins. These are used to cure butyl rubber forming thermally stable carbon-carbon cross-links.

(4) *p*-Benzoquinone dioxime. It is also used to cure butyl and other unsaturated rubbers, following the same mechanism as for phenol-formaldehyde resins. Curing with benzoquinone needs the combination with an inorganic oxidizing agent (lead oxide) or with benzothiazyl disulphide. This system is active at room temperature.

Rubber base adhesives can be used without cross-linking. When necessary, essentially all the cross-linking agents normally used in the vulcanization of natural rubber can be used to cross-link elastomers with internal double carbon-carbon bonds. A common system, which requires heat to work, is the combination of sulphur with accelerators (zinc stearate, mercaptobenzothiazole). The use of a sulphur-based cross-linking system with zinc dibutyldithiocarbamate and/or zinc mercaptobenzothiazole allows curing at room temperature. If the formulation is very active, a two-part adhesive is used (sulphur and accelerator are placed in two separate components of the adhesive and mixed just before application).

4.6. Antioxidants

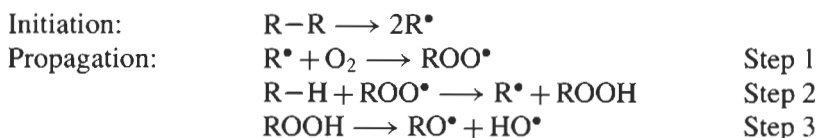
With rubber base adhesives, it is necessary to prevent their properties from changing during service life. Oxidative changes induced by thermal, ozone exposure and UV light can dramatically affect service life of rubber base adhesives. More precisely, the rubber and the resin are quite susceptible to oxidative degradation. Environmental and physical factors exert detrimental effects on rubber base adhesive performance. These effects can be mitigated by the incorporation of low levels of stabilizers during the fabrication process of the adhesive.

Antioxidants and stabilizers occupy a key position in the performance of adhesives. The terms 'antioxidants' and 'stabilizers' are generally used to describe chemical agents that inhibit degradative effects of oxygen, light, heat, and high temperature. Rubber technologists also used the terms 'antidegradants', 'antifatigue agents', 'inhibitors' and 'antiozonants'. It is more convenient to use the term antioxidant to comprehensively describe "all chemical agents that act to inhibit oxidation of a polymer matrix arising from the adverse effects of mechanical, thermal, photochemical, and environmental factors during the manufacture of the polymeric material and throughout the service life of the end-use product".

Most rubbers used in adhesives are not resistant to oxidation. Because the degree of unsaturation present in the polymer backbone of natural rubber, styrene-butadiene rubber, nitrile rubber and polychloroprene rubber, they can easily react with oxygen. Butyl rubber, however, possesses small degree of unsaturation and is quite resistant to oxidation. The effects of oxidation in rubber base adhesives after some years of service life can be assessed using FTIR spectroscopy. The ratio of the intensities of the absorption bands at 1740 cm^{-1} (carbonyl group) and at 2900 cm^{-1} (carbon-hydrogen bonds) significantly increases when the elastomer has been oxidized [50].

Oxygen attacks rubber because of the presence of two unpaired electrons

which may act as two free radical species able to react with the unsaturation in hydrocarbon molecules. Rubber oxidation can be described by a cyclical free radical chain process [51]:



Free radicals are initially generated whenever polymer chains are broken and carbon radicals are formed. These effects occur during manufacture and in service life. Many elastomers are observed to oxidize at relatively low temperature (about 60°C), where carbon-hydrogen and carbon-carbon bond cleavages are highly unlikely. It has been demonstrated [52] that traces of peroxides impurities in the rubber cause low-temperature oxidation of rubber. These initiating peroxides are present in even the most carefully prepared raw rubber polymer [53].

Once free radicals are formed, a chain reaction is set in motion as these radicals rapidly add oxygen in propagation reactions to give the formation of peroxides (step 1). Hydroperoxides are inherently unstable to heat, light, and metal ions and would therefore react immediately after formation. These hydroperoxides abstract a hydrogen from the rubber (step 2), regenerating free radical R^\bullet to continue the cycle. Furthermore, the hydroperoxide formed in step 2 decomposes into two more oxy radicals (step 3). These oxy radicals also react with the rubber, in step 1, and increase the rate of oxidation. It should also be noted that unsaturated polymers oxidize more readily than saturated polymers. This auto-oxidation process normally starts slowly but auto-accelerates, leading to catastrophic damage of the rubber [54].

Oxidation causes rubbers and resins to harden, and also produces colour darkening in resins. The radicals formed in the above chain reaction are highly reactive and very unstable, so they will be rapidly converted to more stable products. For most rubbers and resins, these radicals combine to form cross-links which cause hardening (Fig. 33).

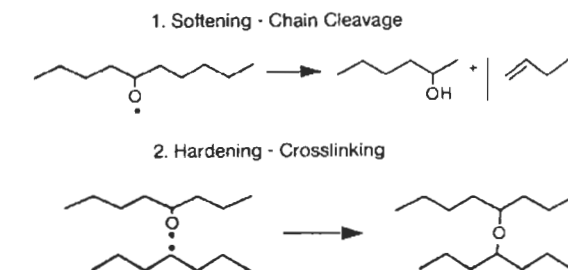


Fig. 33. Hardening process of polymers produced by ageing.

In natural rubber, the cross-linking of these radicals is hindered because of the bulkiness of the methyl side group. Consequently, these radicals prefer to disproportionate and cleave. This reduces the molecular weight and natural rubber softens on ageing.

On the other hand, rubbers are exposed to repeated mechanical flexing and deformation in service. Previous studies [55] have shown that flex cracking of rubber materials is accelerated by the presence of oxygen. Environmental flex cracking is caused by oxidative chain scission of the rubber polymer at mechanically induced cracks.

The oxidation of rubbers and resins can be slowed considerably and the service lifetime extended by adding antioxidants. Antioxidants scavenge and destroy the propagating radicals (ROO^\bullet and R^\bullet) before they have a chance to react with the polymer chains in step 1. Because of this they are referred to as chain braking or primary antioxidants. Primary antioxidants are electron or hydrogen atom donors that are capable of reducing ROO^\bullet to ROOH . Typically secondary aromatic amines and substituted phenols which have very reactive hydrogen atoms act as chain-breaking donor antioxidants. On the other hand, chain-breaking acceptor antioxidants act as oxidizing alkyl radical R^\bullet and are only effective under low oxygen concentration. Quinones are excellent chain-breaking acceptor antioxidants.

Aromatic amines are the most effective *primary antioxidants* (Fig. 34) but they are discolouring and can only be used where the darker colours are acceptable (for instance in rubber adhesive formulations containing carbon blacks as fillers). The

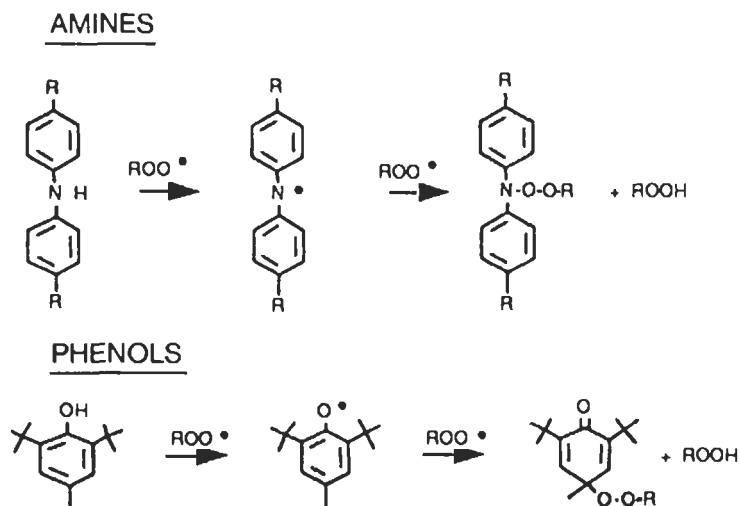


Fig. 34. How primary antioxidants retard oxidation of polymers (see p. 18 in [56]).

secondary diaryl amines (phenyl naphthylamines, substituted diphenylamines, *p*-phenylenediamines), alkyl-aryl secondary amines, ketone-amine condensates, aldehyde-amine condensates, and primary aryl amines are typical primary antioxidants. The polymeric dihydroquinolines are the least discolouring amine antioxidants. All of the *p*-phenylenediamines are highly discolouring but possess the advantage of being metal ion deactivators, antiflex agents and antiozonants. The effectiveness of the amine antioxidants in vulcanizates is frequently improved by adding mercaptobenzimidazole derivatives.

The other class of primary antioxidants are the phenols (hindered phenols, hindered bisphenols, hindered thiobisphenols, polyhydroxy phenols) (Fig. 34). Phenolic antioxidants are generally used when the discolouration of the amine antioxidants cannot be tolerated. Phenols may produce coloured reaction products (yellow, tan or pink) but the discolouration is significantly less than produced with amines.

To obtain maximum lifetime, the oxidants must not be lost during service. A major potential source of loss is the evaporation of the antioxidant. Evaporation is often observed with BHT (butylated hydroxytoluene), a monomeric phenol, and to avoid evaporation less volatile, higher molecular weight antioxidants are used (i.e. bisphenols).

Another method for slowing oxidation of rubber adhesives is to add a compound which destroys the hydroperoxides formed in step 3, before they can decompose into radicals and start the degradation of new polymer chains. These materials are called hydroperoxide decomposers, preventive antioxidants or *secondary antioxidants*. Phosphites (phosphite esters, organophosphite chelators, dibasic lead phosphite) and sulphides (i.e. thiopropionate esters, metal dithiolates) are typical secondary antioxidants. Phosphite esters decompose hydroperoxides to yield phosphates and alcohols. Sulphur compounds, however, decompose hydroperoxides catalytically.

Antioxidant activity is not a linear function of concentration. As the antioxidant level increases, less and less improvement in oxidative stability is noted. Therefore, only enough antioxidant should be added to rubber adhesives, typically 1 to 2 phr.

When two antioxidants are used together, a synergistic improvement in activity usually results. Synergism can arise from three combinations: (1) homosynergism — two chemically similar antioxidants (for instance, two hindered phenols); (2) autosynergism — two different antioxidant functions that are present in the same molecule; (3) heterosynergism — the cooperative effect between mechanistically different classes of antioxidants, such as the combined effect of primary and secondary antioxidants. Thus, combinations of phenols and phosphites are widely used to stabilize synthetic rubbers.

4.6.1. UV absorbers

The UV component of sunlight (wavelength 280–400 nm) can cause degradation of polymers, mainly the UV radiation with a wavelength between 310 and 330 nm. Therefore, *UV absorbers* or light stabilizers are also important components in extending the service life of rubbers. UV absorbers act by absorbing UV light, hence retarding the photolysis of hydroperoxides. The light stabilizers used in polymers can be grouped into four main general functional types (organic UV absorbers, inorganic UV absorbers, free-radical scavengers, and chromophore quenchers), but only the following two are of interest for rubbers.

(1) Organic UV absorbers. These stabilizers operate by absorbing the damaging UV radiation and re-emitting the energy at a longer wavelength as infrared radiation (i.e. heat), which is much more harmless to the polymers. The organic UV absorbers generally absorb wavelengths between 300 and 360 nm, but no absorption in the visible region is produced to avoid colour. The most common organic UV absorbers are modified benzophenones and benzotriazole derivatives. 2-hydroxybenzophenones and 2-hydroxybenzotriazoles are the most typical organic UV absorbers. Both are relatively stable to light between 300 and 360 nm and have high molar absorption in this region [57]. In most cases the degree of UV protection afforded increases with the additive's concentration. Furthermore, the protective effect also depends on the thickness of the rubber material (it is less marked in thin films).

(2) Inorganic (particulate) UV absorbers. These act producing a physical barrier to UV and visible radiation. Carbon black and titanium dioxide, widely used in rubber formulations, have a light-stabilizing effect. Because of their particulate nature and their mode of action, they are often called 'screening agents', 'screeners' or 'light screens'. Carbon black absorbs UV and visible radiation and, as the organic UV absorbers, emits the energy in the IR region; carbon black is also able to capture free radicals. Fine particle grades are more effective and a loading less than 2 phr is sufficient. The screening action of titanium dioxide is mainly due to reflection and scattering of the UV, visible and IR radiations. Although this mechanism is less efficient than that of carbon black (higher loadings are necessary, typically 5 to 15 phr), it can be used in formulations where colour could be a limitation. Zinc oxide can also act as an inorganic screening agent which has a synergistic effect with certain antioxidants.

4.6.2. Antiozonants

Degradation of rubbers and resins can also be produced by *ozone attack*. Ozone directly reacts with, and cleaves, the carbon–carbon double bonds of rubbers and resins. Thus only polymers with backbone unsaturation will be cracked by ozone. Unlike oxidation, ozone attack cannot be accelerated by increasing the

temperature, and it is only produced when the polymer is stretched. Without stretching, the underlying double carbon–carbon bonds are not exposed to ozone, thus cracks do not grow.

Ozone cracking is a physicochemical phenomenon. Ozone attack on olefinic double bonds causes chain scission and the formation of decomposition products. The first step in the reaction is the formation of a relatively unstable primary ozonide, which cleaves to an aldehyde or ketone and a carbonyl. Subsequent recombination of the aldehyde and the carbonyl groups produces a second ozonide [58]. Cross-linking products may also be formed, especially with rubbers containing disubstituted carbon–carbon double bonds (e.g. butyl rubber, styrene–butadiene rubber), due to the attack of the carbonyl groups (produced by cleavage of primary ozonides) on the rubber carbon–carbon double bonds.

Rubbers differ in their resistance to ozone. All the highly unsaturated rubbers (natural rubber, styrene–butadiene rubber, butyl rubber, nitrile rubber) are readily cracked while the deactivated double carbon–carbon bonds rubber (such as polychloroprene rubber) shows moderate ozone resistance.

To be effective, the antiozonants should have two important functions: decrease the rate of crack growth in the rubber, and increase the critical stress value (i.e. the stress at which crack growth occurs). Therefore, the following properties of an antiozonant are desirable.

- (1) A physical antiozonant provides an effective barrier against the penetration of ozone on the rubber surface. This barrier should be continuous at the surface, unreactive and impenetrable to ozone, and also capable of renewing itself if damaged.
- (2) A chemical antiozonant must be extremely reactive with ozone and must not be too reactive with oxygen.
- (3) An antiozonant should have adequate solubility and diffusivity characteristics. Since ozone attack is a surface phenomenon, the antiozonant must migrate to the surface of the rubber to provide protection. Poor solubility in rubber may result in excessive bloom.
- (4) An antiozonant should have no adverse effects on the rubber processing.
- (5) Antiozonants should be effective in both static and dynamic conditions.
- (6) Antiozonants should persist in the rubber over its entire life cycle.
- (7) Antiozonants should have a low toxicity.
- (8) Antiozonants must be non-discolouring and nonstaining.

Ozone attack of rubbers can be prevented in three ways: (1) coating the surface; (2) adding a chemical antioxidant; (3) relieving internal stresses by adding ozone-resistant polymers.

Rubber is protected against ozone attack by addition of physical and/or chemical antiozonants. Hydrocarbon waxes are the most common type of physical antiozonants, and *p*-phenylenediamine derivatives are the prevalent chemical antiozonants. Waxes bloom to the rubber surface and form a protective barrier.

Since this bloom is brittle, it is broken by flexing. Therefore, waxes only protect under static conditions. For serving conditions which involve continuous flexing, *p*-phenylenediamines (*N,N'*-alkyl-aryl derivatives) can be added. These chemical antiozonants scavenge the ozone before it reacts with the rubber. A barrier of ozonized products is created which protects both the rubber and antiozonant from further attack. However, *p*-phenylenediamines are staining compounds. Whenever colour is an important concern, blends of elastomers can be used; elastomers loading should be higher than 30 phr to provide sufficient effectiveness.

A common loading for antiozonants in rubber formulations is 1.5–3 phr. Combinations of waxes and chemical antiozonants are used when the service conditions involve both long periods of static as well as dynamic stresses.

4.7. Solvents

The solvent plays an important role in the performance of rubber base adhesives. The solvent is the carrier for all components of the adhesive. Furthermore, the solvent controls the viscosity, open time, tack and adhesion of rubber base adhesives.

A particular case in which the solvent is important is in contact adhesives, which for some time after application have enough cohesive strength and knitting ability that two surfaces coated with the adhesive have green strength immediately after they are mated. *Knitting ability* is an auto-adhesion phenomenon in which the elastomer molecules are mobile enough to quickly form a bond immediately after contact with little or no applied pressure. Few elastomers have this ability, polychloroprene is one of them. *Green strength* indicates that the adhesive bond is strong enough to be handled a short time after the adherends are mated but much before full cure is obtained. The choice of solvent in contact adhesives is critical because the solvents are chosen in such a way that a rapid evaporating solvent is used as carrier and a slower evaporating solvent provides tack during bonding.

The increase of restrictive regulations on the use of organic solvents favoured the increasing use of latex-based adhesives. Because of the slow evaporation of water, these adhesives show less tack and can suffer bacterial attack. Infrared heaters and ovens can be used to favour the evaporation of water. Often a small amount of solvent (*coalescing aid*) is added to the latex system to improve wetting and coalescence of the latex particles.

5. The most significant rubber base adhesives

5.1. Natural rubber (NR) adhesives

Most often NR adhesives are supplied either as a solvent dispersion or as a latex for coating onto surfaces. Viscosity can range from very low viscosity solutions for

spray application to higher viscosity mastics suitable for trowelling. NR adhesives can also be pre-coated onto fabric, paper or film to provide pressure-sensitive tapes.

NR adhesives can be divided in two types: wet bonding and dry bonding. *Wet bonding* adhesives are applied on substrates in a fluid state, the bond being formed by drying. The *dry bonding* NR adhesives are pressure-sensitive adhesives because the bond is created under pressure.

5.1.1. Properties

Adhesives made from the various forms of NR exhibit similar characteristics, although some properties are altered by adding curatives.

(1) *Excellent tack.* Solvent solutions are very tacky even without addition of a resin. Latex compounds exhibit superior self-adhesion after coated surfaces have dried.

(2) *Very good water and moisture resistance.* Solvent-borne adhesives have an advantage over latex, which contains surfactants.

(3) *High flexibility.*

(4) *High resilience and fatigue resistance.*

(5) *Brittleness with age.* Degradative oxidation can be produced, even after vulcanization, due to oxygen and ozone attack to the carbon-carbon double bonds. Adequate antioxidants must be added if ageing is a key factor in performance.

(6) *Poor resistance to organic solvents and oils.* This can be partially reduced in vulcanized systems.

(7) *Low to moderate cost.*

(8) *A wide range of substrates can be bonded.* The inherent tackiness of natural rubber enables it to coat most non-polar substrates (mainly plastics and rubbers).

(9) *Good electrical and thermal insulators.*

5.1.2. Additives and modifiers

NR adhesives accept a wide variety of compounding ingredients.

(1) *Thickeners* can be added to increase the viscosity of the NR adhesives. Natural materials can be used such as casein or karaya gum, but currently synthetic polymers are used (methyl cellulose and derivatives, polyacrylates).

(2) Most mineral *fillers* can be easily incorporated into solvent-borne and water-borne (adding adequate surfactants and wetting agents) adhesives.

(3) Hydrocarbon *resins*, rosin, rosin ester, coumarone indene resins, and terpene resins can be directly added to solvent-borne adhesives. For latex adhesives, resin emulsification must be produced before addition.

(4) *Reinforcing agents* can be added to increase the cohesive strength of NR adhesives. Carbon blacks have been extensively used, but polyfunctional

isocyanates are currently preferred. The isocyanate must be added to the NR adhesive immediately before use and curing is produced at room temperature. Water must be avoided in the formulation to obtain maximum effectiveness. Finally, chlorinated rubber is a valued reinforcement agent for NR adhesives.

(5) *Plasticizers* and oils, curatives and accelerators may also be added. In solvent-borne adhesives, curing agents are generally packed separately.

(6) *Softeners* (liquid polybutenes and lanolin) can be added.

5.1.3. Formulations of NR adhesives

Specific formulations of NR adhesives can be found in Refs. [59,60].

Solvent-borne adhesives. Although the NR polymer is inherently tacky, tackifying resins are generally added to improve bonding to polar surfaces. Because the solids content in these adhesives is lower than 35 wt%, they are not suitable for gap filling. The quick-grab (cements) adhesives are particular because they contain about 65 wt% rubber, and set within a few seconds under finger pressure.

Water-borne adhesives. These contain between 40 and 80 wt% solids. They are completely untacky in the dried film and auto-adhere to itself under pressure.

Depolymerized latex has intrinsic tack and can be blended with normal latex to improve cohesive strength (Fig. 35a), with tackifiers to improve tack or peel strength (Fig. 35b), or with both.

5.1.4. Adhesion characteristics

NR adhesives perform adequately under peeling stresses. The peel strength can vary from a few N/m in PSA formulations to 'substrate tear' in vulcanized compounds used in hose, belting and tire products.

Nonvulcanizing NR adhesives typically withstand temperature ranges between -30°C and 65°C . Vulcanized NR adhesives can perform between -40°C and 150°C .

The solvent-borne NR adhesives show an important mechanical component in the bonding process, and therefore bulk mechanical and rheological properties (addition of fillers is quite effective) are important. In fact, these adhesives are mainly suitable when at least one of the surfaces to be joined is water-porous (paper, concrete, leather, textiles).

The influence of the gel content in polyisoprene-tackifier blends on creep resistance and peel behaviour have been recently studied [62]. The gel content was achieved by cross-linking the adhesives with electron beam irradiation. The molecular weight of the soluble fraction in the blend was always dominated by that of the initial elastomer. Creep resistance was achieved either through molecular weight increases or gel content increases. However, the peel strength is strongly

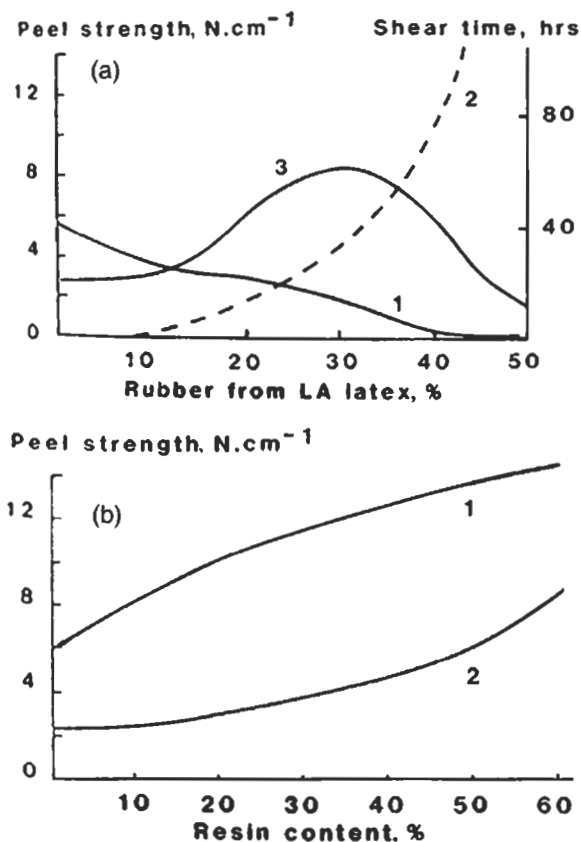


Fig. 35. (a) Blends of depolymerized rubber latex with normal NR latex. $M_w = 160,000$. (1) 180° peel strength on glass; (2) hold time, PSTC7, 500 g; (3) $M_w = 80,000$, 180° peel strength (see p. 175 in [61]). (b) Blends of depolymerized rubber latex ($M_w = 160,000$) with aliphatic hydrocarbon resin. 180° peel strength tested against (1) glass, (2) polyethylene (see p. 175 in [61]).

influenced by the initial elastomer molecular weight and further cross-linking did not provide performance equivalent to that obtained from high molecular weight materials.

5.1.5. Applications

NR pressure-sensitive adhesives with a high tackifier content can be used as commercial tapes and surgical plasters. These PSA require the elimination of the gel fraction and a reduction in molecular weight to facilitate solution.

Solvent-borne NR and quick-grab adhesives are commonly used in the manufacturing of leather footwear for temporary bonding and in rubber footwear

as a curing laminating adhesive. Many off-the-road tires, hoses and belting use vulcanizing grade of solvent-dispersed natural rubber.

Reclaimed rubber can be used in non-vulcanizing general-purpose NR adhesives. It can be used for insulation, packaging materials, and bonding of polyethylene, canvas, metals and wood.

Heveaplus MG has a higher polarity than NR and it is usually used as primer for NR solutions to increase the adhesion of PVC and synthetic upper materials in crepe rubber soles in footwear.

Latex compounds have been typically used in paper, textile and construction. One of the most popular applications is their use in self-sealing envelopes. This application is based on the fact that when NR dries, some soluble non-rubber compounds migrate to the surface by water transport, leaving a thin film when drying is completed. This film reduces the surface tack on the rubber and when pressed against a similar film the non-rubber layer is displaced, allowing the two rubber surfaces to create a bond. Zinc diethyldithiocarbamate is added to prevent degradation by fungi and bacteria. In some cases small amounts of a plasticizer (polybutene) or an adhesion promoter (polyvinyl acetate latex) can be added.

Another important application of NR is for bonding ceramic tiles, although it needs special compounding with clay filler and cellulose thickener. Water-borne NR adhesives can also be used for bonding canvas and leather shoes and interior trim in some automotive applications.

Vulcanizing latex adhesives are used in the manufacture of textiles, rugs and carpets. The vulcanizing ingredients are sulphur, zinc oxide and accelerators (for example, zinc dibutyldithiocarbamate and zinc mercaptobenzothiazole to produce vulcanization at room temperature).

5.2. Butyl rubber (BR) and polyisobutylene (PIB) adhesives

All grades of regular butyl rubber are tacky, rubbery and contain less unsaturation than natural rubber or styrene–butadiene rubber. On the other hand, low molecular weight grades of polyisobutylene are permanently tacky and are clear white semi-liquids, so they can be used as permanent tackifiers for cements, PSAs, hot-melt adhesives and sealants. Low molecular weight polyisobutylenes also provide softness and flexibility, and act as an adhesion promoter for difficult to adhere surfaces (e.g. polyolefins).

Cohesive strength of these adhesives can be modified by blending butyl rubber and polyisobutylene. Higher strength is obtained by using high molecular weight PIB or butyl rubber. On the other hand, blends of butyl rubber or PIB with chlorinated butyl rubber show improved cure properties.

5.2.1. Properties

The extremely diverse nature of the isobutylene family polymers makes it difficult to provide general statements, although the following characteristic properties can be given.

(1) *Superior water and moisture resistance.* Butyl is by far the best elastomer to provide resistance to water and moisture.

(2) *High initial tack.* The adequate choice of butyl or PIB provides excellent building tack (ability to produce quick adhesion by applying low pressure).

(3) *Low air and gas permeability.* The amorphous and highly saturated nature of the polymer chain prevents permeation of air and gases.

(4) *Good resistance to oils.* Mainly polyisobutylene polymers resist high-oil-content foams and rubber. In some cases swelling may occur.

(5) *Good flexibility and impact resistance.* This is due to the amorphous nature of the polymers.

(6) *Excellent ageing.* This is due to the high degree of saturation in the polymer chain.

(7) *Heat resistance.* It depends on the content of PIB in the butyl rubber polymer: the higher the PIB content, the lower the heat resistance and the higher the tack.

(8) *Relatively low strength.* Even when cured or cross-linked, BR tends to creep under load.

(9) *Wide substrate range.* BR and PIB stick to most surfaces, including polyolefins.

5.2.2. Additives and modifiers

BR is similar to NR in its ability to compound with other materials. Some specific aspects related to additives for butyl rubber are given below.

(1) *Pigments and fillers.* In general, BR and PIB polymers are compatible with a wide range of fillers. The same fillers and pigments can be added to BR and PIB. Very fine pigments (clays, precipitated silicas, thermal and furnace carbon blacks) increase cohesive strength and stiffness, and reduces tack, whereas coarser pigments (aluminium hydrate, whiting) increase tack with moderate increase in cohesive strength. Zinc oxide increases tack and cohesive strength, and also influences the vulcanization of BR. Calcium carbonate can also be added to decrease cost without detrimental effect in mechanical properties.

(2) *Tackifiers.* Resins are generally added to adjust the desired tack. In general, resins must be used with plasticizers to obtain a good balance between tack and cohesive strength. Typical tackifiers are polyterpenes, although hydrocarbon resins and modified rosins and rosin esters can also be used. In some cases, terpene-phenolics or phenol-formaldehyde resins are added to increase adhesion.

(3) *Plasticizers*. Polybutene is the most common, although paraffinic oils and certain phthalates (i.e. dithridecyl phthalate) can also be added in the formulations.

(4) *Antioxidants*. Antioxidants are rarely needed because of the highly saturated nature of the polymer chains. If protection against severe environmental ageing conditions is needed, typical antioxidants (Ethanox 702, Irganox 1010) can be added. In some cases, zinc dibutyldithiocarbamate (0.05–0.2 wt%) or butylated hydroxytoluene (BHT) can be used as stabilizers.

(5) *Adhesion promoter*. Epoxy silane can be added to increase adhesion to glass (mainly for BR sealants). In certain textile applications, isocyanates can be added to solvent-borne BR cements.

(6) *Other additives*. Amorphous polypropylene, waxes and asphalt can be added to decrease the cost of BR formulations. On the other hand, PIB can be blended with NR, styrene–butadiene rubber, EVA and low molecular weight polyethylene to impart specific properties.

(7) *Curing systems*. Four curing systems can be used for BR and chlorinated butyl rubber formulations.

- (a) Quinoid cure. This is the most common curing system for BR. *p*-quinone dioxime (QDO) or dibenzoyl *p*-quinone dioxime (DBQDO) combined with manganese dioxide or lead oxide are generally used. Although the cured product has high resistance to chemicals, ozone, heat and ageing, a dark colour is obtained.
- (b) Sulphur or sulphur–donor compounds. Elemental sulphur, thiuram and dithiocarbamate accelerators and thiazole activator are used. Zinc oxide and elevated temperature are necessary to attain satisfactory cure.
- (c) Brominated phenolic resin. Specially used to obtain light coloured and white formulations.
- (d) Zinc oxide. This is intended only for chlorobutyl rubber and has the advantage of producing the cure of this polymer in the presence of other elastomers without affecting them.

5.2.3. Formulations of BR adhesives

Specific formulations of BR and PIB adhesives can be found in [5]. These adhesives are supplied in forms quite similar to those of natural rubber: solvent-borne and water-borne dispersions, and pressure-sensitive pre-coated films.

Butyl latices have a solids content of about 60 wt%, a pH about 5.5, a Brookfield viscosity near 2.5 Pa s and an average particle size of 0.3 μm .

A broad range of solvents can be used in *solvent-borne* BR and PIB adhesives. Hydrocarbon (hexane, heptane, naphtha) and chlorinated solvents (perchloroethylene) can be used; they provide higher viscosities. The presence of small amounts of stabilizer may cause cloudy solutions and settling is rarely produced. There is a logarithmic relationship between viscosity and solids content. In fact, a small

change in the solids may produce large differences in viscosity, especially at high solids levels.

5.2.4. Adhesion characteristics

BR and PIB are used for adhesion of several substrates including nonporous and difficult to adhere materials (e.g. polyolefins). Other common substrates are PVC, polyester film and paper.

The BR and PIB adhesives have permanent tack but relatively low cohesive strength. Cohesive strength is provided by adding natural rubber, fillers or tackifiers. Furthermore, these adhesives have excellent resistance to chemicals, oils and ageing.

BRs were found to have a rate-sensitive mechanical response with very low tensile and shear strengths [63]. The stress-strain curves of the adhesives were characterized by an initial elastic response followed by a region of large plastic flow.

New copolymers based on a copolymerization of isobutylene and *p*-methylstyrene with improved heat resistance have been reported [64]. Once copolymerization was accomplished, the polymer was selectively brominated in the *p*-methyl position to yield a terpolymer called EXXPO. In contrast to butyl and halobutyl, the new terpolymer has no unsaturation in the backbone and therefore shows enhanced thermal stability and resistance to oxidation. Useful solvent-based adhesives can be formulated using the new terpolymer in combination with block copolymers [65]. The hydrocarbon nature of the new terpolymer results in excellent compatibility with hydrocarbon resins and oils.

5.2.5. Applications

Although BR adhesives are used as solvent-borne dispersions, pre-formed tapes and hot-melt PSAs are more common forms.

Tapes and labels. Formulations mainly include blends of BR and tackifier. Permanent tack can be provided using low molecular weight polyisobutylenes, which find application as label PSAs. Cohesive strength of BR adhesives is low compared to natural rubber and can be increased by adding natural rubber or particular resins and fillers. The polymer formulation is pre-coated onto a suitable carrier (film, reinforcement). In this group, general-purpose tapes, surgical tapes, electrical tapes and pipe wrap tapes, can be included. The resistance of BR and PIB to ageing and the permanent tack, also made those materials adequate for removable PSA labels and freezer label adhesives

Pre-formed sealing tapes are widely used in construction applications and for glazing applications in automotive glass.

Hot-melt PSAs. These require heating to melt temperatures and subsequent

cool-down. BR and PIB provide flexibility at low temperature, as well as to ageing and chemicals. Formulations include butyl rubber, petrolatum and amorphous polypropylene, and hydrocarbon oils, polybutenes and microcrystalline waxes (to reduce viscosity). The most common applications include carton closing and appliances manufacture.

Sealants for insulated glass windows are based on butyl polymers. These sealants have excellent weathering and ageing, low-moisture vapour transmission and are non-fogging [66].

Self-curing butyl adhesives can be used for laminating polyethylene film and for flocking adhesives. One of the most important applications is the use of BR as curing, solvent-dispersed and contact-grade for roof manufacturing on industrial buildings.

Precoated butyl latex compounds onto fabric can be used for PSAs in foil and paper lamination. These PSAs are also used in packaging and for bonding polyolefins (require adequate formulation).

Butyl latex can be used in packaging and as a tackifying and flexibilizing additive in higher strength adhesives for adhesion of polyethylene and polypropylene.

5.3. Styrene-butadiene rubber (SBR) adhesives

SBR adhesives are used in applications where low stress but high flexibility and resistance to shock are needed. If ageing is critical, SBR adhesives should not be used. SBR adhesives have relatively low surface energy and therefore can be used as general-purpose adhesive to join several substrates.

5.3.1. Properties of SBR adhesives

Although the emulsion and dispersion SBRs have different properties, the following characteristic properties can be given.

- (1) *Excellent water and moisture resistance.*
- (2) *Poor tack.* Addition of low molecular weight polymers and plasticizers, or addition of tackifiers are mandatory to obtain adequate tack.
- (3) *Excellent flexibility.* Solution SBRs show superior flexibility.
- (4) *Poor resistance to oils and organic solvents.* SBR swells in organic solvents and absorbs oils. Vulcanization is necessary to increase oil and organic solvent resistance.
- (5) *Poor ageing.* This is due to the existence of carbon-carbon double bonds. However, the ageing is better than for natural rubber.
- (6) *Low cost.* Emulsion SBRs are inexpensive compared to most synthetic rubbers.
- (7) *Wide substrate range.* SBRs stick to most surfaces, including polyolefins.

5.3.2. Additives and modifiers

SBR latex and solid SBR have similar ingredients, except for the use of thickeners (only for latex). The major ingredients, in addition to the elastomer, for the SBR adhesives are given below.

(1) *Tackifiers*. SBRs have poor tack, so addition of tackifiers is necessary. The tackifier increases the wetting of the adhesive and also increases the glass transition temperature of the adhesive. Typical tackifiers for SBR adhesives are rosins, aromatic hydrocarbon resins, alpha-pinene, coumarone-indene and phenolic resins.

(2) *Plasticizers/oils*. These are added for several reasons: (a) to improve the compatibility between SBR and the other additives; (b) as extender (to reduce cost); (c) to soften the SBR; (d) to change the wetting properties. The most common additives are organic phosphates, phthalate esters and aromatic hydrocarbon oils.

(3) *Solvents*. Solvents are added for the same purposes as oils and plasticizers, and additionally may interact with the substrate (e.g. by partially dissolving the substrate surface). Aromatic and polar solvents are the most suitable.

(4) *Fillers*. In general, fillers are added to latices to reduce cost, increase volume or weight and/or to modify properties. Addition of fillers produce changes in colour, density, rheology and mechanical properties (increase in stiffness or modulus in the adhesive). Addition of fillers to SBR latices needs the pre-addition of wetting agents and surfactants to facilitate the distribution of filler. Calcium carbonate, clays and silicas are the most typical fillers for SBR adhesives. Barite can be added to increase density. Colour can be controlled by adding titanium dioxide, carbon black or iron oxides.

(5) *Stabilizers*. Antioxidants provide protection against UV light and thermal oxidative degradation. Hindered phenols are the most common nonstaining antioxidants. For SBR latices, two additional type of stabilizers must be used.

(a) Bactericidal agents.

(b) Colloid stabilisers. Three classes can be distinguished:

- Surfactants. These enhance the colloid stability against mechanical and chemical stresses, help to disperse fillers, aid in wetting and enhance foaming. The most common surfactants are dodecylbenzene sulphonates and potassium oleate.

- Wetting agents. These facilitate the wetting of surfaces and aid colloidal stability without foaming. Naphthalene sulphonate/formaldehyde is the most common wetting agent.

- Sequestrants. These protect SBR latex from ions through complex formation. EDTA (ethylenediamine tetraacetic acid) is the most common.

(6) *Thickeners*. They modify the viscosity of SBR latices and control water loss on the substrate surfaces during drying. Several types of thickeners can be used:

natural (starch, gums, alginates), modified natural (carboxymethyl cellulose), and synthetic (polyacrylates) materials.

(7) *Other additives*. It is often necessary to add an antifoaming agent, such as silicones or mineral oils.

(8) *Curing systems*. In general, SBR latices do not require curing agents. However, if curing systems have to be added, there are several choices. For non-carboxylated SBR latex, sulphur or phenolic curing systems can be used. For carboxylated SBR latices some cross-linking agents can be used (melamine formaldehyde, zinc oxide).

5.3.3. Formulation of SBR adhesives

Specific formulations of SBR adhesives are given in the chapter by Midgley and Rea in the *Handbook of Adhesives* [8].

5.3.4. Applications

SBR adhesives can be used as latices or as solvent-borne, pressure-sensitive and tape adhesives.

SBR latex is mainly used in the tufted carpet industry. Carboxylated SBR latex is compounded with up to 500 phr of calcium carbonate or limestone to secure the tufts in the backing and as an adhesive for the secondary backing. The adhesive is normally dried under IR lamps or using hot-air circulating ovens. SBR latices can also be used in laminating or doubling operations in textile, packaging and automotive industries. SBR latices are also employed in construction as wall tile and vinyl floor tile adhesives. In combination with natural rubber, SBR latex is used for coating tire cord.

Solid SBR finds major use as solvent-borne and pressure-sensitive adhesives. Solvent-borne SBRs are widely used as a high-viscosity product for bonding flooring to joists and panels to studs, thereby reducing the amount of nailing and alleviating floor squeaks. On the other hand, sprayable adhesives for tire building and retreading, and the bonding of expanding polystyrene (solvent should be carefully selected to avoid cell collapse in polystyrene) are two major applications. The adhesive must always be applied to the two surfaces to be joined and it should be evaporated before or during the bonding process.

5.4. Nitrile rubber (NBR) adhesives

NBR adhesives are characterized by high resistance to oils and plasticizers, excellent heat resistance and superior adhesion to metallic substrates.

There are several NBRs for adhesive and cement applications, so they should

be properly selected. NBRs containing high acrylonitrile content show outstanding bonding and film properties. Mooney viscosity is related to the bond strength of NBRs, and thus the higher the Mooney viscosity, the higher the strength of the cement adhesive.

Depending on the particular NBR, milling prior to cement preparation can be required. Milling on tight and cold mill rolls is the best way to render NBR soluble in organic solvents. Just after milling, NBR should be put in solution as solubility in milled NBR decreases as time increases.

5.4.1. Properties of NBR adhesives

In general, the NBR adhesives show the following characteristic properties.

(1) *Superior resistance to oils.* NBR has the highest resistance of any of the general elastomers. NBR resists most greases and non-polar solvents.

(2) *High temperature resistance.* If cured, NBR can easily perform at 150–175°C.

(3) *Structural strength.* Combined with phenolic resins or epoxies, high shear strength can be obtained in joints produced with aluminium and other substrates.

(4) *Low initial tack.* NBR needs addition of tackifiers.

(5) *Excellent ageing properties.* The polymer structure combined with adequate antioxidants produces excellent ageing resistance.

(6) *Resistance to moisture and chemicals.* NBR latices show poor resistance to moisture and chemicals than solvent, hot-melt and film NBR grades.

(7) *Good flexibility and tensile strength.* Both properties are improved after curing is produced.

(8) *Medium-to-high cost.*

(9) *Wide substrate range.* NBR adhesives are adequate to bond highly polar surfaces (steel, aluminium) but bond poorly to low-polar surfaces (polyethylene, natural rubber).

5.4.2. Additives and modifiers

NBR is a polar polymer and shows superior compatibility with resins as compared to other elastomers. The major ingredients, in addition to the elastomer, for the NBR adhesives are given below.

(1) *Tackifiers.* Phenolic resins are added to increase strength, oils resistance and resiliency of NBR adhesives. On the other hand, tack and adhesive properties can be improved by adding chlorinated alkyl carbonates. To impart tack, hydrogenated rosin resins and coumarone–indene resins can be added.

(2) *Plasticizers.* Addition of softeners to NBR improve tack and adhesion properties. The most common plasticizers are esters (dibutyl phthalate, tricresyl phosphate), ester gums, alkyd resins, etc.

(3) *Fillers*. They are generally added to reinforce NBR adhesives. However, fillers can be added to promote tack, to increase the storage life, to improve heat resistance or to reduce cost. The most common fillers are carbon blacks. Precipitated silica can be used in applications where black colour is not acceptable, but excessive amounts tend to reduce adhesion. Titanium dioxide can be used to impart whiteness, improves tack and extend storage life.

(4) *Solvents*. NBRs are soluble in aromatic hydrocarbons, chlorinated hydrocarbons, ketones, esters and nitroparaffin compounds. Solvents with high evaporation rate are acetone, methyl ethyl ketone, chloroform and ethyl acetate, among others. Solvents with slow evaporation rate are nitromethane, dichloropentenes, chlorotoluene, butyl acetate and methyl isobutyl ketone.

(5) *Antioxidants*. Amine antioxidants are generally added to NBR adhesives.

(6) *Thickening agents*. When pseudoplasticity is necessary in NBR adhesives (spread coating operations, sprayed cements), carboxylic vinyl polymers can be added.

(7) *Curing systems*. Curing agents are used when high strength and resistance against elevated temperature is a requisite in the NBR adhesives. Typical sulphur curing system are added (sulphur/benzothiazyl disulphide/zinc oxide). Accelerators based on zinc salts of thiuram disulphides are also added when curing is desired to be produced at low temperature.

5.4.3. Adhesion characteristics

NBR adhesives can be used at temperatures between 170°C and -40°C. Bond strength can run above 7 MPa and can provide structural bond to many substrates. Even without curing, NBR adhesives show excellent resistance to organic compounds, acids and alkalis.

5.4.4. Formulation of NBR adhesives

Nitrile rubber is compatible with phenol-formaldehyde resins, resorcinol-formaldehyde resins, vinyl chloride resins, alkyd resins, coumarone-indene resins, chlorinated rubber, epoxies and other resins, forming compositions which can be cured providing excellent adhesives of high strength, high oil resistance and high resilience. On the other hand, NBR adhesives are compatible with polar adherends such as fibres, textiles, paper and wood. Specific formulations of NBR adhesives can be found in [12].

5.4.5. Applications

Applications of NBR adhesives are based on the excellent elastomeric properties of the polymer coupled with its polarity, which provides good solvent resistance

and compatibility with other polymers. Organic solutions of NBR are the most common adhesives, although water-borne and pre-cast films can also be used.

Quite often, NBR adhesives are used to bond various kinds of gasketing (cork, fibre, foam, rubber, metal) to rigid superstructures, such as aircraft. Films cast from solution are often used to fabricate honeycomb structures for aircraft.

Applications of NBR adhesives can be divided in three groups: (1) solely nitrile rubber; (2) nitrile rubber/phenolic blends; (3) nitrile rubber/epoxy blends.

(1) *Nitrile rubber adhesives*. The main application corresponds to laminating adhesives. PVC, polyvinyl acetate and other polymeric films can be laminated to several metals, including aluminium and brass, by using NBR adhesives. NBR adhesives can also be used to join medium-to-high polarity rubbers to polyamide substrates. The adhesive properties of NBR rubbers can be further improved by chemical modification using polyisocyanate or by grafting with methyl methacrylate.

NBR latices can be also used in adhesive applications. The use of latex has the advantage of avoiding the previous solution of the polymer before application and has favourable environmental effects. Compounding with a resorcinol-formaldehyde solution allows one to bond nitrile rubber to cotton or rayon fabric. Nitrile latex can be mixed with PVC latex to give excellent adhesion of polypropylene carpet and plywood backings. Combinations of nitrile latices and styrene butadiene latices provide good laminating bonds for saturated paper and woven fabrics. On the other hand, a versatile adhesive for manufacture of laminates can be obtained by mixing a nitrile latex with a high melting thermoplastic resin called Vinsol [12]. This mixture shows good wettability and improved specific adhesion to metal surfaces, and improve water resistance and moisture vapour transmission of the adhesive film.

(2) *Nitrile rubber/phenolic resin blends*. Blends of equal parts by weight of a nitrile rubber and a phenolic resin in methyl ethyl ketone (at a 20–30 wt% total solids content) is suitable for many adhesive purposes. The more phenolic resin in the formulation, the greater the bond strength and brittleness of the NBR adhesive [67]. Table 10 shows the effect of phenolic resin on nitrile rubber properties. On the other hand, the higher the acrylonitrile content in the rubber,

Table 10

Effect of the phenolic resin content in the mechanical properties of nitrile rubber

Phenolic resin (phr):	50		80		100	
Cure time at 154°C (min):	15	45	15	45	15	45
Tensile strength (psi)	2700	2900	3350	3800	4400	4250
Elongation at rupture (%)	250	200	150	150	100	50

Formulation: 100 phr *Hycar OR-25EP*; different amounts of phenolic resin; 5 phr zinc oxide; 1.5 phr sulphur; 1.5 phr benzothiazol disulphide; 1.5 phr stearic acid [68].

the greater the compatibility with phenolic resins and superior bonding and film properties. Rubbers with lower acrylonitrile content produce adhesives with better low-temperature properties.

Nitrile rubber/phenolic resin blends produce one of the most durable and toughest elastomeric materials developed in the adhesive industry. Further, its resistance to water and to organic solvents is excellent. For these reasons, the nitrile rubber/phenolic resin laminates are used in printed circuit board manufacturing, to bond metallic substrates between themselves (aluminium, steel), and to bond rubber to magnesium. Films of nitrile rubber/phenolic blends have also been used in the aircraft industry for bonding metal to metal surfaces in both plain and honeycomb sandwich constructions. Other applications reported are the bonding of PVC to steel, aluminium foil and copper, the bonding of leather to leather, and for rubber-to-rubber bonding.

(3) *Nitrile rubber/epoxy resin blends*. The flexibility and good low-temperature properties of nitrile rubber is combined with the excellent strength of epoxies in nitrile rubber/epoxy resin blends. These blends were first developed in 1955 and found applications in laminating and structural bonding. The nitrile rubber/epoxy resin blends were developed to meet the need for more temperature-resistant adhesives for aircraft applications. A typical formulation contains the nitrile rubber and the epoxy resin, a high loading of aluminium powder (to retrieve oxygen), and an amine curing agent. A unique feature of this type of adhesive is that the strengths are obtained at relatively low cure temperature (below 100°C).

Elastomers, plastics, fabrics, wood and metals can be joined with themselves and with each other using nitrile rubber/epoxy resin blends cured with amines and/or acidic agents. Ethylene-propylene vulcanizates can also be joined using blends of carboxylated nitrile rubber, epoxy resin and a reactive metal filler (copper, nickel, cobalt). However, one of the largest areas of use of nitrile rubber modified epoxy systems is in the printed circuit board area [12].

Flexibilized epoxy resins are important structural adhesives [69]. Liquid functionally terminated nitrile rubbers are excellent flexibilizing agents for epoxy resins. This liquid nitrile rubber can be reacted into the epoxy matrix if it contains carboxylated terminated functionalities or by adding an amine terminated rubber. The main effects produced by addition of liquid nitrile rubber in epoxy formulations is the increase in T-peel strength and in low-temperature lap shear strength, without reducing the elevated temperature lap shear.

5.5. Polychloroprene (neoprene) rubber (CR) adhesives

Polychloroprene rubber possesses the characteristics of natural rubber and has the advantage of higher polarity.

There are several excellent reviews on polychloroprene adhesives (for specific aspects see [2,14,70]).

5.5.1. Properties of CR adhesives

The general characteristics of the CR adhesives are the following.

- (1) *High green strength.*
- (2) *High ultimate strength.* Addition of phenolic resin is needed.
- (3) *Resistance to moisture, chemicals and oils.* Oil resistance is not as good as for NBR but better than for NR adhesives.
- (4) *Excellent temperature resistance.* With proper compounding, CR adhesives work between -40 and 175°C .
- (5) *Good resilience.* Resilience is better than for natural rubber.
- (6) *Excellent ageing properties.*
- (7) *Wide range of substrates.* CR adhesives bond to almost any high-polar surface, as well as many low-polar surfaces (including polyolefins).
- (8) *Curing system.* The most common room curing agent is zinc oxide. Isocyanates are also very common.

5.5.2. Additives and modifiers

Solvent-borne CR adhesives and polychloroprene latices will be considered separately.

5.5.2.1. Formulation of a solvent-borne CR. A typical formulation of a solvent-borne CR adhesive may include the following components (fillers are not commonly added and curing agents are added to improve heat resistance): (1) polychloroprene elastomer; (2) metal oxides; (3) resins; (4) antioxidants; (5) solvents; (6) fillers; (7) curing agents; (8) other modifiers.

(1) *Polychloroprene elastomer.* *Neoprene AC* and *AD* are the most commonly used, mainly *Neoprene AD* because of its superior viscosity stability. For difficult-to-bond substrates, graft polymers (*Neoprene AD-G* or *AF*) show better performance. For sprayable adhesives or high-viscosity mastics, the *Neoprene AG* offers excellent results. When specific properties (e.g. increase tack, improve wetting, increase peel strength) need to be met, blends of *Neoprene AC* or *AD* with *Neoprene AG* provide adequate performance.

(2) *Metal oxides.* Metal oxides provide several functions in solvent-borne polychloroprene adhesives.

- Acid acceptor. This is the main function of metal oxides in CR adhesive formulations. Upon age, small amounts of hydrochloric acid are released which may cause discolouration and substrate degradation. Magnesium oxide (4 phr) and zinc oxide (5 phr) act synergistically in the stabilization of solvent-borne polychloroprene adhesives against dehydrochlorination.
- Scorch retarder. Magnesium oxide retards scorch during mill processing of polychloroprene adhesives.

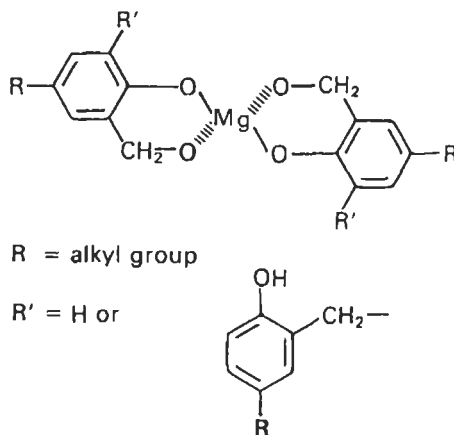


Fig. 36. Structure of magnesium oxide-phenolic resin complex.

- Curing agent. Zinc oxide produces a room temperature cure of solvent-borne CR adhesives, giving increased strength and improved ageing resistance. Magnesium oxide may also act as curing agent but a high amount (20–40 phr) is needed in CR adhesives formulations.
- Reactant for *t*-butyl phenolic resins. Magnesium oxide reacts in solution with *t*-butyl phenolic resin to produce an infusible resinate (Fig. 36) which provides improved heat resistance. The resinate has no melting point and decomposes above 200°C. Although oxides of calcium, lead and lithium can also be used, they are not as efficient as magnesium oxide and also tend to separate from solution. Where clear adhesive solutions are required epoxide resins, zinc-calcium resinates or zinc carbonate can be used.

(3) *Resins*. Addition of resins to solvent-borne CR adhesives serves to improve specific adhesion and autoadhesion, increase tack retention and increase hot cohesive strength. *Para-tertiary* butyl phenolic resins are the most common resins for solvent-borne CR adhesives. Amounts between 35 and 50 phr are generally added. In general, addition of 40–45 phr provides an adequate balance of tack and heat resistance. In general, tack decreases by increasing the phenolic resin content in the CR adhesive, and bond strength reaches a maximum at about 40 phr, decreasing for high amounts of phenolic resin [71].

The high heat resistance produced by adding phenolic resins to solvent-borne CR adhesives is due to the formation of the infusible resinate, which reduces the thermoplasticity of the adhesive and provides good bond strength up to 80°C (Table 11). The resinate also increases the adhesive bond strength development by accelerating solvent release. 4 phr of magnesium oxide for 40 phr of phenolic resin are sufficient to produce a room temperature reaction. A small amount of water (1–2 phr) is necessary as a catalyst for the reaction. Furthermore, the solvent

Table 11

Effect of resin type on heat resistance of solvent-borne CR adhesives

Resin: Solids content (%):	<i>t</i> -Butyl phenolic 24	Hydrocarbon 21	Terpene 26	Terpene phenolic 26
Canvas–canvas bond at R.T. (pli) ^a :				
After 1 day	31 (A)	10 (C)	10 (C)	16 (C)
After 7 days	46 (A)	25 (A)	4 (F)	30 (A)
Canvas–canvas bond at 80°C (pli):				
After 7 days at R.T.	5.5	0.5	0.5	0.5

Formulation: 100 phr *Neoprene AD-20*; 4 phr MgO; 5 phr ZnO; 2 phr hindered phenolic antioxidant; different amount and type of resins; 1 phr water; 100 phr hexane; 400 phr toluene [14].

^a Loci of failure: A, adhesion failure; C, cohesive failure of canvas; F, failure between films.

Table 12

Effect of solvent blend on the rate of magnesium oxide–phenolic resin reaction

Solvent	Reaction time (h)	Ash content of reacted resin (wt%)	Decomposition (D) or melt (M) of reacted resin (°C)
Toluene	1	6.5	250 (D)
	24	6.8	258 (D)
Toluene/ethyl acetate/ <i>n</i> -hexane (1/1/1 by weight)	24	6.9	255 (D)
	96	7.1	255 (D)
Toluene/ <i>n</i> -hexane (1/1 by weight)	24	6.9	264 (D)
Hexane	24	7.0	252 (D)
Acetone	24	0.4	181 (M)
Hexane/MEK	24	0.4	125 (M)
(1/1 by weight)	48	2.9	130 (M)
	72	6.1	226 (M)
	96	6.2	224 (M)

Formulation contained 100 phr elastomer, 10 phr MgO and 1 phr water. More than 6 wt% ash content and melting/decomposition temperature higher than 250°C indicates that a complete reaction is produced [14].

also affects the rate of the magnesium oxide and phenolic resin reaction. Thus, in toluene the reaction is very fast (about 1 h), whereas in polar solvents the reaction is slower (Table 12).

Solutions of polychloroprene adhesives containing metal oxides and *t*-butyl phenolic resin may show phasing (e.g. clear upper layer and flocculated lower layer of metal oxides) on standing for days or months. To recover the full utility

of metal oxides, agitation before use is sufficient. Phasing is ascribed to the wide molecular weight distribution of *t*-butyl phenolic resins. Commercial *t*-butyl phenolic resins with M_n of 900–1200 g/mol contains up to 15 wt% material with a molecular weight lower than 500 g/mol. This low molecular weight material accelerated the phase separation of magnesium oxide–phenolic resin adducts [72]. More precisely, phasing in solvent-borne CR adhesives has been ascribed to *p*-*tert*-butyl phenol dialcohol [73]. This was confirmed by fractionating out the low molecular weight material in the *t*-butyl phenolic resin and adding the resulting product to polychloroprene adhesive formulations. These formulations show no phase separation. Furthermore, phasing in solvent-borne CR adhesives can be minimized by selecting the solvent, optimizing milling time [14], and by adding small amounts of a trifunctional polyisocyanate [74].

Terpene phenolic resins can also be added to solvent-borne CR adhesives to increase open tack time and to provide a softer glue line than *t*-butyl phenolic resins. To provide adequate hot bond strength, these resins are used in combination with a polyisocyanate curing agent.

Chlorinated rubber is also used to promote the adhesion of solvent-borne CR adhesives to metals and plasticized PVC. Addition of a low molecular weight chlorinated rubber (containing about 65 wt% chlorine) improves the shear strength and creep resistance of polychloroprene adhesives [75] but a reduction in open time is also produced. A heat reactivation (process in which the surface of the adhesive film is raised to 90–100°C to destroy the crystallinity of the film and allowing diffusion to produce polymer chain interlocking more rapidly) restores tack to the polychloroprene adhesives.

Isocyanates can be added to solvent-borne CR adhesive solutions as a two-part adhesive system. This two-part adhesive system is less effective with rubber substrates containing high styrene resin and for butadiene–styrene block (thermoplastic rubber) copolymers. To improve the specific adhesion to those materials, addition of a poly- α -methylstyrene resin to solvent-borne CR adhesives is quite effective [76]. An alternative technique is to graft a methacrylate monomer into the polychloroprene [2].

(4) *Antioxidants*. A good antioxidant should be added to CR adhesives to avoid oxidative degradation and acid tendering of substrates. Derivatives of diphenyl amine (octylated diphenyl amine, styrenated diphenyl amine) provide good performance but staining is produced. To avoid staining, hindered phenols or bisphenols can be added. 2 phr antioxidant is sufficient in solvent-borne CR adhesives formulations.

(5) *Solvents*. Solvents affect adhesive viscosity, bond strength development, open time, cost, and ultimate strength. Blends of three solvents (aromatic, aliphatic, oxygenates, e.g. ketones, esters) are generally added, and in their selection environmental and safety regulations must be considered. A graphical method has been proposed to predict the most adequate solvent blends for solvent-borne CR

Table 13

Properties of solvents commonly used in polychloroprene adhesives formulations [77]

Solvent	Solubility parameter (δ) (Hildebrands)	Hydrogen bonding index (γ)	Relative evaporation rate ^a (mPa s)	Viscosity at 20°C
Acetone	10.0	5.9	1160	0.35
Cyclohexane	8.2	2.2	720	1.06
Ethyl acetate	9.1	5.2	615	0.44
Heptane	7.4	2.2	386	0.42
Hexane	7.3	2.1	1000	0.29
Isopropyl alcohol	11.5	8.7	300	2.41
MEK	9.3	5.4	572	0.42
Toluene	8.9	3.3	240	0.59
Xylene	8.8	3.5	63	0.69

^a Reference was taken with respect to *n*-butyl acetate = 100.

adhesives. This method is based in the solubility parameter (δ) and the hydrogen bonding index (γ) of each constituent solvent in the blend (Table 13). For each blend, δ and γ values are obtained by addition, considering the proportion in volume for each one.

Once the δ and γ values of a given blend are determined, the values are positioned in the graphic chart given in Fig. 37 [77]. The blends that fall within the kidney-shaped area yield good solutions with all solvent grade polychloroprene types, except for *Neoprene AH*, and those which fall outside that area will not dissolve the polychloroprene. The solvent blends which fall within the shadow area, may or may not dissolve the polychloroprene depending on the amount of toluene.

The open tack time of the CR adhesives partially depends on the evaporation rate of the solvent blend. If a solvent evaporates slowly, the CR adhesive will retain tack longer, whereas if the solvent evaporates quickly, the cohesive strength will develop more rapidly. According to Table 13, addition of small amounts of xylene (generally lower than 5%) will increase the open time of CR adhesives.

Solvent mixture also affects the application properties of the CR adhesives. Improved application properties are obtained by using a solvent blend which falls closer to the shady area of the kidney-shaped diagram of Fig. 37.

(6) *Fillers*. Fillers are not commonly added to CR adhesives. Calcium carbonate or clay can be primarily added to reduce cost in high-solids CR mastics. Maximum bond strength is obtained using fillers with low particle size (lower than 5 μm) and intermediate oil absorption (30 g/100 g filler). In general, fillers reduce the specific adhesion and cohesion strength of adhesive films. Although polychloroprene is inherently flame retardant, aluminium trihydrate, zinc borate, antimony trioxide or

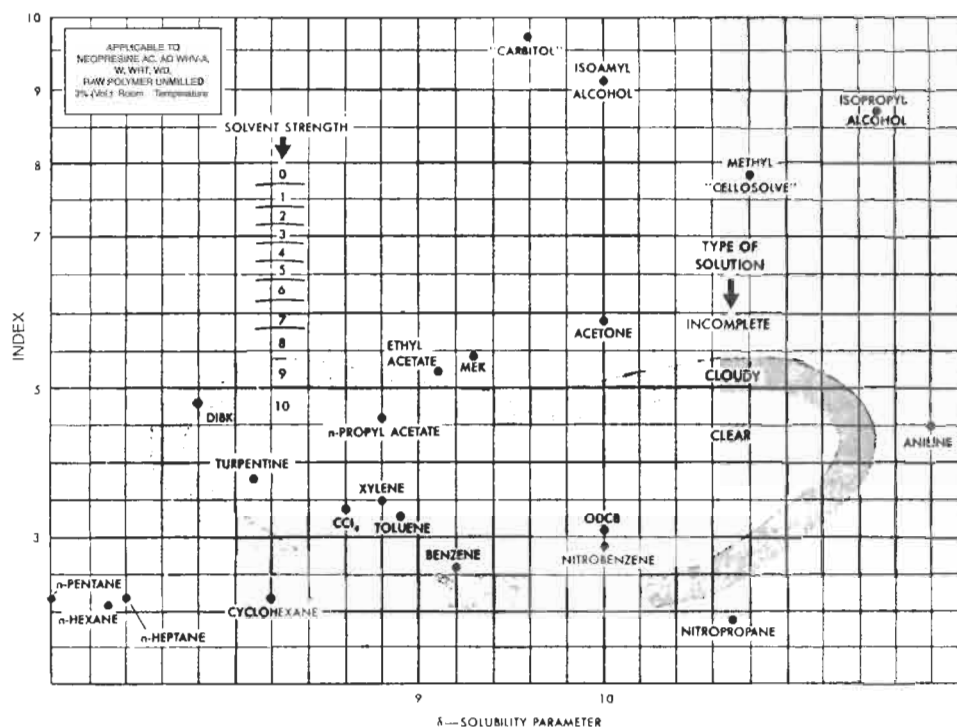


Fig. 37. Solvent strength chart [77].

Table 14

Effect of the addition of polyisocyanate to polychloroprene on ASTM softening point [2]

Isocyanate	Chemical name	Softening point (°C)
None (control)		40
<i>Desmodur R</i> ^a	<i>p,p',p''</i> -triisocyanato triphenylmethane	116
<i>Desmodur RF</i>	thiophosphonic acid tris(<i>p</i> -isocyanatophenyl) ester	97
<i>Desmodur RC</i>	polymeric isocyanate	92

^a *Desmodur* is a trade name from Bayer.

silane (mercapto or chlorosilanes) treated silicas can be added to further improve this property.

(7) *Curing agents*. Curing agents are generally added to CR adhesive formulations to increase heat resistance. Thiocarbanilide and polyisocyanates can be used as curing agents. Table 14 shows the different effectiveness produced with different polyisocyanates in the improvement of heat resistance. On the other hand, the reaction of an isocyanate with polychloroprene that leads to improved

heat resistance has not been fully explained. There are no active hydrogen atoms in the polychloroprene to allow reaction with the isocyanate group, so it has been proposed [2] that the small amount of 1,2 addition in the polymer chain provides allylic chlorine, which can be converted to hydroxyl during manufacturing of polychloroprene.

In formulations based on *Neoprene AF*, metal oxides act as room temperature curative agents, because of their reactivity with the polymer carboxyl functionality.

(8) *Other modifiers*. Although they are not common, additional ingredients can be added to polychloroprene adhesive formulations to improve specific properties.

- **Plasticizers**. Plasticizers can decrease the glass transition temperature, influence crystallization tendency and reduce cost. Highly aromatic mineral oils can be used when reduction in crystallization rate is required.
- **Stearic acid**. Improve processability and reduce mill sticking. Amounts of 0.5 to 1 phr can be added.
- **Resorcinol type resins**. Improve adhesion to textiles and metals.

5.5.2.2. *Polychloroprene latex adhesives*. The formulations of polychloroprene latex adhesives contain essentially the same components as the solvent-borne CR adhesives, except that water-based ingredients have to be used and the compounding is particularly exigent. The following ingredients can be found in most polychloroprene latex adhesive formulations.

(1) *Polychloroprene latex*. Anionic or non-ionic latices can be used. The polymer determines the initial tack and open time, the bond-strength development and hot bond strength, the application properties and the adhesive viscosity. Anionic latices are stabilized with rosin soaps. Carboxylated polychloroprene latex is stabilized with polyvinyl alcohol and provides better freeze–thaw stability than the anionic types [78].

(2) *Emulsifiers*. Non-compounded polychloroprene latex has good mechanical and storage stability, but the addition of other formulating ingredients may require the incorporation of additional surfactants, wetting agents or stabilizers. They function by strengthening the interfacial film by maintaining or increasing the degree of solvation, or by increasing the charge density on the latex particle. More precisely, surfactants are added to improve storage stability, substrate wetting and attain improved freeze resistance. Incorporation of surfactants has an adverse effect on cohesive properties and should be kept to a minimum. Water resistance and tack may also be affected [78]. Emulsifiers are used in polychloroprene latex adhesives to attain stabilization or to convert to liquid, water-insoluble chemicals (e.g. antioxidants, plasticizers) into emulsions. Excessive stabilization of the adhesive mixture may negatively affect coagulation (which is desirable in the wet bonding process). Anionic emulsifiers (alkali salts of long-chain fatty acids, and alkyl/aryl sulphonic acids) or non-ionic emulsifiers (condensation products of long-chain alcohols, phenols or fatty acids with ethylene oxide) can be used.

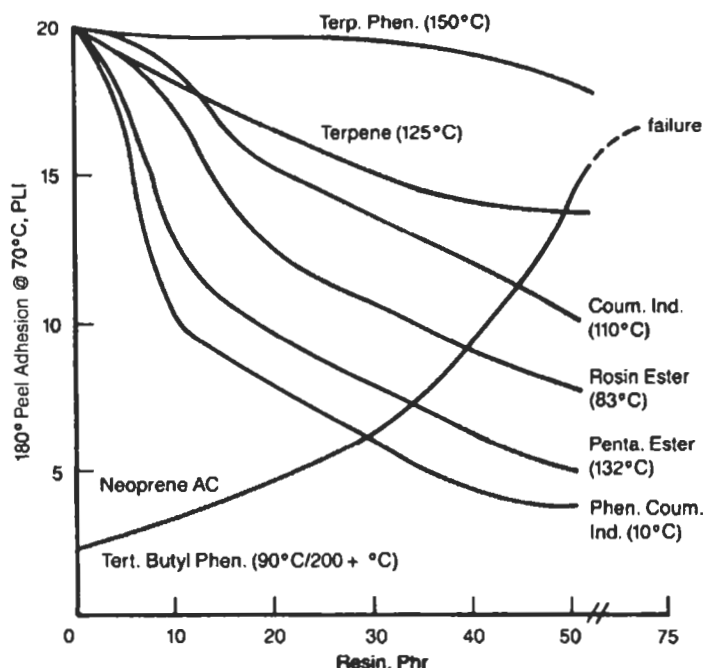


Fig. 38. Effect of resin type in *Neoprene latex 750* adhesives on canvas-to-canvas peel strength. Bonds aged 7 days at room temperature [14].

(3) *Metal oxides*. Zinc oxide is the most effective metal oxide. The zinc oxide should have a low lead content. Zinc oxide has three main functions: (a) promote cure; (b) improves ageing, heat and weathering resistance; (c) acid acceptor. In general, 2–5 phr zinc oxide is added in latex formulations.

(4) *Resins*. Resins influence the adhesion, open time, tack, contactability and heat resistance of polychloroprene latex adhesives. In general, 30–60 phr are added and attention should be paid to the pH and compatibility with the emulsifier systems. The glass transition temperature, the softening point, polarity and compatibility of the resin with the polymer determines the adhesive properties. Thus, hot-bond performance is generally proportional to the softening point of the resin. *t*-butyl phenolic resins cannot be used in polychloroprene latex adhesives because of the colloidal incompatibility. Terpene, terpene phenolic, coumarone-indene, and rosin acids and ester resins can be added to polychloroprene latex adhesive formulations. Fig. 38 shows the peel strength at 70°C of canvas-to-canvas joints against resin level with several different classes of resins.

Terpene phenolic resins can also be added to polychloroprene latex without great reduction in hot strength as the resin content is increased, but contactability is reduced. However, an adhesion failure is obtained, even at the 50 phr level. Furthermore, terpene phenolic resins have relatively poor tack and impart the best

resistance to elevated temperatures, but adhesives based on this class of resin require either heat reactivation or pressure to achieve adequate bond strength. Rosin ester resin emulsions are effective in latex adhesives. These resin emulsions extend the tack life of the polychloroprene latices, but they do not have the reinforcing characteristics of the terpene phenolic or alkyl phenolic resins. Hence, the cohesive strength and heat resistance are sacrificed to obtain surface tack.

(5) *Antioxidants*. Similar antioxidants as for solvent-borne CR adhesives can be used. Addition of antioxidants is important when resins sensitive to oxidation are included in polychloroprene latex formulations. 2 phr is the common amount of antioxidant in latex adhesives.

(6) *Thickeners*. Thickeners increase the viscosity of the polychloroprene latex adhesives. Amounts up to 1% of polyacrylates, methyl cellulose, alginates and polyurethane thickeners can be used. Particular attention should be paid to fluctuations in pH when thickener is added in the formulations. For low-pH (7–10) formulations, fumed silica or some silicates can be used.

(7) *Coagulants*. For some applications (e.g. plastic foam processing) sprayable polychloroprene latex dispersions must be used. In this process, a fast coagulation of latex particles is important to enable immediate bonding of the substrates with exceptional high initial strength. The most common coagulants are carboxylic acids (e.g. lactic acid, citric acid) or salts of multivalent metal ions (e.g. calcium chloride, calcium nitrate, zinc sulphate, aluminium sulphate).

(8) *Fillers*. Addition of fillers is not common in polychloroprene latex formulations. Fillers are used to reduce cost and control rheology, solids content and modulus. However, cohesion and adhesion are reduced. Calcium carbonate, clay and silica are some of the fillers than can be added. Alumina trihydrate is often used when resistance to degradation by flame is important.

(9) *Cross-linking agents*. Curing agents have little effect on the performance of latices with the highest gel content but are sometimes used with low-gel polymers to improve hot bond strength while maintaining good contactability. Suitable curing agents are thiocarbonyl, either alone or in combination with diphenylguanidine, zinc dibutyldithiocarbamate, and hexamethylenetetramine. Two-part systems are also being developed using more active materials such as aqueous suspension isocyanates (e.g. Desmodur VP KA 8768 from Bayer) and hexamethoxy melamine. These agents produce a cross-linking reaction at room temperature and give fast bond development, but exhibit a finite pot life.

The most common use of curing agents is with carboxylic latices. Isocyanates and melamines can be used but zinc oxide is the most common curing agent. Zinc oxide cross-links carboxylated latices and improves bond strength by ionomer formation [78]. Carboxylated polychloroprene reacts slowly with zinc oxide in dispersed form, causing a gradual increase in adhesive gel content. This can lead to restricted adhesive shelf life. Resin acid sites compete with the polymer acid sites for Zn(II). The more resin acid sites, the more stable the adhesive.

(10) *Other ingredients.* Bacterial and fungal attack can be a problem in polychloroprene latex formulations with pH below 10. It is manifested by odour, discolouration and gas evolution; 500–1500 ppm of a biocide should be added.

5.5.3. *Forms of CR adhesives*

About two-thirds of the CR adhesives are solvent dispersions. Solids content ranges from 5 to 90 wt%, the most common range being 15–30 wt%. Properly compounded solvent-borne CR dispersions are resistant to degradation by heat, sunlight, ozone, water, oils and chemicals. Solvent selection allows a great variation in adhesive viscosity and drying rate. Compounding with resins allows specific adhesion to many porous and nonporous substrates to be produced.

Water-borne contact adhesives are growing in importance due to environmental regulations, occupational health and the flammability of solvents. The solids content in the water-borne polychloroprene adhesives varies between 40 and 60 wt%, and viscosities between 15 and 500 mPa s can be obtained. Although polychloroprene latices are water-based they are generally flammable as the resin is dissolved in organic solvents before emulsifying. Thus, these systems combine the two disadvantages of the slowly drying latex system with the flammability of the solvent cement. On the other hand, all polychloroprene latices are susceptible to coagulation by mechanical, thermal and chemical means. To produce a stable adhesive, low-shear mixers are preferred.

It has to be kept in mind that the polymer properties desired in polychloroprene latex formulations may be totally different from those needed in dry grades. Polychloroprene latices generally exhibit lower contactability than dry polychloroprenes because of the presence of residual soaps and salts, appreciable gel content and segregation of tackifier [79]. For this reason, the polychloroprene latices have usually medium to low crystallinity.

Although pressure-sensitive and hot-melt adhesives can be manufactured, they are not common because lower-cost formulations using other elastomers can be prepared.

5.5.4. *Formulation of CR adhesives*

Specific formulations of CR adhesives can be found in Ref. [14].

5.5.5. *Adhesion characteristics*

The properties of the *solvent-borne CR adhesives* depend on the molecular weight, degree of branching and rate of crystallization of the polymer. The ability of polychloroprene adhesives to crystallize is unique as compared to other elastomers. The higher the crystallization rate, the faster the adhesive strength development.

The crystallization is responsible for the quick grab of polychloroprene adhesives. This rapid bond strength development allows the formation of immediate dry bonds without the need of clamping or pressing.

Bond strength can vary from a temporary bond (non-curing compound) to a substrate tearing bond (using phenolic-modified curing products). Solvent-borne CR adhesives can be formulated to have very short open times for fast production operations or to retain contact bond characteristics for up to 24 h. Heat and solvent reactivation can be used to re-impart tack to dried surfaces.

Grafting of acrylic moieties on polychloroprene improves the adhesion properties of solvent-borne adhesives [80]. IR and NMR spectroscopy studies have shown that the mechanism of grafting is a chain transfer as evidenced by the decrease in chlorine content in the graft copolymers [81]. The adhesive formulation containing the graft-polychloroprene exhibited higher peel strength and shear strength in joints produced between upper leather and sole leather.

Latex systems derive their strength characteristics from the gel structure rather than crystallinity as in solution systems. In general, higher gel content leads to the same properties as polymers with higher crystallinity [79]. Polymers with a higher gel content exhibit higher cohesive strength, modulus and heat resistance. Tack, open time and elongation are reduced. An important difference between gel content and crystallinity is that the effects caused by gel content will not disappear as the polymer is heated.

5.5.6. Applications of CR adhesives

Applications of solvent-borne CR adhesives and polychloroprene latices will be considered separately.

(1) Solvent-borne CR adhesives allow almost any two substrates to stick together. The adhesives are extensively used in bonding high-pressure plastic laminates, automotive adhesives, adhesives for construction and shoe adhesives.

Shoe adhesives. CR adhesives are used for the permanent attachment of shoe soles. For difficult-to-bond sole materials (plasticized PVC, EVA foaming soles, thermoplastic rubber, SBR) graft polymer solutions of *Neoprene AD-G* combined with a polyisocyanate provide a good adhesion. Another major area for CR contact adhesives is the manufacture of leather goods, particularly leather shoe sole bonding and belt lamination.

Automotive adhesives. CR adhesives are used to bond recreational vehicle sidewalls, for vinyl trim bonding in panels, and to bond in place truck and trailer roofs.

High-pressure laminates. Solvent-borne CR adhesives are used for bonding foams to wood or fabric, and for bonding metal, fibreglass and plastics.

Construction. CR adhesives find uses in countertops and panel fabrication for curtain walls and partitions. Other large volume applications are the joining of

gypsum dry walls (wallboard), and the joining of core materials in flush doors and curtain wall panels.

(2) Polychloroprene latices are mainly used for high-pressure lamination, for foam bonding and for vinyl adhesion [82]. Also they are used for foil lamination, carpet installation, and PVC floor tile bonding.

High-pressure lamination constitutes a large market for water-borne polychloroprene adhesives. The choice of the polymer has a high impact on end-use properties.

Bonding and shaping of foams are produced with high crystallizable water-borne polychloroprene adhesives. Both one-part and two-part adhesives are used. In both processes, the adhesive is sprayed on the foam and immediately after the foam pieces are placed in contact. The assembly is wet-bonded because no drying is necessary as the water will dissipate into the foam. One-part technology relies on the deliberately unstabilized latex by reducing the adhesive pH to 9.0; the latex is sufficiently stable at that pH to permit spraying but unstable enough to coagulate under light pressure. Further, an antimicrobial agent must be added to prevent bacterial contamination with this low-pH adhesive. However, these adhesives have only moderate hot-bond strength (typically fail below 100°C) which is an important limitation for automotive-interior applications. New polychloroprene latices grades have been recently developed for this purpose [82].

Solvent-borne polychloroprene adhesives are unsuitable for bonding low-energy substrates, such as PVC. However, water-borne polychloroprene adhesives display good peel adhesion to *vinyl substrates*. Addition of an accelerator such as zinc oxide is essential for improved hot bond strength.

6. Summary

This chapter reviews the main aspects of rubber base adhesives. A detailed description of the main ingredients of rubber base adhesive has been given because most of the previous contributions in this area did not consider this important aspect. On the other hand, update of the literature in water-base rubber adhesives has been done.

Acknowledgements

Information provided by Mr. Juan José Hernández-González from Adhesivos Hernán (León, Mexico) on water-borne polychloroprene adhesives is greatly acknowledged. The financial support for research in rubber adhesives from the Spanish Research Agency (MCYT) and the University of Alicante is greatly appreciated. Finally, my deep recognition and acknowledgement to my wife and children for the time I took from them to write this chapter.

References

1. Campion, R.P., *J. Adhes.*, **7**, 1 (1974).
2. Whitehouse, R.S., In: Wake, W.C. (Ed.), *Synthetic Adhesives and Sealants*. John Wiley, Chichester, 1986, pp. 1–29.
3. Coe, D.G., Neoprene solvent based adhesives. Technical Bulletin ADH-100.1 (R1), E.I. Du Pont de Nemours.
4. Gazeley, K.F. and Mente, P.G., Pressure-sensitive adhesives from modified natural rubber latex. *Adhesives, Sealants and Encapsulants Conference*, Kensington, London, 5th November, 1985.
5. Higgins, J.J., Jagish, F.C. and Stucker, N.E., In: Skeist, I. (Ed.), *Handbook of Adhesives*, 3rd ed. Chapman and Hall, New York, 1990, pp. 185–205.
6. Buckley, D.J., *Rubber Chem. Technol.*, **32**, 1475 (1959).
7. Gunner, L.P., *J. Adhes. Sealant Counc.*, **1**, 23 (1972).
8. Midgley, C.A. and Rea, J.B., In: Skeist, I. (Ed.), *Handbook of Adhesives*, 3rd ed. Chapman and Hall, New York, 1990, pp. 227–238.
9. Robinson, H.W., In: *Kirk-Othmer Encyclopedia of Chemical Technology*, Vol. 8, 3rd ed. John Wiley, New York, 1979, pp. 534–546.
10. Morrill, J.P., In: Bobbitt, R.O. (Ed.), *Vanderbilt Rubber Handbook*. RT Vanderbilt Co., Norwalk, CN, 1978, pp. 169–187.
11. Hoffmann, W., *Rubber Chem. Technol.*, **37**, 1 (1964).
12. Mackey, D.E. and Weil, Ch. E., In: Skeist, I. (Ed.), *Handbook of Adhesives*, 3rd ed. Chapman and Hall, New York, 1990, pp. 206–226.
13. Schmolke, R. and Kimmer, W., *Plaste Kautsch.*, **21**, 651 (1974).
14. Guggenberger, S.K., In: Skeist, I. (Ed.), *Handbook of Adhesives*, 3rd ed. Chapman and Hall, New York, 1990, pp. 284–306.
15. Snow, A.M., *Adhes. Age*, **23**, 35 (1980).
16. Autenrieth, J.S. and Foley, K.F., In: Skeist, I. (Ed.), *Handbook of Adhesives*, 3rd ed. Chapman and Hall, New York, 1990, pp. 556–570.
17. Skeist, I. (Ed.), *Handbook of Adhesives*, 2nd ed. Chapman and Hall, New York, 1977.
18. Zinkel, D.F. and Russell, J. (Eds.), *Naval Stores. Production, Chemistry, Utilization*. Pulp Chemical Association, New York, 1989.
19. McReynolds, R.D., Kossuth, S.V. and Clements, R.W., In: Zinkel, D.F. and Russell, J. (Eds.), *Naval Stores. Production, Chemistry, Utilization*. Pulp Chemical Association, New York, 1989, pp. 83–119.
20. Gardner, F.H. Jr., In: Zinkel, D.F. and Russell, J. (Eds.), *Naval Stores. Production, Chemistry, Utilization*. Pulp Chemical Association, New York, 1989, pp. 143–157.
21. McSweeney, E.E., In: Zinkel, D.F. and Russell, J. (Eds.), *Naval Stores. Production, Chemistry, Utilization*. Pulp Chemical Association, New York, 1989, pp. 158–195.
22. Soltes, E.J. and Zinkel, D.F., In: Zinkel, D.F. and Russell, J. (Eds.), *Naval Stores. Production. Chemistry, Utilization*. Pulp Chemical Association, New York, 1989, pp. 261–345.
23. Nyren, V. and Back, E., *Acta Chem. Scand.*, **12**, 1516 (1958).
24. Arimoto, K. and Zinkel, D.F., *J. Am. Oil Chem. Soc.*, **59**, 166 (1982).
25. Mildenberg, R., Zander, M. and Collin, G., *Hydrocarbon Resin*. VCH, Weinheim, 1997, p. 43.
26. Barrueso-Martínez, M.L., Ferrándiz-Gómez, T.P., Martín-Martínez, J.M., Arán-Aís, F., Torró-Palau, A. and Orgilés-Barceló, A.C., *Adhes. Age*, **44**, 32 (2001).

27. Ferrándiz-Gómez, T.P., Fernández-García, J.C., Orgilés-Barceló, A.C. and Martín-Martínez, J.M., *J. Adhes. Sci. Technol.*, **11**, 1303 (1997).
28. Hawley, G.G., *Condensed Chemical Dictionary*, 9th ed. Van Nostrand Reinhold, New York, 1977, p. 223.
29. Ferrándiz-Gómez, T.P., Fernández-García, J.C., Orgilés-Barceló, A.C. and Martín-Martínez, J.M., *J. Adhes. Sci. Technol.*, **10**, 1383 (1996).
30. Wherry, R.W., Resin dispersions for water based pressure sensitive adhesives. *Pressure Sensitive Tape Council Seminar* (May, 1979).
31. Dalhquist, C.A., Adhesion: fundamentals and practice. *Proceedings of Nottingham Conference on Adhesion*. McLaren, London, 1966.
32. Aubrey, D.W. and Sherriff, M., *J. Polym. Sci.*, **16**, 2631 (1978).
33. Class, J.B. and Chu, S.G., *J. Appl. Polym. Sci.*, **30**, 805 (1985).
34. Ferrándiz-Gómez, T.P., Fernández-García, J.C., Orgilés-Barceló, A.C. and Martín-Martínez, J.M., *J. Adhes. Sci. Technol.*, **10**, 833 (1996).
35. Doolittle, A.K., In: Bruins, P.F. (Ed.), *The Technology of Solvents and Plasticizers*. Reinhold, New York, 1965, Ch. 1.
36. Pizzoli, M. and Scandola, M., In: Salamone, J.C. (Ed.), *Polymeric Materials Encyclopedia*, Vol. 7. CRC Press, Boca Raton, FL, 1996, pp. 5301–5308.
37. Katz, H.S. and Milewski, J.V. (Eds.), *Handbook of Fillers and Reinforcements for Plastics*. Van Nostrand Reinhold, New York, 1978.
38. Wypych, G., *Handbook of Fillers*, Ch. 4. ChemTec Publishing, Toronto, ON, 2000.
39. Torró-Palau, A., Fernández-García, J.C., Orgilés-Barceló, A.C., Pastor-Blas, M.M. and Martín-Martínez, J.M., *J. Adhes. Sci. Tech.*, **11**, 247 (1997).
40. Nargiello, M. and Bush, G.J., *Adhes. Age*, **38**, 45 (1995).
41. Torró-Palau, A.M., Fernández-García, J.C., Orgilés-Barceló, A.C., Pastor-Blas, M.M. and Martín-Martínez, J.M., *J. Adhes.*, **61**, 195 (1997).
42. Balard, H. and Papirer, E., *Prog. Org. Coatings*, **22**, 1 (1993).
43. Assai, S. and Sumita, M., *J. Macromol. Sci. B*, **34**, 283 (1995).
44. Domka, L., *Colloid Polym. Sci.*, **272**, 1190 (1994).
45. Krysztafkiewicz, A., Rager, B., Maik, M. and Szymanowski, J., *Colloid Polym. Sci.*, **272**, 1526 (1994).
46. *Basic characteristics of Aerosil*. Degussa Bulletin 11. Degussa, Hanau, 1997.
47. Zaborski, M., Slusarski, L., Donnet, J.B. and Papirer, E., *Kautsch. Gummi, Kunstst.*, **47**, 730 (1994).
48. Norman, D.T., In: Ohm, R.F. (Ed.), *The Vanderbilt Rubber Handbook*, 13th ed. R.T. Vanderbilt Company, Norwalk, CN, 1990, pp. 397–422.
49. Kermadjian, J., *Adhes. Age*, **5**, 34 (1962).
50. Hauser, R.L., Coles, B.A., Elverum, J.A. and Hyta, R.C., *Adhes. Age*, **37**, 36 (1994).
51. Bolland, J.L., *Q. Rev. Chem. Soc.*, **3**, 1 (1949).
52. Shelton, J.R. and Vincent, D.N., *J. Am. Chem. Soc.*, **85**, 2433 (1963).
53. Chakaraborty, K.B. and Scott, G., *Eur. Polym. J.*, **15**, 731 (1977).
54. Al-Malaika, S., In: Cheremisinoff, N.P. (Ed.), *Handbook of Polymer Science and Technology*, Vol. 2. Marcel Dekker, New York, 1989, pp. 261–290.
55. Gent, A.N., *J. Appl. Polym. Sci.*, **6**, 497 (1962).
56. Bobbitt, R.O. (Ed.), *The Vanderbilt Rubber Handbook*, 13th ed. R.T. Vanderbilt Company, Norwalk, CN, 1990.
57. Al-Malaika, S., In: Salamone, J.C. (Ed.), *Polymeric Materials Encyclopedia*, Vol. 1. CRC Press, Boca Raton, FL, 1996, pp. 314–327.

58. Latimer, R.P., Layer, R.W. and Rhee, C.K., In: Cheremisinoff, N.P. (Ed.), *Handbook of Polymer Science and Technology*, Vol. 2. Marcel Dekker, New York, 1989, pp. 243–260.
59. Gazeley, K.F. and Wake, W.C., Natural rubber adhesives. In: Skeist, I. (Ed.), *Handbook of Adhesives*, 3rd ed. Chapman and Hall, New York, 1990, pp. 167–184.
60. De, S.K., Natural rubber-based adhesives. In: Pizzi, A. and Mittal, K.L. (Eds.), *Handbook of Adhesive Technology*. Marcel Dekker, New York, 1994, pp. 315–318.
61. Skeist, I. (Ed.), *Handbook of Adhesives*, 3rd ed. Chapman and Hall, New York, 1990.
62. Yarusso, D.J., Rivard, R.J. and Ma, J., *J. Adhes.*, **69**, 201 (1999).
63. Rao, C.L. and Connor, J.J., *J. Adhes.*, **43**, 179 (1993).
64. McElrath, K.O. and Robertson, M.H., *Adhes. Age*, **38**, 28 (1995).
65. Hubbarb, M., Biddell, B.J. and Fischer, D.K., US Patent 5,234,987, August 10, 1993.
66. Paterson, D.A., *Adhes. Age*, **12**, 32 (1969).
67. Lindner, G.F., Schmelzle, A.F. and Wehmer, F., *Rubber Age*, **56**, 424 (1949).
68. De Lollis, N.J., *Adhesives. Adherends, Adhesion*. Robert E. Krieger Publ., Malabar, FL, 1970.
69. Pocius, A.V., *Rubber Chem. Technol.*, **58**, 622 (1985).
70. Harrington, W.F., *Engineered Materials Handbook. Adhesives and Sealants*, Vol. 3. ASM International, 1990, pp. 143–150.
71. Ackerman, O., *Adhäsion*, **23**, 172 (1979).
72. Garrett, R.R. and Lawrence, R.L., *Adhes. Age*, **9**, 22 (1966).
73. Tanno, T. and Shibuya, L., Special behaviour of para tertiary phenol dialcohol in polychloroprene adhesives. *Adhesives and Sealant Council Meeting*, Spring 1967.
74. E.I. Du Pont de Nemours, *Colloidal stable solvent cement compositions comprising chloroprene polymers, phenolic resins and polyisocyanate*, U.S. Patent 3,318,834, 9 May, 1967.
75. Grant, I., *Adhes. Age*, **11**, 32 (1968).
76. Kelly, D.J. and McDonald, J.W., Solution compatibility of Neoprene with elastomers and resins. *Du Pont Elastomers Bulletin*, October, 1963.
77. Solvent systems for Neoprene – Predicting solvent strength. *Du Pont Elastomers Bulletin*.
78. Lyons, D.F. and Christell, L.A., *Adhes. Sealants Ind.*, December/January, 28 (1997/1998).
79. Lyons, D. and Christell, L.A., *Adhes. Sealants Ind.*, August, 45 (1997).
80. Jannasch, P. and Wessler, B., *J. Polym. Sci. Chem. Ed.*, **A33**, 1465 (1995).
81. Radhakrishnan, N., Periyakaruppan, P. and Srinivasan, K.S.V., *J. Adhes.*, **61**, 27 (1997).
82. Lyons, D.F. and Christell, L.A., *Adhes. Sealants Ind.*, February, 41 (1998).

Fundamental aspects of adhesion technology in silicones

B. PARBHOO *, L.-A. O'HARE and S.R. LEADLEY

Dow Corning Ltd, Barry, UK

1. Introduction

Silicones are used in numerous products, applications, and processes across all industries [1–3]. These polymeric materials combine organic and inorganic character and possess unique physical, chemical, and mechanical properties that are unmatched by any other polymeric materials. Their success in a multitude of technologies is due to a range of properties that include low surface energy, hydrophobicity, chemical resistance, electrical insulation, resistance to weathering, stability to extremes of temperature, resistance to thermal shocks, high elasticity, good tear strengths, capability to seal or bond materials of various natures, biocompatibility, etc. The wide range of polymer molecular structures and chemical functional groups that are possible with silicones further supports their commercial success [1,4]. They can be used as pure polymers or crosslinked to form silicone rubbers [1,5] and resins [1,6]. Silicones address the most demanding needs required by modern, emerging, and future technologies. They have opened ways to applications in fields as varied as aerospace, automobile, building, electronic, energy, healthcare, medical, paper, personal care, plastics, and textiles, to name a few.

Another unique feature of silicones is the possibility of modifying the molecular structure of polymers and composing formulations that will provide specific adhesion properties. This feature led to the development of products where adhesion ranges from very low to very high strength. Typical examples of products where low adhesion strength has led to new product technologies include silicone rubber [7,8] used to mold organic parts, silicone release coatings for organic pressure sensitive adhesives (PSA), and silicone PSAs [9–11]. Product technologies that have high adhesion strength include elastomeric adhesives and sealants. In

* Corresponding author. E-mail: bhukan.parbhoo@dowcorning.com

each of these applications, the adhesion of silicones has been combined with their other unique properties to provide a range of unique product technologies.

The surface of the substrate, the silicone/substrate interface, and the bulk properties of silicones all play significant and influential roles that affect practical adhesion and performance of the silicone. The design of silicone adhesives, sealants, coatings, encapsulants or any products where adhesion property is needed requires the development chemist to have a thorough understanding of both silicone chemistry and adhesion phenomena.

Previous reviews on silicones in relation to adhesion have dealt with specific technologies such as adhesives, sealants, and coupling agents [12–17]. This review attempts to address the fundamental properties of silicones and to relate them to various aspects of adhesion technologies. The perspective taken in this review is from the point of view of a newcomer in the field of adhesion and silicones.

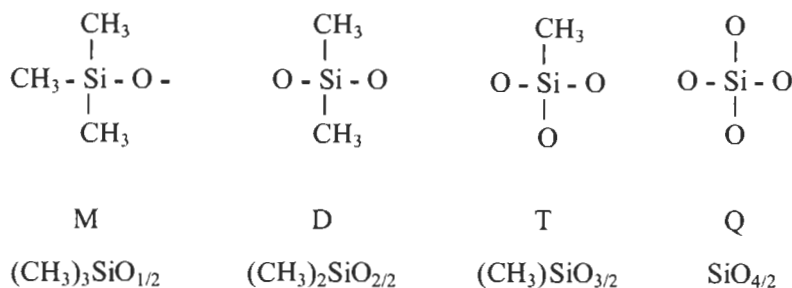
This chapter first reviews the general structures and properties of silicone polymers. It goes on to describe the crosslinking chemistry and the properties of the crosslinked networks. The promotion of both adhesive and cohesive strength is then discussed. The build up of adhesion and the loss of adhesive strength are explained in the light of the fundamental theories of adhesion. The final section of the chapter illustrates the use of silicones in various adhesion applications and leads to the design of specific adhesive and sealant products.

2. Silicone polymers

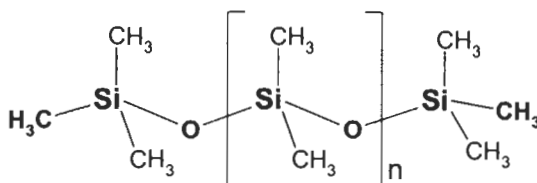
Silicone is the generic name of a unique class of polymers consisting of an inorganic backbone made of alternating silicon and oxygen atoms [1,18]. The Si–O bond, known as *siloxane* bond, confers to the polymer the name *polysiloxane*. The most commonly known silicone is based on the polydimethylsiloxane (PDMS), $(-[(CH_3)_2SiO]_n-)$. However, there are a variety of polysiloxane structures that can be synthesized, from simple linear to highly complex three-dimensional structures that can be further functionalized and designed for specific applications [19]. It is therefore important to discuss the nomenclature associated with silicones in more detail.

2.1. Structures of silicone polymers

A useful notation and abbreviation of the complex silicone structures takes advantage of the number of oxygen atoms around the silicon atom in a *siloxyl* unit [1]. This notation uses the letters M, D, T and Q to represent siloxyl units where the silicon atom is linked with one, two, three or four oxygen atoms, respectively (Scheme 1). Fractions are used in this notation to take into account an equal share of an oxygen atom with adjacent siloxyl monomeric units.



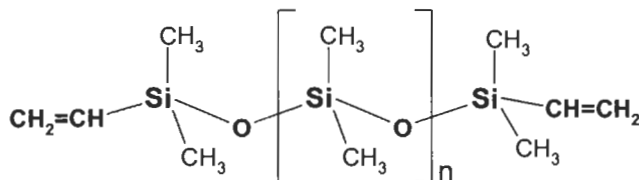
Scheme 1. Notation of siloxy units forming silicone polymers.

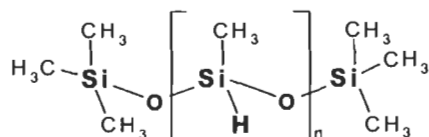
Scheme 2. Structure of trimethylsiloxy-endsblocked-polydimethylsiloxane (MD_nM).

It is generally considered in this notation that methyl groups are attached to silicon atoms. This nomenclature allows structures like trimethylsiloxy-endsblocked-polydimethylsiloxane (TMS-eb-PDMS) to be simply represented as MD_nM (Scheme 2).

When an organofunctional group replaces a methyl group on a siloxy unit, a superscript is used to describe the unit. The most common groups that are encountered can be symbolized as: alkyl (R), hydrogen (H), phenyl (Ph), hydroxyl (OH), trifluoropropyl (F), and vinyl (Vi). Thus, vinyl-endsblocked-PDMS is represented by $\text{M}^{\text{Vi}}-\text{D}_n-\text{M}^{\text{Vi}}$, (Scheme 3), and a trimethylsiloxy-endsblocked-polyhydrogenmethylsiloxane (TMS-eb-PHMS) is symbolized as $\text{M}-\text{D}_x^{\text{H}}-\text{M}$ (Scheme 4). Likewise, for copolymers, a vinyl-endsblocked-polydimethyl-co-methylvinyl-siloxane copolymer will be easily described as $\text{M}^{\text{Vi}}-\text{D}_x-\text{D}_y^{\text{Vi}}-\text{M}^{\text{Vi}}$. By defining the values of n , x and y , the description will be complete.

By combining M, D, T, and Q units, silicones can be made in a variety of structures, which include linear, branched, hyper-branched and cyclic forms.

Scheme 3. Structure of dimethylvinylsiloxy-endsblocked-polydimethylsiloxane ($\text{M}^{\text{Vi}}-\text{D}_n-\text{M}^{\text{Vi}}$).



Scheme 4. Structure of trimethylsiloxy-terminated-polydimethylsiloxane ($M-D^H_n-M$).

Linear polymers are the most commonly found, and consist of chains of D units endblocked by a variety of functionalized M units. Branched-chain silicones consist mainly of D units, with a D unit being replaced by a T or a Q unit at each point of branching. Cyclic PDMS oligomers are also common and can play a role in adhesion. They are usually found as mixtures of structures going from three siloxy units, to four, five, and higher siloxy units. A whole range of analytical techniques can determine the detailed molecular structures of these materials [20,21].

2.2. Properties of silicone polymers

The simultaneous presence of pendant organic groups attached to an inorganic backbone give silicones their unique combination of physical, chemical, and mechanical properties [1]. The low surface tension of liquid PDMS (ca. 20 mN m⁻¹) results from a combination of both the properties of organic side groups and the inorganic backbone [22–24]. The flexible nature of the inorganic backbone, where the energy required to rotate around bonds is practically zero, allows the minimum energy configuration to be easily attained [25]. The methyl groups are able to closely pack at the surface due to their low intermolecular forces and the large Si–O–Si bond angle (149° at equilibrium). The low critical surface tension of wetting of PDMS readily explains one of the most familiar features of silicone polymers: their excellent low adhesion that is at the origin of release behavior which prevents most materials from strongly adhering to them. Conversely, their low surface tension also means that they wet almost all surfaces, thus fulfilling the first requirement of any adhesive system.

The flexibility of the siloxane backbone, in addition to its large free volume and mobility, is used to explain the low glass transition temperatures (T_g –125°C) of PDMS [26]. The polymer also exhibits crystallization behavior [27,28] and displays a melting transition temperature (T_m –40°C) that is dependent on the rate of cooling. The large free volume and mobility of polysiloxanes give rise to a high diffusion coefficient and high permeability of gases or vapors. Oxygen, for example, diffuses through PDMS much more quickly than through other polymers. The particular case of water vapor is interesting. It has a low solubility value but passes through PDMS very quickly due to its high diffusion coefficient. This can be a potential problem for adhesion as water vapor can easily reach

interfaces and interfere with bonding and debonding chemistry, corrosion of metal substrate, cure rate, etc. On the other hand, water is necessary to enhance adhesion build-up at surface of substrates, ensuring complete hydrolysis–condensation reaction and therefore durable bond formation.

As another consequence of the properties of the siloxane bond, the value of n in the common linear trimethylsiloxy-endblocked-PDMS, (M–D_{*n*}–M) can vary from zero to tens of thousands giving a range of viscosity from 0.65 to 2,500,000 centipoise to the polymeric material. This relationship between viscosity and polymer chain length allows PDMS polymers to vary in form from ‘water-like’ fluids to a flowable gum, while retaining the same chemical character.

Another important property of silicones, and one that is particularly relevant to adhesion applications, is their high thermal stability compared to common organic polymers [19,26,29–31]. TMS-eb-PDMS polymers can stay unaffected up to 1000 h when exposed to air at 175°C and indefinitely to inert atmosphere. This outstanding thermal stability of silicone polymers can further be improved by partially replacing methyl groups by phenyl groups. Service temperatures can reach 175 and 260°C in air and nitrogen, respectively. Furthermore, these materials remain fluids at subzero temperatures down to –70°C. This stability towards thermal energy opened a new window of opportunities for silicone adhesives. However, the phenyl group introduces rigidity in the polymer chain and the viscosities of polymethylphenylsiloxane (PMPS) are significantly higher than the corresponding polydimethylsiloxanes.

A chemical property of silicones is the possibility of building reactivity on the polymer [1,32,33]. This allows the building of cured silicone networks of controlled molecular architectures with specific adhesion properties while maintaining the inherent physical properties of the PDMS chains. The combination of the unique bulk characteristics of the silicone networks, the surface properties of the PDMS segments, and the specificity and controllability of the reactive groups, produces unique materials useful as adhesives, protective encapsulants, coatings and sealants.

Silicone adhesives are generally applied in a liquid and uncured state. It is therefore the physical and chemical properties of the polymers, or more precisely of the polymer formulation, that guide the various processes leading to the formation of the cured silicone network. The choice of the cure system can be guided by a variety of parameters that includes cure time and temperature, rheological properties in relation with the application process, substrates, the environment the adhesive joints will be subjected to and its subsequent durability, and of course, cost.

3. Silicone networks

To convert an assemblage of freely moving long chain molecules into an elastic mass capable of sustaining shear and tension, it is necessary to link the chains together by introducing a number of connections or crosslinks between them [1,34]. Crosslinking linear silicone polymer chains results in the formation of a three-dimensional elastomeric network, which has its own physical, mechanical, and chemical properties. Attaching reactive organofunctional groups to the PDMS backbone allows a number of crosslinking reactions; e.g. condensation, addition, or radical reactions. The structure of the network will depend on the nature of the polymers, the number and position of the reactive groups on the polymer chains, and the structure of the organofunctional groups themselves. The proportion of dimethylsiloxy (D) units in the network can reach more than 99% of the polymeric composition. The properties of the polymeric network, and ultimately the performance of the entire polymer matrix, will therefore be determined by the PDMS character.

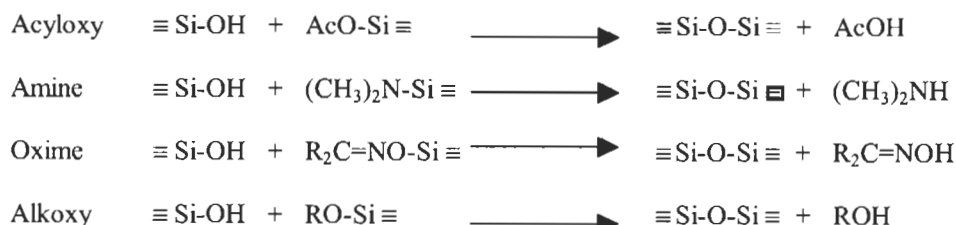
3.1. Structures of silicone networks

The crosslinking systems used in silicone adhesives, coatings and sealants fall into two main categories; condensation cure and addition cure systems [32,33]. Those based on condensation reaction chemistry can be divided in two sub-groups. One sub-group is the moisture condensation cure system where, as the name implies, moisture in the air is utilized for hydrolysis reactions that lead to crosslinking of the polymer chains. These crosslinking reactions proceed from the surface into the bulk and generally take place at room temperature. The second sub-group is based on direct condensation reactions between polymers with different functional groups. These latter cure systems offer adhesive with fast rate of deep section cure at both room and elevated temperature. The addition cure systems can also be divided into two sub-groups, which depend on the source of energy used to trigger the reaction; i.e. heat or UV radiation. The addition cure systems have been developed for rapid processing and fast rate of deep section cure.

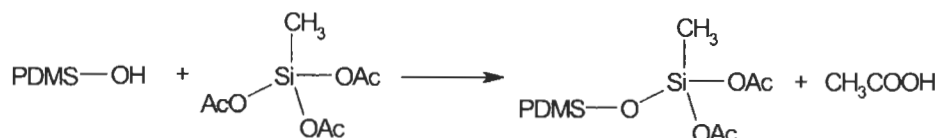
3.1.1. Condensation cure

3.1.1.1. One-part moisture condensation cure. The one-part condensation cure system is a room-temperature vulcanizing (RTV) system that is based on a reactive PDMS polymer that undergoes hydrolysis on contact of air moisture, followed by condensation to yield a crosslinked elastomer. The most common systems [3,12,14,33] are based on the reactions shown in Scheme 5.

These reactions are catalyzed by either carboxylates of tin, zinc, iron or esters



Scheme 5. Common moisture RTV condensation cure systems for silicone adhesives and sealants. R is typically methyl (CH_3 -) or ethyl (CH_3CH_2 -) group.



Scheme 6. In situ formation of the moisture sensitive polymer (II). Only one end of the OH-endblocked PDMS is shown reacting with the silane.

of titanium. The nature of the organic group of the catalyst affects the reaction kinetics.

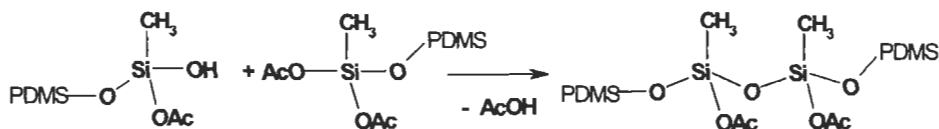
The acetoxy-based moisture sensitive diacetoxymethylsiloxyl-endblocked-PDMS ($\text{M}^{2\text{AcO}}\text{-D}_n\text{-M}^{2\text{AcO}}$) (II) reactive polymer is prepared in situ in the packaging cartridges by mixing silanol-endblocked-PDMS ($\text{M}^{\text{OH}}\text{-D}_n\text{-M}^{\text{OH}}$) (I) with an excess of triacetoxymethylsilane following the reaction shown in Scheme 6. In the sealant cartridge, the silicone is blended with other components such as catalyst, fillers, adhesion promoters, plasticizers, and pigments, which produces a fluid with designed rheological properties.

Upon application of the silicone by extrusion, moisture in the atmosphere comes into contact with the silicone surface. The hydrolysis of an acetoxy siloxy group of the diacetoxymethylsiloxyl-endblocked-PDMS reactive polymer (II) proceeds and leads to a silanol-endblocked polymer as shown in Scheme 7, where OAc represents the acetoxy ($\text{CH}_3\text{COO-}$) group.

The resulting silanol group of a polymer chain condenses with acetoxy siloxy group of another polymer chain to form a siloxane (Si-O-Si) linkage (Scheme 8). Further similar reactions finally result in a crosslinked elastomer. Acetic acid is



Scheme 7. Hydrolysis as the first step reaction in the atmospheric moisture condensation cure system.



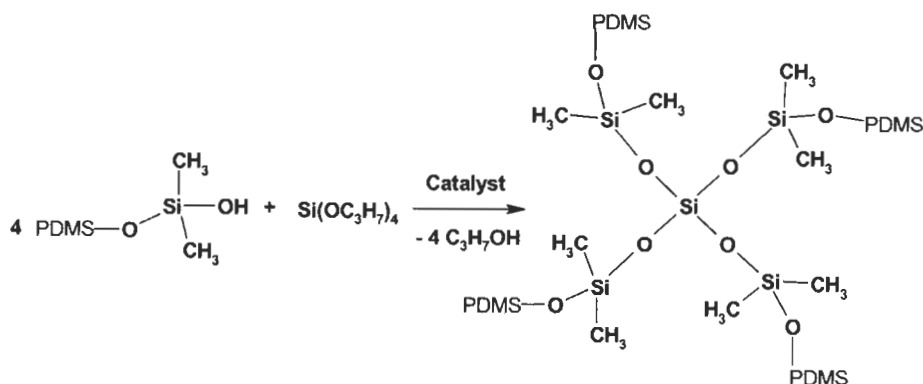
Scheme 8. Condensation reaction as the base of moisture condensation crosslinking system.

released as a by-product in this cure system, which causes corrosion problems with sensitive substrates such as metals or concrete.

The one-part moisture RTV adhesives and sealants are generally cured in an atmosphere of 30–80% relative humidity. As PDMS networks are permeable to water vapor, the cure progresses from the outer surface and continues into the bulk. In general, the silicone can be handled within a few minutes to an hour, when a surface skin begins to form. Depending on the product chosen, greater than 90% of their full physical properties should be attained between 24 and 72 h. Mild heat acceleration of the cure rate may be possible but temperatures above 60°C are not recommended. The silicone will generally cure to about 8 mm in depth from any exposed surface after 7 days. Therefore, these materials are not typically used for highly confined or deep section cures. While the crosslinking reactions proceed to form the elastomeric network, some of the reactive polymer chain ends can react with chemical groups present on surfaces of the substrates. These latter reactions can result in the formation of covalent bonds and subsequent adhesion. Once completely cured, the products resist effects of humidity and temperatures up to 120°C. They are also resistant to other harsh environments. They possess good dielectric properties and good adhesion to a variety of common substrates.

3.1.1.2. Two-part room temperature condensation cure. Silicone can be formulated into two-part systems [3,12,14,33] that prevent the reactive groups from coming into contact before they are needed. The reactions in these systems are based on the condensation of a silanol group with an alkoxy silane group, catalyzed by organo-tin compounds (Scheme 9).

The moisture-sensitive catalyst being maintained in isolation from the reactive polymer species prior to application is an advantage of the two-part system. Due to the high reactivity of the alkoxy silanes, the handling time of the freshly applied adhesive mixture is only a few minutes. Good strength is attained within an hour, but full adhesive and mechanical properties are not reached for a number of days. Because the cured system is the product of a chemical reaction that occurs in the bulk of the material, deep section cure is achieved with this system. When two-part condensation curing materials using organo-tin catalysts are cured in confinement and later subjected to high heat, the curing condensation reaction can be reversed. Thus, in unusual conditions, the cured adhesive can revert back to a flowable polymer. This demonstrates the need for thorough testing of an adhesive in accelerated aging conditions before large-scale production is undertaken.



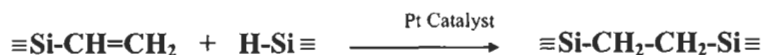
Scheme 9. Crosslinking reaction of a two-part moisture cure silicone adhesive system.

Like the 1-RTV systems, the two-part room temperature vulcanization systems (2-RTV) cure to produce flexible elastomers that resist humidity and other harsh environments. Interestingly, they display primerless adhesion property to many substrates, and are used in silicone adhesives, sealants, seals, and gaskets, to name a few.

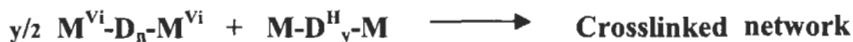
There are many applications for silicone adhesives, sealants, or coatings where the condensation curing systems are not suitable. This is because they are relatively slow to cure, they require moisture to cure that can itself be in some cases uncontrollable, and they evolve by-products that cause shrinkage. Adhesives needed in automotive, electronics, microelectronics, micro electromechanical systems, avionic, and other 'hi-tech' applications are usually confined to very small volumes, which can make access to moisture difficult. Also, their proximity to very sensitive mechanical or electronic components requires a system that does not evolve reactive chemicals.

3.1.2. Addition reactions for crosslinking

Addition cure systems based on thermal or radiation induced reactions respond to the technology needs that are unfulfilled by the condensation cure systems. The crosslinking reactions are fast, adhesion in most cases develops rapidly, and no by-products are formed. The polymers can be selected over a wide range of chain lengths and the resulting materials can have excellent mechanical properties. Thanks to these characteristics, the applications of silicones as adhesives and sealants have been extended to coatings. Of particular interest, the two interfaces of the coatings, namely the air-silicone and the silicone-substrate interfaces, now play two different roles in adhesion. Strong adhesion is generally required with the substrate whereas weak adhesion is sought after for the silicone surface.



Scheme 10. Addition reaction by hydrosilylation catalyzed by a platinum complex.



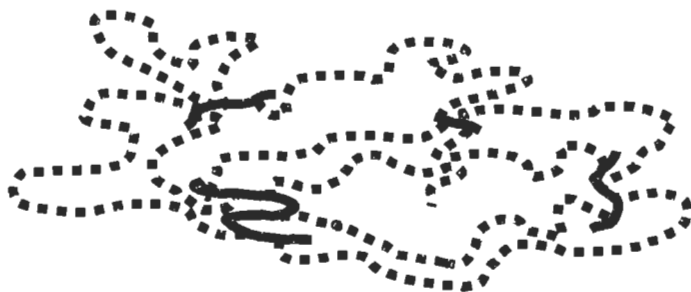
Scheme 11. Basic crosslinking reaction by hydrosilylation catalyzed by a platinum complex.

3.1.2.1. Thermal cure system. The thermal cure system is based on a hydrosilylation addition reaction between vinyl-functionalized and silicon-hydrido functionalized polysiloxanes [32,33,35]. Unsaturated organic groups react with a Si–H functionality in the presence of a platinum-based catalyst (Scheme 10).

In this reaction, no by-products are evolved, and the crosslinking reactions occur within the bulk of the material. A typical hydrosilylation crosslinking system is depicted in Scheme 11, where n and y can vary depending on the required viscosity of the uncured formulation and the final targeted properties of the cured adhesive.

As well as being homopolymers, the vinyl polymers and the SiH crosslinkers can be copolymers such as: $\text{M}^{\text{Vi}}-\text{D}_m^{\text{Vi}}-\text{D}_n-\text{M}^{\text{Vi}}$ and $\text{M}-\text{D}_x^{\text{H}}-\text{D}_y-\text{M}$, where the values of m , n , x , y can also vary widely. A vinyl-functionalized polysiloxane resin or silica ($\text{M}_x\text{M}_y^{\text{Vi}}\text{Q}_z$) can also partially substitute the linear polymer and function as a reinforcing agent.

In addition cure systems, the crosslinker is polymeric with an average degree of polymerization that can range from 3 to 100 reactive Si–H sites per macromolecule. The resulting polymeric network based on Scheme 11 is formed by high molecular weight PDMS of chain lengths ranging from 150 to 1000 siloxy units depending on the polymer selected, attached to the polymeric crosslinkers of chain lengths of 40–60 units (Scheme 12). The theoretical stoichiometric SiH/SiVi ratio



Scheme 12. Schematic structure of vinyl-eb-PDMS chains (dashed line) crosslinked with polymeric TMS-eb-PHMS through the hydrosilylation cure reaction. For illustration purpose the PDMS chains in this scheme are shorter and less abundant relative to PHMS than in real system.

is 1 and is practically maintained above unity to allow complete reaction of the vinyl polymers.

In order to control the cure rate, cure temperature, and the pot life at room temperature, organic or organosiloxane additives are used to inhibit the catalytic activity of the platinum complex. These inhibitors form thermally unstable complexes with the catalyst and decompose at elevated temperatures to allow the cure to proceed. Typical curing temperatures range between 70 and 180°C, depending on processing parameters and the thickness of the applied silicone. The catalyst/inhibitor system and their respective concentrations are selected to give a typical pot life ranging from 1 to 8 h at ambient temperatures.

Although inhibitors are deliberately added to the silicone formulation to control cure rate, unwanted cure inhibition can be caused by other species that react to form strong complexes with the platinum catalyst. Most notable of these undesired inhibitors include organotin and other organometallic compounds, sulfur, polysulfides, polysulfones or other sulfur-containing materials, amines, urethanes or amine-containing materials, unsaturated hydrocarbons in plasticizers, and some solder flux residues.

After the reaction completion in an addition cure silicone system, the cross-linked structure will theoretically not contain any reactive groups. The cured silicone will be composed of dimethylsiloxy units $[(CH_3)_2SiO]$ and some $Si-CH_2-CH_2-Si$ linkages that result from the crosslinking reaction. Moreover, the SiH and $Si-CH=CH_2$ groups are not particularly reactive towards many chemical groups found on surfaces of common substrates. It is therefore expected that no coupling between the polymeric network and the substrate will take place during application and cure. As a consequence, this type of cure system often exhibits very poor adhesion and is ideal for release applications. Exceptions occur when the adhesion of the silicone system is driven by the *mechanical mechanism* or where one of the components of the silicone system can react with the substrate surface to form covalent bonds. Therefore, if strong adhesion is required, it is either necessary to prime the surface of the substrate, or to add adhesion promoters to the thermally activated addition cure system.

Cure systems based on hydrosilylation can be formulated as one and two-part silicone products, that can be either flowing or non-flowing. These formulations provide fast thermal cure rates, they are resistant to humid and other harsh environments, and they have good dielectric properties. These formulations can be self-priming or alternatively the substrate may require priming before application of the silicone.

3.1.2.2. Radiation cure system. Other addition reaction cure systems that have emerged in recent years are the ultra-violet (UV) and electron beam (EB) radiation cure systems. The development of these systems has been prompted by the ever-increasing need for fast cure rates and low cure temperatures. The UV cure system

is more common than the EB based system for general applications in adhesives and coatings. There are several advantages gained from using UV radiation instead of heat for curing solventless silicone systems. A low cure temperature allows deposition and cure on heat sensitive substrates like polyolefins and other plastic materials. Low temperature cure on paper substrates also finds an advantage as the moisture in the paper is retained during cure, which avoids the need for a moisturizing process after coating.

The UV cure system contains an epoxy or a vinyl ether functionalized PDMS polymer and a photo catalyst [36]. This latter, a diaryliodonium salt is photolytically decomposed to form an active acid that polymerizes the epoxy or vinyl ether groups and crosslinks the network.

Theoretically, this system offers the advantages of the thermal cure systems that include fast cure and low temperature processing. However, these systems are sensitive to atmospheric humidity and the possible toxicity of the catalyst may represent an issue.

3.2. Properties of silicone networks

Once cured, PDMS networks are essentially made of dimethylsiloxane polymeric chains crosslinked with organic linkages. The general and inherent molecular properties of the PDMS polymers are therefore conferred to the silicone network. Low surface energy and flexibility of siloxane segments are two inherent properties very useful in adhesion technology.

It is noteworthy that an important industrial application is based on pure silicone network [9]. This is the organic PSA release technology where an uncured silicone is deposited as a thin coating to a flexible substrate. Strong adhesion develops at the silicone–substrate interface whilst the coating cures.

Pure PDMS networks are mechanically weak and do not satisfy the adhesive and cohesive requirements needed for most applications in which the silicone adhesive joint is subjected to various stresses. For crosslinked silicones to become high performing adhesives, they need to be strengthened.

4. Adhesive strength of silicones

The performance of a product where adhesion plays a role is determined both by its adhesive and cohesive properties. In the case of silicones, the promotion of adhesion and cohesion follows different mechanisms [37]. In this context, adhesion promotion deals with the bonding of a silicone phase to the substrate and reinforcement of the interphase region formed at the silicone–substrate interphase. The thickness and clear definition of this interphase is not well known, and in fact depends on many parameters including the surface physico-chemistry of

the substrate, the adhesive, the application technology, etc. Cohesion promotion concerns the bulk of the silicone material. This is easily defined and is measured through classical tests applied to elastomers and plastic materials.

4.1. Adhesion promotion

PDMS based siloxane polymers wet and spread easily on most surfaces as their surface tensions are less than the critical surface tensions of most substrates. This thermodynamically driven property ensures that surface irregularities and pores are filled with adhesive, giving an interfacial phase that is continuous and without voids. The gas permeability of the silicone will allow any gases trapped at the interface to be displaced. Thus, maximum van der Waals and London dispersion intermolecular interactions are obtained at the silicone–substrate interface. It must be noted that suitable liquids reaching the adhesive–substrate interface would immediately interfere with these intermolecular interactions and displace the adhesive from the surface. For example, a study that involved curing a one-part alkoxy terminated silicone adhesive against a wafer of alumina, has shown that water will theoretically displace the cured silicone from the surface of the wafer if physisorption was the sole interaction between the surfaces [38]. Moreover, all these low energy bonds would be thermally sensitive and reversible.

Theoretically, these intermolecular interactions could provide adhesion energy in the order of mJ/m^2 . This should be sufficient to provide adhesion between the adhesive and the substrate. However, the energy of adhesion required in many applications is in the order of kJ/m^2 . Therefore, the intermolecular forces across the interface are not enough to sustain a high stress under severe environmental conditions. It is generally accepted that chemisorption plays a significant role and thus, physisorption and chemisorption mechanisms of adhesion both account for bond strength.

The review of the cure chemistry of silicones has highlighted the reactive nature of the organofunctional groups that can be attached to the PDMS backbone. Potentially, these organofunctional groups can form linkages between the crosslinked network and substrates such as glass, silicon wafers, fabrics, papers, ceramics, reactive metals, plastics, etc. However, for addition cure systems the SiH and Si-CH=CH_2 groups are not particularly reactive towards many chemical groups found on surfaces of common substrates. Therefore, adhesion promotion by either adding a coupling agent into the silicone system and/or pre-treating the substrate will need to be considered. Thus, silicone adhesives, sealants, and coatings are formulated in *unprimed*, *primed*, or *self-primed* forms, which make them suitable for adhesion to almost every substrate.

An unprimed silicone adhesive implies that it is free of any adhesion promoter and that the substrate does not need to be activated or primed; i.e. adhesion relies mainly on *chemical* and/or *mechanical* mechanisms. The chemical adhesion

depends on both the reactivity of the selected silicone cure system and on the natural presence of reactive groups on the surface of the substrates. For example, the condensation based silicone adhesive used to bond the panes of glass of an aquarium relies on both the reactivity of the acetoxo group bonded to silicon atom, and the presence of silanol groups on the surface of glass. Another example of an unprimed silicone is the silicone release coating based on the hydrosilylation reaction, where adhesion to paper substrates relies on penetration and subsequent cure up to a certain depth. The presence of reactive groups on the paper and the reactivity of the chemical crosslinker may also play a role on the chemical bonding mechanism.

Priming a substrate before applying a silicone adhesive chemically functionalizes the surface to provide pathways for chemical bonding with a selected silicone cure system [39]. More importantly priming the substrate results in increasing the concentration of chemical bonds that can be formed across the silicone adhesive/substrate interface. This increase of chemical bonds is definitely improving adhesion durability under severe service-environments (underwater, high/low temperature cycles). The main disadvantage of priming the substrate is the addition of an extra step in the whole process of adhesive application, which brings its own problems and cost. The primer, also called an adhesion promoter or coupling agent, is usually a reactive alkoxy silane. However, a variety of primers have been used for this purpose, and the mechanisms of their adhesion and applications have been studied extensively. A very thin layer of the primer is applied to the substrate before applying the bulk adhesive. The interfacial layer of the primer would be expected to have a defined thickness, which is a function of the amount applied. However, the thin primer coating may well be irregular in thickness, and in the size and distribution of reacted and condensed particles of silane. After curing, it is expected that the highly crosslinked interphase will have a modulus higher than the bulk of the adhesive, but lower than the solid substrate.

Another process that promotes chemical adhesion is the pretreatment of the low energy surface. This can be considered as a 'dry' priming process, as no wet chemicals are used. Various surface pre-treatment techniques can be used to graft chemical functionalities onto the surface of plastics, for example chemical, photochemical, flame, plasma, and corona discharge treatment (CDT) [40–45]. CDT is probably the most widely used technique to pre-treat polyolefin films. The corona discharge contains various excited gaseous molecules of very high chemical reactivity; e.g. electrons, activated elemental oxygen (O^*), activated oxygen molecules (O_2^*), ozone (O_3) and activated nitrogen (N_2^*) [46]. When the substrate is passed through the corona discharge, these reactive elements react with the surface of the substrate. As a result, transient organic radical species, ions, and oxidized groups are formed on the treated surface. This reactive surface allows chemical bonding with the applied adhesive. This is particularly relevant to adhesion of silicone release coatings to substrates such

as polyethylene coated kraft paper, polypropylene and polyethylene terephthalate films.

The ideal silicone adhesive is one that is self-primed; i.e. the adhesion promoter is included in the formulation and is generally part of the curing reaction system [47]. This is the most common type of adhesive, as it provides adhesion without the need of a complicated pretreatment procedure. However, this should not prevent end-users from cleaning the surface of the substrates using the appropriate cleaner (degreasing agents) prior the application of the adhesive layer. All the art and technology of a self-priming polymeric system resides in the choice and chemical design of the adhesion promoter molecules. The simplest approach is to add a coupling agent into the formulation. Silane coupling agents are denoted by the general structure RSiX_3 , where R is a reactive organofunctional group and X is a chlorine atom, or a methoxy, ethoxy, or acetoxy group. The variety of different organosilanes and their respective merits have been discussed in detail elsewhere [48]. Organosilanes are small, surface-active molecules, which can easily diffuse to the interface while crosslinking occurs in the silicone. Once at the interface they can improve adhesion through enhanced wetting and covalent bonding. Hydrolysis of the organosilane provides active SiOH sites for hydrogen bonding. The silanol groups on the organosilane allow condensation reactions to occur, which result in the formation of Si-O-Si bonds between the silane molecule and either the surface of the silicon-containing surface or the silicone network. It is also possible for the organofunctional group on the silane to react with chemically reactive groups present on the substrate surface. Silanes are particularly effective in the promotion of adhesion of silicones to metal, glass, and siliceous surfaces, in general. A study has recently shown that specific mixtures of silanes can provide better adhesive performance than the individual silanes, and that an optimum composition is required [49]. More complex adhesion promoter systems are continually being developed to respond to specific and demanding emerging and future bonding technologies.

4.2. Cohesion promotion

The cohesive strength of a pure non-reinforced silicone network is relatively low, with the fracture energy in the region of several J/m^2 . The need to reinforce the three-dimensional polymeric structure has been long recognized, and inorganic fillers such as silica and calcium carbonate are added to the silicone base to transform the network into a highly elastomeric material. This results in the dramatic improvement of the mechanical properties of silicones, such as tensile strength, tear strength, elongation at break, and hardness. The impact of bulk elastomeric properties on the performance of an adhesive is clear. Indeed, high elongation and low modulus characteristics will help absorb a lot of the stress introduced to the joint. The high tear strength, in general, and the propagation

path of a fracture, in particular, are of importance in adhesion. This is because the fracture of adhesive joints starts from an initial crack.

Silicas are classified as precipitated, aerogel, or fumed silica [50]. The core of silica particles is made of Q siloxy units and the surface is composed of silanol groups (T^{OH}); i.e. the molecular structure of untreated silica can be described as $\text{T}^{\text{OH}}_x\text{Q}_y$ with $x \ll y$. The surface silanol groups are available for interaction with similar groups on the siloxane polymers. Fumed silica is generally surface treated to produce aggregate particles covered with trimethylsiloxy (M) or dimethylsiloxy (D) groups. When completely surface treated with a trimethylsilyl donating agent, the structure can be described as M_xQ_{x+y} . The mechanisms of mechanical reinforcement properties of silicone elastomers are complex [8,51–54].

The rheological properties of the uncured silicone formulation are very important, and optimization of the properties needs to be considered. For example, sealants and adhesives are required to flow easily, but also keep their shapes whilst curing. The choice of filler can often have a dramatic impact on these rheological properties of the silicone. Treated silica readily incorporates into a silicone polymer, increasing its viscosity while reducing its thixotropic structure. Highly active untreated silica will tend to form particle–particle aggregates as well as attachments with silanol groups on the silicone backbone. Untreated silica will be avoided unless it is treated in situ with suitable silanes and catalyst. The physical and chemical interactions between the silica/silica and silica/polymer give rise to two types of structures that affect the rheology of the base: either a highly thixotropic base that can be broken down by shearing, or a permanent structure which, depending on the concentration of active sites and free silanol terminated chains, will considerably enhance the strength and resistance to tear.

Fillers can also be used to promote or enhance the thermal stability of the silicone adhesive. Normal silicone systems can withstand exposure to temperatures of 200°C for long hours without degradation. However, in some applications the silicone must withstand exposure to temperatures of 280°C. This can be achieved by adding thermal stabilizers to the adhesive formulations. These are mainly composed of metal oxides such as iron oxide and cerium oxide, copper organic complexes, or carbon black. The mechanisms by which the thermal stabilization occurs are discussed in terms of radical chemistry.

Another advantage of the addition of inorganic filler is the significant increase in density of the silicone, which helps the dispensing process. The use of fillers also reduces the total cost of the product, as the expensive high performance silicone does not require 100% volume occupancy to fulfil its function.

5. Silicones and mechanisms of adhesion

In the search for an adhesive system, the researcher designs a polymeric network and formulation and builds in adhesive and cohesive strength. A combined

knowledge of silicone chemistry, the surface chemistry of substrates and the mechanisms of adhesion helps in this quest. In this section we examine the concept of adherence and more specifically the mechanisms of adhesion and loss of adhesion encountered in silicones. The distinction between adherence and adhesion is particularly relevant for silicones, as in recent years many studies focused on the measurement of fundamental *adhesion* using the contact mechanic theory and deserves some attention [45,55–59].

5.1. Adherence and adhesion

The term *adherence* is synonymous with the terms *practical adhesion* or *measured adhesive strength*. Adherence is used to describe the adhesive strength of a joint that is measured in a defined adhesion test geometry. The term *adhesion* refers to the fundamental intermolecular forces or bonds acting across the interface created between the adhesive and the substrate. These bonds include all the low- and high-energy interactive molecular forces, which determine the strength of the interface. Adherence and adhesion are interrelated through physical properties of the elastomeric joint. This is expressed in the following empirical relationship:

$$G = G_0[1 + \phi(v, T)] \quad (1)$$

The energy release rate (G) represents adherence and is attributed to a multiplicative combination of interfacial and bulk effects. The interface contributions to the overall adherence are captured by the adhesion energy (G_0), which is assumed to be rate-independent and equal to the thermodynamic work of adhesion (W_a). Additional dissipation occurring within the elastomer is contained in the bulk viscoelastic loss function ϕ , which is dependent on the crack growth velocity (v) and on temperature (T). The function ϕ is therefore substrate surface independent, but test geometry dependent.

The ability to separate the interfacial and bulk factors in Eq. 1 suggests two main approaches for controlling adherence. One approach will be based on changing G_0 through interface modification (adhesion promotion), and the other will be based on altering ϕ by modifying the elastomers bulk properties (cohesion promotion). As we have seen in the previous section, practical adhesion in silicones has exploited both these approaches and has led to the production of highly performing products.

In the case of silicones, there are a variety of chemical ways whereby the cohesive strength can be designed to build the elastomeric network and cope with specific stresses going from pure mechanical to thermal. The adhesive strength, on the other hand, can also be further designed with the aid of adhesion promoters, substrate primers, or substrate pretreatments. The crosslinked polysiloxane network actively participates in various energy absorption processes through its viscoelastic properties, and thereby increases the adherence strength. The inherent

cohesive strength of the silicone material, the adhesive strength of the interface and the energy absorption processes together put adherence energy in the range of kJ/m^2 .

The two following examples illustrate the effect of bulk viscoelastic contributions to adherence in relation with silicone network structures. In silicone release coatings, the silicone crosslinked network is around $1\text{ }\mu\text{m}$ thick and is intrinsically non-elastomeric and brittle. This is due to the short intercrosslink chain lengths and the absence of reinforcing agents. The absence of elastomeric property reduces the contribution of viscoelastic properties of the network to adherence. Any energy applied to the thin coating will be absorbed and dissipated in the fracture of the network. Therefore, the strength of the coating relies on the bonds formed across the interface between the silicone and the substrate (adhesion), and plays a dominant role on the strength of the silicone coating.

In silicone adhesives used to bond structural glazing assemblies, the silicone network is made of very long PDMS chains and is filled with silica that improves the elastomeric properties of the adhesive. The strength of such an adhesive is strongly enhanced through various mechanisms of energy absorption.

A detailed study of adhesion or design of the adhesive performance of a silicone adherent material requires that all possible mechanisms of adhesion be evaluated. The following section focuses on the mechanisms of adhesion that affect G_0 .

5.2. Mechanisms of adhesion

The theories proposed for the mechanisms of adhesion have been reviewed in detail elsewhere [44,45,55–58]. However, for the purpose of this chapter, we are presenting them in the context of silicone adhesion. The various theories underlying each mechanism will be briefly outlined and qualitatively illustrated with specific examples.

5.2.1. Formation of the interface

The primary requirement for good adhesion is the creation of an interface through wetting and spreading of the silicone onto the substrate. The surface tension of silicones is $\sim 22\text{ mN/m}$, which is lower than the critical surface tension of wetting of most substrates. Therefore, PDMS is driven thermodynamically to wet the substrate. However, the low surface tension of PDMS is not the only prerequisite for creating a good interface, and viscosity is also important when considering the spreading of the silicone. When high molecular weight silicone polymers are used in a formulation, the viscosity can be reduced through dissolution in a solvent. Solventless low viscosity formulation may also be achieved with low molecular weight silicone polymers. A combination of these spreading and wetting properties enables the formation of an interface where the silicone is

intimately in contact with the surface of the substrate, which satisfies the primary condition required for good adhesion.

5.2.2. Physical adsorption mechanism

Physical adsorption theory proposes, that if there is intimate contact between the substrate and the adhesive, interatomic and intermolecular forces will operate across this interface, resulting in primary bonding. These interatomic and intermolecular forces include the low energy London dispersion and van der Waals forces, which encompass interactions between both permanent and induced dipoles. Higher energy intermolecular forces such as hydrogen bonding and acid–base interactions are also included in this mechanism. Donor–acceptor interactions are sometimes included in this mechanism, although their bond strength is intermediate between the physical forces and chemical bonds.

Among all the low energy interactions, London dispersion forces are considered as the main contributors to the physical adsorption mechanism. They are ubiquitous and their range of interaction is in the order 2 molecular diameters. For this reason, this mechanism is always operative and effective only in the topmost surface layers of a material. It is this low level of adhesion energy combined with the viscoelastic properties of the silicone matrix that has been exploited in silicone release coatings and in silicone molds used to release 3-dimensional objects. However, most adhesive applications require much higher energies of adhesion and other mechanisms need to be involved.

5.2.3. Mechanical interlocking theory

Mechanical interlocking theory proposes that the adhesive flows into morphological irregularities on the substrate surface before curing. The low surface tension and high spreading coefficient of silicone polymers allows them to rapidly conform to surface irregularities [60,61]. Therefore it is expected that this mechanism of adhesion will play a key role in adhesion of silicones to many different substrates such as leather, textile fabrics, porous metals like anodized aluminium, porous plastic and composite materials, and specialty papers like glassine, super calendered kraft and clay-coated papers.

5.2.4. Diffusion theory

Diffusion theory involves the interdiffusion of macromolecules between the adhesive and the substrate across the interface. The original interface becomes an interphase composed of mixtures of the two polymer materials. The chemical composition of the interphase becomes complex due to the development of concentration gradients. Such a macromolecular interdiffusion process is only

possible if polymer chains in the adhesive and the substrate are both mobile and miscible. The interdiffusion and hence the adherence energy is directly affected by time, temperature and pressure of contact.

Although the diffusion mechanism can be seen as mechanical but occurring at molecular dimensions, van der Waals intermolecular interactions and conformational entropic energy provide an additional mechanism that increases adhesion [62]. It is interesting to note the analogy that exists between this mechanism at the molecular level with the adherence, adhesion and viscoelastic deformations concept applied for a macroscopic adhesive.

5.2.5. Chemical bonding theory

The chemical bonding theory of adhesion applied to silicones involves the formation of covalent bonds across an interface. This mechanism strongly depends on both the reactivity of the selected silicone cure system and the presence of reactive groups on the surface of the substrate. Some of the reactive groups that can be present in a silicone system have been discussed in Section 3.1. The silicone adhesive can be formulated so that there is an excess of these reactive groups, which can react with the substrate to form covalent bonds. It is also possible to enhance chemical bonding through the use of adhesion promoters or chemical modification of the substrate surface.

The mechanism of chemical adhesion is probably best studied and demonstrated by the use of silanes as adhesion promoters. However, it must be emphasized that the formation of chemical bonds may not be the sole mechanism leading to adhesion. Details of the chemical bonding theory along with other more complex theories that particularly apply to silanes have been reviewed [48,63]. These are: the *Deformable Layer Hypothesis* where the interfacial region allows stress relaxation to occur, the *Restrained Layer Hypothesis* in which an interphase of intermediate modulus is required for stress transfer, the *Reversible Hydrolytic Bonding* mechanism which combines the chemical bonding concept with stress relaxation through reversible hydrolysis and condensation reactions.

The adhesion promotion of an organic matrix to an inorganic substrate using a silane has been studied to model the structure of the created interphase [64–66]. The polymer/silane interphase is influenced by the solubility parameter of both the silane coupling agent and the polymer. More interdiffusion occurs when the solubility parameters of the polymer and the silane closely match together. It is believed that this model can be applied to silicone adhesive/solid substrate system.

5.2.6. Electrostatic theory

Electrostatic theory proposes that two materials are held together by electrical charges. Electrons are transported between the adhesive and the substrate forming

an electrical double layer, which gives a force of attraction. Much debate exists as to whether electrostatic attraction forces, or the separation process, of the charges are responsible for the adhesion energy. No studies on this mechanism involving silicones have been published.

5.3. Mechanisms of loss of adhesive strength

Since the locus of failure can clearly distinguish between adhesive and cohesive failures, the following discussion separates loss of adherence into loss of adhesion and loss of cohesion. In the loss of cohesion it is the polysiloxane network that degrades, which can be dealt with independently of the substrate. The loss of adhesion, however, is dependent on the cure chemistry of the silicone, the chemical and physical properties of the substrates, and the specific mechanisms of adhesion involved.

Durability of adhesion is very difficult to predict and control, but the detailed knowledge of the silicone systems in relation with the mechanisms involved in the loss of adherence can help a great deal. As mentioned previously, there are multiple and interrelated mechanisms involved in adhesion, which may follow different mechanistic pathways in debonding. In addition to these complications, the nature of the substrate's surface and its physical and chemical properties are often not known. Although some efforts are currently being employed to address these issues, mastering adhesive durability remains an art. Several reviews have been published on durability of silicone sealants [67–70]. A more recent review discusses the effects of degradation factors on sealant adhesion [71]. The paper focuses on the changes in interfacial stress balanced against the changes in interfacial strength of the sealed joint.

5.3.1. Loss of adhesion

Loss of adhesion occurs at the silicone substrate interface and two main mechanisms can be outlined: the formation of a weak boundary layer (WBL) and the breaking of adhesive bonds.

5.3.1.1. Weak boundary layer. WBL theory proposes that a cohesively weak region is present at the adhesive–substrate interface, which leads to poor adhesion. This layer can prevent the formation of adhesive bonds, or the adhesive can preferentially form bonds with the boundary layer rather than the surface it was intended for. Typically, the locus of failure is interfacial or in close proximity to the silicone–substrate interface. One of the most common causes of a WBL being formed is the presence of contaminants on the surface of the substrate. The formation of a WBL can also result from migration of additives from the bulk of the substrate, to the silicone–substrate interface. Alternatively, molecular

components from within the silicone adhesive formulation could diffuse to the silicone–substrate interface and form the WBL. A noteworthy point is that when adhesive failure occurs, it is important to investigate and assess the mechanism of WBL.

A WBL can also be formed within the silicone phase but near the surface and caused by insufficiently crosslinked adhesive. This may result from an interference of the cure chemistry by species on the surface of substrate. An example where incompatibility between the substrate and the cure system can exist is the moisture cure condensation system. Acetic acid is released during the cure, and for substrates like concrete, the acid may form water-soluble salts at the interface. These salts create a weak boundary layer that will induce failure on exposure to rain. The CDT of polyolefins illustrates the direct effect of surface pretreatment and subsequent formation of a WBL by degradation of the polymer surface [72,73].

5.3.1.2. Breaking of silicone–substrate chemical bonds. In Section 5.2, the important roles played by physical and chemical adsorption were discussed. However, the difficulty with any adhesive system is the identification of the bonds formed at a buried interface. The most common approach for investigating buried interface is to study the surfaces formed from an adhesive test piece that has failed under a variety of environmentally controlled conditions. One such important environmental parameter for silicones is water. The solubility of water in silicones is extremely low but the coefficient of diffusion is very high, and thus, silicones are highly permeable to water vapor and indeed many other gaseous molecules. Depending on the thickness, and surface exposure of the silicone migration of water towards an interface can be very fast. It has been shown that 50% and 95% water vapor saturation of a PDMS adhesive in a lap-shear joint can be attained in 40 min and 2.25 h, respectively [74]. Therefore, it is clear that at equilibrium a silicone adhesive will reflect ambient humidity, and it will be saturated during periods of high humidity. Once at the interface, water can interfere with hydrogen bonding, or could hydrolyse a variety of covalent chemical bonds, resulting in the loss of adhesion.

An investigation of the mechanism of adhesive failure of polydimethylsiloxane elastomers was conducted [75]. The study showed that the total adhesive failure energy could be decomposed into energies for breaking chemical bonds, breaking physical bonds and deforming the bulk viscoelastic elastomer.

5.3.2. Loss of cohesion

Silicone networks that form the matrix of the adhesives are not susceptible to degrade or to depolymerize when exposed to a wide range of conditions of temperature and relative humidity. Therefore, the cohesive strength will not change, as

the polymer intercrosslink chains will maintain their polymeric structures. Moreover, the chemical reactions that lead to crosslinking will not reverse, with the exception of the two-part condensation system under specific conditions. Thus, if the environmental and external conditions of temperature, relative humidity, atmospheric gases, and catalytic residues are within the limits of stability of PDMS polymers, the cohesive strength of the adhesive will remain intact. This property of silicones is behind the unique performance of silicones applied in adhesion.

The thermal stability of the silicone matrix reflects the stability of the polysiloxane polymers. Thus, in the absence of catalyst residue, silanol groups, and moisture, depolymerization, molecular rearrangement, and crosslinking reactions are reduced. The depolymerization of PDMS in vacuum or in inert atmospheres starts in the range of 220°C and leads to the formation of oligomeric cyclosiloxanes. Continuous heating at 350°C will lead to complete degradation, due in part to depolymerization and in part to rearrangement. These limits in temperature degradation suggest an upper use temperature of 200°C for adhesive joints exposed continuously to thermal radiation, and around 300°C for short time exposures. The permeability of silicones to oxygen is very high, which opens the possibility of oxidative degradation mechanisms operating on the organic side chains. Therefore, when the adhesive is continuously exposed to air the upper temperature limit is set to 160°C.

The common atmospheric agents like ultraviolet radiations, ozone, nitrogen oxides, acidic rain, do not noticeably attack silicone materials. However, high-energy radiation does crosslink PDMS networks through radical chemistry of organic groups. This crosslinking increases the cohesive strength of the adhesive, thereby the adhesive strength is overcome by exerting a stress on the adhesive interface [12].

Due to the low glass transition and melting temperatures of PDMS polymer, 100% silicone sealant do not substantially stiffen at lower service temperature. Typically, their Young's modulus is maintained within a $\pm 25\%$ range over a temperature range of -40 to 80°C .

6. Silicone adhesion technologies

The surface, bulk, and rheological properties of silicones, combined with a variety of cure systems, has led to the development of silicone adhesives, sealants, and coatings, which have found applications in various industries. Silicones have become popular because of their capability to bond to a variety of materials and with various degrees of strength, but also because of the range of other unique properties such as low surface energy, excellent resistance to weathering, low sensitivity to a wide range of temperatures, highly elastomeric properties, good electrical resistance, excellent biocompatibility, etc. In addition, the structure of

the uncured materials can be selected to fit a variety of industrial application processes. These include applications in technology fields as varied as aerospace, automobile, building, electronic, healthcare, energy, medical, paper, personal care, plastics, and textiles.

The examples discussed in this section are representative of the breadth of adhesion technologies developed during the past 50 years. The list is by no means exhaustive and they are meant to illustrate some key applications. Novel applications in new and emerging technologies are still being nurtured, and are encouraging the development of highly performing products where adhesion is a key needed property.

Silicone sealants based on condensation cure chemistry are used in the building industry as sealing, adhesive, or coating materials for their outstanding durability under a variety of weathering conditions [67–70]. They provide a barrier against specific environmental influences, which may include humidity, rain, still or pressurized water, draughts, gases, noise, sand, and dust [76]. The durability property is a direct result of the polysiloxane structure, which provides low reactivity and hydrophobic character limiting their contact with many aqueous solutions. They can be used in the presence of many chemical compounds and can be exposed to UV radiation without showing any sign of deterioration. The transparency to light and the ability of incorporating pigments make silicones suitable as building sealants. The low chain-to-chain interaction results in elastomers with very low modulus, which reduces permanent joint stresses and increases longevity of assemblages. The high elastomeric property of silicone sealants gives them the ability to absorb movements. They can sustain 25–30% joint movement as expressed as the percentage of initial joint width. This allows silicone sealants to be used in applications where the adhesive is required to absorb movements of the joint without tearing apart from the substrate. Applications that illustrate this feature include mono-block headlamps in the automobile industry, vapor irons and glass door ovens in the appliances industry.

Although the primary function of sealants is to seal, adhesion promoters are often added, which allows them to adhere to the adjoining base materials. It is therefore sometimes difficult to distinguish between an adhesive and a sealant. For example, structural silicone adhesives are used in the building construction industry owing to their sealing, adhesive, elastomeric properties, and their resistance to harsh environmental conditions [67,70,77].

The role played by the various ingredients in the composition of sealant, and in particular on the durability of adhesion has been discussed recently [77]. Inert plasticizers, such as trimethylsilyl-endblocked-PDMS, are typically added to silicone sealant compositions in order to adjust the rheology of the uncured sealant. They result in a reduction of the modulus and hardness of the cured sealant. Differences in the durability of silicone sealants are found to be due to differences in their cure chemistry, and more specifically to the nature and

Table 1

Typical components of a silicone sealant based on condensation cure system

Component	Typical chemical	Function
Polymer	Hydroxyl $\sim\text{SiOH}$,	Backbone required to form the elastomeric network.
Plasticizer	Trimethylsilyl-endblocked-PDMS	Adjustment of mechanical properties such as hardness, viscoelasticity, rheology.
	Paraffin oil of high boiling point.	Organic plasticizers (diluent) may reduce formulation cost as well as providing some special ease-of-use properties.
Reinforcing fillers (active)	Fumed Silica (SiO_2); precipitated calcium carbonate (CaCO_3); carbon black	Thixotropic reinforcing agents (non-slump), adjustment of mechanical properties (cohesion); provide toughness to the elastomer as opposed to brittle materials.
Non-reinforcing fillers (passive)	Ground calcium carbonate (CaCO_3)	Reduce formulation cost; adjust rheology, and mechanical properties.
Crosslinkers	Acetoxy $\sim\text{Si}(\text{OOCCH}_3)_3$	Crosslinking of the polymeric component; provide network structure.
	Alkoxy $\sim\text{Si}(\text{OR})_3$	
	Oxime $\sim\text{Si}(\text{ON}=\text{CRR}')_3$	
	Amine $\sim\text{Si}(\text{NHR})_3$	
Specific additives	Catalysts: organo-Sn, -Ti, -Pt, -Zn, -Rh	Control of the rate of the curing process.
	Adhesion promoter: $\text{X}-\text{CH}_2\text{CH}_2\text{CH}_2-\text{Si}(\text{OR})_3$	Enhance the adhesive bonding properties against substrates.
	Water scavenger	Prolonging shelf life.
	Pigments	Offering wide range of colors.
	Rheology additive	Adjust <i>ease-of-use</i> characteristics and features.
	Biocides	Provide fungus growth resistance, e.g. sealing of sanitary devices and equipment.

Note typically: R and R' = CH_3 or C_2H_5 ; X = organic functional group, for example amino, mercapto, vinyl, epoxy, methacryloxy.

concentration of the catalyst and crosslinker. The formulation of a typical silicone sealant based on condensation cure may contain up to 10 components as described in Table 1.

Acetoxy sealants are widely being used in a large number of applications in the construction industry. Where they are incompatible with specific substrates, they can be replaced by neutral cure systems. The alkoxy and oxime cure systems are now available in either transparent (silica filled composition only), or non-transparent/solid color (silica and/or chalk filled composition containing appropriate pigment) versions. Their chemical neutrality enables these systems to offer a wide range of adhesive bonding capabilities to metals (copper, brass, zinc, galvanized steel, aluminium), polyester powder coated metals, and all sorts of brick, concrete masonry, and marble. In some applications, a primer might be required with these sealants, particularly with some metals, and where the assemblage will be exposed to severe weathering conditions.

Perfectly smooth and aesthetic glazed facades of buildings are based on structural glazing technique. It is the method of bonding glass, ceramic, metal, stone or composite panels to the frame of a building. The technique utilizes both the adhesive and sealant properties of silicones. The adhesive supports the glazed panels while absorbing differential movements between dissimilar materials, which can be induced by thermal fluctuations, seismic loading, or bomb blasting [78]. The sealant improves the air and weather tightness of the structure. The structural glazing technique provides the architects with limitless design possibilities. One of the most recent prestigious applications of silicone structural sealants is their use in the 32 glazed capsules of the 'London Eye' rotating wheel. Each glazed capsule, completely enclosed by curved glass held together with silicone structural adhesive sealant, can carry up to 25 people on a rotating, 135 meters diameter wheel.

A further use of silicones is in the electronics industry, where they function as adhesives, sealants, coatings, and encapsulants, with the main applications being sealing and/or bonding. Electronic products can experience extremes in temperature, thermal shocks, relative humidity, radiation, vibrations, ageing, and fast accelerations. Therefore, the silicone product must maintain moderate to strong adhesion, as well as durability of the bonds when exposed to these environmental conditions. Sealing leads, gaskets, and attaching base plates are among common uses of silicones. As the electronics industry has progressed from macro- to micro-scale devices, silicones have addressed many of the new challenges in adhesion and encapsulation. For instance, where configurations are intricate, due to micro grooves or miniscule void spaces, the high spreading coefficient of the uncured silicones allows complete penetration, coverage and encapsulation. When cured, in addition of the protective properties required for the application, adhesion is provided to form a tight and intimate seal between the silicone and the surfaces. The adhesion property has also an added benefit in some cases as it helps holding parts of the device together. Silicone adhesives are also used to hold together various parts of a chip in the manufacture of integrated circuits. The same function of holding micro parts together is also provided by silicone adhesive in micro electromechanical systems (MEMS) devices.

Table 2

Typical components of a silicone adhesive based on hydrosilylation addition cure system

Component	Polymer/additive	Function
Polymer	Alkenyl functionalized PDMS	Backbone of silicone cured network
Crosslinker	Si-H functionalized polymer	Crosslink alkenyl PDMS
Catalyst	Platinum-based complex	Fast cure at room or high temperature
Inhibitor	Various organic or organosilicone types	Delays cure at room temperature and increases pot life
Inorganic or organic filler	Silica, carbon black	Reinforces the mechanical strength
Pigment	Various metallic oxides	Color/thermal stability
Adhesion promoter	Various silanes and proprietary complex compounds	Enhance adhesion of silicone to specific substrates. Prolonged durability.

The selection of the cure system in these applications is directed by constraints such as location of the adhesive in terms of confined space, speed and depth of cure, etc. The volumes of silicones typically applied are relatively small. In general, the uncured adhesive needs to be dispensed in a well-defined and limited area, and needs to stay in place without flowing during cure. No by-products of the cure reaction are acceptable as they may contaminate other sensitive areas of the devices. These constraints often direct the choice to the platinum-catalyzed hydrosilylation cure system that is relatively expensive.

Products that are based on hydrosilylation cure system can be packaged in one or two parts. As the term suggests, in one-part systems all the ingredients are formulated together. The catalytic system is inhibited by chemical means that significantly reduces or prevents the cure at room temperature. In the two-part systems, the polymer and the crosslinker are packaged separately in so-called polymer base and crosslinker system. The catalyst, the inhibitor, the fillers and other additives, including the adhesion promoter are formulated with one or the other parts of the package depending on their chemical reactivity. Overall, a silicone adhesive formulation based on the hydrosilylation reaction may contain up to seven components as described in Table 2.

When formulating a silicone adhesive, sealant, or coating, based on hydrosilylation addition cure, one must consider the following properties of the uncured product: pot life, dispensing technique, rheology, extrusion rate, cure performance. These characteristics directly affect the processing properties of the polymer base or crosslinker parts. The degree of cure conversion at the temperature of interest is determined by properties such as tack free time, cure profile and cure time. Once

Table 3

Typical properties of a silicone adhesive based on hydrosilylation addition cure system

	Property	Unit	Value
As supplied	Color		Specified color
	Viscosity at 23°C	MPa s	30,000
	Specific gravity		1.36
Physical properties of cured adhesive at a specified temperature during a specified time	Durometer hardness	Shore A	40
	Tensile strength	MPa	3
	Elongation at break	%	200
	Any other	x	y
Adhesive properties	Lap shear (Al/glass)	MPa	1.5

The range of these properties can be varied very widely depending on the application and these figures are given for illustration. Depending on specialized applications, other specific properties may be provided.

cured, the typical mechanical properties of the cured silicone can be evaluated, which include hardness, tear strength, tensile strength, and elongation at break. In addition to required adhesive properties, considerations should be taken of thermal conductivity, thermal expansion, resistance to flammability, dielectric properties, volume resistivity, and dissipation factors. Typical properties that characterize a silicone adhesive are based on standard published test methods such as ASTM. Table 3 details some properties of silicone adhesive cured through hydrosilylation reaction.

Silicones are being used in advanced fields of technology. One such field is aerospace where extreme environmental conditions are experienced. These applications include coatings for firewalls, windshields and other thermal barriers, and corrosion protection. In all these applications, the silicones are often not visible.

In general, when one refers to adhesion of a material, it is commonly perceived that strong adhesion is required, and yet, there are numerous applications where the adhesion needs to be very low. Such applications include the use of silicone release molds. Silicone rubbers allow fabrication of three-dimensional articles by simple molding technique. The wetting, spreading, flowing properties of silicones allow the reproduction of extremely fine details. Wax representation of famous people in museums, reproduction of art figurines, and archeological artifacts like fossils constitute some examples of applications of the release property of silicones. In some cases, unwanted adhesion can develop between the article and the silicone rubber mold.

As coatings, silicones must exhibit strong and durable adhesion with the substrate on which they are cured. On the other hand, the surface of the cured

silicone has to provide weak adhesion during its lifetime. For example, in the production of automobile airbags [79], a silicone coating is applied onto a nylon fabric. The function of the silicone is to allow fast inflation of the airbag and to act as a temporary gas barrier. The adhesion of the silicone coating to the nylon fabric must be strong. In addition, it must resist the extreme effects of the environment experienced during the potential long life of a car. On the other hand, the silicone coating must retain its non-stick surface properties to allow the air bag to deploy efficiently in case of an accident.

The weak adhesion of silicones towards organic adhesives has led to the development of silicone release coatings used to dispense labels. Adhesion is high enough to hold the adhesive and the label it supports and low enough to release the label at a predesigned force and release speed. The silicone release technology is so advanced that the adhesion strength can be finely tuned to suit very specific application demands.

In all the applications where silicones are used, the design of the polymer reactivity and the composition of the formulation require the development chemist to thoroughly understand both silicone chemistry and adhesion phenomena.

7. Conclusion

The unique and outstanding physical and chemical properties of silicone polymers have helped create products that have been used in many different technologies. These properties have been extended to the cured networks, and in addition have brought mechanical properties that include elasticity, high shear and tear strength, etc. The wide choice of chemical functional groups that can be attached to silicone polymers has offered the possibility of various crosslinking mechanisms. As a consequence, cure conversion rates can proceed from a fraction of a second to hours, in a wide range of temperatures.

The surface energy of silicones, the liquid nature of the silicone polymers, the mechanical properties of the filled networks, the relative insensitivity to temperature variations from well below zero to very high, and the inherent or added reactivity towards specific substrates, are among the properties that have contributed to the success of silicone materials as adhesives, sealants, coatings, encapsulants, etc.

We have attempted to relate the basics of silicone chemistry to applications where adhesion is an important property. These applications cover a vast industrial arena that does not make a review of this sort easy. Instead, we focused on the fundamental aspects of silicone physics and chemistry and related them to adhesion and adherence properties. We have attempted to use a logical structure to help the reader understand silicone adhesion. Adhesion and cohesion have been considered as they both determine the ultimate performance of an adhesive joint.

The design of a silicone adhesive naturally considers both the creation of adhesive and cohesive strengths to provide the performance needed.

Acknowledgements

The authors wish to thank Francois de Buyl and Andy J. Goodwin for their attentive reading and suggestions.

References

1. Noll, W., *Chemistry and Technology of Silicones*. Academic press, New York, 1968.
2. Ranney, *Silicones*. Noyes Data, Park Ridge, NJ, 1977.
3. Colas, A., Silicones: préparation et performances. *Chim. Nouv.*, **8(30)**, 847–852 (1990).
4. Clarson, S.J. and Semlyen, J.A., *Siloxane Polymers, Polymer Science and Technology Series*. PTR Prentice Hall, Englewood Cliffs, NJ, 1993.
5. Lynch, W., *Handbook of Silicone Rubber Fabrication*. Van Nostrand-Reinhold, New York, 1978.
6. LeGrow, G.E., Solventless silicone resins. Relation between polymer structure and engineering properties. *Soc. Plast. Eng., Tech. Pap.*, **21**, 445–446 (1975).
7. Dolgov, O., Voronkov, M. and Grinblat, M., *Organosilicon Liquid Rubber, Rubber and Plastics Research Associates (RAPRA)*, Monograph 1. Internat. Polym. Sci. Technol., Shawbury, UK, 1977.
8. Warrick, E.L., Pierce, O.R., Polmanteer, K.E. and Saam, J.C., Silicone elastomer developments 1967–1977. *Rubber Chem. Technol.*, **52(3)**, 437–525 (1979).
9. Jones, J.D. and Peters, Y.A., Silicone release coatings. In: *Handbook of Pressure Sensitive Adhesive Technology*. Satas Donatas Ed., Van Nostrand Reinhold, New York, 1989, pp. 601–626.
10. Sobieski, L. and Tangney, T.J., Silicone pressure sensitive adhesives. In: *Handbook of Pressure Sensitive Adhesive Technology*. Satas Donatas Ed., Van Nostrand Reinhold, New York, 1989, pp. 508–517.
11. Ulman, K.L. and Thomas, X., Silicone Pressure Sensitive adhesives for healthcare applications. In: *Advances in Pressure Sensitive Adhesive Technology-2*. Satas Donatas Ed., Satas and Associates, Rhodes Island, 1995, pp. 133–157.
12. Wake, W.C., Silicone adhesives, sealants and coupling agents. *Crit. Rep. Appl. Chem.*, **16**, 89–111 (1987).
13. Schorsch, G., Le comportement non adhérent et adhésif des compositions silicones, *Actual. Chim.*, Mars/Avril, 115–123 (1991).
14. de Buyl, F., Silicone sealants and structural adhesives. *Int. J. Adhes. Adhes.*, **21(5)**, 411–422 (2001).
15. Reuther, H., Über Silikonklebstoffe. *Plaste Kautsch.*, **22(6)**, 513–514 (1975).
16. Langer, M., Silikone: absolut verbindlich. *Kleb-Dichtstoffe*, **40(1)**, 26–31 (1996).
17. Tomanek, A., Silicone adhesives. In: *Adhes. '90 Int. Conf.*, 1990, 66, 1–4.
18. Voronkov, M., Mileshekevich, V. and Yushelevski, Y., *The Siloxane Bond*. Plenum, New York, 1978.
19. Kendrick, T.C., Parbhoo, B. and White, J.W., Siloxane polymers and copolymers. In: Patai,

- S. and Rappoport, Z. (Eds.), *The Chemistry of Organic Silicon Compounds, Part 2*. Wiley, Chichester, 1989, Chapt. 21.
20. Lee Smith, A. (Ed.), *The Analytical Chemistry of Silicones, Vol. 112, Chemical Analysis*. Wiley, New York, 1991.
 21. Hayes, R.A. and Ralston, J., Application of atomic force microscopy in fundamental adhesion studies. In: Mittal, K.L. and Pizzi, A. (Eds.), *Adhesion Promotion Techniques — Technological Applications*. Dekker, New York, 1999, pp. 121–138.
 22. Owen, M.J., Why silicones behave funny. *Chemtech*, **11**, 288 (1981).
 23. Owen, M.J., Surface chemistry and applications. In: Clarson, S.J. and Semlyen, J.A. (Eds.), *Siloxane Polymers, Polymer Science and Technology Series*. PTR Prentice Hall, Englewood Cliffs, NJ, 1993, pp. 309–372.
 24. Owen, M.J., The surface activity of silicones: a short review. *Ind. Eng. Chem. Prod. Res. Dev.*, **19**, 97–103 (1980).
 25. Stepto, R.F.T., Theoretical aspects of conformation-dependent properties. In: Clarson, S.J. and Semlyen, J.A. (Eds.), *Siloxane Polymers, Polymer Science and Technology Series*. PTR Prentice Hall, Englewood Cliffs, NJ, 1993, pp. 373–414.
 26. Clarson, S.J., Depolymerisation, degradation and thermal properties of siloxane polymers. In: Clarson, S.J. and Semlyen, J.A. (Eds.), *Siloxane Polymers, Polymer Science and Technology Series*. PTR Prentice Hall, Englewood Cliffs, NJ, 1993, pp. 216–244.
 27. Ohlberg, S.M., Alexander, L.E. and Warrick, E.L., Crystallinity and orientation in silicone rubber. I. X-ray studies. *J. Polym. Sci.*, **27**, 1–18 (1958).
 28. Warrick, E.L., Crystallinity and orientation in silicone rubber. II. Physical measurements. *J. Polym. Sci.*, **27**, 19–38 (1958).
 29. Homma, H., Kuroyagi, T., Izumi, K., Mirley, C.L., Ronzello, J. and Boggs, S.A., Evaluation of surface degradation of silicone rubber using thermogravimetric analysis, *Proc. Int. Symp. Electr. Insul. Mater.*, 2nd. 1998, 1, pp. 631–634.
 30. Budden, G., High temperature properties of silicone elastomers. *J. Coated Fabr.*, **27**, 294–308 (1998).
 31. Gladyshev, G.P., Theory of stabilizing thermally stable polymers. *J. Polym. Sci. Polym. Chem. Ed.*, **14**(7), 1753–1759 (1976).
 32. White, J.W. and Treadgold, R.C., Organofunctional Siloxanes. In: Clarson, S.J. and Semlyen, J.A., *Siloxane Polymers, Polymer Science and Technology Series*. PTR Prentice Hall, Englewood Cliffs, NJ, 1993, pp. 193–215.
 33. Thomas, D.R., Crosslinking of polydimethylsiloxanes. In: Clarson, S.J. and Semlyen, J.A. (Eds.), *Siloxane Polymers, Polymer Science and Technology Series*. PTR Prentice Hall, Englewood Cliffs, NJ, 1993, pp. 567–615.
 34. Clarson, S.J. and Mark, J.A., Siloxane elastomers, In: Clarson, S.J. and Semlyen, J.A. (Eds.), *Siloxane Polymers, Polymer Science and Technology Series*. PTR Prentice Hall, Englewood Cliffs, NJ, 1993, pp. 616–648.
 35. Dow Corning Corporation, Improved composition curable through Si–H and Si–CH=CH₂, GB Patent 1,272,705, Priority: US 21 May 1969.
 36. Stein, J. and Eckberg, R.P., UV Curable silicone release coatings and controlled release additives. *J. Coat. Fabr.*, **20**, 24 (1990).
 37. Mittal, K.L. and Pizzi, A. (Eds.), *Adhesion Promotion Techniques – Technological Applications*. Dekker, New York, 1999.
 38. Allen, K.W., Greenwood, L. and Wake, W.C., The stability of adhesive bonding between silicone rubber and alumina for neural prostheses. *J. Adhes.*, **16**(1), 61–76 (1983).
 39. Harding, P.H. and Berg, J.C., The adhesion promotion mechanism of organofunctional silanes. *J. Appl. Polym. Sci.*, **67**, 1025–1033 (1998).

40. Wertheimer, M.R., Martinu, L., Klemberg-Sapieha, J.E., and Czeremuszkin, G., Plasma treatment of polymers to improve adhesion. In: Mittal, K.L. and Pizzi, A. (Eds.), *Adhesion Promotion Techniques — Technological Applications*. Dekker, New York, 1999, pp. 139–174.
41. Brewis, D.M. and Mathieson, Flame treatment of polymers to improve adhesion. In: Mittal, K.L. and Pizzi, A. (Eds.), *Adhesion Promotion Techniques — Technological Applications*. Dekker, New York, 1999, pp. 175–190.
42. Uehara, T., Corona discharge treatment of polymers. In: Mittal, K.L. and Pizzi, A. (Eds.), *Adhesion Promotion Techniques — Technological Applications*. Dekker, New York, 1999, pp. 191–204.
43. Buchman, A. and Dodiuk-Kening, H., Laser surface treatment to improve adhesion. In: Mittal, K.L. and Pizzi, A. (Eds.), *Adhesion Promotion Techniques — Technological Applications*. Dekker, New York, 1999, pp. 205–244.
44. Packham, D.E. (Ed.), *Handbook of Adhesion, Polymer Science and Technology Series*. Longman, New York, 1992.
45. Pocius, A.V., *Adhesion and Adhesives Technology— An Introduction*. Hanser, Munich, 1997.
46. Amouroux, J., Goldman, M. and Revoil, M.F., Modification of the wettability of a polyethyleneterephthalate film treated by corona discharge in air. *J. Polym. Sci. Polym. Chem. Ed.*, **2**, 13 (1982).
47. Suzuki, T. and Kasuya, A., Adhesion of addition-reaction type silicone elastomers. *J. Adhes. Sci. Technol.*, **3**(6), 463–473 (1989).
48. Plueddemann, E.P., *Silane Coupling Agents*, Plenum, New York, 1982.
49. Van Ooij, W.J. and Jayaseelan, S.K., Bonding metals to rubber using functional and non-functional silanes. In: *Adhes. '99, 7th Int. Conf. Adhes. and Adhes.*, Conference Prep. 1999, pp. 43–48.
50. Patterson, R.E., In: Kirk-Othmer, Ed., Kroschwitz, J.I. and Howe-Grant, M. (Eds.), *Silica — Introduction, Encycl. Chem. Technol.*, 4th ed., Vol. 21. Wiley, New York, 1997, pp. 977–1005.
51. Deng, Q., Hahn, J.R., Stasser, J., Preston, J.D. and Burns, G.T., Reinforcement of silicone elastomers with treated silica xerogels: silica–silicone IPNs. *Rubber Chem. Technol.*, **73**(4), 647–665 (2000).
52. Polmanteer, K.E. and Lentz, C.W., Reinforcement studies. Effect of silica structure on properties and crosslink density. *Rubber Chem. Technol.*, **48**(5), 795–809 (1975).
53. Langley, N.R. and Polmanteer, K.E., Relation of elastic modulus to crosslink and entanglement concentrations in rubber networks. *J. Polym. Sci. Polym. Phys. Ed.*, **12**(6), 1023–1034 (1974).
54. Langley, N.R. and Polmanteer, K.E., Role of chain entanglements in rubber elasticity. *Polym. Prep. Am. Chem. Soc. Div. Polym. Chem.*, **13**(1), 235–240 (1972).
55. Comyn, J., *Adhesion Science*. RSC Paperbacks, The Royal Society of Chemistry, 1997.
56. Kinloch, A.J., *Adhesion and Adhesives—Science and Technology*. Chapman and Hall, London, 1987.
57. Wu, S., *Polymer Interface and Adhesion*. Dekker, New York.
58. Schultz, J. and Nardin, M., Theories and mechanisms of adhesion. In: Mittal, K.L. and Pizzi, A. (Eds.), *Adhesion Promotion Techniques — Technological Applications*. Dekker, New York, 1999, pp. 1–26.
59. Roche, A.A. and Romand, M.J., Adhesion: théories et mesures expérimentales. *Double liaison — Chim. Peintures*, **31**, 503–511 (1984).

60. Packham, D.E., The mechanical theory of adhesion — changing perceptions 1925–1991. *J. Adhes.*, **39**, 137–144 (1992).
61. Packham, D.E. and Johnston, C., Mechanical adhesion: were McBain and Hopkins right? An empirical study. *Int. J. Adhes. Adhes.*, **14**(2), 131–135 (1994).
62. Deruelle, M., Tirrell, M., Marciano, Y., Hervet, H. and Leger, L., Adhesion energy between polymer networks and solid surfaces modified by polymer attachment. *Faraday Discuss.*, **98**, 55–65 (1995).
63. Jones, F.R., Interfacial aspects of glass fibre reinforced plastics. In: Jones, F.R. (Ed.), *Interfacial Phenomena in Composite Materials*. Butterworths, London, 1989, pp. 25–32.
64. Chaudhury, M.K., Gentle, T.M. and Plueddemann, E., Adhesion mechanism of poly(vinyl chloride) to silane primed metal surfaces. *J. Adhes. Sci. Technol.*, **1**(1), 29–38 (1987).
65. Gellman, A.J., Naasz, B.M., Schmidt, R.G., Chaudhury, M.K. and Gentle, T.M., Secondary neutral mass spectrometry studies of germanium–silane coupling agent–polymer interphases. *J. Adhes. Sci. Technol.*, **4**(7), 597–601 (1990).
66. Gentle, T.E., Schmidt, R.G., Naasz, B.M., Gellman, A.J. and Gentle, T.M., Organofunctional silanes as adhesion promoters: direct characterization of the polymer/silane interphase. *J. Adhes. Sci. Technol.*, **6**, 307–316 (1992).
67. Klosowski, J.M., *Sealants in Construction*. Dekker, New York, 1989.
68. Wolf, A.T., Durability of silicone sealants, in press.
69. Wolf, A.T. (Ed.), *Durability of Building Sealants*, State-of-the-Art Report #21 of RILEM Technical Committee 139-DBS, RILEM publication S.A.R.L., 1999.
70. Jacques, L.F.E., Accelerated and outdoor/natural exposure testing of coatings. *Prog. Polym. Sci.*, **25**, 1337–1362 (2000).
71. Shephard, N.E., Klosowski, J.M. and Wolf, A.T., Effects of degradation factors on sealant adhesion, in press.
72. O'Hare, L.-A., Leadley, S.R., Parbhoo, B. and Francis, J.G., Adhesion of silicone coatings to polypropylene films. *Polym. Prep. (Am. Chem. Soc. Div. Polym. Chem.)*, **42**(1), 103–104 (2001).
73. O'Hare, L.-A., Parbhoo, B., Leadley, S.R., Goodwin, A.J., Smith, J.A. and Watts, J.F., Adhesion and surface physico-chemistry of plastic films. In: *Adhes. '99, 7th Int. Conf. Adhes. and Adhes.*, Conference Prep. 1999, pp. 25–30.
74. Comyn J., Communication quoted in Allen, K.W., Greenwood, L. and Wake, W.C., *J. Adhes.*, **16**(1), 61 (1983).
75. Gauthier, L.A., Falender, J.R. and Howell, B.A., An investigation of the mechanism of adhesive failure of polydimethylsiloxane elastomers was conducted. *Polym. Prep. (ACS Div. Pol. Chem.)*, **23**(1), 264–265 (1982).
76. Wolf, A.T., Material properties of construction sealants. *Kautschuk Gummi Kunststoffe*, **41**(2), 173–178 (1988).
77. Lee, T.C.P. and Wolf, A.T., Factors governing the durability of sealant formulations. In: A.T. Wolf (Ed.), *Durability of Building Sealants*, State-of-the-Art Report #21 of RILEM Technical Committee 139-DBS, RILEM publication S.A.R.L., 1999, pp. 203–223.
78. Hautekeer, J.-P., Structural glazing — direction for the future, *Int. Glass Rev.*, **3** (2000).
79. Crouch, E.T., Evolution of air bag components and materials. *Aut. Eng.*, **2**, 99–103 (1994).

Chapter 15

Hot melt adhesives

CHARLES W. PAUL *

National Starch and Chemical, Bridgewater, NJ 08807, USA

1. Introduction

For many bonding applications a variety of adhesives can perform adequately. Hot melt adhesives are normally chosen where process speed is critical. Since hot melts have no carrier vehicle (solvent or water), and thicken rapidly as they cool, they are limited in their ability to: (1) penetrate low porosity substrates or wet out very rough surfaces; (2) cut through or imbibe surface contaminants; and (3) wet out high thermal conductivity substrates (e.g. metals). Nonetheless, hot melts are increasingly the adhesive of choice in automated production environments because of their fast set speed.

The vast majority of hot melts are non-reactive; i.e. they remain thermoplastic during use. In order to achieve adequate strength from a non-reactive hot melt some component of the adhesive must separate out into a dispersed hard phase upon cooling. The hard phases are commonly either glassy styrene domains (for adhesives based on styrenic block copolymers) or organic crystallites (for adhesives based on waxes and/or olefinic copolymers or ethylene copolymers). This chapter will describe first the chemistry of the raw materials used in hot melts, and then typical formulations and general considerations for each of the major applications. Reactive hot melts, a small but rapidly growing class of hot melts, will be discussed in a separate section since these involve unique raw materials and formulating considerations. The chapter concludes with a brief section on equipment and test methods, followed by a discussion of overall trends in hot melt development.

2. Raw materials

Adhesives need to produce high peel forces when the adherends are pulled apart — preferably high enough to induce substrate failure. To accomplish high peel, the

* Corresponding author. E-mail: charles.paul@nstarch.com

Table 1
Primary hot melt ingredients

Ingredient	Physical properties	Function
Polymer	High MW ($> 10,000$) T_g usually $< RT$ Physically crosslinks on cooling Strong	Strength Hot tack Viscous loss \rightarrow peel force
Resin	Low MW (< 5000) T_g usually $> RT$ Amorphous	Lower viscosity Improve wet out Adjust T_g of system
Diluent	Low MW (< 1000) $T_g < RT$ Amorphous	Lower viscosity Improve wet out Adjust T_g of system
Wax	Low MW (< 2000) $T_g < RT$ Crystalline	Speed set Heat resistance Lower viscosity

adhesive must first prevent easy interfacial failure through good wet out, adequate specific adhesion, and for rigid adherends, sufficiently low modulus to induce the deformation to start in the adhesive layer. Secondly, the adhesive must require high levels of irreversible work to be either debonded or fractured. The latter requirement, a rheological requirement, necessitates careful adjustment of the matrix T_g and morphology of the adhesive by the formulator. The roles of the key types of raw materials used in adhesive formulas in accomplishing these tasks are described in Table 1. Polymers provide strength, hot tack (viscous dissipation in the warm fluid state), and fracture energy (high peel resistance in use). Tackifiers and diluents serve similar purposes: reduce viscosity for machinability, improve wet out, and adjust the matrix T_g . Waxes also lower the viscosity, provide rapid set (strength development), and heat resistance in the final product. In what follows, the specific chemistries used in hot melts for each of these ingredient types will be discussed.

2.1. Polymers

2.1.1. Block copolymers and other rubbers

Rubbery materials are defined by ASTM (D1566) as those which will have less than 50% permanent set after one minute when recovering from a strain of 100% applied for one minute. Of the many 'rubbery' materials available, block copolymers are by far the most common used in hot melts.

Non-block polymers which are 'rubbery', such as styrene–butadiene random copolymers, polyisobutylene, butyl rubber, ethylene–propylene, or natural (*cis*-polyisoprene) rubber, are in general of too high a molecular weight (>500,000 g/mol) for incorporation into hot melt adhesives [1]. Most hot melt manufacturing equipment is not capable of handling these materials efficiently if at all, and most hot melt applicators require viscosities of 50,000 cP or below, which would permit incorporation of only very small levels of such high viscosity 'rubbers'. However, even low levels can be of significant utility in improving properties and are employed in special situations.

Block copolymers can contain crystalline or amorphous hard blocks. Examples of crystalline block copolymers are polyurethanes (e.g. B.F. Goodrich's Estane[®] line), polyether esters (e.g. Dupont's Hytrel[®] polymers), polyether amides (e.g. Atofina's Pebax[®] grades). Polyurethanes have enjoyed limited utility due to their relatively low thermal stability; use temperatures must be kept below 275°F, due to the reversibility of the urethane linkage. Recently, polyurethanes with stability at 350°F for nearly 100 h have been claimed [2]. Polyether esters and polyether amides have been explored for PSA applications where their heat and plasticizer resistance is a benefit [3]. However, the high price of these materials and their multiblock architecture have limited their use. All of these crystalline block copolymers consist of multiblocks with relatively short, amorphous, polyether or polyester mid-blocks. Consequently they can not be diluted as extensively with tackifiers and diluents as styrenic triblock copolymers. Thereby it is more difficult to obtain strong, yet soft adhesives — the primary goals of adding rubber to hot melts.

Of the amorphous block copolymers, styrenic block copolymers are the vast majority. These are synthesized anionically in solution, with butyl lithium commonly employed as the initiator [4]. There are three processes for this polymerization:

(1) *Sequential*: one styrene block is polymerized, then the mid-block monomer is added and polymerized, then more styrene is added and the second styrene block polymerized. This process is used to produce 100% triblock rubbers, for maximum strength [5]. Termination is commonly with alcohols, which produces a lithium alkoxide salt as the by-product.

(2) *Coupling*: one styrene block is polymerized, then the mid-block monomer is added and polymerized, and then a coupling agent is added to link two or more of these diblock 'arms' together. Coupling is the most common method. Coupling is never 100%, so some residual diblock is always present. This residual diblock reduces the ultimate strength of the adhesive, but can improve its viscous loss, and thus its presence is often desirable in PSAs [6]. Divalent coupling agents are the most prevalent, a common one is dibromoethane. Tri- and tetra-valent coupling agents are also employed. A common tetravalent coupling agent is silicon tetrachloride. Polymers with more than two and up to four arms are termed 'radial' polymers [7]. Polymers with more than four arms can be obtained by terminating

the chains with a multifunctional crosslinking monomer, such as divinylbenzene [8,9] or a cyclosiloxane [10,11]. Polymers with more than four arms, typically 8–12, are obtained by this method. These materials are generally called ‘star’ polymers. Conventional coupling agents for tri-block or radial polymers produce lithium halide salts as the by-product. This salt can be removed, but complete removal is usually cost-prohibitive. The residual salts reduce the color stability of coupled polymers versus those produced sequentially. Newer coupling agents are being developed that produce more thermo-oxidatively color stable by-products.

(3) *Multiblock process*: Firestone has a trade secret process that produces rubbers with a ‘multiblock’ structure, tapering of the blocks (i.e. there is not a sharp transition between the styrene and mid-block monomer composition), a broader molecular weight distribution (typically $M_w/M_n \sim 2$ versus 1.05–1.1 for the other processes).

The properties of styrenic block copolymers are dependent on many factors besides the polymerization process. The styrene end block is typically atactic. Atactic polystyrene has a molecular weight between entanglements (M_e) of about 18,000 g/mol. The typical end block molecular weight of styrenic block copolymers is less than M_e . Thus the softening point of these polymers is less than that of pure polystyrene. In fact many of the raw materials in hot melts are in the oligomeric region, where properties still depend on molecular weight (see Fig. 1).

The mid-block monomers are primarily isoprene and butadiene. These diolefins can polymerize in several ways. The isomeric structure of the final polymer has a strong impact on its properties and thermal stability. Isomeric composition is easily varied by changing the polymerization solvent or adding complexing agents. The typical isomeric structures for isoprene and butadiene mid-blocks are shown in Fig. 2.

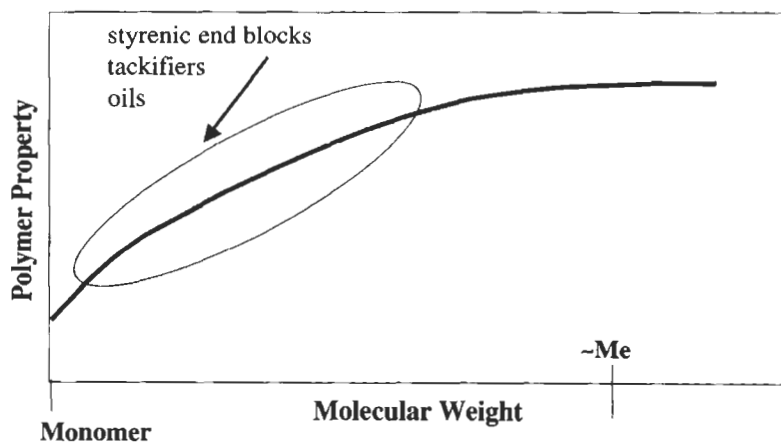
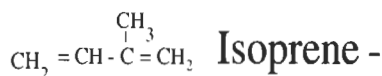

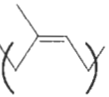
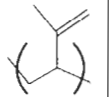
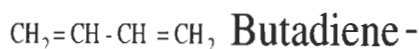


Fig. 1. Polymer property vs. molecular weight.



				For Typical ^a wt. %
	trans 1,4	cis 1,4	"vinyl" 3,4	
typical wt. %	20	73	7	
T _g pure (°C)	-66	-71	20	-60°C
M _e (g/mol)	NA	NA	NA	7,000
^a Note: high "vinyl" SIS (SVS) used for sound dampening				




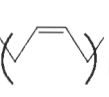
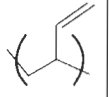
				For Typical ^a wt. %
	trans 1,4	cis 1,4	"vinyl" 1,2	
typical wt. %	50	40	10	
T _g pure (°C)	-83	-95	-10	-85°C
M _e (g/mol)	NA	2,900	1,700	1,700
^a Note: SBS precursors to SEBS have ~30% "vinyl" to avoid crystallization upon hydrogenation.				

Fig. 2. T_g and M_e for isomers of polybutadiene and polyisoprene, and for typical average isomeric compositions in styrenic block copolymers.

Table 2
Comparing block copolymers

	SBS	SIS	SEBS	SEPS	Styrene
Cost (\$/lb)	0.75	1.00	1.90	2.30	
Thermal stability	Fair-poor	Poor	← Excellent →		
Mid-block					
M_e (g/mol)	1700	7000	~1700	1660	17,300
T_g (°C)	-85	-60	-55	-55	95
Solubility parameter (cal/cm ³) ^{1/2}	8.35	8.15	7.75	7.65	9.9

SBS and SIS can be subsequently hydrogenated to form SEBS and SEPS, respectively. SEBS is obtained from SBS with a higher vinyl content (typically around 30%) in order to avoid crystallization of the mid-block. The properties of all four of these common styrenic block copolymers are displayed in Table 2.

In general, the saturated block copolymers are used where long term thermo-oxidative stability is critical, or where compatibility with other low polarity adhesive ingredients is required. SIS is most commonly employed in pressure-sensitive adhesives because of its high M_e and lower solubility parameter in comparison to butadiene. The high M_e allows more polymer of higher molecular weight to be added to the adhesive formula while maintaining adequate softness and an acceptable viscosity. The high M_e and lower solubility parameter of isoprene provides good phase separation between the blocks even at low styrene content, again leading to softer adhesives. SBS is primarily employed where low cost and/or improved thermal stability vs. SIS is needed.

2.1.2. Polyolefins (LDPE and APAO)

The majority of polyolefins used in hot melt adhesives today are synthesized via conventional Ziegler–Natta polymerization. Thus they have relatively broad molecular weight distributions and consequently poor sprayability and machining in general [12]. Compared to plastic or film grade polyolefins, adhesive grade materials are lower in MW, and lower in crystallinity by virtue of high levels of branching and/or comonomer. Low density polyethylene polymers are used in some packaging adhesives where fast set and high crystallinity are needed. Maleated grades are often employed to improve specific adhesion of these relatively non-polar formulas [13].

Where longer open time is needed, atactic olefin homo- and co-polymers (APAOs) are used. These materials incorporate one to three monomers to achieve a desired set of properties. The monomers used are ethylene, 1-butene, propylene, and sometimes 1-hexene [14,15]. Propylene polymerized atactically produces the highest softening points ($\sim 155^\circ\text{C}$) due to a small fraction of high molecular weight isotactic material. Open times are also the shortest and cost is lowest. Butene-based materials combine long open time with high ultimate crystallinity and high strength. These materials all require no formulation to exhibit adhesive properties. Their adhesive properties arise from their low surface tension and long open time (providing excellent wet out) combined with their low crystallinity which minimizes shrinkage stresses, lowers modulus, and reduces strength. Low modulus and strength promote cohesive failure versus interfacial failure. Cohesive failure produces high energy dissipation and thus high peel force on debonding. Tensile strength of the pure materials is generally less than 1/10 that of conventional plastic grade PE or PP. Formulations typically employ low levels of tackifier (10–40%) sometimes in combination with oil (5–15%). Recently, silanated materials have become available which exhibit improved adhesion to polar surfaces [16]. These olefins are sold by Huntsman (Rextac[®]), Eastman (Eastoflex[®]), and Creanova (Vestoplast[®]).

The broad molecular weight distribution (MWD) and low cohesive strength of

Table 3

Effect of base polymer polydispersity on ease of forming a uniform spiral spray pattern from the corresponding adhesives

Polymerization method	Hot melt base polymers	Typical M_w/M_n	Sprayability
Anionic	Styrenic block copolymers (SBS, SIS, SEBS, SEPS)	1.0–1.1	Excellent
Metallocene	Olefin copolymers	1.5–2.5	Very good
Free radical	EVA, EnBA	2.5	Good
Ziegler–Natta	Olefin copolymers	4–8	Marginal

APAOs has limited their utility in a number of applications. The broad MWD produces poor machining and spraying, and the low cohesive strength causes bond failures at temperatures well below the softening point when minimal stress is applied. To address these deficiencies, metallocene–polymerized materials have been developed [17,18]. These materials have much narrower MWDs than Ziegler–Natta polymerized materials and a more uniform comonomer distribution (see Table 3). Materials available commercially to date are better suited to compete with conventional EVA and EnBA polymers, against which their potential benefits have yet to be realized in practice.

2.1.3. Ethylene copolymers (EVA and EnBA)

Ethylene vinyl acetate (EVA) is the most common polymer used in hot melt adhesives for packaging applications [19]. Vinyl acetate levels used in adhesives vary from 6 to 40%. The higher the vinyl acetate the softer and less crystalline the polymer. At about 50% vinyl acetate all crystallinity is lost (see Fig. 3). EVAs exhibit compatibility with a wide range of tackifying resins and waxes. Their recrystallization rate is greatly influenced by the choice of resin. These attributes provide a wide range of formulating latitude to produce customized adhesives. While EVAs exhibit outstanding viscosity stability, they slowly release acetic acid upon thermo-oxidative degradation. Formulations based on ethylene *n*-butyl acrylate (EnBA) were developed to address this deficiency [20]. Alternatively, low application temperature adhesives (250–275°F vs. conventional 350°F grades) based on lower MW EVA base polymers are now available [21].

Since butyl acrylate is higher in molecular weight than vinyl acetate, higher weight fractions are needed to achieve the same final level of crystallinity in the ethylene copolymer. Typically packaging grades contain 33% butyl acrylate. Thermal stability is far better than EVA, with butene rather than acetic acid produced upon decomposition. Acetic acid can catalyze further polymer decomposition and corrosion of the application equipment. Low temperature properties are also

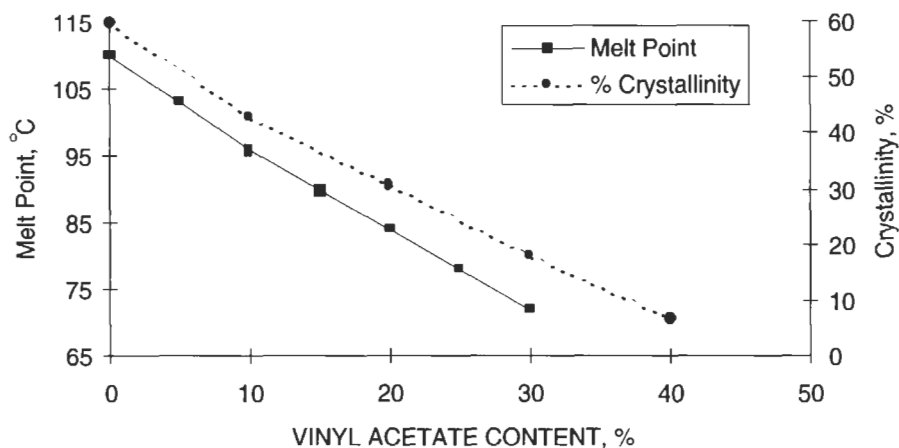


Fig. 3. Melting point and crystallinity vs. weight percent VA in EVA copolymers. (Courtesy of Exxon Chemical Company.)

improved with EnBA, which may be due to its longer open time (and thus better wet out), or the lower T_g of EnBA vs. EVA (-38°C vs. -26°C for 35% BA vs. 28% VA).

2.2. Resins (tackifiers)

In most adhesives, tackifier is the ingredient present in the highest proportion. Tackifying resins are primarily used to reduce adhesive viscosity and adjust the T_g of the adhesive's amorphous matrix phase. Through their effects on the other ingredients and the overall system they can also dramatically affect wet out, hot tack, open time, set speed, and heat resistance.

Tackifiers are high T_g , low molecular weight, amorphous materials. They act as solid solvents for the other ingredients in the adhesive. While they are often selected based on their solubility parameter match up with the other matrix phase components of the formula (see Fig. 4), other properties often dominate tackifier compatibility. These properties are: (1) the enthalpy of the pure tackifier — if it is able to pack well with itself, promoting strong interactions, it will be less prone to dissolve other materials; and (2) molecular weight, i.e. the lower the molecular weight the higher the entropy of mixing with the other ingredients and thus the stronger the solvency power. In practice these considerations result in higher solvency power and thus broader compatibility range for tackifiers with a high content of: (a) rings, particularly fused non-aromatic rings which pack poorly and provide a high T_g for a low molecular weight; and (b) branched vs. linear structures. Thus for instance, while rosin esters (branched, fused three ring structure) have a solubility parameter close to styrene, they are excellent tackifiers

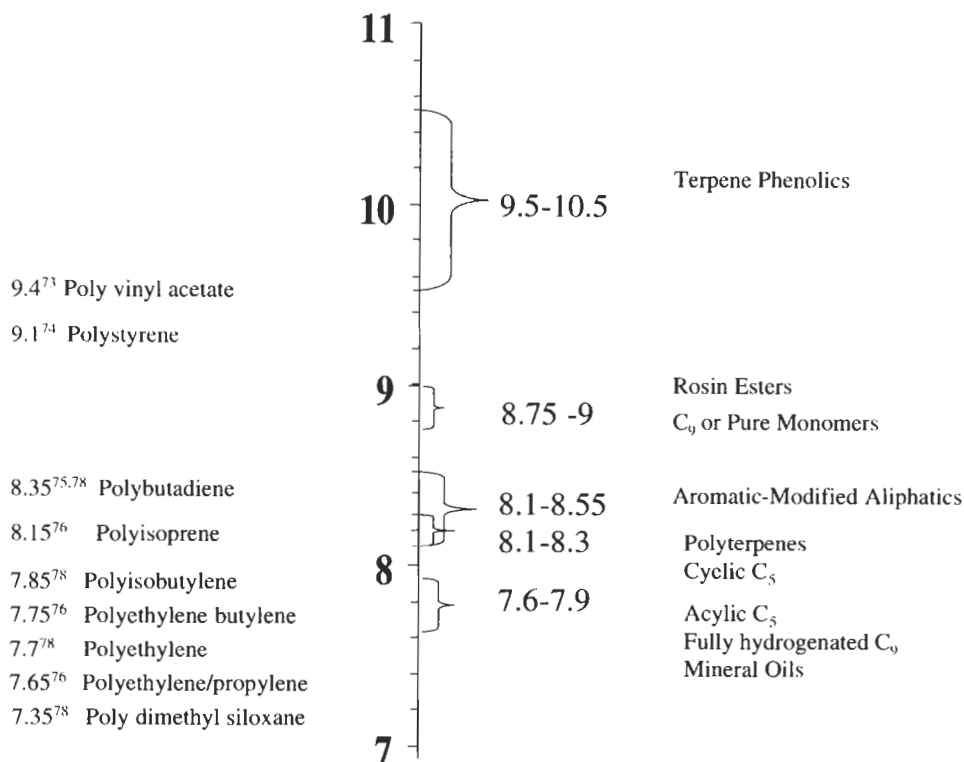


Fig. 4. Solubility parameters of common polymers and classes of tackifiers [77].

for materials ranging from polyisobutylene to polyvinyl acetate. In contrast, pure monomer aromatic resins, which have a solubility parameter close to rosin esters, have much more limited compatibility. These resins can form a separate third phase even in SBS and SIS-based adhesives under certain conditions [100,101].

2.2.1. Naturally derived (rosin and terpene based)

2.2.1.1. Rosin and rosin esters. Rosins are derived from tree stumps (wood rosin), sap (gum rosin), or pulpwood (tall oil rosin). Rosin is a C₂₀ mono-acid with three fused C₆ rings. A variety of isomers occur naturally, the preponderance of which depends on the source of the rosin [22]. Abietic acid is the most common isomer (see Fig. 5). Rosin is an outstanding tackifier. Its fused ring structure provides high solvency power for a wide range of polymers. The acid group improves specific adhesion to most substrates. However, its dark color, strong odor, poor thermo-oxidative stability, and the potential for allergic reactions limit its use. With a softening point of 80°C, rosin is also prone to block and therefore

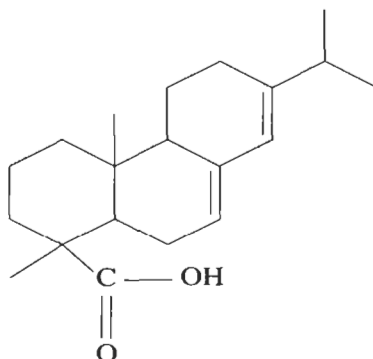


Fig. 5. Abietic acid, the largest component in most resin acids.

is generally sold in solid drums which are 'cracked' on site into chunks of a size suitable for adding to a hot melt mixer. Highly hydrogenated variants overcome some of these deficiencies, but are expensive and prone to crystallize slowly over time in adhesive formulas.

Rosin esters are produced by condensing rosin with various polyols, of which glycerin and pentaerythritol are the most common. Softening points vary with polyol from solid (glycerin and pentaerythritol) to semisolid (diethylene glycol) to liquid (methyl ester). All contain some residual rosin, with acid numbers typically 7–15. Like pure rosin, rosin esters exhibit high solvency power for a variety of polymers. Where polymers are marginally compatible with other synthetic resins, rosin esters are often added as a compatibilizing agent.

2.2.1.2. Polyterpenes. Polyterpenes is one of the first classes of non-polar tackifiers to be developed. Terpene monomers are a by-product in the extraction of rosin from wood stumps or tree sap, and from the extraction of oils from citrus fruits. The latter is the dominant source. As such, polyterpene prices generally mirror those of citrus fruits, which fluctuate substantially from one growing season to the next. Terpenes like rosin are cyclic, see Fig. 6, which is partly responsible for their excellent solvent properties.

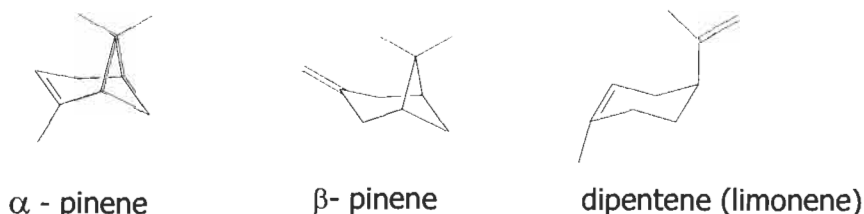


Fig. 6. Terpene monomers.

Polyterpenes enjoy a number of FDA approvals. They are not only suitable for adhesives with indirect food contact, but also for use in both chewing gum and in films that will have direct food contact. Their higher price compared to petroleum-derived equivalents has resulted in a significant decline in usage over the past 10 years, except where FDA approvals dictate their usage.

2.2.2. Petroleum-derived

The refining of oil produces the monomer feed streams for tackifiers as by-products of the process. Tackifiers are low molecular weight polymers, typically 300–5000 g/mol, most often 500–1000 g/mol. Generally molecular weights are well below M_e and thus, within a given class of resins, softening points are controlled primarily by molecular weight (see Fig. 1).

2.2.2.1. C5 resins.

Acyclic C5. The C5 petroleum feed stream consists mainly of isoprene which is used to produce rubber. In a separate stream the linear C5 diolefin, piperylene (*trans* and *cis*), is isolated. Piperylene is the primary monomer in what are commonly termed simply 'C5' resins. Small amounts of other monomers such as isoprene and methyl-2-butene are also present. The latter serves as a chain terminator added to control molecular weight. Polymerization is cationic using Friedel–Crafts chemistry. Because most of the monomers are diolefins, residual backbone unsaturation is present, which can lead to some crosslinking and cyclization. Primarily, however, these are linear acyclic materials. Acyclic C5 resins are sometimes referred to as 'synthetic polyterpenes', because of their similar polarity. However, the cyclic structures within polyterpenes provide them with better solvency power and thus a broader range of compatibility than acyclic C5s.

Cyclic C5. The petroleum stream containing C4–C7 materials is heated prior to further separation to convert, via Diels–Alder chemistry, the cyclopentadiene-containing species to higher adducts such as dimers and other cyclic diene products. This cyclic diene C10–C12 stream is polymerized thermally via further Diels–Alder chemistry and free radical processes to oligomeric materials with a variety of ring, multiring, and bridged ring structures (see Fig. 7). As with polyterpenes, these ring structures reduce the packing efficiency of the oligomers and thus increase their solvency power towards other materials. Commonly, cyclic C5 tackifiers are subsequently hydrogenated to produce water white materials.

2.2.2.2. *Aromatic resins.* Fully aromatic resins are used in block copolymer and ethylene copolymer systems. In the former they are soluble in the styrenic end blocks upon cooling where they serve to increase the strength, stiffness, and creep

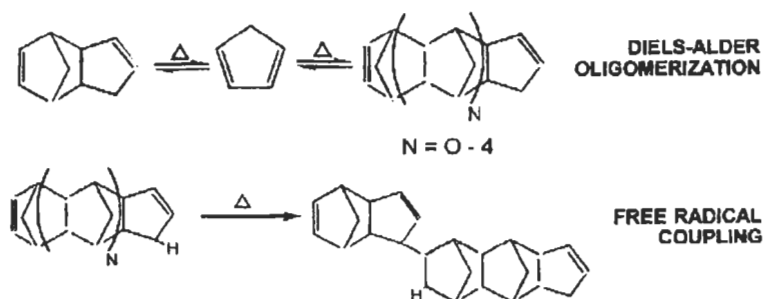


Fig. 7. Thermal oligomerization of dicyclopentadiene.

resistance of the adhesive. In ethylene copolymer-based systems they are used in packaging formulations as part of the resin package to control set speed, hot tack, and heat resistance.

C9. The higher boiling aromatic petroleum stream is fractionated to produce a stream containing C8–C10 vinyl aromatics (see Fig. 8). This monomer stream is normally oligomerized via cationic Friedel–Crafts chemistry. Without subsequent hydrogenation the final products have a strong gasoline-like odor which limits their acceptance. Severe hydrogenation is practised to produce water-white resins with varying amounts of residual aromaticity and cycloaliphatic rings. This method is an alternate route to copolymerization (see discussion below) to produce partially aromatic resins.

Pure monomer. Nearly pure indene, α -methyl styrene, and vinyl toluene are polymerized to make ‘pure monomer’ resins. These resins are an alternative to C9 resins. They offer nearly water white color and vastly reduced odor, but at higher cost. Softening points range as high as 155°C for polyindene, whereas C9 softening points are all below 120°C.

2.2.2.3. Copolymer resins.

Aliphatic/aromatic. Copolymerization of aliphatic monomers (terpenes, cyclic C5, and acyclic C5) with the aromatic C9 petroleum stream is used to produce

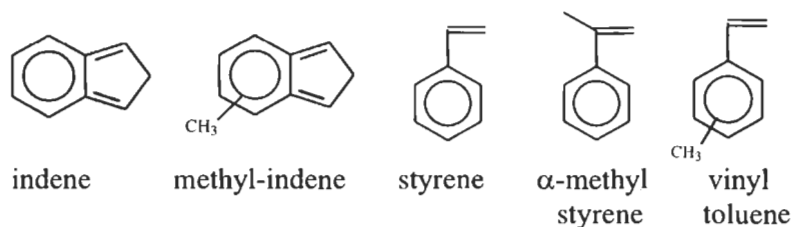


Fig. 8. Vinyl monomers in the C₈–C₁₀ feed stream which polymerize to ‘C₉’ resins.

resins of intermediate polarity. The bulk of the commercial resins are primarily aliphatic (5–30% aromatic), although primarily aromatic resins are also available. As the aromaticity of aliphatic resins increases, their compatibility with packaging grade EVAs and EnBAs improves as does their compatibility with butadiene-based styrenic block copolymers. The viscosity of adhesives based on SBCs (all types) also decreases as the aromaticity of the resin is raised. This effect is due to reduced association of the end blocks in the adhesive melt. Adhesive softening point generally declines since some fraction of the resin will be soluble in the end block and the resin T_g is generally lower than the pure end block T_g . As the aromaticity of the resin increases the amount of resin residing in the end block increases and correspondingly its effect on the softening point.

Phenol modified. Cationic alkylation of phenol by olefins is used to produce resins of high polarity. Terpene phenolics are the most common, although styrene, α -methyl styrene, and rosin-phenolics are also available. Alkylation occurs at the *ortho* and *para* positions, and also the hydroxyl group. Typically about half the phenol groups are alkylated. Softening points up to 150°C are available. These materials tend to have some residual phenolic-type odor. They are used to improve specific adhesion to substrates capable of hydrogen bonding and to improve the heat resistance of ethylene copolymer-based adhesives through hydrogen bonding with the ester groups of the comonomer [23].

2.3. Petroleum-derived oils

While natural oils are occasionally used in hot melt adhesives, this is for specialized purposes. The stronger odor, higher cost, lower thermal stability, and much higher polarity of natural oils (triglycerides) limits their utility. The oils used in hot melts fall into two broad categories based on the crude oil source: naphthenic and paraffinic. Naphthenic crudes are higher in aromatic and cycloparaffin content. Both are unsuitable for hot melt use without significant hydro-finishing. Hydro-finishing at high temperature (250–300°C) and hydrogen pressure (800–2000 psi) eliminates all but traces of sulfur and nitrogen (primarily from heterocyclic species), cleaves some of the fused multiring structures, and converts most of the aromatics to cycloparaffins. Particularly important is the elimination of polyaromatic species, which are carcinogenic. Depending on the degree of hydrogenation, oils are classified as ‘process’ or ‘white’ oils. Process oils are less severely hydrogenated. For medical or skin contact applications USP approval may be needed.

Even after hydrogenation, naphthenic and paraffinic oils differ. Naphthenics will contain a higher level of cycloparaffins (from the higher initial level and the hydrogenated aromatics) whereas paraffinics will contain more branched and linear species. As a result, naphthenic oils have a higher T_g than paraffinic oils

Table 4

Adhesive properties^a vs. oil type

	Oil		
	Napthenic white oil 68 cSt	Paraffinic white oil 68 cSt	Paraffinic white oil 100 cSt
Midblock T_g (°C)	9	8	12
T at which $G' = 10^3$ dynes/cm ² (°C)	87	91	94

^aThe adhesive contained 20/57/23 SBS/C5/C9-resin/oil. The midblock T_g was taken as the peak in tan delta by RDA. The T at which $G' = 10^3$ dynes/cm² is a comparative measure of where the styrene end blocks softened.

(about -55°C vs. about -70°C for paraffinics), yet exhibit a lower cloud point temperature (temperature at which the normal paraffins crystallize). In addition, napthenic oils have higher solvency power (more rings, again), thus more can be added to the formula and they exhibit a greater compatibilizing effect. However, in rubber-based adhesive systems the higher solvency power of napthenics also leads to greater solubility in the styrene end blocks, and thus reduced softening point and heat resistance (see Table 4).

Oils, like tackifiers, are oligomeric species, thus their properties will depend on molecular weight. Solvency power goes down and T_g goes up with molecular weight (see Fig. 9 and Table 5, respectively). Typical molecular weights are in the 300–600 g/mol range. At the lower end of this range flammability can become an issue, particularly in the initial stages of hot melt production where the oil exerts its full vapor pressure. Fires can and have occurred when oxygen is not carefully excluded.

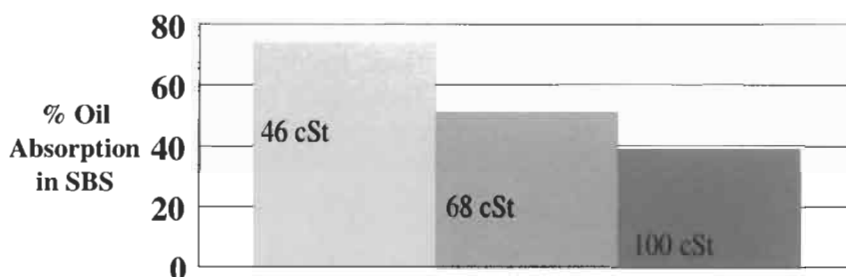


Fig. 9. Oil absorption vs. oil MW. $1 \times 1 \times 0.050$ inch coupons of SBS (Stereon 841A) were immersed in paraffinic process oils of varying molecular weight (kinematic viscosity) for 300 days.

Table 5

Effect of oil MW on oil T_g ^a

Kinematic viscosity (cSt)	13	99
T_g (°C)	-89	-67

^a Paraffinic white oils from the same source but varying in molecular weight as indicated by their viscosity differences.

2.4. Waxes

Waxes fall into two main classes: petroleum fractions and synthetic waxes. Waxes are obtained from crude oil as outlined in Fig. 10. The lower molecular weight 'paraffin' waxes tend to be more highly crystalline by virtue of a higher normal paraffin content (see Table 6). Paraffin wax is also cheaper and very low in viscosity. While its melting point is low ($\sim 65^\circ\text{C}$) it is very sharp, and provides adequate heat resistance for most packaging applications. Microcrystalline waxes at the other extreme, have higher molecular weights and melting points, but have a broad melting peak and are less crystalline. In fact microcrystalline waxes begin to melt before paraffinic waxes (see Figs. 11 and 12) and thus despite their higher final melting point, they generally produce adhesives with less heat resistance.

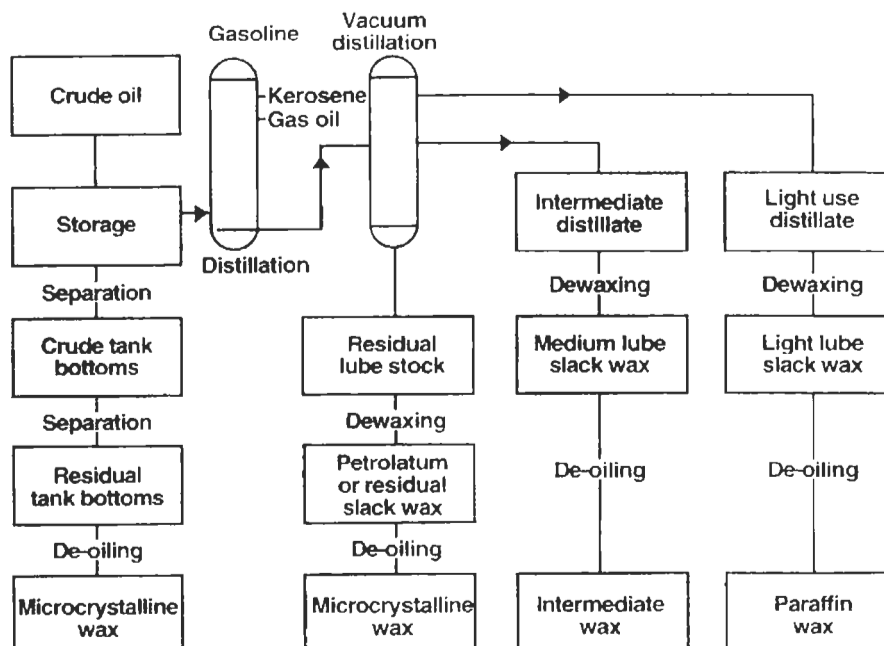


Fig. 10. How wax is extracted from crude oil [24].

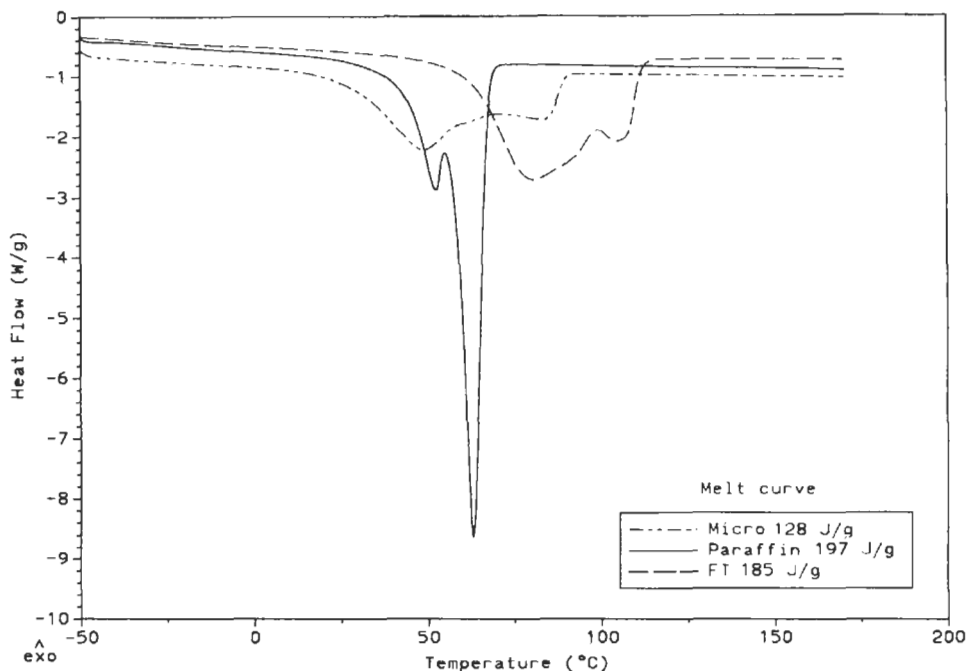


Fig. 11. DSC of microcrystalline, paraffinic, and Fischer–Tropsch waxes on the reheat cycle. Samples were first heated to 175°C, then cooled to –50°C, followed by reheating to 175°C, all at 20°C/min. Heat of fusion for each is shown in the legend.

Rather, microcrystalline waxes are used to provide adhesives with longer open times and better low temperature adhesion, due to better wet out, and toughness.

Synthetic waxes consist of Fischer–Tropsch, polyethylene, and specialty waxes. Fischer–Tropsch waxes are produced from synthesis gas (CO and H₂). They are often termed ‘synthetic paraffin’. Crystallinity is similar to paraffin, but with a higher and bimodal melting point (see Figs. 11 and 12). F–T waxes are used instead of paraffin where higher heat resistance is needed.

Table 6

Petroleum fraction wax compositions [24]

	<i>n</i> -Alkanes (%)	Iso- and cyclo-alkanes (%)	Carbon atoms per molecule
Paraffin	87	13	18–40
Intermediate	60	40	20–60
Microwax			
High melt	30	70	30–80
Plastic	10	90	30–80

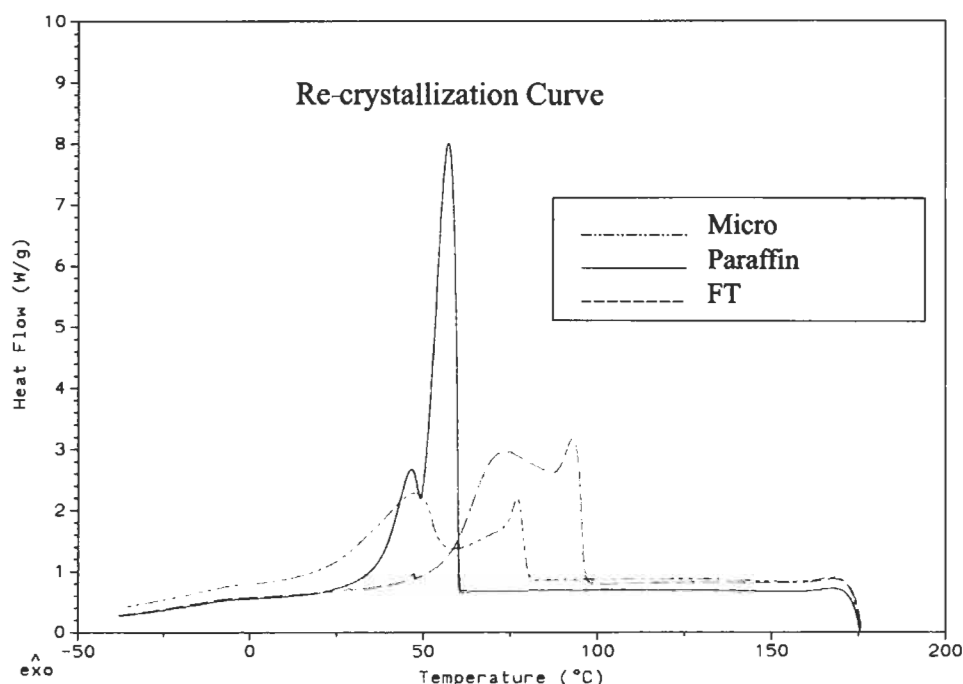


Fig. 12. DSC of microcrystalline, paraffinic, and Fischer–Tropsch waxes on the cool-down cycle. Samples were first heated to 175°C, then cooled to –50°C, all at 20°C/min.

Polyethylene waxes are of two types: by-product and on-purpose. The by-product wax is produced during high MW polyethylene polymerization. It is inexpensive, but very broad in molecular weight distribution. On-purpose PE waxes have a sharper molecular weight distribution and very high melting points (up to ~130°C). Other grades are produced by free-radical cracking of plastic grade PE back to lower molecular weight. This cracking process produces a product with less thermal stability.

Specialty waxes include polar waxes for more polar adhesive systems. Examples would be castor wax (triglyceride of 12-hydroxy stearic acid) or Paracin wax (*N*-(2 hydroxy ethyl)-12-hydroxy stearamide) which are used in polyester, polyamide, or with high VA EVA copolymer-based systems. Other common polar waxes are maleated polyethylenes, which are used to improve the specific adhesion of polyethylene-based adhesives, and low molecular weight ethylene copolymers with vinyl acetate or acrylic acid, which are used to improve low temperature adhesion. High melting point isotactic polypropylene wax ($T_m \sim 155^\circ\text{C}$) and highly refined paraffin wax ($T_m \sim 83^\circ\text{C}$) are used where maximum heat resistance is critical. Needless to say, these specialty waxes also command a premium price, ranging from 2 to 5 times that of conventional paraffin wax.

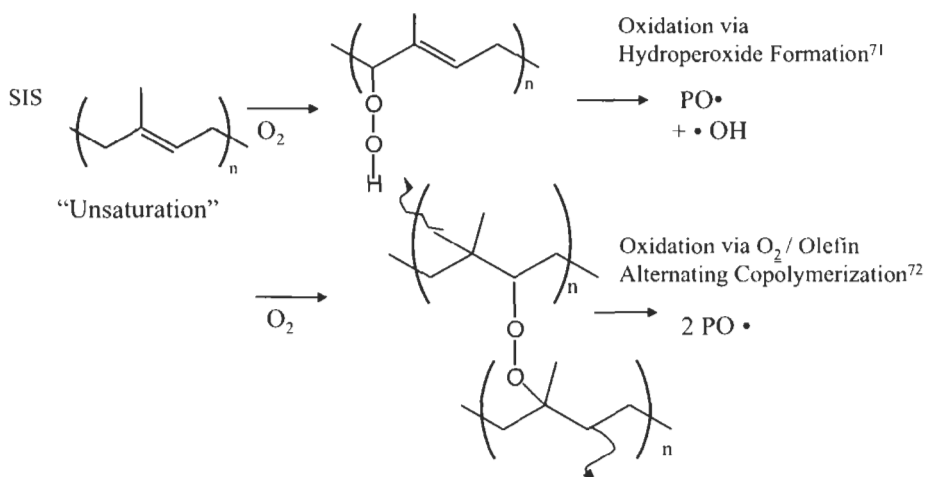


Fig. 13. Auto-oxidation of SIS by air. P represents a polymer chain.

2.5. Antioxidants

Adhesives are prone to degradation due to shear, heat, ultraviolet light, and oxygen. The first three degradative influences are almost insignificant when the fourth factor, oxygen, is completely excluded. However, this is rarely the case. Even under 'vacuum' processing there is generally significant air present, since vacuum levels in most industrial adhesive plants are not very high and mixers are not air tight.

Degradation begins in the bags of raw materials during storage [25]. Unsaturated polymers, resins, or oils will begin oxidizing even at room temperature. Rosin, and rosin esters, and SIS — all of which have allylic hydrogens which can form hydroperoxides in air — are particularly prone to oxidation during storage (see Fig. 13). SIS will become yellow. Rosin and rosin ester when extremely degraded will bubble when heated as they release water — the by-product of oxidative degradation. Thus the adhesive manufacturer must first ensure he has obtained high quality raw materials, properly stabilized and stored, and used within their shelf life.

Secondly, degradation occurs in the mixing process, particularly when styrenic block copolymers are part of the formula. These polymers require shear to break up the rubber pellets and pull the polymer into solution. Unsaturated block copolymers are particularly prone to degradation during mixing, especially SIS, because of the stability of the free radicals formed upon cleavage (Fig. 14). Thus mixing processes are designed to minimize shear within an acceptable processing time. High vacuum batch mixers which apply high shear stresses, but at low shear rates (e.g. sigma blade mixers or continuous extruders) are ideal.

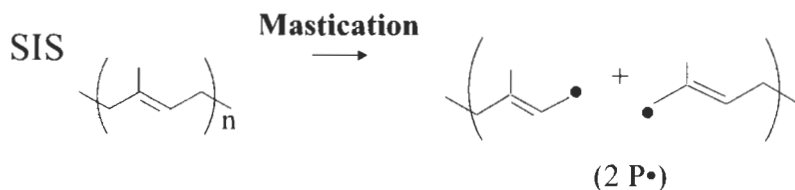


Fig. 14. Stress-induced chain scission of SIS.

Once radicals are generated in the presence of air the reaction becomes autocatalytic (see Fig. 15). Ignoring the relatively infrequent radical combination processes (Fig. 15, Eqs. 8–10) the net reaction (Fig. 15, Eqs. 1–7) shows that for every new radical generated three more are created. Oxidation produces water, and alcohols.

While the process of oxidation is more complicated than this simplified scheme, the general features are correct. The process can be summarized into steps:

- (1) degradation during storage
- (2) creation of alkyl radicals during mixing
- (3) conversion of alkyl radicals to peroxy radicals (Fig. 15, Eq. 1)
- (4) conversion of peroxy radicals to hydroperoxides (Fig. 15, Eq. 2)
- (5) conversion of hydroperoxides into alkoxy and hydroxyl radicals (Fig. 15, Eq. 3)

Means to minimize processes 1 and 2 have already been discussed. Processes 3–5 can be minimized or at least delayed through the choice of suitable antioxidants.

Until fairly recently, there were no antioxidants which could trap alkyl radicals. Recently Sumitomo has developed an acrylated phenol (Sumilizer GM and GS) [26,27] and Ciba-Geigy has developed an aryl benzofuranone (HP 136) [28]. Both

1. $\text{P}\cdot + \text{O}_2 \rightarrow \text{POO}\cdot$
2. $\text{POO}\cdot + \text{PH} \rightarrow \text{POOH} + \text{P}\cdot$
3. $\text{POOH} \rightarrow \text{PO}\cdot + \text{HO}\cdot$
4. $2\text{POOH} \rightarrow \text{POO}\cdot + \text{PO}\cdot + \text{H}_2\text{O}$
5. $\text{PO}\cdot + \text{PH} \rightarrow \text{POH} + \text{P}\cdot$
6. $\text{HO}\cdot + \text{PH} \rightarrow \text{H}_2\text{O} + \text{P}\cdot$
7. $\text{POOP} \rightarrow 2\text{PO}\cdot$

8. $\text{P}\cdot + \text{P}\cdot \rightarrow \text{P-P}$
9. $\text{P}\cdot + \text{POO}\cdot \rightarrow \text{POOP}$
10. $\text{POO}\cdot + \text{POO}\cdot \rightarrow \text{POOP} + \text{O}_2$

Net 1, 2, 3, 5, 6, 7

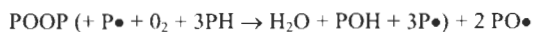


Fig. 15. Free radical induced oxidative degradation reactions.

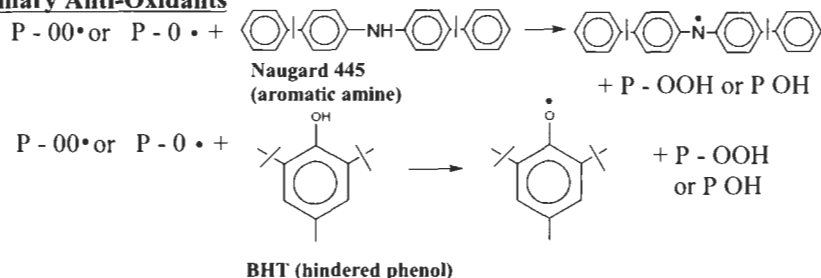
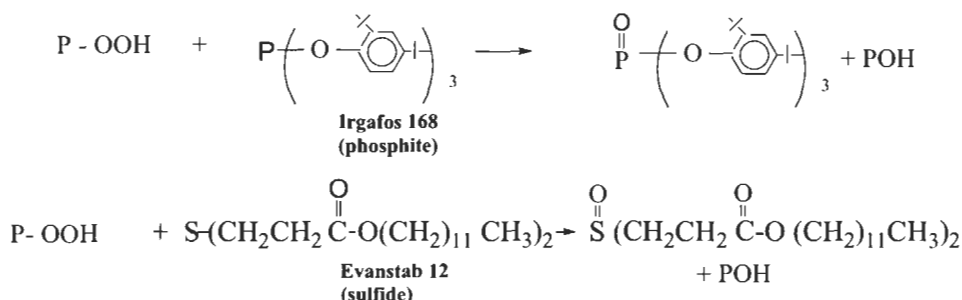
Primary Anti-Oxidants**Secondary Anti-Oxidants**

Fig. 16. Reactions of primary and secondary anti-oxidants.

types are particularly effective with SBS rubbers. The more hindered radicals formed by SIS cleavage may be harder to trap. Such antioxidants are especially useful in low oxygen environments, such as during the initial mixing of adhesives. Rubber manufacturers are increasingly turning to such materials, as their finishing operations often involve extrusion at very high temperatures.

Process 4, conversion of peroxy radicals to hydroperoxides can be interrupted by traditional 'primary' antioxidants (see Fig. 16). The fastest reacting primary antioxidants are the aromatic amines (e.g. Naugard 445). However, these materials yellow upon exposure to UV light which restricts their applications. More common in adhesives are the hindered phenol types of which numerous types are available, with Irganox 1010 the most common choice for adhesives.

Process 5, the conversion of hydroperoxides to alkoxy and hydroxyl radicals, can be interrupted by incorporation of a 'secondary' antioxidant such as phosphites (e.g. Irgafos 168) or thioesters (e.g. Evanstab 12). These materials act as reducing agents, converting hydroperoxides to alcohols and themselves being converted to phosphates or sulfoxides, respectively (see Fig. 16).

For hot melt adhesives there are other considerations as well in choosing an antioxidant. Primary among these are volatility and solubility. Low molecular weight antioxidants (MW <400) should be avoided, for example BHT, as these

can readily volatilize during mixing and/or use. Since most antioxidants are crystalline solids, solubility can be limited. The antioxidant must be soluble to be effective. Solubility in the melt state is not often a problem, whereas solubility after application is more limited. For PSA applications, it is particularly important that the antioxidant not recrystallize or phase separate in the adhesive during use.

3. Reactive hot melts

The vast majority of hot melts are non-reactive. The hard phase(s) formed upon cooling the adhesive impart all of the cohesion (strength, toughness, creep and heat resistance) to the final adhesive. The formulating trade-off for improving the cohesion is higher application viscosity. Reactive hot melts have grown in popularity because of their ability to eliminate this trade-off and provide hot melt adhesives with levels of cohesion heretofore not obtainable. The advantage of hot melt curable adhesives over traditional liquid curing adhesives is their ability to: (1) provide 'green strength' upon cooling and prior to cure, thus eliminating the need for fixturing during the curing process; and (2) provide adhesives of very low crosslink density (high molecular weight reactive species) and thus high levels of flexibility and toughness.

The vast majority of reactive hot melts are moisture-curing urethane adhesives. Radiation (UV/EB) curable adhesives have been explored in the laboratory since the mid-1970s, but are only recently beginning to gain significant market penetration, particularly for PSA applications. The formulation and properties of these two classes of adhesives are discussed below.

3.1. Moisture-curing urethanes

3.1.1. Chemistry overview

These adhesives consist primarily of isocyanate-capped polyurethane prepolymers. These prepolymers are obtained by reacting diols with methylene bisphenyl diisocyanate (MDI), usually pure 4,4' (see Fig. 17a). Pure diols are used primarily, instead of polyols with higher functionality, to avoid excessive branching which can lead to poor pot stability. MDI is favored over lower molecular weight isocyanates to minimize volatility. The mole ratio of NCO/OH is high, typically 1.5–2.0, thus the polyurethanes are oligomeric and the major species is the simple $n = 1$ end-capped polyol. High green strength is obtained by adding higher molecular weight polymers (reactive or not) and/or incorporating crystalline diols, most commonly polyester diols. Cure is obtained through the diffusion of moisture from the atmosphere or the substrates into the adhesive, and subsequent reaction

(see Fig. 17b). The reaction of moisture with residual isocyanate forms carbamic acid. This acid is unstable, decomposing into an amine and carbon dioxide. The amine reacts rapidly with isocyanate to form a urea. The final adhesive product is a lightly crosslinked material held together primarily through hydrogen bonding of urea groups, and to a lesser extent by the urethane groups. These adhesives are extremely tough, with outstanding low temperature flexibility, heat and chemical resistance, and specific adhesion to polar substrates. Adhesion to glass and metal can be improved by using silane coupling agents which are either applied as a primer, or are part of the adhesive itself (as a physical blend or co-reactant (e.g. mercapto silanes), [62]).

3.1.2. Raw materials [34,35]

The polyols used are of three types: polyether, polyester, and polybutadiene. The polyether diols range from 400 to about 10,000 g/mol. The most common polyethers are based on ethylene oxide, propylene oxide, and tetrahydrofuran or their copolymers. The ether link provides low temperature flexibility and low viscosity. Ethylene oxide is the most hydrophilic and thus can increase the rate of ingress of water and consequently the cure rate. However, it will crystallize slowly above about 600 g/mol. Propylene oxide is hydrophobic due to hindered access to the ether link, but still provides high permeability to small molecules like water. Tetrahydrofuran is between these two in hydrophobicity, but somewhat more expensive. Propylene oxide based diols are the most common.

Polyester diols are often combined with polyether diols to provide green strength through crystallization or elevated T_g . Most prevalent and least expensive is hexamethylene diol adipate (HDA) with a T_m of about 60°C. A variety of polyesters are available with various levels of crystallinity — from wax-like to amorphous — and crystallization rate, and with T_g values ranging well below 0°C to above room temperature. Polybutadiene diols are the most expensive and most hydrophobic. They provide low surface tension and thus good wet out of non-polar surfaces.

Isocyanate is added to provide an equivalent ratio of 1.5–2 isocyanate/alcohol. The higher the ratio, the more free isocyanate, and diisocyanate monomer, and the lower the viscosity. Most common is 4,4'-methylene bisphenyl diisocyanate (MDI). Its saturated analog or other aliphatic isocyanates are used where light stability is critical. Most common is isophorone diisocyanate.

Catalysts such as dibutyl tin dilaurate or tertiary amines are added to promote the urethane reaction and/or subsequent moisture cure. Dimorpholine diethyl ether is particularly effective at promoting moisture cure without promoting allophanate side reactions at the application temperature (which leads to instability in the hot melt pot) [29].

Suppliers of these adhesives differentiate themselves by their catalyst pack-

ages and by the other unique resins or polymers added to their formulas. Key attributes thus obtained are: long pot life, high green strength, rapid green strength development, fast moisture cure, and high adhesion to specific substrates. The conventional hot melt raw materials cited in the section above are not generally applicable to urethane formulas due to either limited compatibility or reactivity with the isocyanate groups (e.g. acid, alcohol, amine, phenol, or amide groups). Formulations which successfully incorporate conventional styrenic block copolymers, EVA, or common tackifiers have been patented [30,31]. Unconventional materials have provided greater formulating latitude. For instance, acrylic polymers have broad compatibility and have been used to enhance green strength [32]. Further enhancement is obtained with reactive acrylics (hydroxy functional) [33].

3.1.3. *Synthesis and hot melt processing*

Various processes can be used to synthesize the hot melt adhesive. In part because of the stoichiometric imbalance, the product obtained is highly dependent on the process. Since the diol(s) are present in the largest amount (by weight), they are usually added first to the reactor, and thoroughly devolatilized at elevated temperature (135°C or less) and under vacuum to eliminate any moisture. Any other polymers or tackifiers to be added are dried before addition to the reactor, and would usually be added along with the diol charge. After devolatilization the MDI is added. Because MDI is the excess reagent, the viscosity in the reactor, and the distribution of oligomers will be highly dependent on the stirring and addition process. Heat is usually sufficient to catalyze the urethane reaction, however, the subsequent moisture cure is too slow without catalyst. Thus catalyst is often added at the end of the reaction. The final product is packaged in moisture impermeable containers. Typical properties of a moisture-cure urethane are shown in Table 7.

Pot life is several hours versus several days for conventional non-reactive hot melts. A good reactive urethane is one which exhibits a viscosity rise of less than 10%/h. The slow increase in viscosity with urethane adhesives is due to chain extension via the slow reaction of the active hydrogen of the urethane groups with

Table 7
Effect of moisture cure on properties of a urethane-based hot melt adhesive

	Uncured	Cured
Melt point	60°C	Softens at 60°C without flow; decomposes above 150°C
Viscosity at 250°F	12,000 cP	Infusible
Open time	3 min, tacky, bondable	—
Lap shear strength (wood substrates)	15–20 psi	> 500 psi

the residual isocyanate to form allophanate linkages (see Fig. 17c). To maximize pot stability requires high quality raw materials, minimizing pot temperature (135°C maximum), proper choice and amount of catalyst, and finally appropriate packaging and application equipment. For reactive urethanes, sealed drums or pails are the typical product form, with heated-platen unloaders used to melt and pump material directly from the container. The platen melts only the surface of the adhesive as needed to supply the applicator, thus minimizing the thermal history of the adhesive and consequently the likelihood of gel formation.

Once applied, the cure rate will depend heavily on the moisture content and/or moisture vapor permeability of the substrates between which the adhesive is sandwiched. For wood substrates, typically full cure occurs in a day with the faster systems. Misting of the substrates with water is sometimes conducted prior to adhesive application to further speed cure, or when the substrates are substantially moisture impermeable.

Because the diisocyanate is used in excess, there is usually free monomer present. Isocyanates are hazardous materials particularly upon inhalation and skin contact. Chronic exposure can lead to sensitization. The adhesives must therefore be used with proper ventilation and should not come in contact with the skin in the unreacted state. Vapor monitoring badges for employees and periodic real time vapor monitoring around process equipment is recommended.

3.1.4. Applications

The large volume applications for moisture-curing polyurethanes are discussed briefly in the applications section below. These adhesive offer superior low temperature, high temperature, and specific adhesion performance in comparison to conventional hot melts. These attributes have allowed them to excel in various product assembly applications, including structures such as windows, doors, furniture, and automotive headlamps and trim. Newer applications include book-binding, fabric laminating, and assembly of athletic shoes.

3.2. Radiation (UV/EB) curable hot melts

3.2.1. Hot melt vs. syrup

While the chemistry of radiation curable hot melt adhesives is the same as that used in liquid (syrup) adhesives and coatings discussed elsewhere in this volume, there is a fundamental difference between the objectives of reaction in the two types of systems. Syrups consist largely or entirely of reactive monomeric and/or oligomeric materials. Radiation is used to initiate the polymerization of virtually the entire mass. In contrast, hot melts generally contain polymers initially, and these polymers are capable of reaction via radiation to produce chain extension and

ultimately crosslinking of this portion of the adhesive. Thus the difference is that in syrups the adhesive polymerizes upon irradiation, whereas hot melts chain extend or crosslink lightly. Liquid adhesives have a cured T_g which is much higher than their uncured T_g , since substantial reaction takes place. For hot melts, the T_g of the uncured and cured adhesive is nearly the same, since few new bonds are formed.

3.2.2. *Curing mechanisms*

Radiation can initiate cure by a number of mechanisms. Most common are free radical processes. Free radical cure in liquid adhesives is analogous to addition polymerization. In hot melts the reactions are more complex. In some systems chain transfer and coupling are certainly involved, if not dominant. Most reactive polymers contain pendant or end-linked olefin groups and/or readily abstractable hydrogens. The other ingredients in the system are designed to be free of reactive groups, so that rapid crosslinking of the polymer is obtained at low dose. In addition, the other ingredients should not absorb the incident radiation, as this will limit the thickness of adhesive that can be cured. In practice it has been found that highly hydrogenated aliphatic or cycloaliphatic hydrocarbon resins and petroleum-derived oils provide the least interference with free-radical cure [36,37].

Cationic polymerization in hot melts has been applied to epoxidized polymers [38,39]. No hot melts based on vinyl ether or other cation-sensitive functionalized polymers have been described in the literature. With cationic systems, it is important that the other ingredients in the adhesive be of low basicity to avoid scavenging the initiating acid generated by the photoinitiator.

One key consideration in developing radiation curable adhesive systems is the thermal stability and volatility of any photoinitiators used. These chemicals are designed for liquid systems where these issues do not arise. Few of the commercial photoinitiators have adequate thermal stability at the highest hot melt temperatures (180–200°C) and many are too volatile. Reduced application temperatures and special antioxidant packages are often required.

3.2.3. *E-beam vs. UV*

Electron beam and ultraviolet radiation can initiate cure by either free radical or cationic processes. Electron beam does not require a photoinitiator to produce free radicals since the energies of the impinging electrons exceed the strength of organic covalent atomic bonds by many orders of magnitude (bond strengths are about 4 eV and accelerating voltages are typically about 150 kV). While the exact pathway for cure may differ to some extent for e-beam versus UV, since the source and reactivity of the radicals being generated will not be the same, the overall structure vs. cure rate relationships are similar for both. Some polymers,

particularly those which are highly sterically hindered and thus have a low heat of polymerization, will be prone to chain scission upon exposure to radicals and hydrogen abstraction [40].

Because the energies of electron beams are normally much higher than required to break bonds, they can undergo many chemistry-inducing inelastic collisions before exiting the sample. Consequently, at sufficiently high voltage, typically 150–175 kV, relatively thick films (up to about 4–5 mils) can be cured with high uniformity. Maximum penetration depth is controlled by the accelerating voltage, the thickness and density of the beam exit window material (typically titanium), and the density of the adhesive sample. To ensure good surface cure with a uniform dose, nitrogen blanketing is standard procedure. Without nitrogen, air would scavenge radicals at the surface of the adhesive. Undercure of the surface must be avoided in order to produce tack-free adhesive coatings; however, in pressure-sensitive systems it can actually be a benefit. While UV produces a less uniform dose than e-beam, the surface usually receives a much higher dose than the back side. Thus surface undercure is less of a problem and nitrogen blanketing is not common.

With e-beam the penetration depth and dose is easily varied by altering the voltage and current respectively. With UV systems deeper cure is obtained by using less photoinitiator, a longer wavelength lamp (changing the bulb), and/or a photoinitiator package which absorbs more strongly at longer wavelength. Wattage and line speed are used to control dose. However, with UV there are more restrictions on the adhesive formulator since many common resins and oils are highly UV absorbent (e.g. rosin and derivatives, C9 resins, phenol modified resins, and naphthenic process oils). Hydrogenation to remove visible color from the resin also reduces UV absorbance. E-beam is sensitive to the atomic composition, but not the molecular structure and thus most organic materials absorb similarly.

E-beam is a relatively cold process and so is more suitable for heat-sensitive substrates. UV lamps emit about one third UV light and the rest is visible and IR. Consequently substrates can get very hot, even causing fires if they become stuck beneath the lamp. Safety shutters which close if the line stops are installed on many UV bulbs.

While electron beams can produce cations, they are not effective at producing cationic cure in the absence of suitable photoinitiators. The same cationic photoinitiators used for UV cure are often also e-beam sensitive. Examples are triaryl sulfonium or diaryl iodonium salts [41].

One additional consideration with e-beam, is the effect of radiation on the backing material. If sufficient dose enters into the backing it too can crosslink or otherwise degrade. The nature and extent of the chemical changes depend on the structure and additives in the backing. In general, polyethylene backings crosslink whereas polypropylene will undergo significant chain cleavage at doses as low as 40 kGy. PVC backings should be avoided as they discolor even at much lower

dose and can generate HCl in the process. Partial bonding to the release liner can also occur, particularly if it contains residual unsaturation, such as is present in some addition-cured silicone release coatings.

3.2.4. Polymer systems

As mentioned above, it is the polymer that crosslinks during the radiation cure of hot melts. Various polymer systems have been developed and several of these are now commercial. A brief description of each is summarized below.

3.2.4.1. Unsaturated rubbers. Unsaturated rubbers have been cured by free radical processes using heat activated initiators for many years. The pendant or 'vinyl' double bonds are particularly reactive (see Fig. 2).

Free radical thiol-ene chemistry was one of the first exploited for polymer cure by W.R. Grace in the 1970s [42]. Their examples were liquid systems, but the concept of curing various polyenes such as polyisoprene and polybutadiene was disclosed. Recent work has demonstrated efficient crosslinking of conventional low vinyl SBS block copolymers by adding only 1% of a trifunctional thiol [79,80]. The thiol acts as an alternating comonomer reacting with the olefin bonds of the polymer chain to facilitate crosslinking at low radical concentration (see Fig. 18). Thiol-ene systems have always been constrained in their applications by residual odor; however, manufacturers have continued to reduce odor levels.

Polyisoprene can be UV or e-beam cured [43,44]. The 3,4 units are particularly prone to crosslinking at low dose [45]. SIS and SBS are also crosslinkable, even conventional linear materials with low vinyl content; however, small amounts of liquid trithiol or triacrylate compounds speed cure dramatically [44]. Like UV, e-beam cure is strongly affected by tackifier choice. Hydrogenated, non-aromatic resins provide much less interference with cure [36,37].

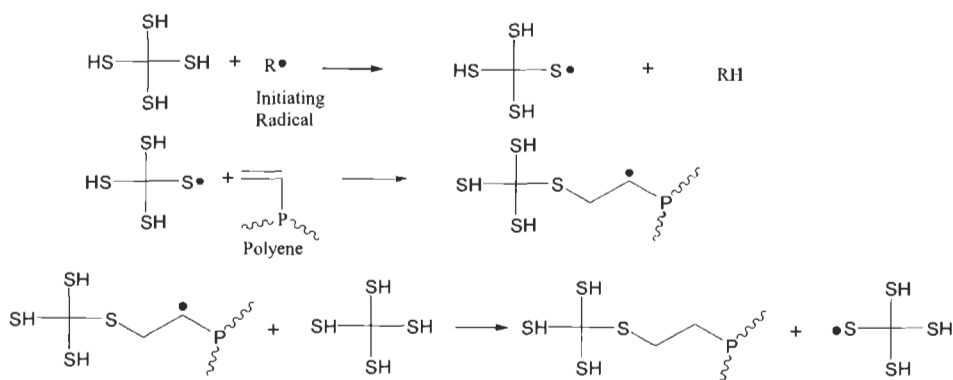


Fig. 18. Thiol-ene free radical copolymerization crosslinking.

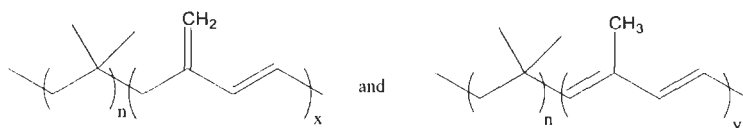


Fig. 19. Conjugated diene butyl rubber ($n \sim 50(x + y)$).

Kraton Polymers has developed a multiarm SIS (Kraton 1320X [37,46,47,50]) and SBS (Kraton KX-222C, [48,49]) for rapid UV/e-beam cure. Besides heat resistance improvements, plasticizer resistance is also improved in cured rubber-based systems. The dioctyl phthalate plasticizer common in PVC backing films is soluble in the styrenic domains of SBCs. Crosslinking of the mid-block provides cohesion even after plasticizer attack [51].

Crosslinking the mid-block of SBCs dramatically improves heat resistance, but with some compromise in peel and tack. Efforts continue to mitigate this compromise. One approach that holds promise is to crosslink the end blocks, rather than the mid-block. Exxon developed such materials in the laboratory by replacing styrene with 2-phenyl-butadiene [52].

3.2.4.2. Functionalized rubbers. Butyl rubber (isobutylene with about 2% isoprene) has been functionalized through the residual double bonds via the bromobutyl intermediate to produce a material with 2% conjugated diene (see Fig. 19). This resin shows high reactivity towards e-beam or UV (free radical or cationic [53]). The bromo butyl intermediate has also been used to attach acrylate or photoinitiator groups to the butyl backbone [54].

More recently, Kraton Polymers has explored various epoxidized rubbers as PSA base polymers [38,49]. They prepare isoprene/butadiene block copolymers and then selectively hydrogenate almost all the double bonds of the butadiene block and some of the double bonds in the isoprene block. The remaining backbone unsaturation in the isoprene block is then epoxidized. These epoxy groups are very reactive towards cationic cure. Most of their effort has been on a material called EKP-207, which has a molecular weight of 6000 g/mol, a hydroxyl on one end (from the termination process) and 8–11 epoxy groups on the other end of the molecule. This material can be co-reacted with other alcohol or epoxy functional resins. The overall chemistry is shown in Fig. 20. Because they cure cationically, there is no termination step, besides that caused by impurities. Thus cure continues after irradiation until the acid is quenched by atmospheric moisture or the reactants can no longer diffuse to one another. This dark cure feature leads to a very low dose requirement for this system, as little as 10 mJ/cm². Like butyl rubber, this material also has the advantage of being saturated and thus not prone to subsequent oxidation. PSA and non-PSA applications have been explored with this technology.

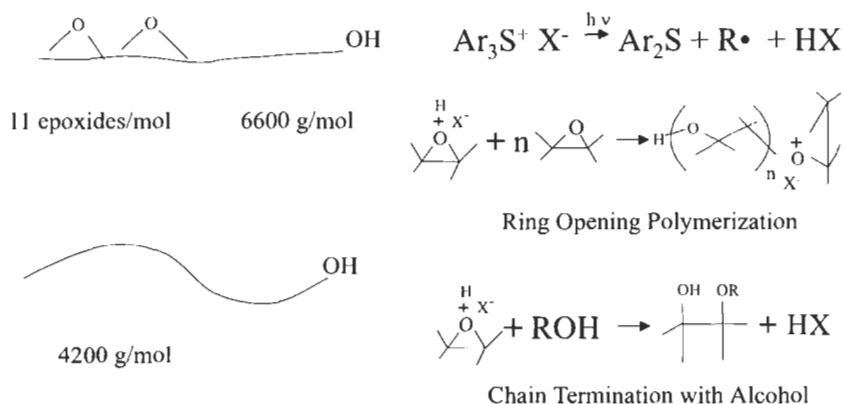


Fig. 20. UV initiated cationic cure of epoxidized block copolymer in the presence of alcohol (Kraton Polymer's EKP-207 and L1203 mono-ol).

Silicone with vinyl-terminal groups is commonly UV-cured for release coatings. These materials have been combined with silicate tackifiers and acrylate monomers to make PSA compositions as well [55].

α -Olefins polymers with low crystallinity have been used as base polymers for PSAs; however, if polymerized randomly their melting points are necessarily very low in order that they be sufficiently amorphous and soft. Thus shear properties are inadequate. 3M found that incorporating 5–10% of divinyl monomers (1,7-octadiene, 4-vinyl-1-cyclohexene, and 5-ethylidene-2-norbornene) provided polymers that could be cured by either UV or e-beam and with the desired heat resistance [56].

Polyalkylene oxides (PAO) are prone to chain transfer. This tendency was used by Union Carbide to graft acrylate side chains via UV exposure of a PAO/acrylic monomer(carbamoyloxy alkyl acrylate)/photoinitiator blend [58]. The final product was a water-sensitive PSA.

3.2.4.3. Acrylics. Acrylics which cure under UV or e-beam have been developed by attaching pendant double bonds through the addition of small amounts of allyl acrylate or methacrylate [59] into the monomer mix or by using pendant hydroxyl groups as a grafting site for an olefin-containing urethane ([60], see Fig. 21). The same researchers synthesized an acrylic monomer with a pendant photoinitiator. This new monomer was copolymerized with conventional acrylic monomers to provide a photoinitiator species attached directly to the acrylic backbone. By attaching the photoinitiator to the backbone cure is more efficient, since one end of the photoinitiator is already attached to the polymer, therefore, fewer free radical crosslinking reactions are needed to effect cure. BASF has developed a similar system, but instead of attaching an α -cleavage photoinitiator they use a diradical forming structure (benzophenone) [61]. This photoinitiator cures the polymer

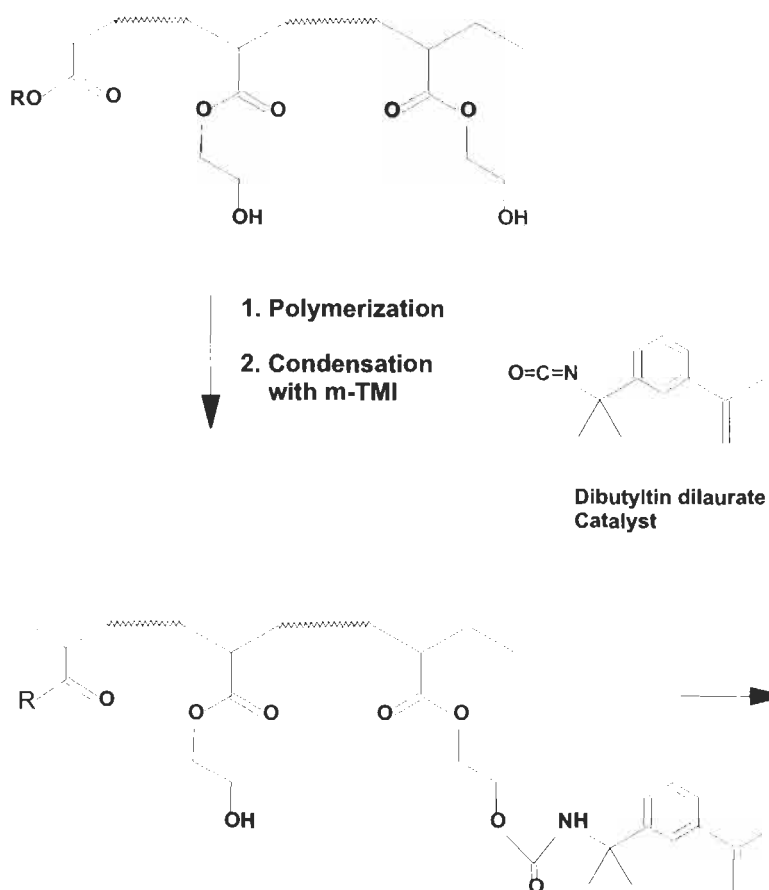


Fig. 21. Olefin functionalization of acrylic polymers through reaction with pendant hydroxyl groups.

without need for olefinic groups and gives faster cure rates since the radicals generated are in close proximity and thus likely to couple leading to crosslinking.

Hot melt acrylic polymers for UV cure are generally of lower molecular weight than their solution counterparts in order to maintain an acceptable application viscosity. Consequently more crosslinks are needed to produce a complete network and thus peel and tack suffer to some degree. Nonetheless, several UV curable materials have been commercialized for PSA tapes and labels.

4. Applications

As mentioned in the introduction, hot melts are used wherever process speed is critical. Described below are some of the major applications for hot melt

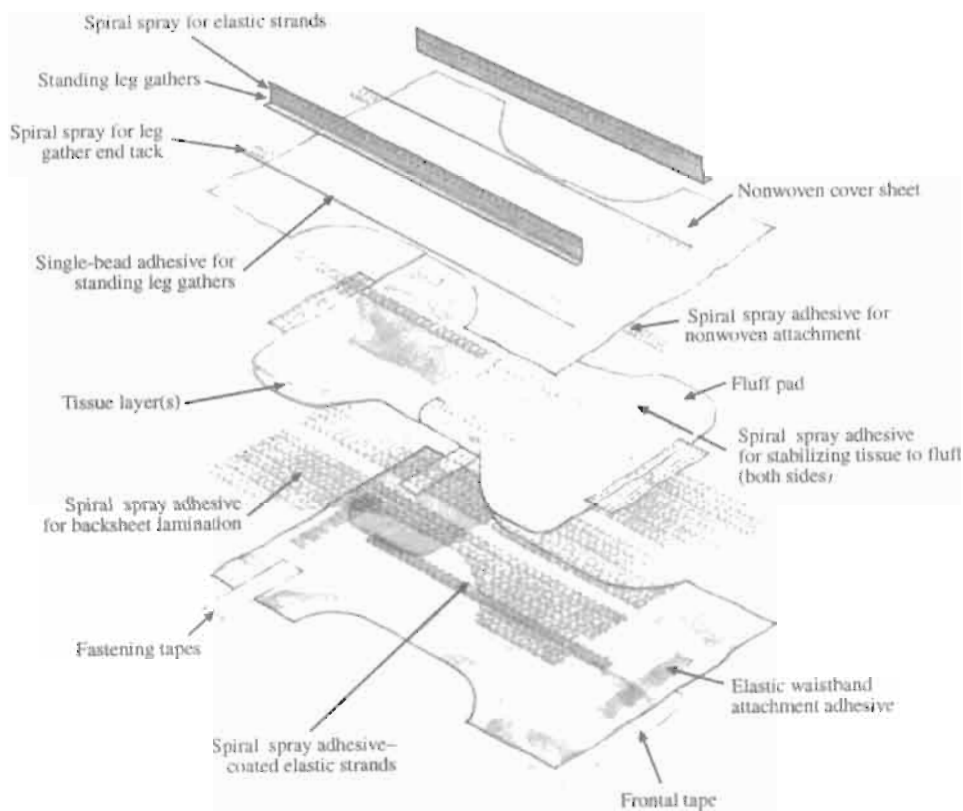


Fig. 22. Common adhesive applications in diapers.

adhesives. Intentionally omitted is a discussion on tapes and labels, since this application is described in detail elsewhere in this volume.

4.1. Non-wovens

The primary non-woven applications for hot melts are in disposable articles such as diapers and sanitary napkins (see Fig. 22). These articles are made by high speed processes and are immediately packaged in sealed plastic bags, thus they are prime candidates for hot melt use. The applications are broken down into three categories, requiring three different types of adhesives: construction, elastic attachment, and garment attachment.

4.1.1. Construction

The construction adhesive is used to bond the layers of the non-woven article together. These layers consist of various non-woven materials and thin polyolefin

films. Very small amounts of adhesive are used, only 1–2 g per diaper. To obtain adequate bond strength, with as little as 1 g/m² of adhesive requires that the adhesive cover only a portion of the substrate. To achieve partial coverage, various spray processes are used. The ability of the adhesive to spray in the desired manner at temperatures low enough to avoid heat distortion of the substrates is a key requirement of the adhesive. Spiral spray is the most common spray process and requires a very ‘short’ (low melt elasticity) adhesive [12]. Narrow molecular weight distribution polymers, such as styrenic block copolymers are ideal. In addition, long open time is required due to the rapid cooling of the thin adhesive filament during spraying. Low surface energy is also critical in order to wet out the polyolefin films and non-wovens employed. Rubber-based adhesives based on SBS multiblock copolymers or low styrene SIS are the most common choices. Formulations are designed with a relatively low T_g (10–17°C) so that the adhesive remains pressure sensitive even at high process speeds. Pressure sensitivity adds to the versatility of block copolymer-based systems. Thus, adequate bonds can be obtained even on very long open time applications, or after a temporary line stoppage (very common).

A typical formula would consist of 18–28 parts of SBS rubber, 50–60 parts of an aliphatic/aromatic tackifier with about 15–30% aromaticity (for long open time), and 15–30 parts of a white oil or a very clean process oil. Formulations are designed to maximize open time, while maintaining adequate heat resistance (maintenance of bond strength upon aging at 40–55°C — warehouse conditions).

Earlier adhesive formulas used APAO polymers as the base. These are still used where the application process does not involve spraying (starved slot or multiline). These formulas are based on 30–40 parts of APAO, 30–40 parts of an aliphatic resin, and 20–30 parts of an oil. Recent work has focused on developing sprayable compositions [63] for the more modern machines which have spray applicators. APAO-based formulas suffer intrinsically from their broad molecular weight distribution, and are still inferior to rubber-based products. In addition they lack pressure sensitivity and the versatility it provides, and further can suffer from having too long an open time, which can lead to debonding in stressed areas shortly after diaper pack off and prior to full set of the adhesive. These deficiencies have led to this market being dominated by rubber-based adhesives.

4.1.2. Elastic attachment

Various elastic elements are added to disposable sanitary products. Strands of lycra, natural rubber, polyurethane foam, and other elastic laminates are applied to provide good fit and avoid leakage. These are attached with adhesives. While non-PSA formulas such as polybutene-based [64] and polyamide [65] adhesives have shown utility, as well as benefits in terms of resistance to baby oils and lotions, adhesives based on styrenic block copolymers still dominate. SBC-based

adhesives offer the advantages of forming softer elasticizing elements, relatively short open time (important since the strands are cut a few seconds after the bond is made), pressure sensitivity, and low cost. Like construction adhesives, elastic attachment adhesives also need a low surface tension for good wet-out of non-polar surfaces, and excellent spiral sprayability, but in addition they need high cohesive strength to hold on to the stretched elastic strands. SIS-based formulas have been prevalent, but are slowly losing ground to cheaper blends with SBS, and entirely SBS-based formulas [66]. Typical formulas are similar to those for construction, but with 5–15 parts more polymer and/or higher molecular weight polymer generally in place of oil. To further boost cohesion, most formulas also contain 5–15 parts of a pure-monomer end block resin (e.g. Herculite 290). Mid-block T_g is normally higher than for construction, as pressure-sensitive bonds are ordinarily not required. Adhesive add-on is 5–15 times higher than for construction so open time is less of an issue, and spraying is facilitated. Since viscosities are higher than for construction, typically 2–20,000 cP at 325°F, higher spray temperatures are needed, and correspondingly higher levels of antioxidant, typical about 1% of a primary antioxidant and 0.5% of a secondary antioxidant.

4.1.3. Garment attachment

The adhesive strip on the outside of sanitary napkins is conventionally applied by hot melt transfer coating in-line with the production of the napkin itself. The adhesive in this application performs a function in the product beyond just holding the parts together. Thus, the requirements are more numerous:

- clean cut off (the application is intermittent so as to provide an adhesive-free tab of release liner at each end of the napkin for the customer to grab)
- high finger tack (the customer should be confident it will hold in place)
- secure hold after bonding (the adhesive must not 'snap-back' and debond after the consumer presses it in place)
- no transfer or excessive adhesion build (upon removal the garment should be free of adhesive, and the removal force should be low enough to prevent ripping of the pad)
- low surface energy (the napkin backing is normally polyethylene)
- no staining of the release liner (oils should not bleed out of the adhesive into the release liner)
- low odor
- non-cytotoxic (the adhesive will be in very close proximity to the skin)
- stable upon storage for up to two years (resist oxidation, phase separation, i.e. no change in adhesive properties).

Because of concerns about long term stability and transfer resistance, adhesives based on saturated SBCs, primarily SEBS, have dominated this application. Over time, cost pressures have encouraged the use of unsaturated rubbers, both SIS and

SBS. These now have a major market share, particularly in developing countries. Traditional formulas have been based on 10–20 parts of SEBS, 50–70 parts of an aliphatic tackifier, and 20–30 parts of oil. Formulas with SIS or SBS have more difficulty passing transfer tests, requiring considerable formulation to meet all the requirements above. Successful formulas rely on higher softening point polymers, by virtue of higher molecular weight styrene end blocks.

4.2. Case and carton sealing

Case and carton sealing is a high volume application for hot melt adhesives. Typical formulas use 20–30% wax, 25–40% polymer, and 35–55% tackifier resin. The basic requirements for packaging adhesives will be described followed by formulating guidelines for specific market areas. The focus of this discussion will be on EVA and EnBA-based systems, which are the most common.

Key requirements are clean processing, fast set, good adhesion, and adequate heat resistance. Case and carton sealing is an intermittent application. Clean processing entails clean cut-off, without stringing. Stringing leads to messy build-up on the equipment. To avoid stringing, adhesives with a 'short' texture are required. Thus narrow molecular weight distribution polymers and excellent melt compatibility for the system, particularly as it cools, are needed.

Setting speed is primarily dependent on the choice of wax and its compatibility in the system. Waxes with a higher T_c (recrystallization temperature) and with marginal compatibility in the system will set quicker.

Adhesion depends on a number of factors. Good adhesion is defined by most customers as substrate failure. The major adhesive manufacturers possess equipment that allows them to make bonds with customer substrates under conditions that closely simulate actual packaging lines. These bonds are peeled either automatically or by hand to gauge adhesion. The most important factors influencing 'adhesion' are the wet-out of the substrate, particularly by the polymer component of the adhesive system, and the specific adhesion with the substrate. Choice of resin is critical for both. Rosin, rosin esters and terpene phenolics are commonly added for these purposes in EVA and EnBA-based systems. 'Adhesion' at low temperatures is also influenced by the overall toughness of the system at the test temperature.

Heat resistance requirements are generally not very severe (warehouse conditions). Various test methods are available although there are few industry standards. Usually the tests involve applying an opening stress (to simulate the spring force of a package flap) to a bond, and determining at which temperature it can resist this stress for some extended period of time, typically 24 h. Thus these are primarily tensile creep tests. Failure occurs in all cases at well below the melting point of the wax component, and well above that of the polymer, thus the interaction of the wax and polymer and the system morphology is critical.

Obviously the main component of the adhesive, the resin, will have a very strong effect on this interaction. Failures can be adhesive or cohesive, depending on the substrate and bonding conditions. The test is most meaningful when it is intentionally made to fail cohesively.

4.2.1. High heat grades

High heat grades generally employ higher and sharper melting point waxes, for example Fischer–Tropsch or PE waxes instead of paraffin. Polymer content is lower and high T_g resins are used (to boost up the amorphous phase T_g). Low application temperature yet high heat resistant adhesives have been developed by formulating to maximize the heat resistance obtained from lower MW paraffin waxes [21].

4.2.2. Freezer grades

Freezer grades normally rely on lower melting paraffin waxes and/or the slower setting and tougher microcrystalline waxes. In direct contrast to the above, polymer content is higher, and resin T_g is lower. The resin system is chosen to maximize the open time of the polymer and also specific adhesion.

4.2.3. High thermal stability 350°F grades

To maximize thermal stability at conventional running temperatures (350°F) EnBA-based systems are chosen [20]. This polymer is much more thermally stable than EVA. Open time is longer than EVA, so special resins are not required for this purpose, even in freezer-grade systems.

4.2.4. Low application temperature adhesives (250–275°F)

Reducing the temperature by 75–100°F dramatically improves the thermal stability of packaging adhesives, resulting in significant cost savings for equipment maintenance, as well as greater worker safety. Such adhesives became possible with the availability of low MW EVA base polymers (MI of 800 and above). They rely on low MW refined paraffin wax and a blend of resins chosen for the specific application [67,68].

4.2.5. Specialty

For particularly difficult to adhere substrates such as metallized or fluorocarbon treated surfaces the same principles that are applied in freezer grade adhesives are used. For especially difficult situations, styrenic block copolymers are added to

maximize flexibility and toughness at low temperatures. However, compatibility is marginal as is processibility. Where chemical resistance is also needed, such as resistance to oils, lotions, greases or fragrances, high levels of terpene phenolic are incorporated.

4.3. Bottle labeling

In the labeling market, hot melts provide the capability to bond non-porous films to plastic cans and bottles. Hot melt usage has grown with the prevalence of such plastic to plastic laminations. The choice of hot melts depends on the equipment, the substrates, whether the bottles are filled or unfilled, and any post-labeling processing (e.g. pasteurization, or heat shrinkage of the film).

The first automated equipment for labeling used a cartridge of pre-cut labels fed one-by-one from a stack. These cartridge-fed machines are still the most common, particularly for applying labels to bottles that are already filled. There are two adhesives applicators, usually both running the same adhesive, but not always. The first applicator puts adhesive onto the bottle. The adhesive must cut off cleanly and then grab and pull out the label from the stack. The second applicator puts adhesive on the trailing edge of the label. Adhesive viscosities are typically in the range of 900–1500 cP. Most of the labels used on these machines are paper, and thus relatively easy to adhere. In addition, paper labels permit running at higher application temperatures (130–170°C). Many machine adjustments are possible which provides some formulation latitude.

Increasingly common are newer machines that apply labels from a roll, usually to unfilled bottles. These machines were well suited to the early plastic labels that were very flexible. Now, label-makers have developed more rigid plastic label stock that can also be used in the older style cartridge-fed machines. Roll-fed machines use one adhesive applicator roll to apply both the leading and trailing edge of adhesive. Viscosities generally need to be lower, 400–1000 cP. With the use of plastic films, especially heat-shrinkable films, lower adhesive temperatures are needed to avoid distortion of the film (120–140°C). At these lower temperatures it becomes more difficult to avoid stringing and resist the heat of subsequent post-processing. Radiation curable warm-melt systems are being explored for these reasons.

For clear labels, which are growing in demand, manufacturers have turned to off-line-produced pressure-sensitive labels, which the labeler purchases and applies to the bottle. However, this option is very expensive, primarily because of the cost of the release paper. The adhesives used for such processes are those used in conventional PSA label manufacturing, as discussed elsewhere in this volume.

The adhesives employed for in-line adhesive application are generally of two types: (1) flexible, but non-pressure-sensitive adhesives based on blends of saturated styrenic block copolymers and wax; and (2) pressure sensitives based

on styrenic block copolymers. Both types are used for both stack and roll-fed labelers. The saturated rubber/wax blend approach provides higher strength and creep resistance, but poorer adhesion due to greater stiffness. Adhesives of this type generally incorporate rosin to improve specific adhesion. They are used where the labels are relatively weak and easy to adhere, such as those based on foamed polystyrene or laminates of clear to opaque (heavily filled) OPP, and only when the bottle is not filled prior to label application.

Filled beverage bottles are frequently cold and often wet from condensation prior to labeling. Such bottles require pressure-sensitive labeling adhesives. The rubber-based PSAs used for bottle labeling are typically lower in rubber-content (10–20%), T_g , and strength than those for tapes and other labels. These soft weak adhesives wet-out easily, and do not debond or ‘flag’ (debonding of the edges) as the bottle expands and contracts with temperature and carbonation level — rather they flex or flow with the bottle.

Because most plastic bottles are recycled, it is necessary to separate the label and adhesive from the bottle. The label is contaminated with ink and not recyclable. The adhesive is also not recycled. Ideally the adhesive will stick tenaciously to the film, but release cleanly from the bottle during the recycling operation. Adhesives designed to aid in recycling have been developed for this market. They incorporate conventional surfactants in place of some or all of the oil in PSA compositions [69] or use ingredients such as rosin which when neutralized by base can function as surfactants. A goal of the recycling industry is to eliminate the need to use base in the process.

4.4. Structural applications

The highest volume applications for hot melts are in the packaging and converting markets (cases, cartons, books, bags, labels, cigarettes, diapers, and sanitary napkins). Structural applications for housing, furniture, and automotive will be described in detail in other chapters of this volume. These applications often entail more severe stress and environmental exposure. Hot melts are suitable in the less-demanding structural applications. The hot melts in use are generally high in viscosity and utilize higher molecular weight polymers at higher concentrations than are used in packaging and converting. The trend has been toward greater use of reactive hot melts. Moisture curing polyurethanes have gained wide acceptance due to their high green strength, excellent adhesion, and outstanding chemical and heat resistance [70].

4.5. Bookbinding

Several types of adhesive are used for attaching the pages of books to the spine. Traditionally, where repulpability is critical, such as phone books, animal glue

is used. For the best 'lay-flat', water-based emulsions are favored. These provide the softest adhesive, yet with adequate strength. Hot melts are used where a more rigid binding is acceptable, and when high production efficiency and low cost are critical.

Adhesives for bookbinding must:

- not crack when the book is opened in the cold (cold crack T)
- must hold the pages strongly as measured by the
page pullout force
cycles to failure when pages are flexed back and forth while under tension
- resist creep at high temperatures as measured by the 'subway' test, where a dowel is placed in the book by the binding, the book is then wrapped into a cylinder with a rubber band, and left in an oven 24 h at the specified T , often 100–120°F.

Hot melts need adequate open time to accept the book cover, but fast set once bound to allow clean trimming shortly after bonding. The adhesive is generally a non-PSA to avoid tack at the exposed edges and for trimming, and is light colored or pigmented for good visual appeal. Most formulas are based on rubber (styrenic block copolymers) or EVA, and contain roughly equal amounts of polymer, wax, and tackifier. Microcrystalline waxes are generally avoided because of their slow set speed and low crystallinity, both of which can lead to gumming during the trimming operation. Polar tackifiers are most common, to maximize the open time of the polymer and the specific adhesion to the paper.

Rubber-based adhesives provide softness and good low temperature flexibility (see Table 8). These properties make them the primary choice for the hinge application, which are two thin glue beads applied to the sides of the book block adjacent to the spine. These adhesive beads allow the book to open with the cover and help to protect the spine glue from stresses. Hinge glues have low if any wax, and are pressure sensitive. When used for the spine application, rubber-based adhesives require a water-based emulsion primer due to their short open time and thus low penetration of paper substrates.

EVA-based adhesives machine more cleanly and are less expensive. For optimum lay-flat and low temperature performance, moisture-curing polyurethane-

Table 8
Comparative properties of bookbinding hot melts

	EVA-based	Rubber-based	Moisture-cure urethane
Viscosity (cP) at 350°F	6000	6000	6000 (250°F)
Yield stress (psi)	700	350	700
Break stress (psi)	900	900	2000
% Elongation at break	1000	1500	1000
Cold crack failure T (°F)	+25	-25	< -40

based adhesive are used. These urethane hot melts are stronger, and thus can be applied at thinner coat weights (about 0.2–0.3 mm vs. 0.5 mm for conventional hot melts). Lower usage helps offset the higher cost and is responsible for the improved lay-flat.

Hot melts are sometimes applied on top of a water-based primer, as mentioned above. The primer penetrates the paper and stiffens the ends of the paper sheets prior to their being attached to the cover with a hot melt overlayer. In some cases a pre-primer is employed which actually penetrates each sheet and stiffens the core of the paper as well.

4.6. Miscellaneous packaging

4.6.1. Cigarettes

Filter cigarettes are assembled with four adhesives: a tow anchor (to bond the filter tow to the filter paper), a seaming adhesive (to bond the paper around the tobacco), a plug wrap adhesive (to create the filter plug), and a tipping adhesive (to attach the filter). Only the plug wrap bond requires a hot melt, since quick set is necessary to prevent the plug from opening up due to the expansive stresses of the compressed filter tow (see Fig. 23). The adhesive is applied as a bead to the filter paper at very fast speeds (up to 24,000 filters/min), the paper is wrapped around the filter tow (just after the tow exits a triacetin dip bath), the adhesive is then reactivated by passing over a heated bar, and then set by contact with a cooler bar. Clean machining, excellent hot tack, and fast set are therefore critical. Other requirements are acceptable taste and odor, and good resistance to triacetin (the solvent used to weld the cellulose acetate fiber tow into a solid bundle of fibers).

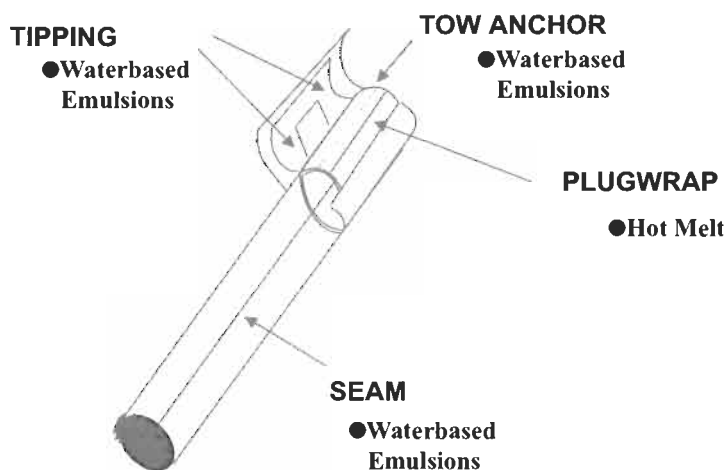


Fig. 23. Adhesive bonding of filter cigarettes.

Triacetin resistance is especially critical when filter tips are made in one location, stored, and then shipped to another location. For these operations, polyethylene-based adhesives are used because of their low polarity and therefore excellent resistance to triacetin. Where filter plugs are attached at the same location shortly after production, EVA-based adhesives are suitable and preferred. Both types of adhesives use low odor, clean tackifiers such as hydrogenated hydrocarbons or pure monomer resins (typically α -methylstyrene based). Rosin, rosin esters, and phenol-containing tackifiers are not acceptable. EVA-based adhesives use a higher level of wax (about 1/3 of the formula) than polyethylene-based adhesives (5–20% wax) due to the lower crystallinity and slower set of EVA vs. PE. Application viscosities are 2000–5000 cP.

4.6.2. Bags

Hot melts are commonly employed in pinch bottom bags. These bags are sealed on one end with hot melt during production of the bag, while on the other end a bead of hot melt is applied, but not bonded. Once the bag is filled, the hot melt bead on the open end is heat reactivated and used to form the final seal on the bag. The hot melts used for this application require a high level of heat and creep resistance in final use. In addition, prior to filling the hot melt must exhibit excellent blocking resistance (i.e. the hot melt beads must not bond the stack of bags together into a block during storage and shipment prior to filling and sealing). Easy heat reactivation and fast set on bonding are also needed. Depending on the content of the bags, chemical or grease resistance may also be necessary.

Both EVA and PE-based adhesives are commonly used for bags. EVA-based formulas typically use lower levels of VA ($\sim 18\%$) compared to case and carton adhesives to improve heat and blocking resistance. For both EVA and PE adhesives high levels of polymer (45–75%) are used for maximum strength. Adhesion is generally better and blocking slightly worse for EVA vs. PE.

For very difficult to adhere bag substrates, such as poly-coated bags, or where extreme chemical resistance is needed, polyamide hot melts are used. These adhesives are very lightly formulated if at all. They provide soft adhesives with outstanding heat and chemical resistance, but at roughly double the price.

4.6.3. Temporary attachment

Examples of temporary attachment applications include securing cases to one another on a pallet during shipping, or attaching inserts into mailings (e.g. credit cards), or onto plastic bottles (e.g. coupons or instruction). For these and other applications where items need to be attached, but then removed without destroying the substrates, rubber-based hot melt adhesives are used. In general stiff, strong rubbers, with good thermo-oxidative stability, such as SEBS, are used at fairly

high levels ($\sim 30\%$), in combination with a high level of oil (about 30%). Such formulas provide a soft, but not pressure-sensitive adhesive (too stiff and with too low a T_g) that exhibits a very low peel force, resists cohesive failure on debonding, and also resists creep and flow during shipping of the bonded product.

5. Equipment and test methods

As should be apparent from the variety of applications, there are many test methods for hot melts, most of which are application specific. Many such tests were developed by adhesive suppliers and are proprietary to them. The use of standardized testing is most common for PSA tapes and labels. These tests are discussed elsewhere in this volume.

The critical equipment for adhesive formulators include:

- Hot melt viscometer. Simple bob in cup viscometers are available which measure viscosity at various temperatures. Fortunately, hot melts are — almost without exception — Newtonian at their application temperatures, so shear rate is not critical.
- Rheometer. Characterizing the elastic and loss modulus over the entire temperature range of potential use and into the melt state is invaluable as a comparative and predictive tool.
- Tensile testing machine operated in a controlled temperature and humidity environment. Many applications involve bonding paper, which exhibits properties that are highly dependent on humidity. In addition, adhesive T_g values are often close to room temperature, and thus properties change substantially over even a few degrees. Therefore, for reproducible comparisons, temperature and humidity control is necessary.
- Application equipment. Laboratory or pilot scale equipment that closely simulates the actual bonding process under production conditions. For some applications this is simple table top equipment, while for others this may be an expensive pilot line with a skilled operator.

6. Trends

Throughout the 1990s a large portion of the research and development effort for hot melt adhesives focused on developing adhesives that are either 'environmentally friendly' or 'functional' [69,81,82]. Environmentally friendly attributes include biodegradability, water dispersibility (repulpability), renewability, and water releasability. Biodegradable adhesives have been developed based on starch esters [83–86] and polyesters such as poly(hydroxy butyrate/hydroxy valerate) [87], poly(lactide) [88–91], and poly(hydroxy ether esters) [92–94]. All but the

latter polymer are, to varying degrees, based on renewable resources. Tackifiers from trees (polyterpenes, rosin) and natural oils and waxes can be employed to raise the level of renewability to more than 75%. Water dispersible adhesives were developed to facilitate the recycling of paper bonded with these adhesives. Adhesives based on starch esters [86], poly(vinyl acetate)/poly(ethylene oxide) graft copolymers [95,96], poly(ethyloxazoline) [81], poly(ethylenimine) [97], and ionic polyesters containing sodium sulfonate groups [57,98] were developed that are water dispersible. The latter have seen the widest applicability. Water releasable PSAs that incorporate surfactant-like diluents were developed primarily for flushable products (e.g. sanitary napkins) and for labeling of plastic bottles that will be recycled.

'Functional' adhesives provide the bonded product with a new or enhanced attribute. For example, adhesives now exist which promote the penetration of fluids into bonded non-woven products by virtue of their low contact angle with water [82]. These materials have been used successfully in both diapers and sanitary napkins for bonding the non-woven cover sheet to the absorbent core. Other examples are water absorbing adhesives that can act as wetness indicators by changing color [69] or can be bonded once moistened [99]. Additional functionalities are currently under development.

Providing these new 'functions' or 'environmentally friendly attributes' increases the cost of the adhesives. When the function was valued and the adhesive delivered it in a suitable and cost-effective manner, commercial success has been realized. Frequently, the economic value of 'environmentally friendly attributes' was overestimated. Without composting facilities biodegradability is rarely of any value, except when the bonded article may end up as litter or is intentionally left to degrade in the environment (e.g. mulch films). Similarly, the attribute of 'repulpability' brings little value to an adhesive unless the manufacturer of bonded paper constructions is also going to be able to repulp some fraction of its product and thus save on disposal costs, or can sell repulpability as an attribute to its customer. In addition, because little make-up water is used in many large commercial repulping operations, dispersible adhesives can build up in the water, eventually redepositing somewhere in the process and causing problems. Therefore, separation by flotation or screening is preferred over dispersibility in most operations. Renewability is of no economic value unless it is required by law, or consumers will place a premium on it. Neither is the case at this time. Water releasability has found niche applications. The ability to better trigger the release in a given removal process will be the key to unlocking greater value.

As mentioned at the outset, hot melt adhesive's primary advantage is process speed. Heat resistance and substrate penetration are typically inferior to liquid adhesives (neat reactive systems, solvent, or water-based). Current research and development is therefore focused on maximizing the process advantages of hot melts and minimizing their performance deficiencies. Optimizing hot melt

processes increasingly involves collaboration with equipment manufacturers developing new systems and more extensive use of a variety of rheological tools. In addition, detailed process analysis using high speed cameras has become common.

Efforts to reduce the processing costs (maintenance, equipment replacement, and down time) and hazards associated with hot melts continue to focus on lowering the application temperature. At 250°F most hot melt formulas become virtually char-free. Thus, both equipment replacement costs and down time due to clogged nozzles are dramatically reduced. Risk of burns is also much lower. Low application temperature adhesives have been developed for most of the major hot melt markets. Broadening the range of product offerings, developing 'cool' technology for the remaining markets, and lowering application temperatures even further are expected to be continuing thrusts for adhesive manufacturers over the next decade.

To improve on penetration and heat resistance (properties normally in opposition when formulating hot melts), reactive hot melt systems are being developed. Moisture curing urethanes have already gained wide acceptance in a number of wood and automotive applications. UV cure is slowly gaining acceptance in PSA, labeling, and other markets.

New raw materials will be the key to unlocking the opportunities above and to creating the possibility for new sets of adhesive properties. On the horizon are new types of moisture curable systems and a variety of novel block copolymers. The future may find entirely new mechanisms or morphologies for strength development on cooling.

References

1. Higgins, J.J., Jagisch, F.C. and Stucker, N.E., Butyl Rubber and Polyisobutylene. In: Skeist, I.S. (Ed.), *Handbook of Adhesives*, 3rd edn. Van Nostrand Reinhold, New York, 1990, p. 185.
2. Vedula, R. and Samms, J.B., Adhesives and Sealants Council, Spring Convention, April, 1999.
3. Foster, M. et al., Canadian patent 2116872.
4. Ewins, E.E., St. Clair, D.J., Erickson, J. and Korcz, W.H., Thermoplastic rubbers: A-B-A block copolymers. In: Satas, D. (Ed.), *Handbook of Pressure Sensitive Adhesive Technology*, 2nd edn. Van Nostrand Reinhold, New York, 1989, p. 317.
5. Tancrede, J.M. and Marchand, G.R., *Adhes. Age*, **June**, (1994).
6. Giordano, S., Parodi, C., Riva, A. and Sacconi, L.V., *Adhes. Age*, Nov., **32** (1994).
7. Diehl et al., US patent 5,292,819.
8. Fetters, L.J., *Macromolecules*, **9**(5), 732 (1976).
9. Kennedy, J. et al., US patent 5,395,885.
10. Kennedy, J. et al., US patent 5,663,245.
11. Omura, N. and Kennedy, J., *Macromolecules*, **30**(11), 3204 (1997).
12. Georjon, O., Faissat, M. and Chambon, F., *Adhes. Age*, **Feb.**, 44 (1999).

13. Godfrey, D.A. et al., US patent 5,763,516.
14. Sustic, A. and Pellon, B., *Adhes. Age*, **Nov.**, 17 (1991).
15. Robe, G., *TAPPI Hot Melt Symposium*, 1992.
16. Robers, W., Vey, M. and Wey, H.G., Adhesives and Sealants Council, Spring Convention, April, 1999.
17. Faissat, M. et al., EP 96/03855 O2.
18. Simmons, E.R. et al., WO 97/33921.
19. Eastman, E.F. and Fullhart, L., Polyolefin and ethylene copolymer-based hot melt adhesives. In: Skeist, I.S. (Ed.), *Handbook of Adhesives*, 3rd edn. Van Nostrand Reinhold, New York, 1990, p. 408.
20. Stauffer, D. et al., US patent 5,331,033.
21. Mehaffy, J.A. et al., US patent 6,117,945.
22. Schlademan, J., Tackifier resins. In: Satas, D. (Ed.), *Handbook of Pressure Sensitive Adhesive Technology*, 2nd edn. Van Nostrand Reinhold, New York, 1989, p. 527.
23. Ruckel, E. and Chu, W., *TAPPI Hot Melt Symposium*, June, 1998.
24. Huntley, M., *Adhes. Age*, 11, 28 (1991).
25. Earhart, N., *TAPPI Hot Melt Symposium*, June, 1994, p. 95.
26. Yachigo, S., Ida, K., Sasaki, M., Inoue, K. and TanakaSumitomo, S., *Polym. Degrad. Stabil.*, **39**, 1 (1993).
27. Miyake, K., Fukuda, K. and Sasaki, M., *TAPPI Hot Melt Symposium*, June, 1998.
28. Knobloch, G., Clauss, M. and Earhart, N., *TAPPI Hot Melt Symposium*, June, 1999.
29. Hung, J.M. et al., US patent 5,550,191.
30. Markevka et al., US patent 4,820,368.
31. Markevka et al., US patent 4,808,255.
32. Stanley, H. et al., US patent 5,012,507.
33. Hung, J.M. et al., US patent 5,866,656.
34. Diller, W., Gupta, P., Haas, P., Schauerte, K., Sundermann, R. and Uhlig, K., Raw materials. In: Oertel, G. (Ed.), *Polyurethane Handbook*, 2nd edn. Hanser, New York, 1994, p. 55.
35. Schollenberger, C.S., Polyurethane- and isocyanate-based adhesives. In: Skeist, I.S. (Ed.), *Handbook of Adhesives*, 3rd edn. Van Nostrand Reinhold, New York, 1990, p. 359.
36. Ewins, E. and Erickson, J., *TAPPI Hot Melt Symposium*, June, 1988, p. 155.
37. Sasaki, Y., *Proceedings of the European Tape and Label Conference*, Brussels, 1993, Paper 7.
38. Erickson, J. et al., US patent 5,686,535.
39. Erickson, J., Zimmermann, E., Southwick, J. and Kiibler, K., *Adhes. Age*, **Nov.** (1995).
40. Charlesby, R., *Atomic Radiation and Polymers*. Pergamon Press, New York, 1960, p. 467.
41. Pappas, S.P., Radiation curing: a personal perspective. In: Pappas, S.P. (Ed.), *Radiation Curing: Science and Technology*. Plenum Press, New York, 1992, p. 1.
42. Barber, R.C. et al., US patent 3,920,877.
43. Berejka, A.J., *Adhes. Age*, **Sept.**, 28 (1997).
44. St. Clair, D.J., *Adhes. Age*, **March**, 30 (1980).
45. Brandes, E.B., Coolbaugh, T.S., Lovelless, F. and Shirazi, F., *Adhes. Age*, **April**, 24 (1998).
46. Erickson, J., *Adhes. Age*, **April**, 22, 1986.
47. Nitzl, K., *Eur. Adhes. Sealants*, **13(4)**, 7 (1996).
48. Dupont, M. and Mayenez, C., *23rd Munich Adhesive and Finishing Seminar*, 1998, p. 122.
49. Dupont, M. and Masse, M., *Adhes. Age*, **March**, 18 (2001).

50. De Craene, L. et al., US 5,777,039.
51. Bradford, W., *Polymer Laminations and Coatings Conference*, 1990, p. 549.
52. Audett, J., US patent 5,135,816.
53. Merrill, N., Radtech '92, p.77.
54. Merrill, N. et al., EP 0609397B1.
55. Mazurek, M. et al., US patent 5,514,730.
56. Babu, G. et al., Eur. Patent Appl. 0416921A1.
57. Miller, R. et al., US patent 5,859,152.
58. Steuben, K., Eur. Patent Appl. 0003741A2.
59. Pastor, S. et al., UK Patent Appl. 2048274A.
60. Ramharack, R. et al., US patent 5,536,759.
61. Auchter, G., Barwich, J., Rehmer, G. and Jager, H., *Adhes. Age*, **July**, 20 (1994).
62. Rumack, D., personal communication.
63. Easymelt®Gold™ Trade Literature — National Starch and Chemical Co., 1997.
64. Harris, B.M. et al., US patent 6,008,148.
65. Paul, C.W. et al., US patent 5,948,709.
66. Sambasivam, M. et al., US patent 6,232,391.
67. Stauffer, D. and Liedermooy, I., *TAPPI Hot Melt Symposium*, June, 1995.
68. Liedermooy, I. et al., US patent 5,670,566.
69. Paul, C.W., Sharak, M.L. and Blumenthal, M., *Adhes. Age*, **July**, 34 (1999).
70. Nowicki, J.W., *Adhesives '91*, Society of Manufacturing Engineers, Sept. 1991, AD91-352.
71. Barnes, C.E., Elofson, R.M. and Jones, G.D., *J. Am. Chem. Soc.*, **72**, 210 (1950).
72. Farmer, E.H., Bloomfield, G.F., Sundralingam, A. and Sutton, D.A., *Trans. Faraday Soc.*, **38**, 348 (1942).
73. Mangaraj, D., Patra, S., Roy, P.C. and Bhatnagar, S.K., *Makromol. Chem.*, **67**, 75 (1963).
74. Small, P.A., *J. Appl. Sci.*, **3**, 714 (1948).
75. Briston, G.M. and Watson, W.F., *Trans. Faraday Soc.*, **54**, 1731 and 1742 (1958).
76. Gergen, W.P. and Davidson, S., In: Holden, G., Legge, N.R., Quirk, R. and Schroeder, H.E. (Eds.), *Styrenic Thermoplastic Elastomers*, 2nd edn. Hanser, New York, 1996, p. 303.
77. Arizona Chemical Company technical literature, Bulletin 8400, Sept., 1993.
78. Marvel, C.S., Riddle, E.H. and Corner, J.O., *J. Am. Chem. Soc.*, **64**, 92 (1942).
79. Decker, C. and Viet, T., *Macromol. Chem. Phys.*, **200**, 1965 (1999).
80. Decker, C. and Viet, T., *Polymer*, **41**, 3905 (2000).
81. Ahmed, S.U., *Adhes. Age*, **Aug.**, 34 (1999).
82. Sharak, M., Paul, C. and Khan, R., *INDA-TEC 97*, p. 280.
83. Billmers et al., US patent 5,321,132.
84. Billmers et al., US patent 5,360,845.
85. Neigel, D. et al., US patent 5,434,201.
86. Blumenthal, M. and Paul, C., *TAPPI Hot Melt Symposium*, June, 1994.
87. Kauffman, T. et al., US patent 5,169,889.
88. Iovine, C.P. et al., US patent 5,252,646.
89. Edgington, G. and Mullikin, L., *Nonwovens World*, summer 1994, p. 31.
90. Edgington, G. and Ryan, L., *Index '93*, III-1.
91. Edgington, G. et al., US patent 5,753,724.
92. Mang, M.N., White, J.E., Kram, S.L., Rick, D.L., Bailey, R.E. and Swanson, P.E., *Polym. Mater. Sci. Eng.*, **76**, 412 (1997).

93. Rick, D.L., Davis, J.W., Lickly, T.D. and Mang, M.N., 6th Annual Meeting of the Bio/Environmentally Degradable Polymer Society, September 1997.
94. Sharak, M. et al., US patent 5,583,187.
95. Schoenberg, J. et al., US patent 3,891,584.
96. Hayes, P.J. and Kauffman, T., TAPPI Hot Melt Symposium, June, 1993.
97. Bunnelle, W.L. et al., US patent 5,459,184.
98. Blumenthal, M. et al., US patent 5,750,605.
99. Blumenthal, M. et al., US patent 6,001,910.
100. Han, C.D., Kim, J., Kim, J.K. and Chu, S.G., *Macromolecules*, **22**, 3443 (1989).
101. Han, C.D., Kim, J., Baek, D.M. and Chu, S.G., *J. Polym. Sci: Part B: Polym. Phys.*, **28**, 315 (1990).

Chemistry and technology of polyurethane adhesives¹

KURT C. FRISCH Jr.^{*}

Bayer Corporation, 100 Bayer Rd, Pittsburgh, PA 15205, USA

1. Introduction

Urethane adhesives are certainly among the most versatile adhesives in the world. A wide variety of urethane raw materials is commercially available, and, as a result, the bonding characteristics of urethanes can vary widely, making them difficult to categorize. One urethane adhesive may bond well to certain types of plastics, while a different urethane adhesive is a poor adhesive for the same plastic. One adhesion scientist may classify all urethanes as ‘flexible’ rubbery adhesives, while another may categorize urethanes as ‘rigid’ plastic-like adhesives. In reality, urethanes can be either flexible or rigid. One of the distinctive characteristics of urethane adhesives, relative to most other structural adhesives, is morphology. The morphology of polyurethanes is a key to the understanding of how the urethane adhesives function. A discussion of structure/property relationships will show the wide versatility of polyurethane adhesives and how scientists can design a urethane to be a plastic or rubber with the desired adhesion and physical properties. While there are over 40 different reactions that may be classed as ‘urethane reactions’, the discussion will be limited to the six most common reactions, which cover over 90% of the urethane adhesives available today. A wide variety of urethane adhesive product types are available, and, within each product type, a wide variety of specific products. While some of the major trends within each product type will be discussed, an exhaustive review within each product type is beyond the scope of this chapter. To aid the discussion, at least one example of each adhesive type will be shown. Certain polyurethane adhesives may be classed as biodegradable and designed for easy hydrolysis, while for other urethane adhesives, such as adhesives for the automotive industry, a high emphasis on durability is mandatory.

¹ This chapter is dedicated to my father, Dr. Kurt C. Frisch (1918–2000), urethane pioneer, founder and director of the Polymer Institute–University of Detroit Mercy. *In pace requiescat.*

^{*} Corresponding author. E-mail: kurt.frisch.b@bayer.com

In order to address these issues, a brief discussion of thermal, oxidative, and hydrolytic stability of urethanes will be offered, so as to aid the adhesion scientist in designing a urethane adhesive with the desired durability.

Urethane adhesives are classified as one-component or two-component adhesives. Each category includes several different types of adhesives.

(A) *One-component adhesives*

- (1) Moisture-curing liquid urethane adhesives
- (2) Moisture-curing hot-melt urethane adhesives
- (3) Solvent-borne urethane adhesives
- (4) Waterborne urethane adhesives
- (5) Blocked urethane adhesives
- (6) Thermoplastic polyurethane adhesives.

(B) *Two-component adhesives*

- (1) Structural urethane adhesives
- (2) Waterborne urethane adhesives
- (3) 'Modified' two-component urethane adhesives

Each of these product types will be discussed, including the method of application, the type of substrates that are bonded by each approach, and one or more typical adhesive formulations. In order to understand the adhesive cure mechanism, a brief review of the common urethane reactions is needed.

2. Major urethane reactions

Over 40 chemical reactions are used in urethane chemistry. The six most common urethane reactions that are relevant to adhesives are shown in Fig. 1. The monomeric forms of the reactions are shown for simplicity's sake; however, most commercially useful products for polyurethanes are based on polyfunctional isocyanates and polyfunctional alcohols or 'polyols'.

Unlike radical or certain ionic reactions, urethanes are based on end-linking reactions, in which the molecular weight is built up gradually. Monomers react to form dimers, then tetramers, and the end-linking process continues until high molecular weight is achieved. For all difunctional components to achieve high molecular weights of 100,000 or more, a high degree of purity is required. Difunctional components can form thermoplastic urethanes, i.e., be melted and reformed into new shapes. Thermoplastic urethane film is sometimes used to bond two dissimilar substrates. A thin aluminum foil may be bonded onto corona-treated polypropylene by extruding a thin layer of a thermoplastic urethane between the substrates and sealing the bond with a nip roller. The great majority of urethanes used in adhesives, however, fall into the thermoset class. They employ multifunctional raw materials, resulting in a crosslinked polymer. Attempts to melt and reform these urethanes are unsuccessful.

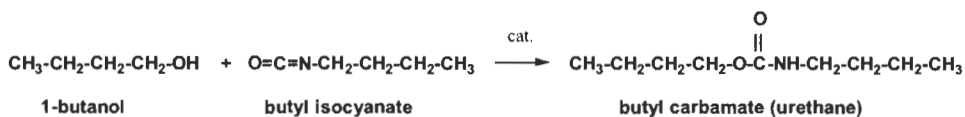
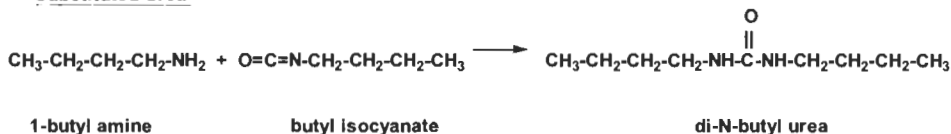
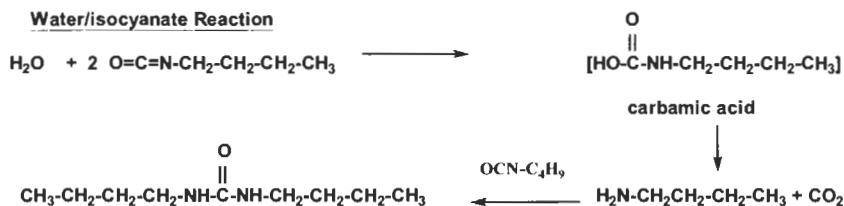
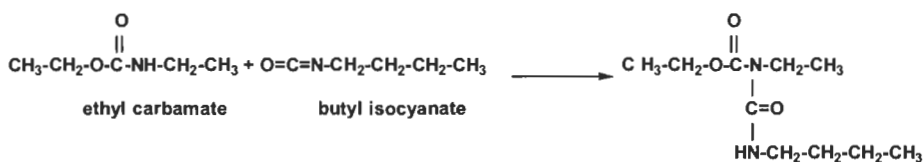
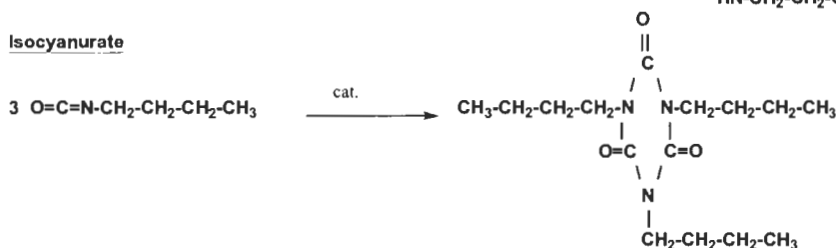
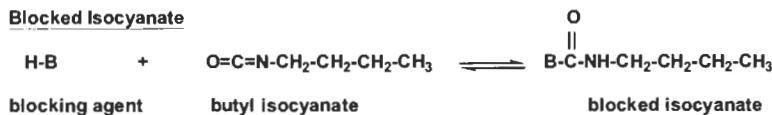
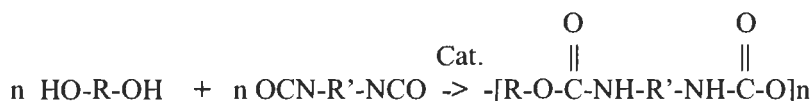
UrethaneSubstituted UreaWater/isocyanate ReactionAllophosphateIsocyanurateBlocked Isocyanate

Fig. 1. Common reactions of urethane chemistry.

2.1. Urethane (carbamate) reaction

The monomeric form of the urethane reaction is shown in the first item of Fig. 1. The urethane or polyurethane reaction for an adhesive would be based

on a diisocyanate and a difunctional alcohol ('diol') or polyfunctional alcohol ('polyol') (see p. 101 in [1]):

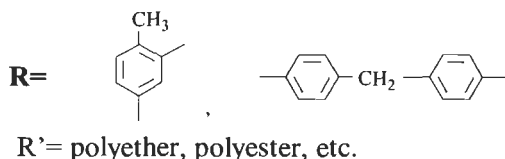
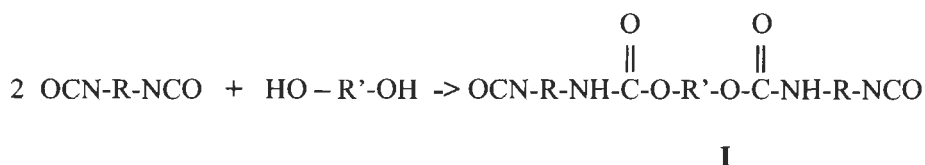


where R is an organic group that represents various polyol backbones. The most common polyol backbones are the polyether polyols, e.g., poly(oxypropylene) polyols (PPG polyols) and poly(tetrahydrofuran), and the polyester polyols, e.g., poly(glycol adipates) and poly(caprolactone) polyols.

R' is an organic moiety, which can be aliphatic or aromatic. Most commonly used in adhesives are the aromatic isocyanates, e.g., methylene diphenylisocyanate (MDI) and toluene diisocyanate (TDI). These polyisocyanates and others will be discussed in Section 3.

In actual practice, catalysts are usually employed to catalyze the isocyanate/alcohol reaction at room temperature. Typical catalysts for this reaction are the tin(IV) salts, e.g., dibutyltin dilaurate, or tertiary amines, such as triethylene diamine [2].

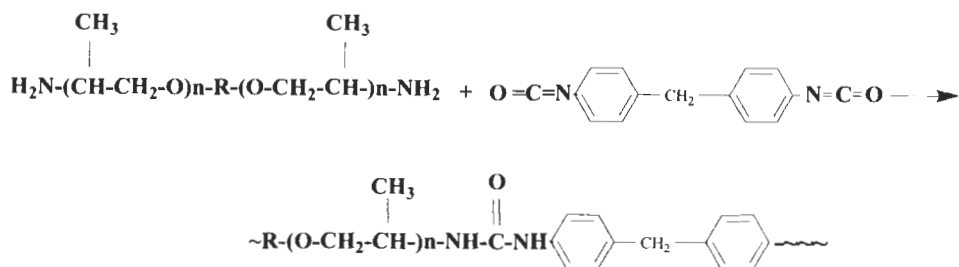
The first urethane reaction in Fig. 1 is used in two major ways in adhesives. In one case, a two-component adhesive usually employs a polyol and polyisocyanate with catalyst. This can react at room temperature to form the polyurethane. The second use of this reaction is to make an isocyanate-terminated prepolymer. Reacting a stoichiometric excess of isocyanate with polyol can produce an isocyanate-terminated prepolymer. A prepolymer is often made with an NCO/OH ratio of 2.0, as shown below, but the isocyanate ratio can range from 1.4 to over 8.0, depending upon the application:



2.2. Substituted urea reaction

The substituted urea reaction is shown as the second item of Fig. 1. The reaction of an amine and an isocyanate is quite rapid at room temperature and often does

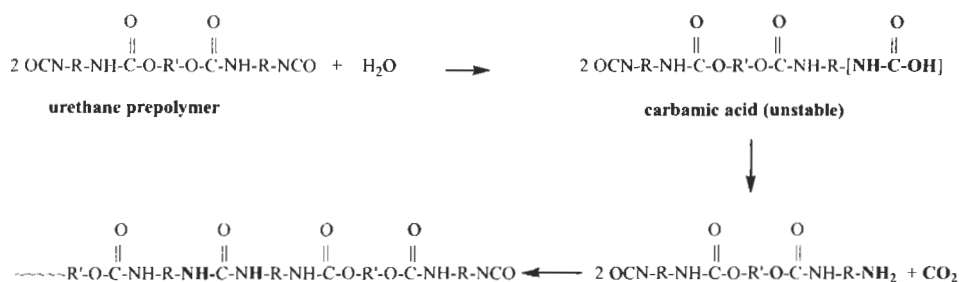
not need a catalyst. Among the fastest of these reactions are the amine-terminated polyether polyols reacting with MDI:



This reaction is reported to proceed at a rapid rate, with over 25% conversion in less than 0.001 s [3]. It can also proceed at very low temperatures, as in the middle of winter. Most primary substituted urea linkages, referred to as urea bonds, are more thermally stable than urethane bonds, by 20–30°C, but not in all cases. Polyamines based on aromatic amines are normally somewhat slower, especially if there are additional electron withdrawing moieties on the aromatic ring, such as chlorine or ester linkages [4]. Use of aliphatic isocyanates, such as methylene bis-4,4'-(cyclohexylisocyanate) (H₁₂MDI), in place of MDI, has been shown to slow the gelation rate to about 60 s, with an amine chain extender present. Sterically hindered secondary amine-terminated polyols, in conjunction with certain aliphatic isocyanates, are reported to have slower gelation times, in some cases as long as 24 h [4].

2.3. Water/isocyanate reaction

The reaction of water with isocyanate is shown in the third item of Fig. 1 [5]. The water/isocyanate reaction is the major curing mechanism for the one-component urethane adhesives. Most one-component urethanes are based on an isocyanate-terminated prepolymer (I). Usually, the moisture in the air is used to cure the adhesive, but in some instances, a fine mist of water may be introduced on top of the adhesive before the bond is closed, in order to facilitate cure:



Initially, the water slowly reacts with the isocyanate. However, the reaction can be catalyzed with an appropriate catalyst, such as dibutyltin dilaurate or a morpholine tertiary amine catalyst. The isocyanate will react with water to form a carbamic acid, which is unstable and splits off carbon dioxide, to produce a terminal amine end group (see p. 76 in [6]). This amine then reacts with more isocyanate-terminated prepolymer, as shown above, to form a polyurea. This process repeats itself, building up molecular weight and curing to become a polyurea–polyurethane adhesive.

For all its benefits, the water/isocyanate reaction can be troublesome as well. All raw materials that go into a one-component moisture-cured adhesive must have very low moisture content, usually less than 0.05% water. If higher water levels are present, the adhesive can start curing in the reactor, causing an increase in viscosity, or, in extreme cases, gelation.

2.4. Allophanate reaction

The allophanate linkage is formed by the reaction of urethane with isocyanate, as shown in the fourth item of Fig. 1 [7]. Isocyanates can react with many active hydrogen compounds. The active hydrogen of the urethane linkage is not very reactive, but if reaction temperatures get high enough (usually in excess of 100°C), or in the presence of certain allophanate catalysts, this reaction can actually become favored over the urethane reaction (see pp. 180–188 in [6]).

In most cases, the allophanate reaction is an undesirable side reaction that can cause problems, such as high-viscosity urethane prepolymers, lower pot lives of curing hot-melt adhesives, or poor shelf lives of certain urethane adhesives. The allophanate reaction may, however, produce some benefits in urethane structural adhesives, e.g., additional crosslinking, additional modulus, and resistance to creep. The same may be said about the biuret reaction, i.e., the reaction product of a substituted urea linkage with isocyanate. The allophanate and biuret linkages are not usually as thermally stable as urethane linkages [8].

R'' can represent a wide variety of backbones, such as polyethers, polyesters, etc. These backbones will be discussed shortly. In actual practice, most prepolymers are made with NCO/OH ratios as low as 1.4, but the ratios can be as high as 3.0 or greater.

The allophanate reaction may occur in the production of a prepolymer if a large exotherm occurs or if certain catalysts are present. This allophanate reaction can lead to branching and high viscosity. If allowed to proceed further, it can lead to gelation. The activation energy to form an allophanate is generally higher than the activation energy of the urethane reaction [9]. Model compound studies of phenyl isocyanate reacting with ethyl phenylcarbanilate determined an activation energy of 16.5 kcal/mol versus 8–9 kcal/mol for the urethane reaction of 1-butanol with phenylisocyanate [10]. Although the allophanate reaction does not normally

occur at room temperature, high levels of catalysts, even standard ones such as dibutyltin dilaurate, can cause a viscosity increase and even gelation of standard prepolymers. Catalysts such as lead naphthanate and cobalt naphthanate may cause allophanate formation even at room temperature (see p. 208 in [6]).

2.5. Isocyanurate reaction

The isocyanurate reaction occurs when three equivalents of isocyanate react to form a six-membered ring, as shown in the fifth item of Fig. 1. Isocyanurate linkages are usually more stable than urethane linkages. Model compound studies show no degradation of the trimer of phenyl isocyanate below 270°C [10,11]. Catalysts are usually needed to form the isocyanurate bond. Alkali metals of carboxylic acids, such as potassium acetate, various quaternary ammonium salts, and even potassium or sodium hydroxide, are most commonly used as catalysts for the isocyanurate reaction. However, many others will work as well [12].

The isocyanurate reaction can be both beneficial and troublesome. It can be the bane of production engineers. Low levels of alkaline impurities present in urethane raw materials such as polyols, tackifiers, etc., can cause problems in prepolymer production, resulting in high viscosity products at levels of 5 ppm or less. At higher levels of alkaline impurities, more serious problems can occur, including poor shelf life, poor caulkability, or poor sag resistance. At levels of 15 ppm or higher, the alkalinity can cause an isocyanurate reaction in a prepolymer that can result in a gelled reactor.

Properly used, the isocyanurate reaction can be highly beneficial in producing two-component structural adhesives. Isocyanurate linkages help to increase modulus and crosslink density. While the isocyanurate linkage is more thermally stable than the urethane linkage, the thermal stability of any polymer is usually controlled by its weakest link. If that weak link is the thermal stability of the urethane linkage, then, as the temperature of the polymer increases, the polymer will degrade based on the urethane linkages present, not the isocyanurate linkages.

2.6. Blocked isocyanate reaction

'Blocked' isocyanate, for our purposes, will refer to the reaction product of a diisocyanate or isocyanate-terminated prepolymer in which the isocyanate functionality has been reacted with a 'blocking agent'. Once 'blocked', the diisocyanate can be added to polyols or certain chain extenders, and these materials will not react at room temperature. The concept is shown in the sixth item of Fig. 1. An adhesive formulated with a blocked isocyanate is basically a two-component adhesive that does not react until heated to the activation temperature. When an adhesive is made with a blocked isocyanate together with hydroxyl-containing curatives, the adhesive has a good long shelf life at room temperature. However, once heated

to the activation temperature, the adhesive can cure in about 30 min. Different blocking agents unblock at different temperatures. Many of the blocking agents volatilize upon deblocking. If the reaction proceeds too quickly, this can cause 'foaming' to occur in the adhesive bond line. 'Foaming' is usually an undesirable effect caused by the volatilization of the blocking agent. This process can generate bubbles in the adhesive bond line. The foaming may decrease the bond strength of the adhesive by up to an order of magnitude. Several of the most common blocking agents are methyl ethyl ketoxime, phenol, and *E*-caprolactam. Methyl ethyl ketoxime is one of the most common blocking agents because it has one of the lowest unblocking temperatures ($\sim 135^{\circ}\text{C}$). Phenol has an unblocking temperature of approximately 150°C but is less commonly used today. *E*-caprolactam unblocks at a relative high 170°C . Its advantage, however, is that it does not volatilize but acts as a plasticizer and may act as an adhesion promoter in some instances. Certain catalysts were found to lower the deblocking temperature [13,14].

Blocked isocyanates are particularly helpful in dual cure mechanisms. In one instance, UV light first polymerizes an acrylate polymer containing hydroxyl groups. The system also contains a malonate ester-blocked isocyanate. The one-component system is heated, which starts the polymerization of the acrylate. Higher temperatures unblock the isocyanate, permitting the cure of the urethane to proceed [15].

In certain cases, even dimers of certain isocyanates, such as toluene diisocyanate or hexamethylene diisocyanate, can act as blocking agents, thermally reversing to regenerate the isocyanate [16,17].

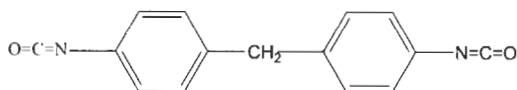
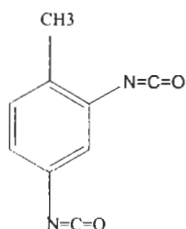
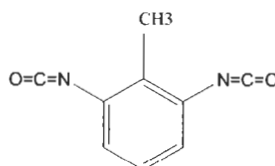
3. Urethane raw materials

Three classes of urethane raw materials will be described: isocyanates, polyols, and chain extenders. The intent is to describe the major types of urethane raw materials used in urethane adhesives, rather than to provide an exhaustive review. The concepts behind the raw materials will be discussed. Once the concepts are understood, it is hoped that the adhesion scientist will then apply the concepts when choosing raw materials for urethane adhesives.

3.1. Isocyanates

The major isocyanates used in urethane adhesives are aromatic isocyanates, i.e., methylene diphenylisocyanate (MDI) and toluene diisocyanate (TDI).

The most commonly used isocyanate in urethane adhesives is MDI. The pure material methylene diphenyl-isocyanate is a solid that melts around 37°C . Many variations of MDI are commercially available, and these variations fall into three major classes: monomeric MDI, 'modified' MDI's, and polymeric MDI's.

**methylene diphenylisocyanate****2,4-toluene diisocyanate****2,6-toluene diisocyanate**

A general description of the three major classes of MDI's and brief descriptions of adhesive applications are shown in Table 1. More recently, MDI has become the isocyanate of choice in adhesives, partly because MDI has a lower vapor pressure than TDI does (see pp. 296–297 in [18]). Isocyanates have been shown to cause an allergic reaction in a small percentage of the population. This reaction can manifest itself in the form of an asthmatic condition [19]. Before starting work with isocyanates, researchers are encouraged to read about the proper precautions to take, in order to work safely with these materials. Researchers should also check with their local health and environmental safety representatives [20].

MDI is known to dimerize slowly at room temperature, so there is a shelf life associated with this raw material.

Toluene diisocyanate has two common isomers; the 2,4- and 2,6-TDI. The most commonly supplied TDI is a combination of 80% 2,4- and 20% 2,6-TDI. A 65/35 ratio of the 2,4-/2,6-TDI is also available, as well as a 100% 2,4-TDI product. The reactivity of the two isocyanates on TDI is different. Once the first isocyanate has reacted, the second is roughly eight times less reactive [21]. TDI produces lower-viscosity prepolymers than does MDI. Pure 4,4'-MDI has a reactivity difference between the isocyanates of approximately 2/1 [22].

In certain niche applications, aliphatic isocyanates, such as isophorone diisocyanate (IPDI), hexamethylene diisocyanate (HDI), methylene 4,4'-biscyclohexylisocyanate (H_{12} MDI), and polymeric versions of these diisocyanates, are used, e.g., in instances where light stability or reduced reactivity is needed. These isocyanates usually cost more than the aromatic diisocyanates. Thus, they are used in adhesive areas that can justify the higher costs.

Table 1
General grades of MDI-adhesive applications

Isocyanate type	Functionality	Physical form	Uses
<i>Monomeric MDI</i>			
Pure 4,4'-MDI	2.0	Solid (MP = 37 C)	Flexible prepolymers Liquid 1-K adhesive Thermoplastic adhesives Curing hot melts Solvent-borne adhesives
<i>Modified MDI's</i>			
Urethane-modified prepolymer	2.0	Clear, light yellow liquid	Flexible, 2-K structural adhesive Thermoplastic adhesives Solvent-borne adhesives
Allophonate-modified MDI	2.0	Clear, light yellow liquid	Flexible, 2-K structural adhesive
Uretonimine-modified MDI	2.15	Clear, to light yellow liquid	Flexible, 2-K structural adhesive Solvent-borne adhesives
<i>Polymeric MDI's</i>			
Low-intermediate polymeric MDI	2.1–2.5	Brown liquid	Semiflexible, 2-K foam adhesive
High-polymeric MDI	2.6–3.0	Brown liquid	1-K liquid rigid adhesives 1-K liquid wood adhesives Foundry binders Wood binders Rigid, 2-K structural adhesives

3.2. Polyols

A wide variety of polyols is commercially available. The major types of polyols used in urethane adhesives are shown in Table 2. Poly(oxypropylene) polyols (PPG's) are usually low-viscosity amorphous liquids and are available in a wide variety of molecular weights. The PPG structure shown in Table 2 is a difunctional polyol, but these materials are also available as triols or even higher functionality. Difunctional materials are used for flexible adhesives, and the higher functionality polyols are used for more rigid applications. The poly(oxypropylene) polyols of PPG's have secondary hydroxyl functionality. Most of these polyols are produced by an anionic ring-opening reaction. A side reaction in the production of these polyols leads to the formation of an allyl-terminated monol, which acts as a chain-stopper, limiting the molecular weight and physical properties of the urethane adhesives. A 4000 molecular weight diol may have up to 33 mole percent of this monol. Recently, low-monomer PPG's have been introduced and have demonstrated improved performance [23].

The PPG polyols are also available with ethylene oxide capping, which pro-

Table 2

Common polyols used in urethane adhesives

Polyol Class	Typical Structure
Polyethers	
Poly(oxypropylene) (PPG)	$\begin{array}{c} \text{CH}_3 \qquad \qquad \text{CH}_3 \\ \qquad \qquad \qquad \\ \text{H}(\text{O}-\text{CH}-\text{CH}_2-\text{O})_n-\text{R}-(\text{O}-\text{CH}_2-\text{CH}-\text{O})_m\text{H} \end{array}$
Poly(tetramethylene oxide) (PTMEG)	$\text{H}(\text{O}-(\text{CH}_2)_4-\text{O})_n-\text{R}-\text{O}-((\text{CH}_2)_4-\text{O})_m\text{H}$
Polyesters	
Crystalline Polyesters	
(symmetrical)	
e.g., poly(hexamethylene adipate)	$\begin{array}{c} \text{O} \qquad \qquad \text{O} \\ \qquad \qquad \\ \text{H}-(\text{O}-(\text{CH}_2)_6-\text{O}-\text{C}-(\text{CH}_2)_4-\text{C}-\text{O})_n-(\text{CH}_2)_6-\text{OH} \end{array}$
Poly(caprolactone)	$\begin{array}{c} \text{O} \qquad \qquad \text{O} \\ \qquad \qquad \\ \text{H}(\text{O}-(\text{CH}_2)_5-\text{C})_m-\text{O}-\text{R}-\text{O}-(\text{C}-(\text{CH}_2)_5-\text{O})_m\text{H} \end{array}$
Amorphous Polyesters	
(asymmetrical)	
e.g., poly(2-methylpropane) adipate	$\begin{array}{c} \text{CH}_3 \qquad \text{O} \qquad \text{O} \qquad \text{CH}_3 \\ \qquad \quad \qquad \qquad \\ \text{H}(\text{O}-\text{CH}_2-\text{CH}-\text{CH}_2-\text{O}-\text{C}-(\text{CH}_2)_4-\text{C}-\text{O})_m-\text{O}-\text{CH}_2-\text{CH}-\text{CH}_2-\text{OH} \end{array}$
Specialty	
Poly(carbonate)	$\begin{array}{c} \text{O} \\ \\ \text{H}(\text{O}-(\text{CH}_2)_6-\text{O}-\text{C}-\text{O})_n-(\text{CH}_2)_6-\text{OH} \end{array}$
Poly(butadiene)	$\begin{array}{c} \text{CH}_2\text{z-OH} \\ \diagup \qquad \diagdown \\ \text{CH}=\text{CH} \\ \diagdown \qquad \diagup \\ \text{HO}-(\text{CH}_2) \qquad \text{CH}_2\text{x}-(\text{CH}_2-\text{CH})_y-(\text{CH}_2) \\ \qquad \qquad \qquad \\ \qquad \qquad \qquad \text{CH}=\text{CH}_2 \end{array}$

vides a primary hydroxyl instead of a secondary hydroxyl. The primary hydroxyl is highly desirable for two-component structural adhesives and improves reactivity. Primary hydroxyls also improve the green strength of one-component moisture-cure systems [24]. Like the standard PPG's, the ethylene oxide-capped PPG's are available in different functionalities and molecular weights. One potential drawback of the ethylene oxide-capped PPG's is increased hydrophilicity of the resulting adhesive, which may lead to water swelling and reduced strength in an aqueous environment.

Poly(tetramethylene oxide) polyols (PTMEG) are high performance polyethers that are crystalline waxes at molecular weights above 650 and liquids at lower molecular weights. They are only available as diols, but they produce adhesives with good hydrolysis resistance and moisture resistance, which is why these adhesives are even used in medical devices, blood bags, catheters, and heart-assist devices [25]. Certain thermoplastic polyurethane adhesives and solvent-borne adhesives are also based on PTMEG's.

Crystalline polyesters are highly important as adhesive raw materials. They are normally crystalline waxes and are highly symmetrical in nature, which can aid the crystallization process [26]. Poly(hexamethylene adipate) and poly(caprolactone), shown in Table 2, are only two of the many crystallizable backbones. Poly(ethylene adipate) and poly(tetramethylene adipate) are also commonly used in urethane adhesives. The crystalline polyesters are used in curing hot melts, waterborne polyurethanes, thermoplastic polyurethanes, and solvent-borne urethane adhesives. The adipates are available mostly as diols. The poly(caprolactones) are available as diols and triols.

The amorphous polyesters are becoming increasingly important for one-component 100% solid moisture-curing adhesives. These materials are usually viscous, amorphous liquids. Poly(2-methylpropane adipate), an example of an amorphous polyester, is a liquid even at a molecular weight of 2000. The amorphous polyesters are usually asymmetrical in structure. In the poly(2-methylpropane adipate) example, the pendant methyl group would be expected to interfere with chain packing, thereby preventing crystallization [27].

The specialty class of polyols includes poly(butadiene) and polycarbonate polyols. The poly(butadiene) polyols most commonly used in urethane adhesives have functionalities from 1.8 to 2.3 and contain the three isomers (x , y and z) shown in Table 2. Newer variants of poly(butadiene) polyols include a 90% 1,2 product, as well as hydrogenated versions, which produce a saturated hydrocarbon chain [28]. Poly(butadiene) polyols have an all-hydrocarbon backbone, producing a relatively low surface energy material, outstanding moisture resistance, and low vapor transmission values. Aromatic polycarbonate polyols are solids at room temperature. Aliphatic polycarbonate polyols are viscous liquids and are used to obtain adhesion to polar substrates, yet these polyols have better hydrolysis properties than do most polyesters.

Numerous other polyols are commercially available, some from renewable resources. Urethanes based on castor oil have been used for many years as encapsulants for electronic components, due to their hydrophobic nature [29].

3.3. Urethane chain extenders

Chain extenders are usually low molecular weight symmetrical diols or diamines. Chain extenders react with isocyanates in the same way as polyols do, but because they are low molecular weight, a high concentration of hydrogen-bonded molecules can associate and phase out of the polyol to form plastic-like domains called 'hard segments'. Hard segments will be discussed in Section 4. Some of the more common diol and diamine chain extenders are shown in Table 3.

3.4. Urethane catalysts

The most common catalyst used in urethane adhesives is a tin(IV) salt, dibutyltin dilaurate. Tin(IV) salts are known to catalyze degradation reactions at high temperatures [30]. Tin(II) salts, such as stannous octoate, are excellent urethane catalysts but can hydrolyze easily in the presence of water and deactivate. More recently, bismuth carboxylates, such as bismuth neodecanoate, have been found to be active urethane catalysts with good selectivity toward the hydroxyl/isocyanate reaction, as opposed to catalyzing the water/isocyanate reaction, which, in turn, could cause foaming in an adhesive bond line [31].

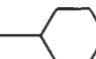

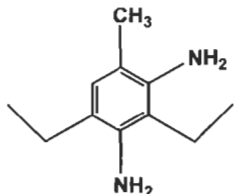
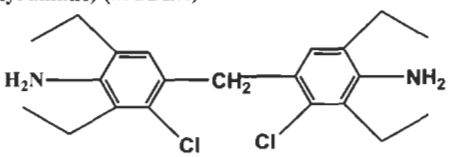
Most tertiary amines are not suitable for use in one-component, moisture-curing adhesive systems, especially in the presence of a reactive isocyanate such as MDI. Tertiary amines, due to their high alkalinity (high pK_a), may catalyze side reactions, which can cause poor shelf life, i.e., slowly increasing viscosity of the adhesive and possibly even gelation. However, dimorpholinodiethyl ether (DMDEE) is an exception to this rule. DMDEE has a low alkalinity, thereby avoiding the side-reaction problem associated with most tertiary amine catalysts. DMDEE is a favorite catalyst for curing hot-melt urethane adhesives and fast-curing MDI moisture-curing systems.

Delayed action catalysts are used in certain two-component adhesives systems but will not be discussed here. A review of delayed action catalysts can be found elsewhere [32].

4. Structure/property relationships of urethanes

In order to understand the widely varying physical properties and adhesion properties of urethanes, it is important to understand the different classes of urethane raw materials and their functions in urethane adhesives. In order to

Table 3
Common urethane chain extenders

<u>Diols</u>	<u>Chemical Structure</u>
1,4-butanediol	$\text{HO-CH}_2\text{-CH}_2\text{-CH}_2\text{-CH}_2\text{-OH}$
ethylene glycol	$\text{HO-CH}_2\text{-CH}_2\text{-OH}$
diethylene glycol	$\text{HO-CH}_2\text{-CH}_2\text{-O-CH}_2\text{-CH}_2\text{-OH}$
1,4-cyclohexane dimethanol	$\text{HO-CH}_2\text{-}$  $\text{-CH}_2\text{-OH}$
bis(2-hydroxyethyl) hydroquinone	$\text{HO-CH}_2\text{-CH}_2\text{-O-}$  $\text{-O-CH}_2\text{-CH}_2\text{-OH}$
<u>Diamines</u>	
diethyltoluene diamine (major isomer)	
ethylene diamine	$\text{H}_2\text{N-CH}_2\text{-CH}_2\text{-NH}_2$
4,4'-methylene bis(3-chloro-2,6-diethyl aniline) (MCDEA)	

understand how urethanes function as adhesives, it is also important to understand the morphology of urethanes.

4.1. Morphology of urethanes

Most structural adhesives would be classified as plastics, i.e., they have a glass transition temperature higher than room temperature (25°C). Pure plastic adhe-

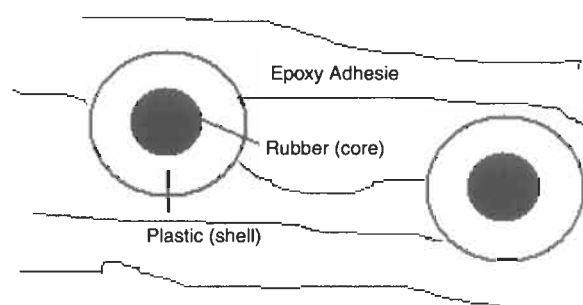


Fig. 2. Morphology model of a core-shell, rubber-toughened epoxy adhesive.

sives, while having high modulus, may have a tendency toward brittleness. If the adhesive bond receives a sharp impact perpendicular to the bond line, this may cause the plastic to fracture, resulting in bond failure. 'Toughened' structural adhesives may have a distinct rubber phase amidst the continuous plastic matrix, e.g., the rubber-toughened epoxy shown in Fig. 2. If the toughened epoxy receives the same sharp impact perpendicular to the bond line, the starting fracture propagates directly into the rubber particle, a desirable effect. Since the crack propagates into the rubber particle, the stress is relieved and the propagation of the crack stops [33].

Urethane structural adhesives have a morphology that is inverse to the toughened epoxy just described. The urethanes have a rubber continuous phase, with glass transition temperatures of approximately -50°C . This phase is referred to as the 'soft segment'. Often, a discontinuous plastic phase forms within the soft segment, and that plastic phase may even be partially crystalline. This is referred to as the 'hard segment'. A representation of the morphology is shown in Fig. 3 [34].

The hard segments may be formed by the reaction of a diisocyanate and a 'chain extender'. Early in the history of polyurethanes, high molecular weight urethanes were formed in two steps. The prepolymer step was the reaction between an excess

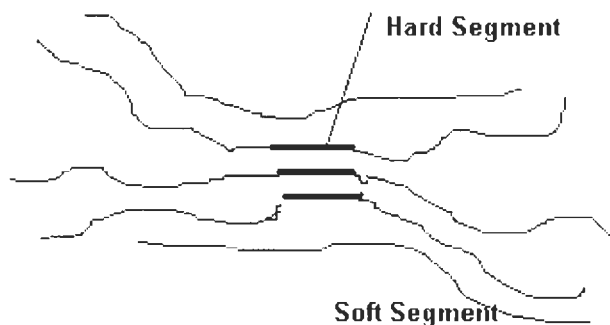
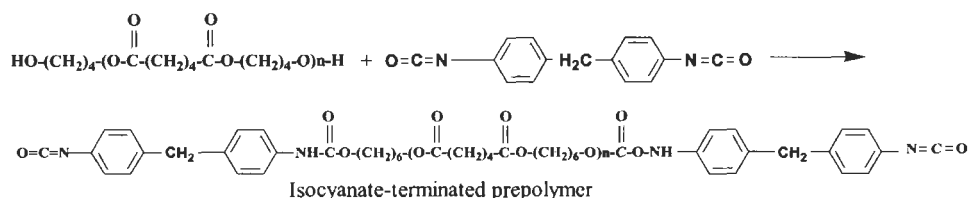
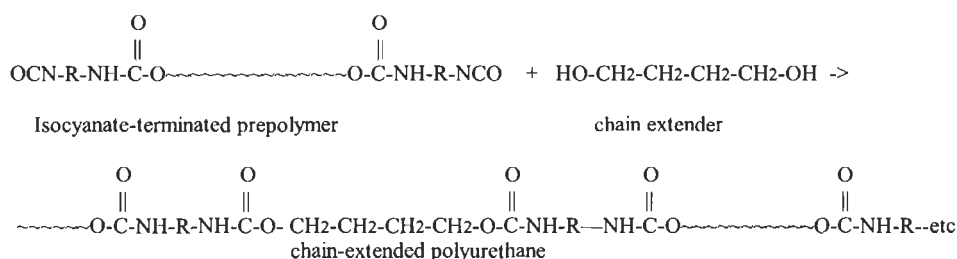


Fig. 3. Morphology of a typical polyurethane adhesive.

of diisocyanate and a polyol, creating a low molecular weight oligomer that was isocyanate-terminated:



In a second step, the prepolymer was then reacted with a low molecular weight difunctional alcohol, commonly referred to as a 'diol' or a diamine, to connect the prepolymer oligomers into a high molecular weight polyurethane. This step was referred to as the 'chain extension', resulting in the use of the term 'chain extenders' to describe the low molecular weight diols or diamines that reacted with the prepolymer oligomers.



Chain extenders are used to increase modulus and tensile properties. Over the years, as instrumentation to characterize polyurethanes improved, it was discovered that chain extenders were responsible for forming separate plastic-like domains with varying degrees of molecular association, as a result of hydrogen bonding [35]. Blackwell established the fact that annealing increases the molecular ordering of the hard segments made from 1,4-butanediol and MDI. At least two crystalline forms were characterized by X-ray diffraction. It is believed that annealing of the urethane at elevated temperature (70°C) may permit enough mobility in the hard segment to allow a re-alignment, which improves molecular associations and packing, as a result of hydrogen bonding [36].

Some of the unique properties of polyurethanes may be derived from hydrogen bonding. The hard segments are, first of all, plastic domains with a glass transition temperature above room temperature. Within these plastic domains are wide ranges of molecular ordering, leading up to the most ordered crystallinity. In actual practice, it is rarely feasible to post-cure or anneal polyurethane adhesives, but the hard segments are important in aiding the adhesive physical properties at elevated temperatures. As temperatures increase in a rubber, modulus and bulk viscosity usually drop, causing a reduction in strength. The hard segments may

act as a physical crosslink, holding the rubbery soft segments together. This may delay failure until the crystalline melting point of the hard segment is reached. For certain chain extenders, such as most diamines, the melting point of the crystalline hard segment may exceed the degradation point of the polyurethane itself, making it for most practical purposes a thermoset [37]. Most diol chain extenders have a crystalline melting point below the degradation point of the polyurethane. If the polyurethane is built with not much more functionality than 2.0, the urethane may be a thermoplastic. If the urethane has higher functionality than 2.0, it will act like a thermoset.

4.2. Morphology of urethanes contributes to adhesive properties

The morphology of urethane adhesives, i.e., hard segments amid low T_g rubbery soft segments, provides certain advantages and disadvantages. If a high flexural modulus is desired, urethanes may not be the best choice. Equally disadvantageous would be other adhesives with similar morphologies, i.e., plastic domains within a rubbery matrix, e.g., a high rubber SBS triblock, flexible epoxies, etc. Urethanes can be designed to approach the structural modulus of some of the rigid epoxies, cyanate esters, etc., and this will be discussed later. In order to raise the modulus of the adhesive, it is necessary to raise the glass transition temperature of the soft segment, thereby moving away from the standard urethane morphology of hard segments in a rubber matrix. Increased modulus within the standard urethane morphology can be accomplished by raising the level of hard segment (chain extender) and adding certain fillers [38]. Higher levels of chain extenders would also be expected to increase shrinkage in the bond line, if the reaction takes place within the confines of the bond itself. If too much chain extender is added to the urethane, a phase inversion may occur, in which the plastic portion of the urethane, derived from the chain extender/isocyanate reaction, becomes the continuous phase. The rubber portion of the urethane, from the polyol/isocyanate reaction, becomes the discontinuous phase. At these high chain extender levels, increased modulus is achieved, but this creates a network that may easily undergo brittle fracture.

Fig. 4 shows the major stresses that may be placed on a bond line. Structural adhesive joints should be designed for shear or tensile stresses and should avoid the cleavage and peel modes. A 'garden variety' epoxy structural adhesive would typically produce bonds with 3000 pli in tensile, 3000 psi in shear but only 100 psi in cleavage and as low as 3 pli in peel [39]. Epoxies can be rubber-toughened to improve strength in the cleavage and peel modes, as shown in Fig. 4, but there are limitations. Urethanes are often preferred when it comes to bonding dissimilar substrates, such as metal to plastic. Large inherent differences in the thermal expansion coefficients of dissimilar substrates can create stresses in the bond line. Strong vibrations have also been known to cause premature failure. The average

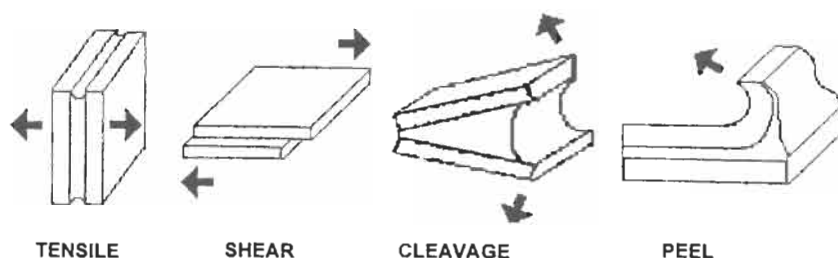


Fig. 4. Four major stresses possible in an adhesive bond.

urethane structural adhesive has peel properties of 60 pli and, in some cases, can exceed 100 pli. In rubber-toughening epoxies, however, peel strengths of over 30 pli are easily attained, and, in rare cases, 60 pli [40]. Improvements beyond this 60 pli usually require a change in morphology to more closely resemble the standard urethane morphology shown in Fig. 3.

5. Controlling the physical properties of urethane adhesives

It is difficult to generalize regarding adhesion properties and physical characteristics of urethanes, because both the adhesion properties and physical properties can vary widely. One two-part urethane adhesive may be an outstanding adhesive for bonding SMC/SMC. Another urethane adhesive may fail miserably using the same SMC, due to delamination at the interface or adhesive failure.

A urethane may have bulk properties of some of the stiffest plastics, on one extreme, or it may be as flexible and conformable as a PSA, on the other extreme. This section will give qualitative guidelines to achieving the desired adhesion characteristics of 'properly prepared' substrates.

5.1. Morphology and adhesion properties of urethanes

The morphology of a typical urethane adhesive was previously shown in Fig. 3. The continuous phase usually comprises the largest part of the adhesive, and the adhesion characteristics of the urethane are usually controlled by this phase. From a chemical standpoint, this continuous phase is usually comprised of the polyol and the small amount of isocyanate needed to react the polyol chain ends. A wide variety of polyols is commercially available. A few of the polyols most commonly used in urethane adhesives are shown in Table 2. As a first approximation, assuming a properly prepared bonding surface, it is wise to try to match the solubility parameters of the continuous phase with that of the substrate to be bonded. The adhesion properties of the urethane are controlled to a great extent by the continuous phase. Adhesion to medium polarity plastics, such as

SBR, polycarbonates, etc., can often be achieved by choosing a polyol backbone that is similar in polarity to the substrate to be bonded. For example, polyethers often work well for obtaining adhesion to these medium polarity plastics, whereas polyesters usually work better for polar substrates, such as glass and metal.

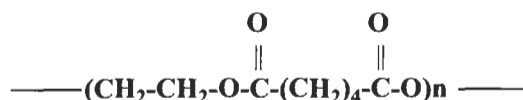
5.1.1. The role of crystallizable soft segments in urethane adhesives

Some polyols with a symmetrical structure may be partially crystalline, while other polyols may be totally amorphous. This crystallinity can be a very important feature for certain types of urethane adhesives. In most curing hot-melt adhesives, certain types of waterborne polyurethane adhesives, and some thermoplastic polyurethane adhesives, the crystallinity of the 'soft segment' (continuous rubbery phase) is utilized to obtain 'fixturing strength'. Fixturing strength is the minimum amount of strength necessary for an adhesive to be able to hold two substrates together without using clamps or fixtures to hold the substrates in place. Poly(hexamethylene adipate) polyols, for example, have a very symmetrical structure, i.e., no pendant side groups (methyl, ethyl, etc.) that could be a hindrance to chain packing and crystallization. Poly(hexamethylene adipate) has a crystalline melting point range of 55–65°C [41]. Urethane adhesives utilizing a crystallizable backbone, such as poly(hexamethylene adipate), are applied with heat. This heat is necessary in order to melt the crystalline component within the polyol; the molten liquid can then be applied to the two substrates and the bond closed. Usually, the lower the viscosity of the material in this molten state, the more easily it can 'wet' the interface: a crucial requirement for a durable bond. Once the bonding has occurred, the temperature at the interface begins to cool below the crystalline melting point of the soft segment. The time to achieve fixturing strength is, therefore, dependent upon the temperature of the interface, the viscosity, and the crystallization kinetics. Poly(hexamethylene adipate) is among the fastest crystallizing backbones for urethanes, and fixturing strength may usually be achieved in 60–120 s. When crystallization occurs, the polymer chains pack together and align themselves. The act of crystallization physically ties one polymer chain to another, locking them in place, and the viscosity rises dramatically, creating the desired fixturing strength. The role that the crystallization plays in achieving fixturing strength will be discussed later for each type of urethane adhesive. Some polyol backbones may have no crystalline character at all or may be slowly crystallizing, e.g., poly(neopentyl adipate). If crystallization occurs at all in poly(neopentyl adipate), it may take weeks at ambient temperature.

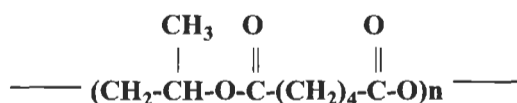
5.1.2. The role of non-crystallizing soft segments in urethane adhesives

The most common non-crystallizing soft segment in urethane adhesives is based on poly(oxypropylene) polyols, shown in Table 2. Most non-crystalline soft

segment polyols have an asymmetrical structure, i.e., contain pendant methyl, ethyl, etc. moieties, which sterically hinder chain packing. Poly(oxypropylene) polyols are prime examples of this point. They contain a pendant methyl group that hinders the packing together of the polymer chains. If the polymer chains cannot pack closely enough, crystallization within the soft segment is unlikely. Almost without exception, the non-crystallizable polyols are liquids at room temperature. Many asymmetrical polyester polyols can be liquids, albeit high-viscosity liquids. An example of a symmetrical polyester polyol is poly(ethylene adipate), which has a crystalline melting point of around 50°C and a glass transition temperature of -35°C. Poly(1,2-propylene adipate) is a non-symmetrical structure related to the symmetrical poly(ethylene adipate):



Poly(ethylene adipate)



Poly(1,2-propylene adipate)

The two structures appear very similar. Poly(1,2-propylene adipate) has the same basic structure as poly(ethylene adipate), except for a pendant methyl group. This pendant methyl group on the poly(1,2-propylene adipate) makes a large difference, however. Poly(1,2-propylene adipate) has no crystalline melting point. Trappe theorizes that the pendant methyl prevents chain packing and therefore, prevents crystallization [42].

The soft segments made from asymmetrical (amorphous) polyols are important for two-component structural adhesives and one-component moisture-curing adhesives. These materials are applied and usually cured at room temperature.

Not all symmetrical polyols are crystalline solids. Low molecular weight symmetrical polyols, such as poly(oxytetramethylene) polyols, of approximately 650 molecular weight and less, as well as low molecular weight symmetrical polyester polyols, such as poly(hexamethylene adipate) or poly(caprolactone) polyols, are liquids at room temperature. In a study, Penning demonstrated that there were marked differences in the crystallinity of a certain symmetrical polyester, depending upon the molecular weight of the polymer. In general, lower molecular weight polyesters had lower crystallinity. This led to the hypothesis that chain ends themselves were crystal defects, causing a decrease in crystallinity

[43]. Low molecular weight symmetrical polyester polyols may be liquids as a result of many chain ends that disrupt crystalline packing entirely.

5.1.3. The role of isocyanates in urethane adhesives

Isocyanates are polar, reactive molecules. Isocyanates, either alone or in conjunction with certain resins, have been established as excellent primers for metal, glass, rubber, and fibers [44].

The isocyanates are believed to aid wetting of metals by interacting with the metal oxides and hydroxides (M-OH) present on the surface. The isocyanates can then react with water to form a rigid polyurea network which interacts at the metal surface through hydrogen bonding. The isocyanates also react to form 'hard segments', which will be explained shortly.

5.2. Structure/property relationships of polyurethanes

5.2.1. Role of the polyols

As previously mentioned, polyurethanes can be either rubbers or plastics. Table 4 shows the various glass transition temperatures of two types of polyurethanes, depending on the molecular weight of the polyol. Note that polyurethanes made from poly(caprolactone) polyols can yield either plastics (T_g above room temperature) or rubbers (T_g below room temperature) (see p. 50 in [45]). The data for both the poly(caprolactone) urethanes and poly(oxypropylene) urethanes show a trend. As the molecular weight of the polyol decreases, the glass transition temperature of the resulting polyurethane increases. As the polyol molecular weight decreases, more diisocyanate is needed. The diisocyanate is a rigid component

Table 4

Effect of varying polyol molecular weight on the glass transition temperature of polyurethanes

Poly(caprolactone) polyol (PCI) PCI/MDI/BD = 1/2/1		Poly(oxypropylene) polyol (PPG) PPG/TDI/MOCA = 1/2/1	
Polyol MW	T_g (°C)	Polyol MW	T_g (°C)
340	53	1000	-40
530	25	1250	-50
830	-10	1500	-55
1250	-27	2000	-56
2100	-40		
3130	-43		

Ref. [45].

of the polyurethane. Therefore, an increase in the amount of diisocyanate (corresponding to a decrease in the molecular weight of the polyol) used to react with the polyol usually results in an increase in the glass transition temperature of the resulting urethane. It should be apparent from Table 4 that urethane adhesives can be formulated as either rigid plastic adhesives or flexible rubber adhesives. Usually, many different molecular weights of a given polyol are offered, in order to give the scientist the maximum flexibility in designing the proper adhesive for the task.

5.2.2. Role of the isocyanate

The isocyanate is that which distinguishes polyurethanes from other structural adhesives. In the process of reacting an isocyanate with a polyol, the urethane linkage is formed, which provides hydrogen-bonding capabilities that are lacking in most other structural adhesives. Isocyanates are also the key element in the hard segment in the urethane. Hard segments are best described as rigid segments that associate through hydrogen bonding to form plastic-like domains. These hydrogen-bonded domains may even be partially crystalline. As a rule of thumb, the more the isocyanate level increases in a urethane adhesive, the more rigid that adhesive becomes.

Rules of symmetry apply to isocyanates. The odd/even rule, put forth by Buist and Gudgeon, shows that urethanes based on aliphatic isocyanates with an even number of carbons have a higher crystalline melting point than urethanes based on isocyanates with an odd number of carbons, as shown in Table 5 [46].

Rules of symmetry apply to the aromatic isocyanates as well. Polyurethanes based on ethylene glycol (EG) and aromatic isocyanates were also studied by Buist and Gudgeon. Aromatic isocyanates with a plane of symmetry had higher crystalline melting points than did those without a plane of symmetry. Therefore, EG derivatives made with toluene diisocyanate, an asymmetrical diisocyanate, had a lower crystalline melting point than those made with methylene diphenyliso-

Table 5
Crystalline melting points of aliphatic polyurethanes

Diisocyanate $\text{OCN}-(\text{CH}_2)_x-\text{NCO}$ $x =$	Diol $\text{HO}-(\text{CH}_2)_y-\text{OH}$ $y =$	Melting point ($^{\circ}\text{C}$)
4	4	193
5	4	159
6	4	183
8	4	160
11	4	143–146

cyanate, a symmetrical diisocyanate. The crystalline melting points were reported as 185°C and 255°C, respectively. Of the commercially available isocyanates, *para*-phenylene diisocyanate (PPDI) and naphthalene diisocyanate (NDI) reportedly performed the best. The urethane decomposition point for the PPDI/EG adduct (340°C) was reached before the crystalline melting point was reached. The crystalline melting point for the NDI/EG adduct was 304°C. These latter two isocyanates are generally reserved for the highest performance applications. Certain applications require a higher-temperature service life than is possible from normal urethanes. Assuming no thermal or oxidative degradation, a urethane adhesive may continue to perform in heated conditions up to the temperature of the crystalline melting point of the hard segment.

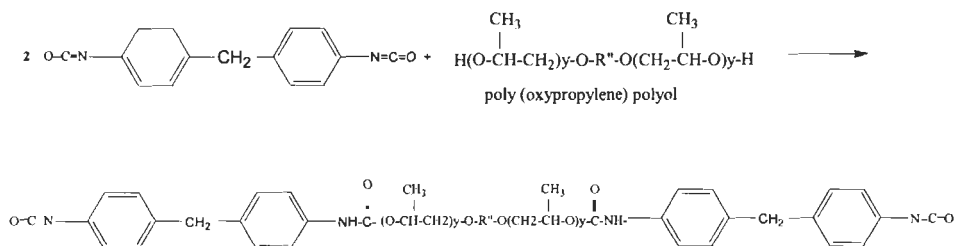
6. One-component urethane adhesives

6.1. Moisture-curing liquid urethane adhesives

The moisture-curing liquid adhesives of today contain little or no solvent, in order to comply with VOC (volatile organic compound) guidelines. Most of today's liquid adhesives are based on methylene diphenylisocyanate (MDI), although some adhesives still contain toluene diisocyanate (TDI). It is easier to formulate a low-viscosity liquid adhesive based on TDI. Unfortunately, toxicity concerns (associated with inhalation of even low levels of TDI) preclude its safe use, unless excellent ventilation and/or respiratory protection is provided for the end user, under conditions carefully defined by a trained industrial hygienist. Several manufacturers produce prepolymers with very low levels of monomeric TDI (<0.07%). The free TDI monomer has been stripped from the prepolymer, which greatly reduces the toxicity hazard, so that these prepolymers may be considered for some MDI-based applications. Most liquid adhesives are based on MDI and have higher viscosity than their TDI counterparts. As previously mentioned, the vapor pressure of MDI is substantially lower than that of TDI, making it much easier to use safely.

Several large applications for one-component moisture-cure urethane adhesives are available. Polymeric MDI is an exceptional binder for wood products, such as oriented strand board and particleboard. One-component urethane windshield adhesives are used almost exclusively in both the OEM and automotive aftermarket. One-part urethane adhesives are used to assemble the sidewalls for recreational vehicles (RV's), manufactured housing, and mobile homes. In construction applications, one-part urethanes are used to bond metal doors, hardwood flooring, panels, and partitions.

The basis of most one-component, moisture-curing urethanes is the synthesis of an isocyanate-terminated prepolymer, as shown:



A variety of applications exist for liquid, '100% solid' adhesives. (An adhesive is considered '100% solid' if there is no solvent in the adhesive.) Some of the largest uses include structural wood adhesives and adhesives used for the transportation industry, such as windshield adhesives and those used for bonding composite sidewalls of a recreational vehicle (RV). Structural wood adhesives are often made of a polymeric MDI with functionality of approximately 2.7 or higher. Rigid assemblies often utilize polymeric MDI, whereas flexible adhesive assemblies will more often utilize pure MDI, a solid waxy material that melts at around 37°C, or a 'modified MDI', i.e., MDI that has been modified to make it a liquid at room temperature. Prepolymers are made with ratios of anywhere from $\text{NCO}/\text{OH} = 1.6$ to 3.0 or higher.

Most moisture-curing liquid adhesives utilize poly(oxypropylene) (PPG) polyols, as shown above. These raw materials produce among the lowest-viscosity prepolymers but may not have sufficient modulus at higher temperatures for some applications. A certain percentage of polyester polyols may also be utilized to boost performance, but these may cause a large increase in viscosity, and so they are more often used in conjunction with polyether polyols to provide a high-performance adhesive with workable viscosities. Poly(butadiene) polyols may be utilized for specific adhesion characteristics.

Common plasticizers are used to reduce viscosity and to aid adhesion. Most plasticizers commonly utilized in PVC are also used in urethanes. One of the most common plasticizers is diisodecyl phthalate, though many others are used equally effectively. In some cases tackifiers, such as certain esters or terpene phenolics, are utilized to obtain specific adhesion characteristics.

Catalysts serve a dual purpose in one-component moisture-curing urethanes. The first purpose is to accelerate the prepolymer synthesis. The second purpose is to catalyze the curing reaction of the adhesive with moisture. The most common catalysts used to promote both prepolymer formation (NCO/OH) and later the adhesive curing reaction ($\text{NCO}/\text{H}_2\text{O}$) are dibutyltin dilaurate and DMDEE ((*dimorpholinodiethyl*) ether), a tertiary amine. A stabilizer such as 2,5-pentanedione is sometimes added when tin is used, but this specific stabilizer has fallen from favor in recent years, due to toxicity concerns. DMDEE is commonly used in many one-component moisture-curing urethanes. DMDEE is one of the few tertiary amines with a low alkalinity and a low vapor pressure. The latter

characteristic is desirable in order to minimize the 'fishy' odor common to many tertiary amine catalysts. The odor is most noticeable during adhesive application.

In recent years, the push for fast reacting, room temperature curing adhesives has created a dilemma for the urethane adhesive producers. The one-component, liquid urethanes can be applied to a substrate, followed by a fine mist of water. The bond is then closed, and fixturing strength can be achieved in 15 min or less at room temperature. The fast water/isocyanate reaction has both positive and negative effects. On the positive side, very low levels of adhesives may be used, even on rough surfaces. Instead of the expected problems associated with bond line starvation, i.e., the use of too little adhesive to bond two substrates, the water/isocyanate reaction produces carbon dioxide, causing the adhesive to foam and expand to fill the bond line completely. The negative feature associated with this foaming is a reduction in the overall strength of the bond. A specific example of this reduction in strength is the performance of a standard one-component wood adhesive based on a polymeric MDI prepolymer:

	pbw
Ethylene oxide capped poly(oxypropylene) diol, MW 2800	100
Polymeric MDI, functionality 2.7	100
Dibutyltin dilaurate	50 ppm

An overlap shear test (pine/pine) of this standard adhesive usually produces a bond that cures slowly (3–4 h handling strength) and results in substrate failure of the wood, i.e., the adhesive was stronger than the wood itself. The strength of the bond must usually be in excess of 300 psi to achieve this desired substrate failure. Suppose 0.75% DMDEE catalyst is added to this same wood adhesive. This adhesive is then applied to the same wood substrates and water is then misted into the bond line prior to closure. Handling strength of this accelerated adhesive can be obtained in less than 5 min, but the curing process results in cohesive failure (not substrate failure) of the adhesive with only 22 psi overlap shear, a loss of over an order of magnitude in strength.

The addition of defoamers can restore some of this lost strength, but only to a certain point. The defoaming mechanism usually relies upon diffusion of gas bubbles together in the liquid adhesive to form larger bubbles, which, in turn, rise to the surface and break. Diffusion generally decreases with increasing viscosity and stops when the gel point is reached, i.e., when the viscosity approaches infinity, accordingly:

$$g = 1/f - 1$$

where g is the gel point and f is the functionality of the system [47]. Therefore, as the functionality of the system increases, the gel point is reached earlier. The defoamer usually becomes ineffective after the gel point. Defoamers are most effective for flexible adhesives with a functionality of 2.0. If the use of a defoamer

is anticipated, adhesion properties should be monitored, especially if the defoamer is silicone-based.

Foaming in the bond line is also related to the viscosity of the adhesive and rate of carbon dioxide evolution. Assuming that water is misted on the adhesive prior to closure, high viscosity of the adhesive and a fast cure encourage foaming in the bond line. In some cases, this is desirable for gap-filling purposes. In order to minimize foaming in the bond line, one should use low-viscosity, low T_g polyols with a functionality of 2.0, together with a slow rate of cure and addition of defoamers.

Windshield sealants comprise some of the most significant applications of one-component urethane adhesives. Several years ago, the requirements for these sealants were increased. In an accidental rollover, in certain automobiles, the windshield becomes a structural part of the car. Therefore, the windshield adhesive, which holds the windshield in place, must have structural strength. An example of a one-component windshield sealant is shown below [48]:

	pbw
MDI prepolymer (10/4 PTMEG 2000 MW/6000 PPG triol, NCO/OH = 2.0)	53.1
Fumed silica	5.0
Zinc oxide	1.8
Talc	17.7
Acrylic tackifier (95/5 isooctylacrylate-acrylic acid)	7.1
Hydrogenated terphenyl plasticizer	7.1
Toluene	5.5
Bis (<i>N,N'</i> -dimethyl-aminoethyl) ether	0.1
Silane adduct (mercaptopropyltrimethoxysilane/biuret of HDI)	2.6

6.2. Moisture-curing hot-melt urethane adhesives

Most moisture-curing hot-melt adhesives utilize a crystallizable backbone and are based almost exclusively on monomeric MDI at NCO/OH ratios of 1.5 to 2.2. Poly(hexamethylene adipate) polyol is the workhorse of the curing hot-melt adhesives.

Moisture-curing hot melts are a small but fast growing segment of the urethane adhesive market. They are used mostly in construction and furniture assembly applications. Recent applications include RV sidewall assembly and other OEM automotive applications. Smaller applications include bookbinding and footwear.

A typical adhesive is shown below:

100 parts	poly(hexamethylene adipate) 3750 MW
11.7 parts	4,4'-methylene di(phenylisocyanate) (NCO/OH = 1.75)
0.2 parts	dimorpholinodiethyl ether catalyst

Warm MDI ($\sim 40^\circ\text{C}$) is added to a vessel equipped with stirring and nitrogen. It is then heated to 90°C . Poly(hexamethylene adipate) is slowly added to the vessel. After an exotherm, the catalyst is added to complete the reaction. The product may

be dumped into 5-gallon or 55-gallon open head drums under nitrogen. Since this product is moisture sensitive, care must be taken to exclude water vapor.

The curing hot-melt adhesives are usually crystalline waxes at room temperature. When heated to the 250°F (125°C) application temperature, they become low-viscosity liquids. They are applied to one substrate as a one-surface bond. The second substrate is then joined with minimal pressure. Within 2 min or less, the bond temperature cools below the crystallinity point of the polyester. Crystallization occurs, resulting in a sharp increase in viscosity, thereby locking the chains in place and providing enough fixturing strength so that the temporary fixturing clamps can be removed. At this point, the bond has no more strength than that of a crystalline wax and can be easily broken. The adhesive is, however, a moisture-curing adhesive and over a period of 24–48 h develops the strength of a structural adhesive.

These adhesives differ from normal hot-melt adhesives, such as the standard ethylene vinyl acetate hot melts. Standard hot-melt adhesives like EVA have no curing mechanism. They are heated above the crystalline melting point and applied as a low-viscosity liquid in the same manner as is the curing hot melt. The bond is closed in the same manner and strength is developed upon crystallization.

Curing hot melts usually have less fixturing strength than do standard hot-melt adhesives but eventually develop structural strength. Once the moisture cure is complete, the curing hot melt has good structural properties and has better elevated heat strength than does a traditional hot melt such as EVA.

While the curing hot melts provide some quick fixturing strength without the use of solvent, when first applied, prior to cure, the fixturing strength of the bond is nothing more than that of a crystalline wax. In recent years, new developments have made the curing hot melts a more viable option to replace solvent-borne adhesives. By using higher melting points (60–100°C) intermediate molecular weight polyesters based on azaleic acid or dodecanedioic acid, the initial bond strength has been improved [49,50]. Another approach to improving green strength involves incorporation of high melt flow thermoplastics, such as polyurethane thermoplastics [51]. In a third approach, acrylates are polymerized in the polyester polyol prior to prepolymer formation. The polymerized acrylate provides the improved fixturing strength upon application [52]. Other improvements include catalyst enhancements to lengthen the heated working life of curing hot melts [53].

Potential disadvantages of curing hot melts are both equipment- and material-related. The equipment for applying curing hot melts has improved greatly in recent years. As with standard hot melts, all adhesive delivery lines must be heat-traced to prevent 'cold spots', in which the adhesive could solidify and create a blockage. The equipment differs from that for standard hot-melt adhesives in that great care must be taken to exclude water, since this starts the curing process. Most equipment uses 5-gallon or 55-gallon open head drums. A 'follower plate' is used to provide additional pressure, which aids delivery of the adhesive and

seal off the bulk material from moisture. Most curing hot melts have a limited application time at the 250°F application temperature, as a result of side reactions at elevated temperatures. The viscosity of the product will generally increase as time goes by, making the product more difficult to dispense. Heated pot life can be as short as 3 h, or, in some instances, may exceed 48 h. This is one of the inherent complexities of the product.

6.3. Solvent-borne urethane adhesives

Solvent-borne adhesives are of two different types: reactive and non-reactive. The reactive solvent-borne adhesives are usually high molecular weight oligomers with isocyanate functionality. When applied, these adhesives can react further, increasing physical properties. The non-reactive solvent-borne adhesives will not react further after application.

Solvent-borne urethanes are still widely used to bond leather and athletic shoes. The OEM automotive market uses some solvent-borne urethanes together with chlorosulfonated polyethylene as a primer. Some urethane solvent-borne packaging adhesives are used for cap liners and for paper and foil lamination. Some textile laminating applications are still based on solvent-borne urethanes.

As a general class of adhesives, the solvent-borne polyurethanes are gradually being replaced by other adhesive types, such as waterborne polyurethane dispersions and curing hot melts. Increasing regulations regarding volatile organic compounds (VOC's) have restricted their use, and regulators are beginning to be levy fines. Chlorinated solvents, such as methylene chloride, were commonly used in solvent-borne urethanes but now have nearly been eliminated. The most common solvents are the aromatics, such as toluene and xylene, as well as some esters, such as ethyl and butyl acetate, and various ketones. In some cases, acetone is used, since, as of this writing, acetone is considered to be a HAPS-free material and, therefore, excluded from the regulations associated with VOC's. Commonly, two or more solvents are employed for solvent-borne urethanes. A low-boiling solvent is present to assure rapid flash-off of the majority of the solvent after the adhesive is applied. A second (higher-boiling) solvent has several functions. The higher-boiling solvent helps to control the crystallization kinetics of the soft segment (e.g., crystalline polyester) or phase out of the hard segment, in the case of TPU, thereby helping to extend the open time of the adhesive. Once crystallization of the soft segment or phase-out of the hard segment occurs, the bond can no longer be closed and the open time has expired. The second function is to keep viscosity of the urethane low. This helps the adhesive wet the substrate, by helping the urethane to penetrate the surface of the substrate to be bonded, thereby extending the interphase region and improving mechanical interlocking of the adhesive and the substrate. The commonly used terminology for this mechanical interlocking with the substrate is 'bite'. Bite is a qualitative term, referring to the ability

of the adhesive to wet the substrate, thereby penetrating the surface and 'biting' into the substrate to accomplish bonding. This 'bite' effect is the reason that it has been so difficult to replace solvent-borne urethanes. Without the solvent present, the viscosity of the urethane is higher, and penetration of anything but the first monolayers of the substrate is difficult to accomplish. Common consequences of the inability of an adhesive to properly wet the surface of the substrate are adhesive failure of the bond and/or a shortening of the durable life of the bond. Solvent-borne urethanes have proved difficult to replace by alternative adhesives. The shoe industry, for example, still uses solvent-borne adhesives, as of this writing.

The polymer part of solvent-borne urethane adhesives may be purchased in the form of pellets or chips, which are later dissolved in such solvents as toluene or various esters, as previously mentioned. Alternatively, the urethane adhesive can be synthesized in the solvent and sold in liquid form. Tackifiers, plasticizers, and other additives are used to obtain specific adhesion to certain substrates. A good review of crystallization rates and the effect of tackifiers is given by Penczek and Kujawa-Penczek [54]. Certain solvent-borne urethanes can meet the requirements of a room temperature contact bond adhesive, in which the solvented adhesive is applied to both substrates. After several minutes, most of the solvent has evaporated; the two substrates are then mated to obtain instant fixturing strength. Very few polymers meet the auto-adhesion requirements of a good contact adhesive, but certain urethanes, natural rubber, chloroprenes, and a few others do meet these requirements. High-performance solvent-borne urethanes are made with a crystalline polyester backbone. They must be heat-activated. Once the solvent is flashed off these high-performance urethanes, the bonding must occur above the crystalline melting point of the polyester, producing a bond with good fixturing strength. The open time is controlled by the crystallization kinetics of the polyester backbone. Fast crystallizing, high-performance solvent-borne urethanes continue to be widely used in the shoe industry today, but they are beginning to be replaced by waterborne urethanes. Early indications are that thermoplastic hot-melt urethanes could also replace solvent-borne urethanes, but this should take longer to occur because of the vastly differing equipment requirements. While extruders to process the urethane hot melts are commonplace, they are not part of the equipment commonly used today for bonding shoe soles. Waterborne urethanes are the more logical choice to replace the solvent-borne urethanes because the equipment used is similar. Some minor changes are needed, usually in the form of the additional heat required to flash off water instead of a solvent.

An example of a solvent-borne adhesive is shown below:

	<u>pbw</u>
Polyurethane HP9 resin	18
Dispersed fumed silica	2
Methylethyl ketone	60
Ethyl acetate	20

Internal surfactants, i.e., surfactants that are incorporated into the backbone of the polymer, are commonly used in PUD's. These surfactants can be augmented by external surfactants, especially anionic and nonionic surfactants, which are commonly used in emulsion polymerization. Great attention should be paid to the amount and type of surfactant used to stabilize urethane dispersions. Internal or external surfactants for one-component PUD's are usually added at the minimum levels needed to get good stability of the dispersion. Additional amounts beyond this minimum can cause problems with the end use of the PUD adhesive. At best, additional surfactant can cause moisture sensitivity problems with the PUD adhesive, due to the hydrophilic nature of the surfactant. Problems can be caused by excess (or the wrong type of) surfactants in the interphase region of the adhesive, affecting the ability to bond.

A tertiary amine such as triethylamine is then added to the isocyanate-terminated prepolymer (containing carboxylic acid groups). The tertiary amine reacts with the pendant carboxylic acid groups, forming a carboxylic acid salt. The presence of this salt, together with adequate stirring, allows the dispersion of the prepolymer in water by the so-called 'melt dispersion process' [57].

The chain extension step may then take place in the water phase. Hydrazine and ethylene diamine are commonly used chain extenders for waterborne urethane dispersions. The isocyanates react with the diamine chain extenders much faster than with the water, thus forming polyurea linkages and building a high molecular weight polymer. More detailed information regarding the synthesis and process of making waterborne polyurethane dispersions is found in Dieterich's review article [58].

Fig. 5 shows the details of bonding of the two substrates by a waterborne PUD adhesive. The figure shown assumes a PUD adhesive with a fast crystallizing backbone [59].

As shown in Fig. 5, the adhesive is applied to one substrate and undergoes some heating, usually by infrared lamps. During phase I, the water in the PUD comes off, causing the viscosity to rise and a continuous film to form on the substrate. Phase II is marked by a sharp decrease in viscosity. There are two reasons for this sharp decrease in viscosity: (1) as a result of the water flashing off, the temperature of the adhesive can exceed 100°C, causing a bulk decrease in viscosity; (2) the melting of the crystalline polyester backbone also results in a decrease in viscosity, allowing the adhesive to wet the substrate.

As a result of the reduction in viscosity, the adhesive is now fully activated. The heating of the bond line ceases. The viscosity of the adhesive is now low enough so that the adhesive can be mated with a second substrate, and proper wetting of the second substrate can occur.

Phase III in Fig. 5 is marked by a cooling of the bond line, which causes the bulk viscosity of the adhesive to rise. During phase IV, another sharp increase in viscosity is observed. This is caused by the re-crystallization of the polymer

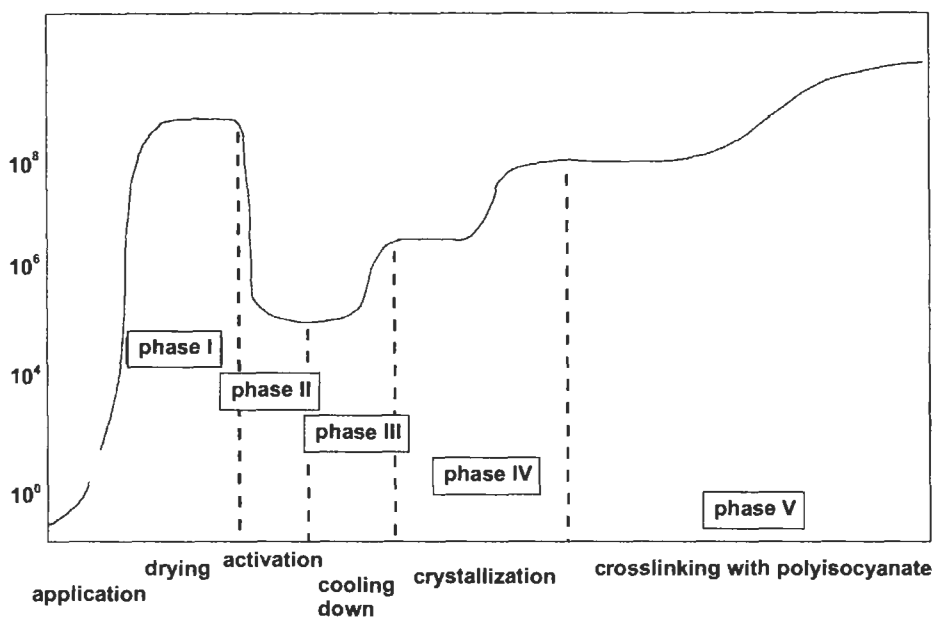


Fig. 5. Viscosity versus time — bonding process for a waterborne polyurethane dispersion.

backbone. Phase V deals with crosslinking of the polyurethane dispersion, which will be discussed later in the two-component waterborne adhesives section.

Waterborne urethane adhesive dispersions are usually high molecular weight linear polyester urethanes. The adhesive characteristics are most often defined by the crystalline melting point and crystallization kinetics of the backbone. The crystallization temperature of the backbone has both positive and negative aspects. It is highly desirable to activate the adhesive at room temperature or slightly above so that bonding can occur. As previously mentioned, polyurethanes based on hexamethylene adipate have a crystalline melting point with the 55–65°C range. These adhesives do not require large amounts of heat in order to form a bond. On the other hand, it is desirable for adhesives to have good heat resistance. In addition, the adhesive bond strength is related to the temperature by virtue of the crystalline melting point of the backbone. The urethane based on hexamethylene adipate would be expected to lose bond strength when exposed to temperatures in excess of the crystalline melting point of the backbone. The crystalline melting points of polyester urethanes can be varied and in some cases can exceed 100°C. Such an adhesive must be activated in excess of 100°C in order to form the bond.

One interesting advantage of the one-component waterborne adhesives is that many are re-positionable. For example, if, for some reason, the two substrates are poorly aligned when the bonding occurs, this problem can be corrected by heating the bonded substrates above the bond activation temperature. The two substrates

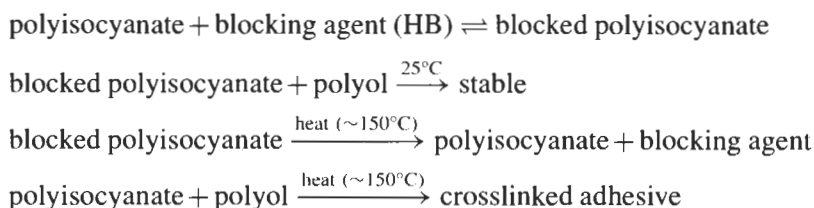
can be pulled apart and re-aligned correctly, with little or no penalty to the bond strength.

The crystallization kinetics defines the open time of the bond. For automated industrial processes, a fast crystallizing backbone, such as hexamethylene adipate, is often highly desirable. Once the bond line cools, crystallization can occur in less than 2 min. Thus, minimal time is needed to hold or clamp the substrates until fixturing strength is achieved. For specialty or non-automated processes, the PUD backbone might be based on a polyester polyol with slow crystallization kinetics. This gives the adhesive end user additional open time, after the adhesive has been activated, in which to make the bond. The crystallization kinetics for various waterborne dispersions were determined by Dormish and Witowski by following the Shore hardness. Open times of up to 40 min were measured [60].

6.5. Blocked urethane adhesives

'Blocked' urethane adhesives are termed 'blocked' by virtue of the fact that one of the key reactants is chemically blocked to prevent reaction. The concept of a blocked isocyanate has already been discussed.

The concept of utilizing a blocked isocyanate in a one-component adhesive system is shown below:



Applications for blocked urethane adhesives are small. However, they may be used as flocking adhesives or as crosslinkers for solvent-borne adhesives. Blocked urethane adhesives are also used as splicing adhesives for belts. Blocked isocyanates based on TDI, IPDI, and derivatives of hexamethylene diisocyanate are most commonly commercially available.

The blocked isocyanate does not react with the polyol at room temperature because it has already reacted with the blocking agent. Normally, if one adds polyols to the blocked isocyanates, the viscosity of the system is stable over long periods of time at room temperature. A good review of blocked isocyanates is found elsewhere [61].

The blocked isocyanate systems (with curative present) are latent cure systems. In order to create a latent curing adhesive, the blocked isocyanate is added to a catalyzed polyol component without a reaction occurring at room temperature. In theory, the blocked adhesive system is relatively stable at room temperature. When this system is heated to the unblocking temperature, the chemical reaction, which

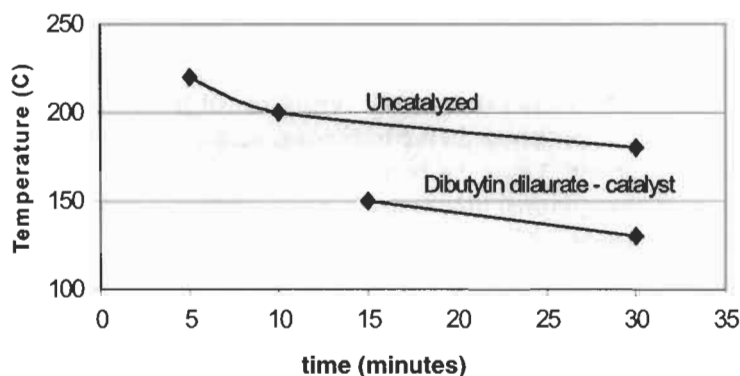


Fig. 6. Curing temperature of phenol-blocked TDI, catalyzed and uncatalyzed.

had caused the blocking reaction to take place (last reaction in Fig. 1), reverses to generate the unblocked isocyanate. The isocyanate can then react with the polyol (or other active hydrogen component) to form a tough, crosslinked adhesive.

The unblocking temperature usually refers to the temperature at which the blocked urethane system must be heated for 30 min in order to achieve cure. The reaction can be accelerated by curing at higher temperatures and/or by the addition of catalyst, as shown in Fig. 6 [62]. Common urethane catalysts like dibutyltin dilaurate are known to decrease the unblocking temperature.

If blocking agents come off too quickly, foaming in the bond line can result, especially if the substrates are non-porous. One exception to this rule is *E*-caprolactam. It remains in the adhesive and can act as a plasticizer, which can aid adhesion at elevated temperatures.

Most blocked isocyanates are solids at room temperature and thus may require the use of solvent. The unblocking temperatures are often fairly high and are energy intensive. Furthermore, certain blocking agents may qualify as volatile organic compounds. For these reasons, the blocked isocyanate adhesives occupy a small, but important segment of the adhesive marketplace.

An interesting blocked room-temperature curing urethane windshield adhesive is described by Barrons [63]:

	pbw
Phenolic-blocked isocyanate prepolymer	100
Thixotrope (Thixin R)	15.7
Filler	42.5
3-Aminopropyl trimethoxysilane	1.0
Methyl triethoxysilane	3.5
Methanol	0.88
Plasticizer (processing oil)	15.9
Ketamine (400 MW amine-terminated PPG/acetone)	8.5

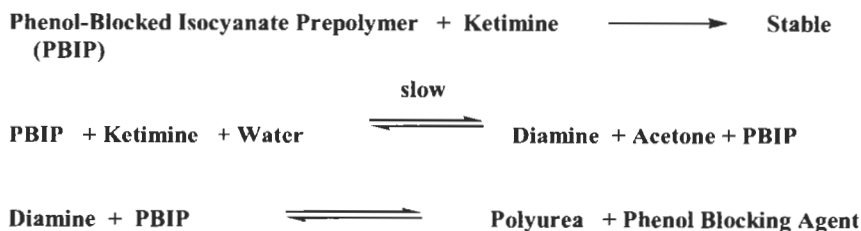


Fig. 7. Room-temperature curing concept for a phenol-blocked isocyanate-terminated prepolymer.

The ketimine is an acetone-blocked diamine. The synthesis and applications of ketimines will be discussed later. The curing concept for the adhesive is shown in Fig. 7. Phenol-blocked prepolymers would normally unblock at approximately 150°C. However, an aliphatic diamine, generated by the hydrolysis of the ketimine to an aliphatic diamine and ketone as a result of exposure to the moisture in the air, is sufficient to cure the windshield adhesive at room temperature.

6.6. Thermoplastic polyurethane adhesives

The thermoplastic polyurethane (TPU) adhesives must, of necessity, contain low gel content because they must be processable in an extruder. Most adhesives are relatively linear, with a functionality of 2.0, although small amounts of branching may be introduced, usually at the expense of a lower melt flow. Good physical properties of TPU's are obtained when the thermoplastic urethanes have molecular weights of 100,000 or higher (see p. 56 in [63]). Most TPU adhesives are based on symmetrical polyesters with a fast crystallizing backbone or a backbone slightly modified to increase the open time.

The market for polyurethane thermoplastic adhesives is small, but growing. TPU's are used to produce some solvent-borne adhesives and also are used in laminating textiles and films for labels and emblems. In addition, they are being considered as an alternative to solvent-borne adhesives in the shoe market.

Thermoplastic urethane adhesives may be processed into an adhesive film. Lamination of two substrates can, in theory, be done immediately, but the film is often extruded onto one substrate, covered by a release liner, and allowed to cool. Crystallization follows to create a non-tacky film that may be cut into specific shapes. The release liner is then removed, and the shaped adhesive can be heat-activated on one substrate, using infrared lamps. The second substrate is then nipped under pressure, followed by a cooling press to speed crystallization. Once the backbone has crystallized, the bond should be strong.

Although not in wide use, a fast crystallizing TPU adhesive can be used in the shoe industry as an alternative to solvent-borne urethane adhesives. The TPU adhesives have good holding strength soon after crystallization, which can be a distinct advantage over curing hot-melt adhesives. TPU adhesives normally have

better properties than the bulk hot-melt adhesives, such as EVA. Unfortunately, like the bulk hot-melt adhesives, TPU adhesives lose most of their strength above the crystalline melting point of the polyester backbone. Some TPU adhesives have low amounts of diol chain extenders, which produce high melting hard segments. These hard segments can extend the useful temperature range of the adhesive. TPU adhesives normally cost more than the majority of the bulk hot melt adhesives and are therefore used in higher-performance applications. TPU adhesives are especially effective in applications where softness, high flexibility, and toughness are required. An example of a thermoplastic polyurethane adhesive is shown below:

	<u>pbw</u>
<i>Polyol component</i>	
Poly(tetramethylene adipate) MW = 2000	100
1,4 butandiol	4
dibutyltin dilaurate	0.005
<i>Isocyanate component</i>	
4,4'-methylene diphenylisocyanate	23.6

The components may be mixed at 60°C, cast into a slab, and allowed to cure. Temperatures may rise to 150°C or higher. Once cured, the slab is broken up and granulated into a powder using a cryogenic granulator. The granulate may then be put through an extruder, followed by pelletization [64]. Alternatively, the TPU could be made in a twin screw extruder [65]. The output of the extruder, i.e., the TPU 'rope', then goes through a cooling bath. The TPU rope is cut into pellets. The pellets are then packaged in airtight bags in order to minimize the water content.

The adhesive pellets are processed in an extruder at 170–210°C [66]. Addition of 0.5–1.0% of a carbodiimide is recommended for TPU polyester adhesive applications. The role of carbodiimides will be discussed later. Even though polyesters are more resistant to oxidation than are polyethers, antioxidants are often added to prevent chain scission. In a shoe cap application, the adhesive web can be applied to a substrate on one side and a release liner on the other side. The bond is then cooled and cut into the proper shape. The shoe cap may be assembled by first heating the TPU adhesive to the proper temperature, using infrared lamps. The cap is then joined with the second substrate, followed by pressure and cooling, until crystallization is complete.

7. Two-component urethane adhesives

7.1. Structural urethane adhesives

The two-component urethane structural adhesives are among the most difficult to characterize, simply because of the widely varying properties that are possible. These adhesives may be rigid plastics similar in modulus to standard epoxy adhesives, with glass transition temperatures of the cured adhesive being approximately 60°C.

Two-component urethane adhesives are used to bond sheet molding compound (SMC) panels for automotive OEM and aftermarket applications. Two-part urethanes are used as laminating adhesives in the RV industry.

Like the epoxies, the rigid urethane adhesives may have overlap shear strength and tensile strength approaching 3000 psi. However, they suffer from two of the same problems as do the epoxies: a brittle bond line that has little tolerance for sharp impact and relatively low peel strengths of less than 30 pli. On the other end of the spectrum, two-component urethanes can be flexible, tough adhesives with glass transition temperatures of -50°C or lower. Flexible urethane adhesives have a flexural modulus below that of the average epoxy, as well as lower overlap shear, and tensile strength of 1000–3000 psi. They do, however, provide a flexible bond line capable of absorbing a sharp impact (even at -20°C without failure). In addition, they may have peel strengths even exceeding 100 pli. It is here that they find their niche [67].

Epoxies can be modified to improve their impact and peel properties. Rubber-toughened epoxies have previously been mentioned. They provide an impressive combination of high flexural modulus with improved impact and peel properties both approaching that of the average urethane. Two-component urethanes are often employed when a more flexible bond line is required. In general, the morphology of urethanes, i.e., hard segments amid a rubbery soft segment matrix (see Fig. 3), makes urethanes the best choice to handle large mismatches in thermal expansion coefficients of two dissimilar bonded substrates. Two dissimilar substrates, such as metal to plastic, can create stresses in the bond line. This thermal expansion coefficients mismatch can lead to embrittlement and bond failure, when exposed to the normal thermal cycling expected in actual use. The low glass transition temperature (usually -20°C or lower) of the continuous phase soft segment in the urethane gives it superior ability to conform to these stresses.

With the exception of fillers, the raw materials used in two-component urethanes are all liquids. The two components have an isocyanate side and a polyol side. The raw materials are combined in various ways in order to produce with liquids that are combined at a 1:1 volume ratio, preferably, thus keeping the dispensing equipment as simple as possible. Fixed ratios of 3:2 or 1:2 are also commonly used. Ratios other than these are possible, but require the use of a

variable ratio machine, which costs more than the fixed ratio machines. A static mixer is usually employed to mix the two components.

It would not be possible to discuss the infinite variations of two-component urethane adhesives in this writing. In order to demonstrate the extremes possible with two-component urethanes, two simplified adhesives are shown below with widely differing properties:

Rigid adhesive

Isocyanate component:

Liquid MDI prepolymer — 2.0 functionality, equivalent wt = 182

Polyol component:

Liquid poly(caprolactone) triol — 540 MW

Dibutyltin dilaurate catalyst — 0.001% by weight

Bulk properties of the adhesive:

Flexural modulus — 960 Ksi

Tensile properties — 2860 psi

Elongation at break — 4%

Overlap shear, 5 mil bond line, Al/Al — 3200 psi

90 Peel strength, Al/Al — 10 pli

Flexible adhesive

Isocyanate component:

Liquid polyester MDI prepolymer, 9% NCO	pbw
-----------------------------------------	-----

Liquid polymeric MDI, 2.2 functionality	52.3
-----------------------------------------	------

Polyol component:

Aromatic amine-terminated poly(tetrahydrofuran) — 650 MW	47.7
----------------------------------------------------------	------

Amine chain extender — 4,4'-methylene bis(3-chloro-2,6-diethyl aniline)	82
-------------------------------------------------------------------------	----

Note: the amine chain extender must be melted into the polyol at 160°C for 3 hrs under stirring, until completely melted. Once cooled, the chain extender remains liquid in the polyol.

Physical properties:

Flexural modulus — 16 Ksi

Tensile strength — 4500 psi

Elongation at break — 820%

Overlap shear (5 mil bond line) — Al/Al = 2450 psi

90 Peel strength (5 mil bond line) — CRS/CRS — 80 pli

Open times of two-component urethanes can vary widely, depending on the level of catalyst. Reaction times can vary from 90 s to over 8 h. Dibutyltin dilaurate is the most common catalyst employed to catalyze the urethane reaction. This is normally added to the polyol side. A tertiary amine may also be added in small amounts. Tin catalysts do not catalyze the amine/isocyanate reaction very well. Acids, such as 2-ethyl hexanoic acid, may be employed to catalyze the amine/isocyanate reaction where needed.

One application for a two-part urethane adhesive is a windshield adhesive/sealant

for the automotive aftermarket. A formulation utilizing a new delayed action catalyst system is described elsewhere [68].

Various additives and fillers may be employed. Calcium carbonate, talc, carbon black, titanium dioxide, and wollastonite are commonly used as fillers. Plasticizers are often utilized also. Plasticizers may reduce viscosity and may help adhesion to certain substrates. Thixotropes such as fumed silica, structured clays, precipitated silica, PVC powder, etc. can be added. Adhesion promoters, such as silane coupling agents, may also be used in the formulation [69].

7.2. Waterborne urethane adhesives

Two-component waterborne urethane dispersions are similar to the one-component PUD's in that a polyurethane dispersion comprises one of the two components. The second component is usually a crosslinker from the following classes of materials; (a) polyisocyanates, (b) aziridines, (c) polycarbodiimides, and (d) epoxies. Many of the crosslinkers are not inherently water-soluble or water-dispersible. Therefore, they must be modified with surface active agents themselves, so as to become emulsifiable in water.

Two-component waterborne urethanes are the preferred choice to replace solvent-borne urethane adhesives, especially in the packaging and shoe industries. At this time, the packaging area is the largest application of two-part waterborne urethanes. Good strides have been made by the two-part waterborne urethanes in the shoe industry, especially in the athletic shoe market. Waterborne urethanes are also replacing the solvent-borne products in the OEM door panels.

The two-component waterborne urethanes are similar in nature to the one-component waterborne urethanes. In fact, many one-component PUD's may benefit from the addition of a crosslinker. The two-component urethanes may have higher levels of carboxylic acid salt stabilizer built into the backbone than is actually needed to stabilize the urethane in water. As a result, if these two-component urethane dispersions were to be used as one-component adhesives by themselves (without crosslinker), they would show very poor moisture resistance. When these two-component urethane dispersions are used in conjunction with the crosslinkers listed in Fig. 8, the crosslinkers will react with the carboxylic pendant groups built into the urethane, as previously shown in the one-component waterborne urethane section. This accomplishes two tasks at the same time: (1) when the crosslinker reacts with the carboxylic acid salt, it eliminates much of the hydrophilicity associated with urethane dispersion, and (2) it crosslinks the dispersion, which imparts solvent and moisture resistance to the urethane adhesive (see phase V in Fig. 5). As a result of crosslinking, the physical properties may be modified. For example, the results may be an increase in tensile properties and a decrease in elongation. Depending upon the level of crosslinking, the dispersion may lose the ability to be repositionable. (Many of the one-component PUD's may

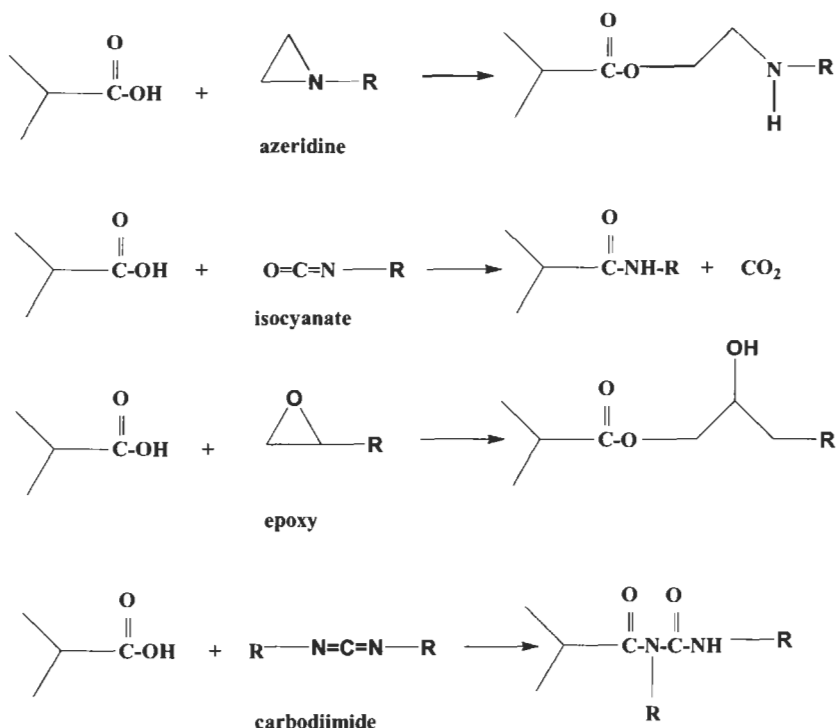


Fig. 8. Crosslinking reactions of carboxylated waterborne polyurethane dispersions.

be repositioned after bonding. By heating the bond above the crystalline melting point of the polyester backbone, the bond may be reset and pressure applied to remake the bond.)

The crosslinkers are normally added to the PUD and simply stirred in. The water is then flashed off, using a combination of forced-air drying and infrared lamps. The pot life associated with most of the crosslinkers varies between 30 and 180 min, but may exceed this in some cases. The common crosslinking reactions for a PUD containing carboxylic acid are shown in Fig. 8. Coogan evaluated various crosslinkers using a PUD containing both carboxylic acid groups and hydroxyl groups. Water-dispersible isocyanates were found to give the best cure, followed by aziridines, carbodiimides, and epoxies. If the PUD contained only carboxylic acid groups, aziridines gave the best improvement in solvent resistance and mechanical properties, followed by the carbodiimides and water-dispersible isocyanates, and, finally, the waterborne epoxies [70].

Common crosslinkers for hydroxyl-terminated PUD's are water-dispersible isocyanates and melamines. Unlike other crosslinkers, melamine crosslinkers usually have good stability in water. Two major drawbacks are associated with melamine crosslinking. In the first place, the bond must be heated. It will not

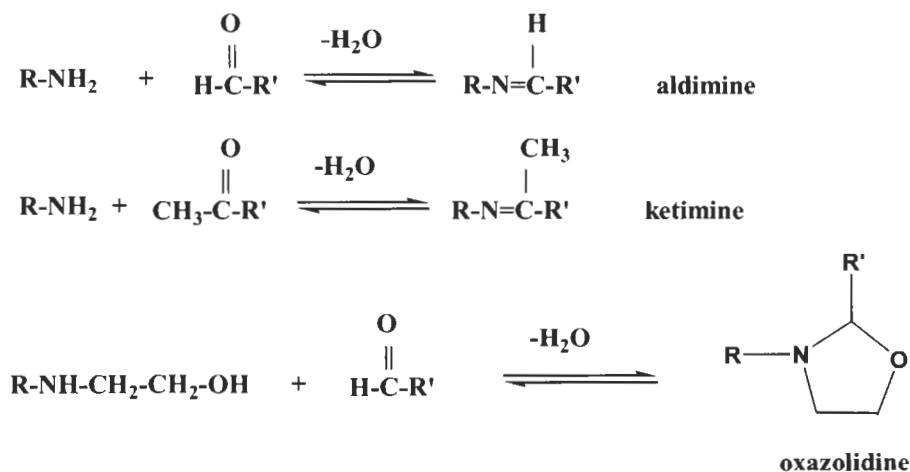
crosslink at room temperature. Secondly, methanol or formaldehyde may be given off in the heated curing cycle [71].

Once the crosslinker is added, it is important to apply the adhesive and dry off the water. Most of the commonly used crosslinkers will react with water over a period of time and lose effectiveness. In some two-component PUD's, the system may increase in viscosity and even gel, giving the user some idea of when the useful life of the crosslinker is approaching its end. In other instances, no viscosity increases or other visible indications signal that the crosslinker has reached the end of its useful life. The improvements in physical properties, solvent resistance, and water resistance normally provided by a crosslinked PUD adhesive would not be fully realized, in this case.

7.3. 'Modified' two-component urethane adhesives

The term 'modified' two-component urethanes refers to systems in which one or more of the reactants in a two-component system are temporarily blocked to prevent reaction. The modified two-component system does not have the long shelf life of a standard one-component blocked system.

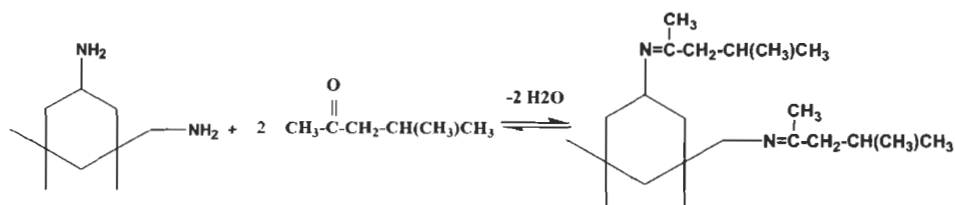
Several blocked diamines or amino-alcohols are commercially available. The 'aldimine' is an aldehyde-blocked diamine. The 'ketimine' is a ketone-blocked diamine. The oxazolidine is a five-membered ring containing oxygen and nitrogen. The oxazolidine ring shown below is an aldehyde-blocked amino alcohol. The basic synthetic concepts of an aldimine, a ketimine, and an oxazolidine are shown below:



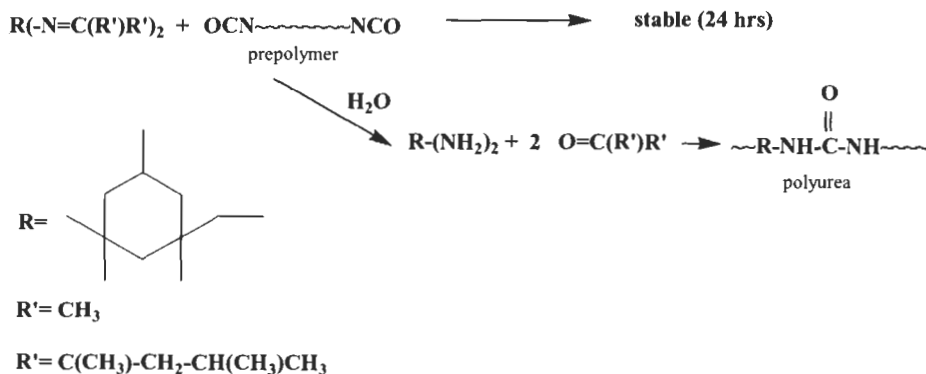
Note that, in each case, water is split off to form each derivative. These blocked amines and blocked amino-alcohols can be stirred into isocyanate-terminated urethane prepolymers. Each system has a certain pot life. The pot life can vary from

several seconds to a system that is relatively shelf stable and, in some cases, may even qualify as a one-component system, as long as there is no exposure to moisture. In general, the longest pot life can be obtained when aliphatic-based isocyanate-terminated prepolymers are used, particularly those based on isophorone diisocyanate (IPDI) and methylene 4,4'-dicyclohexylisocyanate (H12MDI). Side reactions can limit the pot life of these materials, which often react even in the absence of water. Certain aldimines are reported to be relatively shelf stable but cure when exposed to humidity [72,73]. Certain oxazolidines, together with the aliphatic isocyanate-terminated prepolymers just described, have sufficient pot life to be classed as one-component systems [74].

An example of the synthesis and curing reactions of a specific ketimine is shown below:



The ketimine of isophorone diamine is formed by reacting it with methyl isobutylketone, splitting off water in the process. When said ketimine is added to an isocyanate-terminated prepolymer based on IPDI, a semi-stable system is established with a pot life of several hours. The ketimine is a Schiff base and thus can react even in the absence of water. The complexities and advantages of this system are reviewed by Bock and Halpaap [75]:



Once the adhesive system is applied, water reacts preferentially with the more reactive ketimine, instead of with the slower reacting isocyanate. In the presence of water, the ketimine unblocks to reform the ketone and diamine. Once formed, the diamine will react quickly with the isocyanate to form a polyurea,

which can attain good strength within 30 min at room temperature. Despite the relatively fast cure of these systems at room temperature, no foaming appears in the bond line. Foaming would be associated with a normal fast, moisture-curing isocyanate prepolymer. Since the water reacts faster with the ketimine than with the isocyanate-terminated prepolymer, no carbon dioxide, which could get trapped in the bond line, is formed. Instead of carbon dioxide, methyl isobutylketone is formed, which can diffuse slowly out of the bond line. In this manner, even relatively thick bond lines can be formed without foaming in the bond line. The major disadvantage of these types of systems is the higher cost of the raw materials; these systems are, therefore, utilized only for niche applications.

Methylene dianiline is normally a very reactive diamine in the presence of diisocyanates. However, a sodium chloride complex that is relatively unreactive at room temperature is commercially available. When the complex is heated to 127°C, it activates to quickly cure the urethane [76].

8. Thermal, oxidative and hydrolytic stability of polyurethanes

There appear to be conflicting reports regarding the degradation of urethanes. For example, some urethanes are reported to have relatively poor hydrolysis resistance and good biodegradability [77], while other urethanes are reported to be so hydrolytically stable that they have been successfully used as an artificial heart [78]. Both reports are correct. It will be shown that the thermal, oxidative, and hydrolytic stability of urethanes can be controlled, to some degree, by the choice of raw materials used to make the urethane.

8.1. Thermal stability of urethanes

Urethanes, as a general class, are not as thermally resistant as are most epoxies, cyanate esters, bismaleimides, engineering thermoplastics, etc. Within the class of urethanes, a certain amount of latitude is available, enabling the scientist to design the thermal stability, based on the choice of raw materials and the chemical bonds formed to make the polyurethane. Although there can be exceptions, isocyanurate and oxazolidone linkages are generally more stable than ureas (mono-substituted), which, in turn, are more stable than urethane linkages [79,80]. Biurets and allophanates are reported to be less stable than urethane linkages [81].

isocyanurate > oxazolidine > urea > urethane > allophanate and biuret

Two major mechanisms for thermal degradation and one minor mechanism are shown in Fig. 9. The first mechanism is the reverse of urethane formation. The second mechanism, which was proposed by Fabris, forms a primary amine and an olefin. It involves a six-member intermediate, as shown in Fig. 10. A thermal

1. Thermal Dissociation2. Olefin Formation3. sec-Amine Formation

Fig. 9. Mechanisms of thermal degradation.

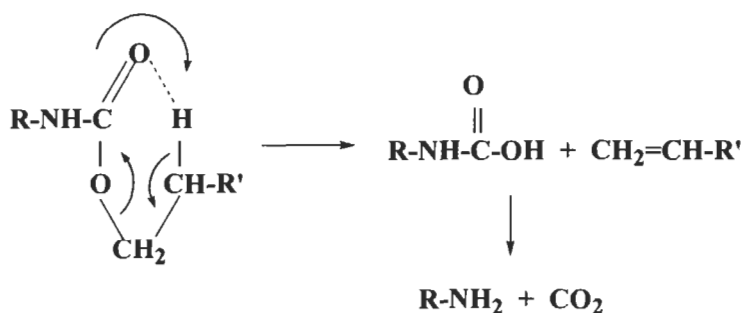
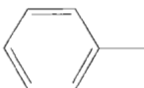

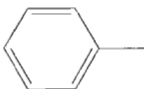
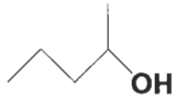
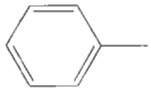
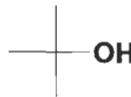


Fig. 10. Proposed mechanism for olefin formation.

stability study was run on model compound urethanes and the data are shown in Fig. 11. It is apparent from the study that urethanes based on primary hydroxyls should have better thermal stability than those based on secondary or tertiary alcohols.

8.2. Oxidative stability of urethanes

Oxidative stability is highly important because it deals with the degradation of polymers under actual performance conditions. Oxidative stability, as applied to urethanes, refers to the combination of oxygen and heat or oxygen and light that causes degradation of urethanes.

$\begin{array}{c} \text{O} \\ \\ \text{R-NH-C-O-R'} \end{array}$		
R=	R'=	T (°C)
		235
		200
		166

conditions: 10°C/min. in Argon

Fig. 11. Thermal stability of model urethanes.

8.2.1. Oxidative stability of urethanes — oxygen and heat

The combination of heat and oxygen poses a difficult challenge for any adhesive. The thermal degradation mechanisms still apply, as discussed previously, but now may be accelerated by the addition of oxygen. Of particular importance is the susceptibility of the urethane soft segment to oxidation. Polyols (which usually make up the majority of the soft segment) may show good thermal stability in the absence of oxygen, but may now be prone to attack. Polyether polyols are especially prone to oxidation. The proposed mechanism for oxidation of a urethane based on PPG is shown in Fig. 11 [82].

Polyesters and polycarbonate polyols show improved resistance to oxidative attack, compared with that of the polyethers. Stress relation studies run at 130°C, comparing a urethane based on a poly(oxypropylene) polyol and a urethane based on poly(butane adipate) polyol show that, after 60 h, the urethane based on PPG lost most of its strength, while the polyester retained most of its strength [83].

Urethanes made from poly(butadiene) polyols are also susceptible to oxidation, but they show good resistance to air-oven aging with antioxidants present (see p. 290 in [45]).

A study was done measuring the thermal oxidative stability of polyurethanes made from PPG polyols, varying the isocyanate curative. Oxygen absorption was

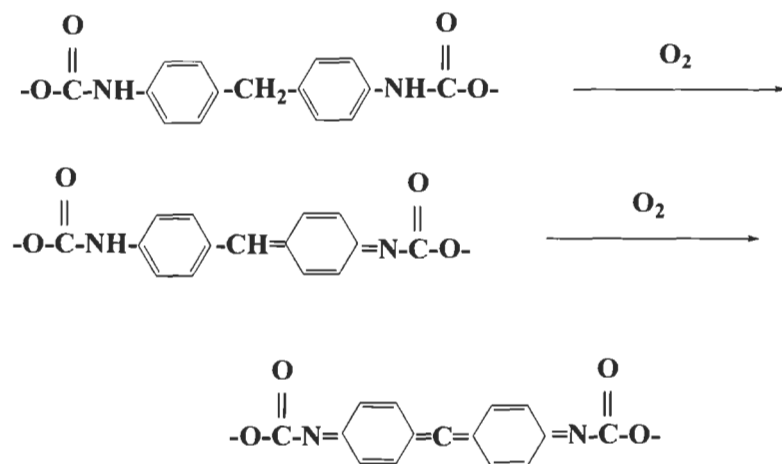
correlated to oxidation of the urethane. Aromatic diisocyanates were found to have better oxidation resistance than an aliphatic diisocyanate [84].



where NDI is naphthalene diisocyanate, MDI is methylene diphenylisocyanate, TDI is toluene diisocyanate and HDI is hexamethylene diisocyanate.

8.2.2. Oxidative stability of urethanes — oxygen and light

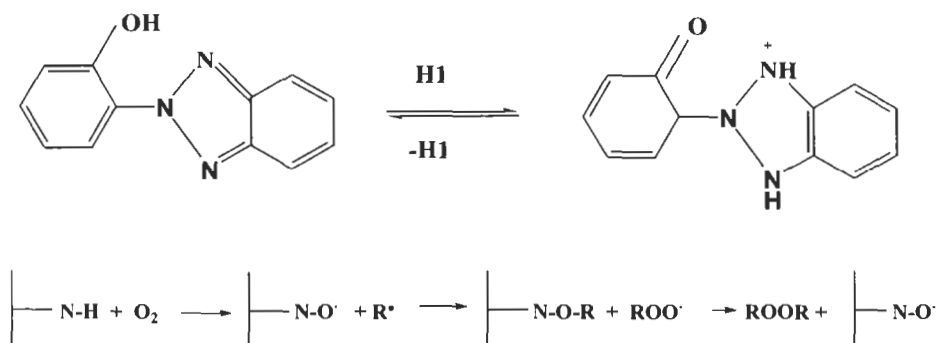
The combination of light and oxygen can have a deleterious effect on the stability of urethanes. It is well established that urethanes based on aromatic amines will yellow, especially in combination with oxygen and U.V. light. Schollenberger and Dinsbergs established the mechanism by discovering quinoid formation, resembling that of azo dyes [85]:



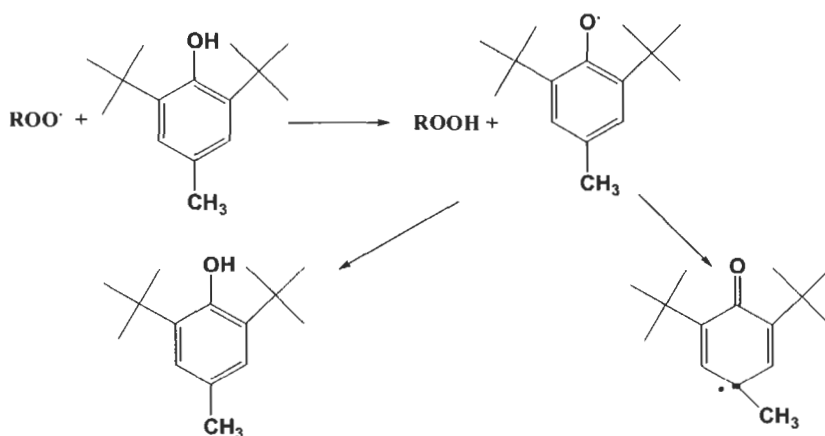
8.2.3. Role of U.V. stabilizers and antioxidants

In order to protect urethanes from the deleterious effects of oxygen and U.V. light, U.V. stabilizers have been developed. Some of the more common U.V. stabilizers are the hydroxybenzotriazoles and hydroxybenzophenones. These stabilizers absorb U.V. light in the aromatic range (300–400 nm), dissipating the energy in the form of heat. A hindered amine light stabilizer often works synergistically with

antioxidants, in a mechanism reviewed by Capocii [86]:



A hindered phenol is one of the most common antioxidants used in urethanes. This antioxidant traps radicals, which can degrade the polymer chain. The proposed mechanism is as follows [87]:



Certain metal catalysts, such as tin(IV) salts and tertiary amines, may work synergistically with oxygen to cause oxidative degradation of urethanes [88].

Certain fillers are commonly added to protect the urethane backbone from oxidative degradation. Carbon black and titanium dioxide are commonly used in conjunction with antioxidants to protect polyether polyurethanes in exterior adhesive applications that may be exposed to oxygen and light (Fig. 12).

Despite all precautions, urethanes can be used most effectively within certain thermal and oxidation limits. Outside these parameters, other adhesives, such as certain epoxies, cyanate esters, and other high-temperature adhesives, should be considered.

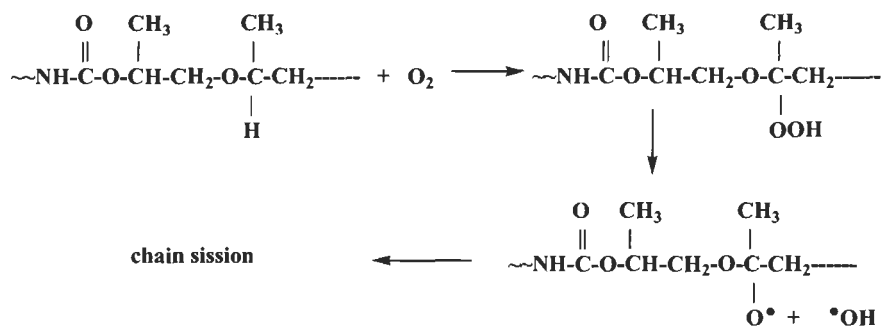


Fig. 12. Oxidative degradation of a polyether polyol.

8.3. Hydrolytic stability of polyurethanes

As previously mentioned, some urethanes can biodegrade easily by hydrolysis, while others are very resistant to hydrolysis. The purpose of this section is to provide some guidelines to aid the scientist in designing the desired hydrolytic stability of the urethane adhesive. For hydrolysis of a urethane to occur, water must diffuse into the bulk polymer, followed by hydrolysis of the weak link within the urethane adhesive. The two most common sites of attack are the urethane soft segment (polyol) and/or the urethane linkages. Urethanes made from PPG polyols, PTMEG, and poly(butadiene) polyols all have a backbone inherently resistant to hydrolysis. They are usually the first choice for adhesives that will be exposed to moisture. Polyester polyols and polycarbonates may be prone to hydrolytic attack, but this problem can be controlled to some degree by the proper choice of polyol.

Schollenberger and Stewart studied the hydrolysis of various polyester urethanes by immersing the materials in water at 70°C for several weeks and measuring the tensile properties. The data are shown in Table 6 [89]. The urethane

Table 6

Effect of chain structure on the hydrolysis of polyester polyurethanes

Polyester	Tensile (psi)				
	0 weeks	1 week	3 weeks	5 weeks	7 weeks
PEA	7000	5700	2800	NA	NA
PTMA	9200	8000	5500	2000	NA
PHMA	9000	8900	6300	4200	2000

Synthesis: MDI prepolymer with 1000 MW polyester polyol, NCO/OH = 2.0, chain-extended with 1,4-butanediol, acid number of polyester ~0.6.

Note: PEA = poly(ethylene adipate), PTMA = poly(tetramethylene adipate), PHMA = poly(hexamethylene adipate).

Table 7

Effect of acid number on the hydrolytic stability of urethanes made from poly(tetramethylene adipate)

Acid # PTMA	Tensile (psi)				
	0 weeks	1 weeks	3 weeks	5 weeks	7 weeks
3.66	8300	4100	575	NA	NA
2.50	8100	4300	900	300	NA
0.6	9000	7800	5400	2200	NA
0.1	9200	9200	8300	8200	6000

Synthesis: MDI prepolymer with 1000 MW poly(hexamethylene adipate) polyol, NCO/OH = 2.0, chain extended with 1,4-butanediol.

Ref. [89].

made from poly(ethylene adipate) retained only 40% of its original strength, while poly(tetramethylene adipate) retained 60%, and poly(hexamethylene adipate) retained 70% of its original strength. The conclusion is that urethanes based on polyesters made from long hydrocarbon diols (e.g., poly(hexamethylene adipate)) have better hydrolysis resistance than the polyester urethanes based on short chain diols (e.g., poly(ethylene adipate)). In the same study, the authors measured the effect of the acid number of the polyester polyol on the hydrolysis of the resulting urethane. These data are shown in Table 7. Higher levels of acid are clearly detrimental to the tensile properties of the polyester urethane. A polyurethane based on poly(tetramethylene adipate) with an acid number of 3.66 retained only 7% of its original strength after 3 weeks of water immersion at 70°C. At the other extreme, the same polyester urethane with an acid number of 0.1 retained 90% of its original strength under the same conditions. Free acid clearly catalyzes hydrolysis of the polyester urethanes and might be considered counterproductive to a highly durable urethane adhesive. On the other hand, if the urethane is to function as a temporary bond, with the intent of biodegradation, the acid-catalyzed hydrolysis could be a useful reaction.

Schollenberger added 2% of a polycarbodiimide additive to the same poly(tetramethylene adipate) urethane with the high level of acid (AN = 3.66). After 9 weeks of 70°C water immersion, the urethane was reported to retain 84% of its original strength. Carbodiimides react quickly with residual acid to form an acyl urea, removing the acid catalysis contributing to the hydrolysis. New carbodiimides have been developed to prevent hydrolysis of polyester thermoplastics. Carbodiimides are also reported to react with residual water, which may contribute to hydrolysis when the urethane is exposed to high temperatures in an extruder [90].

Hillshafer et al. reported that aromatic polyester urethanes based on orthophthalic anhydride had better hydrolysis resistance than polycaprolactone urethanes, despite high acid numbers [91].

Hydrolysis studies compared a polycarbonate urethane with a poly(tetramethylene adipate) urethane and a polyether urethane based on PTMEG. After 2 weeks in 80°C water, the polycarbonate urethane had the best retention of tensile properties [92]. Polycarbonates can hydrolyze, although the mechanism of hydrolysis is not acid-catalyzed, as in the case of the polyesters. Polycarbonate polyurethanes have better hydrolysis resistance than do standard adipate polyurethanes, by virtue of the highest retention of tensile properties. It is interesting to note in the study that the PTMEG-based urethanes, renowned for excellent hydrolysis resistance, had lower retention of physical properties than did the polycarbonate urethanes.

It is speculated that the water does not diffuse as easily into the polycarbonate as into the PTMEG urethane, making the polycarbonate more resistant to plasticization by water and subsequent hydrolysis. The tensile properties of the PTMEG polyurethane eventually returned to nearly the original tensile properties, if the material was allowed to dry at room temperature for 2 weeks. This observation lends credence to the idea that the PTMEG urethane was plasticized by water.

9. Special adhesion problems for polyurethane adhesives

Thus far, the discussion has dealt with the versatility of urethane adhesives, the wide variety of substrates urethanes can bond, and the infinite variations of one-component and two-component urethanes. Some substrates have posed particular challenges for urethanes. Many adhesion problems have been discussed, but not all can be covered in this brief synopsis. However, two of the more common problems, with possible solutions, will be mentioned.

9.1. Urethane adhesives and metal bonding

Urethanes can bond very well to metal. To improve bond durability, abrading off the metal oxides from the surface of the metal is highly recommended. These metal oxides can be a weak boundary layer, which can interfere with the ultimate strength and durability of the bond. If the adhesive bond line is exposed routinely to moisture, the metal surface may start to oxidize, forming metal oxides within the interphase region, thus undercutting the adhesive and shortening the service life [93]. As mentioned previously, the correct choice of raw materials can slow this advance to acceptable levels, in many cases. Sometimes, additional help is needed. Various primers which prevent the ingress of water into the interphase region of the bond line are commercially available.

The other problem that can occur with metals is the presence of various machine oils on the surface, such as might be used in the automotive area. Oil serves as a low surface energy barrier to adhesion, in most instances. Abrading and solvent wipe are recommended or else degreasing. Removing the surface oil is

recommended. If surface preparation is not a possibility, some types of adhesives, such as epoxies and acrylics or even a urethane IPN (Interpenetrating Polymeric Network), may still accomplish the bonding.

9.2. Urethane adhesives and low surface energy plastics

Thermoplastic polyolefins, polyethylenes, polypropylenes, and other low surface energy substrates have caused particular problems over the years. Substrate preparation is always recommended, but particularly for the low energy plastics. Many low surface energy substrates have a low molecular weight weak boundary layer that should be removed by abrading the surface of the plastic [94]. The second problem is the inability of the urethane adhesive to wet the substrate in order to form a bond. Recommended surface treatments are corona, plasma, or flame treatment, or, in some cases, acid oxidation. Oxidizing the surface of a polyolefin accomplishes two tasks: it raises the surface energy of the polyolefin to facilitate wetting of the substrate by the polyurethane adhesive, and it provides polar groups on the surface to which the adhesive can chemically bond.

If corona, plasma, or flame treatment is chosen as the surface treatment, it is important to bond quickly after the treatment. Waiting several hours will reduce the effectiveness of the treatment. In some cases, attempts to bond 24 h after the treatment can give the same poor bonding results as if the plastic had never been surface treated. If surface oxidation is not possible, priming the surface with a chlorinated polyethylene primer is a second choice [95].

References

1. Uhlig, K., *Discovering Polyurethanes*. Hanser, 1999.
2. Axelrood, S., Hamilton, C. and Frisch, K., *Ind. Eng. Chem.*, **53**, 889 (1961).
3. Pannone, M. and Macosko, C., *J. Appl. Polym. Sci.*, **34**, 2409 (1987).
4. Casey, J., Milligan, B. and Fasolka, M., *Proc. SPI 28th Annu. Technical/Marketing Conf., San Antonio*, p. 220 (1984).
5. Wicks, D. and Yeske, P., *Proc. 19th Annu. Waterborne, Higher Solids and Powder Coating Symp.*, p. 182 (1993).
6. Saunders, J. and Frisch, K., *Polyurethanes — Chemistry and Technology*. Wiley, New York, NY, 1962.
7. Gilbert, D., *Proc. Polyurethane World Congr. 1987, Aachen*, p. 167 (1987).
8. Kogon, I.C., *J. Org. Chem.*, **24**, 83 (1959).
9. Kogon, I.C., *J. Org. Chem.*, **24**, 83 (1958).
10. Kogon, I.C., *J. Org. Chem.*, **26**, 3004 (1961).
11. Nicholas, L. and Gmitter, G., *J. Cell. Plast.*, **1**, 85 (1965).
12. Reegen, S. and Frisch, K., In: Frisch, K. and Reegen, S. (Eds.), *Advances in Urethane Science and Technology*. Vol. 1. Technomic Publishing Co., Las Vegas, NV, 1971, p. 208.
13. Koch, H., Mennicken, G., Mueller, F., Toepsch, H. and Traubel, H., In: Oertel, G. (Ed.),

- Polyurethane Handbook*. Hanser, 1985, p. 523.
14. Nachtkamp, K. et al., U.S. Patent 4,373,081 (1983) assignee: Bayer A.G.
 15. Vasta, J., U.S. Patent 4,727,100 (1988) assignee: DuPont de Nemours.
 16. Potter, T. et al., In: Nelson, G. et al. (Eds.), *Proceedings of 13th Annual Waterborne and Higher-Solids Coating Symposium*. Hattisburg, MS, 1986, p. 162.
 17. Chandalia, K. et al., In: Storey, R. and Thames, S. (Eds.), *Proceedings of 28th International Waterborne, High-Solids and Powder Coating Symposium*. New Orleans, LA, 2001, p. 77.
 18. Woods, G., *The ICI Polyurethanes Book*. Wiley, New York, NY, 1987.
 19. Bailey, R., Gilbert, S. and Kitahara, H., *Polyurethane World Congress 1991, Nice*. Technomic Publishing Co., Las Vegas, NV, 1991, p. 17.
 20. *Bulletin 107*. 2nd edn., revised, 1981, The Upjohn Company.
 21. Evans, R., In: Frisch, K., Jr. (Ed.), *Recent Advances in Polyurethanes and Interpenetrating Polymeric Networks*. Technomic Publishing Co., Las Vegas, NV, 1988, p. 104.
 22. Evans, R., *Polyurethane Sealants*. Technomic Publishing Co., Las Vegas, NV, 1993, p. 31.
 23. Seneker, S.D., Barksby, N. and Lawrey, B.D., *Proceedings of the SPI Polyurethanes Expo 96*. Technomic Publishing Co., Las Vegas, NV, 1996, p. 305.
 24. Schumacher, G., U.S. Patent 4,511,626 (1985) assignee: Minnesota Mining and Manufacturing.
 25. Ulrich, H., Bonk, H. and Colovos, G., In: Szycher, M. and Robinson, W. (Eds.), *Synthetic Biomedical Polymers*. Technomic Publishing Co., Las Vegas, NV, 1980, p. 29.
 26. Billmeyer, F., Jr., *Textbook of Polymer Science*, 2nd edn. Wiley, New York, NY, 1971, p. 224.
 27. Trappe, G., In: Buist, J. (Ed.), *Advances in Polyurethane Technology*. Imperial Chemical Co., Maclaren, 1968, p. 79.
 28. Frisch, K. et al., *Proceedings of UTECH 96*, paper 46. Crain Communications, 1996.
 29. Wong, S. and Wang, S., In: Frisch, K. and Klemptner, D. (Eds.), *Advances in Urethane Science and Technology*, Vol. 13. Technomic Publishing Co., Las Vegas, NV, 1996, p. 74.
 30. Frisch Jr., K., *J. Elastomers Plast.*, **19**(3), 170–187 (1987).
 31. Arenivar, J., *Proc. SPI 32nd Annu. Technical/Marketing Conf.*, p. 623 (1989).
 32. Frisch, K., Jr., *Proc. 60 Years of Polyurethanes Symp., Detroit, MI*, pp. 287–303 (1998).
 33. Pocius, A., *Adhesion and Adhesive Technology — An Introduction*. Hanser, 1997, pp. 202–209.
 34. Frisch, K., Jr. and Hartshorn, S., *Proc. 25th Anniversary Symp. Polymer Institute, Detroit, MI*, p. 276 (1994).
 35. West, J. and Cooper, S., *J. Polym. Sci., Polym. Symp.*, **60**, 127 (1977).
 36. Blackwell, J. and Lee, C., *J. Polym. Sci. Polym. Phys. Ed.*, **21**, 2169 (1983).
 37. Gall, H. and Wolf, K., In: Oertel, G. (Ed.), *Polyurethane Handbook*. Hanser, 1985, p. 579.
 38. Amato, T., Pannone, M. and Bityk, D., In: *Proceedings of the SPI — 32nd Annual Technical/Marketing Conference*. Technomic Publishing Co., San Francisco, CA, 1989, pp. 269–279.
 39. Frisch, K., Jr., *Adhesion Principles and Practice for Coatings and Polymer Scientists*, short course. Kent State University, Kent, OH, May, 2000.
 40. Stamper, D., In: Wake, W. (Ed.), *Synthetic Adhesives and Sealants*. Wiley, Chichester, 1986, Chapter 3.
 41. *Technical Data Sheet — Polyester Diol S-105*. Ruco Polymer Corporation, Oct. 1995.
 42. Trappe, G., In: Buist, J. and Gudgeon, H. (Eds.), *Advances in Polyurethane Technology*. Maclaren, 1968, p. 80.
 43. Penning, A., In: McIntyre, D. (Ed.), *Characterization of Macromolecular Structure*. National Academy of Sciences, Publ. No. 1573, Washington, D.C., 1968, pp. 2144–244.

44. Schollenberger, C., In: Skeist, I. (Ed.), *Handbook of Adhesives*, 2nd edn. Van Nostrand Reinhold, 1977, pp. 450–452.
45. Wright, P. and Cummings, A., *Solid Polyurethane Elastomers*. Gordon and Breach, 1969.
46. Buist, J.M. and Gudgeon, H., *Advances in Polyurethane Technology*. Elsevier, Amsterdam, 1968, p. 72.
47. Flory, P., *Principles of Polymer Chemistry*. Cornell University Press, 1953, p. 353.
48. Schumacher, G., U.S. Patent 4,511,626, assignee: 3M.
49. Stobbie, C., Kangas, L. and Tangen, J., U.S. Patent 5,436,302, assignee: 3M.
50. Huber, H. and Muller, H., *Adhes. Age*, **30**, 32–34 (1987).
51. Merz, P.W. and Zabel, L.D., S. African Patent # 8798302 (1988) assignee: Sika.
52. Stanley, H., Davis, I. and Chiao, W.B., U.S. Patent 5,021,507, assignee: National Starch.
53. Hung, J.M. and Graham, M., U.S. Patent # 5,550,191, assignee: National Starch.
54. Penczek, P. and Kujawa-Penczek, B., In: Frisch, K. and Klemptner, D. (Eds.), *Advances in Urethane Science and Technology*, Vol. 11. Technomic Publishing Co., Las Vegas, NV, 1992, pp. 192–216.
55. Dolhausen, M., In: Oertel, G. (Ed.), *Polyurethane Handbook*. Hanser, 1985, p. 555.
56. Rosthauser, W. and Nachtkamp, K., In: Frisch, K. and Klemptner, D. (Eds.), *Advances in Urethane Science and Technology*, Vol. 10. Technomic Publishing Co., Las Vegas, NV, 1987, pp. 121–162.
57. Dieterich, D. and Reiff, H., In: Frisch, K. and Reegen, S. (Eds.), *Advances in Urethane Science and Technology*, Vol. 4. Technomic Publishing Co., Las Vegas, NV, 1976, p. 112.
58. Dieterich, D., *Prog. Org. Coat.*, **9**, 281–340 (1981).
59. Lucas, H., Festel, G., Ramthun, I., Witowski, R. and Dormish, J., *Journal Adhesion and Sealants Council, 1996 International Conference*. Adhesive and Sealants Council, Inc., San Francisco, CA, 1996, pp. 237–257.
60. Dormish, J. and Witowski, R., *Proceedings of the Adhesive and Sealant Council — Fall Meeting, Oct. 2000*. Adhesive and Sealants Council, Inc., Minneapolis, MN, 2000.
61. Wicks Jr., Z., *Prog. Org. Coat.*, **3**, 73 (1975).
62. Kock, H. et al., In: Oertel, G. (Ed.), *Polyurethane Handbook*. Hanser, 1985, p. 523.
63. Barrons, L., U.S. Patent 4,507,443 (1985) assignee: B.F. Goodrich.
64. Saunders, J. and Pigott, K., U.S. Patent 3,214,411 (1965) assignee: Mobay.
65. Frye, B., Pigott, K. and Saunders, J., U.S. Patent 3,233,025, assignee: Mobay.
66. Atwater, A. et al., In: Oertel, G. (Ed.), *Polyurethane Handbook*. Hanser, 1985, p. 408.
67. Reid, T. and Wright, C., Eur. Patent Appl. EP 91-302701 (1991) assignee: 3M.
68. Engen, P., World Patent Appl. WO 96/20967 (1996) assignee: 3M.
69. Frisch, Jr., K., *Sealants and Caulks II — Short Course, 'Urethane Sealants'*. Adhesives and Sealants Council, Inc., 1994.
70. Coogan, R.G., *Proc. 22nd Int. Conf. Organic Coatings, Athens*, pp. 81–100 (1996).
71. Frisch, K. and Kordomenos, P., In: Tess, R. and Poehlein, G. (Eds.), *Applied Polymer Science*, 2nd edn. American Chemical Society, 1985, p. 1010.
72. Schleier, G. and Gerold, F., *Polyurethane World Congress*. Technomic Publishing Co., Aachen, 1987, pp. 323–327.
73. Aoki, M. et al., *Polyurethane World Congress*. Technomic Publishing Co., Vancouver, B.C., 1993, p. 341.
74. Bock, M. and Halpaap, R., *J. Coat. Technol.*, **59(755)**, 131 (1987).
75. Bock, M. and Halpaap, R., *Polym. Mater. Sci. Eng.*, **55**, 448 (1986).
76. Griffin, G. and Willwerth, L., *IEC Product Res. Dev.*, **1**, 265 (1962).
77. Kelly, P. et al., *Proceedings of the API Polyurethanes Conference 2000*. Technomic Publishing Co., 2000, p. 535.

78. Coury, A., In: Frisch, K. and Eldred, E. (Eds.), *Proceedings from the 25th Anniversary Symposium of the Polymer Institute*. Technomics Publishing Co., Univ. of Detroit Mercy, Detroit, MI, 1994, pp. 206–256.
79. Tilley, P., Nadeau, H., Reymore, H., Waszwciak, P. and Sayigh, A., *J. Cell. Plast.*, **4**, 56 (1968).
80. Tilley, P., Nadeau, H., Reymore, H., Waszwciak, P. and Sayigh, A., *J. Cell. Plast.*, **4**(1), 22 (1968).
81. Fabris, H., In: Frisch, K. and Reegen, S. (Eds.), *Advances in Urethane Science and Technology*, Vol. 6. Technomic Publishing Co., 1978, p. 173.
82. Griffith, R., *Eur. Polym. J.*, **29**, 437 (1993).
83. Singh, A., Weissbein, L. and Mollica, J., *Rubber Age*, **98**(12), 77 (1966).
84. Tarakanov, O. and Kondrateva, L., *Polym. Sci. USSR* **A13**, 642 (1971).
85. Schollenberger, C. and Dinsbergs, K., *SPE Trans.*, **1**(1), 31 (1961).
86. C. Capocci, *Plastics Comp.*, **5–6**, 13 (1987).
87. Scott, G., *J. Appl. Polym. Sci.*, **33**, 131 (1979).
88. Abramoff, C., *Modern Plastics Encyclopedia*. McGraw-Hill, New York, NY, 1978, Vol. 54, 10A, p. 144.
89. Schollenberger, C. and Stewart, F., In: Frisch, K. and Reegen, S. (Eds.), *Advances in Urethane Science and Technology*, Vol. 1. Technomic Publishing Co., 1972, p. 73.
90. McAfee, E., *Proceedings of the SPI 34th Annual Technical/Marketing Conference*. Technomic Publishing Co., New Orleans, LA, 1992, pp. 122–127.
91. Hillshafer, D., O'Brien, M. and Knudsen, K., *SPI Polyurethanes Expo '96*. Technomic Publishing Co., 1996, pp. 530–538.
92. Atwater, A., In: Oertel, G. (Ed.), *Polyurethane Handbook*, 2nd edn. Hanser, 1993, p. 401.
93. Wegman, R., *Surface Preparation Techniques for Adhesives*. Noyes Publishing Co., 1989.
94. Lees, W., *Polym. Paint Colour J.*, **4054**(171), 8 (1981).
95. Schneberger, G., *Adhes. Age*, **28**(6), 9 (1985).

The chemistry of bis-maleimides used in adhesives

MIKIO KAJIYAMA *

Institute of Agriculture and Forest Engineering, University of Tsukuba, 1-1 Tennodaiitcho, Tsukuba-si, Ibaraki 305-8572, Japan

1. General introduction to bis-maleimides

In the narrow sense, 'bis-maleimide resin' means the thermosetting resin composed of the bis-maleimide of methylene dianiline (BMI, bis(4-maleimidophenyl)-methane) and methylene dianiline (MDA, bis(4-aminophenyl)methane) (Fig. 1). Because of the addition mechanism, the resin is cured without elimination, which is a characteristic of this resin. Bis-maleimide resin is used as a thermally stable matrix up to 204°C (400°F) which typical epoxy resins may not normally be used. However, in spite of having an imide structure, bis-maleimides are classified as being 'moderately' thermally stable resins. The aliphatic structure of the resin is not stable for long periods above 232°C (450°F.) If a 'highly' aromatic thermally stable thermosetting resin is necessary, acetylene end-capped aromatic imide-based oligomers should be used.

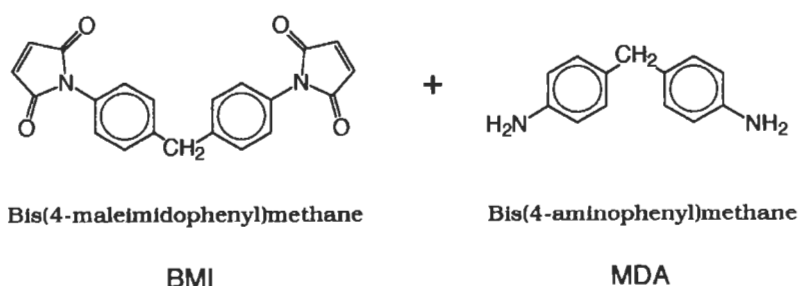


Fig. 1. The chemical structure of BMI and MDA.

* E-mail: mkd@sakura.cc.tsukuba.ac.jp

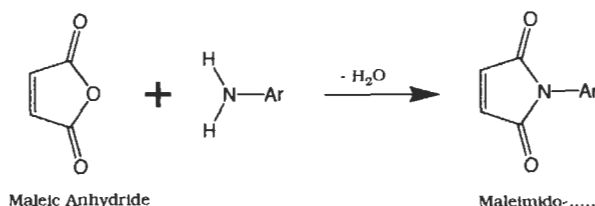


Fig. 2. Formation of a maleimide.

The original compound, maleimide (2,5-dioxo- Δ^3 -pyrroline), is synthesized by the cyclo-condensation of ammonia and maleic acid. Similarly, primary amine is added to maleic anhydride, followed by cyclocondensation, to form N-substituted maleimide (Fig. 2). This reaction is applied to the preparation of bis-maleimides (BMI) [1]. At first, BMI was used as a crosslinking agent for natural rubber (NR). An *o*-dichlorobenzene solution of NR was crosslinked by BMI at 108–150°C in the presence of peroxides. The radicals generated from peroxides react with the double bonds of both BMI and NR [1].

BMI was also used as a crosslinking agent for poly(iminoethylene). The Michael addition takes place with the nucleophilic nitrogen of the imino group and the double bonds of the electrophilic BMI. The Michael addition of BMI is now adopted as a crosslinking reaction for polymers with amino end groups [2].

Bis-maleimide resins composed of BMI and diamines have been reported in the early 1960s in the patent literature. Since that time, a number of patents have appeared describing improvements in their properties and uses [3]. Although many bis-maleimide resins are commercially developed, relatively few reports of their use as adhesives are to be found in scientific journals [4–10]. Improvements of maleimide resins are mirrored in the improvements of thermosetting polyimides. For example, the method of in situ polymerization of monomer reactants (PMR method) was developed [6].

2. Chemistry of monomeric bis-maleimides

Maleimides have three principal reaction pathways. These are: radical addition to vinyl compounds; the Michael addition with compounds having active hydrogens; and the Diels–Alder reaction with dienes (Fig. 3). Any of the three can be tools for forming thermosetting adhesives.

A typical maleimide resin is synthesized by the Michael addition of MDA and BMI (Fig. 4). If the stoichiometrically equal amounts of MDA and BMI are added into the reaction solvent under controlled temperature, linear, high molecular weight polyaminoimide (PAI) results. To obtain crosslinkable oligomer (pre-polymer) with maleimide end groups, a calculated 1.1–1.8 times an excess

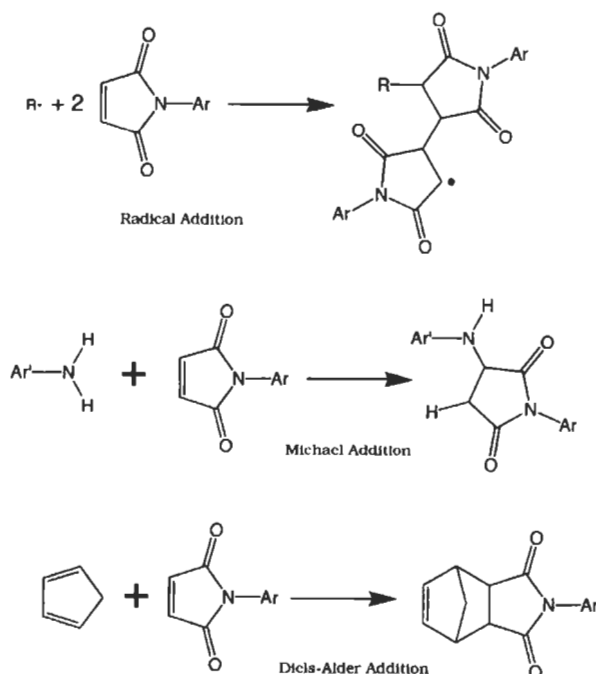


Fig. 3. Reactions of maleimides.

amount of BMI should be used. These maleimide end groups can radically react with each other and at the same time further react with the secondary amino groups in the maleimide resins at elevated temperatures.

Instead of preparing a pre-polymer, BMI can itself be mixed with MDA and cured in an in situ reaction. BMI and MDA were mixed and processed from the melt. About 1 MPa pressure and 170–200°C of temperature were applied to cast the parts [10]. More conveniently, maleic anhydride and MDA could be ground with a mortar and pestle and heated to 140°C for 1 h to prepare adhesive films. The resultant resins are highly crosslinked by simultaneous radical and Michael addition reactions (Fig. 5). These products are often brittle. To avoid being too brittle, oligomers having only a few repeating units with maleimide end groups are preferred as the maleimide resin [7–9] or certain additives are used [8,11].

BMI also reacts with dienes to form Diels–Alder adducts [12]. When BMI reacts with a α,ω -biscyclopentadienyl compound or other bis-diene resin, the bis-maleimide chain is extended by the Diels–Alder reaction. Bis-maleimide, chain extended with bis-diene, is not used in adhesives. However, as the Diels–Alder reaction is reversible, there may be a possibility of recyclability of the cured resin by depolymerization of the backbone (Fig. 6).

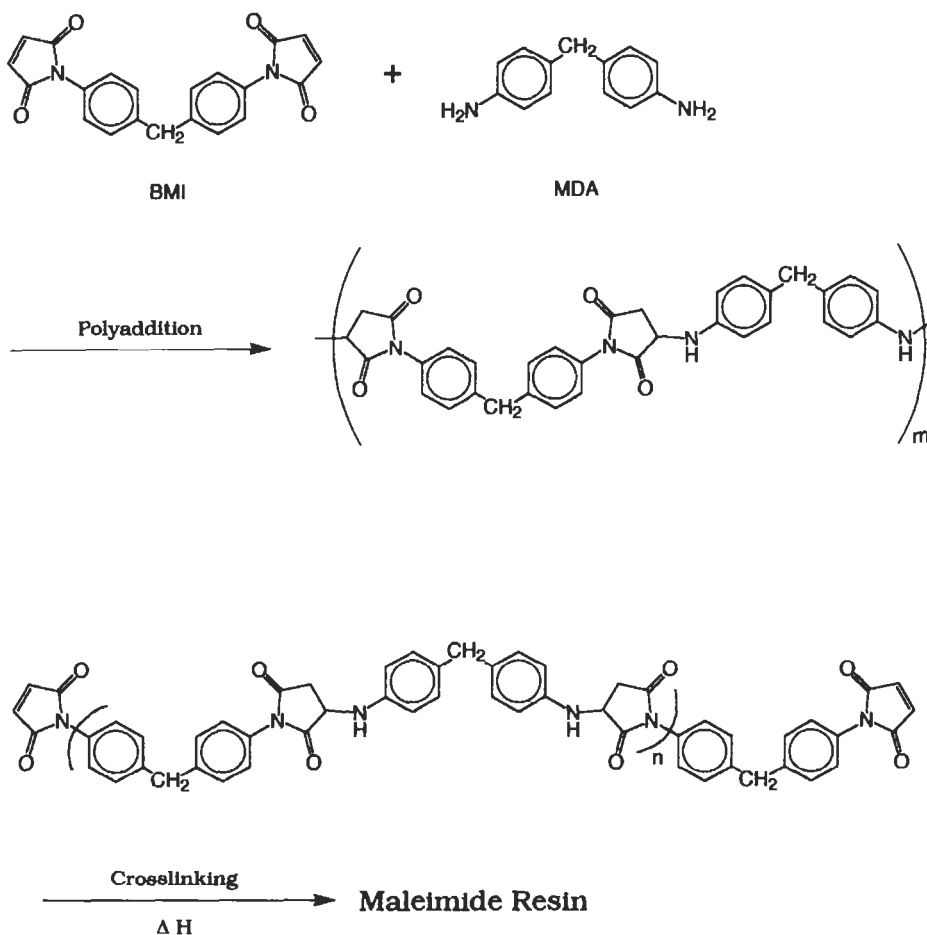


Fig. 4. Preparation of a maleimide resin.

Tan et al. investigated polymers made from bis-benzocyclobutenes [13–15]. As the benzocyclobutane is analogous to the dien, the Diels–Alder addition takes place. This reaction is applied to the preparation of polyimides. The advantage of this system is that the resultant polymer is oxidized to form thermally stable aromatic polyimides (Fig. 7).

One can vary the chemical composition of the bis-maleimide system by replacing the MDA with other diamines. The nature of the resin is not that different from that using MDA because the resins are so highly crosslinked. Based upon availability, ease of use and cost, BMI and MDA are most often used. However, one commercial maleimide resin, Techochemie's Compimide H795™ has an original structure. As shown in Fig. 8, it is composed of BMI and *m*-aminobenzoyl hydrazide [10].

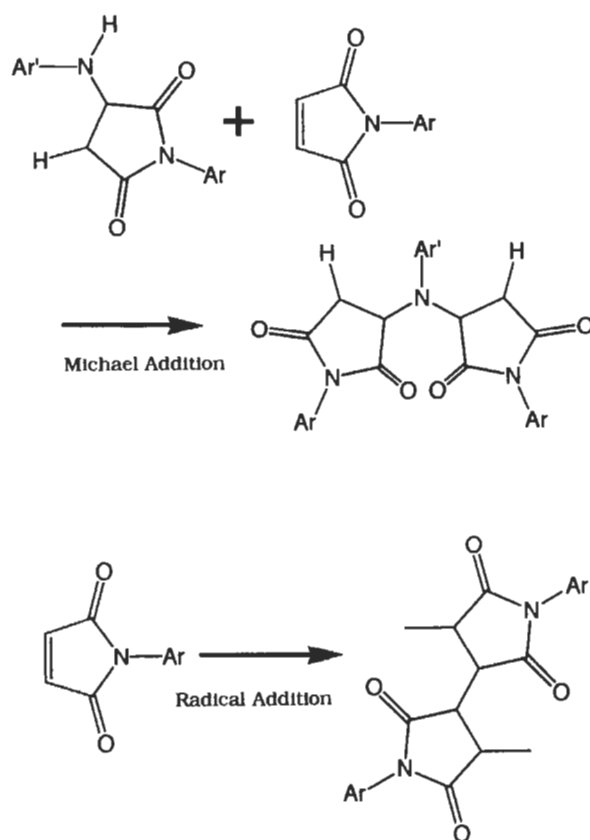


Fig. 5. Curing mechanism of a maleimide resin via Michael addition.

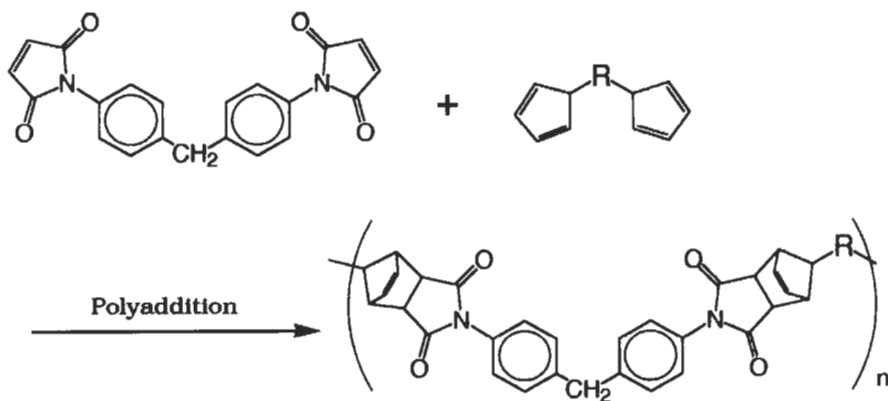


Fig. 6. Curing mechanism of a maleimide resin via Diels-Alder reaction [12].

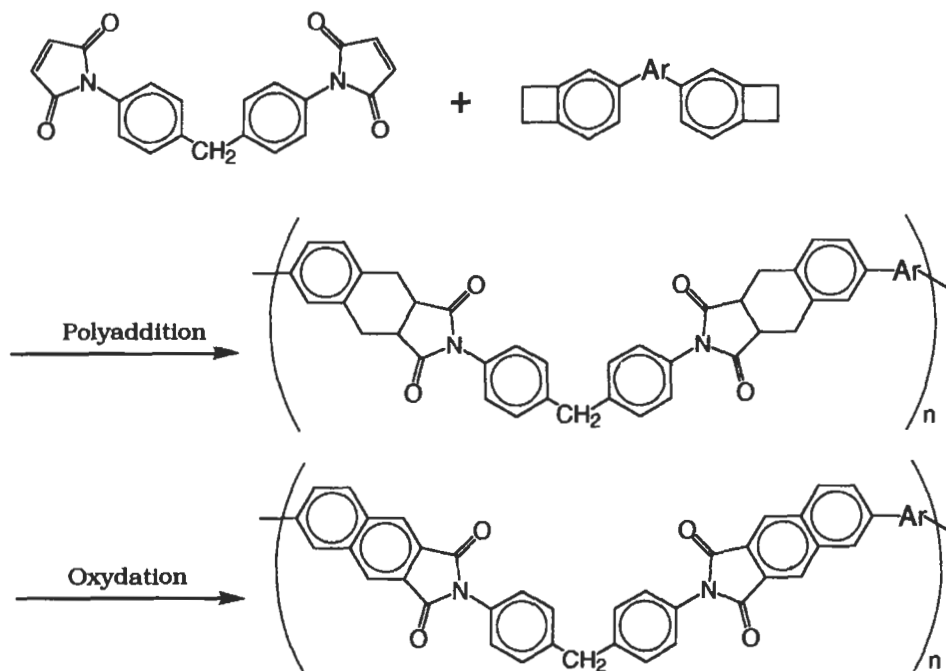


Fig. 7. Polyimide formation by the Diels–Alder reaction [15].

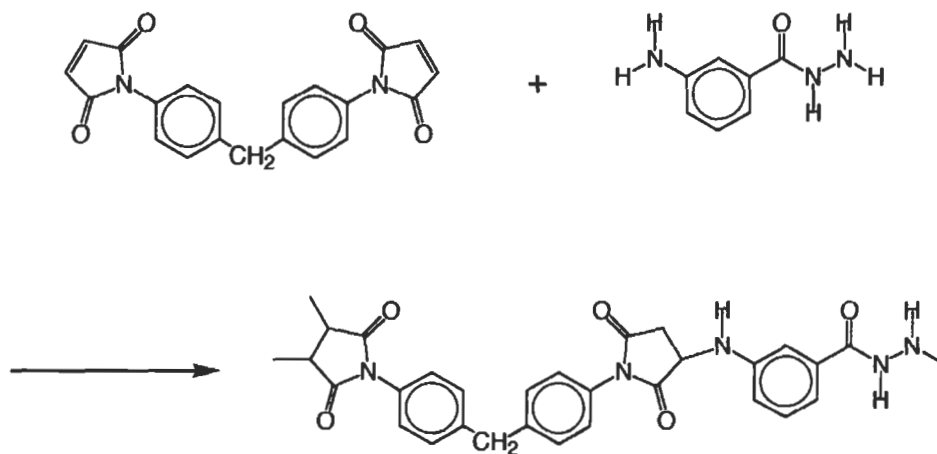


Fig. 8. Preparation of Compimide H795™ [10].

To improve upon their inherent brittleness, bis-maleimide resins are often mixed with other compounds and materials. Glass fabric and carbon fiber fabric are immersed in uncured maleimide resin and plied are layed up, followed by

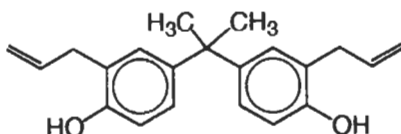


Fig. 9. Chemical structure of DAP (2,2-bis(3-allyl-4-hydroxyphenyl)propane).

curing of the resin. Thus, multilayer circuit boards were obtained, having about 12 MPa of interlaminar shear strength. Vinyl monomers and polymers are also added to the uncured maleimide resin to enhance the flexibility of the cured resin so that interlaminar shear strength of the resultant composite was enhanced by about 5 times over the unmodified resin [10]. Improved maleimide resins are also applied to prepreps and reactive hot melt adhesives.

Another original approach is exemplified by Ciba-Geigy's XU292. BMI is mixed with *o,o'*-diallylbisphenol A (DAP, 2,2-bis(3-allyl-4-hydroxyphenyl)propane; Fig. 9) followed by heating to 110–125°C to obtain a liquid pre-polymer. The pre-polymer could be cured in the same way as common maleimide and epoxy resins are done [16,17].

Although the reaction mechanism with DAP is rather more complicated than that which occurs with diamines [16], DAP was formulated with bis-maleimide prepolymers as one of the additives to improve the properties of bis-maleimide resins [18]. In one Japanese patent [18], the 90° peel strength between copper foil and polyimide circuit board was compared. Lamination of copper onto polyimide with adhesives containing 33 wt% BMI, 33 wt% synthetic rubber, 14 wt% methacryloyl novolac resin and 10 wt% DAP, gave a peel strength of 1.8 kN/m, while without DAP, it only provided a peel strength of 0.2 kN/m. As described above, vinyl monomers and polymers are known to be common additives to toughen bis-maleimide resins. However, the use of vinyl polymers in bis-maleimide compositions may hurt the thermal stability of the cured composition, so aromatic oligomers terminated with maleimide end groups were developed.

3. Maleimide terminated oligomers and other maleimide-like resins

As already mentioned, aromatic polymers are thermally stable but aliphatic portions of them are not as thermally stable. Typical maleimide resins have aliphatic units. This is inevitable because the Michael addition was used to prepare the maleimide-based oligomers. On the other hand, if an adhesive consists of a linear thermoplastic polymer, it is not usable at temperatures above its softening temperature. Introducing chemical crosslinking is one way to prevent thermal weakening of a material.

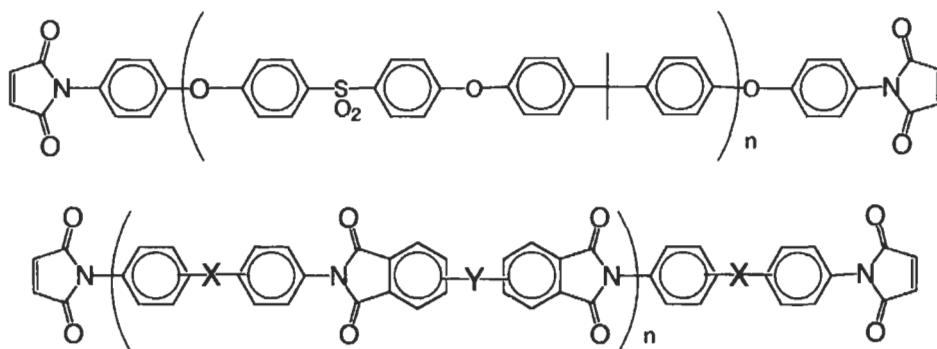
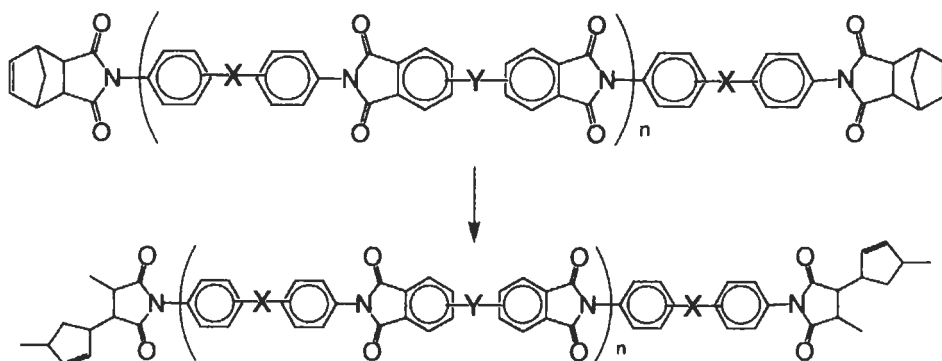
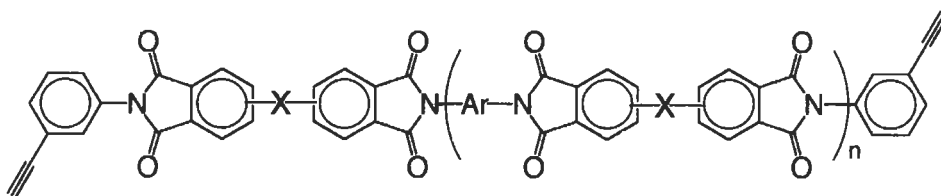


Fig. 10. α,ω -Maleimide terminated polyethersulfone and polyimide.

Aromatic oligomers having maleimide groups in the α and ω positions have been developed [7,8]. A thermoplastic polyimide, for example, is prepared with a diamine and a tetracarboxylic anhydride in a polar, aprotic solvent. Addition of a calculated amount of maleic anhydride into the reaction mixture causes formation of an α,ω -maleimide terminated polyimide polymer. This oligomer acts as a thermoplastic before curing and it should be crosslinked to enhance thermal stability for prepreg-type adhesives. This type of resin still has an aliphatic group, but the aliphatic to aromatic ratio in the resin is relatively lower than in monomeric materials. Additionally, less crosslinked structures usually means that the resulting cured resin is less brittle. It is possible to use these resins without additives such as synthetic rubbers and plastics. For example, it was reported that aluminum single lap joints bonded with an α,ω -maleimide terminated polyethersulfone (degree of polymerization = 2; Fig. 10) had a lap shear strength of 14 MPa [7].

Crosslinkable oligomers are not limited to the maleimide end group. Maleimide reacts with cyclopentadiene to form the nadimide. Like preparation of the α,ω -maleimide terminated oligomers, the α,ω -nadimide terminated oligomers are used as thermosetting resins and adhesives (Fig. 11). The nadimide itself no longer reacts electrophilically, so the pot-life of adhesives is improved. The ring opening reaction, the radical addition and the reverse Diels–Alder will take place only at elevated temperatures.

St. Clair et. al. investigated a series of maleimide and nadimide terminated polyimides and developed LARC-13™ [8,9]. Changing the terminal group from maleimide to nadimide, the value of the lap shear strength of a titanium lap shear joint increased from 7 to 19 MPa [9]. They also added an elastomeric component to the adhesive formulation. The introduction of 15 wt% of a rubbery component, ATBN (amine terminated butadiene nitrile polymer) and ADMS (aniline terminated polydimethyl siloxane) enhanced the adhesive properties as follows: 19 MPa to 25 MPa (ATBN); titanium T-peel strength 0.2 kN/m to 1.4

Fig. 11. α,ω -Nadimide terminated polyimide.Fig. 12. α,ω -Acetylene terminated polyimide.

kN/m (ADMS); fracture toughness (G_{Ic}) 70 N/m to 317 N/m (ADMS) and 370 N/m (ATBN) [9].

Polyimide by the PMR method should also belong to this category, however, before reaching the final stage of curing, elimination of the alcoholic component seems to be causing reduction of performance.

Introduction of acetylene derivatives at the end of the oligomer gives reactive bis-acetylene terminated oligomers (Fig. 12). Three acetylene end groups react together to form an aromatic crosslinking point. The advantage of this system is the aliphatic free curing system. A higher curing temperature is needed for this curing system than the other, and these systems are applied to thermosetting resins and adhesives that are highly thermally stable.

References

1. Kovacic, P. and Hein, R.W., *J. Am. Chem. Soc.*, **81**, 1187 (1959).
2. Kovacic, P. and Hein, R.W., *J. Am. Chem. Soc.*, **81**, 1190 (1959).
3. U.S. Patent 3,380,964 (1964); U.S. Patent 3,127,414 (1964); and British Patent 1,190,718 (1968).
4. Crivello, J.V., *J. Polym. Sci. Polym. Chem. Ed.*, **13**, 1819 (1973).

5. Serafini, T.T., *J. Appl. Polym. Sci.*, **16**, 905 (1972).
6. Serafini, T.T. and Delvigs, P., *J. Appl. Polym. Sci. Appl. Polym. Symp.*, **13**, 961 (1973).
7. Kwiatkowski et al., G.T., *J. Polym. Sci. Polym. Chem. Ed.*, **13**, 961 (1973).
8. St. Clair, A.K. and St. Clair, T.L., *Int. J. Adhes. Adhes.*, **1**, 249 (1981).
9. St. Clair, A.K. and St. Clair, T.L., *Polym. Eng. Sci.*, 22(9) (1982).
10. Stenzenberger, H.D., *Br. Polym. J.*, **15**, 2 (1983).
11. Japanese Patent, JP P2000-265149A (2000).
12. Stille, J.K., *Adv. Polym. Sci.*, **3**, 48 (1961).
13. Tan, L.S. and Arnold, F.E., *J. Polym. Sci. A Polym. Chem.*, **25**, 3159 (1987).
14. Tan, L.S. and Arnold, F.E., *J. Polym. Sci. A Polym. Chem.*, **26**, 1819 (1988).
15. Tan, L.S., Arnold, F.E. and Soloski, E.J., *J. Polym. Sci. A Polym. Chem.*, **26**, 3103 (1988).
16. King et al., J.J., *Natl. SAMPE Symp. Exhib.*, **29**, 392 (1984).
17. Chaudhari et al., M., *Natl. SAMPE Symp. Exhib.*, **30**, 735 (1985).
18. Japanese Patent, JP P2000-273425A (2000).

Structural acrylics

ROBIN F. RIGHETTINI*

Omnova Solutions Inc., 1476 J.A. Cochran Bypass, Chester, SC 29706, USA

1. Introduction

Acrylic and anaerobic adhesives cure by the free radical polymerization of unsaturated compounds, most often methacrylate esters. Acrylic adhesives are two-part structural adhesives. Anaerobic adhesives are one-part products commonly used for thread-locking and other applications where tight tolerances are possible. These adhesives have a unique set of properties due to their cure chemistry. Advantages of these products include room temperature cure, fast strength build, good adhesion to a wide range of substrates including some oily metal, easy application, and tolerance to variation in mix ratios. Acrylics can give good adhesion to plastics (in some cases even unprepared polyolefin), metals, ceramics, and many thermoset polymers including unsaturated polyester. These products also have their own set of disadvantages, which explains their limited penetration into the adhesive market. Early acrylic adhesives were notable for their flammability and pungent odor. Some products have mix ratios well away from 1 : 1, which complicates application. Others show an air inhibition that manifests itself as poor surface cure. Although cure inside the bond line is complete, fluid or tacky uncured material at the surface can give the appearance of lack of cure. Finally, in part due to the low volume of these products, they tend to be fairly expensive. As will be discussed below, this is not inherent to the technology.

A recent reference [1] lists twenty suppliers of structural acrylic adhesives. Many other companies have been involved in this area, and it is often felt that acrylic adhesives have unrealized technical potential [2]. Acrylic adhesives are not commonly found in the consumer market, but fill an important niche there in the bonding of rear view mirrors to windshields in automobiles.

* E-mail: robin.righettini@omnova.com

Table 1
Acrylic adhesive formulation

Side A	Side B
80 parts methyl methacrylate	80 parts methyl methacrylate
15 parts Neoprene [®] (solution grade)	15 parts Neoprene [®]
5 parts <i>N,N</i> -dimethylaniline	5 parts benzoyl peroxide

In the laboratory, acrylic adhesives are easy to prepare and fun to work with. Small batches can easily be prepared by hand. The low viscosity of many of the components often makes it possible to manipulate many of their mixtures as master batches, minimizing the number of weighing operations. The only time-consuming step is the preparation of solutions of solid rubbers. This can conveniently be done by rolling mixtures of solid rubber and methacrylate monomers overnight on a conventional paint roller [3]. The room temperature curing of these products eliminates the need for complicated baking cycles, and allows the preparation and evaluation of a large number of samples in a given study.

The development of acrylic adhesives is well documented, although most of the publications are in the patent literature. Much early work was done by Bäder and coworkers [4–7] at Degussa (Deutsche Gold- und Silber-Scheideanstalt vormals Roessler), and provides a good source for starting formulations.

Acrylic adhesive formulations can be amazingly simple. The formulation given in Table 1 is a simplification of the Bäder work, and provides an excellent starting point for screening studies.

Although the B-side is only stable for about a day, this composition gives surprisingly good performance on a range of substrates, as Table 2 illustrates [8].

These results demonstrate some interesting chemical principles of the use of acrylic adhesives. They stick to a broad range of substrates, with some notable exceptions. One of these is galvanized steel, a chemically active substrate which can interact with the adhesive and inhibit cure. Another is Noryl[®], a blend of polystyrene and polyphenylene oxide. It contains phenol groups that are known polymerization inhibitors. Highly non-polar substrates such as polyolefins and silicones are difficult to bond with any technology, but as we shall see, the initiator can play a big role in acrylic adhesion to polyolefins.

Acrylic polymers are also important in the preparation of other classes of adhesives, especially pressure sensitive adhesives. This discussion will be limited to adhesives that cure by the reaction of unsaturated acrylic functional groups. These adhesives are also sometimes termed 'Methacrylic', 'Methacrylic' or 'Structural Acrylic' adhesives. This is consistent with the long-standing habit of organic chemists to assign multiple names to the same substance.

Table 2

Performance of formulation in Table 1 on a range of substrates

Substrate	Lap shear strength		Failure mode
	psi	MPa	
Steel	1037	7.15	Adhesive
Oily metal	1230	8.48	Adhesive
Aluminum	701	4.83	Adhesive
Galvanized steel	54	0.37	Thin cohesive
Glass	16	0.11	Stock break
Sheet molding compound-1	567	3.91	Mixed
Sheet molding compound-2	960	6.62	Stock break
Plexiglas [®] (PMMA)	577	3.98	Stock break
Lexan [®] (polycarbonate)	1032	7.12	Stock break
Cyclac [®] T (ABS)	691	4.77	Stock break
Noryl [®] 751 (PPO-polystyrene)	42	0.29	Thin cohesive
Ortho-phthalate fiberglass	1049	7.24	Stock break
Vinyl ester fiberglass	1319	9.09	Thin cohesive
Silicone rubber	6	0.04	Adhesive
EPDM rubber	21	0.15	Adhesive
Polypropylene	75	0.51	Adhesive

2. Chemistry of cure

Acrylic adhesives cure by a free radical chain growth mechanism. In contrast, epoxy and urethane adhesives cure by a step growth mechanism. This has a major impact on the cure kinetics, as well as the composition of the adhesive during cure ([9], pp. 6–9). Cyanoacrylate adhesives (such as Super Glue[®]) also cure by chain growth, but the mechanism is ionic with initiation by surface moisture.

Free radical chain growth polymerization takes place through three distinct chemical steps. These are shown in Fig. 1.

The first is the generation of a free radical, which is a chemical species bearing an unpaired electron. This initiator fragment adds to a molecule of monomer to form a growing polymer chain. These two steps are termed initiation. Many free radicals are highly reactive species capable of adding to a molecule containing a double bond to yield a growing polymer chain. The reaction product between a free radical and an organic molecule containing an even number of electrons is by necessity another free radical. This addition reaction can occur again and again, and the process is termed propagation. As long as the free radical adds species containing an even number of electrons, another larger reactive species is formed, and propagation continues. Although the interaction of two growing chains is of low probability (due to their dilute nature), eventually they do interact to end the polymerization, a process termed termination. At any time during the

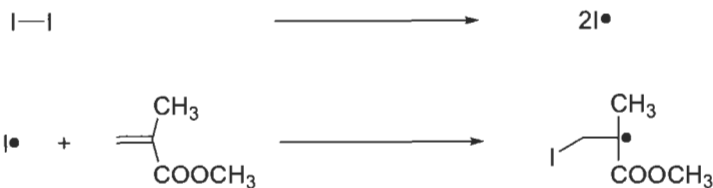
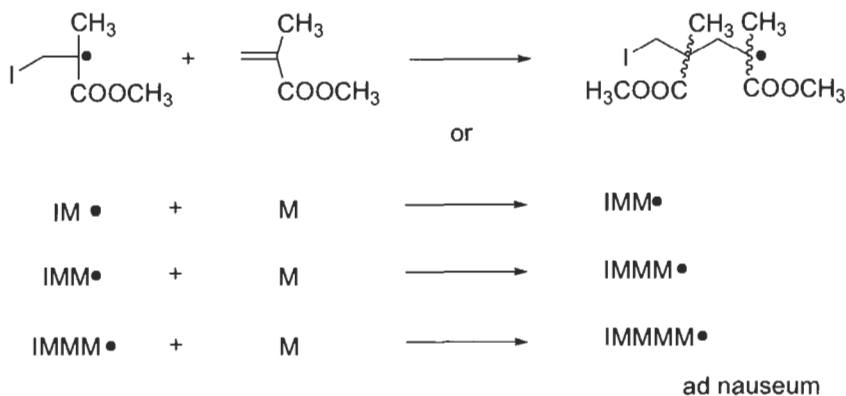
Initiation:Propagation:Termination:

Fig. 1. Mechanism for free radical chain growth polymerization.

polymerization, the reacting mixture contains monomer, terminated high polymer and a small number of growing chains. In contrast, epoxy and urethane adhesives cure by a step growth mechanism. Monomeric species react to form dimers, trimers, and higher oligomers. High polymer only appears at the very end of the reaction.

2.1. Redox initiation

Free radicals are generated through a process known as redox (reduction–oxidation) initiation; general reviews on redox chemistry include Refs. [10–

13]. Generally the oxidant is compounded in one part of the adhesive, and the reductant in the other. Redox initiation and cure occur when the two sides of the adhesive are mixed. There also exist the one-part aerobic adhesives, which use atmospheric oxygen as the oxidant. The chemistry of the specific redox systems commonly used in adhesives will be discussed later. The rates of initiation and propagation are given by the following equations ([9] p. 221).

$$R_i = k_d[\text{reductant}][\text{oxidant}] \quad (1)$$

$$R_i = k_p[M]\sqrt{\frac{k_d[\text{reductant}][\text{oxidant}]}{2k_t}} \quad (2)$$

where k_d , k_p and k_t are rate constants for initiator disassociation, monomer propagation and termination respectively, and $[M]$ is monomer concentration.

A practical insight to be obtained from this equation is that the rate of cure is proportional to the square root of initiator concentration. This is partly why acrylic adhesives are relatively insensitive to variations in mix ratio. As long as enough initiator is present to complete the reaction, high molecular weight polymer is formed. In step growth polymerizations (such as those encountered in the cure of epoxy or two-part urethane adhesives for example), molecular weight is strongly influenced by the ratio of the monomers.

2.2. Polymerization

The kinetics of reaction of free radical chain reactions are complicated compared to the second-order kinetics of epoxy and urethane adhesives. Many of these complications offer practical advantages to the process of using acrylic adhesives.

In contrast to ionic chain polymerizations, free radical polymerizations offer a facile route to copolymers ([9] p. 459). The ability of monomers to undergo copolymerization is described by the reactivity ratios, which have been tabulated for many monomer systems; for a tabulation of reactivity ratios, see Section II/154 in Brandrup and Immergut [14]. These tabulations must be used with care, however, as reactivity ratios are not always calculated in an optimum manner [15]. Systems in which one reactivity ratio is much greater than one (1) and the other is much less than one indicate poor copolymerization. Such systems form a mixture of homopolymers rather than a copolymer. Uncontrolled phase separation may take place, and mechanical properties can suffer. An important ramification of the ease of forming copolymers will be discussed in Section 3.1.

The generation of free radicals usually does not immediately start polymerization in commercial adhesives. These contain small amounts of inhibitors, which are chemical compounds that prevent free radical polymerization. Inhibitors are purposely added to acrylic adhesives to obtain practical shelf life. Inhibitors stop polymerization by reacting with active free radicals to form a less reactive species

incapable of adding to monomer. The first free radicals generated react with these inhibitors, and no cure of the adhesive takes place. This adds open time or work time to the adhesive by delaying cure until a significant time after mixing. Once all the inhibitors are consumed, cure begins. Since cure is a chain reaction, a small amount of inhibitor can have a large effect on rate of cure. Some common inhibitors are capable of destroying more than one initiating radical [16], thus preventing the reaction of thousands of monomer molecules.

Atmospheric oxygen is a ground state free radical, and hence a powerful inhibitor of free radical polymerization. The inhibitor constant of oxygen in MMA polymerization is over an order of magnitude higher than that of any other known material ([9] p. 263). In a small bead or thin film, the presence of oxygen can increase open time, or the time the adhesive can sit before mating the parts. This is desirable in certain manufacturing processes. The presence of oxygen can also cause poor cure of squeeze-out (the adhesive fillet, or material that is squeezed out of the bonded area when the parts are mated). This may be an advantage or a disadvantage depending on the application. Uncured squeeze-out can give the perception that the adhesive inside the bond line is also uncured, which it is not. Inside the bond line there is no oxygen to inhibit the cure. In the auto industry, however, this lack of cure in the squeeze-out is an advantage. Small amounts of adhesive on cosmetically important substrates can be easily removed long after application. This preserves the appearance of the final product.

Once polymerization begins, it takes place rapidly. Acrylate and methacrylate monomers have relatively high propagation rate constants; for a tabulation of propagation rate constants, see Section II/67.1 in Brandrup and Immergut [14]. As discussed previously, the rate of polymerization is linear with monomer concentration. This is in contrast to step growth polymerization, where the rate decreases as the multiplication product of the concentrations of the reactive species decreases. If the concentrations in a step growth polymerization are nearly equal (as often is the case), rate decreases as the square of concentration. This causes a steeper decrease in rate at high conversion for step growth reactions than for chain reactions.

Another theoretical consideration with real practical impact on ease of application is autoacceleration, also called the Trommsdorff Gel Effect or the Norrish–Smith Effect. Organic reactions commonly decrease in rate as the reactants are consumed. Radical polymerizations done at high concentrations of monomer often undergo an increase in reaction rate at a critical level of conversion ([9] p. 286). As the reaction proceeds, high molecular weight polymer is formed. This polymer increases the viscosity of the reaction medium. A point is reached where the mobility of free radicals at the end of growing chains is restricted, and the probability that they get close enough to each other to react and terminate the polymerization decreases. The decrease in termination results in an increase in the rate of polymerization. As a consequence, polymerization (and hence strength development)

proceeds rapidly once the induction period has ended. This is commonly called 'snap cure' and is especially desirable for rapid line speed assembly processes.

3. Raw materials

In formulating adhesives, it is desirable to use materials with low cost. For specialty adhesives such as the acrylics, it is preferred to use commodity chemicals with a range of other uses. Minor components such as reactive rubbers, functional monomers and some additives are specially synthesized for acrylics, but these are expensive due to low volume.

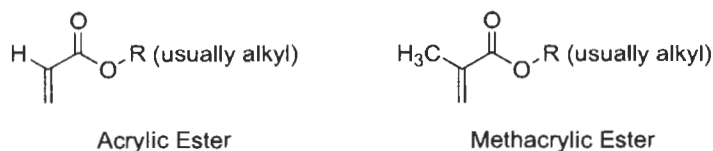
3.1. Monomers

Esters of methacrylic acid (also called methacrylates) are most commonly used for adhesives. This is slightly different from UV curable coatings, where acrylic esters are generally preferred. These differ by a methyl group as in Scheme 1.

Methacrylates in general have modestly slower propagation constants, and higher glass transition temperatures than acrylates.

Methyl methacrylate (MMA) is still commonly used in acrylic adhesives. This monomer is used to prepare poly(methyl methacrylate) (PMMA) which is sold under trade names Plexiglas[®], Perspex[®], and Lucite[®] [17]. MMA has many advantages including low cost, low viscosity and powerful solvating capability. Its polymer is notable for a high glass transition temperature, transparency and good resistance to weathering. On the negative side, MMA has a pungent and characteristic odor, and a low flash point.

Flammability can be reduced by using methacrylates bearing larger alkyl groups. The boiling points of many organic compounds increases by 20–30°C for each added $-\text{CH}_2-$ group [18]. Some common examples include 2-ethylhexyl, cyclohexyl, and tetrahydrofurfuryl methacrylates. Higher molecular weight often, but not always, also correlates with lower odor. Cyclohexyl methacrylate is an exception, and has a notably nasty odor. Methacrylates bearing a phenyl group such as benzyl or 2-phenoxyethyl methacrylate reportedly give transparent adhesives for glass [19]. Dimethacrylates are also used, especially in anaerobic adhesives. An example is diethylene glycol methacrylate. As this is a dimethacrylate, it



Scheme 1. Acrylic and methacrylic esters.

polymerizes to form a highly crosslinked system. Small amounts of difunctional monomers can be used with monofunctional monomers to control crosslinking.

Mixtures of monomers can be used to balance properties. This is possible due to the ease of copolymer formation via free-radical polymerization. The glass transition temperature of acrylic copolymers can be predicted from the weight fraction of the component monomers and the glass transition temperatures of the respective homopolymers [20]. Eq. 3 (commonly known as the Fox equation) is reported:

$$\frac{1}{T_g} = \frac{w_1}{T_g(1)} + \frac{w_2}{T_g(2)} \quad (3)$$

where T_g is the glass transition of the copolymer, $T_g(n)$ is the glass transition temperature of monomer n , and w_n is the weight fraction of monomer n . This relationship only holds for systems without gross phase separation.

Even the earliest reports discuss the use of components such as polymer syrups bearing carboxylic acid functionality as a minor component to improve adhesion [21]. Later, methacrylic acid was specifically added to adhesive compositions to increase the rate of cure [22]. Maleic acid (or dibasic acids capable of cyclic tautomerism) have also been reported to increase both cure rate and bond strength [23]. Maleic acid has also been reported to improve adhesion to polymeric substrates such as Nylon[®] and epoxies [24]. Adducts of 2-hydroxyethyl methacrylate and various anhydrides (such as phthalic) have also been reported as acid-bearing monomers [25]. Organic acids have a specific role in the cure of some blocked organoboranes, as will be discussed later.

Methacrylates possess many advantages, and alternatives to them are rarely seen in the marketplace. An early example using styrene in a structural adhesive has been reported [26]. The combination of styrene with unsaturated polyester is commonly used as a filler and bonding putty.

3.2. Tougheners and other polymers

Pure PMMA and other acrylic polymers are somewhat brittle materials. Also, pure MMA is slow to react completely and undergoes a great deal of shrinkage during cure. All of these issues can be dealt with by adding additional polymer to the system. An excellent example is the composition given in Table 3 [27], which, although lacking in shelf stability, is extremely simple.

The polymer plays several roles in this composition. First, it reduces shrinkage. Second, it increases the viscosity of the adhesive to the point where it can be easily applied. It also speeds the rate of cure. As will be discussed in the section on initiators, the boron compound reacts with atmospheric oxygen to form free radicals.

The use of rubbers (low glass transition polymers) to toughen acrylic adhesives

Table 3

Example of a formulation with an added polymer

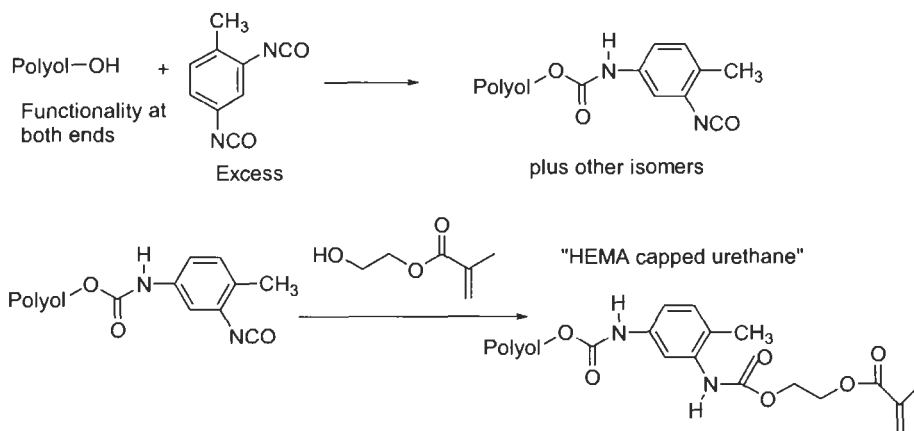
Component	Parts
Methyl methacrylate	10
PMMA	10
Tributylboron	0.2

dates back to some of the earliest reports, where a polychloroprene derivative was used [28]. A graft copolymer was formed by the reaction of polychloroprene with a mixture of MMA and styrene in the presence of a free radical initiator. Such products are called termed prepolymer syrups. The grafted copolymer gives improved compatibility over the pure polychloroprene. This grafting under thermally initiated conditions has recently been investigated [29]. Another early report describes the mixture of an unsaturated polyester (prepared from two moles of maleic acid, one mole of phthalic acid, and 3.1 moles of 1,3-propanediol) and poly(vinyl methyl ether) [30]. Polybutadiene and its copolymers have also been used at levels of up to 30% [31]. Styrene–butadiene–styrene block copolymers have also been used as tougheners at similar levels [32]. Even though the polymer is not chemically bound in these systems, good toughness is obtained. These systems may not be optimal for resistance to aggressive organic solvents however.

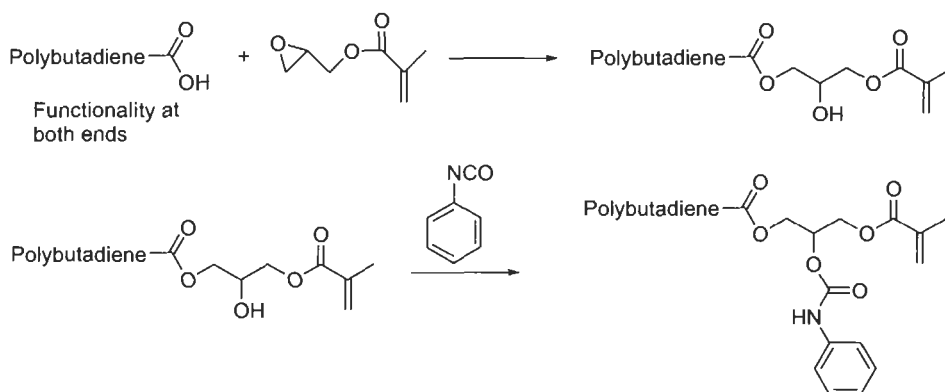
These are all examples of soluble polymers. Combinations of soluble with insoluble polymers have also been reported. Polychloroprene or chlorosulfonated polyethylene was combined with core-shell polymer particles to give an adhesive with improved cold impact resistance [33]. The fascinating chemistry of chlorosulfonated polyethylene in acrylic adhesives will be further discussed in the section on initiators. In many cases chlorosulfonated polyethylene is chemically attached to the acrylic matrix.

Liquid organic rubbers with reactive functionality can be prepared by several methods. End-functional oligomers are preferred. Chains attached to the network at only one end do not contribute as much strength to the network as those attached at both ends [34]. Urethane chemistry is a handy route to such molecules. A hydroxy-terminated oligomer (commonly a polyester or a polyether) can be reacted with excess diisocyanate, and then with a hydroxy methacrylate to form a reactive toughener [35]. The methacrylate ends undergo copolymerization with the rest of the acrylic monomers. The resulting adhesive is especially effective on poly(vinyl chloride) shown in Scheme 2.

An alternative route starts with a carboxy-terminated oligomer [36]. This is reacted with glycidyl methacrylate to provide the methacrylate-terminated polymer. The resulting linkage is susceptible to hydrolysis, so the hydroxy group may be reacted with an isocyanate to improve environmental resistance (Scheme 3).



Scheme 2.

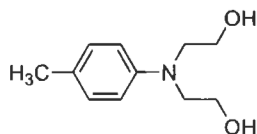


Scheme 3. Synthesis of methacrylated rubber.

A hydroxy-terminated oligomer can be converted into a carboxy-terminated one by reaction with an anhydride [37]. Such an oligomer can also be used to synthesize a methacrylated rubber as above [38].

3.3. Initiators

The cure reaction of structural acrylic adhesives can be started by any of a great number of redox reactions. One commonly used redox couple is the reaction of benzoyl peroxide (BPO) with tertiary aromatic amines. Pure BPO is hazardous when dry [39]. It is susceptible to explosion from shock, friction or heat, and has an autoignition temperature of 79°C. Water is a very effective stabilizer for BPO, and so the initiator is often available as a paste or a moist solid [40]. The

Scheme 4. *N,N*-dihydroxyethyl-*p*-toluidine.

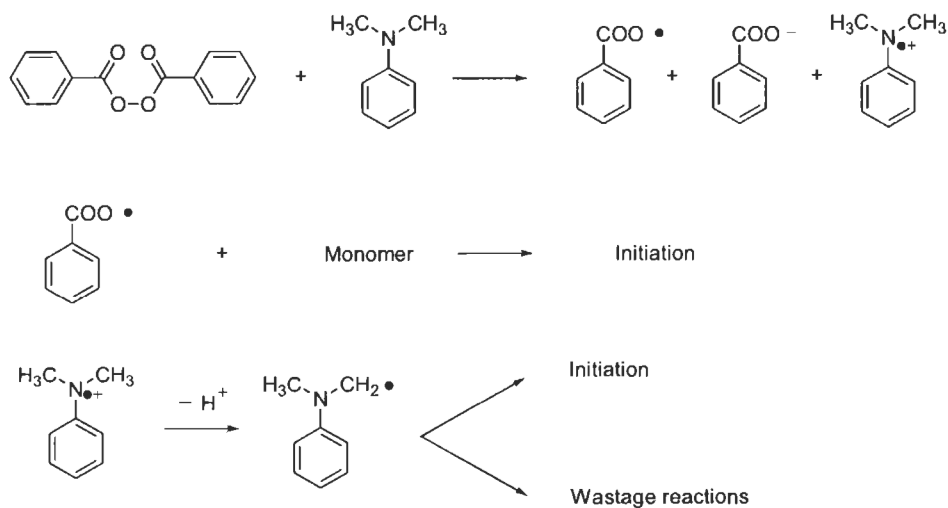
compounding of BPO with acrylate functional ingredients is usually avoided (for shelf stability considerations), but some examples of this combination are reported [41]. Although water is usually the preferred stabilizer for BPO, dispersion in a liquid or solid plasticizer (such as a phthalate ester) is sometimes encountered in adhesives.

Ethyoxylates or propoxylates of *p*-toluidine are commonly used tertiary aromatic amines (Scheme 4).

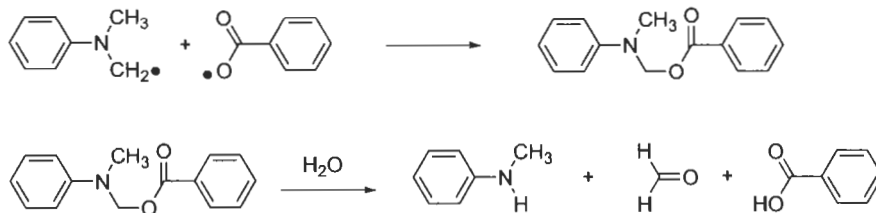
This compound is also described as diethanol-*p*-toluidine in the older literature. Anilines bearing hydroxyl groups are preferred because they are less volatile than anilines without polar substituents. Tertiary aromatic amines with *para*-halogen substitution have also been reported for use in adhesives [42].

The reaction between benzoyl peroxide and *N,N*-dimethylaniline has been the subject of many examinations over the years. The following mechanism of initiation is fairly well accepted in the polymerization of styrene. It seems likely that a similar mechanism is followed for other free-radical polymerizations (Scheme 5).

Some fraction of the benzoyl radicals may lose carbon dioxide to give phenyl radicals, which also initiate polymerization [43]. The nature of the initial inter-



Scheme 5. Mechanism of initiation.

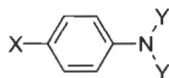


Scheme 6. A wastage reaction.

action between the peroxide and aniline has been a matter of debate [44]. Both $\text{S}_{\text{N}}2$ and electron transfer mechanisms have been proposed. The radical derived from loss of a proton from the aniline radical cation (see above) has been trapped with 2-methyl-2-nitrosopropane [45]. It is interesting to note that the benzoyl radical is not directly trapped, but its addition product with a molecule of styrene is. In the absence of monomer, the reaction product (after work-up) from BPO and *N,N*-dimethylaniline is a nearly quantitative yield of benzoic acid, *N*-methyl aniline and formaldehyde [46]. These likely result from the hydrolysis of the recombination product of the radical resulting from the tertiary amine and a benzoyl radical (Scheme 6).

Solvent can have an effect on the reaction path. The reaction between benzoyl peroxide and *N,N*-dimethylaniline in carbon tetrachloride is complicated by the strong chain transfer tendencies of this solvent [47].

Calorimetry has been used to measure the rate of reaction for several tertiary amines with benzoyl peroxide [48]. The relative rate results are in line with the predictions from general organic chemistry. The rates given in Table 4, see also Scheme 7, are based on *N,N*-dimethylaniline = 1.00.

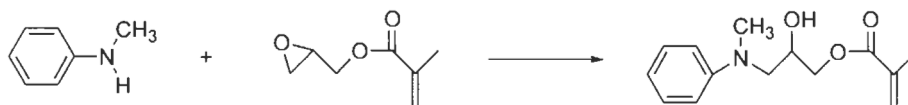


Scheme 7. Substituted dialkylanilines.

Table 4

Reaction rates relative to *N,N*-dimethylaniline. See Scheme 7 for X and Y

X	Y	Relative rate
-H	-CH ₃	1.00
-CH ₃	-CH ₃	3.57
-H	-(CH ₂) ₂ -OH	0.33
-CH ₃	-(CH ₂) ₂ -OH	2.26
-COOH	-CH ₃	0.00
-CHO	-CH ₃	0.00



Scheme 8. Synthesis of polymerizable tertiary amine.

Further aspects of the reaction of aromatic tertiary hydroxyl amines have been examined by more sophisticated techniques [49]. 2-Methyl-2-nitrosopropane was used as a radical trap, and the endgroups on PMMA resulting from its addition were detectable by ultraviolet spectroscopy. Electron spin resonance results on the same system have also been reported [50].

Possible impurities of the tertiary amine include primary and secondary amines. The presence of aniline slows the reaction, while the presence of *N*-methylaniline actually accelerates the polymerization [51]. As the secondary amine may be formed during polymerization (especially in the presence of water) reaction kinetics may be complicated.

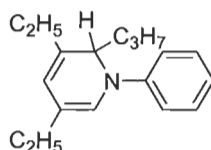
As small molecule fragments resulting from the initiator may plasticize the polymer and lower performance, approaches have been developed to avoid this. A dihydroxyamine can be used to form a polyester [52]. This accelerator gave a modest increase in the strength of unsaturated polyester resins. A polymerizable tertiary amine has been prepared by the reaction of *N*-methylaniline with glycidyl methacrylate [53] (Scheme 8).

It has been reported that tertiary aromatic amines can be encapsulated in formaldehyde-crosslinked microbeads, and used in an adhesive [54]. These microbeads burst when the joint is mated, and cure is accelerated.

Another common initiator system is based on chlorosulfonated polyethylene (trade-name HYPALON®). Adhesives based on this technology were referred to as RF (short for Reactive Fluid) or DH (DuPont HYPALON®) in the early literature. Chlorosulfonated polyethylene reacts with an amine (and optionally a peroxide) to form free radicals [55].

Many factors make this chemistry delightfully well suited for use in adhesives. Chlorosulfonated polyethylene is a synthetic elastomer used in applications requiring resistance to heat and oil [56]. It is produced in large volume for a number of applications, and hence is inexpensive. The amine can be applied as a primer, and so cure begins when the parts are mated. This gives excellent rate of bond strength development for an adhesive with a long open time. Other oligomers or polymers such as poly(vinylidene fluoride), polychloroprene or its copolymers, epoxy resins, or even a polyurethanes may be chlorosulfonated [57]. The chlorosulfonation procedure has been described, and soluble chlorosulfonates may contain 0.1 to 8% sulfur and 25 to 70% chlorine.

The most common amine used to cure chlorosulfonated polyethylene is the condensation product between butyraldehyde and aniline. This material is also de-

Scheme 9. VANAX[®] 808

scribed as VANAX[®] 808 or ACCELERATOR[®] 808. The active compound responsible for cure is *N*-phenyl-2-propyl-3,5-diethyl-1,2-dihydropyridine (Scheme 9).

Aromatic tertiary amines can also be used as part of the initiator system [58]. Glycidyl methacrylate or methacrylic acid have been used to hybridize acrylic adhesives based on this cure chemistry with epoxies [59]. The epoxy functionality is reactive with the carboxylic acid groups on the monomer.

Alkylboron compounds are another interesting class of initiators, discovered in the late 1950s [60,61]. These are of special importance as adhesives prepared with them bond well to polyolefins [27]. At first it was thought that alkylborons initiate by an ionic mechanism, but copolymerization studies confirmed a radical mechanism [62]. Oxygen was identified as a reactant, and vinyl acetate was not polymerized under nitrogen [63]. Trialkylboranes add to oxygen to form boron peroxides, which can then rearrange to boronic esters [64]. The first C–B bond is oxidized the most quickly [65], and the kinetics of oxidation have been measured [66–68]. The chemistry of boron peroxides has been reviewed [69]. Due to the stability of boron peroxides, it seems unlikely that these initiate polymerizations alone [70]. It has been suggested that the boron peroxide reacts with an additional molecule of trialkylboron [71] or trialkylboron–monomer complex [72]. Some of the proposed mechanisms have been reviewed [73]. Combining the above references, the following mechanism (Fig. 2) for the production of radicals may be suggested as plausible, but subject to discussion.

Polymerizations using trialkylborons are not slowed as much as is normal by the presence of conventional inhibitors such as *p*-phenylenediamine, hydroquinone, benzoquinone, phenothiazine or others [74]. This has been attributed to

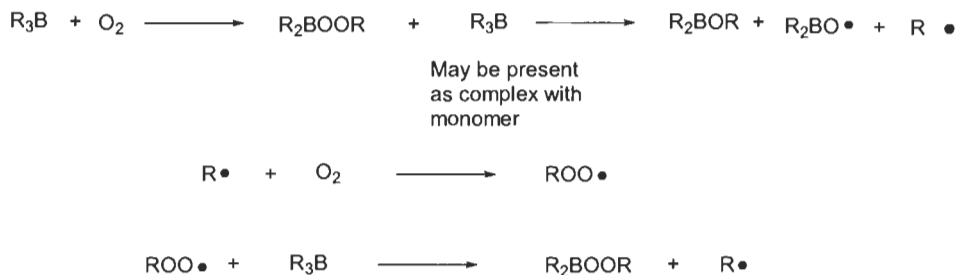
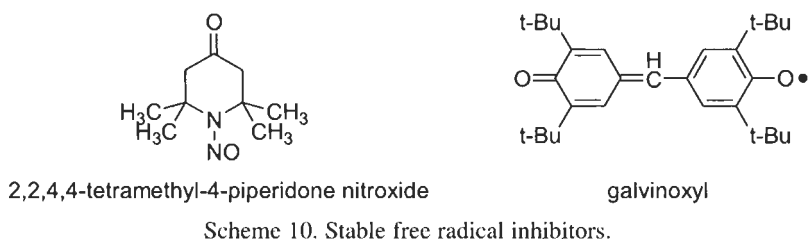


Fig. 2. Proposed mechanism for the production of radicals.



Scheme 10. Stable free radical inhibitors.

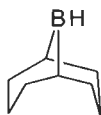
complex formation between the propagating radical and an additional molecule of trialkylboron. This proposal has been the subject of some debate in the literature [75]. Inhibitors such as 2,2,4,4-tetramethyl-4-piperidone nitroxide, or the stable free-radical galvinoxyl are effective however [76] (Scheme 10).

Trialkylboranes are pyrophoric, but can be stabilized by a number of bases [77,78]. Amines work well, and the resulting complex can be activated by amine acceptors such as isocyanates, acid chlorides or sulfonyl chlorides [79]. Aldehydes and organic acids have also been used as deblockers [80,81]. The amine has a major effect on polymerization reactivity, and so the amine strength must be chosen with care [82,83]. Pyrophoricity studies have been done, and the complexes containing 1,6-hexanediamine are especially nice in that regard [84]. Oligomeric amine complexes have also been prepared [85]. The 1,6-hexanediamine can then be consumed by a polyaziridine, which can also react with the carboxylic acid deblocking agent [86].

An alternative route towards stabilizing alkylborons is partial oxidation. Trialkylboranes can be reacted with 0.3–0.9 moles oxygen give a more stable product [87]. The procedure for preparing partially oxidized tributylborane has been described in detail, and about an hour is needed to prepare 204 grams [88]. Partially oxidized boranes are reported to be commercially available [89]. Iso-cyanatomethacrylates have been cured by this initiator. Compositions containing partially oxidized boranes have been used as dental and surgical cements.

Simple one-part acrylic compositions containing 9-borabicyclo-[3,3,1]-nonane (often called 9-BBN) cure and give good adhesion to wood [90]. It has also been used to cure a reactive acrylic hot-melt [91] (Scheme 11).

A complex of 9-BBN with MMA can be formed and compounded with sodium borohydride [92]. Derivatives from the combination of 9-BBN with fatty acid or fatty alcohol give an initiator with improved stability [93]. Stability appears to improve with increasing molecular weight, so oligomeric and polymeric analogs



Scheme 11. 9-Borabicyclo-[3,3,1]-nonane or 9-BBN.

have also been made [94]. These are some examples of aerobic acrylic adhesives, other types of which will be discussed later.

Cumene hydroperoxide [95], benzoyl peroxide, or *tert*-butyl peroxide [96], can be used as accelerators with alkylboron initiators. The chain transfer constant for MMA to tributylborane has been estimated to be 0.647, which is comparable to tripropylamine [97].

Atmospheric oxygen has always been a desirable oxidant. Its presence in the atmosphere allows the formulation of one-part reactive adhesives with good stability. Such compositions are commonly called aerobic adhesives. In an early example, an adhesive containing a combination of *t*-butyl perbenzoate and ferric sulfate is applied and mated with a surface coated with the condensation product between butyraldehyde and aniline (VANAX® 808) [98]. More work on aerobic adhesives has been done recently. *N*-substituted dihydropyridines can be combined with an organic acid and a cobalt catalyst to give an adhesive that cures on exposure to air [99]. Hydrogen peroxide has been identified as an intermediate in the reaction chemistry [100]. Onium salts such as diazonium, iodonium and sulfonium can be used in place of the weak acid [101]. A composition initiated by the combination of ferric acetylacetonate and *N*-phenyl-2-propyl-3,5-diethyl-1,2-dihydropyridine is especially effective in the bonding of poly(vinyl chloride) [102]. The shelf stability of air-activated adhesives has been investigated [103]. Finally, a hybrid adhesive incorporating moisture cure has been disclosed [104].

There are other initiator systems of lesser commercial importance. Cumene hydroperoxide is reported to cure acrylic adhesives in the presence of alkyl or pyridyl thioureas [105]. These initiators have been combined with a phosphated acrylate to promote adhesion to metal [106]. Thiourea-based initiators can be applied as a one-part on galvanized metal, where the metal surface provides the second part of the redox initiator [107].

Another interesting system has been developed to use a metal surface as part of a redox couple to give a one-part reactive adhesive. The combination of a sulfonyl halide (usually the chloride), an organic or inorganic acid, and a transition metal salt (such as copper) are combined to form the initiator [108]. A version that does not contain halogen has also been developed [109]. This technology can be converted to a two-part adhesive by providing a curative containing a metal powder [110].

Activation by a metal surface also takes place in the commercially important anaerobic adhesives. These one-part adhesives are stable in the package, but cure quickly in an oxygen-free environment such as a tightly controlled bond line. Important applications include thread-locking, sealing, retaining, and some structural bonding [111]. A representative model formulation has recently been described [112] (Fig. 3).

Anaerobic adhesive chemistry has been reviewed [113], so only a few recent developments will be covered here. Many of the components of anaerobic adhesives,

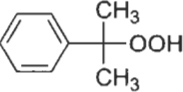
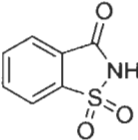
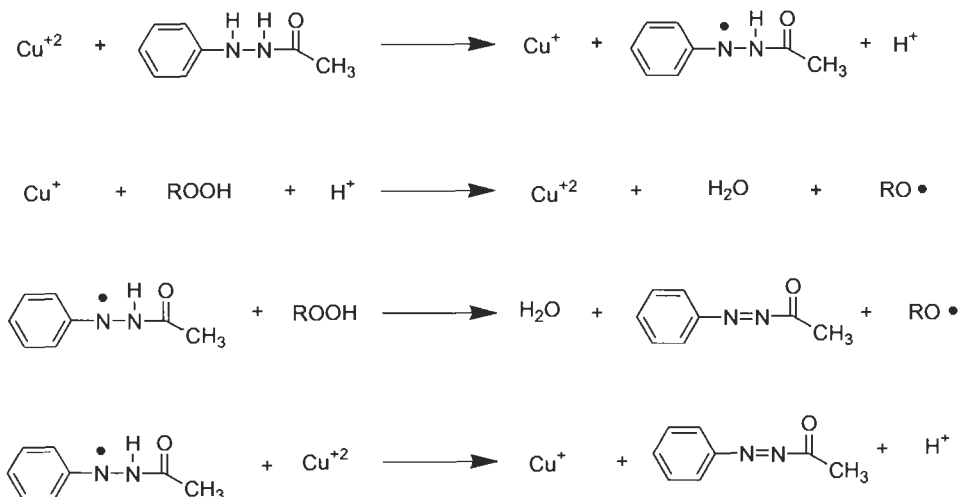
Component:	Parts:
Triethyleneglycol dimethacrylate	The remainder
Cumene hydroperoxide	2.64
Saccharin	0.85
	
Cumene hydroperoxide	Saccharin or O-benzoic sulfimide

Fig. 3. A representative model formulation that is activated by a metal surface.

including copper(II), iron(III), poly(ethylene glycol) dimethacrylate, cumene hydroperoxide, and *N,N*-dimethyl-*p*-toluidene, can be quantified using differential pulse voltammetry [114]. Gas and liquid chromatography have also been used [115]. The kinetics of polymerization of the initiator system saccharin/*N,N*-dimethyl-*p*-toluidene/cumene hydroperoxide has been reported to be (Eq. 4)

$$R_p = k[\text{saccharin}]^{0.36}[\text{N,N-dimethyl-}p\text{-toluidene}]^{0.34} \quad (4)$$

with the kinetics being zero order in cumene hydroperoxide [116]. Several interesting recent papers discuss new methods for the observation of cure. It has been known that metal ions also play an important role in cure, as evidenced by the usefulness of metal ion containing primers. The cure across gaps as a function of these primers has been examined using dynamic mechanical analysis and dielectric thermal analysis [117]. FTIR spectroscopy has been used to assess the effect of copper catalysis [118], cure profile on different metals [119], and has been correlated with dielectric spectroscopy [120]. The use of dielectric spectroscopy to investigate anaerobic adhesives has been reviewed [121]. Polarography has also been a useful tool in the investigation of the mechanism of cure. The interactions of metal ions with saccharin [122] as well as with 1-acetyl-2-phenylhydrazine, 1-acetyl-2-phenyldiazene, and 1,2,3,4-tetrahydroquinoline [123] have been reported. Polarography has also been used to examine the reaction of metal ions with peroxides [124]. The lower oxidation state metal ions are often quite active. This information has been combined to yield a recent mechanism of cure for 1-acetyl-2-phenylhydrazine based systems [125] (Scheme 12).



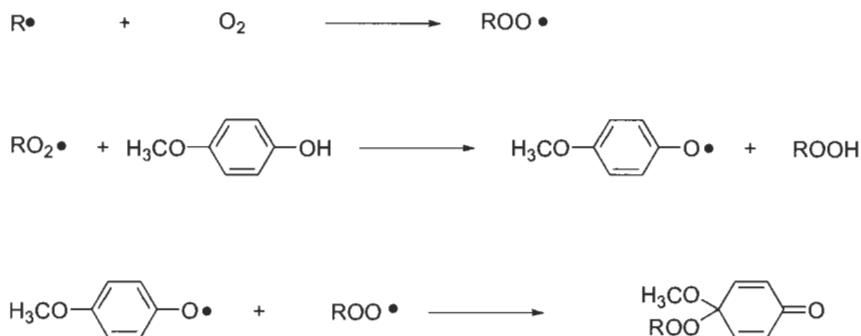
Scheme 12. Mechanism of cure for 1-acetyl-2-phenylhydrazine based systems.

3.4. Additives

It is difficult to obtain information about additives in the open literature. Typically, the additive packages are held as trade secrets. Some limited information has been published, however. Wax has long been used to promote surface cure [126]. Such waxes include paraffin, montan wax, beeswax, ceresin and spermaceti. Redox indicators have been proposed, as a visual measure of open time [127]. These additives include alkali metal salts of dichlorophenolindophenol (i.e. 2,6-dichloro-*N*-(4-hydroxyphenyl)-1,4-benzoquinonimine), *m*-cresolindophenol and thymolindophenol.

Polymerization inhibitors are key additives which prevent premature gelation of the adhesive. The formulator must carefully balance shelf stability and the required cure on demand. Due to its high propagation rate, MMA is difficult to inhibit. Some comments on specific inhibitors follow. The most common inhibitor to be found in component monomers is 4-methoxyphenol, which is also called the methyl ether of hydroquinone. This inhibitor is effective only in the presence of oxygen. A mechanism has been proposed, and is illustrated in Scheme 13 [128].

Some other inhibitors from the patent literature include hydroquinone [129], 'ionol' [130], and quinone [131]. Other inhibitors used to stabilize MMA include butylated hydroxy toluene (BHT), phenothiazine, methylene blue, hydroxydiphenylamine and di-*beta*-naphthol [132]. Several good reviews of inhibition and inhibitors have been written [133–136]. The mechanisms of inhibition are subtle and complicated. For example, it has been reported that highly purified benzoquinone acts as a retarder rather than an inhibitor [137]. It has been proposed



Scheme 13. Mechanism of inhibition by 4-methoxyphenol.

that quinhydrone (the charge transfer complex between benzoquinone and hydroquinone) is the active inhibitor, and that the complex has some stable free-radical character [138]. Metal chelators also have a role in stabilization [139], especially EDTA [140].

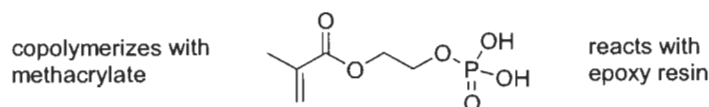
The role of atmospheric oxygen is complex, both inhibiting and promoting polymer formation [141]. Oxygen is a ground state diradical, and so rapidly adds to a propagating free radical to give a stable species. On the other hand, oxygen can cause peroxide formation, destabilizing the monomer. The interaction of oxygen with phenolic stabilizers has been well documented [142].

Inorganic materials (fillers) can be used to lower raw material cost and provide some special properties [143]. Careful attention must be paid to processing and dispersion, however [144].

Hybrid systems of acrylics with other technologies have been reported. Acrylic and epoxy polymers can be coupled through the use of 2-methacryloxyethyl phosphate. The phosphoric acid functionality reacts with epoxy and the methacrylate group copolymerizes with the acrylic backbone [145] (Scheme 14).

Such compositions give good heat resistance and adhesion to unprepared metal. Adhesives based on chlorosulfonated polyethylene have also been modified by an epoxy resin [146].

There are two approaches to forming urethane-acrylic hybrids. First, an acrylate terminated urethane oligomer can be used [147]. Alternatively, polyisocyanate and benzoyl peroxide can be combined in one side of the adhesive, and methacrylate monomers and urethane curatives (especially polyols) in the other [148].



Scheme 14. 2-Methacryloxyethyl phosphate.

4. Applications

Most acrylic adhesives are used by industrial customers. They are well suited to manufacturing environments. The adhesive bonding of fiberglass boats is often done with acrylic adhesives [149]. Their ability to bond unprepared composites, combined with the broad range of cure speeds available, make acrylics well suited for boat-building applications. Deck-to-hull joints of 29-foot boats are held together with a combination of acrylic adhesive and mechanical fasteners. Self-tapping screws can be driven through the joint before the adhesive sets. Other structural elements such as stringers and bulkheads can also be adhesively bonded.

The ability to tailor acrylic adhesives to fast cure times allows their use on fast, highly mechanized production lines such as those for audio speakers [150].

The robust nature of acrylics make them useful in repair shops such as those for automobiles. For example, exterior roof panels can be repaired with acrylics [151]. Acrylics are also suitable for repair of some trim components on automobiles [152].

Acrylic adhesives can also be used in automotive assembly. For example, the hem flanges between the inner and outer panel of automotive doors can be bonded with acrylic adhesives [153]. There are many smaller industrial assembly applications where acrylic adhesives are applicable. An interesting recent example is the bonding of cable splice enclosures, using a borane initiated adhesive [154].

References

1. Hussy, B. and Wilson, J., *Structural Adhesives Directory and Handbook*. Chapman and Hall, London, 1996, pp. 67–68.
2. Hartshorn, S.R. (Ed.), *Structural Adhesives — Chemistry and Technology*. Plenum Press, London, 1986, p. 235.
3. Briggs, P.C. and Muschiatti, C.L., U.S. Patent 4,106,971.
4. Bäder, E. and Koert, H., U.S. Patent 2,894,932.
5. Bäder, E. and Schweitzer, O., U.S. Patent 2,981,650.
6. Bäder, E., U.S. Patent 3,321,351.
7. Bäder, E., U.S. Patent 3,333,025.
8. Lap shear samples performed according to ASTM-D1002 or D3163. Oily metal was coated with hexadecane. All other substrates were bonded unprepared.
9. Odian, G., *Principles of Polymerization*, 3rd ed. Wiley, New York, 1991.
10. Bacon, R.G.R., *Q. Rev. (London)*, **9**, 287 (1955).
11. Nayak, P.L. and Lenka, S., *J. Macromol. Sci. Rev. Macromol. Chem.*, **C19(1)**, 83 (1980).
12. Misra, G.S. and Bajpai, U.D.N., *Prog. Polym. Sci.*, **8**, 61 (1982).
13. Sarac, A.S., *Prog. Polym. Sci.*, **24**, 1149 (1999).
14. Brandrup, J. and Immergut, E.H., *Polymer Handbook*, 3rd ed. Wiley, New York, 1989.
15. O'Driscoll, K.F. and Reilly, P.M., *Makromol. Chem. Macromol. Symp.*, **10/11**, 355 (1987).
16. Tüdös, F. and Földes-Berezsnich, T., *Prog. Polym. Sci.*, **14**, 717–743 (1989).
17. Braun, D., *Simple Methods for the Identification of Plastics*, 2nd ed. Hanser Publishers, Munich, 1986, p. 21.

18. Morrison, R.T. and Boyd, R.N., *Organic Chemistry*, 3rd ed. Allyn and Bacon, Newton, MA, 1973, p. 85.
19. Skoultschi, M.M. and Ray-Chaudhuri, D.K., U.S. Patent 5,310,835.
20. Fox, T.G., *Bull. Am. Phys. Soc., Ser. II*, **1**, 123 (1956).
21. Bäder, E., U.S. Patent 3,333,025.
22. Owston, W.J., U.S. Patent 3,725,504.
23. Bachmann, A.G., U.S. Patent 4,429,088.
24. Briggs, P.C. and Gosiewski, D.E., U.S. Patent 4,959,405.
25. Masuhara, E. et al., U.S. Patent 3,527,737.
26. Bäder, E. and Schweitzer, O., U.S. Patent 2,981,650.
27. Imai, Y. et al., Chemical Abstracts 80: 134385, translation from Japanese, 1974.
28. Bäder, E., U.S. Patent 3,333,025.
29. Cangialosi et al., D., *Eur. Polym. J.*, **37**, 535 (2001).
30. Bäder, E. and Koert, H., U.S. Patent 2,894,932.
31. Owston, W.J., U.S. Patent 2,832,274.
32. Briggs, P.C. and Muschiatti, L.C., U.S. Patent 4,182,644.
33. Briggs, P.C. and Gosiewski, D.E., U.S. Patent 4,942,201.
34. Sperling, L.H., *Introduction to Physical Polymer Science*, 2nd ed. Wiley, New York, 1992, p. 414.
35. Owston, W.J. and Howard, D.D., U.S. Patent 3,873,640.
36. Dawdy, T.H., U.S. Patent 4,769,419.
37. Boeckeler, R.H., U.S. Patent 5,587,433.
38. Abbey, K.J. and Quarmby, I.C., U.S. Patent 5,710,235.
39. Paquette, L.A. (Ed.), *Encyclopedia of Organic Synthesis*, Vol. 3. Wiley, New York, 1995, p. 1529.
40. Howe-Grant, M. (Ed.), *Encyclopedia of Chemical Technology*, 4th ed., Vol. 18. Wiley, New York, 1996, p. 230.
41. Wolinski, L.E. and Berezuk, P.D., U.S. Patent 4,126,504.
42. Righettini, R.F., U.S. Patent 5,932,638.
43. Ayrey, G., *Chem. Rev.*, **63**, 645 (1963).
44. Pryor, W.A. and Hendrickson, W.H., *J.A.C.S.*, **97**, 1580 (1975).
45. Sato et al., T., *Makromol. Chem.*, **176**, 561 (1975).
46. Walling, C. and Indictor, N., *J.A.C.S.*, **80**, 5814 (1958).
47. Lokaj, J. and Hrabak, F., *Macromol. Chem.*, **119**, 23 (1968).
48. Mallon et al., H.-J., *Acta Polym.*, **41**, 460 (1990).
49. Fu et al., J., *Acta Polym. Sin.*, **1**, 67 (1990).
50. Qui et al., K., *Acta Polym. Sin.*, **1**, 84 (1991).
51. Wahid et al., A.K., *Iraqi J. Sci.*, **25**, 21 (1984).
52. Pittman, C.U. and Jada, S.S., *Ind. Eng. Chem. Prod. Res. Dev.*, **21**, 281 (1982).
53. Wolinski, L.E. and Berezak, P.D., U.S. Patent 4,155,950.
54. Wolinski, L.E. and Berezuk, P.D., U.S. Patent 4,080,238.
55. Briggs, P.C. and Muschiatti, L.C., U.S. Patent 4,106,971.
56. Howe-Grant, M. (Ed.), *Encyclopedia of Chemical Technology*, 4th ed., Vol. 8. Wiley, New York, 1996, p. 956.
57. Briggs, P.C. and Muschiatti, L.C., U.S. Patent 4,182,644.
58. Briggs, P.C. and Muschiatti, L.C., U.S. Patent 4,106,971.
59. Briggs, P.C., U.S. Patent 4,426,243.
60. Kolesnikov, G.S. and Fedorova, L.S., *Bull. Acad. Sci. USSR, Div. Chem. Sci.*, 251 (1957).
61. Furukawa et al., J., *J. Polym. Sci.*, **26**, 234 (1957).

62. Fordham, J.W.L. and Sturm, C.L., *J. Polym. Sci.*, **33**, 503 (1958).
63. Furukawa, J. and Tsuruta, T., *J. Polym. Sci.*, **28**, 227 (1958).
64. Abraham, M.H. and Davies, A.G., *J. Chem. Soc.*, 429 (1959).
65. Mirviss, S.B., *J.A.C.S.*, **83**, 3051 (1961).
66. Welch, F.J., *J. Polym. Sci.*, **61**, 243 (1962).
67. Hansen, R.L. and Hamann, R.R., *J. Phys. Chem.*, **67**, 2868 (1963).
68. Hansen, R.L., *J. Polym. Sci. Part A*, **2**, 4215 (1964).
69. Sosnovsky, G. and Brown, J.H., *Chem. Rev.*, **66**, 529 (1966).
70. Hansen, R.L. and Hamann, R.R., *J. Phys. Chem.*, **67**, 2868 (1963).
71. Grotewold, J. et al., *J. Chem. Soc. (B)*, 182 (1971).
72. Bawn, C.E.H. et al., *Proc. Chem. Soc.*, 397 (1959).
73. Yoshikuni et al., M., *J. Polym. Sci. Polym. Chem. Ed.*, **2**, 3115 (1973).
74. Arimoto, F.S., *J. Polym. Sci. Part A-1*, **4**, 275 (1966).
75. Grotewold et al., J., *J. Polym. Sci. Part A-1*, **6**, 3157 (1968).
76. Brindley, P.B. and Pearson, R.G., *Polym. Lett.*, **6**, 831 (1968).
77. Frankland, E., *Philos. Trans. (London)*, **152**, 167 (1862).
78. Russell, C.A., *Edward Frankland — Chemistry, Controversy and Conspiracy in Victorian England*. Cambridge University Press, 1996.
79. Fujisawa, S. et al., Chemical Abstracts 73: 88532, translation from Japanese, 1970.
80. Skoultchi, M.M. and Merlo, N.V., U.S. Patent 5,143,884.
81. Skoultchi, M.M., U.S. Patent 5,286,821.
82. Mottus, E.H. and Fields, J.E., U.S. Patent 3,275,611.
83. Mottus, E.H. and Fields, J.E., *Polym. Prepr.*, **4**, 1 (1963).
84. Zharov, J.V. and Krasnov, J.N., U.S. Patent 5,539,070.
85. Pocius, A.V., U.S. Patent 5,621,143.
86. Pocius, A.V. and Deveny, E.J., U.S. Patent 5,935,711.
87. Masuhara, E. et al., Chemical Abstracts 80: 41060, translation from German, 1974.
88. Nakabayashi, N. and Masuhara, E., *J. Biomed. Mater.*, **12**, 149 (1978).
89. Chappelow et al., C.C., *J. Appl. Polym. Sci.*, **58**, 1147 (1995).
90. Ritter, W. and Gruber, W., U.S. Patent 4,831,386.
91. Ritter, W., U.S. Patent 4,921,921.
92. Ritter, W., U.S. Patent 4,385,153.
93. Ritter, W., U.S. Patent 4,515,724.
94. Ritter, W., U.S. Patent 4,638,092.
95. Skoultchi, M.M. and Merlo, N.V., U.S. Patent 5,106,928.
96. Contreras et al., I., *J. Polym. Sci. Part A*, **7**, 2341 (1969).
97. Huff, T. and Perry, E., *J. Polym. Sci. Part A*, **1**, 1553 (1963).
98. Bachmann, A.G., U.S. Patent 4,348,503.
99. Kneafsey, B. et al., European Patent 92301899.8.
100. Raftery et al., D.P., *Anal. Commun.*, **33**, 375 (1996).
101. Kneafsey, B., PCT Int. Appl. WO 94/19418.
102. Kneafsey, B., U.S. Patent 5,683,536.
103. Lyons et al., E., *Int. J. Adhes. Adhes.*, **21**, 35 (2001).
104. Huver, T. et al., U.S. Patent 5,744,543.
105. Zimmermann, W.D. and Temin, S.C., U.S. Patent 4,469,976.
106. Taguchi et al., K., *J. Jpn. Soc. Adhes.*, **36**, 136 (2000).
107. Fisher, E., U.S. Patent 4,645,810.
108. Damico, D.J., U.S. Patent 4,703,089.
109. Holmes-Farley, S.R. and Abbey, K.J., U.S. Patent 5,096,962.

110. Damico, D.J. et al., U.S. Patent 4,857,131.
111. Skeist, I. (Ed.), *Handbook of Adhesives*, 3rd ed. Chapman and Hall, London, 1990.
112. Yang, D.B., *J. Adhes.*, **43**, 273 (1993).
113. Hartshorn, S.R. (Ed.), *Structural Adhesives — Chemistry and Technology*. Plenum Press, London, 1986, pp. 217–235.
114. Hai-Lin et al., G., *Anal. Chim. Acta*, **217**, 335 (1989).
115. Leonard et al., R.G., *Anal. Proc.*, **29**, 393 (1992).
116. Hudak et al., S.J., *Surf. Interface Anal.*, **15**, 167 (1990).
117. McArdle et al., C., *Plastics, Rubber Composites Proc. App.*, **16**, 245 (1991).
118. Yang, D.B., *J. Adhes.*, **43**, 273 (1993).
119. Yang et al., B.D., *J. Adhes. Sci. Technol.*, **9**, 1369 (1995).
120. McGettrick et al., B.P., *J. Appl. Polym. Sci.*, **52**, 737 (1994).
121. McGettrick et al., A., *Int. J. Adhes. Adhes.*, **14**, 211 (1994).
122. Raftery et al., D., *J. Polym. Sci. Part A: Polym. Chem.*, **35**, 3327 (1997).
123. Raftery et al., D., *Int. J. Adhes. Adhes.*, **17**, 9 (1997).
124. Moane et al., S., *Int. J. Adhes. Adhes.*, **19**, 49 (1999).
125. Raftery et al., D., *Int. J. Adhes. Adhes.*, **17**, 151 (1997).
126. Baeder, E., Canadian Patent 617,637 (1961).
127. Hechenberger, D.A. and Gollub, H.J., U.S. Patent 4,467,079.
128. Kurland, J.J., *J. Polym. Sci. Polym. Chem. Ed.*, **18**, 1139 (1980).
129. Bader, E., U.S. Patent 3,333,025.
130. Briggs, P.C., U.S. Patent 4,536,546.
131. Bachmann, A.G., U.S. Patent 4,429,088.
132. Leonard, E.C. (Ed.), *Vinyl and Diene Monomers*. Wiley-Interscience, New York, 1970, p. 168.
133. Bovey, F.A. and Kolthoff, I.M., *Chem. Rev.*, **42**, 491 (1948).
134. Mark, H. (Ed.), *Encyclopedia of Polymer Science and Technology*, Vol. 7. Wiley, New York, 1967, p. 644.
135. Novak, J., *Prog. Org. Coatings*, **16**, 231 (1988).
136. Tüdös, F. and Földes-Bereznich, H., *Prog. Polym. Sci.*, **14**, 717 (1989).
137. Bonsall et al., E.P., *Trans. Faraday Soc.*, **49**, 686 (1953).
138. Kharasch et al., M.S., *J.O.C.*, **19**, 1977 (1954).
139. Mark, H. (Ed.), *Encyclopedia of Chemical Technology*, 3rd ed. Wiley, New York, 1978, p. 128.
140. Moane et al., S., *Int. J. Adhes. Adhes.*, **19**, 49 (1999).
141. Anonymous du Pont workers, *Ind. Eng. Chem.*, **28**, 1160 (1936).
142. Caldwell, R.G. and Ihrig, J.L., *J.A.C.S.*, **84**, 2878 (1962).
143. Wypych, G., *Handbook of Fillers*, 2nd ed. ChemTec Publishing, 1999.
144. Patton, T., *Paint Flow and Pigment Dispersion*, 2nd ed. Wiley, New York, 1979.
145. Dawdy, T.H., U.S. Patent 4,467,071.
146. Briggs, P.C., U.S. Patent 4,426,243.
147. Shah, D.N. and Dawdy, T.H., U.S. Patent 5,232,996.
148. Chung, D.A., PCT Int. Appl. WO 98/33845.
149. Pfund, B., *Professional Boatbuilder*, **60**, 104 (1999).
150. Suto, H. and Taguchi, K., U.S. Patent 6,166,146.
151. Staquet, E.T. and Anderson, W.J., U.S. Patent 5,968,298.
152. Gascoigne, B., *Adhes. Age*, **42**, 16 (1999).
153. Herring, J.M. and Greve, B.N., U.S. Patent 6,074,506.
154. Pulido, J.J. et al., U.S. Patent 5,912,433.

Cyanoacrylate instant adhesives

PHILIP KLEMARCYK^{*}

Henkel Loctite Corporation, 1001 Trout Brook Crossing, Rocky Hill, CT 06067, USA

1. Introduction

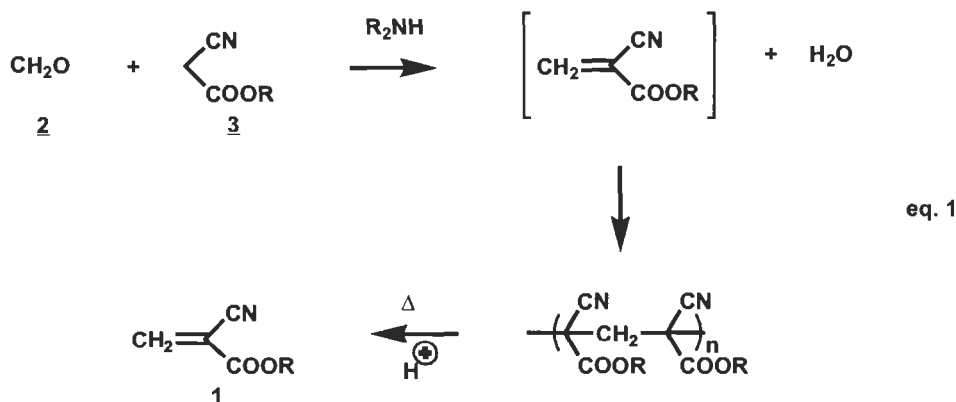
The preparation of alkyl cyanoacrylate esters was first reported by scientists at B.F. Goodrich in 1949, and these monomers were observed to produce hard, glassy polymers after thermal polymerization [1]. However, the desirable adhesive properties of the polymers formed from these substituted acrylic esters were not recognized until 1951, when researchers at Tennessee Eastman attempted to measure the refractive index of these materials on an Abbe refractometer. After obtaining the measurement, they discovered that the prisms of refractometer had been bonded together [2]. These researchers then realized that alkyl cyanoacrylate esters could effectively perform as one-part, liquid adhesives, which would cure rapidly at room temperature. Unlike epoxy or acrylic adhesives, alkyl cyanoacrylate adhesives will polymerize, in many cases, without the need for an added initiator or curing agent. The first cyanoacrylate instant adhesive, Eastman 910[®], which utilized methyl cyanoacrylate as the monomer, was marketed in 1958. After that initial product introduction, a large number of improvements and modifications have been developed for cyanoacrylate technology, which has led to the manufacture of a large variety of instant adhesive products.

Because of their ability to bond a wide variety of substrates, cyanoacrylate instant adhesives are now produced in multi-ton quantities for both industrial and consumer applications [3].

^{*} E-mail: phil.klemarczyk@Loctite.com

2. Chemistry

The manufacture of alkyl cyanoacrylate monomers, **1**, involves the Knoevenagel reaction of formaldehyde, **2**, with an alkyl cyanoacetate, **3**, and a base, such as a secondary amine, as the catalyst, shown in Eq. 1.

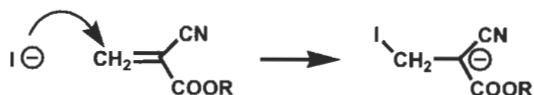
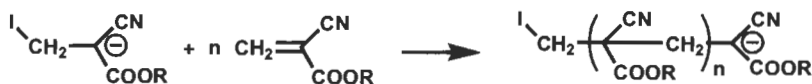
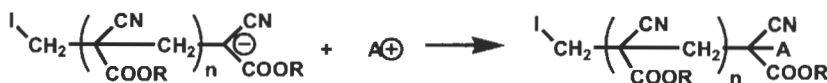


Since amines initiate cyanoacrylate polymerization, the monomer cannot be isolated directly, because a polymer is generated immediately after formation of the monomer. An acid is then added to the polymer, and heat (140–180°C) is applied to the reaction mixture. Because of the relatively low ceiling temperature of the polymer, the pure monomer can be isolated, in greater than 80% yield, by the thermal reversion of the polymer back to the free monomer [4,5].

3. Polymerization

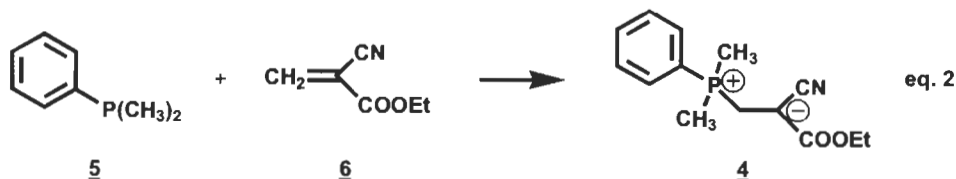
One of the reasons for the effectiveness of cyanoacrylate instant adhesives is the rapid rate of initiation by trace amounts of base on the substrate surface, subsequent high rate of polymerization, and the formation of high molecular weight polymers. The stabilization of the propagating anion by the two strongly electron-withdrawing groups, –CN and –COOR, facilitates the polymerization [6,7]. Since the polymerization is propagated anionically, it can be terminated by the addition of any cationic species, most commonly a proton from a strong acid. The initiation, polymerization, and termination mechanisms, with basic initiator I[–] and cationic termination species A⁺, are outlined in Scheme 1 [3].

The initiation mechanism is well defined because of the recent isolation and spectroscopic characterization of the initial zwitterion from ethyl cyanoacrylate (ECA) and a phosphine [8,9]. Specifically, zwitterion **4** was prepared from the reaction of equimolar amounts of dimethylphenyl phosphine, **5**, and ECA, **6**,

1. Initiation**2. Propagation****3. Termination**

Scheme 1.

as shown in Eq. 2 [8]. The addition of excess ECA monomer yields the ethyl cyanoacrylate homopolymer.



The formation of polymer can be considered as a quasi-living polymerization. After the polymerization is complete, it can be reinitiated with the addition of more monomer to the unquenched polymer. However, the degree of polymerization cannot be predicted by the monomer/initiator molar ratio, the polydispersity is 1.5–2.0, and water, or even carboxylic acids, act as inhibitors and do not terminate the polymerization [10].

Polymerization can also be effected with latent base photoinitiators. The one-part formulations are stable at ambient temperature, and will only polymerize after exposure to UV light.

4. Stabilizers

To prevent premature polymerization, a strong protic or a Lewis acid is added to the distilled monomer and to adhesive formulations. A wide variety of materials have been utilized as acidic stabilizers in the alkyl cyanoacrylate monomers. A list of some of these materials is shown in Table 1 [2,11–14].

Table 1

Acid stabilizers for alkyl cyanoacrylate monomers

-
- Aliphatic and aromatic sulfonic acids
 - Sulfuric acid
 - Sulfur dioxide
 - Nitric oxide
 - Hydrogen fluoride
 - Lewis acids
-

These acids can be used alone or as mixtures. It is especially advantageous to use a mixture of liquid and gaseous acids. The gaseous acid will stabilize free monomer in the headspace of a container, while the liquid acid will prevent premature polymerization of the bulk monomer or adhesive. However, it is important to use only a minimum amount of acid, because excess acid will slow initiation and the formation of a strong adhesive bond. It can also accelerate the hydrolysis of the alkyl cyanoacrylate monomer to 2-cyanoacrylic acid, which inhibits the polymerization of the monomer and reduces molecular weight of the adhesive polymer. While carboxylic acids inhibit the polymerization of cyanoacrylate monomer, they do not prevent it completely [15]. Therefore, they cannot be utilized as stabilizers, but are used more for modifying the reactivity of instant adhesives.

Because they are acrylic monomers, alkyl cyanoacrylate esters still require the addition of radical polymerization inhibitors, such as hydroquinone or hindered phenols, to prevent radically induced polymerization over time [3]. Since basic initiation of alkyl cyanoacrylate monomers is the predominant polymerization mechanism, large quantities of free radical inhibitors can be added, with little or no effect on adhesive performance.

5. Monomers

Several different monomers are available for use in commercial products. Table 2 lists the most commonly utilized monomers and some of their physical properties.

Ethyl cyanoacrylate is the monomer which is most widely used in both consumer and industrial applications, because of its combination of fast cure speed and ease of manufacture.

Blooming is the phenomenon of the formation of a white residue of cured adhesive near a bond line. It is the result of the evaporation of a small amount of the adhesive monomer from where it was applied onto the adjoining surface and its subsequent polymerization. The use of higher molecular weight monomers, such as the alkoxy esters, eliminates this problem.

All of the commercially available monomers are monofunctional, leading to

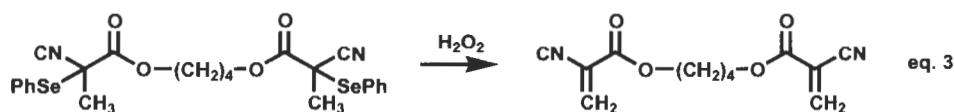
Table 2

The most common alkyl cyanoacrylate monomers

$\begin{array}{c} \text{CN} \\ \diagup \\ \text{CH}_2=\text{C} \\ \diagdown \\ \text{COOR} \end{array}$				
Type (R)	CAS Registry Number	Boiling Point (°C/kPa)	Density (g/cm ³)	Uses
Methyl (CH ₃)	137-05-3	48/0.33	1.10	Original product
Ethyl (C ₂ H ₅)	7085-85-0	54/0.21	1.05	General purpose
Isopropyl (C ₃ H ₇)	10586-17-1	53/0.27	1.01	Rubber bonder
Butyl (C ₄ H ₉)	6066-65-1	83/0.40	0.98	Medical, Veterinary
Methoxyethyl (CH ₃ -O-C ₂ H ₄)	27816-23-5	96/0.35	1.06	Low odor, Low bloom
Allyl (CH ₂ =CH-CH ₂)	7324-02-9	78/0.80	1.05	Crosslinking site

the formation of a thermoplastic adhesive polymer with poor solvent resistance toward polar organic solvents, such as acetone or methylene chloride. This could be an advantage in the cases where skin is accidentally bonded to a surface, but some applications do require good solvent resistance. One general method for the improvement of solvent resistance is the addition of difunctional monomers to crosslink the resulting adhesive polymer.

Literature articles, which report the formation and evaluation of difunctional cyanoacrylate monomers, have been published. The preparation of the difunctional monomers required an alternative synthetic method than the standard Knoevenagel reaction for the monofunctional monomers, because the crosslinked polymer thermally decomposes before it can revert back to the free monomer. The earliest report for the preparation of a difunctional cyanoacrylate monomer involved a reverse Diels–Alder reaction of a dicyanoacrylate precursor [16,17]. Later reports described a transesterification with a dicyanoacrylic acid [18] or their formation from the oxidation of a diphenylselenide precursor, seen in Eq. 3 for the dicyanoacrylate ester of butanediol, **7** [6].



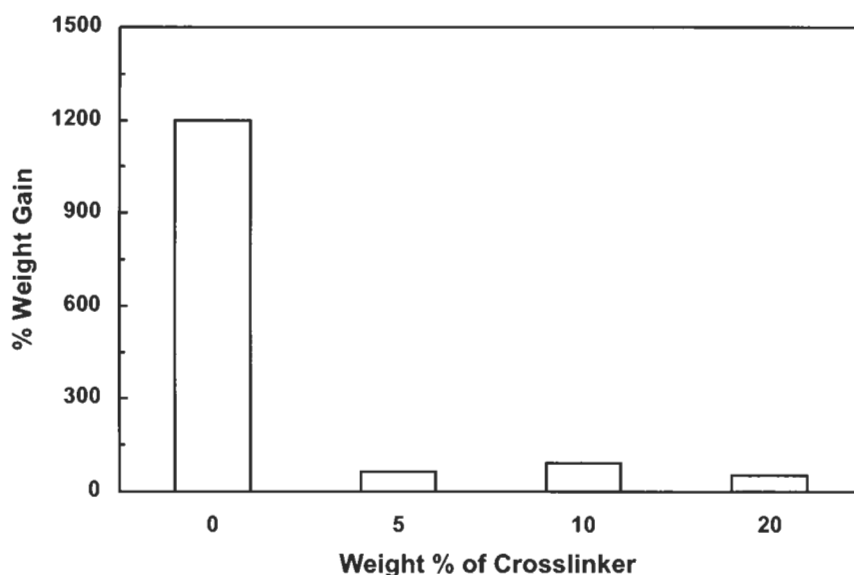


Fig. 1. Solvent swelling experiments with ECA polymers crosslinked with 7.

Solvent swelling experiments, with CH_2Cl_2 and ECA polymer crosslinked with 7, demonstrate that the addition of a difunctional cyanoacrylate monomer does improve solvent resistance [6], shown in Fig. 1.

Crosslinking has been claimed to improve thermal resistance of the cyanoacrylate adhesive [18]. However, in other reports [6], little or no improvement in thermal resistance of the adhesive was demonstrated by the addition of a difunctional monomer. As seen in Fig. 2, the addition of varying amounts of crosslinker 7 provided no improvement in the tensile adhesive strength of ethyl cyanoacrylate on steel lapshears after thermal exposure at 121°C for up to 48 h.

6. Copolymers

Alkyl cyanoacrylate monomers have been copolymerized with a variety of monomers, both by radical and anionic initiation. The radical-initiated copolymerization with acrylic monomers was performed with a sufficient amount of an acid stabilizer present to suppress polymerization by anionic means [19]. This investigation has been covered extensively elsewhere.

More recently, the copolymerization of ethyl cyanoacrylate with other 1,1 disubstituted electron deficient monomers and the effect of the monomers on adhesive properties have been studied. Monomers, such as diethyl methylenemalonate (DEMM), 8, were prepared [6,7]. Their homopolymers and copolymers

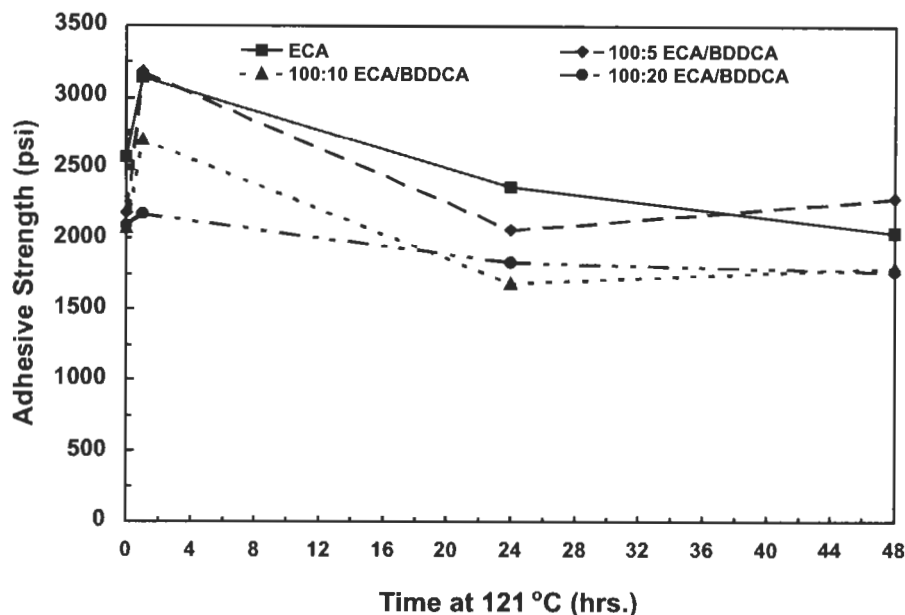
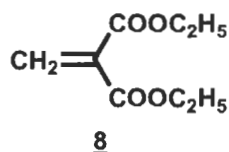


Fig. 2. Adhesion tests after thermal exposure with ECA crosslinked with the dicyanoacrylate ester of butanediol, 7.

with ECA were prepared with a basic initiator, pyridine. The GPC analysis of the homopolymers and copolymers are shown in Fig. 3. The fact that the copolymer GPC curve is monomodal and its molecular weight is intermediate between those of the homopolymers are good indicators that a copolymer was formed. It is not just a mixture of the two homopolymers.



The molecular weights of the polymers are much larger than would be predicted from the monomer/initiator ratio, as seen in Fig. 4. However, this effect is most evident for the polymerization of ethyl cyanoacrylate alone.

The adhesive properties the other monomers were also evaluated, alone and as mixtures with ethyl cyanoacrylate. The addition of DEMM to ECA has an obvious negative effect on adhesion, as can be seen in Fig. 5.

Even low concentrations of DEMM in ECA significantly reduce lapshear adhesive strength, probably because of the reduction in molecular weight of the adhesive polymer. However, even though the initial adhesive strength is lower,

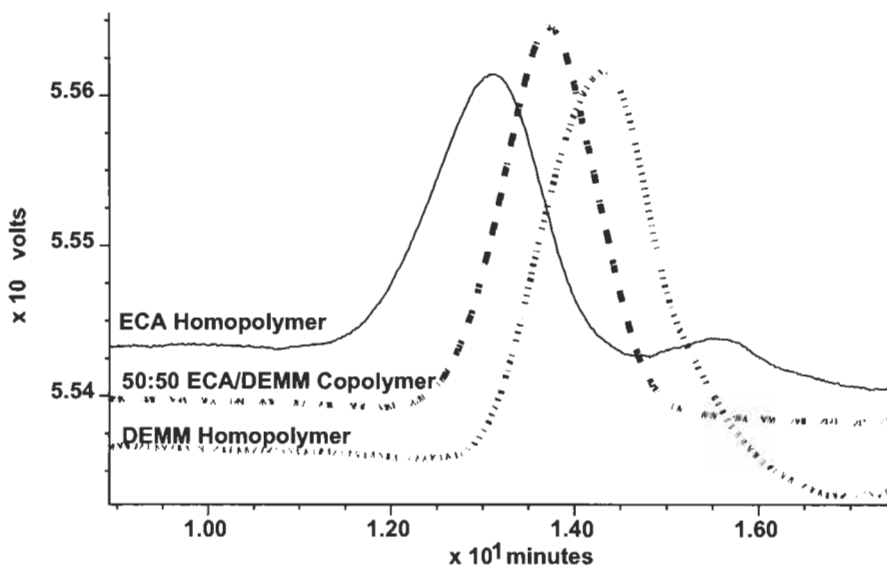


Fig. 3. GPC analysis of ECA homopolymer, 50:50 ECA/DEMM copolymer, and DEMM homopolymer.

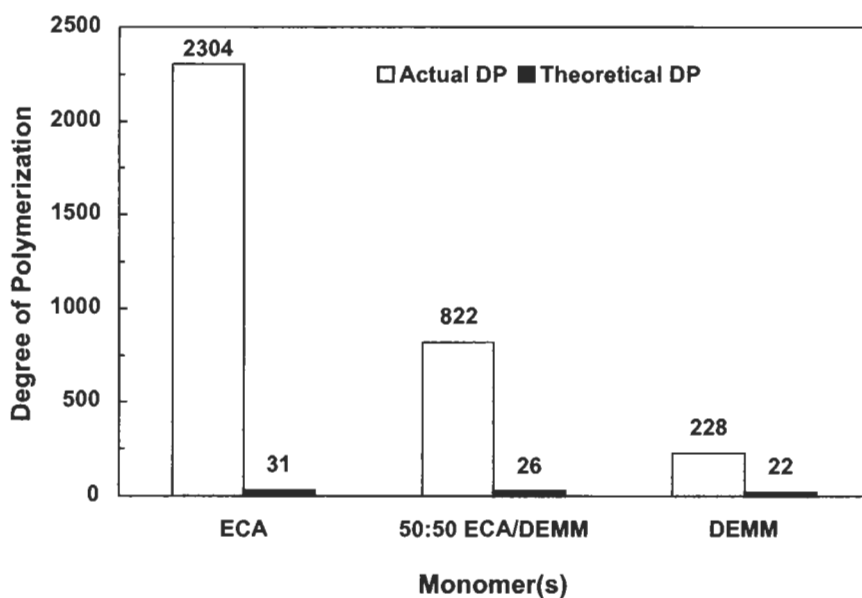


Fig. 4. Degree of polymerization for ECA homopolymer, 50:50 ECA/DEMM copolymer, and DEMM homopolymer.

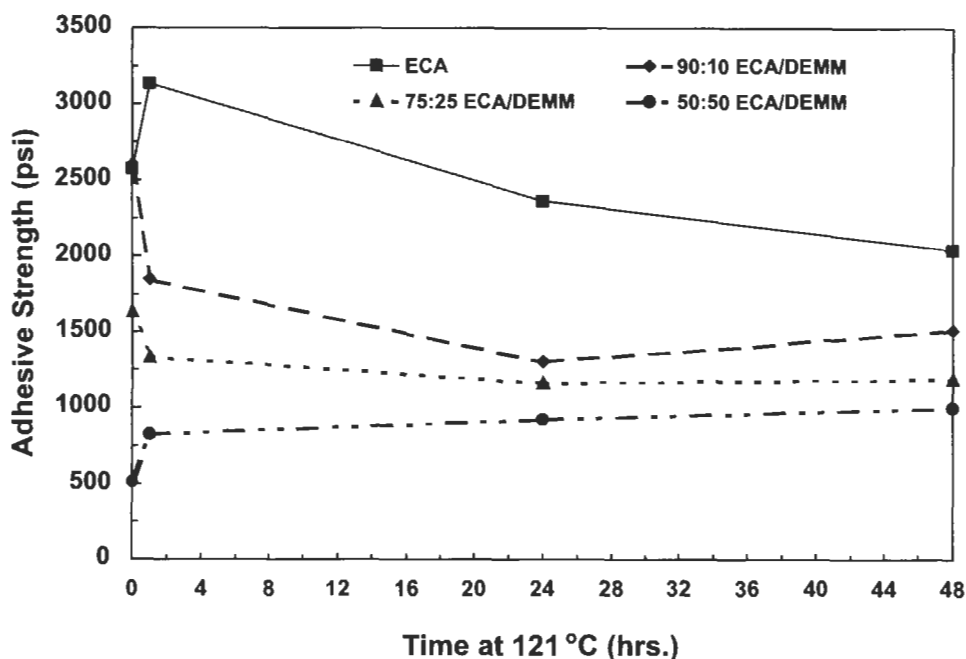


Fig. 5. Lapshear strengths for ECA and DEMM monomer mixtures after thermal exposure.

Table 3

Fixture time (s) of ECA/DEMM mixtures on glass and steel

Monomers	Glass (s)	Steel (s)
ECA	1	1
90:10 ECA/DEMM	1	2
50:50 ECA/DEMM	1	3
DEMM	1	Evaporation, no fixture

there is no loss of adhesion after thermal exposure, but the absolute value is still lower than ECA alone after 48 h at 121°C. There is an unacceptable trade-off between an improvement in thermal stability and overall adhesive properties. The presence of DEMM also reduces fixture time on steel, although the fixture time on glass is unaffected, as seen in Table 3.

No adhesion or fixture time data on steel could be obtained for DEMM alone because it was insufficiently reactive on the steel surface and evaporated before an adhesive bond could form.

7. Product development

The early cyanoacrylate instant adhesives possessed a number of advantages over existing adhesive technology, such as ease of use, small quantity, one-part, room temperature cure, fast fixture, high strength, and effectiveness on a variety of substrates. However, they also exhibited a number of disadvantages, among them: useful only on thin gaps, limited thermal stability, brittleness, odor, and limited solvent resistance. Product development efforts have concentrated on overcoming these disadvantages, with minimal loss of the advantages [20].

As demonstrated earlier, the addition of other electron deficient monomers to copolymerize with the cyanoacrylate monomer has not proven to be an effective means of modifying the physical properties of cyanoacrylate-based adhesives. The most effective adhesive improvements have come through the incorporation of various additives, which modify the adhesive physical properties but do not copolymerize with the monomers. These product development efforts have been quite successful in improving the properties of alkyl cyanoacrylate-based adhesives to the point where they can now be used in a huge variety of applications.

8. Viscosity control agents and plasticizers

All of the commercial alkyl cyanoacrylate monomers are low-viscosity liquids, and for some applications this can be an advantage. However, there are instances where a viscous liquid or a gel adhesive would be preferred, such as for application to a vertical surface or on porous substrates. A variety of viscosity control agents, depending upon the desired properties, have been added to increase the viscosity of instant adhesives [21]. The materials, which have been utilized, include polymethyl methacrylate, hydrophobic silica, hydrophobic alumina, treated quartz, polyethyl cyanoacrylate, cellulose esters, polycarbonates, and carbon black. For example, the addition of 5–10% of amorphous, non-crystalline, fumed silica to ethyl cyanoacrylate changes the monomer viscosity from a 2-cps liquid to a gelled material [22]. Because of the sensitivity of cyanoacrylate esters to basic materials, some additives require treatment with an acid to prevent premature gelation of the product.

To minimize the gradual embrittlement that can occur on aging of cyanoacrylate adhesives, plasticizers are added. Some of the materials, which have been used as plasticizers, include phthalates, phosphonates, acyl esters, succinates, and cyanoacetates. The use of allyl, methallyl, and crotyl phthalates is also claimed to improve thermal resistance properties in addition to plasticizing the adhesive [23].

9. Toughening agents

The homopolymers, which are formed from alkyl cyanoacrylate monomers, are inherently brittle. For applications which require a toughened adhesive, rubbers or elastomers can be added to improve toughness, without a substantial loss of adhesion. The rubbers and elastomers which have been used for toughening, include ethylene/acrylate copolymers, acrylonitrile/butadiene/styrene (ABS) copolymers, and methacrylate/butadiene/styrene (MBS) copolymers. In general, the toughening agents are incorporated into the adhesive at 5–20 wt.% of the monomer.

An example of this improvement in toughness can be demonstrated by the addition of Vamac B-124, an ethylene/methyl acrylate copolymer from DuPont, to ethyl cyanoacrylate [24–26]. Three model instant adhesive formulations, a control without any polymeric additive (A), a formulation with poly(methyl methacrylate) (PMMA) (B), and a formulation with Vamac B-124 (C), are shown in Table 4. The formulation with PMMA, a thermoplastic which is added to modify viscosity, was included to determine if the addition of any polymer, not only rubbers, could improve the toughness properties of an alkyl cyanoacrylate instant adhesive. To demonstrate an improvement in toughness, the three formulations were tested for impact strength, 180° peel strength, and lapshear adhesive strength on steel specimens, before and after thermal exposure at 121°C.

The impact strength data for ambient temperature and 121°C cure are shown in Fig. 6. While the addition of the rubber does not initially improve impact strength, it does increase over time at ambient temperature, and after thermal exposure, this improvement is even greater.

The addition of Vamac B-124 to ethyl cyanoacrylate has a more pronounced effect on peel strength, both at ambient temperature and after thermal exposure. After 24 h at ambient temperature, the peel strength of the rubber-toughened formulation is almost 40% greater than the control formulation A without rubber. After heating the test specimens for 2 h at 121°C, the peel strength of formulation A, is almost non-existent, while that of C has increased significantly, as seen in Fig. 7.

An unexpected benefit of the rubber addition to alkyl cyanoacrylate adhesives is

Table 4
Ethyl cyanoacrylate formulations with and without polymeric additives

Material	A (phr)	B (phr)	C (phr)
Ethyl cyanoacrylate	100	100	100
PMMA	–	5	–
Vamac B-124	–	–	10

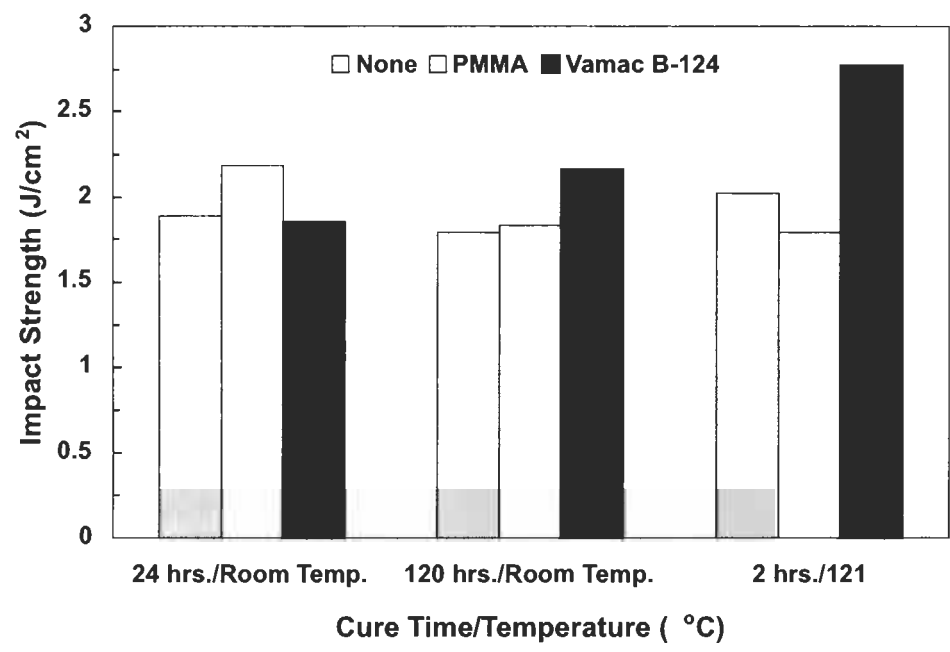


Fig. 6. Impact strengths for ECA, ECA/PMMA, and ECA/Vamac B-124, in the text respectively indicated by A, B and C, with and without thermal exposure at 121°C.

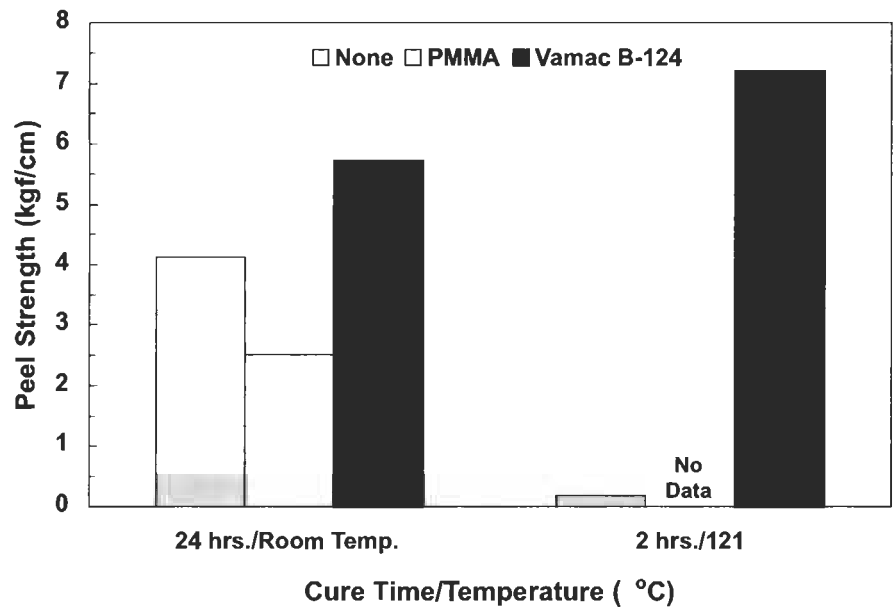


Fig. 7. Peel strengths for ECA, ECA/PMMA, and ECA/Vamac B-124 with and without thermal exposure at 121°C.

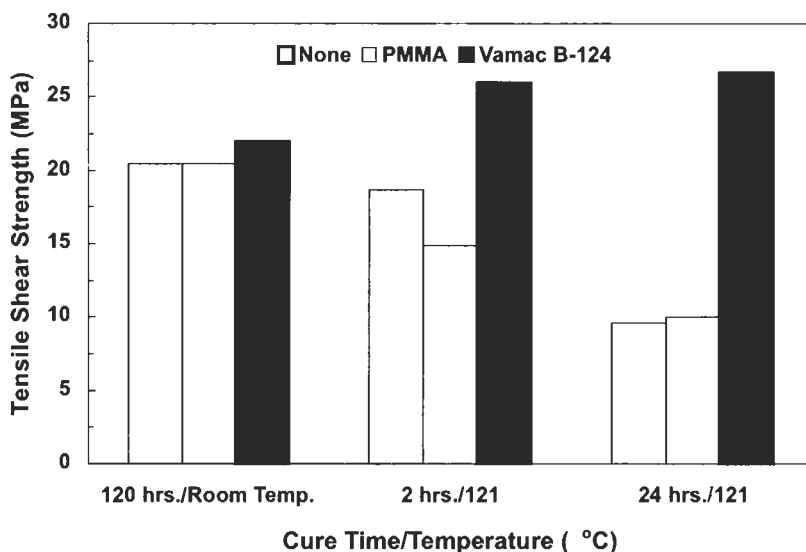


Fig. 8. Steel lapshear tensile shear strengths for ECA, ECA/PMMA, and ECA/Vamac B-124 with and without thermal exposure at 121°C.

the maintenance of tensile shear strength after thermal exposure, as demonstrated in Fig. 8.

The lapshear tensile shear strength of formulation A without any rubber, declines to ca. 50% of its original strength after 24 h at 121°C. In contrast, the lapshear tensile shear strength of formulation C exhibits no loss of adhesion under the same conditions.

The data also demonstrate that the addition of the thermoplastic, PMMA, does not have the significant effect on the toughness or adhesion properties as does the addition of the rubber, Vamac B-124. Clearly, the physical properties of the polymeric additive determine the magnitude of the adhesive physical property modifications, which result from their addition to an alkyl cyanoacrylate monomer.

Care must also be taken in the choice of rubber to insure that the rubber, or one of its additives, does not initiate the premature polymerization of the monomer. Even very low concentrations of a basic or nucleophilic material in the rubber or elastomer will cause the premature polymerization of an alkyl cyanoacrylate adhesive formulation.

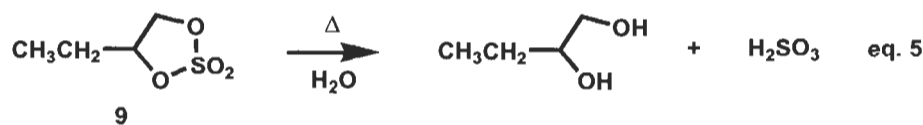
10. Thermal stabilizers

As has been mentioned earlier, polycyanoacrylates possess a relatively low ceiling temperature, because the polymer will thermally revert back to monomer by an

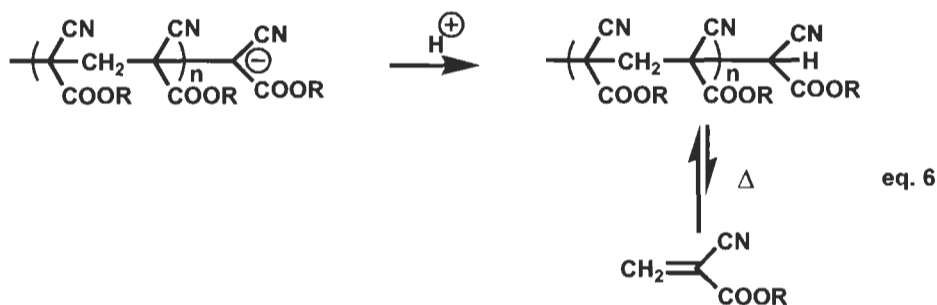
'unzipping' mechanism, as shown in Eq. 4 for the polymer formed from ECA [27].



However, certain additives can decrease the rate of thermal decomposition [28]. These additives include cyclic sulfates, sulfones, sultones, aliphatic and aromatic anhydrides, and polymers with pendant carboxylic acid functional groups. Most of these materials are latent acids, which decompose on heating in the presence of moisture to form a strong acid, as shown for cyclic sulfate, **9**, in Eq. 5.



The liberated acid can then react with the anionic chain ends to inhibit the thermally activated decomposition of the polymer chain, outlined in Eq. 6.



This phenomenon can be demonstrated by both measuring the changes of the thermal properties of the ECA homopolymer and in adhesion tests. The addition of only 1 wt.% of **9** to a sample of the ECA homopolymer significantly increases the onset of decomposition in the thermogravimetric analysis (TGA) of the polymer, as seen in Fig. 9 [29].

This increase in polymer thermal stability translates to improved thermal stability of the adhesive, as shown in Fig. 10 for the steel lapshear adhesive strength after thermal aging at 121°C for 48 h.

Interestingly, this same effect has been observed for the addition of a rubber toughening agent to ethyl cyanoacrylate-based adhesives, as was reported previously. The rubber must contain enough latent acid functionality on the polymer backbone or in an additive to inhibit the thermally activated decomposition of the alkyl cyanoacrylate adhesive polymer.

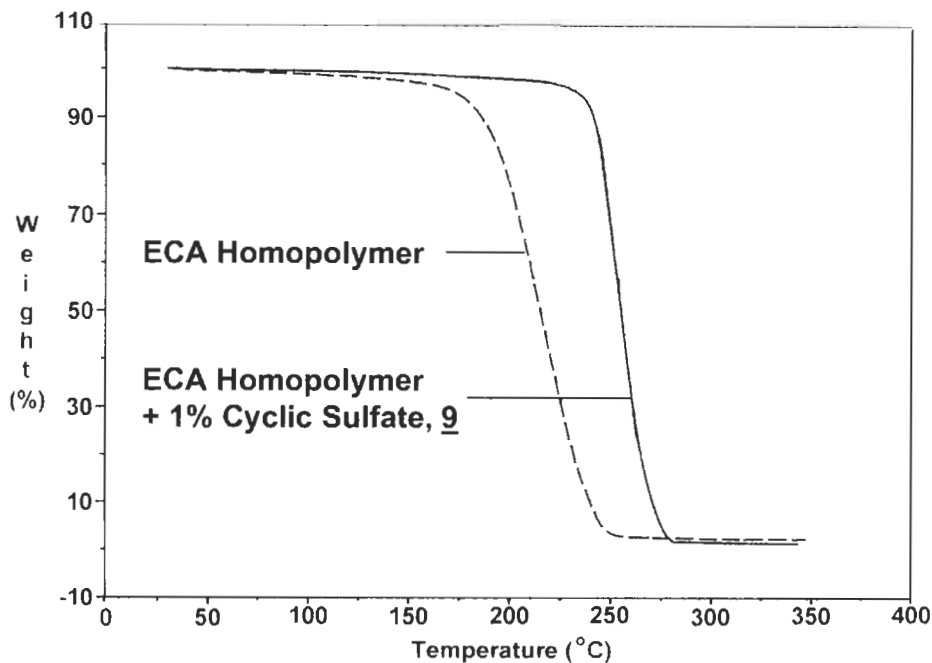
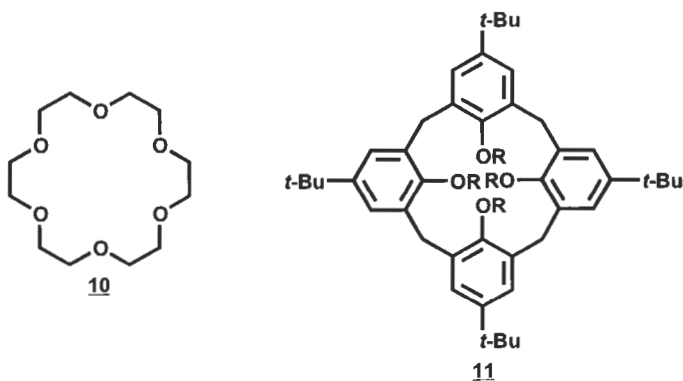


Fig. 9. TGA analysis of ECA homopolymer with and without cyclic sulfate, **9**.

11. Surface insensitivity additives

Because of the need for basic initiators, cyanoacrylate adhesives do not perform well on acidic surfaces, such as wood. However, the addition of sequestering agents, such as crown ethers [30], **10**, or calixarenes [31], **11**, and others [32] to the adhesive improves the reactivity of the adhesive on less active surfaces.



It is assumed that the sequestering agents can complex with trace amounts of

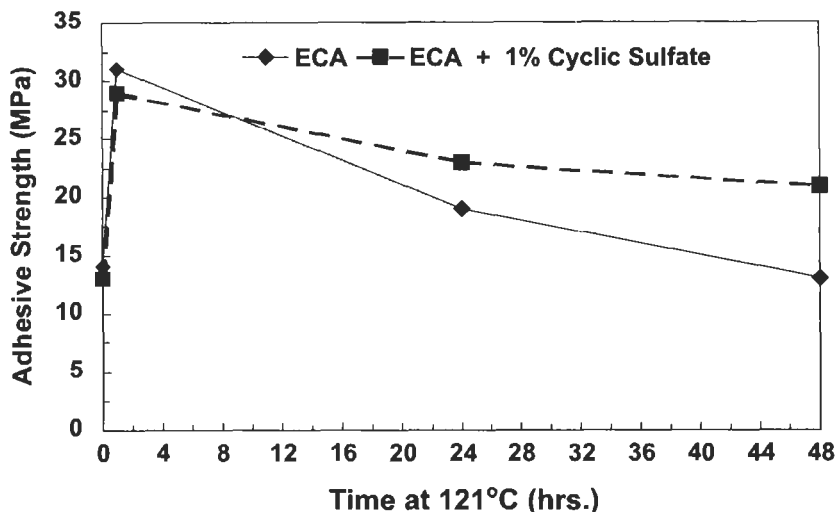


Fig. 10. Tensile shear strength of ECA homopolymer after heat aging at 121°C with and without cyclic sulfate, **9**, on steel lapshears.

surface metallic cations and, therefore, act as a phase transfer reagent to make their counteranions more readily available for initiating polymerization of the adhesive monomers.

12. Primers

Low surface energy substrates, such as polyethylene or polypropylene, are generally difficult to bond with adhesives. However, cyanoacrylate-based adhesives can be effectively utilized to bond polyolefins with the use of the proper primer/activator on the surface. Primer materials include tertiary aliphatic and aromatic amines, trialkyl ammonium carboxylate salts, tetraalkyl ammonium salts, phosphines, and organometallic compounds, which are initiators for alkyl cyanoacrylate polymerization [33–36]. The primer is applied as a dilute solution to the polyolefin surface, solvent is allowed to evaporate, and the specimens are assembled with a small amount of the adhesive. With the use of primers, adhesive strength can be so strong that substrate failure occurs during the course of the shear tests, as shown in Fig. 11.

The mechanism by which the primers are thought to work is relatively straightforward. The primer first diffuses into the polyolefin surface, and subsequently becomes entangled in the polyolefin. The primer molecule can then act as an anchor in the substrate surface for the adhesive polymer, which forms after the primer initiates polymerization of the alkyl cyanoacrylate monomer [37].

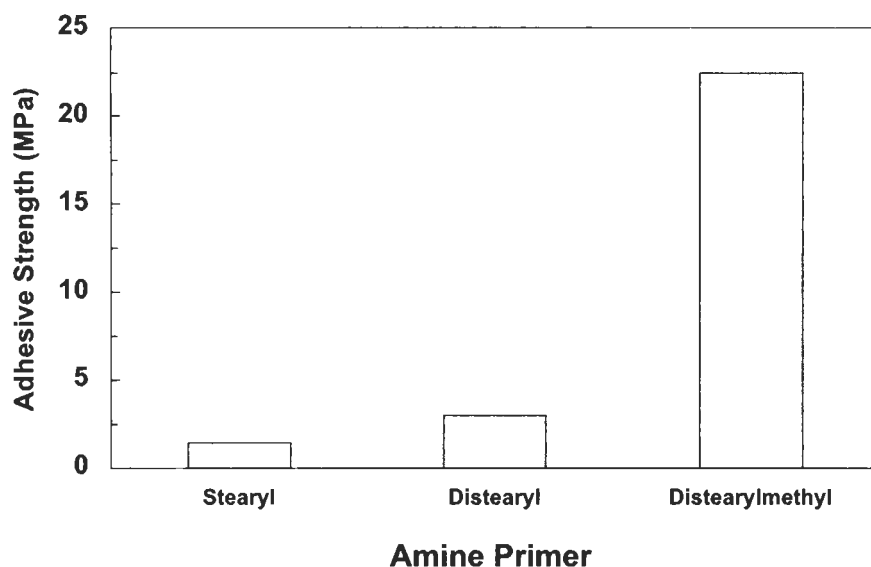
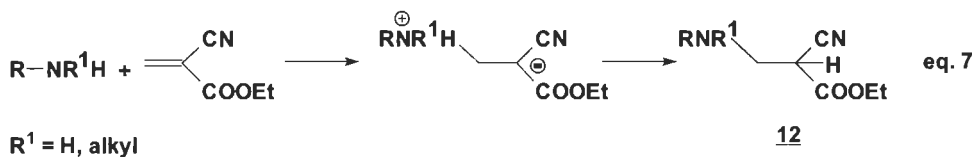


Fig. 11. Block shear strength of ECA on polypropylene blocks with different amines as primers.

However, as can also be seen in Fig. 11, primary and secondary amines do not perform very effectively as primers, compared to tertiary amines, even though they also contain long alkyl chains. It has been demonstrated that, instead of directly initiating ECA polymerization, primary and secondary amines first form aminocyanopropionate esters, **12**, because proton transfer occurs after formation of the initial zwitterionic species, as shown in Eq. 7 [8,9].



In contrast, tertiary amines do not possess a proton to transfer, and the reaction of the Michael-type addition adduct with ECA can only initiate polymerization to form high molecular weight adhesive polymer, as shown earlier in Scheme 1.

This difference in reactivity between the different classes of amines explains the difference in the primer performance on polyolefin substrates with ethyl cyanoacrylate-based adhesives [37]. Since primary and secondary amines form low molecular weight species, a weak boundary layer would form first, instead of high molecular weight polymer. Also, the polymer, which does ultimately form, has a lower molecular weight, which would lower adhesives strength [8,9].

For surfaces which do not readily polymerize alkyl cyanoacrylate monomers, the adhesive monomer can be applied, a part assembled and repositioned, if

necessary, and the adhesive subsequently polymerized by an overspray of an initiator [38]. Tertiary aromatic amines, such as *N,N*-dimethyl-*p*-toluidine are particularly effective for this purpose. Not only do they initiate polymerization, but they also provide good depth of cure and surface cure because the polymerization is not inhibited by oxygen like the polymerization of acrylates or methacrylates. While tertiary alkyl amines initiate polymerization, they create a skin-over effect, where the surface of a drop of the adhesive is cured, but the interior remains a liquid.

13. Manufacturers

Cyanoacrylate adhesives are ubiquitous with several major manufacturers around the globe. They include, along with their brand names, Alpha Giken (Alpha Ace and Alpha Techno), Henkel/Loctite (Prism, Sicomet, Superbond, and Quicktite), National Starch (Permabond), Three Bond (Super Three), and Toa Gosei (Aron Alpha and Crazy Glue).

14. Applications

Because they can rapidly bond a wide variety of substrates and because of their recent improvements in performance, cyanoacrylate instant adhesives have found uses in a wide variety of industrial and consumer applications.

They are utilized for home use to repair broken rubber, metal, and ceramic objects. They can even be used to bond plastics, with the use of an appropriate primer. A few of the home applications include:

- Repair of loose side-panel stripping on car doors.
- Door gasketing reattachment.
- Small interior vinyl or plastic repairs in automobiles.
- Creating crafts, decorations, or models.
- Small reattachments for loose tiles, wallpaper, or linoleum.

Industrial uses include automotive, small, close fitting parts in machinery, hardware, speaker magnets, toys, and sporting goods. Specific industrial applications include:

- Speaker magnet assembly.
- Gasket adhesive on transformers.
- Assembly of medical and veterinary devices made of polypropylene.
- Non-structural applications on the space shuttle.

Law enforcement agencies even use cyanoacrylates to obtain fingerprints on irregularly shaped objects and porous surfaces [39]. They first place the object to be tested in a tank with warmed ethyl cyanoacrylate. The ECA vapor migrates onto

the natural oils, which remain from the fingerprint, and the monomer selectively polymerizes at that site to reveal the presence of the fingerprint.

15. Medical

Despite the universal use of sutures for wound closure, there is a need to utilize adhesives instead, because of their ease of use and the reduced risk of infection. Alkyl cyanoacrylate adhesives have been studied extensively for this use, and a significant amount of research has been performed to evaluate their interaction with living tissue [40,41]. They have been approved for external use only, because of concerns with the fact that the polymers do not readily biodegrade and can cause inflammation around the area to which it was applied. However, these concerns are reduced for *n*-butyl cyanoacrylate, as compared to the ethyl cyanoacrylate. There is even some evidence that their use as liquid sutures actually reduces the rate of infection around the healing wound or surgical incision [42].

16. Packaging

Given the high reactivity of cyanoacrylate adhesives, creating packaging which is unreactive toward the adhesive is critical in obtaining a reasonable shelf-life for commercial products. The interior package surface must be neutral or slightly acidic, impermeable to water, and allow for multiple adhesive uses. Most packages are composed of polyolefins, such as polyethylene or polypropylene, which are free of any basic contamination from stabilizers, processing aids, or mold release. The packaging itself can take several forms, bottles, tubes, bottles with brush applicators, syringes, and even pen-like dispensers.

17. Health and safety

While alkyl cyanoacrylate-based adhesives are used globally in a large variety of domestic and commercial settings, their physical and toxicological properties must be considered. Alkyl cyanoacrylate polymerization is a very exothermic reaction, so care must be taken to prevent the contamination of large quantities with any materials, which might initiate a very rapid, runaway reaction. Also, alkyl cyanoacrylate monomers and the polymers which they form, will burn, and users should avoid their use near sparks or open flames.

Their vapors are irritating to nasal passages and to the throat. These effects are noticeable in airborne concentrations of 2–5 ppm [43,44]. When large quantities of these materials are used, efficient ventilation is required. Because alkyl

cyanoacrylate monomers rapidly polymerize when they come into contact with skin or eye tissue, care must be taken in their handling to avoid direct contact. However, if contact does occur, soaking in warm water will eventually loosen the adhesive bond, which is formed.

Polymeric ethyl cyanoacrylate exhibits very low toxicity properties. In tests with laboratory rats, oral administration of 6400 mg/kg of the polymer failed to harm the test animals. Some skin irritation did occur in tests on guinea pigs, but skin sensitization or absorption through the skin was not observed [45].

Acknowledgements

The author wishes to acknowledge his Loctite colleagues, many of whom have spent much of their careers advancing cyanoacrylate adhesive technology, for their help in the preparation of this chapter, especially John O'Connor, John Woods, Shabbir Attarwala, and David Melody. He also wishes to thank librarian Margaret Orszak for her assistance with the literature search.

References

1. Ardis, A.E., U.S. Patent 2,467,926, 1949.
2. Coover, H.W., Jr. and Shearer, N.H., U.S. Patent 2,794,788, 1957.
3. Lee, H. (Ed.), *Cyanoacrylate Resins — The Instant Adhesives*. Pasadena Technology Press, Los Angeles, CA, 1986.
4. Ardis, A., U.S. Patent 2,467,927, 1949.
5. Joyner, F. and Hawkins, G., U.S. Patent 2,721,858, 1955.
6. Klemarczyk, P., *Polymer*, **39**(1), 173 (1998).
7. Coover, H., Dreifus, D. and O'Connor, J., In: Skeist, I. (Ed.), *Handbook of Adhesives*, 3rd edn. Van Nostrand Reinhold, New York, NY, 1990, p. 463.
8. Klemarczyk, P., *Polymer*, **42**(7), 2837 (2001).
9. Krylova, T., Kolomnikova, G., Garbuzova, I. and Golobolov, Y., *Russ. J. Gen. Chem.*, **64**(3), 371 (1994).
10. Pepper, D., *J. Polym. Sci. Polym. Symp.*, **62**, 65 (1978).
11. Joyner, F. and Shearer, B., U.S. Patent 2,756,251, 1956.
12. Ito, K. and Kondo, K., U.S. Patent 3,557,185, 1971.
13. Lizardi, L., Malofsky, B., Liu, J.C. and Mariotti, C., U.K. Patent GB 2,107,328B, 1985.
14. Kawamura, S. et al., U.S. Patent 3,652,635, 1972.
15. Pepper, D., *Makromol. Chem. Macromol. Symp.*, **60**, 267 (1992).
16. Buck, C., U.S. Patent 4,012,402, 1977.
17. Kennedy, J., Midha, S. and Godhari, A., *J. Macromol. Sci., Chem.*, **A**, **28**(2), 209 (1991).
18. Golobolov, Y., Gruber, W. and Nicolaisen, C., U.S. Patent 6,096,848, 2000.
19. Guest, A., In: Lee, H. (Ed.), *Cyanoacrylate Resins — The Instant Adhesives*. Pasadena Technology Press, Los Angeles, CA, 1986, p. 56.
20. O'Connor, J., *ChemTech*, September, 51 (1994).
21. Wicker, T. and Shearer, N., U.S. Patent 3,178,379, 1965.

22. Litke, A., U.S. Patent 4,447,606, 1984.
23. Wicker, T., U.S. Patent 3,354,128, 1967.
24. O'Connor, J. and Liu, J.C., U.S. Patent 4,440,910, 1984.
25. O'Connor, J. and Zimmerman, W., *Factors affecting adhesion of cyanoacrylate adhesive to bright, anodized surfaces*. Paper to American Electroplaters Society, Denver, CO, 1976.
26. O'Sullivan, D. and Melody, D., U.S. Patent 3,832,334, 1974.
27. Birkinshaw, C. and Pepper, D., *Polym. Degr. Stab.*, **16**, 241 (1986).
28. Attarwala, S. and Klemarczyk, P., U.S. Patent 5,328,944, 1994.
29. Klemarczyk, P., *J. Adhes.*, **69**, 293 (1999).
30. Motegi, A., Isowa, E. and Kimura, K., U.S. Patent 4,171,416, 1979.
31. Harris, S., McKervey, M., Melody, D., Woods, J. and Rooney, J., U.S. Patent 4,556,700, 1985.
32. Liu, J.C., U.S. Patent 4,906,317, 1990.
33. Liu, J.C., U.S. Patent 5,079,098, 1992.
34. McDonnell, P. and Kneafsey, B., U.S. Patent 4,869,772, 1989.
35. Kimura, K. and Ito, K., U.S. Patent 5,110,392, 1992.
36. Okamoto, Y. and Klemarczyk, P., U.S. Patent 5,066,743, 1991.
37. Courtney, P. and Salerni, C., *Adhes. Age*, **44(2)**, 38 (2001).
38. Buck, C., U.S. Patent 3,903,055, 1975.
39. Bourdon, L., U.S. Patent 4,297,383, 1981.
40. Forseth, M., O'Grady, K. and Toriumi, D., *J. Long Term Eff. Med. Impl.*, **2(4)**, 221 (1992).
41. John, G., In: Zimmerman, T. (Ed.), *Textbook of Ocular Pharmacology*. Lippincott-Raven, Philadelphia, 1997, p. 671.
42. Eiferman, R. and Snyder, S., *J. Arch. Ophthalmol.*, **101**, 958 (1983).
43. McGee, W., Oglesby, F., Raleigh, R. and Fassett, W., *Am. Ind. Hyg. Assoc. J.*, **29**, 558 (1968).
44. *TLV for Chemical Substances in Work Room Air*. American Conference of Government Industrial Hygienists, Cincinnati, OH, 1975.
45. Thomsen, W., In: Schneberger, G. (Ed.), *Adhesives in Manufacturing*. Marcel Dekker, New York, NY, 1983, p. 305.

Phenolic resins: some chemistry, technology, and history

William D. Detlefsen^{*}

Springfield, OR, 97477, USA

1. Introduction

Thousands of technical papers and many books have been written on the subject of phenolic resins. The polymer is used in hundreds of diverse applications and in very large volumes. It is used worldwide. In fact the term ‘phenolic resin’ encompasses a wide variety of materials based on a broad range of phenols and co-monomers. In this short article, we cannot expect complete coverage. Our hope is that we can provide an understanding of the fundamental chemistries, uses, and values of these materials as well as enough references to permit the interested reader to begin his own exploration of the topic.

2. History

Phenolic resins were the first totally synthetic plastics invented. They were commercialized by 1910 [1]. Their history begins before the development of the structural theory of chemistry and even before Kekulé had his famous dreams of snakes biting their tails. It commences with Gerhardt’s 1853 observations of insoluble resin formation while dehydrating sodium salicylate [2]. These were followed by similar reports on the behavior of salicylic acid derivatives under a variety of reaction conditions by Schroder et al. (1869), Baeyer (1872), Velden (1877), Doebner (1896 and 1898), Speyer (1897) and Baekeland (1909–1912) [3–17]. Many of these early reports appear to involve the formation of phenolic polyesters rather than the phenol–aldehyde resins that we think of today. For

^{*} Corresponding author. E-mail: wdetlefsen@aol.com

the first four or five decades, these resins were viewed as nuisances interfering with purification of phenolic compounds. Scientists of the day had no concept of polymers or macromolecules.

Adolph Baeyer is credited with the first recognition of the general nature of the reaction between phenols and aldehydes in 1872 ([2,5–7]; [18], Table 5.1). He reported formation of colorless resins when acidic solutions of pyrogalllic acid or resorcinol were mixed with oil of bitter almonds, which consists primarily benzaldehyde. Baeyer also saw resin formation with acidic and basic solutions of phenol and acetaldehyde or chloral. Michael and Comey furthered Baeyer's work with additional studies on the behavior of benzaldehyde and phenols [2,19]. They studied a variety of acidic and basic catalysts and noted that reaction vigor followed the acid or base strength of the catalyst. Michael et al. also reported rapid oxidation and darkening of phenolic resins when catalyzed by alkaline materials.

Prior to 1890, formaldehyde was not commercially available [2]. Thus the first phenol–formaldehyde resins were made using formaldehyde equivalents such as methylene diacetate or methylal [2,20]. The first true phenol–formaldehyde resin was made by Kleeberg at the direction of Emil Fisher in 1891 [2,21]. Saliginen (*o*-hydroxymethyl phenol) was recognized as a condensation product of phenol and formaldehyde in 1894 and was the subject of United States patents in 1894 and 1896 [22,23].

There was significant interest in developing commercial processes based on phenolic resins in the 1890–1910 era. By this time, cellulose nitrate, vulcanized rubber, and viscose rayon had all found places in commerce [24]. Smith patented processes for manufacture of commercially useful molded articles from phenolic in 1899–1900 [2,25–28]. His products were made with phenol, paraldehyde (2,4,6-trimethyl-1,3,5-trioxane) or paraformaldehyde, and additives in the presence of HCl at elevated temperatures.

Blumer, Meyer, and Zwickau described methods for making varnishes and coatings from phenol or α -naphthol and aqueous formaldehyde solutions at about the same time ([2]; [18], Table 5.1; [29–33]). Luft suggested the use of phenolics for fabric and leather coatings, billiard balls, buttons, electrical insulators, and linoleum and celluloid substitutes. He also proposed the carbonization of phenolic threads for incandescent bulb filaments [2,34–38]. Story developed casting methods for phenolic materials [1,14–17,39–41]; and Baekeland introduced his Bakelizer and received his patents for forming molded articles under heat and pressure in 1907–1909 ([2]; [18], Table 5.1; [42,43]). With the exception of Baekeland's inventions, none of these early phenolic-based technologies saw significant commercial success at the time, though phenolics were successfully used in many of these applications later on [44]. The General Bakelite Co. was established in the U.S. to manufacture phenolic molding compounds in 1910 [45,46]. A German company was also formed for the same purpose, also in 1910. Both were based on the Bakelite process technology.

Table 1
U.S. phenolic resin volume growth

Year	Production (kt)	Average growth rate (%)
1910 ^b	0	—
1920 ^c	2	20
1925 ^c	5	17
1930 ^c	8	9
1943 ^a	66	12
1944 ^a	107	62
1956 ^f	227	6
1966 ^f	442	6
1975 ^d	500	2
1983 ^b	1022	8
1985 ^h	1287	3 ⁱ
1993 ^e	1400	3 ⁱ
1995 ^h	1672	3 ⁱ
2000 ^{g,h}	1909	3
2005 ^{g,h}	2168	2

^a Carswell [44]. ^b Knop and Pilato [45]. ^c Ellis [48]. ^d Seymore and Carraher [24]. ^e Fried [49].

^f Kirk-Othmer [50]. ^g Estimated. ^h North American. ⁱ Ten-year average.

The largest share of the early uses of phenolic resins fell into the molded article category. Until about 1920, most of the material was used for electrical insulators and industrial parts. However, after 1920, phenolic began to see use in a wide variety of consumer products, jewelry, and even art objects [47]. Much of the jewelry is highly valued by collectors today. The list of Bakelite objects available for sale on the Internet today is illustrative. It includes candlesticks, an owl lamp, a nail-polishing machine, cruets, scent bottles, carved powder boxes, necklaces, belt buckles, bangles, coasters, cigarette cases, a watch, and many others. Bakelite radios, telephones, and other appliances are also collectors items. A detailed review of the early development of phenolics is provided by Carlton Ellis [2]. Table 1 shows some selected market volume data illustrating the growth of phenolic use.

In 1932, the first plywood hot press was installed in the United States. This marked the advent of the large market for phenolic wood adhesives [51]. By 1962, the volume of phenolic wood adhesives had reached about 33 kt (solids) in the U.S. Growth was accelerated in 1962 with the development of Southern pine plywood. By 1979, the consumption of phenolic plywood adhesives exceeded 220 kt or about 25% of phenolic resin production [51]. Phenolic adhesive demand for wood products took another jump in 1964 with the commencement of waferboard production. The first oriented strandboard (OSB) plants were built in 1981 [52]. OSB soon replaced most of the waferboard production and began a period of

rapid growth, which continues to the present. This new material raised worldwide phenolic consumption in wood panel products to over 1600 kt in 1995. Wood products now claim 55–65% of all phenolic made and account for approximately 75% of phenolic growth in North America since 1985 ([53]; [18], Table 6.3). The range in these figures is indicative of some disagreement between various estimates. North America accounts for slightly over half of the global phenolic resin demand. Automotive, foundry, and oilfield uses have also been important growth areas.

Despite its advanced age, as technologies go, phenolic technology is far from geriatric. It has not undergone the obsolescence that is the normal result of the technology cycle [54]. Phenolic resins continue to be an important part of the world economy and phenolic resin volumes continue to grow at about 2–4% annually despite their large volume base.

3. Phenolic capability and value

The reasons for the long-term, commercial robustness of phenolic technology include low cost, versatility, heat and flame resistance, durability, strength and stiffness, low toxicity, and ease of processing. Some key factors are discussed in detail below.

By far the preponderance of the 3400 kt of current worldwide phenolic resin production is in the form of phenol–formaldehyde (PF) reaction products. Phenol and formaldehyde are currently two of the most available monomers on earth. About 6000 kt of phenol and 10,000 kt of formaldehyde (100% basis) were produced in 1998 [55,56]. The organic raw materials for synthesis of phenol and formaldehyde are cumene (derived from benzene and propylene) and methanol, respectively. These materials are, in turn, obtained from petroleum and natural gas at relatively low cost ([57], pp. 10–26; [58], pp. 1–30). Cost is one of the most important advantages of phenolics in most applications. It is critical to the acceptance of phenolics for wood panel manufacture. With the exception of urea–formaldehyde resins, PF resins are the lowest cost thermosetting resins available. In addition to its synthesis from low cost monomers, phenolic resin costs are often further reduced by extension with fillers such as clays, chalk, rags, wood flours, nutshell flours, grain flours, starches, lignins, tannins, and various other low cost materials. Often these fillers and extenders improve the performance of the phenolic for a particular use while reducing cost.

Phenolic resins are adaptable to many applications. The list is very long, however, the major uses are wood binders, glass insulation binders, molding compounds, laminates, foundry binders, coatings, friction linings, abrasives, and oil well propants [59–66]. They have found their way into a number of new, high technology uses such as rocket motor wear parts, military armor, sports equipment,

photoresists for computer chip manufacture, epoxy crosslinkers, circuitboard binders, and microchip module packaging. There has been a renewal of interest in the use of phenolics for aircraft construction because of their excellent flame resistance and low smoke generating properties ([18], p. 117). This great versatility stems from the excellent native properties of phenolic polymers and the wide range of phenolic formulas available. The polymer properties follow from its high cross-link density and chemical stability. The wide range of formulations follows from the compatibility of phenolic resins with a great number of fillers, compounding materials and solvents; response to a variety of catalysts; the commercial availability of a number of phenols; and the ability of phenols to react with a range of co-monomers. In addition to aldehydes, alkenes such as styrene, dicyclopentadiene, vinyl benzenes, polyhydric alcohols, and various drying oils are also popular co-monomers.

The physical properties of phenolics are often a major factor in their selection. They have sufficient strength to permit their use in many applications where metals and ceramics have been the traditional materials of choice [59,60]. Phenolics have the best heat resistance of any organic polymer ([18], p. 117). Outstanding dimensional stability and creep resistance are also phenolic strengths [67–72]. Phenolics may be formulated with excellent resistance to acids, organic solvents, and water [70]. They are subject to attack by strong base and formic acid, though this weakness can be mitigated by proper selection of the phenol. Phenolics make excellent electrical insulators [72]. Their high crosslink density and adhesive properties provide high mechanical strength. Though our focus here will not be on applications, we hope to be able to relate the chemistry of phenolics to some of their performance capabilities as we go. We will try to include elements of both chemistry and practice in our discussions.

4. Overview: the basics

It is traditional to divide phenolics into two main categories. These are novolacs and resoles. This system of classification is consistent with the division of applications as well as the compositions and conditions of resin manufacture. Novolacs are used primarily in the molding industries and electronics applications. Resoles are used primarily as binders for other materials.

The term novolac refers to the early use of phenolic to replace expensive shellac-based coatings. Novolacs are now those resins made at formaldehyde-to-phenol molar ratios of less than one-to-one. They are generally, though not always, manufactured under acidic conditions. Sulfuric or oxalic acids are most often chosen as catalyst though aromatic sulfonic acids and phosphoric acid are also quite common. Many other acids are used for special purposes. The finished novolac resin is incapable of further polymerization or crosslinking and therefore

requires the addition of a methylene donor or other aldehyde equivalent for curing. In other words it is thermoplastic. Hexamethylenetetramine (hexa) is the most common material used to provide the needed crosslinking capability. In addition to a crosslinker, elevated temperatures and, sometimes, additional catalysts are required. Resorcinol-formaldehyde and phenol-resorcinol-formaldehyde are novolac resins that are exceptions to these heat requirements. They generally cure well at room temperature. They are also exceptional in that they are usually base-catalyzed novolacs. Paraformaldehyde is most commonly used as a formaldehyde source during the curing of resorcinolic novolacs, though other patented systems based on oxazolidines and the like are also available [73–75].

Though novolacs usually start out in aqueous solution, they generally become water-insoluble as the reaction proceeds. The aqueous phase is usually distilled or decanted off of the resin. During this process, the resin must be maintained at a temperature above its freezing point. Novolacs are usually discharged from the reactor in a molten state and allowed to solidify before further processing or packaging. Often they are dropped onto a cooled metal conveyor belt to speed solidification and facilitate handling. In other cases, they are discharged into cooling pans or simply onto a cooling floor. Novolacs are sold in several solid forms, which include chunks, flakes, powders, and pastilles. Methods for obtaining these forms range from breaking up cooled resin with a sledge hammer to highly automated grinding and pellet formation. For some applications, photoresists for example, the novolacs are often taken up in solvent and shipped as liquids.

Resoles are usually those phenolics made under alkaline conditions with an excess of aldehyde. The name denotes a phenol alcohol, which is the dominant species in most resoles. The most common catalyst is sodium hydroxide, though lithium, potassium, magnesium, calcium, strontium, and barium hydroxides or oxides are also frequently used. Amine catalysis is also common. Occasionally, a Lewis acid salt, such as zinc acetate or tin chloride will be used to achieve some special property. Due to inclusion of excess aldehyde, resoles are capable of curing without addition of methylene donors. Although cure accelerators are available, it is common to cure resoles by application of heat alone.

Most resole products are currently shipped and applied in aqueous solution, though spray-dried resoles are also made in fairly large volumes. Solid, ground resoles are produced for a few special applications, however, these are somewhat difficult and relatively expensive to make and do not show superior performance in most applications. The bulk of the resole production goes into adhesives for plywood, laminated veneer lumber, oriented strandboard, hardboard, and other wood products. Significant amounts are also used as glass binders for fiberglass insulation, glass laminating and impregnating, foundry binders, and paper saturation. Much of the phenolic paper is destined to become an overlay for other phenolic-containing wood-panel products.

5. Safety issues with phenolic resins

Before we discuss the synthesis of phenolic resins, it is fitting that we mention safety issues surrounding this activity. The manufacture of phenol–formaldehyde resins, or any phenolic resin, is a potentially dangerous undertaking both in the laboratory and in the manufacturing facility. There are several levels of danger of which chemists and reactor operators should be well aware. The resins themselves are generally, though not universally, rated non-hazardous, however, the monomers may be highly toxic, flammable, or corrosive to human flesh. When toxic monomers remain in the finished resin at sufficient levels, the resin may also carry a hazardous rating.

Phenol is a highly corrosive and toxic material with regard to human tissue. It penetrates skin readily and causes severe chemical burns. Exposure of relatively small skin areas can result in death. A worker fatality relating to phenol exposure occurred in Wisconsin in late 1999. Some phenolics, such as cashew nut oils, are also sensitizers and show long-term exposure effects similar to those seen with poison ivy. Some *para*-alkyl phenols have shown estrogen-mimicking effects with chronic exposure. These may produce symptoms such as breast enlargement and development of other female secondary traits in males. Estrogen-mimicking activity appears to be confined to a definite range of alkyl chain lengths and ring positions that permit them to act as estrogen receptor agonists.

Formaldehyde has been rated as a possible carcinogen by the United States Occupational Safety and Health Act (OSHA) rules and should be handled with due caution. It is also a strong lacrymator and choking respiratory irritant. It irritates the skin, eyes, and mucous membranes [76]. Since it is used for tanning leather, it is obvious that formaldehyde has a high potential for reactions with proteins. Formaldehyde gas is flammable and most formalin solutions contain significant amounts of methanol, which is also volatile, toxic, and flammable.

The alkalis and acids used to catalyze phenolic reactions are highly corrosive and any exposure is a potentially serious health threat. Those handling these materials should be thoroughly familiar with the appropriate Material Safety Data Sheets and emergency procedures. We do not purport to provide any specific health guidance here except to say that one should consult the appropriate references and be properly trained when making phenolic resins.

In addition to the health hazards mentioned above, it is important be aware of the potential for explosions due to the Cannizzarro reaction ([77], pp. 36–37). When strong alkali is mixed with formaldehyde solutions, the Cannizzarro reaction will result in a rapid and spontaneous reaction even at relatively low temperatures. Depending on conditions, an induction period may be seen. The main organic products of this reaction are methanol and formic acid (salt form). In addition, significant amounts of hydrogen are evolved. The potential for explosions in closed containers is high, and even open containers will often erupt.

The Cannizzarro can best be avoided by mixing ingredients in the right order to insure that the phenate salt is formed prior to introduction of formaldehyde and that the desired competing reactions are faster than the Cannizzarro under the prevailing conditions. In general this would involve premixing the strong base with phenol and water before any formaldehyde is introduced. Slow addition of formaldehyde to such mixtures at temperatures greater than 60°C makes it probable that the concentration of formaldehyde is never high enough to promote much Cannizzarro. Cannizzarro also leads to solids yield losses so its avoidance has economic as well as safety benefits.

The Cannizzarro occurs with aldehydes containing no α -hydrogen such as formaldehyde or benzaldehyde. With α -hydrogens present, as with acetaldehyde, ketones, or other higher aliphatic aldehydes, the aldol reaction is prevalent ([77], pp. 6–9). This reaction is also rapid and quite vigorous once initiated. Like the Cannizzarro, there may be a deceptive induction period before the reaction takes off. Once these reactions begin to occur, the rates increase rapidly due to autocatalytic behavior. Aldols are seen under either basic or acidic conditions. Although the aldol is a useful synthetic reaction, it is usually an unwanted side reaction during phenolic manufacture.

Reasonable procedures for manufacturing resoles and novolacs are presented in subsequent sections. These procedures utilize the a concept known in the industry as programmed formaldehyde addition to avoid the problems mentioned above as well as aiding in control of the exothermic reactions resulting from the manufacture of the desired phenol–aldehyde products. These reactions are also extremely exothermic.

An example of what can happen in a production situation is provided in Fig. 1. This photo shows the devastation resulting from a phenol–formaldehyde reactor explosion that occurred at the Borden Chemical plant in Demopolis, Alabama on June 28, 1974. In this explosion, the stainless steel reactor was blown to bits. The reactor operators' control room was obliterated. Two people were killed and several others were injured. All nearby property was demolished and windows were broken in homes for a distance of five miles from the plant.

As a result of the explosion in Demopolis, Borden Chemical developed some new concepts with regard to reactor safety. These included new rules for maximum batch size calculated on the basis of reactor relief areas, cooling capacities, and reagent concentrations, as well as a continued effort to improve PF manufacturing safety. This attention led to adoption of the programmed formaldehyde technique, a system originally developed by Monsanto. Through an unprecedented cooperative effort, all of the major PF resin manufacturers in North America have joined forces to reduce PF manufacturing risks. This group has also received much help from Fauske and Associates, OSHA, and the EPA. As a result of these efforts, a number of other technical innovations were developed including automatic control loops for temperature control and deluge, improved



Fig. 1. Demopolis 1974 explosion. (Photo courtesy of Don Schaechtel and Borden Chemical.) The reactor and the operator's station were located approximately in the center of this photo before the explosion. The large tanks in the background hold about 10,000 gallons (U.S.).

maintenance and testing of safety systems, and better calculations of relief area requirements.

The Reactive System Screening Tool (RSST) developed by Fauske and Associates provided the key to understanding the thermal potential of PF reactions in relationship to the composition and temperature variables available. Figs. 2 and 3 show RSST results for some resoles and novolacs, respectively. In all cases, these are production formulas that are adjusted for solids by water addition. The benefits of water for absorption of heat and reducing the reaction rates is clear in the figures. The reaction initiation temperatures are also clearly defined with resoles showing significant reaction rates at 40–50°C and novolacs beginning to react at about 70°C. It is important that the reaction mixtures be above these minimum temperatures during the programming of the formaldehyde. This insures that formaldehyde reacts as it is added and does not build up to dangerous concentrations. Programmed formaldehyde addition is appropriate for both resoles and most novolacs.

The RSST charts also point out another important difference between resoles and novolacs. Fig. 2 shows that resole reactions take place in two distinct stages with initiation temperatures at about 40–50°C and 100–140°C, respectively.

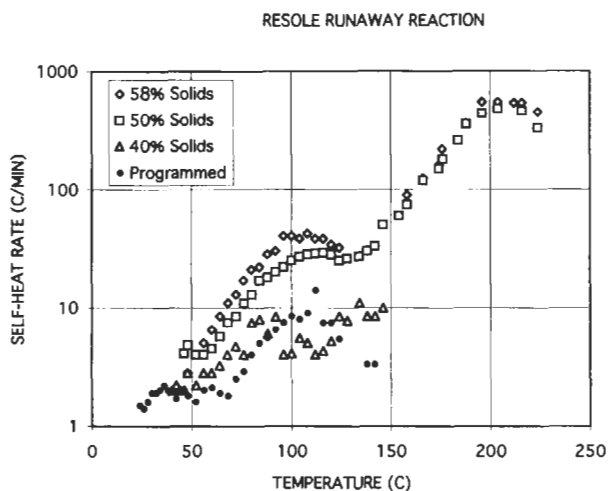


Fig. 2. RSST results on various resoles. The three bulk-charged resoles are at approximately 58% solids, 50% solids, and 40% solids. The programmed formaldehyde has no water charged except that contained in the 50% formaldehyde. The 50 and 58% solids resins reach self-heat rates of nearly 600°C/min. The 40% solids resin does not exceed 10°C/min. (Chart courtesy of Borden Chemical and Bill Burleigh.)

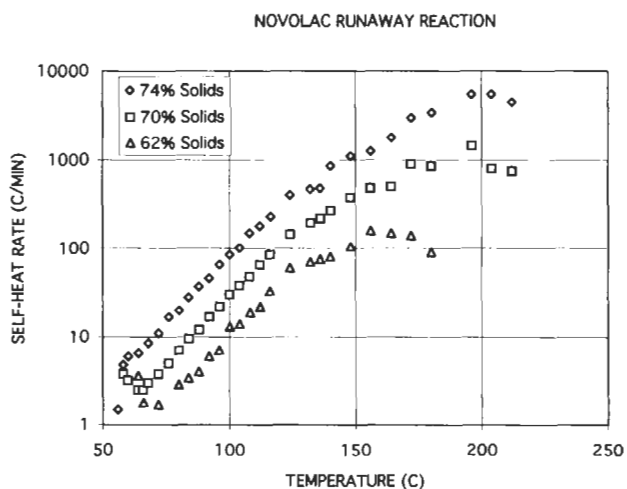


Fig. 3. RSST results on some typical production novolacs. The solids on these materials are 74, 70, and 62%, respectively. Note that the reaction does not become initiated significantly below 70°C and that the high solids system is capable of self-heating rates as high as 5500°C/min under these conditions. (Chart courtesy of Borden Chemical and Bill Burleigh.)

The two reaction stages represent those of the methylation and condensation polymerization reactions. It is difficult to decide exactly where the polymerization reaction is initiated due to the dominance of methylation data in the lower temperature region where the two are overlaid. We must bear in mind that these tests start with raw phenol and formaldehyde. Therefore, there is nothing available for condensation polymerization early in the process. Methylation must occur first. From practice, we know that condensation occurs at a significant rate at 75°C and at a slow rate even in frozen resins. The apparent initiation temperatures are somewhat dependent on heating rate when using the RSST with these high monomer reaction mixtures. It is clear from the figure that, when the solution is sufficiently dilute, the condensation reaction is highly suppressed and poses little danger. The exotherm rate of the programmed formaldehyde batch could have any form and is a consequence of formaldehyde charging rate, which is under the control of the operator. The heat of reaction for the methylation reaction is reported to be about 247 cal/g (1033 J/g) formaldehyde for a solution with about 0.7 formaldehyde-to-phenol and 0.1 sodium hydroxide-to-phenol molar ratios, respectively [78]. The total heat evolution for the methylation and condensation polymerization reactions is reported to be from 580–809 cal/g (2424–3385 J/g) formaldehyde [78]. Notice that these numbers are reported on a formaldehyde basis, not a PF resin basis.

In Fig. 3 there appears to be only one reaction step for the novolac from beginning to end. This indicates that novolac methylation and condensation reactions occur simultaneously at all temperatures. This, in turn, shows that the activation energy for the condensation reaction is similar to or less than that for the methylation. In other words, the methylation is the rate-determining step in the process.

The specific heat of the PF polymer system is on the order of 0.5–0.6 while that of water is 1.0 [78]. Water therefore exerts a double effect in the control of exotherm through raising the ability of the system to absorb heat and through dilution to reduce reaction rates. Water provides additional safety through its high heat of vaporization and low boiling point, relative to other PF components. To initiate boiling of water consumes about 7 times as much energy as is required to heat it from 20 to 100°C. This is why most PF reactors are equipped with vacuum-based temperature control systems in addition to cooling coils.

There are two philosophies regarding how to best slow a runaway reaction. One view holds that simple water deluge is the best method as it provides immediate cooling and dilution. The anti position is that the batch should be deluged and neutralized simultaneously. Kumpinsky reports that minimum self-heat rates occur between pH 4 and 7 [78]. Since neutralization involves production of additional heat, because the pH of a runaway batch is rarely known, and since the phenolic reactions are catalyzed by acid, base, and salt it seems likely that simple deluge is the surest method.

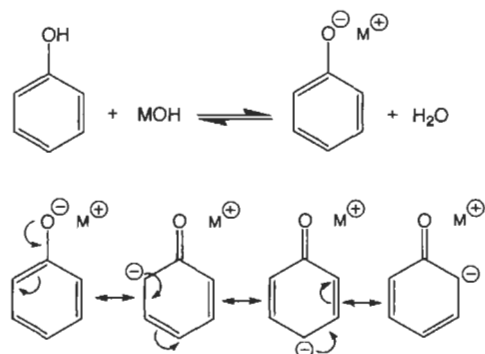
Despite all of the work that has gone into PF reactor safety, PF reactor accidents continue to occur. There have been seven serious incidents in the U.S. alone in the last 10 years. On September 10, 1997, Georgia-Pacific Resins suffered a serious explosion of an 8000-gallon reactor at their facility in Columbus, OH. In this incident, one worker was killed and four more were injured. The explosion was reportedly felt as far as seven miles from the plant [79]. This was a relatively small reactor by today's standards. The incident was a result of human error. An operator failed to follow the instructions in the formula, charging a material before it was called for. Although many things have been done to reduce the probability of human error through automation, redundancy in procedures, better record keeping, and so on, it is impossible to eliminate human error from these or any other processes requiring operator participation. Equipment failures are also impossible to eradicate. Thus, though the frequency of error will no doubt decrease, there will remain a finite potential for PF reactor explosions and continuous safety improvement will be an ongoing requirement.

6. General synthesis of resoles

The formation of a phenolic resin is often formally separated into two steps, though it probably should be three. If we use a three-step model, the first step is activation of the phenol or aldehyde. The second step is methylation, and the third is condensation or chain extension. In addition to the clarity provided by the formalism, these steps are also generally separated in practice to provide maximum control of exothermic behavior, with the strategy being to separate the exotherm from each step from that of the others as much as possible. As there are significant differences in the activation step and in the details of the methylation and condensations steps of novolacs and resoles, we will treat the two types separately.

In some of the older literature, it is common to classify phenolic resins as A-stage, B-stage, and C-stage resins. By this method, an A-stage resin corresponds to mixture of methylol phenols without much polymerization. This class only fits resoles. B-stage resin is a material that is condensed significantly, but which is not cured. Virtually all phenolic resins fall into this group when shipped from the manufacturing plant. C-stage resin is a cured or cross-linked phenolic. Modern practice and understanding of PF chemistry makes these classifications less useful than they were at one time, and they are not often used at present. Occasionally, the terms resitol and resite are also encountered to indicate uncured and cured resins, respectively.

Resoles are normally catalyzed with strong base ($pK_a > 14$), though weaker bases such as amines and carbonates ($pK_a \approx 10-11$) are also used. They typically remain in aqueous solution until the user applies them to the substrate to be



Scheme 1. Phenol activation by base. Phenol is treated with a metal hydroxide or other strong base to form the activated salt.

glued or saturated. In addition to catalysis, the base provides aqueous solubility to the polymer when strong enough. Treatment of the phenol ($pK_a \approx 10$) with base causes a salt to form. The salt has enhanced electron density at the reactive ring positions over that of the alcoholic form of phenol. This is the source of the activation (Scheme 1). As shown in Scheme 1, the charge developing as a result of salt formation is dispersed across the ring with higher electron densities appearing at the positions *ortho* and *para* to the original phenolic hydroxyl. It should be noted that neutral phenols in the alcohol form can react with aldehydes, but the rates are enhanced by as much as 10,000-fold by salt formation ([57], p. 30). This has caused unsalted phenol to be viewed as a by-stander or solvent in some cases [80].

As opposed to the intensity of electron charge, the ring positions receiving electron density enhancement do not depend on salt formation. Even in unsalted phenol, the carbons *ortho* and *para* to oxygen have enhanced electron density relative to the *meta* carbons. The nature of the ring substituent, hydroxyl in this case, and the principles of resonance determine the position of activation. Most activating groups are *ortho*-/ *para*-directing, while deactivating groups tend to be *meta*-directing. Selection of base can affect the distribution of substituents among activated ring positions through secondary mechanisms. These secondary mechanisms tend to enhance selectivity toward certain activated sites, typically the *ortho* positions. The judicious choice of base catalyst will not result in *meta*-substitution.

Occasionally, a phenol may have more than one substituent on the ring before alkylation with aldehyde. If the groups are *meta* to one another and activating, they will enhance the electron density of the same ring positions and reinforce one another. If they are *ortho* or *para* to one another, they may increase or reduce reactivity, depending on the nature of the groups. The most common

activating groups encountered are alkyl, ether, or another hydroxyl, which are all *ortho*-/*para*-directing.

It is rare to encounter deactivating groups in resole chemistry with the exception of sulfonate groups. Sulfonates may be directly substituted to the ring or attached to an alkyl substituent on the ring. Methanesulfonate groups are the most commonly encountered, though direct ring sulfonation is used in some phenolic drilling muds. Occasionally, capping, or protecting, groups are used to reduce methylol or phenolic hydroxylic reactivity. Ether or ester caps are the most common. Esters are not stable in the presence of aqueous base.

In instances where the second ring substituent is alkyl, the hydroxyl group will dominate the situation both in terms of reactivity and substitution pattern under resole synthesis conditions. The primary effect of alkyls will be slight electronic enhancements, which usually lead to modest increases in reaction rates, steric hindrance of adjacent sites, and blockage of the alkyl-substituted position. For example, Reddy and colleagues report that 4-*t*-amyl phenol reacts with formaldehyde at about 1.5 times the rate of phenol itself, showing that the alkyl group provides a small enhancement of the reactivity of the positions *ortho* to the phenolic hydroxyl despite its *meta* relationship to the alkyl [81]. Eapen and Yeddnapalli show that the *ortho* positions of 4-methyl phenol are about 1.8 times as reactive as those of phenol [82]. The electron-donating effects of alkyl groups are thought to be both inductive and mesomeric through hyperconjugation. Conner has demonstrated that the reactivity of phenols correlates well to the electron density of the reactive site [83]. Alkyl groups can also have significant effects on the solubility of polymers as they develop. If the polymer leaves the phase containing the monomers, methylation or chain growth rate may be greatly altered. In most cases, this means that it will be retarded or stopped.

A second ring hydroxyl group will more strongly conflict with or enhance the activity of the first in comparison to the effect of alkyl groups. Hydroxyl groups are actually electron withdrawing in terms of their inductive effects on the ring. Such effects are felt to the greatest extent at positions *meta* to the electron-withdrawing group. If this is a reaction site for aldehyde, it will react less readily than were it not exposed to the inductive effects of the additional hydroxyl. Electron-withdrawing groups deactivate aromatic rings toward electrophilic attack. The net activating behavior of ring hydroxyl is due to the overpowering effects of electron sharing with the ring through resonance. Monomers such as resorcinol, where the hydroxyl groups compliment one another, are far more reactive and more acidic than ordinary phenol. Catechols and *p*-hydroquinones, where the hydroxyls are activating different sites, are less reactive than phenol toward aldehydes. In these situations, the site *ortho* or *para* to one hydroxyl is *meta* to the other. The acidity of the second hydroxyl on a given ring is also considerably reduced by the first dissociation or salt formation. This is particularly true when resonance sharing enhances the electron density of the hydroxyl-bearing ring position.

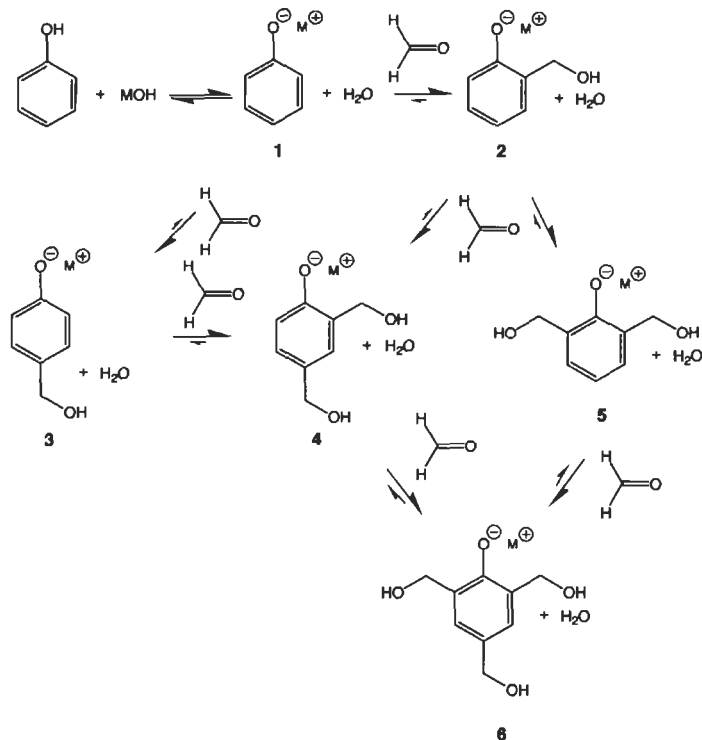
Ethers are stronger activators than alkyl groups. They are capable of resonance interactions with the ring. However, electron sharing results in the development of some positive charge on the ether oxygen. This limits ether activation effects. In a resole, they will be weaker activators than hydroxyl because they cannot form salts. In novolacs, however, they may be slightly stronger activators than hydroxyl because they can make resonance contributions similar to hydroxyl, and they provide slightly higher electron density due to the inductive contribution of the alkyl. This activating effect may be reduced if the aromatic ether is protonated to any extent under novolac manufacturing conditions. The same can be said of hydroxyls. The alkyl group of the ether may also exert steric effects depending on its size. These, of course, will inhibit reactions within the Van der Waals radius of the alkyl group.

While discussing ethers we should mention that the presence of unreacted anisoles or methyl anisoles is highly undesirable in the manufacture of phenol-formaldehyde resoles. These materials tend to be unreactive relative to phenol under normal resole conditions. They are also volatile and have odors detectable at very low concentrations. They have been the source of worker complaints and costly claims in the wood products industry. Benzophenones and methyl phenyl ketones are also common phenol contaminants that are problematic in this regard.

In general, the reaction between a phenol and an aldehyde is classified as an electrophilic aromatic substitution, though some researchers have classed it as a nucleophilic substitution (S_N2) on aldehyde [84]. These mechanisms are probably indistinguishable on the basis of kinetics, though the charge-dispersed sp^2 carbon structure of phenate does not fit our normal concept of a good nucleophile. In phenol-formaldehyde resins, the observed hydroxymethylation kinetics are second-order, first-order in phenol and first-order in formaldehyde.

Regardless of the thought model chosen, the driving force for the reaction is the sharing of the relatively high electron density of the ring with the electron-deficient carbon of the aldehyde. Obviously, increases in charge density increase the need for charge dispersion (i.e. reaction), thus the effectiveness of acids and bases in catalysis of the phenol-aldehyde reactions in novolacs and resoles, respectively. Both methylation and condensation-polymerization reactions are driven by the same thermodynamic forces, though the rates differ due to activation details and steric considerations. There are also slight differences in the stability gained from the two processes.

The second phase in resole formation is reaction of the activated phenol with the aldehyde to form the phenol alcohol derivative. When the aldehyde is formaldehyde, the derivative is a hydroxymethyl phenol and the process is known as methylation. Scheme 2 illustrates this reaction. Since resoles are usually made with excess aldehyde, more than one substitution may be made on the ring. When the reactants are phenol and formaldehyde, up to three methylol groups may be substituted. This reaction has been extensively studied and the rates of



Scheme 2. Methylation under basic conditions.

each successive substitution have been quantified [80,84–99]. The rates of the substitutions may vary considerably. We will describe the reaction rates in detail when we explore the kinetics of hydroxymethylation.

A nice thing about working with resoles is that all of the intermediates shown or mentioned in Scheme 2 can be isolated conveniently and quantified at any point during the reaction. The 2,6-dimethylol product 5 in Scheme 2 is very reactive and somewhat difficult to isolate from a PF resin in comparison to the others, though good syntheses are available [82]. Despite this minor problem, the phenol–formaldehyde reaction can be stopped fairly cleanly at the methylation stage by prudent control of reaction temperature and reagent concentrations. This means that a sample taken from a reaction mixture followed by immediate dilution and cooling will analyze for the expected benzyl alcohols. The same is not true of novolac intermediates, which must be largely inferred by analysis of downstream products or viewed *in situ* by spectroscopy. The difference occurs because the intermediates formed in a novolac reaction are sufficiently reactive to go directly to dimers and higher oligomers without buildup of significant quantities of the benzyl alcohol intermediates at any point in the

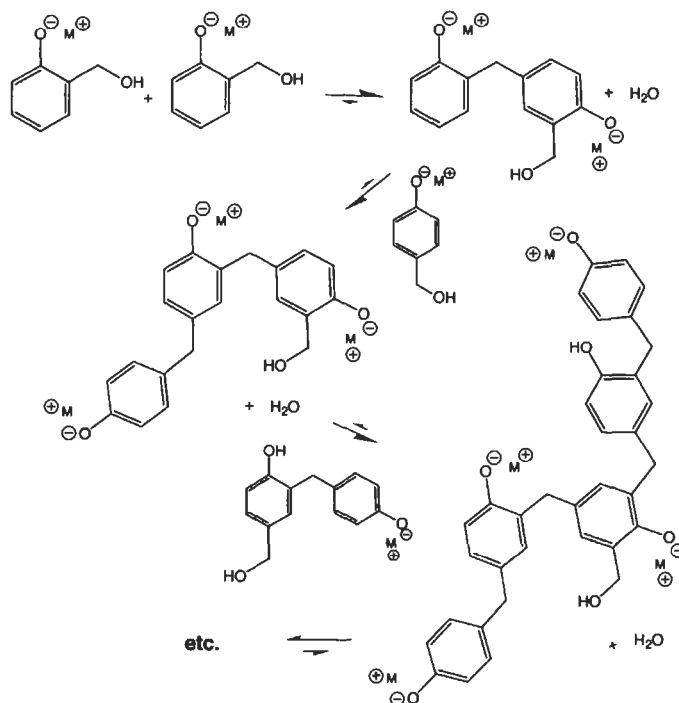
reaction. Novolac reaction stoichiometry also favors immediate conversion of methylols.

The methylation reaction is extremely vigorous when the resin is catalyzed by a strong base, such as sodium hydroxide. It has been the main cause of the serious reactor explosions that we discussed in the previous section [79]. Phenolic reactors of 20,000-gallon capacity are common today. These are considerably larger than most of the reactors that exploded in the past. Equipment engineering solutions alone are inadequate to deal with the problem, though the advent of automated temperature control loops, automatic quenching systems, and accurate methods for estimating reactor vent sizes are improving their effectiveness [78,100–107]. Many of the problems encountered have been due to operator error to some extent. Thus, exotherm control requires both engineering and process solutions.

Older cook styles called for addition of phenol, formaldehyde, and water followed by alkali. Once the alkali was added, strict temperature control was the only barrier to a runaway reaction. A power or equipment failure at this point was likely to lead to disaster. Every batch made involved a struggle between the skill of the operator and capability of the equipment to control the exotherm versus the exothermic nature of the reactants. Most of the disasters that have occurred were due to utilization of this cooking method.

Newer cooks rely on the use of programmed formaldehyde additions. This involves charging the phenol and the base to the reactor prior to addition of the formaldehyde. If water is added to the formula, some of it would also be added with the phenol and base before formaldehyde. The technique separates the exothermic hydration and neutralization reactions that occur between the phenol, base, and solvent water from the heat production of the methylation. After forming the salt, the solution is best heated to 60°C or above to insure that methylation will occur quickly as formaldehyde is introduced. Failure to observe this step may nullify the effectiveness of the programming strategy. The formaldehyde is then added at a slow to moderate rate to insure that the equipment is capable of controlling the batch temperature and exotherm throughout the process. If heat production rate exceeds the capacity of the exchange devices, the formaldehyde addition can be interrupted. This quickly reduces the exotherm rate and allows the engineering controls to regain effectiveness. The formaldehyde charging rate and maximum allowable exotherm rate can be preset in the electronic system controls.

It is important that the formaldehyde addition rate be balanced with the alkali content of the system and the engineering control capability. At high alkali contents, the exotherm will be more vigorous and create more load on the heat exchangers. At low alkali contents, the reaction rate may be quite slow. While this temporarily reduces the difficulty in instantaneous heat load, it may permit potentially hazardous levels of unreacted formaldehyde to accumulate. Such accumulations could become dangerous as batch temperature rises. In both cases,



Scheme 3. Condensation polymerization.

slower formaldehyde addition rates and higher charging temperatures provide maximum safety.

In practice, a hold period is often included in the early stages of resin manufacture to promote extensive methylolation before beginning the polymerization step. This has utility that goes beyond the safety requirements. By including this step, the formulator can ensure that the free formaldehyde is low when the viscosity endpoint is reached. If the batch is cooked at higher temperatures without this step, resins with high free formaldehyde may result, though this depends on the resin solids, alkali content, and molar ratio of formaldehyde to phenol as well as cooking process.

The final phase of resole manufacture is known as the condensation stage (Scheme 3). This is the actual process by which molecular weight is developed and involves the combination of the hydroxymethyl phenol intermediates to form oligomers. It can be reasonably well separated from the resole methylolation reaction in practice by maintaining reaction temperatures below about 70°C. The activation energy for condensation is higher than that for methylolation. This is not to say that condensation does not occur at temperatures below 70°C. It simply means that the methylolation is much faster than condensation at this temperature.

Furthermore, 70°C is a temperature that promotes the methylation at a rate that is usually acceptable for manufacturing productivity.

The general definition of a condensation reaction is a one that involves product formation by expulsion of water (or other small molecule) as a by-product. By this definition, activation and methylation are also condensations. In more precise terms the chain-building process should be described as a condensation polymerization, however, in the jargon of the phenolics industry, the term condensation is usually reserved for the chain-building process. This terminology is not necessarily observed in the literature [88]. Many literature reports correctly refer to methylation as a condensation reaction. The molecular weight development of the phenol alcohol adducts may also be classified as a step-polymerization.

An important feature of Scheme 3 shows the addition of both simple methylol phenols and oligomers to other oligomers to form higher oligomers. Such is not the case with all polymers, e.g. paraformaldehyde, which increases chain length only by monomer addition ([58], Chapter 3). In the case of PF resins, the higher oligomers are usually more reactive than their lower molecular weight analogs. This is because of the principle of equal reactivity of functional groups. This principle, which applies to virtually all polymerizations, states that all functional groups of a given type are similar in reactivity regardless of the size of the oligomer in which they occur, assuming equal activation and steric availability [108]. Also, unlike some polymerizations, there are no problems with critical functional group balances in phenol-formaldehyde resins. As long as there is a sufficiency of hydroxymethyl, polymerization will proceed. Thus, the higher molecular weight phenolic molecules tend to be more reactive toward condensation because of the greater number of reactive sites that they contain. This appears to hold true until diffusion rates of the large molecules become limiting in the final stages of cure. These facts are important to understanding the curing behavior of resoles.

Cure occurs through extension of the condensation process. The highest molecular weight fractions react most rapidly and also increase more rapidly in mechanical strength for each condensation reaction occurring. They influence cure speed disproportionately in situations where attaining a certain minimum strength is required to permit terminating the curing process, such as in hot pressing plywood. The presence of lower molecular weight oligomers and monomers reduce cure speed by providing alternative reactive partners for high molecular weight molecules. This may be desirable or undesirable depending on the circumstances. Formulations are normally determined by compromises that must be made to accommodate limitations in the resin manufacturing and customers' plants.

It is probably obvious at this point that the molecular weight distribution of a resole is an extremely important characteristic. It has major influence on such important performance capabilities as cure speed, viscosity, green strength development (or prepress), assembly time tolerance, required application rates,

substrate penetration, and adhesion. Molecular weight, in turn, is determined by the resin design parameters, particularly alkalinity, solids, and viscosity. These parameters exert great influence because most applications are limited by their viscosity tolerance. The viscosity limitations are usually the result of equipment design or storage requirements. The equipment design limits are often found in the sizing or power of resin transfer pumps, piping, or application equipment. In general, resole storage life decreases with increased viscosity. Shipping times, temperatures, and inventory requirements often place strict limits on the reactivity of the resin and the viscosity range available to the formulator.

Prior to about 1980, most resole manufacturers had no idea what the molecular weights of their products were. PF resoles were simply formulated on the basis of alkalinity, solids, formaldehyde-to-phenol molar ratio, and viscosity. Since resin formulas must always add up to 100% and since viscosity is a function of solids, alkalinity, and molecular weight, it was impossible to separate the controlling variables. This is to say the variables are not independent and that, with the exception of viscosity, it is impossible to vary one parameter at a time. Even though viscosity can be varied independently, its meaning is tied to the composition variables. This created much confusion among formulators and was a major hurdle in the development of improved PF technology. The effects of additives also clouded the picture. To further complicate things, customers often arbitrarily specified the resin solids and viscosities that they wanted, thus removing important control variables. These specifications were usually imposed for contract reasons or mechanical convenience with no thought to performance.

In the early 1980s, phenolic resin producers began adapting high-pressure liquid size exclusion or gel permeation chromatography (SEC or GPC) to their needs. Despite the fact that most of the columns of the day would not tolerate water or base, and that derivatizing resoles to make them compatible with these systems invariably perturbed their molecular weight distributions, effective methods were developed for determining PF molecular weights. Since these early days, many improvements in GPC methods have been devised. Some of the newer columns are tolerant of water and base. The plate counts are higher. Flow controls are better. The availability of low angle laser light scattering (LALLS) detectors makes absolute calibration possible. Detector capabilities are improved and the use of multiple detectors facilitates analysis of functional group distribution and molecular shape factors across molecular weight distribution, among others. Low-pressure gel filtration methods have also been devised [109].

Direct measurement of PF molecular weight distributions led to great progress in PF performance and demystified many areas of product formulation [110]. For example, the effects of base could be evaluated with molecular weight held constant or *visa versa*. Such evaluations led to much new knowledge that produced great benefits for commercial users. Fig. 4 shows a GPC molecular weight distribution for a typical plywood resin using one proprietary test method. Molecular

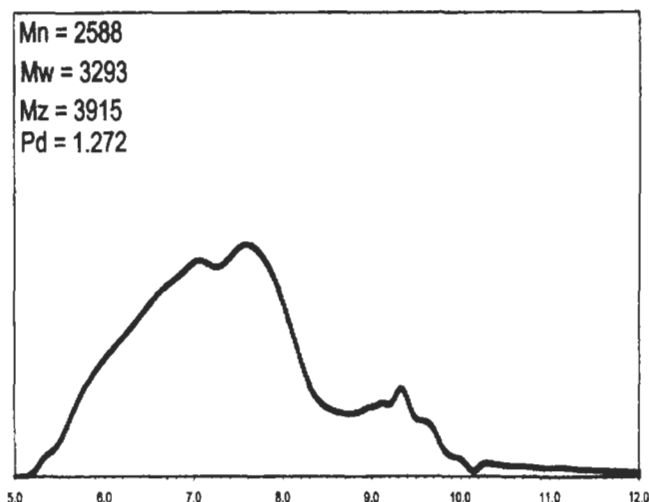


Fig. 4. GPC scan of a typical plywood resin. (Chart courtesy of Borden Chemical.)

weight distributions became the focus for formulating resin performance, and many correlations were developed.

As mentioned earlier, cure speed was one of several performance areas that benefited greatly from molecular weight knowledge. These improvements in cure speed were very important to maintaining the wood products market for phenolic adhesives as they met competition from highly efficient, faster curing, but more costly, isocyanates. Fig. 5 shows the progress in molecular weight development and cure speed for PF OSB resins in North America. The correlation in available pressing times and resin molecular weight is very strong. These data imply that mills in the year 2000 have press productivities that are about three times what they were in the early 1980s without press modification. Although this productivity is provided largely through improvements in PF adhesive technology, use of faster closing schedules and higher pressing temperatures have also been useful and have improved board quality in ways that permit attainment of the PF cure speed potential.

Despite the statements above, one should not conclude that additional mill productivity did not require capital investment. Removal of the pressing bottlenecks invariably moved bottlenecks upstream into the forming, drying, or flaking operations. Solutions to these problems usually required capital investment.

7. Examples and practice of resole synthesis and formulation

The manufacturing instructions and formula for a typical commercial resole to be used in a plywood adhesive application are shown in Table 2. Such resin

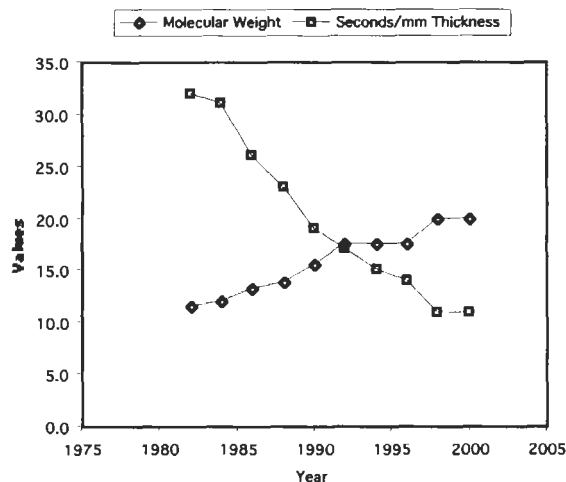


Fig. 5. Commercially available pressing times and relative molecular weights for PF OSB resins [109,110]. Note that the molecular weight values are made relative to fit the scale. The pressing times are for 3/4-inch OSB in s/mm. The coefficient of determination between relative molecular weight and cycle time is 0.96.

would normally be mixed with various fillers, extenders, water, and more alkali before use [111,112]. This could happen on the resin manufacturer's site, and the material supplied as a complete adhesive, or in the user's mill. The selection of filler materials and the construction of the mix are not trivial matters and may greatly enhance or detract from the performance potential of the resin. The additives chosen are usually selected to reduce penetration of the adhesive, to provide 'prepress' or green strength, and to insure minimum adhesive usage while attaining adequate bonding.

Typical features of a plywood resole formulation are a formaldehyde-to-phenol molar ratio in the 2.0:1 to 2.5:1 range, programmed formaldehyde, an alkali content from 4 to 8 wt% (calculated as sodium hydroxide), and pan solids of 40–50%. Resins used for laminated veneer lumber (LVL) tend to be similar to plywood resins in composition and molecular weight, though they are often designed for high-end cure speed.

Molecular weight assignments for such resins will be dependent on the method used for measurement. Each manufacturer has his own relative scale. In practice, absolute molecular weight determination is not important. The method used must discriminate between resins with sufficient resolution to allow prediction of resin performance in the applications of interest.

In addition to the formulation parameters mentioned above, selection of the base used for catalysis has strong implications. Bases commonly used are sodium hydroxide, potassium hydroxide, lithium oxide, calcium hydroxide, barium hy-

Table 2
A typical plywood resol formula

Material	Relative moles	%
Phenol, 100%	1.0	27.65
Water-I	NA	13.82
Sodium Hydroxide-I, 50%	0.2	4.71
Formaldehyde, 50%	2.0	35.28
Water-II	NA	13.83
Sodium hydroxide-II, 50%	0.2	4.71
Total		100.00

Charge phenol and water-I to the reactor. Start agitation. Charge sodium hydroxide-I. Heat to 60°C. Charge formaldehyde at a uniform rate over a period of 60 min while holding temperature at 60–70°C. The batch will exotherm significantly as formaldehyde is charged and cooling will be required. After the formaldehyde is all in the reaction mixture and the exotherm has subsided, heat to 95°C and hold to a Gardner viscosity of 'C'. Cool the batch to 85°C and hold to a Gardner 'T'. Cool the batch to 70°C. Charge water-II and sodium hydroxide-II at 65–75°C. After charges are complete, hold batch to Gardner 'T' at 70–75°C. Apply full cooling to 25°C. Discharge from the reactor through a 20-mesh screen and store at 18–22°C. This will yield a resin of approximately 43% solids. The alkalinity will be about 4.71%, and the viscosity will be approximately 550 cps.

dioxide, amines, and organic zinc salts. Calcium and barium hydroxides are normally selected for applications where the manufacturer wishes to remove the catalyst from the finished resin before shipment. These materials are easily removed by formation of the carbonate, sulfate, or other insoluble salt followed by filtration. Calcium and other divalent metal salts are known to promote *ortho* substitution during methylation. Zinc salts are also used for this purpose.

The use of potassium hydroxide catalyst in combination with sodium hydroxide has led to some unexpected performance results of great significance to the plywood and LVL industries, especially in the U.S. [113,114]. In addition to providing faster cure, potassium hydroxide greatly increased the ability of plywood resoles to tolerate moisture during the curing process. Although the mechanism leading to these benefits has not been thoroughly studied, it seems likely that most of the benefits stem from the reduced hydration requirements and the greater mobility of the potassium cation in comparison to sodium.

Fully hydrated potassium ion coordinates about 10–11 molecules of water, whereas sodium coordinates about 16–17 molecules [115]. The ionic mobility of potassium is about 50% greater than that of sodium. In simple terms, this means that more of the water in a potassium-catalyzed resin will be available as free water for viscosity reduction and that movement of water from a glue line into the wood will have less effect in moving the adhesive off of the glue line with it.

The viscosity reducing effects of potassium hydroxide modifications during resin manufacture allow a formulator to produce a higher molecular weight PF polymer while remaining within the viscosity restrictions imposed. The higher molecular weight implies faster cure and reduced penetration of the adhesive into the wood. Polymer diffusion rates are inversely proportional to the square of molecular weight in view of the Stokes–Einstein scheme [116]. The retention of resin on the glue line permits lower spreads, which, in turn, accelerate cure. Faster cure allows attainment of the necessary bond strengths to permit press opening even in the presence of moisture from the veneer.

Moisture normally retards the development of mechanical strength during PF cure [117,118]. This looks like a slower reaction rate, though it is not exactly the same thing. Moisture also tends to cause over-penetration of the glue due to viscosity thinning during the gluing process. Normally, when PF adhesive is applied to dry wood, it begins to lose moisture to the atmosphere and wood at a significant rate. This causes the resin to gain viscosity as it sits on the wood. Unless the adhesive dries out too much and loses flow, this drying process tends to be beneficial, improving prepress, adhesion, and cure speed in the process. If wood moistures are high enough, however, moisture may move out of the wood and into the glue prior to pressing. This counteracts the moisture loss to atmosphere and keeps the glue viscosity low. Furthermore, the adhesive cure speed has been slowed because of the dilution. The use of potassium hydroxide reduces the tendency of the adhesive to draw moisture from the wood in these situations, in comparison to sodium-based systems.

When moisture gain from wet veneer is combined with the natural viscosity reduction occurring when the glue is initially heated in the press, over-penetration and poor gluing can result. The lower hydration requirements of potassium appear to significantly reduce this occurrence. The higher molecular weights attained further reduce the affinity of the potassium-modified systems for moisture. While these ideas are somewhat speculative, they are reasonable, self-consistent, and have served well as a model for thinking about the use of potassium hydroxide in formulating superior plywood and LVL resins. They help to rationalize the observation that the potassium-modified PF systems are capable of gluing high moisture veneer, whereas strictly sodium-based resins are not as well adapted to this use.

Table 3 shows a typical U.S. West Coast plywood adhesive mixing procedure. The most common fillers for plywood mixes in the U.S. are grain flours, wood flours, bark flours, and shell flours. Grain flours are most likely to be wheat or sorghum flours. Wheat flours are preferred for roll coaters and curtain coaters while sorghum flours are better for plywood spray systems, for sprayability reasons. Resin manufacturers are often very concerned with the type of wheat from which the flour was derived and its grind as well as its total protein, gluten, and moisture contents. The most common shell flours are from walnut and pecan

Table 3

A typical U.S. plywood mix

Ingredient	Pounds
Water	950
Resin, 43%	932
Wood flour	220
Wheat flour	294
<i>Mix for 5 min at 2000 rpm</i>	
Sodium hydroxide, 50%	138
<i>Mix for 8 min at 2000 rpm</i>	
Resin, 43%	1466
<i>Mix for 1 min at 2000 rpm</i>	
Total	4000

This makes a mix with a viscosity of 5000–7000 centipoise. The total mix solids are 40% and the resin solids in the mix are 26%. A mix like this would be used on Douglas fir veneer at the rate of about 55 pounds per 1000 square feet of veneer surface (double glue line basis). The 43% solids resin would be used at about 500 cps viscosity.

sources, though filbert and almond shells are also used. In general the finer the grind, the better the performance of shell flours. Wood flours are also selected for wood species, grind, and moisture content. Douglas fir, pine, and birch flours are widely used. Alder bark is also used on the West Coast.

Clays are also common fillers in plywood resins. Clays have a cost advantage over most of the materials mentioned above, though there are some drawbacks to their use, particularly in terms of consistent quality. All fillers present some problems in this regard, though some are worse than others.

In other parts of the world, plywood adhesive fillers are obtained from local sources and may be quite different than those used in North America. In Southeast Asia, banana flour is quite important. In Europe, calcium carbonate (chalk) is often used. Nearly any fibrous material or fine particulate material capable of forming a functionally stable suspension can be made to work if the formulator is sufficiently skillful. However, the mix formulator will be very specific about the type and grade of filler to be used in a particular mix. Substitutions may lead to serious gluing problems.

Carbonates, especially sodium and potassium carbonates, are often added to plywood and LVL mixes to accelerate cure and reduce delaminations and blows. Calcium carbonates do not show a significant accelerating effect. Occasionally esters are used to accelerate plywood mixes [119]. Carbon dioxide also accelerates PF cure [120].

The selection of mix ingredients may depend heavily on the type of adhesive application equipment used. The main types of equipment for plywood and LVL are roll coaters, spray systems, curtain coaters, and foam extruders. When foam extruders are used, animal blood and surfactants are usually added to the mill mix. For other application systems, resin producers typically supply the non-filler additives as part of the resin composition.

Oriented strandboard (OSB) resins are quite similar to plywood resins, though they tend to be lower in alkalinity and higher in solids. Since OSB resins are sprayed onto dry wood in small discrete droplets rather than applied in glue lines, the problems associated with holding the glue on the wood surface are not usually issues of concern. Adhesive dry-out and loss of flow displace over-penetration as major difficulties.

In most cases, OSB resins are designed for use in either the surface or core of the board. Face resins are usually designed for maximum resistance to pre-cure and dry-out during the period when they are in contact with the hot press platens before and during press closing. If the resin cures before proper wood-to-wood contact is made and sufficient contact pressure develops, there will be no bond formed. Core resins are designed primarily for rapid cure though they must also resist dry-out to a lesser extent. Much of the performance difference between face and core resins is the result of molecular weight distributions. Surface resins are designed at lower molecular weight than core resins. Surface and core resins also tend to contain different additives. OSB resins also contain a different selection of additives than plywood resins.

Urea is sufficiently important as an additive to PF resins for OSB to warrant some discussion. It has had a large favorable economic impact on the OSB industry. When used, it is generally added after the polymerization is complete. Thus, it is not part of the polymer and does not have any direct effect on polymer resistance to hydrolysis, as might be expected if it was part of the polymer backbone. Under alkaline pH conditions, urea-formaldehyde adducts do not polymerize at a rate that is significant compared to the PF polymerization; therefore, the urea does not participate significantly in the curing process of the PF, despite the fact that it is present during the cure. Since urea is not present in the cured PF polymer per se, it does not detract from the durability of the polymer. Despite this, it is possible to see reduced OSB durability as a result of formulated urea if its use has led to actual PF polymer application rates that are too low.

Though urea and its adducts do not co-polymerize significantly with PF under alkaline resole conditions, urea does react rapidly with formaldehyde under these conditions to form non-polymerizing adducts. This makes it useful as a scavenger for any formaldehyde that may remain after the PF manufacturing reactions have been completed or that might be condensed out during curing. This scavenging ability has great benefits for the workplace and for the environment [121]. Since urea-formaldehyde adducts are less thermodynamically stable than

phenol-formaldehyde adducts, if the polymer needs formaldehyde during the curing process it may extract it from the UF adducts present.

Even though UF adducts are known to be present in OSB, formaldehyde emissions are not elevated over those expected of an unmodified PF. There are three reasons for this. First, the molar ratio of formaldehyde-to-urea in these situations is very low. It is at least an order of magnitude lower than practical molar ratios for curable UF resin binders. Second, UF adducts are quite stable under the alkaline conditions that prevail in PF-bonded OSB. Finally, the urea only reacts with the formaldehyde that was left behind during polymerization and would have been largely emitted in pressing and cool-down. Urea additions have been shown to reduce PF formaldehyde emissions from hot pressing [121].

In addition to its scavenging effects, urea has considerable ability to reduce the viscosity of aqueous PF resins. Thus it serves as a non-volatile solvent, allowing solids to increase while viscosity is reduced. This thinning ability at high solids is particularly important in OSB resins because moisture control is critical to high productivity and board quality. As discussed earlier, moisture slows the development of mechanical strength during cure, reduces minimum panel temperature in the press, and reduces finished panel dimensional stability when later exposed to liquid water [117,118]. This latter moisture effect is related to both the temperature reduction just mentioned and to the reduction in cure level of the resin [122–124]. The viscosity thinning of urea allows the formulator to raise the molecular weight of the PF resin to give a faster-curing polymer. Urea has only a minor direct negative effect on the resin cure speed. This is greatly outweighed by the positive effects on moisture reduction and cure speed enhancement through higher molecular weight. The benefits of urea are similar in some ways to those described earlier for potassium hydroxide although the effects of urea on prepress are dramatically different, making it less useful for many plywood processes.

Other effects of urea include improvement in resin dry-out resistance during the gluing process, lower cost, and improved storage stability. The dry-out resistance benefits the adhesion of the resin and allows low resin application rates. This is especially true with high molecular weight systems which naturally tend to dry faster than lower molecular weight resins, although urea is also used extensively in low molecular weight surface resins to impart additional dry-out resistance in the face of hot platen exposure.

The lower cost of the urea-modified PF resins is a combination of PF solids extension by lower cost urea and improved adhesion and distribution capabilities. The improvements in storage stability stem from the thinning and dilution effects as well as from the formaldehyde scavenging. Liquid PF resins with high free formaldehyde contents tend to be less stable in storage.

Though the discussion above was aimed primarily at wood binders, many of the ideas carry over into foundry and glass binding applications. For example, potassium hydroxide is used extensively in foundry binders as are esters and

organic carbonates. Urea is used extensively to modify glass insulation binders. Motivations for using materials may be somewhat different. Ester-curing systems are often selected in preference to amine-curing foundry systems for their reduced toxicity or lower tendencies toward veining defects. Glass insulation binders are often made at very high formaldehyde-to-phenol molar ratios and urea is essential for mill health considerations as well as stability, but it may also provide some flame resistance.

8. Methylation kinetics and mechanisms in resoles

Up to this point, we have presented only a general overview of phenolic chemistry with some illustration of applications. We now turn to a more detailed and quantitative discussion of the methylation process. Though other aldehydes are occasionally used, formaldehyde is overwhelmingly the aldehyde of choice, and we will limit our discussions to phenol-formaldehyde reactions.

The classic study on methylation of phenol is a 1953 report by Freeman and Lewis [125]. In their work, Freeman and Lewis used paper chromatography to separate the various methylolated species [126,127]. Prior to their work, only an overall rate relationship in phenol and formaldehyde had been reported. They were able to provide a rate constant for formation of each species that we have shown in Scheme 2. Their work was done in concentrated solutions in the presence of sodium hydroxide catalyst. Reaction mixtures contained a 1:1 molar ratio of base to phenol and a 3:1 molar ratio of formaldehyde to phenol. Where a methylolphenol was used as starting material, they employed a molar ratio of 1:1 formaldehyde to available phenolic reactive site. Formalin solutions were of 37% concentration and probably contained methanol, though they do not mention it. Their experiments were done at 30°C. They followed the reactions for up to 1000 h. The samples collected were diluted 10:1 with 75% methanol before analysis.

Freeman and Lewis reported that all rate constants are second-order as expected. This was at odds with previous literature. Referring to Scheme 2, we will describe the rate constant for converting species **1** to species **2** (**1**→**2**) as k_{12} and so on. On this basis, Freeman and Lewis report the rates for each conversion as shown in Table 4. They indicate that their analyses of rates are consistent to within about 16% and their chemical analyses to within about 5%, though their quantitative assessments relied on the weights of spots from paper chromatography.

The rate constants reported in Table 4 are double the specific rate constant for a given site when two identical sites are present, so that the actual position reactivity is half of the level indicated. Since the rates are reported as second order, the

Table 4

Freeman and Lewis second-order rate constants at 30°C (l/mol s)

Conversion	Rate constant $\times 10^6$	Relative rate	Relative reactivity
1-2	10.5	1.69	0.85
1-3	6.2	1.00	1.00
2-4	7.3	1.18	1.18
2-5	8.7	1.40	1.40
3-4	7.5	1.21	0.61
4-6	9.1	1.47	1.47
5-6	41.7	6.73	6.73

methylation reactions are expected to fit

$$-\frac{dP_i}{dt} = \sum k_{ij}[P_i][F] \quad (1)$$

which gives the rate of disappearance of phenol and methylolphenols in the presence of formaldehyde. F is the formaldehyde concentration. P_i is the concentration of an individual phenol derivative as determined by previous substitutions on the phenolic ring. k_{ij} is the rate constant associated with a particular conversion. Obviously, ' i and j ' refer to the appropriate possible conversions as listed in Table 4. If a conversion does not take place $k_{ij} = 0$.

An example of the application of Eq. 1 is

$$-\frac{dP_1}{dt} = (k_{12} + k_{13})[P_1][F] \quad (2)$$

for the conversion of phenol to monomethylolphenols. The subscripts relate to the species in Eq. 1 and Tables 4 and 5. Since phenol must be converted to a

Table 5

Some literature methylation rates $\times 10^3$

Ref.	Year	°C	k_{12}	k_{13}	k_{24}	k_{25}	k_{34}	k_{46}	k_{56}
[125]	1953	30	0.0105	0.0062	0.0073	0.0087	0.0075	0.0091	0.0417
[84]	1998	30	0.00588 ± 0.0003	0.00860 ± 0.0003	0.0197 ± 0.0005	0.0110 ± 0.0003	0.00538 ± 0.0003	0.0103 ± 0.0003	0.0278 ± 0.0012
[80] ^a	1968	30	0.0387	0.0275	0.0349	0.0482	0.0415	0.0246	0.1028
[80] ^a	1968	57	0.510	0.339	0.360	0.495	0.558	0.265	1.077
[90] ^b	1983	30	0.0836	0.0479	0.0776	0.0848	0.0769	0.0619	0.155
[90]	1983	70	4.94	2.56	3.06	4.38	4.55	2.56	6.51
[90]	1983	80	11.9	6.01	6.72	10.2	10.9	5.69	14.5
[90]	1983	90	27.1	13.5	14.2	22.7	25.0	12.1	30.9

^a Rate constants written in terms of phenate salt only and corrected for formaldehyde equilibria.

^b Calculated from Ferrero and Peretti [90].

monomethylolphenol before anything else can be made, this scheme is a complete description of the disappearance of phenol.

The data in Table 4 show clearly that the reactivity of the *para* position is slightly higher than that of the *ortho*; however, once the *ortho* position has been methylolated, it activates the other ring positions, particularly the remaining *ortho*. The details of Freeman and Lewis' results have been challenged by others [80].

The high reactivity of the di-*ortho* hydroxymethyl derivative has stimulated a great deal of effort toward formulation of fast curing systems based on high-*ortho* polymer structures. Grenier-Loustalot and co-workers have reported that *o,o'*-linkages do not form under typical resole conditions [128]. Techniques have been developed for manufacture of highly *ortho* polymers. Industrial products are available that are greater than 85% *ortho*-linked. Such polymers must be manufactured under the influence of special salts or acids. In order to develop the fast speeds expected in a resole, one would have to make a high *ortho* polymer under suitable conditions then transfer it into base. Such polymers have not shown the cure speed expected based on the Freeman and Lewis methylolation rate constants, however, they are faster curing than ordinary PF resins.

Freeman and Lewis attribute the special reactivity of the *ortho*-dimethylol adduct to the stabilization of the quinoid resonance form shown in Fig. 6 due to hydrogen bonding of the methylol substituents to the phenolate oxygen (7). That *ortho* methylol groups hydrogen bond to the phenolic oxygen is also supported by other observations of increased acidity of *o*-dihydroxymethyl phenols [129]. If this species is indeed the source of the fast methylolation reaction at phenolic C4, it also explains why highly *ortho* polymers have not met fast-curing expectations of Freeman and Lewis. Obviously, the *ortho* hydrogen bonding disappears as *ortho* polymerization proceeds (8, see Fig. 6) and the electron density on the ring will attain a more normal distribution among the activated ring positions.

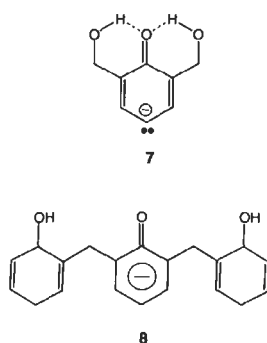


Fig. 6. Freeman and Lewis stabilized structure and the likely results of *ortho*-polymerization. As polymerization consumes *o*-hydroxymethyl groups, the hydrogen-bonded species cannot form.

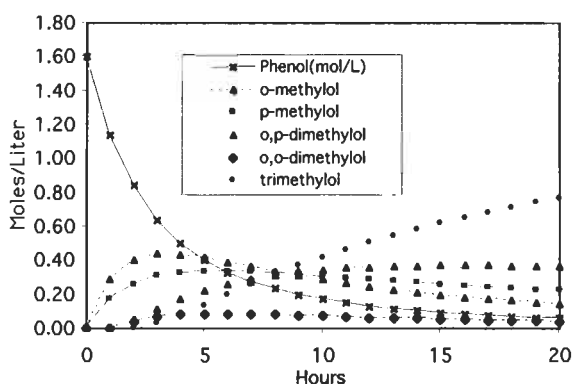


Fig. 7. Calculated species development using Freeman and Lewis rate constants.

As mentioned, highly *ortho* polymers are somewhat faster than others. This is probably due to a slight elevation in electron density that is the general case for *para* positions [91,96].

When the Freeman and Lewis rate constants are applied to an experimental situation and integrated, Fig. 7 results. This figure shows the same fundamental trends seen in the data. There are some differences, however. The Freeman and Lewis measurements, as presented in their Fig. 2, appear to exceed the available phenol by about 39%. This is probably one reason why Zavitsas et al. state that the Freeman rate constants do not fit the data [80]. However, the calculations made using their rate constants do maintain the overall material balance. As presented here, they are not as precise as they could be because the calculation interval has been set at 1 h. However, they are as good as the data at this level.

Another difference between the data and the calculations shows up at extended reaction times. Freeman and Lewis show a maximum concentration of trimethylolphenol at about 50 h reaction time. After this point, the concentration falls dramatically. This is apparently due to formation of condensation products which reach noticeable, but low, levels at about 50–60 h. After the reaction has been allowed to proceed for 1000 h, the level of the condensation product reported is equivalent to that of trimethylolphenol, which has fallen to about one third of its maximum concentration. This accounts reasonably well for the loss in trihydroxymethyl phenol, since two moles are consumed to make one mole of dimer. As the calculation contains no information about the condensation reaction, it predicts that the level of trimethylolphenol plateaus at about 98% yield on phenol.

The observation of condensation products at 30°C may seem to contradict statements made earlier regarding our ability to separate the methylation and condensation reactions by holding reaction temperatures below 70°C. However, there is no conflict. The differences in the situations are primarily matters of absolute rate. The relative rates are still similar for methylation and condensation. No

dimer (condensation product) is seen in the Freeman experiments until the phenol has been more than 99% converted to methylolphenols. Formaldehyde conversion is about 87% at this time. Furthermore, except for a fairly low concentration of *o,p*-dimethylolphenol, there are no significant amounts of any species remaining that are capable of methylation. Thus, condensation is about the only thing that can happen at this point and we see that the methylation and condensation reactions have indeed been separated. The situation is analogous at 70°C though all of the rates are faster. The rate of methylation is still much faster at temperatures approaching 70°C than the condensation, though the rates are converging.

The condensation product formed in Freeman's experiments is diphenyl-4,4'-dihydroxy-3,3',5,5'-tetrahydroxymethyl methane. The fact that this dimer develops primarily at the expense of the trimethylol phenol at this low temperature is a little surprising at first glance. It implies that formaldehyde is lost from the ring during the condensation. Jones has studied this condensation in detail and shows that it is a first-order process consistent with slow formation of a reactive intermediate, which is rapidly consumed by available nucleophile [130]. Under conditions of high alkalinity, the quinone methide proposal by Jones seems to account well for most of the observed kinetic results. Von Euler reports isolation of a quinone methide trimer at 140°C [131]. However, other researchers have stated that quinone methide formation requires high temperature [132]. Furthermore, quinone methides should be sufficiently reactive to form bonds with any nucleophile present. This fact has been demonstrated through use of model phenolic compounds in the presence of ester accelerators [133]. In this case, the most abundant nucleophile is hydroxymethyl, though the most powerful nucleophile is probably phenoxide. This should lead to at least traces of dimethylene or methylene-phenyl ether linkages between rings. These were not observed by Freeman and Lewis. Dimethylene ethers should be stable at 30°C. Murray reports methylene-phenyl ethers, though his work shows loss of formaldehyde to form methylene linkages between rings rather than dimethylene ether linkages when quinone methide reacts with methylolphenol. He also states that the methylene-phenyl ethers are labile and difficult to isolate. Thus, Murray's work supports Jones in part. Failure to report the formation of a particular product does not mean that it was not formed, only that it was not identified. The strength of the anti arguments lies in the energy required to create quinone methides when esters are not present. Leading references on quinone methides are provided [134–136]. Some relevant studies on solvent effect on C- versus O-alkylation are provided by Kornblum and co-workers [137–140].

Since few commercial phenol-formaldehyde resins are made at molar ratios of 3 : 1 (*F* : *P*), Fig. 8 was generated at a molar ratio of 2 : 1 to see how Freeman's predictions would look. The concentration of reagents is still quite low compared to most commercial resins, but a comparison of species is easier if we maintain the same initial concentration of phenol used by Freeman and Lewis. As expected,

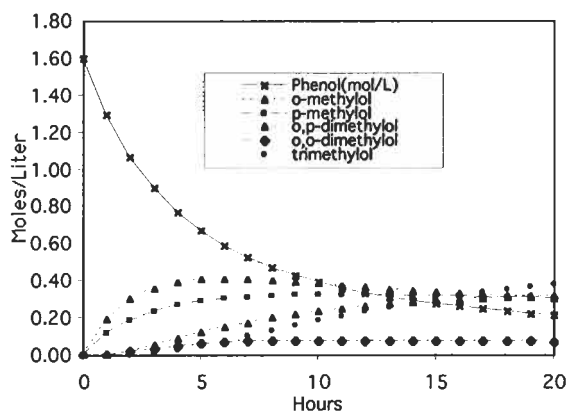


Fig. 8. Freeman and Lewis-based calculations at a 2 : 1 formaldehyde-to-phenol molar ratio.

phenol is not as completely converted, the mono-substituted phenols are more dominant, and the trimethylolphenol is greatly reduced.

Whereas Freeman and Lewis reported the first comprehensive analysis of hydroxymethylation of phenol, they were not the last to study this system. A number of reports issued since their work have confirmed the general trends that they discovered while differing in some of the relative rates observed [80,84–99]. Gardziella et al. have summarized a number of these reports ([18], pp. 29–35). In addition to providing new data under a variety of conditions, the other studies have improved on the accuracy of Freeman and Lewis, provided activation parameters, and added new methodologies for measuring product development [97–99].

Zavitsas et al. added terms for the extent of hemiformal and paraformaldehyde formation. Hemiformal formation slows the methylolation reaction as does the presence of paraformaldehyde. They report that only monomeric methylene glycol appears to methylolate. They point out that the terms for the two polyoxymethylene species partially cancel one another, as depolymerization of paraformaldehyde naturally occurs while hemiformal formation is increasing due to methylolation. They observe that hemiformals form only on the methylolphenol hydroxyls and not on the aromatic hydroxyl. They calculate that the average number of methoxy groups involved in each of the hemiformals is about two in addition to the original methylol. There is no selectivity for *ortho* versus *para* positions in hemiformal formation.

Zavitsas et al. account for the effects of water in their calculations. Water promotes depolymerization of the paraformaldehyde as well as the hemiformals. Their modifications correct for the apparent reduction in methylolation rate as the extent of reaction proceeds, in that the hemiformals remove formaldehyde reactivity from the reaction mixture. Their rate constants look large because they are written for phenate concentrations rather than phenol and because of the formaldehyde equilibrium adjustments. They note that unsalted phenol is a by-

stander in the reaction mixture and acts only as solvent. A ratio for correction of formaldehyde present to the monomeric methylene glycol form is part of their rate scheme. Zavitsas' observations regarding the effects of water on hemiformal and paraformaldehyde depolymerization probably explain why higher solids PF resins tend to have higher final free formaldehyde content.

Zavitsas et al. take the alkalinity of the reaction mixture and the relative acidity of the various phenol derivatives into account in their study. Their rate scheme is corrected for the acidity of each individual species as it forms. They state that alkalinity has no appreciable effect on the availability of methylene glycol.

Activation data are also provided by Zavitsas. Thus, the Zavitsas study adds significantly to the work of Freeman and Lewis and gives a thorough analysis of the methylation in the presence of strong base such as sodium or potassium hydroxide. Work done since Zavitsas has generally been aimed at providing new and more convenient methodology for analyzing PF reactions or in the area of special catalyst effects. The Higuchi studies are similar to Zavitsas and may be more accurate due to the availability of modern analytical techniques [84]. Like Zavitsas, the Higuchi work is comprehensive.

The activation data collected by Zavitsas et al. at 30 and 57°C was extrapolated to 70–90°C by Ferrero and Panetti and tested against experiment. The data fit well throughout the temperature range. Fig. 9 and Table 6 show these activation data for each species involved in the methylation process.

Eq. 3 is the function developed by Henry Eyring to describe equilibrium activation free energy relationships [141].

$$k = \frac{\kappa T}{h} \exp\left(\frac{-\Delta G^*}{RT}\right) \quad (3)$$

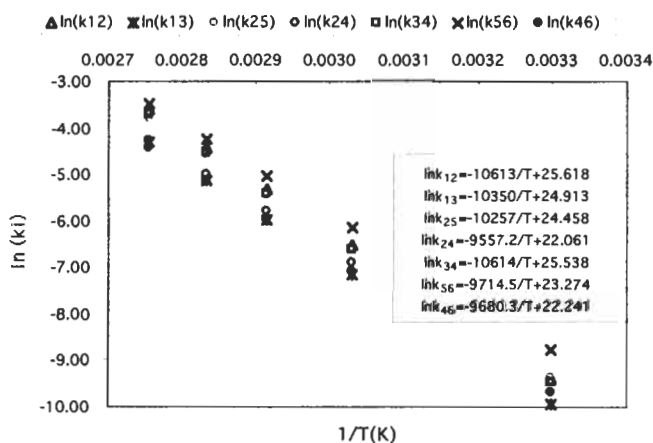


Fig. 9. Activation parameters for resole methylation in the presence of NaOH in concentrated solutions [80,90].

Table 6

Eyring activation parameters for NaOH-catalyzed methylation in relatively concentrated aqueous solutions

Substitutions (number prior)	Positions substituted	Reaction position	ΔH^* (kcal/mol)	ΔS^* (cal/mol K)
0	none	<i>ortho</i>	20,430	-09.83
1	<i>ortho</i>	<i>ortho</i>	19,722	-12.14
1	<i>para</i>	<i>ortho</i>	20,433	-09.99
2	<i>ortho, para</i>	<i>ortho</i>	18,576	-16.54
0	none	<i>para</i>	19,907	-12.66
1	<i>ortho</i>	<i>para</i>	18,333	-16.90
2	<i>ortho, ortho</i>	<i>para</i>	18,644	-14.97

where κ is the Boltzmann constant, h is Planck's constant, R is the universal gas constant, T is in K, and ΔG^* is the Gibbs free energy of activation.

When the expanded expression for Gibbs free energy is substituted for ΔG^* , as shown in Eq. 4, it becomes possible to calculate the enthalpy and entropy of activation when rates are available across a range of temperatures. These parameters are calculated in Table 6 using the data supplied by Zavitsas and Ferrero [80,85,90].

$$k = \frac{\kappa T}{h} \exp \left(\frac{-\Delta H^*}{RT} + \frac{-\Delta S^*}{R} \right) \quad (4)$$

Here ΔH^* is the enthalpy of activation and ΔS^* is the activation entropy.

That the entropies of activation in Table 6 are significantly negative confirms the second-order (bimolecular) nature of the rate-determining step in the methylation process and indicates requirements for highly organized transition states. ΔS^* appears to be significantly less negative for *ortho* methylations, except where *ortho* methylation has already taken place. One *ortho* substitution makes the second *ortho* position essentially equivalent to the *para* position on an unsubstituted ring in terms of entropy requirements. This could be interpreted in several ways. One might be that the lower entropy requirements for the initial *ortho* substitution are the result of having two equivalent *ortho* positions. This reasoning is supported by the fact that the reactivity of an individual *ortho* position is less than that of the *para* position. If interactions of the incoming methylene glycol with the ring were somehow stabilized by *ortho* interactions, such as hydrogen-bonding to the phenolic oxygen, a similar effect might be seen. This author favors the first argument.

Another interesting idea that can be drawn from Table 6 is with regard to the relative rate of substitution of the last reactive ring position in dimethylol derivatives. It is clear that there is no favorable change in the activation enthalpy

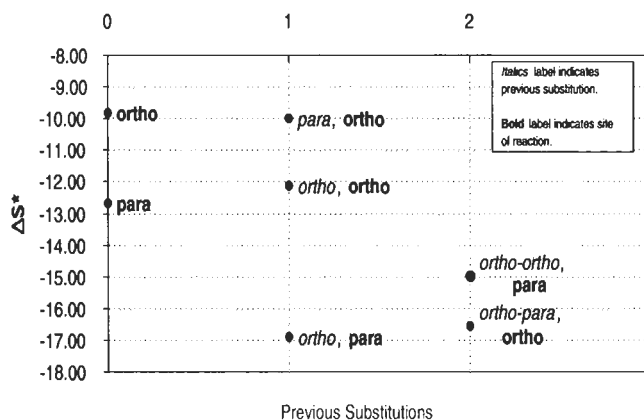


Fig. 10. Activation entropy requirements by reacting position as affected by previous substitutions based on Zavitsas [80]. As the activation entropy becomes more negative, steric demands on the transition state are more stringent. The effect of previous *ortho*-substitution on reaction at the *para* position is hard to explain, in light of both the reciprocal effect of *para* substitution on *ortho* and the effect seen with the di-*ortho* pre-substitution.

in the 2,6-dimethylol phenol versus the 2,4-dimethylolphenol. However, there is a favorable change in ΔS^* of about 1.5 eu in favor of the 2,6-derivative. When this fact is combined with the general decrease in required activation enthalpy that follows greater substitution, a fast reaction results. If the hydrogen bonding proposal of Freeman and Lewis provided electronic driving force for the rapid *para*-methylation of the 2,6-derivative, one would expect to see a favorable change in ΔH^* for the final methylation in the 2,6- versus the 2,4-derivative. This is not seen. The activation enthalpies for the two species are nearly identical. Thus, it seems likely, based on these calculations, that steric factors, rather than electronic activation, account for most of the differences in the rates of the last methylations. Figs. 10–12 further illustrate these points.

It is quite possible that the hydrogen-bonded structure proposed by Freeman and Lewis is partially responsible for the favorable steric situation. The hydrogen-bonded structure would tend to hold the relatively large methylol hydroxyls closer to the plane of the ring. This would reduce their interference to the approach of methylene glycol to the reactive *p*-surface of the ring. If we see the methylation of phenol as an interaction with the ring π -system, a perpendicular approach is required relative to the plane of the ring. There is a conflict between this thinking and the observed ΔS^* for *para*-reaction of the mono-*ortho*-substituted phenol.

In summary, it is clear that methylation is a bimolecular, second-order reaction. As methylol groups are added to the ring, the ring undergoes general activation. Addition of *o*-methylol groups increases the acidity of the phenolic hydroxyl, which could increase reaction rates. However, all methylol groups ap-

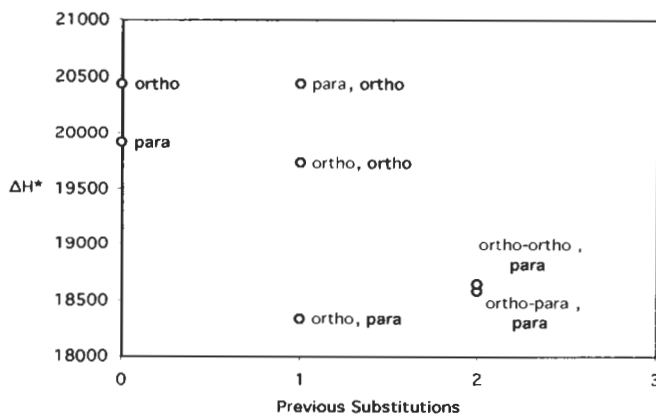


Fig. 11. Activation enthalpy requirements by reactive position in light of previous substitutions [80].

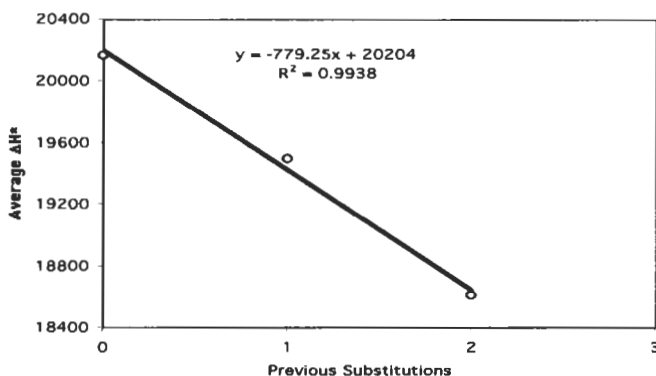


Fig. 12. Average effect of substitution on activation enthalpy.

pear to be activating. *Para* ring positions are somewhat more reactive than *ortho* positions. Only salted phenol reacts appreciably, with the unsalted form serving as solvent. Only methylene glycol reacts with phenol to any extent. Paraformaldehyde polymers do not react directly with phenol under resole conditions. Once methylol phenols begin to form there is competition between the ring positions and the methylol groups for methylene glycol. When the methylol groups react with formaldehyde hemiformals are formed. These slow methylolation. The phenolic hydroxyl does not form these hemiformals. Base does not have much effect on the depolymerization of paraformaldehyde nor on the formation or decomposition of hemiformals. Several models are available for calculation of methylol phenol formation. The best of these are probably those derived by Zavitsas and Higuchi.

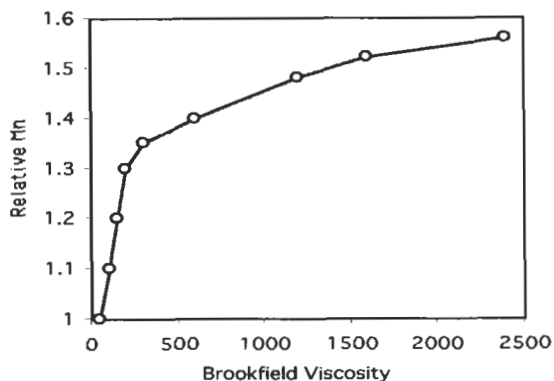


Fig. 13. The relationship between viscosity and relative number-average molecular weight for a certain resole. Different resoles will have different relationships. Note the non-linearity.

9. Condensation kinetics and mechanisms in resoles

As we stated earlier, the molecular weight advancement in phenolics occurs through a step-wise condensation process. Depending on the intermediates involved the molecule condensed out of the structure may be either water or formaldehyde. An overview of this process was provided in Scheme 3.

Early work on condensation leaned heavily on changes in physical characteristics to indicate reaction rates. These studies relied on changes in viscosity, density, refractive index, cloud points, and gel times to estimate molecular weight development [142]. Unfortunately, most of these parameters do not enjoy linear relationships with molecular weight throughout the normal molecular weight range, and there are often critical points in the relationships. For example, Fig. 13 shows the relationship between viscosity and the relative number-average molecular weight in a certain resole. It should be obvious from Fig. 13 that viscosity is a poor measure of polymer development. The same is true of all physical parameters. It should be mentioned here that, though viscosity is not a good tool for predicting molecular weight, it makes an excellent tool for controlling condensation reactions. Viscosity effects at higher molecular weights are greatly magnified so that a large change in viscosity signifies only a small change in molecular weight. This high viscosity sensitivity provides excellent molecular weight control.

Average molecular weight development can be measured directly through GPC or SEC, as we mentioned earlier. These measurements have their own problems, but can be very useful when properly tested and interpreted. They provide an excellent basis for predicting PF performance. They can also give an overview of PF condensation kinetics and even some information about polymer shapes. However, they do not provide detailed information on the chemical structure of the polymer. Such information is required to propose reasonable mechanisms. ¹³C-

NMR, IR, and HPLC have become the tools of choice for such mechanistic studies [128,132,143–159]. CP-MAS based on ^{13}C -NMR has been useful in studying the condensations in solid PF [143].

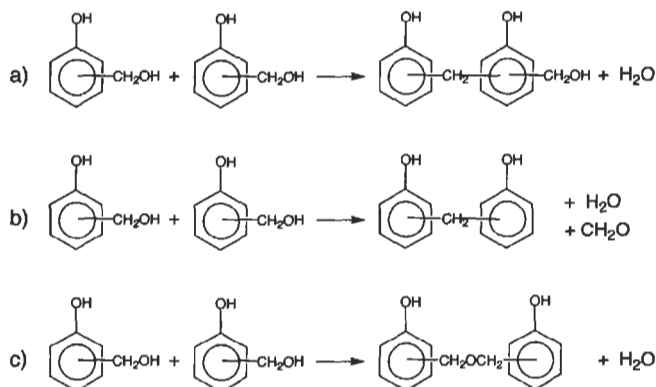
The study of PF polymerization is far more difficult than that of methylation due to the increased complexity of the reactions, the intractability of the material, and a resulting lack of adequate analytical methods. When dealing with methylation, we saw that every reactive ring position had its own reaction rate with formaldehyde that varied with the extent of prior reaction of the ring. Despite this rate sensitivity and complexity, all reactions kinetics were second-order overall, first-order in phenol reactive sites and first-order in formaldehyde. This is not the case with the condensation reactions.

There are still a number of unresolved disputes regarding the mechanisms of the resole condensation reactions. For example, Jones reports that the base-catalyzed condensation of 2,4,6-trihydroxymethyl phenol (THMP) occurs through a first-order process [147]. Higuchi et al. report that Jones was in error and that condensation of THMP occurs through a second-order process [149]. This is not the first time this has happened [154,155]. Higuchi et al. have determined that the base-catalyzed condensation of the various hydroxymethyl phenols are of order 1.0 for 2-hydroxymethyl phenol (2-HMP), 1.33 for 4-hydroxymethyl (4-HMP), and 1.12 for 2,4-dihydroxymethyl phenol (2,4-DHMP). Kim et al., on the other hand, felt justified in reporting second-order rate constants for their resole condensation studies [144]. Several other authors have reported condensations of hydroxymethyl phenols as first-order processes [125,152,156,157]. In addition to these fundamental problems, phenolic condensation mechanisms are known to vary with pH and they may also vary with temperature and concentration [143,132,147]. Most researchers agree that the condensation of hydroxymethyl phenols is second-order in phenol alcohol concentration under acidic conditions [147,150,151].

Another thing that everyone seems to agree on is that there are three general mechanisms through which condensation may take place [128,147]. These are illustrated in Scheme 4a, b, and c.

Scheme 4a shows the condensation of a benzyl alcohol group with a phenolic ring position occupied by hydrogen to produce a methylene linkage between two phenolic rings and producing one mole of water as a by-product. This type of condensation occurs at both high and low pH. It is the type most commonly seen in both resoles and novolacs.

Scheme 4b depicts condensation between a hydroxymethyl group and a phenolic ring where the hydroxybenzyl attacks at a ring position that is already hydroxymethylated. In this case, a methylene linkage is produced between the rings with concurrent loss of one mole each of formaldehyde and water. Both Jones and Grenier-Loustalot et al. demonstrated the occurrence of this reaction pathway beyond doubt under basic conditions.



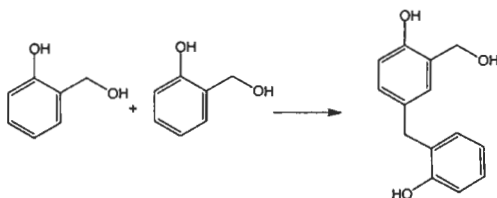
Scheme 4. Condensation mechanisms for hydroxymethyl phenols.

Sprung and Gladstone were the first to show the formation of dibenzyl ether linkages during the condensation of hydroxymethyl phenols, as depicted in Scheme 4c [152]. These results have been corroborated by a number of researchers since [128,144,147,148]. This condensation was reportedly second-order and takes place at pH conditions near neutral and at temperatures less than 130°C [128,147,153]. At temperatures of 160°C the dibenzyl ethers are converted to something else, most likely to methylene linkages and formaldehyde [132].

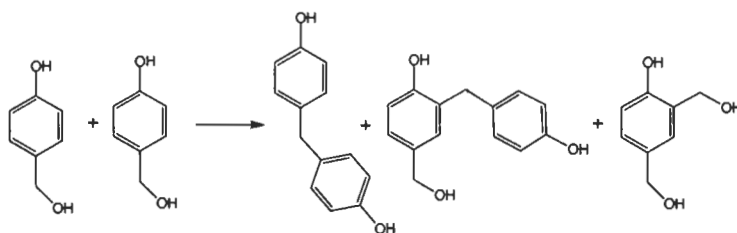
The pathways described above lack description with regard to ring position effects. As mentioned earlier, each ring position has its own reaction mechanisms available and these will vary across other reaction conditions, e.g. pH. ¹³C studies by Grenier-Loustalot et al. and by Kim and co-workers have clearly shown differences in reactivity for the various ring positions in their various states of substitution [128,144].

The primary results of all of these studies are that condensation occurs far more readily at the *para* position than at *ortho* and that methylation tends to activate condensation much as it does methylation. An important inference from these results is that steric factors appear to be quite influential in the condensation process.

Kim et al. observed a number of facts gleaned from ¹³C-NMR that led to an overall picture of the reactivity of various hydroxymethyl phenols (HMPs) [144, 148]. Grenier-Loustalot and co-workers did a number of important experiments that expanded Kim's findings and clearly delineated the reactivity of the various functional groups position-by-position [128]. The two studies show excellent agreement. The materials that follow are drawn from these two reports without further citation. As shown in Scheme 5, the condensation of 2-HMP at pH 8 and 60°C resulted in only one product. This product is the result of *p*-attack on the ring by the hydroxymethyl group.



Scheme 5. Condensation of 2-HMP.

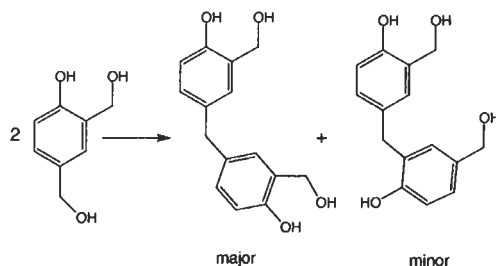


Scheme 6. Condensation of 4-HMP.

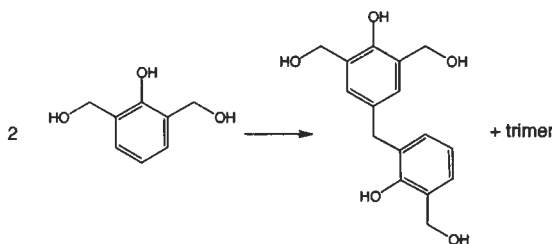
Several products resulted when 4-HMP was allowed to condense under the same conditions. These are provided in Scheme 6. These products indicate that a *p*-hydroxymethyl group can react with either an unsubstituted *ortho* position or through an ipso-attack on a hydroxymethyl-substituted *para* position. The two condensation products were formed at approximately equal rates. Since there were two unoccupied *ortho*s, it seems that the specific reaction rate for the *ortho* site is about half that of the occupied *para* position in this situation. The condensation rate for 4-HMP was about 5 times the rate for 2-HMP overall.

These two experiments make a number of important points. An *o*-HMP will not react with an *ortho* position as long as a *para* reaction site is available. A *p*-HMP will react with unoccupied *ortho* position at about half the rate that it reacts with a substituted *para* position. This suggests that there is something special about the repulsion between the phenolic hydroxyls. Since the pH was only 8, it is clear that there was ample opportunity for a salted 2-HMP to find and react with an unsalted 2-HMP. Both species were present. On this basis, we cannot invoke repulsion of like-charged ions. According to Jones salted species probably react with unsalted species and this is one reason that reaction rate drops rapidly when PF pH gets much above 9.0 [147]. Yet the phenolic hydroxyl appears to be the cause of the reduced reactivity of the *ortho* position. Unfortunately, Jones did much of his work in a carbonate buffer. He did not realize the pH-dependent accelerating effects of carbonate on PF condensation.

It would not be unreasonable to suggest that the dipole moment of the phenolic system has a negative skew toward the aromatic hydroxyl and that the electronic repulsion of these groups in an *ortho-ortho* situation greatly reduces the likelihood



Scheme 7. Condensation of 2,4-DHMP.



Scheme 8. Condensation of 2,6-DMPH.

of reaction. It would likewise be reasonable to believe that the phenolic hydroxyl is hydrogen-bonded to the aqueous solvent and that the size of this complex provides more hindrance than might be expected on the basis of hydroxyl size alone. This latter argument seems weaker since the *p*-HMP is able to react.

When 2,4-DHMP was allowed to condense, 3,3'-dihydroxymethyl-4,4'-dihydroxydiphenyl methane was the main product. Scheme 7 shows the two main products developed. It seems likely that both products have reacted through loss of a *p*-HMP group. There is some confusion in the paper regarding the identity of the minor product, however, the structure shown appears to be the most likely one [128].

The 2,6-DHMP condensation produced only one dimer and a significant amount of trimer as depicted in Scheme 8. The structure of the trimer was not reported. The reaction path is analogous to that of 2-HMP, but occurred at a faster rate. 2,6-DHMP was the only derivative to form a significant amount of trimer under the reaction conditions studied. This supports the idea that *ortho*-linked PF polymers should have a faster cure than others. It also points out the futility of attempting to manufacture an *ortho*-linked polymer under alkaline conditions. Extension of the polymerization process as depicted in Scheme 8 leads to a continual reduction in the amount of *para* functionality available for condensation as shown in Table 7.

Table 7 shows that if we start making our resole with pure 2,6-DHMP, only about 5% of the reactive sites will still be *para* functions when we reach a

Table 7

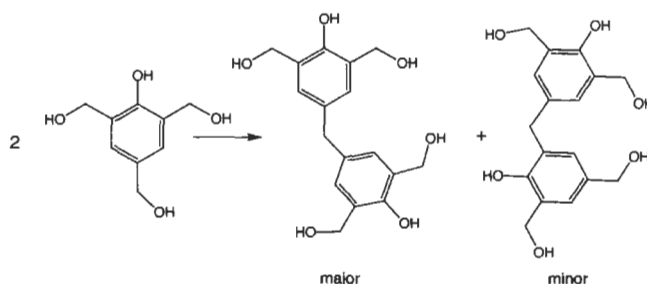
Percent *para* functionality with degree of polymerization of 2,6-DHMP

DP	1	2	4	8	16
% <i>para</i>	25	20	14.3	9.1	5.3

molecular weight of 2200. This is a molecular weight that would be fairly typical of a plywood resin at use. It is possible that 5% is enough to show acceleration, but it is clearly sub-optimal. It is not enough, then, to *ortho*-methylolate, to optimize one must also polymerize 2,6-DHMP through *o,o*-linkages. Unfortunately, 2,6-DHMP is the best case and it is highly unlikely that we will start with much of it in the resin (see Figs. 6 and 7). All of the other monomers converge to zero *para* at much earlier stages. Both the 2,4-DHMP and the 2,4,6-trihydroxymethyl phenol (THMP) go to practically no *para* functionality at the dimer stage. Only the minor products retain any active *para* functionality.

Scheme 9 shows the condensation of THMP. The major product is formed through *p,p*-condensation with loss of formaldehyde. The minor material is probably formed through *ortho* methylol attack on the *p*-HMP partner with formaldehyde loss from the *para* position. Again there was no sign of *ortho-ortho* coupling. Kim et al. show that materials containing 2,6-dihydroxymethyl functionality build up during the condensation of PF, thus confirming the low *o*-hydroxymethyl reactivity. Unlike Grenier-Loustalot and company, who find no evidence of *o,o*-coupling (8 h at 60°C, pH 8, and $F/P \leq 3.0$), Kim and co-workers show the development of a small amount of *o,o*-linkage at extended condensation times (8 h at 70°C, pH 10.2, $F/P = 2.51$). This suggests that condensation between hydroxymethylated *ortho* groups does occur slowly under conditions of high pH and at higher temperatures. This is highly fortunate.

Since the functionality available for curing most commercial PF resins is likely to consist mainly of *o*-hydroxymethyl units, it is obvious that these groups do condense at significant rates under the high temperature curing conditions that



Scheme 9. Condensation of THMP.

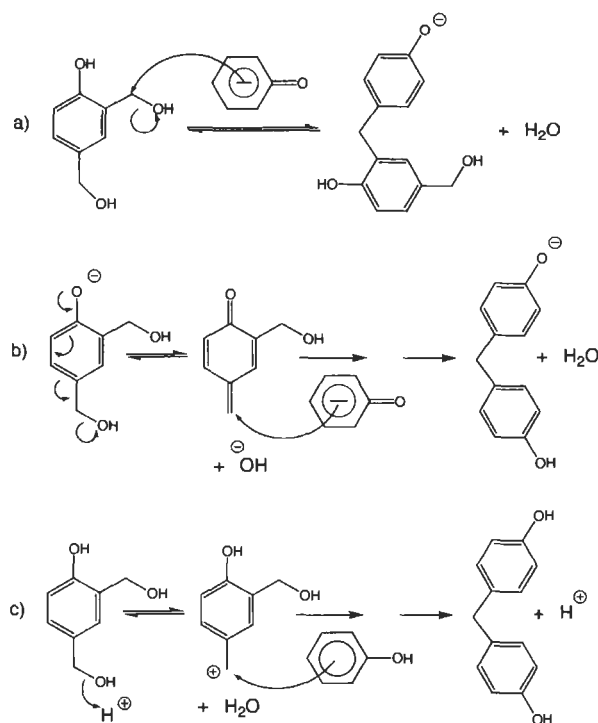
prevail. Typically, plywood resins will see a minimum curing temperature of 104°C while OSB resins usually experience curing temperatures of 115°C or higher. If the problems in attaining *o,o*-linkages stem from steric interactions due to water complexation with the phenolic hydroxyl, this fact, coupled with the requirement that most commercial PF must cure through *o,o*-interactions, would explain much about the observed sensitivity of PF resin curing to moisture.

Grenier-Loustalot shows that there is a general increase in PF reactivity toward condensation as hydroxymethyl groups are added. This is analogous to the situation with the methylation reaction [128]. Freeman and Zavitsas also report activation with more hydroxymethylation. The two most reactive monomers toward condensation are 2,6-DHMP and THMP. So and Rudin support this idea with data showing increased cure speed with rising molar ratio. The reactivity of THMP is somewhat surprising in view of the steric requirements for ipso-attack on the *para* position. Apparently, the ring activation attained outweighs the steric factors in this case. Many researchers have reported ipso-attack and formaldehyde loss to form methylene linkages between rings, involving *o*-hydroxymethyl in some cases. Thus, the steric restrictions must not be too severe.

Despite much talk of mechanisms, there are no solid, detailed mechanisms available for the condensation of PF resoles. In this context, 'detailed' means that transition states and intermediates have been identified or reasoned with a high degree of reliability. There are three strong possibilities for PF condensation mechanisms that are widely accepted and reasonable. However, with the exception of the acid-condensation case, it has been impossible to tell when each is acting. This will not be cleared up until such time as the condensation reaction order questions have been well answered. The three widely accepted possibilities under ionic reaction conditions are shown in Scheme 10. As we have noted, there are difficulties with mechanisms 10a and 10b that have not yet been rationalized. Perhaps there are some possibilities that have not yet been recognized. There is still room for some good mechanistic work. A situation exists where the use of esters to accelerate the cure of PF resoles goes through the quinone methide. Under these conditions, the expected methylene-phenyl ether is formed [119,133]. The quinone methide intermediate is well established through ¹⁸O studies and product analysis in this case [133].

10. Resole curing

As we have already mentioned, the cure of resoles takes place primarily through further extension of the condensation process, though the conditions are usually considerably different from those of synthesis. The changes in conditions normally include exposure to much higher temperatures and higher concentrations of polymer than are seen in resin synthesis. The pH of the medium may also



Scheme 10. Mechanistic possibilities for PF condensation. Mechanism a involves an S_N2 -like attack of a phenolic ring on a methylol. This attack would be face-on. Such a mechanism is necessarily second-order. Mechanism b involves formation of a quinone methide intermediate and should be first-order. The quinone methide should react with any nucleophile and should show ethers through both the phenolic and hydroxymethyl oxygens. Reaction c would not be likely in an alkaline solution and is probably illustrative of the mechanism for novolac condensation. The slow step should be formation of the benzyl carbocation. Therefore, this should be a first-order reaction also. Though carbocation formation responds to proton concentration, the effects of acidity will not usually be seen in the reaction kinetics in a given experiment because proton concentration will not vary.

be different. For example, OSB is pressed at platen temperatures up to 440°F (227°C). The surface of the board gets pretty close to the platen temperature and the core of the board may reach 260°F (127°C) or more on thinner panels. OSB moistures usually start at 6–8% of total wood weight and drop to around 1–3% during pressing. The wood pH usually starts out somewhere between 4 and 6, so that considerable neutralization of the resole is likely to occur during cure. The resin is only about 3% of wood weight.

There are some reports proposing that structures not present in the aqueous resole are formed during cure, to include 2,2-diphenyl ethanol and 1,1,3,3-tetraphenyl propane crosslink structures [132,158,159]. However, these have not

been confirmed in careful ^{13}C NMR studies. It is possible that the alkali in the system can extract a small equilibrium amount of methylene proton between rings in a manner analogous to base-catalyzed aldol reactions, though it is doubtful that enough alkali is present to make this an important mechanism for cure. It is not likely that temperatures get high enough to produce significant amounts of free radicals under these conditions. Most phenolics show no signs of decomposition below 180°C . Furthermore, aromatic rings are excellent radical scavengers, further reducing the likelihood of reactions between aliphatic moieties.

In the wood products panel industry, cure is intended to develop physical strength and stiffness in the product being manufactured and to permit the phenolic to reach a high state of durability. The amount of hot-press time required in manufacturing is not usually limited by these two goals. Instead, it is determined by the time required by the phenolic to develop enough strength to permit opening of the press without blows or delaminations. Blows are failures that occur when the gas pressure of the steam in the pressed board exceeds the strength of the board. They usually occur in hot, high density, or high moisture spots in the panel. Delaminations are separations that result from areas where the resin strength cannot withstand the internal stresses imposed by changes in wood dimensions during press opening. They usually occur at the corners or cold spots in the pressed panel. Normally, the phenolic has received enough heat in the press to facilitate development of the required stiffness and durability in use before it has sufficient strength at pressing temperatures to permit press opening. This is largely because the curing process continues long after the board is removed from the press by virtue of residual heat. Therefore, development of physical strength is the key to high mill productivity, in most cases.

Geimer and a group from the USDA Forest Products Laboratory in Madison (WI) have studied the cure of phenolic resins using dynamic mechanical analysis (DMA), a technique that allows simultaneous measurement of strength development and heat flow [117]. Study parameters included the effects of moisture, temperature, and initial PF resin molecular weight on the rates of mechanical strength development. They compared the rates of strength development to the heat generated by the resins during the curing process and noticed that the comparisons varied with conditions. As a result, they developed the concepts of mechanical cure and chemical cure.

Geimer et al. first ran a series of experiments using high and low molecular weight PF resins at 140°C under dry conditions. These tests showed that high molecular weight resins developed higher mechanical strength at lower degrees of chemical cure. In the case studied, the high molecular weight resin developed about 70% of its ultimate strength at only about 5% chemical cure, while the low molecular weight PF required about 25% chemical cure to reach the same level. Whereas the relationship between chemical and mechanical cure is linear to 100% mechanical cure for the low molecular weight resin, the high molecular

weight resin shows diminishing returns after the initial 70% mechanical cure. Both systems reach maximum available mechanical cure with only about 30% chemical cure under these dry conditions. Our perception of PF cure speed is also, no doubt affected by this fact and it has often been observed that moisture slows PF resin cure in wood products processes. We have mentioned some chemical possibilities for this phenomenon already as well as showing the impact of dilution on the RSST results. Now we see that there may be both physical and chemical aspects to the effects of water.

The Geimer group goes on to report the effects of moistures up to 91% relative humidity (RH) at 115°C on the curing phenomenon. Both the high and low molecular weight resins required higher levels of chemical cure to reach a given level of mechanical cure as moisture increased. At 41% RH the low molecular weight resin required about 45% cure to reach complete mechanical cure while the high molecular weight system needed about 20% chemical cure. Both resins also needed more time to achieve a given level of chemical cure. The impact of moisture was greater on the low molecular weight resin.

Despite the rate reduction seen, however, the higher moisture had beneficial effects on the ultimate strength achieved with the high molecular weight system, though not with the low molecular weight resin. Apparently, strength development is limited by strength development. It seems likely that the higher humidity provided opportunity for flow in the system and permitted a more thorough curing process at 115°C. The 140°C temperature imparted sufficient flow to achieve the required cure under dry conditions but 115°C only permitted about 40% of the mechanical strength development under dry conditions. Chemical cure was not inhibited to the same extent as mechanical cure, at least up to 25% chemical cure.

In some of our own studies with thin PF films using differential scanning calorimetry (DSC), we saw corroborative results [160]. In this work, we noted that reaction initiation occurred at progressively higher temperatures as moisture content rose. This implies slower reaction rates. On the other hand, curing temperature had to be pushed higher to attain full cure as moisture was reduced. The curing peaks split into two parts at low MC, indicating that cure stopped at some point and temperature had to be raised to restore reactivity. A relationship between moisture and molecular mobility appears consistent with these results. Overall the low moisture materials showed larger areas under the curing peaks. This suggests that moisture reduces ultimate cure as well. The DSC scans are shown in Fig. 14.

All of the observations above relate well to our own with respect to the effects of molecular weight on the available cure speed in manufacturing, both in plywood and OSB. They also correlate with our experience on the effects of molecular weight and dry-out on bond quality.

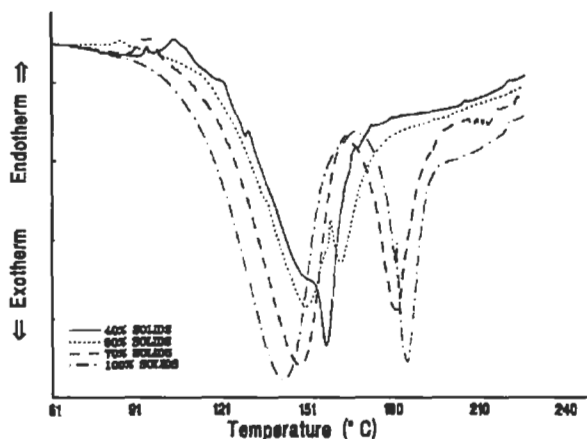


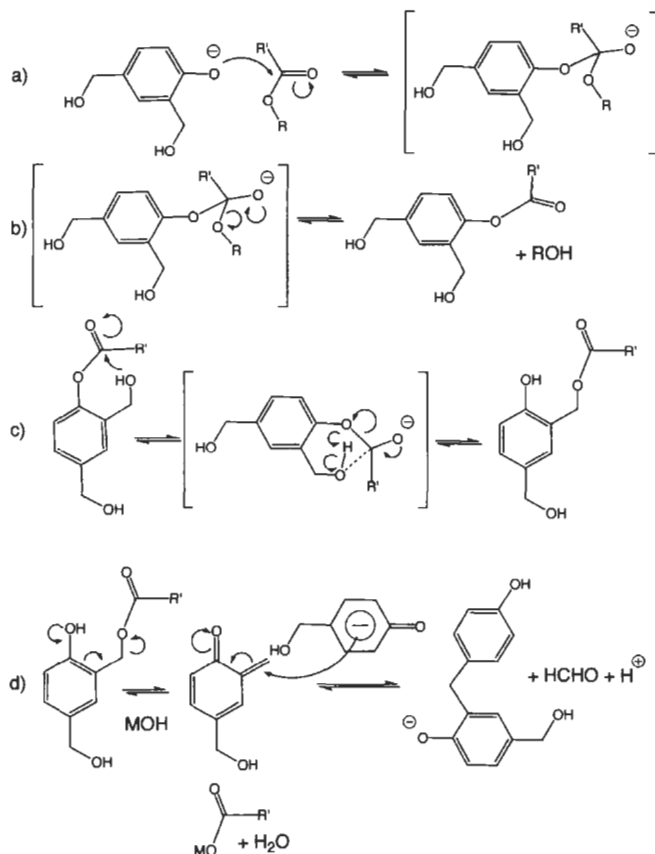
Fig. 14. DSC evaluation of the effects of moisture content (by weight) on the reactivity of a PF film [160].

11. Cure accelerators for resoles

Helmut Orth first reported the use of lactones to accelerate phenolic resole cure in 1957 [161]. A year later, Orth discovered that this effect could be extended to aliphatic esters as well [162]. Despite the dramatic nature of the acceleration seen, Orth's observations were not applied in industry for a decade. In 1967, Sumitomo and BASF applied esters to soil grouting and wood uses [133,163, 164]. Neither of these applications were commercially successful, however, and commercial success would not occur until 1980 when Borden introduced ester-cured sand binders for foundry [165]. This technology was highly successful in UK and spread to the US, where it was applied immediately to foundry in 1981 and eventually to wood products in 1990 [119,166–173]. Esters are capable of reducing the gel times of resoles from several weeks to less than 30 s at room temperature. Both gaseous and liquid esters are applicable [119,166].

The mechanism of this reaction has been studied by several groups [133,174–177]. The consensus is that interaction of ester with the phenolic resole leads to a quinone methide at relatively low temperature. The quinone methide then reacts rapidly leading to cure. Scheme 11 shows the mechanism that we believe is operative. This mechanism is also supported by the work of Lemon, Murray, and Conner. It is challenged by Pizzi et al. Murray has made the most complete study available in the literature [133]. Ester accelerators include cyclic esters (such as γ -butyrolactone and propylene carbonate), aliphatic esters (especially methyl formate and triacetin), aromatic esters (phthalates) and phenolic–resin esters [178]. Carbamates give analogous results but may raise toxicity concerns not usually seen with esters.

Esters and the like only provide acceleration under basic pH conditions. In



Scheme 11. Proposed quinone methide condensation mechanism. Work by Murray (and Lemon unpublished) showed clearly that the quinone methides formed from *o*-hydroxymethyl and not *p*-hydroxymethyl groups in the presence of ester.

some alkali ranges, base addition further speeds the process. However, base competes with phenate for the ester and too much will result in the need for high ester usage or reduced cure. A mole of acid is produced each time a crosslink is formed so that the system is self-neutralizing. The need for base provides some support for the mechanism proposed, as does the observed self-neutralization. That only *o*-hydroxymethyl phenols participate in the ester cure provides additional support. This fact was gleaned from model compound studies [133]. The ¹⁸O studies and identification of a quinone methide dimer also add strength to the mechanism in Scheme 11.

Murray remarks that ester-cured phenolics do not produce the strength seen in some other systems. This could be due to several factors. First it may be due to incompleteness of cure under the conditions provided. We have noticed that

ester cure at room temperature stops or slows remarkably at gel when liquid esters are used. It stops well short of full crosslinking. This may be analogous to the situation described earlier for mechanical cure. Heat assistance may be required to drive the cure to completion due to loss of mobility. Conner et al. added ester at different stages of cure and showed that, under their conditions, ester depletion had occurred and that more ester led to more cure [174]. The same could be true of alkali. In addition, with liquid esters, carboxylate and alcohol residues may remain in the cured resin to act as plasticizers and soften the resin. Though plasticizers may improve PF durability in some cases, they nearly always detract from strength and stiffness. We have noticed that ester-cured PF resins are slightly more susceptible to water absorption and thickness swell in OSB. Since ester-cured resin is likely to achieve a high level of cure in OSB, the plasticizer effect is probably important in some cases.

Another approach for speeding PF resin cure utilizes faster phenolics as accelerators. The most popular of these has been resorcinol. Many different approaches have been tried. Resorcinol has often been cooked into the PF resin. This is probably the least effective approach available. Depending on the amount of resorcinol used and other reaction conditions, different results are obtained. If enough resorcinol is added to the beginning of the cook, a resorcinol-formaldehyde polymer will rapidly form. This polymer will contain little or no phenol. Thus, in a viscosity-limited system, the resin may hit the viscosity endpoint while still containing large quantities of raw phenol and formaldehyde. Meanwhile, the resorcinol-formaldehyde polymer will have exhausted all of the resorcinol functionality during its formation. Such a polymer will not show the rapid curing characteristics hoped for and will have high VOC emissions. If only a small amount of resorcinol is used, it will become thoroughly incorporated into the phenolic polymer and will show no special reactivity in cure. Sometimes, the resorcinol polymer made in the first case will break down in the presence of the excess phenol to give the same result as the second case. This will only happen if the reaction time and conditions are sufficient to allow it.

A second approach involves addition of resorcinol after forming the PF polymer. This is basically the approach used for manufacture of phenol-resorcinol-formaldehyde (PRF) resins. In the case of a PRF, the amount of resorcinol is usually on the order of 20% of the final resin composition. When someone is basically trying to make a PF that is a little faster curing, they normally try to add only 1–5% resorcinol. If the phenolic part is a normal resole, the resorcinol will react rapidly until its functionality is used up. Since resorcinol will react at significant rates at temperatures as low as 4°C, a resin of this type has no storage stability under normal conditions if there is enough resorcinol to create fast cure. This approach will result in a high molecular weight, which will be somewhat fast curing on that basis. However, the resorcinol reactivity is normally expended in the course of thickening the resin in storage and will have little to offer during cure.

Resorcinol will react rapidly with hydroxymethyl as well as free formaldehyde; thus only a resin with low-to-nonexistent methylol will be stable in its presence. Such a resin is not likely to show good cure speed unless some sort of latent, protected methylene donor is present. This approach may be viable in a user's mill where the storage time after resorcinol addition is relatively short. If the resorcinol is dissolved, in-line mixing with the PF would be a reasonable approach.

Resorcinol additions just prior to use provide acceleration, though they are still not the most cost effective nor technically effective use of resorcinol. In-line addition of a PRF resin just before application of the resin to the adherend achieves better results at less than half the cost of resorcinol chemical, in most cases; and it is easier to handle. A variant of this concept is application of the resorcinol and PF resins to the substrate separately but in a way that permits them to come into contact during the curing process. Such methods are sometimes called honeymoon systems.

Recently, a two-part cross-catalyzed system has been developed that takes advantage of both the acceleration abilities of resorcinol resin and ester [179]. The term 'cross-catalyzed' is applied because the phenolic resin contains an accelerator-crosslinker for the resorcinol resin while the resorcinol resin carries an accelerator for the PF, in addition to itself being capable of improving PF cure speed. In each part, the resin carrier for the accelerator is not susceptible to acceleration by the material contained. It is only when the systems are mixed that the accelerators are activated. This system is faster and lower in cost than most of the resorcinol accelerators and gives better bonds (in wood products) than the ester cure alone [179]. Another variant of the resorcinol approach utilizes resorcinol-glutaraldehyde resins [180–182].

Perhaps the lowest cost accelerators for PF resoles are inorganic carbonates and carbon dioxide [118,183,184]. Potash and soda ash have been added to PF plywood mixes for many years. Though the results are not as dramatic as those seen with organic esters, resorcinol, and related derivatives, they work well and are cost effective. The mechanism by which they operate is not known. Levels between 0.25 and 2%, based on liquid resin are normally used.

12. General synthesis of novolacs

While resoles account for most of the volume in phenolic products, novolacs account for most of the diversity. They are used in a wide variety of applications. They also tend to be significantly more expensive than resoles. The higher cost and pricing structure permits more creativity in their formulation. Many novolacs are made in small volumes and are formulated for very specific purposes. It is, therefore, rather difficult to make meaningful generalizations about novolacs beyond a few basic concepts.

Novolacs are usually made under acidic conditions. Oxalic, sulfuric, toluene sulfonic, phenyl sulfonic, methane sulfonic, hydrochloric, and phosphoric acids are the most common catalysts, though nearly any moderately strong acid will probably do. Often selection of the acid has significant effects on the resultant polymer structure or performance. Sometimes acids are selected for their volatility, as it may be necessary to distill the acid off in some processes.

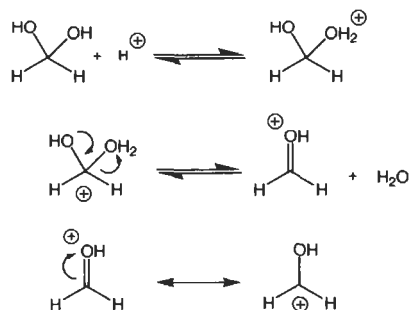
While phenol is the most common monomer for novolac manufacture, it is far more common to see incorporation of other phenolic materials with novolacs than with resoles. Cresols, xlenols, resorcinol, catechols, bisphenols, and a variety of phenols with longer alkyl side chains are often used. While most resoles are made with a single phenolic monomer, two or more phenolic materials are often seen in novolac formulae. These additional monomers may be needed to impart special flow characteristics under heat, change a glass transition temperature, modify cure speed, or to adjust solubility in the application process among others.

Novolacs are often modified through alkylations based on reactions with monomers other than, and in addition to, aldehydes during their manufacture. Examples might be inclusion of styrene, divinyl benzene, dicyclopentadiene, drying oils, or various alcohols. Despite significant production of all of these variants, most novolac volume is produced using phenol and formaldehyde.

Novolac manufacturing processes often call for much higher temperatures than resoles. Most resoles are aqueous and therefore manufactured at temperatures on the order of 100°C or below. It is not uncommon for novolacs to require temperatures in excess of 300°C for successful processing.

Many applications of novolacs are found in the electronics industry. Examples include microchip module packaging, circuit board adhesives, and photoresists for microchip etching. These applications are very sensitive to trace metal contamination. Therefore the applicable novolacs have stringent metal-content specifications, often in the low ppb range. Low level restrictions may also be applied to free phenol, acid, moisture, and other monomers. There is often a strong interaction between the monomers and catalysts chosen and attainment of low metals levels. These requirements, in combination with the high temperature requirements mentioned above, often dictate special materials be used for reactor vessel construction. Whereas many resoles can be processed in mild steel reactors, novolacs require special alloys (e.g. Inconel[®]), titanium, or glass for contact surfaces. These materials are very expensive and most have associated maintenance problems as well.

The formaldehyde-to-phenol molar ratios of most novolacs lie somewhere between 0.30 and 0.99. This is a very broad range in the eyes of a novolac chemist. Novolacs are extremely sensitive to molar ratio variation and they are usually specified to the nearest 0.001 molar ratio unit or less. Also unlike resoles, one does not have the option of selecting the development of molecular weight through viscosity control. The molecular weight and viscosity are largely determined by



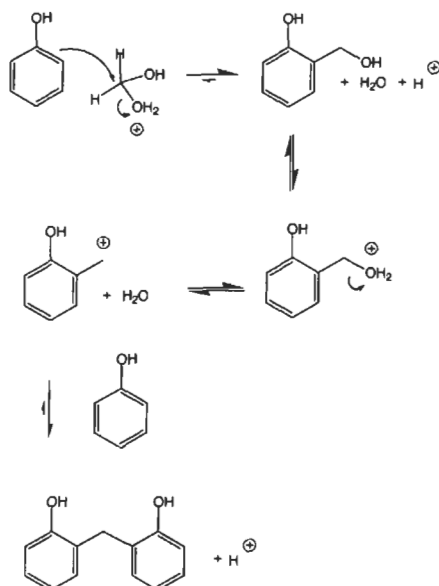
Scheme 12. Formaldehyde activation in novolac synthesis. Any of the charged species shown would be a suitable reaction partner for a phenol. The stability of the cation under the reaction conditions that prevail will determine predominance. Regardless of which is favored, the outcome will be the same.

the ratio of monomers available. The reaction proceeds until all of the aldehyde is consumed. Excess phenolic monomer is then often recovered through distillation.

As with resoles, we can use a three-phase model to discuss formation of a novolac. Whereas the resole is activated through the phenol, activation in novolacs occurs with protonation of the aldehyde as depicted in Scheme 12. The reader will note that the starting material for the methylation has been depicted in hydrated form. The equilibrium level of dissolved formaldehyde gas in a 50% aqueous solution is on the order of one part in 10,000. Thus, the hydrated form is prevalent. Whereas protonation of the hydrate would be expected to promote dehydration, we do not mean to imply that the dehydrated cation is the primary reacting species, though it seems possible.

Methylation occurs next, and the methylolated phenol goes on to build polymer as shown in Scheme 13. A practical difference between novolacs and resoles lies in the relative rates and activation energies of the methylation and condensation steps. As mentioned earlier, we can separate these reactions in resoles by controlling the reaction temperature and reagent concentrations. With novolacs, methylation is the slow step and condensation is faster, thus both reactions proceed simultaneously with little if any methylol phenol accumulating at any point during the synthesis. The condensation step is 5–13 times faster than methylation depending on the phenol and conditions. Though this comment is based on observation, it is also reasonable due to the greater stability of the benzylic cation versus the protonated formaldehyde carbonyl. Whereas the carbonyl cation can spread its charge across only two atoms, the benzyl can dissipate the positive charge across a system of four nearly equivalent resonance hybrids. The hydrated forms of aldehyde may be able to stabilize the charge across three atoms, however, the presence of the extra electron-withdrawing oxygen may negate this stability advantage.

The speed of condensation in novolacs relative to methylation is also the



Scheme 13. Methylation and condensation in novolacs.

primary reason that novolac molar ratios are confined to the region below 1 : 1 *F* : *P*. Anything higher than this leads to gelation and crosslinking during the manufacturing process. Thus novolacs are always made by a two-stage process wherein the polymer is made in the first stage and additional aldehyde is added in a second stage. In most cases, the additional crosslinker is added in the mill; however, it may also be compounded with the novolac when it is shipped in powder form. Such pre-compounded adhesives will have a more restricted storage life than the novolac thermoplast alone. They will also be more sensitive to storage moisture and temperature.

Unlike resoles, which show a definite preference for methylation and condensation at the *para* position, ring positions in novolacs are less differentiated. The normal ratio of *o,o*-, *o,p*-, and *p,p*-linkages in a novolac will be 1 : 2 : 1. This may be affected by the choice of catalyst, and much work has been done to control this aspect of novolac synthesis, with the emphasis on producing highly *ortho*-linked resins. In some cases, the judicious choice of protic acid may lead to the desired result. More commonly, a Lewis acid salt is chosen as the catalyst. These are usually divalent metal salts of acetates or similar small carboxylates. Zinc acetate is probably the most common example. Often resins made using these salts cannot be cleanly characterized as resole or novolac. They may have a resole molar ratio and a novolac pH or they may be made near neutral conditions. As mentioned before, commercial phenolic polymers showing 85% *ortho* linkage are available. Solvent choices may also be important to determination of substitution patterns.

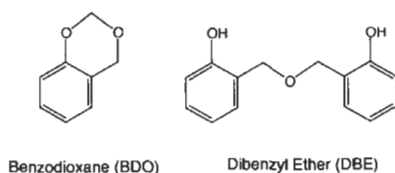


Fig. 15. Some common novolac by-products.

In addition to the normal methylene linkage formation involved in polymerization with both resoles and novolacs, other, usually less desirable, condensation by-products are also seen in novolac synthesis. Among these are benzodioxanes and dibenzyl ethers. The reaction pH has significant effect on the relative amounts produced. Fig. 15 shows typical structures for these by-products. When such by-products are present, the meaning of the molar ratio changes and variability with respect to molecular weight development, glass transition point, and solubility may be seen. They also lead to poor raw material utilization.

An example of a novolac formula is presented in Table 8. A resin of this type might be used to manufacture electronics composites. Formulae for other applications might show considerable differences in molar ratio, monomer choice,

Table 8
A novolac formula example

Material	Relative moles	%
Phenol, 100%	1.000	129.600
Oxalic acid, reagent	0.006	0.455
Formaldehyde, 50%	0.494	40.865
Distillate	—	—70.900
Total		100.00

Charge phenol and oxalic acid into a glass reactor. Heat to $100 \pm 1^\circ\text{C}$ at 760-mm mercury total pressure. Program formaldehyde into the reactor at 1% of total charge per minute. If batch temperature does not exceed 115°C within 10 min, stop charging and wait for 15 min. Call supervisor if temperature does not reach 118°C within 15 min. If exotherm is normal, charge formaldehyde over a 100-min period maintaining temperature between 99 and 120°C . The 120°C is a peak that should be reached when about 15% of the formaldehyde has been added. As addition continues, the batch temperature should naturally drop to about 100°C and level off there. After all formaldehyde is in, reflux until the free formaldehyde is less than 0.6%. When formaldehyde target is reached, begin distillation at atmospheric pressure under full steam. The batch temperature will rise as water is removed. When batch temperature reaches 140°C , gradually apply vacuum until reactor pressure is less than 35 mm mercury. Continue to distill until the free phenol is less than 1100 ppm by GC. The temperature will be about 200°C . Discharge molten resin into decontaminated cooling table. The resin should be a colorless solid with a cone and plate viscosity of about 300–450 cps at 125°C .

catalyst selection, cook style, etc. The variants available through novolac chemistry are virtually unlimited.

13. Novolac curing

Polymerization and curing rates of novolacs depend strongly on the acidity of the reaction mixture. Fig. 16 depicts the general pH dependence. Fig. 17 shows a partial structure for a hexa-cured novolac. Incorporation of amine is widely, though not universally, reported in hexa-cured novolac structures. In addition to the structure shown in Fig. 17, *N,N*-dibenzyl and *N,N,N*-tribenzylamine linkages have been reported [185–192]. The main by-products of hexa-curing conditions are water and ammonia, though formaldehyde is also produced. The structure and abundance of the amino portions of the cured polymer vary considerably with conditions.

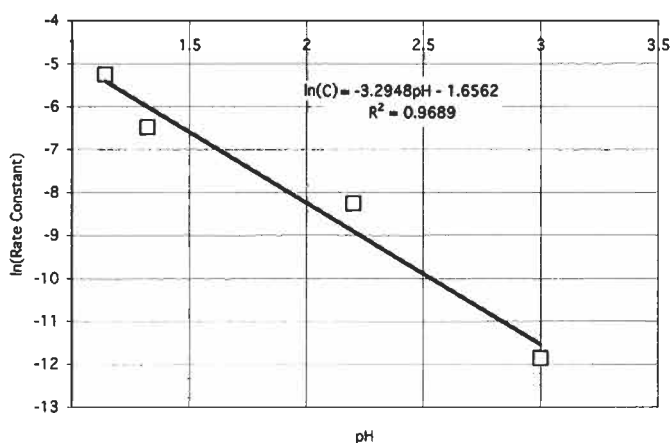


Fig. 16. Effects of acidity on novolac reaction rate in the normal pH range at 80°C.

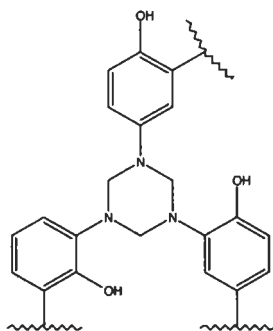


Fig. 17. The structure one linkage in a hexa-cured novolac. Many other linkages are also found.

Cured phenolics are universally brittle in nature. This is true of both resoles and novolacs and does not depend much on the source of methylene used to promote cure. Consequently, the fillers used in molded articles are highly important to the design of the manufactured product. With resoles, the fiber or filler are usually the primary component of the final composite, with the resole acting as a binder or impregnating agent. With novolacs the resin may be the major component in the molded part. Poly-silanes and other organic polymers are also added in some applications to promote impact resistance and toughness [192].

Free phenol is a major concern in the manufacture of novolac resins. This is true for several reasons. The strongest drivers are probably EPA classification of phenol as a Hazardous Air Pollutant and worker safety concerns. However, free phenol also has significant technical effects on such parameters as melt flow characteristics. In this role, free phenol may undermine the desired effects of a molecular weight design by increasing flow beyond the desired point. Since free phenol is often variable, the effects on flow may also cause variation in product performance from batch to batch. Fig. 18 shows the effects of free phenol on the flow across a series of molecular weights. Free phenol contents between 1 and 10% are commonly seen. In recent years, much work has been aimed at reducing the free phenol.

As with resoles, the central issue in design of novolacs is molecular weight. The effects of formaldehyde-to-phenol molar ratio and formaldehyde conversion on molecular weight of novolacs has been well studied and reported [192,193]. The effects of molecular weight on most of the important properties are also available [193]. These include T_g , melt viscosity, gel time, hot-plate flow, glass-plate flow,

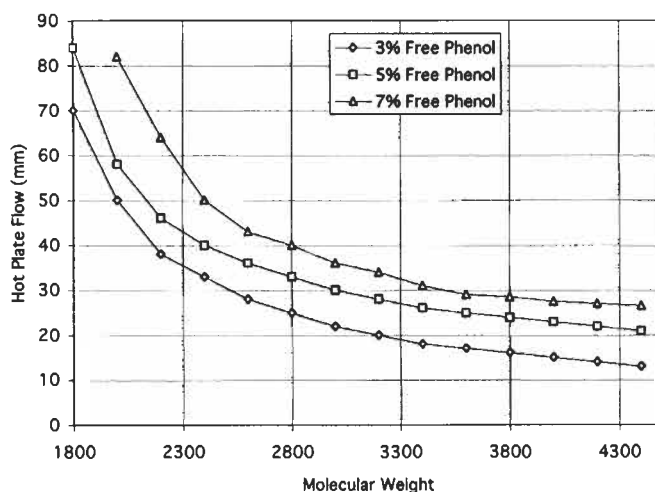


Fig. 18. The effects of free phenol and molecular weight on glass-plate flow by one standard test method. (Data courtesy of R. Boudreau and Borden Chemical, Inc.)

and others. Besides molecular weight and free phenol, the structure of the phenolic pre-polymer, cured composite moisture, hexa content, catalyst type and catalyst content all have important effects on the properties of the cured material. Hexa content will normally comprise between 5 and 20% of the cured polymer weight. Moistures generally range between 0.1 and 1.5% depending on manufacturing objectives. Curing temperature and time are also effective in determining the nature of the final cured product [192]. Typically, curing temperatures between 130 and 250°C are used, although there may be processes that go beyond this range. The required processing temperature and time is linked to the service temperature expectations for the part. It is not unusual to have a two-stage process wherein a part is formed in a first stage then baked to promote further cure.

This concludes our discussion of novolac systems. We have covered only the most basic chemistry and formula strategies. To go further would lead us into technology issues that lie beyond the scope of this discussion and could go on indefinitely. The references provided will lead the interested reader more deeply into the subject.

14. Phenolics as additives for adhesives

14.1. Antioxidants and performance stabilizers

There are many horror stories about the early use of rubber. In 1937, Waldo L. Semon of the B.F. Goodrich company writes: “The deterioration of rubber has been a vexing problem for the last century, as evidenced by several early examples. The flourishing trade in rubber soles, which were prepared from latex in South America and sold in New England in 1830 prompted manufacture at Roxbury, Massachusetts, of substitutes made from crude rubber. The factory-made shoes, however, would not last through the summer, but softened to so great an extent and developed so offensive an odor that many were buried . . . MacIntosh, after whom the water-proof coat was named, had many sad experiences with the deterioration of rubber. When he dissolved it in turpentine and spread the cement on fabric, the rubberized cloth often became brittle and malodorous . . . Goodyear thought he had succeeded in making rubber articles serviceable when he utilized Hayward’s sulfur treatment and ‘dried up’ the surface. Relying on this treatment, he took a contract from the government for making mailbags. The mineral pigments which he had incorporated caused the rubber to age so poorly that the bags soon decomposed and fell away from the handles” ([194], p. 414). Most of these problems were attributed to oxidation.

Without antioxidants virtually all rubber products, including those made from modern synthetic rubbers, undergo unacceptable performance degradation upon aging [195]. Various aromatic materials and particularly phenols have proven to

be among the most useful antioxidants, thus phenolic materials were introduced to the rubber industry early and continue to be useful antioxidants. The first U.S. Patent (US 99,935) for use of phenolic antioxidants in rubber was issued to Murphy in 1870 ([194], p. 429). Due to phenolic functional equivalent weight and polymerizability, the best phenolic antioxidants may not be polymers. However, phenolic polymers, particularly those based on alkyl phenols, are capable antioxidants and one of their valued uses is prevention of both softening and hardening of various elastomers with age. Part of this performance is probably due to antioxidant activity. It is of particular interest with pressure sensitive adhesive (PSA) and in contact adhesives based on polychloroprene [196,197].

14.2. Structural adhesives

14.2.1. Polyvinyl-phenolics

Phenolics are used extensively with polyvinyl acetals, poly(acrylonitrile) copolymers, and epoxies as the basis for reactive metal bonding systems. The poly(vinyl formal)-phenolic combination (PVF-P) was the first of the phenolic-polyvinyl structural adhesive systems. It was known early as the Redux adhesive system or the Redux process ([198], pp. 11–14). ‘Adhesives of particularly high quality’ are obtained by this technique ([198], pp. 25–39). Redux adhesives still find considerable use in the aircraft industry in structural metal-to-metal bonding, joining metal skins to honeycomb constructions, and metal-to-wood applications where service temperatures will not exceed 80°C. They generally exceed unmodified epoxy performance and equal nitrile-phenolic (except at high temperatures) in high-strength sandwich applications ([198], pp. 25–39). The adhesives are available as two-part systems, one-part emulsions, or films. PVF-P is known for its good weathering capability, fatigue resistance, and its performance retention when exposed to fungi, salts, humidity, water, and oil. Creep resistance at temperatures exceeding 90°C may or may not be good, depending on the specific adhesive formula. Shelf lives normally exceed 1 year.

PVF-P adhesives have been used at de Havilland in Hatfield, England since 1936 for the manufacture of ‘air screws’ [199]. Aero Research Ltd. of Duxford, England, which became CIBA (A.R.L.), originally developed them ([200], pp. 76–83). Currently, the Redux[®] business and trademark belongs to the Hexcel Composites Ltd. and is applied to the original polyvinyl-phenolic alloys as well as epoxies and bismaleimide adhesives that give structural performance at even higher temperatures [201].

One of the first applications of the Redux process was in construction of structural aluminum parts for the de Havilland bomber ‘Sea Hornet’ produced during World War II ([198], pp. 80–81; [202,203]). In the original form, it consisted of a two-part adhesive including a low viscosity liquid phenolic known

as K6 and a poly(vinyl formal) powder with the trade name Formvar[®] C, originally a product of the Shawinigan Products Corporation. Formvar[®] products are now made by the Monsanto Corporation ([200], pp. 76–83; [204,205]. After proper preparation of the metal surfaces, the adhesive was applied by brushing (or by dipping) the liquid phenolic on both metal surfaces to be joined. The PVF powder was then applied by sprinkling and the adhesive was allowed to stand for an hour or more to permit loss of solvent water. The parts were then joined under 50–100 psi (0.3–0.7 MPa) pressure and typically cured for 4 min at 180°C or for 30 min at 145°C, for examples. The cured system is said to be a poly(vinyl formal)–phenolic copolymer.

The PVF is made by acidic reaction between poly(vinyl alcohol) (PVA) and formaldehyde. The poly(vinyl alcohol) is, in turn, made by hydrolysis of poly(vinyl acetate) or transesterification of poly(vinyl acetate). Thus, residual alcohol and ester functionality is usually present. Cure reportedly occurs through reaction of phenolic polymer hydroxyls with the residual hydroxyls of the PVA [199]. The ester residues are observed to reduce bond strength in PVF-based systems [199]. This does not necessarily extend to PVF-P adhesives. PVF is stable in strong alkali, so participation of the acetals in curing is probably unimportant in most situations involving resoles. PVF is physically compatible with many phenolic resins.

Redux was soon extended to other aircraft including the DeHavilland civilian airliner ‘Dove’ and the jetliner ‘Comet’ [202]. In the Fokker F27/F50 ‘Friendship’, it accounted for about 70% of structural bonds (about 550 parts). Over 1000 F27/F50 aircraft were constructed and were in service for over 30 years, indicating high fatigue resistance and durability ([198], pp. 80–81). When attempts were used to substitute low-temperature curing epoxies for PVF, joint corrosion due to salt spray exposure required expensive repairs.

The original two-part PVF-P system used during WWII was still in use in 1983 ([198], pp. 25–39). By 1957, several other grades of Redux[®] adhesives were available from CIBA. These included a one-part emulsion known as Redux[®] 120, a product formulated especially for binding friction linings to brake shoes designated Redux[®] 64, Redux[®] 775 (which resembled the original liquid–powder system), and Redux[®] films 775 and 775R. The films were an unsupported and a glass cloth-supported film, respectively. These are of great utility in gluing metal skins to honeycomb ([200], pp. 76–83). Currently, there are 15 Redux[®] products available. Product 775 is still among them. The modern Redux[®] family includes products capable of extended service at temperatures as high as 230°C or brief service up to 270°C [201]. A minimum service temperature of –55°C is typically available. Lap shear strengths available on 1.63 mm aluminum with a 12.5 mm overlap at room temperature will typically be between 2200 and 7000 psi (15 and 50 MPa), depending on the adhesive chosen [201]. The PVF-P system specifically has shown room-temperature shear of about 5000 psi (35 MPa) with no losses up

to 82°C. Strength falls off rapidly above 90–120°C (formula dependent) ([200], pp. 30–33). A list of physical properties is provided by Wakeman [204].

Poly(vinyl butyral)–phenolic (PVB-P) adhesives are used in many applications similar to those of PVF-P. They show the same good weathering, fungal, salt, humidity, water, and creep resistance as PVF-P. They bond metals and reinforced plastics to paper honeycomb, cork, and rubber. They find use in binding Kevlar® in the manufacture of bulletproof vests and military armor [204]. They are usually a little less rigid than the PVF-P systems and, thus, develop slightly lower structural strength. Their additional flexibility, however, may improve performance when gluing dissimilar materials or in constructions where failure through vibrational fatigue is likely ([198], pp. 25–39; [206]). It also enhances impact resistance. Excellent metal sandwich constructions are made from PVB-P adhesives. PVBs also find considerable use in coatings for electrical wire (also the major use of PVF) and magnetic tape, where a long-term tolerance to bending is needed. They are also used in printing inks and toners for copying machines and printers, which requires excellent flexibility and pigment binding [206]. Useful hot-melt adhesives are also based on PVB. Of course, the main use of the PVB is in binding safety glass for automobiles. In 1984, it was reported that in the prior 50 years of use, no safety glass failure had been attributed to PVB failure do to old age [207]. Monsanto, DuPont, and Union Carbide all produce poly(vinyl acetal) resins for this purpose.

14.2.2. Nitrile rubber–phenolics

Structural adhesives based on nitrile rubber–phenolic (NR-P) show exceptional bond strength and resistance to high temperature effects in both structural and non-structural applications ([198], pp. 25–39). They are particularly useful for structural metal–metal bonding. NR-P alloys are useful at continuous service temperatures as high as 140°C with short-term exposures to temperatures up to 260°C tolerable. Consequently, these alloys are often selected for use in brake linings, clutch disks, engine gaskets, joining airframes, helicopter rotor blade construction, fuel tank liners, and many other aircraft applications. DeLollis states that, due to their low flow during cure, they are not suitable for skin to honeycomb applications [208]. They show excellent resistance to water, oil, fuels, salt, and biological attack. They have relatively poor low-temperature properties, though service temperatures as low as –51°C are reported ([200], pp. 29–30). Strengths actually increase on NR-P adhesives as they are cooled, but they become increasingly subject brittle failure. Despite this shortcoming, DeLollis characterizes NR-P as one of the toughest and most durable products developed for the adhesive industry [208].

Curing temperatures of 150–250°C are required. The best strengths are developed at the highest curing temperatures ([200], pp. 29–30). Cure times are

relatively long, typically about 2 h at 150°C or 8 min at 220°C. Pressures of 10–200 psi (0.1–1.4 MPa) are used during cure [209]. At room temperature, NR-P adhesives typically show shear strengths on the order of 4000 psi (28 MPa) and good resistance to impact and cold flow ([200], pp. 29–30). Shear strengths at 260°C are about 25% of RT values. NR-P shows high tensile, shear, and peel strengths. It is unusual for an adhesive to have all of these attributes. Good bonding is obtained on metals, plastics, rubber, wood, glass, and ceramic. An extended discussion of NR-P physical properties is found in DeLollis [208].

NR-P adhesives are normally used as supported or non-supported tapes, but are also available as liquids ([209]; [210], pp. 206–226). Depending on the formula and application, they may be used with or without primers. A one-to-one mixture of nitrile rubber-to-Durez® 12687 phenolic diluted to 20–30% solids in MEK is widely applicable to a range of gluing applications ([210], pp. 206–226). When making this adhesive, both polymers are dissolved in the MEK separately before blending. As the proportion of phenolic is increased, bond strength tends to increase, but the adhesive becomes more brittle. Adhesive performance is also sensitive to the acrylonitrile content of the nitrile rubber copolymer. In general, increases in acrylonitrile content increase the compatibility with phenolic but decrease low temperature performance. Suitable nitrile rubbers are manufactured by B.F. Goodrich (Hycar®), Uniroyal (Paracril®), and Goodyear (Chemigum®).

Mackey and Weil provide the general formula for a NR-P tape adhesive as shown in Table 9 ([210], Table 21, p. 219). They also give brief descriptions of the various grades of nitrile rubber available.

Mackey and Weil also list specific NR-P formulas for adhesives for printed circuits, leather-to-leather, bonding steel plates, and Nomex® paper ([210], Tables 8 and 19, p. 219). The formula in Table 10, for a general structural adhesive, is also from Mackey and Weil ([210], Table 22, p. 219).

Table 9

General formula for a nitrile rubber–phenolic tape adhesive

Component	Parts (by weight)
1. Nitrile rubber	100
2. Phenolic resin	75–200
3. Zinc oxide	5
4. Sulfur	1–3
5. Accelerator	0.5–1
6. Antioxidant	0–5
7. Stearic acid	0–1
8. Carbon black	0–20
9. Filler	0–100
10. Plasticizer	0–10

Table 21 (p. 219) from ref. [210].

Table 10

General formula for a nitrile rubber–phenolic structural adhesive

Component	Parts (by weight)
<i>Part A</i>	
1. Phenolic resin SP-8855 ^a	45
2. MEK/ <i>m</i> -chlorobenzene (70/30 v/v)	90
<i>Part B</i>	
1. Hycar [®] 1001CG ^b	100
2. Carbon black	50
3. ZnO	5
4. Stearic acid	0.5
5. Sulfur	3
6. Benzothiazyl disulfide (Altax)	1.5
7. MEK/ <i>m</i> -chlorobenzene (70/30 v/v)	

Table 22 (p. 21) from ref. [210].

^a Schenectady.^b 41% acrylonitrile at a Mooney viscosity of 80 B.F. Goodrich.

14.2.3. Epoxy–phenolic adhesives

Epoxy–phenolic (EP) blends are among the best adhesives for long-term high-temperatures service ([198], pp. 25–39). They were developed around 1955 [208]. Temperatures as high as 260°C for periods of up to thousands of hours are available. Extended exposures to temperatures above 260°C result in oxidative degradation [211]. EP adhesives such as Bloomingdale's HT-424 are capable of withstanding exposure to temperatures exceeding 530°C for short periods, making these adhesives useful for construction of supersonic jet aircraft [211]. Shear and tensile strengths are good across a wide temperature range, making them far superior to most unmodified epoxies in this respect. HT-424 retains about 1000-psi (7 MPa) tensile shear strength at 530°C. It also shows tensile shear strength of over 3000 psi (21 MPa) at –218°C [211]. The general RT range of tensile shear strengths for EP resins is 2000–3200 psi (14–22 MPa) [212]. Some EP adhesives are rated to –260°C service temperature [212]. Resistance to weathering, aromatic fuels, glycol, hydrocarbons, and water is high. High cost and poor peel and impact strengths detract from performance. The materials are useful in metal, glass, phenolic composite, and ceramic bonding. The metals include aluminum, stainless steel, copper, copper alloys, titanium, galvanized iron, and magnesium ([198], pp. 25–39; [212]). EP finds much use in honeycomb and metal sandwich constructions for aircraft. Epoxy curing is a low shrinkage process in general. Better thermal stability is seen on aluminum than on stainless steel or titanium [211].

In addition to epoxy-phenolic adhesives three-part epoxy-phenolic-nitrile rubber systems are used in metal-metal edge joints and honeycomb constructions [208]. These add toughness not available in most EP systems and improve peel strengths. When used on honeycomb, the NR-P is normally applied to the aluminum skin and the EP to the honeycomb for assembly. Service temperature limitations are those imposed by the NR-P part.

One of the primary virtues of epoxy-phenolics is their low curing temperature requirements. EP adhesives cured at 74–95°C retain reasonably good strengths at 482°C [208,212]. Higher cure temperatures, often around 165–175°C, lead to better structural properties. Curing often occurs in three stages. In the first stage, the adhesive is applied and solvents are dried off of the open assembly at up to 90°C. The second step involves baking under 10–58 psi (0.07–0.40 MPa) pressure for 30 min to 2 h at temperatures in the 165°C area [212]. Final cure is attained by post curing at elevated temperatures. The tendency of some EP to foam during cure makes them excellent for bonding where tolerances are not close, e.g. honeycomb constructions and glass laminates. The reactivity of EP at low temperatures limits storage stability, making cold storage at –18°C common practice. The use of high curing temperatures allows formulation of single part systems with better storage life.

EP adhesives come as fabric- or glass-supported films, pastes, and viscous liquids [208,212]. They are often supplied in solvent. The pastes are most useful in situations where gap filling is required [208]. A wide variety of epoxies are available. Some of the producers are Bloomingdale, Shell (Epon®), ICI [formerly Hysol] (Hysol®), CIBA-Geigy (Araldite®), 3M (Scotch Weld®), and Amicom (Uniset®). There are many more.

Tobiason furnishes us with two examples of EP formulations for electronic encapsulation and primer coating applications as shown in Tables 11 and 12, respectively [213]. The coating formula was obtained from a Union Carbide Technical Bulletin.

Table 11
Epoxy-phenolic suitable for electronic encapsulation

Component	Parts (by weight)
1. Epoxidized novolac	20
2. Phenolic resin	10
3. Silica flour	70
4. Lubricant (stearate)	1
5. Catalyst	0.4–2

From ref. [213].

Table 12

Epoxy–phenolic coating formula

Component	Parts (by weight)
1. Synthetic iron oxide	37.5
2. EPON [®] -1007 (Shell)	17.5
3. UCAR [®] BKR-2620 (phenolic resin)	11.0
4. Toluene	15.7
5. Methyl propasol [®] (Union Carbide)	7.5
6. MEK	4.5
7. Methyl propasol acetate [®]	2.3
8. <i>n</i> -Butanol	4.0

From ref. [213].

15. Phenolic in elastomeric adhesives

15.1. Pressure-sensitive adhesives

Standard-grade PSAs are usually made from styrene–butadiene rubber (SBR), natural rubber, or blends thereof in solution. In addition to rubbers, polyacrylates, polymethylacrylates, poly(vinyl ethers), polychloroprene, and polyisobutenes are often components of the system ([198], pp. 25–39). These are often modified with phenolic resins, or resins based on rosin esters, coumarones, or hydrocarbons. Phenolic resins improve temperature resistance, solvent resistance, and cohesive strength of PSA ([196], pp. 276–278). Antioxidants and tackifiers are also essential components. Sometimes the tackifier will be a lower molecular weight component of the high polymer system. The phenolic resins may be standard resoles, alkyl phenolics, or terpene–phenolic systems ([198], pp. 25–39 and 80–81). Pressure-sensitive dispersions are normally comprised of special acrylic ester copolymers with resin modifiers. The high polymer base used determines adhesive and cohesive properties of the PSA.

One of the important uses of phenolic in PSA is to impart heat resistance to masking tape used in factory automotive painting ([196], pp. 276–278). This tape must be able undergo baking at up to 130°C for about 40 min. After baking, the tape must be removed while still warm without leaving a residue on the part. Without phenolic, most rubbers would soften too much for this application, thus most construction masking tape contains phenolic resin. The natural cure speed, non-staining properties, lack of corrosiveness toward metals (particularly copper), and low cost of phenolics make them ideal for this use. The phenolics chosen must be heat curable (resoles) and have excellent compatibility with the rubber high polymer. Compatibility is generally attained through use of an alkyl phenol in making the resin. Bemmels described a nonyl phenol-based resole suitable for

Table 13

A natural rubber–phenolic construction masking tape

Component	Parts (by weight)
1. Natural rubber, pale crepe	100
2. Piccolyte [®] S115 tackifier	65
3. Schenectady 1056 (brominated PF)	10
4. Zinc resinate accelerator	10
5. Satovar [®] A antioxidant	1
6. Ionol [®] antioxidant	1
7. Zinc dibutyl dithiocarbamate	1

From ref. [196], pp. 277 and British Patent 1,172,670 (1969) Johnson and Johnson.

the purpose [196,214]. Bemmels claims that the alkyl phenol used in making his resin must have at least 8 carbons on the side chain. When a faster phenolic cure is desired, cure accelerators may be added. Organic complexes of group IV metals are said to be efficacious accelerators. Examples offered by Satas include zirconium tetraisopropoxide and titanium tetrabutoxide ([196], pp. 276–278). Octyl phenyl acid phosphate is also mentioned as a good accelerator in this application ([196], pp. 276–278). A halogenated phenolic resin in combination with a zinc resinate is also reportedly an effective modifier for automotive masking tapes ([196], pp. 276–278).

Satas provides the formula for construction grade masking tape in Table 13 ([196], pp. 276–278).

In addition to heat resistance, PF is also used to improve the solvent resistance of PSA. Formulas for attaining this property are similar to the one in Table 13, but would contain 20–30 parts of phenolic resin rather than 10. Such PSAs require cure times up to 3 h at 150°C.

The high temperatures required for phenolic cure are generally viewed as positive characteristics, as they insure that the phenolic does not cure at normal room-temperature storage conditions. This keeps the adhesive soft so that it retains the desired adhesive properties.

A general formula for an SBR-based PSA is found in Table 14 ([196], p. 519). A typical blended natural rubber and SBR formula is given in Table 15 ([196], p. 519).

One way to obtain enhanced heat and solvent resistance in SBR-based PSA is sulfur addition. It is difficult to obtain sufficient cure with sulfur during normal drying cycles (2–5 min at 150–180°C). Furthermore, cure via sulfur may continue after leaving the oven, thus degrading adhesion. When used in contact with copper, the sulfur may promote corrosion. The use of phenolic overcomes all of these problems despite the fact that its natural cure speed is also insufficient for the time frame available. This is overcome through addition of one of the accelerators

Table 14

A pressure-sensitive SBR–phenolic adhesive

Component	Parts (by weight)
1. Butadiene–styrene copolymer (75 : 25)	50
2. Tackifying resin	25
3. Heat-reactive PF resin	7.5
4. Zinc resinate accelerator	2.5
5. Antioxidant	1

From ref. [196], p. 519 and US Patent 3,535,153 (Korpman, 1970) Johnson and Johnson.

Table 15

A pressure-sensitive blended rubber–phenolic adhesive

Component	Parts (by weight)
1. Natural rubber, pale crepe	25
2. SBR copolymer (71 : 29)	25
3. ZnO	47.5
4. Polyterpene resin (m.p. 115°C)	15
5. Glycerol ester of rosin hydrogenate	20
6. Zinc resinate accelerator	5
7. Octyl phenol–formaldehyde resin	5
8. 2,5-di- <i>tert</i> -amyl hydroquinone	1

From ref. [196], p. 519 and US Patent 3,051,588 (Lavanchy, 1962) Johnson and Johnson.

Table 16

SBR-based PSAs

Component	Parts (by weight)	
1. SBR 4502 copolymer (72 : 25) Goodrich Gulf Chemical Co.	100	100
2. TPO #1 tackifier	125	0
3. Ambersol® ST137 <i>para</i> -octyl phenol–formaldehyde resole	30	0
4. Picco® L-30-3 tackifier	0	150
5. Schenectady SP-1056 brominated phenolic resin	0	150
6. Zinc resinate accelerator	20	5
7. Antioxidant	2	2
8. Percent solids by weight in toluene	40	50

From ref. [196], p. 519 and US Patent 3,725,322 (Weidner, 1973) Johnson and Johnson.

mentioned. After acceleration, the PF is capable of adequate cure in 1 min at 120°C or 30 s at 175°C. Two more specific examples of an SBR-based PSAs, again from Satas, are shown in Table 16 ([196], p. 519).

Table 17

Water-resistant butadiene–phenolic PSA

Component	Parts (by weight)
1. 1,4-Polybutadiene	100
2. Polyterpene resin S-1010	50
3. Polyterpene resin S-115	20
4. Phenol–formaldehyde resin	35
5. Dioctyl phthalate	10
6. Heptane	500
7. Ethanol	10

From ref. [196], p. 522 and US Patent 3,451,537 (Freeman and Sauer, 1969) 3-M.

Finally, Satas gives us a PSA example based on synthetic polybutadiene is shown in Table 17 [196]. Good water resistance and bonds are claimed for this formula.

Binder formulas for carpet backing, aluminum foil to paper, vinyl flooring, tire cord, paper labeling, masking tape, and oriented polypropylene tape applications are available from Midgley and Rea in Skiest [215].

15.2. Contact adhesives

High quality contact adhesives are normally based on polychloroprene ([198], pp. 11–14). Many modifying resins are compatible with polychloroprene [197]. Phenolic, terpene–phenolic, or phenolic-modified rosin esters are among those used in contact cements [197]. Alkyl phenol-based phenolics are the most common. “With the exception of alkaline phenolics, all other resin types catalyze the oxidative degradation of polychloroprene elastomers and hence bond durability” [197]. The antioxidant properties of some alkyl phenolics have provided durability in for periods exceeding 20 years. Low molecular weight phenolics (number-average \approx 500 Da) and significant amounts of dimethylol phenol have been known to cause ‘phasing’ problems. This is easily avoided by using resins with number-average molecular weights exceeding 900 Da. Schenectady SP-154 and Union Carbide CK-1636 are phenolic resins that do not cause phasing ([216], pp. 284–306).

As with PSA, the phenolics are added primarily for increased cohesive strength and temperature resistance ([216], pp. 284–306). More phenolic is used in adhesives with higher strength requirements, e.g. for metal–metal bonding. Resins based on *p*-*t*-butyl phenolics are most commonly selected ([216], pp. 284–306). They are usually present in the adhesive at 35–50 parts per 100 rubber (phr), with typical optima at 40–45 phr ([216], pp. 284–306). Significant deviation from this optimum may have drastic effects.

Magnesium salts are sometimes added to chloroprene–phenolic alloys for improved heat resistance [197]. The magnesium resinate has no melting point and does not decompose at temperatures below 200°C ([216], pp. 284–306). Typically, about 10 parts of magnesium oxide per 100 parts of phenolic resin will give maximum effect. This raises the service temperature of the adhesive to 80°C or higher, depending on the formula and performance demands of the composite. For some grades of neoprene, the use of the magnesium *t*-butyl phenolic resinate is absolutely essential, e.g. DuPont Neoprene AF ([216], pp. 284–306). The use of the magnesium oxide alone would cause premature gellation. A small amount of water must be present to allow formation of the phenolic–magnesium complex. The organic solvents also affect the rate of complex formation.

Phenolic–neoprene contact cements are used for structural metal–metal bonding, especially where fatigue resistance and low temperature performance are important [209]. They are also used for bonding textiles, wood, rubbers, plastics, ceramics, and glass to metal and to one another. Solvent toxicity and flammability has greatly reduced the use of contact cements in the wood products industry. Water-based contact cements persist, but generally do not perform as well as the solvent systems, thus allowing market erosion by alternative binders.

There are 16 grades of DuPont neoprene alone. They vary in crystallization rate and potential, viscosity, molecular weight, additive content, and other properties ([216], pp. 284–306). Selection of the right materials requires sophisticated knowledge of both the neoprenes and the phenolic additives. Guggenberger provides a good overview of this situation and some basic formulation information ([216], pp. 284–306). She also provides a prototype formula for a heat-resistant contact cement as shown in the Table 18 ([216], source Table 10, p. 293).

The amount of phenolic resin strongly affects the rate of strength development and its ultimate heat resistance. Phenolic has positive effects in both contexts. Strength retained at 80°C with 46-phr phenolic exceeds that with 33 phr by 10-fold

Table 18

Heat resistant neoprene–phenolic contact cement

Component	Parts (by weight)
1. Neoprene AD	100
2. MgO	4
3. ZnO	5
4. Antioxidant	2
5. Phenolic resin	33–46
6. Water	1
7. Hexane	100
8. Toluene	400

Table 10 (p. 293) from ref. [216].

Table 19
General purpose neoprene–phenolic contact cement

Component	Parts (by weight)
1. Anionic neoprene latex	100
2. Surfactant	AR ^a
3. ZnO	5
4. Antioxidant	2
5. Terpene phenolic	50
6. Liquid polyterpene resin	25
7. Thickener	AR

Table 17 (p. 305) from ref. [216].

^a AR = as required.

([216], source Table 10, p. 293). Further improvements in heat resistance may be had by incorporation of curing agents such as thiocarbanilide, triethyl trimethylene triamine, polymeric isocyanates (e.g. Bayer Desmodur RF), or mixtures of sulfur with Vanax[®] 808 or 833 (R.T. Vanderbilt).

The formula in Table 19 is from Guggenberg ([216], source Table 17, p. 305). It is a starting point formula for general-purpose contact cement. The proportions are as dry parts.

References

1. Pilato, L.A. and Michno, M.J., *Advanced Composite Materials*. Springer-Verlag, Berlin, 1994, pp. 18–23.
2. Ellis, C., *The Chemistry of Synthetic Resins*, 2nd edn., Vol. 1. Reinhold, New York, 1935, Chapt. 13.
3. Gerhardt, C.F., *Ann. Chem.*, **87**, 159 (1853).
4. Schroder, Prinzhorn and Kraut, K., *Ann. Chem.*, **150**, 1 (1869).
5. Baeyer, A., *Ber. Dtsch. Chem. Ges.*, **5**, 25 (1872).
6. Baeyer, A., *Ber. Dtsch. Chem. Ges.*, **5**, 280 (1872).
7. Baeyer, A., *Ber. Dtsch. Chem. Ges.*, **25**, 1094 (1872).
8. v.d. Velden, R., *J. Prakt. Chem.*, **15**(2), 164 (1877).
9. v.d. Velden, R., *Jahresber. Leist. Chem. Tech.*, **5**, 337 (1877).
10. Doebner, O., German Patent 94,298, 1896.
11. Doebner, O., *Chem. Zentr.*, **1**, 299 (1898).
12. Speyer, A., German Patent 99,570, 1897.
13. Speyer, A., *Chem. Zentr.*, **1**, 462 (1898).
14. Baekeland, L.H., *Ind. Eng. Chem.*, **1**, 149 (1909).
15. Baekeland, L.H., *Ind. Eng. Chem.*, **1**, 545 (1909).
16. Baekeland, L.H., *Ind. Eng. Chem.*, **3**, 518 (1911).
17. Baekeland, L.H., *Ind. Eng. Chem.*, **4**, 737 (1912).
18. Gardziella, A., Pilato, L.A. and Knop, A., *Phenolic Resins: Chemistry, Applications*,

- Standardization, Safety and Ecology*, 2nd edn. Springer, Berlin, 2000.
19. Michael, A. and Comey, A.M., *J. Am. Chem. Soc.*, **5**, 349 (1883–1884).
 20. ter Meer, E., *Ber. Dtsch. Chem. Ges.*, **7**, 1200 (1874).
 21. Kleeberg, W., *Ann. Chem.*, **263**, 283 (1891).
 22. Manasse, O., United States Patent 526,786, 1894.
 23. Lederer, L., United States Patent 563,975, 1896.
 24. Seymore, R.B. and Carraher, C.E., *Polymer Chemistry: An Introduction*, 2nd edn. Marcel Dekker, New York, 1988, Chapter 1.
 25. Smith, A., United States Patent 643,012, 1900.
 26. Smith, A., British Patent 16,247, 1899.
 27. Smith, A., German Patent 112,685, 1899.
 28. Smith, A., *J.S.C.I.*, **18**, 1029 (1899).
 29. Blumer, L., British Patent 12,880, 1902.
 30. Blumer, L., British Patent 6,823, 1903.
 31. Blumer, L., German Patent 172,877, 1902.
 32. Blumer, L., *J.S.C.I.*, **22**, 705 (1903).
 33. Blumer, L., *J.S.C.I.*, **23**, 448 (1904).
 34. Luft, A., United States Patent 735,278, 1903.
 35. Luft, A., British Patent 10,218, 1902.
 36. Luft, A., German Patent 140,552, 1902.
 37. Luft, A., *J.S.C.I.*, **21**, 1085 (1902).
 38. Luft, A., *J.S.C.I.*, **21**, 1012 (1903).
 39. Story, W.H., British Patent 8,875, 1905.
 40. Story, W.H., German Patent 173,990, 1905.
 41. Story, W.H., Belgian Patent 210,965, 1908.
 42. Baekeland, L.H., United States Patent 939,966, 1909.
 43. Baekeland, L.H., United States Patent 942,699, 1909.
 44. Carswell, T.S., Phenoplasts: their structure, properties, and chemical technology. In: Mark, H. and Melville, H.W. (Eds.), *High Polymers*. Interscience, New York, 1947, Chapter 1.
 45. Knop, A. and Pilato, L.A., *Phenolic Resins*. Springer-Verlag, Berlin, 1985, p. 3.
 46. Saunders, K.J., *Organic Polymer Chemistry*, 2nd edn. Chapman and Hall, New York, 1989, pp. 316–340.
 47. Fadem, L. and Fadem, S.Z., Bakelite: a revolutionary early plastic. <http://www.deco-echoes.com/bakelite.html>, Deco Echoes, 1996.
 48. Ellis, C., *The Chemistry of Synthetic Resins*, 2nd edn., Vol. 1. Reinhold, New York, 1935, Chapt. 1.
 49. Fried, J.R., *Polymer Science and Technology*. Prentice Hall, Englewood Cliffs, NJ, 1995, Chapter 1.
 50. *Kirk-Othmer Encyclopedia of Chemical Technology*, 2nd edn., Vol. 15. Interscience, New York, 1968, p. 178.
 51. Sellers, T., *Plywood and Adhesive Technology*. Marcel Dekker, New York, 1985, Chapter 17.
 52. Spelter, H., McKeever, D. and Durbak, I., Review of Wood-Based Panel Sector in United States and Canada, General Tech. Rpt. FPL-GTR-99, U.S. Department of Agriculture, Forest Service, Madison, WI, 1997.
 53. Sellers, T., Adhesive Innovation and Production of North American Glued-Wood and Related Products, XXI IUFRO World Congress, Kuala Lumpur, Malaysia, 7–12 August 2000.
 54. Tushman, M.L. and O'Reilly, C.A., Winning through innovation: a practical guide to

- leading organizational change and renewal, Harvard Business School Press: Boston, 1997, Chapters 2 and 7.
55. Anonymous, *Chem. Week*, **160(7)**, 46 (1998).
 56. Anonymous, *Chem. Week*, **160(17)**, 30 (1998).
 57. Knop, A. and Shieb, W., *Chemistry and Application of Phenolic Resins*. Springer-Verlag, Berlin, 1979.
 58. Walker, J.F. *Formaldehyde*, 3rd edn. Robert E. Krieger, Huntington, NY, 1964.
 59. Lampman, H.F. and Reidenbach, F. (Eds.), *Engineered Materials Handbook*. ASM International, The Materials Information Society, Materials Park, OH, 1995, pp. 157–286.
 60. Rogers Corporation, Molded Materials Div., <http://www.rogers-corp.com/mmd/phenolic.htm>, 1999.
 61. Stokes, E.H., *40th SAMPE Symposium*, **40(1)**, 59 (1995).
 62. Taylor, J.G., *40th SAMPE Symposium*, **40(1)**, 596 (1995).
 63. McDonald, R.A. and Quereschi, S.P., *41st SAMPE Symposium*, **41(2)**, 1573 (1996).
 64. Ostberg, D.T., *41st SAMPE Symposium*, **41(2)**, 1459 (1996).
 65. Moreau, W.M., *Semiconductor Lithography, Principles, Practices, and Materials*. Plenum, New York, 1988, pp. 1–79.
 66. Seymore, R.B. and Carraher, C.E., *Polymer Chemistry: An Introduction*, 2nd edn. Marcel Dekker, New York, 1988, pp. 259–263.
 67. Findley, W.N., *Mod. Plastics*, **Dec.**, 153 (1944).
 68. Telfair, D., Carswell, T.S. and Nason, H.K., *Mod. Plastics*, **Feb.**, 137 (1944).
 69. Gailus, W.J. and Telfair, D., *Mod. Plastics*, May, 149 (1945).
 70. Carswell, T.S., In: Mark, H. and Melville, H.W. (Eds.), *Phenoplasts: Their Structure, Properties, and Chemical Technology. High Polymers*. Interscience, New York, 1947, Chapter VII.
 71. Carswell, T.S. In: Mark, H. and Melville, H.W. (Eds.), *Phenoplasts: Their Structure, Properties, and Chemical Technology. High Polymers*. Interscience, New York, 1947, Chapter VIII.
 72. Carswell, T.S. In: Mark, H. and Melville, H.W. (Eds.), *Phenoplasts: Their Structure, Properties, and Chemical Technology. High Polymers*. Interscience, New York, 1947, Chapter X.
 73. Phillips, E.K., Garwood, A.J. and Detlefsen, W.D., New Zealand Patent 323176, 2000.
 74. Phillips, E.K., Garwood, A.J. and Detlefsen, W.D., Australian Patent 700953, 1999.
 75. Wu, G., United States Patent 5,912,317, 1999.
 76. Budavari, S., O'Neil, M.J., Smith, A. and Heckelman, P.E. (Eds.) *The Merck Index*, 11th edn. Merck, Rahway, NJ, 1989, pp. 662, 1150.
 77. Mundy, B.P. and Ellard, M.G., *Name Reactions and Reagents in Organic Synthesis*. Wiley-Interscience, New York, 1988.
 78. Kumpinsky, E., *Ind. Eng. Chem.*, **34**, 3096 (1995).
 79. Anonymous, How to Prevent Runaway Reactions, EPA 550-F99-004, U.S. Environmental Protection Agency Office of Solid Waste and Emergency Response, August 1999. In addition to the accidents mentioned in the reference, a significant number occurred prior to the 1989 time frame. Serious incidents are recorded as early as 1957. Accident recording before 1957 was incomplete.
 80. Zavitsas, A.A., Beaulieu, R.D. and LeBlanc, J.R., *J. Polym. Sci.*, **6**, 2541 (1968).
 81. Venkatachalam, R., Reddy, B.S.R. and Rajadurai, S., *Indian J. Chem.*, **25A**, 1134 (1986).
 82. Eapen, K.C. and Yeddanapalli, L.M., *Makromol. Chem.*, **119**, 4 (1968).
 83. Conner, A.H., *J. Appl. Polym. Sci.*, in press.
 84. Higuchi, M., Nohno, S. and Tohmura, S., *J. Wood Sci.*, **44**, 198 (1998).

85. Zavitsas, A.A., *J. Polym. Sci.*, **6**, 2533 (1968).
86. Astarloa-Aierbe, G., Echeverria, J.M., Egiburu, J.L., Ormaetxea, M. and Mondragon, I., *Polymer*, **39**(14), 3147 (1998).
87. DeJong, D.J. and DeJonge, J., *Rec. Trav. Chim.*, **72**, 497 (1953).
88. Grenier-Loustalot, M., Larroque, S., Grenier, P. and Bedel, D., *Polymer*, **37**(6), 939 (1996).
89. Grenier-Loustalot, M., Larroque, S., Grenier, P., Leca, J. and Bedel, D., *Polymer*, **35**(14), 3046 (1994).
90. Ferrero, F. and Panetti, M., *Eur. Polym. J.*, **19**(12), 1153 (1983).
91. Eapen, K.C. and Yeddnapalli, L.M., *Die Makromol. Chem.*, **119**, 4 (1968).
92. Dijkstra, R., DeJonge, J. and Lammers, M.F., *Rec. Trav. Chim.*, **76**, 92 (1957).
93. Dijkstra, R. and DeJonge, J., *Rec. Trav. Chim.*, **81**, 295 (1962).
94. Debing, L.M., Murray, G.E. and Schatz, R.J., *Ind. Eng. Chem.*, **44**, 356 (1952).
95. Minami, T. and Ando, T., *J. Chem. Soc. Jpn. Indus. Chem.*, **59**, 668 (1956).
96. Francis, D.J. and Yeddnapalli, L.M., *Makromol. Chem.*, **119**, 17 (1968).
97. Sebnik, A. and Lapanje, S., *Angew. Makromol. Chem.*, **63**, 139 (1977).
98. Sebnik, A., *J. Chromatogr.*, **106**, 205 (1978).
99. Sebnik, A. and Lapanje, S., *Angew. Makromol. Chem.*, **70**, 59 (1978).
100. Kumpinsky, E., *Ind. Eng. Chem.*, **33**, 285 (1994).
101. Booth, A.D., Karmarkar, M., Knight, K. and Potter, R.C.L., *Inst. Chem. Eng.*, **58**, 75 (1980).
102. Creed, M.J. and Fauske, H.K., *Chem. Eng. Prog.*, **March**, 45 (1990).
103. Anonymous, RSST, The Reactive System Screening Tool, Fauske and Assoc., Burr Ridge, IL.
104. Anonymous, V2P2 — The Premier Process Hazard Calorimeter System, Fauske and Assoc., Burr Ridge, IL.
105. Anonymous, Vent sizing Software, Fauske and Assoc., Burr Ridge, IL.
106. Leung, J.C. and Fauske, H.K., *Thermochim. Acta*, **104**, 13 (1986).
107. Schaechtel, D. and Moore, D., *Proceedings from the International Conference and Workshop on Risk Analysis in Process Safety*, October 21–24, 1997, Atlanta, GA, Sponsored by CPS, EPA, HS and E, Eur. Fed. of Chem. Eng., 285.
108. Odian, G., *Principles of Polymerization*, 3rd edn. John Wiley and Sons, New York, 1991, pp. 40–46.
109. Wooten, A.L., Prewitt, M.L., Sellers, T. and Teller, D.C., *J. Chromatogr.*, **345**, 371 (1988).
110. Detlefsen, W.D., *6th Panel and Engineered Wood Technology Conference*, 37 (1998).
111. Robertson, J.E. and Robertson, R.R., *For. Prod. J.*, 30 (1977).
112. Nuss, D. and Atchison, D., *Proceedings of the APA Conference on Structural Panels and Timber*. The Engineered Wood Research Foundation, American Plywood Assn., September 18, 1998.
113. Daisy, N.K. and Leeper, D.L., United States Patent 4,758,478, 1988.
114. Detlefsen, W.D., *Plywood and Panel World*, Aug–Sept., 22, 1987.
115. Cotton, F.A. and Wilkinson, G., *Advanced Inorganic Chemistry*, 5th edn. Wiley-Interscience, New York, 1988, pp. 123–124.
116. Kumar, A. and Gupta, R.K., *Fundamentals of Polymers*. McGraw-Hill, New York, 1998, p. 421.
117. Geimer, R.L., Follensbee, R.A., Christiansen, A.W., Koutsky, J.A. and Meyers, G.E. In: Maloney, T.M. (Ed.), *Proceedings 24th International Particleboard Composite Materials Symposium*, WSU. Washington State University Press, Pullman, WA, 1990, pp. 65–83.
118. Detlefsen, W.D. In: Kerwood, T. (Ed.), *Proceedings APA Conference on Structural Panels*

- and Timber. Engineered Panel Research Foundation, APA — the Engineered Wood Assn., September 18, 1998.
119. Detlefsen, W.D., Phillips, E.K. and Norton, R.V., United States Patent 4,961,795, 1990.
 120. Phillips, E.K., Detlefsen, W.D. and Creel, L.D., Canadian Patent 2101765, 1999.
 121. Carlson, F.E., Phillips, E.K., Tenhaeff, S.C. and Detlefsen, W.D., *Measuring and Controlling Volatile Organic Compound and Particulate Emissions from Wood Processing Operations and Wood-Based Products*. Forest Products Society, Madison WI, 1995, pp. 52–61.
 122. Hsu, E. In: Maloney, T.M. (Ed.), *Proceedings 21st International Particleboard Composite Materials Symposium*, WSU. Washington State University Press, Pullman, WA, 1987, pp. 219–236.
 123. Hsu, E. In: Maloney, T.M. (Ed.), *Proceedings 23rd International Particleboard Composite Materials Symposium*, WSU. Washington State University Press, Pullman, WA, 1989, pp. 37–53.
 124. Wolcott, M.P., Kamke, F.A. and Dillard, D.A., *Wood Fiber Sci.*, **22**(4), 345 (1990).
 125. Freeman, J.H. and Lewis, C.W., *J. Am. Chem. Soc.*, **76**, 2080 (1953).
 126. Freeman, J.H., *J. Am. Chem. Soc.*, **74**, 6257 (1952).
 127. Freeman, J.H., *Anal. Chem.*, **24**, 955 (1952).
 128. Grenier-Loustalot, M., Larroque, S., Grenier, P. and Bedel, D., *Polymer*, **37**(6), 939 (1996).
 129. Sprengling, G.R. and Lewis, C.W., *J. Am. Chem. Soc.*, **75**, 5709 (1953).
 130. Jones, B.T., *J. Polym. Sci.*, **21**, 1801 (1983).
 131. Megson, N.J.L., *Phenolic Resin Chemistry*. Butterworths, London, 1958, pp. 50–80.
 132. Maciel, G.E., Chuang, I.-S. and Gollob, L., *Macromolecules*, **17**, 1081 (1984).
 133. Murray, G.S., *An Investigation into the Chemistry of the Reactions of Phenol-Formaldehyde Compounds with Novel Crosslinking Agents*, Ph.D. Thesis. Portsmouth University, Portsmouth, 1993.
 134. Yoshikawa, T. and Kumantani, J., *Makromol. Chem.*, **165**, 11 (1973).
 135. Schleigh, W.R., *Eastman Org. Chem. Bull.*, **43**(1), 1 (1971).
 136. Wan, P., Barker, B., Diao, L., Fischer, M., Shi, Y. and Yang, C., *Can. J. Chem.*, **74**, 465 (1996).
 137. Kornblum, N., Berrigan, P.J. and le Noble, W.J., *J. Am. Chem. Soc.*, **85**, 1141 (1963).
 138. Kornblum, N., Seltzer, R. and Haberfield, P., *J. Am. Chem. Soc.*, **85**, 1148 (1963).
 139. Kornblum, N., Berrigan, P.J. and le Noble, W.J., *J. Am. Chem. Soc.*, **82**, 1257 (1960).
 140. Kornblum, N., Smiley, R.A., Blackwood, R.K. and Iffland, D.C., *J. Am. Chem. Soc.*, **77**, 6269 (1955).
 141. Lowry, T.H. and Richardson, K.S., *Mechanism and Theory in Organic Chemistry*, 3rd edn. Harper and Row, New York, 1987, pp. 202–229.
 142. Martin, R.W., *The Chemistry of Phenolic Resins*. John Wiley and Sons, New York, 1956, pp. 249–270.
 143. So, S. and Rudin, A., *J. Appl. Polym. Sci.*, **41**, 205 (1990).
 144. Kim, M.G., Amos, L.W. and Barnes, E.E., *Ind. Eng. Chem. Res.*, **29**, 2032 (1990).
 145. Astarloa-Aierbe, G., Echeverria, J.M., Ormaetxea, M. and Mondragon, I., *Polymer*, **39**(14), 3147 (1998).
 146. Ishida, S.-I., Tsutsumi, Y. and Kaneko, K., *J. Polym. Sci.*, **19**, 1609 (1981).
 147. Jones, R.T., *J. Polym. Sci.*, **21**, 1801 (1983).
 148. Kim, M.G., Tiedeman, G.T. and Amos, L.W., *Phenolic Resins — Chemistry and Applications*, Weyerhaeuser Science Symposium. 1, Weyerhaeuser, Tacoma, WA, 1981, pp. 263–287.

149. Higuchi, M., Morita, M., Urakawa, T., Yoshimatu, T. and Kamo, N., *Adhesives 2000 Symposium*. Lake Tahoe, NV, Forest Products Soc., in press.
150. Yeddanapalli, I.M. and Kuriakose, A.K., *J. Sci. Ind. Res. (India)*, **18B**, 467 (1962).
151. Little, G.E., *J. Appl. Chem.*, **12**, 196 (1962).
152. Sprung, M.M. and Gladstone, M.T., *J. Am. Chem. Soc.*, **71**, 2907 (1949).
153. Rodia, J.S. and Freeman, J.H., *J. Org. Chem.*, **24**, 21 (1959).
154. Freeman, J.H., *Am. Chem. Soc. Div. Org. Coat. Plast. Chem. Pap.*, **27(1)**, 84 (1967).
155. Sekhar, N., Kucharska, H. and Vasisth, R.C., *Am. Chem. Soc. Div. Polym. Chem. Polym. Prep.*, **12(1)**, 585 (1971).
156. Francis, D.J. and Yeddanapalli, L.M., *Makromol. Chem.*, **125**, 119 (1969).
157. Yeddanapalli, L.M. and Francis, D.J., *Makromol. Chem.*, **55**, 74 (1962).
158. Zinke, A., *J. Appl. Chem.*, **1**, 257 (1951).
159. Conley, R.T. and Metil, I., *J. Appl. Polym. Sci.*, **7**, 37 (1963).
160. Phillips, E.K., Detlefsen, W.D. and Carlson, F.E., *Proc. Int. Particleboard and Composite Matls. Symp.*, **25**, 231 (1991).
161. Orth, H., German Patent 1065605, 1957.
162. Orth, H., German Patent 1171606, 1958.
163. Sumitomo, United States Patent 3,599,433, 1967.
164. BASF, British Patent 1374332, 1967.
165. Lemon, P.H.R.B., European Patent 0085512, 1982.
166. Hickson, C.H., United States Patent 4,937,024, 1990.
167. Iyer, R.S. and Trika, S.K., United States Patent 4,988,745, 1991.
168. Laitar, R., United States Patent 4,246,157, 1981.
169. Gerber, A., United States Patent 4,994,505, 1991.
170. Lemon, P.H.R.B. and Baker, D., United States Patent 5,032,642, 1991.
171. Iyer, R.S. and Trika, S.K., United States Patent 5,036,116, 1991.
172. Chandramouli, P., Iyer, R.S. and Johnson, C., United States Patent 5,043,412, 1991.
173. Lemon, P.H.R.B., King, J.G., Murray, G., Leoni, H. and Gerber, A., United States Patent 5,051,454, 1991.
174. Conner, A.H. and Lorenz, L.F. In: Bauman, M.G.D. (Ed.), *Wood Adhesives 2000*, Extended Abstracts. Forest Products Soc., Madison, WI, 2000, 95.
175. Pizzi, A. In: Bauman, M.G.D. (Ed.), *Wood Adhesives 2000*, Extended Abstracts. Forest Products Soc., Madison, WI, 2000, 45.
176. Miller, T.R. and Detlefsen, W.D. In: Bauman, M.G.D. (Ed.), *Wood Adhesives 2000*. Forest Products Soc., Madison, WI, in press.
177. Higuchi, M., Tohmura, S. and Sakata, I., *Mokuzai Gakkaishi*, **40(6)**, 604 (1994).
178. Lemon, P.H.R.B., King, J.G., Murray, G., Leoni, H. and Gerber, A., United States Patent 5,340,888, 1994.
179. Phillips, E.K., Detlefsen, W.D. and Carlson, F.E., United States Patent 5,684,114, 1997.
180. Shiau, D.W., Detlefsen, W.D. and Phillips, E.K., United States Patent 5,700,587, 1997.
181. Shiau, D.W., Detlefsen, W.D. and Phillips, E.K., United States Patent 5,637,374, 1997.
182. Shiau, D.W., Detlefsen, W.D. and Phillips, E.K., United States Patent 5,498,647, 1996.
183. Phillips, E.K., Detlefsen, W.D. and Creel, L.D., United States Patent 5,902,442, 1999.
184. Detlefsen, W.D., *Proceedings Pete Conference*, 37 (1998).
185. Zinke, A., Hanus, F. and Pichelmayer, H., *Monatsh. Chem.*, **78**, 311 (1948).
186. Zinke, A., Zigeuner, G. and Weiss, G., *Monatsh. Chem.*, **80**, 148 (1949).
187. Zinke, A., Zigeuner, G., Weiss, G. and Schaden, W., *Monatsh. Chem.*, **81**, 999 (1950).
188. Zinke, A., Zigeuner, G., Weiss, G. and Wiesenberger, E., *Monatsh. Chem.*, **80**, 160 (1950).

189. Martin, R.W., *The Chemistry of Phenolic Resins*. John Wiley and Sons, New York, 1956, pp. 152–164.
190. Redman, L.V., Weith, A.J. and Brock, F.P., *Ind. Eng. Chem.*, **6**, 3 (1914).
191. Pilato, L.A. and Michno, M.J., *Advanced Composite Materials*. Springer-Verlag, Berlin, 1994, pp. 18–23.
192. Gardziella, A., Pilato, L.A. and Knop, A., *Phenolic Resins: Chemistry, Applications, Standardization, Safety and Ecology*, 2nd edn. Springer, Berlin, 2000, pp. 66–77.
193. *Encyclopedia of Polymer Science and Technology*. Interscience, New York, 1969, v. 10.
194. Semon, W.F., History and use of materials which improve aging. In: Davis, C.C. and Blake, J.T. (Eds.), *The Chemistry and Technology of Rubber*, ACS Monograph Series No. 74. Reinhold, New York, 1937.
195. Schildtknect, C.E. (Ed.), *Polymer Processes, High Polymers X*. Interscience, New York, 1956, pp. 532–540.
196. Satas, D., Miscellaneous polymers. In: Satas, D. (Ed.), *Handbook of Pressure-Sensitive Adhesive Technology*, 2nd edn. Van Nostrand Reinhold, New York.
197. Whitehouse, R.S., Contact adhesives. In: Wake, W.C. (Ed.), *Synthetic Adhesives and Sealants, Critical Reports on Applied Chemistry*, Vol. 16. John Wiley and Sons, New York, pp. 9–10, 1987.
198. Gierenz, G. and Karmann, W., *Adhesives and Adhesive Tapes*. Wiley-VCH, New York, 2001.
199. Bishopp, J.A., A brief history of the redux bonding process, structural adhesives in engineering V, *5th Int. Structural Adhesives in Engineering Conference (SAE-V)*. Bristol, UK, 1998.
200. Hurd, J., *Adhesives Guide*. Cable Printing and Publishing, London, 1959.
201. Anonymous, www.hexcelcomposites.com, 2001.
202. Allbericci, P., Aerospace applications. In: Kinlock, A.J. (Ed.), *Durability of Structural Adhesives*. Applied Science Publishers, London, 1983, Ch. 8.
203. Powis, C.N., Some applications of structural adhesives. In: Alner, D.J. (Ed.), *Aspects of Adhesion-4*. CRC Press, Cleveland, OH, 1968, pp. 107–116.
204. Wakeman, R.L., *The Chemistry of Commercial Plastics*. Reinhold, New York, 1947, pp. 375–390.
205. Chapman, F., Synthetic resin adhesives. In: DeBruyne, N.A. and Houwink, R. (Eds.), *Adhesion and Adhesives*. Elsevier, New York, 1959, pp. 201–249.
206. Farmer, P.H. and Jemmot, B.A., Polyvinyl acetal adhesives. In: Skeist, I. (Ed.), *Handbook of Adhesives*, 3rd edn. Van Nostrand Reinhold, New York, 1990, pp. 423–436.
207. St. Clair, J.R., How high quality laminated glass is made. *Glass Industry*, **Nov.** (1964).
208. DeLollis, N.J., *Adhesives for Metals, Theory and Technology*. Industrial Press, New York, 1970, pp. 81–119.
209. Guttman, W.H., *Concise Guide to Structural Adhesives*. Reinhold, Chapman Hall, London, 1961, pp. 7–8.
210. Mackey, D.E. and Weil, C.E., Nitrile rubber adhesives. In: Skeist, I. (Ed.), *Handbook of Adhesives*, 3rd edn. Van Nostrand Reinhold, New York, 1990.
211. Kreiger, R.B. and Politi, R.E., High temperature structural adhesives. In: Alner, D.J. (Ed.), *Aspects of Adhesion-3*. CRC Press, Cleveland, OH, 1967, pp. 47–57.
212. Landrock, A.H., *Adhesives Technology Handbook*. Noyes, Park Ridge, NJ, 1985, pp. 149–150.
213. Tobiason, F.L., Phenolic Resin Adhesives. In: Skeist, I. (Ed.), *Handbook of Adhesives*, 3rd edn. Van Nostrand Reinhold, New York, 1990, pp. 316–337.
214. Bemmels, B.W., US Patent 2,987,420 (1964). Related patents assigned to Johnson and

- Johnson include the following British Patents: BP 960,509 (1963); BP 975,971(1964); BP 1,172,670 (1969).
215. Midgley, C.A. and Rea, J.R., Styrene–butadiene rubber adhesives. In: Skeist, I. (Ed.), *Handbook of Adhesives*, 3rd edn. Van Nostrand Reinhold, New York, 1990, pp. 227–234.
 216. Guggenberger, S.K., Neoprene (polychloroprene)-based solvent and latex adhesives. In: Skeist, I. (Ed.), *Handbook of Adhesives*, 3rd edn. Van Nostrand Reinhold, New York, 1990.

Surface treatments of metal adherends

GUY D. DAVIS^{a,*} and JOHN D. VENABLES^b

^a *DACCO SCI, INC., Columbia, MD 21046, USA*

^b *Venables and Associates, Baltimore, MD 21204, USA*

1. Introduction

Proper preparation of an adherend surface is one of the most important factors in assuring adequate joint strength and durability of high-performance adhesive joints [1–9]. In the case of a structural bond, stresses must be transferred from one adherend to the other adherend through the adhesive. The interface or interphase between the adhesive and the adherend is critical to this stress transfer. The goal of a surface treatment is to form a strong and stable interface or interphase that is stronger and more durable than the adhesive being used so that bond failure is cohesive within the adhesive, both initially and throughout the joint's service lifetime.

There are several requirements for a good surface preparation.

- (1) The surface must be cleaned of any contamination or loosely bound material that would interfere with the adhesive bond.
- (2) The adhesive or primer must wet the adherend surface (Chapter 10).
- (3) The surface preparation must enable and promote the formation of bonds across the adherend/primer–adhesive interface. These bonds may be chemical (covalent, acid–base, van der Waals, hydrogen, etc.), physical (mechanical interlocking), diffusional (not likely with adhesive bonding to metals), or some combination of these (Chapters 7–9).
- (4) The interface/interphase must be stable under the projected use conditions for the lifetime of the bonded structure (Chapter 17 of Volume I).
- (5) The surface formed by the treatment must be reproducible. Reproducibility requires that the prepared surface be independent of surface contamination, mill-scale, and other variations of nominally identical alloy surfaces. Reproducibility is facilitated if the treatment has wide processing windows so that

* Corresponding author. E-mail: gddaccosci@aol.com

processing variables, such as pH, solution contamination, solution chemistry, temperature, and time do not have to be narrowly controlled. An added level of reproducibility would be independence of metal alloy or heat treatment.

Different industries assign different roles to surface preparation. The aerospace industry, with relatively low throughput and extreme emphasis on safety, carefully prepares the surface prior to bonding during original manufacture and repair to assure the best practical bond strength and durability. This is done even when the bonding areas are very large as in the Space Shuttle where insulating tiles are adhesively bonded to virtually the entire surface area of the Orbiter and an insulating urethane foam is bonded to over 1/4 acre of the External Tank surface. On the other hand, the automotive industry, with high throughput, prefers almost no surface preparation and therefore uses contamination-tolerant adhesives and overdesign of joints. Likewise, the packaging industry, with very high throughput but relatively low requirements for stress and durability, also minimizes surface preparation. This chapter will focus on surface treatments used for high-performance bonds, primarily of the type used in the aerospace industry.

2. Surface preparation issues

Most high-performance surface treatments of metal adherends, such as those used in the aerospace industry, involve several steps. These include cleaning the surface of undesired contamination, removing the as-received oxide layer, and growing or depositing an oxide or other coating designed to provide good bonding properties.

2.1. Cleaning

Cleaning the surface of undesirable organic and inorganic material is the first step in preparing an adherend for bonding. The organic contamination originates from rolling oils at the mill, oils and greases applied for temporary corrosion protection, machining oils used during fabrication, release agents, and contamination from the atmosphere. Unless the adhesive is specifically designed to absorb this material, such contamination will prevent wetting and strong bonds across the interface and the joint will readily fail. Although the importance of surface contamination has been known for many years,

“When a plate of gold shall be bonded with a plate of silver or joined thereto, it is necessary to beware of three things, of dust, of wind, and of moisture: for if any come between the gold and silver they may not be joined together. . . .”

De Proprietatibus Rerum (The Properties of Things) (written in 1250 AD)

the ability to detect and measure it is much more recent, as discussed in Section 5 and in Chapter 6.

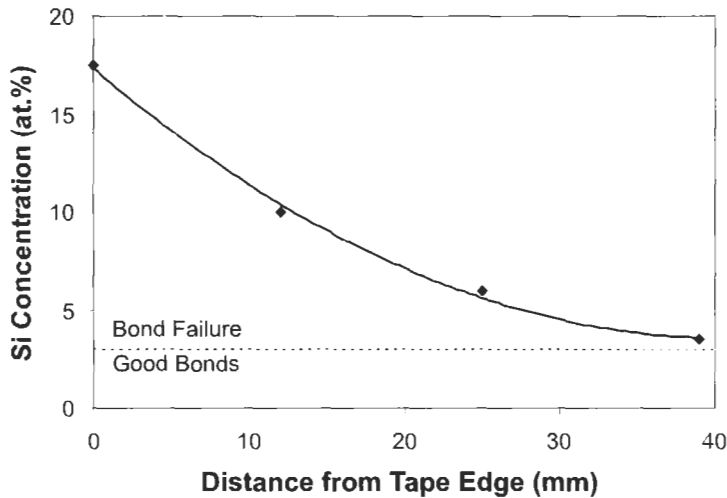


Fig. 1. Silicone contamination, as measured by XPS, as a function of distance from the edge of a silicone tape after a heat treatment to simulate a curing cycle. The dashed line represents the silicone level that would produce delamination. Adapted from Ref. [11].

The amount of acceptable contamination varies and can be very small [10]. Silicones and other mold release agents are designed to be very effective at preventing adhesives and primers from wetting adherend surfaces in order to form good bonds. Accordingly, even small amounts can cause bond failure. Aluminum surfaces with one-third to one molecular layer of silicone (~ 3 at.% Si as measured by X-ray photoelectron spectroscopy (XPS)) will not bond well [11]. Unfortunately, silicones are very mobile and can readily migrate. An example is shown in Fig. 1. A silicone adhesive tape was used at the edge of an aluminum/phenolic structure to hold the end of the phenolic tape in place prior to curing. After curing, the phenolic heat shield exhibited delamination near the edge where the tape was used. XPS analysis showed that silicone from the tape had migrated under the phenolic to prevent bonding.

The sensitivity of a system to contamination depends on many factors. Rubbers are more tolerant of contamination than epoxies. Rougher surfaces tend to be more tolerant than smoother surfaces. In general, water-borne or high-solid adhesives and primers are more sensitive to surface contamination than solvent-borne materials. As adhesives and coatings are reformulated to become more environmentally acceptable, contamination may become a greater issue. This is illustrated in Fig. 2, which shows the solvent-borne system to be very tolerant of grease while the aqueous system is approximately an order of magnitude more sensitive [12]. Accordingly, the first step in an adherend preparation process is usually a degreasing step. Traditionally this was done with chlorinated solvents, but regulations have required substitution of more environmentally acceptable cleaners.

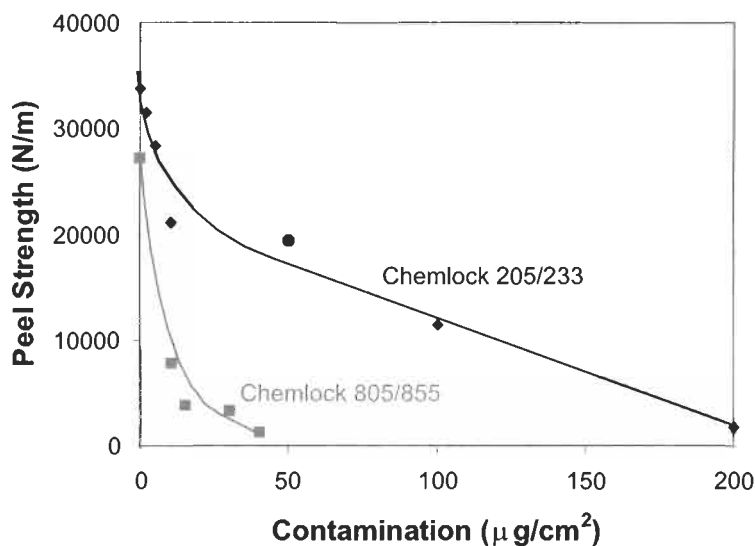


Fig. 2. Peel strength of NBR rubber as a function of HD2 grease contamination level on grit-blasted steel using the solvent-borne Chemlock 205/233 primer/adhesive and the aqueous Chemlock 805/855. Adapted from Ref. [12].

2.2. Deoxidizing

In addition to organic contamination, most as-received metal alloys have a thick oxide/hydroxide film formed during heat treatment, fabrication, and other processing. The coating's composition, morphology, thickness, and mechanical properties will vary from fabricator to fabricator and lot to lot and is not reproducible. In the case of aluminum alloys containing magnesium, such as the 5000, 6000, and 7000 series alloys, the mill-scale on heat-treated material will be all or mostly MgO because of the high mobility of Mg in the aluminum alloy and its preferential oxidation when exposed to the atmosphere at high temperatures [13–15]. In copper-containing alloys, such as the 2000 and 7000 series, there often is a buildup of copper at the oxide–metal interface. Copper has been shown to degrade bond durability, especially in the absence of a corrosion-preventative primer [14,15]. The degradation of bond durability with increasing copper is illustrated in Fig. 3. It is believed that the copper serves to promote corrosion via galvanic coupling with the aluminum. The effect of magnesium is less clear. Some authors report degraded durability with increasing magnesium [7,16,17] while others have shown improvements in wedge test crack growth with certain ranges of magnesium concentration in the oxide (3–12 wt.%) [14,15]. Differences in surface morphology and other variables may have played a role in the different results. To assure reproducible bonding surfaces, the second step in the treatment process utilizes mechanical abrasion or a deoxidizing agent (a strong acid or alkaline solution

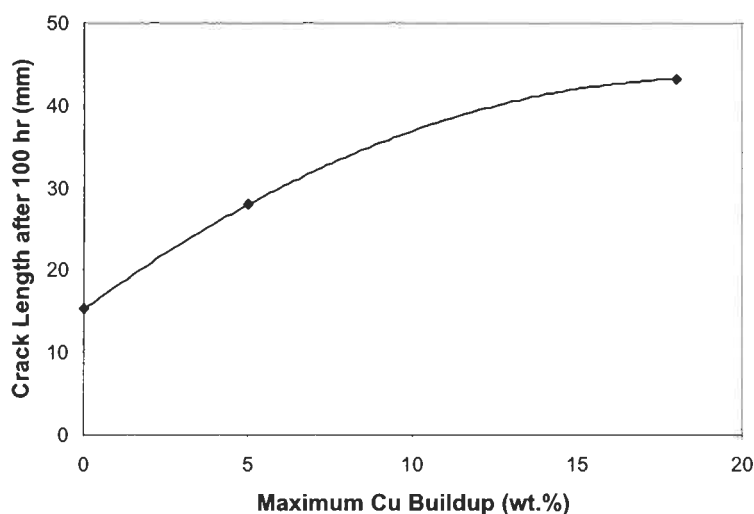


Fig. 3. Wedge test crack length as a function of maximum Cu buildup at the oxide-metal interface. The adhesive was Cytec FM-123. The surfaces were prepared with the Forest Products Laboratory etch. The oxide morphology was kept constant. Data are from Ref. [15].

as indicated in Tables 1–5) that removes the original mill-scale leaving the bare metal or a thin native oxide surface. The adherend is then ready for the next step in which a stable oxide or coating is grown or deposited.

2.3. Surface engineering

The final step in providing an acceptable bonding surface is to grow or deposit an oxide or other surface film designed to promote good, stable bonds with the primer or adhesive. As mentioned earlier, the bonding can be either chemical or physical. Durable covalent chemical bonding across the interface is generally achieved with phenolic adhesives [18], but not the more common epoxies without the use of coupling agents [19,20] or sol-gel films [21–25]. In most cases, a microscopically rough surface is needed to achieve mechanical interlocking. This can be achieved mechanically (e.g., grit blasting, sanding, or Scotch-Briting[®]), chemical etching, anodization, or deposited coating (e.g., conversion coating, plasma spray coating). Specific surface treatments for different metals are given in Section 3.

The scale of the microscopic surface roughness is important to assure good mechanical interlocking and good durability. Although all roughness serves to increase the effective surface area of the adherend and therefore to increase the number of primary and secondary bonds with the adhesive/primer, surfaces with features on the order of tens of nanometers exhibit superior performance to those with features on the order of microns [9,14]. Several factors contribute to this difference in performance. The larger-scale features are fewer in number

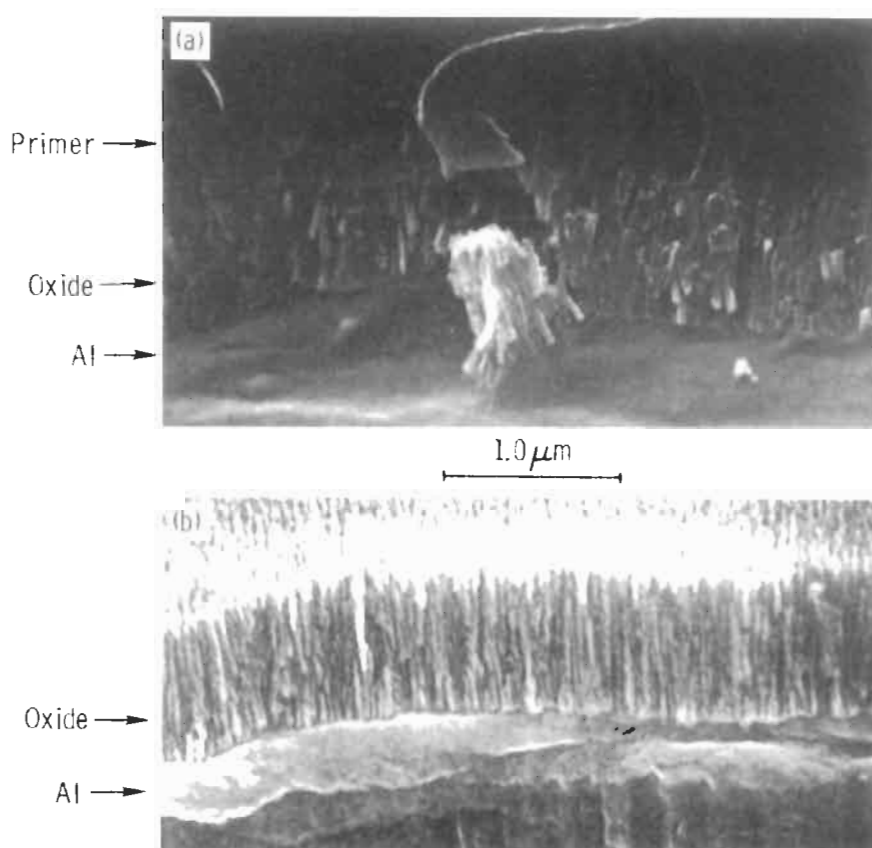


Fig. 4. Cross-sectional electron micrographs of (a) primed PAA interphase and (b) unprimed PA oxide showing complete penetration of primer into the oxide pores [9].

and generally are smoother (even on a relative scale) so that interlocking is less effective. Depending on the particular treatment used, there may also be loosely bound detritus that prevent bonding to the integral adherend surface [26]. In addition, the larger-scale roughness frequently allows trapped air and surface contaminants to remain at the bottoms of troughs and pores [11,26,27]. These unbonded regions limit joint performance by reducing both chemical and physical bonds and serving as stress concentrators. In contrast, smaller-scale microroughness tends to be more convoluted in morphology and generates strong capillary forces as the primer wets the surface, drawing the polymer into all the 'nooks and crannies' of the oxide and displacing trapped air and some contaminants to form a microcomposite interphase [11]. Indeed, cross-sectional micrographs show complete filling of the micropores [9,26–31] by primers and some adhesives (Fig. 4).

This dependence on the degree and scale of roughness is illustrated in Fig. 5,

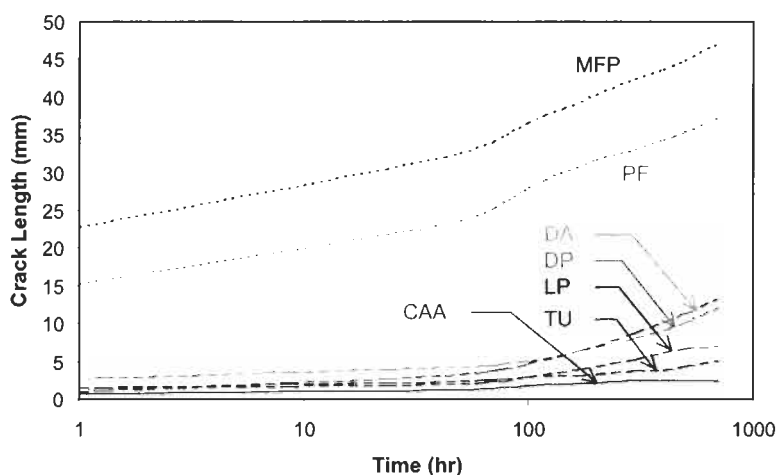


Fig. 5. Wedge test results for Ti adherends with several different surface treatments having differing degrees and scales of roughness. Specimens were exposed to 100% relative humidity at 60°C. Data from Ref. [32].

which shows wedge test results of titanium bonds with several surface preparations [32]. Because the titanium surface is stable under these conditions (see below), differences in the joint performance can be attributed solely to differences in the polymer-to-oxide bonds and correlate very well with adherend roughness [33]. The poorest performing group of pretreatments [Class I: phosphate fluoride (PF) and modified phosphate fluoride (MPF)] produced relatively smooth surfaces. The intermediate group [Class II: Dapcotreat (DA), dry Pasa Jell 107 (DP), liquid Pasa Jell 107 (LP), and Turco 5578 (TU)] exhibited macrorough surfaces with no microroughness. They had significant improvements in durability over the smooth adherends, but not as good as the Class III pretreatment [chromic acid anodization (CAA)] which provided a very evolved microroughness. Subsequent Class III surfaces prepared using sodium hydroxide anodization (SHA) and plasma spray provide further evidence to this correlation [34–36]. Both of these give very good durability performance and exhibit high levels of microroughness. Because of the importance of small-scale roughness, high-quality micrographs with magnifications in the order of 50,000 \times , such as those shown below in Figs. 14–18 are critical in evaluating surface morphology [9].

2.4. Processability issues

2.4.1. Critical process parameters

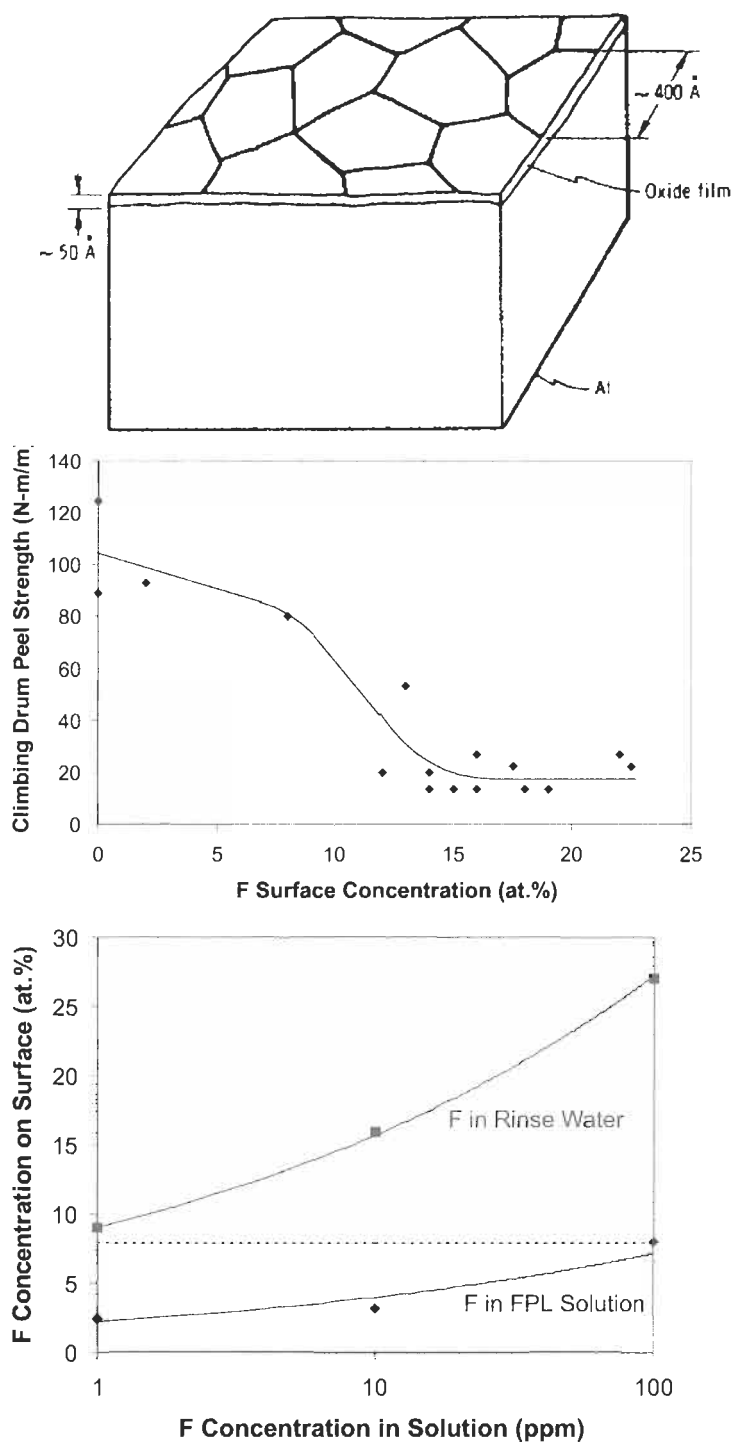
For a surface treatment process to be practical, not only does it have to produce a clean, stable surface suitable for chemical or physical bonding to the

primer/adhesive, but it must be able to do this reliably in a production environment. An important aspect of processability is the acceptable window for the different process variables. That is, how much can a parameter vary from its nominal value before the performance of the bonded structure is compromised and degraded? The narrower the acceptable window, the tighter the processing controls must be. Tight controls, in turn, are associated with high cost for implementation of the controls, the inspection of the part or processing variable, and the waste from out-of-specification parts that must be reprocessed or discarded. In contrast, a robust process will have wide processing windows so that the prepared surface will still be acceptable despite the inevitable processing discrepancies that occur.

The critical processing parameters (those which must be controlled most closely) will depend on the specific process, the material, and the performance requirements. Typical parameters include solution composition/concentration, pH, bath temperature, time of each step and time between each step, anodization voltage and current, etc. For the most part, proper ranges for these parameters are given in the various ASTM or manufacturer standards for the process, but frequently other factors involving accidental contamination of solutions or parts being processed may lead to unexpected and sometimes serious problems that must be handled on a case-by-case basis. One illustration will serve to emphasize the importance of having available expertise and analytical procedures required to maintain acceptable parts for bonding.

In an actual example, it was found that climbing drum peel tests used for quality control of an FPL process in a production setting for aluminum bondments occasionally showed low strength values especially during hot, humid summer days [37]. Characterization of both sides of the peeled surfaces and of unbonded ends using high-resolution scanning electron microscopy (HR-SEM) showed that the FPL surfaces were very smooth without the shallow cell/whisker structure of a normal FPL surface (Fig. 6, as compared to Fig. 14). With no physical bonding, the joint had to rely solely on whatever chemical bonds were formed and these were not sufficient to give good joint strength, especially when the joints were exposed to moisture, even for a short time. In addition, surface analysis using X-ray photoelectron spectroscopy (XPS) and Auger electron spectroscopy (AES) showed fluorine contamination on the surface and that high fluorine levels (>8 at.%) were correlated with poor bond strength.

Fig. 6. Top: Morphology of FPL surface following fluorine contamination. This is to be compared to the standard FPL morphology of Fig. 14. Middle: Climbing drum peel (CDP) strength as a function of F surface concentration. Bottom: F concentration on FPL surfaces following doping the FPL etch solution and the rinse water with NaF. The dotted line corresponds to the surface concentration with which the CDP strength began to decrease. Adapted from Ref. [37].



To determine the source of the fluorine contamination, an FPL etch solution and final rinse water were doped with NaF in the laboratory (Fig. 6). Other specimens were held over a HNO_3/HF chemical milling solution used in the processing of titanium adherends in the same facility. Each potential contamination source could transfer fluorine to the surface. However, contamination from the etch bath could be eliminated as a probable cause of failure because adsorption of sufficient fluorine would have required ~ 100 ppm NaF in the solution, which was monitored and controlled to less than 1 ppm. Likewise, although 1 ppm of fluorine in the rinse water gave the same adsorption as 100 ppm in the etch solution, this source was eliminated because controls of the rinse water kept the fluorine levels below this amount. The real culprit turned out to be the fluorine vapor above the titanium milling solution where it was found that exposure for only 15 min resulted in five times the fluorine needed for bond degradation. With a relatively large amount of fluorine on the otherwise normal FPL surface, exposure to only 2 h at 80% relative humidity (RH) in the environment caused the oxide protrusions to disappear, presumably the result of forming HF-like species on the surface that etched the oxide.

As a result of this investigation many steps were taken to prevent fluorine adsorption and loss of microroughness including relocation of the titanium etching tank and much better control on the ambient environment. Moreover, recognition that the surface morphology of the surface oxide was extremely important in assuring good bond strength led to the development of a program whereby witness panels were inspected weekly by HR-SEM to detect variations from the standard process. (See Section 5.5 for details.)

2.4.2. Quality control

Because of the critical nature of adhesive bonds in the aerospace industry, among others, it is essential to inspect the process to assure quality. This inspection can involve monitoring the critical process parameters, testing of witness specimens prepared at the same time as the structure, or evaluating the surface to be bonded. The best surface to inspect is the actual surface to be bonded, but techniques available for inspection, especially large surface area bondments such as on the Space Shuttle, are limited. Witness specimens allow a broad range of techniques, including those requiring small sizes, vacuum, or highly trained personnel. They also allow bonding and destructive testing.

Approaches and examples to quality control are given in Section 5. Laboratory techniques to evaluate surfaces are discussed in Chapter 6.

2.4.3. Health and safety concerns

A separate set of processability issues involves health, safety, and environmental concerns. Ozone-depleting compounds (ODCs), such as trichloroethane and

trichloroethylene, have been banned. Hexavalent chromium is a carcinogenic toxin and is heavily regulated. Disposal is becoming increasingly difficult and expensive. Other materials are either strong acids or strong bases that require appropriate safety precautions. As a result, considerable research has recently been aimed at developing more environmentally acceptable and less hazardous processes. These will be discussed below along with the more conventional treatments.

3. Surface/bondline degradation mechanisms

It is important to understand the various degradation mechanisms in order to make intelligent choices regarding the appropriate surface treatment to use for a specific application. As discussed earlier and in Chapter 17 of Volume 1, secondary bonds at a metal (oxide)–polymer interface can readily be disrupted by moisture. However, once high-quality physical or chemical bonds are formed across the interface, the interface will not fail unless it degrades in some manner to break the interlocking or allow crack growth through the oxide or at the oxide/metal interface. The mechanism of degradation will depend on the adherend/adhesive materials and the exposure conditions.

3.1. Aluminum adherends

For aluminum adherends, moisture causes hydration of the surface, i.e., the Al_2O_3 that is formed during the surface treatment is transformed into the oxyhydroxide AlOOH (boehmite) or trihydroxide $\text{Al}(\text{OH})_3$ (bayerite) [9,38,39]. The transformation to the hydroxide results in an expansion of the interphase (the volume occupied by the hydroxide is up to three times larger than that originally occupied by the Al_2O_3). This expansion and the corresponding change in surface morphology induce high stresses at the bondline. These stresses coupled with the poor mechanical strength of the hydroxide, promote crack propagation near the hydroxide–metal interface, as shown schematically in Fig. 7 [9].

The rate of hydration of the aluminum oxide depends on a number of factors, including surface chemistry (treatment), presence of hydration/corrosion inhibitors in the primer or applied to the surface, temperature, and the amount of moisture present at the surface or interface. One surface treatment that provides an oxide coating exhibiting good hydration resistance is phosphoric acid anodization (PAA) [28]. Its stability is due to a layer of phosphate incorporated into the outer Al_2O_3 surface during anodization; only when this phosphate layer goes into solution does the underlying Al_2O_3 hydrate to AlOOH [38]. The hydration process is illustrated in the surface behavior diagram of Fig. 8 [38,40]. It shows hydration to occur in three stages: (1) a reversible adsorption of water, (2) slow dissolution of the phosphate layer followed by rapid hydration of

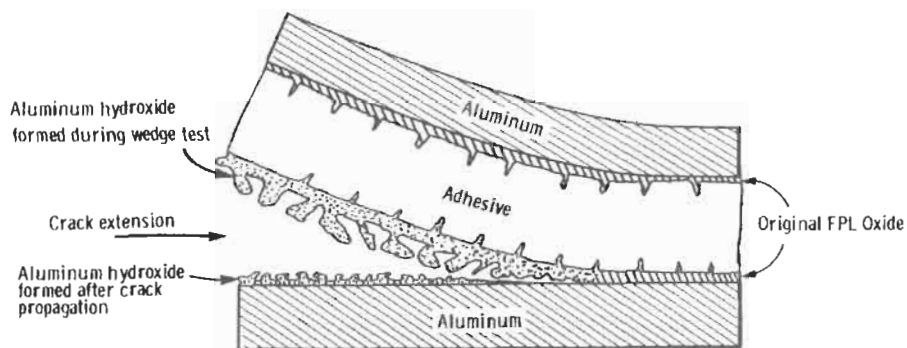


Fig. 7. Schematic representation of hydration causing crack propagation in a wedge test specimen. The increase in volume upon hydration induces stresses at the crack tip that promote crack growth [9,39].

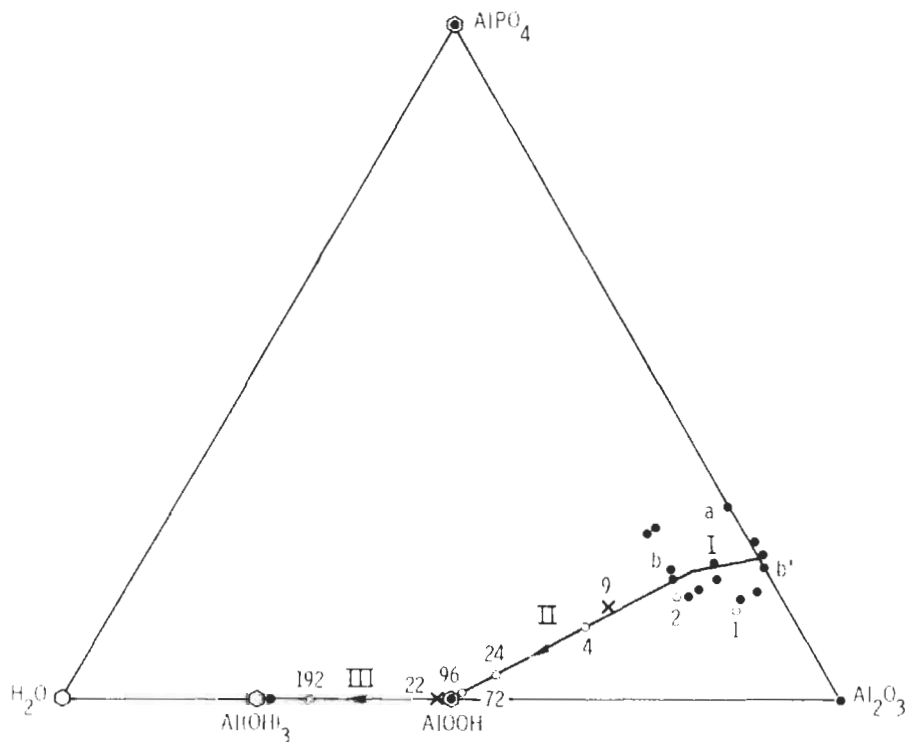


Fig. 8. Surface behavior diagram showing hydration of the PAA surface. Hydration occurs in three stages: I, reversible adsorption of moisture; II, hydration of the Al₂O₃ to AlOOH; and III, further hydration to Al(OH)₃. The numbers represent hours of exposure to high humidity. Adapted from Refs. [38,40].

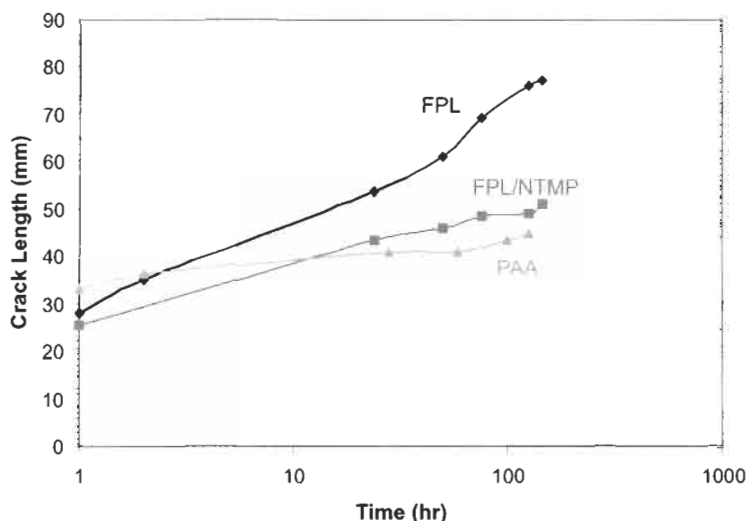


Fig. 9. Wedge test results of aluminum adherends with the following surface preparations: FPL, PAA, and FPL followed by an NTMP treatment. Adapted from Ref. [42].

the freshly exposed Al_2O_3 to AlOOH , and (3) further hydration of AlOOH to $\text{Al}(\text{OH})_3$.

Another means of providing a hydration-resistant surface is its treatment with a hydration inhibitor [41]. Fig. 9 shows wedge tests results for a Forest Product Laboratory (FPL) bond [43], an FPL bond pretreated with nitrilotrismethylenephosphonic (NTMP) acid [42,44,45], and a PAA bond. The monolayer coverage of NTMP stabilizes the FPL surface against hydration and provides wedge test bond performance similar to that of PAA-treated adherends.

Although the above experiments involved exposure to the environment of unbonded surfaces, the same process occurs for buried interfaces within an adhesive bond. This was first demonstrated by using electrochemical impedance spectroscopy (EIS) on an adhesive-covered FPL aluminum adherend immersed in hot water for several months [46]. EIS, which is commonly used to study paint degradation and substrate corrosion [47,48], showed absorption of moisture by the epoxy adhesive and subsequent hydration of the underlying aluminum oxide after 100 days (Fig. 10). After 175 days, aluminum hydroxide had erupted through the adhesive.

Subsequent investigations proved that identical hydration reactions occur on bare aluminum surfaces and bonded surfaces, but at very different rates of hydration [49]. An Arrhenius plot of incubation times prior to hydration of bare and buried FPL surfaces clearly showed that the hydration process exhibits the same energy of activation (~ 82 kJ/mole) regardless of the bare or covered nature of the surface (Fig. 11). On the other hand, the rate of hydration varies dramatically, de-

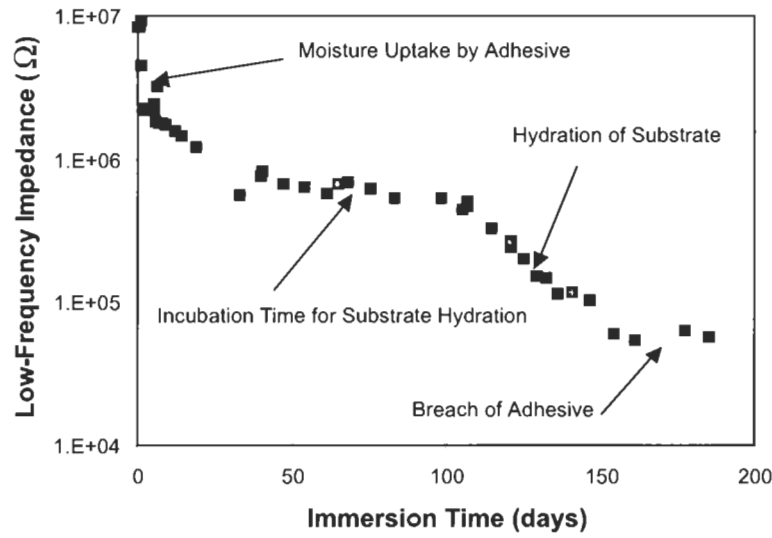


Fig. 10. Low-frequency electrochemical impedance of an epoxy-coated FPL aluminum adherend as a function of immersion time in 50°C water. Adapted from Ref. [46].

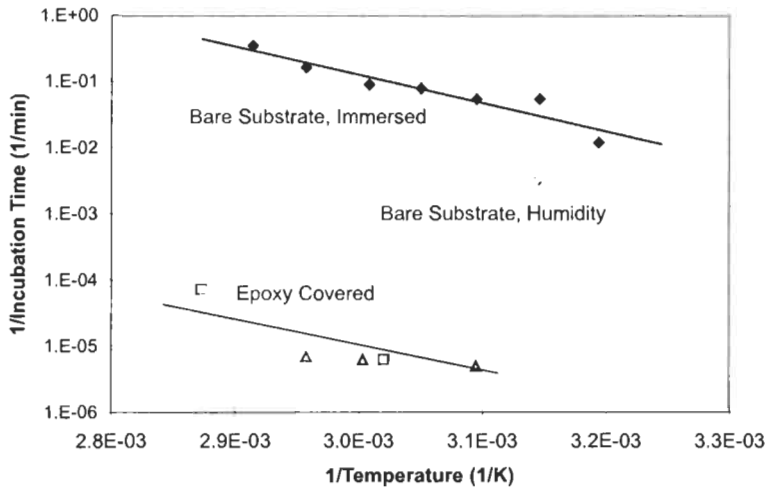


Fig. 11. Arrhenius plot of incubation times prior to hydration of FPL aluminum under various conditions. Adapted from Ref. [49].

pending on the concentration of moisture at the oxide interface/surface available to react. The epoxy-covered surfaces have incubation times three to four orders of magnitude longer and rate constants similarly smaller than bare, immersed specimens, reflecting the limited amount of moisture absorbed by the epoxy and free to react with the oxide.

The beginnings of hydration have also been detected in advance of the crack tip of a PAA/epoxy tapered double cantilever beam using transmission electron microscopy (TEM) [27]. Following cyclic loading in distilled water and crack arrest, the outer 20 nm of the PAA oxide at the adhesive interface had become denser and lost its original porosity (in this specimen, there was little interpenetration of the adhesive into the oxide because of high viscosity during cure). This change in morphology was identified as the very early stages of hydration. A companion specimen that had been primed did not show any signs of hydration. The primer with low viscosity during cure had completely penetrated the oxide pores. This penetration and the addition of phenolic- and silane-based additives to couple with the oxide reduced the amount of moisture available to react with the oxide and increased the oxide stability. Thus the hydration reaction had been significantly inhibited.

The slow rate of hydration for buried surfaces is desirable from a service point of view, but makes the study and evaluation of the durability of surface treatments difficult unless wedge tests (ASTM D3762) or similar tests are used to accelerate the degradation. As for the wedge test, the stress at the crack tip, together with the presence of moisture at the tip, make this a more severe test than soaked lap shear specimens or similar types and therefore a better measure of relative durability.

3.2. Titanium adherends

In contrast to aluminum, titanium adherends are stable under conditions of moderately elevated temperatures and humidity. Although moisture has been shown to accelerate the conversion of the amorphous CAA oxide on titanium adherends to crystalline anatase [50], the crystallization, along with the resulting morphology change, is very slow relative to the changes observed with aluminum and steel. In the wedge test results of Fig. 5, for example, the adherend surfaces underwent no change in morphology or crystallinity. Failure of the CAA specimens remained within the adhesive, with the physical bonds provided by the microscopically rough oxide remaining intact [50]. For moderate conditions, the key requirement for a titanium treatment is a convoluted microrough surface to promote physical bonding.

At elevated temperatures where titanium alloys could be the adherend of choice, a different failure mechanism becomes important. The solubility of oxygen is very high in titanium at high temperatures (up to 25 at.%), so the oxygen in a CAA or other surface oxide can and does dissolve into the metal (Fig. 12). This diffusion leaves voids or microcracks at the metal–oxide interface and embrittles the surface region of the metal (Fig. 13). Consequently, bondline stresses are concentrated at small areas at the interface and the joint fails at low stress levels [51,52]. Such phenomena have been observed for adherends exposed to 600°C for as little as 1 h or 300°C for 710 h prior to bonding [52] and for bonds using

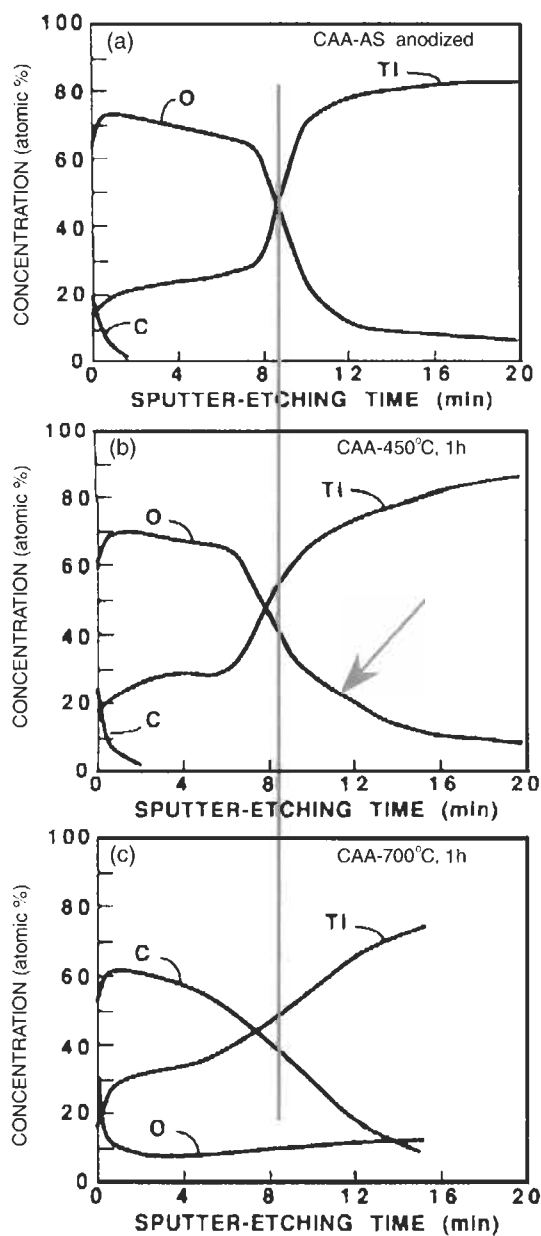


Fig. 12. Auger electron spectroscopy (AES) sputter-depth profile of CAA-treated titanium after various exposures in vacuum: (a) as anodized, (b) 450°C for 1 h, and (c) 700°C for 1 h. The sputter etch rate is ~ 1.5 nm/min. The line indicates the original interface. The arrow denotes oxygen diffused into the substrate. Adapted from Ref. [51].

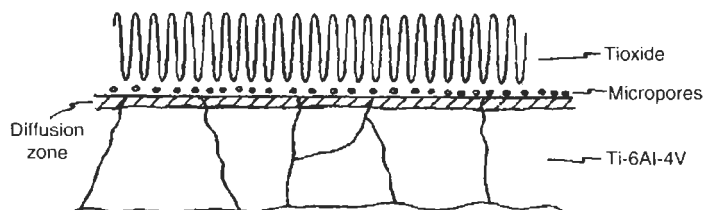


Fig. 13. Schematic representation of oxygen dissolving from the oxide into the titanium metal at high temperatures. The interface is weakened with the formation of voids, porosity, and microcracks and with the embrittlement of the interfacial metal region [52].

a high-temperature adhesive cured at 371°C [53] or 400°C [52]. To prevent this failure mode, thick oxides, such as those grown by CAA, must be avoided in high-temperature applications. Surface treatments that show compatibility with high temperatures are discussed in Section 4.2.

3.3. Steel adherends

Despite intense commercial interest in the bonding of steel structures and considerable research efforts toward the goal of forming durable, structural bonds to steel surfaces, no general-purpose pretreatments for steel substrates have been developed [54]. Unlike aluminum and titanium, iron does not form coherent, adherent oxides, so that it is difficult to create a stable film with the fine microroughness needed for good adhesion. Accordingly, grit blasting, by default, has become the pretreatment process of choice even though it has a number of serious drawbacks. Among these is the fact that impurities in or on the grit blast material itself may lead to the formation of a contaminated surface that may overcome the advantages of the roughened surface. Another drawback is the fact that, except on stainless steels, the newly exposed surface will tend to rust and corrode very easily if not immediately covered with a corrosion inhibiting primer. And even then, since these primers are not 100% effective, once moisture reaches the surface, before or after bonding, the non-coherent oxide that forms will lead to a degradation of bond strength.

For stainless steels the problem is somewhat different. Here, the oxides can be quite stable but they are extremely thin and very smooth with none of the type of microroughness that leads to excellent bond strength and durability for aluminum and titanium. Attempts to introduce microroughness by surface etching designed to preferentially attack grain boundaries or microstructure can be successful but each alloy and each heat treatment may require special etchants and processing to be effective, thus adding immensely to the cost of surface preparation.

For most applications the strength requirements for steel bonding may not be as demanding as for aluminum and titanium so some sacrifice in bondment

properties may be tolerated. Additionally, it has been found that certain epoxy adhesives (that cure at high temperatures) can form durable bonds directly to oily steel coil surfaces. The mechanisms proposed by Debski et al. [55,56] involve: (1) thermodynamic displacement of oil from the steel surface, and (2) absorption of oil into the adhesive. Such a situation is fortunate because many steel bonding applications, especially in the automotive and appliance industries, are of the high-volume type for which elaborate surface preparation is undesirable or even impossible.

In Section 4.3 several recently developed and experimental surface preparation methods for steel such as conversion coatings, plasma spray and sol-gel that attempt to simultaneously improve durability and bond strength over grit blasting will be discussed.

4. Treatments for specific metals

4.1. Aluminum

4.1.1. Etching

The FPL and other chromic–sulfuric acid etching (CAE) processes are the oldest surface pretreatments for aluminum adherends [43] other than simple degreasing or mechanical abrasion. Variations in the performance of clad material as a function of age of the etch solution, led to the optimized FPL etch which includes the prior dissolution of Cu-containing aluminum (typically 2024) in the acid bath [57,58]. The etching solution dissolves the initial oxide (hence their use as deoxidizers in anodization processes) and grows a thin oxide [14]. The FPL oxide morphology is shown in the HR-SEM stereo micrograph and isometric drawing [9] in Fig. 14. The oxide consists of a network of shallow pores and protrusions or whiskers on top of a thin barrier layer. While this roughness is less evolved and complex than the PAA oxide, it is sufficient to provide at least some mechanical interlocking between the adhesive and the oxide surface. Chemically, the FPL film is amorphous Al_2O_3 with varying quantities of adsorbed water [41] that can be removed by heating, vacuum exposure, or adsorption with certain organic hydration inhibitors.

A more recent process, the P2 etch [60], which uses ferric sulfate as an oxidizer in place of sodium dichromate avoids the use of toxic chromates, but still provides a similar oxide surface morphology (Fig. 15) allowing a ‘mechanically interlocked’ interface and strong bonding [9]. The P2 treatment has wide process parameter windows over a broad range of time–temperature–solution concentration conditions and mechanical testing confirms that P2-prepared surfaces are, at a minimum, equivalent to FPL-prepared specimens and only slightly inferior to PAA-prepared surfaces [61].

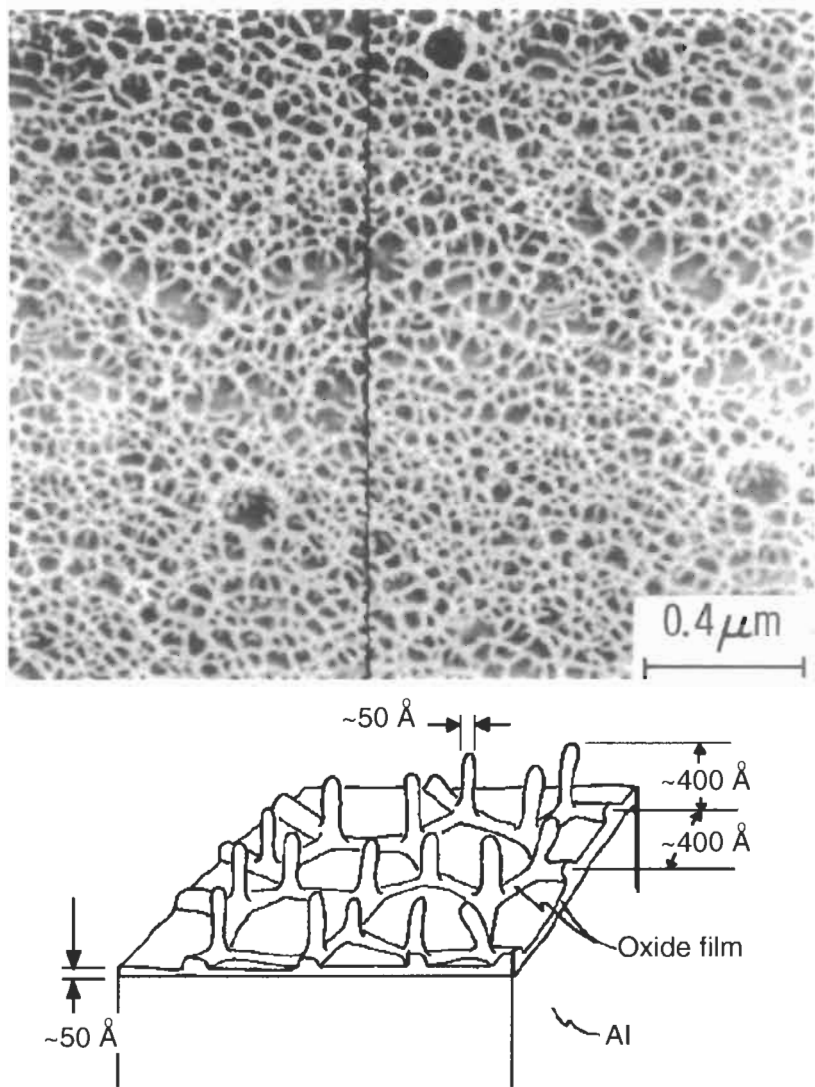


Fig. 14. Top: High-resolution stereo micrograph of an FPL-etched 2024 aluminum surface. Bottom: Schematic diagram of the oxide structure. Diagram is from Refs. [9,59].

Processing details for the optimized FPL etching procedure, other chromic-sulfuric acid etches and the P2 etch are summarized in Table 1 [2,62].

4.1.2. Anodization

4.1.2.1. PAA. Phosphoric acid anodization (PAA) was developed by the Boeing Company in the late 1960s and early 1970s to improve the performance of bonded

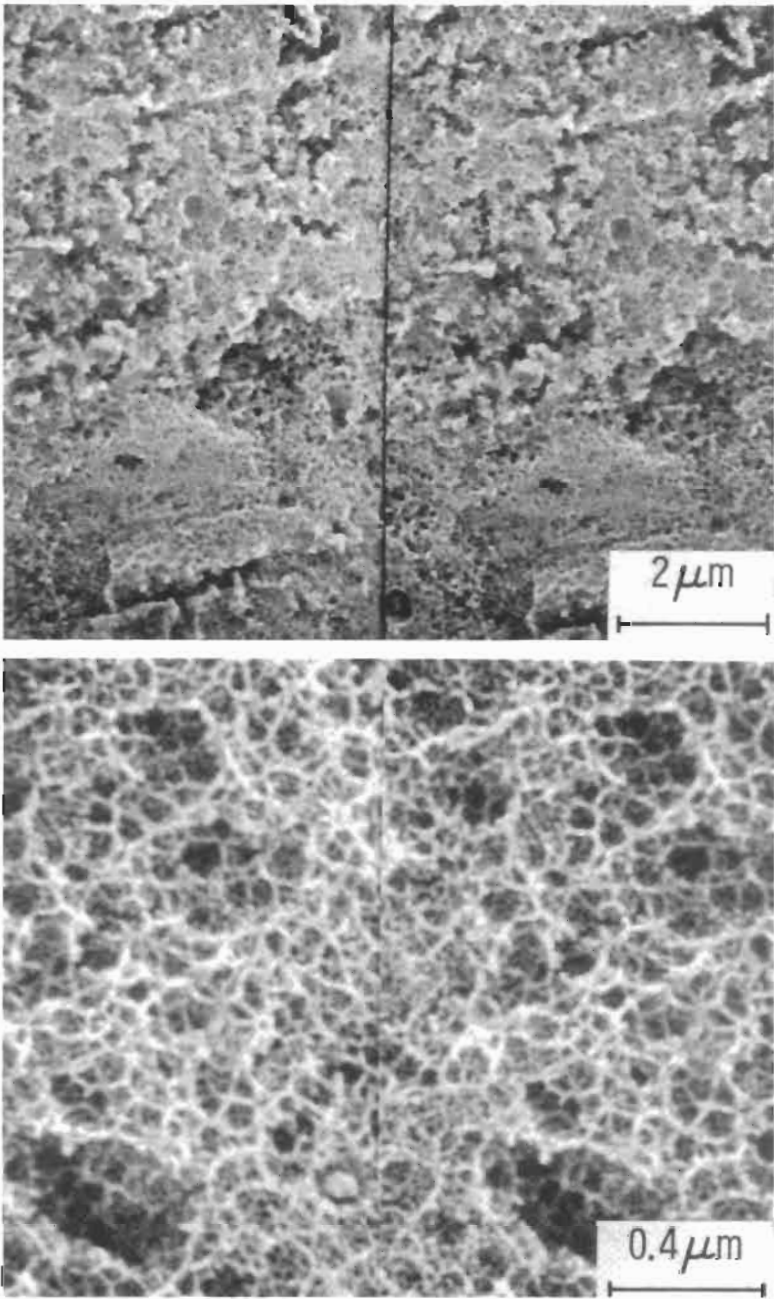


Fig. 15. High-resolution stereo micrographs of P2-etched 2024 Al.

Table 1

Etch bath composition (wt.%)

Process	$\text{Na}_2\text{Cr}_2\text{O}_7 \cdot 2\text{H}_2\text{O}$	H_2SO_4	H_2O	Temperature ($^{\circ}\text{C}$)	Time (min)
FPL	2.5	24.3	73.2	68	15–30
UK Defense 03-2/1	6.4	23.3	70.3	60–65	30
DIN 53 281	7.5	27.5	65.0	60	30
Alcoa 3	3.2	16.5	80.3	82	5
Optimized FPL ^b	5.0	26.7	68.3	65	10
FPL-RT	6.4	23.4	70.2	22	240
P2	(15.0 ^c)	37.0	48.0	60–70 ^d	8–15

^a From Refs. [2,62].^b Also 1.9 g/l 2024 Al.^c FeSO_4 instead of $\text{Na}_2\text{Cr}_2\text{O}_7 \cdot 2\text{H}_2\text{O}$.^d Can also be performed at room temperature.

primary structures [63–65]. Bonds formed with PAA-treated adherends exhibit superior durability during exposure to humid environments compared to those formed with FPL-treated adherends, especially when epoxy adhesives are used. In addition, PAA bonds are less sensitive than FPL bonds to processing variables, such as rinse-water chemistry and time before rinsing. As a result, the PAA procedure has become the treatment of choice in the United States for critical aerospace applications.

The one outstanding feature that accounts in great part for the popularity of the PAA process is shown in Fig. 16. The HR-SEM micrograph and isometric drawing indicate an oxide with an open cell structure approximately 400 nm in height on top of a much thinner barrier layer [9,59]. The structure appears to be formed by a competition between the anodically induced growth process through the barrier layer and the inherent chemistry of the anodizing solution which simultaneously tends to dissolve the oxide. Thus, as the oxide builds up in thickness, the cell walls tend to be dissolved by the electrolyte to become thinner and thinner especially near the outer surface where only remnants of the walls remain leaving a whisker-like structure. As noted in Section 2.3, the fine pores exert strong capillary forces on the wetted adhesive or primer when they are applied thereby drawing the polymer into the structure to form a very strong interlocking interphase.

Chemically, the PAA film is amorphous Al_2O_3 [9,66–70] with the equivalent of a monolayer of phosphate incorporated onto the surface [16,17,38,71–73]. Alloying constituents of the adherend are not generally found in the as-anodized oxide. Depending on the storage conditions, some water can adsorb on the surface, but is readily removed by heating or storing in a dehydrating environment (e.g., a desiccator or a vacuum). The monolayer of phosphate protects the oxide from hydrating and only as the phosphate is slowly removed in an aqueous environment does hydration of the underlying oxide occur [38].

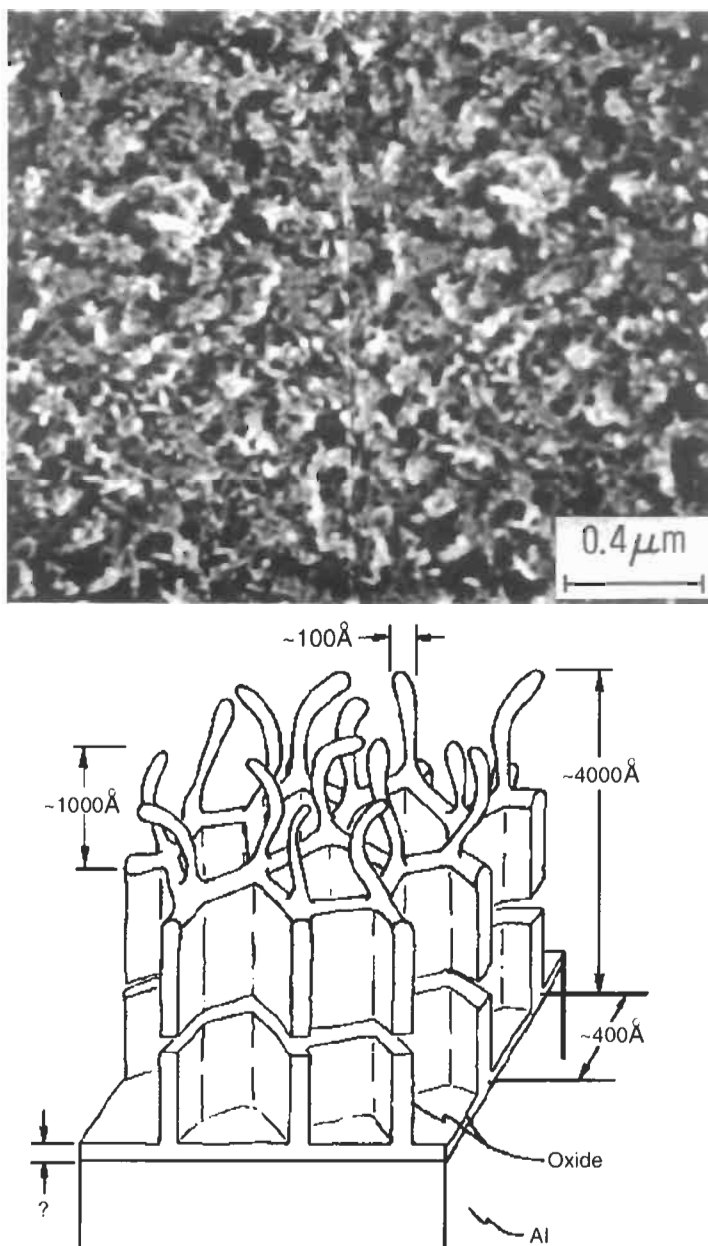


Fig. 16. Top: High-resolution stereo SEM micrograph of the PAA oxide on 2024 aluminum. Bottom: Schematic drawing of the oxide structure. Diagram from Refs. [9,59].

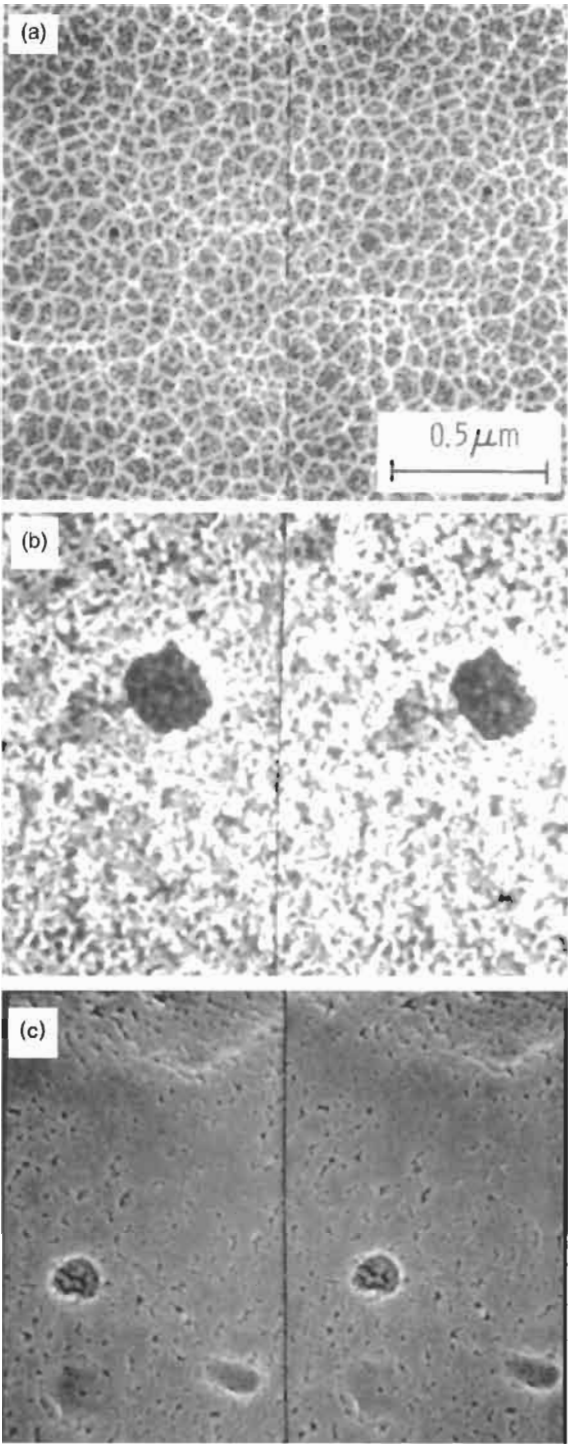
4.1.2.2. CAA. Chromic acid anodization [74–76], was developed initially as a treatment to improve the corrosion resistance of aluminum surfaces, but it is also used as a surface treatment for adhesive bonding especially in Europe where it is used extensively in aerospace applications [29,77].

The CAA oxide (Fig. 17) differs in several important aspects from the PAA oxide. First, and most important, it is much less porous overall than PAA due to the fact that the oxide is not soluble in the electrolyte and the mechanism that leads to the highly porous PAA oxide does not apply. Second, because the oxide has no solubility in the electrolyte, the morphology of the top surface is completely determined by whatever surface treatment precedes the anodizing process. Thus, if the FPL process is used as a de-oxidizing treatment, then the upper surface after anodizing will exhibit the FPL morphology and likewise a pretreatment by PAA will result in a PAA surface (Fig. 17). Third, the total oxide thickness is 1–2 μm , which is much greater than that provided by most other surface treatments and the barrier layer at the bottom of the columns is also relatively thick (40 nm) due to the high anodization voltages used [78,79].

The chemistry of the CAA oxide also differs from that of PAA. Although the upper portion is amorphous Al_2O_3 , like that of PAA, indications are that the lower part is crystalline [68–70,73,80,81]. Also, in contrast to the phosphate incorporated in the PAA oxide, little chromate is incorporated in or on the CAA oxide [68,69,82]. In spite of this, hydration of the CAA oxide generally occurs at a slower rate than the PAA which may be due to the crystallinity or the greater thickness [83] but the evidence is not clear on this point.

As a consequence of these factors, it is important to realize that success in developing good bonds to a CAA surface depends critically on the type of surface preparation used immediately prior to anodization. When this is taken into account and a FPL or PAA treatment precedes anodization, then the CAA process can yield excellent results. Moreover it has also been shown that the CAA oxide, overall, is less friable, i.e., less susceptible to damage, than PAA, or other thinner oxides [29,84].

4.1.2.3. BSAA. As hexavalent chromium has significant health and safety issues and is strictly regulated, several nonchromate processes have been developed. One of these is boric–sulfuric acid anodization (BSAA) [85], which, while not as popular as PAA or CAA, is used in several aerospace applications by the Boeing Corporation. The BSAA oxide has not been fully characterized as yet, but recent information indicates it exhibits a porous morphology intermediate to those of PAA and CAA (Fig. 18) although its total oxide thickness is perhaps closer to that of CAA. With regard to its chemistry, XPS surface analysis shows a small amount of sulfur incorporated in the oxide surface, but no detectable boron. Durability results (see below) show similar results to PAA and CAA.



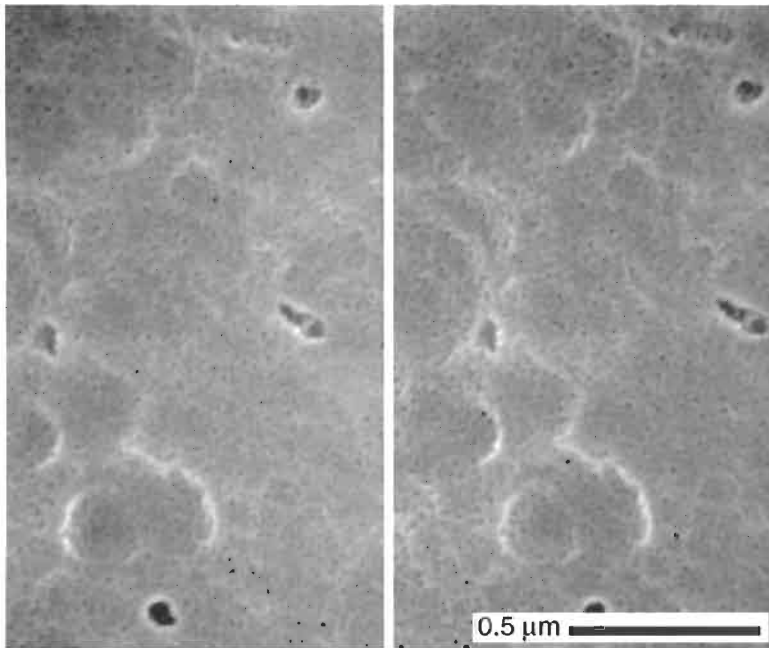


Fig. 18. High-resolution stereo SEM micrograph of BSAA oxide.

4.1.2.4. Processing steps. The anodization processes used commonly for aluminum adherend preparation share many common features. Table 2 gives the processing steps outlined for several of these. As outlined above, they consist of cleaning, deoxidizing, and anodization steps with rinsing and drying at the end. In some cases, one of the etching treatments, which can be used alone, is also used as the deoxidizing step before the anodic oxide is grown.

4.1.3. Emerging processes

Although the most popular of the processes described above (PAA and CAA) perform very well, there is a continuing need to develop processes that are less hazardous (no chromates, no strong acids or bases) or that are suitable for treatment of repair areas in the field. Two of these treatments are grit blasting coupled with silane coupling agents and sol-gel.

Fig. 17. High-resolution stereo SEM micrograph of CAA oxide: (a) with FPL pretreatment; (b) with PAA pretreatment; (c) production CAA surface. (a) and (b) are from Ref. [9].

Table 2

Processing steps for anodization of aluminum^a

Step	CAA				
	PAA (Ref. [64])	MIL SPEC (Ref. [74])	Bell helicopter (Ref. [75])	Fokker-DIN (Ref. [76])	BSAA (Ref. [85])
Cleaning	Alkaline	Alkaline	Alkaline	Alkaline	Alkaline
Deoxidation	FPL ^b	FPL	FPL	CAE	BAC5765
Anodization	100–120 g/l H ₃ PO ₄ 22–33°C 3 V/min to 15 V for 20–25 min	40–50 g/l CrO ₃ 32–38°C 8 V/min to 40 V, hold 55 min	60–700 g/l CrO ₃ 33–37°C 3–5 V/min to 40 V, hold 30–35 min	50 g/l CrO ₃ 38–42°C 5 V/min to 40 V, hold 20 min, raise to 50 V, hold for 10 min	30.5–52.0 g/l H ₂ SO ₄ , 5.2–10.7 g/l H ₃ BO ₃ 24.5–29°C 5 V/min to 15 V, hold for 18–22 min
Rinse	5–15 min, <43°C air dry, <i>T</i> < 71°C	1–5 min, 20°C oven dry, <i>T</i> < 65°C	20–25°C seal 75–125 ppm CrO ₃ , 82–85°C, 7–9 min, air dry	5 min, 20–25°C air dry, <i>T</i> < 60°C	3–15 min, <35°C air dry, <i>T</i> = 88°C

^a Adapted from Ref. [2].^b FPL was the original deoxidizer. Alternative, nonchromate processes include P2 and phosphoric acid deoxidizer (BAC6004-RH).

4.1.3.1. Grit blast/silane. The grit blast/silane (GBS) treatment was initially developed for use with bonded repair patches by AMRL (Aeronautical and Maritime Research Laboratory) in conjunction with the RAAF (Royal Australian Air Force) [86]. One example is their repair of C-130 outer wing fatigue cracks, in which over 1000 bonded doublers have been applied to primary structures. Airplanes with these repairs have been flying with no crack growth or patch failures for twenty years. More recently, Wright Laboratory has extended this technology and optimized a grit blast/silane surface treatment [87–89] for patching C-5 and C-141 aircraft, among others. Both laboratory and field-compatible process versions have been developed and are given in Table 3.

In contrast with the oxide treatments discussed above where mechanical interlocking is the key to obtaining good bond strength and durability, the GBS treatment utilizes the functionality of the silane to form chemical bonds with both the metal oxide surface and the adhesive/primer to couple the two materials [90–92]. Silane coupling agents have the form R–SiX₃, where R is an organic functional group and X is a hydrolyzable group. The GBS treatment uses γ -glycidoxypolytrimethoxy silane (γ -GPS), in which R is an epoxy group

Table 3

Grit blast/silane treatment ^a

	Laboratory-optimized process	Field repair process
Solvent degrease	Wipe with MEK (Methyl Ethyl Ketone)	Wipe with MEK and Duralace aerospace wipes over large area; each succeeding step is to be performed over a slightly smaller area.
Abrade	Hand abrade with Scotch-Brite® wet with MEK until the surface is shiny.	Use fine-grit, dry Scotch-Brite® pads on high-speed grinder driven by dry, oil-free N ₂ until the surface is shiny.
Solvent clean	Wipe with MEK until no evidence of soil appears on wipes. Use each wipe one time only.	Wipe with MEK until no evidence of soil appears on wipes. Use each wipe one time only.
Grit blast	Grit blast with virgin 50- μ m Al ₂ O ₃ using dry, oil-free N ₂ .	Grit blast with virgin 50- μ m Al ₂ O ₃ using dry, oil-free N ₂ . Extreme care is needed to contain and clean up the grit.
Grit removal	Clean with dry, oil-free N ₂ at 70–80 psi.	Clean with dry, oil-free N ₂ at 70–80 psi.
Silane hydrolysis	Stir 1–3 wt.% γ -GPS ^b (Dow Corning Z-6040) in DI water for 1 h using a magnetic stir bar. Water pH should be ~5.	Mix 2 1-ml vials of silane for each 150 ml of distilled or deionized water. Adjust pH of water using acetic acid, if necessary. Hydrolyze for 1 h as goal, but no more than 4 h.
Silane application	Flood horizontal panel with silane solution. Use camel's hair brush to keep the surface wet for 10 min; add more solution if necessary.	Using clean acid brushes, brush solution on aircraft. Keep the surface wet for 10 min.
Silane drying	Blow excess silane off panel with 30 psi dry, oil-free N ₂ . Place in preheated 220°F (104°C) circulating air oven for 1 h.	Blow excess silane off panel with dry, oil-free N ₂ . Use heat lamps or other heating sources to maintain 200–220°F (93–104°C) for 1 h. Use appropriate thermocouples to assure temperature and uniformity. The time between silane application and start of heating should be minimized and no more than 1 hour.
Prime	Prime with appropriate primer.	After the surface has cooled to 90°F (32°C), apply primer and cure with heat lamps.

^a From Ref. [89].^b Epoxy-functional γ -glycidoxypolytrimethoxy silane.

connected to the Si by a propylene chain and X is a methoxy. In an aqueous solution, the methoxies hydrolyze to form the trisilanol (R–Si–(OH)₃). For this application, the epoxy group reacts with epoxy adhesive while the silanols react

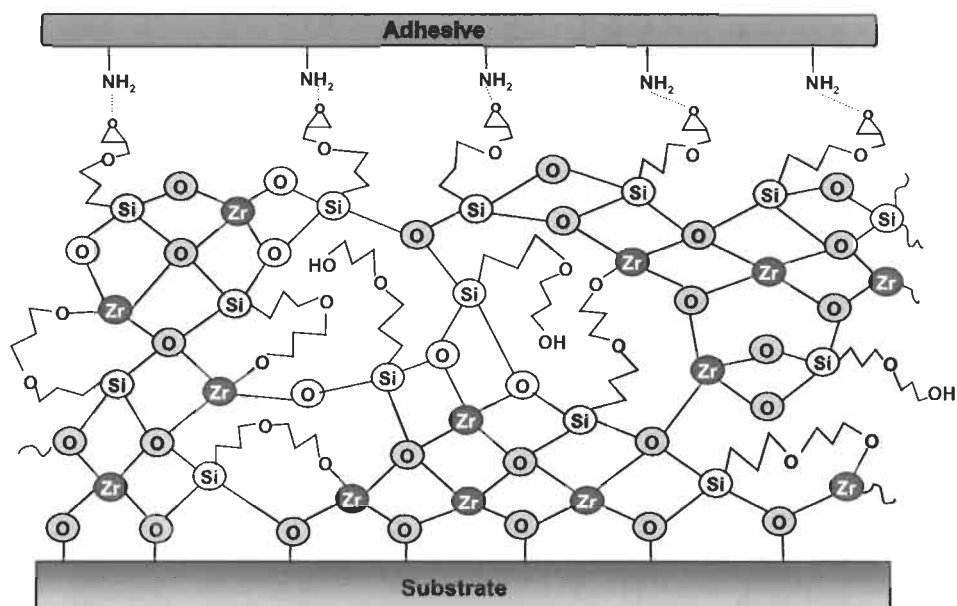


Fig. 19. Schematic representation of a typical sol-gel thin film coating. Diagram adapted from Ref. [95].

with the metal oxide surface. These bonds are stable against moisture attack and can provide excellent bond durability.

One issue with the GBS treatment (and silane-coupling treatments, in general) is that the performance can be highly dependent on processing conditions, especially hydrolysis and drying conditions. Nonetheless, process controls suitable for field application of bonded repair patches are possible.

4.1.3.2. Sol-gel coatings. Sol-gel is a contraction of 'solution-gelation'. It is based on hydrolysis and condensation reactions to form inorganic polymer networks, Fig. 19. The Boeing process involves a dilute aqueous alkoxide solution containing zirconium isopropoxide (tetra-*n*-propoxyzirconium, TPOZ) and a silane-coupling agent [21,22,93–96]. The silane constituent can be chosen or designed to be compatible with the primer and to form strong, durable chemical bonds. A glycidoxyl group, such as that of glycidoxytrimethoxysilane (GTMS), is typically used for epoxies. A small amount of acetic acid is added to control reactions and stabilize the mixture. The hydrolyzed aluminum oxide surface promotes the condensation reactions. The part to be treated can be sprayed, drenched, or immersed. No rinsing is required.

A thin film (typically 50–200 nm) is grown from solution to serve as a hybrid inorganic/organic gradient between the metal (oxide) surface and the organic primer or adhesive. XPS indicates that the surface is silane-rich and the

interface near the metal substrate is zirconia-rich. EXAFS and XANES suggest the formation of Zr–O–metal substrate chemical bonds [22].

The goal is covalent bonding throughout the gradient coating. In this way, the sol-gel treatment differs from all the traditional oxide treatments discussed above in that chemical bonding and not physical bonding is the key component of a strong and durable joint.

Although sol-gel treatments are still being developed, their performance is very promising. They have potential to be an environmentally compliant surface treatment for both original manufacture and repair. In some applications, they may eliminate the need for separate primers.

4.1.4. Relative performance

Bonds made with PAA adherends exhibit greater inherent durability than those made with FPL adherends [8,9,42] (Fig. 9) due to both the better hydration resistance of PAA surfaces [38] and the evolved microroughness and subsequent interlocking that occurs between the oxide and the adhesive [9,39]. For PAA surfaces, hydration occurs via a three-step process: (1) reversible adsorption of water, (2) slow dissolution of the surface phosphate followed by rapid hydration of the freshly exposed Al_2O_3 to boehmite (AlOOH), and (3) further hydration of the boehmite to bayerite ($\text{Al}(\text{OH})_3$) [38]. For FPL surfaces, which contain no phosphate (unless specially treated) the initial part of the second step is missing and hydration to boehmite leading to crack propagation proceeds more rapidly. Nonetheless some improvement in the performance of FPL-treated surfaces can be achieved by intentionally introducing an adsorbed layer of phosphonate-containing hydration inhibitor as described in Section 3.1. In addition, of course, further improvements in bond-durability can be obtained by using moisture-resistant adhesives or primers.

Because of their greater thickness, CAA oxides serve to protect the metal surface from corrosion better than thinner oxides but the important factor for bond durability is the stability of the outer oxide structure when water diffuses to the oxide–polymer interphase. Accordingly, it would be expected that the performance of CAA treated adherends would be similar, although no better, than that of PAA, or BSAA. The wedge test data shown in Fig. 20 and other work [29,77,97,98] support this and demonstrate that when these processes are done correctly the wedge test crack will be forced to propagate entirely within the adhesive. Similar arguments are likely with BSAA adherends, also.

Optimized grit blast/silane treatments can provide wedge test durability as good as PAA with failure entirely cohesive within the adhesive (Fig. 21) [89]. Maintaining the process parameters within acceptable tolerances is critical with the heat drying of the silane on the treated surface being the most sensitive process parameter.

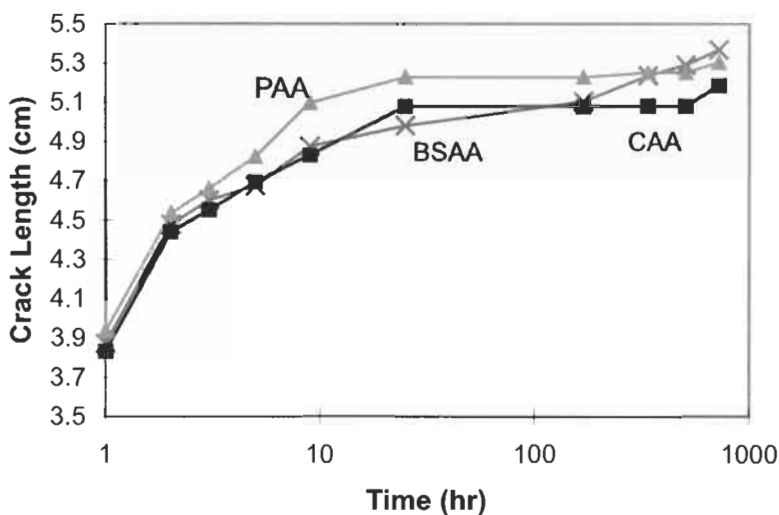


Fig. 20. Wedge test results showing PAA, CAA, and BSAA treated aluminum bonds. (Note that this test involved thicker adherends than is typical and therefore crack lengths cannot be compared to those of other tests.)

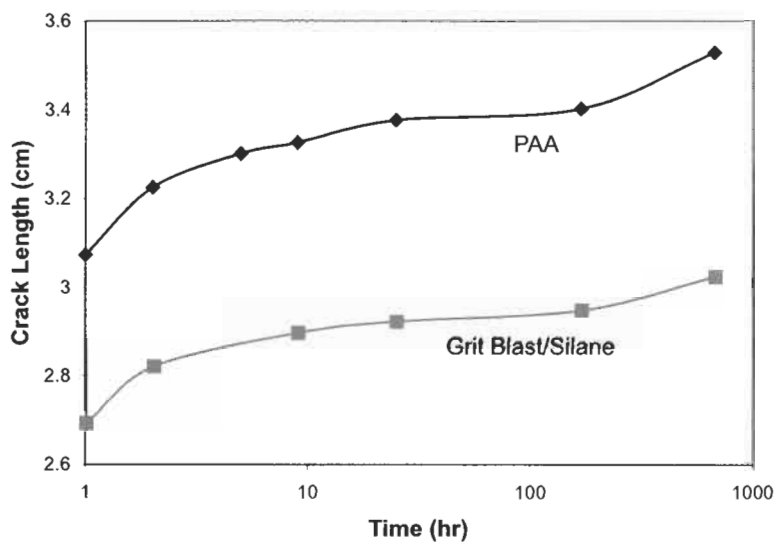


Fig. 21. Wedge test results for grit blast/silane surface treatment compared to PAA. Both surfaces were primed with BR127. Note the expanded crack length scale compared to other figures. Data are from Ref. [89].

Sol-gel films deposited on a grit-blasted aluminum surface give performance close to PAA bonds (Fig. 22) with generally cohesive failures observed in wedge tests. Given that one application of this treatment is repair, the performance is

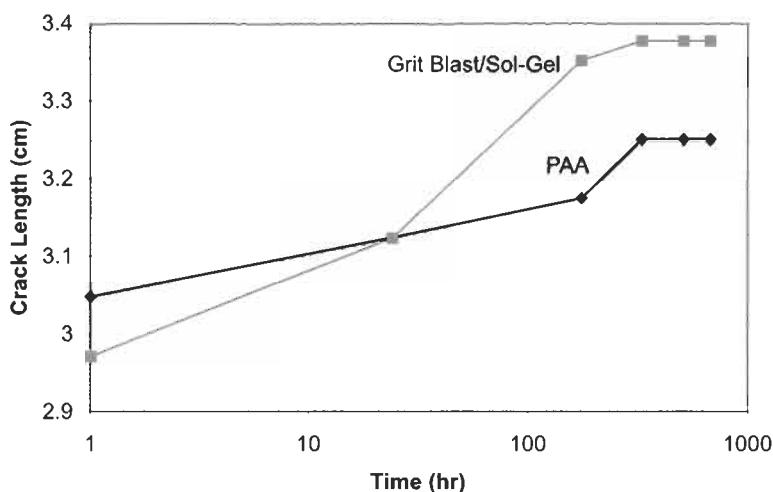


Fig. 22. Wedge test results for PAA and grit-blasted/sol-gel-treated aluminum. Data are from Ref. [22].

quite good and can exceed that of the paste–acid treatments designed for repair operations [99].

4.2. Titanium

4.2.1. Anodization, etches, and other processes

Titanium alloys are particularly attractive for aerospace structures due to their high strength-to-weight ratio. In addition, they retain their mechanical properties at high temperatures, so that they can be used as components in structures where operating temperatures up to 370°C (and possibly beyond) are expected. The desire to adhesively bond to titanium and use the resulting structure at elevated temperatures for programs such as the High Speed Civil Transport (HSCT) has played a key role in the development of high-temperature adhesives [23,24,53]. In this section, surface preparations for titanium alloys and the durability of the subsequent adhesive bonds are described.

Like Al, durable surface preparations for Ti can be achieved by forming porous oxides in anodizing and/or etching solutions. Several surface treatments have been developed for Ti over the years, including those shown in Fig. 5 and more recently others have shown promise including sodium hydroxide anodization (SHA) [100,101], NaTESi [102], plasma spraying [31,51,52], and sol-gel [22–25,53]. Typically, anodization results in the best bond durability for Ti alloys under moderate conditions, primarily due to the microrough surface morphology that results from the treatment. The most commonly used process is CAA [32,103–

Table 4
CAA process for titanium ^a

Step	Process
Degrease	TCE or MEK vapor for 10 min.
Pickling	15 vol% of 70% HNO ₃ + 3 vol% of 49% HF at room temperature for 30 s.
Rinse	Deionized water at 25°C for 1–5 min.
Anodization	50 g/l CrO ₃ + 1 g/l NH ₄ HF ₂ , 10 V, 20 min, 20–25°C.
Rinse	Deionized water for 5–20 min.
Air dry	25–60°C

^a Adapted from Ref. [31].

108] (in a different form than for aluminum adherends) but Pasa Jell 107, Turco 5578 and alkaline peroxide [80] etches are also popular.

The general steps used to provide an anodized surface on titanium adherends, Table 4, are similar to those used for aluminum adherends. Initially, the adherend must be degreased to remove organic contaminants and then an acid etch is used to remove the oxide scale. The anodization is done at constant voltage and the adherend is rinsed and dried. Grit blasting is often included in the process; however, studies suggest that it provides no gain in durability [2].

The oxide morphology formed by the CAA process on Ti-6Al-4V is shown in Fig. 23 [29,33,50–52]. At low magnifications, a two-level morphology is evident. One of these is due to the two-phase nature of the alloy, i.e., large grains of the aluminum-rich alpha phase with an intergranular, vanadium-rich beta phase. The other, revealed at higher magnifications, is a honeycomb-like structure similar to that produced by PAA on aluminum adherends [9,31,51]. The thickness of the amorphous TiO₂ oxide depends on the concentration of the solution and the anodization voltage used. Typically, when anodizing at 10 V for 20 min at room temperature, as outlined in Table 4, an oxide that is 120–130 nm thick results. Cross-sectional transmission electron micrographs reveal that a 100 nm thick honeycomb structure resides on top of a thin (20–30 nm), dense, barrier layer.

Processing steps for selected etches (Pasa Jell 107, alkaline peroxide (AP), and Turco 5578) are given in Table 5. The AP process gives a Class III microrough oxide morphology (Fig. 24) having an average pore size somewhat larger than that of CAA. The oxide thickness varies from 60 to 200 nm, depending on bath temperature and immersion time [51]. One drawback of this process is the instability of the H₂O₂ solution; the peroxide must be replenished every 30 min. The other two etches provide oxides approximately 20 nm thick having larger-scale features that provide some physical bonding with an adhesive (Figs. 25 and 26).

Several different sol-gel chemistries have been described: the TPOZ/GTMS chemistry used for aluminum (Section 4.1.3.2), an aromatic silane (*m*- and *p*-

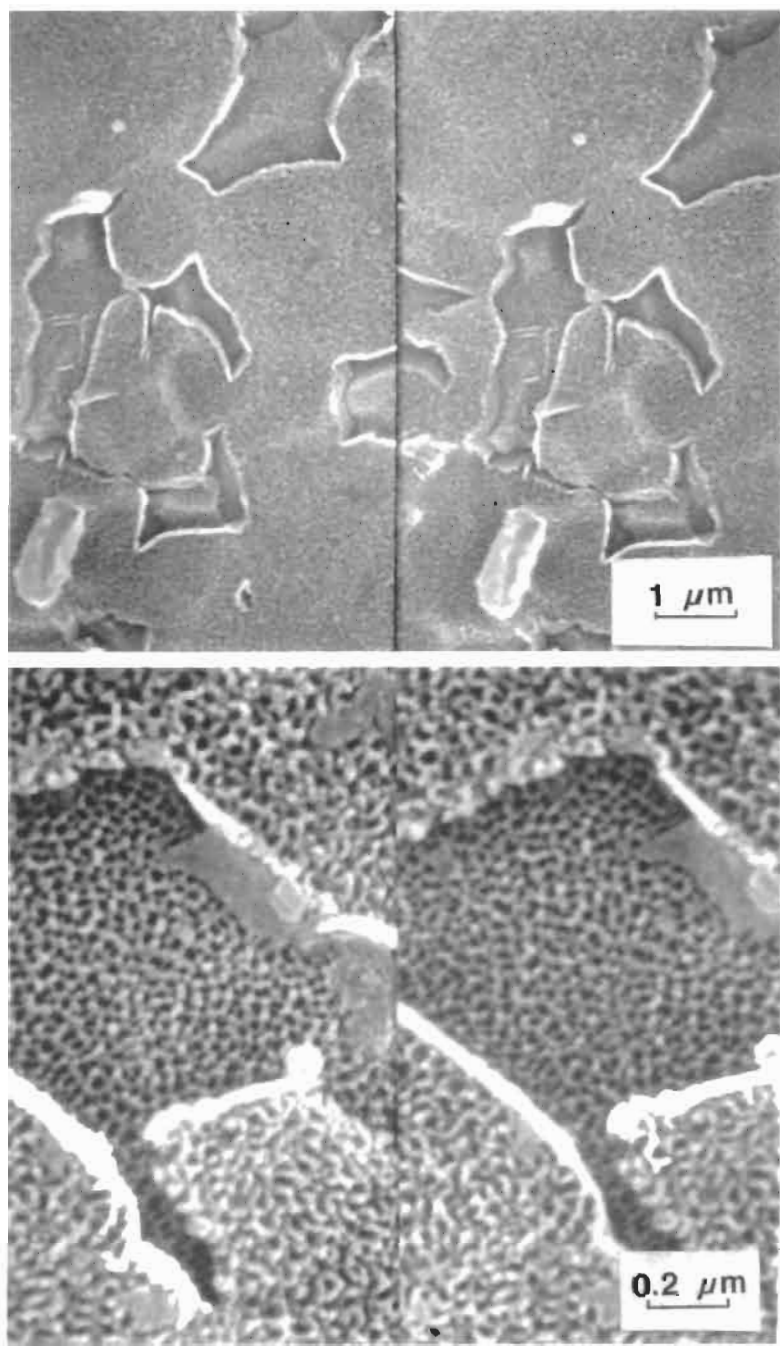


Fig. 23. Stereo micrographs of CAA-treated Ti-6Al-4V.

Table 5

Etching processes for titanium ^a

Step	Pasa Jell 107	Alkaline peroxide	Turco 5578
Solvent degrease	MEK or 1,1,1-TCA	MEK	
Alkaline degrease	300–364 g/l Turco alkaline rust remover, 20–30 min, 93–100°C	Kelite 19, 3–5 min, 60–71°C	45–140 g/l Turco 5578, 15 min, 74–79°C
Rinse	Spray tap water, 2–4 min	Immerse deionized water, 2–5 min, spray deionized water 1–2 min, RT	Flowing deionized water, 5 min, 71–82°C
Dry			Air, 54°C
Etch	10 vol% Pasa Jell 107-CV, 21 vol% HNO ₃ , 30 g/l CrO ₃ flake, 15–20 min, ≤38°C	0.5 M NaOH + 0.4 M H ₂ O ₂ , 23–27 min, 55–65°C	364–485 g/l Turco 5578, 8–10 min, 82–88°C
Rinse	Immerse in deionized water, RT, spray deionized water, 2–4 min	Immerse deionized water, 2–5 min, spray deionized water 1–2 min, RT	Spray deionized water, 5–10 min, 74–79°C
Dry	Air, 30 min, 38–65°C	Air, 60 min, 65°C	Air, 54°C

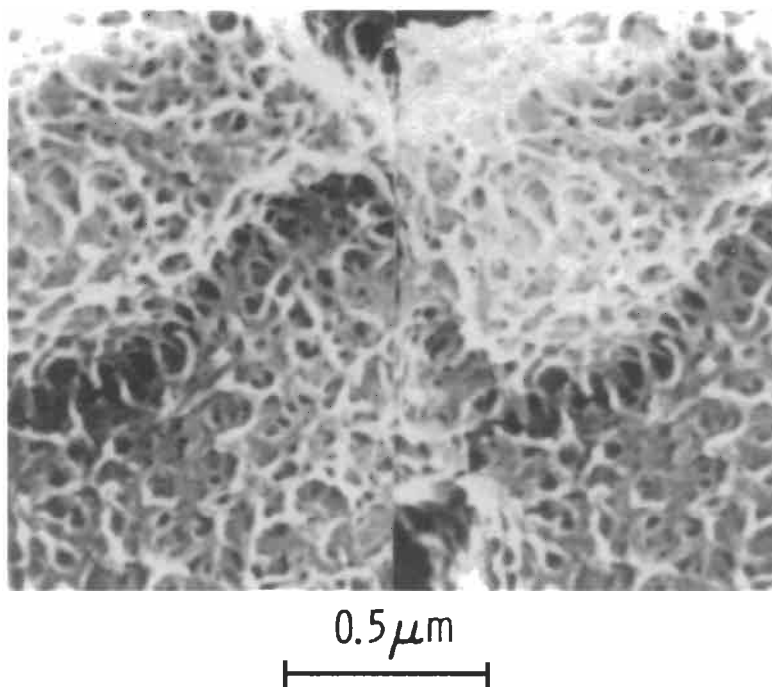
^a Adapted from Ref. [80].

Fig. 24. Stereo micrograph of alkaline peroxide-treated Ti-5Al-4V.

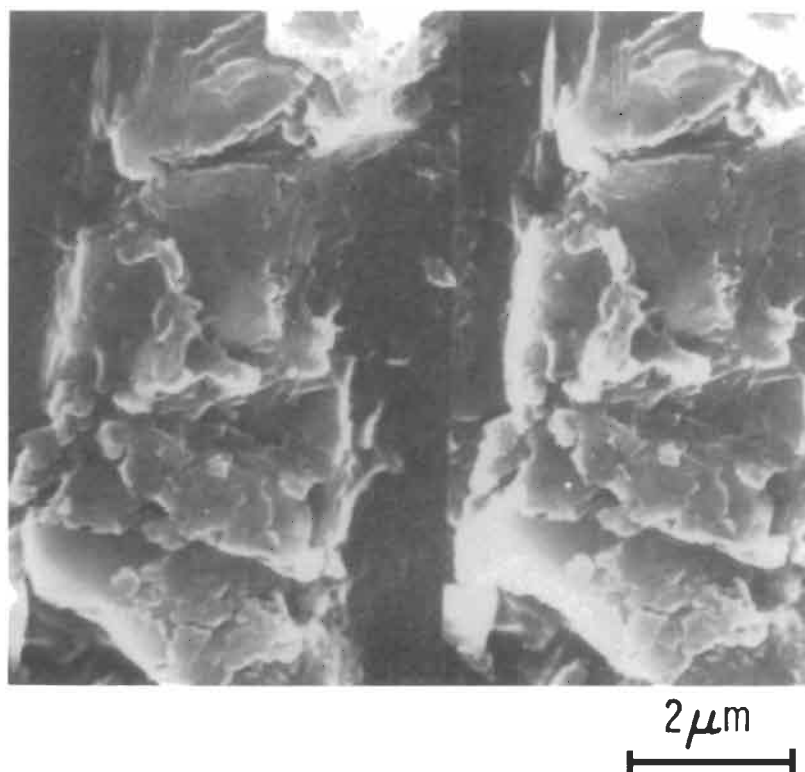


Fig. 25. Stereo micrographs of Pasa Jell 107-treated Ti-6Al-4V.

aminophenyltriethoxysilane), an aliphatic silane (3-aminopropyltriethoxysilane), and polyimide-silica hybrids (pendent phenylethynyl imide oligomeric disilanes/tetraethoxysilane or PPEIDA/TEOS and phenylethynyl terminated imide oligomer/aromatic phenylethynyl imide silane/TEOS or PETI-5/APEIS/TEOS) [22–25,53]. The later chemistries include high-temperature-stable components similar to those used in the high-temperature FM-x5 adhesive. The surface morphology has not been investigated or reported upon in as much detail as CAA and the other oxide surfaces. However, Cobb et al. describe it as being similar to that of Turco 5578 provided that the Turco process is used as a precursor to the sol-gel process [109]. Because it relies on chemical bonding between the adhesive and the hybrid organic/inorganic structure, it does not require the fine microscopic features to form physical bonding that the anodized surface does.

4.2.2. Relative performance

In early studies, the durability of Ti-6Al-4V bondments was determined as a function of surface preparation for several adherend preparations and several adhesives

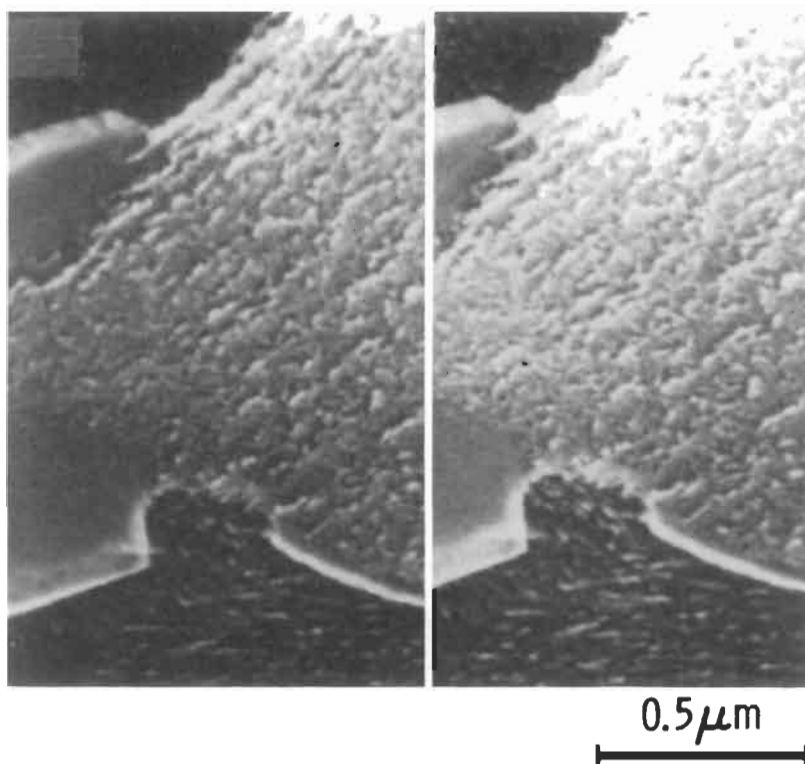


Fig. 26. Stereo micrographs of Turco 5578-treated Ti-6Al-4V.

[9,32,110]. As reported earlier (Fig. 5), surface preparations that produce oxides with no roughness (macro- or micro-) yield the poorest bond durability (Class I adherend), those that produce a large degree of macroroughness, with little or no microroughness, fall into an intermediate class of moderate-to-good durability (Class II adherend), and those preparations that produce oxides with significant microroughness lead to the best durability (Class III). This improvement in performance with microroughness is due to the interlocking nature of the interphase that results when strong capillary forces induced by the small cell size cause the polymer to displace all air and completely fill the oxide pores. This is a different situation from that of sol-gel surfaces that provide chemical bonding between the metal and the adhesive and, hence, are less dependent on physical (interlocking) bonding.

In general, the stability of titanium oxide surfaces in moist environments is less of a concern than it is for aluminum oxide surfaces. For example, an FPL or PAA oxide on aluminum would be completely converted to hydroxide in less than 5 min after exposure to boiling water, whereas even after 24 h only slight changes such as crystallite formation and reduction in density of the cell structure occur for

titanium oxides [104,105]. (After 72 h exposure to boiling water the honeycomb structure on titanium is completely disrupted and the surface is covered with crystallites.) Nonetheless, titanium adherends are chosen specifically for their use at elevated temperatures and so precautions must be taken to assure that these durability factors are taken into consideration.

Unlike aqueous environments, dry, high-temperature environments have little or no obvious effect on CAA morphology but they may effect bond strength. For example, bare CAA adherends exposed to air (330°C) for 1200 h and to vacuum (400°C) for 165 h retain their morphology, however, bonds formed after such exposures failed under minimal force [51,52,105]. In these cases, failures occurred at the oxide-metal interface, caused by the dissolution of some of the oxide into the base metal at the exposure temperature [110]. Because oxygen is highly soluble in the metal, dissolution of the oxide occurs and defects such as voids or microcracks form at the oxide-metal interface. Under these conditions, very little tensile force is needed to pull the oxide away from the metal. This phenomenon, discussed previously in Section 3.2 and shown schematically in Fig. 13 [52], has been observed for adherends exposed in vacuum at 400°C for as little as 1 h [36,110]. Moreover, it has also been observed in bonded structures exposed for much longer times at temperatures as low as 200–250°C [52,111,112]. All of this suggests that for those applications where very high temperatures will be anticipated, it might be worthwhile to consider other types of surface preparation such as the sol-gel process which appears to provide the best high-temperature performance for titanium [22,24,53].

The titanium sol-gel treatment performs as well as CAA under moderate conditions [22] and recent indications are that it exhibits high-temperature durability as well. This has mostly been evaluated with lap shear joints after exposure to 177°C for long periods of time [24,53,109]. Fig. 27 gives the fracture toughness determined from crack-lap shear specimens bonded with FM-x5 following 5000 h at 177°C <10% RH or 71°C at >95% RH [109]. The sol-gel treatment outperforms Pasa-Jell 107 and Turco 5578 initially and following both exposures. Very little decrease in fracture toughness is seen for the sol-gel treatment under the hot/wet conditions — a result consistent with the very little crack growth seen in wedge tests [22]. At the higher temperature, the fracture toughness decreases by approximately 50%, but remains considerably higher (both in absolute and relative terms) than the other two treatments. The locus of failure remained largely within the adhesive although regions of interfacial failure were also seen.

Finally, it should be noted that an important problem in developing high-temperature-compatible surface treatments (and adhesives) is the testing and screening procedure. Bonded joints cannot be exposed to temperatures much higher than the projected service temperature of the component without degrading the adhesive. The risk of inducing new degradation mechanisms is also present for accelerated testing at higher temperatures so testing is usually done at near service

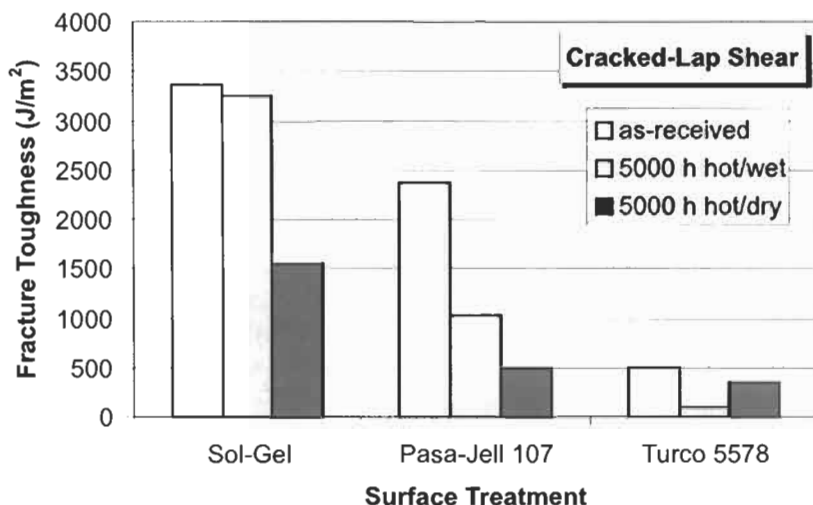


Fig. 27. Fracture toughness of cracked-lap shear specimens made with FM-x5 adhesive. Adapted from Ref. [109].

temperatures and for long periods of time. For example, one test that provided results compatible with proposed service conditions involved long-term exposure to 95% RH for 10,000 h at 177°C [53]. No matter what the value is of such a test, it definitely imposes severe limitations on the rate of feedback of results.

4.3. Steel

4.3.1. Conventional treatments

4.3.1.1. Direct bonding. In many high-volume production applications (i.e., the automotive and appliance industries), elaborate surface preparation of steel adherends is undesirable or impossible. Thus, there has been widespread interest in bonding directly to steel coil surfaces that contain various protective oils [55,56,113–116]. Debski et al. proposed that epoxy adhesives, particularly those curing at high temperatures, could form suitable bonds to oily steel surfaces by two mechanisms: (1) thermodynamic displacement of the oil from the steel surface, and (2) absorption of the oil into the bulk adhesives [55,56]. The relative importance of these two mechanisms depends on the polarity of the oil and the surface area/volume ratio of the adhesive (which can be affected by adherend surface roughness).

In other studies [115], the bond strengths of joints made from steel substrates coated with a variety of oils and waxes ($\sim 6 \text{ mg/cm}^2$) and joined with acrylic adhesive were investigated. Lap-shear strengths up to 15 MPa were obtained with room temperature curing. Very little degradation was seen after 1000 h of

exposure at 40°C and 95% relative humidity. However, the shear strength dropped by roughly half when the joints were subjected to a 30-min bake at 200°C. Although the reported bond strengths do not approach those reported for Al, Ti, or Cu adherends, they are adequate for the intended application.

4.3.1.2. Surface cleaning/etches. As with aluminum and titanium, the most critical test for bonded steel joints is durability in hostile (i.e., humid) environments. The fact that the problem is a serious one for steel was illustrated in a study [117] that compared solvent cleaned (smooth) 1010 cold-rolled steel surfaces with FPL aluminum (microrough) substrates. Although the dry lap-shear strengths were not markedly different, stressed lap-shear joints of steel adherends that were exposed to a humid environment failed in less than 30 days, whereas the aluminum joints lasted for more than 3000 days.

A number of novel techniques have been attempted to provide (atomically) clean steel surfaces for optimal chemical bonding, but generally there has been no improvement over grit blasting. Ultraviolet light/ozone exposures have been used very successfully to provide extremely clean surfaces for semiconductor processing. However, when this technique was applied to oily steel, the cleaned surfaces showed no improvement in bond strength compared to control specimens [118]. Glow-discharge etching, which is another method of providing very clean semiconductor surfaces, was used to prepare steels for an anti-corrosion, polymer-film-coating process [119] but the results were no better than wiping with a solvent cloth. Neither was the result of another scheme [120] that incorporated cleaning components into the adhesive itself.

Although chemical treatments for cleaning steel surfaces have been widely used for many years, there are no general chemical treatments designed to prepare steels for adhesive bonding. Much research has been done to find such a treatment, but with limited success. In one case, a superheated steam treatment was used following etching in dilute HCl to induce a 'microfibrous topology' similar to aluminum and titanium bonding surfaces [121]. However, bonded surfaces treated in this way failed at the oxide-metal interface and at lower stress levels than expected for normally prepared, smoother steels.

One of the main problems with chemical-etch treatments of low-carbon steels is the formation of a loosely adhering layer of iron oxide 'smut' on the adherend surface. The oxide is difficult to remove before bonding, but easily pulls away with the adhesive when the joint is stressed. Fig. 28 shows an electron micrograph of an A606 steel surface after etching in phosphoric acid [54]. Despite vigorous rinsing, the steel surface is mostly obscured by Fe_3O_4 smut. Attempts to suppress the formation of the smut by using acid etches in alcohol solutions [122,123] yielded results that were no better than grit blasting in stressed durability testing. Even so, in some applications, a treatment that is 'as-good-as-grit-blasting' is still acceptable and, for example, Soviet researchers indicate that a chemical-

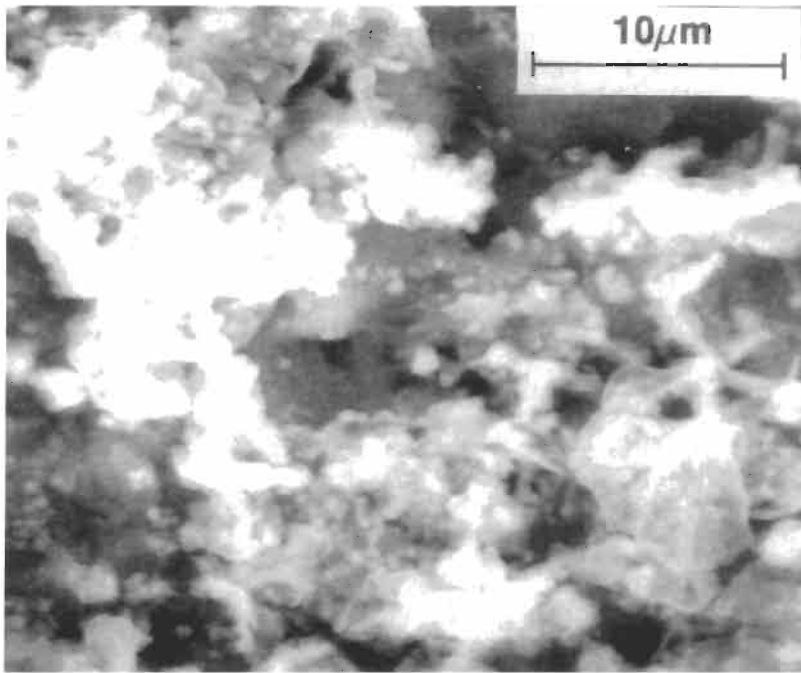


Fig. 28. Phosphoric acid etched A606 steel surfaces showing normal heavy smut formation [54].

etch/corrosion-inhibitor treatment can reduce the cost of surface preparation to 15% of that for grit blasting [124].

Another major problem with chemical etches is that the resulting morphology is a function of the metallurgy of the substrate. Figs. 29 and 30 show electron micrographs of clean A606 and A514 steel surfaces after a phosphoric-acid-etch treatment [54]. Even though A606 and A514 substrates are chemically similar high-strength, low-alloy steels, their etched surfaces offer different bonding/interlocking potentials because different heat treatments are used to purposely change their microstructure. In both, the acid primarily attacks grain boundaries, etching out surface grains. However, the A606 surface has smooth-sided, dimpled morphological features, similar to grit-blasted surfaces, whereas the A514 surface has small crevices that can allow adhesive penetration. Etched A514 performs much better than either grit-blasted A514 or etched A606 surfaces in wedge/crack-propagation tests.

The adherend metallurgy also indirectly determines the degree of smut buildup because the rate of smut formation is proportional to the etch rate [54]. For instance, the etch rate of A606 is four times greater than that of A514, due to differences in grain size, etc. As a result, a different etch treatment is required for each. In general, the roles of alloy and heat-treatment differences have not

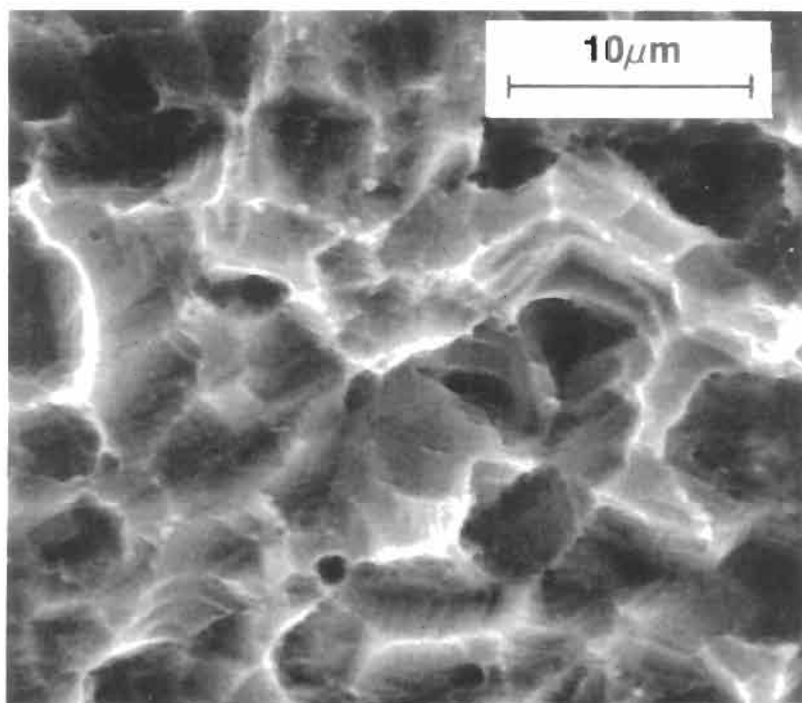


Fig. 29. Phosphoric acid etched A606 steel surface showing smut-free, smooth-walled crevice morphology [54].

been widely investigated in bonding research on steel; details of the substrate metallurgy are usually not reported.

The high etch rates for standard, cold-rolled steels cause smut buildup that is difficult to eliminate. Simply reducing the activity of the etch solution is frequently not possible because many steel surfaces do not react at all to weak etching solutions. Using surface analysis techniques, it has been shown that standard processing can cause graphite and other carbonaceous species to coat the steel [125]. A similar effect has also been observed with 'drawing quality' steel [126]. These layers are relatively impervious to mineral acids, and must be undercut to be removed. Other research has shown that carefully controlled phosphoric acid solutions can be used to clean steel [127]. However, because they do not consistently provide an improved bonding morphology, they offer no performance enhancement compared with normal, more easily monitored techniques, such as grit blasting.

Although there is considerable evidence that chemical surface treatments improve the substrate bondability of stainless steels, there is no general agreement on which is the best. One etchant commonly used with stainless steels is an HNO_3 -HF mixture [128–131]; others are chromic acid and ferric chloride/hydrochloric

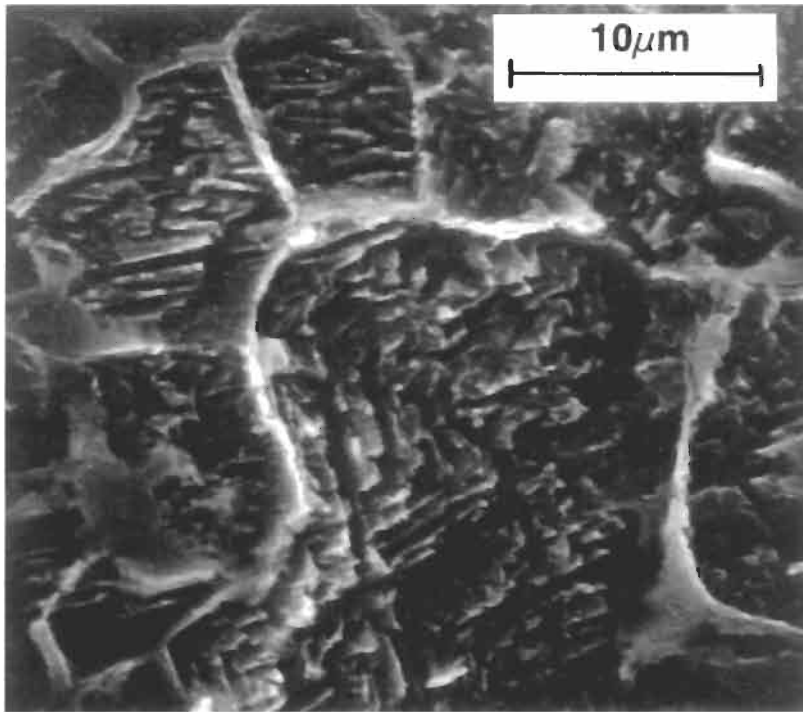


Fig. 30. Phosphoric acid etched A514 steel surface showing extensive etching along martensite boundaries. This alloy contains the same constituents as A606, but has been given a different heat treatment [54].

acid [22]. Various solutions based on sulfuric acid have also been beneficial [132–134], and several researchers recently investigated a wide variety of solutions based on acids with dichromates added, with and without anodization [135–138]. The treatment judged to be the best by one researcher did not receive the same ranking from another. They all used a highly concentrated, very active solution that attacked grain boundaries and the chromium-poor regions around chromium carbide particles. One common finding by researchers who used peel tests [131,134–136] was that surface roughness correlated with bond performance and it has been noted [117], for example, that peel performance could be correlated to the microscopic surface roughness seen in a scanning electron microscope. However, the type of substrate alloy and heat treatment were different in many cases so that the treatment that worked best for any one researcher may have done so only because of the sample metallurgy and not the chemistry of the etches. For example, Hirko [138] reported that three different treatments — a nitric acid anodization, a sulfuric acid/dichromate etch, and a sulfuric acid/dichromate anodization — provided essentially equivalent wedge/crack-propagation test performance.

4.3.1.3. Grit blasting. There is no question that grit blasting is the surface preparation method of last resort. One of the problems is that the grit-blast material itself is often found to contain contaminants that are transferred to the surface being cleaned thereby exacerbating the problem. But even when chemically analyzed virgin grit material is used, tests have shown that the method yields bonds to steel adherends exhibiting poor durability. For example, it was observed that wedge-test specimens prepared in this manner exhibited rapid crack growth during humidity-chamber exposure [139]. In the same study, electron micrographs taken of failure surfaces in the crack-growth region indicated that the failures were purely interfacial and what is more the metal surface showed no signs of corrosion, nor was there visual evidence of moisture attack on the polymer. Gledhill and Kinloch who investigated joints immersed in water obtained similar results [140]. They concluded, "Thermodynamics indicate that if only secondary forces are acting across the interface, water will virtually always desorb an organic adhesive from a metal oxide surface." This suggests that simply cleaning the adherend surface is not an adequate treatment for structural bonding applications. However, for less demanding applications, such as rubber bonding, it can give adequate performance.

Further work has been done in an effort to optimize mechanical cleaning. Gilbert and Verchery tried different types of grinding and grit blasting and found that grit blasting outperformed fine or coarse grinding [141]. They concluded that the best results were obtained when the grit size was matched to the size of the filler material in the adhesive. Watts and Castle also investigated a variety of mechanical cleaning treatments and judged grit blasting to be the best [142]. They concluded that some improvements they observed in durability were strictly related to the increased surface area of the grit-blasted surfaces. Such improvements, however, can be negated significantly if the grit blast material happens to be contaminated.

4.3.1.4. Conversion coatings. A better approach to forming durable bonded joints with steels is to use a conversion-coating process to deposit a rough, corrosion-resistant layer on the adherend. To achieve such a coating, zinc and iron phosphate solutions are used to precipitate crystallites onto the steels. This frequently provides good bonding morphology [54,143] (as shown in Fig. 31). Research at the West German Academy of Science showed that even though iron and zinc phosphate surfaces had 15% lower bonding strengths when tested under dry conditions, they typically had 100% better values than a ground steel surface after the bonds had been soaked in water [144]. Work done by Trawinski and Miles [145] using carefully controlled zinc phosphate treatments, supports this finding. They demonstrated lap-shear strengths equivalent to those on grit-blasted steel substrates but greatly improved wedge/crack-propagation test performances in humid conditions [139].

Recent efforts to improve the performance of conversion coatings have led

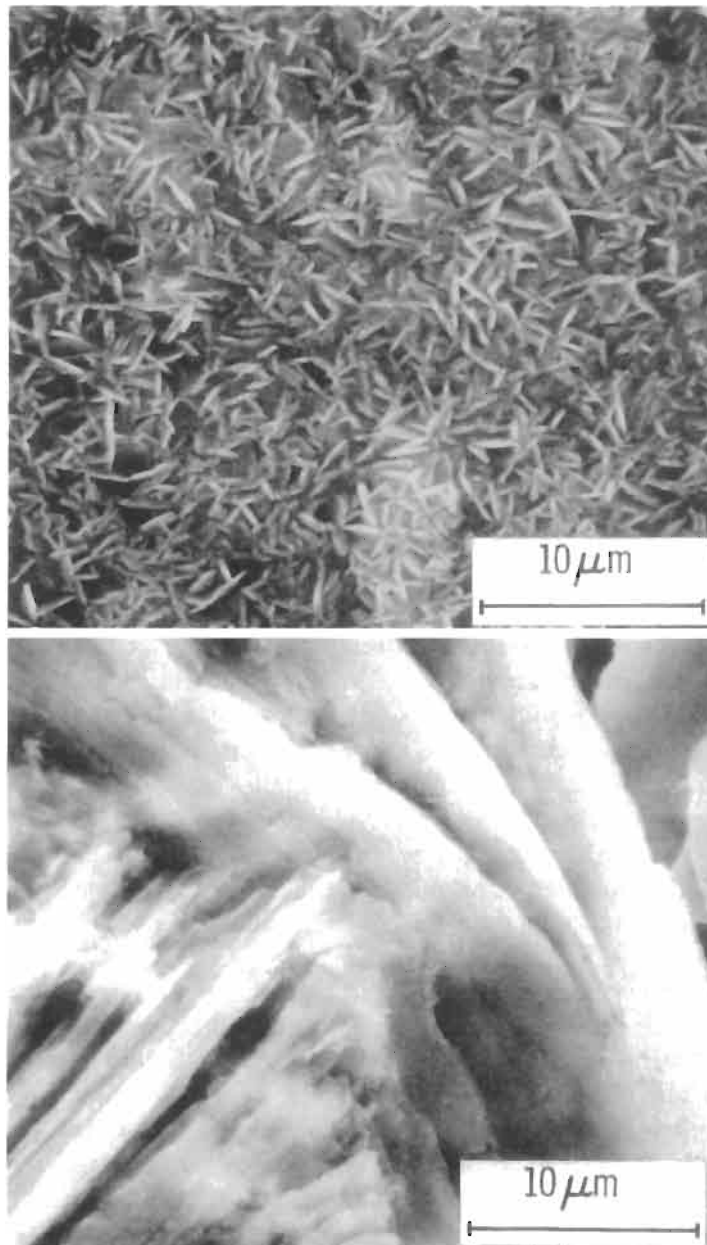


Fig. 31. Electron micrographs that compare crystal size of (top) a grain-refined microcrystalline coating and (bottom) a conventional zinc phosphate conversion coating [54].

to the development of grain refiners and initiators that allow small-grained zinc phosphate coatings to be readily deposited [146–150]. If the grain size is not controlled, the coating becomes so thick that one phosphate crystal precipitates

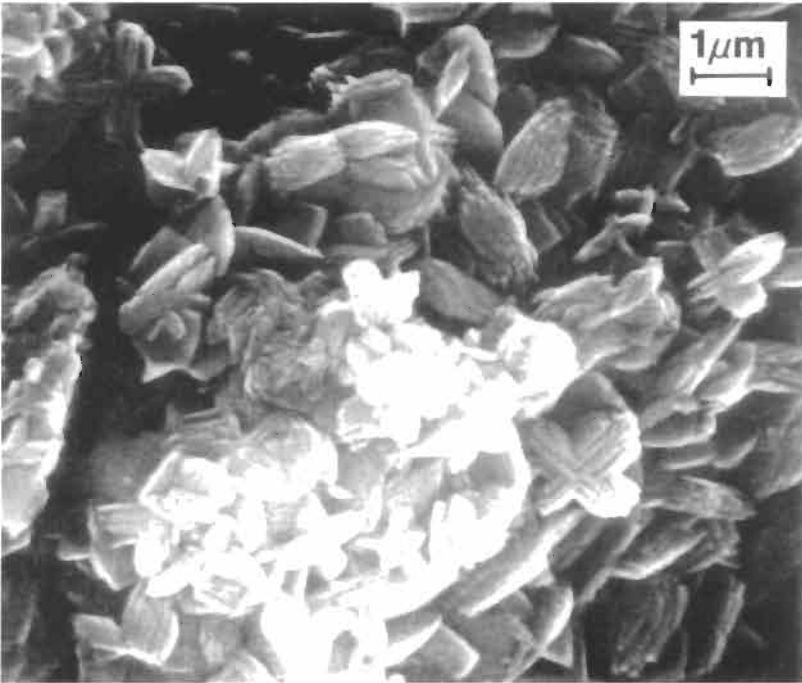
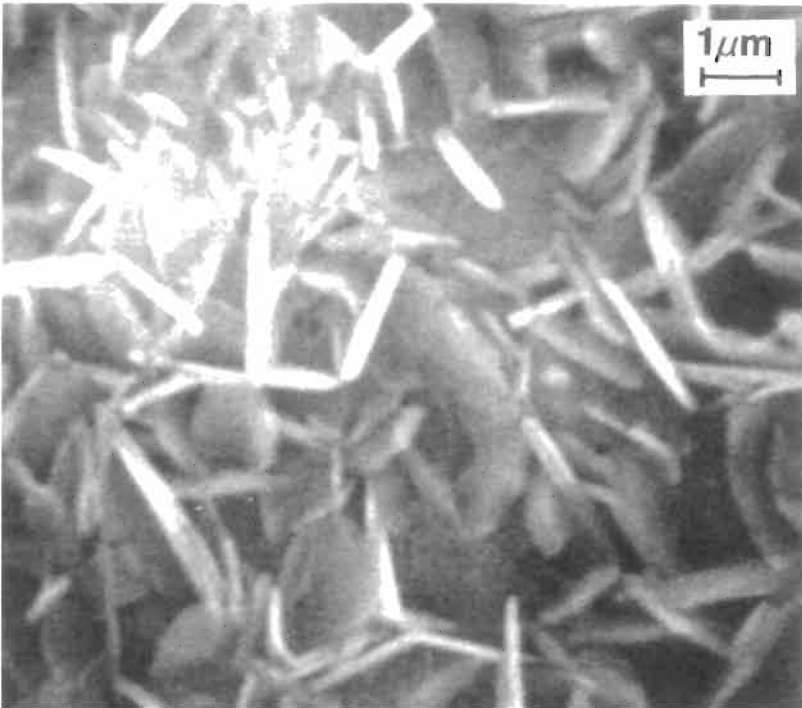
on another, and a weak interface is introduced (Fig. 31). This may explain why, in earlier studies [151], heat-curing epoxies were not compatible with conversion coatings: thermal stress between the thick conversion coating and the steel substrate may have caused fracture in the coating. Gan et al. investigated the relationship between the surface condition before phosphatization and the strength of the coating and found “that the phosphate layer had failed” for all coatings tested [152]. In this case, electron micrographs of the coatings showed large phosphate crystals but in a subsequent study, they demonstrated improved performance using a finer-grained coating, although failures still occurred within the coating layers albeit at somewhat higher strength levels [153].

As with chemical etches, developing optimum conversion coatings requires assessment of the microstructure of the steel. Correlations have been found between the microstructure of the substrate material and the nature of the phosphate films formed. Aloru et al. demonstrated that the type of phosphate crystal formed varies with the orientation of the underlying steel crystal lattice [154]. Fig. 32 illustrates the different phosphate crystal morphologies that formed on two heat-treated surfaces. The fine flake structure formed on the tempered martensite surface promotes adhesion more effectively than the knobby protrusions formed on the cold-rolled steel.

4.3.2. *Emerging treatments*

4.3.2.1. *Plasma spray.* Each one of the above treatments for steel adherends has some drawbacks. The chemicals used for solvent cleaning are hazardous and ozone depleting, the effectiveness of etches often depends in unpredictable ways on the underlying microstructure, grit-blasting is ineffective because it provides no corrosion protection, and conversion coatings tend to exhibit strengths (in the coating) that are somewhat less than desirable. To overcome these difficulties some recent studies have focused on developing plasma spray coatings as a surface treatment for steels [155–157]. This type of surface treatment has been used extensively to provide improved wear resistance, thermal barriers (for turbine blades), corrosion resistance, etc., in many industrial applications. For adhesive bonding, the prospect of being able to apply a coating having superior corrosion resistance than the underlying steel adherend, while at the same time exhibiting controlled roughness and porosity to improve mechanical interlocking, provided the incentive for the studies.

Plasma spraying is a process in which an electric arc is struck between a cathode and an anode (nozzle), both of which are water-cooled. A working gas, typically a mixture of argon and hydrogen (or nitrogen and hydrogen), is forced through the arc, creating a plasma. A powder of the material to be deposited (e.g., nickel–chrome alloys) is injected into the plasma either within or downstream from the nozzle, and the plasma softens or melts the powder in flight. The



molten particles, traveling at supersonic velocities, strike the substrate and splat cool. The result is a microrough, metallic coating exhibiting some porosity that can be controlled by the spraying conditions. In addition, it is also found that sufficient control can be exercised to avoid undesirable increases in the substrate temperature.

In one study, plasma spray coatings of nickel–chrome–zinc alloys were developed for treating the internal surfaces of Solid Rocket Motor (SRM) cases [155–157]. To protect the steel case from burning propellant, a rubber insulation is adhesively bonded to the steel. The steel is typically grit blasted prior to bonding, but corrosion of the surface either during hold times during manufacture or following recovery in the ocean (for reusable motors) can reduce adhesion. The intent of the study was to develop a corrosion resistant coating that would exhibit adequate surface roughness for good adhesive bonding.

Initially, nickel–chrome plasma sprayed coatings were studied and it was shown that they exhibited sufficient roughness (Fig. 33) to provide excellent adhesion to either acrylonitrile butadiene rubber (NBR) or ethylene propylene diene monomer (EPDM) as well as epoxy adhesives. Even if greases were present, the coatings were shown to be much less susceptible to this type of contamination than grit blasted surfaces. However, it was observed that the coatings were not completely protective of the casing from salt water exposure and so various approaches were taken to improve the corrosion resistance. Additions of small quantities of zinc to the plasma spray powders resulted in dramatic improvements in corrosion resistance even under conditions where a scratch was intentionally made in the coating. Studies showed that the small additions of zinc served to galvanically protect the steel surface but since the concentrations of zinc were so low, chemical changes occurring in the salt water, such as the conversion of Zn to Zn(OH)_2 , did little to degrade the bondline strength.

In summary, preliminary studies indicate that plasma spray coatings show great potential for improving the bondability of steel. Potential drawbacks include the requirement for relatively expensive plasma spray equipment and the necessity to keep the substrate temperature below that which would lead to undesirable metallurgical changes.

4.3.2.2. Sol-gel. A limited evaluation of sol-gel coatings on stainless steel has been reported with the goal of reducing hazardous wastes and other environmentally undesirable materials [22]. In this study, the GTMS/TPOZ sol-gel discussed

Fig. 32. Micrographs of microcrystalline zinc phosphate coatings on (top) A514 and (bottom) A606 steel substrates showing the very different morphologies produced by identical processes [54].

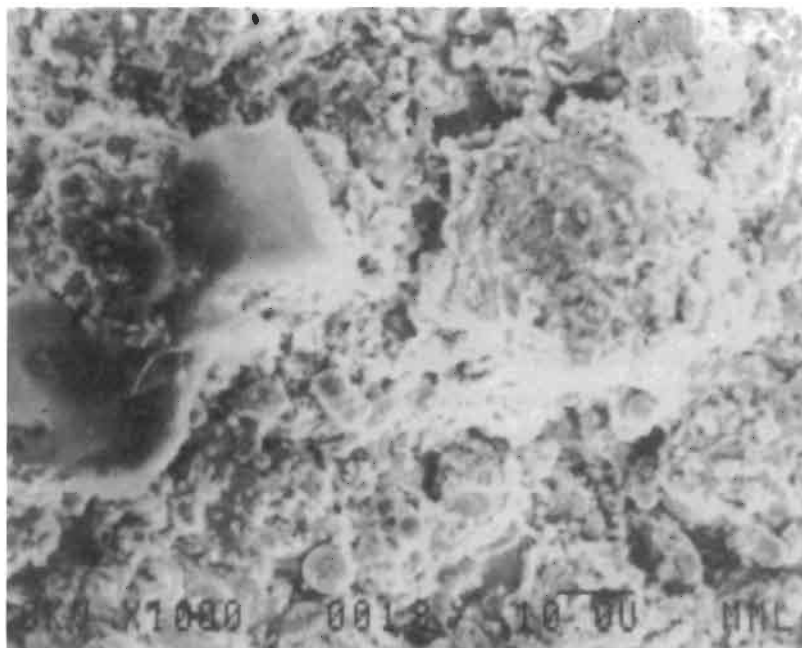


Fig. 33. Ni-Cr-Zn plasma spray coating on D6AC steel showing complex morphology ideal for adhesive bonding [155].

in connection with aluminum bonding gave wedge test performance as good, if not better than, the conventional ferric chloride/hydrochloric acid etch on 301 stainless steel. The ability of the same sol-gel coating to provide bondable surfaces with different metal adherends contrasts with the different chemical etches or anodization processes that must be tailored to different materials. Only deposited coatings, such as sol-gel or plasma spray, have the potential to be a universal treatment for multiple metals.

5. Surface inspection methods

During the past twenty or so years numerous sophisticated surface analytical techniques have been successfully employed to investigate and understand the nature of bonding surfaces and their interaction with the environment. Some of these, e.g., HR-SEM and XPS have been mentioned above, with details of these and many more techniques covered in Chapter 6. In this section emphasis will be placed on those somewhat less sophisticated techniques that are employed in or in close conjunction with bond shops. What they lack in sophistication they often make up for in the ability to quickly and cheaply evaluate whether problems such as surface contamination or out-of-spec surface treatment procedures are

developing in the bonding facility. It is convenient to discuss these inspection methods in terms of those used to inspect (1) the actual part, and (2) witness panels that are processed along with the actual part.

5.1. Part inspection

The extremely fine, porous oxide morphologies illustrated in this chapter are a requisite for making high quality aerospace type bonds, but on the minus side they can be perfect traps for oils found on fingers (which should never be used to handle bondments) and on virtually all bond shop materials such as, nylon gloves, Kraft paper, silicone rubber, and Teflon [158]. Contaminant layers that fill the pores and cover the surface, as shown in Fig. 34, will prevent wetting by the adhesive and, consequently, prevent mechanical interlocking from forming thereby leading to low-strength bonds. Note that surface contact can also damage the oxide asperities, but the overall hardness of the oxides ensures that such damage may be limited to relatively small areas.

To inspect for contaminants, a water break test is frequently employed. Water, being a polar molecule, will wet a high-energy surface (contact angle near 180°), such as a clean metal oxide, but will 'bead-up' on a low-energy surface characteristic of most organic materials. If the water flows uniformly over the entire surface, the surface can be assumed to be clean, but if it beads-up or does not wet an area, that area probably has an organic contaminant that will require the part be re-processed.

In some cases, it is not possible to use water break testing because water would be deleterious to the surface as for freshly cleaned steel. The steel solid rocket motor (SRM) cases of the Space Shuttle are examples where the actual bonding surface must be 100% inspected for cleanliness to verify that the preservative grease intentionally applied to prevent corrosion has been removed prior to priming and application of a rubber insulation layer. In this case, optically stimulated electron emission (OSEE) [159,160] is used because large areas can be inspected in reasonable times without the need for contacting the surface [161]. In OSEE, the surface is illuminated with an ultraviolet light, the low-energy photoelectrons emitted from the steel surface are collected and the photocurrent measured. If the surface is contaminated, the organic material will absorb the photoelectrons and a lower current will be measured. This is illustrated in Fig. 35 for two different contaminants. The silane contamination completely attenuates the substrate signal, but grease does not because it is slightly photoemitting itself and the OSEE signal begins to increase at high levels of coverage. Although this can present conflicting evidence with both high and low levels of contamination giving the same OSEE signal, high levels can be detected visually so that clean surfaces can be assured. OSEE works best on steel but not as well on aluminum because the oxide also attenuates the photoelectron signal from the substrate.

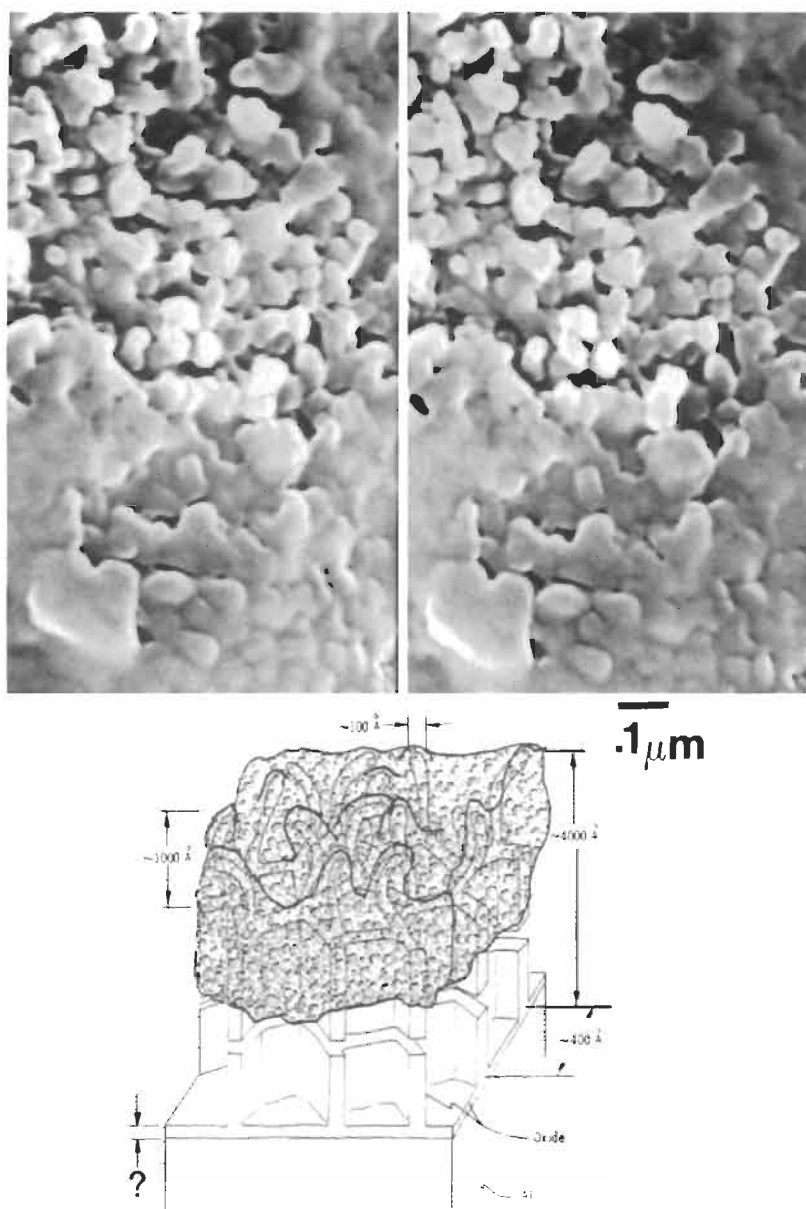


Fig. 34. PAA aluminum surface covered with a thin layer of grease that masks the oxide morphology.

Other techniques to inspect bonding surfaces for contamination have also been proposed, including ultraviolet fluorescence [162]. Pulsed ultraviolet light incident on the surface excites fluorescence of organic contamination, which can

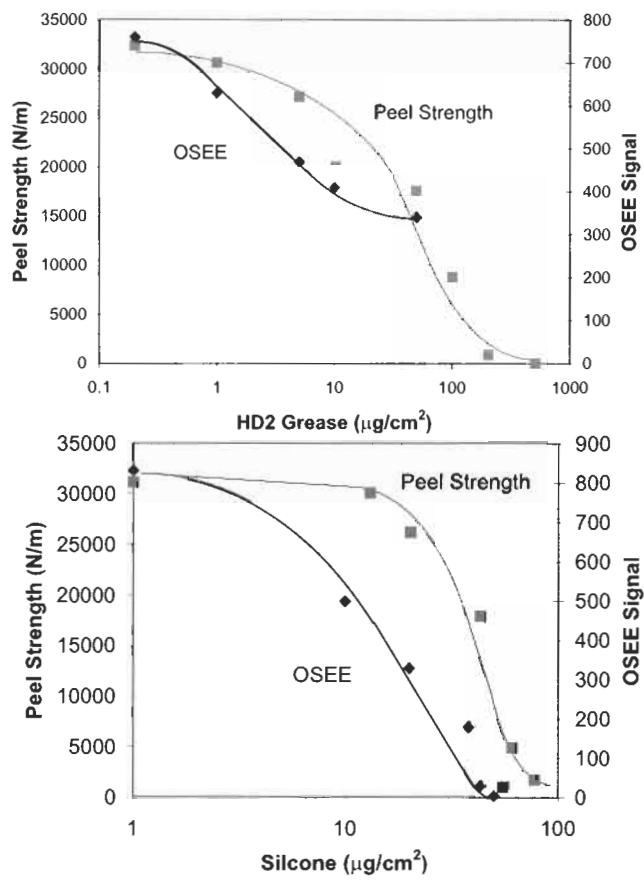


Fig. 35. OSEE response and peel strength of NBR rubber on steel for HD2 grease (data from Ref. [162]) and silicone release agent contamination (data from R.L. Gause, unpublished work and Ref. [10]). The HD2 grease is slightly photoemitting so the OSEE signal does not decrease to zero at high contamination levels.

be imaged using a low-light video camera. Because the metal surface does not fluoresce, organic contamination at levels as low as $1 \mu\text{g}/\text{cm}^2$ can be detected and mapped quickly. Similar contamination maps can be obtained with infrared imaging [12,163], and here again emphasis is placed on contamination detection not on identification. This allows broad energy (wavelength) filters to be used, which speed up inspection but provides for little or no molecular identification through spectral analysis.

In addition to inspecting for possible contamination, it usually is also of interest to determine whether the chemical etching or anodization process has actually produced the desired oxide. For this purpose, anodization has somewhat of an advantage over etching (FPL, for example) because the thicker oxide developed

by the former process can be readily detected optically by observation with crossed polarizers [54]. This method is useful for determining if the oxide is present but it does not reveal anything about the oxide morphology which must be examined by more sophisticated techniques. Thus, when bonding problems arise which are not resolved by less sophisticated techniques, it may be necessary to employ the use of analytical laboratories having high resolution HR-SEM and other sophisticated scientific apparatus. At such times, witness panels can play a crucial role in the investigation as discussed in the next section.

5.2. Witness specimen inspection

A large fraction of quality control (QC) procedures cannot be performed on actual parts but must be done on witness panels. This practice relaxes the constraints that actual bonding surfaces impose (too big to get in the microscope, for example) but introduces the question 'Is the witness specimen identical to the production part or structure?' The affirmative assumption is usually valid provided the witness specimens are actually prepared along with the production part, and extreme care is used in dealing with them after processing as outlined in ASTM documents for handling bonding hardware [164,165]. Notwithstanding such potential problems, witness specimens are used universally with great confidence for quality control on everything from Space Shuttle components to flight hardware on commercial and military aircraft.

A list of tests that can be performed on witness panels includes numerous analytical procedures as well as destructive testing (climbing drum peel, T-peel, lap shear, or wedge tests). Of these mechanical properties tests, the wedge test is usually the most discriminating because it involves testing in a humid environment where the real weaknesses of many types of bonded joints evidence themselves. It is relatively easy to obtain good initial bond strength, in the absence of significant contamination or other serious processing problems, but durability under hot, moist conditions with opening stresses is more elusive. The wedge test also has the advantage that humidity exposures of only 1 h [166–168], are frequently sufficient to detect processing problems, a period which is generally acceptable within production time constraints. Other durability tests involving lap shear or tensile buttons require extensive time for moisture to penetrate the adhesive and reach the interface so they usually are not appropriate for production durability testing [46,49].

Another major advantage of witness panels is that they make it possible to employ sophisticated analytical procedures to investigate the cause of serious bonding problems. Instrumentation such as HR-SEM, XPS, AES, FTIR, etc., which are discussed in detail in Chapter 6, are not customarily available in a production environment but there are many independent analytical laboratories that offer such services and whose personnel can be extremely helpful in diag-

nosing the difficulty. This is especially true if baseline micrographs and analyses are available showing what acceptable bonding surfaces are like. In addition, one bond shop had prepared a series of HR-SEM micrographs showing how various out-of-spec procedures and contaminants modified the oxide morphology. Part of this 'Morphology Catalog' [169] is shown in Figs. 36 and 37, which illustrate the effect of (1) contaminants in the FPL bath, and (2) 'forgetting' to do the FPL treatment. (These should be compared with Fig. 14, a normal FPL oxide morphology.) Since the catalog covered virtually all possible things that could go wrong in the etching or anodization process, it became a simple matter for the QC department to compare the recent morphologies with the catalog to quickly identify the source of any difficulty.

Finally, no matter what the investment needed to finance a witness panel program or a collection of baseline micrographs and data, when things start to go wrong and extremely expensive parts start piling up on the scrap heap, the benefits brought about by a well thought out crisis avoidance program will be very welcome.

6. Summary

This chapter has reviewed many of the most widely accepted procedures and processes used to treat metal adherends for the purpose of making strong and durable metal-polymer bonds. Not surprisingly, most of these surface treatments were developed by or for the aerospace industry because of that industry's emphasis on safety and reliability. Early on, some important processes were developed empirically using more-or-less an Edisonian approach but in recent years a more scientific approach has been fostered by the industry and The Adhesion Society. Indeed, through the efforts of that Society there has been a virtual invasion of electron microscopists, surface scientists, physicists, material scientists, organic chemists and the like into the field that has put the entire industry on a much firmer scientific footing than it was many years ago.

One of the important lessons that has been learned by the more recent work is that the morphology, the fine structure, of the surface or surface oxide that is formed by many of the surface treatments is crucial to the development of strong, durable bonds. This realization was brought about by examining the surface of metal adherends in the electron microscope at high magnifications ($50,000\times$) and finding a fine porous structure that correlated well with good bond strength and bondment durability. Specifically, these studies were able to show very convincingly that metal treatment processes such as PAA, FPL and CAA, for aluminum, and a modified CAA for titanium, were successful because they developed oxides having a porous and microscopic roughness that interlocked with the polymer. This formation of an interlocked interphase is responsible for

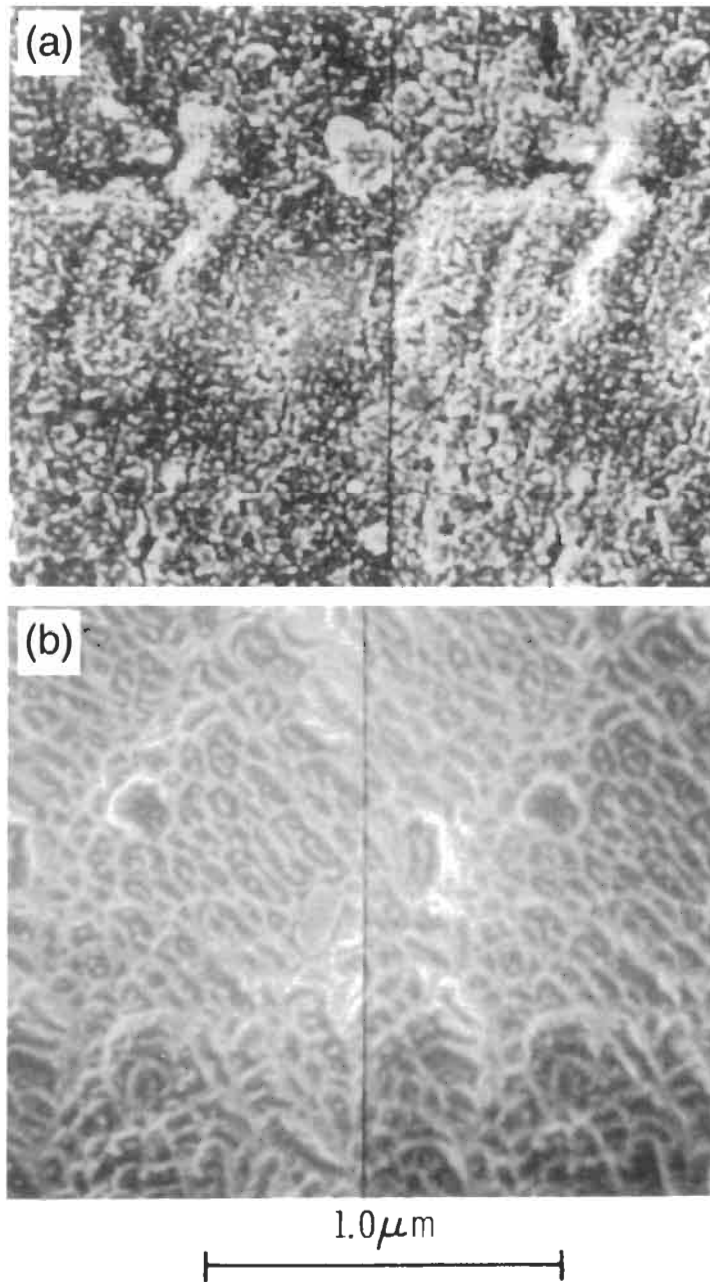


Fig. 36. Part of a 'Morphology Catalog' illustrating the unacceptable morphologies resulting from incorrect surface treatment: (a) Turco alkaline clean with no FPL etch, and (b) Amchem deoxidizer with no FPL etch [169].

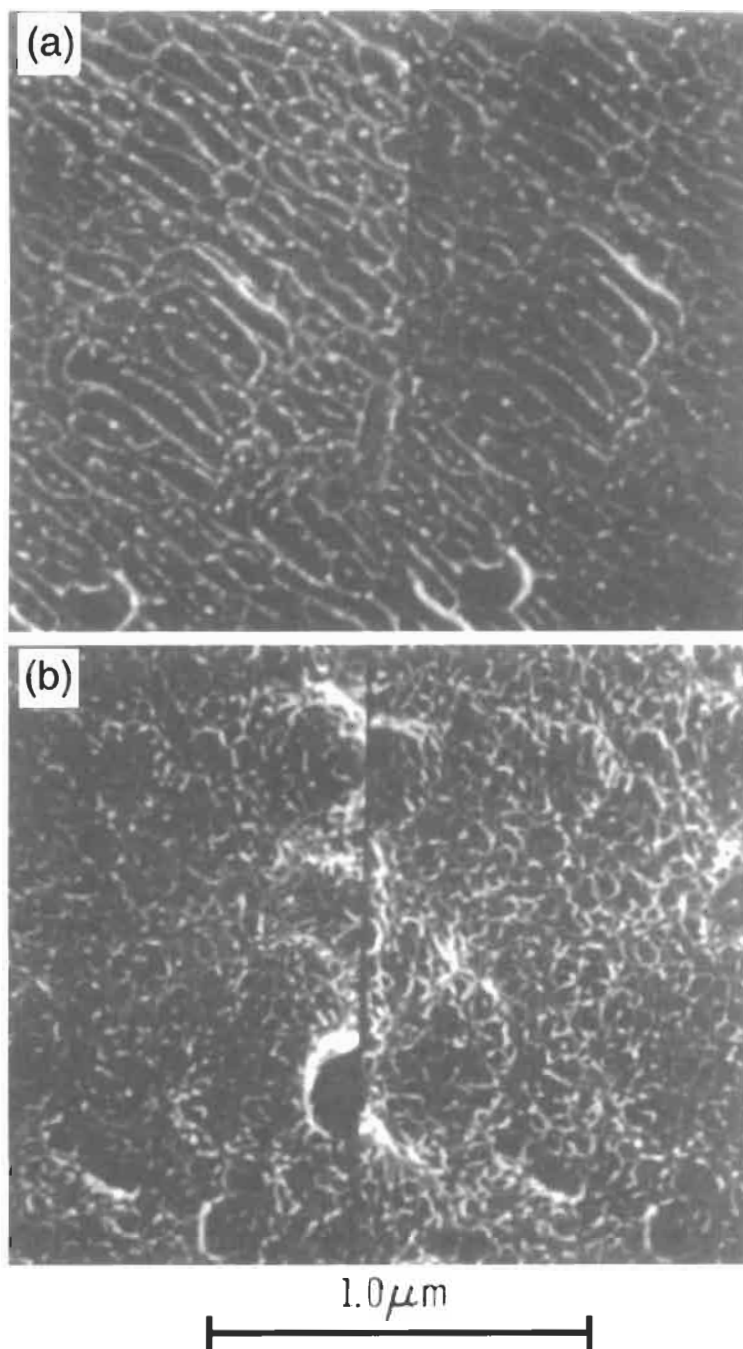


Fig. 37. Part of a 'Morphology Catalog' illustrating the unacceptable morphologies resulting from contaminated etch solution: (a) FPL with ~ 600 ppm F^- , and (b) FPL with ~ 400 ppm Cl^- [169].

producing much stronger and more durable bonds than if the metal surface were smooth. In addition, the ability to view this fine structure led to the discovery that the surface morphology on the CAA process for aluminum depended solely on what pre-treatment was used. That is, a pre-treatment of PAA resulted in a PAA surface morphology after being anodized by the CAA method and likewise an FPL pre-treatment gave an FPL outer surface. The message was very clear-pay attention to what pre-treatment is used when using the CAA process.

Surface scientists have also contributed greatly to the development of reliable bonds. For example, the use of XPS revealed that extremely low concentrations of silicone on an adherend can lead to poor bond strength because the contaminant prevents the polymer from wetting the oxide and thereby prevents penetration of the polymer into the porous structure. The interlocking interphase never forms or forms only poorly. In addition, surface behavior diagrams using XPS data have provided a great deal of insight into bond degradation mechanisms and what might be done to improve the situation. This, in turn, has led to the development of EIS that has been used on an experimental scale to monitor bond degradation in the presence of a humid environment. In the future this may become a health monitoring technique that could prevent catastrophic failures such as that occurring on an Aloha airliner several years ago.

Despite the progress outlined in this chapter, much work remains to be done in the metal surface preparation arena. For example, there is still no ideal surface preparation method that does for steel what anodization processes do for aluminum and titanium. The plasma spray process looks encouraging but because it is slow for large areas and requires rather expensive robot controlled plasma spray equipment, its use will probably be limited to some rather special applications. For more general use, the sol-gel process has potential if future studies confirm recently reported results.

Finally, an equally pressing need is for processes that are more environmentally friendly than those that currently use chromates, volatile solvents, etc. This is an area where the recently developed scientific tools described in this and other chapters will play a major role in assuring that the results are not only 'greener' but are also just as effective or more so than currently used methods.

References

1. Davis, G.D., *Handbook on Engineered Materials Vol. 3: Adhesives and Sealants*. Brinson, H.F., Chm., ASM International, Metals Park, OH, 1990, p. 235.
2. Clearfield, H.M., McNamara, D.K. and Davis, G.D., *Handbook on Engineered Materials, Vol. 3: Adhesives and Sealants*. Brinson, H.F., Chm., ASM International, Metals Park, OH, 1990, p. 259.
3. Boerio, F.J., Davis, G.D., deVries, J.E., Miller, C.E., Mittal, K.L., Opila, R.L. and Yasuda, H.K., In: Czanderna, A.W. and Landgrebe, A.R. (Eds.), *Current Status, Research Needs*,

- and Opportunities in Applications of Surface Processing to Transportation and Utilities Technologies. National Renewable Energy Laboratory, Golden, CO, 1992, p. 23-1; and *Crit. Rev. Surf. Chem.*, **3**, 81 (1993).
4. Kinloch, A.J., *Adhesion and Adhesives: Science and Technology*. Chapman and Hall, London, 1987.
 5. Landrock, A.H., *Adhesives Technology Handbook*. Noyes Publications, Park Ridge, NJ, 1985.
 6. Pocius, A.V., *Adhesion and Adhesives Technology*. Hanser/Gardner Publications, Cincinnati, 1997.
 7. Minford, J.D., *Handbook of Aluminum Bonding Technology and Data*. Marcel Dekker, New York, 1993.
 8. Davis, G.D. and Shaffer, D.K., In: Mittal, K.L. and Pizzi, A. (Eds.), *Handbook of Adhesive Technology*. Marcel Dekker, New York, 1994, p. 113.
 9. Venables, J.D., *J. Mater. Sci.*, **19**, 2431 (1984).
 10. Davis, G.D., *Surf. Interface Anal.*, **20**, 368 (1993).
 11. Davis, G.D., *Surf. Interface Anal.*, **17**, 439 (1991).
 12. Davis, G.D. Davidson, T.F. and Gause, R.L., *Proc. 1994 JANNAF Nondestructive Evaluation and Structures and Mechanical Behavior Meeting*. Chemical Propulsion Information Agency, Columbia, MD, 1994.
 13. Sun, T.S., Chen, J.M., Viswanadham, R.K. and Green, J.A.S., *J. Vac. Sci. Technol.*, **16**, 668 (1979).
 14. Sun, T.S., Chen, J.M., Venables, J.D. and Hopping, R., *Appl. Surf. Sci.*, **1**, 202 (1978).
 15. Chen, J.M., Sun, T.S., Venables, J.D., McNamara, D.K. and Hopping, R.L., *Proc. 24th Nat. SAMPE Symp.*, SAMPE, Azusa, CA, 1979, p. 1188.
 16. Kinloch, A.J. and Smart, N.R., *J. Adhes.*, **12**, 23 (1981).
 17. Kinloch, A.J., Bishop, H.E. and Smart, N.R., *J. Adhes.*, **14**, 105 (1982).
 18. Lewis, B.F., Bowser, W.M., Horn Jr., J.L., Luu, T. and Weinberg, W.H., *J. Vac. Sci. Technol.*, **11**, 262 (1974).
 19. Gettings, M. and Kinloch, A.J., *J. Mater. Sci.*, **12**, 2511 (1977).
 20. Miller, J.D. and Ishida, H., In: Lee, L.H. (Ed.), *Fundamentals of Adhesion*. Plenum, New York, 1991, p. 291.
 21. Blohowiak, K.Y., Osborne, J.H., Krienke, K.A. and Sekits, D.F., *Proc. 28th Int. SAMPE Tech. Conf.*, Covina, CA, 1996, p. 440.
 22. Blohowiak, K.Y., Krienke, K.A., Osborne, J.H. and Greigor, R.B., *Proc. Workshop on Advanced Metal Finishing Techniques for Aerospace Applications*, Keystone, CO, 1998.
 23. Park, C., Lowther, S.E., Smith, J.G. Jr., Connell, J.W., Hergenrother, P.M. and St. Clair, T.L., In: Speth, D.R. (Ed.), *Proc. 22nd Annual Meeting Adhesion Society*. Blacksburg, VA, 1999, p. 361.
 24. Park, C., Lowther, S.E. and Smith, J.G. Jr., *Proc. PMSE Meeting*, 81, p. 403, American Chemical Society, 1999.
 25. Park, C., Lowther, S.E., Smith Jr., J.G., Connell, J.W., Hergenrother, P.M. and St. Clair, T.L., *Int. J. Adhes. Adhes.*, **20**, 457 (2000).
 26. Bishopp, J.A., Sim, E.K., Thompson, G.E. and Wood, G.C., *J. Adhes.*, **26**, 237 (1988).
 27. Kinloch, A.J., Little, M.S.G. and Watts, J.F., *Acta Materialia*, **48**, 4543 (2000).
 28. Marceau, J.A., In: Thrall, E.W. and Shannon, R.W. (Eds.), *Adhesive Bonding of Aluminum Alloys*. Marcel Dekker, New York, 1985, p. 51.
 29. Brockmann, W., Hennemann, O.D., Kollek, H. and Matz, C., *Int. J. Adhes. Adhes.*, **6**, 115 (1986).

30. Clearfield, H.M., McNamara, D.K. and Davis, G.D., In: Lee, L.H. (Ed.), *Adhesive Bonding*. Plenum, New York, 1991, p. 203.
31. Clearfield, H.M., McNamara, D.K. and Davis, G.D., In: *Engineered Materials Handbook Vol. 3: Adhesives and Sealants*. chm., Brinson, H.F., ASM International, Metals Park, OH, 1990, p. 259.
32. Brown, S.R., In: *Proc. 27th Natl. SAMPE Symp.* SAMPE, Azusa, CA, 1982, p. 363.
33. Ditchek, B.M., Breen, K.R., Sun, T.S. and Venables, J.D., In: *Proc. 12th SAMPE Tech. Conf.*, SAMPE, Seattle, WA, 1980, p. 882.
34. Kennedy, A.C., Kohler, R. and Poole, P., *Int. J. Adhes. Adhes.*, **3**, 133 (1983).
35. Filbey, J.A., Wightman, J.P. and Polgar, D.J., *J. Adhes.*, **20**, 283 (1987).
36. Shaffer, D.K., Clearfield, H.M., Blankenship, C.P. Jr., and Ahearn, J.S., In: *Proc. 19th SAMPE Tech. Conf.*, SAMPE, Azusa, CA, 1987, p. 291.
37. Chen, J.M., Sun, T.S., Venables, J.D. and Hopping, R., In: *Proc. 22nd Natl. SAMPE Symp.*, Azusa, CA, 1977, p. 25.
38. Davis, G.D., Sun, T.S., Ahearn, J.S. and Venables, J.D., *J. Mater. Sci.*, **17**, 1807 (1982).
39. Venables, J.D., McNamara, D.K., Chen, J.M., Ditchek, B.M., Morgenthaler, T.I., Sun, T.S. and Hopping, R.L., In: *Proc. 12th Nat. SAMPE Tech. Conf.*, Azusa, CA, 1980, p. 909.
40. Davis, G.D., *Surf. Interface Anal.*, **9**, 421 (1986).
41. Davis, G.D., Ahearn, J.S., Matienzo, L.J. and Venables, J.D., *J. Mater. Sci.*, **20**, 975 (1985).
42. Ahearn, J.S., Davis, G.D., Sun, T.S. and Venables, J.D., In: Mittal, K.L. (Ed.), *Adhesion Aspects of Polymer Coatings*. Plenum Press, New York, 1983, p. 281.
43. Eichner, H.W. and Schowalter, W.E., Report 1813, Forest Products Laboratory, Madison, WI, 1950.
44. Venables, J.D., Tadros, M.E. and Ditchek, B.M., US Patent 4,308,079 (1983).
45. Ahearn, J.S. and Davis, G.D., *J. Adhes.*, **28**, 75 (1989).
46. Davis, G.D., Whisnant, P.L. and Venables, J.D., *J. Adhes. Sci. Technol.*, **9**, 433 (1995).
47. Mansfeld, F., Kendig, M.W. and Tsai, S., *Corrosion*, **38**, 478 (1982).
48. Scully, J.R., *J. Electrochem. Soc.*, **136**, 979 (1989).
49. Davis, G.D., Krebs, L.A., Drzal, L.T., Rich, M.J. and Askeland, P., *J. Adhes.*, **72**, 335 (2000).
50. Natan, M. and Venables, J.D., *J. Adhes.*, **15**, 125 (1983).
51. Shaffer, D.K., Clearfield, H.M. and Ahearn, J.S., In: Minford, J.D. (Ed.), *Treatise on Adhesion and Adhesives, Vol. 7*. Marcel Dekker, New York, 1991, p. 437.
52. Clearfield, H.M., Shaffer, D.K., VanDoren, S.L. and Ahearn, J.S., *J. Adhes.*, **29**, 81 (1989).
53. Hergenrother, P.M., *SAMPE J.*, **36**, 30 (2000).
54. McNamara, D.K. and Ahearn, J.S., *Int. Mater. Rev.*, **32**, 292 (1987).
55. Debski, M., Shanahan, M.E.R. and Schultz, J., *Int. J. Adhes. Adhes.*, **6**, 145 (1986).
56. Debski, M., Shanahan, M.E.R. and Schultz, J., *Int. J. Adhes. Adhes.*, **6**, 150 (1986).
57. Pocius, A.V., In: Mittal, K.L. (Ed.), *Adhesion Aspects of Polymeric Coatings*. Plenum Press, NY, 1983, p. 173.
58. Pocius, A.V., Wilson, T.H. Jr., Lunquist, S.H. and Sugii, S., In: Bartelds, G. and Schliekilmann, R.J. (Eds.), *Progress in Advanced Materials and Processes: Durability, Reliability, and Quality Control*. Elsevier, Amsterdam, 1985, p. 71.
59. Venables, J.D., McNamara, D.K., Chen, J.M., Sun, T.S. and Hopping, R.L., *Appl. Surf. Sci.*, **3**, 88 (1979).
60. Rodgers, N.L., In: *Proc. 13th Natl. SAMPE Tech. Conf.*, SAMPE, Azusa, CA, 1981, p. 640.
61. Desai, A., Ahearn, J.S. and McNamara, D.K., Cleanliness of external tank surfaces.

- Martin Marietta Laboratories, Baltimore, MD, Technical Report MML TR 85-65, 1985 (unpublished).
62. Olefjord, I. and Kozma, L., *Mater. Sci. Technol.*, **3**, 860 (1987).
 63. Kabayashi, G.S. and Connelly, D.J., Boeing Co. Report No. DG-41517, 1974.
 64. BAC5555, Phosphoric acid anodization of aluminum for structural bonding. Boeing Aircraft Company, 1974.
 65. ASTM D3933, Standard Guide for Preparation of Aluminum Surfaces for Structural Adhesives Bonding, Phosphoric Acid Anodization, ASTM, West Conshohocken, PA.
 66. El-Mashri, S.M., Jones, R.G. and Forty, A.J., *Philos. Mag. A*, **48**, 665 (1983).
 67. Olsen, R.H., In: *Proc. 11th Natl. SAMPE Tech. Conf.*, SAMPE, Azusa, CA, 1979, p. 770.
 68. Franz, H.E., *Z. Werkstofftech.*, **14**, 164 (1983).
 69. Franz, H.E., *Z. Werkstofftech.*, **14**, 290 (1983).
 70. Koliek, H., *Int. J. Adhes. Adhes.*, **5**, 75 (1985).
 71. Solomon, J.S. and Hamlin, D.E., *Appl. Surf. Sci.*, **4**, 307 (1980).
 72. Poole, P. and Watts, J.F., *Int. J. Adhes. Adhes.*, **5**, 33 (1985).
 73. Abd Rabbo, M.F., Richardson, J.A. and Wood, G.C., *Corros. Sci.*, **16**, 689 (1976).
 74. Mil Spec MIL-A-8625C.
 75. Process Specification 4352, Bell Helicopter Textron, Inc.
 76. Process Specification TH 6.7851, Fokker VFW B.V.
 77. Brockmann, W. and Hennemann, O., In: *Proc. 11th SAMPE Tech. Conf.*, Boston, MA, November 1979, pp. 804–816.
 78. Singh, V., Rama, P., Cocks, G.J. and Taplin, D.M.R., *J. Mater. Sci. Lett.*, **14**, 745 (1979).
 79. Csanady, A., Imre-Baan, I., Lichtenberger-Bajza, E., Szontagh, E. and Domolki, F., *J. Mater. Sci.*, **15**, 2761 (1980).
 80. Wegman, R.F., *Surface Preparation Techniques for Adhesive Bonding*. Noyes Publications, Park Ridge, NJ, 1989.
 81. Cagle, C.V. (Ed.), *The Handbook of Adhesive Bonding*. McGraw Hill, New York, 1973.
 82. Yaniv, A.E., Fin, N., Dodiuk, H. and Klein, I.E., *Appl. Surf. Sci.*, **20**, 538 (1985).
 83. McNamara, D.K. and Venables, J.D., unpublished work, Martin Marietta Laboratories.
 84. Allen, K.W. and Stevens, M.G., *J. Adhes.*, **14**, 137 (1982).
 85. BAC5632. Boric acid-sulfuric acid anodizing. Boeing Aircraft Company, 1990.
 86. Baker, A.A., Bonded Composite Repair of Metallic Aircraft Components — Overview of Australian Activities, AGARD (Advisory Group for Aerospace Research and Development) Conference of Composite Repair of Military Aircraft Structures, 3–5 October 1994, Seville.
 87. Kuhbender, R.J. and Mazza, J.J., *Proc. SAMPE Int. Symp.*, **38**, 1211 (1993).
 88. Fredell, R., Guyt, C., Mazza, J., Knighton, S. and Collar, E., *Proc. SAMPE Int. Symp.*, **41**, 962 (1996).
 89. Mazza, J.J. and Kuhbender, R.J., Grit blast/silane (GBS) aluminum surface preparation for structural adhesive bonding, WL-TR-94-4111. Materials Laboratory, Air Force Materiel Command, September 1999.
 90. Plueddemann, E.P., *Silane Coupling Agents*. Plenum Press, New York, 1982.
 91. Walker, P., Silane and other adhesion promoters in adhesive technology. In: Mittal, K.L. and Pizzi, A. (Eds.), *Handbook of Adhesive Technology*. Marcel Dekker, New York, 1994, p. 47.
 92. Bascom, W.D., In: *Engineered Materials Handbook Vol. 3: Adhesives and Sealants*. chm., Brinson, H.F., ASM International, Metals Park, OH, 1990, p. 254.
 93. Pike, R.A., *Int. J. Adhes. Adhes.*, **5**, 3 (1985).
 94. Blohowiak, K.Y., Krienke, K.A., Osborne, J.H., Mazza, J.J., Gaskin, G.B., Arnold, J.R.,

- DePiero, W.S. and Brescia, J., *Proc. 2nd DoD/FAA/NASA Conf. on Aging Aircraft*, Williamsburg, VA, 1998.
95. Osborne, J.H., Blohowiak, K.Y., Taylor, S.R., Hunter, C., Bierwagen, G., Carlson, B., Du, J., Damron, M., Bernard, D. and Donley, M.S., *Proc. 2nd DoD/FAA/NASA Conf. On Aging Aircraft*, Williamsburg, VA, 1998.
 96. Pike, R.A., *Int. J. Adhes. Adhes.*, **6**, 21 (1986).
 97. Brewis, D.M., In: Kinloch, A.J. (Ed.), *Durability of Structural Adhesives*. Applied Science Publishers, Essex, pp. 215–254.
 98. Arrowsmith, D.J. and Clifford, Q.W., *Int. J. Adhes. Adhes.*, **5**, 40 (1985).
 99. McCray, D.B. and Mazza, J.J., *Proc. SAMPE 2000*, SAMPE, Covina, CA, 2000.
 100. Kennedy, A.C., Kohler, R. and Poole, P., *Int. J. Adhes. Adhes.*, **3**, 133 (1983).
 101. Progar, D.J., NASA Tech. Mem. 89045, 1986 (unpublished).
 102. Matz, C., *Int. J. Adhes. Adhes.*, **8**, 17 (1988).
 103. Ditchek, B.M., Morgenthaler, T.I., Sun, T.S. and Hopping, R.L., In: *Proc. 25th Natl. SAMPE Symp.*, SAMPE, Azusa, CA, 1980, p. 909.
 104. Natan, M., Venables, J.D. and Breen, K.R., In: *Proc. 27th Natl. SAMPE Symp.*, SAMPE, Azusa, CA, 1982, p. 178.
 105. Clearfield, H.M., Shaffer, D.K. and Ahearn, J.S., In: *Proc. 18th Natl. SAMPE Tech. Conf.*, SAMPE, Azusa, CA, 1986, p. 921.
 106. Clearfield, H.M., Shaffer, D.K., Ahearn, J.S. and Venables, J.D., *J. Adhes.*, **23**, 83 (1987).
 107. Assefpour-Dezfuly, M., Viachos, C. and Andrews, E.H., *J. Mater. Sci.*, **19**, 3626 (1984).
 108. Moji, Y. and Marceau, J.A., U.S. Patent No. 3959091 (assigned to the Boeing Company), 1976.
 109. Cobb, T.Q., Johnson, W.S., Lowther, S.E. and St. Clair, T.L., *J. Adhes.*, **71**, 115 (1999).
 110. Wegman, R.F. and Levi, D.W., In: *Proc. 27th Natl. SAMPE Symp.*, SAMPE, Azusa, CA, 1982, p. 440.
 111. Progar, D.J. and St. Clair, T.L., *Int. J. Adhes. Adhes.*, **6**, 25 (1986).
 112. Peters, P.D., Ledbury, E.A., Hendricks, C.L. and Miller, A.G., In: *Proc. 27th Natl. SAMPE Symp.*, SAMPE, Azusa, CA, 1982, p. 940.
 113. Hsu, N.N.C., Noland, J.S., Brinen, J.S. and Graham, A.W., In: *Proc. 7th Annual Meeting of the Adhesion Society*. Jacksonville, FL, 1984.
 114. Commercon, P. and Wightman, J., *J. Adhes.*, **22**, 13 (1987).
 115. Charnock, R.S., *Int. J. Adhes. Adhes.*, **5**, 201 (1985).
 116. Arnold, J.R., In: *Proc. Automotive and Corrosion Prevention Conference*. Society of Automotive Engineers, Warrendale, PA, 1986, p. 21.
 117. Pocius, A.V., Wangness, D.A., Almer, C.J. and McKown, A.G., In: *Proc. Adhesion Society Meeting*. Jacksonville, FL, 1984.
 118. Andrews, E.H. and King, N.E., *J. Mater. Sci.*, **11**, 2004 (1976).
 119. Zadorozhnyi, V.G., Rafalovich, D.M. and Roikh, I.L., *Elektronnaya Obrab. Mater.*, **1**, 43 (1977).
 120. Ruhlsland, K., In: Mittal, K. (Ed.), *Adhesive Joints: Formation, Characteristics and Testing*. New York, Plenum Press, 1984, p. 257.
 121. Hine, P.J., Packham, D.E. and El Muddarris, S., In: *Proc. Int. Adhesion Conf.*, Plastics and Rubber Institute, Nottingham, September 1984, pp. 10.1–10.4.
 122. Russell, W., Rosty, R. and Levi, D.W., Technical Report ARSCD-TR-82005, ARRAD-COM, Dover, NJ, June 1982.
 123. Russell, W.J., Rosty, R., Adelson, K.M., Bodner, M.J., Wegman, R.F., Garnis, E.A. and Levi, D.W., Technical Report ARSCD-TR-83014, U.S. Army Research and Development Center, Dover, NJ, October 1983.

124. Mindyuk, A.K., Lavrishin, B.N. and Krutsan, A.M., *Soc. Mater. Sci.*, **19**, 560 (1983).
125. Leroy, V., *Mater. Sci. Eng.*, **42**, 289 (1980).
126. Hsu, N.N.C., Noland, J.S., Brinen, J.S. and Graham, A.W., In: *Proc. 7th Annual Adhesion Society Meeting*. Jacksonville, FL, 1984.
127. Podoba, E.A., Kodaii, S.P., Curley, R.C., McNamara, D.K. and Venables, J.D., *Appl. Surf. Sci.*, **9**, 359 (1981).
128. Bottrell, N.L., *Sheet Metal Ind.*, **42**, 667 (1965).
129. Henderson, A.W., In: *Aspects of Adhesion*. University of London Press, London, 1965. pp. 33–46.
130. David, H.L., *Met. Deform.*, **26**, 45 (1974).
131. David, H.L., *Met. Deform.*, **19**, 27 (1973).
132. Rodgers, N.L., In: *Proc. Conf. Specialized Cleaning, Finishing and Coating Processes*. American Society for Metals, Los Angeles, CA, Feb. 1980, pp. 63–77.
133. Allen, K.W., *J. Adhes.*, **8**, 183 (1977).
134. Look, L.G., In: *Proc. Conf. Technology Transfer*, SAMPE, Mount Pocono, PA, 1981, p. 150.
135. Pocius, A.V., Almer, C.J., Wald, R.D., Wilson, T.H. and Davidian, B.E., *SAMPE J.*, **20**, 11 (1984).
136. Smith, T., *J. Adhes.*, **17**, 1 (1984).
137. Haak, R.P. and Smith, T., *Int. J. Adhes. Adhes.*, **1**, 5 (1983).
138. Hirko, A.G., In: *Proc. Conf. Hi-Tech Review 1984*, SAMPE, Reno, NE, April 1984.
139. Trawinski, D.L., McNamara, D.K. and Venables, J.D., *SAMPE Q.*, **15**, 6 (1984).
140. Gledhill, R.A. and Kinloch, A.J., *J. Adhes.*, **6**, 315 (1974).
141. Gilibert, Y. and Verchery, G., In: Mittal, K. (Ed.), *Adhesive Joints: Formation, Characteristics, and Testing*. Plenum Press, New York, 1984, p. 69.
142. Watts, J.F. and Castle, J.E., *J. Mater. Sci.*, **19**, 2259 (1984).
143. Trawinski, D.L., In: *Proc. Conf. Advancing Technology in Materials and Processes*. SAMPE, Anaheim, CA, 1985, pp. 1065–1072.
144. Bishof, C., Bauer, A., Kapelle, R. and Possart, W., *Int. J. Adhes. Adhes.*, **5**, 97 (1985).
145. Trawinski, D.L. and Miles, R.D., In: *Proc. Conf. Hi-Tech Review 1984*, SAMPE, Albuquerque, NM, 1984, p. 633.
146. Chandler, H.E., *Met. Prog.*, **121**, 38 (1982).
147. Sugama, T., In: *Proc. Conf. Structural Adhesives Needs Through the 1990s*. Army Research Office, Raleigh, NC, 1985, p. 11.
148. Spaeth, F.J., In: *Proc. Conf. Finishing '83'*, Society of Manufacturing Engineers, Warrendale, PA, February 1983, pp. T-1 through T-4.
149. Kronstein, M., In: *Proc. SAE Congress*. Society of Automotive Engineers, Detroit, MI, 1980, paper 800444.
150. Janssen, E., *Mater. Sci. Eng.*, **42**, 309 (1980).
151. Ross, M.C., Wegman, R.F., Bodner, M.J. and Tanner, W.C., *SAMPE J.*, **12**, 4 (1976).
152. Gan, L.M., Ong, H.W. and Tan, T.L., *J. Adhes.*, **16**, 233 (1984).
153. Ong, H.W.K., Gan, L.J. and Tan, T.L., *J. Adhes.*, **20**, 117 (1986).
154. Aloru, S., Bartoli, P., Leoni, M. and Memmi, M., In: *Proc. Int. Deep Drawing Research Group Conference*. Amsterdam, Netherlands, 1985, Hoogoven IJmuiden BV, Paper 19.
155. Davis, G.D., Groff, G.B., Biegert, L.L. and Heaton, H., *J. Adhes.*, **54**, 47 (1995).
156. Davis, G.D., Cooke, A.V., Rooney, M., Groff, G.B., Boothe, R., Simmons, C., Swauger T.R. and Graham, P., In: *Proc. 1995 JANNAF Propulsion and Subcommittee Joint Meetings Technology*. Chemical Propulsion Information Agency, Columbia, MD, 1995.
157. Davis, G.D., Groff, G.B. and Zatorski, R.A., *Surf. Interface Anal.*, **25**, 366 (1997).

158. McNamara, D.K., Venables, J.D., Sun, T.S., Chen, J.M. and Hopping, R.L., In: *Proc. 11th Natl. SAMPE Tech. Conf.*, SAMPE, Azusa, CA, 1979.
159. Smith, T., *J. Appl. Phys.*, **46**, 1533 (1975).
160. Arora, A., *Proc. 31st Tech. Meeting Inst. Environmental Sciences*, Mount Prospect, IL, 1985.
161. Gause, R.L., A noncontacting scanning photoelectron emission technique for bonding surfaces cleanliness inspection. NASA Technical Memorandum NASA TM-100361, 1989.
162. Schirato, R.C., Polichar, R.M. and Shreve, D.C., In: *Proc. JANNAF Nondestructive Evaluation Subcommittee Meeting*. Chemical Propulsion Information Agency, Columbia, MD, 1992.
163. Davis, G.D. and Kolonko, L.L., Process control methodology — process sensitivity evaluation of the case to insulation bondline, In: *Proc. JANNAF Structure and Mechanical Behavior Subcommittee Meeting, Publ. 591*. Chemical Propulsion Information Agency, Columbia, MD, 1992, p. 67.
164. ASTM E1829, Standard guide for handling specimens prior to analysis. ASTM, West Conshohocken, PA.
165. ASTM E1078, Standard guide for procedures for specimen preparation, mounting, and analysis in auger electron spectroscopy, X-ray photoelectron spectroscopy, and secondary ion mass spectrometry. ASTM, West Conshohocken, PA.
166. Marceau, J.A. and Thrall, E.W., In: Thrall, E.W. and Shannon, R.W. (Eds.), *Adhesive Bonding of Aluminum Alloys*. Marcel Dekker, New York, 1985, p. 177.
167. Marceau, J.A., Moji, Y. and McMillan, J.C., *Adhes. Age*, **20**, Oct. (1977).
168. Kuperman, M.H. and Horton, R.E., In: *Engineered Materials Handbook Vol. 3: Adhesives and Sealants*. chm., Brinson, H.F., ASM International, Metals Park, OH, 1990, p. 801.
169. Venables, J.D., *J. Adhes.*, **39**, 79 (1992).

Electron beam processed adhesives and their use in composite repair

VINCENT J. LOPATA^{a,*}, ALLAN PUZIANOWSKI^a and MORRIS A. JOHNSON^b

^a *Acsion Industries Incorporated, Ara Mooradian Way, Pinawa, MB R0E 1L0, Canada*

^b *UCB Chemicals Corporation, 2000 Lake Park Drive, Smyrna, GA 30080, USA*

1. Introduction

Electron-beam (EB) processing has been used extensively in the adhesive field. It is primarily used as a manufacturing step to cure the adhesive gum used in the production of tapes. However, the use of EB processing to join two or more materials together has been very limited. Two reasons can be attributed to the limited use of EB processing in this field. First was the lack of electron accelerators with the combination of high energy for the required penetration of the required material and the power for the throughput. The second was the lack of development in aerospace-quality EB-curable adhesives. The last 15 years has seen the development of high-energy, high-power electron accelerators [1,2]. This development gives potential users the equipment to penetrate materials such as aluminum and composites as well as curing large quantities of materials extremely quickly. The development of EB-curable epoxy resins [3–5] has given users EB-curable materials with the mechanical properties of traditional room temperature or thermally cured epoxies.

Considerable research has been done to look at the processing and development of EB-curable epoxy resins [6,7]. Much of the resin development work has focused on toughening and improving the interlaminar shear properties of the resins. However, little research has been done to develop EB-curable adhesives. There are two groups that have been developing adhesives to be used exclusively for EB processing. One group is the consortium of Acsion Industries and UCB Chemicals that is focused primarily on developing EB-curable epoxy adhesives.

* Corresponding author. E-mail: lopata@acsion.com

The second group is Electron Solutions and University of Delaware that have focussed primarily on the vinyl-based adhesives [8].

Over the years there have been several studies examining electron-curable adhesives [9–12]. Off-the-shelf acrylate adhesives were the primary focus of the studies. These adhesives, that have potential use for the repair of advanced composites using high-energy electron accelerators, offer several advantages over conventional repair systems, including [6]:

- (1) curing at ambient temperatures, which eliminates the use of thermal blankets typically used for conventional repair of composites;
- (2) less energy consumption because of the elimination of autoclaves and curing ovens;
- (3) simplified processing at contact pressures;
- (4) ability to focus the electron beam on the damaged area only, minimizing internal stresses and possible damage to surrounding material;
- (5) shorter turn around time and, because of the speed of EB curing, repairs can be completed more quickly than conventional means; and
- (6) ability to cure thick parts using either high-energy electrons (<2 cm for 10 MeV electron) or X-rays (<10 cm for 3-MeV X-rays).

Although the acrylate adhesives are readily available and studies have shown that they can produce reasonable bonding properties, they have the disadvantages of having high shrinkage, high fluid absorption, and low service temperatures. Acrylate adhesive applications would be limited. The development of EB-curable epoxy adhesives would have applications in the aerospace and automotive industry and potential wider uses. The most immediate application for these resin systems is composite repair of commercial and military aircraft.

2. Adhesive systems

Adhesives are widely used and offer many advantages over conventional welding and solvent cementing techniques. Adhesives are easy to apply and particularly useful in bonding dissimilar materials. In general, the main disadvantages are a slow cure speed and the need for surface treatment, prior to bonding. One of the most attractive features of EB-curable adhesives is that they can be cross-linked rapidly at ambient or near-ambient temperatures. This feature, coupled with the control the user can exercise over the curing process, makes the EB-cured product attractive for high-speed operations. Also, EB-curable adhesives do not contain solvents or release volatile organic compounds upon curing making them environmentally attractive.

2.1. Adhesion mechanism

In order for adhesives to function, there are a number of chemical and physical forces involved. Several principal mechanisms can play a role in adhering two substrates, including [13]:

- (1) *Absorption and wetting*. Generally, it is necessary for the adhesive resin to wet the substrate surfaces. The surface energy of the composite substrate must be greater than the surface energy or surface tension of the resin in order for effective wetting to occur.
- (2) *Interdiffusion*. An effective bond may be formed when the molecules of one substrate diffuse into the surface layers of the other. Such interdiffusional processes will cause a localized molecular entanglement, contributing significantly to interfacial adhesion. In most instances, however, these interdiffusional processes are limited. Various chemical additives, particularly those that depress glass transition temperatures and enhance molecular mobility, can significantly enhance diffusional processes.
- (3) *Electrostatic attraction*. A difference in electrostatic charge between the substrates at the interface may contribute to the adhesion between them.
- (4) *Chemical covalent bonding*. The formation of covalent chemical bonds between elements at an interface may be an important factor. Such direct chemical bonding would greatly enhance interfacial adhesion, but specific chemical functional groups are required for the reactions to occur.
- (5) *Chemical secondary bonding*. Low-energy bonds, dipolar interactions, dispersion may all play an important role in the development of interfacial adhesion.
- (6) *Mechanical adhesion*. Mechanical interlocking between the two substrates can also contribute to adhesion. This mechanism would function most effectively with fibers with rough surfaces and irregular or non-circular cross-sectional shapes.

In any given system all of the above adhesion mechanisms are probably occurring to varying degrees. In certain systems one or another of the mechanisms can play a greater role [14].

2.2. Surface treatment

Surface treatment of the composite can have a significant effect on adhesion. Surface treatment enhances one or more of the mechanisms described previously. Wu et al. [15] studied the effects of surface treatment on adhesive bonding for AS-4/APC-2 laminates. They found that the greatest bond strength was achieved from acid etching and plasma etching the composite surface. Table 1 summarizes the various surface treatments that were evaluated.

Table 1

Effects of various surface treatments on AS-4/APC-2 laminate for adhesive bonding [15]

Surface treatment	Lap shear (MPa)		Ratio element to carbon			
	EM-300	EA-9673	O/C	N/C	Si/C	S/C
Solvent wipe		5.08	0.337	0.020	0.083	0.009
SCOTCH-BRITE	4.41					
SCOTCH-BRITE/BON AMI	13.58	8.94	0.192	0.006	0.022	0.005
Chromic-sulfuric acid etch	30.27	21.29	0.708	0.105	0.091	0.108
Coupling agent:						
Q1-6106, 5% ^a	19.41	8.66				
Q1-6106, 2% ^a	14.61					
Q1-6106, 0.5% ^a	17.02					
X1-6100, 2% ^a	14.61	7.42				
A-1100, 5% ^a	11.68					
Tetra-etch ^a	19.35					
Plasma	27.82		0.472	0.006	0.072	0.000
De Soto Primer ^a		8.98				

AS-4 = low modulus graphite fiber produced by Hercules.

APC-2 = a polyetheretherketone, thermoplastic polymer matrix from ICI Fiberite.

^a All AS-4/APC-2 surfaces were cleaned with SCOTCH-BRITE and BON AMI before the surface treatment.

Acid and plasma etching greatly increase the bond strength for graphite composite joints. The acid etch gave the best bond strength overall. For both the acid and plasma etching, the amount of surface oxygen had increased significantly compared to the other treatments. For each acid treatment, which showed the largest increase in bond strength, there were also large increases in the elements, nitrogen, silicon, sulfur and chromium on the surface. Other than silicon that probably came from the release agent used, the other elements were expected to play a part in enhancing the bond strength. The increase in oxygen on the surface was not sufficient alone to explain the magnitude of the increase in bond strength. Acid etching increases the size of micro-cracks in the substrate, allowing adhesive to penetrate, improving mechanical adhesion.

2.3. Adhesive functional groups

An EB-curable structural adhesive formulation usually consists of one or more crosslinkable oligomeric resins or prepolymers, along with such additives as reactive diluents, plasticizers, and wetting agents. The oligomer is an important component in terms of the development of mechanical properties. The adhesive and cohesive properties depend on the crosslink density, chemical group substitution, and molecular organization within the polymer matrix. Adhesion is achieved

Table 2

Typical structures contributing to rigidity and flexibility in polymer chains

Rigid groups		Flexible groups	
$-\text{C}(\text{O})\text{NH}-$	Amide, urethane	$-\text{OCH}_2\text{CH}_2-$	oxyethylene
$\text{PhC}(\text{O})-\text{O}-$	Aromatic ester	$-\text{Si}(\text{CH}_3)_2\text{O}-$	dimethylsiloxane
$-(\text{O})\text{C}-\text{NH}-\text{C}(\text{O})-$	Imide	$-\text{CH}_2\text{C}(\text{CH}_3)_2-$	isobutylene

through a combination of chemical and/or physical bonding at the adhesive interface.

The most commonly used resins for EB-cured adhesives are multifunctional oligomers containing two or more reactive groups, principally acrylates and epoxides. Two distinct types of chemical structures are important; those that cause stiffening or rigidity of the polymer chains and those that form flexible, free-moving groups. Table 2 shows examples of both types of structures. The majority of adhesive resins contain a blend of both structural types. Good mechanical properties are due to the micro-phase separation of the various segments containing different structural types.

Stiffening groups are beneficial because they provide adhesives with strong cohesive properties. Cohesive strength is promoted because the stiff segments tend to form laterally ordered groups, through which intermolecular bonding occurs. Under stress, the relatively weak intermolecular bond can easily be broken and re-formed, providing a mechanism for relieving the stress without damage to the polymer backbone and consequent adhesive joint degradation. Bonding is improved by the interaction of the polar groups of the stiffening segment with polar functions on the surface of the adherend and by direct covalent bonding with surface-bound hydroxyl functions. This type of bonding is beneficial because it may improve the environmental resistance of the adhesive joint, since H_2O ingressing along the interface does not disrupt the relatively strong covalent bond.

Flexible groups tend to be molecularly disordered and randomly oriented. In this state, intermolecular bonding is slight and cohesive strength consequently low. Flexibilizing groups are necessary to provide bond toughness. If the flexible backbone is sufficiently long, a certain amount of coiling can occur, giving rise to rubbery domains within the adhesive matrix. Such dispersed phases contribute to the toughness of the adhesive and are important for preventing crack propagation. For most structural adhesive systems, there is a correlation between the flexible group component and characteristics such as peel strength, impact resistance and fracture strength.

2.4. Adhesive properties

2.4.1. EB-curable acrylate adhesives

Table 3 lists the selected properties [16] that we have measured for several commercially available acrylate resins manufactured by the Sartomer Company and the Rohm and Haas Company. The resins were cured in an AECL Gammacell Model 240. The temperature rise was measured for an 8-g sample using Acsion's (formerly AECL Radiation Applications Branch) Gamma Calorimetry method [17]. All of this information is being used to evaluate the applicability of EB-cured acrylate adhesives for repairing composite structures. Combinations of these adhesives can be used to create electron-curable adhesives suitable for composite repair.

Loctite has developed several acrylate adhesives that can be used as EB-curable adhesives [12]. Some of the resins were cured and tested for EB curing properties

Table 3
Selected properties of EB-cured acrylic adhesives

Product code ^a	Product description	Polymer density (kg/m ³)		Polymer shrinkage (%)	Curing dose (kGy) ^b	Temp. rise (°C)
		Cured	Uncured			
238	Hexanediol dimethacrylate	1175	1035	14	9	165
297	Butylene glycol dimethacrylate	1175	944	25	23	86
306	Tripropylene glycol diacrylate	1165	1030	13	11	106
344	Polyethylene glycol diacrylate	1201	1113	7	6	84
368	Isocyanurate triacrylate	1396	1300	7	5	118
399	Dipentaerythritol pentaacrylate	1310	1192	10	11	6
604	Polypropylene monomethacrylate	1079	1010	7	44	38
9035	Trimethylol propane triacrylate	1182	1149	6	6	66
9040	Aliphatic diacrylate ester	1125	1016	11	16	–
9503	Aliphatic urethane acrylate	1215	1200	1	7	27
C2000	C ₁₄ –C ₁₅ acrylated monomer	1017	934	9	20	77
CN111	Epoxidized oil acrylate	1081	1040	4	23	26
CN114	Epoxy acrylate	1400	1150	22	10	–
CN962	Urethane acrylate	1131	1080	5	9	15
CN964	Urethane acrylate	1160	1080	7	6	25
QM589	Proprietary	1065	972	10	9	64
CD-502	Proprietary	1184	1100	8	5	81
CD-504	Proprietary	1070	1030	4	16	34
PRO-636	Proprietary	1203	1140	6	62	32

^a All of the resins were supplied by Sartomer except QM58, which was supplied by Rohm and Haas.

^b kGy = SI unit for a measure of absorbed dose; 1 kGy = 1 kJ/kg.

Table 4

Lap shear strengths for EB-cured acrylic adhesives on graphite composites

Adhesive	Curing dose (kGy)	Man. specs.	Lap shear strength (MPa)					
			Thermal cured ^a			Electron cured ^b		
			None	Sanded	Acid ^c	None	Sanded	Acid ^c
Loc-206	17		16.3	20.5		14.5		
Loc-306	18	13.8	13.2	7.0				
Loc-312	29	20.7	15.7	16.9				
Loc-317	22	17.2	13.1	8.3				
Loc-324	7	19.3	15.6	20.4	16.8	12.6	16.5	
Loc-352	8	20.7	16.0	18.5	17.8	12.4	22.1	
Loc-363	14	22.1	12.8	18.4	22.1	9.8	17.7	8.6
Loc-392	9	19.3	13.6	17.3		10.4	19.4	
Loc-398	10	9.6	8.2	9.7				
FW4 ^d	50		12.6			3.5		
BMI4 ^d	50		12.6	8.1				
AD01 ^e				7.6			12.4	
AD02 ^e				5.1			13.3	
AD03 ^e				11.4			16.3	
AD04 ^e				8.5			13.8	

Man. specs. = Manufacturer specification. Lap shear strength on steel.

^a Thermal-cured panel; Hercules AS4, 5HS, 6K fiber, Ciba Geigy's R-6376 epoxy resin.^b Electron-cured panel; Hercules AS4, 5HS, 6K fiber, FW3 epoxy acrylate resin.^c Hot chromic acid etch for 30 min.^d Adhesive provided by Applied Polaramics.^e Adhesives developed at AECL Whiteshell.

by AECL. Table 4 summarizes the properties of this study. These resins are all cured by free-radical polymerization. Several of these adhesives, when EB-cured, give lap shear strengths similar to the manufacturer's specifications. Table 4 shows the lap shear strengths for various EB-curable adhesives, and compares the shear strengths with thermal-cured and EB-cured graphite composites.

A structural adhesive joint must not only develop good strength properties during or shortly after cure, but it must be capable of maintaining an acceptable fraction of its load bearing characteristics over the expected lifetime of the joint. It is well established that an adhesive joint gradually loses strength with exposure to the environment. The factors that contribute most to the deterioration of adhesive properties are heat and moisture [12]. Some commercially available adhesives, when EB-cured on graphite composites, produce adhesive strengths that are acceptable (Table 4). Our lab has not yet tested the adhesives listed in Table 4 for environmental exposure. Campbell and Brenner [9] performed environmental tests on a number of similar adhesives. These results are summarized in Table 5. Most

Table 5
Environmental effects on EB-cured acrylic adhesives

Adhesive	Lap shear strength (MPa)				
	Initial	Air at 177°C	Water at 25°C	JP-4 at 25°C	Acetone at 25°C
Loc-306	13.0	12.6	12.6	13.0	12.8
Loc-312	13.5	13.4	13.7	12.9	1.9
Loc-317	14.3	10.6	12.5	12.1	14.3
Loc-X-353	13.4	12.3	10.4	13.0	12.3

Test samples were aged in medium for 500 h. Curing dose for adhesive was 100 kGy. Adherends were 7075-T6 aluminum.

of the adhesives retained acceptable strengths after 500 h storage in the respective medium, with the exception of Loctite 312 in acetone. This adhesive exhibited substantial loss of shear strength (retained only 14% of initial strength).

Another factor that can have an effect on adhesion is adhesive shrinkage during curing. Excessive shrinkage can be expected to weaken bond strengths. Poor adhesion of some EB-cured products has been attributed to the rapid cure rates that lock shrinkage-induced stresses into the adhesive layer. Structural adhesives are generally designed to minimize shrinkage or negate its effect. This is most frequently achieved by optimization of the molecular structure of both the resin and monomer components, by the use of fillers and/or plasticizers, and by the use of specific adhesion promoters that form direct chemical links between the adhesive and the adherend. Adhesive strength may also be improved by annealing at elevated temperatures either during or following the curing process. Another way of minimizing the stresses from shrinkage, when using EB curing, is to employ a two step curing cycle. An initial dose that is just below the gel point of the adhesive is given in the first application. Below the gel point, no internal stresses are introduced because the molecules can freely re-orient themselves. About 70% of the shrinkage will occur prior to gelation [18]. The second step would involve applying the remaining dose required to cure the resin to maximum strength. Table 6 shows the EB-cure and shrinkage properties of the EB-cured acrylate adhesives listed in Table 2.

2.4.2. EB-curable epoxy adhesives

There has been very little work done on the development of EB-curable epoxy adhesives. When undertaking this development work the authors had two objectives. The first objective was to develop a series of adhesives for bonding aluminum-to-aluminum (Al–Al) and composite-to-composite (C–C) with lap shear strengths of 30 MPa or greater at room temperature. The second objective was that the

Table 6
EB curing and shrinkage properties for selected EB-cured acrylic adhesives

Adhesive	Gel point (kGy)	Curing dose (kGy)	Volume shrinkage (%)
Loc-206	2.3	17	5.3
Loc-306	1.5	18	13.0
Loc-312	1.9	29	8.1
Loc-317	1.8	22	7.0
Loc-324	1.0	7	4.0
Loc-352	0.9	8	4.4
Loc-363	1.4	14	8.2
Loc-392	1.6	9	
Loc-398	1.3	10	
FW3	1.0	50	16.8
BMI2	1.0	100	10.8
BMI4	5.0	70	10.8

adhesives developed should have service temperatures in excess of 180°C. A large number of resin formulations were tried with mixed success. The development work included looking at gamma calorimetry [17] to determine the curing parameters of the epoxy adhesives. Samples were also cured using Acsion's 10 MeV 1 kW electron accelerator to determine the rheological properties. Table 7 summarizes the resulting properties of some of the adhesives looked at.

One of the important properties epoxy adhesives require for the manufacture and repair of composite aircraft structures is low fluid uptake. This is particularly important when dealing with aircraft structures. The introduction of fluids into the resin matrix can result in the lowering of the service temperature, reduction in mechanical properties at high temperatures and the eventual overall deterioration of the structure with prolonged use. We studied a number of fluids that EB-curable epoxy adhesives may come in contact with particularly if these resins were being considered for manufacture and repair of aircraft components. The fluids that were looked at include: water, skydrol (hydraulic fluid), jet fuel, and de-icing fluid. The adhesives were fully immersed in the fluids until the fluid uptake was in equilibrium. Table 8 summarizes the uptake of various fluids with various EB-curable epoxy adhesives. The values shown here are taken from long term equilibrium studies. The table shows that water uptake for the EB-cured adhesives averages around 3%. When compared with thermally cured epoxy resins these values are considerably lower. Our work showed that 997-2 and 3501-6, Hexcel epoxies that are used routinely for aircraft components, gave values of 5% under the same conditions. The difference in the values is attributed to the higher crosslink densities of the EB-cured systems.

Table 7

EB processing and rheological properties of EB-cured epoxy adhesives

Adhesive	Gel point (kGy)	Curing dose ^a (kGy)	Service temp. ^b (°C)	Glass transition temperature (°C)			
				Loss modulus		Tan δ	
				α	β	α	β
611	1.5	49	78	213	80	231	151
613	6.9	117	178	168	80	168	85
631	0.9	41	123	208	103	221	135
632	1.4	25	171	196	90	218	120
633	5.1	117	206	233	83	253	95
671	2.1	49	133	201	100	213	130
681	2.5	48	153	201	108	218	123
682	1.3	30	166	176	80	208	88
EB2000			157	200		215	
GM27V3B			121	141		156	

^a Curing dose was determined by multiplying by 10 the dose at which the resin reaches maximum temperature from the gamma calorimetry experiment.

^b Service temperature is the temperature at which the flexural modulus from a DMA plot is 50% of that at room temperature.

Table 8

Fluid uptake for selected EB-cured epoxy adhesives

Adhesive	Fluid uptake, %					
	Graphite composite			Neat resin		
	Water	Skydrol	Jet fuel	Water	Skydrol	Jet fuel
611				2.9		
613				5.6		
631				2.7		
632				3.2		
633				5.6		
671				2.8		
681				2.7		
682				3.1		
EB2000	1.2	3.5	1.1	1.9	4.5	

We have also looked at the lap shear strength of selected EB-curable epoxy adhesives. Because the adhesives being developed were being used for both aluminum-to-aluminum and composite-to-composite applications the lap shear strengths for both adherends was measured. Aluminum adherends were T2024 phosphoric acid anodized according to ASTM 3933. The composite adherends

Table 9

Lap shear strengths (MPa) of selected EB-cured epoxy adhesives at various temperatures

Adhesive	Aluminum					Composite			
	−55°C	25°C	93°C	121°C	149°C	−196°C	−54°C	25°C	120°C
611		7						4	
613		7						11	
631		14						3	
632		22						4	
633		10						4	
671		17						3	
681		32						4	
682		18						4	
EB2000						10	7	7	10
11L						10	8	9	9
GM27V3B	12	6	12	10	5				

were thermally cured AS-4 3K GP with Epocast 50A resin. Table 9 summarizes these results.

There are two crucial observations from Table 9. The first observation is that even though a good lap shear value may be obtained for an aluminum-to-aluminum joint, this does not translate into getting a good value for a composite-to-composite joint. Adhesive #632 gave 22 MPa for an Al–Al joint, but only 4 MPa for a C–C joint, while adhesive #613 gave only 7 MPa for an Al–Al joint and 11 MPa for a C–C joint. The reason for this difference is that the resin formulation is tailored for the adherend. Each adherend has different surface properties such as surface energy and molecular structure requiring the use of different adhesion promoters and surfactants to effect good bonding properties.

The second observation is that the EB-curable adhesive resins show no change in adhesive properties from liquid helium temperatures up to temperatures just below their service temperatures. This can be seen for the adhesives, EB2000 and 11L. At this time there is no explanation for this behavior.

A study of several EB-curable epoxy adhesives was also conducted on the effects of various surface preparations on lap shear strength for the two adherends, Al–Al and C–C, used. Table 10 summarizes the results from these tests. The two adhesives, GM27V3A and GM27V3B, were specifically formulated to give good lap shear strengths for C–C joints. The abrasion-only surface preparation shows a higher lap shear strength for the composite adherend. However, when other surface preparations such as the various acid etchants are used, there is an increase in the lap shear strength in favor of the aluminum adherend. In the case of the aluminum adherends the acid etchs would change the surface morphology as well as the chemistry of the surface. The strong oxidizing acids would tend to

Table 10

Effects on lap shear strength of EB-cured epoxy adhesives from different surface preparations on aluminum and composite adherends

Adhesive designation	Surface preparation	Lap shear strength (MPa)	
		Al–Al	C–C
GM27V3A	Abrasion only	8.8	12.4
	Phosphoric acid anodizing	11.8	
	AMPS-sulfuric acid etchant		23.5
	AMPS-sulfuric acid paste, electrochemical etching	11.6	7.1
	Pasa-jell chromic acid etchant	11.3	7.8
GM27V3B	Abrasion only	8.4	11.8
	Fumed silica/sulfuric acid paste		18.7
	Fumed silica/sulfuric acid paste, electrochemical etch	21.7	10.7
	Phosphoric acid anodizing	8.0	
	Pasa-jell chromic acid etchant	9.6	7.1

increase the size of small cracks or fissures in the composite surface by chemically destroying the epoxy matrix of the composite. However, the acid could also be partially destroying the graphite fiber resulting in loss of carbon fiber strength. The oxidizing acids in the case of composites should produce some active chemical sites on the surface. These sites then should be able to interact with the adhesive to produce chemical bonds between the graphite fiber and the polymerized adhesive. However, the subsequent washing and drying cycles to remove the acid from the surface may have destroyed these active sites and introduce other species that would produce a deterioration in the shear strength. The results we see from Table 10 shows mixed results for the acid etchants.

2.5. Curing mechanisms

Of the commercially available EB-curable adhesives [9–12], the resins fall within one of two categories based on their curing mechanisms. The majority of EB-curable resins are based on (meth)acrylate-functionalized oligomers involving a free-radical curing mechanism. The second category is the epoxy resins that cure by a cationic mechanism.

2.5.1. Free radical curing mechanism

Methacrylates and acrylates are readily synthesized from low-cost commercially available resins and (meth)acrylate intermediates or (meth)acrylic acid [19]. A wide range of structural backbones are available, including epoxies, urethanes,

amides, imides, ethers, hydrocarbons, esters and siloxanes. EB curing of these resins is rapid (generally less than 60 kGy) and the polymers exhibit durable adhesive properties under extreme environmental conditions. A wide variety of isocyanates, that contribute to rigidity, and hydroxy-functionalized resins, that contribute flexibility, are readily available. By altering the molecular weights, functionality, substitution pattern and stoichiometry of these various resins, an almost limitless variety of structural adhesives, to suit particular physical property requirements, can be produced. In addition to the oligomer, a typical acrylate-based, EB-curable adhesive composition also contains EB reactive diluents, such as monofunctional (meth)acrylate monomers, used to control viscosity and modify physical properties. The adhesive may also contain small amounts of cross-linking agents and adhesion promoters to control adhesive and cohesive properties.

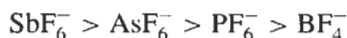
Oxygen inhibition is a major drawback of free radical curing systems. Oxygen interferes with the curing mechanism, resulting in tacky and incompletely cured material. This effect is minimized in a number of ways, including increasing the instantaneous dose rate of the EB process, or by placing an oxygen-impermeable layer, such as aluminum foil or thin plastic sheet, over the surface of the resin before curing. Chain transfer agents, such as amines and thiols, that convert non-propagating radicals into propagating radicals, tend to lessen the inhibiting effects. This mechanism is outlined in Woods [12]. Aromatic carbonyl compounds such as benzophenone and acetophenone derivatives are also used to promote surface curing by reducing the inhibitory effects of oxygen.

2.5.2. Cationic curing mechanism

With the development of iodonium and sulfonium salt cationic catalysts the range of epoxy-based oligomeric resins suitable for use in EB-curable compositions has been greatly extended. Epoxy resins are frequently used for adhesive applications. All of the commercially important epoxies are currently used for formulating EB-curable adhesives, including cycloaliphatics and bisphenol-A epoxy resins, epoxidized Novolacs, glycidyl polyethers, and esters such as acrylic copolymers of glycidyl (meth)acrylate. In general, epoxy resins need higher curing doses than acrylate monomers of equivalent molecular weight and functionality. They have advantages over acrylates; oxygen does not interfere with the cationic polymerization; and shrinkage on curing is considerably reduced because of the epoxy ring opening. Of the monomers listed above, the cycloaliphatic epoxies cure at lower doses. However, cycloaliphatic epoxy monomers produce relatively brittle polymers that exhibit poor adhesive characteristics without a flexibilizing component. The addition of hydroxyl-functionalized poly(oxyalkylene) ethers and related products reduces brittleness and improves adhesive strength. In addition to improving flexibility, the polyol component was also found to accelerate the curing.

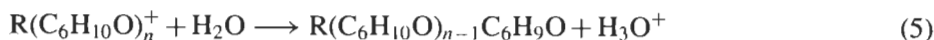
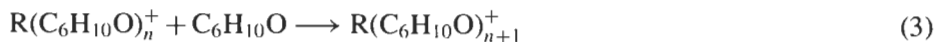
Radiation curing of epoxies with cationic initiators is well known [20–28]. UV–visible light has been the predominant radiation source; the process has been limited to thin coatings due to the low penetration of the visible–UV light [22,23]. Thermal and mechanical properties of these materials are low and the curing is incomplete. Several studies have shown that commercially available epoxies with various cationic initiators can be polymerized with EB curing [20,29–34].

Most of the commercially available initiators are diaryliodonium or triarylsulfonium salts of weak bases. The diaryliodonium salts are known to be more effective initiators than the triarylsulfonium salts of the same anion [20]. The anion also influences the effectiveness of the cationic initiator in catalyzing the EB curing. The anion effect is inversely related to the nucleophilicity of the anion [18]. Lopata et al. [17] showed that the cationic initiators can have a significant effect on the dose required to cure the epoxy resin as well as the resulting polymer's morphology. Within a given initiator family, the following anion effects on the curing efficiency prevailed:



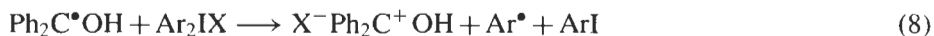
Triarylsulfonium salts cure at a lower dose but have poorer rheological properties than diaryliodonium salts. Gamma calorimetry studies [17] also showed the higher the heat generated from polymerization the better the rheological properties and the lower the dose required to cure. Formulating of EB-curable epoxy resins involves mixing a cationic initiator at a concentration of 1% to 3% with conventional epoxy resins (bisphenol-A, bisphenol-F, epoxy novolacs, glycidyl ethers, and/or cycloaliphatics).

Several mechanisms for the polymerization of vinyl ether and epoxies have been suggested [20,22,23,25,27,28,33–35]. On irradiation with gamma rays or electrons, pure epoxies polymerize via a cationic mechanism [35]. However, this cationic polymerization is inhibited by just traces of moisture, as shown below for cyclohexene oxide in reaction 5.



Since polymerization of epoxies proceeds in the presence of onium salts [17,33,34,29], it is most likely that the above-mentioned cationic mechanism proceeds in their presence, and that the onium salts prevent water from inhibiting the cationic polymerization.

Lapin [33] suggested that photoinitiated cationic polymerization can proceed through reactions of free radicals, as shown below for benzophenone sensitized photoinitiation:



Since free radicals are formed on irradiation of all organic systems [36], free radicals formed in epoxies would also lead to polymerization by an analogous mechanism.

Lapin [33] also suggests the following cationic mechanism for the polymerization of vinyl ethers



An analogous mechanism should also produce polymers on irradiation of epoxies. Crivello's recent mechanistic suggestions [29] are consistent with the mechanisms given above. One can conclude that radiation-induced polymerization of epoxies can proceed via several mechanisms. However, further work is needed to determine the relative contributions of the different mechanisms, which might vary from one epoxy to another. As part of the "Interfacial Properties of Electron Beam Cured Composites CRADA" [37], an in-depth study of the curing mechanism for the cationic-initiated epoxy polymerization is being undertaken.

Materials and additives that are chemically basic in nature have a detrimental effect on the curing of cationic-initiated epoxy systems. These substances can either stop the curing mechanism completely or produce under-cured polymers. Therefore such additives as amines or imides that are known to be adhesion promoters cannot be used in the EB-curable epoxy adhesive formulations.

3. Composite repair

3.1. Types of composite damage

The type of damage an advanced composite sustains plays an important role in the type of repair that can be implemented. Damage to advanced composites can be

Table 11

Flaw/damage size for type of damage

Scratches	A surface scratch that is 100 mm long and 0.50 mm deep.
Delamination	Separation of fiber layers that have an equivalent to a 50 mm diameter circle with dimensions critical to its location.
Impact damage	Damage caused by the impact of a 25 mm diameter hemispherical impactor with 135 J of kinetic energy, or with that kinetic energy required to cause a dent 2.5 mm deep, whichever is least.

divided into three main categories, scratches, delamination and impact. Table 11 summarizes the characteristics associated with each category of damage.

In general, composites sustaining damage in the last two categories would be the major focus for repair using electron and X-ray curing. Delamination damage can be either visible or invisible. In the case of the visible delamination, the repair may just involve applying the adhesive with external pressure to compact the fracture as well as maintain the original shape without loss of mechanical properties. The invisible delamination (sub-surface) fracture may require injecting the resin into the fracture and curing in situ. In the case of impact damage, the damaged area would require cleaning, application of the adhesive and insertion of a composite plug, followed by curing. The repair techniques applied may be very simple or may involve very complex lay-ups, depending on the type of damage, time, and integrity of the repair techniques employed for advanced composites.

3.2. Composite repair techniques

Laminates can be repaired by three basic methods; bolting or bonding a patch over the damaged area, injecting resin into the delaminated area, or removing the damaged area and replacing the plies (see Table 12) [38]. The quickest repair method is to leave the damaged area intact, and bolt or bond a patch over it. Bolting is fast, requiring little or no surface preparation with minimal equipment requirements. Bolt holes, however, weaken the structure, and bolts can pull out. If the patch is a metal plate, weight gain may also be a consideration. Bolting will be adequate for a lightly loaded structure or as a temporary repair. Bonding a patch is more reliable than bolting. Holes are regions of increased stress and also expose the area around them to moisture and corrosion. Bonding allows both metal and composite patches to be applied over the damaged part. At present, depending on the adhesive used, heating blankets may be required to raise the temperature for curing. The repair time will depend on the curing cycle of the adhesive.

When the part will experience higher temperatures or greater stresses than a patch can normally tolerate, the flush aerodynamic technique is often the solution. This technique consists of removing the damaged area and replacing the plies.

Table 12
Summary of repair techniques [38]

Method	Advantages	Disadvantages	Ease of repair	Structural integrity
Bolted patch	No surface treatment; no refrigeration, heating blankets, or vacuum bag required	Bolt holes weaken structure; bolts can pull out	Fast	Low
Bonded patch	Flat or curved surface; field repair	Not suitable for high temperature or critical parts	Fast but depends on cure cycle of adhesive	Low to medium
Flush aerodynamic	Restores full strength; high-temperature capability	Time consuming; usually limited to depot; requires refrigeration	Time consuming	High
Resin injection	Quick; maybe combined with external patch	May cause plies to separate further	Fast	Low
Honeycomb; fill in with body filler	Fast; restores aerodynamic shape	Limited to minimal damage	Fast	Low
Honeycomb; remove damage, replace with synthetic foam	Restores aerodynamic shape and full compressive shape	Some loss of impact strength, gain in weight	Relatively quick	High
Honeycomb; remove damage, replace with another piece of honeycomb	Restores full strength with nominal weight gain	Time consuming; requires space honeycomb	More difficult	High

Unlike bolt or bond patch repair, this type of repair can restore full design strength. However, this technique is expensive. If the laminate requires a high temperature resistance, then heating the prepreg and structure adhesive would be required. This would usually require the repair to be done at a repair depot. Furthermore, heating the composite part to the original cure temperature can be dangerous, as the remaining adhesive may soften and the internal pressure blow the skin from the sound cells adjacent to the repair. A repair adhesive curing 25–50°C lower should be selected [39].

When one or more plies delaminate, one technique is to remove the damaged area and replace the plies, in the similar manner to the flush aerodynamic technique. Another technique is to inject resin directly into the delaminated area,

without removing the damaged plies. Resin injection can be performed quickly. One problem with this technique is that the plies can separate even further. Thus, ply replacement is preferred. Another common type of damage occurs when an adhesive debonds. The straightforward technique is to clean the area, apply the adhesive, clamp and cure, with heat if needed.

All of the types of repairs described can be accomplished using electron/X-ray curing and suitable electron-curable adhesive systems. The advantages of using an electron accelerator are faster curing cycles, short turn-around time, and higher-temperature-resistant bonds, cured at ambient temperatures.

4. Electron/X-ray curing

The end-user has to decide if a beam of electrons should be used directly for curing or should X-rays, produced by the interaction of the electron beam with a high-atomic-number material such as tungsten, be used for curing. The production of X-rays is a simple but inefficient process with a conversion efficiency of less than 10%. The determining factor for what type of radiation to use, is the required penetration of the energy. Fig. 1 shows the depth of penetration in such materials as aluminum, water, graphite composite, fiberglass composite and lead as a function of the electron beam's energy. The electron penetration is inversely proportional to the density of the material and directly proportional to the energy of the beam. The figure shows that composite structures with a normal thickness of 3 mm require electron energies of 3 MeV or greater. However, if one is looking at materials such as steel for automotive applications, then electrons of higher

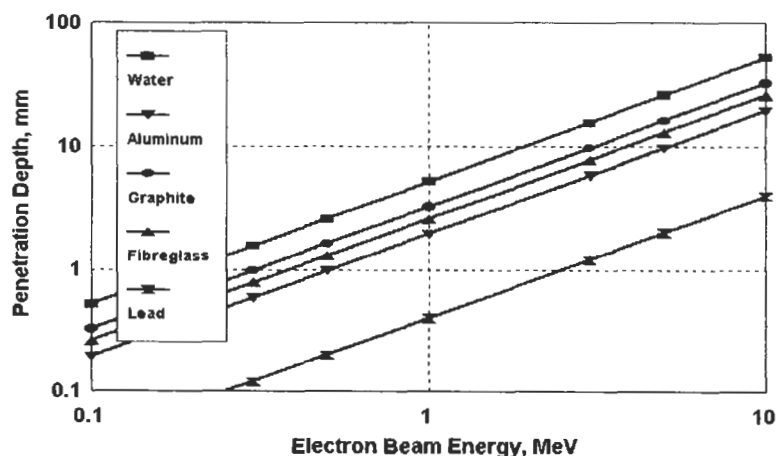


Fig. 1. Electron beam penetration in various materials as a function of electron beam energy.

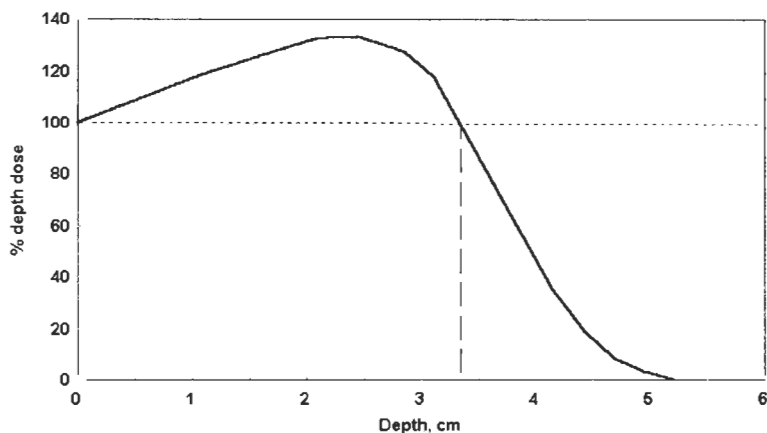


Fig. 2. Dose profile for 9-MeV electrons in polyethylene.

energies such as 10 MeV are required. A 10-MeV electron will only penetrate approximately 2 mm. Fig. 2 shows the dose profile for 9-MeV electrons into polyethylene. The penetration depth is defined as the depth at which the effective dose is the same as the surface dose. It should be noted that there is a steady increase in the dose through the object and then a sudden decrease in the effective dose. The increase is due to the production of secondary electrons as the primary electron is passing through the material. These secondary electrons have energies sufficient to produce chemical reactions. The sudden drop is due to electrons that do not have sufficient energy to go further.

One solution to the penetration problem for thick parts or dense materials is to convert the electrons to X-rays. Fig. 3 shows the attenuation of gamma rays

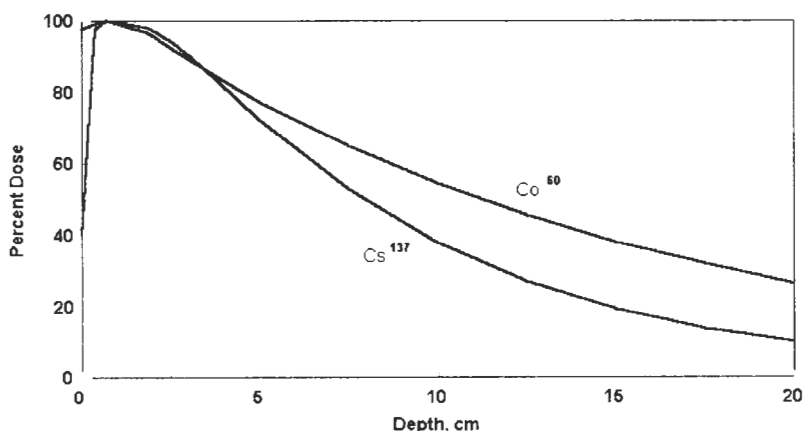


Fig. 3. Dose profile curves for cesium¹³⁷ and cobalt⁶⁰.

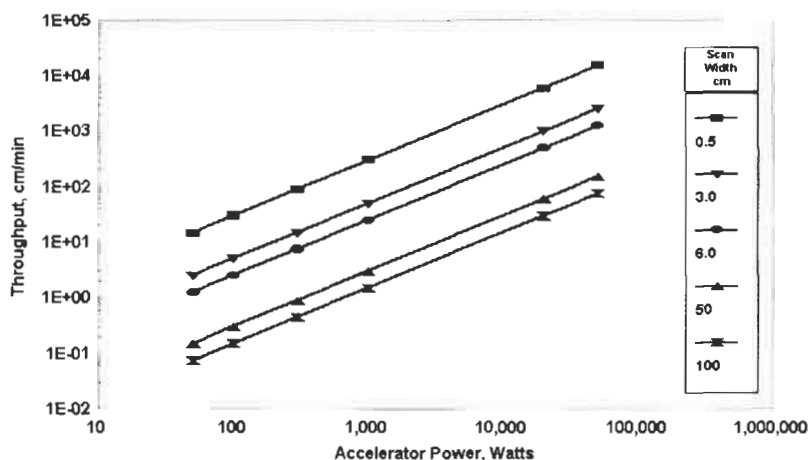


Fig. 4. Throughput versus dose for different accelerator powers.

from two isotopic sources, Cs^{137} and Co^{60} , as function of penetration depth for graphite composite. Gamma rays, from a radioactive source such as cobalt⁶⁰, are equivalent to machine-generated X-rays. In the case of X-rays or gamma rays, there is a gradual decrease in the dose on penetrating a material. Fig. 3 shows that at 50% of the surface dose gamma rays from Co^{60} (Energy: 1.2 MeV) penetrate approximately 10 cm of graphite composite. To achieve maximum properties throughout the composite, surface doses for adhesives and parts will experience significant overdoses. Because of this overdose, these materials would have to be radiation stable in order to maintain their properties. As noted previously, all of the electron-curable resins/adhesives studied are stable to overdoses of at least one order of magnitude

In order to determine the throughput for a particular part, there are several points which must be considered:

- (1) the dose required to cure the adhesive,
- (2) the dose rate of the radiation source (X-ray gamma or electron),
- (3) The absorption efficiency; how much of the available energy is actually absorbed by the adhesive.

For most electron-curable adhesives, a dose of 100 kGy is required to cure. Fig. 4 shows the speed of curing various widths of material as a function of accelerator power. A reasonably controllable speed for moving parts through an accelerator would be approximately 10 m per minute. Based on this criterion, the lower wattage limit for an accelerator curing an adhesive strip 5 cm wide would be 5 kW. For curing very large parts a 50 kW accelerator would be more suitable.

5. Equipment

5.1. General

There are three options for remote repair of composite structures using electron curing; a portable accelerator, X-rays generated from such an accelerator and radioisotopic sources, such as Co^{60} .

5.2. Electron accelerators

There are seven types of electron accelerator available for industrial uses [41]: (1) Van de Graaff generator; (2) Cockcroft–Walton generator; (3) insulated core transformer; (4) parallel coupling, cascading rectifier accelerator; (5) resonant beam transformer; (6) RhodetronTM; (7) linear accelerator (LINAC).

The use of a beam of energetic electrons for repair of advanced composites is feasible if one uses a linear electron accelerator. In this type of accelerator, the electrons move along a straight path either arriving at appropriate gaps in the accelerating structure at the correct time in the period of radio-frequency excitation, or, alternately keeping in step with a moving electromagnetic field, i.e. with a moving wave. The travelling wave accelerator has been shown to be a practical source of high-power beams at reasonable energy and the conversion efficiency from radio-frequency (rf) power to electron beam power can be very high. This type of accelerator is the most economical source when energies in excess of 3 MeV are required [42].

The simplest arrangement for a linear accelerator is shown in Fig. 5. Here a single source, either a self-oscillating magnetron or klystron amplifier with appropriate drive stages, feeds power into a single length of accelerator wave-

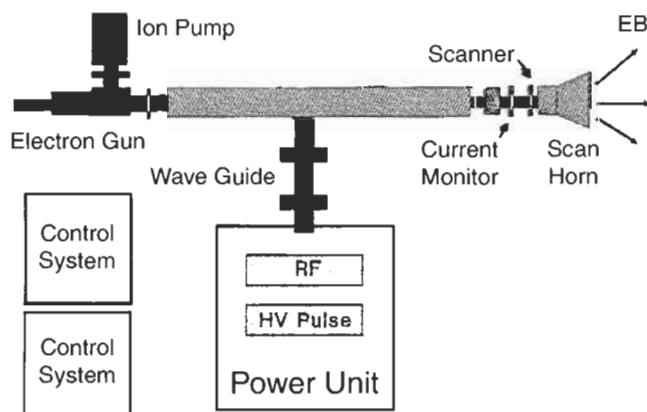


Fig. 5. A simple linear accelerator with radio-frequency feedback.

guide structure. The transition from the normal rectangular wave-guide carrying power from the source into the accelerator, is accomplished by means of a wave-guide transformer. This transition not only provides a matched transfer of the rf power, but also enables a beam of electrons to be fed from an electron gun into the accelerator. A similar arrangement at the output end of the machine allows the accelerated electron beam to exit the accelerator via a thin metallic window. The electron gun may take several forms, the simplest being a diode operating at the same voltage as the rf power source. This allows both to be operated from the same pulser unit. An axial magnetic field is required for focusing. This is easily provided by current-carrying solenoids surrounding the accelerating guide. The above described arrangements may be used for accelerating structures of 1 or 2 m in length. These usually provide energies in the 2–6 MeV range with power outputs of 1 kW when a magnetron power source is used. If a klystron source is used, the power output may be several times greater [42]. An arrangement that has advantage in special circumstances is the use of radio-frequency power feedback. It consists essentially of the combination of any remnant rf power from the output end of the accelerator with the incoming power from the source. The combinations are accomplished in some form of wave-guide bridge circuit. Its most apparent advantage is the elimination of power wastage at the output end of the accelerator, but of course in an efficient accelerator this remnant power would normally be small. The real advantage is rather more subtle, in that the designer is able to produce high-energy accelerators in a compact form. It is best used in accelerators that are arranged to have appreciable remnant rf power at the output, and this when combined with the incoming power creates an increased power flux in the accelerator and thus increases the energy of the electron beam [42].

There are several suppliers of electron accelerators suitable for remote repair of composites, including Varian, Siemens, and Schonberg. At present, the only manufacturer of suitable portable electron accelerators is Schonberg Radiation Corporation of Santa Clara, California. Field repair of damaged aircraft components can be accomplished with a remotely controlled, truck-mounted accelerator. Table 13 gives the characteristics for several electron accelerators, all portable, supplied by Schonberg. Fig. 5 shows a schematic layout of a 10-MeV accelerator [43]. The weights for each component shown indicate that this particular accelerator is suited for mounting on a truck or trailer. The distances between each component are employed to ensure the safety of the workers involved in the repair (see Safety Requirements section).

The technology to routinely cure applied adhesives for repairing damaged composite structures at remote repair stations is currently available. There are already systems that use portable accelerators for X-ray radiographic inspection of aircraft components [43]. Fig. 6 shows a conceptual picture of a portable accelerator unit that would contain the power unit, vacuum systems, and computer

Table 13
X-ray and electron beam characteristics of a typical S-band electron accelerator [40]

Electron beam characteristics	Energy level (MeV)			
	1.5	4.0	6.0	9.0
RF frequency (GHz)	9.3	9.3	9.3	9.3
Accelerator peak current (mA)	30	50	50	20
Accelerator avg. current (mA)	30	50	50	20
Electron beam peak power (kW)	45	200	300	200
Electron beam avg. power (W)	45	200	300	200
Magnetron peak RF power (MW)	0.2	1.5	1.5	1.5
Magnetron avg. RF power (kW)	0.2	1.5	1.5	1.5
Pulse voltage (kV)	23	35	35	35
R.P.F. (pulses/second nominal)	250	250	250	250
Pulse width (microseconds)	4	4	4	4
Duty cycle	0.001	0.001	0.001	0.001
Injection voltage (kV)	17	17	17	17
Gun filament voltage (V)	6	6	6	6
Gun filament current (A)	1.6	1.6	1.6	1.6
Power requirements (VAC)	115/220 1 phase	208–220 3 phase	208–220 3 phase	208–220 3 phase
<i>X-ray output/penetration</i>				
Radiation output (Gy/h), 1 m	1.8	60	180	180
Leakage (%)	1.0	1.0	1.0	1.0



Fig. 6. A 10-MeV portable electron accelerator.

to control the robotics for doing the composite repair. With minor modifications, a tungsten target can be placed in front of the electron horn for X-ray radiography work.

A typical mobile repair station would consist of the following components: (1) a portable power generator; (2) a trailer with the control console, a power conditioning system and protective shielding for the operator; (3) the linear accelerator mounted on a motorized pointing device; (4) a TV monitoring system; and (5) constant speed controls to ensure that the desired dose, with the needed uniformity, is applied to the repair.

6. Safety requirements

Whether a radioisotope or electron accelerator is used for remote repair, its method of operation must be such that during normal use any radiation exposure to workers is very low and there is no significant exposure to individual members of the public. X-ray and electron beam sources produce high dose rates, and personnel cannot be in the immediate vicinity of the equipment during operation. As an alternative, temporary shielding, usually lead blocks, can also be used as an additional safety feature. The risk of accidental exposure can be kept to a minimum by proper design, with specific attention to such areas as shielding and interlocks, and a good radiation protection program.

The objectives of radiation safety are [44]:

- (1) To ensure that during normal operation, maintenance and decommissioning, and in emergency situations, the radiation exposure to both workers and the public is kept as low as reasonably achievable, economic and social factors being taken into account.
- (2) To ensure that during normal operation, maintenance and decommissioning, and in emergency situations, the radiation exposure to workers and the public is kept below the dose limits given in the Basic Safety Standards for Radiation Protection (BSS). The standards are set at a maximum of 5 REM annually and a maximum of 3 REM quarterly.
- (3) To ensure that the probability of events giving rise to significant exposures and the magnitude of such exposures are kept as low as reasonably achievable, economic and social factors being taken into account.

A specific system design for a remote repair depends heavily on several factors, as discussed. In order to achieve and maintain the required reliability, the following design principles should be applied.

- (1) *Defence in depth*. The design process should ensure that multiple levels of protection are provided and the necessity of human intervention is minimized.
- (2) *Redundancy*. Redundancy is the use of more than the minimum number of items required to accomplish a given safety function. This allows the failure or unavailability of one item to be tolerated without loss of function.
- (3) *Diversity*. Diversity is applied to redundant systems or components that

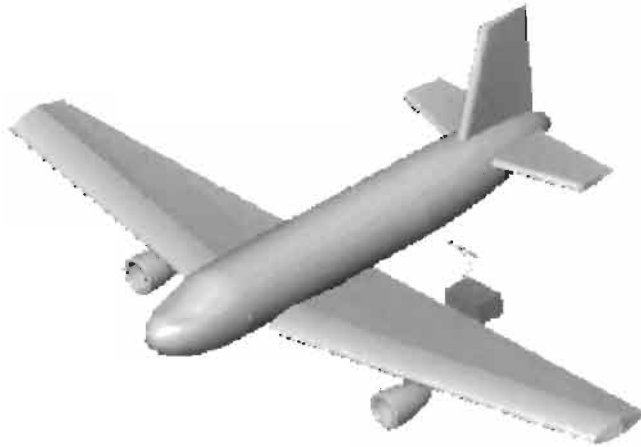


Fig. 7. Portable electron accelerator setup for on-aircraft repair.

perform the same safety function by incorporating different attributes into the systems or components.

- (4) *Independence*. Independence is achieved in the design of systems through functional isolation and physical separation.
- (5) *Programmable electronic systems*. Increasing programmable electronic systems are being used in safety control applications. Problems can arise relating to the integrity of the hardware and validation of the software, leading to faults in the system.
- (6) *Safety analysis*. A formal method of assessment should be used. Each component within the system should be considered in turn. The likely types of failure and their consequences for the system should be taken into account. This should include consideration of the reliability of operating procedures, where safety depends upon them, and should encompass both inadvertent and deliberate failure to follow procedures.

The main safety consideration when using a high-energy electron source for repair of aircraft components in the field is the protection of workers operation. Fig. 7 shows a particular repair using a portable accelerator. There are two ways of protecting the worker. One way is to remove the worker to a distance from the electron source where the radiation fields produced were not harmful. The second method would be to provide adequate shielding for the worker. The most economical method would be using distance from the radiation source. The worker could control the repair process from a remote trailer which was located a safe distance from the component being repaired. A suitable, quickly dismantled enclosure such as a curtain could be placed around the perimeter of the safe distance to prevent other people from entering the area.

Table 14

Basic component costs (in \$, times 1000) for remote repair facility

Equipment	Beam energy (MeV)			
	1.5	4.0	6.0	9.0
Electron accelerator	215	375	425	525
Field generator	2	3	3	3
Robotic system	200	200	200	200
Total	417	578	628	728

7. Facility costs

The facility costs are based on the concept of a mobile remote repair facility. The advantages of this concept are low-cost, minimal shielding requirements, and flexible use of the overall repair facility. The main components for a remote repair are the electron accelerator, the power supply, and the robotic control system including the remote video system. Table 14 shows the estimated costs for these main components.

The cost of the vehicle to move the accelerator, and temporary shielding, if needed, have not been included in Table 14. The vehicle houses the control console, video system, and robotic controls. A trailer would carry the main robotic system, the electronic accelerator, magnetron, and the supplies. The cost for such a vehicle and trailer is estimated at \$100,000.

8. Summary

Advanced composites, like other materials, are subject to damage and can be repaired. Electron curing can be used for repairing advanced composites, particularly for delamination and impact damage. The advantages of using an electron accelerator are faster curing cycles, short turn-around time, and higher-temperature-resistant bonds cured at ambient temperatures.

An electron-curable structural adhesive formulation usually consists of one or more crosslinkable oligomeric resins or prepolymers, along with such additives as reactive diluents, plasticizers, and wetting agents. The most commonly used resins for electron-curable adhesives are oligomers containing two or more reactive groups. The two principal classes of oligomer are acrylates and epoxides. Acrylates cure by free radical mechanisms and epoxides cure by cationic mechanisms in the presence of certain initiators. The development of iodonium and sulfonium salt cationic initiators, has greatly increased the number of resins suitable for electron curing, including traditional epoxies. Several commercially

available adhesives (acrylates and methacrylates), when electron cured, meet the manufacturer's specifications for mechanical strength.

Penetration energy and cure speed are two key design parameters when considering electron curing of adhesives. The penetration limit of 10-MeV electrons is about 2 cm in graphite composite. If a penetration greater than 2 cm is needed, then X-rays generated from 10-MeV electrons (~ 3 -MeV X-rays) can penetrate about 10 cm of composite. For most electron-curable acrylate adhesives, the dose required to cure is about 50 kGy. With an expected absorption efficiency of about 10%, a 1-kW electron accelerator can routinely cure about 7 kg/h of adhesive. There are commercially available portable accelerators that are well-suited for remote repair of composites. A mobile repair station consists of a power supply, a trailer with control console, a power conditioning system and protective shielding, a linear accelerator, and a beam delivery system. Electron accelerators produce radiation, and personnel cannot be near the beam. The risk of accidental exposure can be kept to a minimum by proper design, with specific attention to such areas as shielding and interlocks, and a good radiation protection program.

The cost of a remote repair facility ranges from about \$500,000 to \$730,000, depending on the beam energy and power required. The current power range available for a portable accelerator is 45 to 300 W, with the energies varying from 1.5 to 9 MeV.

Glossary

APC-2	Aromatic Polymer Composite-2. This is a polyether-etherketone, thermoplastic polymer matrix from ICI Fiberite.
AS-4	Fiber produced by carbonizing precursor fibers based on polyacrylonitrile. AS-4 is produced by Hexcel Corporation and is available with 3000, 6000 and 12000 filaments per tow. For example 'AS-4 3K GP' is AS-4 fiber with 3000 filaments and with GP epoxy sizing applied.
BON AMI	A scouring cleanser from Faultless Starch/Bon Ami Company.
Cockcroft-Walton Generator	Named after John Douglas Cockcroft (1897-1967) and Ernst Thomas Sinton Walton (1903-), the Cockcroft-Walton Generator is based on a voltage multiplier scheme that produces a graded series of voltages. This system has the advantage of dissipating much less power than a resistive voltage divider.

CRADA	Cooperative Research and Development Agreement. A CRADA is designed to involve industrial and government labs in cooperative research programs. A CRADA typically has provisions for sharing technical resources, protecting confidentiality, and treatment of intellectual property. The subject CRADA was sponsored by the US Department of Energy (DOE).
Gammacell	The Gammacells utilize the radioisotope cobalt-60 (Co-60) that decays to nickel-60 by beta (electron) emission along with two gamma rays. Gamma rays and X-rays are essentially the same, differing only in their origins: gamma rays are produced by an excited nucleus in an attempt to reach a ground state; X-rays come from the orbiting electrons as they move from a higher to lower shell level.
kGy	SI unit for a measure of absorbed dose. $1 \text{ kGy} = 1 \text{ kJ/kg}$.
Rhodetron	A compact, high power electron beam accelerator that can be configured with outputs ranging from 3 to 10 MeV in a continuous wave mode. The Rhodetron derives its name from the pattern of the electrical field in the single coaxial-shaped cavity that is rose-shaped ('rhodos' in Greek). IBA of Belgium is the supplier of this accelerator.
SCOTCH-BRITE	A product of 3M TM Company. SCOTCH-BRITE hand pads come in general purpose and ultra fine grade.

References

1. Kerluke, D.R. and McKeown, J., The commercial launch of IMPELA. *Radiat. Phys. Chem.*, **42**, 511–514 (1993).
2. Ungrin, J., Drewell, N.H., Ebrahim, N.A., Labrie, J.-P., Lawrence, C.B., Mason, V.A. and White, B.F., IMPELA: An industrial accelerator family. *Proc. Eur. Part. Acc. Conf., EPAC*, p. 1515, 1988.
3. Crivello, J.V., Electron beam curable epoxy compositions, US Patent 5,260,349, 1993.
4. Janke, C.J., Dorsey, G.F., Havens, S.J. and Lopata, V.J., A toughened epoxy resin system and a method thereof, US Patent 5,726,216, 1998.
5. Janke, C.J., Lopata, V.J., Havens, S.J., Dorsey, G.F. and Moulton, R.J., High energy electron beam curing of epoxy resin systems incorporating cationic photoinitiators, US Patent 5,877,229, 1999.
6. CRADA, No. Y1293-0233; Electron Beam Curing of Polymer Matrix Composites; Department of Energy Defense Programs; Participants: Lockheed Martin Energy Systems Inc., Lockheed Martin Sandia Corporation, AECL Technologies Inc., Applied Poleramics Inc., The Boeing Company, Ciba-Geigy Corporation, E-Beam Services Inc., Nicolet Corporation, Lockheed Martin Tactical Aircraft Systems, Lockheed Martin Aero and Naval

- Systems, Northrop-Grumman Corporation, UCB Radcure Inc., 1994.
7. CRADA, DOE Contract: DE-AC05-96OR22464; Interfacial properties of Electron Beam Cured Composites; Participants: US Department of Energy, Oak Ridge National Laboratory, Air Force Research Laboratory, NASA Langley, Acsion Industries, Adherent Technologies, Applied Poleramics, The Boeing Company, BP Amoco, E-BEAM Services, Hexcel, Lockheed Martin Aeronautics Corporation, STERIS Isomedix Services, UCB Chemicals Corp., YLA Inc., Michigan State University, Canadian National Research Council Industrial Materials Institute, and Canadian National Research Council Institute for Aerospace Research, 1999.
 8. Goodman, D.L. and Byrne, C.A., Phase-separated dual-cure elastomeric adhesive formulations and methods of using the same. US Patent 5,997,682.
 9. Campbell, F.J. and Brenner, W., Curing high performance structural adhesives by electron-beam radiation. *Nav. Eng. J.*, June, p. 160 (1982).
 10. Lopata, V.J., Chung, M., McDougall, T.E. and Weinberg, V.A., Electron-curable adhesives for high-performance structures. *39 Int. SAMPE Symp.*, Apr. 11–14, 1994.
 11. Huber, H.F., Radiation cured adhesives. *Beta-Gamma*, **1**, 3 (1992).
 12. Woods, J.G., Radiation-curable adhesives. In: Pappas, S.P. (Ed.), *Radiation Curing, Science and Technology*. Plenum Press, New York, 1992.
 13. Rebenfeld, L., The research approach to fiber composites. *Proc. Annu. Ind. Fabr. Assoc. Int. Conv.*, 74th, 13–21. Ind. Fabr. Assoc. Int., St. Paul, MN, 1986.
 14. Petrie, E.M., *Handbook of Adhesives and Sealants*. McGraw-Hill, 2000.
 15. Wu, S.Y., Schuler, A.M. and Keane, D.V., Adhesive bonding of thermoplastic composites 1. The effect of surface treatment on adhesive bonding. *19th Int. SAMPE Symp.*, Oct. 13–15, 1987.
 16. Saunders, C.S. and Lopata, V.J., Electron beam processing of advanced composites; DREP Final Report (1994); Contract No. W7708-2-0001/01-XSA; Department of National Defence Defence Research Establishment Pacific, FMO Victoria, Canada, 1994.
 17. Lopata, V.J., Chung, M., Janke, C.J. and Havens, S.J., Electron curing of epoxy resins: initiator and concentration effects on curing dose and rheological properties. *28th Int. SAMPE Technical Conference*, 901, 1996.
 18. Luck, R.M. and Sadhir, R.K., Shrinkage in conventional monomers during polymerization. In: Sadhir, R.K. and Luck, R.M. (Eds.), *Expanding Monomers, Synthesis, Characterization and Applications*. CRC Press, Boca Raton, FL, 1992, p. 5.
 19. Packham, D.E. (Ed.), *Handbook of Adhesion*. Wiley, New York, 1992, pp. 369–371.
 20. Crivello, J.V., Lam, J.H.W., Moore, J.E. and Schroeter, S.H., *J. Radiat. Curing*, **5**, 2 (1978).
 21. Crivello, J.V., Diaryliodonium salts. US Patent 4,310,469, 1982.
 22. Crivello, J.V., *Adv. Polym. Sci.*, **61**, 1 (1984).
 23. Crivello, J.V. and Lee, J.L., The synthesis, characterization and photoinitiated cationic polymerization of silicon-containing epoxy resins. *J. Polym. Sci. Polym. Chem. Ed.*, **28**, 479–503 (1990).
 24. Crivello, J.V., Electron beam curable epoxy compositions. US Patent 5,260,349, 1993.
 25. Fox, F.J. and Noren, R.W., Catalyst for condensation of hydrolyzable silanes and storage stable compositions thereof. US Patent 4,101,513, 1978.
 26. McGinniss, V.D., *Photogr. Sci. Eng.*, **23**, 124 (1979).
 27. Koleske, J.V., Photocopolymerizable compositions based on epoxy and polymer/hydroxyl-containing organic materials. US Patent 4,593,051, 1986.
 28. Davidson, S.R. and Wilkinson, S.A., electron-beam-induced polymerization of epoxides. *J. Photochem. Photobiol. A: Chem.*, **58**, 123–134 (1991).
 29. Crivello, J.V., Walton, T.C. and Malik, R., *Chem. Mater.*, **9**, 1273–1284 (1997).

30. Janke, C.J., Dorsey, G.F., Havens, S.J. and Lopata, V.J., Electron beam curing of epoxy resins by cationic polymerization. *41st International SAMPE Symposium*, 196, 1996.
31. Janke, C.J., Dorsey, G.F., Havens, S.J. and Lopata, V.J., Toughened epoxy resins cured by electron beam radiation. *28th International SAMPE Technical Conference*, 877, 1996.
32. Janke, C.J., Electron beam curable cationic epoxy resin systems and composites. *1st Annual Electron Beam Curing of Composites Workshop*, September 18–19, Oak Ridge, TN, Ref. 1D, 1996.
33. Lapin, S.C., *Proc. RADCURE '86*, Baltimore, MD, p. 15-15, 1986.
34. Dougherty, J.A., Vara, F.J. and Anderson, L.R., *Proc. RADCURE '86*, Baltimore, MD, p. 15-1, 1986.
35. Dickson, L.W. and Singh, A., *Radiat. Phys. Chem.*, **31**, 587 (1988).
36. Tabata, Y., Ito, Y. and Tagawa, S., *CRC Handbook of Radiation Chemistry*. CRC Press, Boca Raton, FL, 1991.
37. CRADA, ORNL99-0544, Interfacial Properties of Electron Beam Cured Composites, 1999.
38. Klein, A.J., Repair of composites. *Adv. Composites*, June/July, p. 50 (1987).
39. Armstrong, K.B., In: Packham, D.E., (Ed.), *Handbook of Adhesion*, with references. Wiley, New York, 1992, pp. 374–378.
40. Technical Datasheet, MINAC System, Schonberg Radiation Corporation, Santa Clara, CA 95054.
41. Sheien, B. and Terpilak, M.S. (Eds.), *The Health Physics and Radiological Health Handbook*. Nucleon Lectern Associates, Inc., 1984.
42. Miller, C.W., Power sources for irradiation processing the linear accelerator. In: Charlesby, A. (Ed.), *Radiation Sources*. The MacMillan Company, New York, 1964, pp. 197–219.
43. Schonberg, R.G., Radiation considerations for operation of a portable 6-MeV Electron Linear Accelerator. *Proceedings 20th Midyear Topical Symposium, Health Physics Society*, Reno, NV, February 8–12, 1987, p. 297.
44. Radiation Safety of Gamma and Electron Irradiation Facilities, Safety Series No. 107, International Atomic Energy Agency, Vienna, 1992.

Wood adhesives

M. DUNKY ^a and A. PIZZI ^{b,*}

^a *DYNEA, Krems, Austria*

^b *ENSTIB, University of Nancy 1, Epinal, France*

1. Introduction

Progress in research and development in the wood-based industry and in the adhesive industry has shown many successes during the last decades. On the other hand, many industrial requirements still require considerable and important developments in this area. The main driving forces today are ‘cheaper’, ‘quicker’ and ‘more complex’. The first two are caused by the heightened competition in the above-mentioned industries and the attempt to minimize costs while maintaining a certain level of product quality and performance. The key word ‘more complex’ stands for new and specialized products and processes. Adhesives play a central role in wood-based panel production. The quality of bonding, and hence the properties of the wood-based panels, are determined mainly by the type and quality of the adhesive. Development in wood-based panels, therefore, is always linked to development in adhesives and resins.

Both the wood-based panel industry and the adhesive industry show a high commitment to and great capability towards innovation. The best evidence for this is the considerable diversity of types of adhesives used for the production of wood-based panels. Well-known basic chemicals have been used for a long time for the production of the adhesives and their resins, the most important ones being formaldehyde, urea, melamine, phenol, resorcinol and isocyanate. The greater portion of the currently used adhesive resins and adhesives for wood-based panels is produced with these few raw materials. The ‘how to cook the resins’ and the ‘how to formulate the adhesive’ become more and more complicated and sophisticated and are key factors to meet today’s requirements of the wood-based panel industry.

* Corresponding author. E-mail: pizzi@enstib.uhp-nancy.fr

The quality of bonding and hence the properties and the performance of the wood-based panels and beams are determined by three main parameters: (1) the wood, especially the wood surface, including the interface between the wood surface and the bond line; (2) the adhesive; (3) the working conditions and process parameters.

Good-quality bonding and sufficient properties of the wood-based panels can be attained only if each of these three parameters contributes to the necessary extent to the bonding and production process.

2. Wood as a substrate

Wood is a natural composite made of approximately 60–65% carbohydrate fibers, 25–30% of a random polyphenolic branched polymer (lignin, functioning as a binder) and 10% of residues, extractables or cellular waste infiltrates (oleoresins, tannins, starches, some inorganic salts etc.) coating the porous cellular surfaces. The carbohydrate fraction is composed of linear cellulose homopolymers (40–45%) interspersed and intertwined with heterogeneous short-chain polysaccharides called hemicelluloses (20–25%). As much as cellulose and lignin present specific gravities of 1.4 and 1.5, respectively, wood itself has a much lower density due to its porous, honeycomb structure in which the longitudinally aligned intracellular matrix cellulose fibers, or tracheides, have inner open spaces with diameters of 4–25 μm . Depending on the type of wood species the fiber cells may present open or closed ends as well as interconnected pits, each of roughly 200 nm diameter, which may or may not allow liquids and air to penetrate from one fiber into another [1]. Wood is then volumetrically of much lower density than its own fibers and of synthetic resins and fibers. The cellulose fibers are polar and shrink and swell on drying or wetting, and are useful in adhesion to wood.

In hardwoods, morphological structural elements in longitudinal series comprise the segmented structure termed 'vessel'. Vessels, which are exposed in transverse section, constitute about 10–46% of the stem volume in deciduous hardwoods and are cells of relatively large diameters (50–300 μm). Vessels have in short the appearance of open vertical tubes within the wood structure because their end walls have partially dissolved. By comparison, the hardwood vessel diameter can be as much a 10 times the diameter of a softwood fiber.

Because the porous growth patterns of wood vary, the densities of various dry woods also vary (200–1200 kg/m^3). The porosity of wood, of course, greatly influences the wood's utility as a substrate. The wood porosity affects also the type and form of the adhesive as it affects the ability of the substrate to absorb water and other solvents from the adhesive, as well as allowing some of the adhesive to be absorbed over larger surface areas.

Lignin, a random and branched polyphenolic polymer, encrusts and bonds the

intracellular cellulose fibers. It is only moderately polar. The cavities or lumens of dried wood cells are lined with a variety of organic compounds deposited there after having been generated by the tree. Collectively these materials are called 'extractives' as they are relatively easy to extract with water or organic solvents; they also tend to determine the pH of the wood surface. Depending on the nature of these compounds, they may strongly hinder or favor wood bonding, and notwithstanding their low proportion, these wood metabolites play an inordinately important role in wood glueing.

3. Types of wood adhesives

In the wood and building industry a great variety of adhesives is currently in use, with the greatest variety being used in the wood panel industry. Condensation resins based on formaldehyde represent the biggest volume within the wood adhesives industry. These resins are formed by the reaction of formaldehyde with various chemicals like urea, melamine, phenol or resorcinol or with combinations of these substances. These adhesive resins are mainly liquid and consist of primarily linear or branched oligomeric and polymeric molecules in an aqueous solution but also, partly, of a dispersion of molecules in the same aqueous solutions. During hardening and gelling they convert to insoluble and non-melting three-dimensionally crosslinked networks. The hardening conditions can be acidic (aminoplastic resins), highly alkaline (phenolic resins) or neutral to light alkaline (resorcinol resins, tannins). Isocyanates (especially PMDI, polymeric 4,4'-diphenyl methane diisocyanate) are another important chemical group of adhesives used for various applications in the wood industry. These latter are not based on formaldehyde. Table 1 gives an overview on the fields of application for various wood adhesives.

4. Overview of requirements concerning wood adhesives

The consumption of resins for wood adhesives in North America and Europe in 1997 and 1999, respectively, based on resin solids, were as shown in Table 2.

The necessity to achieve shorter press times is omnipresent within the wood industry, based on the constant pressure on costs and prices. Increased production rate gives the chance to reduce production costs, as long as the market takes up the surplus products.

Shorter press times in a given production line for a certain type of wood-based panel can be attained, in the following ways:

- Highly reactive adhesives with quick gelling and hardening behavior and steep increases in bonding strength even at a low degree of chemical curing.

Table 1
Fields of application for various wood adhesives

Type	V20	V100	V313	FP	MDF	PLW	HLB	MH	Ven.	Furn.
UF	x				x	x	x	x	x ^a	x ^a
MUF	x ^b				x					
MF/MUF		x ^c	x		x	x	x	x		
MUPF		x			x	x				
PF/PUF		x		x	x	x				
RF							x			
PMDI	x	x			x					
PVAc							x	x	x	x
Old nat. adhesives										x
Nat. BM	x	x	x		x	x				
Inorg. BM	x			x ^d						
Activation				x						

UF: urea-formaldehyde resin.

MUF: melamine-fortified UF-resin.

MF/MUF: melamine- and melamine-urea-resins; MF-resins are only used mixed with UF-resins.

MUPF: melamine-urea-phenol-formaldehyde-resin.

PF/PUF: phenol-formaldehyde and phenol-urea-formaldehyde-resin.

(P)RF: resorcinol-(phenol-) formaldehyde-resin.

PMDI: polymethylenediisocyanate(polymeric 4,4'-diphenylmethane diisocyanate).

PVAc: polyvinylacetate adhesive.

Old nat. adhesives: old (historic) natural adhesives, e.g. starch, gluten, casein adhesives.

Nat. adhesives: natural adhesives (tannin, lignin, carbohydrates).

Inorg. adhesives: inorganic adhesives: cement, gypsum.

Activation: activation of wood inherent adhesives.

V20: particleboard interior according to EN 312-2 to 4 and -6 [2].

V100: particleboard exterior according to EN 312-5 and 7, option 2 [2] (internal bond after boil test according to EN 1087-1 [3]).

V313: particleboard exterior according to EN 312-5 and 7, option 1 [2] (cycle test according to EN 321 [4]).

FP: hardboard (wet process) according to EN 622-2 [5].

MDF: medium-density fiberboard according to EN 622-5 [6].

PLW: plywood according to EN 636 [7] with various resistance against influence of moisture and water.

HLB: laminated beams.

MH: solid wood panels according to prEN 12775, prEN 13353 part 1 to 3, prEN 13017-1 and 2, prEN 13354 [8].

Ven.: veneering and covering with foils.

Furn.: production of furniture.

^a Partly powder resins.

^b Boards with reduced thickness swelling, e.g. for laminate flooring.

^c Only possible as MUF + PMDI.

^d Special production method.

Table 2

Estimated consumption of wood adhesives solids in North America and Western Europe (in 1000 metric tons)

Polymer type	North America ^a	Western Europe ^b	Total
Urea-formaldehyde (UF)	960	2600	3560
Melamine-urea-formaldehyde (MUF)	—	350	350
Phenol-formaldehyde (PF)	567	260	827
Isocyanates	50	100	150
Resorcinols (PRF)	12	6	18

^a 1997.

^b 1999.

- Highly reactive adhesive mixes produced by including accelerators, special hardeners, crosslinkers and other materials.
- Optimization of the pressing process, e.g. by increasing the effect of the steam shock by (1) increased press temperatures, (2) additional steam injection, or (3) an increased gradient in the moisture content difference between surface and core layer.
- By maintaining constant, as long as possible, as many parameters of the production process as possible.

Cheaper raw materials are another way to reduce production costs. This includes, e.g., the minimization of the melamine content in a MUF-resin. An impeding factor can be the (often temporary) shortage of raw materials for the adhesives, as it was the case with sudden price increases for methanol (from which formaldehyde is obtained industrially) and melamine within the last decade.

Adhesives and resins are one of the most important raw materials in wood-based panels. Thus, each question concerning the life cycle assessment and the recycling of bonded wood panels does bring into question the adhesive resins used. This includes, for example, the impact of the resin on various environmental aspects such as waste water and effluents, emission of noxious volatile chemicals during production and from the finished boards, or the reuse for energy generation of wood panels. The type of resin has also a crucial influence on feasibility and efficiency for several material recycling processes.

Emission of volatile noxious chemicals from wood-based panels during their production can be caused by chemicals inherent to wood itself, like terpenes or free acids, as well as by volatile compounds and residual monomers of the adhesive. The emission of formaldehyde as well as free phenol effluents is a matter of concern.

Formaldehyde emission from finished panels is due to the residual formaldehyde present as a gas in the wood and recesses of UF-bonded and MUF-bonded boards as well as dissolved in the boards residual moisture content. On the other

Table 3

Actual regulations conc. the subsequent formaldehyde emission from wood-based panels (Germany) according to the German Regulation of Prohibition of Chemicals (former Regulation of Hazardous Substances)

-
- (a) Maximum steady-state concentration in a climate chamber:
0.1 ppm (prEN 717-1; 1995 [8])
- (b) Laboratory test methods (based on experimental correlation experiences):
- PB: 6.5 mg/100 g dry board as perforator value (EN 120; 1992 [10])
 - MDF: 7.0 mg/100 g dry board as perforator value (EN 120; 1992 [10])
 - Plywood: 2.5 mg h⁻¹ m⁻² with gas analysis method (EN 717-2 [11])
- PB and MDF: correction of the perforator value to 6.5% board moisture content
-

hand the hydrolysis of weakly bonded formaldehyde from *N*-methylol groups, acetals and hemiacetals as well as in more severe cases of hydrolysis (e.g. at high relative humidity or higher temperatures) from methylene ether bridges, increases further the content of emittable formaldehyde. Contrary to phenolic and polyphenolic resins where an emission problem does not occur, in aminoplastic resin-bonded wood panels, a permanent stream of supplementary, emittable formaldehyde is generated from these weakly bonded structures. This explains the constant (although nowadays low) release of formaldehyde from UF-bonded wood-based panels even over longer periods. However, unpleasantly high emissions of this excess of emittable formaldehyde depend on conditions. The higher the hydrolysis rate, the higher is the proportion of formaldehyde which contributes to the subsequent formaldehyde emission from the wood panel.

The so-called E1-emission class describes a wood panel presenting formaldehyde emission which is low enough to prevent any danger, irritation or inflammation of the eyes, nose and mouth mucous membranes. However, it is important that not only the boards themselves, but also the veneering and carpenter's adhesive resins, laquers, varnishes and other sources of formaldehyde are under control, since they also might contribute to the mixture steady state formaldehyde concentration [9]. Table 3 gives an overview on some European regulations. However, it is necessary here to introduce the principal types of composite wood products, especially panels, that are produced in this industry:

Particleboard: a flat pressed wood composite panel composed of randomly oriented wood chips bonded by hot-pressing by using thermosetting adhesive resins, mainly urea-formaldehyde (UF), melamine-urea-formaldehyde (MUF), phenolic resins (PF and TF) and isocyanates (pMDI). The board is generally composed of three distinct layers, the surface layers being composed of finer wood chips than the coarser core layers. Some processes yield a continuously chip-size-graded board along the surface/core/surface thickness. The panel has generally a density of 680–700 kg/m³ and the average amount of resin solids in

the board core section is between 6% and 12% on dry wood (although lower and much higher percentages are also sometime used). Panels of the same type but composed of wood chips of greater length and greater width but similar thickness are called also *flakeboard* and *waferboard*.

Medium-density fiberboard (MDF): a flat pressed wood composite panel composed of randomly oriented wood fibers obtained by thermomechanical wood pulping and bonded by hot-pressing by using thermosetting adhesive resins. The panel has generally a density of approximately 850 kg/m^3 and the average amount of resin solids in the board core section is between 11% and 14% on dry wood.

Oriented strand board (OSB): a flat pressed three-layer wood composite panel composed of oriented wood wafers bonded by hot-pressing by using thermosetting adhesive resins. The very thin wafers (length and width are very much bigger than in particleboard and of the order of $100 \times 20 \text{ mm}$, respectively) are oriented in the same direction within the same layer and at 90° of each other in adjacent layers yielding a particularly strong panel very suitable for structural applications. It is the modern competitor of plywood but at a much cheaper price. The lower surface area of the wafers in relation to other types of panel yield panels that need to be bonded with only 4–5% adhesive solids on dry wood. It is today the main substitute panel for the rather more expensive plywood, but presenting the same advantages.

Hardboard (high-density fiberboard): a flat pressed wood composite panel composed of randomly oriented wood fibers obtained by thermomechanical wood pulping and traditionally bonded without any adhesive by hot-pressing simply by the very high density ($900\text{--}1100 \text{ kg/m}^3$) and the high-temperature-induced flow of the lignin component of the fibers. Panels containing a small amount of adhesives (2–3% adhesive solids on dry fiber), generally PF resins, are often produced today to upgrade the properties of the panel.

Plywood: a flat pressed multilayer wood panel composed of oriented wood veneers bonded by hot-pressing by using thermosetting adhesive resins. The veneers wood grain is oriented at 90° of each other in adjacent layers yielding a particularly strong panel. As a consequence this is the panel with the best strength/weight ratio but is rather expensive in relation to the equally strong OSB.

Laminated veneer lumber (LVL): a flat pressed multilayer wood panel similar to plywood composed of oriented wood veneers but differently from plywood oriented all in the same direction in all the layers and bonded by hot-pressing by using thermosetting adhesive resins.

Laminated beams (glulam), parallam (or LSL) and fingerjoints: a flat pressed multilayer wood beam, thick wood planks constituting the layers, used for structural exterior applications and bonded with PRF (phenol–resorcinol–formaldehyde) cold-setting resins, or MUF cold-setting resins, or even with certain types of polyurethanes (although the use of these latter ones is only established in one country and can show creep and temperature-induced creep problems). The indi-

vidual wood planks are bonded to the necessary length to compose the beam by fingerjoints bonded with one of the same three adhesives above.

Parallam, or laminated strand lumber (LSL) is a beam made by a continuous manufacturing process composed of bigger-size wood needles (very elongated wood particles) reassembled with a structural exterior grade adhesive, the favorite adhesive being isocyanates (pMDI) when heat-curing and PRFs when cold-curing.

This problem, namely the formaldehyde emission of the wood panel in service, after its manufacture, can be fortunately regarded to day as more or less solved, due to unequivocal and stringent regulations in many European countries, and successful long-term joint R&D in the adhesives and wood-working industries.

5. UF-resins

Urea-formaldehyde resins [9,12–18] are based on the manifold reactions of urea and formaldehyde. Using different conditions of reaction and preparation a more or less innumerable variety of condensed structures is possible. UF-resins are thermosetting resins and consist of a mix of linear or branched oligomers and polymers, always containing some amount of monomers. Unreacted urea is often welcome to achieve special effects, e.g. a better storage stability. Free formaldehyde, however, can have an ambivalent role. On the one hand it is necessary to induce the hardening reaction, while on the other hand it causes a certain amount of formaldehyde emission during the press cycle. At times, even in the hardened state some residual formaldehyde leads to some displeasing subsequent emission from the finished boards. This fact has changed significantly UF-resin composition and preparation during the last 20 years. The problem of the subsequent formaldehyde emission can be attested to have now been solved for at least the last 10 years. This is especially true in parts of Europe, where the most stringent formaldehyde emission regulations are in place.

After hardening, UF-resins consist of insoluble, more or less three-dimensional networks and cannot be melted or thermoformed again. At their application stage, UF-resins are still soluble or dispersed in water or are spray dried powders, which in most cases are redissolved and redispersed in water for application.

Despite the fact that the two main components of UF-resins are urea and formaldehyde, a broad variety of possible reactions and structures in the resins can be obtained. At the molecular level, the basic characteristics of UF-resins can be explained as follows: (1) high reactivity; (2) water solubility and dispersibility, which renders the resins ideal for use in the woodworking industry; and (3) the reversibility of the aminomethylene link, which also explains the low resistance of the UF-resins against the influence of water and moisture, especially at higher temperatures. This is also one of the reasons for the subsequent formaldehyde emission.

The reaction of urea and formaldehyde to form UF-resins is basically a two-step process, usually an alkaline methylation followed by an acidic condensation.

The methylation step, which usually is performed at high formaldehyde (F) to urea (U) molar ratio ($F/U = 1.8$ to 2.5), consists of the addition of up to three (four in theory) molecules of the bifunctional formaldehyde to one molecule of urea to give the so-called methylolureas. The types of methylolureas formed and their relative proportions depend on the molar ratio, F/U . Each methylation step has its own rate constant k_i , with different values for the forward and the backward reaction. The formation of these methylols mostly depends on the molar ratio, F/U , and tends with higher molar ratios to the formation of higher methylolated species.

The UF-resin itself is formed in the acid condensation step, where the same high molar ratio as in the alkaline methylation step is used ($F/U = 1.8$ to 2.5): the methylolureas, urea and the residual free formaldehyde react to form linear and partly branched molecules with medium and even higher molar masses, forming polydispersed UF-resins composed of oligomers and polymers of different molar masses. Molar ratios lower than approx. 1.7 – 1.8 during this acid condensation step might cause resin precipitation.

The low molar ratio of the final UF-resin is adjusted by the addition of the so-called second urea, which might also be added in several steps [16–18]. Particular care and know-how are needed during this acid condensation step in order to produce resins of good performance, especially at the very low molar ratios usually in use today in the production of particleboard and MDF. This last reaction step generally also includes the vacuum distillation of the resin solution to the usual 63–66% solid content syrup in which form the resin is delivered. The distillation is performed in the manufacturing reactor itself or in a thin layer evaporator. Industrial preparation procedures are usually proprietary and are described in the literature in only a few cases [17–19].

The type of bridges existing between the urea molecules in the resin depends on the conditions used. Methylene ether bridges ($-\text{CH}_2-\text{O}-\text{CH}_2-$) as well as the more stable methylene bridges ($-\text{CH}_2-$) are both formed in different relative proportions according to the conditions used. Methylene ether bridges rearrange with temperature-induced relative ease to methylene bridges with emission of one molecule of formaldehyde. One ether bridge needs two formaldehyde molecules to form it and, additionally, it is not as stable as a methylene bridge. It is highly recommended to avoid and minimize, when possible, the proportion of such ether groups in UF-resins.

In the literature, various other types of resin preparation procedures are described, e.g. yielding uron structures [20–22] or triazinone rings in the resins [23,24]. The last ones are formed by the reaction of urea and an excess of formaldehyde under basic conditions in the presence of ammonia or an amine, respectively. These resins are used to enhance the wet strength of paper.

In the UF-resin itself, different chemical species are present:

- Free formaldehyde, which is in steady state equilibrium with the remaining methylol groups and the post-added urea
- Monomeric methylols, which have been formed mainly by the reaction of the post-added urea with the high content of free formaldehyde at the still high molar ratio of the acid condensation step
- Oligomeric methylols, which have not reacted further in the acid condensation reaction or which have been formed by the above-mentioned post-added urea reaction
- Molecules with higher molar masses, which are resin molecules in the closer sense of the word.

The condensation reaction and the increase of the molar mass can also be monitored by GPC [25]. With longer duration of the acid condensation step, oligomers of higher molar masses are progressively formed.

Forced by the necessity to limit the subsequent formaldehyde emission, the UF-resin molar ratio, F/U, has been progressively decreased to very low values. The main differences between UF-resins with high and with low content of formaldehyde, are: (1) the reactivity of the resin due to the different content of free formaldehyde, and (2) the degree of crosslinking in the cured network.

For example, a UF-resin for particleboard at the end of the 1970s would have had a F/U molar ratio of approx. 1.6–1.8. To day a UF-resin for the same application has a molar ratio of between 1.02 and 1.08, but the requirements for the boards, as given in the quality standards, are still the same. The degree of crosslinking of the cured resins as well as the reactivity of the hardening reaction depends on the availability of free formaldehyde in the system.

However, it has to be considered that it is neither the content of free formaldehyde itself nor the molar ratio which eventually should be taken as the decisive and the only criterion for the classification of a resin concerning the subsequent formaldehyde emission from the finished board. In reality, the composition of the glue mix as well as the various process parameters during the board production also determine both performance and formaldehyde emission. Depending on the type of board and the manufacturing process, it is sometimes recommended to use a UF-resin with a low molar ratio F/U (e.g. $F/U = 1.03$), hence low content of free formaldehyde, while sometimes the use of a resin with a higher molar ratio (e.g. $F/U = 1.10$) and the addition of a formaldehyde catcher/depressant will give better results [17]. Which of these two, or other possible approaches, is the better one in practice can only be decided in each case by trial and error.

The higher the F/U molar ratio, the higher is the content of free formaldehyde in the resin. Assuming stable conditions in the resins, that means that post-added urea has had enough time to react with the resin, and the content of free formaldehyde is very similar even for different cooking procedures. In a coarse scale, the content of free formaldehyde in a straight UF-resin is approx. 0.1% at

Table 4

Influences of the molar ratio on various properties of UF-bonded wood panels

Decreasing the molar ratio leads to:	
a decrease of	the formaldehyde emission during the production of the wood based panels the subsequent formaldehyde emission the mechanical properties the degree of hardening
an increase of	the thickness swelling and water absorption the susceptibility to hydrolysis

Table 5

Molar ratios F/U and F/(NH₂)₂, respectively, of pure and melamine-fortified UF-resins currently in use in the wood-based panels industry

1.55 to 1.85	Classical plywood UF-resin, also cold setting; use is only possible with special hardeners and additives, e.g. melamine containing glue mixes for an enhanced water resistance.
1.30 to 1.60	UF-plywood resin; use for interior boards without special requirements concerning water resistance; in order to produce panels with low subsequent formaldehyde emission, the addition of formaldehyde catchers is necessary.
1.20 to 1.30	Plywood or furniture resin with low content of formaldehyde; also without addition of catchers, products with low subsequent formaldehyde emission can be produced.
1.00 to 1.10	E1-particleboard and E1-MDF-resins; especially in the MDF-production further addition of catchers is necessary. In case of modification or fortification with melamine.
Below 1.00	Special glue resins for boards with a very low formaldehyde emission; in most cases modified or fortified with melamine.

F/U = 1.1 and 1% at F/U = 1.8 [25–27]. It also decreases with time due to ageing reactions and to the free formaldehyde reacting further.

Table 4 summarizes the various influences of the molar ratio on various properties of wood-based panels. Table 5 summarizes the molar ratios F/U and F/(NH₂)₂, respectively, of pure and melamine-fortified UF-resins currently in use in the wood-based panels industry

6. MUF and MU(P)F adhesives

Whereas UF-resins are mainly used for interior boards (for use in dry conditions, e.g. in furniture manufacturing), a higher hydrolysis resistance can be achieved by incorporating melamine and phenol into the resin (melamine-fortified UF-resins,

MUF, MUPF, PMF). In UF-resins, the aminomethylene link is susceptible to hydrolysis and is therefore not stable at higher relative humidity, especially at elevated temperatures [28]. Hardened UF-resins can also be hydrolyzed under the influence of humidity or water, due to the weak bonding between the nitrogen of the urea and the carbon of the methylene bridge, especially at higher temperatures. During this reaction formaldehyde can be liberated [29,30]. The amount of this liberated formaldehyde can be taken under certain circumstances as a measure of the resistance of a resin against hydrolysis. The main parameters upon which resin hydrolysis depends are the temperature, pH and the degree of hardening of the resin [27]. The acid which was used to harden the resin can also induce its hydrolysis. Resin hydrolysis also leads to a loss of bonding strength. The degree of melamine fortification, and especially the way in which melamine is incorporated in the resin, can be very different. The different resistance of formaldehyde polycondensation resins against hydrolysis is based on their differences in behavior at the molecular level. The chemical bond between the nitrogen of the urea or the melamine, respectively, and the carbon of the methylol group can be easily split in UF-resins but not so easily in MF-resins. In the latter case, this is mainly due to the conjugated double bonds of the quasi-aromatic triazine ring of melamine. The methylene bridges connecting phenolic nuclei in phenolic resins are very stable against hydrolytic attack, making of PF-resins the only true exterior formaldehyde-based thermosetting resins. The melamine-fortified products are much more expensive due to the manyfold price increase of melamine in recent years compared to urea. The content of melamine in these resins, therefore, is always as high as strictly necessary but as low as possible.

Melamine can also be added to a UF-resin in the form of melamine salts like acetates, formates or oxalates [31–34]. These decompose in the aqueous resin mix at higher temperatures and enable considerable savings of melamine for the same degree of water resistance compared to traditionally prepared MUF-resins. These salts can act additionally as hardeners.

Another approach to increase the resistance of UF-resins against hydrolysis is based on the fact that the acid hardening of the resin causes residue of acids or acidic substances in the glue line. Myers [35] pointed out that in the case of an acid hardening system the decrease in the durability of the adhesive bonds can be initiated by the hydrolysis of the wood cell wall polymers adjacent to the glue line as well as by an acid-catalyzed resin degradation in the case of UF-bonded products. A neutral glue line, therefore, should show a distinctly higher hydrolysis resistance. The amount of hardener (acids, acidic substances, latent hardeners), therefore, always should be adjusted to the desired hardening conditions (press temperature, press time and other parameters) and never be like 'the more the better'. Just the opposite is the case: too high an addition of hardener can cause brittleness of the cured resin and a very high acid residue level in the glue line.

The necessary melamine content in the resin depends on various parameters,

e.g. the type of wood furnish (i.e. the type of wood particles mat formed), the pressing parameters (pressure profile, density distribution) and the resin consumption; it can vary from a few percent to more than 30%, based on liquid resin. Due to the considerable costs, the content of melamine always must be as high as necessary but as low as possible. Other important parameters are the cooking procedure of the resin, which considerably influences the board thickness swelling in water even at the same resin solids content and at the same content of melamine.

The deterioration of a bond line can occur due to: (1) the failure of the resin (low hydrolysis resistance, degradation of the hardened resin causing loss of bonding strength); (2) the failure of the interface between resin and wood surface (replacement of secondary forces between resin and reactive wood surface sites by water or other non-resin chemicals); (3) the breaking of bonds due to mechanical forces and stresses (the influence of water will cause swelling and therefore movement of the structural components of the wood-based panels).

The production of melamine-fortified UF-resins and of MUF-resins can follow various paths.

(1) Co-condensation of melamine, urea and formaldehyde in a multistep reaction [36–40]. A comprehensive study of various reaction types has been done by Mercer and Pizzi [41]. They especially compare the sequence of the additions of melamine and urea, respectively.

(2) Mixing of a MF-resin with an UF-resin according to the desired composition of the resin [42–44].

(3) Addition of melamine in various forms (pure melamine, MF/MUF-powder resin, melamine acetates) to an UF-resin during the application of the glue mix. In the case of the addition of pure melamine the UF-resin must have a rather high molar ratio, otherwise there is not enough formaldehyde available to react with the melamine in order to incorporate it into the resin.

The higher the content of melamine, the higher is the stability of the hardened resin against the influence of humidity and water (hydrolysis resistance) [17, 45,46]. Resins containing melamine can be characterized by the molar ratio $F:(NH_2)_2$ or by the triple molar ratio $F:U:M$. The mass portion of melamine in the resin can be described as being based on the liquid resin or based on the total mass of urea and melamine in the resin (Table 6). MUF-resin hardener addition usually is distinctly higher than in UF-resins.

MUPF-resins (PMUF-resins) are mainly used for the production of so-called V100-boards according to EN 312-5 and -7, option 2 [2]. They contain small amounts of phenol. Production procedures are described in patents and in the literature [47–51].

PMF-resins usually contain little or no urea. The analysis of the molecular structure of these resins has shown that there is no co-condensation between the phenol and the melamine, but that there are two distinct networks [52–55]. The

Table 6

Molar ratios $F/(NH_2)_2$ of MUF/MUPF-resins currently in use in the wood based panels industry

1.20 to 1.35	Resins for water-resistant plywood, in case addition of a formaldehyde catcher.
1.08 to 1.15	E1-particleboard- and E1-MDF-resin for water-resistant boards (EN 312-5 and 312-7 [2]). For boards according to option 1 (V313-cycle test) MUF-resins can be used; for boards according to option 2 (V100-boiling test) MUPF with approval are necessary. In case, especially for the MDF-production, formaldehyde catchers are added.
1.00 to 1.08	Similar to E1-resins above.
below 1.00	Special resins for boards with a very low subsequent formaldehyde emission.

reason for this is the different reactivity of the phenol and the melamine methylols, depending on the existing pH.

7. Reactivity and hardening reactions of aminoplastic adhesive resins (UF/MUF)

During the curing process of a thermosetting adhesive resin, a three-dimensional network is built up. This yields an insoluble resin which is not longer thermoformable. The hardening reaction is the continuation of the acid condensation step during resin production. The acid hardening conditions can be adjusted (1) by the addition of a so-called latent hardener, or (2) by the direct addition of acids (maleic acid, formic acid, phosphoric acid and others), or of acidic substances, which dissociate in water (e.g. aluminum sulfate). Common latent hardeners are ammonium sulfate and ammonium chloride. The latter, however, is no longer in use in the particleboard and MDF industry because of the generation of hydrochloric acid during combustion of wood-based panels causing corrosion problems. It is also no longer used because of the suspected formation of dioxins and due to the need to decrease chloride pollution of the environment (now limited by government regulations). Ammonium sulfate reacts with the free formaldehyde in the resin to generate sulfuric acid, which decreases the pH. Low pH and, hence, the acidic conditions so generated, enable the condensation reaction to start again and eventually the gelling and hardening of the resin. The rate of decrease of pH depends upon the amount of available free formaldehyde and of hardener and is greatly accelerated by heat [56,57].

MUPF/PMUF-resins harden in the main under similar acid conditions to UFs and MUFs. Because MUF-resins harden in the acid pH range, but phenolic resins have a minimum reactivity under these conditions, there is the real danger that the phenolic portion of the resin might not really be incorporated into the aminoplastic

portion of the resin during hardening. This does indeed occur if the sequence of reaction is not well chosen, often negating any advantage that could be derived by addition of phenol [51]. Proper reaction sequences do however yield acceptable copolymers and resins of acceptable performance [51].

During the hardening of PMF-resins no co-condensation occurs; in the hardened state two independent interpenetrating networks exist [58]. Indications for a co-condensation via methylene bridges between the phenolic nucleus and the amido group of the melamine had been found by ^1H -NMR only in model reactions between phenolmethyllols and melamine.

In order to increase the capacity of a production line especially by reducing the necessary press times, adhesive resins with a reactivity as high as possible should be used. This includes two parameters: (1) a short gelation time: and (2) a rapid bond strength increase, and this even at a low degree of chemical curing.

The reactivity of a resin at a certain molar ratio F/U or F/(NH₂)₂ is mainly determined by its preparation procedure and the quality of the raw materials

8. Correlations between the composition of aminoplastic resin and the properties of wood-based panels

Only a small amount of work has been done up to now concerning the prediction of bond strengths and other properties based on the results of the analysis of the resin. Ferg et al. [59] worked out correlation equations evaluating the chemical structures in various UF-resins with different F/U molar ratios and different types of preparation on the one hand and the achievable internal bond as well as the subsequent formaldehyde emission on the other hand. These equations are valid only for well defined series of resins. The basic aim of such experiments is the prediction of the properties of the wood-based panels based on the composition and the properties of the resins used. For this purpose various structural components are determined by means of ^{13}C NMR and their ratios related to board results. Various papers in the chemical literature describe examples of such correlations, in particular for UF, MF, MUF and PF resins [59–62]. For example one type of equation correlating the dry internal bond (IB) strength (tensile strength perpendicular to the plane of the panel) of a particleboard bonded with PF adhesive resins is as follows [17]

$$\text{Resin cross-linking} \approx \text{IB} = \frac{aA}{A+B+C} + \frac{b(Mo)}{A+B+C} + \frac{c(Me)}{A+B+C} \quad (1)$$

where the IB strength is expressed in MPa, A is the sum of peak areas of phenolic ortho and para sites still free to react (110 to 122 ppm), B is the sum of peak areas of phenolic meta sites (125 to 137 ppm), C is the sum of peak areas of phenolic ortho and para sites already reacted (125 to 137 ppm), Mo is the sum of

peak areas of phenolic methylol groups (59–66 ppm), Me is the sum of peak areas of methylene bridges connecting phenolic nuclei (30–45 ppm). The coefficients a , b and c are characteristic of a type of resin and depend from a variety of manufacturing parameters. Eq. 1 is one of the simpler equations of this type, the equations for UF-resins in particular being in general more complex. Similar equations correlating the level of crystallinity of a hardened aminoplastic resin, the IB strength of the board prepared with it, the level of crosslinking of the resin and the formaldehyde emission of the panel and resin with the ^{13}C NMR spectrum of the liquid resin have also been presented [17,59–62].

For certain boards, some good correlations exist. However, it must be assumed, that a general correlation for various resins and various panels will not exist and that maybe other correlation equations must be used. Nevertheless, these results are rather important, because they show that at least for a special combination of resin type and board type, correlations exist. Furthermore, it can be assumed that the various parameters as mentioned above also will be the decisive parameters for other combinations, even the numbers within the individual equations might differ. However, it also must be considered that the range of molar ratio under investigation in the papers mentioned above is rather broad. At the moment it is not possible to use these equations for predictions within narrow ranges of the molar ratio, e.g. the usual range of an E1-UF-resin with $F/U = \text{approx. } 1.03 \text{ to } 1.10$. It also will have to be shown how different cooking procedures at the same molar ratio can be included in these correlation equations.

9. Phenolic resins

Disadvantages of the phenolic resins are the necessary longer press times compared to UF-resins, and the dark color of the glue line and the board surface. There is also the possibility of a higher moisture pickup of the boards when stored at higher relative humidity due to the hygroscopicity of the high alkali content of the resin.

Special resins consist of a two-phase system composed of a mix of a highly condensed, and no longer soluble, PF-resin with a standard type PF-resin [63]. Another two-phase resin is composed of a highly condensed PF-resin, still in an aqueous solution, and of a PF dispersion [64]. The purpose of such special resins is the gluing of wet wood, where the danger of overpenetration of the resin into the wood surface exists and would cause a starved glue line.

Usually alkaline NaOH is used as catalyst, in an amount up to one mole per mole phenol (molar ratio NaOH/P), which corresponds to approx. 10 mass% alkali in the liquid resin. The pH of a phenolic resin is in the range of 10–13. The biggest part of the alkali is free NaOH, a smaller part is present as sodium phenate. The alkali is necessary to keep the resin water-soluble via the

phenate ion formation in order to achieve a resin of a degree of condensation as high as possible but at a viscosity which is still easy to handle during resin application. Additionally, the alkali significantly drops the viscosity of the reaction mix. Hence, the higher the content of alkali, the higher is the possible degree of condensation of the resin, hence the higher is the hardening reactivity of the resin and therefore, the shorter is the necessary press time.

On the other hand, a higher alkali content has some disadvantages. The equilibrium moisture content in humid climates increases with the alkaline content, and some hygroscopic (longitudinal stability, thickness swelling, water absorption) and mechanical properties (creep behavior) become worse. The alkali content also causes cleavage of the acetyl groups of the hemicelluloses; this leads to an enhanced emission of acetic acid compared to UF-bonded boards. The higher the content of alkali, the higher is the emission of acetic acid. In EN 312-5 and 312-7 [2] the content of alkali is limited to 2.0% for the whole board and 1.7% of the face layer.

Besides NaOH, other basic catalysts can be used, e.g. $\text{Ba}(\text{OH})_2$, LiOH, Na_2CO_3 , ammonia or hexamine, some of these being effectively used and others not. The type of catalyst significantly determines the properties of the resins [65–67]. Replacing alkali in PF-bonded boards could give some advantages. Ammonia gas evaporates during the hot-press process and does not therefore contribute to the alkali content and the hygroscopicity of the boards. It is important to hold the pH high as long as possible during board hot-pressing in order to guarantee a high reactivity of the resin and hence a short press time of the board [68,69].

The penetration behavior highly depends on the molar masses present in the resin: the higher the molar masses (more or less equivalent to the viscosity of the resin at the same solid content), the worse is the wettability and the lower is the penetration into the wood surface [70,71]. The lower molar masses are responsible for good wettability; however, too low molar masses can cause overpenetration and hence starved glue lines. Contact angles of phenolic resins on wood increase strongly with a higher viscosity of the resins, according to higher molar masses [72]. The higher molar masses remain at the wood surface and form the glue line, but they will not anchor as well in the wood surface. Depending on the porosity of the wood surface, a certain portion with higher molar masses must be present to avoid an overpenetration into the wood, causing a starved glue line; that means a certain ratio between low and high molar masses is necessary [15,73–77]. Some authors found a decrease of the wood failure with increased molar mass averages of PF-resins [78].

The penetration behavior of resins into the wood surface also is influenced by various parameters, like wood species, amount of glue spread, press temperature and pressure and hardening time. The temperature of the wood surface and of the glue line and hence the viscosity of the resin (which itself also depends on the already reached degree of hardening) influence the penetration behavior of the resin [79].

10. Reactivity and hardening reactions of PF adhesive resins

PF core layer resins usually have the highest molar masses and hence show a high reactivity and quick gelation. They contain higher amounts of alkali than face layer resins in order to keep the resin soluble even at higher degrees of condensation. The higher the degree of condensation during the production process (the higher the viscosity), the shorter is the gelling time [80]. The limits of the increase of the degree of condensation in the production process of the resin are given by (1) the viscosity of the resin (the resin must be able to be pumped, a certain storage stability as well as a proper distribution of the resin on the particles during blending is required), and (2) the flow behavior of the resin under heat, guaranteeing wetting of the unglued second wood surface and a sufficient penetration into the wood surface. Decreasing the solid content of the resin is limited by a possible too high moisture content of the glued particles.

Alkaline PF-resins contain free reactive methylol groups in sufficient number and can harden even without any further addition of formaldehyde, of a formaldehyde source or of catalysts. The hardening reaction is initiated by heat. The methylol groups thereby react to methylene and methylene ether bridges. Under high temperatures, ether bridges can be retransformed to methylene bridges. The lowest possible temperature for a technically sufficient gelation rate is approximately 100°C. In some cases potash in the form of a 50 mass% solution is added in the core layer resin mix in an amount of approximately 3–5% potash solid based on resin solid content.

Pizzi and Stephanou [81] investigated the dependence of the gel time on the pH of an alkaline PF-resin. Surprisingly they found an increase in the gel time in the region of very high pH values (above 10). Such pH values, however, are obtained in the case of the usual PF-resins at a content of NaOH of 5 to 10 mass%. A decrease of the pH in order to accelerate the hardening process is not possible, because spontaneous precipitation would occur. A change of the pH of the resin, however, might occur when the resin comes into contact with the acid wood surface. Especially with rather acidic wood species, the pH of the resin could drop significantly [82].

Lu and Pizzi [83] showed that lignocellulosic substrates have a distinct influence on the hardening behavior of PF-resins, whereby the activation energy of the hardening process is much lower than for the resin alone [84]. The reason is a catalytic activation of the PF-condensation by carbohydrates like crystalline and amorphous cellulose and hemicellulose. Covalent bonding between the PF-resin and the wood, especially lignin, does not play any role [84].

Acid-induced gelling reactions of PF resins can cause severe deterioration of the wood substrate and therefore have lost any importance in the wood adhesives field. Pizzi et al. [85] describe a procedure for the neutralization of acid-hardened PF glue lines by partly using as hardener a mix of *p*-toluene sulfonic acid with a

complex of morpholine and a weak acid in order to partly prevent the acid-induced deterioration of the wood substance. Several other attempts, which however failed, have been done by Christiansen [86], incorporating the acid by chemical means into the resin or fixing the hardeners (high molecular polystyrenesulfonic acids) physically within the glue line.

Acceleration of the hardening reaction is possible by using an as high as possible degree of condensation. Another way is the addition of esters such as propylene carbonate [81,87–92] or, even better, glycerol triacetate (triacetin) [81,93,94] or guanidine carbonate [94]. The mechanism of this acceleration, however, is not yet clear. It might be due to the hydrogen carbonate ion formed after hydrolysis of the propylenecarbonate [92], or due to the formation of hydroxybenzyl alcohols and aromatic carbonyl groups in the reaction of the propylene carbonate with the aromatic ring of the phenol [87,88]. The higher the addition of ester, the faster the gel time of the PF-resin [81].

Other accelerators for PF-resins are potassium carbonate, sodium carbonate [91,92] or sodium and potassium hydrogen carbonate. Also wood-inherent chemicals might have an accelerating influence on the hardening reactivity of PF-resins [91].

Since phenolic resins harden only thermally, post-curing during hot-stacking is very important. Different from UF-bonded boards, PF-bonded boards should be stacked as hot as possible to guarantee a maximum post-curing effect. On the other hand, very high temperatures during stacking might already cause partial deterioration (seen as discoloration) of the wood.

11. Modification of phenolic resins

11.1. Post-addition of urea

The addition of urea to a phenolic resin causes several effects: (1) decrease of the content of free formaldehyde; (2) decrease of the viscosity of the glue resin; (3) acceleration of the hardening reaction via the higher possible degree of condensation of the resin at the same viscosity; (4) reduction of the costs of the resin.

The urea usually is added to the finished PF-resin and causes a distinct decrease of the viscosity due to disruption of hydrogen bonds [95] and due to dilution effects. There is obviously no co-condensation of this post-added urea with the phenolic resin. Urea only reacts with the free formaldehyde of the resin forming methylols, which, however, do not react further due to the high pH [19]. Only at the higher temperatures of the hot-press does some phenol–urea co-condensation occur [93,94,96].

The higher the amount of post-added urea, the worse are the properties of

the boards. A reason for this might be the diluting effect of urea on the PF-resin. Amelioration of the co-condensation process also could help in the optimization of the urea addition. Surprisingly, Oldörp and Marutzky [97] have found better board properties with an increased urea addition. However, the full amount of added urea could be extracted from the boards, therefore no significant co-condensation between the urea and the phenolic resin seems to have occurred.

Using such PUF-resins, the resin content of the board should be calculated only based on the PF-resin solids in the PUF-resin.

11.2. Co-condensation between phenol and urea

A real co-condensation between phenol and urea can be performed by two ways: (1) reaction of methylol phenols with urea [98–101]; (2) acidic reaction of UFC (urea–formaldehyde concentrate) with phenol followed by an alkaline reaction [102,103].

Alkaline co-condensation to yield commercial resins and the products of reaction obtained thereof [93,94] as well as the kinetics of the co-condensation of mono methylol phenols and urea [104,105] have also been reported [17]. Model reactions in order to prove an urea–phenol–formaldehyde co-condensation (reaction of urea with methylolphenols) are described by Tomita and Hse [98,102, 106] and by Pizzi et al. [93,104] (Fig. 1).

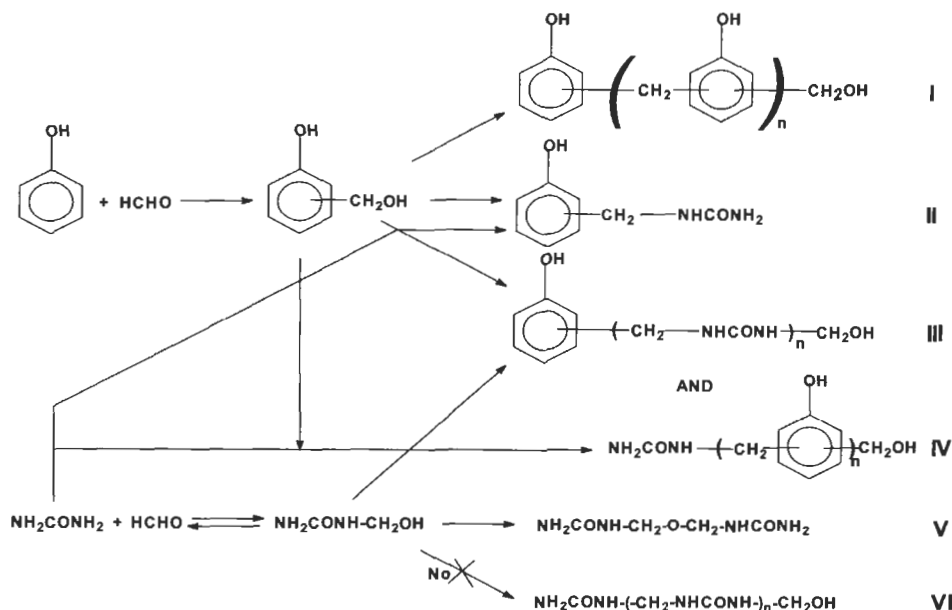


Fig. 1. Schematic representation of the coreaction of urea and phenol with formaldehyde to give PUF resins when reacted under alkaline reaction conditions.

11.3. Addition of tannins

The purposes of the addition of tannins are the following.

(1) The acceleration of the hardening reaction [107,108]. This is unsuccessful with the hydrolyzable chestnut tannins used in ref [107] but successful with the use of polyflavonoid tannins such as in Ref. [108].

(2) The replacement of phenol or part of the PF-resin [16,109–111].

11.4. Addition of lignins

The addition of lignins to phenolic resins can be (1) as an extender, e.g. in order to increase the cold tack or to reduce costs, or (2) to chemically modify the resin, whereby the lignin is chemically incorporated into the phenolic resin. The basic idea behind its addition is the chemical similarity between the phenolic resin and lignin or between phenol and the phenylpropane unit of the lignin. The lignin can be added at the beginning, during the cooking procedure or at the end of the condensation reaction (with a subsequent reaction step between the lignin and the phenolic resin). It is not fully clear that the lignin really is incorporated into the phenolic resin. In practice, lignin is used, if at all, as a neutral filler in adhesive resins, without yielding any special advantage (sometimes even not in terms of costs).

11.5. Addition of isocyanate

The use of isocyanate as a fortifier for phenolic resins was not thought to be worthwhile. Deppe and Ernst [112] had reported a precuring, hence a negative reaction between the isocyanate and the phenolic resin, even if both components have been applied separately to the particles. However, extensive industrial applications of pre-mixed glue mixes of isocyanate and phenolic resin in water to bond wood panel products have been shown to yield excellent bonding results [113,114], to yield copolymers linked by urethane bridges during curing of the wood panel in the hot-press. The reactions involved and their reasons for occurring have also been clarified and presented [113]. Hse et al. [115] have described a similar system, although with the isocyanate and the phenolic resins added separately to the wood. This also gave good results but worse than pre-mixing the two resins before application. This is due to the decreased mobility and diffusion hindrance rendering impossible to optimize the in situ reaction between the two resins.

12. Resorcinol adhesives

Resorcinol–formaldehyde (RF) and phenol–resorcinol–formaldehyde (PRF) cold-setting adhesives are used primarily in the manufacture of structural, exterior-

grade glulam (timber-laminated beams), fingerjoints, and other exterior timber structures. They produce bonds not only of high strength, but also of outstanding water and weather resistance when exposed to many climatic conditions [16,17, 116,117]. PRF-resins are prepared mainly by grafting resorcinol onto the active methylol groups of low-condensation resols obtained by the reaction of phenol with formaldehyde. Resorcinol is the chemical species that gives these adhesives their characteristic cold-setting behavior. At ambient temperature and on addition of a hardener, it provides accelerated and improved crosslinking not only to resorcinol-formaldehyde resins but also to the phenol-formaldehyde resins onto which resorcinol has been grafted by chemical reaction during resin manufacture. Resorcinol is an expensive chemical, produced in very few locations around the world (to date only three commercial plants are known to be operative in the United States, Germany, and Japan). Its high price is the determining factor in the cost of RF and PRF adhesives. It is for this reason that the history of RF- and PRF-resins is closely interwoven, by necessity, with the search for a decrease in their resorcinol content, without loss of adhesive performance.

In the past decades, significant reductions in resorcinol content have been achieved: from pure resorcinol-formaldehyde resins, to PRF-resins in which phenol and resorcinol were used in equal or comparable amounts, to the present-day commercial resins for glulam and fingerjointing. In these the percentage, by mass, of resorcinol based on liquid resin is of the order of 16 to 18%. A step forward has also been the development and commercialization of separate applications very fast-setting adhesives (the so-called 'honeymoon' fast-set system) [16,18,118], coupled with the use of tannin extracts, which in certain countries are used to obtain PRFs of 8 to 9% resorcinol content without loss of performance and with some other advantages (such as gluing of high moisture content timber). This was a system improvement, not an advance on the basic formulation of PRF-resins.

12.1. Chemistry of RF-resins

The same chemical mechanisms and driving forces presented for phenol-formaldehyde resins apply to resorcinol resins. Resorcinol reacts readily with formaldehyde to produce resins (Fig. 2) which harden at ambient temperatures if formaldehyde is added. The initial condensation reaction, in which A-stage liquid resins are formed, leads to the formation of linear condensates only when the resorcinol/formaldehyde molar ratio is approximately 1 : 1 [119]. This reflects the reactivity of the two main reactive sites (positions 4 and 6) of resorcinol [120]. However, reaction with the remaining reactive but sterically hindered site (2-position) between the hydroxyl functions also occurs [119]. In relation to the weights of resorcinol-formaldehyde condensates which are isolated and on a molar basis, the proportion of 4- plus 6-linkages relative to 2-linkages is 10.5 : 1. However, it must be noted that the first-mentioned pair represents two condensa-

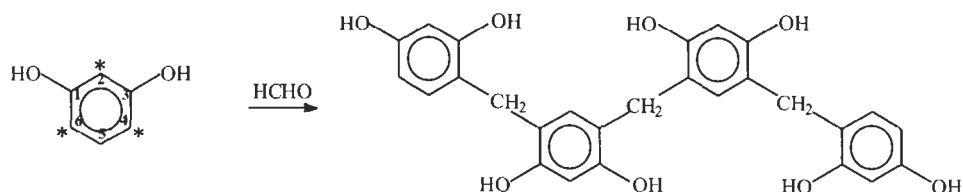


Fig. 2. Schematic representation of the reaction of resorcinol and formaldehyde to give linear resorcinol-formaldehyde oligomers.

tion sites relative to one. The difference in reactivity of the two types of sites (i.e., 4- or 6-position relative to the 2-position) is then 5 : 1 [119]. Linear components always appear to form in preference to branched components in A-stage resins [119]; that is, terminal attack leads to the preferential formation of linear rather than branched condensates. This can be attributed to the following.

(1) The presence of two reactive nucleophilic centers on the terminal units, as opposed to single centers of doubly bound units already in the chain.

(2) The greater steric hindrance of the available nucleophilic center (nearly always at the 2-position) of the doubly bound units as opposed to the lower steric hindrance of at least one of the nucleophilic centers of the terminal units (a 4- or 6-position always available). The former is less reactive as a result of the increased steric hindrance. The latter are more reactive.

(3) The lower mobility of doubly bound units which further limits their availability for reaction.

The absence of methylol ($-\text{CH}_2\text{OH}$) groups in all six lower molecular weight resorcinol-formaldehyde condensates which have been isolated [119] reflects the high reactivity of resorcinol under acid or alkaline conditions. It also shows the instability of its *para*-hydroxybenzyl alcohol groups and their rapid conversion to *para*-hydroxybenzyl carbonium ions or quinone methides. This explains how identical condensation products are obtained under acid or alkaline reaction conditions [119]. In acid reaction conditions methylene ether-linked condensates are also formed, but they are highly unstable and decompose to form stable methylene links in 0.25 to 1 h at ambient temperature [121,122].

From a kinetic point of view, the initial reaction of condensation to form dimers is much faster than the subsequent condensation of these dimers and higher polymers.

The condensation reaction of resorcinol with formaldehyde, on an equal molar basis and under identical conditions, also proceeds at a rate which is approximately 10 to 15 times faster than that of the equivalent phenol-formaldehyde system [16-18,123]. The high reactivity of the resorcinol-formaldehyde system renders it impossible to have these adhesives in resol form. Therefore, only resorcinol-formaldehyde novolaks, i.e. resins not containing methylol groups can be produced. All the resorcinol nuclei are linked together through methylene

bridges with no methylol groups being present and generally without any presence of methylene ether bridges either.

The reaction rate of resorcinol with formaldehyde is dependent on the molar ratio of the two constituents, the concentration of the solution, pH, temperature, presence of various catalysts, and amount of certain types of alcohols present [124–127]. The effect of pH and temperature on the reactivity and gel time of the resorcinol–formaldehyde system presents the same trend as for all phenolic–formaldehyde reactions, with a minimum of reactivity at around pH 4 and with the rate of reaction becoming rapidly faster at progressively more alkaline and more acid pH values [127,128]. Methanol and ethanol slow down the rate of reaction. Other alcohols behave similarly, the extent of their effect being dependent on their structure. Methanol lengthens gel time more than that of other alcohols, higher alcohols being less effective. The retarding effect on the reaction is due to temporary formation of hemiacetals between the methanol (or other alcohols) and the formaldehyde. This reduces the reaction rate because of the lower concentration of available formaldehyde [125,126]. Other solvents also affect the rate of reaction by forming complexes or by hydrogen bonding with the resorcinol [125,128].

In the manufacture of pure resorcinol resins, the reaction can be violently exothermic unless controlled by the addition of alcohols. Because the alcohols perform other useful functions in the glue mix, they are left in the liquid adhesive. PRF adhesives are generally prepared firstly by reaction of phenol with formaldehyde to form a PF resol polymer, that has been proved to be in the greatest percentage, and often completely, linear [95]. In the reaction step that follows the resorcinol chemical is added in excess to the PF-resol to react it with the PF-resin $-\text{CH}_2\text{OH}$ groups to form PRF polymers in which the resorcinol groups can be resorcinol chemical or any type of resorcinol–formaldehyde polymer.

Where resorcinol adhesives are not suitable, resins can be prepared from modified resorcinol [128]. Characteristic of these types of resins are those used for tyre cord adhesives, in which a pure resorcinol–formaldehyde resin is used, or alternatively, alkyl resorcinol or oil-soluble resins suitable for rubber compounding are obtained by prereaction of resorcinol with fatty acids in the presence of sulfuric acid at high temperature followed by reaction with formaldehyde. Worldwide more than 90% of resorcinol adhesives are used as cold-setting wood adhesives. The other most notable application is as tyre cord adhesives, which constitutes less than 5% of the total use.

12.2. Phenol–resorcinol–formaldehyde adhesives

PRF adhesives in which a liquid phenol–resorcinol–formaldehyde adhesive and a powder or liquid hardener are used are currently the most commonly used industrially. Pure resorcinol–formaldehyde (RF) adhesives were used extensively

up to a few years ago. They fell into disfavor because of the high price of the resorcinol. They are still used industrially when particularly difficult wood-gluing problems arise. PRF adhesives in which a liquid phenol–resorcinol–formaldehyde adhesive and a liquid hardener, are used quite extensively in Europe, as they have several handling advantages for this market. These adhesives are mixed before use in a mass/mass ratio of liquid adhesive resin (50 to 60% solid content) to powder hardener of 5:1, or when using a liquid hardener of 4:1, 2:1 or even 1:1 (depending from the type). The powder hardener is generally a mixture of equal parts fine paraformaldehyde powder and fillers, these latter being comprised of 200-mesh wood flour or a mixture of wood flour and nutshell flour (also 200 mesh). Adhesives with a liquid hardener use formaldehyde and formurea as hardeners and when needed, oxazolidine. The latter is used to reduce formaldehyde odor.

All properly formulated resorcinol-based adhesives must have a viscosity low enough in aqueous–alcoholic solutions to flow with ease into the interstices of the wood surface. Wetting ability is promoted by the alcohol. The paraformaldehyde powder, used in solid hardeners, is an addition polymer composed of a few to over 100 formaldehyde monomers. It dissolves slowly in water by depolymerization to formaldehyde monomers. The rate of depolymerization depends on the degree of polymerization of the paraformaldehyde, the size of the particles, and the pH. Therefore, the working life or pot life of a glue mix can be adjusted by selecting the type of paraformaldehyde and the pH correctly, as its success also depends on the rate of supply of formaldehyde monomer. Fillers are added to give consistency to the glue mix, to control viscosity and thixotropic characteristics, to form a fibrous reinforcement of the adhesive film, and to decrease the cost. Wood flour is used as a filler to obtain better gap filling where rough or uneven surfaces must be bonded, or where low bonding pressures must be used. Nutshell flours, such as coconut shell flour, walnut shell flour, peach pip shell flour, macadamia nut shell flour, or even olive stone flour are used as fillers to lower absorptive qualities and to provide smoothly flowing mixtures. Inorganic fillers are also used, especially in Europe, although this is a practice to avoid as it is very hard on saws afterwards. Clays and silica smokes can also be used in very small amounts to control the thixotropic consistency of the glue mix.

As the formaldehyde reacts with the resorcinol-based resin, condensation occurs, with the formation of high molecular weight polymers. There is a considerable secondary force interaction between the growing resorcinol polymers and the noncrystalline hemicellulosic and lignocellulosic molecules of the substrate. The highly polar methylol groups and the phenolic hydroxy groups link to cellulose and lignin groups by van der Waals, hydrogen, and electrostatic bonds. The growing adhesive polymers continue to interact to form colloidal particles and then a gelatinous film. This mechanism depends strongly on the moisture content of the wood, which determines the rate of water and solvent absorption.

Table 7

Typical tensile strength and percentage wood failure results obtainable with synthetic PRF resins

Dry test		24-h cold-water soak		6-h boil test	
Strength (N)	Wood failure (%)	Strength (N)	Wood failure (%)	Strength (N)	Wood failure (%)
3000–3500	90–100	2600–3200	75–100	2500–3000	75–100

Refs. [18,129,130].

The advantage of ambient-temperature curing is that the moisture escapes gradually from the hard film formed on curing, inducing a minimum of residual stresses on the joint and allowing the glue line to assume the aspect of a molecularly porous solid. As a consequence, the hard film is able to transpire in the same way as wood, which minimizes checking or crazing and allows the glued joint to survive exposure to the extremes of humidity cycles. Typical levels of strength and wood failure results obtained in specified standard tests are shown in Table 7.

12.3. Special adhesives having reduced resorcinol content

12.3.1. Fast-setting adhesives for fingerjointing and glulam

Together with the more traditional fingerjointing adhesives that have just been discussed, a series of ambient-temperature fast-setting separate application systems, have also been developed. These eliminate the long delays caused by the use of more conventional phenol–resorcinol–formaldehyde adhesives, which require lengthy periods to set. These types of resorcinol adhesives are applied separately. They were first developed in the United States [131–134] to bond large components where presses were impractical. Kreibich [134] describes these separate application or ‘honeymoon’ systems as follows: “Component A is a slow-reacting phenol–resorcinol–formaldehyde resin with a reactive hardener. Component B is a fast-reacting resin with a slow-reacting hardener. When A and B are mated, the reactive parts of the component react within minutes to form a joint which can be handled and processed further.” Full curing of the slow-reacting part of the system takes place with time. The *m*-aminophenol used for component B is a frightfully expensive chemical, and for this reason these systems were discarded and not used industrially [118,134]. In their original concept component A is a traditional phenol–resorcinol–formaldehyde cold-setting adhesive at its standard pH of between 8 and 8.5 to which formaldehyde hardener has been added. Flour fillers may be added or omitted from the glue mix. Component B is a phenol/meta-aminophenol/formaldehyde resin with a very high pH

(and therefore a high reactivity), which contains no hardener or only a very slow hardener.

More recently, a modification of the system described by Kreibich has been used extensively in industry with good success. Part A of the adhesive is again a standard phenol–resorcinol–formaldehyde (PRF) cold-setting adhesive, with powder hardener added at its standard pH. Part B can be either the same PRF adhesive with no hardener and the pH adjusted to 12, or a 50 to 55% tannin extract solution at a pH of 12–13, provided that the tannin is of the condensed or flavonoid type, such as mimosa, quebracho, or pine bark extract, with no hardener [118,135–137]. The results obtained with these two systems are good and the resin not only has all the advantages desired but also the use of vegetable tannins and the halving of the resorcinol content makes the system considerably cheaper [118,135–137].

The adhesive works in the following manner. Once the component A glue mix is spread on one fingerjoint profile and component B on the other fingerjoint profile and the two profiles are joined under pressure, the reaction of component B with the hardener of part A is very fast. In 30 min at 25°C fingerjoints prepared with these adhesives generally reach the levels of strength that fingerjoints glued with more conventional phenolic adhesives are able to reach only after 6 h at 40–50°C or in 16–24 h at 25°C [118,136]. Clamping of laminated beams (glulam) bonded with these fast-set honeymoon adhesives averages only 3 h at ambient temperature compared with the 16 to 24 h necessary with traditional PRF resins [135–137]. These adhesives present two other advantages: (1) they are able to bond without any decrease of performance at temperatures down to 5°C, and (2) they are able to bond ‘green’ timber at high moisture content, a feat which has been used in industrial glulam bonding since their commercial introduction in 1981.

13. Isocyanates

13.1. Adhesives for wood-based panels (polyisocyanates)

Adhesives based on isocyanate (especially PMDI, polymethylene diisocyanate, more exactly polymeric 4,4′-diphenylmethane diisocyanate) have been used for more than 25 years in the wood-based panel industry [88], but still have a low market value in the wood-working industry compared to systems based on UF-, MUF- or PF-resins. The main application is the production of waterproof panels, but also the production of panels from raw materials that are difficult to glue, like straw, bagasse, rice shells or sugar cane bagasse. They can be used as adhesives for wood-based products like particleboard, oriented strandboard (OSB), laminated strand lumber (LSL), medium-density fiberboard (MDF) or

other special engineered composites. Today PMDI is quite extensively used to produce exterior-grade OSB and particleboard.

Like other adhesives, PMDI is a specific mixture of different molecules. The greater part of the functional groups of polyisocyanates are of low reactivity because of the different positions. The molecular weight distribution influences the reactivity, but also the typical properties of adhesives like viscosity, wetting and fluidity. In the monomer form (MDI) the functionality is 2 and the NCO-content is 33.5%, while PMDI has an average functionality of 2.7 with a NCO-content of approximately 30.5%. The HCl-content is usually below 200 ppm. PMDI is used whenever the color of the finished adhesive is not of concern [138].

The excellent application properties of PMDI and of the produced wood-based panels are based on the special properties of PMDI, e.g. the excellent wetting behavior of a wood surface as compared to aqueous condensation resins. Due to this fact, surfaces with poor wetting behavior can be glued, e.g. straw. The wetting angles for PMDI on various surfaces are much lower than for UF-resins. Additionally, good penetration into the wood surface is observed, which seems to be provided by the small molar mass of PMDI as compared with condensation resins. Marcinko et al. [139] found that PMDI can penetrate 5–10 times further into wood than PF-resins. PMDI not only penetrates the macroscopic hollows of the wood substance, but also penetrates the polymer structure of the wood. This enables a good mechanical anchoring. Good wetting and penetration behavior might cause starved glue lines.

Johns [116] could show that isocyanate spreads easily on a wood surface. 4% of isocyanate give panels the results which are comparable to those of boards bonded with 8% of a phenolic resin. The good mobility of MDI is based on several parameters [140]: (1) MDI contains no water, and it cannot lose its mobility during adsorption on the wood surface; (2) it has a low surface tension (ca. 50 dyn/cm) as compared to water (76 dyn/cm); (3) it has a low viscosity.

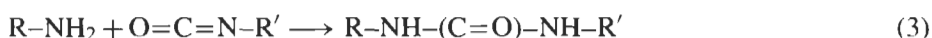
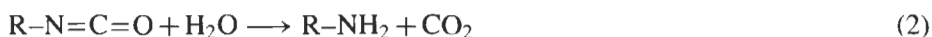
PMDI is produced on an industrial scale by the phosgenation of diaminodiphenylmethane. Structure and molar mass of PMDI depend on the number of aromatic rings in the molecule. For PMDI the distribution of the three monomeric isomers has a great influence on the quality, because the reactivities of the various isomers (4,4'-, 2,4'- and 2,2'-MDI) differ significantly. The greater the portion of the 2,2'- and 2,4'-isomers, the lower is the reactivity. This can lead to different bonding strengths as well as to residual isomers in the produced wood-based panels.

PMDI also contains isocyanates with higher molar masses (triisocyanates, tetraisocyanates, polyisocyanates), whereby the structure and the molar mass depend on the number of phenyl groups. This distribution influences, to a great extent, the reactivity, but also the usual properties like viscosity, flowing and wetting behavior as well as the penetration into the wood surface.

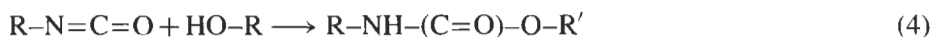
The impossibility of diluting PMDI with water was solved by the introduction

of emulsified PMDI, often called EMDI, which allows a regular distribution of the adhesive during the gluing process. EMDI is a product of the reaction of PMDI with polyglycols. The system is manufactured under high pressure and dispersed in water.

The isocyanate group in PMDI is characterized by a high reactivity towards all substances which contain active hydrogen. The main hardening reaction occurs via water attack onto the amine group, with emission of CO₂. It is applied together with the PMDI (by spray applying them simultaneously or by applying an aqueous dispersion) or it may be already present in the wood in a sufficient amount. The amine group reacts further with another isocyanate group to a polyurea structure:

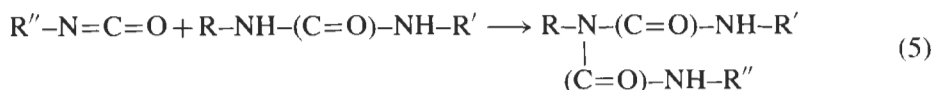


The reaction of an isocyanate group with an hydroxylgroup leads to the urethane bond:



Such a reaction theoretically can also be established between an isocyanate group and an OH group of the cellulose or the lignin forming a covalent bond. Such bonds usually are of higher durability than pure physical bonds. If it can be managed that the reaction of the isocyanate groups of the PMDI with water can be suppressed, the chance for forming such covalent bonds improves. Covalent bonds lead to higher adhesive bond strengths and especially higher resistance against the influence of humidity. It has been clearly shown, however, that under the fast pressing conditions prevalent in wood panel bonding, covalent bonds between the adhesive and the wood substrate do not form. The presence of some (low amount) of isocyanate/wood covalent bonds can be envisaged to some extent where the assembly is in direct contact with the 200°C hot platen of the press, or for unrealistically long pressing or heating times, but not in the strength-determining board core where the temperature reaches a maximum of 110–120°C for not more than 60 to 120 s.

If an isocyanate group reacts with a hydrogen within the polyurea structure, a branching point is formed, a biuret group:



During the hardening of PMDI urethanes, polyureas, biurets and triurets/polyurets have been found [16,17,141,142]. The proportions of the various compounds depend on the working and hardening conditions. The forming of the network is especially influenced by the ratio between isocyanate and water.

Table 8

Advantages and disadvantages of PMDI compared to other adhesives, especially UF-resins

Advantages	<ul style="list-style-type: none"> • high storage stability • formaldehyde-free gluing, despite the fact that formaldehyde is used in the production of MDI/PMDI • high reactivity • high bonding strength • high tolerance against humidity • low consumption of adhesive
Disadvantages	<ul style="list-style-type: none"> • higher price, which fact is partly diminished by the low adhesive consumptions and sometimes shorter press times • the adhesion behavior towards all other surfaces, e.g. also press platens, which needs the use of (i) special internal or external release agents, (ii) special types of PMDI or (iii) different types of adhesives used in the board surface • the use of special emulsified (EMDI) or special dosing and gluing systems • higher requirements concerning EHS due to the toxicity and the low but nevertheless existing vapor pressure of the monomeric MDI, which need special precautions during use

Usually no hardeners are added during the production of wood-based panels (PB, MDF, OSB, engineered wood products). With special additives, an acceleration of the hardening reaction and hence shorter press times or lower press temperatures can be achieved. This is especially interesting for cold-setting systems as well as for the production of particleboards. Possible catalysts are those traditionally used for the promotion of urethane formation [17,143].

Compared to other adhesives PMDI shows various advantages, but also some disadvantages (Table 8).

Isocyanates by themselves cannot be used to bond plywood due to the balance of rheology and rate of hardening which are characteristic of PMDI.

13.2. Polyurethane adhesives

Polyurethane adhesives are formed by the reaction of various types of isocyanates with polyols. The polar urethane group enables adhesion to various surfaces. Depending on the raw materials, glue lines with rubber-like elastic to brittle-hard behavior can be achieved. The presence of reactive terminal groups provides a chemically hardened adhesive. When polymerized to a high enough molecular weight, the adhesive can be physically rather than chemically hardened, i.e. a hot melt.

One-component systems are starting to be used for structural glulam and fingerjointing applications. The bond line reaches the necessary green strength

within a few hours and hardens after a few days. During the reaction of the active isocyanate groups present in the adhesive with the moisture in the wood, CO₂ is formed, which may cause some foaming of the bond line. The cured bond lines themselves are more or less resistant against humidity and water.

Two-component systems consist of (1) polyol or polyamine, and (2) isocyanate. The hardening starts with the mixing of the two components. Due to the low viscosities of the two components, they can be used without addition of solvents. The mass ratio between the two components determines the properties of the bond line. Linear polyols and a lower surplus of isocyanates give flexible bond lines, whereas branched polyols and higher amounts of isocyanates lead to hard and brittle bond lines. The pot life of the two-component systems is determined by the reactivity of the two components, the temperature and the addition of catalysts. The pot life can vary between 0.5 and 24 h. The cure at room temperature is completed within 3 to 20 h.

14. Wood adhesives based on natural resources

Bio-based glue resins have been investigated for many years. However, a real breakthrough in their industrial utilization, at least in Europe, has not yet occurred. However, their successful industrial use has been in full development for many years in several countries of the Southern Hemisphere, such as Australia, South Africa, Zimbabwe and to a much lesser extent Chile, Argentina and Brazil [16,17]. The use and application of adhesives based on natural and renewable resources by industry and the general public is often thought of as a new approach that requires novel technologies and methods to implement. Despite the increasing trend toward the use of synthetic adhesives, processes based on the chemical modification of natural products offer opportunities for producing a new generation of high-performance, high-quality products. The distinct advantages in the utilization of natural materials, e.g. lower toxicity, biodegradability and availability, need to be paralleled by more efficient and lower-cost methods of production. We have to use factors such as regional and species variation as an aid in selecting the optimum feedstock for a particular process. Additionally, we have to develop cost-effective manufacturing techniques that will enable these materials to capture a wider percentage of the world market.

Manufacturers need to have confidence that a continual uninterrupted supply of raw material can be sustained throughout the life cycle of a product. It is of equal importance that the feedstock should not be restricted by geographical and climatic conditions or that yield does not dramatically vary when harvested in different locations and at a particular time of the year. The key to an increased usage of natural products by industry is in the control of the above variables so that the end performance of the product remains consistent.

14.1. Tannins

Tannins are polyhydroxyphenols. They are soluble in water, alcohols and acetone and can coagulate proteins. They are yielded by extraction from wood substance, bark, leaves and fruits. Other components of the extraction solutions are sugars, pectins and other polymeric carbohydrates, amino acids and other substances. The content of non-tannins can reduce wood failure and water resistance of glued bonds. The polymeric carbohydrates especially increase the viscosity of the extracts.

Usually spray-dried powders are sold. A purification step is not usually done on the industrial scale. The modification of the extracts are especially aimed at decreasing the sometimes too high viscosity to achieve better handling and application, but also a longer pot life and a better crosslinking [16,17,144].

As tannins contain many 'phenolic'-type subunits (Fig. 3), one may be tempted to think that they will exhibit a similar reactive potential to that of phenol, and that therefore procedures used in standard PF production can be transferred to those containing tannin. This, however, is not the case. The real situation is that tannin is far more reactive than unsubstituted phenol due to the resorcinol and catechol rings present in the tannin. This increase in hydroxyl substitution on the two aromatic rings affords an increase in reactivity to formaldehyde by 10 to 50

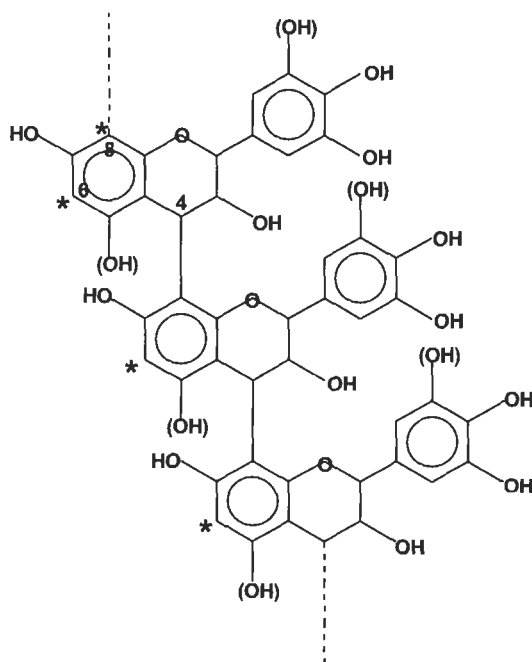


Fig. 3. The regular structure of a procyanidin-type condensed tannin showing characteristic 4,8 interflavanoid bonds linking the flavonoid units.

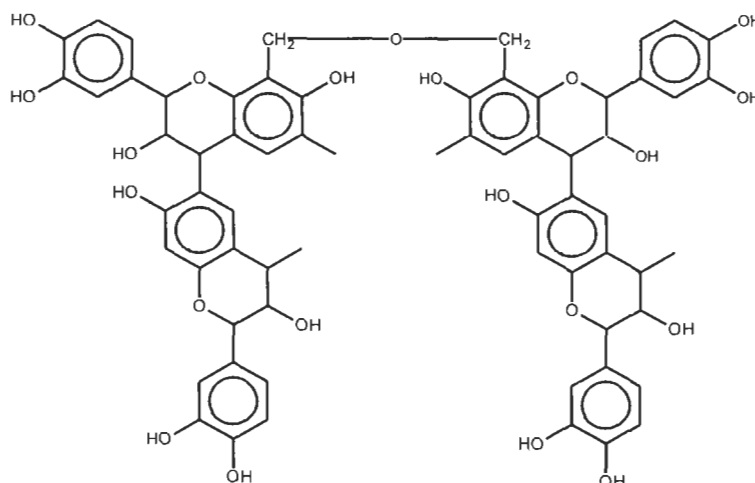


Fig. 4. Two 4,6-linked biflavonoid units linked to each other through a methylene ether bridge formed by reaction with formaldehyde.

times when compared to simple phenol. While this initially sounded promising, it creates additional problems with respect to producing an industrially applicable resin, due to limited pot lives of the ready-to-use formulations.

Crosslinking via methylene or methylene ether bridges (Fig. 4) in a polycondensation reaction is necessary for the tannins to fulfill their traditional role as exterior weather-resistant adhesives. Tannin reactions are based on their phenolic character similar to those of phenol with formaldehyde. Formaldehyde reacts with tannin in an exothermic reaction forming methylene bridges. At neutral or even slightly acid pH, formaldehyde reacts rapidly with the tannin. This leads to the advantage that no (high) alkaline pH is necessary to achieve quick gelling and that a neutral, hardened glue line is obtained with consequent improvement in resistance to water and weather.

From a purely technological point of view the gelation time may not be reduced without limit. Decisive factors are the pot life, the viscosity of the tannin solution as well as the rate of the steam escaping from the mat and the board. One possible way is the separate addition of the crosslinker, e.g. by dosing paraformaldehyde via a small screw conveyor directly to the particles in the blender. Also a liquid crosslinker, e.g. a urea-formaldehyde prepolymer concentrate (formurea) (UFC), can be mixed with the tannin solution in a static mixer shortly before the blender. The higher viscosity of the tannin solution at higher pHs, even without addition of the crosslinker, can be overcome by warming up to 30–35°C or by adding water. A higher moisture content of the glued particles is no disadvantage with these adhesives, but rather necessary to guarantee a proper flow of the tannin [16,17,145–147].

Possible formaldehyde crosslinkers are paraformaldehyde [16,17,144,145], methylolurea mixtures such as urea-formaldehyde precondensate or formurea [145], or urea and phenol methylols with longer chains to overcome steric hindrance.

Tannins can also be hardened by addition of hexamethylenetetramine (hexamine) [146,147], whereby these boards show very low formaldehyde emission [16–18,148–151].

The autocatalytic hardening of tannins without addition of formaldehyde or another aldehyde as crosslinker is possible, if small traces of alkaline SiO_2 are present as catalyst and also a high pH is used, or with certain tannins just by the catalytic action induced by the wood surface [152–160].

Tannin adhesives are the class of modified natural adhesives which are used and have been used industrially for more than 25 years, mainly in South Africa and Australia, but also in Zimbabwe, Chile, Argentina, Brazil and New Zealand. It is mainly the still limited raw material supply that limits their use to approximately 30,000 tons resin solids per year [16,17].

14.2. Lignins

Lignins are large three-dimensional polymers produced by all vascular terrestrial plants. They are second only to cellulose in natural abundance and are essentially the 'natural glue' that holds plant fibers together. Lignins have polymeric and phenolic characters. Lignins are primarily obtained as a by-product in wood-pulping processes with estimates exceeding 75 million tons per annum. Therefore great interest exists for possible applications. Lignins of very different chemical composition and possible applications in the wood-based panel industry (adhesives, additive to or partly replacing adhesives, raw material for synthetic resins) have been described in a huge number of papers and patents. Research into lignin-based adhesives dates back over 100 years with many separate examples of resins involving lignin being cited. In reality, existing applications are very rare. No industrial use as a pure adhesive for wood is currently known, despite the fact that considerable research activity has been directed toward producing wood adhesives from lignins. By themselves, lignins offer no advantages in terms of chemical reactivity, product quality or color when compared to conventional wood composite adhesives. The greatest disadvantages of lignins in their application as adhesives are (1) their low reactivity and therefore the slow hardening compared to phenol due to the lower number of reactive sites in the molecule, causing increased press times, and (2) the concern of chemical variation in the feedstock. The chemical structure of lignin is very complex with the added difficulty (unlike tannin) that the individual molecules have not a fixed, well defined molecular structure. Therefore no true generic molecule exists for lignin from softwood, hardwood or cereals.

Lignosulfonates can be added to synthetic glue resins as extenders (under partial replacement of resin) [161]. The partial replacement of phenol during the cooking procedure of PF-resins has no present industrial application, but the addition of between 20% and 50% pre-methylolated lignin (pre-reacted with formaldehyde) to synthetic phenol-formaldehyde resins is used industrially in some North American plywood mills [162,163]. Lignin and methylolated lignin added to synthetic adhesives slow down proportionally the pressing time which can be used in board production, rendering such processes less economically viable. However, plywood production is much less economically dependent from achieving shorter pressing times. Consequently a fairly reactive form of lignin such as pre-methylolated lignin is useful to decrease costs without decreasing performance when added to synthetic adhesives for plywood. Methylolated lignin can react rapidly with isocyanates. Adhesive formulations for panel products successfully using 20–30% isocyanates added in the glue mix to methylolated lignin have been reported [164,165]. They can compete successfully with synthetic adhesives in the case of the very short press times needed for the adhesive to be of industrial significance for particleboard or other composite wood panels [164,165].

14.3. Use of lignins as adhesive without adding other synthetic resins

The application of lignin as an adhesive is possible in principle. The first attempt needed very long press times due to the low reactivity (Pedersen process) [161]. This process was based on lignin polycondensation under strong acidic conditions, which led to considerable corrosion problems in the plant [161]. The particles had been sprayed with spent sulfite liquor (pH = 3–4) and pressed at 180°C. After this step, the boards were tempered in an autoclave under pressure at 170–200°C, whereby the sulfite liquor became insoluble after splitting off water and SO₂.

Shen [166–168] modified this process by spraying the particles with spent sulfite liquor containing sulfuric acid and pressing them at temperatures well above 210°C.

Nimz et al. [161,169] described the crosslinking of lignin after an oxidation of the phenolic ring in the lignin molecule using H₂O₂ in presence of a catalyst, especially SO₂ [169]. This leads to the formation of phenoxy radicals and with this to a radical coupling (but not to a condensation reaction), whereby inter- and intra-molecular C–C-bonds are formed. This reaction does not necessarily need heat and also no acidic conditions, but is accelerated by higher temperatures (max. 70°C) as well as lower pHs. In this way the disadvantages of the processes mentioned above (high press temperatures, long press times, use of strong acids) could be avoided [161,169].

An oxidative activation of the lignin also can be achieved in a biochemical way by adding enzymes (phenol oxidase laccase) to the spent sulfite liquor, whereby

a polymerization via a radical mechanism is initiated. The enzymes are obtained from nutrient solutions of white fungi. Preparing the two-component adhesive is done by mixing the lignin with the enzyme solution (after filtration of the mycelium). At the beginning of the press cycle the enzyme still works, as it is stable up to a temperature of 65°C. If a higher temperature is reached, then the enzyme is deactivated. At that time, however, the level of quinone methides generated is high enough to initiate the crosslinking reaction by phenoxy coupling [170,171]. While this approach is of interest it has a few severe drawbacks, primarily the system works only with very long press times. For example press times as long as 15 min for 3 mm thick panels have been reported but industrially viable press times for this panel thickness are around 20–30 s today using the same press technology. This far too long a press time can be improved, and the authors have experimented with this [171], by adding a reduced amount of a very strong adhesive, namely isocyanate to the panel. The press time obtained is still about 10 times longer than what would be industrially significant today. The prospects for such systems are then not very exciting today: or one uses only enzymes on wood, without adding any adhesive, and produces board of unacceptably long press times, or one uses enzymes to pretreat the wood while also adding a reduced amount of some adhesive and still produces boards at faster press times but still unacceptably long. None of these systems is used industrially.

15. Thermoplastic wood adhesives

15.1. Hot melts

Hot melts are 100% solid thermoplastic compounds. They are compounded and applied in the molten state at elevated temperatures. The resultant properties are obtained by cooling. Due to the quick cooling, bonds can be established in a very short time.

Advantages of hot melts:

- 100% solid, contain no organic solvents; no water or solvent to be evaporated; low requirements concerning working and environmental safety
- easy use, short set time allows high speed operation (up to 100 m/min)
- quick forming of bond strength
- high seal strength
- effective bonding even of difficult surfaces: PE, PP, varnishes and others
- combine flexibility and toughness
- adhesion on a wide variety of substrates even without primer
- formulation latitude (color, viscosity during application, temperature and others)
- more or less unlimited storage life, easy storage

- no time limitations in application, no pot life
- no pollution of machinery and adherends, because of exact application
- good temperature controlling of application, easy use in automated production systems

Disadvantages of hot melts:

- cold flow: hot melts creep under mechanical load, even far below the melting temperature; bonds can open slowly; this effect is accelerated by higher temperatures
- low heat resistance at elevated temperatures due to thermoplastic behavior; loss of bond strength
- sensitivity of certain substrates to the required application temperature
- degradation at elevated temperature (color, viscosity)

15.1.1. Composition of hot melts

15.1.1.1. Polymer. The polymer determines the properties of the hot melt; variations are possible in molar mass distribution and in the chemical composition (copolymers). The polymer is the main component and backbone of hot-melt adhesive blend; it gives strength, cohesion and mechanical properties (filmability, flexibility). The most common polymers in the woodworking area are EVA and APAO.

Ethylenevinylacetate (EVA) is the most used type (approximately 80%); it can be varied in viscosity (melt index) and content of acetate in broad ranges. It is semicrystalline. The vinyl acetate groups provide improved adherability towards many materials. The low heat stability, however, limits the areas of application.

With increasing content of the vinyl acetate comonomer, the adhesion ability, the wetting behavior and the flexibility increase, but also the setting time and the price, heat resistance and cohesion properties become worse. The higher the molecular weight of the polymer, the worse is the EVA wetting behavior, but the better the cohesion properties, the heat and temperature resistance and the higher the melting viscosity at a given temperature.

Ethylene–acrylic acid ester copolymerisate, EEA, shows high heat resistance and high elasticity at low temperatures.

In amorphous poly- α -olefins (APAO), the main monomer is propylene. Compared to EVA, it provides better heat resistance. APAO shows good adhesion properties to nonpolar surfaces, good flexibility and high resistance to temperature and moisture.

Polyamides give high setting speed, good cohesion and very high heat resistance; they are oil- and solvent-resistant. Due to the narrow melting region (sharp transition between the elastic and plastic areas) a short setting time during cooling is given. Depending on the type, the melting temperature is between 105 and 190°C. Advantages are the low melt viscosity, high bond strength and a high green

tack. Disadvantages are the high price and the susceptibility for carbonization at high temperatures in the presence of oxygen.

Thermoplastic polyurethanes have no reactive isocyanate groups and cannot crosslink.

Thermoplastic, linear and saturated polyester give, depending on their chemical composition, hard or elastic and tacky bond lines; they have relatively high melting viscosities; bond lines are resistant against moisture, water and UV.

15.1.1.2. Tackifiers. The tackifiers usually are hydrocarbon resins (aliphatic C5, aromatic C9) or natural resins (polyterpenes, rosin and rosin derivatives, tall oil rosin ester). They improve hot tack, wetting characteristics and open time and enhance adhesion. The content on tackifiers in a hot melt can be in the region of 10–25%.

15.1.1.3. Other components. Waxes increase the resistance against water and moisture (hydrophobication). Anorganic fillers (CaCO_3 and/or BaSO_4) reinforce the cohesion (small particle size), decrease sagging, adhesion and the price of the product. Also used are pigments (e.g. TiO_2), plasticizers which decrease the viscosity and heat resistance while improving wetting behavior and bond line flexibility (cold flow can occur however), and stabilizers which improve thermooxidative behavior (heat and aging stability).

15.1.2. Curing hot melts

Curing hot melts are easily meltable polyurethane prepolymers (polyaddition of polyvalent alcohols and isocyanate) with reactive isocyanate end groups ($-\text{N}=\text{C}=\text{O}$), which react with the moisture content of the wood under hardening. This leads to the formation of a crosslinked polymer. After cure, they are no longer thermoplastic, they cannot melt and are insoluble. This provides good mechanical and chemical resistance. During processing a two-step bonding takes place; the two steps run parallel, but with different speeds:

- quick physical solidification due to cooling: high green strength for quick further processing
- slower chemical hardening by crosslinking: the reaction of the free isocyanate groups is initiated by the moisture content of the surrounding air and of the adherend.

Advantages:

- higher resistance against heat, moisture and steam
- higher mechanical bond strength
- lower application temperatures: lower molar masses and softening and melting temperatures; processing of heat-susceptible adherends, e.g. PVC foils, is

possible. Example: processing temperature 70°C; heat-resistance temperature of the bond line 120°C.

- high aging resistance.

Disadvantages:

- contain monomeric isocyanates (workers' safety)
- higher requirements concerning packaging and application: preventing access of water during storage and application
- high price

Two-component curing hot melts consist, e.g., of (1) polyamide and epoxy as crosslinker, or (2) polyolcomponent + isocyanate. After the mixing of the two components only a limited pot life is given. Advantages are the good heat, aging and long-term stability due to the duroplastic character.

15.2. Polyvinyl acetates

PVAc is another important type of adhesive, especially in furniture manufacturing and for carpentry. They form the bond line in a physical process by losing their water content to the two wooden adherends. PVAc adhesives are ready to use, have short setting time and give flexible and invisible joints. They are easy to clean and show long storage life. Limitations are their thermoplasticity and the creep behavior.

PVAc is a thermoplastic polymer; due to the manifold variations (homo- or copolymerizate, unmodified or modified, with or without plasticizers) it shows a great variety of processing and bonding properties. The various formulations differ in viscosity, drying speed, color of the bond line, flexibility or brittleness, hardness or smoothness and other criteria.

The bonding principle of PVAc is based on the removal of the water by penetration into the wood substance or by evaporation to the surrounding air. Bond line formation also requires a proper pressure. The final bond strength is reached after migration of the residual water from the bond line. The minimum temperature of the film formation (white point) is 4–18°C, depending on the type of the adhesive and the addition of plasticizers. This temperature mainly is determined by the glass transition temperature T_g of the polymers (second-order transition temperature). It is the border between the brittle and the elastic state of the polymer; for PVAc this temperature is approx. 28°C. Parameters that influence the drying time are the type of the adhesive, the wood surface, the absorption behavior of the wood surfaces, the wood moisture content, the relative humidity and the temperature of the surrounding air, the amount of adhesive applied and the temperature of the adhesive and the wood surfaces.

Depending on the formulations various grades of water resistance can be achieved according to EN 204 (D1–D4) [172]. For the two-component PVAc adhesives crosslinking and hence a duroplastic behavior is effectuated by addition of hardening resins (e.g. on basis of formaldehyde), complex forming salts (based

on chromium Cr III, e.g. chromium nitrate, or aluminum Al III, e.g. aluminum nitrate) or isocyanate. The bond lines are resistant against higher temperatures and the influence of water.

The addition of comonomers during the polymerization enables a higher flexibility compared to PVAc-homopolymerizates. This results in a lower glass transition temperature and a lower minimum temperature of the film formation. Possible comonomers are acrylic acid esters (butylacrylate, 2-ethylhexylacrylate), dialkylfumarates, ethylene and others.

Plasticizers soften the film and increase the adhesion and the setting speed. The most common are phthalates, adipates and benzoates. The amount added can be in a broad range of 10–50%. They affect the swelling and softening of the PVAc emulsion particles, ensure film formation at room temperature, and the tack of the still wet adhesive. They also provide improved moisture resistance of the bond. Disadvantages are the lower resistance of the bond line against heat, possible migration of the plasticizers and enhanced cold flow.

Fillers (calcium carbonate, calcium sulfate, aluminum oxide, bentonites, wood flour) increase the solid content of the dispersion. They are added up to 50%, based on PVAc. The purpose of the addition is the reduction of the penetration depth, provision of thixotropic behavior of the adhesive, gap filling properties and the reduction of the costs. Disadvantage can be the increase of the white point and a possible higher tool wear.

Other components in PVAc-formulations are defoamers, stabilizers, filler dispersants, preservatives, thickeners (hydroxyethylcellulose, carboxymethylcellulose), polyvinyl alcohols, starch, wetting agents, tackifiers, solvents (alcohols, ketone, esters), flame retardants and others.

The PVAc bond strength decreases due to the thermoplastic behavior with higher temperatures. The higher the molecular weight, the smaller is this loss of strength. Additionally, PVAc-bond lines, subjected to long-term load, may cold flow, especially when plasticizers are comprised in the formulation. Both effects limit the heat resistance of a PVAc-bond line as well as generally the long-term strength under load at higher temperatures ($>40^{\circ}\text{C}$).

16. Influence of the adhesive on the bonding process and the properties of wood products

For the production of wood-based panels various adhesives are in use like aminoplastic resins (UF, MU(P)F), phenolic resins (PF) or isocyanate (PMDI). The proper choice of the adhesive depends on the required properties of the wood-based panels, on the working conditions during the production as well as often on the costs for the adhesive system; this not only means the net price of the adhesive but the overall costs of the gluing system including glue spread factor,

Table 9

Evaluation of the three adhesive types UF, PF and PMDI concerning various parameters

Property	UF	PF	PMDI
Price	low	medium	high
Necessary hardening temperature	low	high	low
Susceptibility against wood species	high	low	low
Efficiency	low	medium to high	high
Manipulation	easy	easy	difficult
Resistance against boiling water	no	high	high

capacity of the line and other parameters. Also environmental aspects can have a significant influence on the choice of the adhesive system.

Table 9 evaluates the three adhesives UF, PF and PMDI concerning various parameters.

16.1. Viscosity

The viscosity of a glue mix is determined by the viscosity of the resin (mainly depending on the degree of condensation and the solid content) and the composition of the glue mix. If the viscosity or the degree of condensation, resp., of the resin is too low, a big portion of the resin might penetrate into the wood, causing a starved glue line. In such a case no glue line and hence no bonding strength can be formed. At a too high viscosity on the other side there might lack a proper wetting of the non-glued wood surface with no or a very low penetration into the wood surface and hence no mechanical locking. Also in these cases a low bonding strength will be caused.

Beside of the viscosity of the glue resin itself also the viscosity of the glue mix plays an important role. A higher dilution of the resin gives a higher volume to be spread and with this a better distribution of the resin on the particles or fibers with hence better bonding strength [173]. This also saves costs.

16.2. Flow behavior

The flow ability of a resin depends on its viscosity, the solid content as well as the changes in the viscosity at elevated temperatures in the hardening glue line. A low flow ability causes a poor penetration of the resin into the wood surface and low bonding strengths. A too high flow ability on the other side leads to an overpenetration of the resin into the wood and to a starved glue line. Flow ability and hardening run in opposite directions during the hot press process. Main parameters are the molar mass distribution and the concentration on reactive sites on the molecules.

16.3. Surface tension and wetting behavior

Aqueous adhesives behave similar to water concerning surface tension and wetting behavior. The higher the molar ratio, F/U, the lower is the surface tension. The surface tension can be decreased adding a detergent or few percent of a PVAc-adhesive [174,175]. The wetting behavior also depends strongly on the molecular composition of an UF-resin [174,175]. Proper wetting of the wood surface is a prerequisite for high adhesive bond strength.

16.4. Reactivity

The target of the development of adhesive resins is to achieve high reactivities mitigated by consideration of the storage stability of the resin or the pot life of the glue mix. The reactivity of a glue resin and of a glue mix is determined by various parameters:

- type of adhesive resin;
- composition and cooking procedure;
- type and amount of hardeners;
- additives, might accelerate or retard;
- hardening temperature;
- properties of the woodsurfaces.

16.5. Combination of various adhesives

For the purpose of special effects, combinations of adhesives or glue resins might be used, e.g.:

- addition of PVAc to UF-resins in order to get a better wetting of the wood surface [148,149] and a more elastic glue line
- UF/MUF + PMDI
- combination of adhesives in the particleboard or OSB-production, i.e.
core layer – PMDI
face layer – MUF-resin or PF-resin
- production of a MUF-resin by mixing an UF- and a MF-resin or an UF-resin with a MF-powder resin.

17. The wood component as influence parameter in wood gluing

The properties of wood-based panels are determined in principle by three influence parameters: (1) wood component; (2) adhesive; (3) production conditions. Only if all three parameters are appropriately considered, can proper bonding results can achieved.

The influence of wood includes a variety of topics. Wood bonding is often described as a chain of several links: wood (substance), wood surface, interface between wood and adhesive, surface of the glue line (boundary layer), glue line itself. As with all chains, the weakest link determines the strength of the chain. In wood gluing, in most cases, the interphase is the weakest link.

The strength of a glue bond depends on various parameters:

- strength of the glue line and its behavior against stresses
- influence of humidity, wood moisture content and wood preservatives
- wood properties, which can influence the strength of the glue line
- wood properties, which might cause internal stresses
- mechanical properties of the wood material.

Hence the wood, especially the wood surface (including the interface to the bond line), plays an crucial role for the quality of bonding and hence for the quality of the wood-based panels. Low or even no bonding strength can be caused by unfavorable properties of the wood surface, e.g. due to low wettability.

17.1. Influence of the wood species on properties of wood-based panels

In the wood-based panels industry, various wood species are in use. Often the choice of the used wood species is determined by the availability and price of the raw material. Additionally, in recent times higher amounts of residual wood materials as well as old wood are used. It is more than a proverb, that the quality of a wood-based panel already is established by the wood storage area. The composition of the mix of wood species as well as of the various types of origins and preparation modes usually are held as constant with time as possible for a certain board type. For various board types different wood mixes (species, shape and size of the particles) are used. The choice is based upon empiricism and is not scientifically based. Economic reasons (availability of special wood assortments, price) can play an important role, as already mentioned. Although there is a long list of papers, too long to be all reported here, dealing with special wood species in the production of wood-based panels, an overall view, however, is lacking.

17.2. Wood structure before pressing, size and shape of particles

The strength of a bond increases with the wood density in the region of approx. 0.7 to 0.8 g/cm³. Above this density, a decrease of the bond strength occurs. Performance and properties of wood-based panels are strongly influenced by the properties of the used wood. The anisotropy as well as the heterogeneity, the variability of various properties and the hygroscopicity have to be taken into account. Also the orientation of the wood fibers bonding solid wood has to be considered.

Particles as raw material for particleboards show a great variety in wood

species, origin, method of preparation and age and especially a great variety of size and shape. If wood is disintegrated to particles, a mixture of particles of very different sizes and shapes is always generated. They can be described in a simple way as square flat pieces with: length l (mm), width b (mm), thickness d (mm) and slenderness ratio $s = l/d$. The volume of a particle size is given as:

$$V = l \times b \times d \text{ (mm}^3\text{)}.$$

Considering particles with $l \gg d$, the gluing efficient surface area is:

$$F = 2 \times l \times b \text{ (mm}^2\text{)}.$$

The area form factor [176] can be considered as a measure of the gluing efficient surface area based on the volume and is inversely proportional to the thickness of the particles: $F/V = 2/d = 2 \times s/l$.

The influence of the particle size and shape on mechanical and hygroscopic properties of boards is described in several papers in the literature [177–181]. The central statement of these papers is that an increase of bending strength, compression and tension strength in the board plane, but a decrease of internal bond with greater particle length is obtained. In particleboard the particles overlap. These overlapping areas must be large enough to guarantee the transfer of the strength of the wood substance into the assembly.

17.3. Chemical behavior of wood

Wood-inherent chemicals (extractives) can influence the gluing process in physical as well as in chemical sense. Zavarin [182], Jaic et al. [183] and Liptakova et al. [184] have indicated that the chemical composition of a wood surface after processing might differ due to the concentration of polar and non-polar substances from the chemical components of wood itself. Additionally, the orientation of the wood surface (longitudinal, radial, tangential) can influence this composition. Extractives soluble in water or steam can migrate during the drying process to the wood surface and can decrease the wettability; especially fatty substances and waxes might cover the surface. Therefore, so-called chemical weak boundary layers (CWBL) are formed [185]. If extractives have a strong acidic or a strong alkaline behavior, this might cause acceleration or retardation of the hardening process using condensation resins.

Between various wood species great differences can occur in pH as well as in the buffer capacity. Even within the same wood species, differences might occur due to seasonal variations, portion of the wood substance under investigation, pH of the soil, age of the tree, time span after cutting, drying and processing parameters.

17.4. Wood surfaces

The wood surface is a complex and heterogeneous mixture of polymeric substances like cellulose, hemicellulose and lignin. It also is influenced by parameters like polymer morphology, wood extractives and processing parameters. During the processing of wood and the generation of new surfaces, damaging of the wood material and the surface can occur. This might have negative consequences in gluing (low quality of bondings, low bond strengths). The fracture picture often shows only weak wood failure or only a thin fiber layer. Reason for this can be a mechanical destruction of the uppermost wood layer, usually described as a mechanical weak boundary layer (MWBL) [185–187]. This layer consists of damaged wood cells caused by processing. A fracture of an adhesive bond at the interface between wood and adhesive can be a cohesion fracture of such a weak boundary layer [185] or a real adhesion fracture in the interface [186].

17.4.1. Contact angles of wood surfaces

A prerequisite for the gluing of two wood surfaces is the wetting of these surfaces by the liquid or liquified adhesive. Wetting includes the formation of a contact angle, the spreading of the liquid on the surface and the penetration of the liquid into the porous adherend. Good wetting enables the forming of high adhesion forces between the wood surface and the adhesive. However, direct correlations between the contact angle and the achieved bonding strength are rather rare [188] or seem not to be universal [189]. Low contact angles ($\Theta < 45^\circ$) indicate a good wetting behavior. Contact angles $>90^\circ$ indicate an incomplete wetting, which might be predictive of low bond strengths.

The primary parameters that influence surface energy and resultant bond strengths are:

- wood species [174,175,190]
- roughness of the surface [191–193]
- cutting direction radial/tangential [174,175]
- earlywood, latewood [174,175]
- direction of the spreading of the droplet during measuring the contact angles (along or lateral to the direction of the fibers) [194,195]
- wood moisture content [196–198]
- fiber angle [199]
- age of the wood surface [200,201]
- pH of the wood surface [202–204]
- type and amount of wood-inherent chemicals [205,206]
- pretreatment of the surface, e.g. by extraction with various solvents
- type of adhesive
- UF-resins [174,175]

- PF-resins [193].

During the production of wood-based panels, part of the adhesive penetrates into the wood surface. An overpenetration causes starved glue lines, whereas a low penetration limits the contact surface between wood and the adhesive; low penetration often is the consequence of bad wetting behavior.

17.4.2. Modifications of the wood surface

Modifications of the wood surface can be performed by various physical, mechanical and chemical treatments. Chemical treatments especially are performed in order to enhance the dimensional stability, but also for amelioration of physical and mechanical properties or a higher resistance against physical, chemical and biological degradation.

Increasing the water repellency of the wood substrate, e.g. by acetylation, decreases the number of hydrophilic sites on the wood surface [207]. OH-groups of the cellulose react with acetic anhydride, forming an ester. Hygroscopicity of the wood substance decreases, and in this way swelling and shrinking can be lowered. Use of acetylated fibers for the production of MDF boards gave distinct reduction of thickness swelling.

17.4.3. Seasonal variations of the wood quality in the panel board industry

The experience of the particleboard industry on the influence of seasonal variations of the wood quality has been reported. Problems occur especially using wood which has been harvested in the wintertime and which goes into board production immediately.

The contact angles of water and adhesive resin on wood are higher in the case of freshly harvested wood compared to stored chips. This means that the surface of particles from this fresh wood is more hydrophobic. This influences the wetting and the penetration negatively and with this the gluability. Reason for this lower wettability of freshly harvested wood is a higher content of some wood chemical components, or wood extractives, as has been determined by water extraction. This result, however, must not be confused with the better wettability of a freshly cut surface, independently if it is freshly harvested or stored wood.

Back [208] had found that hydrophobic wood-inherent chemicals oxidize or polymerize during storage after harvesting, as also can be seen from their lower extractability. With this effect, the ability of the wood extractives to migrate to a new surface is reduced.

The water extracts from particles made from freshly harvested wood have higher pH-values, but lower buffer capacities than surfaces made from stored chips. The former might lead to prehardening using the usual amount of hardener with the consequence of a decrease of the board strength.

18. Conditions during production as influence parameters in wood gluing

18.1. Adhesive resin consumption and glue spread

The amount of adhesive acting in the particleboard production has to be evaluated in various respects:

- quantitative portion of adhesive on individual particles
- quantitative portion of adhesive in particle mixtures and fractions
- quantitative portion of adhesive in the total particle mix
- distribution of the adhesive on the surface of the particles, portion of the surface covered with adhesive.

The gluing factor (the resin solids content on wood) as a measure of the consumption of adhesive is one of the central values during the production of particleboards. From the technological standpoint a certain minimum of resin is necessary to obtain the desired properties of the boards resulting in sufficient bonding of the individual particles. However, an excessive gluing factor imparts some technological disadvantages, like high moisture content and hence possible problems with high vapor pressure during hot-pressing. Also for economical reasons the consumption of glue resins should be as low as possible, because the resin contributes directly to the costs of the boards. The usual gluing factor, however, is only an overall average of the total mixture of particles, but without concern to differences in particle size distribution and to the shape of the individual particles. Furthermore, the gluing factor gives no direct indication of the amount of resin solids content which remains on the surface of the particles and that has not been absorbed by the wood. The former contribute to bond effectiveness, while the latter does not. The expression 'resin voracity' of the fines is well known and describes the exceedingly high consumption of adhesive based on mass of particles owing to the great surface area of the fine particles.

The gluing factor can be described in two ways:

- mass gluing factor of a fraction (% or g resin solid contents/100 g dry particles);
- surface-specific gluing factor (g resin solid contents/m² surface area).

If one of the two terms is known, the other one can be calculated assuming an uniform distribution of the resin on the particle surfaces.

In the production of particleboards, mixtures of particles are often used as raw material. The particles differ in size and shape. A particle size distribution can be done by screening, and two of the three dimensions of the particle must be smaller than the standard measure of the screen to be passed. An exact screening of the particles to their size is only possible for rather similar shapes. Particles, however, can widely differ in shape. For a simplifying description, the shape is assumed as a flat square of length l , width b and thickness d for medium and coarse particles and cubic for the fines. The mechanical screens are graded in

such a way that the particle size distribution obtained has generally Gaussian distribution. Distributions in industrial scale might differ from this model, but this is without influence on the basic results and conclusions which are given below.

Each particle fraction has a certain relation to its gluing factor according to the size of the particles. Because of the great surface area of the fine particles their gluing factors increase strongly (linearly with the term $1/d$). If there is only a small mass fraction of very fine particles in the mixture, the high consumption of resin solid content of these fractions might have a negative impact on the gluing factor of the coarse particles.

Because of the reasons described above, the core layer and face layers are glued separately, that is, the core layer contains rather coarse particles, but the face layers contains rather fine particles. However, the two distributions might overlap to some extent. This separate gluing enables one to use different compositions of the glue resin mixes (e.g. different addition of water and hardener) and different gluing factors for the individual layers.

Samples of industrial unglued and glued core layer and face layer particles, respectively, can be fractionated by sieving. Sampling has to be done at about the same time before and after the blender. Each unglued and glued particle fraction can be investigated for its nitrogen content. Knowing (1) the content of nitrogen as well as the resin solid content in the glue mix, and (2) the moisture content of the glued as well as of the unglued particles in the various fractions, the mass gluing factor of each glued particle size fraction can be determined.

Assuming that the gluing of particles of different sizes is performed randomly with their surface area as decisive parameter, for various homogeneous particle size fractions and for different particle size mixtures, the theoretical mass gluing factors and the distribution of the resin solid content can be calculated.

There are some indications [209–211], however, that gluing is not performed exactly based on surface of the particles, but with a certain preference to coarser particles. The reasons for this fact may be the performance of the gluing itself, separation and distribution of glue droplets or post-mixture of the glue on the particles (wiping effect). The area-specific gluing principle obviously loses its validity if glue droplets and the surface to be glued have similar size. Meinecke and Klauditz [209] mentioned diameters of glue droplets of 8 to 110 μm , depending on the type of spraying. Lehmann [212] mentioned diameters of up to 200 μm . The latter numbers are in the same order of magnitude as the size of the finest particles used for the calculations above.

In addition to the surface area of the particles, several other parameters have some influence on the necessary resin consumption, e.g. the type of the boards, thickness of the sanding zone, type and capacity of the blenders, separation and spraying of the glue resin (only wiping effect or spraying of the resin by air or liquid pressure), shape of the particles for the same particle sizes, dependence of

the slenderness ratio on particle length, concentration and viscosity of the glue resin or the deterioration of the coarser particles in the blender. Other parameters might also have some influence.

New strategies in blending pay tribute to the fact of the higher resin consumption of the finer particles and intend to remove the dust and the finest particles from the particle mix before blending. An exact screening and classifying of the particles before blending can improve the distribution of the resin on the particle surfaces and can help to spare resin. A lower consumption of resin not only means lower costs for the raw materials, but also helps to avoid various technological disadvantages. As the adhesive resin is applied to the particles, so is water. As long as this amount of water is low enough, especially in the core layer, no problems should occur with a too high vapor pressure during hot-pressing. Often the moisture content of the glued core particles is too high, due to an excessive gluing factor. The high vapor pressure in the board at the end of the press cycle tends to increase the fresh board thickness, this effect being called 'springback'. If venting is not done very carefully, blistering of the boards after the continuous press or after the opening of the press might occur. Additionally, the heat transfer can be delayed if the vapor pressure difference between the face layer and the core layer is smaller. If the moisture content of the glued core layer particles is high, the moisture of the glued face layer particles must be reduced. Spraying water onto the belt before the forming station and to the surface of the formed mat cannot be performed due to problems with a too high moisture content in the mat and hence with too high vapor pressure.

Gluing of particles usually is done in high-speed rotating blenders by spraying the resin mix into the blender. Due to the high rate of rotation of the blender, the particle size distribution changes during blending due to mechanical degradation of the particles. When blending OSB-strands, this destruction must be avoided. This is done by using slowly rotating large blender drums with a diameter of approx. 3 m. The liquid adhesive is applied to the wood particles by several spraying nozzles in this blender drum.

Gluing of fibers in the MDF-production usually is done in the so-called blowline between the refiner and the dryer. Advantages compared to the blending of dry fibers include avoiding resin spots at the surface of the board. The disadvantage, however, is the fact, that the resin passes the dryer and can suffer some prehardening. This causes some loss of usable resin (approx. 0.5 to 2% in absolute figures); therefore, the gluing consumption in blow line blending is higher than in mechanical blending. Due to this fact, mechanical blenders have started to be installed recently. The theory of the blow line gluing process is not yet clear [213,214].

18.2. Wood moisture content

Wood moisture content influences several important processes like wetting, flow of the adhesive, penetration into the wood surface and hardening of the adhesive in gluing and production of wood-based panels. Usually, a wood moisture content of 6–14% is judged as optimal. Lower wood moisture contents can cause a quick dryout of the glue spread due to strong absorption of the water into the wood surface as well as wetting problems. High moisture contents can lead to high flow and an enhanced penetration into the wood, causing starved glue lines. Additionally, high steam pressure can be generated within the board during hot-pressing which might give problems with blistering when the press opens. The hardening of a condensation resin can be retarded as a consequence of this.

During the hot press cycle of the particleboard or MDF production quick changes of temperature, moisture content and steam pressure occur. The established gradients of the temperature and the moisture content determine the forming of the board properties and the hardening of the resin. The combination of these gradients with the mechanical pressure applied to densify the mat is decisive for generating the density profile and hence the application properties of the boards. The higher the moisture content of the glued face layer particles, the steeper is the moisture gradient between the surface and the core of the mat and the quicker the heating up of the mat is realized. In the fiber mat no differences exist between the initial moisture content values of surface and core layers. However, due to the temperature applied to the mat surfaces a surface/core vapor pressure gradient within the board does nevertheless occur.

The moisture content of the glued particles is the sum of the wood moisture content and the water which is part of the applied glue mix. Therefore, the moisture content of the glued particles mainly depends on the gluing factor. Usual moisture contents of glued particles are 6.5–8.5% in the core layer and 10–13% in the face layer for UF, and 11–14% in the core layer and 14–18% in the face layer for PF.

The optimal moisture content of the glued and dried MDF fibers in the mat before the press is in the region of 9–11%.

Blistering at the end of the press cycle or at the end of the continuous press occurs, if the steam pressure within the fresh and still hot board exceeds the internal bond of the board. It has to be considered that the bond strengths are lower just after the press than after the board cools. Water and steam within the board are the causes of blisters. If blistering occurs using resins with low formaldehyde content, press time should be shortened instead of lengthened, because a longer press time would rather not increase the bond strength but certainly will increase the steam pressure in the board. Careful venting as well as decreasing the moisture content of the glued particles and reducing the press temperature will help.

The higher the moisture content of the particles, the easier can the face layer be densified at the start of the press cycle; this leads to a lower density in the core layer.

18.3. Pressing

During the hot press cycle (170°C to 220°C depending from the nature and age of the press), the hardening of the adhesive resin and possible reactions of the adhesive with the wood substrate take place. Pressing takes place according to well defined pressure variations (Fig. 5): a zone A from contact of the unpressed mat with the hot platens of the press to maximum pressure which also forces the steam in the core of the press, followed by a zone B of rapid decrease of pressure starting to drive the superheated steam in the board core to exit through the porous board edges. Follows then a phase C where the board is maintained to thickness and allowed to eliminate through the board edges the greatest amount possible of water under the form of steam. It is a phase of steady state in which the steam generated at the surfaces in contact with the hot press platens travels to the center of the panel and from there streams out through the board edges. In the panel industry jargon this is called the degassing phase. The last phase, phase D, is the press opening phase.

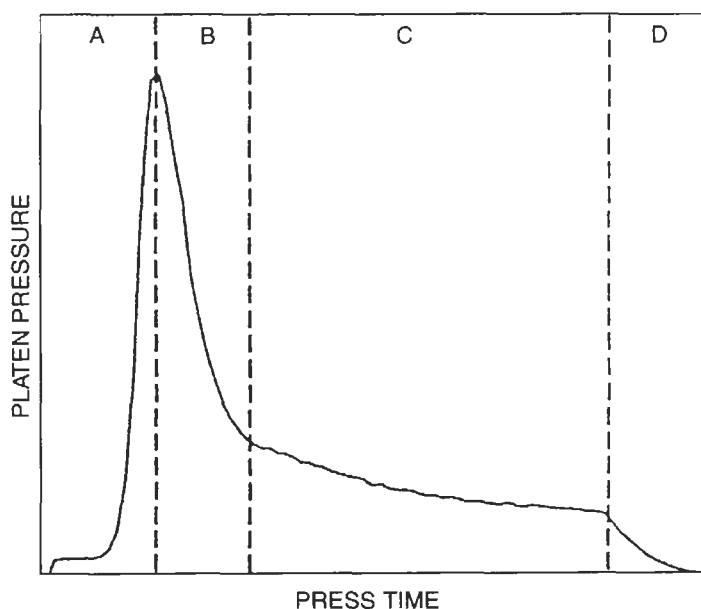


Fig. 5. Schematic diagram of pressure variation as a function of pressing time during the manufacture of wood panels. The diagram is divided into four distinct stages.

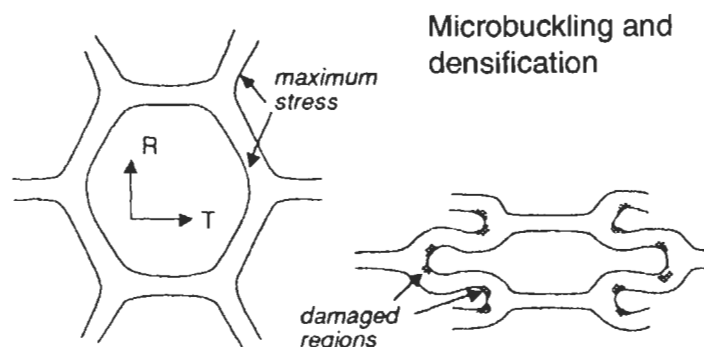


Fig. 6. Stress propagation across the wood cell walls, cell walls microbuckling and wood densification leading to the characteristic plastic deformation which wood undergoes during panel manufacture and hot-pressing.

Influence parameters are especially the press temperature and the moisture content in the mat. Additional parameters are the wood density, the porosity, the swelling and shrinking behavior of the wood, the structure at the surface and the wetting behavior. During the press cycle several mechanisms are in operation:

- transport of heat and moisture
- densification with first increasing stresses, followed by relaxation processes
- adhesion between the particles or fibers
- forming of the bond strength in the glue line (cohesion).

Simulation models describe the various conditions occurring during a press cycle (gradients of the temperature, the moisture content, the steam pressure and the formed bond strengths) which lead both to microbuckling of the wood cell walls by their moisture and temperature-induced densification (Fig. 6) [215–218].

The warming up of the mat is performed by the so-called steam shock effect [173,219]. A prerequisite for this is the high permeability of the particle or fiber mat. Higher moisture contents of the face layers and spraying of water sustain this effect.

The press temperature influences the possible press time and therefore the capacity of the production line. The minimal press time has to guarantee that the bond strength of the still hot board can withstand the internal steam pressure as well as the elastic spring back of the board when the press opens or when the board leaves the continuous press.

19. Correlation between pressing parameters and physical properties

The wood panel industry is in need of new technologies to overcome the problems associated with conventional pressing methods such as high wood dryer tempera-

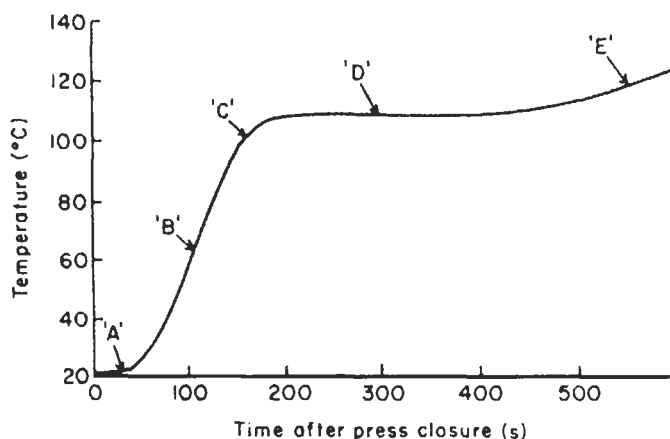


Fig. 7. Schematic representation of the temperature increase in wood particleboard core as a function of hot-pressing time.

tures, lack of tolerance by dense wood species and dimensional stability problems of the panel after manufacture. For example, when wood-based composites are hot-pressed under conditions of high temperature and low moisture content, compressive stresses are imparted to the individual wood cells resulting in damaged wood cell walls and strength losses [220–222]. The subsequent moisture release of these residual stresses, associated with microfractures of the cell walls, will lead to excessive thickness swelling of the finished board.

As regards the use in panels of high-density woods, a greater compressive pressure is required to attain a similar degree of interparticle contact when using high-density species [223,224]. The consequence of this is an increase in the board thickness swelling when immersed in water or placed in a high moisture content environment [224].

The temperature profile, namely the increase in board temperature as a function of the time after press closure can be divided into five periods [225] (Fig. 7).

The initial phase, A, corresponds to the phase of heat transfer from the press platens to the wood mat just after press closure. Phase B is a rapid temperature rise in the core of the board, such an increase corresponding to steam flow and condensation in the cold areas of the wood mat. The steam flow is governed by the vapor pressure gradient between the surfaces and the core layer. The main heat transfer mechanism is by convection. A fast press closing rate will then lead to a higher vapor pressure in the surface layers and hence to a marked vapor gradient across the thickness of the board. Phase B, contrary to what is stated in the literature [219,225], does not present a linear trend in the case of high moisture content (MC) tolerant adhesive in Figs. 8–10 but is divided in an earlier slower rise in temperature followed by a period of much more rapid temperature rise.

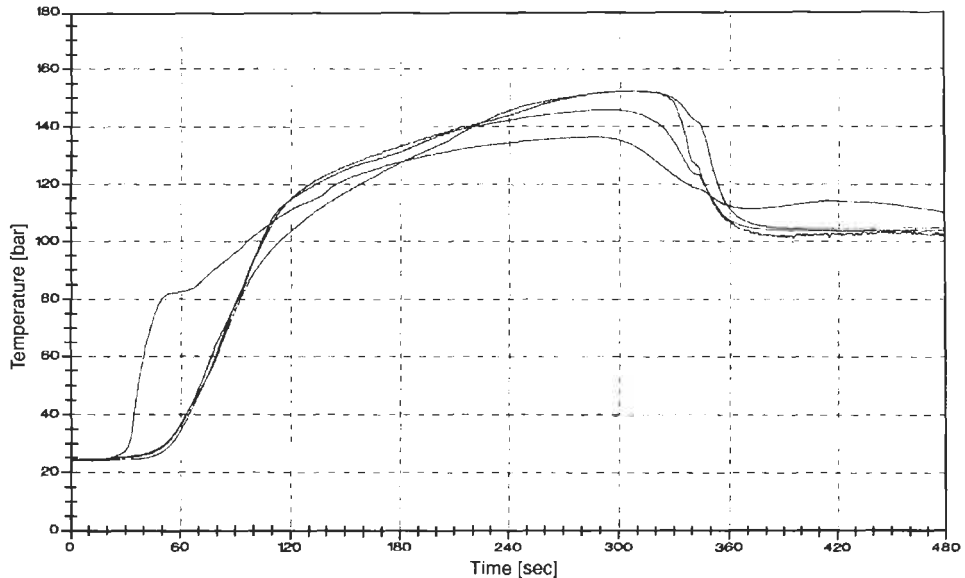


Fig. 8. Temperature increase as a function of pressing time in the core layer of an industrial OSB of $2440 \times 1220 \times 12$ mm dimensions. The highest temperature is reached in the region of the panel comprised between the panel center and 500 mm from the board edge. The fastest initial increase in temperature but lowest max. temperature is for the region nearest to the board edge (100 mm from the board edge).

Phase C corresponds to a decreasing rate of temperature rise in the board core at about 100°C . It is followed by stabilization of the temperature, namely phase D. This latter being due to decrease of the steam gradient due to moisture escape from the board edges, and the increase and decrease of the wood wetting heat, respectively, near the board surface and in the core layer. Phase E, a new slow increase in temperature is observable in standard moisture content boards [225] but is absent at high moisture content (due to the maintenance of some moisture in the core layer), contrary to the case of traditional moisture content adhesives, as shown in Fig. 8.

When pressing at higher moisture content (MC) the initial temperature rise lengthens for longer closing times while it is faster at faster press closing rates. The latter is due to rapid mat densification inducing better strand contact and hence faster heat conduction [226]. Thus, in spite of the lower permeability of the wood mat induced by the greater densification at faster press closures the steam continues to flow by convection between the wood strands and continues to condense onto the colder material. At longer press closing times, heat transport is slower and moreover the steam will follow the way of least resistance and hence flow along the steam pressure gradient toward the board edges. There steam

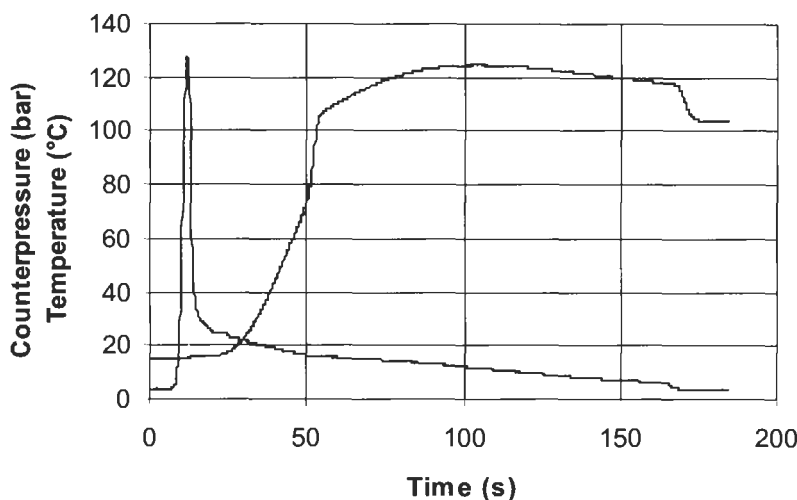


Fig. 9. Effect of press closing rate: variation of counterpressure and temperature increase as a function of pressing time in the core layer of an OSB panel at a press closing time of 10 s.

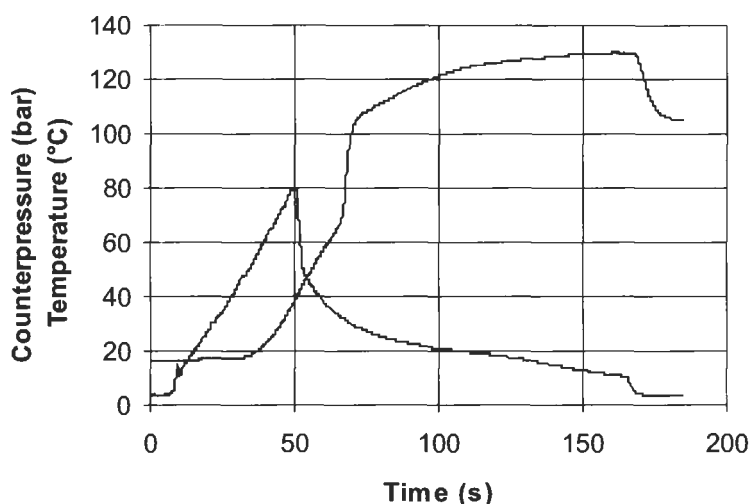


Fig. 10. Effect of press closing rate: variation of counterpressure and temperature increase as a function of pressing time in the core layer of an OSB panel at a press closing time of 50 s.

escape is easier as mat density is still low and permeability parallel to the board surfaces is relatively favorable.

The press closing time also influences the relative densifications of the surface and core layers of the wood mat during pressing (Figs. 9 and 10). Fig. 11 details the density profile of the particleboard panels prepared at short and longer press closing times [226]. The two cases differ in several aspects. (1) A short

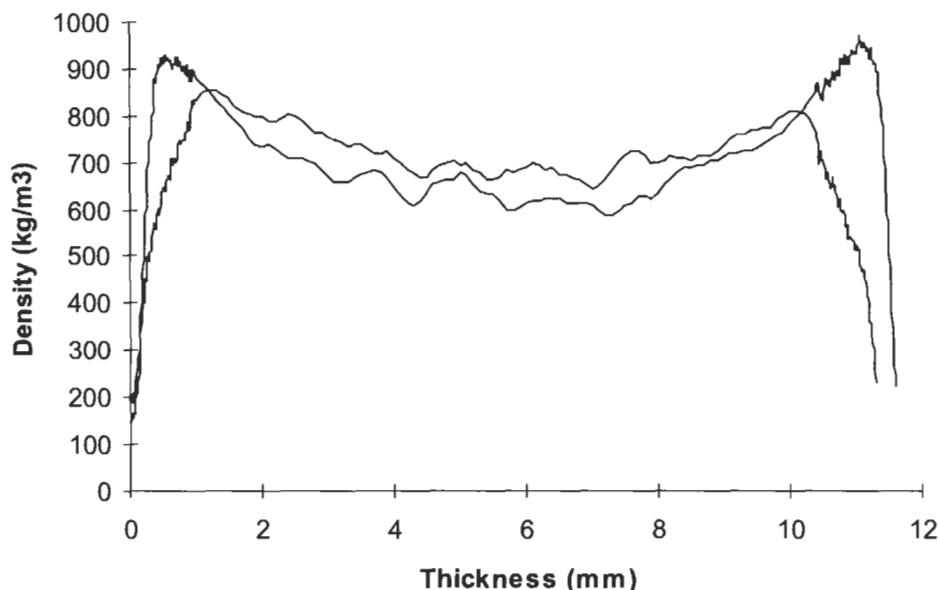


Fig. 11. Laboratory OSB board density profile as a function of board thickness when using 10 s and 50 s press closing times. Note the much higher peaks of surface density for the 10 s case, and the more even density profile for the slower press closing time.

press closing time induces a 'U-shaped' density profile of the panel. Density is highest in the middle of the surface layer and decreases along a regular gradient to a minimum in the core. (2) A longer closing time induces an 'M-shaped' configuration of the density profile. The density near the panel surface is somewhat lower than deeper inside the outer core of the panel.

In the case of the faster press closure, rapid steam generation occurs directly after the press hot platen contact. The high temperature and moisture content at the surface layer enables greater wood plasticization, hence considerably reducing the surface layer resistance to compaction and resulting in its marked densification. However, the closing time is too short to allow the steam front to reach the central core layer, which consequently remains at its initial temperature and is hence not very pliable and densifies much less. At longer press closing times the steam generated at the surface can more rapidly flow to the mat core layer. Because of the quick water depletion of the board surface, less plasticization of the surface layer will occur yielding board faces of lower density. The moisture lost by the board face is gained by the adjacent layer, at approximately 2 mm depth. This layer, which now becomes more pliable, yields the density peak observed in Fig. 11. As steam flow proceeds during closing time, the high mat permeability allows the steam front to reach the core layer of the board, where water condensation leads to moisture and temperature increases, in the most favorable case up to 50°C.

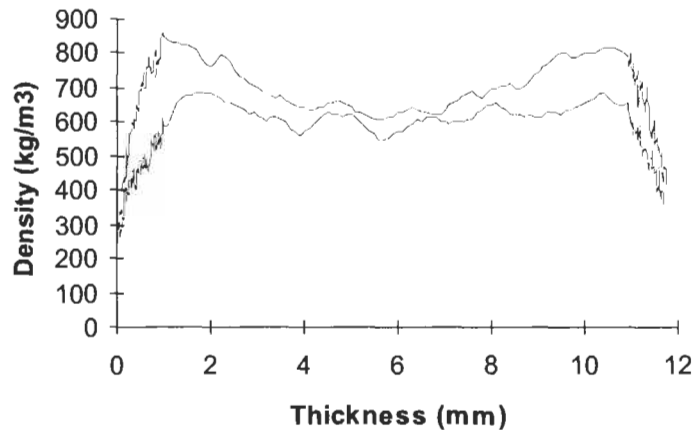


Fig. 12. Laboratory OSB board density profile as a function of board thickness when the board average density of the panel is different (590 kg/m^3 and 690 kg/m^3). Note the much higher peaks of surface density for the panel of higher average density, and the more even density profile for the panel of lower average density.

The temperature of pressing has also a noticeable effect [226,227] as it does influence the surface/core temperature gradient and has a direct influence on the temperature rise in the board core layer. In short, the higher the press temperature, the faster the heat conduction and the faster the development of the steam gradient across the wood mat. The press temperature will influence the steam front transfer time to the core layer. The higher the initial temperature, the faster the steam front enters the mat core. Increasing the press temperature will cause the maximum steam pressure peak to appear earlier but does not result in a higher core temperature.

Overall board density will strongly affect core layer plasticization and density profile (Fig. 12), as at the highest overall board density a steep density gradient appears between the surface and core layers of the board. This is due to the greater difficulty encountered by the steam to penetrate and plasticize it. At lower density, the greater mat permeability enables a faster steam throughflow of the board, comparable to a steam injection process. The final result is similar as the overall board density is closer in value to both core and surface densities.

The initial moisture content is a determinant factor in the rate of heat transfer to the center of the core mat [226,227]. At short press closing times the rapid temperature rise occurs at the same time for both lower and higher moisture content percentages indicating that the steam condensation front reaches the core at the same rate and that this is then determined more by local permeability rather than local moisture content. The slope of the rise is similar as it is the balance of horizontal and vertical permeability which controls the rate of steam flow to the core layer. Furthermore, water remains in the surface layer in a quantity such as

to enable steam generation at a rate greater than such steam can escape through the mat edges. One major difference is, however, in the maximum temperature attained. A higher temperature maximum of the core temperature occurs at higher moisture content and a lower maximum temperature is reached for lower moisture content boards. Phase D is controlled by the edge steam escape rate, the rate of vapor flow from the surfaces and the rate of vapor generation in the core layer. This result indicates that the moisture content of the surface layer will deplete faster for the lower moisture content cases and hence limit the maximum steam pressure in the board core. As the pressure closely controls the temperature this explains the much higher temperature measured for higher moisture content cases. The situation is different at longer closing times; although the first temperature rise appears at the same time, the rise is faster at higher MC than at lower MC. Since temperature rise depends upon mat permeability, this remaining high during press closing, steam escape through the edges depletes the MC of the surface layers, hence slowing down the rate at which heat enters the board core. This occurrence is all the more marked the lower the MC is.

The wood mat environment during hot-pressing is rather different in industrial boards since the size of the panel is a determining parameter as regards internal permeability and steam flow. For example Humphrey and Bolton [218,228] found pressures three times higher in industrial boards than in laboratory boards as well as differences in heating rates. In reality steam pressure increases until the degassing period begins. The edge effect appears clearly on steam pressure curves (the curve shifts progressively to lower pressure nearer the site is to the board edge) as a gradient of pressure develops from the board center to the edges. Gas flow through particleboard can be described by Darcy's law which shows that increasing the length of the steam path, hence the dimensions of the wood mat with all the other parameters held constant, will result in a smaller volumetric steam flow rate. Clearly, a given steam volume at 100 mm from the board edge will escape from the edge with greater ease than an equivalent steam volume in the board center. This leads to greater steam accumulation in the board center than in sites nearer to the board edges. Thus, the steam pressure gradient, which is observed during particleboard pressing, is merely the result of Darcy's law and the gradient is steeper towards the board edges. As resin hardening is strongly temperature dependent [16,83], the lower temperature due to lower steam pressure at the board edges will noticeably decrease the cure rate of the adhesive with consequent fall off of board properties at the edges. This is supported by the dry internal bond (IB) strength results for industrial OSB panels [226,227] showing that a temperature difference of 25°C induces a strength reduction of 0.25 MPa, or expressed in percentage, a decrease of approximately 70% in IB strength. This is furthermore related to density profile at the different sites. Samples at the board edge show a much lower core layer density than in the board middle. As the difference noticed was shown not to be ascribed to a

variable rheological behavior of the strands [226,227] this effect can be ascribed to adhesive strength development which appears to strongly influence the final board density profile [83,226,227]. A way to understand this relation is to consider the measured IB strength as a macroscopic, apparent strength parameter resulting from the difference between the net strength of the hardened network less the residual stress of the board remaining at the end of the pressing cycle (i.e. $IB_{macro} \approx IB_{network} - \text{Residual Stress}$). Thus, bonding which is so poor that it cannot withstand the excess of residual stress in the board at the end of the press cycle will allow some strain recovery, hence damaging the hardened network, in turn impairing the final IB_{macro} strength of the panel.

Liquid water has also been found to act as a transport medium and hence can contribute to heat transfer during hot-pressing, although its total contribution to total heat transfer cannot be easily evaluated [226,227]. Furthermore, Humphrey and Bolton [217,228] have pointed out that only part of the water brought through the liquid adhesive application process is absorbed by wood (if equilibrium is achieved before pressing) the rest being retained by the resin. It is also possible that some capillary translation of resin through the board could contribute to heat transfer, this becoming more pronounced at high quantity of free water. Unfortunately, a high proportion of water in the adhesive will also cause extensive resin flow which can alter bonding quality and result in poorer internal bond values. This underlines one of the essential characteristics of suitable wood adhesives, namely their capacity of developing more quickly a hardened network resistant to solution in water.

References

1. Kollmann, F.F.P., Kuenzi, E.W. and Stamm, A.J., *Principles of Wood Science and Technology, Vol. II, Wood-Based Materials*. Springer, New York, 1975, pp. 34–93.
2. European Norm EN 312, Wood particleboard — Specifications, 1995.
3. European Norm EN 1087-1, Wood particleboard. Determination of resistance to humidity. Boiling water test, 1997.
4. European Norm EN 321, Wood fibre panels — cycle tests under humid conditions, 1994.
5. European Norm EN 622-2, Wood fibre panels — Specification requirements for hard-board, 1998.
6. European Norm EN 622-5, Wood fibre panels — Specification requirements for dry panels (MDF), 1998.
7. European Norm EN 636, Plywood panels — Specifications, 1997.
8. Committee of European Norms (CEN), provisional norms prEN.
9. Dunky, M., Aminoplastic glue resins. In: Woebecken, W. (Ed.), *Duroplastics*, Vol. 10. Carl Hanser, Munich, 1988, pp. 593–614.
10. European Norm EN 120, Wood-based panels. Determination of formaldehyde content. Perforator extraction method, 1995.
11. European Norm EN 717-2, Wood-based panels. Determination of formaldehyde emission.

- Formaldehyde emission by gas analysis method, 1996.
12. Dunky, M., Urea-formaldehyde glue resins. In: Salamone, J.C. (Ed.), *Polymeric Materials Encyclopedia*, Vol. 11. CRC Press, Boca Raton, FL, 1996.
13. Lederer, K., Aminoplaste. In: Batzer, H. (Ed.), *Polymere Werkstoffe*, Vol. III. Thieme, Stuttgart, 1984, pp. 95–291.
14. Meyer, B., *Urea-formaldehyde Resins*. Addison-Wesley, London, 1979.
15. Petersen, H., Aminoresins. In: Büchel, K.H. (Ed.), *Methods of Organic Chemistry*, Vol. E20, *Macromolecular substances*, Bartl, H. and Falbe, J. (Eds.), G. Thieme, Stuttgart, 1987, pp. 1811–1890.
16. Pizzi, A., *Wood Adhesives, Chemistry and Technology*. Marcel Dekker Inc., New York, 1983.
17. Pizzi, A., *Advanced Wood Adhesives Technology*. Marcel Dekker Inc., New York, 1994.
18. Pizzi, A. and Mittal, K.L., *Handbook of Adhesive Technology*. Marcel Dekker Inc., New York, 1994.
19. Kim, M.G., Amos, L.W. and Barnes, E.E., *Ind. Eng. Chem. Res.*, **29**, 2032–2037 (1990).
20. Soulard, C., Kamoun, C. and Pizzi, A., *J. Appl. Polym. Sci.*, **72**, 277–289 (1999).
21. Brunnmüller, F., Grabowsky, O., Petersen, H., Lenz, J., Wittmann, O., Mayer, J., Erhardt, K. and Reuther, W., German patent DE 2207921, assigned to BASF AG, 1972.
22. German patent DE 2550739, assigned to BASF AG, 1975.
23. United States patent USP 2,605,253, assigned to Röhm and Haas Co., 1950.
24. United States patent USP 2,683,134, assigned to Allied Chemical and Dye Co., 1951.
25. Dunky, M., Lederer, K. and Zimmer, E., *Holzforsch. Holzverwert.*, **33**, 61–71 (1981).
26. Dunky, M., *Holzforsch. Holzverwert.*, **37**, 75–82 (1985).
27. Myers, G.E., In: *Wood Adhesives in 1985: Status and Needs*, Proceedings, Madison, WI, 1985, pp. 119–156.
28. Yamaguchi, H., Higuchi, M. and Sakata, I., *Mokuzai Gakkaishi*, **26**, 199–204 (1980).
29. Myers, G.E., *Wood Sci.*, **15**, 127–138 (1982).
30. Myers, G.E. and Koutsky, J.A., *For. Prod. J.*, **37**, 56–60 (1987).
31. Cremonini, C. and Pizzi, A., *Holzforsch. Holzverwert.*, **49**, 11–15 (1997).
32. Cremonini, C. and Pizzi, A., *Holz Roh- Werkst.*, **57**, 318 (1999).
33. Kamoun, C. and Pizzi, A., *Holz Roh- Werkst.*, **56**, 86 (1998).
34. Prestifilippo, M., Pizzi, A., Norback, H. and Lavisci, P., *Holz Roh- Werkst.*, **54**, 393–398 (1996).
35. Myers, G.E., *For. Prod. J.*, **33**, 49–57 (1983).
36. Czepel, H., German patent DE 2455420, assigned to Lentia GmbH, 1976.
37. German patent DE 3442454 (1984), European patent EP0185205, B1 (1986). Process for the preparation of melamine-urea-formaldehyde condensates. Assigned to BASF AG.
38. Hoetjer, J.J., European patent EP 0062389, B1. Manufacture of chipboard and a novel suitable bonding agent. Assigned to Methanol Chemie Nederland, 1982.
39. McCaskey, H.O. Jr., United States patent USP 4,123,579. Resin coated substrate using a short-set, high-flow melamine-formaldehyde impregnating resin. Assigned to Westinghouse Electric Corp., 1978.
40. Breyer, R.A., Hollis, S.G. and Jural, J.J., United States patent USP 5,681,917. Low mole ratio melamine-urea-formaldehyde resin. Assigned to Georgia-Pacific Resins, Inc., 1997.
41. Mercer, T.A. and Pizzi, A., *Holzforsch. Holzverwert.*, **46**, 51–54 (1994).
42. Maylor, R., In: *Wood Adhesives 1995*, Proceedings, Portland, OR, 1995, pp. 115–121.
43. Kaesbauer, F. and Bolz, W., German patent DE 3116547. Assigned to BASF AG, 1981.
44. Dudeck, C., Diem, H., Etling, H. and Siegler, M., European patent EP 0052212, B1. Method of preparing aminoplast resins. Assigned to BASF AG, 1981.

45. Chow, S. and Pickles, K.J., *Wood Sci.*, **9**, 80–83 (1976).
46. Neusser, H. and Schall, W., *Holzforsch. Holzverwert.*, **24**, 108–116 (1972).
47. German patent DE 2020481, Wood adhesive. Assigned to BASF AG, 1970.
48. Diem, H., Fritsch, R., Lehnert, H., Matthias, G., Schatz, H. and Wittmann, O., German patent DE 3125874. Process for the preparation of cocondensates which form weather-proof adhesive bonds. Assigned to BASF AG, 1981.
49. Diem, H., Fritsch, R., Lehnert, H., Matthias, G., Schatz, H. and Wittmann, O., German patent DE 3145328. Process for the preparation of cocondensates which form a weatherproof adhesive bond. Assigned to BASF AG, 1981.
50. Prestifilippo, M. and Pizzi, A., *Holz Roh- Werkst.*, **54**, 272 (1996).
51. Cremonini, C., Pizzi, A. and Tekely, P., *Holz Roh- Werkst.*, **54**, 85–88 (1996).
52. Braun, D. and Krauß, W., *Angew. Makromol. Chem.*, **108**, 141–159 (1982).
53. Braun, D. and Krauß, W., *Angew. Makromol. Chem.*, **118**, 165–182 (1983).
54. Braun, D. and Ritzert, H.-J., *Angew. Makromol. Chem.*, **125**, 9–26 (1984).
55. Braun, D. and Ritzert, H.-J., *Angew. Makromol. Chem.*, **125**, 27–36 (1984).
56. Higuchi, M. and Sakata, I., *Mokuzai Gakkaishi*, **25**, 496–502 (1979).
57. Higuchi, M., Shimokawa, H. and Sakata, I., *Mokuzai Gakkaishi*, **25**, 630–635 (1979).
58. Higuchi, M., Tohmura, S. and Sakata, I., *Mokuzai Gakkaishi*, **40**, 604–611 (1994).
59. Ferg, E.E., Pizzi, A. and Levendis, D., *J. Appl. Polym. Sci.*, **50**, 907–915 (1994).
60. Mercer, T.A. and Pizzi, A., *J. Appl. Polym. Sci.*, **61**, 1697–1702 (1996).
61. Mercer, T.A. and Pizzi, A., *J. Appl. Polym. Sci.*, **61**, 1687–1696 (1996).
62. Panamgama, L.A. and Pizzi, A., *J. Appl. Polym. Sci.*, **59**, 2055–2068 (1996).
63. Steiner, P.R., Troughton, G.E. and Andersen, A.W., In: *Adhesives and Bonded Wood Products*, Proceedings, Seattle, WA, 1991, pp. 205–214.
64. Clarke, M., Steiner, P.R. and Anderson, A.W., United States patent USP 4,824,896. Phenol formaldehyde adhesives for bonding wood pieces of high moisture content and composite board and veneers bonded with such adhesive. Assigned to the inventors, 1989.
65. Duval, M., Bloch, B. and Kohn, S., *J. Appl. Polym. Sci.*, **16**, 1585–1602 (1972).
66. So, S. and Rudin, A., *J. Appl. Polym. Sci.*, **41**, 205–232 (1990).
67. Wagner, E.R. and Greff, R.J., *J. Polym. Sci.*, **A1(9)**, 2193–2207 (1971).
68. Oldörp, K., In: Klein, J. and Marutzky, R. (Eds.), *Klebstoffe für Holzwerkstoffe und Faserformteile*, Proceedings, Braunschweig, 1997.
69. Oldörp, K. and Miertzsch, H., *Holz Roh- Werkst.*, **55**, 97–102 (1977).
70. Johnson, St.E. and Kamke, F.A., *J. Adhes.*, **40**, 47–61 (1992).
71. Johnson, St.E. and Kamke, F.A., *Wood Fiber Sci.*, **26**, 259–269 (1994).
72. Haupt, R.A. and Sellers Jr., T., *For. Prod. J.*, **44(2)**, 69–73 (1994).
73. Ellis, S., *For. Prod. J.*, **43(2)**, 66–68 (1993).
74. Ellis, S. and Steiner, P.R., In: *Wood Adhesives 1990*, Proceedings, Forest Products Society, Madison, WI, 1990, p. 76–85.
75. Ellis, S. and Steiner, P.R., *Wood Fiber Sci.*, **23(1)**, 85–97 (1991).
76. Nieh, W.L.-S. and Sellers Jr., T., *For. Prod. J.*, **41(6)**, 49–53 (1991).
77. Stephens, R.S. and Kutscha, N.P., *Wood Fiber Sci.*, **19**, 353–361 (1987).
78. Gollob, L., Krahmer, R.L., Wellons, J.D. and Christiansen, A.W., *For. Prod. J.*, **35(3)**, 42–48 (1985).
79. Young, R.H., In: *Wood Adhesives in 1985: Status and Needs*, Proceedings, Forest Products Society, Madison, WI, 1985, pp. 267–276.
80. Haupt, R.A. and Sellers Jr., T., *Ind. Eng. Chem. Res.*, **33**, 693–697 (1994).
81. Pizzi, A. and Stephanou, A., *J. Appl. Polym. Sci.*, **49**, 2157–2170 (1993).
82. Pizzi, A. and Stephanou, A., *Holzforschung*, **48**, 35–40 (1994).

83. Lu, X. and Pizzi, A., *Holz Roh- Werkst.*, **56**, 339–346 (1998).
84. Pizzi, A., Mtsweni, B. and Parsons, W., *J. Appl. Polym. Sci.*, **52**, 1847–1856 (1994).
85. Pizzi, A., Vosloo, R., Cameron, F.A. and Orovan, E., *Holz Roh- Werkst.*, **44**, 229–234 (1986).
86. Christiansen, A.W., *For. Prod. J.*, **35**(9), 47–54 (1985).
87. Pizzi, A., Garcia, R. and Wang, S., *J. Appl. Polym. Sci.*, **66**, 255–266 (1997).
88. Pizzi, A. and Stephanou, A., *Holzforschung*, **48**, 150–156 (1994).
89. Riedl, B. and Park, B.-D., In: *Wood Adhesion Research*, Proceedings, Forest Products Society, Merida, MX, 1998, pp. 115–121.
90. Steiner, P.R., Troughton, G.E. and Andersen, A.W., *For. Prod. J.*, **43**(10), 29–34 (1993).
91. Tohmura, S., *J. Wood Sci.*, **44**, 211–216 (1998).
92. Tohmura, S. and Higuchi, M., *Mokuzai Gakkaishi*, **41**, 1109–1114 (1995).
93. Zhao, C., Pizzi, A. and Garnier, S., *J. Appl. Polym. Sci.*, **74**, 359–378 (1999).
94. Zhao, C., Pizzi, A., Kühn, A. and Garnier, S., *J. Appl. Polym. Sci.*, **77**(2), 249–259 (2000).
95. Gramstad, T. and Sandstroem, J., *Spectrochim. Acta*, **25A**, 31 (1969).
96. Scopelitis, E. and Pizzi, A., *J. Appl. Polym. Sci.*, **48**, 2135–2146 (1993).
97. Oldörp, K. and Marutzky, R., *Holz Roh- Werkst.*, **56**, 75–77 (1998).
98. Tomita, B. and Hse, C.-Y., *J. Polym. Sci., Polym. Chem.*, **30**, 1615–1624 (1992).
99. Tomita, B. and Hse, C.-Y., *Mokuzai Gakkaishi*, **39**, 1276–1284 (1993).
100. Tomita, B., Ohyama, M. and Hse, C.-Y., *Holzforschung*, **48**, 522–526 (1994).
101. Tomita, B., Ohyama, M., Itoh, A., Doi, K. and Hse, C.-Y., *Mokuzai Gakkaishi*, **40**, 170–175 (1994).
102. Tomita, B., Yoshida, Y. and Hse, C.-Y., In: *Adhesive Technology and Bonded Tropical Wood Products*, Proceedings, USDA Forest Service and Taiwan Forestry Research Institute, Taipei, 1993, pp. 71–83.
103. Ohyama, M., Tomita, B. and Hse, C.-Y., *Holzforschung*, **49**, 87–91 (1995).
104. Pizzi, A., Stephanou, A., Antunes, I. and de Beer, G., *J. Appl. Polym. Sci.*, **50**, 2201–2207 (1993).
105. Yoshida, Y., Tomita, B. and Hse, C.-Y., *Mokuzai Gakkaishi*, **41**, 652–658 (1995).
106. Tomita, B. and Hse, C.-Y., *Int. J. Adhes. Adhes.*, **18**, 69–79 (1994).
107. Kulvijk, E., *Adhes. Age*, **20**, 33–34 (1977).
108. Trosa, A. and Pizzi, A., *Holz Roh- Werkst.*, **55**, 306 (1997).
109. Chen, C.M., *Holzforschung*, **36**, 65–70 (1982).
110. Dix, B. and Marutzky, R., *Adhäsion*, **26**(12), 4–10 (1982).
111. Driljic, R.M., FAO-Bericht World Consultation on Wood Based Panels, New Dehli, 1975.
112. Deppe, H.-J. and Ernst, K., *Holz Roh- Werkst.*, **29**, 45–50 (1971).
113. Pizzi, A. and Walton, T., *Holzforschung*, **46**(6), 541–547 (1992).
114. Pizzi, A., Valenzuela, J. and Westermeyer, C., *Holzforschung*, **47**(1), 69–72 (1993).
115. Hse, C.-Y., Geimer, R.L., Hsu, W.E. and Tang, R.C., *For. Prod. J.*, **45**(1), 57–62 (1995).
116. Dinwoodie, J.M., Properties and performance of wood adhesives. In: Pizzi, A. (Ed.), *Wood Adhesives Chemistry and Technology*, Ch. 1. Marcel Dekker, New York, 1983, pp. 1–58.
117. Kreibich, R.E., In: Pizzi, A. (Ed.), *Wood Adhesives: Present and Future*. Applied Polymer Symposium, 40, 1984, pp. 1–18.
118. Pizzi, A., Rossouw, D. du T., Knuffel, W. and Singmin, M., *Holzforsch. Holzverwert.*, **32**(6), 140–151 (1980).
119. Pizzi, A., Horak, R.M., Ferreira, D. and Roux, D.G., *Cell. Chem. Technol.*, **13**, 753–767 (1979).
120. Raff, R.A.V. and Silverman, B.M., *Ind. Eng. Chem.*, **43**, 1423–1430 (1951).

121. Rossouw, D. du T., Pizzi, A. and McGillivray, G., *J. Polym. Sci., Polym. Chem.*, **18**, 3323–3334 (1980).
122. Pizzi, A. and van der Spuy, P., *J. Polym. Sci., Polym. Chem.*, **18**, 3477–3483 (1980).
123. Marra, G.G., *For. Prod. J.*, **6**, 97–101 (1956).
124. Raff, R.A.V. and Silverman, B.M., *Can. Chem.*, **29**, 857–862 (1951).
125. Ingram, A.R., *Can. Chem.*, **29**, 863–868 (1951).
126. Liu, C.T. and Naratsuka, T., *Mokuzai Gakkaishi*, **15**, 79–85 (1969).
127. Rhodes, P.H., *Mod. Plast.*, **24**(2), 145–148 (1947).
128. Moul, R.H., In: Skeist, I. (Ed.), *Handbook of Adhesives*, 2nd ed. Reinhold, New York, 1977, pp. 417–423.
129. Specification for synthetic resin adhesives for wood, Part 2; Close contact joints. *British Standard BS 1204-1965*, 1965.
130. Standard specification for phenolic and aminoplastic adhesives for laminating and finger-jointing of timber, and for furniture and joinery. *SABS 1349-1981*, South African Bureau of Standards, 1981.
131. Baxter, G.F. and Kreibich, R.E., *For. Prod. J.*, **23**(1), 17–27 (1973).
132. Caster, R.W., *For. Prod. J.*, **23**(1), 26–28 (1973).
133. Ericson, H., *Papper Tra*, **1**, 19–21 (1975).
134. Kreibich, R.E., *Adhes. Age*, **17**, 26–28 (1975).
135. Pizzi, A. and Cameron, F.A., *For. Prod. J.*, **34**(9), 61–67 (1984).
136. Pizzi, A. and Cameron, F.A., In: Pizzi, A. (Ed.), *Wood Adhesives Chemistry and Technology*, Vol. 2. Marcel Dekker, New York, 1989, pp. 229–306.
137. Scopelitis, E. and Pizzi, A., *J. Appl. Polym. Sci.*, **47**, 351–362 (1993).
138. Lay, D.G. and Cranley, P., Polyurethane adhesives. In: Pizzi, A. and Mittal, K.L. (Eds.), *Handbook of Adhesive Technology*, Ch. 24. Marcel Dekker Inc., New York, 1994, pp. 405–430.
139. Marcinko, J.J., Phanopoulos, C. and Teachey, P.Y., In: *Wood Adhesives 2000*, Proceedings, Forest Products Society, Madison, WI, 2001.
140. Johns, W.E., The chemical bonding of wood. In: Pizzi, A. (Ed.), *Wood Adhesives: Chemistry and Technology*, Ch. 3, Vol. 2. Marcel Dekker Inc., New York, 1989, pp. 75–96.
141. Wendler, S.L. and Frazier, C., *Int. J. Adhes. Adhes.*, **16**(3), 179–186 (1996).
142. Pizzi, A. and Owens, N.A., *Holzforschung*, **49**, 269–272 (1995).
143. Frisch, K.C., Rumao, L.P. and Pizzi, A., Diisocyanates as wood adhesives. In: Pizzi, A. (Eds.), *Wood Adhesives: Chemistry and Technology*, Ch. 6. Marcel Dekker Inc., New York, 1983, pp. 289–316.
144. Pizzi, A., *For. Prod. J.*, **28**(12), 42–48 (1978).
145. Pizzi, A. and Sorfa, P., *Holzforsch. Holzverwert.*, **31**, 5–7 (1979).
146. Pizzi, A., In: *Wood Adhesion Research*, Proceedings, Forest Products Society, Merida, MX, 1998, pp. 13–30.
147. Pichelin, F., Kamoun, C. and Pizzi, A., *Holz Roh- Werkst.*, **57**(5), 305–317 (1999).
148. Heinrich, H., Pichelin, F. and Pizzi, A., *Holz Roh- Werkst.*, **54**(4), 262 (1996).
149. Pizzi, A., Stracke, P. and Trosa, A., *Holz Roh- Werkst.*, **55**(3), 168 (1997).
150. Wang, S. and Pizzi, A., *Holz Roh- Werkst.*, **55**(3), 174 (1997).
151. Pizzi, A., Roll, W. and Dombo, B., United States patent USP 5,532,330. Heat-curable tannin-based binding agents. Assigned to Rutgerswerke AG, 1996.
152. Meikleham, N., Pizzi, A. and Stephanou, A., *J. Appl. Polym. Sci.*, **54**, 1827–1845 (1994).
153. Pizzi, A., Meikleham, N. and Stephanou, A., *J. Appl. Polym. Sci.*, **55**, 929–933 (1995).
154. Pizzi, A. and Meikleham, N., *J. Appl. Polym. Sci.*, **55**, 1265–1269 (1995).

155. Masson, E., Merlin, A. and Pizzi, A., *J. Appl. Polym. Sci.*, **60**, 263–269 (1996).
156. Masson, E., Pizzi, A. and Merlin, A., *J. Appl. Polym. Sci.*, **60**, 1655–1664 (1996).
157. Masson, E., Pizzi, A. and Merlin, A., *J. Appl. Polym. Sci.*, **64**, 243–265 (1997).
158. Pizzi, A., Meikleham, N., Dombo, B. and Roll, W., *Holz Roh- Werkst.*, **53**, 201–204 (1995).
159. Garcia, R. and Pizzi, A., *J. Appl. Polym. Sci.*, **70**(6), 1093–1109 (1998).
160. Garcia, R. and Pizzi, A., *J. Appl. Polym. Sci.*, **70**(6), 1111–1119 (1998).
161. Nimz, H.H., Lignin-based wood adhesives. In: Pizzi, A. (Eds.), *Wood Adhesives: Chemistry and Technology*, Ch. 5. Marcel Dekker Inc., New York, pp. 247–288, 1983.
162. Tahir, P. Md. and Sellers, T. Jr., 19th IUFRO World Congress, Montreal, QC, August, 1990.
163. Calvé, L., 19th IUFRO World Congress, Montreal, QC, August, 1990.
164. Stephanou, A. and Pizzi, A., *Holzforschung*, **47**(5), 439–445 (1993).
165. Stephanou, A. and Pizzi, A., *Holzforschung*, **47**(6), 501–506 (1993).
166. Shen, K.C., *For. Prod. J.*, **24**(2), 38–44 (1974).
167. Shen, K.C., *For. Prod. J.*, **27**(5), 32–38 (1977).
168. Fung, D.P.C., Shen, K.C. and Calvé, L., *Report OPX 180 E*, Eastern Forest Products Laboratory, Ottawa, ON, 1977.
169. Nimz, H.H. and Hitze, G., *Cell. Chem. Technol.*, **14**, 371–382 (1980).
170. Kharazipour, A., Haars, A., Shekholeslami, M. and Hüttermann, A., *Adhäsion*, **35**, 30–36 (1991).
171. Kharazipour, A., Hüttermann, A., Biotechnological production of wood composites. In: Bruce, A. and Palfreyman, J.W. (Eds.), *Forest Products Biotechnology*, Ch. 9. Taylor and Francis, London, 1998, pp. 141–150.
172. European Norm EN 204, Water resistance of PVAc adhesives, 1992.
173. Kollmann, F., Schnülle, F. and Schulte, K., *Holz Roh- Werkst.*, **13**, 440–449 (1955).
174. Scheikle, M. and Dunky, M., *Holzforsch. Holzverwert.*, **48**, 55–57 (1996).
175. Scheikle, M. and Dunky, M., *Holzforsch. Holzverwert.*, **48**, 78–81 (1996).
176. Duncan, T.F., *For. Prod. J.*, **24**(6), 36–44 (1974).
177. Post, P.W., *For. Prod. J.*, **8**, 317–322 (1958).
178. Neusser, H. and Krames, U., *Holzforsch. Holzverwert.*, **21**, 77–80 (1969).
179. May, H.-A. and Keserü, M., *Holz Roh- Werkst.*, **40**, 105–110 (1982).
180. Rackwitz, G., *Holz Roh- Werkst.*, **21**, 200–209 (1963).
181. Lehmann, W.F., *For. Prod. J.*, **24**(1), 19–26 (1974).
182. Zavarin, E., Activation of wood surface and non-conventional bonding. In: Rowell, J. (Ed.), *The Chemistry of Solid Wood*, Chapter 10. Advances in Chemistry Series, American Chemical Society, Washington, DC, 1984, pp. 349–400.
183. Jaic, M., Zivanovic, R., Stivanovic-Janezic, T. and Dekanski, A., *Holz Roh- Werkst.*, **54**, 37–41 (1996).
184. Liptakova, E., Kudela, J., Bastl, Z. and Spivorova, I., *Holzforschung*, **49**, 369–375 (1995).
185. Bikerman, J.J., *The Science of Adhesive Joints*, Academic Press, New York, 1961.
186. Good, R.J., *J. Adhes.*, **4**, 133–154 (1972).
187. Stehr, M., Seltman, J. and Johansson, I., *Holzforschung*, **53**, 93–103 (1999).
188. Chen, C.M., *For. Prod. J.*, **20**, 36–41 (1970).
189. Scheickl, M., Dunky, M. and Resch, H., In: *Wood Adhesives 1995*, Proceedings, Forest Products Society, Madison, WI, 1995, pp. 43–46.
190. Kazayowoko, M., Neumann, A.W. and Balatinecz, J.J., *Wood Sci. Technol.*, **31**, 87–95 (1997).
191. Bogner, A., *Holz Roh- Werkst.*, **49**, 271–275 (1991).

192. Gray, V.R., *For. Prod. J.*, **12**(9), 452–461 (1962).
193. Hse, C.-Y., *Holzforschung*, **26**(2), 82–85 (1972).
194. Shen, Q., Nylund, J. and Rosenholm, J.B., *Holzforschung*, **52**, 521–529 (1998).
195. Shen, Q., Mikkola, P. and Rosenholm, J.B., *Colloids Surf. A.*, **145**, 235–241 (1998).
196. Elbez, G., In: *Wood-based Composite Products*, Proceedings, Vol. 6, Pretoria, 1985.
197. Rozumek, O. and Elbez, G., *Holzforschung*, **39**, 239–243 (1985).
198. Wellons, J.D., *For. Prod. J.*, **30**(7), 53–55 (1980).
199. Suchsland, O., *For. Prod. J.*, **17**(2), 51–57 (1967).
200. Herczeg, A., *For. Prod. J.*, **15**(11), 499–505 (1965).
201. Nguyen, T. and Johns, W.E., *Wood Sci. Technol.*, **13**, 29–40 (1979).
202. Kehr, E. and Scilling, W., *Holztechnologie*, **6**(4), 225–232 (1965).
203. Plath, E., *Holz Roh- Werkst.*, **11**, 392 (1953).
204. Popper, R., *Holzbau*, **44**(6), 168–170 (1978).
205. Chen, C.M., *For. Prod. J.*, **20**(1), 36–41 (1970).
206. Narayanamurti, D., *Holz Roh- Werkst.*, **15**(9), 377–378 (1957).
207. Rowell, J. (Ed.), *The Chemistry of Solid Wood*. Advances in Chemistry Series, American Chemical Society, Washington, DC, 1984.
208. Back, E.L., *For. Prod. J.*, **41**(2), 30–36 (1991).
209. Meineke, E. and Klauditz, W., On the physical and technical processes during gluing of particles in the production of particleboard. Nordrhein-Westfalen Report, 1962.
210. Wilson, J.B. and Hill, M.D., *For. Prod. J.*, **28**(2), 49–54 (1978).
211. Eusebio, G.A. and Generalla, N.C., *FPRDI J.*, **12**(3/4), 12–19 (1983).
212. Lehmann, W.F., *For. Prod. J.*, **15**, 155–161 (1965).
213. Robson, D.J., In: *25th Int. Particleboard/Composites Symposium*, Proceedings, Washington State University, Pullman, 1991, pp. A67–179.
214. Robson, D.J., In: *1st European Panel Products Symposium*, Proceedings, Llandudno, Wales, 1991, pp. 203–210.
215. Humphrey, P.E., In: *25th Int. Particleboard/Composites Symposium*, Proceedings, Washington State University, Pullman, 1991.
216. Humphrey, P.E. and Ren, S., *J. Adhes. Sci. Technol.*, **3**, 397–413 (1989).
217. Humphrey, P.E. and Bolton, A.J., *Holzforschung*, **43**, 199–206 (1989).
218. Humphrey, P.E. and Bolton, A.J., *Holzforschung*, **43**, 401–405 (1989).
219. Strickler, M.D., *For. Prod. J.*, **9**, 203–215 (1959).
220. Geimer, R.L., Mahoney, R.J., Loehnertz, S.P., Meyer, R.W., Influence of process induced damage on the strength of flakes and flakeboards. Research Paper FPL 463, USDA Forest Products Lab., Madison, WI, 1985.
221. Jahan-Latibari, A., In: *16th International Particleboard Symposium*, Proceedings, Washington State University, Pullmann, 1982.
222. Price, E.W., *For. Prod. J.*, **16**, 50–53 (1976).
223. van Niekerk, J. and Pizzi, A., *Holz Roh- Werkst.*, **52**, 109–112 (1994).
224. Hse, C.-Y., *For. Prod. J.*, **25**, 48–53 (1975).
225. Bolton, A.J., Humphrey, P.E. and Kavvouras, P.K., *Holzforschung*, **43**, 265–274 (1989).
226. Pichelin, F., Pizzi, A., Frühwald, A. and Triboulot, P., *Holz Roh- Werkst.*, 2001, in press.
227. Pichelin, F., 1999. *Herstellung von OSB mit feuchtetoleranten Klebstoffen*. Doctoral Thesis, University of Hamburg.
228. Bolton, A.J., Humphrey, P.E. and Kavvouras, P.K., *Holzforschung*, **43**, 345–349 (1989).

Tissue adhesives and hemostats: new tools for the surgeon

WILLIAM SPOTNITZ^{a,*}, DAVID MERCER^b and SANDRA BURKS^b

^a *Division of Thoracic and Cardiovascular Surgery, University of Florida College of Medicine, P.O. Box 100286, Gainesville, FL 32610-0286, USA*

^b *Surgical Therapeutic Advancement Center, University of Virginia Health System, Charlottesville, VA 22908, USA*

1. Introduction

Tissue adhesives and hemostats are important new tools which may be used as adjuncts in a wide variety of surgical procedures [1]. Modern surgical practice is moving toward minimally invasive approaches for all forms of operations. As technical challenges increase with this trend, efforts to improve the tools available to clinicians will enhance the quality of clinical care and reduce the challenges facing the operator. Tissue adhesives and hemostats will become a useful part of the armamentarium. They will be required to maintain outstanding results and patient satisfaction as new and old procedures are performed with less invasive, more technically challenging methods. These new materials are the beginning of large families of agents which will be available for a wide variety of applications. At present a handful of materials are approved for specific on-label indications (Table 1). New agents will continue to enter the marketplace and the indications for the existing ones will also expand with new on-label as well as off-label uses. The objective of this review is to provide insight into the recently developed agents and describe both the approved and unapproved indications for their use.

The extent to which these new tissue adhesives and hemostats will influence surgical procedures can be seen in the following analogy. An effective carpenter cannot create a masterpiece without a saw to cut wood, nails to ensure local fixation of separate pieces of wood, and glue to cause broad surface apposition between wood surfaces. Similarly, the surgeon presently uses a scalpel to cut and divide tissues as well as a suture to create local fixation of tissues, but until

* Corresponding author. E-mail: spotnwd@mail.surgery.ufl.edu

Table 1
Presently approved new tissue adhesives and hemostatic agents

Product name (Generic, Trade Names, Manufacturer/ Distributor)	Fibrin Sealant, Hemaseel APR, Haemacure, Tisseel VH, Baxter Healthcare	Platelet Gel, Medtronic Harvest Technologies, and others	Collagen Enhanced Fibrin Sealant, CoStasis, Cohesion Technologies, US Surgical	Collagen + Thrombin, FloSeal, Fusion Medical, Proceed Sulzer Medica
Components/ mechanism of action	Human plasma, fibrinogen and thrombin, virally inactivated, hemostat, sealant.	Autologous fibrinogen + platelet-rich plasma, hemostatic gel.	Bovine collagen, bovine thrombin, plus autologous human plasma, hemostatic agent.	Bovine collagen and bovine thrombin. Expands 20% which aids in hemostatic effect.
Approved indications	FDA-approved in May, 1998, for hemostasis in cardiopulmonary bypass procedures, splenic trauma, and for the sealing of colon anastomoses. Large 'unapproved' off-label clinical use literature.	Clinical literature supporting use as hemostatic agent and tissue sealant, promoting wound healing due to presence of growth factors and platelet-rich gel formulation.	FDA-approved in June, 2000, as device to stop active surgical bleeding during general, hepatic, orthopedic, and cardiovascular procedures.	FDA-approved in December, 1999, as an adjunct to hemostasis in all surgical procedures (except urologic and ophthalmic) where control of bleeding is impractical or unresponsive to conventional methods.
Ease of use	2–6°C storage. Multiple application devices (linear, spray tips, endoscopic, etc.), 20 min preparation time. Set-up time = 30 s–3 min. May 'wash away' in presence of active bleeding.	Requires trained personnel to operate equipment.	Preparation time required to obtain plasma component.	Room temperature storage. 5 min preparation time. Single syringe applicator per kit. Set-up time = 3 min. Effective at site of active bleeding.
Cost information	About \$100 per ml kit.	<\$10/patient use with appropriate preexisting instrumentation and equipment.	\$100–150 per 1 ml kit. Requires centrifuge to obtain autologous plasma.	\$120 per ml kit.

Table 1
(Continued)

Product name (Generic, Trade Names, Manufacturer/ Distributor)	Polyethylene Glycol (PEG) Polymer,FocalSeal-L, Focal Technologies, Genzyme	Cyanoacrylate, Dermabond, Closure Medical, Ethicon, Johnson and Johnson	Gluteraldehyde Cross-linked Albumin, BioGlue, CryoLife/Gynzme
Components/ mechanism of action	Light-activated polyethylene-glycol (PEG) polymer sealant for lung tissue.	Monomeric (2-octyl cyanoacrylate) formulation tissue adhesive for skin closure.	Bovine albumin cross-linked with gluteraldehyde tissue adhesive/sealant.
Approved indications	FDA-approved in May, 2000, as lung sealant.	FDA-approved in 1998 for skin closure of external lacerations and simple incisions. Avoid high tension.	FDA-approved in December, 2001, as an adjunct in vascular surgical anastomoses.
Ease of use	−20 to −4°C storage. 3-step application over 10–15 min using light source, wand, cable, primer, sealant.	Room temperature storage. Single dose, crushable ampule for linear application only. Immediate availability.	Room temperature storage. Single use applicator 'gun'. 1–2 min preparation time. 2–3 min maximum bonding strength.
Cost information	\$450 per 8 ml/kit.	\$22 per 0.5-ml vial.	Approx. \$450 per 5 ml kit.

recently there have been no surgical tissue adhesives to assist with adhesion of tissues. Thus a truly significant change in the surgical armamentarium of tools is occurring with the introduction of tissue adhesives and hemostats capable of effectively assisting the surgeon during operative procedures.

Although it would appear inherently obvious that surgical glues would have existed for quite some time, this is actually not the case. In fact although sutures have been available as early as the second century BC [2], the widespread use of tissue adhesives has only become practical in the latter half of the 20th Century [2]. Fibrin sealant as a prototype tissue adhesive and hemostat was approved in Europe for commercial use in 1972 and in essence represents the first widespread clinical use of such a material. Although efforts were made at the time to achieve simultaneous approval through the Food and Drug Administration (FDA) in the United States, it took approximately 25 years to gain final approval for this material in the American marketplace. The delay, which occurred over significant concerns related to viral safety and hemostatic efficacy, illustrates the fact that the introduction of these new materials has been challenging not only in the research and development phases but in the regulatory ones as well. This tissue adhesive and hemostat received FDA approval in May of 1998. Its introduction has set the stage and increased the interest of a large number of surgeons. Now, a wider variety of tissue adhesives and hemostats are entering, have entered or have completed the regulatory process. Thus, an increasing number of materials are available for surgical use.

As with any new technology, the ability to successfully employ such agents is dependent on a thorough understanding of their appropriate use as well as experience with the materials. In fact, a significant learning curve exists with these agents. The surgical specialty is predicated on an apprenticeship process which facilitates the development of increasing levels of skill and knowledge over a period of years characterized by increasing graded responsibilities. This practical experience has evolved and developed to train the best qualified individuals as surgeons. During this process the physician learns clinical judgement as well as how to cut, sew, and perform a wide variety of different operations. Up to the present time, however, the use of tissue adhesives and hemostats has not been an element of this practical educational process. In fact, during residency training, young surgeons have had some experience with a variety of different hemostatic agents other than the newly evolving agents. It is not generally accepted that skill in the use of these hemostatic agents is required. Rather it is assumed to be a simple intervention that can be easily done to stop bleeding. Thus many surgeons are under the misunderstanding that these newer agents do not require significant learning and experience for successful use. This could not be further from the truth, as the new agents do require skill in application for efficacious results. Improved technical understanding of the use of these materials significantly enhances their efficacy.

The educational issue becomes even more complex as the requirements in each surgical specialty for tissue adhesives and hemostats may vary significantly. For example a cardiac surgeon who requires rapid and effective hemostasis when using these materials needs an agent that will polymerize immediately and rapidly cause bleeding to stop. On the other hand, a plastic surgeon who wishes to place a split thickness skin graft upon a recipient's wound site, would like for the skin graft to not only adhere to the underlying tissues, but for the agent to polymerize slowly. This is desirable because it allows modifications in the position of the skin graft in order to achieve the best positioning and maintain maximum graft survival. Thus, one specialist desires a rapidly polymerizing hemostatic agent while the other desires a slowly polymerizing malleable tissue adhesive. Even when the specialists desire similar agents for example a rapidly polymerizing hemostat that can stop the leakage of liquids, the needs of the specialist may be different. Again the cardiac surgeon desires a rapidly polymerizing agent to stop bleeding. Once the bleeding has been stopped and the body's normal clotting mechanisms reinforce the tissue adhesive, the long-term persistence of the tissue adhesive is no longer required as the body will maintain effective hemostasis and healing. Alternatively, the neurosurgeon who is attempting to stop the leakage of cerebrospinal fluid during a procedure wants a rapidly polymerizing material to stop fluid leakage, but does not have the advantage of an inherent clotting system. Cerebrospinal fluid has no clotting ability and will clot to reinforce the tissue adhesive or hemostat. Thus the neurosurgeon requires a persistent tissue adhesive which assures an absence of cerebrospinal fluid leakage for a prolonged period of time during which the body's healing capacity can eventually prevent fluid leakage. Clearly, a family of agents or agents with adjustable characteristics will be required to fulfill all of the criteria which will be created by surgical specialists for these materials.

Prior to reviewing the specific indications and agents which are presently available for use, it may be helpful to create a construct which can be used to identify the specific characteristics of an ideal agent [3] in order to help evaluate the present agents and the directions in which future research and development will proceed. Specifically, a construct can consist of five different categories.

- (1) *Safety*. The agent must be safe and there must be no adverse effects as the result of the material itself or any possible biodegradation products of the material. An ideal agent might be completely degradable so that there will be no short-term or long-term adverse effects as a result of the agent or any of its metabolites.
- (2) *Effectiveness*. The material must be highly effective so that surgeons find its use helpful in the performance of the operative procedure. Effectiveness, however, may be different for each particular specialty. Slowly polymerizing agents may be favored by the plastic surgeon adjusting the exact position of a skin graft while rapidly polymerizing agents may be favored by the cardiac surgeon attempting to stop life threatening bleeding.

- (3) *Usability*. The ability to easily obtain the agent and reconstitute it if necessary within a reasonable period of time is extremely important. In addition, the ability to easily apply the material in a variety of different settings is also significant. Specifically, the ability to deliver the material through an operative instrument such as an endoscope or laparoscope and the ability to deliver the agent over broad surface areas or to specific localized punctate regions is required. In order for the surgeon to use the agent it must be readily available and obtainable in a brief period of time with minimal reconstitution. A number of instruments to apply the agent in a variety of settings is also desirable.
- (4) *Affordability*. The use of the agent should result in a reduction in cost of the overall operative procedure so that the material pays for itself and also results in an overall net cost savings.
- (5) *Approvability*. The product must be able to meet satisfactory criteria for efficacy and safety such that it is approvable by regulatory agencies responsible for the protection of patients.

In fact, it would be almost impossible for any one agent to satisfy all of the above criteria. Thus, the future would appear to consist of families of products which are capable of clinical benefit in a variety of different surgical applications ranging from skin closure and hemostasis to drug delivery and wound healing. This is an exciting period of time with innovative technologies being brought to the operating room. Tissue adhesives and hemostats will be valuable tools which will enhance the safety, efficacy and cost effectiveness of surgical operations.

In the following sections, a variety of different applications for tissue adhesives and hemostats will be reviewed and specific new agents presently available for clinical use will be discussed.

2. Indications

2.1. Skin closure

2.1.1. Cyanoacrylates

At present there is only one commercially available tissue adhesive with approved on-label indications for skin closure. 2-Octyl-cyanoacrylate (Dermabond, Ethicon, Inc., Somerville, NJ) is presently indicated for skin closure in wounds which are not under extreme tension. This tissue adhesive is approved for topical skin application only. It is not indicated for internal use. The material is useful in closing traumatic skin lacerations [4,5] after wounds have been thoroughly cleaned as well as for minimally invasive surgical incisions and even larger surgical incisions in elective cases. The cyanoacrylate is applied while the skin



Fig. 1. Cyanoacrylate application to close a skin incision (arrow points to adhesive).

edges are held in apposition and polymerization of the tissue adhesive occurs when it comes in contact with hydroxyl ions in the skin. This combination causes a release of heat which can be noted by the patient as a sensation of warmth. The manufacturer recommends that three successive layers be applied to the incision separated by 30 s of waiting after each application. The material should be applied over an area extending for about 1 cm to either side of the skin incision (Fig. 1). The material is not recommended for high tension areas of an incision such as across joint surfaces. Although the cyanoacrylate itself is extremely strong, its ability to maintain wound closure is limited by the strength of the skin itself as the cyanoacrylate bonds with only the superficial layers of skin. Thus, it is not suitable for wounds which are under significant tension. The material is sloughed approximately 7–10 days after application as the superficial layers of the skin are normally replaced with new epithelium. This exfoliative process allows the adhesive to be removed without a return visit to a physician's office. If it is necessary to remove the material prior to exfoliation of the superficial skin layers, the application of petroleum based products to the cyanoacrylate reduces its strength and results in its effective removal. Although the use of cyanoacrylates for internal wound management and tissue apposition would be a desirable goal, at present the agent is approved for external use only. There have been reports of significant carcinogenicity in animals and humans treated with cyanoacrylates internally [6]. Thus internal use cannot be recommended at this time. 2-Octyl cyanoacrylate is presently provided in a crushable ampule which can be stored at room temperature. This single-dose delivery system is very easy to use and is effective at delivering the tissue adhesive to the skin surface. The crushable ampules contain 0.5 ml 2-Octyl cyanoacrylate. 2-Octyl cyanoacrylate

costs approximately \$50 per ml. The material is readily obtainable in most emergency rooms and is becoming increasingly available in hospital operating rooms.

As always, meticulous aseptic technique should be used in closing wounds which cyanoacrylate. Excellent hemostasis and thorough cleansing of the wound including irrigation should be performed prior to closure of the incision. Careful approximation of the skin edges is important using forceps or fingers and some have recommended placement of a subcutaneous layer of sutures prior to application of the cyanoacrylate in order to minimize wound dimpling which may accentuate the appearance of the scar. Proper preparation of the wound is essential, and a good technique is to prepare the wound as if you were preparing to suture it. This includes using local anesthetic where indicated. In general, clinical reports suggest that wounds closed with cyanoacrylate result in less traumatic and painful closure and that cosmesis is equivalent to wounds closed with standard suture techniques. Reports of using 2-Octyl cyanoacrylate in a variety of elective surgical procedures are increasing with excellent cosmesis being achieved particularly in facial and plastic reconstructive surgery [7].

Thus 2-Octyl cyanoacrylate can be used as an effective means of achieving skin closure in wounds which are not under high tension or across joint surfaces. In addition, in wounds which have been closed using a combination of subcutaneous and subcuticular sutures, the cyanoacrylate can still be applied over the surface of the wound to act as a barrier against the leakage of serous fluids. This may be particularly effective in lower extremity incisions which occasionally leak such fluids and may thus be predisposed to infection. Thus, the cyanoacrylate can be used as an adjunctive measure to support routine suture closure and may reduce the need for frequent postoperative dressing changes as well as the risk of infection associated with weeping surgical incisions. Cyanoacrylate use could potentially be enhanced by new forms of this material which may be more easily biodegradable and have less potential carcinogenic effect.

None of the other presently available tissue adhesives are approved for skin closure and their use in this setting is not presently recommended.

2.2. Hemostasis

2.2.1. Fibrin sealant, thrombin and collagen, fibrin sealant plus collagen, and platelet gels

There are a number of tissue adhesives currently approved as adjuncts to hemostasis. Each agent has specific properties which enhance intraoperative hemostasis in particular situations. All forms of surgical bleeding are not alike. Bleeding can be fast or slow, diffuse or punctate, arterial or venous, capillary or larger vessel. Thus one agent may be more efficacious than another in a specific clinical situation.

2.2.2. Fibrin sealant

Fibrin sealant is a hemostatic agent which is presently approved by the FDA in a liquid two-component form. The commercial agent consists of concentrated human thrombin and human fibrinogen with trace amounts of Factor XIII and calcium which, when combined, cause fibrinogen to be cleaved and cross-linked to produce fibrin. The fibrin is stabilized by the addition of bovine aprotinin. The polymerization process is rapid and is influenced by the concentration of thrombin. The higher the concentrations of thrombin, the more rapid the polymerization. The commercially available FDA-approved product is now widely available in the United States (Tisseel VH, Baxter Healthcare, Glendale, CA and Hemaseel APR, Haemacure Corporation, Sarasota, FL). Both the fibrinogen and thrombin components are derived from pooled human plasma sources obtained from carefully screened and tested donors to reduce the potential risk of viral disease transmission. In addition, the materials are processed with techniques including heat pasteurization and ultrafiltration to remove viral particles. Bovine aprotinin has been added to this commercial fibrin sealant in order to reduce fibrinolysis and stabilize the components. The normal biologic degradation of fibrin sealant occurs by fibrinolysis and antifibrinolytics such as aprotinin are used to modify the rate of degradation. Calcium is added to the mixture to function as a catalyst and enhance the polymerization reaction.

This two-component tissue adhesive requires refrigeration with temperature regulation of 2–4°C. In order to use the material during a surgical operation, the fibrinogen and thrombin, which are supplied as lyophilized powders, must be reconstituted with saline containing calcium chloride and bovine aprotinin. The entire process of thawing, mixing, and reconstituting the components takes approximately 20 min and is customarily a function performed by operating room personnel. In order to most effectively complete this process the commercial distributors provide a special warmer and mixing device which facilitates preparation.

In 1998, the FDA approved fibrin sealant for three specific indications. These include hemostasis at the time of cardiac surgical operations [8] (Fig. 2) as well as at the time of operative procedures to treat splenic trauma. The application of the fibrin sealant which consists of normal biologic components in the body's clotting cascade creates a localized clot which further enhances inherent clotting ability. Although approved for these specific hemostatic indications only, fibrin sealant is useful as a hemostat in a wide variety of off-label clinical situations as well [9,10]. These include such applications as hemostasis for liver trauma or resection [11], vascular anastomoses [12], tonsillectomy [13], peripheral joint replacement [14], dental extractions [15], and burn debridement [16].

There is a learning curve associated with the use of fibrin sealant and the application devices which are used to apply the agent can significantly influence

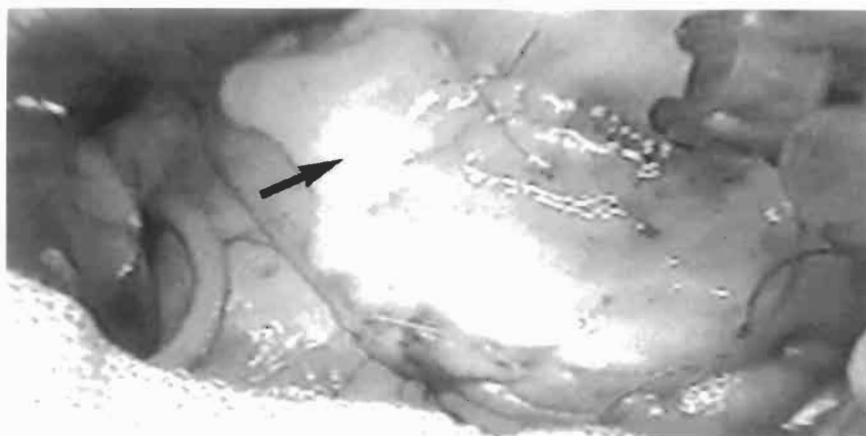


Fig. 2. Fibrin sealant spray application at site of left ventricular aneurysm repair to facilitate hemostasis (arrow points to adhesive).

hemostatic effectiveness. The applicators produce a mixing of fibrinogen and thrombin. The device available for linear application of the tissue adhesive uses a dual syringe holder which is capable of manually delivering the components through a blunt-tipped 19-gauge needle. This device is particularly useful for applying fibrin sealant to localized suture lines. Recently introduced compressed-air-driven spray units allow for the effective aerosolization of small droplets of the adhesive components for application over a broad surface area. This allows for a particularly effective distribution and mixing of the agents and also can reduce costs by most efficiently using a limited amount of tissue adhesive to cover a large region of tissue.

In order to employ fibrin sealant an effective hemostatic agent, it is desirable to apply it to a dry field. Because fibrin sealant is presently applied as a liquid which polymerizes into a solid form, it is best to apply it when active bleeding is reduced. Otherwise, the active bleeding may wash away the liquid fibrin sealant before it can polymerize. Such situations of reduced rate bleeding occur for example when an extremity is under tourniquet control in orthopaedic surgery or when vascular clamps are in place during a bypass graft procedure or when an aortic cross-clamp is in place during cardiac surgical operations. All of these situations create opportunities to enhance hemostasis using fibrin sealant when minimal active bleeding is occurring. In these situations the fibrin sealant polymerizes completely over a period of 2–3 min. After polymerization is complete, the tourniquet can be released, the vascular clamps can be removed, or the aortic cross-clamp can be opened allowing for return of active blood flow. Because the fibrin sealant has polymerized in a bloodless field, it is extremely effective at maintaining control of bleeding. Repressurization of blood vessels in this situation does not usually result in a return of bleeding. Clearly such applications require anticipation on the

part of the surgeon who may note that tissues are fragile and potentially subject to bleeding or that an extremely complex surgical procedure has been performed in a coagulopathic patient which may require additional hemostatic support.

However, it is not always possible for the surgeon to anticipate when active bleeding may occur or when the need for a local hemostat may be required. If localized capillary bleeding occurs, there is no doubt that fibrin sealant spray can be effective at controlling a small arterial or venous ooze from capillaries. However, if significant faster bleeding occurs particularly in an arterial setting other techniques must be employed. A suture remains the best means of controlling such hemorrhage. If on the other hand, the bleeding is not suturable, fibrin sealant may still be of clinical value. The best way to use the fibrin sealant in an active bleeding situation is to combine it with a carrier sponge [9]. The sponge will enable the fibrin sealant liquid to be delivered to the bleeding site without having the liquid sealant be washed away by the active bleeding. Specifically the carrier sponge of cellulose or collagen can be soaked initially with fibrinogen and then the thrombin component of fibrin sealant is added to the side of the sponge to be applied to the bleeding site just prior to application. The sponge with the active sealant is then held in place with manual pressure over the site of active bleeding. As long as the bleeding can be controlled with pressure in this fashion hemostasis will be achieved after 2–3 min polymerization of the adhesive. Obviously, however, if hemostasis cannot be achieved using manual pressure on the carrier sponge, 2–3 min of pressure will not result in hemostasis. Although liquid fibrin sealant begins to polymerize rapidly in a period of 20–30 s, the full polymerization process continues for a number of minutes. The carrier sponge method of using fibrin sealant can be a particularly effective way of dealing with active bleeding in a wide variety of clinical situations.

The advantage of the recently introduced commercial form of fibrin sealant is that a highly concentrated form of human thrombin and fibrinogen which has been virally inactivated and combined with an antifibrinolytic is now available. As noted above, the transformation of fibrin sealant from a liquid form to a firm gelatin requires approximately 30 s to 3 min and is influenced by the extent of mixing in the application device. The thrombin concentration is a significant determinate of the rate of this reaction and is presently 500 IU/ml in the commercial product. The fibrinogen concentration, which affects the internal bonding strength of the tissue adhesive, is 75–115 mg/ml. The distributors provide a variety of volume choices including kits with 1, 2, and 5 milliliters of each component. The final fibrin sealant product costs approximately \$75–100 per ml.

Prior to May of 1998 when the commercial product was approved by the FDA in the United States, surgeons in this country formed fibrin sealant by using topical bovine thrombin, which is a commercially available product, together with concentrated fibrinogen most frequently obtained from the blood bank. Standard blood bank cryoprecipitate is a good source of concentrated fibrinogen. Also

concentrated fibrinogen can be obtained in a cryoprecipitation process from the patient's own blood [17] or from outdated plasma which is devoid of unstable clotting factors [18,19]. The advantage of the latter methodology is that it avoids a waste of unstable clotting factors which are present in cryoprecipitate and are valuable means of reversing coagulopathies in patients requiring systemic clotting factors. Outdated plasma treated with a freeze/thawing process, on the other hand, creates concentrated fibrinogen, a stable clotting factor. Such a method avoids the waste of valuable unstable clotting factors while still producing concentrated fibrinogen. Thus traditional cryoprecipitate can be preserved for patients requiring unstable transfusable clotting factors. The fibrinogen concentrations obtained using blood bank techniques vary between 15 and 35 mg/ml. This is significantly less than that obtainable in the commercial product and may reduce strength of the final form of fibrin sealant. To use blood-bank-produced concentrated fibrinogen in order to create sealant, one also requires commercially available topical bovine thrombin. At present, no human thrombin stand-alone product is available in the United States. Thus a bovine product is the only available source of concentrated thrombin. Coagulopathy is a rarely reported complication as a result of antibody formation to human clotting factors which may occur because of using bovine thrombin [20,21].

2.2.3. Collagen and thrombin

This product consists of bovine thrombin and bovine collagen and has been recently approved as an adjunct to hemostasis in surgical procedures when control of bleeding by ligature or conventional procedures is ineffective or impractical. This device is particularly effective at controlling active bleeding since it is delivered as a granular gel rather than a liquid [22] (Fig. 3). The toothpaste-like consistency of the material allows it to be placed at the site of active bleeding without being washed away. Immediate manual pressure with a sponge for a period of 2–3 min facilitates the achievement of hemostasis. The sponge will not stick to the device as only the portions of the device coming in contact with blood enhance coagulation. The collagen and thrombin combination works by causing clotting of inherent fibrinogen in the patient's own blood. The process is enhanced by the collagen. In addition, the collagen matrix which is formed swells approximately 20% within the first 10 min. A significant tamponade effect is thus added to enhance the ability of the device to achieve hemostasis. Because of the swelling effect, collagen and thrombin are not recommended for use in ophthalmic or urologic procedures. Although currently marketed for use in cardiovascular and spinal procedures, the material is approved for bleeding of any type. The agent comes in a 3-ml kit (FloSeal, Fusion Medical Technologies, Mountain View, CA and Proceed, Sulzer Medica, Minneapolis, MN). The agent can be conveniently stored at room temperature. The mixing of the collagen and thrombin prior to

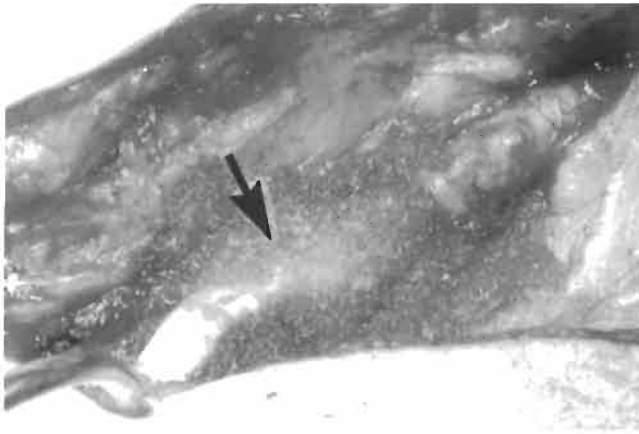


Fig. 3. Collagen and thrombin gel applied to achieve hemostasis at a vascular anastomosis (arrow points to gel).

application requires approximately 5 min. The material can be used repeatedly if initial application does not achieve hemostasis. This is done by applying new layers of the agent through the previously applied material directly at the site of bleeding. This device costs approximately \$40 per ml.

In order to reduce the risk of potential antibody formation creating coagulopathy, the bovine thrombin employed in this product is highly purified. Coagulopathy which has been noted on rare use of bovine thrombin [20,23] appears to be related to the production of antibodies by the patient against bovine thrombin and/or Factor V which can cross-react with human Factor V. This cross-reaction can result in a deficiency in human Factor V thus causing a potentially significant coagulopathy. This adverse effect is more likely to occur upon repeated exposures to bovine thrombin. The potential complication should be considered by the surgeon prior to using this agent in a re-exposure setting. The hemostatic device is biodegraded over a period of 6–8 weeks.

The unique advantage of this agent is that it is able to stop active bleeding because it is applied as a gelatin matrix. This matrix tends to remain at the site of active bleeding and is not washed away as might occur with a liquid material. After application of the gel to the site of bleeding, 2 min of pressure is used to allow for clot formation to occur. This material, however, would not be as efficacious as a preventive agent at a site which is not presently actively bleeding because it requires the body's blood as a source of fibrinogen in order to create a stable hemostatic effect. Therefore, as an example, it is not effective at preventively sealing a vascular anastomosis which is not pressurized with blood and not actively bleeding.

2.2.4. Thrombin, collagen, and plasma

This new agent uses the body's own plasma as a source of fibrinogen which can then be combined with topical bovine thrombin and collagen to form fibrin sealant plus collagen (CoStasis, Cohesion Technologies, Palo Alto, CA). In essence this agent uses the patient's own blood which has been fractionated into plasma and red cells. The plasma, in combination with the supplied thrombin and collagen, forms a collagen-augmented form of fibrin sealant based on the patient's own plasma fibrinogen. This material, which is approved as a hemostatic adjunct [24–26] in general hepatic, cardiovascular and vascular operations, is prepared in the operating room at the time of a surgical procedure. A small table-top centrifuge allows the patient's blood to be separated into red cells and plasma. The plasma fraction can then be obtained in a syringe as a source of the patient's own fibrinogen. This material is then combined with bovine thrombin and collagen which are available in a second pre-filled syringe. Using a proprietary dual syringe applicator, the two components, fibrinogen and thrombin with collagen, are thoroughly mixed in a spray application. This mixture produces a fibrin sealant which is enhanced with collagen and platelets. This material is biodegraded over a period of 8 weeks in the body. The commercial product comes in a variety of different kit sizes for specific clinical uses and the collagen and thrombin pre-filled syringes can be kept in the refrigerator for a period of up to 24 months. Current kit sizes for the product include 1, 2, and 4.5 ml collagen/thrombin suspension syringes, which are combined with equal volumes of the patient's own fibrinogen. Plasma collection devices are priced separately. The cost of this material is estimated to be \$100–\$150 per ml. The usual cautions mentioned above for products containing bovine thrombin [20,23] should be followed.

2.2.5. Platelet gels

This product can be used at the time of cardiac surgical operations to improve hemostasis and is often prepared by the perfusionist who is familiar with auto transfusion and other hemoconcentrating or blood containing devices. The platelet gel [27,28] can be prepared from the disposables provided by the manufacturers of cell washing equipment for cardiopulmonary bypass and other surgical procedures. These systems (Sorin, Harvest, Haemonetics, Medtronic, and Cobe) can be used to create a hemostatic agent from the patient's own blood. Specifically, the platelet gel contains human plasma with fibrinogen and also contains concentrated platelets and white blood cells which may enhance blood clotting and facilitate effective wound healing. When combined with commercially available bovine thrombin and calcium chloride, a platelet gel clot is formed. Thus, not only is fibrin created, but other natural components of the blood including platelets are

used to enhance the effectiveness of this material. It has been suggested that this material may be more cost effective than commercial fibrin sealant.

2.3. Lymphostasis

2.3.1. Fibrin sealant

Fibrin sealant is not only capable of functioning as a hemostatic agent, but it can seal other vascular structures such as lymphatic ducts. This may be particularly important in surgical operations which involve removal or dissection of lymphatic tissues. Examples of such procedures include axillary and groin dissections for breast cancer [29] (Fig. 4) or melanoma. In these operations, drains are frequently required for prolonged periods of time in order to evacuate serous or lymphatic drainage from the wound and prevent the formation of a seroma. These seromas can be associated with significant morbidity including pain, discomfort, wound dehiscence, and infection. Fibrin sealant has been found in a variety of different studies to be an effective agent at reducing lymphatic leakage. Its prophylactic use at the time of a surgical operation may reduce the time required for drains to remain in place and may potentially enable procedures to be performed without the need for long-term drainage [30]. Although this use of the material remains controversial, many reports of successful use in stopping lymphatic drainage exist



Fig. 4. Application of fibrin sealant (arrow points to spray head for applying two-component adhesives) at the time of mastectomy and axillary dissection to reduce seroma formation.

in the literature. In fact, there have been anecdotal reports of using fibrin sealant to treat thoracic duct injuries and to eliminate recurrent lymphoceles.

2.4. Pneumostasis

Surgical operations which are performed on the lung can be associated with the leakage of air from resected portions of the lung parenchyma. Traditional means of performing lung resection include parenchymal suturing or stapling. Because the lung parenchyma is heavily laden with alveolar spaces, any manipulations of the lung tissue can be easily associated with air leaks. This becomes even more significant in patients who have parenchymal degenerative diseases such as emphysema. In such settings the tissues become even more fragile and friable. Surgical manipulations may then be even more likely to result in significant air leaks. Thus tissue adhesives which can reduce air leakage and the need for prolonged chest tube drainage could not only enhance patient care by reducing morbidity and even mortality, but could also be significant in reducing length of stay and hospital costs.

2.4.1. Polyethylene glycol (PEG) polymers

A number of new synthetic agents are under development as tissue adhesives capable of enhancing pneumostasis. A family of agents known as hydrogels polymerize to form strong adhesives. A form of polyethylene glycol (PEG) polymer is presently approved for commercial sale in the United States by the FDA as a means of achieving pneumostasis at the time of lung resection. This is a proven effective means of reducing air leaks at the time of lung resections and may also be effective at reducing the length of time required for chest tube drainage [31]. This commercial PEG polymer (Focalseal L, Focal Incorporated, Lexington, MA) requires light activation for final polymerization (Fig. 5). The adhesive comes as a two-component material consisting of a primer which is then followed by application of the PEG polymer. The primer and polymer require storage at -20 and 4°C , respectively. In order to successfully apply this agent three steps are followed. The first step is the generous brush application of the primer to the surface of the lung parenchyma. This is then followed by the application of PEG polymer which is carefully worked into the tissues using a second brush applicator. Finally, the material is light-activated by a light source (470–520 nanometers) consisting of a cable and wand. The entire process of application takes approximately 10–15 min. The commercially available kit has a volume of 8 ml. This PEG polymer costs approximately \$55 per ml.

This agent was approved by the FDA in May of 2000 and is the first tissue adhesive to be specifically approved for use on lung parenchyma. It is extremely strong and has excellent adherence strength on the surface of the lung. Approval



Fig. 5. Light activation (arrow points to light wand) of polyethylene glycol (PEG) polymer on the surface of the lung as an adjunct to pneumostasis.

for this material was obtained in a pivotal trial in patients undergoing surgical lung resection [31]. PEG polymer-treated patients were three times less likely to have postoperative lung leaks than patients who were treated with a standard therapy. This relatively new tissue adhesive is slowly biodegraded and approximately 36% of the PEG polymer remains present 6 months after use. Long-term clinical safety data are not yet available and thus physician vigilance has been encouraged with respect to potentially increased infection rates and long-term carcinogenicity.

2.4.2. Fibrin sealant

Fibrin sealant, as described earlier, is a two-component biologic adhesive consisting of fibrinogen and thrombin which can function as a hemostatic agent. This material, however, is also available for off-label use as a pneumostatic material. There is extensive literature supporting its beneficial use in pulmonary surgical resections [32]. The overall effectiveness of this material as a pneumostat remains controversial, however, with some papers supporting its use and others suggesting a lack of effect. The lung during respiration is a dynamic structure which actually expands and contracts with respiration. Thus, a tissue adhesive capable of achieving pneumostasis must be able to adhere to the lung surface which is changing shape. The tissue adhesive must be flexible and elastic but must also have very

strong adherence strength. The fibrin sealant internal bonding strength remains excellent but its internal flexibility and adherence strength may not be sufficient for it to remain intact on the surface of the dynamic lung. The following example will clarify this challenge. In order to apply tissue adhesives to the surface of the lung, the lung must be partially deflated and have a reduced air pressure. Thus, the tissue adhesive can be applied when minimal air leak is occurring in order to allow the adhesive to satisfactorily form along the parenchyma of the lung without dislodgment by leaking air. After the tissue adhesive has polymerized the lung is re-inflated and normal respirations are resumed. However, in the process of re-inflation, the lung re-expands and significant changes in surface area occur. Thus, the tissue adhesive is exposed to significant expansile forces. In order to avoid rupturing of the tissue adhesive off the surface of the lung, the adhesive must be elastic enough to satisfactorily expand and it must adhere strongly enough to the surface of the lung to avoid breakdown of the adherence bond between the tissue adhesive and the lung parenchyma. The elasticity and adherence strength of the current forms of fibrin sealant are less than that required for ideal achievement of pneumostasis at the surface of the lung parenchyma.

Fibrin sealant has been reported to be extremely effective at reducing air leak from broncho-pleural fistulas following pulmonary resections [33]. This material can be delivered by the fiberoptic flexible bronchoscope throughout the bronchial tree using local anesthesia alone. This procedure significantly reduces morbidity associated with more aggressive surgical approaches and is effective in 60–80% of patients with small broncho-pleural fistulas less than 0.5 cm. Repeated applications of the fibrin sealant through a silastic catheter placed down the biopsy channel of the bronchoscope may be required. It is important to remove any granulation tissue at the site of the broncho-pleural fistula prior to applying the fibrin sealant in order to maximize the adherence of the sealant to the bronchial tissues. Application of approximately 1 ml of fibrin sealant using this technique may not only improve clinical results in the patient but they may also result in major cost savings.

2.5. Tissue sealing and apposition

2.5.1. Albumin cross-linked with glutaraldehyde

This tissue adhesive, which has only recently completed multi-center clinical trials and was recently approved by the FDA for treatment of patients undergoing vascular surgical procedures, consists of albumin and glutaraldehyde. The bovine albumin is cross-linked by glutaraldehyde as the two components mix in an applicator gun which is supplied by the manufacturer (BioGlue, CryoLife, Incorporated, Kennesaw, GA). This material solidifies in a period of 20–30 s and maximum bonding strength is reached within a period of 2–3 min. This strong

adhesive has improved the results of aortic dissection surgical operations to such an extent that it initially received a HDE from the Food and Drug Administration in the treatment of aortic dissection (Summary of Safety and Probable Benefit, CryoLife, Inc., BioGlue Surgical Adhesive, HDE # H990007). Careful application of a thin layer of this material between the layers of the dissected aorta results in a re-adherence of the intima and adventitia which had been separated during the pathologic process of aortic dissection. An aortic dissection classically occurs when an intimal tear of the aorta allows blood to move from the intraluminal space into the medial layer dissecting through this layer and causing significant injury. In type A aortic dissections which require emergency surgical treatment to avoid hemorrhage, cardiac tamponade, and death, the use of surgical tissue adhesives as a tissue sealing agent may be extremely valuable. In this setting albumin cross-linked by glutaraldehyde can be used to facilitate surgical repair of the dissection. Dissection repair is classically achieved by replacement of the ascending aorta with a tube graft. The anastomoses between the tube graft and the aorta involve sewing to extremely friable tissues of the injured aorta. This new tissue adhesive can be used to help obliterate the false lumen space between the adventitia and intima by gluing these tissues back together. In addition, the friable layers of the aorta can be strengthened by the tissue adhesive which results in layers that are much less fragile and much more receptive to suture placement. Initial work suggests that perioperative morbidity associated with hemorrhage as well as a perioperative mortality are significantly reduced by the use of this material. Long-term studies with respect to tissue effects or injuries caused by the adhesive are still pending. This particular biodegradable agent is different from previous forms of similar tissue adhesives. Glutaraldehyde, resorcinol, and formaldehyde glue (GRF glue) otherwise known as 'French Glue' which has been previously used as a similar treatment for aortic dissection has been associated with some long-term complications including tissue degeneration which may be linked with aortic root dissection, aortic insufficiency, and false aneurysm formation [34]. Long-term studies with respect to albumin cross-linked with glutaraldehyde are pending. Other clinical studies to expand the applications of this material into other forms of surgery are in progress.

Albumin cross-linked with glutaraldehyde is sold at a cost of approximately \$90 per ml and comes in a 5 ml kit. The adhesive can be stored at room temperature and preparation time including assembly of the applicator 'gun' can be completed in several minutes.

Meticulous care needs to be used in the application of this tissue adhesive. Only a very thin layer of adhesive should be used to assist with reapproximation of the intima and adventitia. It is important to remember that the material should not be allowed to drip into or onto critical areas such as the ostium of the coronary arteries. Inadvertent placement of this agent in such areas can result in blockage of a critical artery and a potentially fatal myocardial infarction. In addition,

placement of an extremely firm reinforcing sealant such as albumin cross-linked with glutaraldehyde in pediatric tissues which are subject to growth may result in restriction of normal development. This restriction of normal growth could create a functional stenosis similar to that seen with running sutures. Thus just as interrupted and/or absorbable sutures are more desirable in allowing for tissue growth in pediatric surgical procedures, it may be best to avoid the circumferential use of albumin cross-linked with glutaraldehyde in such cases.

2.5.2. Fibrin sealant

As mentioned earlier fibrin sealant is an effective sealing agent particularly when applied at the sites of potential future bleeding prior to pressurization of the structures. Thus fibrin sealant applied to an anastomosis in a surgical operation involving vascular structures can help reduce bleeding from friable tissues particularly if applied while vascular clamps are still in place. Fibrin sealant polymerizes prior to pressurization of the blood vessel and the onset of active bleeding. In this setting fibrin sealant is an effective hemostat and may be valuable in vascular operations in which tissues are friable including aortic dissections [9].

The third FDA-approved on-label indication for fibrin sealant after hemostasis at the time of cardiac surgery and splenic trauma surgery is sealing of colonic anastomoses at the time of colostomy closure. Thus fibrin sealant has been approved as an agent which may be valuable in sealing colonic anastomoses. Such anastomoses, whether hand sewn or created with stapling devices, may be associated with a defined leak rate which can result in peritonitis, abscess formation, sepsis, and even death. Agents capable of sealing such anastomoses are clinically useful. When using fibrin sealant in such settings, it is important to have the tissues as dry as possible in order to maximize the adherence capacity of the fibrin sealant to the outer serosal surface of the bowel.

Fibrin sealant can be a useful method of achieving tissue plane apposition in order to eliminate potential spaces of fluid accumulation. Specific examples include mastectomy with axillary dissection [29,30] which frequently is subject to the development of subcutaneous seroma formation as a result of leakage of blood, lymph, and serous fluid following the surgical procedure. Fibrin sealant which has an effective hemostatic and lymphostatic effect is a valuable agent in such procedures. However, in addition to its vascular sealing effect, fibrin sealant is capable of gluing tissues together in an efficacious manner to avoid and eliminate potential spaces subject to fluid accumulation. In other words, it is possible during a mastectomy and axillary dissection to glue the overlying skin down to the underlying chest wall musculature so that potential fluid accumulations cannot develop. This may result in a decreased period of time required for postoperative drainage and may even allow for such procedures to be performed without drains.

This particular application provides an excellent example of the extent to which physicians and surgeons must clearly understand the use of tissue adhesives and learn to use them in the most efficacious fashion. Paradoxically this excellent tissue adhesive, fibrin sealant, can actually function as an anti-adhesive. If fibrin sealant is applied to the underlying musculature following a mastectomy and axillary dissection and the overlying skin is rapidly closed and placed on top of the underlying muscle so that the muscle and skin become in contact as the fibrin sealant is initially polymerizing, then the two tissues are effectively glued together. If, however, a period of delay occurs between the application of fibrin sealant to the underlying chest wall musculature and the closure of the skin with apposition of the skin and underlying muscle, so that polymerization is complete before these tissues come in contact, then the fibrin sealant functions as an anti-adhesive. In fact in this setting the fibrin sealant will prevent adhesion and healing of the two tissue layers. It may even create more potential for seroma formation and drainage than would have been present without its use in the first place. It is also important to note that if effective, rapid closure of the wound is achieved so that the skin and underlying muscle tissues are effectively adherent, it is equally important to not inadvertently disrupt this bond by pulling up on the skin at a later time. Disruption of this bond creates a situation in which the fibrin sealant may again function as an anti-adhesive.

2.6. Drug delivery

Substances which function as tissue adhesives have the unique ability to remain in contact with tissues in localized areas for prolonged periods of time. Not only does the tissue adhesive function as a 'glue' but it has the capacity to serve as a slow release mechanism for drug delivery as it is biodegraded.

2.6.1. Fibrin sealant

The most extensive experience with tissue adhesive drug delivery exists in the fibrin sealant literature. This is clearly an off-label use of this agent as it is only currently approved for hemostasis in cardiac and splenic trauma surgery and for colon sealing at the time of colostomy closure.

The concept of using tissue adhesives as a means of slow release of drugs is extremely exciting. A wide variety of medications can be slowly released to the local site. These include antibiotics, chemotherapeutic agents, and growth factors [35,21]. The potential therapeutic applications include delivery of antibiotics to an abscess site or to osteomyelitic bone, delivery of chemotherapeutic agents to the site of the tumor resection to prevent localized recurrence, and delivery of growth factors to enhance the seeding of cultured cells into absorbable frameworks to create biologic vascular grafts.

As an example of such a function, recently some of the unusual characteristics of fibrin sealant, specifically its anti-adhesive capacity and its drug delivery potential were evaluated in a simulated burn wound model [36]. This in-vivo rat work showed that preformed clots of fibrin sealant containing silver sulfadiazine appeared more effective at reducing bacterial counts in a simulated burn wound infection than was the traditional cream containing silver sulfadiazine. Not only were bacterial counts reduced during the use of preformed fibrin sealant clots containing silver sulfadiazine, but the dressings were changed less frequently and visually appeared to promote better healing. A wide variety of creative uses of fibrin sealant as a carrier for medications in localized areas can still be envisioned. This represents one of the future areas in which tissue adhesive development will continue.

3. Summary

In this chapter, a review of the new currently available FDA-approved tissue adhesives and hemostats has been provided. Both on and off-label uses have been described. These agents will be joined by second generation materials in the coming years which will continue to increase safety and efficacy of these products. The future of this technology will continue to enhance the quality of surgical operations and allow for less invasive procedures to be performed. It has not been possible in this chapter to provide an extensive review of all of the available literature on new tissue adhesives and hemostats with respect to each specialty of surgery. This literature is now large and suggests that this field is attaining a level of maturation which will assure its acceptance and growth as a new tool in the armamentarium of the modern surgeon.

References

1. Schlag, G. (Ed.), *Fibrin Sealing in Surgical and Nonsurgical Fields*. Springer, Berlin, 1994, Volumes 1–8.
2. Spotnitz, W.D., Falstrom, J.K. and Rodeheaver, G.T., The role of sutures and fibrin sealant in wound healing. In: Barbul, A. (Ed.), *Surgical Clinics of North America — Wound Healing*. W.B. Saunders, London, 1997, pp. 1–19.
3. Spotnitz, W.D., History of tissue adhesives. In: Sierra, D. and Saltz, R. (Eds.), *Surgical Adhesives and Sealants, Current Technology and Applications*. Technomic, Lancaster, PA, 1996, pp. 3–11.
4. Quinn, J., Drzewiecki, A., Li, M., Stiell, I., Sutcliffe, T., Elmslie, T. and Wood, W., A randomized, controlled trial comparing a tissue adhesive with suturing in the repair of pediatric facial lacerations. *Ann. Emerg. Med.*, **22**, 1130–1135 (1993).
5. Quinn, J., Wells, G., Sutcliffe, T., Jarmuske, M., Maw, J., Stiell, I. and Johns, P., A randomized trial comparing octylcyanoacrylate tissue adhesive and sutures in the management of

- lacerations. *JAMA*, **277**, 1527–1530 (1997).
6. Samson, D. and Marshall, D., Carcinogenic potential of isobutyl-2-cyanoacrylate. *J. Neurosurg.*, **65**, 571–572 (1986).
7. Toriumi, D.M., O'Grady, K., Devang, D. and Bagal, A., Use of octyl-2-cyanoacrylate for skin closure in facial plastic surgery. *Plast. Reconstruct. Surg.*, **102**, 2209–2219 (1998).
8. Rousou, J., Gonzalez-Lavin, L., Cosgrove, D., Weldon, C., Hess, P., Joyce, L., Bergsland, J. and Gazzaniga, A., Randomized clinical trial of fibrin sealant in patients undergoing re sternotomy or reoperation after cardiac operations. *J. Thorac. Cardiovasc. Surg.*, **97**, 194–203 (1989).
9. Spotnitz, W.D., Fibrin sealant in the United States: Clinical use at the University of Virginia. *Thromb. Haemost.*, **74**, 482–485 (1995).
10. Spotnitz, W.D., New developments in the use of fibrin sealant: a surgeon's perspective. *J. Long-Term Eff. Med. Implants*, **7**, 243–253 (1997).
11. Uranüs, S., Mischinger, H.-J. and Pfeifer et al., J., Hemostatic methods for the management of spleen and liver injuries. *World J. Surg.*, **20**, 1107–1112 (1996).
12. Padybidri, A.N., Brown, E. and Kononov, V., Fibrin glue-assisted end-to-side anastomosis of rat femoral vessels: Comparison with conventional suture method. *Ann. Plast. Surg.*, **34**, 41–47 (1996).
13. Schlosser, R.J., Gallagher, R., Burks, S.G., Flanagan, H.L., Mintz, P.D., Avery, N.L., Mayers, S.L., Spotnitz, W.D. and Gross, C.W., Autologous fibrin sealant reduces pain following tonsillectomy. *Laryngoscope*, **111**, 259–263 (2001).
14. Levy, O.L., Martinowitz, U., Oran, A., Tauber, C. and Horoszowski, H., The use of fibrin tissue adhesive to reduce blood loss and the need for blood transfusion after total knee arthroplasty: a prospective, randomized, multicenter study. *J. Bone Joint Surg.*, **81A**, 1580 (1999).
15. Rakocz, M., Lavie, G. and Martinowitz, U. Glanzmann's thrombasthenia, 1995. The use of autologous fibrin glue in tooth extractions. *J. Dent. Child.*, **62**, 129–131 (1995).
16. Stuart, J.D., Kenney, J.G. and Spotnitz et al., W.D., Application of single donor fibrin glue to burns. *J. Burn Care Rehabil.*, **9**, 619–622 (1988).
17. Siedentop, K., Harris, D., Ham, K. and Sanchez, B., Extended experimental and preliminary surgical findings with autologous fibrin tissue adhesive made from patient's own blood. *Laryngoscope*, **96**, 1062–1064 (1986).
18. Spotnitz, W.D., Dalton, M.S., Baker, J.W. and Nolan, S.P., Reduction of perioperative hemorrhage by anterior mediastinal spray application of fibrin glue during cardiac operations. *Ann. Thorac. Surg.*, **44**, 529–531 (1987).
19. Spotnitz, W.D., Mintz, P.D., Avery, N., Bithell, T.C., Kaul, S. and Nolan, S.P., Fibrin glue from stored human plasma: An inexpensive and efficient method for local blood bank preparation. *Am. Surg.*, **53**, 460–464 (1987).
20. Daniels, T.M. and Fisher et al., P.K., Antibodies to bovine thrombin and coagulation factor V associated with the use of topical bovine thrombin or fibrin glue: a frequent finding. *Blood*, **82**, 59a (1993).
21. MacPhee, M., Singh, M., Brady, R., Akhyani, N., Liao, G., Lasa, C., Hue, C., Best, A. and Drohan, W. Fibrin sealant: A versatile delivery vehicle for drugs and biologics. In: Sierra, D. and Saltz, R. (Eds.), *Surgical Adhesives and Sealants, Current Technology and Applications*. Technomic, Lancaster, PA, 1996, pp. 109–120.
22. Oz, M.C., Cosgrove, D.M., Badduke, B.R., Hill, J.D., Flannery, M., Palumbo, R., Topic, N. and The Fusion Matrix Study Group, Controlled clinical trial of a novel hemostatic agent in cardiac surgery. *Ann. Thorac. Surg.*, **69**, 1376–1382 (2000).
23. Ortel, T.L., Mercer, M.C., Thames, E.H., Moore, K.D. and Lawson, J.H., Immunologic

- impact and clinical outcomes after surgical exposure to bovine thrombin. *Ann. Surg.*, **233**, 88–96 (2001).
24. Prior, J., Wallace, D., Harner, A. and Powers, N., A sprayable hemostat containing fibrillar collagen, bovine thrombin, and autologous plasma. *Ann. Thorac. Surg.*, **68**, 479–485 (1999).
 25. Chapman, W., Sherman, R., Boyce, S., Malawer, M., Hill, A., Buncke, G., Block, J., Fung, J., Clavien, P., Lee, K., Lebovic, G., Wren, S., Diethrich, E. and Goldstein, R., A novel collagen-based composite offers effective hemostasis for multiple surgical indications: Results of a randomized controlled trial. *Surgery*, **129**, 445–450 (2001).
 26. Chapman, W., Clavien, P., Fung, J., Khanna, A. and Bonham, K., Effective control of hepatic bleeding using a novel collagen-based composite combined with autologous plasma: Results of a randomized controlled trial. *Arch. Surg.*, **13**, 1200–1204 (2000).
 27. Hill, A.G., Hood, A.G., Reeder, G.D., Potter, P.S., Iverson, L.I.G., Keating, R.F., Speir, A.M. and Lefrak, E.A., Perioperative autologous sequestration II: A differential centrifugation technique for autologous component therapy: Methods and results. *Am. Acad. Cardiovasc. Perfus.*, **14**, 122–125 (1993).
 28. Hood, A.G., Hill, A.G., Reeder, G.D., Potter, P.S., Iverson, L.I.G., Keating, R.F., Speir, A.M. and Lefrak, E.A., Perioperative autologous sequestration III: A new physiologic glue with wound healing properties. *Am. Acad. Cardiovasc. Perfus.*, **14**, 126–129 (1993).
 29. Moore, M.M., Nguyen, D.H.D. and Spotnitz, W.D., Fibrin sealant reduces serous drainage and allows earlier drain removal after axillary dissection: a randomized prospective trial. *Am. Surg.*, **63**, 97–102 (1997).
 30. Moore, M., Burak Jr., W., Nelson, E., Kearney, T., Simmons, R., Mayers, L. and Spotnitz, W., Fibrin sealant reduces the duration and amount of fluid drainage after axillary dissection: A randomized prospective clinical trial. *J. Am. Coll. Surg.*, **192**, 591–599 (2001).
 31. Macchiarini, P., Wain, J., Almy, S. and Dartevell, P., Experimental and clinical evaluation of a new synthetic, absorbable sealant to reduce air leaks in thoracic operations. *J. Thorac. Cardiovasc. Surg.*, **117**, 751–758 (1999).
 32. Spotnitz, W.D., Clinical applications of fibrin sealant in thoracic and cardiovascular surgery. In: Sierra, D. and Saltz, R. (Eds.), *Surgical Adhesives and Sealants, Current Technology and Applications*. Technomic, Lancaster, PA, 1996, pp. 239–244.
 33. Matthew, T.L., Spotnitz, W.D., Daniel, T.M. and Kron, I.L., Closure of small bronchopleural fistulas using fibrin sealant through the flexible fiberoptic bronchoscope. *Chest*, **94**, 77S (1988).
 34. Bingley, J.A., Gardner, M.A.H., Stafford, E.G., Mau, T.K., Pohlner, P.G., Tam, R.K.W., Jalali, H., Tesar, P.J. and O'Brien, M.F., Late complications of tissue glues in aortic surgery. *Ann. Thorac. Surg.*, **69**, 1764–1768 (2000).
 35. MacPhcc, M.J., Campagna, A., Best, A., Kidd, R. and Drohan, W., Fibrin sealant as a delivery vehicle for sustained and controlled release of chemotherapy agents. In: Sierra, D. and Saltz, R. (Eds.), *Surgical Adhesives and Sealants, Current Technology and Applications*. Technomic, Lancaster, PA, 1996, pp. 145–154.
 36. Wang, J., Neisley, H., Moody, D., Dobraz, J., Spotnitz, W.D. and Rodeheaver, G., Fibrin sealant delivery system increases the effectiveness of silver sulfadiazine. *Surg. Forum L*, 624–626 (1999).

Applications of adhesives in aerospace

KEVIN D. PATE*

The Boeing Company, Seattle, WA, USA

1. Introduction

Adhesives and aircraft have a long and interesting joint history. Even though flying vehicles have progressed from glorified kites to commercial jet transports, supersonic missiles and space vehicles, adhesively bonded structure has been crucial to virtually every one. The use of adhesive bonding is widespread in the aerospace industry because it has characteristics that are particularly well suited to aerospace applications: weight efficiency, fatigue resistance, sonic vibration damping and the ability to easily produce aerodynamically smooth surfaces, to name a few. Likewise, the aerospace industry is well suited to adhesive bonding. The industry learned early that building and flying aircraft is not a forgiving practice. Safe manufacture and flight requires well-defined and controlled materials and practices and meticulous craftsmanship. Successful use of structural adhesive bonding requires the same control and care and fits into this environment well.

The aerospace field is a broad one and has a complex history. A comprehensive review of structural adhesive applications on currently flying aerospace vehicles alone could fill its own book. Hence this chapter will concentrate on the aerospace commercial transport industry and its use of adhesives in structural applications, both metallic and composite. Both primary structure, that is structure which carries primary flight loads and failure of which could result in loss of vehicle, and secondary structure will be considered. Structural adhesives use and practice in the military aircraft and launch vehicle/spacecraft fields as well as non-structural adhesives used on commercial aircraft will be touched on briefly as well.

While the use of adhesive bonding is widespread among all aerospace firms, the author is most familiar with history and practice at The Boeing Company and will of necessity draw primarily on that resource. Adhesive bonding use at other firms will be included as much as possible.

* E-mail: kevin.d.pate@boeing.com

2. The advantages of adhesive bonding

As mentioned above, there are many aspects of adhesive bonding which make it attractive for use on aerospace vehicles. Listed below are the primary advantages noted by aerospace designers when considering bonding as a fabrication technology.

2.1. Weight efficiency

An adhesively bonded joint is typically more structurally efficient than a mechanically fastened joint. Fasteners introduce discrete, or at least concentrated, points at which load is transferred from one component to another. Therefore the peak stress at each fastener is much higher than overall joint stress and the joint must be suitably designed to withstand these peak stresses. Compounding this is the fact that aerospace components are typically quite thin with proportionately low fastener bearing strength. The most efficient way to mechanically fasten thin members is with numerous small fasteners which add weight and cost.

In contrast, a bonded joint can transfer load more uniformly across its area. If designed correctly bonded joints take full advantage of this ability to gradually react load from one component to another resulting in thinner and hence lighter components. This is a greatly simplified description; more detail regarding proper adhesive joint design is contained elsewhere in this compilation.

2.2. Fatigue resistance

Fatigue, or the gradual cracking of a material when repeatedly loaded well below its normal failure stress, is a primary design consideration for commercial aircraft. Fatigue cracking is such a problem that a large number of joints on modern commercial aircraft are sized by fatigue considerations and not by ultimate strength requirements. A joint of thin components made with many small fasteners is highly susceptible to fatigue cracking because of the high stress concentrations at the edges of the fastener holes.

Again, a properly designed adhesively bonded joint eliminates or reduces the stress concentration at fasteners and increases the fatigue life of a given joint. Adhesively bonded doublers are also more effective at slowing or stopping the growth of fatigue cracks in an adjacent field than a mechanically fastened doubler. Finally, bonded components can be used to introduce dual load-carrying capability. Adhesively laminated sheets tend to resist propagation of cracks from one component to another, resulting in an inherently fail-safe design.

2.3. Aerodynamic smoothness

Of obvious importance to aircraft is the smoothness of exterior surfaces. Smooth aerodynamic surfaces reduce aerodynamic drag, resulting in higher airspeeds and increased efficiency. Mechanical fasteners, even countersunk flush fasteners, introduce disruptions in the airflow over the exterior surface. Even the slight deformation of thin sheets around fasteners produces drag. Adhesively bonded structure has no fasteners to disrupt airflow and is more capable of producing the smooth continuous contours that are so common on aircraft.

2.4. Sonic damping/fatigue resistance

Two related but distinct advantages of adhesively bonded structure are sonic vibration damping and sonic fatigue resistance. Structural adhesives are typically fairly compliant materials and can be further modified with rubber particles if necessary. The adhesive layer in a bonded joint can act as a sonic dampener, absorbing some of the acoustic energy and reducing the need to increase component thickness or use other means of reducing high frequency noise propagation.

Sonic fatigue occurs when unsupported sheet vibrates in response to sonic noise to the point that fatigue cracks initiate and propagate. This phenomenon can be eliminated by introducing a compliant adhesive layer as mentioned above, increasing the sheet thickness to increase its stiffness, or adding support by other means such as honeycomb sandwich bonding. Bonded honeycomb sandwich construction has been very successful in solving sonic fatigue problems on lightly loaded structure such as flight control surfaces and fairing panels. In honeycomb sandwich bonding the adhesive does not act as a sonic dampener, but allows the honeycomb to support the facesheet almost continuously. This not only increases the overall stiffness of the panel much more weight efficiently than merely increasing the gauge of the skin, it also reduces the size of the area of unsupported skin to the size of the honeycomb cell, making it very resistant to sonic fatigue.

2.5. Labor savings

As mentioned above, aircraft structure is typically quite thin with numerous small fasteners to achieve efficient load transfer through joints. Mechanical fasteners are laborious to install. Adhesive bonding of large area doublers and joints can be accomplished at significant labor hour savings over equivalent mechanically fastened designs.

2.6. Tailored properties

The number of basic polymeric resin chemistries available for use as adhesives is large and each has their own set of application and performance properties. The ability to further modify these with other chemical or physical additives means that adhesives can be tailored for particular application or performance requirements quite readily.

2.7. Joint sealing

Structural adhesive bonding produces joints which are air and fluid-tight, environmentally stable and resistant to aggressive aircraft liquids such as cleaning solutions, fuels and hydraulic fluids. Bonded joints can prevent fuel leakage, pressure leakage and joint corrosion. Certain applications such as integral fuel tank structure can take advantage of these capabilities to achieve even more savings over mechanically fastened joints which must be fay or fillet sealed with standard elastomeric sealants.

2.8. Composite substrate compatibility

Composite materials have greatly increasing popularity in the aerospace industry during the last quarter century and adhesive bonding is an integral part of composite part manufacture for various reasons. The matrix polymer for a given composite system, whether it is epoxy, bismaleimide or polyimide, can usually be formulated into a suitable adhesive. This virtually guarantees chemical compatibility and good adhesion between the adhesive and matrix resin. Also, composite materials are not high in fastener bearing strength and are prone to damage during hole drilling, meaning that mechanically fastening composites is laborious and disadvantageous. Lastly, fabrication processes to mold and cure composite parts are virtually identical to those necessary to cure adhesive bonds. Many times the two operations can be combined, achieving great savings in fabrication costs.

3. Early history: wooden aircraft

Adhesives have been an integral part of aircraft construction from the very first flights. One of the more interesting facets of studying adhesive bonding in aerospace is tracing this early history, learning how bonding has adapted to the tremendous changes in the industry and how it has remained the same.

The early decades of bonding in aerospace were dominated by the need to join wood. The first aircraft builders worked with wood of necessity because metallurgy and associated joining technologies of the late 19th and early 20th

centuries were not up to the challenge of providing plane builders with high-strength lightweight structure. Wood was the natural choice, being the material from which most other contemporary transport structure was fabricated, and the natural choice for joining wood was adhesive bonding. Early adhesives were glues, or adhesives derived from natural proteins, so adhesive bonding was commonly referred to as gluing. Glued wooden aircraft were prevalent in the early days of flight up through the 1920s and 1930s, were not uncommon in the 1940s, and remained aloft in day-to-day use even in the 1950s and 1960s.

Gluing was used then for many of the same reasons it is used today, such as weight efficiency, ease of fabrication, redundant load paths and damage tolerance. It was much easier to join wood details together and maintain high strength in the substrates by gluing them than it was to use nails, screws or bolts. The relatively low strength of wood was a good match for the low-strength glues available; a common bond quality measure of the time was the ability to fail primarily within the wood substrate rather than in the glue line during a bond strength test.

It is interesting to note that many of the concerns of the early wooden aircraft industry were similar to those of today: glue quality and consistency, glue pot life, substrate surface preparation, bondline thickness, application skill, curing requirements, and in-service resistance to moisture exposure [1]. The solutions to many of these problems came about through the use of detailed specifications controlling materials and processes. The military was involved early on in aircraft research and development and brought with it the practice of tight control of quality and consistency through specifications. The fledgling industry benefited from this practice and civil aircraft manufacturers adopted specifications for materials and processes as well, a practice that continues as a key part of the control and certification of production of modern aircraft.

3.1. Glues

A number of different glues were utilized on early aircraft. Since these craft were manufactured during the infancy of synthetic polymeric chemistry, all were of natural origin. These glues are still in use today, though not for aerospace bonding.

Despite its relative brittleness and moisture sensitivity, the most common glue for early wooden aircraft structure was casein. Casein is a glue made from the proteins in skim milk. Cured casein is somewhat water-resistant but degrades in long-term moist conditions, is similarly sensitive to repeated wetting and drying, and is furthermore prone to fungal attack when kept moist. Later formulations contained preservatives to prevent fungal attack, but the inherent impermanence of the glue remained a factor throughout its use in aircraft. Early aircraft were relatively fragile in most respects and were coddled for many reasons, so the sensitivity of the glue was not a conspicuous limitation. In addition, advancement in aircraft design and performance was so rapid that aircraft hardly had time

to grow old and degrade before they were eclipsed by faster, safer and cheaper models.

Another widely used glue was blood glue. As its name suggests, blood glue is made by extracting albumin protein from animal blood and drying it to a powder that is re-mixed with water for use. Blood glues are more resistant to moisture than animal and casein glues, though still not waterproof.

Animal glue, obtained by boiling hide and bones, is one of the oldest glues known and in fact was the substance originally referred to by the word 'glue'. Hide and bones are boiled to extract the primary protein present, collagen, which is then further boiled to drive off water and cause the collagen molecules to join together to form long polymeric chains. The dried material is ground into chunks or a powder that is soaked in water and heated on use. Although animal glue is a relatively tough glue with high initial bond strength, exposure to water or high humidity causes rapid degradation. This lack of durability meant that animal glues were only used in protected applications such as laminated propellers, which had to be sealed to prevent warping caused by water absorption.

Other natural glues common at the time, such as plant starch and fish glues, were not used for aircraft structure because they are even more sensitive to moisture.

As polymer chemistry advanced in the 1930s and 1940s, stronger and more durable synthetic adhesives such as early phenol, resorcinol and urea formaldehydes began to supplant natural glues in wood aircraft manufacture. Around this time however, metal began to replace wood as the dominant material for aircraft manufacture. Aerospace adhesives research and development moved on to focus on metals, primarily aluminum, as the substrates of interest.

3.2. Applications

Simply in terms of bonded area, the most common use of glue on early aircraft was to fabricate plywood. Plywood was used for exterior coverings such as 'turtle' decks, wing leading edges, wing and fuselage coverings, internal components such as wing and empennage rib webs, main wing spar webs and fuel tank walls, and interior surfaces such as walkways, bulkheads, cabin surfaces and instrument panels.

Glue was also used to join the numerous small plywood and wood details necessary to fabricate the structural frameworks typical of early aircraft. Fig. 1 shows a monoplane wing circa 1930 fabricated primarily from wood that was joined via more than one thousand glued joints [2]. Note the many small stringers and gussets bonded together to form the ribs and spars of the wing.

Monocoque structure fabricated by molding wood veneer with glue to shape under pressure was successfully used as early as 1916 in the LWF Model V complete molded fuselage and probably most famously in the monocoque fuselage

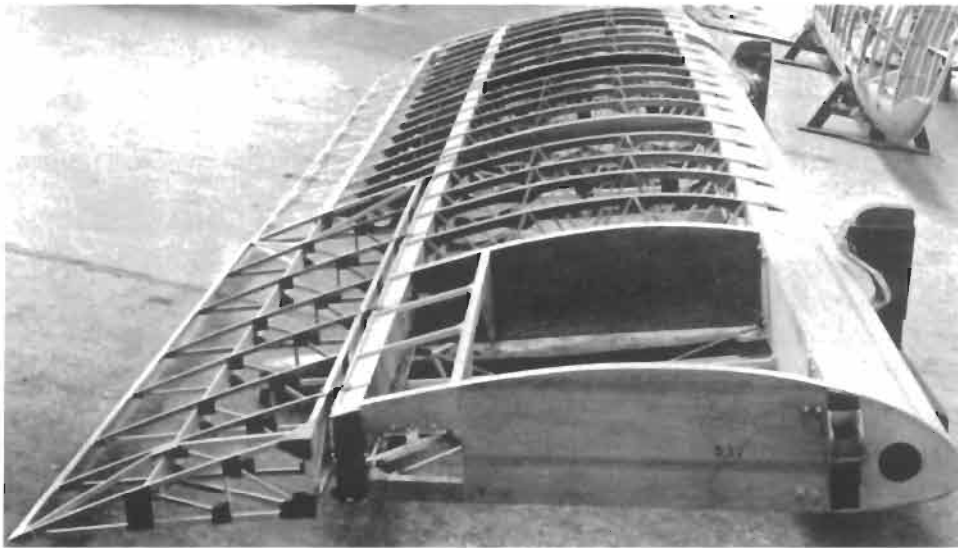


Fig. 1. Glued wing structure ca. 1930.

of the de Havilland Mosquito of WWII. Numerous other small molded laminate parts were fabricated by using matched metal dies, pressure bladders inside female tools, vacuum under bags on male tools and in later years, autoclaves. This type of molded wood laminate structure was the early forerunner of today's autoclave-bonded metal and composite semi-monocoque structure.

3.3. Examples

Because gluing of wood members was a very common method of fabricating aircraft during this time, there are innumerable examples. One unusual and interesting example, as mentioned above, is the de Havilland Mosquito of 1940. In many respects the Mosquito was a bridge between the old world of wood aircraft and the increasingly predominant world of aluminum aircraft (Fig. 2).

The Mosquito was made almost entirely of wood and for that reason was nearly canceled by the British before it was even built; wood aircraft were viewed as fragile and slow based on the previous 40 years of aerospace history. Fortunately the designers of the Mosquito were able to overcome this bias and the Mosquito went on to become one of the best-performing fighter/bombers of the war.

The Mosquito was a laminated wood monocoque design that although unusual, was not new. More uniquely, the monocoque shell was fabricated by gluing plywood skins to balsa wood core. This construction foreshadowed the popular honeycomb core/facesheet aluminum and composite designs of later years. Fuselage halves of the Mosquito were formed in closed wooden female tools (tools



Fig. 2. de Havilland Mosquito. Canada Aviation Museum, Ottawa.

were concrete in later years) using bladder pressure and joined with screws and more glue. Casein glue was used at first but later changed to synthetic adhesive because of the moisture sensitivity of casein. The rest of the aircraft was of more conventional glued wood construction with plywood covering.

The innovative design of the Mosquito worked around many of the strategic materials shortages of war-time Britain by using wood and even more importantly produced one of the highest performance and versatile military aircraft of the time. Due in part to the extremely aerodynamically smooth exterior and strong, lightweight structure made possible by gluing, the Mosquito was a remarkably fast and long-range aircraft able to outrun most contemporary aircraft.

4. Post-WWII

The era following the war was an interesting one for adhesive bonding in aerospace for numerous reasons. It was a period in which the change in bonding substrates from wood to aluminum and other metals and composites became almost total, bringing with it a raft of new technical challenges. It was a period in which great strides in bonding materials (adhesives, primers, etc.) and support processes (machining, tooling, autoclaves, etc.) enabled more ambitious bonded

structure. Perhaps most interestingly, it was a period of great innovation and experimentation with adhesive bonding of large primary structure for European civil airframe manufacturers and one of relative timidity for manufacturers in the U.S.

It is clear that European civil aircraft manufacturers adopted adhesive bonding for major structural elements much more rapidly than their American counterparts, but it is difficult to determine exactly why. Certainly a number of contributing factors are obvious. One was a history of success in incorporating adhesively bonded structure in military aircraft such as the Mosquito. Although the Mosquito was the most unusual and extreme example of adhesively bonded structure, other European wartime aircraft contained bonded structure as well. American military craft of the time were almost exclusively riveted aluminum structure.

Another significant factor was the British invention of a strong and durable synthetic adhesive for aluminum metal to metal bonding, Redux, in 1942. Redux, a creation of George Newell and Norman de Bruyne of Aero Research Ltd., was a mixed phenolic/polyvinyl formal (PVF) system that had relatively high strength, excellent environmental durability and good toughness [3]. The first version was applied by coating the bond surfaces with liquid phenolic and sprinkling on PVF powder. Later the two components were combined in a film adhesive. Redux was wildly successful in the European aerospace market and is still used in virtually the same form on production aircraft today.

De Bruyne himself was undoubtedly no small factor in the spread of adhesive bonding through the European aerospace community. In addition to co-inventing the Redux family of adhesives, he was involved in the conceptual development of the Mosquito and numerous other aircraft and sponsored (and taught) a series of educational sessions on the benefits of structural bonding during the post-war years.

Virtually all military and commercial aircraft designed in Europe after WWII relied significantly on structural bonding. The de Havilland Comet, the first commercial jet transport, first flew in 1951 and employed Redux adhesive extensively for bonding much of its structure. Redux bonding was used for joining fuselage doublers to skins, fuselage and wing stringers to skins, stiffeners to wing ribs and spars, flight control surfaces, etc. [3]. The list of European commercial aircraft fabricated with Redux adhesive in following years is quite impressive: Fokker F27 (1955), Vickers Vanguard (1959), Vickers VC-10 (1962), Hawker-Siddely Trident (1962), de Havilland 125 (1962), Fokker F28 (1967), BAe 146 (1981), Fokker F50 (1985), Fokker 100 (1988), and the BAe RJ series (1989) [4]. The Fokker F27, shown in Fig. 3, was typical of these aircraft. Virtually all major structural elements were adhesively bonded in some way.

Meanwhile, adhesive bonding came into use in the U.S. at a more gradual rate. The major U.S. large civil airframe manufacturers began using adhesive bonding for the fabrication of secondary structure such as fairings and flight

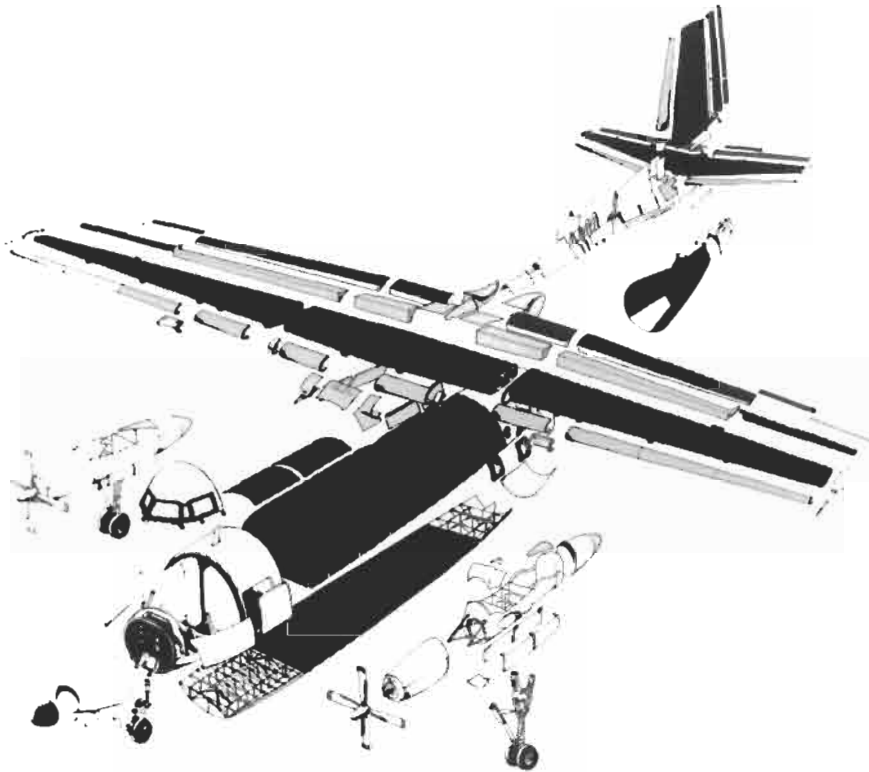


Fig. 3. Adhesively bonded structure (shaded) on the Fokker F27. Reproduced by permission of Stork Fokker.

control surfaces, but application in primary structure was virtually nonexistent. As manufacturers shifted from turbo-prop aircraft to high-speed jets, they found that traditional riveted secondary structure such as fairings and flight control surfaces were prone to rapid sonic fatigue [5]. This secondary structure typically had thin, flexible skins that were prone to cracking in severe sonic vibration areas such as wing trailing edges. For example (albeit from a military aircraft) Fig. 4 shows a B-52 landing gear door of traditional riveted design that failed due to sonic fatigue. Assemblies such as these were redesigned as bonded metal-to-metal and aluminum honeycomb core sandwich panels to take advantage of the sonic fatigue resistance, weight efficiency and cost effectiveness of such a design.

Unlike European manufacturers, U.S. manufacturers never made the leap to primary structural metallic bonding on civil aircraft. In the late 1950s the Boeing 707 (first flight 1954) and Douglas DC-8 (first flight 1959) kicked off the U.S. entry into the jet transport age. Both incorporated metal-to-metal and honeycomb bonded parts such as fairings and flight control surfaces. As adhesives and

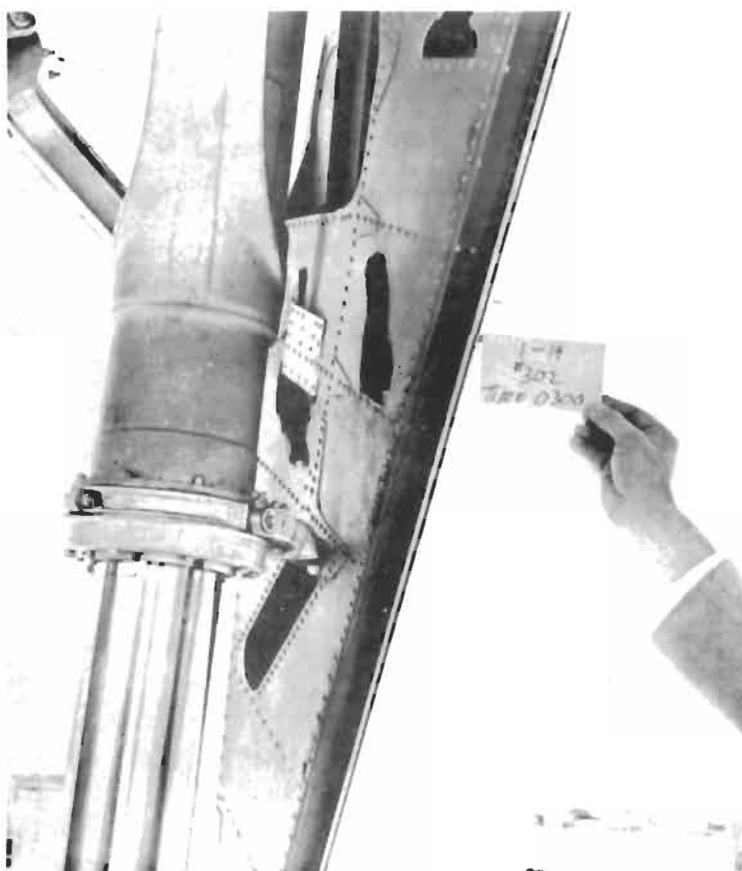


Fig. 4. B-52 landing gear door damage from sonic fatigue. Reproduced by permission of the Boeing Company.

adhesive bonding manufacturing technologies advanced and designers became more comfortable with the technology, adhesive bonding usage increased.

Fig. 5 charts the growth of adhesively bonded structure on Boeing aircraft through the 1980s. The arcs traced by the bottom two lines, metal-to-metal and metallic honeycomb usage, are a good approximation of the arc of metallic adhesive bonding popularity in civil aircraft. As with all new technologies there was a latent period during the 1950s when the technology was too new and unfamiliar for widespread use (at least in the U.S.). Then followed a period of booming popularity where designers embraced adhesive bonding as the solution to many problems and rushed to apply it to as many areas of the aircraft as possible. The honeymoon ended before widespread adhesive bonding of primary structure was accomplished. By the mid-1970s recognition of the practical limits of the technology, extensive corrosion and delamination problems in service

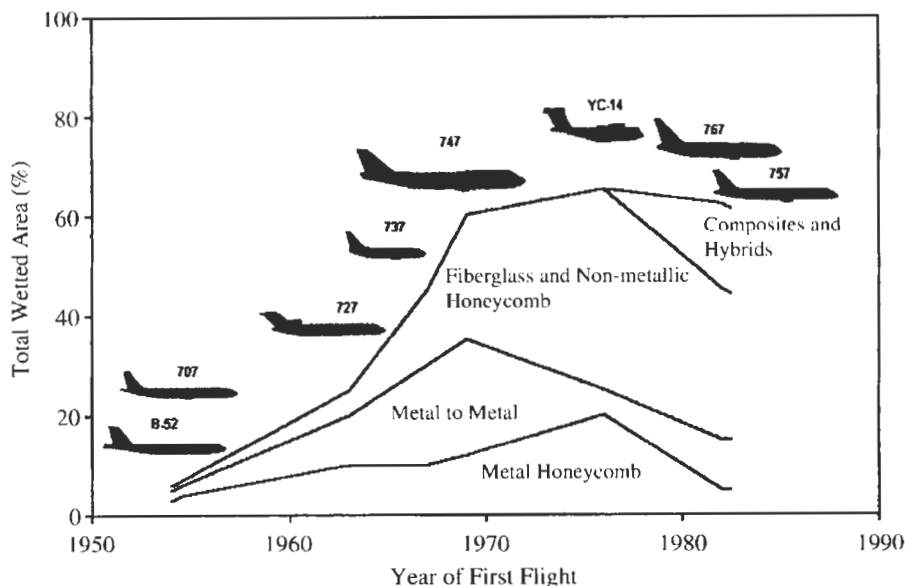


Fig. 5. Growth of adhesive bonding on Boeing Aircraft. Reproduced by permission of the Boeing Company.

and the new cachet of advanced composite materials combined to reduce the enthusiasm for metal bonding. Metal bonding continued to be, and still is today, an important technology for commercial transports, but it is only one of a number of technologies that designers have to choose from.

4.1. Adhesives

Early synthetic polymer adhesives that were more than adequate for wood were not acceptable for aluminum aircraft. The unmodified phenol, resorcinol and urea formaldehydes developed for wood were too brittle and weak for aluminum structure. As mentioned previously, the first successful adhesive for metallic bonding was phenolic resin toughened with PVF particles. Similar toughened phenolic film adhesives such as neoprene-phenolics and nitrile-phenolics were developed in the 1950s that also produced strong, tough metal-to-metal bonds. All of these systems exhibited a number of shortcomings however. All evolved significant volatiles during cure from solvents and condensation-reaction cure mechanisms and had low flow at cure temperature, requiring high bonding pressures and special tooling. All also required high cure temperatures (350°F) that affected the temper of increasingly common precipitation-hardened aluminum alloys such as 2024-T3. Epoxies were targeted early on as the potential replacement for phenolics because of their potential for high flow, low cure temperatures and volatile-free

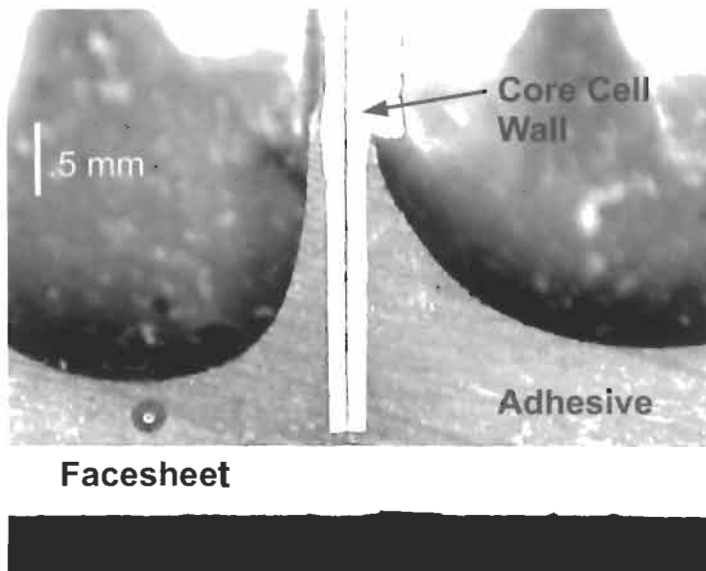


Fig. 6. Adhesive fillet on honeycomb core. Reproduced by permission of the Boeing Company.

cure mechanisms. Although the first epoxies were untoughened and exhibited inadequate fracture toughness, later versions modified with nylon and nitrile rubber produced high strength, tough bonds and largely supplanted toughened phenolics for metal-to-metal bonding, at least in the U.S.

Adhesives for sandwich bonding progressed similarly. Early low-flow adhesives were used with plastic foam cores and end-grain balsa to manufacture sandwich assemblies. The development of less dense honeycomb cores necessitated a change in adhesive. Development of good bond strength to honeycomb core requires relatively high flow so that an adhesive fillet forms on the core walls (Fig. 6).

Sandwich bonding with low-flow toughened phenolics was attempted but was marked by low peel strength from small adhesive fillets and the large amount of volatiles evolved during cure. Perforations in the honeycomb core were required to vent the gases and subsequent in-service protection from moisture ingress through the perforations relied upon post-cure sealing. Although the assemblies were supposedly initially leak-free, in-service pressure and temperature cycling during flight found or eventually caused leaks and allowed water into the sandwich. Even small amounts of water readily attacked the skins and core surfaces, resulting in widespread delamination and corrosion (Fig. 7). Alternate freezing and thawing of larger amounts of water caused physical bursting of the core cells and bulging of the skins. Subsequent duplex adhesives combined a high-flow epoxy layer for good core adhesion with a phenolic layer for a tough facesheet bond. Eventually toughened epoxies progressed to the point that the phenolic



Fig. 7. Corrosion of honeycomb sandwich assembly. Reproduced by permission of the Boeing Company.

layer was unnecessary and was discarded. The lower cure temperatures of the epoxies (250°F) simplified tooling and the lack of cure volatiles allowed lower cure pressure and the use of non-perforated core. Service durability was greatly improved.

4.2. Adhesive bonding processes

By the time aluminum structural bonding began in earnest, large-scale processes for gluing and molding wood using vacuum bags, heated presses or autoclaves were, if not common, at least known technologies. For aluminum bonding their use was expanded, scaled up to fit the increasingly larger size of metal airplanes and refined. Vacuum bag bonding, or drawing a vacuum under a bag sealed around the part and tool, is by definition limited to less than one atmosphere pressure and so has limited usefulness. Vacuum bag bonding was limited mostly to repair of bonded parts where small patches were being applied. Heated presses remained

in use for curing selected parts, but limitations of heat-transfer and pressure uniformity meant that they were restricted mostly to thin, flat assemblies. Autoclaves became the dominant means of applying cure pressure and heat to bonded assemblies because of their flexibility, pressure and temperature uniformity and potential for more efficient heat transfer.

Interestingly, a process similar to the practice of using nails to tack wood members together while the glue cured also survived the transition to metal substrates and was known as rivet-bonding. In this practice adhesive was applied between metal details and fasteners installed to hold the two together while the adhesive was cured, either in an oven or at room temperature. The fasteners did double duty as the means of applying bond pressure as well as to carry loads in service. Because of the very non-uniform bond pressure, this method had the potential to introduce voids that in some cases became sites for corrosion initiation and delamination.

4.3. Substrate surface preparation

As with the use of structural bonding in general, surface preparation of substrates took two quite different paths in the United States and Europe, with significant effects on the success and popularity of adhesive bonding. There were of course variations between manufacturers in both countries, but general observations can be made. European commercial aircraft manufacturers typically used a chromic–sulfuric acid etch when bonding metal-to-metal with the early phenolic systems and achieved relatively good service experience. They learned early on the benefits of a durable surface treatment and designs that protected bondlines from corrosive environments. When epoxies and honeycomb sandwich bonding became practical, they found that an unsealed chromic acid anodize treatment was necessary to guarantee bond durability and adopted it in the late 1950s [6].

American manufacturers, on the other hand, cut their teeth on aluminum bonding during the 1950s in the military world. Military flight durations are shorter, flights are much less frequent and higher maintenance costs are more easily tolerated than in the commercial world. Durability of bonded structure using acid etch surface treatments was known to be a problem, but the cost and trouble was not enough to drive any significant changes in the industry. American manufacturers continued to use chromic–sulfuric acid etch on civil aircraft well into the 1970s. The boom in usage of bonded structure on U.S. commercial aircraft designed in the early to mid-1960s resulted in a tidal wave of delaminated and corroded bonded structure in the late 1960s and early 1970s that cost commercial operators dearly.

Fig. 8 shows the number of bonded metallic parts completely rebuilt during the 1960s and 1970s by a U.S. operator with a large fleet of U.S.-manufactured aircraft [7]. The vast majority of these parts had to be rebuilt because of moisture-

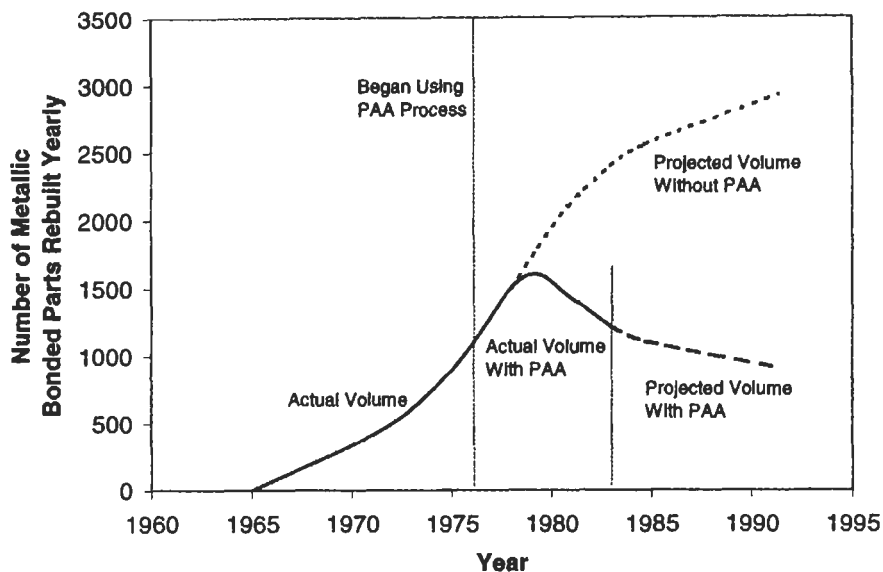


Fig. 8. Repair of bonded assemblies. Reproduced by permission of the Boeing Company.

induced delamination and corrosion. The costs to this one operator in aircraft downtime and labor to remove and replace these parts and completely rebuild them were tremendous. Manufacturers responded to airline pressure with the development and implementation of more durable surface treatments such as phosphoric acid anodize as well as corrosion inhibiting adhesive primers. These advances demonstrably solved the environmental durability problem of bonded structure. However, the reputation of bonded aluminum structure was already severely damaged. Advanced (graphite and aramid fiber) composite technology had reached sufficient maturity to be production ready and replaced aluminum bonded structure in many applications. Thoughts of bonded aluminum primary structure, such as that manufactured in Europe for decades, receded further from the minds of American aircraft designers.

4.4. Composite bonding

Early composite structure was primarily fiberglass, which has relatively low strength properties and was mainly used for non-structural fairings. The development of higher strength advanced fibers such as boron, graphite and aramid gave new life to composites and widened their potential to include structural applications. On commercial aircraft, application of advanced composites grew to include critical structure such as elevators and rudders and eventually to primary structure such as horizontal and vertical stabilizers.

Adhesive bonding is an integral part of virtually all composite structure. Early composite matrix resins could in some cases act as an adhesive, such as with 'self-filleting' systems used for honeycomb sandwich fabrication. As composite systems became more optimized for minimum resin content and limited flow, supplementary adhesives became more common. Modern-day composite structure relies on adhesives almost as much as bonded metallic structure.

5. Current production aircraft

Current production aircraft include bonded structure designed up to 20 years ago as well as more recent designs on newer aircraft or derivatives. Materials, processes and design philosophy for metallic bonded structure have remained relatively stable over that period, while composite bonded structure has advanced significantly. Both will be reviewed and contrasted in the following sections.

5.1. Metallic bonded structure

5.1.1. Adhesives and associated materials

Though toughened phenolic adhesives remain in use for specific applications, toughened epoxy adhesives have dominated metallic bonding on civil aircraft since their development in the 1960s. Advances since then have been incremental and mostly revolving around manufacturing issues such as handleability and allowed out-time.

Toughened epoxy metalbond adhesives are manufactured as films of various thickness (typically ~ 0.005 – 0.015 ") for different applications. The thinner products are used for metal-to-metal bonding and will produce a bondline thickness of ~ 0.003 – 0.008 ". The thicker films are used for bonding honeycomb sandwich where additional adhesive is needed to form fillets on the core cell walls. Most modern film adhesives are cast from a resin melt, as opposed to casting from resin thinned with solvent, to simplify the adhesive manufacturing process and to reduce volatile outgassing during cure. The films are cast around or onto a loose-woven or random mat carrier or 'scrim', usually made of nylon, for ease of handling during part layup and for cured bondline thickness control. The carrier prevents metal-to-metal bonds from squeezing down to very thin bondlines in areas of high pressure. Carriers are available woven or non-woven (random-mat). Early experience suggested that woven carriers exacerbated bondline corrosion by providing an easier path for moisture to wick into the bondline. This concern has faded significantly with the development of more durable aluminum surface treatments. The adhesive film is usually wound on a roll up to a few feet in

Table 1

Adhesive property requirements for metallic bonding

Property	Requirement
Lap shear at 75°F	4200 psi
Lap shear at -67°F	4200 psi
Lap shear at 180°F	3100 psi
Lap fatigue at 75°F	10 ⁷ cycles at 1500 psi
Creep rupture deformation at 75°F under 1600 psi load for 192 h	0.015" max.
Creep rupture deformation at 180°F under 800 psi load for 192 h	0.015" max.
Lap shear at 75°F after 30 days exposure to 100 percent R.H. at 120°F	No significant change from room-temperature lap shear strength
Lap shear at 75°F after 30 days salt spray exposure at 95°F	Less than ~15% loss from room-temperature lap shear strength
Lap shear at 75°F after 7 days immersion in jet fuel at 75°F	No significant change from room-temperature lap shear strength
Lap shear at 75°F after 7 days immersion in hydraulic fluid at 150°F	No significant change from room-temperature lap shear strength
Metal-to-metal climbing drum peel at 75°F	45 lb-in/in (Grade 5) 55 lb-in/in (Grade 10) Not required (Grade 15)
Crack extension (fracture toughness)	$G_{Ic} = 8$ lb/in
Sustained stress loading in 140°F, 100% R.H.	No failures in 90 days at 900 psi

width and a few hundred feet in length with release paper or plastic interleaved to prevent the adhesive from sticking to itself.

Adhesives are controlled by airframe manufacturer's or industry specifications that lay out requirements for both engineering and manufacturing properties. Engineering properties are those necessary for good performance in service and include properties such as shear strength, peel strength, fracture toughness, environmental durability, resistance to common aircraft fluids, etc. Manufacturing properties such as out-time and storage life are controlled to ensure the adhesive can be used in a realistic manufacturing environment without significant waste or extra labor.

Table 1 contains the metal-to-metal engineering property requirements for Boeing Material Specification (BMS) 5-101, a structural film adhesive for metal to metal and honeycomb sandwich use in areas with normal temperature exposure. The requirements are dominated by shear strength tests. Shear strength is the most critical engineering property for structural adhesives, at least for the simplistic joint analysis that is commonly used for metal-to-metal secondary structure on commercial aircraft. Adhesive joints are purposefully loaded primarily in shear as opposed to tension or peel modes as adhesives are typically stronger in shear than in Mode I (load normal to the plane of the bond) loading.

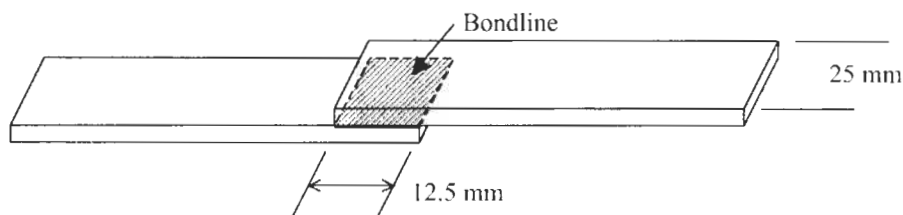


Fig. 9. Standard single overlap shear specimen.

Shear strength is measured via a simple single overlap shear specimen of standard dimensions (Fig. 9). In contrast to its simple appearance, the forces in a thin-adherend shear specimen can be quite complex due to the inherent offset loading of the specimen and subsequent bending in the substrates. The single overlap shear test is anything but a pure shear test, but the configuration is easy to manufacture, simple to test and is firmly entrenched in the industry as a primary examination technique for materials qualifications, inspection and process control.

Adhesive strength is evaluated at room temperature as well as at the extreme temperatures of -65°F and 180°F . Aircraft structure can reach -65°F at cruise altitudes and 180°F on the ground in a hot, sunny location. The types of toughened epoxies commonly used for metal bond adhesives have glass transition temperatures not much greater than 200°F , so properties fall off drastically at higher temperatures.

Resistance to common aircraft fluids such as water, salt water, hydraulic fluid and jet fuel is determined by additional shear testing after exposure to these fluids. Since adhesives are typically only exposed at bond edges, are protected by secondary primers and enamels and are not expected to be exposed to these fluids (save for water) for extended periods, exposure time prior to testing is relatively short. Lastly, the adhesive is tested for propensity to creep rupture under load in standard and aggressive environments. This testing indicates whether the polymer is crosslinked sufficiently to resist long-term creep under low load.

Peel strength is characterized via various methods including climbing drum peel (ASTM D1781), shown in Fig. 10, T-peel (ASTM D1876), and floating roller, or 'Bell', peel. Even though adhesive bonds are purposefully not loaded significantly in peel or Mode I, most shear joints have some Mode I loading component. The peel strength requirement is primarily a legacy of the early days of adhesive bonding when brittle, low peel strength adhesives were common. Delaminations during manufacture and premature failures in service were not unusual because of the delicacy of the bonded joints. Controlling peel strength was a 'gut-feel' way of reducing these problems. More modern methods of bond analysis and design rely on adhesive stress-strain curves and Mode I fracture energy properties such as G_{Ic} and G_{Ia} , though these are still seldom used in the civil aircraft world where bonded primary structure is rare.

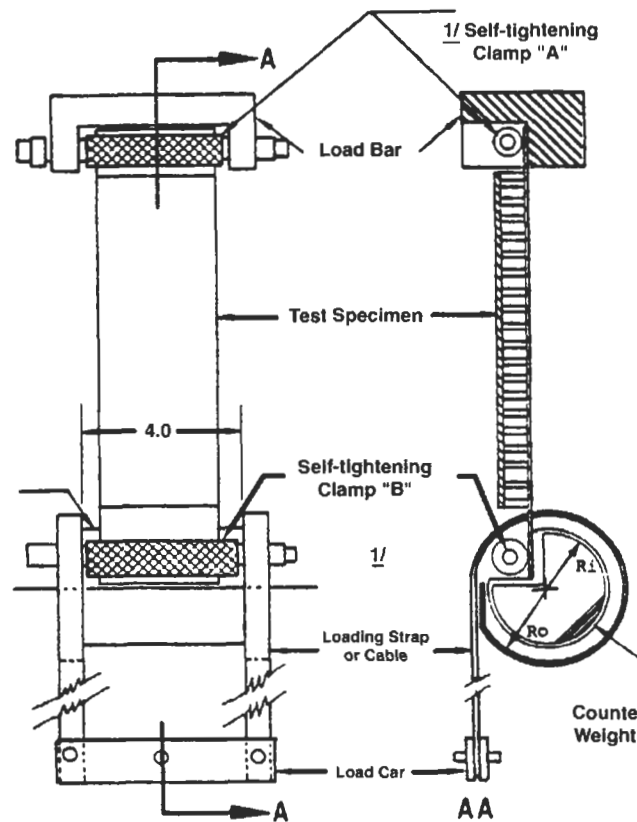


Fig. 10. Climbing drum peel apparatus (honeycomb shown). Reproduced by permission of the Boeing Company.

Table 2 contains the honeycomb sandwich bonding property requirements for the same adhesive. Note that 0.005" thick adhesive has no sandwich bond requirements because it does not contain enough adhesive to form effective fillets and so is not used for sandwich bonding.

Adhesive properties for honeycomb bonding differ substantially from metal-to-metal applications. The honeycomb core used is lightweight and will not sustain significant shear loads (in comparison to the adhesive), so peel and flatwise tension testing is the primary means of evaluation. Peel is performed on the same climbing drum apparatus as metal-to-metal peel (ASTM D1781). Flatwise tension testing (ASTM C297) is performed by secondarily bonding thick load blocks to a 2 × 2" sandwich specimen and applying load normal to the facesheet until failure of the adhesive or core occurs (Fig. 11). High strength indicates that the adhesive flows and wets the cell walls during cure, forming fillets, and is compatible with

Table 2
Adhesive strength requirements for honeycomb core bonding

Property	Strength requirement (minimum)	
	Adhesive thickness	
	0.010"	0.015"
Honeycomb peel at 75°F	45 lb-in/3 inch	75 lb-in/3 inch
Honeycomb peel at 75°F after 30 days exposure at 95°F, 100 percent R.H.	75% of actual room temperature peel strength	
Honeycomb peel at 75°F after 30 days salt spray exposure at 95°F	75% of actual room temperature peel strength	
Flatwise tensile at 75°F	900 psi	1100 psi
Flatwise tensile at 180°F	500 psi	750 psi

the surface treatment on the honeycomb core. Again, performance at various temperatures and after environmental exposure is evaluated.

Manufacturing properties such as 'tack' and 'out-time' are important to the cost-effective manufacture of bonded hardware. The tack of an adhesive, or its propensity to stick to itself or other materials, can have a large effect on the cost of bonding. Layup of bonded assemblies is a labor-intensive task full of intricate



Fig. 11. Flatwise tensile test specimen. Reproduced by permission of the Boeing Company.

handwork. Sections of adhesive film are placed on part details and must have enough tack to remain in place, even on vertical surfaces. If the adhesive has not enough tack, extra procedures such as heat tacking (using a small iron or blower to heat-weld the adhesive to the part) or vacuum consolidation (placing the adhesive and part under a vacuum bag to achieve adherence) become necessary. Too much tack, on the other hand, makes repositioning film sections difficult or impossible, making layup a frustrating and lengthy ordeal.

Out-time is the maximum time an adhesive can be at room temperature before it must be cured. Most modern structural adhesives contain cure catalysts that require high temperature (250–350°F) to initiate crosslinking, but crosslinking does occur slowly at room temperature. This crosslinking eventually increases the melt viscosity of the adhesive, reducing the ability of the adhesive to wet bond surfaces and form fillets on adhesive core. To prevent this, adhesives are shipped and stored frozen and out-time is controlled. Out-time during layup of bonded parts is tracked so that maximum out-time is not exceeded before the assembly is cured. Early film epoxies had short out-times of 5 days or less. Since out-time includes the length of time the roll of adhesive sits waiting to be used as well as time during layup, 5 days was a significant hardship for cost-effective manufacturing. Improved products with allowed out-time of 10 days or more were introduced in the late 1960s and are now standard.

Structural adhesives are also available in paste form. Bondline thickness control and void elimination are more difficult with paste materials but they can be very useful for unusual designs and innovative manufacturing methods.

5.1.1.1. Product qualification versus consistency control and design values. Engineering property requirements such as those discussed above are used for two separate and distinct purposes, both of which have little to do with the actual performance expected of the adhesive in a real part. Adhesives requirements in a specification are used for both initial product qualification and batch consistency control. New products are tested to the requirements of the specification, or qualified, in order to determine whether it meets those requirements. The requirements are relatively limited in scope and test configurations are simple and not typically representative of actual part designs. Qualification serves to indicate whether the product in question has the properties required to justify further effort. For new specifications that push available technology, this process is often iterative, with requirements raised or lowered (within limits) to match the product that is available. For existing specifications, the qualification merely serves to indicate that the product is equivalent or better than the existing qualified materials. The same requirements are then used to guarantee batch to batch consistency for ongoing production. Governmental agency regulations for aircraft require a manufacturing control system that guarantees consistent quality of materials and processes. As applied to adhesives, that means that there must be certainty that a new batch of

adhesive is equivalent to the batch used to determine properties for the original part design.

All of these requirements and testing are only peripherally related to the adhesive properties used by actual design engineers to design hardware. Because of the complex stresses and strains in bonded aircraft parts, simple adhesive shear strengths (for instance) obtained from a specimen of standard dimensions and materials are not adequate to enable efficient design. After qualification, adhesives are tested much more rigorously to develop statistically valid properties called allowables. Adhesive strength in relation to temperature, substrate thickness, bond length and width, etc., is determined by testing multiple specimens of multiple batches of adhesive. The results are analyzed to produce statistically valid minimum properties, or allowables, that can be used for a reasonable variety of part designs. 'A-basis' allowables are defined as having a 95% confidence that at least 99% of the population will exceed the allowable. 'B-basis' allowables are defined as having a 95% confidence that at least 90% of the population will exceed the allowable. A- and B-basis allowables are used (depending on the criticality of the part) to size bonds to take expected loads.

Since it is not cost-effective to test all foreseeable bond configurations, occasionally actual parts, or specimens containing features that are very similar to specific parts, are tested to generate 'point-design allowables'.

The brute force allowables method described above of testing numerous substrate thicknesses and bond widths is still not that much more cost-effective than a point-design approach. A more efficient and analytical method of designing and analyzing adhesive bonds relies on more detailed knowledge of adhesive mechanics. Mechanics of bonded joints become very complex very quickly because of the large difference in stiffness and strength of the adhesive and adherends, the significant deformations these adhesives exhibit before ultimate fracture, and the common need to bond adherends of different thicknesses and shapes. Modeling these complex joints requires knowledge of the adhesive stress-strain response up to ultimate fracture at temperatures of interest. This information has been gathered by various methods such as the napkin ring shear and thick-adherend lap shear (ASTM D5656) extensometer testing. Fig. 12 shows typical thick adherend stress-strain data for a standard 250°F curing epoxy film adhesive.

5.1.1.2. Higher-temperature applications. Bonded aluminum assemblies are also present in areas that experience higher than normal temperatures, such as engine cowls and noise attenuation linings, and so require adhesives with higher temperature capabilities. Higher-temperature cure epoxies are used for these applications. Cure temperature is typically 350°F and cured shear strength properties are still quite significant at 350°F (Table 3). Even high-temperature epoxies, though tested for performance at 350°F, are not durable enough for continuous operational use at 350°F. The lifetime of a civil aircraft can reach 80,000 flight hours or more. The

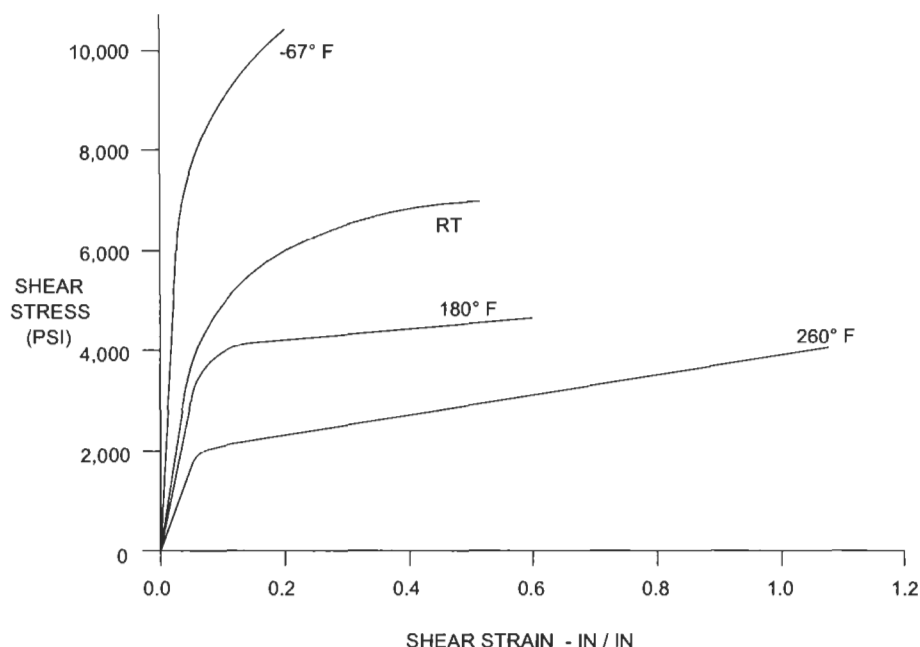


Fig. 12. Adhesive thick adherend shear stress/strain. Reproduced by permission of the Boeing Company.

particular applications in service today may reach 350°F for only a few minutes of every flight cycle. Others may only experience high temperatures in the event of a failure in another system, such as an anti-icing duct failure that leaks hot engine-bleed air adjacent to a bonded leading edge slat trailing edge wedges. The adhesives are tested for residual shear strength after some limited exposure to 350°F, typically 1000 h.

Applications such as the noise attenuation panels that line engine inlets and exhausts require a special form of high temperature adhesive known as a reticulating adhesive. These bond honeycomb sandwich assemblies have inner facesheets with numerous small holes (Fig. 13). The holes and underlying honeycomb core

Table 3

Lap shear requirements for an elevated temperature adhesive

Test temperature (°F)	Shear strength requirement (psi)
-67	2500
75	3200
350	1500



Fig. 13. Engine inlet noise attenuation panel. Reproduced by permission of the Boeing Company.

cells form many small chambers that are carefully sized to attenuate specific frequencies of the noise created by the air rushing through the inlet and exhaust. In order to achieve maximum attenuation, the facesheet must be bonded to the core without covering a significant number of the openings with adhesive. This is accomplished by using reticulating adhesive, a special resin film that does not have a carrier fabric. The adhesive film is placed on the honeycomb core or the facesheet and passed over a hot air blower. The hot air is blown up through the core or through the openings in the facesheet, melting the resin enough to form bubbles that expand and burst, retracting to leave adhesive only on the core cell edges or on the solid facesheet. The core is then bonded to the facesheet with a standard autoclave cure cycle, blocking a minimum number of holes with adhesive.

5.1.1.3. Adhesive primers. Metal adherends are coated with adhesive primers after cleaning and surface preparation. Adhesives primers are specially formulated to be a strong intermediate layer between the aluminum surface and the adhesive bondline. The primer is designed to wet the aluminum surface well, penetrating the anodize and developing a strong, durable bond to the aluminum surface. Adhesive primers are formulated to be chemically compatible with the adhesive, intermixing and forming a strong bond during adhesive cure. The primer also serves as a protective layer for the delicate and contamination-sensitive anodize

layer. Anodized and primed details can be handled and stored for relatively long periods of time, unlike details with unprotected anodize. Many primers can be solvent cleaned to remove incidental contamination without adversely affecting subsequent bond strength and durability.

Primers are required to be resistant to all of the same fluids and environments as the adhesive, and are in addition expected to be compatible with secondary finishes such as corrosion and fluid resistant primers applied to cured bond assemblies. The most commonly used primers for 250°F cured epoxy adhesives also have active corrosion inhibitors themselves to combat corrosion at bondlines. This last requirement is somewhat dated, evolving from the severe corrosion and delamination problems experienced before U.S. airframe manufacturers adopted durable surface treatments.

5.1.1.4. Foaming adhesives. Film adhesives are used to bond honeycomb core to facesheets but are not suitable for splicing core sections or for bonding core peripheries to embedded solid members such as spars or actuator fittings. The cut edges of the core are irregular, present little area to obtain a strong bond to and are difficult to apply in-plane pressure to maintain contact between the adherends. For these reasons foaming adhesive is used. Foaming adhesives contain a blowing agent that expands during cure and causes the adhesive to expand to contact the adherends (Fig. 14). The expansion ratio, usually two or three hundred percent, is critical to proper usage. Too little expansion produces inadequate contact and bond strength between adherends and the adhesive while too much expansion can push details out of position or compress the honeycomb core. Early foaming adhesives had an open cell structure and on occasion were found to be paths for water ingress when the adhesive was exposed to the environment at panel edges. More recent versions are closed cell and are tested for resistance to water passage.

5.1.1.5. Potting compounds. Potting compounds are highly filled epoxies used to fill honeycomb core areas where additional compression strength is needed such as locations where fasteners pass through. Though not adhesives in a traditional sense, they too must exhibit good adhesion to other bond materials and adhesives and be resistant to the same environmental factors.

5.1.2. Adherends

5.1.2.1. Honeycomb core. Honeycomb core used for aluminum bonded sandwich structure is exclusively aluminum. The core is fabricated by printing offset stripes of adhesive (the 'node' adhesive) on aluminum foil, stacking a large number of these foils and then curing the adhesive in a heated press. The resulting block is called a hobe. Slices are machined from the edge of the hobe and then expanded to

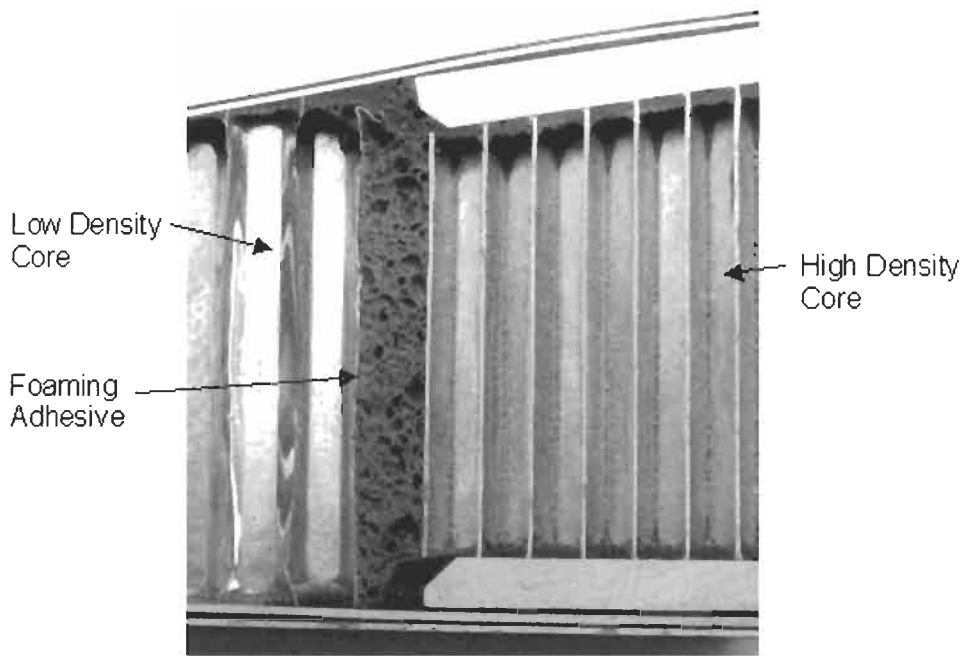


Fig. 14. Foaming adhesive joint. Reproduced by permission of the Boeing Company.

form honeycomb core (Fig. 15). Spacing of the adhesive stripes, which determines the honeycomb cell size, and foil thickness control density and strength of the core. High-density core with foil too thick to expand without breaking the node bonds is made by pre-corrugating the foil strips and bonding the core slices individually. Honeycomb core is most commonly manufactured with 5052 aluminum alloy foil, though 5056 and other alloys are also available and are stronger (and more expensive).

Surface preparation of the core foil was originally simple acid etching. As the importance of durable surface treatments became known, a more stable chemical conversion coating with an organic primer-like coating became standard. Still, water ingress into honeycomb structure continued to cause the occasional

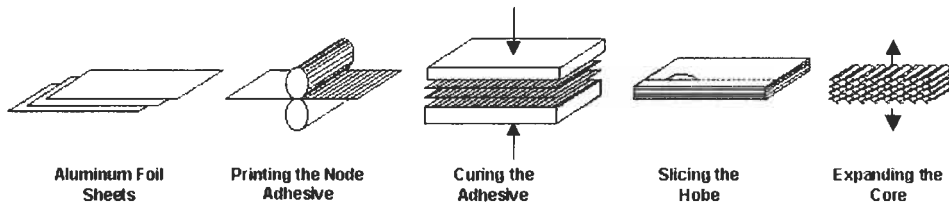


Fig. 15. Aluminum honeycomb core fabrication.

delamination in service. A contributing factor to these failures was determined to be the honeycomb core surface treatment. Within the last ten years honeycomb core with a phosphoric acid anodize coating and epoxy primer has been developed and become common for aircraft structure. Though the anodize and priming process has been optimized for high-speed continuous treatment of aluminum foil, durability is equivalent to that of the surface treatment on other aluminum details.

5.1.2.2. Metals. Aluminum is by far the most commonly bonded metal used in civil aircraft construction. For the most part this is due to the preponderance of aluminum in transport aircraft structure. Steel and titanium are used in areas where high strength or high temperature requirements make aluminum unwieldy or unsuitable such as landing gear, the engine, engine strut and wing control surface tracks, carriages and actuators. Most, if not all, of these applications have temperature or configuration limitations that have in the past made the application of adhesive bonding technically difficult or of little benefit. A contributing factor is the lack of success in developing cost-effective, robust, durable surface treatments for metals such as titanium and steel. In recent years advances have been made in high-temperature composite and adhesive materials as well as titanium and steel surface treatment processes that allow the use of adhesive bonding in new areas, particularly the engine. In pursuit of increased efficiency and power, engine manufacturers have been quite aggressive in taking advantage of adhesive bonding for new applications such as composite fan blades.

The aluminum alloys most commonly bonded are 2024 bare, 2024 clad and 7075 bare. Clad 7075 was also used extensively in early bonded structure but was largely abandoned after service performance demonstrated that it was susceptible to rapid dissolution or corrosion of the clad layer. Naturally aged tempers such as T3, in particular 2024-T3 because of its widespread use, are restricted to bonding with adhesives that cure at 250°F or below in order to avoid adversely affecting the temper. Various other alloys and tempers are bonded to a lesser extent, though the dominance of 7075 and 2024 is decreasing as higher-performance alloys and tempers are adopted.

5.2. Composite bonded structure

5.2.1. Adhesives

Adhesives for bonding composites are very similar to those used for bonding metallic structure. In fact, early epoxy film adhesives for metal-bond were used for bonding fiberglass as well. This gradually changed with the development of advanced composite systems such as graphite and aramid-reinforced epoxies. In order to produce a resin matrix glass transition temperature that is high enough to maintain properties in hot conditions (160°F) after exposure to humidity, these

Table 4
Adhesive for composite substrates, requirements

Property	Requirement, minimum average (psi)
<i>Double lap shear</i>	
−65°F	3300
75°F	3500
160°F	2700
270°F	950
75°F after 1000 hours at 160°F, 95% RH	2400
75°F after 14 days min. at 160°F, 95% RH	2400
<i>Honeycomb flatwise tensile</i>	
−65°F	600
75°F	600
160°F	500
160°F after 14 days min. at 160°F, 95% RH	390
<i>Sandwich beam shear</i>	
−65°F	500
75°F	500
160°F	500

systems normally cure at 350°F. New adhesives were developed that matched these cure temperatures and were compatible with the matrix resin of the composite. Table 4 contains the property requirements for a typical 350°F curing adhesive for composite adherends.

Lap shear strength of composite adhesives is measured using composite laminate adherends in a double-overlap lap shear configuration (Fig. 16). Double overlap is used to minimize peel stresses during the shear test. Because of the relatively low fracture toughness of the matrix resin, significant peel stresses during shear testing can cause failure in the adherends before the adhesive. Likewise, adhesive peel strength is difficult to measure with composite adherends. Double-cantilever beam fracture toughness tests are more common. Honeycomb bond strength characterization is accomplished with flatwise tensile and beam shear

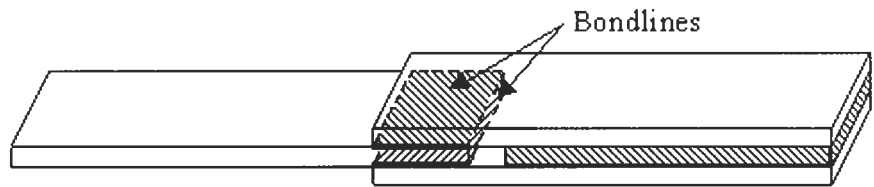


Fig. 16. Double-overlap shear specimen.

tests. Property requirements for honeycomb bonding are relatively low compared to adhesives for aluminum bonding because of the use of non-metallic core, which has much lower strength than aluminum core.

Until relatively recently adhesive films for composites were also used to enhance the surface finish of composite parts. Because advanced composite systems have the minimum amount of matrix resin necessary in order to maximize mechanical properties, surfaces of parts made with these systems can be of poor cosmetic quality. Small pits and depressions due to 'resin starvation' and telegraphing of the honeycomb core pattern through thin facesheets are typical. When these problems occur on aerodynamic surfaces, labor-intensive secondary operations such as filling and hand-sanding are necessary to produce an acceptable appearance. Adhesive films placed on these exterior surfaces during layup of the composite plies add enough extra resin to greatly reduce these problems. During the 1990s specific products for improving surface quality of cured parts were developed and adhesive films were no longer required to perform both functions.

5.2.2. *Adherends*

5.2.2.1. Honeycomb core. Honeycomb core used with composites is typically non-metallic, though aluminum core has been used in fiberglass sandwich panels with particularly high compression strength requirements. Non-metallic core is usually aramid or fiberglass based. For both types of core, manufacturing techniques are somewhat similar to those used to fabricate aluminum core. Adhesive stripes are printed on aramid paper or light fiberglass and the adhesive is cured. Unlike aluminum core, the hobe is expanded prior to machining. The expanded hobe is dipped into a phenolic resin bath and the resin cured. The hobe is dipped a number of times to build up wall thickness and increase mechanical properties until the target density is reached. This also serves to lock the hobe into the honeycomb shape. Core slices of desired thickness are then machined off the hobe. One disadvantage of non-metallic core, in particular aramid fiber-based core, is the tendency to absorb atmospheric moisture. If the core is not baked dry prior to use, absorbed water can evolve during curing of the composite assembly and cause problems such as porosity and poor mechanical properties.

5.2.2.2. Composite adherends. Composite adherends are bonded in both the cured and uncured states. Wherever possible the adhesive and all adherends are cured simultaneously to avoid the added cost of additional autoclave cure cycles. In many cases this is not practical due to part size and complexity. Cured parts can be bonded to uncured parts, which is known as cobonding, and fully cured parts can be bonded together, which is known as secondary bonding. Adhesives for composites are formulated to be compatible with matrix resins in either cured or uncured states.

5.3. Design, manufacture and fleet performance of bonded structure

5.3.1. Aluminum

As stated previously, most uses of adhesively bonded aluminum assemblies on large commercial transports are in secondary structure. The majority of these applications can be generally divided into three major design categories: structural skins of various types with metal-to-metal bonded doublers (triplers, etc.), stiffened fairing panels with one or no aerodynamic surfaces, and trailing edge wedge assemblies. The first category describes skins with additional bonded layers placed for such reasons as local load distribution, fatigue life enhancement and crack stopping purposes. The second category is usually comprised of lightly loaded aerodynamic fairings that can also contain metal-to-metal doublers, though most modern designs for panel stiffening are of honeycomb sandwich construction. Stiffened panels are typically fastened to surrounding structure on all sides, though fastening on three sides is not unknown. Trailing edge wedges are most often the aft-most section of a flight control surface, taper to a point and are fastened along the forward edge. There are of course numerous bonded assemblies that do not fall into these categories, but these categories cover by far the majority of the area of adhesive bonding on an aircraft.

A significant portion of design, fabrication and in-service processes and practices are common to all three of these categories of assemblies. These common issues will be explored first, followed by more detailed examination of the genesis and issues particular to each of the three major categories listed above.

5.3.1.1. Design. Detailed adhesively bonded joint design and analysis methods are discussed elsewhere in this volume. General issues associated with bonded assembly design will be considered here.

Successful design of adhesively bonded metal structure must take into account not only operating and ground loads but tooling considerations, autoclave capacity, inspection requirements, other manufacturing issues, in-service environment and repair scenarios. The first few considerations are relatively straightforward and familiar to designers. Is the assembly capable of carrying design loads without failure? Does it require complex tooling that will be expensive to build and delicate, requiring constant maintenance? Will the tool fit in existing autoclaves or will it require a larger autoclave? Is it such an odd shape that it will require its own lengthy and expensive cure cycle, or can it be cured along with other assemblies?

The remaining requirements for a bonded assembly that a designer must consider are more difficult to delineate and their boundaries are expanding as manufacturing and service experience with metal-bond structure grows. A designer must be well aware of the capabilities and limitations of adhesively bonded structure in general, not to mention the particular adhesive system being used, as

well as the service environment of the part. This is obviously true of all fabrication technologies but like any other, adhesive bonding has its particular quirks. Some of these quirks are best illustrated with brief examples.

During the late 1970s an adhesive was developed for higher-temperature applications that was rather brittle at room temperature, exhibiting low peel strength and fracture toughness. This adhesive was used to bond many types of assemblies including engine inlets and leading edge slat trailing edge wedges. Manufacturing bonded assemblies with this adhesive proved to be difficult. Assemblies were prone to delamination during trimming and general handling in the factory because of the low fracture toughness of the adhesive.

Designers must keep in mind that modern aircraft will likely be in service for thirty years and that repair of adhesive bonded structure will be inevitable. They must allow for reasonable disassembly of bonded structure for repair access as well as anticipate repair procedures that will not be unduly difficult for airline repair stations.

An aircraft maintenance issue that has become more of a concern of aircraft operators over the years is materials proliferation, particularly of adhesives and composite materials. Advancement of adhesive and composite technologies have been rapid and designers of each new aircraft model wish to take advantage of the improved properties of the newest generation of materials to reduce weight and cost. A large operator with numerous models from various manufacturers is faced with stocking increasing numbers of unique adhesives and composite preregs for repairs. The vast majority of these require refrigeration, have a relatively short storage life and require periodic testing to audit properties. The cost to the operator can be tremendous. There is increasing pressure on airframe manufacturers to limit the number of new materials, or at least make sure that new materials are backward compatible with older designs.

Design example. This example explores the process that a typical bond assembly designer might use in designing a simple aerodynamic fairing.

The designer would first determine the loads to which his assembly is subject. With a aerodynamic fairing loading will be primarily aerodynamic. Normal operating loads and boundary conditions are determined. An aerodynamic assembly might be limited to a maximum deflection from nominal contour under normal operating loads in order to maintain expected aerodynamic performance and efficiency. There may be structural loads from deflection of substructure to take into account as well, but for a fairing these are usually small. The appropriate worst-case loads are determined, possibly a high speed emergency descent or a higher than normal emergency maneuver load. These are known as design ultimate loads, or the highest loads that might be encountered during the life of an aircraft. The bonded part will be designed to withstand the ultimate load, plus a safety factor, without failure.

Next, the operating environment is considered. Assemblies that are not near heat sources such as engines are designed to temperature limits of -65°F to 180°F . Adhesive bond strength between these temperature limits is used to evaluate the strength of the bond assembly. External damage sources such as hail would be considered. The external skins and honeycomb core of upper wing surface fairings would be sized to withstand impact by certain hailstone sizes and speeds.

The designer might perform a trade study to determine the best option for manufacturing the assembly. Using the load and operating environment requirements, the designer would size a number of different panel configurations such as composite and metal sandwich designs with various facesheet thicknesses and core densities. The designer might also consider the slight weight savings made possible by combining 2 or more adjacent fairing panels into one assembly versus the added cost of making the larger, more complex assembly. In addition to well-defined requirements such as loads, the selection of metal versus composite sandwich might be influenced by such intangibles as the proposed market for the target aircraft. Customers for a long-range trans-oceanic aircraft might view the extensive use of lightweight but somewhat delicate and expensive advanced composites more favorably than would the customers for a short-hop feeder-route plane.

After resolving the trade study and selecting the general configuration of the assembly, the detailed design work would commence. The exact size and shape of all components would be defined and detailed analyses performed to show that all design requirements were met. Though the broad part configuration would be defined in the initial trade study, there are numerous detail decisions to be made in this phase. Most can be summarized as performance (weight, strength) versus cost (both original manufacture cost and in-service cost). For example, if an assembly will be removed for frequent maintenance of underlying systems, the designer might choose to specify thicker skins than required in anticipation of rough handling. Or the designer might choose to specify more steps in the gauge reduction of the exterior skin from the edge to the center in order to eke out every last ounce of weight, but at slightly increased manufacturing cost.

5.3.1.2. Manufacture.

Detail preparation. Manufacture of a bonded assembly begins with preparation of the adherends, or details. The details are formed and machined as appropriate and all edges are deburred. Imperfections as small as edge burrs can prevent details from fitting together properly and result in voids or pinched off bondlines. The dimensionally complete parts are then placed into their proper place in the bonding tool to check for proper fit. If hand pressure cannot be used to bring details into contact, it is possible a void will occur during bonding and the parts are reworked to improve fit.

The details are then removed from the tool for anodizing and priming. They are first processed through a multi-tank anodize line that consists of a vapor degreaser

or emulsion cleaner and alkaline cleaner to remove organic contaminants, an acid etch to remove the existing surface oxide layers and finally the anodize tank to create a strong, durable and porous oxide layer. Rinse tanks of increasing purity are used between each of these tanks to prevent contamination and after the anodize tank to produce a clean, neutral surface. Each of the tanks in these lines can be between tens of gallons and tens of thousands of gallons in size to accommodate details many feet in length and width. And each tank is closely monitored to insure that it has the correct chemistry and temperature required to produce a bondable, durable surface. From this point on the details are handled only with clean, gloved hands to prevent damage or contamination of the bond surfaces.

After drying, the anodized parts are primed with the adhesive primer. Time between anodize and priming is limited to prevent contamination of the active oxide layer. The primer is air-dried for a time to allow the solvents to evaporate and then baked at elevated temperature to cure. Many adhesive primers have very tight thickness requirements, for instance 0.00015" to 0.001", and require skilled spray operators to apply. A primer layer that is too thick can result in low peel strength while a layer that is too thin might not be continuous and could result in insufficient wetting of the surface by the adhesive during cure.

Honeycomb core parts are usually supplied from the core manufacturer clean and packaged in such a way that additional cleaning is not necessary. If this is not the case or if secondary machining is necessary, the core detail is cleaned by vapor degreasing or emulsion cleaning to remove organic contaminants.

Layup and adhesive cure. After surface treatment the details are again placed in the tool, but this time with adhesive. Film adhesive is placed between all adherends except for the peripheries of core details. Core peripheries, whether they are adjacent to other core sections, spars or other machined details, are bonded with foaming adhesive. High-temperature tape or tooling features are used to keep small details from moving out of place during cure. Thermocouples are placed in areas of high and low assembly/tool mass to insure that all the adhesive in an assembly is kept within the required temperature range during cure. If the assembly will be autoclave or vacuum bag cured, a flexible, high-temperature resistant film (typically nylon) is placed over the part and sealed to the tool base with high-temperature resistant bag sealant. Air ports are installed through the bag to allow evacuation of the air under the bag during layup to seat details and check for leaks prior to cure and venting to atmosphere during the cure cycle. Then the tool is placed in the press, oven or autoclave for adhesive cure.

The vast majority of metallic bonded assemblies are cured in autoclaves. A small number are cured using mechanical pressure application devices (clamps, presses) or by drawing a vacuum under a bag over the part in an oven. Mechanical pressure is rarely used for a few reasons. For all but completely flat assemblies it

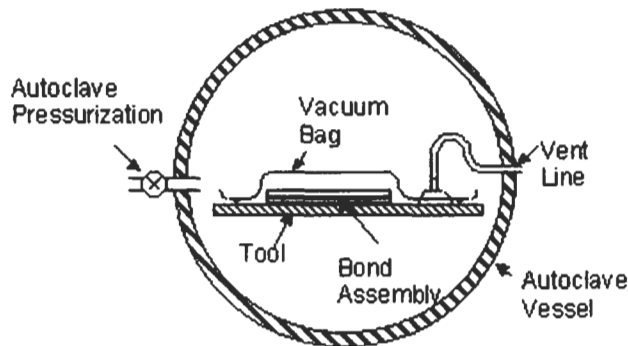


Fig. 17. Autoclave schematic.

is difficult to maintain adequate and consistent pressure over all areas of the part. Matched metal dies necessary to apply mechanical pressure to contoured parts are expensive and sensitive to minute variation in detail part dimensions. They may also vary in thickness substantially, interfering with temperature uniformity during adhesive cure. Particularly for metal-to-metal assemblies, bonding pressure required necessitates huge hydraulic presses for all but the smallest assemblies.

Vacuum bag bonding is restricted by definition to less than 1 atm (<15 psi) which can be insufficient to achieve good part contact and prevent bondline voids. Hence vacuum bag bonding is rarely used outside of repair situations.

Autoclave bonding has none of the limitations listed above. Uniform fluid pressure is applied to the part by the pressurized medium in the autoclave (typically air, or nitrogen for safety reasons) acting on the flexible plastic bag over the part and tool. The inside of the bag is vented to the atmosphere so bonding pressure can be as high as the autoclave is capable of sustaining (Fig. 17). Numerous parts of various sizes can be placed in the autoclave, limited only by tool size and autoclave volume and heating capacity. Lastly, the pressurized gases in the autoclave have better heat transfer characteristics than unpressurized ovens, making it easier to maintain heat-up rate and temperature uniformity requirements. Disadvantages include sensitivity to leaks in the vacuum bag surrounding the part. A pinhole leak can result in loss of pressure and a ruined assembly. Also, autoclaves are complex and expensive systems, and are essentially just as costly to operate when they contain one small assembly as when they contain a dozen.

Fig. 18 shows a trio of autoclaves. In the foreground is a bond assembly on a wheeled tool ready to be placed in the autoclave. A technician stands at a control console next to a two-level rack used for holding multiple bond tools in the autoclave.

The air in the autoclave is slowly heated to the cure temperature of the adhesive. Heating rate is monitored and controlled to within a given range. Increasing the temperature too slowly can cause partial cure of the adhesive at lower temperature



Fig. 18. Autoclaves and bond tools. Reproduced by permission of the Boeing Company.

than intended and a corresponding increase in the melt viscosity. This can produce poor fillet formation on honeycomb core and poor wetting of substrate surfaces.

The thermal mass of parts and tools and the heating capacity of the autoclave naturally limit the maximum heating rate. Attempting to increase the heat-up rate by overheating the autoclave air can result in overheating of areas of the assembly with low thermal mass.

During the temperature ramp period, pressure is applied. How much pressure is applied depends on the adhesive and the type of assembly. Honeycomb assemblies are limited by the compression strength of the honeycomb core, so cure pressure is typically limited to ~ 50 psi for aluminum core of standard density. Metal to metal assemblies can withstand higher pressures and usually have fewer bondline voids when cured at higher pressures. Metal-to-metal assemblies bonded with standard modified epoxies are cured at ~ 90 psi.

Upon completion of adhesive cure, the assembly is removed from the tool. In some cases this first assembly is but a sub-assembly of the final bonded component. One of the most common uses of a first-stage cure is to bond together a honeycomb core blanket from various densities of core. Another use of multi-stage curing, though less common with modern wedge designs, is to bond the honeycomb core, spar and one facesheet of a trailing edge wedge together. The contour of the remaining core surface is then machined and the remaining facesheet bonded in the second cure cycle. Care must be taken with secondary bond cycles to avoid weakening the first-stage adhesive. Although the first-stage adhesive has been crosslinked, it is weak at the elevated cure temperature. If the

first-stage bond is stressed during the second-stage cure cycle, for instance from a second-stage bond tool that does not perfectly fit the part, the bond can fully or partially fracture. Partial bond fractures may not be detectable by post-bond inspection and can fail in service.

Inspection. After the final adhesive cure cycle, the bonded assembly is removed from the tool and inspected. The first and most cursory inspection is a simple visual check. Major problems such as crushed core and significantly mislocated details can be seen with the unaided eye. A lack of continuous adhesive squeeze-out ('flash' or 'spew') around the periphery of details can be indicative of insufficient adhesive and subsequent voids.

Instrumented non-destructive testing (NDT) is sometimes performed, usually to inspect for bondline voids and occasionally to inspect for damaged or mislocated details. In addition to obvious visual indicators, the need to perform instrumented NDT in general is based on complexity, criticality and past history. A particularly critical and complex part may require NDT of every assembly to give sufficient confidence in part quality, while a simple part with no history of production rejections may only require NDT of every 50th assembly. Sampling plans such as this can be employed because NDT is not the sole basis for insuring bonded part quality. First part qualification (discussed below) is initially used to verify that the processes and tools used to fabricate the assembly produce a good part. Constant monitoring of detail part fabrication processes and bond processes and process parameters are the primary means of ensuring quality.

The most common NDT methods used for bonded metal assemblies are based either on transmitting ultrasonic energy through the part and measuring changes in the signal (through-transmission, pulse echo or reflector plate) or exciting the panel directly using an ultrasonic transducer and measuring the response (resonance impedance). Through-transmission ultrasonic (TTU) inspection uses either a water jet as a carrier medium between both the transmitter and receiver and the part, or immerses all three in a water bath. TTU inspection is particularly well suited to automated scanning ('C-scan') and interpretation of the results via computer and so is commonly used for high-volume production inspection. TTU C-scan inspection can produce graphical maps of the part (Fig. 19) with disbonds or questionable areas determined by increased attenuation of the signal. TTU cannot distinguish which of many different layers of a bonded assembly contains a disbond, so more detailed characterization of a defect is left to other NDT methods.

The pulse-echo and resonance impedance techniques are capable of determining which layer contains a disbond, given an appropriate standard to compare against. Inspection standards are bond assemblies made to simulate specific areas of a part with disbonds purposefully placed in them. By comparing the signal response of a suspected void to that of a known disbond in the standard, the

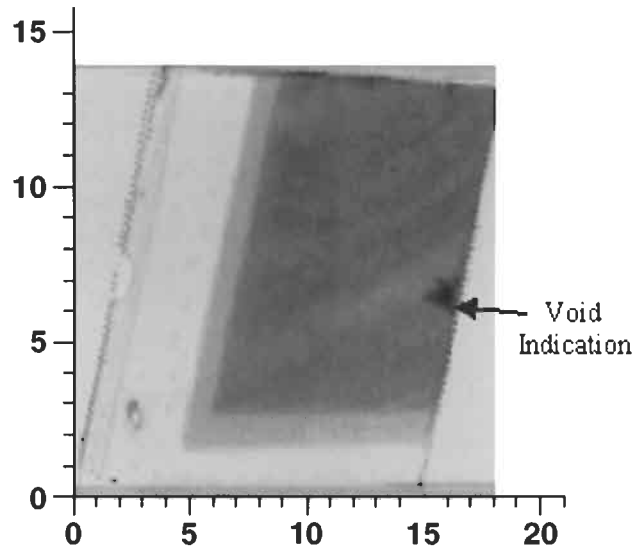


Fig. 19. TTU of Sandwich Assembly. Reproduced by Permission of The Boeing Company.

location of the void can be more accurately determined. Resonance impedance is better suited to small parts or localized inspection of larger parts since it requires physical contact between the transducer and the assembly. Although pulse echo can be performed with an immersion-coupled transducer, it also is typically used in contact mode.

X-ray radiography can be used to detect mislocated and damaged details such as blown or crushed core (Fig. 20). It is not useful in detecting voids since the change in X-ray opacity through a void is negligible.

All of the inspection methods above are incapable of detecting what is called a 'kissing bond'. A kissing bond is a no- or low-strength bond in which the adherends are in intimate contact. Acoustic energy is transmitted across the low-strength interface with little attenuation, resulting in the flaw being invisible to standard NDT techniques. Causes of kissing bonds can include such things as local areas of bond surface contamination or small pieces of release film or adhesive backing paper being left in the bondline. These flaws may be undetectable immediately after manufacture but can become evident in service as flight or environmental loads stress the bond and cause the defect to grow.

There are numerous other inspection techniques that have been developed in the last couple of decades such as holographic interferometry, acoustical holography, acoustic emission, thermal emission scanning, etc. They all have been developed to address shortcomings of more popular inspection techniques but for the most part remain niche techniques.

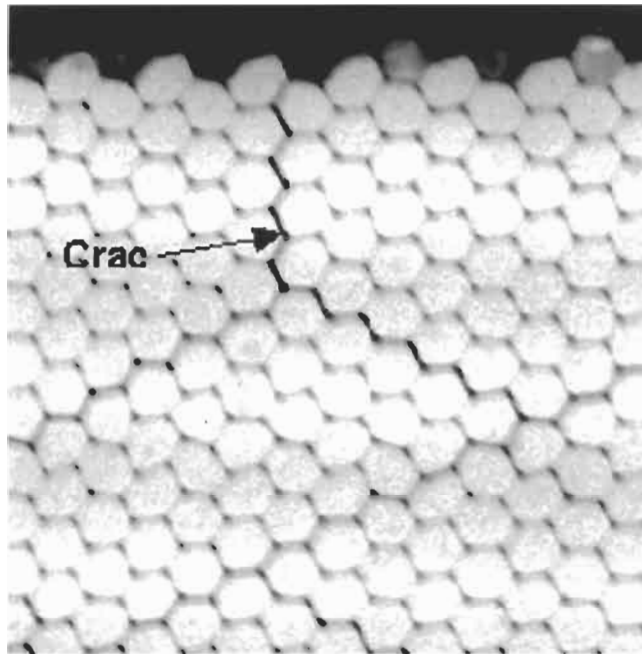


Fig. 20. X-ray image of potted honeycomb core. Reproduced by permission of the Boeing Company.

First part qualification. First part qualification is a process performed the first time a new bonded assembly is manufactured or the first time a new tool is used to manufacture a bonded assembly. First part qualification provides assurance that all of the aspects that control bond assembly quality, such as the design dimensions, detail part manufacturing techniques, tool dimensions, layup procedures and autoclave cure cycle parameters are correct and will produce a bond assembly that meets the engineering requirements.

The specific steps that make up a first part qualification depend on details of the bond assembly such as complexity and history of the part and complexity of the tooling. First part qualification of a simple flat sheet metal assembly is likely to be not much different than standard production, while qualification of a new and complex part is a lengthy and detailed process that often results in significant changes to details and tools.

For a typical assembly, first part qualification begins with a rigorous dimensional check and painstaking proof of all details on the bond tool. The assembly details are placed on the tool without adhesive, close contact between bond surfaces is verified and any detail or tool interference is corrected prior to proceeding. This is followed by fabrication of a 'verification film', or a simulated bond cure cycle of the assembly to allow measurement of the adhesive bondline thickness.

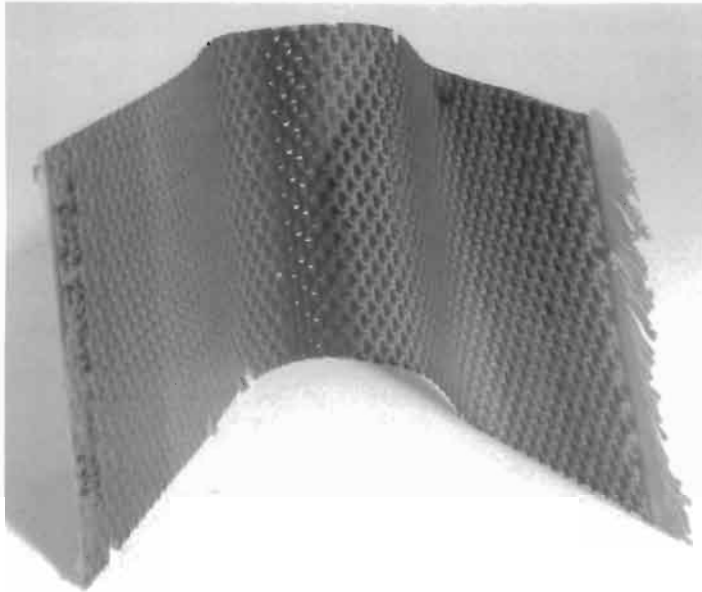


Fig. 21. Adhesive verification film. Reproduced by permission of the Boeing Company.

The assembly details are placed in the tool with adhesive, but the adhesive is sandwiched between release film so that it does not adhere to the details during the cure cycle. After cure the adhesive can be removed and the bondline thickness measured without destructively inspecting an assembly. Fig. 21 shows the verification film from a tightly curved fin leading edge honeycomb sandwich assembly (Fig. 32). The honeycomb core imprint in the adhesive is clearly visible. The darker area at the center of the photograph indicates thicker adhesive caused by poor contact between the honeycomb core and the facesheet. Areas such as this that are too thick or thin must be addressed because adhesive bond shear strength can be affected by the thickness of the adhesive layer. Poor contact between honeycomb core and facesheets can produce small or non-existent adhesive fillets on the core, resulting in low bond strength. Thin adhesive layers (less than approximately 0.002" for common aerospace adhesives) between solid adherends can rupture prematurely because of an inability to withstand the displacement of the adherends at the joint edge. Likewise adhesive joints of certain dimensions are weaker with thick bondlines (greater than approximately 0.020").

Verification film has drawbacks that render it useless for some assemblies. For bonded assemblies with complicated tooling and/or multiple layers of adhesive, the additional thickness of the release film plies can cause the verification film to be non-representative of an actual bonded assembly. Details can be moved out of their normal positions just enough to prevent them from fitting correctly or tooling from performing correctly, resulting in false indications of problems

or lack of problems. In these cases destructive inspection of the assembly must be performed. Verification film is also less useful for honeycomb sandwich assemblies. The release film prevents the honeycomb core from penetrating the adhesive the way it does in a real assembly, again potentially causing false indications. Sharp honeycomb core edges can pierce the release film and allow adhesive to partially bond the details together, ruining the details and preventing interpretation of the verification film.

After a satisfactory verification film is produced, an assembly may be fabricated specifically for destructive inspection to validate that the verification film was accurate. This correlation allows the use of verification film rather than more expensive destructive inspection for future changes such as duplicate tool fabrication and tool or detail modification. Simple assemblies are usually not destructively inspected because of high confidence that the verification film is entirely representative of the expected bondlines. Complex or large parts may not be destructively inspected because of the cost of the details and assembly time. In these cases other means of validating the verification film are used. Meticulous pre-bond detail and post-bond assembly thickness measurements may be sufficient to prove bondline thickness control. Ultrasonic inspection and X-ray photography (discussed previously) may be sufficient to prove that details are in the correct places and bonds are good.

If an assembly is destructively inspected, the verification film is used to identify potential problem areas for particular attention. These areas and others randomly selected are cross-sectioned to determine bondline thickness (Fig. 22), bond details are peeled apart to inspect for voids and honeycomb core bonds are

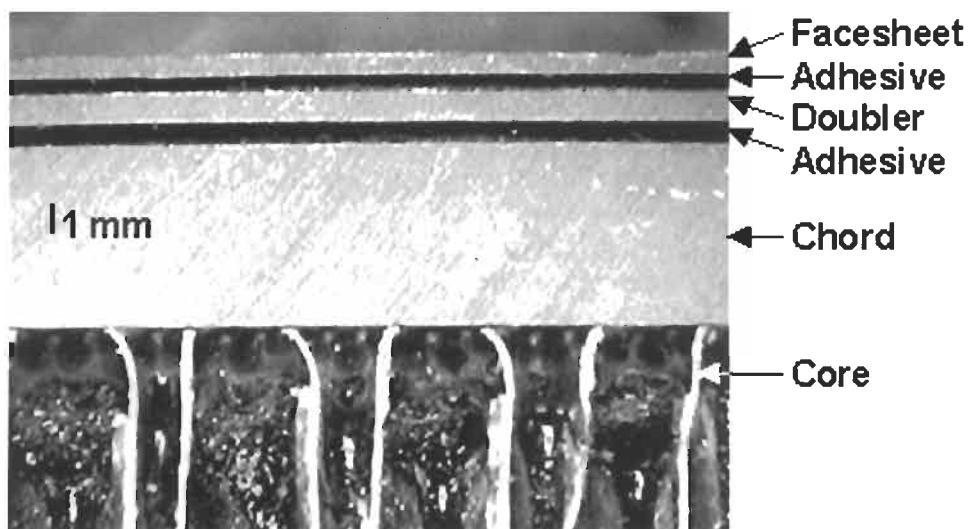


Fig. 22. Bonded assembly cross-section. Reproduced by permission of the Boeing Company.

examined for good adhesive filleting. Once correlation between the destructive test article and the verification film has been established, the verification film can be used for periodic process validation and qualifying tool modifications and repairs, new tools, etc.

In-service issues. As mentioned previously, many early service failures of bonded structure were due to adherend surface treatments that were unstable in long-term exposure to water. A majority of these problems were resolved by the adoption of surface treatments such as chromic and phosphoric acid anodize for aluminum details. The remaining few were alleviated by the adoption of phosphoric acid anodized honeycomb core and foaming adhesives resistant to water passage. Other service durability issues such as the cracking of brittle potting compound used to seal honeycomb sandwich assemblies, and subsequent delamination, have been minor in scope.

Environmental factors such as severe hailstorms and human errors such as impact by aircraft service equipment also cause in-service damage to bonded assemblies. Bonded honeycomb sandwich assemblies are particularly prone to such damage because of their customary use as lightly loaded fairings and flight control surfaces and subsequent thin facesheets and relative fragility.

Repair. Repairs for damaged bonded structure can be either mechanical or adhesively bonded. Mechanical repairs are metallic doublers on one or both sides of a damaged component, held on by fasteners. The fasteners transfer the load through the doubler around the damaged site and restore part functionality. Although common for metal-to-metal bonded structure, mechanical repair of sandwich structure is rare because of the risk of further delamination. Unless the doubler and fasteners are perfectly sealed, water can travel into the honeycomb core eventually causing freeze–thaw damage and delamination.

Bonded repair sizes, shapes and configurations vary greatly depending on the type of structure and size and location of damage. Typically the damaged area is removed and replacement details of like material and size are prepared to fit. Larger doublers and possibly triplers are installed over the replacement details to hold them in place and transfer load to them. Fig. 23 shows a typical bonded repair for a small damaged area on honeycomb bonded structure.

Occasionally a repair is needed that will maintain an aerodynamically smooth surface on exterior surfaces of sandwich structure. In this case an internal doubler is used to hold the filler detail (called a ‘dime-dollar’ repair for obvious reasons; Fig. 24). Damaged trailing edges can be the most difficult to repair because of the difficult geometry (Fig. 25). Repairs of larger areas follow the same general concepts but must be engineered individually to account for specific part shape and load requirements.

The processes used to prepare and bond repair patches are more difficult

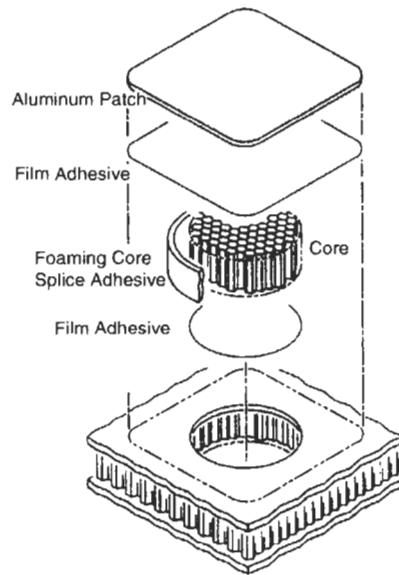


Fig. 23. Typical one-side honeycomb assembly repair. Reproduced by permission of the Boeing Company.

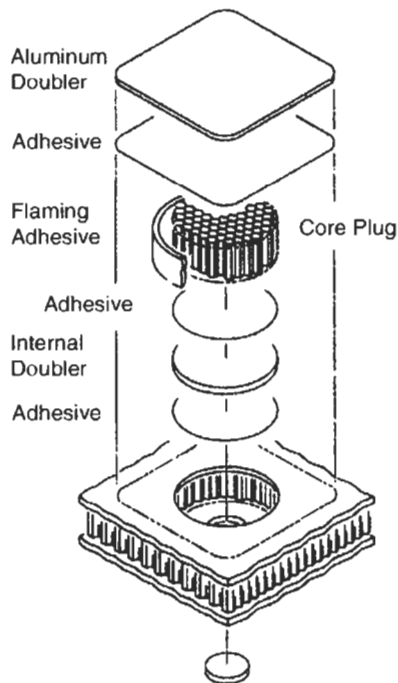


Fig. 24. Typical flush repair. Reproduced by permission of the Boeing Company.

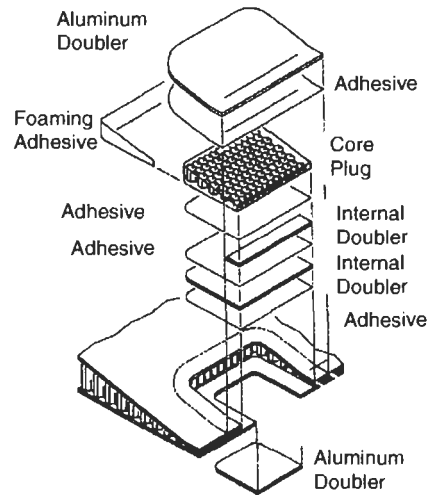


Fig. 25. Typical trailing edge repair. Reproduced by permission of the Boeing Company.

and time-consuming than those used to fabricate the assembly initially. Surface preparation in particular is a challenge. Although it is easy enough to clean, anodize and prime the repair details, correctly treating the areas of the damaged assembly to which they will be bonded is not simple. Solvent cleaning and sanding can replace the alkaline cleaners and acid etches used in anodize tank lines, but the anodize itself is critical. There are methods of anodizing a small area using either gelled acid or a bag sealed against the surface. Acid solution is pumped through the bag, which also contains the cathode to which the power supply is attached for the anodization. The gelled acid also has an anode embedded in it. These methods work, but are time consuming and not very robust. Far more common is the use of chemical conversion coating, even though it is known to produce a bond that is less durable and lower in peel strength. In this method the surface is solvent cleaned, sanded and the solution swabbed on the surface for a number of minutes. After rinsing and drying, it is ready for priming. All of these procedures carry the risk of contaminating honeycomb core when performed on sandwich assemblies. Repair surface preparation processes based on mixed organic-inorganic sol-gel technologies are becoming available but still have the requirement for a clean, oxide-free surface prior to application.

Application of adhesive primer presents another challenge. Most adhesive primers require a high-temperature cure, which presents the potential for damaging existing bondlines. Infrared curing can be used to reduce the likelihood of problems.

Most bonded repairs are cured using electric heat blankets and vacuum bags, shot bags or clamps for applying pressure. Programmable heat blanket controllers

that monitor thermocouples in the part and control power to the blanket to maintain proper temperature ramp rates and dwell times are available commercially. Autoclaves are rarely used because of the difficulty in properly supporting the rest of the structure during cure so as not cause damage to existing cured adhesive.

Operators select methods of repair for damaged bonded structure depending on the cause of the damage, size of the damage, type of bonded assembly and even the length of time until the next major overhaul of the aircraft.

Local repair of delamination originally caused by non-durable surface treatment is only temporarily successful at best. The surface treatment on the unrepaired portion of the assembly remains susceptible to attack and the area of delamination will likely continue to grow once the assembly is put back into service and exposed to moist conditions. Replacement or complete remanufacture of the component is the only way to permanently address this type of damage. However, time-limited repairs using bonded or mechanical methods can be used to extend the life of the component until a major overhaul is scheduled. In some cases such as widespread disbond of fuselage doublers, mechanical repairs (rivets and fastened doublers) and continued inspection are used to extend the life of the skin indefinitely because of the high cost of replacement.

Local repair of bonded structure damage from mechanical sources (bird-strike, equipment impact, etc.) can either be bonded or mechanically fastened patches. In general it is more likely that sandwich structure is repaired using bonded patches because of the limited compression capability of sandwich structure and the risk of introducing water into the honeycomb from penetrating fasteners.

5.3.1.3. Case studies.

Metal-to-metal bonded doublers. This category of bonded assembly is typified by a fuselage skin with localized reinforcement around cutouts for windows, doors, access hatches, etc., or other localized increases in load. Bonded doublers increase the cross-sectional area of the skin to compensate for increased load or loss of load carrying capability from a cutout without the parasitic weight of an overall thicker skin or the need for gauge reduction of a thicker skin by extensive machining or chemical milling. In addition to the simple cost of the operation, machining or chemical milling of aluminum skins reduces the inherent corrosion resistance of the skin by removing the surface cladding, a layer of lower strength but substantially more corrosion resistant aluminum alloy usually added to wrought aluminum products. A bonded doubler allows retention of clad surfaces in both the full and reduced thickness areas of the skin assembly. Lastly, skins with bonded doublers are inherently more resistant to fatigue cracking than an equivalent monolithic skin. The compliant adhesive layer tends to blunt the stress concentration at a growing crack tip, reducing the speed of crack growth and resisting crack initiation in adjacent layers. For example, Fig. 26 shows a flat pattern view of a section of bonded fuselage skin with local doublers around cutouts.

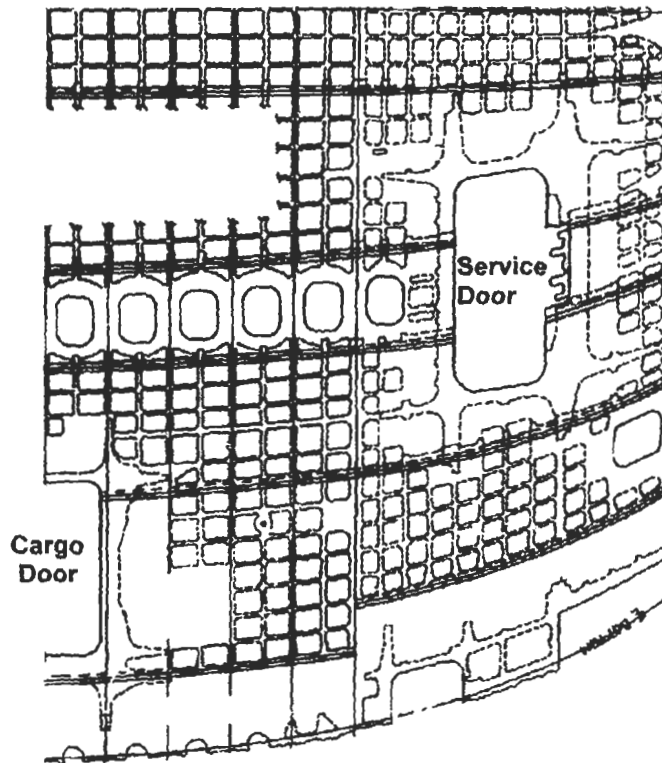


Fig. 26. Bonded fuselage doubler pattern. Reproduced by permission of the Boeing Company.

Note also the regular grid pattern of doublers that follow stringer and frame locations. These doublers are referred to as fail-safe doublers, or tear straps. Fail-safe doublers are meant to control the growth of potential cracks from pressurization loads and allow the fuselage to decompress in a controlled and relatively safe way in the event of a serious event. The tear straps affect the stress field at the tip of a growing crack in the skin and cause it to turn as it approaches the doubler. Full-scale fatigue testing confirmed that the ends of the crack would turn and form a skin flap, which allowing controlled decompression. This flapping prevents externally induced damage or a fatigue crack from growing to a size sufficient to cause catastrophic failure of an airframe.

Skins with bonded doublers have been used successfully on a large number of civil aircraft and are still used on new designs. The only widespread in-service problem with bonded doubler assemblies has been delamination caused by unstable surface preparation. Early fuselage skins with bonded doublers and inadequate surface preparation experienced severe delamination and subsequent corrosion. A majority of these delaminated doublers were the fail-safe tear straps (Fig. 27). Although the tear strap bond does not carry structural load, the bond



Fig. 27. Bonded fuselage skin corrosion. Reproduced by permission of the Boeing Company.

is necessary to maintain overall damage tolerance of the structure. Significant in-service repairs were necessary, up to and including replacement of entire body skin sections on many aircraft.

Stiffened panel designs. Stiffened panels are exterior fairing panels that are attached on three or four sides. They carry little to no structural loads; they are designed primarily to take air loads. Early designs using simple riveted concepts were heavy and prone to rapid sonic fatigue.

The first type of bonded design for this application was the beaded doubler panel (Fig. 28). This design was fairly successful at addressing the problems with simple riveted structure but had two primary drawbacks. The area under the 'beads' remained a single thickness sheet and was still prone to fatigue. Reducing the unbonded areas under the beads was not a solution because it reduced the overall stiffness of the panel. Secondly, tooling for these panels was complex and not very robust. Autoclave pressure applied to the beaded areas of the doubler would cause them to collapse, so thick frames were fabricated with cutouts for the beads to protect them. A rubber layer bonded to the surface of the frames

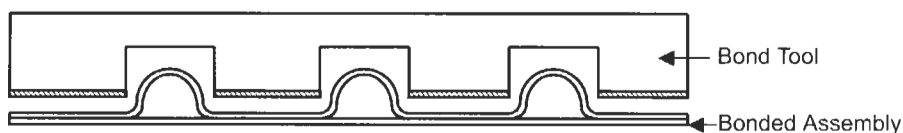


Fig. 28. Beaded doubler assembly and tool.

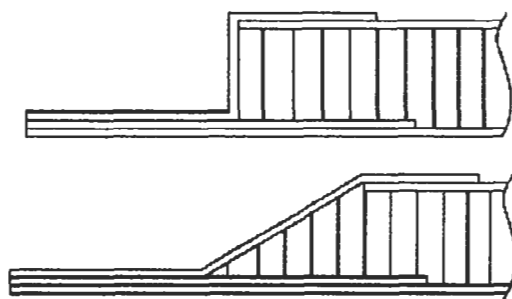


Fig. 29. Early enclosed sandwich designs.

that contacted the doubler tended to degrade after only a few autoclave cycles and reapplication was time consuming. Fit between the bead cutouts and the bead was critical. If the gap was too small the rubber would ride up on the bead, partially collapsing it. Too great a gap and insufficient pressure would produce voids in the bondline at the bead edge.

Stiffened panels soon migrated to the use of honeycomb sandwich. Two early sandwich designs were the enclosed square-edge and tapered-edge honeycomb sandwich designs (Fig. 29). Honeycomb core was bonded between two aluminum facesheets. The honeycomb core supported the skins almost continuously, preventing sonic fatigue and enabling the use of very thin facesheets. In the square-edge design the inner facesheet followed the contour of the rectangular core detail, making a box that enclosed the core. The core in the tapered sandwich panel tapered at the edges to allow the facesheets to come together gradually at the edgeband. Fabrication of the enclosed square-edge design was difficult because of the many details required to make the box and the difficulty in achieving a leak-free part. The tapered-edge design was more foolproof in that regard, but achieving good fit between the core detail and the inner facesheet was still challenging. The 'crushed core' method achieved good fit by stamping a rectangular core detail along with the pre-formed inner facesheet between matched metal dies. The core crushed along the edges to the same contour as the inner facesheet, guaranteeing good fit for the adhesive bonding cycle (Fig. 30).

As core and facesheet surface preparation became more environmentally durable, the need to fully enclose the core waned. The open square-edge de-



Fig. 30. Crushed core sandwich design.

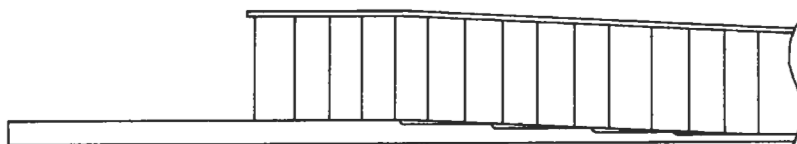


Fig. 31. Square-edge sandwich design. Reproduced by permission of the Boeing Company.

sign took advantage of this by not extending the inner facesheet into the edgeband (Fig. 31). This greatly simplifies the detail fabrication and bonding processes by removing the need to form either the honeycomb core or inner facesheet. The core and facesheet are usually flexible enough to form under autoclave pressure to the slight contours of the inner surface of the outer skin. Protection from moisture ingress is achieved by coating the outer few cells of honeycomb core with 'pour-coat' adhesive. Pour-coat adhesive is essentially a liquid version of the film adhesive. It fully coats the core cell walls, improving resistance to water and increasing bond strength between the film adhesive and core. Fig. 32 shows a cross-section of a 757 stabilizer leading edge utilizing square-edge construction.

Square-edge stiffened panels are used extensively on current production aircraft such as the 737, 757 and 767, primarily in the aft fuselage (unpressurized section),

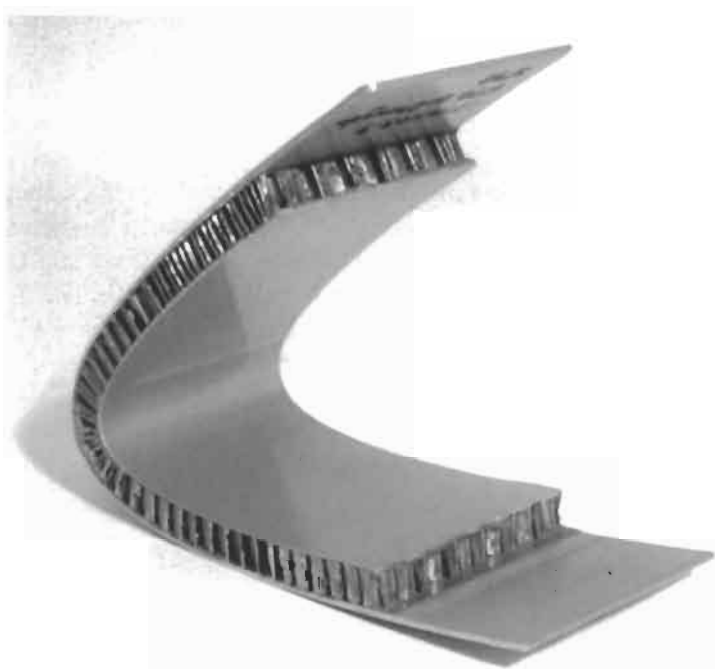


Fig. 32. Empennage leading edge square-edge panel. Reproduced by permission of the Boeing Company.

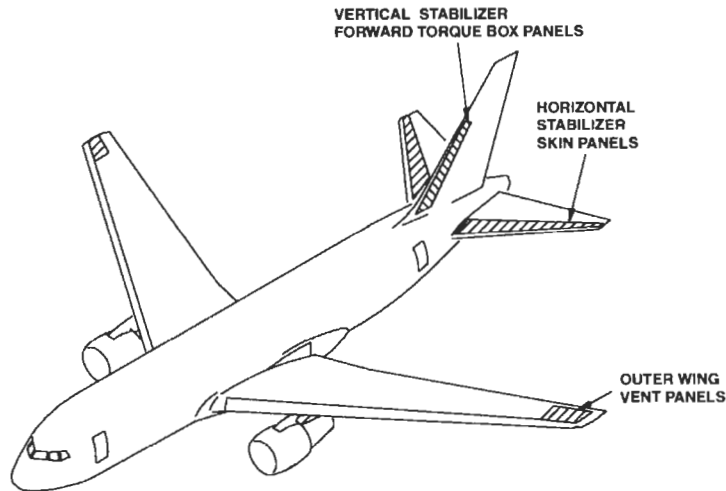


Fig. 33. Typical square-edge panel locations. Reproduced by permission of the Boeing Company.

empennage leading edge (Fig. 32), empennage auxiliary torque boxes (Fig. 33) and outboard wing.

Trailing edge wedge. Trailing edge wedges are the aft-most portions of flight control surfaces such as leading edge slats, flaps, ailerons, spoilers, etc. (Fig. 34). Wedges taper to a point either to fair in against underlying structure as with leading edge slats or because the wedge is the aft edge of the wing (Fig. 35). As with stiffened panels, design of trailing edge wedges has changed significantly through the years because of manufacturing improvements and service performance issues.

Early trailing edge design was comprised of a C-shaped spar bonded to upper and lower facesheets with honeycomb core between (Fig. 36). The spar was either a simple extrusion of constant dimension, or built-up from two L-shaped legs if it needed to taper from one end to the other. Facesheets were simple constant-thickness sheet material.

The primary disadvantages of this design were associated with contouring of the honeycomb core. This type of assembly was usually manufactured by bonding the spar and rectangular honeycomb core block to the lower skin. The upper surface contour was machined into the honeycomb core using the spar and lower skin to provide stability while machining. The upper facesheet was then bonded on in a second autoclave cycle. Besides the cost of the second bonding operation, this process entailed a number of added costs. In order to achieve a good bond, the core had to be machined very close to the surface of the spar (say, within 0.005"). Invariably the honeycomb core cutter contacted the spar slightly, removing the surface preparation and primer from the spar surface. The finish on these areas had to be manually repaired using aggressive chemicals, risking further damage and

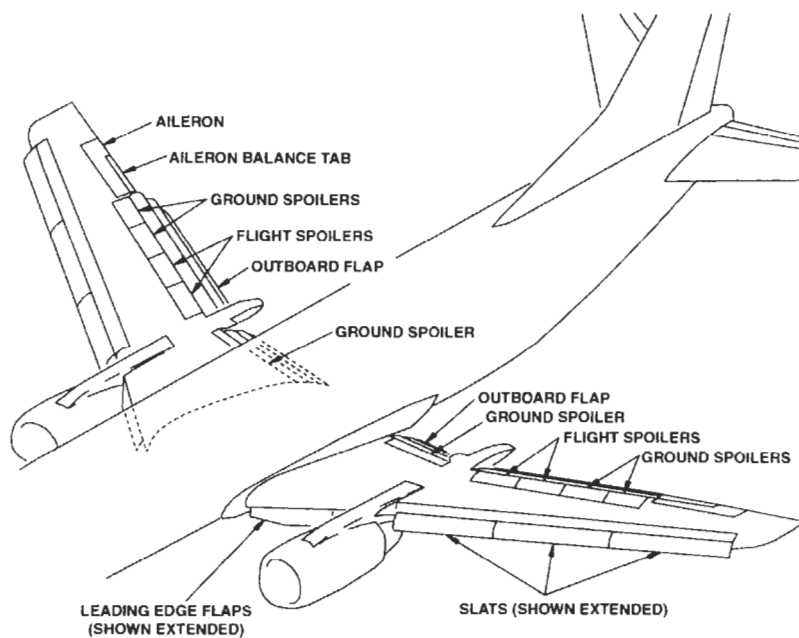


Fig. 34. Flight control surfaces with trailing edge wedges. Reproduced by permission of the Boeing Company.

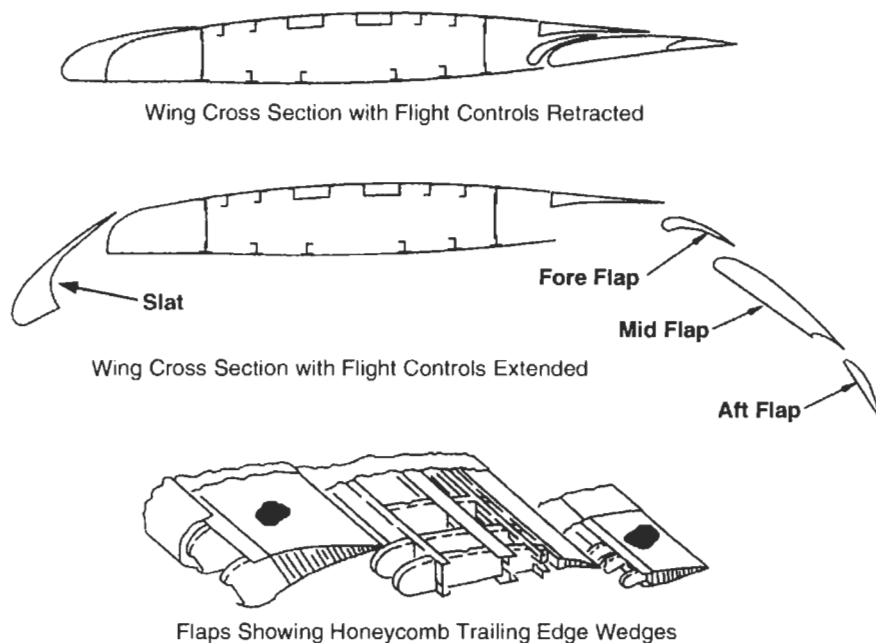


Fig. 35. Trailing edge wedges. Reproduced by permission of the Boeing Company.

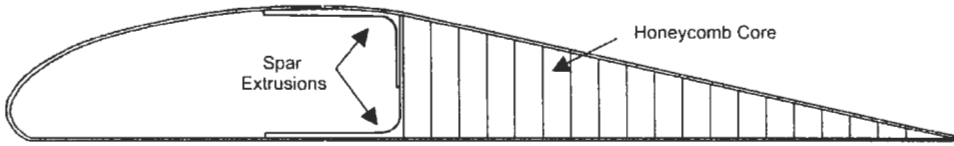


Fig. 36. Early trailing edge wedge design. Reproduced by permission of the Boeing Company.

contamination of the honeycomb core immediately adjacent. The touch-up surface preparation method was also less durable than the original anodize, contributing to the risk of in-service delamination.

An alternate method involved pre-machining the core detail to contour while it was stabilized in a frozen block of water or other medium. This entailed the expense and time to freeze the block and keep it frozen during machining as well as the risk of contaminating the core bond surfaces. In addition it was difficult to maintain the dimensional tolerances necessary to match the spar dimensions to the core adequately. Both spar and core details had machining tolerances and significant hand sanding of the core was often required to match the details.

Occasional in-service delaminations occurred at the aft tip of the wedge. Because there was no metal-to-metal closeout bond at the aft tip, any slight incidental damage could easily crack the bond slightly and allow moisture to enter the core. Eventually, freeze-thaw damage and delamination would occur.

The next design iteration of trailing edge wedges was an interesting sparless concept adopted in the early 1980s (Fig. 37). This design was used on the leading edge slats of the 757, 767 and 737-300/400/500 family of aircraft. The sparless

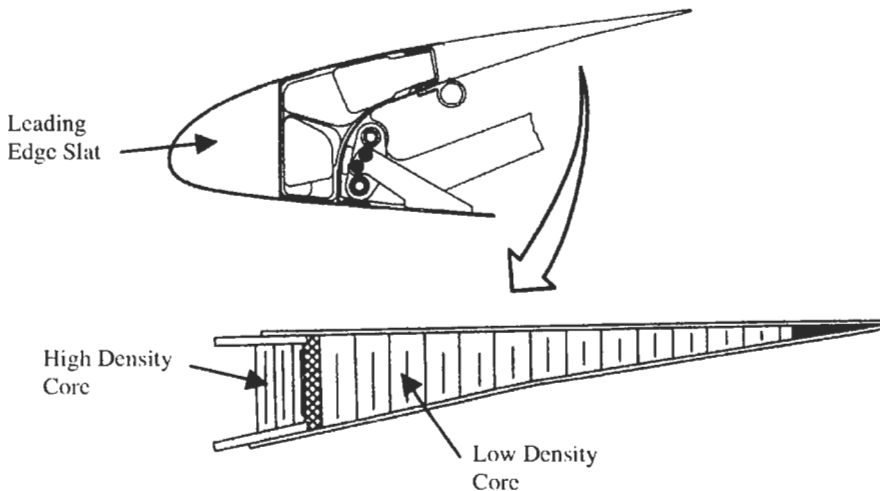


Fig. 37. Sparless trailing edge wedge design. Reproduced by permission of the Boeing Company.

design took advantage of improvements in speed and accuracy of aluminum honeycomb machining to create an elegant, highly weight-efficient assembly.

The design was referred to as sparless because there was no true spar in the traditional sense. The spar was built-up from a section of high-density core and two lightly machined wrought aluminum chords. The advantages in manufacturing were significant. The aft low-density core section was machined to net shape prior to expansion. The pre-machined high and low density core sections were spliced together with foaming adhesive, which did not require an autoclave and could be performed under a vacuum bag in an oven. The high-density core acted to stabilize the subassembly for machining of doubler and chord pockets. During the only bond cure cycle the core subassembly acted partially as a tool, locating the chords in both position and orientation. There was no need for multiple autoclave cycles and substantial hand work with this design as there was with the preceding design.

Note also that the aft tip of the wedge was filled with a fiberglass/epoxy wedge. This strengthened the tip and makes it more resistant to delamination.

Unfortunately and in spite of the improvements, this design had manufacturing and in-service problems. The bond assembly tooling was somewhat complex in order to keep the details in location, prevent autoclave pressure from reacting on the forward portions of the spar chords and yet allow autoclave pressure to reach the remainder of the assembly. In practice the tooling occasionally interfered with movement of the chords and skins, resulting in mis-oriented chords and voids between the chord and skin. In addition, potting compound placed in the ends of the wedges to seal off the honeycomb had a tendency to erode and crack, allowing the entry of moisture and subsequent delamination. The wedge was not designed to be removable and was a significant structural member of the slat. Replacement of delaminated wedges in service was difficult and time-consuming, requiring a special tool to hold the remainder of the slat in proper shape while the new wedge was installed.

The most recent trailing edge design is shown in Fig. 38. This design relies on highly accurate extrusion and honeycomb machining to produce spar and core details that fit together without multiple cure stages, hand work, or complex tooling. This assembly illustrates the movement in recent years towards designs that are more cost efficient and robust, both in manufacturing and in service.



Fig. 38. Improved trailing edge wedge design. Reproduced by permission of the Boeing Company.

5.3.2. Composite adhesive bonding

Even though the substrates are quite dissimilar, adhesive bonding of composite material is comparable to that of aluminum. Only aspects unique to composites will be discussed here. There are many details of composite part design, manufacture and performance that are not necessarily related to adhesive bonding that also will not be discussed.

5.3.2.1. Design. Many design considerations for adhesive bonding of composite structure are similar to that of aluminum bonding, with the added flexibility of being able to adhesively bond during various stages of the manufacturing process. Depending on tooling requirements, part sizes and manufacturing flow, the adhesive bond can be cured at the same time that the adherends are cured (cocuring), during the curing of one adherend being bonded to another already-cured adherend (cobonding) or as a final operation between two already-cured adherends (secondary bonding). With this flexibility comes the ability to utilize the most efficient manufacturing sequence by balancing the number of cure cycles against tooling and layup process complexity.

There are, of course, many more aspects of composite hardware design that differ from metallic bonded structure but do not necessarily involve adhesive bonding. For instance there are many types of reinforcement tape and fabric to choose from, the orientation of the plies must be chosen, the ply stackups must be balanced to avoid part warping after cure, a minimum number of plies must be used to prevent non-visible impact damage that significantly affects the load carrying capability of the part, etc.

5.3.2.2. Manufacture. Surface treatment of composite details is obviously quite different from that of aluminum. Uncured composite materials require no surface treatment. The resins and adhesives are formulated to be compatible and intermix to some extent during cure, forming a very strong interface. Precured composite details surfaces which are to be secondarily bonded require some sort of surface treatment to reactivate the surface and remove contamination, such as mold release agents, that may have been picked up during initial cure. There are two primary methods of surface preparation, surface abrasion and peel ply. Surface abrasion, by machine or by hand, removes the outermost layer of matrix resin, exposing fresh active material and removing contamination. The drawbacks of this method are the extensive hand labor required and the non-uniformity. Adequacy of the surface treatment depends on the operator removing enough material to effectively clean the surface while not removing so much that fibers in the composite are damaged.

Peel ply is a sacrificial layer of dry or resin-impregnated fabric that is placed on the bond surface during initial part fabrication. The peel ply is cured along

with the initial subassembly and then peeled off of the bond surface immediately before the secondary bond operation. This exposes a clean, active surface for the adhesive to bond to. Resins in impregnated peel plies are preferably the same as the base matrix resin so as to avoid concerns of resin compatibility. Peel ply fabric, typically a lightweight glass or polymer fiber weave, is sometimes treated to weaken the bond between the fibers and matrix resin, easing removal. However, this practice carries the risk of leaving behind a contaminant or weak resin layer that will interfere with adhesion or interfacial bond strength of the secondary bond.

5.3.2.3. In-service performance. Service performance of bonded composite hardware has been good, at least from the standpoint of adhesive bonding. Like all aerospace hardware there have been occasional in-service problems with materials, design and manufacture of composite parts, but few have been related to adhesive bonding.

Repair. Repair of damaged bonded composite structure is in many respects similar to that of metal bond structure and in some respects simpler. Surface treatment of the structure being repaired is significantly easier; sanding is sufficient to ensure a durable bond. The damaged area is removed and the surrounding composite material tapered, or scarfed, to accept the repair plies. A ply of adhesive is placed on honeycomb core in the repair area and as required on the composite surfaces as well. A generic repair of a composite honeycomb sandwich panel is shown in Fig. 39. Bagging practices, bond pressure application and heat sources for composite repair are the same as metal bond repair. As with metal bond, care must be taken to support surrounding structure to prevent deformation and delamination during exposure to high cure temperatures. Care must also be taken to ensure that all contamination is removed from the honeycomb core prior to cure. Non-metallic cores, particularly aramid-based core, will readily absorb water and other fluids if exposed by a damaged facesheet. Heat applied to cure a repair can

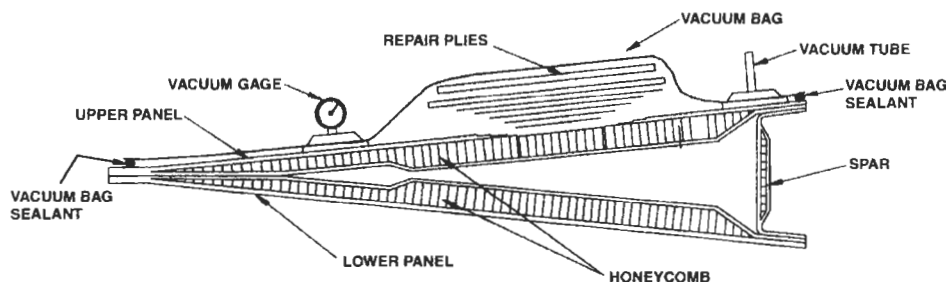


Fig. 39. Typical composite assembly repair. Reproduced by permission of the Boeing Company.

cause liquid and absorbed water in the surrounding area to vaporize, resulting in porosity in the composite and adhesive plies at best and catastrophic delamination of the whole area at worst.

5.3.2.4. Secondary composite structure. Secondary structure composite hardware generally falls into the same three categories as metal-bond parts: laminate with local reinforcement, stiffened panels, and trailing edge wedges. However, the laminate with local reinforcement group is inherently different than with metal substrates because local reinforcement is usually achieved by adding plies of composite material and does not rely on adhesive bonding. One exception to this is structure such as skin/stringer monocoque where the stringers are bonded to the skins with adhesive in a cobond or secondary bond cycle.

Composite trailing edge wedges and stiffened panels are quite similar to their metal-bond counterparts and are used in many of the same applications (Fig. 40). Composite stiffened panels have an advantage over metallic bonded panels in that multiple core bays can easily be incorporated in one assembly (Fig. 41).

The capability of bonded composites, particularly advanced composites such as carbon fiber, to achieve even greater weight savings than bonded metallic design has meant that composites are used for components that were metallic bonded designs on earlier aircraft or derivatives. For example, flaps on the 757, 767 and 777 are bonded carbon fiber–epoxy assemblies. On the 737, an earlier aircraft, they are of aluminum with significant use of bonded structure. It is interesting to note that though the 737 has gone through two major design updates (in the early 1980s and mid-1990s), the flaps remain aluminum (built-up and adhesively

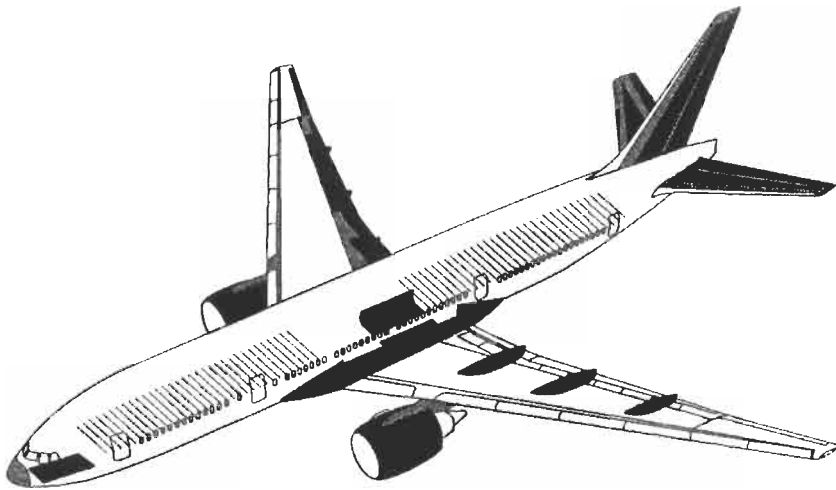


Fig. 40. Composite structure locations on Boeing 777. Reproduced by permission of the Boeing Company.

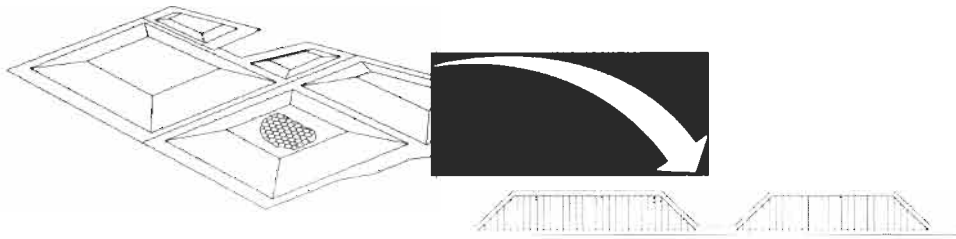


Fig. 41. Typical composite sandwich. Reproduced by permission of the Boeing Company.

bonded). This is primarily because of the different target markets for these aircraft and the perceived durability and ease of repair of aluminum structure (even including bonded structure) compared to composite structure.

5.3.2.5. Primary composite structure. Bonded composite structure has been put to use in primary load-bearing applications as well. Commercial designs that incorporate composite bonded primary structure such as the Beech Starship (composite fuselage and wing), Boeing 777 (composite horizontal tail) and Airbus A340 (composite horizontal tail) have been flying for years. Both the A340 and 777 tail structures are of composite laminate skins with bonded composite stringer design. The Starship has a unique composite sandwich design, with the major components secondarily bonded together with paste adhesives (Fig. 42). While there are few other examples of primary bonded composite structure in large commercial transports, small commercial aircraft have seen much experimentation with bonded composites as primary structure.

6. Non-structural applications on commercial aircraft

Adhesives are not used just for structural applications on modern aircraft. In fact, the number of non-structural applications of adhesives vastly outnumbers the structural applications. Adhesives are used for everything from assembling lavatory walls to attaching the 'No Smoking' sign to cabin partitions. Just a sampling of adhesive types and applications are discussed below.

Pressure-sensitive adhesives (PSAs) based on acrylic, natural rubber and silicone are employed primarily for ease of application. To name just a few applications, PSAs bond decals to surfaces, interior decorative surfaces to interior panels, interior trim pieces in place directly or hook and loop tape for the same purpose, structural shims in place during manufacturing and acoustic (sound deadening) materials to body skin interior surfaces. Tape products with pressure-sensitive adhesive on one or both surfaces are used for such functions as cargo compartment sealing, as a fluid barrier to prevent spills and leaks in the lavatories and

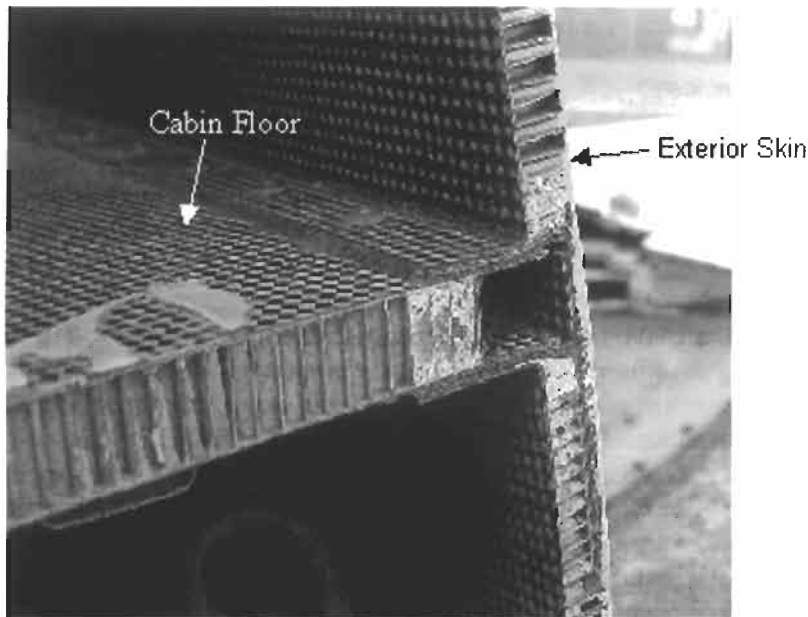


Fig. 42. Starship fuselage bonded composite joint. Reproduced by permission of the Boeing Company.

galleys from corroding the underlying structure and to hold carpets and mats to the passenger compartment floor.

Room-temperature curing epoxies are useful for applications that need higher strength and durability than adhesives such as PSAs and urethanes, but do not require the very high strength of elevated temperature curing structural adhesives. Room-temperature curing epoxies are used for such purposes as bonding rub strips to sliding components such as flaps, to apply permanent identification plates to major assemblies, and to bond composite sandwich panels together to form interior assemblies such as stow bins, lavatories, galleys and closets.

Polysulfides are more commonly used as sealants but are occasionally employed as adhesives as well. Polysulfides adhere well to a wide range of materials and are useful where some flexibility is needed in the joint.

Contact adhesives. Natural and synthetic rubber-based contact adhesives are used for bonding various interior decorative materials such as fabrics and decorative laminates to underlying surfaces.

Cyanoacrylates. Fast curing cyanoacrylates are used for holding shims in place during assembly of components and other applications where fast cure is useful.

Silicones. Silicones are useful where high temperature resistance or compatibility with silicone components such as molded seals are needed. Silicone firewall insulation materials and silicone gaskets and seals are bonded with silicone rubber adhesives.

7. Future technology and applications on commercial aircraft

To some extent, modern applications of adhesive bonding of metal and composites exhibit the maturation of adhesive bonding as just one component of the aircraft designer's toolbox. Neither technology dominates the aircraft; each has its place. Decades of production and service experience with adhesive bonding, combined with the advancement of other fabrication technologies such as automated riveting, high speed machining, welding, super-plastic forming, etc., have given designers a number of options when designing a part. They trade the requirements of a specific application against the advantages and drawbacks of the available manufacturing options to arrive at the lightest, cheapest, most robust design possible.

Maturation as a technology does not mean that advancement and innovation has ceased. Adhesive bonding is so essential to the aerospace field that as long as there is a desire to go higher, faster and farther more efficiently, there will be an incentive to develop new materials and processes for adhesive bonding. Areas of particular interest for future applications are high-temperature adhesives, fiber-reinforced metal laminates and more efficient bond assembly techniques.

There are many applications for which adhesives capable of operating at high temperatures for long periods of time are useful, such as on aircraft engines. Although the cores of modern turbines operate at extremely high temperatures, high bypass ratios mean that a significant portion of the engine is at a much lower temperature.

High-speed aircraft also benefit greatly from high-temperature adhesives. Supersonic flight can produce significant frictional heating of aerodynamic surfaces. Military craft, with their much shorter lives and ability to absorb high fabrication and operational costs, have been able to take advantage of metals such as titanium and high-temperature composites to enable supersonic flight. A cost-effective supersonic commercial aircraft, however, is not possible without significant advances beyond the current technology of high temperature composites and adhesives. The structure of a supersonic commercial aircraft would need to withstand tens of thousands of hours at temperatures approaching 350°F (or higher, depending on cruising speed) without significant degradation as well as have affordable materials and fabrication costs. There have been advances in resin chemistry, particularly with polyimides, that hold out the promise of such materials but they are not yet totally proven or commercially available at reasonable cost. They also require curing at very high temperature (700°F and higher) that necessitates the use of expensive high-temperature tooling and expendable materials and increases fabrication costs. Adhesives based on polymers with slightly lower temperature capabilities such as bismaleimides have been developed and are in use on selected applications.

Fiber-reinforced metal laminates have been developed in recent years and are slowly finding their way onto commercial aircraft. Fiber-reinforced metal

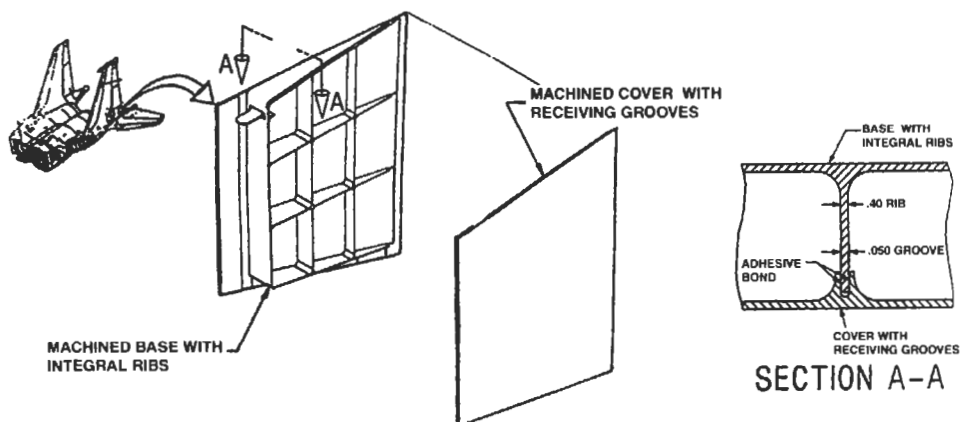


Fig. 43. Grid-lock F-15 rudder fairing. Reproduced by permission of the Boeing Company.

laminates are composite materials comprised of layers of fiber-reinforced resins between layers of metal sheet or foil. The fiber-resin layers act as an adhesive between the metal layers and in some cases the fiber layer matrix is in fact an adhesive film. Various fiber layers such as glass, graphite and aramid fibers can be combined with metals such as aluminum and titanium to tailor the properties of the material to the application. Fiber-metal laminates combine the best properties of metallic structure such as ease of fabrication, damage visibility and lightning strike durability with the fatigue resistance of bonded structure and the high specific strength of composites.

As always, there is constant interest in reducing the fabrication costs of bonded structure. On the composites side of the house this has resulted in continued research into automated (robotic) means of applying composite raw materials to the tool. Although this is most often used to lay down composite fabrics and tapes, it is occasionally used to apply adhesive film as well. Metallic bonded structure has seen the development of concepts such as Grid-Lock[®], a combination of the advantages of accurate high-speed machining and adhesive bonding. Grid-Lock[®] is probably most useful for fabricating assemblies such as flight control surfaces. In the Grid-Lock[®] concept, components of the bonded assembly (skins, ribs, spars, etc.) are machined to size with grooves at the bondlines between the details. For simple assemblies, two major details can be machined. One skin is machined with integral ribs and spars, the other with receiving grooves (Fig. 43). After surface treatment and priming, adhesive in paste form is applied to the grooves, the details assembled and the adhesive cured. Because of the self aligning grooves and precision machining, Grid-Lock[®] assemblies require minimal tooling to assemble and little pressure during adhesive cure.

Commercial transports will undoubtedly follow the lead of their smaller business jet brethren and utilize more bonded primary structure, probably in the form

of advanced composites. As the industry gains experience and confidence and as materials and manufacturing costs are driven down, the advantages of bonded structure become more compelling. Because of continuing advancements in other materials and joining technologies we may not see a completely bonded airframe, but it seems clear that we will see increased use of bonded structure. Both Boeing and Airbus, the remaining large commercial transport manufacturers, have plans for new aircraft that contain significantly increased amounts of bonded primary structure and continue to rely on bonded metal and composite secondary structure.

8. Military applications

The military has historically led the way in the development and application of adhesive bonding on aircraft. This practice continues today, primarily with bombers, fighter and attack aircraft where weight is a critical consideration, but also with support craft such as reconnaissance aircraft and freighters.

The military embraced adhesive bonding earlier and more extensively than the civil aviation industry for two primary reasons, basic factors that dominate many of the differences between military and civil aviation. Much more so than the commercial world, military aviation is concerned with aircraft performance. The advantages that adhesive bonding brings, such as weight efficiency and aerodynamic smoothness, result in significant airframe performance improvements over mechanically fastened structure. Secondly, the military is largely insulated from the risk and cost constraints that limit the use of new and unfamiliar technology on commercial aircraft. Military aircraft designers recognized the potential that adhesive bonding had for improving aircraft performance and were willing to spend the resources to develop the new technology and continue to do so today. Virtually all advancements and innovations in adhesive bonding on commercial aircraft were first developed for military craft. In addition, the military is less constrained by the inevitable higher production and maintenance costs associated with working the bugs out of new technologies. As mentioned previously, early adhesive bonded structure was notorious for in-service delamination and corrosion problems. These problems severely impacted the growth of adhesive bonded aluminum structure on commercial aircraft but were much less detrimental to the use of bonding on military craft.

Because of this continued emphasis on adhesive bonding technology development over the years, the airframes of modern front-line aircraft such as the B-2 bomber and the F-117 and F-22 fighters are largely structurally bonded advanced composites. They tend to be comprised of materials that are more advanced (expensive) than commercial aircraft such as carbon and boron fiber reinforcements with cyanate esters, bismaleimides, polyimides or other high-temperature resin matrices and adhesives.

9. Space applications

Space applications have traditionally pushed the envelope of adhesive bonding technology in selected areas, and continue to do so. The extreme weight sensitivity of spacecraft is the primary driving force behind this interest in bonding. The very high cost of boosting spacecraft structure into orbit makes it cost-effective to spend significant resources to save weight. Exotic materials and processes that are too expensive for use on commercial aircraft are commonplace in the space vehicle industry.

Typical requirements for adhesively bonded structure for space applications vary widely and differ substantially from those for atmospheric vehicles. Because of widespread use of cryogenic rocket fuels, adhesives near tank structure must maintain adequate properties at very low temperatures. At the other extreme, adhesives have been used to bond ablative or insulative heat shields to the bottom of re-entry vehicles since the advent of manned space flight (see pages 33 and 34 in [8]). The expected service life of bonded structure on spacecraft varies tremendously as well. Adhesives on expendable booster structure may have a life measured in minutes, while reusable structure such as the shuttle has a much longer life. Adhesives that are used on structure that reach and remain in orbit for some time, such as satellites and space stations, can be subject to large swings in temperature from varying sun load and must be protected from attack by atomic oxygen. The widely varying requirements are mentioned merely to illustrate the futility of making broad, all-encompassing summaries of adhesives on space vehicles.

Virtually all of the early manned space flight programs (Mariner, Mercury, Apollo) used structural adhesive bonding of large structural assemblies in both booster and payload modules (see p. 546 in [9]). Urethane adhesive was used on some early rocket structure because of low modulus at cryogenic operating temperature [10]. Elevated temperature cure epoxy film and paste adhesives supplanted the urethanes and are standard today in areas of low- to moderately high-temperature exposure because of their ease of fabrication and high strength. Other adhesives such as silicone elastomers, cyanoacrylates and room-temperature epoxies are used to bond many non-structural joints.

As with commercial aircraft, modern spacecraft take advantage of the extreme weight savings potential of bonded composite structure. Solid and liquid tank structure are often filament-wound or fiber-placed carbon fiber–epoxy composite construction, which lends itself well to secondary bonding of support structure with epoxy adhesives. Where service temperatures allow, other graphite–epoxy composites components such as satellite structural members are bonded with epoxy film and paste adhesives to metallic (typically titanium) and composite components. In bonded structure with higher temperature requirements such as payload fairings (aerodynamic heating) or satellite structural radiators (waste heat

from satellite electronics), more heat-resistant cyanate esters and bismaleimides are used.

There has been concerted effort in recent years to develop next generation launch vehicles that are significantly less expensive to operate than traditional expendable boosters. Many of these efforts center on reusable launch vehicles with very low structural mass. Although there have been setbacks such as the failure of the X-33 composite fuel tank during development testing and subsequent program cancellation, it is quite likely that any successful vehicle will contain significant bonded composite structure. The weight savings potential is too great for spacecraft designers to ignore. However, as the X-33 program also illustrated there is significant development work remaining before we are able to take advantage of adhesive bonding for such large, complex structure.

References

1. Truax, T.R., *Gluing Practice at Aircraft Manufacturing Plants and Repair Stations*. Technical Note No. 291, National Advisory Committee for Aeronautics, Washington, DC, 1928.
2. Truax, T.R., *Gluing Wood in Aircraft Manufacture*. Technical Bulletin No. 205, United States Department of Agriculture, Washington, DC, 1930.
3. Bishop, J.A., The history of Redux[®] and the Redux bonding process. *Int. J. Adhes. Adhes.*, **17**, 287–301 (1997).
4. Higgins, A., Adhesive bonding of aircraft structures. *Int. J. Adhes. Adhes.*, **20**, 367–376 (2000).
5. Sorenson, A., Sonic fatigue testing and development of aircraft panels. *Symposium on Structural Adhesives and Sandwich Construction*. Wright Air Development Center, Wright Patterson Air Force Base, Ohio, 1957.
6. Thrall, E.W. Jr., Failures in adhesively bonded structures. *AGARD Lecture Series No. 12, Bonded Joints and Preparation for Bonding*. North Atlantic Treaty Organization Advisory Group for Aerospace Research and Development, London, 1979.
7. Kuperman, M. and Seidl, T., Improved structural adhesive bonding at United Airlines. *Boeing Airliner*, April–June p. 9 (1985).
8. National Materials Advisory Board, National Research Council, *Structural Adhesives with Emphasis on Aerospace Applications*. Marcel Dekker, Inc., New York, 1976.
9. Minford, J.D., *Handbook of Aluminum Bonding Technology and Data*. Marcel Dekker, Inc., New York, 1993.
10. Long, R.L., Cryogenic adhesive application. Papers from the Structural Adhesive Bonding Conference Presented March 15–16, 1966, NASA Marshall Space Flight Center, Clearinghouse for Federal Scientific and Technical Information, 1966.
11. *Adhesive Bonding Alcoa Aluminum*. Aluminum Company of America, Pittsburgh, PA, 1967.
12. Alldredge, J.D. and Holmquist, H.W., Adhesive bonding. *Boeing Airliner*, April–June, 6–8 (1985).
13. Bodnar, M.J., *Structural Adhesives Bonding*. Interscience Publishers, New York, 1966.
14. *Wood Aircraft Inspection and Fabrication*. Bulletin ANC-19, Munitions Board Aircraft Committee, Washington, DC, 1951.

15. Grimes, D.L., *Application of Structural Adhesives in Air Vehicles*. Advisory Group for Aeronautical Research and Development, North Atlantic Treaty Organization, Paris, 1958.
16. Lockshaw, J.J. et al., United States Patent 5,273,806, Structural Element with Interlocking Ribbing, United States Patent Office, 1993.
17. Potter, D.L. et al., *Primary Adhesive Bonded Structure Technology (PABST) Design Handbook for Adhesive Bonding*. Report AFFDL-TR-79-3129, Douglas Aircraft Co., Air Force Flight Development Laboratory (FBA), Air Force Systems Command, WPAFB (November, 1979).
18. Schliekelmann, R.J., *Adhesive Bonding in the Fokker-VFW F-28 Fellowship*. National Technical Information Service, Springfield, VA, 1973.
19. Structural adhesive bonding. *Boeing Airliner*, February, 3–8 (1959).
20. Thrall, E.W. and Shannon, R.W., *Adhesive Bonding of Aluminum Alloys*. Marcel Dekker, Inc., New York, 1985.

Author Index

Berg, J.C., 1
Boerio, F.J., 243
Brown, H.R., 221
Burks, S., 1105

Clemens, L.M., 465

Davis, G.D., 947
Detlefsen, W.D., 869
Dillingham, G., 433
Dunky, M., 1039

Everaerts, A.I., 465

Falsafi, A., 75
Frisch, Jr., K.C., 759

Johnson, M.A., 1009

Kajiyama, M., 813
Kinning, D.J., 535
Klemarczyk, P., 847

Leadley, S.R., 677
Lopata, V.J., 1009

Mangipudi, V.S., 75

Martín-Martínez, J.M., 573
Mercer, D., 1105

O'Hare, L.-A., 677
Owen, M.J., 403

Packham, D., 317
Parbhoo, B., 677
Pate, K.D., 1129
Paul, C.W., 711
Pizzi, A., 1039
Puzianowski, A., 1009

Quesnel, D.J., 139

Righettini, R.F., 823
Rimai, D.S., 139

Schneider, H.M., 535
Spotnitz, W.D., 1105
Syed Asif, S.A., 193

Venables, J.D., 947

Wahl, K.J., 193
Wool, R.P., 351

Subject Index

A

- ablative shields, 1190
- acid acceptors,
 - and neoprene-based adhesives, 661*ff*
 - and rubber base adhesives, 590
- acid-base interactions,
 - and adhesion, 38*ff*
 - and particle adhesion, 178*ff*
- acidic solids, 39*ff*
- acrylic-based adhesives, 823*ff*
- acrylic-based pressure sensitive adhesives, 485*ff*
 - advantages, 486
 - and plasticizers, 504
 - and tackification, 504
 - and crosslinking, 492*ff*
- acrylonitrile–butadiene–styrene copolymers in cyanoacrylate adhesives, 857
- addition crosslinking of
 - silicone-based PSAs, 507
- addition cure silicones, 682, 685*ff*
- adherence, 693
- adhesion, 694
 - hysteresis, 341
 - measurements from contact mechanics, 91*ff*
 - mechanisms, 1011
 - of elastomers, effects of interfacial chains, 115
 - parameter in contact mechanics, 97
 - promotion and silicone-based adhesives, 689*ff*
- adhesive bond strength requirements
 - for aircraft bonding, 1146
 - adhesive bonding advantages, 1130–1132
 - adhesive layup, 1162
 - adhesive shrinkage, 1016
 - adhesively bonded doublers, 1130
 - adsorption, 35
 - adsorption mechanism of adhesion, 11*ff*
 - advancing contact angle, 29
 - aerobic acrylic adhesives, 838
 - aerodynamics of adhesive bonds, 1131
 - AES, 288*ff*
 - AFM, 198*ff*
 - aircraft fluids, resistance of adhesives to, 1147
 - aircraft adhesive bonding process, 1142–1143
 - albumin with glutaraldehyde, 1122–1124
 - aldimine curative in urethane adhesives, 799
 - aliphatic/aromatic resin tackifiers, 722
 - alkaline peroxide treatment of titanium, 980
 - alkyl boron, 836
 - N*-alkyl carbamates, 550*ff*
 - alkyl side chain polymers as release materials, 550*ff*
 - allophanate reaction, 764–765
 - aluminum,
 - boric–sulfuric anodization of, 969
 - chromic acid anodization of, 969
 - chromic–sulfuric acid etching of, 964
 - P2 etch, 964

phosphoric acid anodization of, 965
aluminum trihydrate, 637
aminoplast resin, wood panel
 properties, 1053–1054
 reactions and crosslinking, 1052–1053
anaerobic adhesives, 823, 828
analysis depth in XPS, 267
anionic polymerization of
 cyanoacrylates, 848–849
anisotropic self consistent spring
 model, 229
antimony trioxide, 637
antioxidants, 640ff
 in hot melt adhesives, 728
antiozonants, 644ff
apposition, 1122
aramid-based honeycomb core, 1183
aromatic amine antioxidants, 642, 730
aromatic amines, as primers, 862
aromatic resin tackifiers, 721
associate solution, 48
A-stage phenolic resin, 880
athermal solution, 48
atmospheric oxygen and acrylic
 adhesives, 828, 841
atomic force microscopy, 195, 198ff
ATR-IR, 244ff
attenuated total reflection infrared
 spectroscopy, 244ff
Auger,
 depth profile, 291ff
 electron, 263
 electron emission, 262ff
 process, 288
Auger Electron Spectroscopy, 288ff
autoadhesion, 575
autoclave, 1162–1167

B

Bakelite, 871
barrier primer, 458
basic solids, 39ff
beaded doubler panel, 1175
benzoyl peroxide, 832
bifunctional adhesives, 40ff
bis-maleimide,
 chemistry, 814ff
 resin, 813
bismuth neodecanoate, 771
block copolymers,
 as pressure sensitive adhesives, 479ff
 in hot melt adhesives, 712ff
 as coupling agent, 413–414
blocked isocyanates, 765, 766, 791
blocked urethane adhesives, 791
blood glue, 1134
BMI, 813
bond design, 1159–1161
bonded doublers, 1173
bonding process and wood products, 1078–1080
bookbinding and hot melt adhesives, 748–750
bottle labeling and hot melt adhesives, 747
Boussinesq and Cerruti formalism, 144ff
bovine collagen, 1116
bovine thrombin, 1116
B-stage phenolic resin, 880
t-butyl phenolic resin in rubber-based
 adhesives, 597
butyl rubber, 584, 739
butyl rubber-based adhesives
 formulation and applications, 650ff
butylated hydroxy toluene, 840
butyraldehyde–aniline condensate, 835

C

- C-5 tackifiers, 721
- C-9 tackifiers, 722
- calcium carbonate, 636
- calixarenes, 861
- capillary force, 197
- capillary number, 25
- carbamate formation, 761, 762
- carbon black, 636
- carboxylated latex styrene-butadiene latex, 587
- carton sealing and hot melt adhesives, 745
- casein adhesive, 1133
- Cassie-Baxter equation, 28ff
- centrifuged latex rubber, 582
- chain extenders in urethane adhesives, 771, 772
- chain pull-out,
 - in glassy polymers, 224ff
 - role of friction, 236
- chemical behavior of wood in wood bonding, 1082
- chemical bonding theory, 696
 - of coupling agents, 415-419
- chemical conversion coating, 1172
- chemical interactions and release, 541
- chemical patterning and release, 539
- chemically modified natural rubber, 583
- chlorinated polyolefin, as a primer, 461
- chlorobutyl rubber, 585
- chloroprene-based pressure sensitive adhesives, 511
- chlorosulfonated polyethylene in acrylic adhesives, 831, 835
- chromates, 439ff
- chromic acid anodization, 969, 1143
- chromic acid anodization of titanium, 978
- chromic-sulfuric acid (FPL) Etch, 954, 964, 1143
- chromium complex coupling agent, 411-412
- cigarette manufacture and hot melt adhesives, 750
- cis-poly(1,4-isoprene), 582
- clay, 629, 632
- cleaning of metals, 948
- climbing drum peel, 1147
- coalescing aide, 646
- co-curing, 1182
- coefficient of friction and release coatings, 566
- cohesive energy density, 50
- cohesive zone, 352
 - viscoelastic effects, 127
- compatibility/penetration theory and coupling agents, 424
- composite bonding, 1144-1145, 1156-1158, 1182-1185
- composite repair techniques, 1024
 - and electron beam curable adhesives, 1023
- condensation cure silicones, 682
- condensation kinetics in resole synthesis, 906
- condensation stage,
 - in novolac synthesis, 921
 - in phenolic resin synthesis, 886
- contact adhesion hysteresis, 104
- contact adhesives in aerospace applications, 1186
- contact angle, 8ff
- contact mechanics, 81ff
- contact stiffness, 198ff
 - mechanical properties, 208
 - and glass transition, 204
 - of polydimethylsiloxane, 200
- controlled release additive, 548
- conversion coating of steel, 989
- corrosion-inhibiting primers, 439ff

- coumarone-indene tackifiers, 603ff
- coupling agent, 45ff, 403, 434ff
 - adhesion mechanisms, 414, 415
 - characterization by NMR, 418
- coupling to a mineral surface, 435
- covalent contribution, 42
- craze, 227ff
- creamed latex rubber, 582
- creep compliance function, 180
- critical crack opening displacement, 352
- critical fracture stress, 355
- critical speed of crack propagation, 117
- critical stress intensity factor, 389
- critical surface tension, 23
- crosslinking of rubber base adhesives, 639
- crown ethers, 861
- crushed core honeycomb sandwich, 1176
- C-stage phenolic resin, 880
- cumene hydroperoxide, 838
- cure mechanisms for electron beam curable adhesives, 1020–1023
- curing hot melts, 1076–1077
- curing of rubber base adhesives, 638ff
- cyanoacrylate adhesives, 847ff
 - applications, 864ff
 - co-polymers for, 852
 - in aerospace applications, 1186
 - in wound closure, 865, 1110ff
 - monomers, 850ff
 - primers for, 460
- cyclic PDMS oligomers, 680
- D**
- Dahlquist criterion, 466
- Debye force, 22
- decomposition from ion bombardment, 296
- decorative coatings, primers for, 455
- deformable layer theory and coupling agents, 425
- dendritic zinc, 325
- deoxidizing of metals, 950
- depolymerized liquid natural rubber, 583
- Derjaguin model of particle adhesion, 147ff
- Derjaguin–Muller–Toporov model, 196ff
- design ultimate loads, 1160
- detail preparation, 1161
- dewetting, 240
- di-block content in block copolymer PSAs, 481
- dibutyl tin dilaurate, 733, 762, 771, 782
- Diels–Alder addition in
 - bis-maleimide adhesives, 815, 817
- di-ethanolamine adsorption on aluminum analyzed by SIMS, 299
- diethanol-*p*-toluidine, 833
- diffusion and adhesion, 15ff, 358, 695
- difunctional cyanoacrylate monomers, 851
- N,N*-dimethyl aniline, 833
- dimorpholine diethyl ether in urethane adhesives, 733, 771, 782
- dipole moment, 167
- dipole–dipole interaction, 170ff
- dispersion component of surface energy, 537
- dispersion force, 22ff, 172ff
- dissociation energy of bond, 238
- DMT model, 86ff, 196ff
- double overlap shear, 1157
- Drago constants, 42ff
- drug delivery patches, 504

drying time of rubber-based
adhesives, 575
duct tape, 474
Dugdale crack, 124
Dugdale model, 385
Dupre equation, 7ff, 77, 197
dynamic contact angle, 25
dynamic SIMS, 297

E

elastic modulus from contact
stiffness, 211
elastomeric adhesives, 573ff
electrodynamic interaction, 169
electroforming to produce rough
surfaces, 334
electroless deposition to produce
rough surfaces, 334
electron accelerators, 1029–1032
electron beam curable,
acrylate adhesives, 1014–1016
adhesives, 1012
epoxy adhesives, 1016–1018
block copolymer PSAs, 484
electron beam cure, 496
in hot melt adhesives, 740
electron beam processing, 1009ff
electropriming, 442
electrostatic contribution, 42
electrostatic forces and adhesion, 17,
162, 696
emulsified PMDI, 1067
energies of adsorption and adhesion,
36
energy of activation in hydration
process, 960
epoxized butadiene in hot melt
adhesives, 739
epoxy silicones, 544
epoxy–phenolic adhesive, 931, 932
epoxy–phenolic–nitrile adhesive, 932
equilibrium contact angle, 320

etching of steel, 985ff
ethylene–acrylate copolymers in
cyanoacrylates, 857
ethylene–ethyl acrylate (EEA), 1075
ethylene–vinyl acetate (EVA), 1075
evaporated latex rubber, 581
evaporated metal films on polymers
analyzed by XPS, 273ff

F

Factor V, 1117
Factor XIII, 1113
fail-safe doublers, 1174
fatigue resistance of adhesive bonds,
1130
fibrin sealant, 1113–1116
and pneumostasis, 1121
and drug delivery, 1125–1126
and tissue sealing, 1124–1125
application methods, 1115
fillers,
and rubber base adhesives, 578,
628ff
and silicone-based adhesives, 691ff
in phenolic resin adhesives, 892
fingerjointing, 1064
finite size effects in contact
deformation, 88, 133
first part qualification, 1167
flame treatment of high-density
polypropylene analyzed by
XPS, 280
flame treatment of low-density
polypropylene analyzed by
XPS, 279
flatwise tension test, 1148
Flory–Huggins theory, 393
Flory–Huggins theory of polymer
solubility, 58
fluoroalkyl side chain polymers as
release materials, 555

fluoropolymers as release materials, 549
fluorosilicone release liners, 509
fluorosilicones as release materials, 550
foam tapes, 516ff
foaming adhesives, 1154
formaldehyde emission, 1043
Fox equation, 830
Fox-Flory equation, 476
FPL Etch, 954
fractal dimension, 328
fractal surface, 327ff
 produced by diffusion, 337
fractional polarity, 33
fracture,
 by bond rupture, 389
 by disentanglement, 386
 of entangled polymers, 381ff
fracture energy, 321–322, 352, 1147–1148
 and interface thickness, 338
fracture strength, relationship to solubility parameters, 53
fracture toughness, 225
free radical addition cure of acrylic adhesives, 825–826
free volume, 575
Fuller and Tabor parameter, 185
fumed silica, 633
future adhesive technologies in aerospace applications, 1187–1189

G

gamma ray penetration depth, 1027
garment attachment and hot melt adhesives, 744
GBS (grit blast/silane) treatment of aluminum, 972
gel point in urethane adhesives, 783
generalized fracture mechanics, 129

Gent-Schultz model, 238
geometric mean method and work of adhesion, 33
Gibbs adsorption equation, 9
Gibbs surface free energy, 318
glassy polymers,
 in contact mechanics studies, 105
 joining immiscible, 231
glulam, 1064
Good-Girifalco equation, 22, 113ff, 322
Good-van Oss equation, 323
 γ -GPS adsorption on aluminum analyzed by SIMS, 298
graded layer transition in priming, 451
gradient percolation theory, 391
green strength and rubber-based adhesives, 646
Griffith crack, 124
grit blasting of steel, 989
group contribution methods, 60ff
group interaction parameters, 60
Gutman acceptor number, 41
Gutman donor number, 41

H

Hamaker constant, 147ff
hardness, 42
harmonic mean method and work of adhesion, 33
hemostasis, 1112ff
hemostats, 1105
Hertz equation, 212
Hertz theory, 82ff
Hertzian indenter, 151
heterogeneity,
 and contact angle, 26
 and release, 539
hexamethylene diisocyanate, 767
hexamethylene tetraamine in novolac cure, 924–926

hide and bone glue, 1134
high density fiberboard, 1045
high density polyethylene oxidation
 analyzed by SIMS, 309
high styrene block copolymers in
 PSAs, 482
high temperature adhesives and
 aerospace applications, 1151
hobe, 1158
honeycomb core and adhesive
 bonding, 1154–1156
honeycomb sandwich, 1176
honeycomb sandwich bonding,
 1141–1142, 1145
hot bond fracture stress, 383
hot melt adhesives, 711*ff*
 applications, 741–752
 in wood bonding, 1074–1077
human fibrinogen, 1113
human thrombin, 1113
hybrid acrylic adhesives, 841
hydration inhibitor, 957
hydration of alumina and locus of
 failure, 957
hydrocarbon tackifiers, 606*ff*
hydrogen abstraction, 495
hydrolysis of urea–formaldehyde
 resins, 1051
hydrolytic stability of urethane
 adhesives, 806*ff*

I

implantation of source ions, 296
induced dipole force, 22
Inelastic Electron Tunneling
 Spectroscopy, 417
inhibitor of free radical
 polymerization, 827
initiator of free radical
 polymerization, 832
inorganic primers, 443*ff*
interdiffusion,

 and coupling agents, 421–424
 of polymer chains, 235
 and release, 540
 of random coils, 353
interdigitation of monolayers, 110
interface shape, 229
interface slip, 240
 and release, 542
interfacial free energy, 7*ff*
interfacial restructuring and release,
 553, 557, 560
interfacial strength,
 and group contribution parameter,
 65
 with influxes, 372
interpenetrating network hypothesis
 and silanes, 421–424
interphase, 9*ff*, 433
interstitial voids, 457
inverse gas chromatography, 34*ff*
iodonium salts, 1023
ionic crosslinking, 498
isocyanates in wood adhesives,
 1065*ff*
isocyanurate reaction, 765
isophorone diisocyanate, 767

J

James–Martin correction factor, 35
J-integral, 353*ff*, 384
JKR apparatus, 94
JKR theory, 83*ff*, 150*ff*, 324
Johnson–Kendall–Roberts theory,
 83*ff*, 150*ff*, 324

K

k1 spectrum, 251
Keesom interaction, 22*ff*, 170*ff*
ketimine curative in urethane
 adhesives, 799
knitting ability, 646
knock-on effect, 296

L

lactones in resol cure, 916
 Lake–Thomas model, 238
 laminated beams, 1045
 laminated veneer lumber, 1045
 Langmuir–Blodgett monolayer in
 contact mechanics studies, 110
 Laplace Transform in IR absorption,
 246
 lateral contact stiffness, 202
 Lewis acid catalysis in novolac
 synthesis, 922
 Lifshitz model of interfacial
 interaction, 148ff
 Lifshitz–van der Waals interactions,
 30ff
 lignin, 1040, 1072ff
 lignosulfonates, 1073
 London force, 22ff
 London–van der Waals constant, 147
 longitudinal modulus in a craze, 228
 loop tack test, 471
 lymphostasis, 1119–1120

M

macromers, 500
 magnesium oxide, 629, 635,
 maleic acid, 830
 maleimide terminated oligomers, 819
 maleimide terminated polyimides,
 820
 matrix effects in SIMS, 297
 Maugis–Pollock model, 158
 MDI, 766
 mean free path of electron in XPS,
 267
 mechanical adhesion, 342
 mechanical interlocking,
 in adhesion, 16ff, 695, 972
 and surface preparations, 951ff
 mechanisms of adhesion, 694ff
 medium density fiberboard, 1045

melamine–urea–formaldehyde resins,
 1049ff
 metal aircraft and adhesives,
 1136–1140
 methacrylate monomers, 829
 methacrylate–butadiene–styrene
 copolymers in cyanoacrylate
 adhesives, 857
 methacrylate-terminated polyurethane
 in acrylic adhesives, 831
 4-methoxy phenol, 840
 methyl methacrylate, 829
 methylene 4,4′-biscyclohexyl
 isocyanate, 767
 methylene diphenyl isocyanate, 766
 methylation, 880, 883
 in novolac synthesis, 921
 kinetics in phenolic resin
 adhesives, 896
 Michael addition in bis-maleimide
 adhesives, 813
 microcrystalline waxes in hot melt
 adhesives, 725
 microfibrinous oxide, 325
 microscopic roughness and adhesion,
 951
 minor chain reptation, 360
 mode coupling, 366
 Mode I fracture, 353
 modified Auger parameter, 266
 moisture blooming, 575
 moisture-cure hot melt adhesives,
 731, 784ff
 moisture-cure urethane adhesives,
 781ff
 morphology modification and
 coupling agents, 426
 MQ resin, 506, 548, 549

N

nail solution of weak interfaces, 369

nanindentation and depth sensing, 206
nanoscale roughness, 338
natural rubber-based adhesives, 581
 formulation and applications, 646ff
natural rubber-based pressure
 sensitive adhesives,
 choice of tackifier, 478
 coating, 474
 formulation, 473ff
 phenolic crosslinking, 475
 sulfur crosslinking, 475
negative SIMS, 299
negative spreading coefficient, 537
neoprene rubber,
 and rubber base adhesives, 589ff
 microstructure, 592
 types, 593ff
neoprene rubber-based adhesives,
 formulation and applications,
 660ff
neoprene-phenolic adhesive, 1140
net solution of strong interfaces, 376ff
nitrile rubber and rubber-base
 adhesives, 587ff
nitrile rubber phenolic adhesive,
 929-931
nitrile rubber-based adhesives,
 formulation and applications,
 656ff
nitrile-phenolic adhesive, 1140
non-destructive testing, 1165
non-ideal particles, adhesion of, 183
non-woven fabrics and hot melt
 adhesives, 742
normal operating loads, 1160
novolac cure, 924-926
novolac phenolic resins, 873
 applications, 920
 synthesis, 919ff

O

2-octyl cyanoacrylate, 1110
one-part moisture cure silicones,
 682ff
open time of rubber-base adhesives,
 575
operating environment, 1161
organosilane coupling agent, 435ff
organo-tin catalysts, 684
oriented strand board, 871, 1045
orthoesters, 412
orthosilicates, 405, 409, 410
out-time of adhesives in aerospace
 applications, 1150
overlap shear test, 1147
Owens-Wendt equation, 323
oxidation mechanism, 729
oxidative stability of urethane
 adhesives, 802ff
oxygen inhibition of electron beam
 cure, 1021

P

packaging and masking tapes, 512ff
paper bags and hot melt adhesives,
 751
paraffin waxes in hot melt adhesives,
 725
particle adhesion, effect of asperities,
 184
particle radius and adhesion, 154ff
particleboard, 1044
PASA jel surface preparation for
 titanium, 978
Paschen limit, 167
peel energy, 374
peel force build in acrylic PSAs, 490
peel ply, 1182
peel strength and etching, 247
peel test, 469ff
penetration depth in ATR, 245
permanent dipole force, 22ff

- permanent-induced dipole
 - interactions, 171ff
- petroleum-derived oils, 723–725
- phase separation, 480
- phenol–formaldehyde adhesives,
 - addition of isocyanates, 1059
 - addition of lignins, 1059
 - addition of tannins, 1059
 - addition of urea, 1058
 - reactions and crosslinking, 1056–1057
- phenol–formaldehyde reaction
 - products, 872
- phenolic resins, 869ff
 - safety issues, 875ff
 - general properties, 873
 - in contact adhesives, 936–938
 - in pressure sensitive adhesives, 933–936
 - in wood adhesives, 1054–1055
- phenolic wood adhesives, 871
 - effect of alkali, 1055
 - effect of molecular weight, 1055
- phenolic–poly(vinyl formal) adhesive, 1140
- phenolics as antioxidants, 926–927
- phenol–resorcinol–formaldehyde,
 - adhesives, 1062ff
 - resins, 918
- N*-phenyl-2-propyl-3,5-diethyl-1,2-dihdropyridine, 836
- phosphates as hydration inhibitors, 957
- phosphoric acid anodization, 965, 1144
- phosphoric acid ionization analyzed by XPS, 281
- photoelectron, 262
- photo-induced crosslinking, 495
- physical adsorption theory, 695
- physical crosslinking, 499
- plasma polymerization, 445ff
- plasma spray,
 - of steel, 991
 - to produce porous surface, 335
- plastic adhesive bonding, primers for, 458
- plastic deformation and particle
 - adhesion, 179
- plasticizer migration, 502
- plasticizers,
 - and rubber base adhesives, 578, 624ff
 - in cyanoacrylate adhesives, 856
- platelet gel sealant, 1118–1119
- platinum catalysts, 687
- plywood, 1045
- PMMA in XPS studies, 270
- pneumostasis, 1120–1122
- Poiseuille's equation, 332
- polar comonomers in acrylic PSAs, 487ff
- polar component of surface energy, 537
- polyacrylic acid interacting with metal oxide, analyzed by XPS, 271
- poly(acrylonitrile-co-butadiene) in phenolic adhesives, 927
- poly- α -olefins, 1075
- poly(α -olefin)-based pressure sensitive adhesives, 510
- polyamides, 1075
- poly(butadiene) polyol, 770
- poly(caprolactone) polyols, 762, 764, 770
- polycarbonate polyol, 770
- poly(chloroprene) and rubber base adhesives, 589
- poly(dimethyl siloxane), 678
- polydimethylsiloxane in contact mechanics studies, 102ff
- polyester diols, 733

- polyester polyols, 762
- polyether polyols, 762
- poly(ethylene glycol) and pneumostasis, 1120
- poly(ethylene-co-*n*-butyl acrylate) in hot melt adhesives, 717–718
- poly(ethylene-co-vinyl acetate) in hot melt adhesives, 717–718
- polyethylene waxes in hot melt adhesives, 727
- poly(hexamethylene adipate) polyol, 770
- polyimide, analyzed by XPS, 311
- polyisobutylene, 584
- poly(isobutylene)-based pressure sensitive adhesives, 511
- polyisoprene rubber in contact mechanics studies, 106
- polymer–polymer welding, 390ff
- polymethylene diisocyanate (PMDI), 1065
- poly(2-methylpropane adipate) polyol, 770
- polyolefins,
 - as release materials, 563ff
 - in hot melt adhesives, 716–717
- polyols in urethane adhesives, 768ff
- poly(oxypropylene) polyols, 768
- polyphenylene ether (PPE), analyzed by XPS, 274
- polypropylene oxidation, analyzed by SIMS, 309
- polyterpene tackifiers, 620ff, 720
- poly(tetramethylene oxide) polyol, 770
- polyurethane adhesives, 759ff
 - in wood bonding, 1068
- polyurethane dispersions, 788
- poly(vinyl acetals) in phenolic adhesives, 927–929
- poly(vinyl acetate), 1077–1078
- polyvinyl butyral–phenolic adhesive, 929
- polyvinyl ether-based pressure sensitive adhesives, 509ff
- polyvinyl formal–phenolic adhesive, properties, 927–929
- pore penetration, 331ff
 - kinetics, 332
- Post-It™ Notes, 523ff
- potting compounds, 1154
- pour-coat adhesive, 1177
- practical adhesion, 9, 321ff
- precipitated silicas, 634
- press cycle and wood bonding, 1085–1097
- pressure sensitive adhesive tapes,
 - and graphics applications, 527ff
 - and medical applications, 525ff
 - and office supplies, 522
 - tests, 468ff
 - and the electronics industry, 517ff
 - and the transportation industry, 514ff
- pressure sensitive adhesives,
 - applications, 511ff
 - block co-polymer-based, 479ff
 - criteria, 466
 - definition, 466
 - history, 465
 - natural rubber-based, 472ff
 - tackification, 476
 - types, 466–467
 - in aerospace applications, 1185
- primary composite structure, 1185
- primers, 1153
 - for aerospace applications, 437ff
 - for cyanoacrylate adhesives, 862
- priming and silicone-based adhesives, 690
- printable release liners, 564
- probe tack test, 471
- product qualification, 1150

protective coatings, primers for, 455
pull-off energy, 84
pulse-echo impedance testing, 1165

Q

Quesnel model, 157

R

radial block co-polymers, 482
radiation curable hot melt adhesives, 735
radiation cure silicones, 687
RAIR, 248ff
 microscopy, 261
 studies of plasma polymerized primer, 254
randomization of polymer chains, 359
receding contact angle, 29
receptor groups and adhesion, 397
reconstructive surgery, 1112
recycled rubber in rubber-based adhesives, 583
redox initiation of acrylic adhesives, 826–827
reduced spreading coefficient, 321
reduction–oxidation initiation of acrylic adhesives, 826–827
reflection Fresnel coefficients, 250
reflection–absorption infrared spectroscopy, 248ff
regular solutions, 48
reinforcement of incompatible interfaces, 393ff
relative retention volume, 35
reorganization of surfaces, 341
repair, 1170
reptation, 360ff
repulpable PSAs, 491, 499
resins and rubber-based adhesives, 578
resole cure, 912ff

resole cure accelerators, 916ff
resole phenolic resins, 874
 moisture effect on cure, 892
 in plywood, 890
 synthesis, 880ff
resonance impedance testing, 1165
resorcinol in resole cure, 918
resorcinol–formaldehyde adhesives, 1059ff
restrained layer theory and coupling agents, 424
reticulating adhesive, 1152
reversible hydrolysis theory and coupling agents, 419
reversible work of adhesion, 449
rheological contribution to release phenomena, 542–543
ripple experiment, 363ff
rivet-bonding, 1143
rolling ball tack test, 471
room-temperature curing epoxies in aerospace applications, 1186
rosin tackifiers, 598ff, 719
roughness and contact angle, 26
Rouse dynamics, 366
Rouse relaxation time, 361
RTV silicones, 682ff
rubber base adhesives, 573ff
 features, 576ff
 ingredients, 578ff
rubber–metal priming, 451–452
rugosity factor, 28

S

safety considerations for electron beam cure, 1032–1034
SAFT, 471
scaling laws for interdiffusion, 362
Scatchard–Hildebrand theory of solubility, 49ff
Schapery's theory, 125
scintered steel surface, 335

- scrim, 1145
- sealing of joints, 1132
- SEBS in PSAs, 483, 643
- secondary antioxidants, 730
- secondary composite structure, 1184
- Secondary Ion Mass Spectroscopy, 295ff
- secondary structure, 1159
- self-affine fractal in a grit-blasted surface, 337
- self-assembled monolayers, in adhesion studies, 101 as coupling agent, 412
- self-priming silicone-based adhesives, 691
- semi-structural pressure sensitive adhesives, 505
- shake-up satellite in XPS, 264
- shear adhesion failure test, 471
- shear modulus in a craze, 228
- shear holding power, 470ff
- shear strength, 1146
- shock release, 565
- side chain mobility and release, 553
- silane coupling agent, 403ff
 - analyzed by XPS, 287ff
 - in epoxy coatings, 407
 - in fiberglass, 406
 - in polyurethane coatings, 408
 - types, 404–406
 - and silicone-based adhesives, 691
- silicone acrylates, 546
- silicone adhesives, formulation and applications, 699ff
- silicone networks, 682ff
- silicone organic polymers as release materials, 558ff
- silicone polymers, properties, 680ff
- silicone release coating, 543ff
- silicone release liner chemistry, 543
- silicone-based adhesives, 677ff
 - silicone-based pressure sensitive adhesives, 505ff
- silicones,
 - and mechanisms of adhesion, 692ff
 - in aerospace applications, 1186
- siloxane bond formation, evidence in plumbosiloxane, 416
- siloxane nomenclature, 678ff
- siloxyl unit, 678
- SIMS, 295ff
- small-spot XPS delamination study, 284ff
- smut buildup on steel, 986
- snap cure of acrylic adhesives, 829
- softness, 42
- sol-gel coating,
 - as adhesion primer, 974
 - on steel, 993
 - primer, 444
 - technologies, 1172
- solubility parameter, 51ff
- solvent-borne urethane adhesives, 786ff
- solvents and rubber-based adhesives, 646
- sonic damping by adhesive bonds, 1131
- space applications of adhesives, 1190
- specialty waxes in hot melt adhesives, 727
- spreading coefficient on rough surface, 325
- spreading energy, 321
- spreading pressure, 8ff, 99, 322
- sputtering, 289
 - preferential, 296
 - DC mode, 298
 - pulsed mode, 298
- stabilizers for cyanoacrylates, 849, 850
- stable release force, 553
- stannous octoate, 771

- static SIMS, 297
 - static toughness, 449
 - steel, surface preparation for
 - adhesion, 963ff, 984ff
 - sticker group and adhesion, 354, 395
 - stiffened fairings, 1159
 - stiffened panel designs, 1175
 - strain energy release rate, 90
 - stress singularity, 123
 - structural urethane adhesives, two component, 795ff
 - styrene–butadiene,
 - block copolymers, 479
 - cold latex, 586
 - hot latex, 586
 - and pressure-sensitive adhesives, 510
 - and rubber base adhesives, 585
 - styrene–butadiene rubber-based adhesives formulation and applications, 654ff
 - styrene–ethylenebutylene–styrene block copolymers in block copolymer PSAs, 483
 - styrene–isoprene block copolymers, 479
 - styrene-modified coumarone–indene tackifiers, 605ff
 - substituted urea reaction, 761–762
 - sulfonium salts, 1023
 - surface approach, 356
 - surface chemistry of wood, 1083–1084
 - surface energy, 319
 - and adhesion, 320
 - and coupling agents, 419–421
 - surface forces apparatus, 95ff
 - surface insensitivity additives for cyanoacrylate adhesives, 861
 - surface inspection methods, 994ff
 - surface preparation, 1143–1144
 - surface preparation of aluminum,
 - comparisons, 975
 - surface preparation of titanium,
 - comparisons, 981ff
 - surface rearrangement in adhesion, 356
 - surface roughening from ion bombardment, 296
 - surface roughness,
 - and adhesive joint strength, 334ff, 342ff
 - and wetting, 329ff
 - in inorganic primer films, 446
 - surface tension, 8ff
 - surface tension and wood bonding, 1080
 - surface treatment of composites, 1011
 - surface treatment of metals, 947ff
 - critical processing parameters, 953ff
 - requirements, 947
 - synthetic isoprene, 583
 - synthetic waxes in hot melt adhesives, 726
- T**
- Tabor parameter and the DMT to JKR transition, 86
 - tack and aerospace applications, 1149
 - tack test, 471ff
 - tackification,
 - and storage modulus, 476
 - of block copolymers PSAs, 484
 - tackifier function, 619ff
 - tackifier physical property tests, 612ff
 - tackifiers in hot melt adhesives, 718ff
 - take-off angle in XPS, 267
 - talc, 629, 632
 - Tanner's law, 25
 - tannins, 1070ff
 - tape pop-off, 470

- TDI, 766
tear straps, 1174
tertiary aliphatic amines as primers, 862
tertiary amines in urethanes, 762, 771
tertiary aromatic amines, 832
textured surface and priming, 446
thermal cure addition silicone, 686
thermal stability of urethane adhesives, 801–802
thermal stabilizers in cyanoacrylate adhesives, 859–860
thermodynamic work of adhesion, 7ff, 77ff, 536
thermoplastic urethane adhesives, 793ff
thick-adherend lap shear, 1151
thiol-ene chemistry in hot melt adhesives, 738
thiuram disulphide, 590
three dimensional solubility parameter, 55
threshold toughness, 117
thrombin, collagen and plasma sealant, 1118
through-transmission ultrasonic testing, 1165
time of flight SIMS, 296ff
tissue adhesives, 1105ff
tissue sealing, 1122–1124
titanium, surface preparation of, 961ff, 977ff
titanium oxide, 629–634
toluene diisocyanate, 766
topology and release, 539
toughened epoxy adhesives, 1141, 1145
tougheners,
 in acrylic adhesives, 830
 in cyanoacrylate adhesives, 857ff
trailing edge wedge, 1178–1181
transfer tapes, 520
Trommsdorff Gel Effect and acrylic adhesives, 828
tube renewal time, 360
two-part condensation cure silicones, 683ff
- U**
UNIFAC, 60ff
urea in phenolic resin adhesives, 894
urea-formaldehyde resins, 1046ff
urethane,
 catalysts, 771
 chemistry, 760ff
 morphology, 772ff
 reaction, 761
 structure-property relationship, 779, 780
UV absorbers, 644
UV cure acrylics in hot melt adhesives, 740
- V**
vacuum bag, 1142
valence electron in XPS, 264
vector percolation model of fracture, 377
viscoelastic contact, 203
viscoelastic energy dissipation in elastomers, 238
viscoelastic polymer adhesion and contact mechanics, 122
viscoplastic processes at interface, 374ff
viscosity control,
 and wood bonding, 1079
 in cyanoacrylate adhesives, 856
vulcanization of rubber-based adhesives, 638
- W**
waferboard, 871
Washburn equation, 332

- water/isocyanate reaction, 763
 - water-based primers, 437
 - water-borne urethane adhesives, 788ff
 - two component, 797ff
 - waxes, 725–728
 - in acrylic adhesives, 840
 - weak boundary layer, 354
 - and release, 541
 - theory of adhesive bonding, 697
 - weight efficiency of adhesive bonds
 - of adhesive bonds, 1130
 - welding and crack healing, 355ff
 - Wenzel equation, 28
 - Wenzel roughness factor, 325ff
 - wetting,
 - and adhesion, 357–358
 - and coupling agents, 419–421
 - and solid surface energy, 19ff
 - requirements in adhesion, 17ff
 - windshield sealants, 784
 - wood adhesives, 1039ff
 - requirements, 1041–1043
 - types, 1041
 - wood composition, 1040–1041
 - wood moisture content, 1084–1085
 - wood properties, 1080–1085
 - wood species, 1081
 - wood structure, 1040–1041
 - wooden aircraft and applications of
 - adhesives, 1132–1136
 - work of adhesion, 150, 196, 321
 - work of cohesion, 321
 - work of peel, 536
 - Wu's equation, 323
- X**
- XPS, 261ff
 - X-ray photoelectron spectroscopy, 261ff
 - X-ray radiography, 1166
- Y**
- Young–Dupre equation, 9ff
 - Young's equation, 9ff, 98, 320ff
- Z**
- z-axis conductive tapes, 519
 - zinc oxide, 629, 635
 - Zisman plot, 21
- Greek**
- χ parameter, 59

ISBN 0 444 51140 7



9 780444 511409